N80 75348

QUIET CLEAN SHORT-HAUL EXPERIMENTAL ENGINE (QCSEE)

Under-the-Wing (UTW) Final Design Report

June, 1977

by

Advanced Engineering & Technology Programs Department
Group Engineering Division

GENERAL ELECTRIC COMPANY

(NASA-CR-134847) QUIET CLEAN SHORT-HAUL EXPERIMENTAL ENGINE (QCSEE) UNDER-THE-WING (UTW) DESIGN REPORT Final Report (General Electric Co.) 730 p

N80-75348

Unclas
00/07 17913

Prepared For

National Aeronautics and Space Administration

NASA-Lewis Research Center

Contract NAS3-18021

1. Report No.
NASA CR-134847

2. Government Accession No.

3. Recipient's Catalog No.
CR134 847

4. Title and Subtitle
QUIET CLEAN SHORT-HAUL EXPERIMENTAL ENGINE (QCSEE) UNDER THE WING (UTW) FINAL DESIGN REPORT

5. Report Date
May 1977

6. Performing Organization Code

7. Author(s)
Advanced Engineering & Technology Programs Department
Group Engineering Division

8. Performing Organization Report No.

9. Performing Organization Name and Address
General Electric Company
Aircraft Engine Group
Cincinnati, Ohio 45215

10. Work Unit No.

11. Contract or Grant No.
NAS3-18021

12. Sponsoring Agency Name and Address
National Aeronautics & Space Administration
Washington, D.C. 20546

13. Type of Report and Period Covered
Contractor Report

14. Sponsoring Agency Code

15. Supplementary Notes
Design Report, Project Manager, C.C. Ciepluch, QCSEE Project Office, Technical Advisor, N.E. Samanich, NASA-Lewis Research Center, Cleveland, Ohio 44135

16. Abstract

The QCSEE Program provides for the design, fabrication, and testing of two experimental high-bypass geared turbofan engines and propulsion systems for short-haul passenger aircraft. The overall objective of the program is to develop the propulsion technology required for future externally blown flap types of aircraft with engines located both under-the-wing and over-the-wing. This technology includes work in composite structures and digital engine controls.

17. Key Words (Suggested by Author(s))
Aerodynamics
Aircraft propulsion and power
Composite materials
Acoustics

18. Distribution Statement

19. Security Classif. (of this report)
Unclassified

20. Security Classif. (of this page)
Unclassified

21. No. of Pages

22. Price

NASA-C-168 (Rev. 6-71)

FOREWORD

The Quiet Clean Short-Haul Experimental Engine (QCSEE) Program is currently being conducted by the General Electric Company, Aircraft Engine Group under NASA Contract NAS3-18021. The QCSEE Program is under the direction of Mr. C.C. Ciepluch, NASA Project Manager.

This report presents results of the Under-the-Wing (UTW) experimental engine detail design effort. An oral review covering the results of UTW detail design activity was presented at NASA-Lewis Research Center January 20 and 21, 1975. The UTW system design and analysis effort was conducted under the direction of Mr. N.E. Samanich, NASA UTW Systems Manager.

TABLE OF CONTENTS

Section Page

1.0 INTRODUCTION 1

2.0 SUMMARY 3

2.1 Program Objectives 3
2.2 Specific Technical Objectives 4

2.2.1 Noise 4
2.2.2 Pollution 4
2.2.3 Thrust-to-Weight 4
2.2.4 Thrust Reversal 5
2.2.5 Engine Bleed 6
2.2.6 Power Extraction 6
2.2.7 Dynamic Thrust Response 6
2.2.8 Distortion Tolerance 6
2.2.9 Oil Consumption 6
2.2.10 Dumping 6
2.2.11 General Design Criteria 6

2.3 Operating Requirements 8

2.3.1 Life and Duty Cycle 8
2.3.2 Flight Attitudes 9

2.4 UTW Experimental Propulsion System 9
2.5 UTW Flight Propulsion System 14

3.0 ACOUSTIC DESIGN 17

3.1 Summary 17
3.2 Design Requirements 18
3.3 System Acoustic Design Considerations 21
3.4 Noise Components 22

3.4.1 Takeoff Noise 22
3.4.2 Approach Noise 22
3.4.3 Reverse Thrust Noise 26

3.5 Component Design 26

3.5.1 Fan Inlet Design 28
3.5.2 Fan Exhaust Design 28
3.5.3 Core Exhaust Design 43

3.6 System Noise Levels 51

TABLE OF CONTENTS (Continued)

Section		Page
4.0	EMISSIONS CONTROL	54
	4.1 Summary	54
	4.2 Exhaust Emissions Design Goals	55
	4.3 Selected Combustor Design	57
	4.4 Predicted UTW Engine Emissions Characteristics with Selected Version of F101 PV Combustor	64
	4.4.1 Smoke Emissions	64
	4.4.2 Gaseous Emissions	64
	4.5 Pertinent Emissions Reductions Design Technology	66
	4.6 Predicted UTW Emissions Characteristics - with Added Emissions Control Features	80
5.0	ENGINE CYCLE AND PERFORMANCE	89
	5.1 Summary	89
	5.2 Cycle Selection Criteria	89
	5.3 Engine and System Performance	93
6.0	FAN AERODYNAMIC DESIGN	107
	6.1 Summary	107
	6.2 UTW Fan Aerodynamic Design	108
	6.2.1 Operating Requirements	108
	6.2.2 Basic Design Features	108
	6.2.3 Reverse Flow	112
	6.2.4 Performance Representation with Variable Pitch	114
	6.2.5 Detailed Configuration Design	114
	6.2.6 Rotor Blade Design	122
	6.2.7 Core OGV Design	139
	6.2.8 Transition Duct Strut Design	153
	6.2.9 Vane-Frame (Fan Bypass OGV) Design	153
	6.2.10 Fan Performance Based on Scale Model Tests	168
7.0	VARIABLE-PITCH FAN ACTUATION SYSTEMS	182
	7.1 Summary	182
	7.2 Design Requirements and Criteria	185
	7.3 Hamilton Standard Cam-Harmonic Drive Variable-Pitch Actuation System	187

TABLE OF CONTENTS (Continued)

Section | Page

7.3.1 System Description 187
7.3.2 Component Design 193
7.3.3 Actuator System Lubrication 220
7.3.4 Blade Pitch Angle Range 225
7.3.5 Actuation System Weight 226

7.4 General Electric Ball Spline Variable-Pitch Actuation System 226

7.4.1 System Description 226
7.4.2 Component Design 230
7.4.3 Lubrication System 260
7.4.4 Maximum Blade Pitch Angle Actuation Range 260
7.4.5 Actuation System Weight 260
7.4.6 Design Blade Angle Setting Accuracy 260

8.0 FAN ROTOR MECHANICAL DESIGN 264

8.1 Summary 264
8.2 Composite Fan Blades 266

8.2.1 Design Requirements 266
8.2.2 Basic Design Features 267
8.2.3 Design Analysis 282

8.3 Fan Disk 307
8.4 Blade Support Bearing 307
8.5 Blade Trunnion 316
8.6 Fan Spinner 322
8.7 Fan Attachment Hardware 322

9.0 FAN FRAME MECHANICAL DESIGN 325

9.1 Summary 325
9.2 Design Requirements 331

9.2.1 Loads 331

9.3 Structural Description 331
9.4 Structural Functions 339
9.5 Structural Concept 339
9.6 Design Analysis 345

TABLE OF CONTENTS (Continued)

Section Page

9.6.1 Thermal Analysis 351
9.6.2 Dynamic Analysis 356
9.6.3 Weight Analysis 356

9.7 Supporting Data 356

9.7.1 Element Test Program 356
9.7.2 Fluid Exposure Tests 360
9.7.3 Subcomponent Tests 366

10.0 REDUCTION GEAR DESIGN 371

10.1 Summary 371
10.2 Design Requirements 373
10.3 Design Description 373
10.4 Design Approach 373
10.5 Design Analysis and Results 378

10.5.1 Design Conditions 378
10.5.2 Materials 379
10.5.3 Reduction Gear Geometry 379
10.5.4 Stress Analysis 379
10.5.5 Design Oil Flow Rates 381
10.5.6 Reduction Gear Efficiency 386
10.5.7 Heat Rejection 386
10.5.8 Gear Scoring 386
10.5.9 Star Gear Bearing 386
10.5.10 Weight 390

10.6 Component Test Programs 390

10.6.1 Star Gear Bearing Tests 390
10.6.2 Reduction Gear Back-to-Back Test 394

11.0 ENGINE CORE AND LOW PRESSURE TURBINE DESIGN 397

11.1 Summary 397
11.2 Design Requirements 397
11.3 Engine Core Modifications 398

11.3.1 Accessory Drive Gear Mount 398
11.3.2 Compressor IGV Inner Flowpath 398
11.3.3 Compressor Stator Actuator 398
11.3.4 Compressor First Stage Rotor Blade Airfoil 402
11.3.5 Combustor 402
11.3.6 HP Turbine Diaphragm Area 404

TABLE OF CONTENTS (Continued)

Section Page

11.3.7 LP Turbine Diaphragm 404
11.3.8 Low Pressure Turbine Second Stage Blade 404
11.3.9 Turbine Frame 404
11.3.10 Balance Piston 404
11.3.11 PV Turbine Shrouds 408
11.3.12 Warm Bridge HP Turbine Blade 408

11.4 Low Pressure Turbine Frame Aerodynamic Design 408

11.4.1 Introduction 408
11.4.2 Design 408
11.4.3 Off-Design Study 414

11.5 Low Pressure Turbine Frame Mechanical Design 422

11.5.1 Summary 422
11.5.2 Design Requirements 422
11.5.3 Design Description 422
11.5.4 Design Analysis 429

12.0 BEARINGS AND SEALS DESIGN 448

12.1 Summary 448
12.2 Design Requirements 449
12.3 Lubrication System 449

12.3.1 Oil Supply System 450
12.3.2 Oil Scavenge Subsystem 457
12.3.3 Vent Subsystem 467
12.3.4 Flight Engine Thermal Balance 468
12.3.5 Heat Exchanger 468
12.3.6 Hydraulic System 468
12.3.7 Seal Pressurization Subsystem 472

12.4 Rotor Thrust Balance 473

12.4.1 Fan Rotor Balance 473
12.4.2 Core Engine 477
12.4.3 Low Pressure Turbine Rotor 477

12.5 Bearings, Seals, and Sumps Design 483

12.5.1 Forward Sump 485
12.5.2 Aft Sump 488

TABLE OF CONTENTS (Continued)

Section		Page
	12.6 Accessory Drive Design	500
	12.6.1 Accessory Gearbox	504
	12.6.2 Scavenge Pump	509
13.0	CONTROLS AND ACCESSORIES DESIGN	511
	13.1 Summary	511
	13.2 Design Requirements	512
	13.3 Engine Control System	512
	13.3.1 General Description	513
	13.3.2 Automatic Control	513
	13.3.3 Manual Control	539
	13.3.4 Hydromechanical Control	539
	13.3.5 Digital Control Subsystem	543
	13.4 Fuel Delivery System	565
	13.5 Variable-Geometry Actuation Systems	565
	13.5.1 Hydraulic Supply System	565
	13.5.2 Fan Nozzle Actuators	571
	13.5.3 Fan Pitch and Fan Nozzle Servovalves	573
	13.5.4 Core Stator Actuation and Feedback	576
	13.6 Sensors	576
	13.6.1 Low Pressure Turbine (LPT) Speed Sensor	576
	13.6.2 Core Engine Speed Sensor	577
	13.6.3 Fan Inlet Temperature (T12) Sensor	579
	13.6.4 Absolute and Differential Pressure Sensors	581
	13.6.5 Position Feedback Sensors	581
14.0	NACELLE AERODYNAMIC DESIGN	584
	14.1 Summary	584
	14.2 Design Requirements	587
	14.3 Component Design	588
	14.3.1 Inlet	588
	14.3.2 Fan Bypass Duct and Exhaust Nozzle	594
	14.3.3 Core Nozzle	605
	14.3.4 Pylon	605
	14.4 References	608

TABLE OF CONTENTS (Concluded)

Section Page

15.0 NACELLE MECHANICAL DESIGN 609

15.1 Summary 609

15.1.1 Flight Propulsion System 609
15.1.2 Experimental Propulsion System 611

15.2 Design Criteria 615
15.3 Composite Nacelle Design 616

15.3.1 Inlet 617
15.3.2 Fan Bypass Duct 625
15.3.3 Fan Nozzle 631
15.3.4 Core Cowl 645
15.3.5 Core Nozzle Design 645
15.3.6 Mounting System 651
15.3.7 Accessories 659

15.4 Boiler Plate Nacelle Design 662

15.4.1 Inlet 662
15.4.2 Fan Bypass Duct 663
15.4.3 Core Cowl 671
15.4.4 Boiler Plate Nacelle Pylon-Skirt Assembly 671
15.4.5 Composite Nacelle Pylon-Skirt Assembly 671

16.0 SYSTEM VIBRATION ANALYSIS 674

16.1 Summary 674
16.2 Design Requirements 674
16.3 Vibration Analysis 676

16.3.1 Method of Analysis 676
16.3.2 Vibration Model 677
16.3.3 Analysis Results 679
16.3.4 Conclusions 681

17.0 WEIGHT 689

LIST OF ILLUSTRATIONS

Figure		Page
2-1.	QCSEE Operating Envelope.	10
2-2.	QCSEE Design Loads.	11
2-3.	QCSEE Flight Attitudes.	12
2-4.	UTW Experimental Propulsion System.	13
2-5.	UTW Flight Propulsion System.	15
3-1.	UTW Experimental Engine Acoustic Configuration.	19
3-2.	QCSEE Acoustic Requirements.	20
3-3.	Takeoff Noise Constituents.	24
3-4.	Approach Noise Constituents.	25
3-5.	Reverse Thrust Noise Constituents.	27
3-6.	Inlet Noise Reduction Concepts.	29
3-7.	Summary - Inlet Acceleration Suppression.	30
3-8.	Inlet Noise Reduction Concepts.	31
3-9.	Inlet Noise Reduction Due to Treatment.	32
3-10.	Accelerating Inlet Configurations.	33
3-11.	Low Throat Mach Number Configurations.	34
3-12.	Effect of Angle of Attack on Acceleration Suppression.	35
3-13.	UTW Fan Spectra.	37
3-14.	Cold Flow Duct Test Results.	38
3-15.	Phased Treatment Suppression.	39
3-16.	Rotor, OGV Treatment Suppression.	40
3-17.	Slant Cell Treatment Suppression Results.	41
3-18.	Flow Noise Effects.	42

LIST OF ILLUSTRATIONS (Continued)

Figure		Page
3-19.	Effect of Vane-Blade Ratio on Rotor 55 Second Harmonic.	44
3-20.	UTW Side-Branch Resonator Treatment Configuration.	45
3-21.	UTW Core Stacked SDOF Treatment Configuration.	46
3-22.	Core Suppressor Cold Flow Duct Tests.	47
3-23.	F101 Core Noise Measurement.	48
3-24.	Farfield Core Noise Measurements Vs. Predictions.	49
3-25.	Probe Measured Vs. Predicted Combustor Noise.	50
3-26.	Effect of Constituent Suppression on UTW System Noise.	52
3-27.	UTW Approach and Takeoff EPNdB Contours.	53
4-1.	EPA Smoke Emission Standards.	58
4-2.	F101 PV Combustor.	59
4-3.	F101 PV Air Blast Carburetor and Low Pressure Fuel Injector.	60
4-4.	Comparison of CO and C_xH_y Emissions of the PFRT Combustor and Selected F101 PV Combustor at UTW Ground Idle Conditions.	62
4-5.	Exit Temperature Characterisitcs of QCSEE UTW Engine Equipped with Modified PV Combustor.	63
4-6.	Peak Smoke Emission Characteristics of GE-AEG Class T2 Engines.	65
4-7.	Estimated Gaseous Exhaust Characteristics of QCSEE UTW Engine Based on CFM56 Component Test Data.	67
4-8.	C_xH_y Emissions Characteristics of AEG Commercial Engines (Class T2).	71
4-9.	NO_x Emissions Characteristics of AEG Commercial Engines (Class T2).	72
4-10.	CO Emissions Characteristics of AEG Commercial Engines (Class T2).	73

LIST OF ILLUSTRATIONS (Continued)

Figure		Page
4-11.	CO and C_xH_y Emissions Characteristics of Selected F101 PV Engine Combustor.	75
4-12.	Relationships Between CO and H/C's Emissions and Combustion Efficiency.	76
4-13.	C_xH_y and CO Reductions in CF6-6 Engine with Increased CDP Bleed Air Extraction.	79
4-14.	Fuel Staging Methods at Idle in the CF6 Engine.	81
4-15.	C_xH_y and CO Reductions in a CF6-50 Engine Combustor.	82
4-16.	C_xH_y and CO Reductions in Higher Pressure Ratio Engine Equipped with a PFRT and a PV Combustor.	83
4-17.	Characteristics of UTW Combustor Inlet Conditions with Increased Flat Pitching of Variable Fan.	86
4-18.	Idle Emissions Characteristics of UTW with Increased Combustor Inlet Temperature for Increased Fan Flat Pitching.	87
5-1.	QCSEE Inlet Ram Recovery Characteristics.	90
5-2.	QCSEE Inlet Characteristics.	91
5-3.	Predicted Fan Performance, Nominal Pitch.	95
5-4.	Predicted Fan Performance, Takeoff Pitch.	96
5-5.	Predicted Fan Performance, Cruise Pitch.	97
5-6.	Cooling Flow Schematic.	98
5-7.	Station Designations - Forward Thrust Mode.	102
5-8.	Station Designations - Reverse Thrust Mode.	103
5-9.	UTW Operating Characteristics During Approach.	105
6-1.	UTW Variable-Pitch Fan Design Requirements.	109
6-2.	Cross Section of UTW Variable-Pitch Fan.	110
6-3.	UTW Fan Blade Geometry at Different Pitch Angle Settings.	113

LIST OF ILLUSTRATIONS (Continued)

Figure		Page
6-4.	UTW Fan Stage Characteristics at 100% Speed for Various Pitch Settings.	115
6-5.	Radial Distribution of Rotor Total Pressure Ratio.	117
6-6.	Radial Distribution of Rotor Efficiency.	118
6-7.	Radial Distribution of Rotor Diffusion Factor.	119
6-8.	Radial Distribution of Rotor Relative Mach Numbers.	120
6-9.	Radial Distribution of Rotor Relative Air Angles.	121
6-10.	Radial Distribution of Design Parameters for Core OGV.	123
6-11.	Rotor Incidence, Deviation, and Empirical Adjustment Angles.	138
6-12.	Rotor Throat Margin Distribtution.	140
6-13.	UTW Fan Rotor Blade Plane Sections.	141
6-14.	UTW Fan Rotor Camber and Stagger Angle Radial Distributions.	147
6-15.	Rotor Thickness Distributions.	148
6-16.	Core OGV Aerodynamic Design Characteristics.	149
6-17.	Core OGV Geometry Parameters.	150
6-18.	Cylindrical Section of Core OGV at the Pitch Line Radius.	151
6-19.	Transition Duct Flowpath.	154
6-20.	Nominal and Modified Transition Duct Strut Cylindrical Sections.	155
6-21.	Vane-Frame (Fan Bypass OGV) Aerodynamic Environment.	157
6-22.	Vane-Frame (Fan Bypass OGV) Diffusion Factor for Nominal Vanes.	158
6-23.	Vane-Frame (Fan Bypass OGV) Unwrapped Section at ID.	160
6-24.	Vane-Frame (Fan Bypass OGV) Unwrapped Section at ID - Detail Near Pylon LE Fairing.	161

LIST OF ILLUSTRATIONS (Continued)

Figure		Page
6-25.	Vane-Frame (Fan Bypass OGV) Stagger and Camber Distributions.	169
6-26.	Vane-Frame (Fan Bypass OGV) Solidity and Chord Distributions.	170
6-27.	Fan Bypass Stream Performance Map at Design Rotor Stagger Setting.	171
6-28.	Fan Bypass Stream Performance at Cruise Rotor Stagger Setting.	173
6-29.	Fan Bypass Stream Performance Map at Estimated Takeoff Rotor Stagger Setting.	174
6-30.	Fan Hub Pressure Ratio Correlation (Forward Mode).	175
6-31.	Fan Hub Efficiency Correlation (Forward Mode).	176
6-32.	Reverse Mode Fan Performance.	178
6-33.	UTW Fan Scale Model Gross Reverse Thrust, Scaled to Engine Size.	179
6-34.	UTW Fan Reverse Mode Universal Characteristics.	180
6-35.	UTW Fan Reverse Mode Adiabatic Efficiency.	181
7-1.	Hamilton Standard Cam-Harmonic Drive Actuator System.	183
7-2.	General Electric Ball Spline Actuator System.	184
7-3.	UTW Mission Duty Cycle.	186
7-4.	Net per Blade Twisting Torque at 3244 rpm, SLS Standard Day.	189
7-5.	Beta Regulator Schematic.	191
7-6.	Blade Trunnion Arm and Roller.	195
7-7.	Trunnion Arm Bending Moment Distribution from Centrifugal Force at 3347 rpm.	196
7-8.	Roller Cyclic Load Conditions.	199

LIST OF ILLUSTRATIONS (Continued)

Figure		Page
7-9.	Cam Assembly.	200
7-10.	Harmonic Drive.	203
7-11.	No-Back.	209
7-12.	Torque Limiter Brake.	212
7-13.	Differential Gear Assembly.	214
7-14.	Flexible Shaft.	216
7-15.	Beta Regulator.	218
7-16.	Beta Regulator.	219
7-17.	Beta Regulator - Hydraulic Motor Torque/Speed Performance.	221
7-18.	Beta Regulator - Hydraulic Motor Flow/Speed Performance.	222
7-19.	Lubrication Schematic.	224
7-20.	GE Ball Spline Actuation System.	228
7-21.	GE Ball Spline Variable-Pitch Mechanism Schematic.	229
7-22.	Actuator Design Speed and Load Characteristics.	231
7-23.	Bevel Gear Geometry.	232
7-24.	Forward Ring Gear Deflections.	235
7-25.	Aft Ring Gear Deflections.	236
7-26.	Forward Ring Gear Design Loads and Stresses.	237
7-27.	Aft Ring Gear Design Loads and Stresses.	238
7-28.	Axial Support Link Design Loads and Stresses.	239
7-29.	Ring Gear Sliding Thrust Bearing Design Loads.	240
7-30.	Forward Drive Cone Design Loads and Stresses.	242
7-31.	Aft Drive Cone Design Loads and Stresses.	243

LIST OF ILLUSTRATIONS (Continued)

Figure		Page
7-32.	Ball Spline.	244
7-33.	Ball Spline Outer Diameter Member Design Loads and Stresses.	246
7-34.	Ball Spline Midmember Design Loads and Stresses.	247
7-35.	Ball Spline Inner Diameter Member Design Loads and Stresses.	248
7-36.	Ball Screw Assembly.	249
7-37.	Ball Screw.	250
7-38.	Ball Nut.	251
7-39.	Ball Screw Thrust Ball Bearing.	252
7-40.	Axial Dynamic Stop (Forward).	254
7-41.	Hydraulic Motor.	255
7-42.	Hydraulic Motor Characteristics Torque Versus Speed.	256
7-43.	LVDT Drive Schematic.	257
7-44.	Differential and No-Back.	259
7-45.	Actuation Lubrication System.	261
8-1.	UTW Fan Rotor Configuration.	265
8-2.	UTW Composite Fan Blade and Platform.	268
8-3.	UTW Composite Fan Blade.	270
8-4.	Molded Fan Blade.	271
8-5.	Blade Airfoil Sections.	272
8-6.	Radial Sections Through the Molded Blade.	274
8-7.	Ply Layup and Material Arrangement.	275
8-8.	UTW Composite Blade.	277
8-9.	Dovetail Molded Section.	281

LIST OF ILLUSTRATIONS (Continued)

Figure		Page
8-10.	Platform Design.	283
8-11.	UTW Blade Resultant Radial Stress - 3326 rpm.	284
8-12.	Calculated Blade Radial Stress.	285
8-13.	Calculated Blade Chordal Stress.	286
8-14.	Calculated Blade Interlaminar Shear Stress.	287
8-15.	UTW Blade Displacements and Twist.	288
8-16.	Calculated Blade Relative Radial Stresses for First Flexural Mode.	289
8-17.	Calculated Blade Relative Radial Stresses for Second Flexural Mode.	290
8-18.	Calculated Blade Relative Radial Stresses for First Torsional Mode.	291
8-19.	Allowable Stress Range Diagram - Blade Radial Stress.	292
8-20.	Allowable Stress Range Diagram - Blade Radial Stress.	294
8-21.	Allowable Stress Range Diagram - Dovetail Shear Stress.	295
8-22.	Platform Cross Section.	296
8-23.	Limit Cycle Boundaries.	301
8-24.	Campbell Diagram - UTW Composite Blade.	302
8-25.	UTW Blade Transferred Impact Energy for a 1.81 kg (4 lb) Bird.	304
8-26.	Composite Blade Predicted Gross Impact Capability.	305
8-27.	UTW Blade Impact Momentum for a 0.68 kg (1.50 lb) Bird.	306
8-28.	Fan Rotor.	308
8-29.	Bearing and Disk Seat.	309
8-30.	Fan Disk Stresses with Hamilton-Standard Actuator.	311

LIST OF ILLUSTRATIONS (Continued)

Figure		Page
8-31.	Blade Thrust Bearing.	312
8-32.	Blade Trunnion.	317
8-33.	UTW Blade Trunnion Stresses.	318
8-34.	GE Ball Spline Actuation System.	320
8-35.	Hamilton-Standard Variable Pitch Interface.	321
8-36.	Fan Flowpath Adapters.	323
9-1.	OTW Fan Frame.	326
9-2.	Simulated Composite Frame.	327
9-3.	QCSEE Composite Frame.	328
9-4.	Frame Assembly.	329
9-5.	QCSEE Fan Design Bypass OGV/Frame Aero Design Air Loads - Closed 2°, Open 2°, and Nominal Vanes.	334
9-6.	Fan Core OGV Assembly.	335
9-7.	Fan Frame Service Areas.	336
9-8.	Fan Frame Service Areas.	337
9-9.	Fan Frame Service Areas (Forward Looking Aft).	338
9-10.	Composite Frame.	340
9-11.	UTW Frame Midwheel.	342
9-12.	Nominal Bypass Vane Skin.	343
9-13.	Core Strut Skin.	344
9-14.	Fan Blade Containment Ring.	346
9-15.	Fan Frame Acoustic Treated Areas.	347
9-16.	Computer Analytical Model of Composite Frame.	348

LIST OF ILLUSTRATIONS (Continued)

Figure		Page
9-17.	Computer-Generated 3-Dimensional Finite Element Model - Composite Frame.	349
9-18.	Computer-Generated End View Finite Element Model - Composite Frame.	350
9-19.	First Flexural Mode of Composite Frame Bypass Vanes.	357
9-20.	Graphite/Epoxy AS 3501 Exposed to Skydrol 500C for 5 Minutes at 356 K (180° F), Tested at 356 K (180° F).	365
9-21.	Frame Subcomponent Test Areas.	368
10-1.	UTW Engine Low Pressure Rotor Configuration.	372
10-2.	Main Reduction Gear Configuration.	374
10-3.	Curtiss-Wright YT49-W-1 Reduction Gear.	376
10-4.	Sun Gear Stresses.	382
10-5.	Star Gear Stresses.	383
10-6.	Ring Gear Stresses.	384
10-7.	Star Gear Spherical Roller Bearing.	389
10-8.	Bearing Test Rig Schematic.	392
10-9.	Bearing Test Rig.	393
10-10.	Main Reduction Gear Test Rig Schematic (Back-to-Back Test).	396
11-1.	Accessory Drive Gear Mount.	399
11-2.	Compressor IGV Inner Flowpath.	400
11-3.	UTW Compressor Stator Schedule.	401
11-4.	UTW Engine Frequency Margin, Takeoff.	403
11-5.	Compressor Characteristics.	405
11-6.	High Pressure Turbine Stator Assembly.	406

LIST OF ILLUSTRATIONS (Continued)

Figure		Page
11-7.	Low Pressure Turbine Stage 1 Stator Assembly.	407
11-8.	QCSEE OGV/Frame Flowpath.	411
11-9.	QCSEE Turbine Frame Axisymmetric Flow Analysis.	412
11-10.	QCSEE Vane Modification.	413
11-11.	CASC Mach Number Distributions.	415
11-12.	CASC Mach Number Distributions.	416
11-13.	Turbine Frame Axisymmetric Flow Analysis.	418
11-14.	Off-Design Study, CASC Results, Root Section.	419
11-15.	Off-Design Study, CASC Results, Pitch Section.	420
11-16.	Off-Design Study, CASC Results, Tip Section.	421
11-17.	Turbine Frame Assembly Features.	423
11-18.	Turbine Exit Gas Profile.	425
11-19.	Rear Mount System.	426
11-20.	Outer Ring Support.	427
11-21.	QCSEE and F101 Mounting System.	428
11-22.	Turbine Frame Strut, Cross Section.	430
11-23.	Turbine Frame Strut Fishmouth Seal, Forward Looking Aft.	431
11-24.	Turbine Frame Stresses and Loads - Max. Sea Level Steady State plus 10 g Landing.	433
11-25.	Turbine Frame Transient Average Temperatures for Start to Maximum Sea Level.	435
11-26.	Turbine Frame Strut Buckling.	436
11-27.	Turbine Frame Stresses and Loads - 50 Second Transient plus 1 g Load.	437
11-28.	Frame Stress Range Diagram - Foot/Skin Weld Line.	439

LIST OF ILLUSTRATIONS (Continued)

Figure		Page
11-29.	Frame Stress Range Diagram - Hub.	440
11-30.	Turbine Frame Ring Support Lug Analysis.	445
11-31.	Turbine Frame External Loads for One Airfoil Out.	446
11-32.	QCSEE Turbine Frame (UTW) Stresses Due to 2-1/2 Blade-Out Load.	447
12-1.	Engine Lube System Schematic.	451
12-2.	Facility Lube System Schematic.	453
12-3.	Lube Tank Cross Section.	456
12-4.	Lube Supply Pump Flow Vs. Inlet Pressure at 5977 rpm.	458
12-5.	Lube Supply Pump Flow Vs. Discharge Pressure at 5977 rpm.	459
12-6.	Relief Valve Flow Vs. Discharge Pressure at 5977 rpm.	460
12-7.	Lube Filter.	461
12-8.	QCSEE Scavenge Pump Schematic.	463
12-9.	Scavenge Pump Main Element Flow Vs. Inlet Pressure.	465
12-10.	Scavenge Pump Gearbox and Rear Element Flows Vs. Inlet Pressure.	466
12-11.	Schematic of Conventional and Geared LP Drive Systems.	474
12-12.	Fan Thrust Load Vectors.	475
12-13.	HP Spool Thrust Load Vectors.	478
12-14.	LP Turbine Thrust Load Vectors.	480
12-15.	LP Turbine Thrust Balance System.	481
12-16.	Schematic of OTW Engine Bearing Arrangement.	484
12-17.	UTW Forward Sump.	486
12-18.	Forward Sump Stationary Structure Deflections.	489

LIST OF ILLUSTRATIONS (Continued)

Figure		Page
12-19.	Forward Sump Rotating Structure Deflections.	490
12-20.	Forward Sump Stationary Structure Stresses.	491
12-21.	Forward Sump Rotating Structure Stresses.	492
12-22.	Flex Coupling Stresses.	493
12-23.	UTW Maximum Steady-State Temperatures.	494
12-24.	Aft Sump Stationary Structure Deflections.	496
12-25.	Aft Sump Rotating Structure Deflections.	497
12-26.	Aft Sump Stationary Structure Stresses.	498
12-27.	Aft Sump Rotating Structure Stresses.	499
12-28.	Accessory Drive System.	501
12-29.	Accessory Gearbox System.	502
12-30.	Inlet Gearbox Assembly.	503
12-31.	Accessory Gearbox.	505
12-32.	Accessory Gearbox Housing.	506
12-33.	Starter Torque Vs. Rotor rpm at Various Starter Pressure Ratios.	508
12-34.	Scavenge Pump and Drive System.	510
13-1.	Control System Schematic.	514
13-2.	Overall Control Room Functional Block Diagram.	515
13-3.	Base Schedule for TP5 Maximum Climb Power.	521
13-4.	Engine Core Pressure Ratio for Maximum Climb Power on Reference Climb Path.	522
13-5.	Fan Nozzle Effect on Inlet Mach Number.	525
13-6.	Fuel Control Loop.	527

LIST OF ILLUSTRATIONS (Continued)

Figure		Page
13-7.	Fan Nozzle Area Control Loop.	528
13-8.	Fan Pitch Control Loop.	529
13-9.	UTW Engine 2nd Control System Hunting at Nominal Design Conditions, SLS, Standard Day.	530
13-10.	UTW Throttle Burst from 62 to 100% Net Thrust at SLS, Standard Day, Zero Bleed.	531
13-11.	Preliminary Performance Constant NIK Control Configuration Percent Net Thrust Versus Time.	533
13-12.	Preliminary Performance Constant NIK Control Configuration Acceleration Time Versus Maximum A_{18}.	534
13-13.	Control Model Effect on Transient Response Hybrid Model Data.	535
13-14.	Fan Pitch Effect on Cruise SFC.	537
13-15.	Fan Nozzle Effect on Cruise SFC (Mach 0.7, 25,000 ft).	538
13-16.	Hydromechanical Control Schematic.	542
13-17.	F101 Fuel Pump and Control.	544
13-18.	Digital Control Subsystem.	545
13-19.	Digital Control Schematic.	549
13-20.	Central Processor Unit.	554
13-21.	Digital Control.	556
13-22.	Typical Digital Control Module.	558
13-23.	Digital Control Command and Monitor Equipment.	560
13-24.	Engineering Control Panel.	561
13-25.	Operator Control Panel.	562
13-26.	Fuel Delivery System.	566
13-27.	Hydraulic System.	569

LIST OF ILLUSTRATIONS (Continued)

Figure		Page
13-28.	Hydraulic Pump.	570
13-29.	Variable Nozzle Actuation Schematic.	572
13-30.	Exhaust Nozzle Actuator.	574
13-31.	Electrohydraulic Servovalve.	575
13-32.	Alternating Current Generator.	578
13-33.	Fan Inlet Temperature (T12) Sensor.	580
13-34.	Pressure Sensor.	582
14-1.	Engine/Flap Relationship, Inboard Station.	585
14-2.	Nacelle Aerodynamic Flowpath.	586
14-3.	STOL Aircraft Design Envelope, YC15 EBF and QCSEE.	589
14-4.	Flight Placard Airflow Characteristics for QCSEE and CTOL Aircraft.	590
14-5.	Inlet Throat Mach Number Selection.	591
14-6.	30.5 cm (12 in.) Inlet Model in NASA-Lewis 2.7 x 4.6 m (9 x 15 ft) Wind Tunnel.	592
14-7.	Inlet Performance Comparison Versus Angle of Attack.	593
14-8.	30.48 cm (12 in.) Inlet Wall Mach Number Distribution.	595
14-9.	Inlet Aerodynamic Design.	596
14-10.	Fan Duct and Nozzle Design Experimental Nacelle.	597
14-11.	Fan Duct and Nozzle Design Flight Nacelle.	598
14-12.	Experimental Nacelle Fan Duct Mach Number Distribution, Takeoff Power Boiler Plate and Composite Nacelle.	599
14-13.	14.0 cm (5.5 in.) Exlet Model Typical Tunnel Installation.	601
14-14.	14.0 cm (5.5 in.) Exlet Model in NASA-Lewis 2.7 x 4.7 m (9 x 15 ft) Wind Tunnel.	602

LIST OF ILLUSTRATIONS (Continued)

Figure		Page
14-15.	14.0 cm (5.5 in.) Exlet Model Test Configurations.	603
14-16.	Performance Summary - 13.97 cm (5.5 in.) Exlet Tests.	604
14-17.	QCSEE UTW Core Nozzle Design.	606
14-18.	Contoured Pylon Nose Section.	607
15-1.	Baseline QCSEE UTW Propulsion Unit.	610
15-2.	Accessory Access Provisions.	612
15-3.	UTW Experimental Propulsion System.	613
15-4.	QCSEE Inlet Axial Cross Section.	618
15-5.	Inlet Wall Local Load Resistance.	622
15-6.	Inlet Anti-Icing Schematic.	623
15-7.	Outer Cowl Cross Section.	626
15-8.	Development - Outer Cowl/Nozzle.	627
15-9.	Nacelle/Pylon Hinge and Seal.	628
15-10.	Outer Cowl/Fan Frame Attachment.	629
15-11.	Actuator/Flap Link Installation.	630
15-12.	Outer Cowl, Forward Hook Latch Installation.	632
15-13.	Flare Nozzle Flap Schematic.	634
15-14.	Variable Flap Nozzle.	635
15-15.	Intraflap Seal Schematic.	637
15-16.	Outer Cowl/Nozzle Flap Circumferential Seal.	638
15-17.	Flap/Pylon Interface Seal.	639
15-18.	Nozzle Flap Cross Section.	641
15-19.	Fan Nozzle Segment.	642

LIST OF ILLUSTRATIONS (Continued)

Figure		Page
15-20.	Inner Cowl Schematic.	646
15-21.	Inner Cowl Estimated Temperatures.	647
15-22.	Location of Air Passages and Radiation Shield.	648
15-23.	Core Exhaust Nozzle.	649
15-24.	Engine Change Unit.	652
15-25.	Engine Mounting System.	655
15-26.	Load Nomenclature.	660
15-27.	UTW Experimental Engine Accessories.	661
15-28.	Bellmouth Inlet.	664
15-29.	Inlet Mounted on Test Stand at Peebles Proving Grounds.	665
15-30.	Typical Decoupled ("Load-Break") Joint.	666
15-31.	Typical Splitter Installation.	668
15-32.	Outer Fan Doors Support.	669
15-33.	Fan Nozzle Assembly Attached to Fan Duct.	670
15-34.	Core Cowl.	673
16-1.	UTW Engine Rotating Subsystems.	675
16-2.	UTW Vibration Model Installed Engine.	678
16-3.	Fan Reference, Configuration 1.	685
16-4.	LP Reference, Configuration 1.	686
16-5.	HP Reference, Configuration 1.	687

LIST OF TABLES

Table		Page
2-I.	Flight Duty Cycle.	8
3-I.	UTW System Noise Levels.	17
3-II.	UTW Aircraft Flight Characteristics for Acoustic Calculations.	18
3-III.	UTW Design Parameters.	23
4-I.	EPA Gaseous Emissions Standards for Class T_2 Engines.	56
4-II.	EPA Gaseous Emissions Standards - Turbojets and Turbofans.	56
4-III.	Ignition Test Results.	64
4-IV.	Emissions Calculations Using Prescribed EPA Landing-Takeoff Cycle (Constant Fan Pitch).	68
4-V.	Emissions Calculations Using Prescribed EPA Landing-Takeoff Cycle (Constant Fan Speed).	69
4-VI.	Predicted QCSEE UTW Engine Emissions Characteristics.	70
4-VII.	Comparison of Operating Conditions of UTW and a Higher Pressure Ratio Engine at Ground Idle and Takeoff.	74
4-VIII.	Predicted UTW Engine Emissions Characteristics.	85
5-I.	UTW Engine Performance Objectives.	92
5-II.	Experimental Engine Performance.	99
5-III.	Separated-Flow Turbofan Nomenclature.	100
6-I.	UTW Variable-Pitch Fan Design Requirements.	108
6-II.	Design Blade Element Parameters for QCSEE UTW Fan.	124
6-III.	UTW Fan Rotor Blade Coordinates.	142
6-IV.	UTW Fan Core OGV Coordinates at the Pitch Line Radius.	152
6-V.	Vane-Frame (Fan Bypass OGV) Coordinates.	162
7-I.	Variable-Pitch System Design Requirements.	188

LIST OF TABLES (Continued)

Table		Page
7-II.	Component Operating Characteristics.	194
7-III.	Trunnion Arm Stresses.	198
7-IV.	Trunnion Arm Deflections.	198
7-V.	Cam Support Housing Stresses.	202
7-VI.	Harmonic Drive - Design and Operating Characteristics.	206
7-VII.	Harmonic Drive Radial Deflection at Tooth Mesh and Loss of "d".	207
7-VIII.	Harmonic Drive Flex Spline/Circular Spline Tooth-Bearing Stress.	208
7-IX.	Flex Spline Stresses.	208
7-X.	No-Back Design Characteristics.	211
7-XI.	Differential Gear Data.	215
7-XII.	Feedback Loop Accuracy in Terms of Fan Blade Angle.	217
7-XIII.	Bearing Data.	223
7-XIV.	Hamilton Standard Actuation System.	227
7-XV.	Pinion Gear Teeth Design Data.	233
7-XVI.	Experimental Engine Actuation System Weights.	262
7-XVII.	Mechanical System Backlash in Terms of Fan Blade Angle.	263
8-I.	UTW Composite Fan Blade Design Summary.	269
8-II.	PR288/AS Prepreg Properties.	279
8-III.	Composite Material Properties.	280
8-IV.	Platform Stresses and Margins of Safety.	298
8-V.	Platform Natural Frequencies.	299
8-VI.	Composite Fan Blade Weight Breakdown.	303

LIST OF TABLES (Continued)

Table		Page
8-VII.	Fan Disk Design Data.	310
8-VIII.	UTW Blade Support Bearing, Operating Conditions of Mission Duty Cycle.	314
8-IX.	UTW Blade Support Bearing Loads and Life Predictions.	315
8-X.	Trunnion Retainer (Nut).	319
8-XI.	Disk Cone Flange Bolts.	324
9-I.	QCSEE Engine Loads.	332
9-II.	Frame Radial Bearing Loads.	333
9-III.	Geometry of Composite Frame Components.	352
9-IV.	Frame Component Stresses.	353
9-V.	Bond Shear Stresses.	354
9-VI.	Effect of Different Thermal Coefficients.	355
9-VII.	Composite Frame Weight Breakdown.	358
9-VIII.	Test Specimen Configurations.	359
9-IX.	Tensile Test Results.	361
9-X.	Compression Test Results.	362
9-XI.	Shear Test Results.	363
9-XII.	Bolt Hole Test Results.	364
9-XIII.	Exposure Evaluation - MIL-L-23699.	367
9-XIV.	Composite Frame Subcomponents Test Plan Summary.	369
9-XV.	Subcomponent Test Results.	370
10-I.	UTW Reduction Gear Design Details.	375
10-II.	Comparison of UTW and YT49 (1st Stage) Reduction Gear Data.	377

LIST OF TABLES (Continued)

Table		Page
10-III.	Reduction Gear Detail Design, Flight Cycle.	379
10-IV.	Reduction Gear Detail Design, Experimental Engine Cycle.	380
10-V.	Gear Set Materials.	380
10-VI.	Reduction Gear Geometry.	381
10-VII.	Reduction Gear Oil Flow Rates (Flight Cycle).	385
10-VIII.	Reduction Gear Efficiency.	387
10-IX.	Reduction Gear Heat Rejection.	388
10-X.	Reduction Gear Scoring Index.	388
10-XI.	Star Gear Bearing Life Prediction.	390
10-XII.	Reduction Gear Weight Summary.	391
10-XIII.	Star Gear Bearing Test Results.	395
11-I.	Low Pressure Turbine Operating Point Data.	409
11-II.	Fan Turbine Operating Point Data.	417
11-III.	Summary of Design Changes.	424
11-IV.	Turbine Frame Maneuver Stresses, Maximum Steady-State plus 10 G Down Loading.	434
11-V.	Turbine Frame Stresses Thermal Loading and 1 G Engine Loading, Start to Maximum Sideline Thrust.	438
11-VI.	Turbine Frame Mount Reactions, 2.22 cm (7/8 in.) Pin Mount, 2-1/2 Blades Out.	441
11-VII.	Engine Mount Reaction Load Due to Maneuver, 2.22 cm (7/8 in.) Pin Mount.	442
11-VIII.	Engine Mount Reaction Loads for 2.22 cm (7/8 in.) Pin.	443
12-I.	QCSEE Lube Flows - UTW.	454
12-II.	Scavenge Element Predicted Performance.	464

LIST OF TABLES (Continued)

Table		Page
12-III.	Heat Study Conditions.	469
12-IV.	Predicted Heat Loads and Oil Flows.	470
12-V.	Predicted Temperatures, 100 gpm [26.7° C (80° F)] Cooling Water.	471
12-VI.	Derated Reduction Gear Efficiency, 100 gpm [26.7° C (80° F)] Cooling Water.	472
12-VII.	Fan Rotor Thrust (No. 1B) Bearing Axial Loads.	476
12-VIII.	Core Engine Rotor Thrust (No. 3) Bearing Axial Loads.	479
12-IX.	Low Pressure Turbine Rotor Thrust (No. 2) Bearing Axial Loads.	482
12-X.	No. 1 Seal Design.	485
12-XI.	No. 1R Bearing Design.	487
12-XII.	No. 6 Seal Design.	495
12-XIII.	Inlet Gearbox Design Data.	500
13-I.	Thrust Functions Evaluated for UTW Control.	517
13-II.	Tolerance Study Results.	519
13-III.	Tolerances and Variations Used.	520
13-IV.	Digital Control Instrumentation Input Signals.	550
13-V.	Digital Control Engine Sensor and Transducer Signals.	550
13-VI.	Alternator and Digital Signals to Digital Control.	551
13-VII.	Digital Control Outputs.	551
13-VIII.	Pump Characteristics (F101 Pump).	567
15-I.	Experimental and Flight Propulsion System Comparison.	614
15-II.	Inlet Stresses and Deflections at Maximum Combined Load Condition.	620

LIST OF TABLES (Concluded)

Table		Page
15-III.	Critical Buckling Loads.	621
15-IV.	Inlet Latch Loads.	624
15-V.	Fan Duct Hinge/Skin Stresses.	633
15-VI.	Nozzle Flap Design Conditions.	643
15-VII.	Nozzle Critical Loads/Stresses.	644
15-VIII.	UTW Experimental Propulsion System Mount Loads, Boiler Plate Nacelle.	657
15-IX.	UTW Experimental Propulsion System Mount Loads, Composite Nacelle.	658
16-I.	Critical Speeds, Fan Reference, UTW Configuration 1.	680
16-II.	Critical Speeds, LP Reference, UTW Configuration 1.	680
16-III.	Critical Speeds, HP Reference, UTW Configuration 1.	682
16-IV.	Critical Speeds, Fan Reference, UTW Configuration 2.	683
16-V.	Critical Speeds, LP Reference, UTW Configuration 2.	683
16-VI.	Critical Speeds, HP Reference, UTW Configuration 2.	684
17-I.	UTW Engine Weight.	690
17-II.	Propulsion System Weight.	691
17-III.	Experimental and Flight Engine Weight Differences.	692

SECTION 1.0

INTRODUCTION

The Quiet Clean Short-Haul Experimental Engine (QCSEE) Program provides for the design, fabrication, and testing of experimental, high-bypass, geared turbofan engines and propulsion systems for short-haul passenger aircraft. The overall objective of the program is to develop the propulsion technology required for future externally blown flap types of aircraft with engines located both under-the-wing and over-the-wing. This technology encompasses the following elements:

- Variable-pitch and fixed-pitch fans
- Geared fans
- Low noise
- Low exhaust emissions
- High thrust-to-weight ratio
- Composite fan blades
- Composite fan frames
- Lightweight, low-drag nacelles
- Digital electronic controls
- Thrust reverse means
- Rapid response to thrust demand
- Low fan pressure ratio, low fuel consumption cycles

Two experimental propulsion systems are being developed and will be tested as a part of the QCSEE Program (Contract NAS3-18021). The under-the-wing (UTW) engine features a low-tip-speed, low-pressure-ratio variable-pitch fan, while the over-the-wing (OTW) engine features a fixed-pitch fan having a higher design pressure ratio accomplished with a higher tip speed.

The overall engine design process included preliminary design of optimized UTW and OTW flight engine configurations during the initial phase of the program, which involved participation of representatives of NASA-Lewis, Douglas Aircraft Company, Boeing Company, and American Airlines.

Preliminary design of the two experimental engines was conducted in parallel with design of the flight engines. Design of the experimental engines duplicated the flight engines in all areas except those where considerable cost savings could be accomplished through simplification or utilization of existing hardware without compromising the basic program objectives.

Following approval of the preliminary engine designs by NASA, detail design of the experimental engines was initiated. This report summarizes the final detail design of the UTW experimental engine. Any discussions relating to the UTW flight engine are included only for the purpose of defining specific differences which exist between experimental and flight engine configurations. Reference to the OTW engine in certain sections is made only where it was felt necessary to provide a better understanding of the overall engine design process.

SECTION 2.0

SUMMARY

This report summarizes the detail design of the under-the-wing (UTW) experimental engine. Results of the detail design provide a high degree of confidence that the experimental engine will meet all stated program objectives. Design simplification in certain areas and application of available component hardware to the experimental engine design to minimize program expenditures have not resulted in any compromise of the program technical objectives.

2.1 PROGRAM OBJECTIVES

The major purpose of the QCSEE Program is to develop and demonstrate the technology required for propulsion systems for quiet, clean, and economically viable commercial short-haul aircraft. This comprehensive program includes the following objectives:

- To develop propulsion system technology which will permit a short-haul aircraft, to achieve the system noise goal of 95 EPNdB along a 152 m (500 ft) sideline when the engines are scaled to a total installed thrust of 400,300 N (90,000 lb). The design shall also minimize the ground area (footprint) exposed to objectionable noise levels.

- To demonstrate a propulsion system which will meet advanced pollution goals under all operating conditions.

- To develop the technology for very high bypass ratio engines with quiet low pressure ratio geared variable-pitch fans.

- To develop technology required to meet propulsion system performance, control, weight, and operational characteristics.

- To develop material, design, and fabrication technology for quiet propulsion systems which will yield engine designs which have an uninstalled thrust-to-weight ratio greater than 6 to 1 and installed thrust-to-weight ratios greater than 3.5 to 1.

- To develop technology which will yield engine thrust response characteristics required for powered-lift operations.

- To provide the technology which will permit design of quiet, efficient, lightweight thrust-reversing systems for powered-lift aircraft.

- To provide the technology to permit design of integrated engine and nacelle installations which will be tolerant to aerodynamic distortion expected with operating flight conditions such as high crosswinds, large angles of attack, and side slip, and still provide good cruise performance.

- To provide the digital electronic engine control technology required to improve engine and fan pitch control, thrust response, operational monitoring, and to relieve the pilot's workload especially during powered-lift flight operations in the terminal area.

2.3 SPECIFIC TECHNICAL OBJECTIVES

The following specific design objectives have been established for flight and experimental UTW propulsion systems:

2.2.1 Noise

The UTW experimental engine shall be designed to meet the following noise objectives when scaled to fit a four-engine 400,300 N (90,000 lb) thrust aircraft:

Takeoff and Approach	-	95 EPNdB @ 152 m (500 ft) SL
Max. Reverse Thrust (35% Max. Forward Thrust)		100 PNdB @ 152 m (500 ft) SL

The conceptual flight design engine will meet these same noise objectives when installed on a typical short-haul commercial aircraft. The design shall also minimize the aircraft acoustic footprint.

2.2.2 Pollution

The engines shall be designed to meet EPA exhaust emission standards specified for 1979 aircraft.

2.2.3 Thrust-to-Weight

The full-scale UTW experimental engine shall be designed to meet the following thrust and thrust-to-weight objectives:

	Uninstalled	Installed
Thrust	81,400 N (18,300 lb)	77,400 N (17,400 lb)
Thrust/wt.	6.2	4.3

Uninstalled thrust includes all engine internal pressure losses up to the nozzle throat; installed thrust includes additional losses due to inlet ram recovery and core cowl scrubbing drag.

Uninstalled weight includes the dry weight of all engine components and engine accessories. Installed weight includes the following additions:

- Inlet and inlet anti-icing system
- Exhaust ducts and nozzles
- Fan duct and splitter
- Engine mounts to interface with pylon
- Nozzle controls and hydraulic system
- Fire detection and extinguishing system
- Drains, vents, and oil cooler
- Instrumentation

Thrust/weight shall be representative of a flight engine design. This shall include analytical predicted flight weight of all boilerplate and nonflight design components.

2.2.4 Thrust Reversal

The UTW propulsion system shall provide the following thrust reversal capacity:

- Operation down to 5.1 m/sec (10 knots)
- Max. forward to max. reverse thrust transient in less than 1.5 seconds
- At least 35% static take-off thrust in reverse
- Noise levels as specified in Section 2.2.1

2.2.5 Engine Bleed

The engine shall be capable of safely providing up to 13% engine core bleed.

2.2.6 Power Extraction

Engines shall be capable of supplying a minimum of 1640 W/4448 N (2.2 horsepower per 1000 lb) of installed thrust for customer takeoff power.

2.2.7 Dynamic Thrust Response

Engine thrust response shall be designed to meet an acceleration from 62% to 95% thrust in one second [sea level to 1830 m (6000 ft) altitude].

2.2.8 Distortion Tolerance

The engine shall be capable of satisfactory operation at inlet upwash angles of 0 to 50°, with 18 m/sec (35 knot) 90° crosswinds.

2.2.9 Oil Consumption

Engine oil consumption shall not exceed 0.906 kg/hr (2 lb/hr).

2.2.10 Dumping

No fuels or lubricants shall be dumped.

2.2.11 General Design Criteria

In addition to the specific objective listed above, the experimental engine shall meet the following general criteria:

1. The propulsion system shall be designed for ground static, wind tunnel, and altitude chamber operation.
2. The propulsion system shall be designed for flight operation except in specific areas where nonflight hardware can be used to save costs.
3. Propulsion system characteristics, such as temperatures, specific fuel consumption, and overall pressure ratio shall be selected to be appropriate for short-haul commercial aircraft.
4. All propulsion system components shall be designed for life which is compatible with expected commercial short-haul operation.

5. The propulsion system control system shall be designed with digital logic and signal paths capable of interfacing with an aircraft onboard flight digital computer. The control system shall be designed to provide selectable programmed power management and failure indication and/or corrective action over the entire propulsion system operating envelope.

6. The propulsion system shall be designed with the objective of achieving high performance, but it is not essential that hardware development be carried to the point where ultimate performance is achieved for the experimental propulsion system. The Contractor shall show that his analytical extrapolation of performance data to a fully developed propulsion system is reasonably accurate, and that deviations in performance do not significantly affect acoustic or pollution characteristics of the experimental propulsion systems.

The experimental engine nacelle shall be designed with the following features:

1. An accurate representation of external and internal aerodynamic contours of the flight nacelle
2. Accurate acoustic representation of the flight-type design
3. All electrical, fuel, oil, cooling, fire detection and prevention, control, and instrumentation systems required to test the propulsion systems
4. Convenient access for maintenance

The propulsion system shall be designed for the following maintenance features:

1. The engine shall be easily removable from the nacelle without requiring removal of the fan exhaust duct.
2. The engine shall be capable of being trimmed on a test stand with no additional trimming required if installed on an aircraft.
3. Accessories shall be located for easy inspection.
4. Access to borescope ports shall be provided without requiring removal of any engine component.
5. Any propulsion system accessory shall be replaceable in 45 minutes*.

---

*Exception to this objective has been taken in the design of the experimental engine in those areas where significant cost savings could be effected through utilization of existing accessory component hardware.

6. Fans shall have an even number of blades to permit replacement in pairs without rebalancing. Blades shall be capable of rapid inspection and replacement.

7. Modular construction is used to facilitate maintenance.

The propulsion system shall be designed to perform within the flight maneuver forces envelope per MIL-E-5007C data December 30, 1965, paragraph 3.14, with the exception of conditions of catapult flight maneuver and precession rates.

2.3 OPERATING REQUIREMENTS

The foregoing specific objectives and general criteria are further amplified by the following propulsion system operating requirements.

2.3.1 Life and Duty Cycle

The engines shall be designed for a useful life of 36,000 hours over a 15 year period, based on the typical 403 km (250 mile) mission cycle shown in Table 2-I.

Table 2-I. Flight Duty Cycle.

Segment	Altitude km	Altitude ft	Mach No.	% Power	Time Min.	% Time
Start	0	0	0	-	0.5	1.11
Idle-Taxi	0	0	0	4-20	3.1	6.89
Takeoff	0	0	0.12	100	1.22	2.71
Climb (1st seg)	0-3.05	0-10K	128.6 m/sec (250 kts) IAS	Max. Cont.	5.0	11.11
(2nd seg)	3.05-7.63	10-25K	154.3 m/sec	Max. Cont.	5.0	11.11
Cruise	6.41-7.63	21-25K	.70	Max. Cruise	14.0	31.11
Descent	6.1-.06	20K-200 ft	.60	F.I.	10.0	22.22
Approach	.06	200 ft	0.12	65	3.0	6.67
Reverse Thrust	0	0	0.12-0	Max. Rev.	0.08	0.18
Idle-Taxi	0	0	0	4-20	3.1	6.89
					45.0	100.00

Cyclic life shall be based on 48,000 mission cycles plus 1000 ground checkout cycles to full power.

The engine shall be capable of operation throughout the flight envelope shown in Figure 2-1. The combustor shall meet commercial relight requirements as shown on the flight envelope.

The engine and its supports shall withstand without permanent deformation the conditions specified on Figure 2-2.

The engine shall be capable of withstanding loads caused by seizure of either rotor with deceleration from maximum rpm to zero rpm in one second.

Composite parts shall be capable of withstanding unbalanced loads caused by loss of five adjacent composite fan blades at maximum rpm. Metal parts shall be capable of withstanding loss of one equivalent metal blade.

2.3.2 Flight Attitudes

The engine shall be capable of operating within the range of flight attitudes shown in Figure 2-3.

2.4 UTW EXPERIMENTAL PROPULSION SYSTEM

The UTW experimental propulsion system, shown in Figure 2-4, features: a composite high Mach (accelerating) inlet; a gear-driven, variable-pitch fan with composite fan blades; a composite fan vane-frame; a treated fan duct with an acoustic splitter ring; a variable-geometry fan exhaust nozzle, an advanced (F101) core and low pressure turbine; a treated core exhaust nozzle; top-mounted engine accessories; and, a digital electronic control system combined with a hydromechanical fuel control.

The fundamental design criterion which established the engine design approach was the fan engine cycle required to meet the noise objective. The fan and core exhaust pressure ratios were dictated by jet-flap noise constraints.

The fan is a low pressure ratio (1.27)*, low tip speed [289.6 m/sec 950 ft/sec]* configuration sized to provide 405.5 kb/sec (894 lb/sec)* of corrected airflow. The fan contains 18 composite, variable-pitch fan blades with flight-weight disks and blade supporting system. The fan is driven by the F101 low pressure turbine through a main reduction gear. The reduction gear is a six-star epicyclic configuration with a gear ratio of 2.465 and a takeoff power rating of 9806 kw (13,145 HP).

---

*Takeoff power setting.

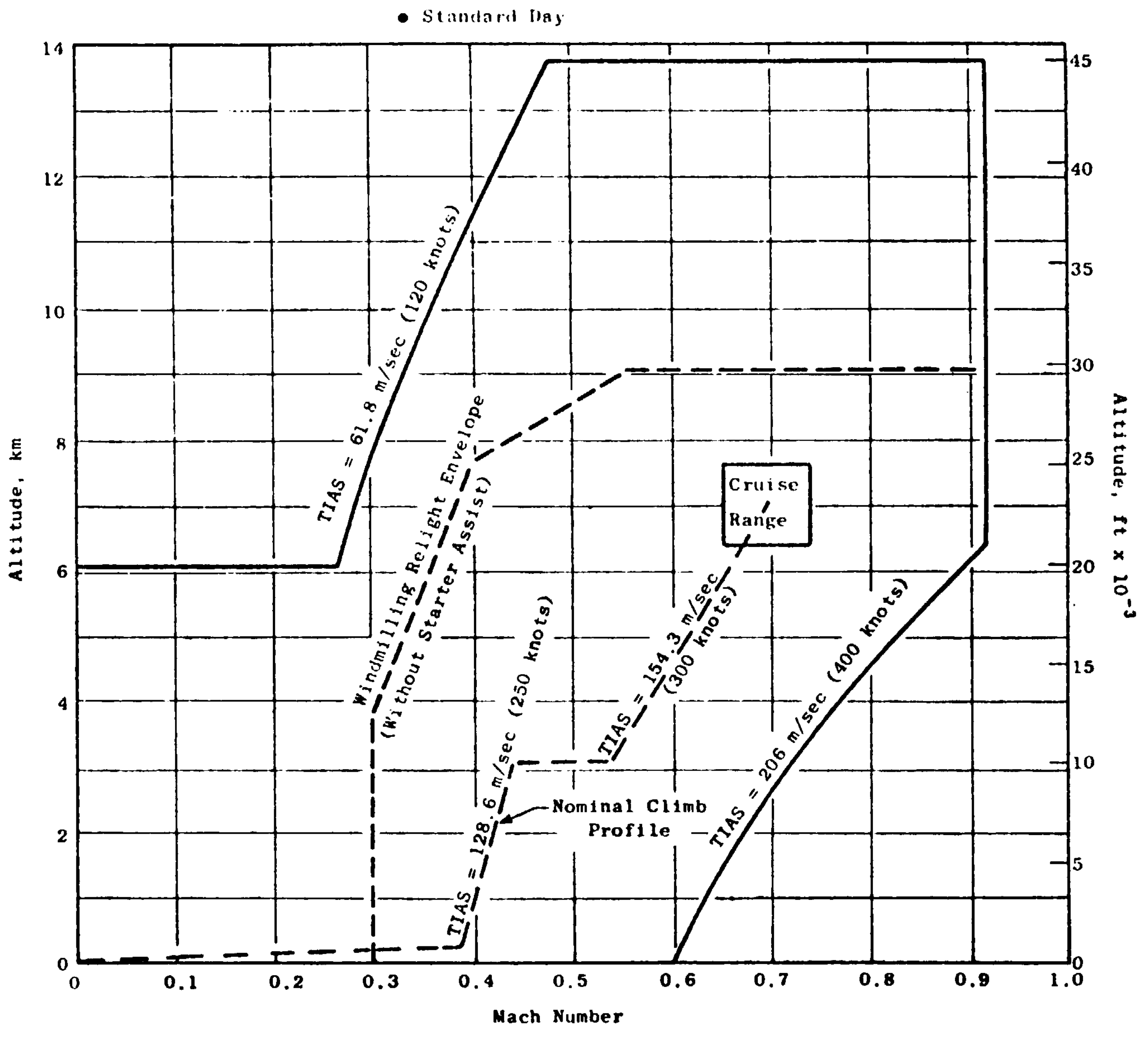

Figure 2-1. QCSEE Operating Envelope.

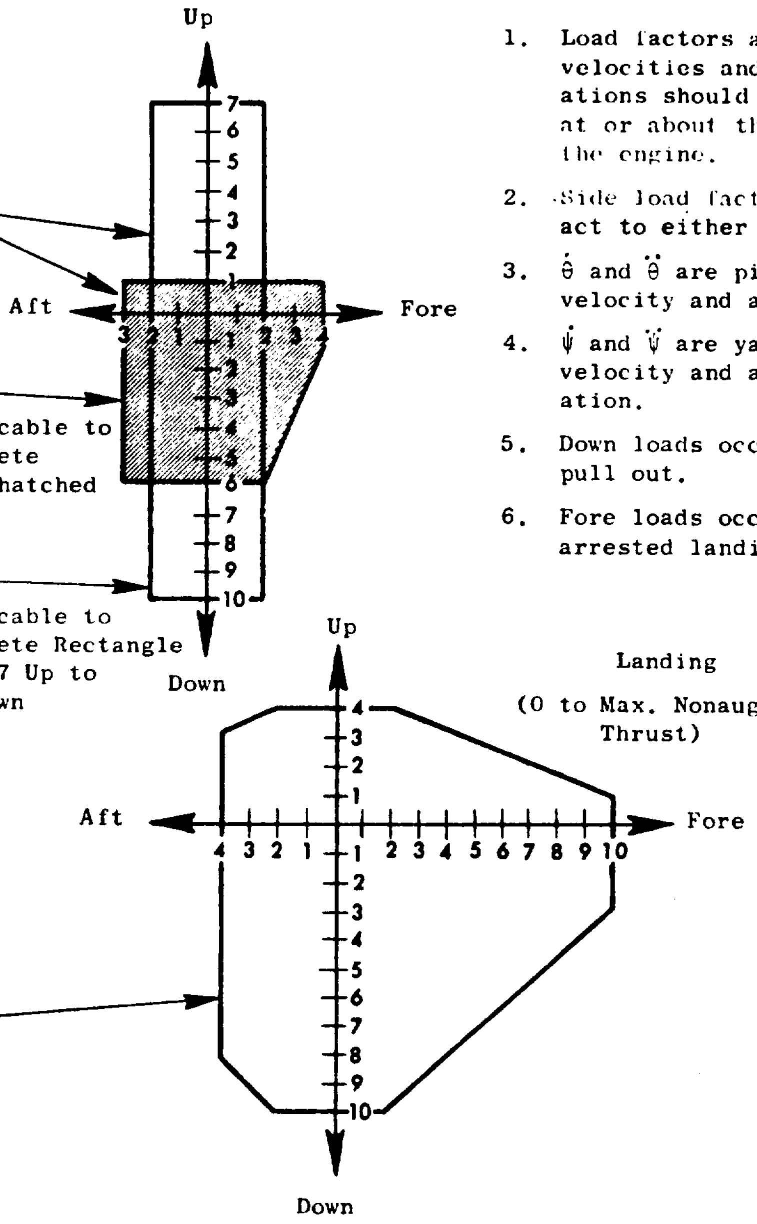

Up
7
6
5
4
3
2
1
Aft
Fore
3 2 1
1 2 3 4
1
2
3
4
5
6
7
8
9
10
Down
Up
4
3
2
1
Aft
Fore
4 3 2 1
1 2 3 4 5 6 7 8 9 10
1
2
3
4
5
6
7
8
9
10
Down

Flight

(0 to Max. Thrust)

$\ddot{\theta} = \pm 6\ \text{rad/sec}^2$

$\ddot{\psi} = 0$

$\dot{\psi} = 0$

$\dot{\theta} = \pm 1\ \text{rad/sec}$

or

S.L. = 4.0

Applicable to Complete Crosshatched Area

$\dot{\theta} = 0$

S.L. = 1.5

Applicable to Complete Rectangle from 7 Up to 10 Down

Landing

(0 to Max. Nonaugmented Thrust)

S.L. = 2.0

$\dot{\theta} = 0$

$\dot{\psi} = 0$

$\ddot{\theta} = \pm 14\ \text{rad/sec}^2$

$\ddot{\psi} = \pm 6\ \text{rad/sec}^2$

1. Load factors and angular velocities and accelerations should be taken at or about the C.G. of the engine.
2. Side load factors (S.L.) act to either side.
3. $\dot{\theta}$ and $\ddot{\theta}$ are pitching velocity and acceleration.
4. $\dot{\psi}$ and $\ddot{\psi}$ are yawing velocity and acceleration.
5. Down loads occur during pull out.
6. Fore loads occur during arrested landing.

Figure 2-2. QCSEE Design Loads.

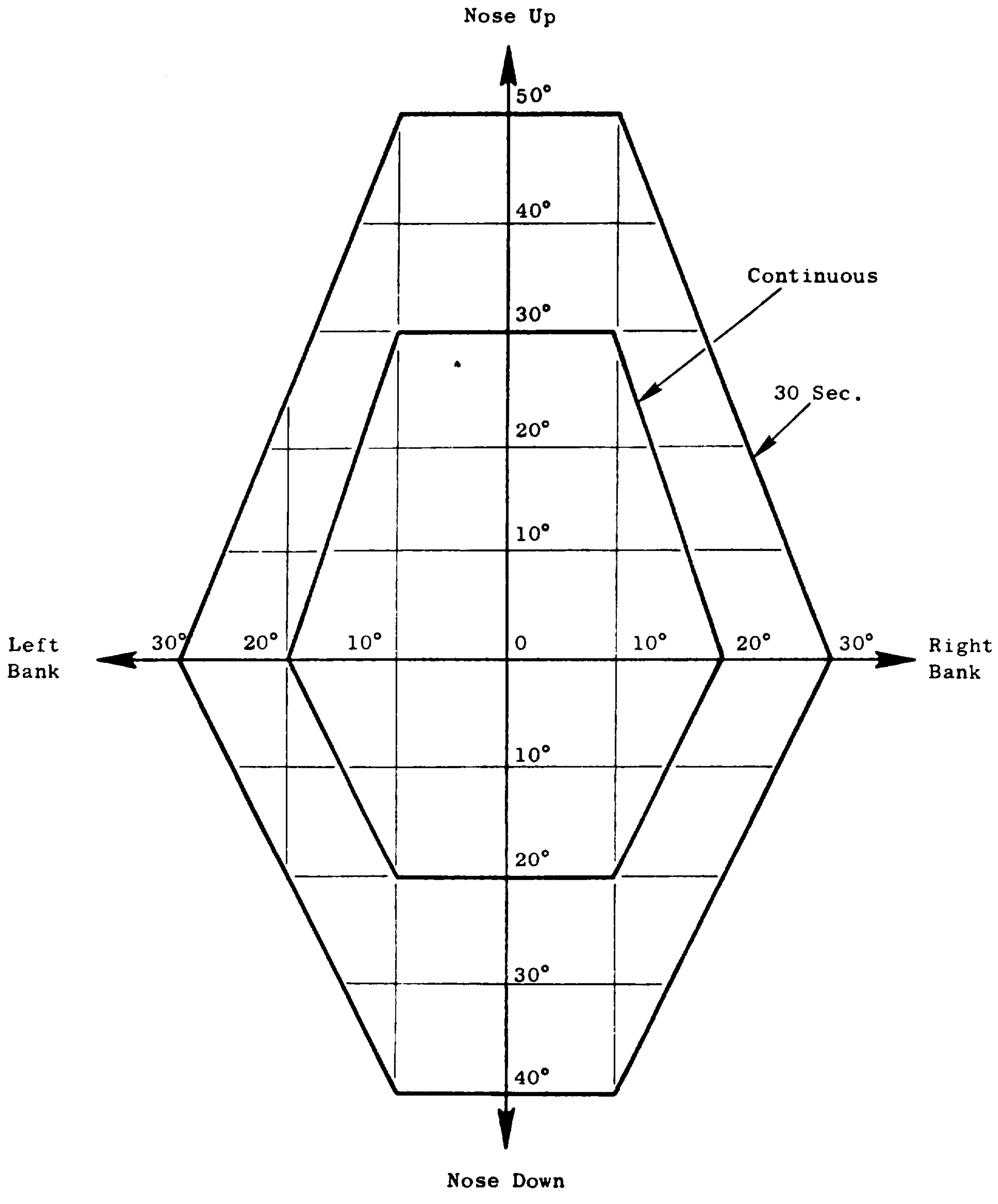

Figure 2-3. QCSEE Flight Attitudes.

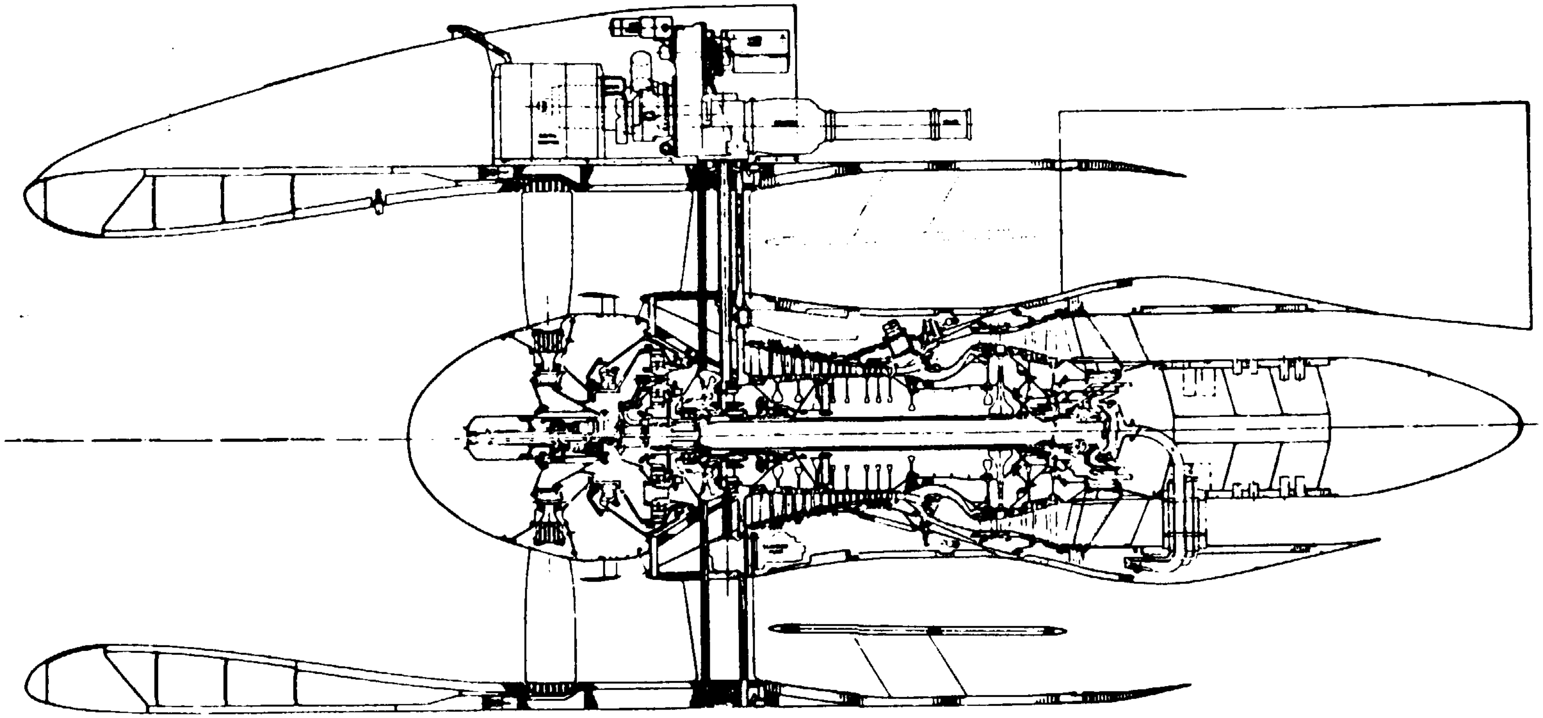

Figure 2-4. UTW Experimental Propulsion System.

The fan is capable of blade pitch change from forward to reverse thrust through either flat pitch or stall pitch. Two variable-pitch fan actuation systems are being developed for the UTW experimental engine. A cam/harmonic drive system is being developed by the Hamilton Standard Division of United Technology Corporation under subcontract to the General Electric Company. The second system is a ball spline actuation system being developed by GE. The rotary motion power required to drive both systems is provided by hydraulic motors. Both systems are designed to move the blades from their forward thrust position to reverse in less than one second at the reverse power setting.

The fan frame is a flight-weight composite structure containing integral acoustic treatment, outer casing, containment, and fan tip treatment. Thirty-three integral outlet guide vanes also act as structural struts. The outer casing of the frame provides both inner and outer nacelle flow paths and also containment for failed airfoils. Core inlet flow path and mounts for the forward bearings, gears, radial drive, etc., are also integrally provided.

The nacelle components include a lightweight composite hybrid inlet providing acoustic suppression by means of a high throat Mach number (0.79) and integral acoustic treatment. The composite fan duct, acoustic splitter, and core cowl are hinged from the pylon to provide access for engine maintenance. The core exhaust nozzle and nozzle plug are acoustically treated to reduce aft radiated noise. The fan exhaust nozzle is a variable-area, four-flap design capable of area change from takeoff to cruise, as well as opening to a flared position to form an inlet in the reverse thrust mode. The nozzle flaps are hydraulically actuated.

Engine fuel flow, blade pitch angle, and exhaust nozzle area are controlled by a digital electric control, which modifies the fuel demand of a modified F101 hydromechanical control. Major engine accessories are mounted on a boiler plate gearbox on top of the fan frame.

All experimental engine components have been designed to meet the engine life and operating requirements defined in Section 2.3.

The UTW experimental propulsion system is designed to provide 81,400 N (18,300 lb) of uninstalled thrust and 77,400 N (17,400 lb) of installed thrust at takeoff on a 305.6 K (90° F) day. Analysis indicates that, when scaled in accordance with the specified ground rules, the engine will meet all of the program noise objectives.

2.5 UTW FLIGHT PROPULSION SYSTEM

The UTW flight propulsion system cross section is shown in Figure 2-5. Comparing Figure 2-5 with Figure 2-4, it can be seen that the major configuration difference between the flight and experimental propulsion systems is the modified fan duct and elimination of the acoustic splitter ring required to satisfy the experimental engine noise goal. The noise goal for the

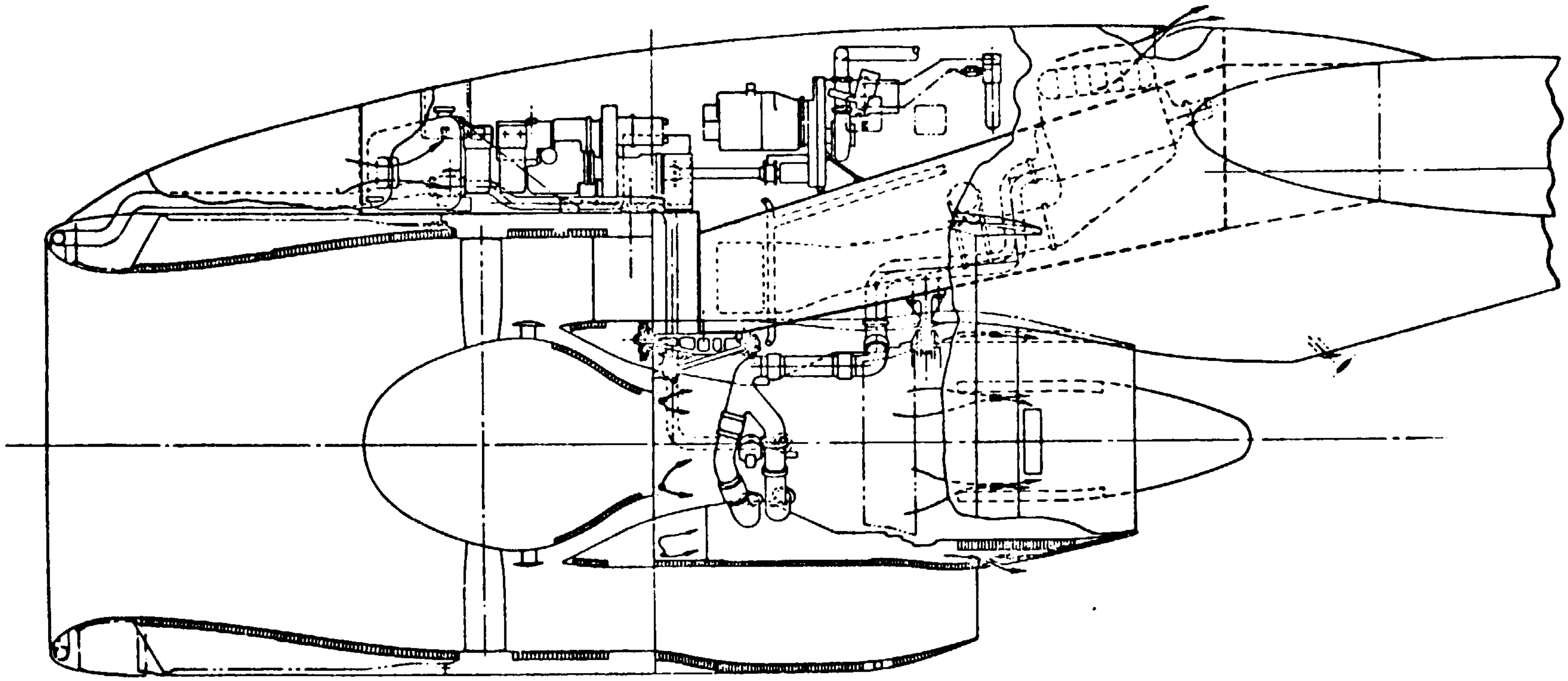

Figure 2-5. UTW Flight Propulsion System.

experimental engine is based on a 609.6 m (2000 ft) takeoff while acoustic design of the flight propulsion system is based on a noise goal set for a 914.4 m (3000 ft) takeoff.

Major structural component differences are in areas of the turbine rear frame and core nozzle. The experimental engine utilizes a modified F101 rear frame, while the flight engine configuration is based on an optimized flight-weight design. The core nozzle of the experimental engine is boiler plate design to minimize cost.

Other differences between the two configurations are primarily in areas of material substitutions and utilization of existing accessory components in the experimental engine to minimize program cost. For example, the experimental engine uses steel rather than titanium for fan shafting, reduction gear carrier, and bearing support cones. Cost savings in the accessory area are based on utilization of an available oil tank, heat exchanger, pumps, filters, etc., which would be optimized in the flight engine. Several changes in the core have also been considered, consistent with the lower UTW cycle compressor discharge pressure.

The flight propulsion system also includes: inlet anti-icing provision, which is not included in the experimental system inlet; a flight-type fire detection and extinguishing system, in place of a facility system; and a double-wall fuel system. The flight system would also include the necessary bleed manifolding for cabin air conditioning and for high lift systems requiring engine bleed air.

Both the experimental and flight UTW engines are top mounted from a pylon, with mounts on the fan frame and turbine frame. By opening bypass duct and core cowl, the engine and inlet can be removed from the pylon in the downward direction. A hinged sliding accessory cover provides access to engine accessories located in front of the pylon in the flight engine, whereas a bolted cover is utilized for the experimental engine.

Analyses conducted to date indicate that the uninstalled thrust/weight of the flight engine will be within 3 or 4% of meeting the program goal of 6.2, and that the installed (total propulsion system) thrust/weight will meet the program goal of 4.3.

SECTION 3.0

ACOUSTIC DESIGN

3.1 SUMMARY

The acoustic design of the UTW engine has resulted in a configuration which meets takeoff, approach, and reverse thrust noise goals. Table 3-I summarizes the system noise levels at the three engine operating conditions.

Table 3-I. UTW System Noise Levels.

	Requirement	Current Status
Takeoff	95 EPNdB	94 EPNdB
Approach	95 EPNdB	90.5 EPNdB
Reverse thrust	100 PNdB	100 PNdB

The noise levels have been obtained by estimating unsuppressed noise from existing test data of similar fan and core configurations, suppressing the dominant engine noise sources with the advanced technology concepts to be developed under the QCSEE program, and extrapolating these levels to in-flight conditions. Jet/flap noise was added to the engine noise levels to obtain total system or aircraft noise levels.

The preliminary acoustic design effort has attempted to establish UTW engine configurations which have balanced suppression in the fan inlet, fan exhaust, and core. To establish the balanced system suppression, detailed predictions have been made for the following 10 different noise sources:

1. Fan inlet
2. Fan exhaust
3. Turbine
4. Combustor
5. Compressor
6. Gears
7. Flow
8. Struts
9. Splitter
10. Jet/Flap

By predicting the noise level of various sources which could represent noise floors, the required treatment can be determined and applied to the engine only to the extent which is beneficial to the total system.

Figure 3-1 summarizes the main acoustic features of the UTW engine. A high inlet throat Mach number (0.79) is used to suppress inlet noise at takeoff. Wall treatment having a length equal to 0.74 fan diameters is added to provide suppression at approach and in reverse thrust. The rotor-stator combination has 1.5 tip chords spacing and a vane-blade ratio selected to reduce second harmonic noise. Fan exhaust suppression utilizes inner and outer wall treatment with varying thickness to obtain increased suppression bandwidth. A 101.6 cm (40 in.) splitter is necessary to obtain the required suppression level. A major concern in the aft duct is noise generated by flow over the treated surfaces, struts, and splitter. To keep these sources below the suppressed fan noise, the average duct Mach number is limited to 0.47. Core suppression utilizes a low frequency design for combustor noise reduction with thinner treated panels on the inner and outer walls to reduce the high frequency turbine noise. Treatment is also applied in the core inlet to reduce forward radiated compressor noise.

3.2 DESIGN REQUIREMENTS

Noise requirements for the UTW engine are specified as a total system or aircraft noise level at the operating conditions associated with takeoff and approach operation. A reverse thrust requirement is also specified for static aircraft conditions. These are shown graphically on Figure 3-2.

The takeoff noise requirement is 95 EPNdB on a 152.4 m (500 ft) sideline with the aircraft at 61.0 m (200 ft) altitude and engines at 100% thrust. Takeoff flap angle and aircraft speed are defined in Table 3-II. Also shown in Table 3-II are inlet angle of attack and upwash angles which must be accounted for with regard to fan inlet noise generation and high Mach inlet suppression.

Table 3-II. UTW Aircraft Flight Characteristics for Acoustic Calculations.

Flight Conditions	Takeoff	Landing
Aircraft speed	41.15 m/sec (80 knots)	41.15 m/sec (80 knots)
Flap angle	0.524 rad (30°)	1.047 rad (60°)
Climb or glide angle	0.218 rad (12.5°)	0.105 rad (6°)
Angle of attack	0.105 rad (6°)	0.035 rad (2°)
Upwash angle	0.262 rad (15°)	0.192 rad (11°)
Percent installed net thrust	100	65

- p/p = 1.27
- Tip Speed = 290 m/sec (950 ft/sec)
- Blade No. = 18

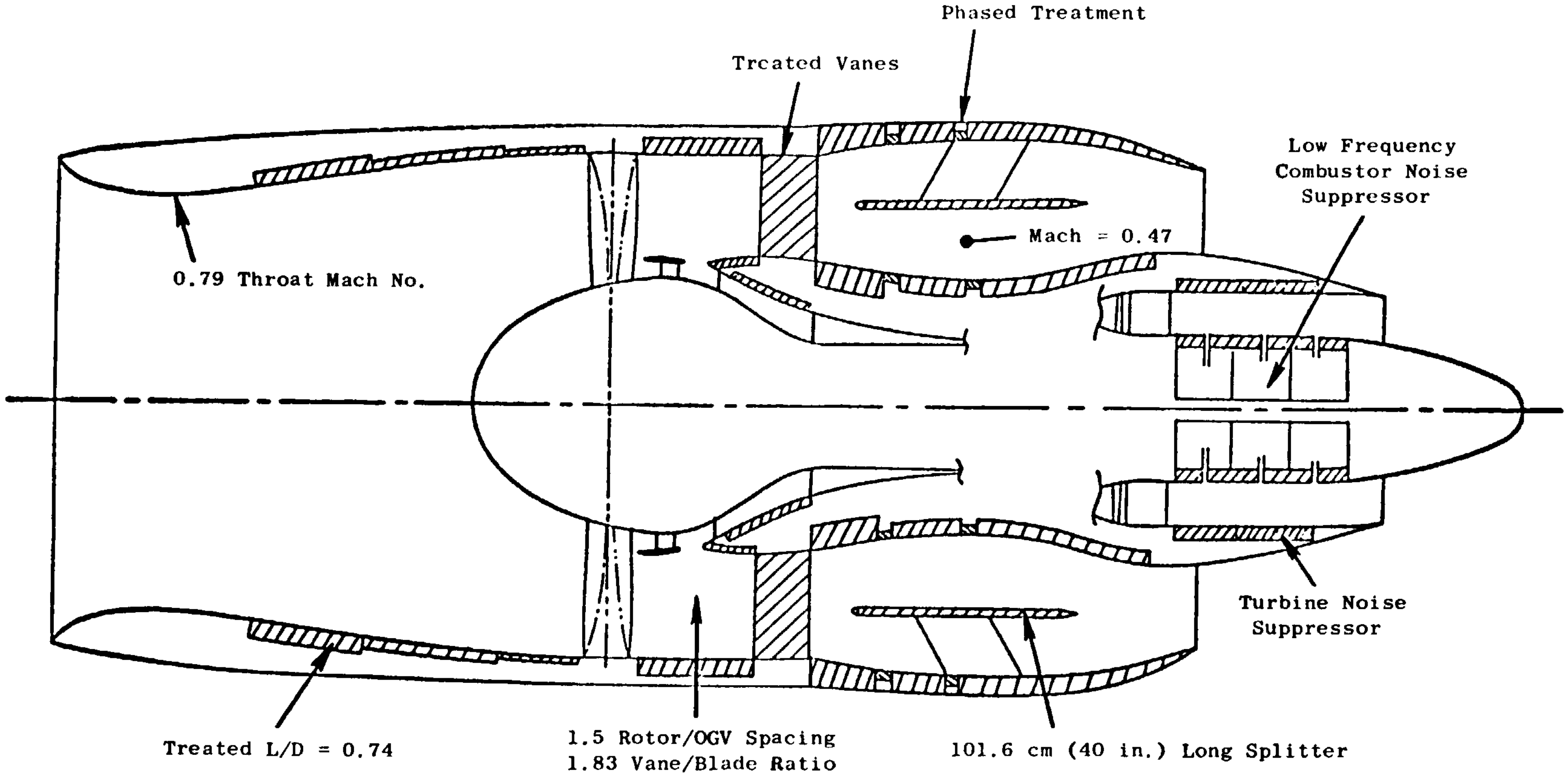
Phased Treatment
Treated Vanes
Low Frequency Combustor Noise Suppressor
Mach = 0.47
0.79 Throat Mach No.
Turbine Noise Suppressor
Treated L/D = 0.74
1.5 Rotor/OGV Spacing
1.83 Vane/Blade Ratio
101.6 cm (40 in.) Long Splitter

Figure 3-1. UTW Experimental Engine Acoustic Configuration.

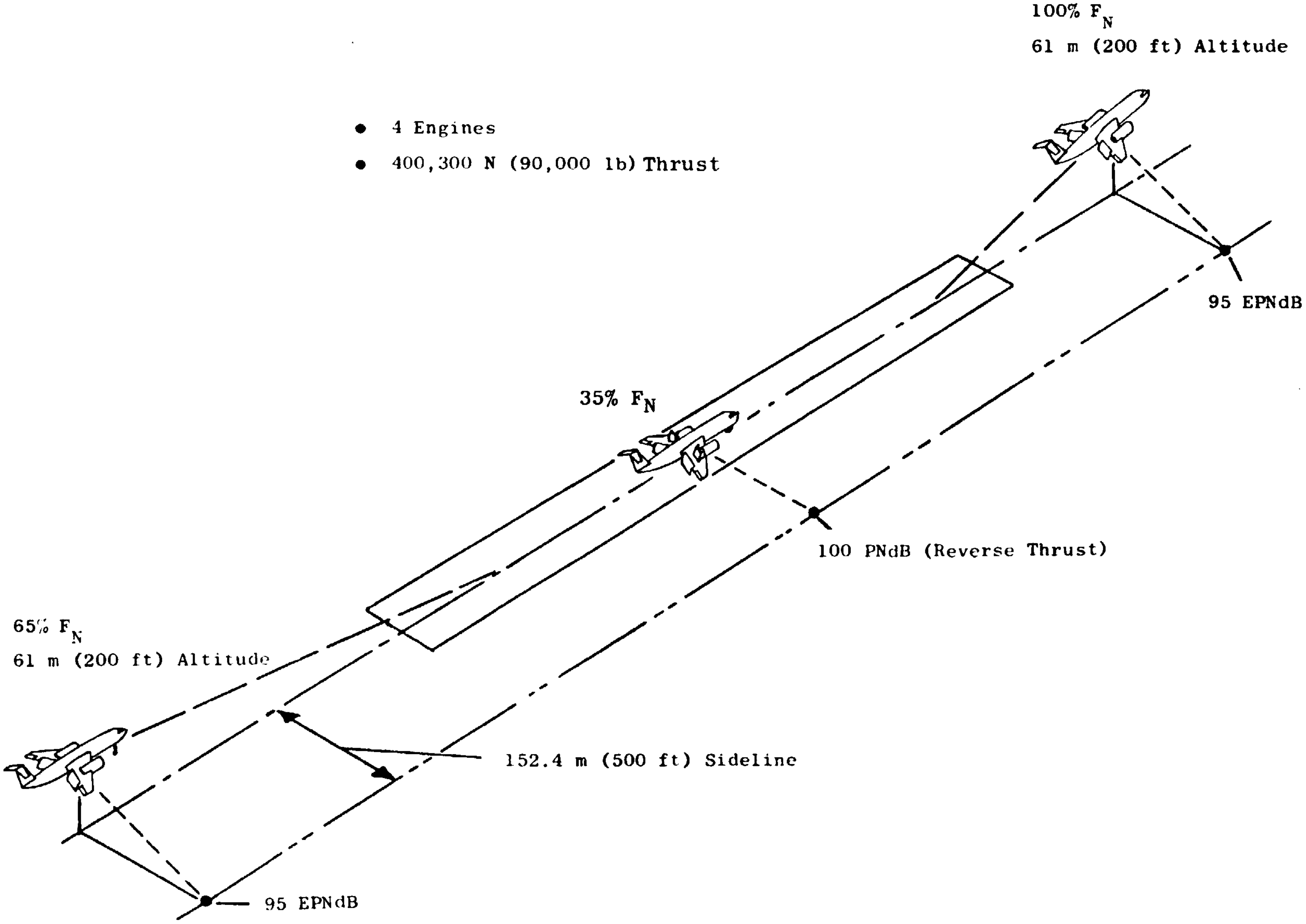
100% F_N
61 m (200 ft) Altitude
• 4 Engines
• 400,300 N (90,000 lb) Thrust
95 EPNdB
35% F_N
100 PNdB (Reverse Thrust)
65% F_N
61 m (200 ft) Altitude
152.4 m (500 ft) Sideline
95 EPNdB

Figure 3-2. QCSEE Acoustic Requirements.

At approach, the noise requirement is the same as takeoff, but the engine is operated at 65% thrust. Flap angles, defined in Table 3-II, however, are increased for the powered-lift approach.

Reverse thrust noise is limited to 100 PNdB at 35% reverse thrust with the aircraft static.

Since the engine noise levels can be measured only during static testing, a procedure for determining inflight EPNdB levels from static data has been established as part of the contract. This procedure, Appendix I of the contract, establishes the following:

1. Jet/flap noise calculation procedure
2. Extrapolation procedures
3. Doppler shift correction
4. Dynamic effect correction
5. In-flight clean-up and upwash angle correction
6. Relative velocity correction for jet/flap noise
7. Fuselage shielding and OTW wing shielding
8. PNdB to EPNdB calculation

This procedure has been used in all noise estimates for the UTW engine.

3.3 SYSTEM ACOUSTIC DESIGN CONSIDERATIONS

Many features of the UTW engine design have been selected based on the low system noise requirements for a 100,080 N (22,500 lb) thrust engine installed in an under-the-wing configuration. The two major noise sources considered were fan noise and jet-flap noise. Forward radiated fan noise is primarily a function of fan tip speed. Fan noise in the inlet quadrant can be reduced with lower tip speed, and tip speeds lower than 366 m/sec (1200 ft/sec) avoid increased noise levels due to the multiple pure tones associated with supersonic tip speed fans. The lowest tip speed, 289 m/sec (950 ft/sec), consistent with other engine cycle requirements was therefore selected for the UTW fan.

Aft radiated fan noise levels have been correlated primarily with fan pressure ratio. In addition to controlling aft fan noise, the fan pressure ratio also determines the fan jet velocity. Since the jet/flap noise is proportional to the velocity to the sixth power, low fan pressure ratios result in rapidly reduced aft system noise levels. Since aft generated fan noise can be suppressed with acoustic treatment, the fan-pressure ratio was selected primarily based on need to achieve low levels of jet flap noise.

Fan source noise reduction features were selected to provide noise reduction at the source with minimum weight and performance impact. A rotor-OGV spacing of 1.5 rotor chords was selected in order to reduce fan source noise levels and minimize the need for splitters in the fan inlet and exhaust. Additional reductions could be achieved with wider rotor-OGV spacing or a lengthened exhaust splitter. The latter approach results in a smaller weight increase than that associated with the frame length increase required for additional spacing. A vane-blade ratio of 1.83 has been selected to minimize the fan tone second harmonic level which makes a large contribution to the perceived noise levels. The variable-pitch fan also provides an additional degree of flexibility in optimizing fan performance for minimum noise.

Table 3-III shows the major design features in the UTW design which contribute to determination of the projected noise levels. The engine system trades discussed above have produced an engine design which meets noise goals of the program as well as performance and thrust-to-weight requirements.

3.4 NOISE COMPONENTS

Details of the critical noise sources were presented in the preliminary design report (References 1 and 2). Presented in the following sections are updated noise levels which are based on the data and prediction procedures discussed.

3.4.1 Takeoff Noise

Noise levels for the UTW engine at takeoff are shown in Figure 3-3 in bar chart form. Unsuppressed noise is dominated by the fan in the forward and aft quadrants. Suppressed noise levels are balanced between the fan and jet/flap noise in the aft quadrant and are dominated by jet/flap noise in the forward quadrant. The constituent levels shown are at the angle of maximum noise for the suppressed engine; thus, in the forward quadrant 1.4 radians (80°) is selected since the dominant source (jet/flap noise) is a maximum at that angle. As shown, fan inlet noise has been suppressed well below the jet/flap noise. Gear noise and compressor noise are not shown, since their contribution as noise sources was found to be insignificant.

3.4.2 Approach Noise

To obtain 65% thrust at approach, the UTW fan may be operated at a variety of engine speeds, blade pitch angles, and fan nozzle exit area combinations. For the current acoustic noise predictions, engine speed was 100% (to satisfy wave-off engine response requirements) with a nozzle area opened to the maximum allowable area. This combination of fan speed and nozzle area results in a blade pitch angle of 1.4° (closed) to obtain the desired thrust level. The approach noise constituents are shown on Figure 3-4. Jet/flap noise in the forward quadrant is the dominant source

Table 3-III. UTW Design Parameters.

- 41.16 m/s (80 knots) aircraft speed
- 60.96 m (200 ft) altitude
- Take-off power

Number of fan blades	18
Fan diameter	180.3 cm (71 in.)
Fan pressure ratio	1.27
Fan rpm	3089
Fan tip speed	289.6 m/sec (950 ft/sec)
Number of OGV's	33 (32 + Pylon)
Corrected inlet airflow	405.5 kg/sec (894 lb/sec)
Inlet Mach number (throat)	0.79
Rotor/OGV spacing	1.5 Rotor tip chords
Fan exhaust area	16,155 cm^2 (2504 $in.^2$)
Core exhaust area	3484 cm^2 (540 $in.^2$)
Uninstalled net thrust (SLS)	81,400 N (18,300 lb)
Blade passing frequency	920 Hz
Corrected core airflow	30.6 kg/sec (67.5 lb/sec)
Fan exhaust velocity	197.8 m/sec (649 ft/sec)
Core exhaust velocity	239.0 m/sec (784 ft/sec)

- EPNdB = 94
- 152.4 m (500 ft) Sideline at 61.0 m (200 ft) Altitude
- 100,080 N (22,500 lb) Installed Thrust

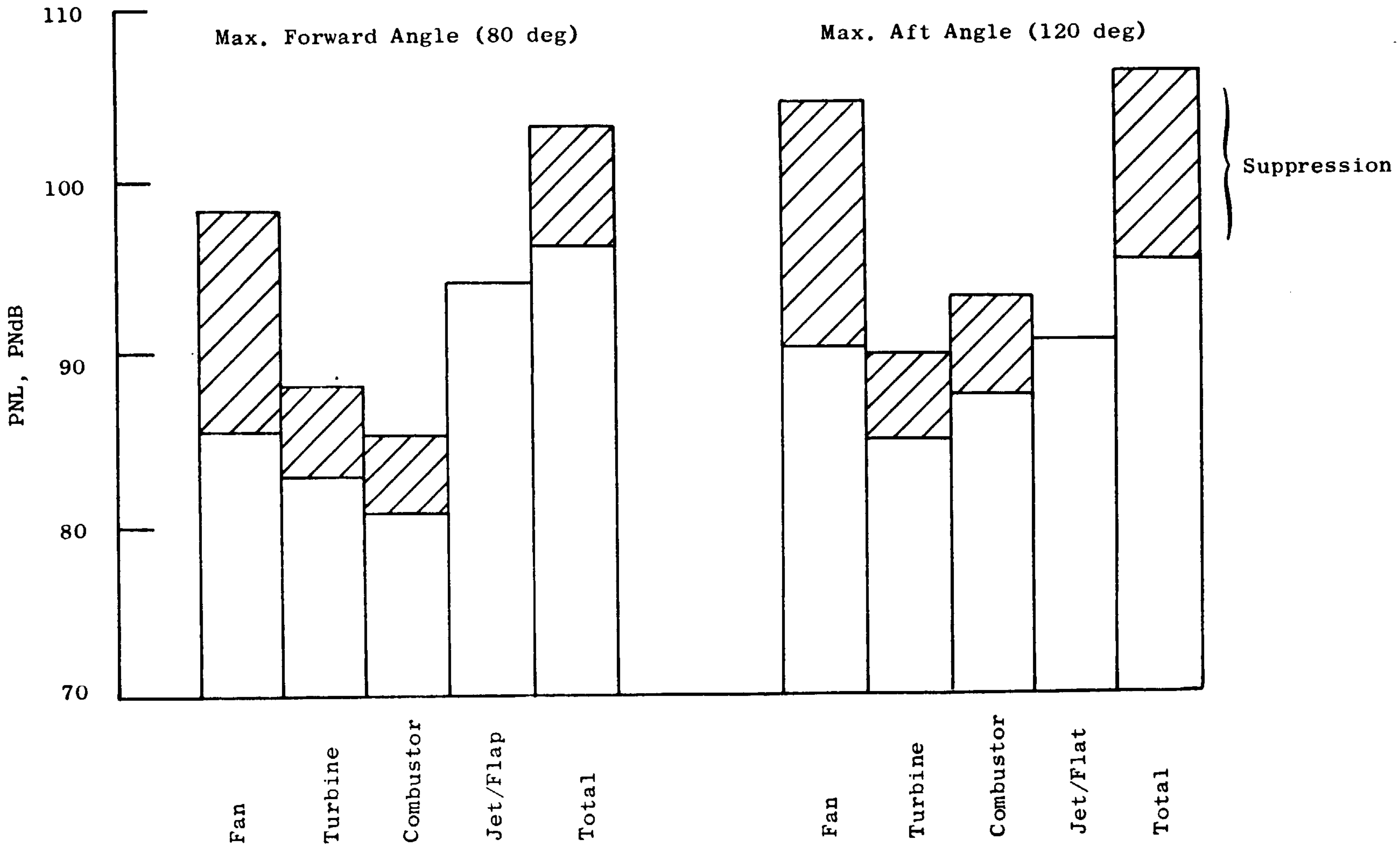

Figure 3-3. Takeoff Noise Constituents.

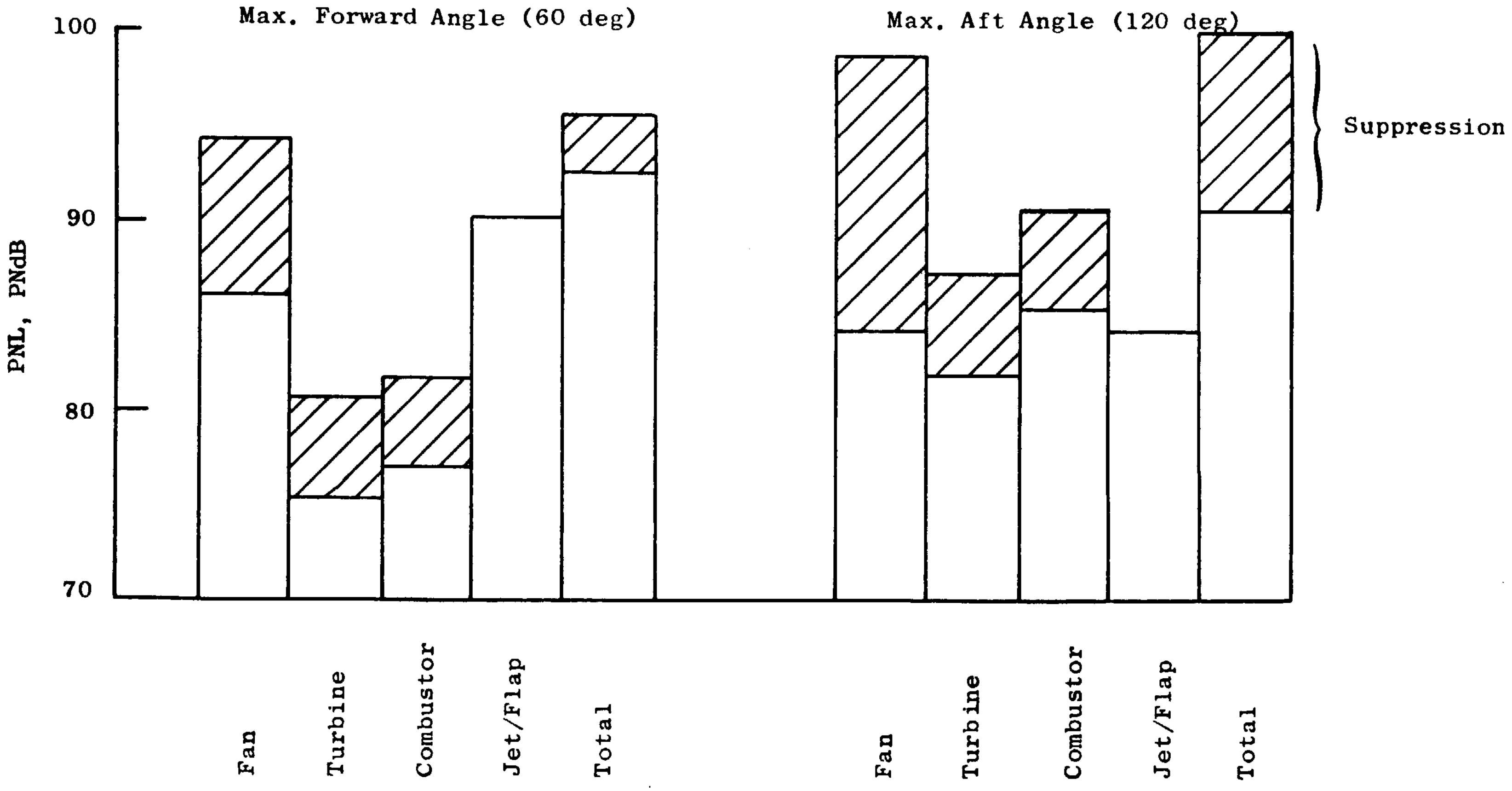

- EPNdB = 90.5
- 152.4-m (500-ft) Sideline at 61.0 m (200 ft) Altitude
- 65% of Take-off Thrust
- Take-off Fan Speed

Figure 3-4. Approach Noise Constituents.

for the suppressed levels with fan inlet, exhaust, and aft jet/flap noise approximately 4 to 8 PNdB lower. Unsuppressed, the fan aft noise is dominant. During preliminary design studies a combination of takeoff speed and nozzle area with the blades closed 8° was utilized to obtain 65% thrust. The current procedure of opening the nozzle area to reduce fan nozzle exit velocity was adopted to reduce the jet-flap noise.

3.4.3 Reverse Thrust Noise

Predicted noise constituents for the UTW engine operating in the reverse thrust mode are presented in Figure 3-5. The constituents are at a 152.4 m (500 ft) sideline at 90 percent fan speed (reversed through stall pitch) with a corresponding thrust level of 35 percent of engine rated thrust in the forward mode at takeoff power. The major noise source in reverse thrust is fan noise in the forward quadrant. All other sources are well below the 100 PNdB requirement.

3.5 COMPONENT DESIGN

This section provides the acoustic design approach selected for each critical noise source and the design status. These suppression techniques were selected for detailed study as part of the acoustic design development programs and were based on studies conducted after the Preliminary Design Review (PDR). In several cases, the design approach is the same as that presented in the PDR, but additional substantiating data were obtained to confirm the earlier selections.

Since the PDR, the following tasks have been completed:

1. Vane blade ratio selected
2. Rotor stator spacing selected
3. Treated vane-frame defined
4. Fan inlet throat Mach number selected
5. Fan inlet length defined (Preliminary Design)
6. Exhaust splitter length selected
7. Aft duct Mach number distribution defined
8. Core nozzle length defined
9. Core compressor inlet treatment defined

A detailed discussion of the critical design items follows.

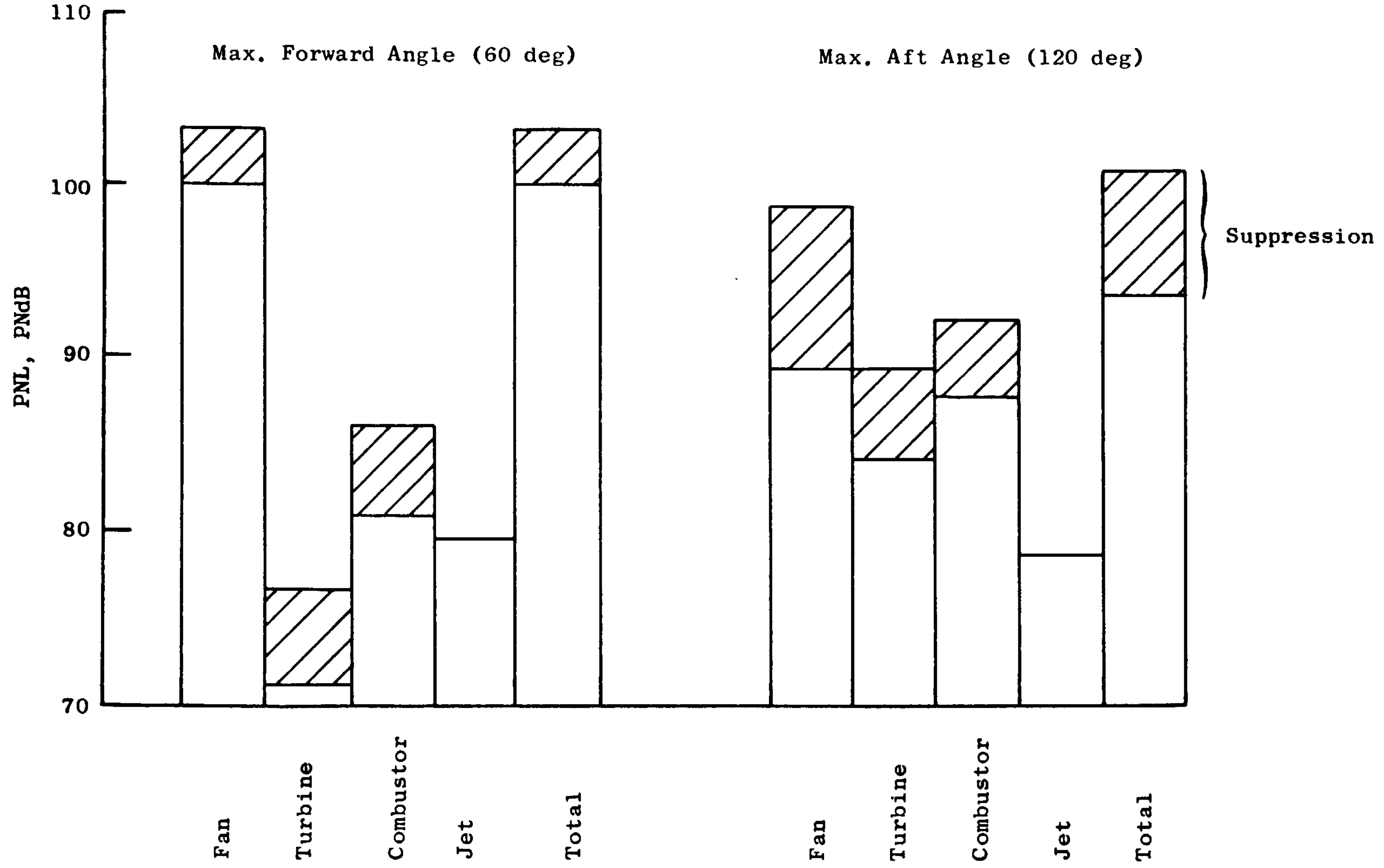

- Fan Blades Rotated Through Stall
- Max. PNdB = 100
- 152.4 m (500 ft) Sideline
- 35% of Takeoff Thrust
- 90% of Take-off Fan Speed

Figure 3-5. Reverse Thrust Noise Constituents.

3.5.1 Fan Inlet Design

The accelerating inlet (Figure 3-6) has been selected as the primary design. This inlet provides suppression at takeoff with a 0.79 throat Mach number. In reverse thrust and approach, suppression is obtained through the use of wall treatment. Since the PDR, a detailed study of existing acoustic data from accelerating inlets was made and is summarized in Figure 3-7. Aerodynamic and control studies resulted in the selection of Mach 0.79 as the maximum allowable inlet throat Mach number. From the data of Figure 3-7, a correlation of design parameters was obtained at 0.79 throat Mach number which predicted 10.5 PNdB suppression for the UTW engine. The inlet treatment would thus have to contribute an additional 2.5 PNdB to achieve the inlet suppression goal of 13 PNdB. Due to the suppression variation seen in the data of Figure 3-7, an alternate design has also been selected. This design (Figure 3-8) uses wall treatment which has been designed for takeoff suppression. The approach and reverse thrust acoustic suppression is, therefore, a by-product. Based on existing data (Figure 3-9), this design requires a longer inlet to obtain the desired 13 PNdB suppression. The accelerating inlet has a treated length of 0.74 fan diameters while this design will require a 0.85 to 1.1 L/D. The accelerating inlet will be tested on the UTW fan 50.8 cm (20 in.) simulator in the General Electric Anechoic Chamber at Schenectady. Depending on the results of these tests and other program considerations, the low Mach inlets may or may not be tested as a part of this program. The accelerating inlet configurations to be tested are shown in Figure 3-10. Candidate low throat Mach number configurations are illustrated in Figure 3-11.

The aerodynamic lines for the accelerating inlet have been selected as a result of 30.48 cm (12 in.) inlet tests at the NASA-Lewis 2.74 × 4.57 m (9 × 15 ft) wind tunnel. During these tests, noise data were obtained with the accelerating inlet operating at 0.79 throat Mach number and various angles of attack. These data, presented in Figure 3-12, indicate that the inlet is acoustically insensitive to angle of attack.

3.5.2 Fan Exhaust Design

Several techniques have been introduced in the engine design to achieve a 14.5 PNdB aft fan noise reduction. These are:

1. Phased wall treatment
2. Acoustic splitter
3. Rotor - OGV Treatment
4. Vane-blade ratio for second harmonic reduction
5. Slant cells

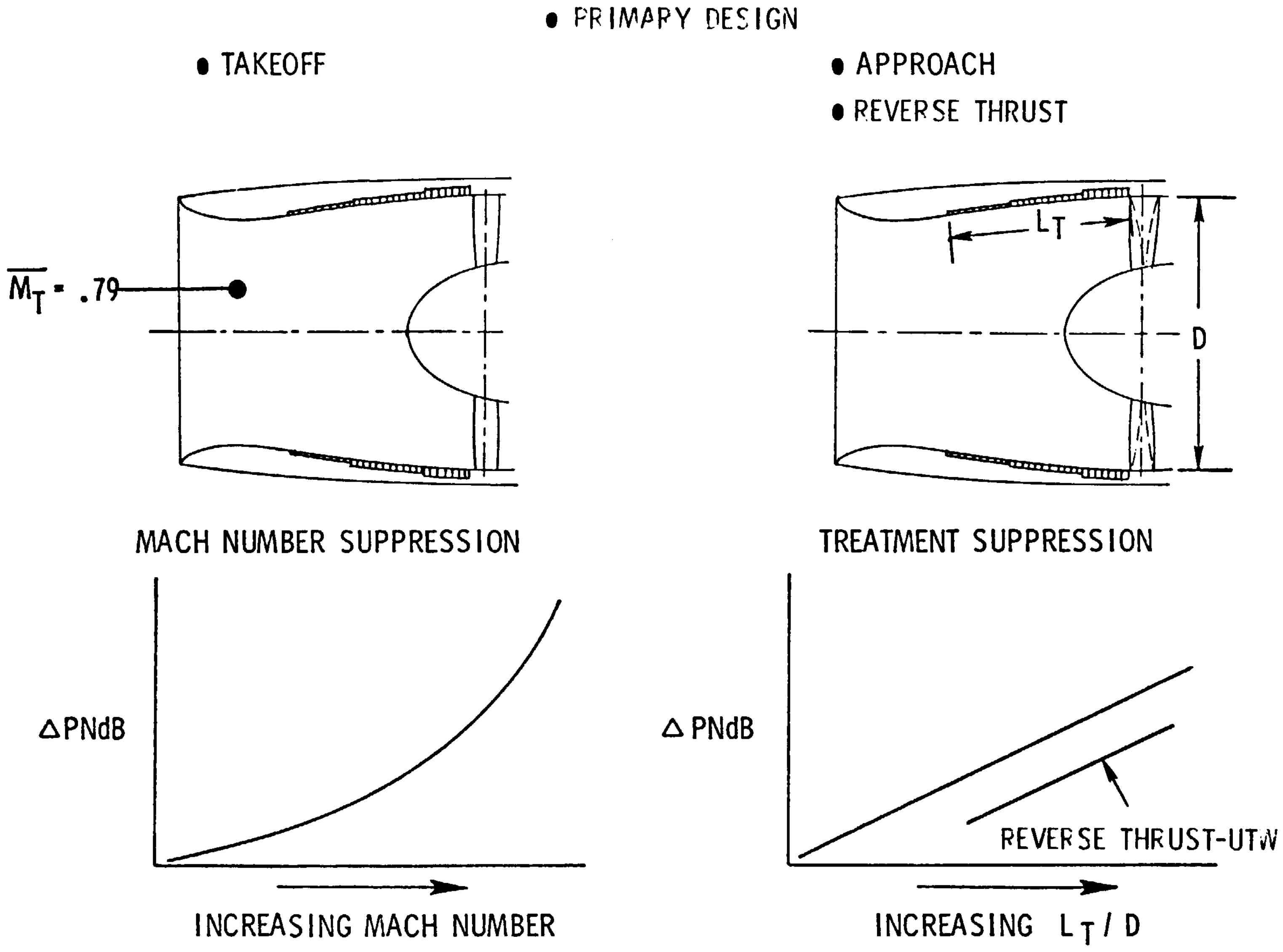
• PRIMARY DESIGN
• TAKEOFF
• APPROACH
• REVERSE THRUST
$\overline{M_T} = .79$
L_T
D
MACH NUMBER SUPPRESSION
TREATMENT SUPPRESSION
ΔPNdB
ΔPNdB
REVERSE THRUST-UTW
INCREASING MACH NUMBER
INCREASING L_T / D

Figure 3-6. Inlet Noise Reduction Concepts.

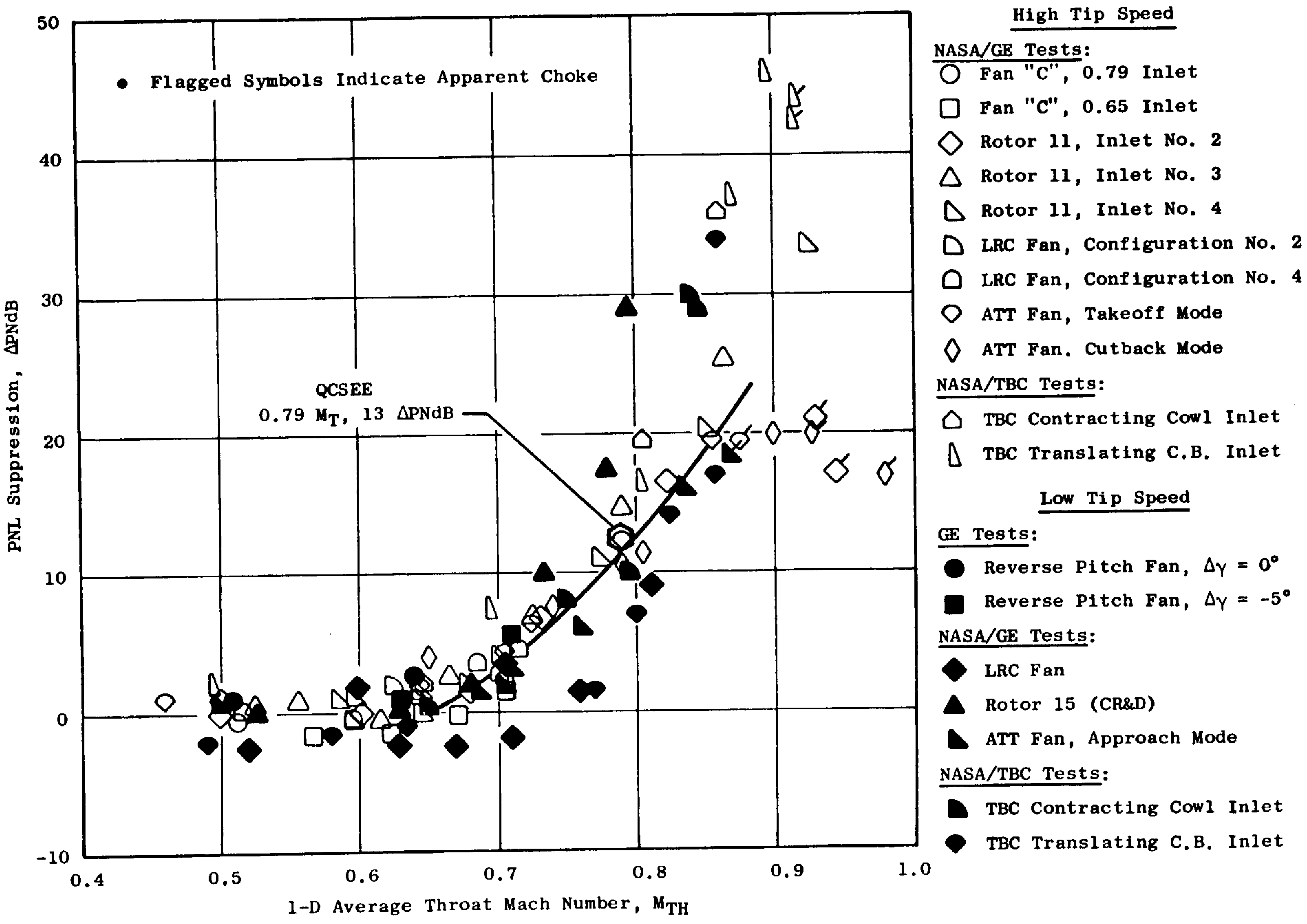

Figure 3-7. Summary - Inlet Acceleration Suppression.

- Alternate Design

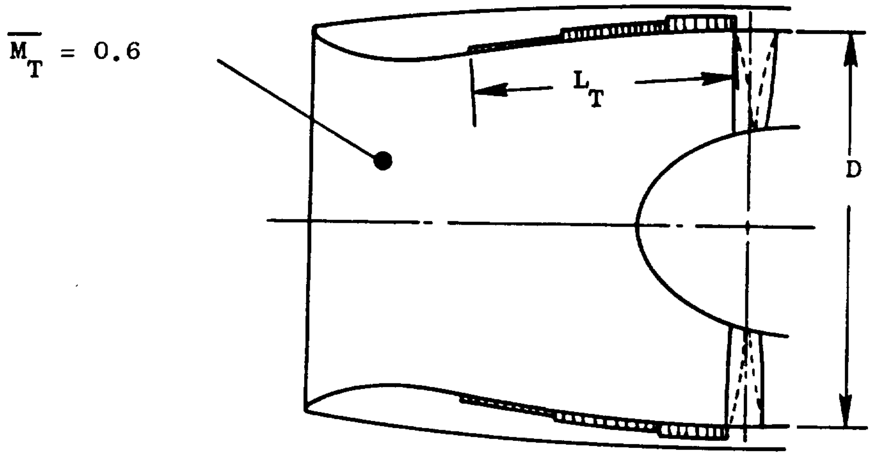
$\overline{M}_T = 0.6$
L_T
D

Treatment Suppression

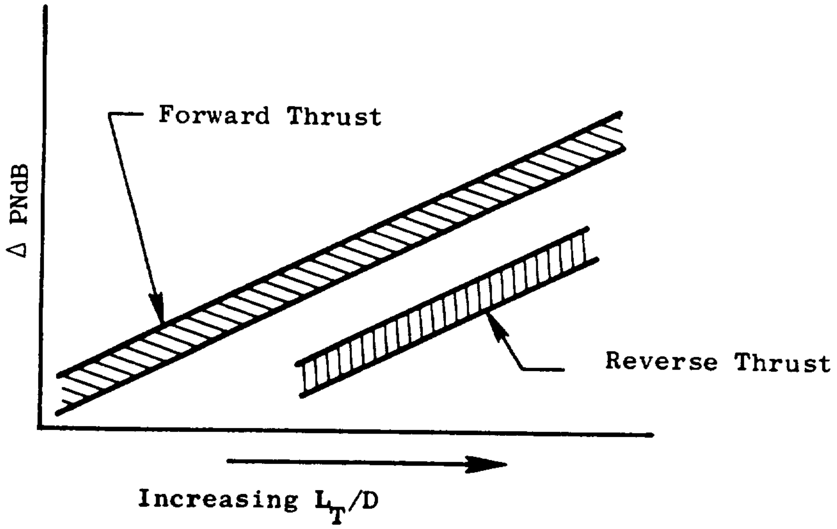

Figure 3-8. Inlet Noise Reduction Concepts.

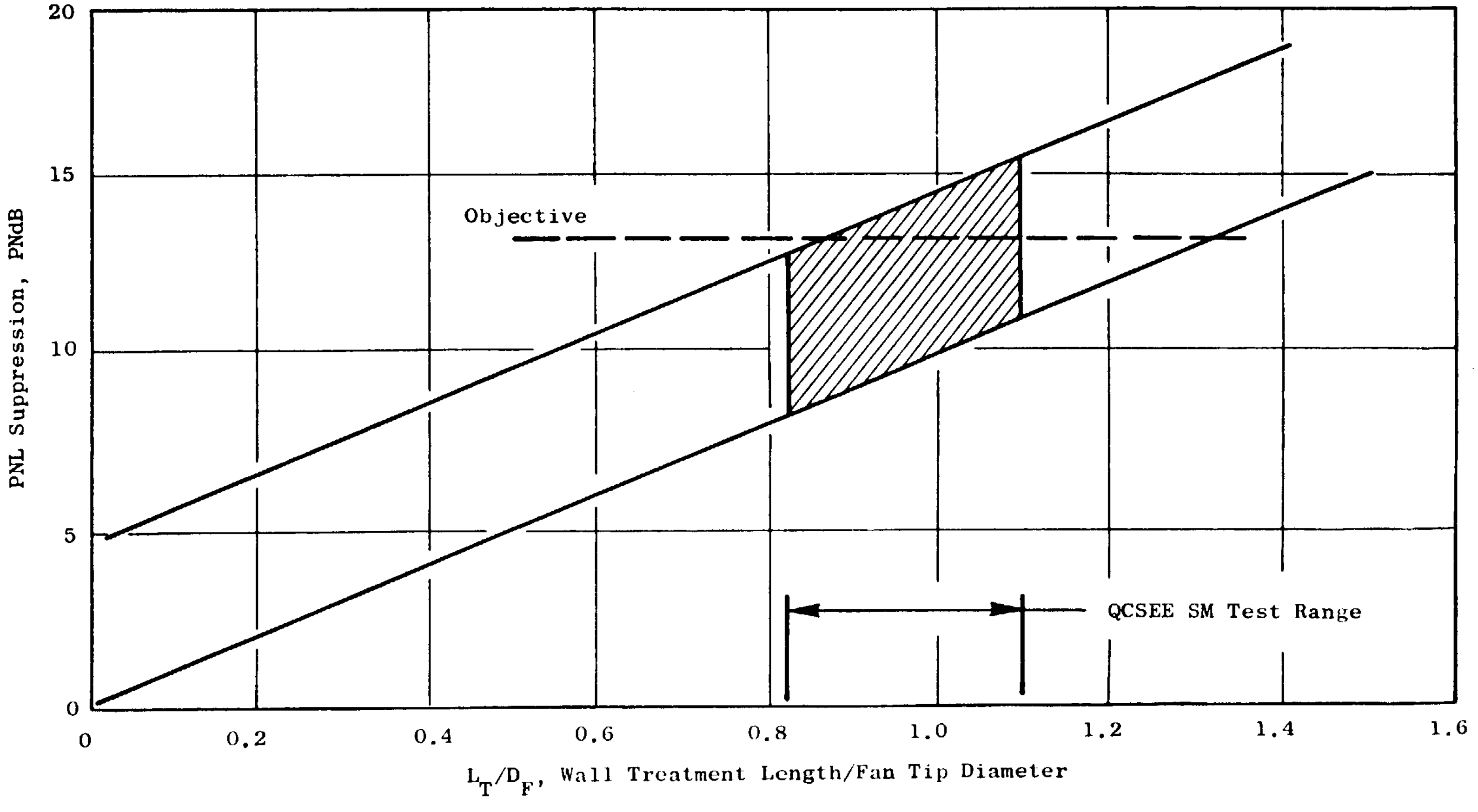

Figure 3-9. Inlet Noise Reduction Due to Treatment.

1. Hardwall with Aero/Acoustic Lip

2. Treated Wall with Aero/Acoustic Lip
   - 3 Diffusers Designed for Reverse Thrust Suppression

3. Treated Wall with Flight Lip

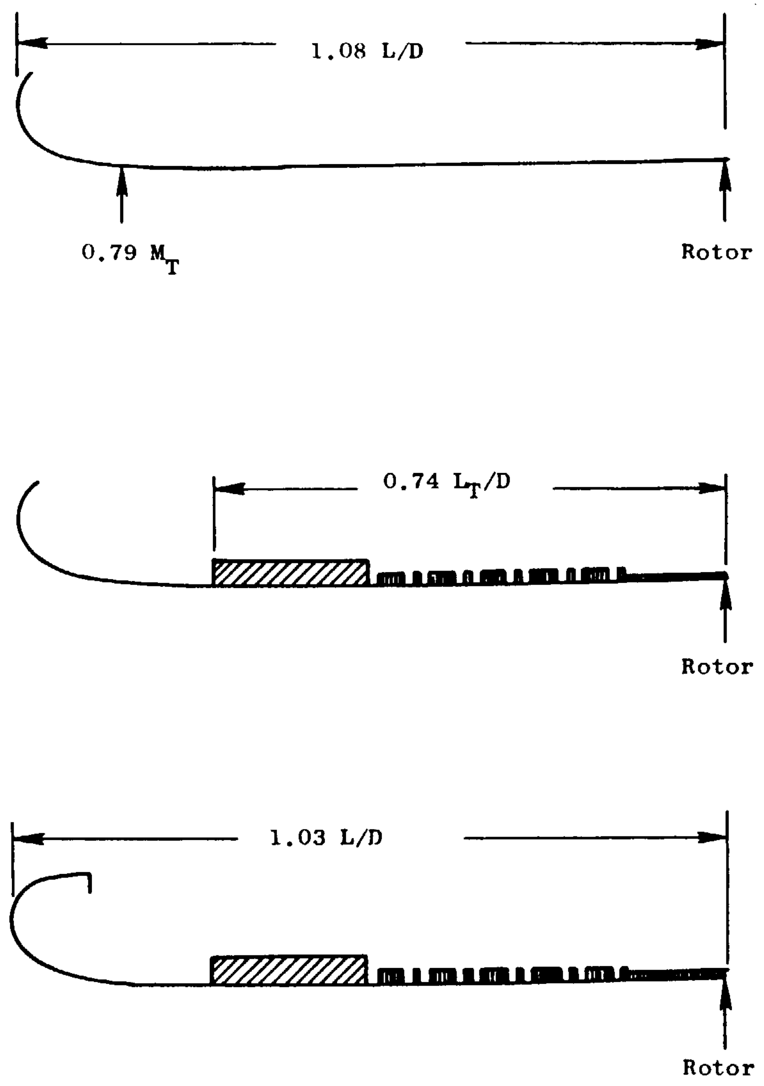
1.08 L/D
0.79 M_T
Rotor
0.74 L_T/D
Rotor
1.03 L/D
Rotor

Figure 3-10. Accelerating Inlet Configurations.

1. Hardwall with Aero/Acoustic Lip

2. Treated Wall with Aero/Acoustic Lip
   - 4 Diffusers (0.575 L_T/D)
   - 2 Spools (0.275 L_T/D)

3. Treated Wall with Aero/Acoustic Lip
   - 2 Spools (0.25 L_T/D)

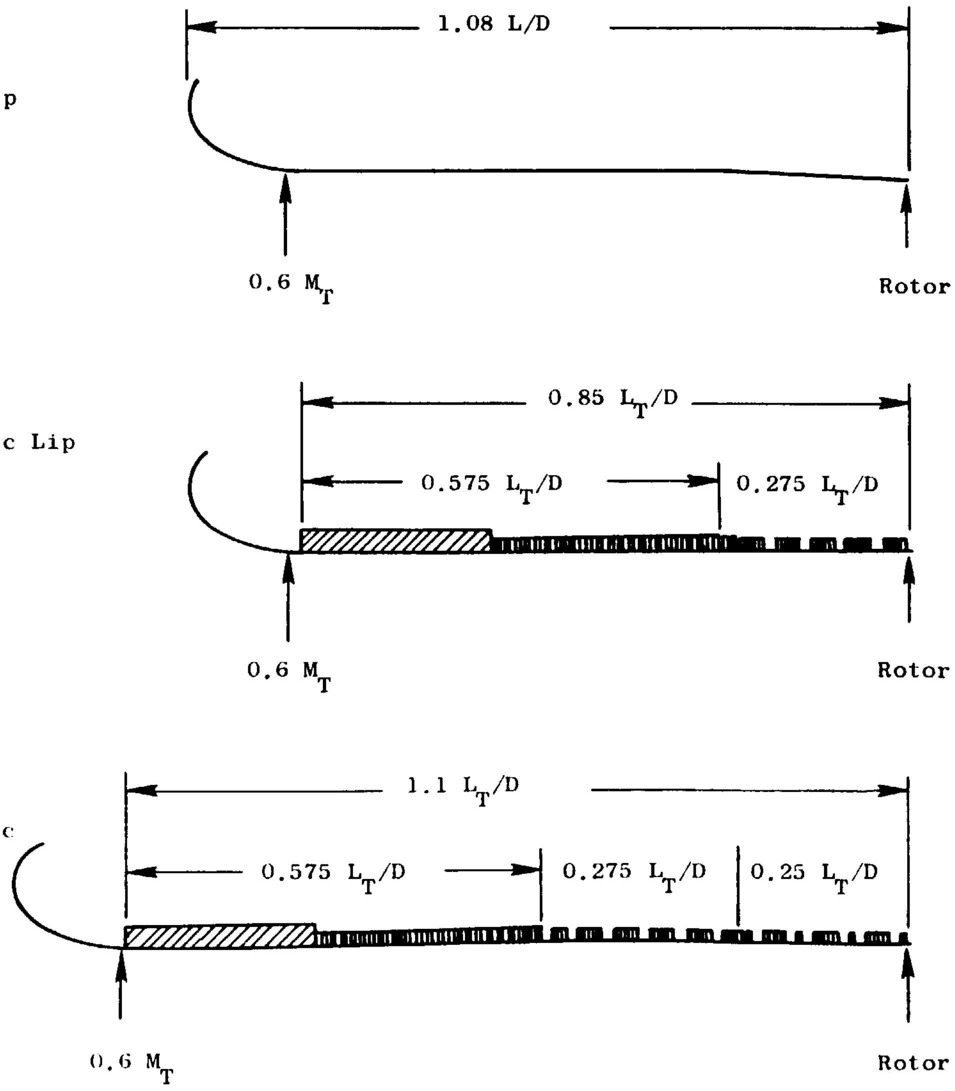
1.08 L/D
0.6 M_T
Rotor
0.85 L_T/D
0.575 L_T/D
0.275 L_T/D
0.6 M_T
Rotor
1.1 L_T/D
0.575 L_T/D
0.275 L_T/D
0.25 L_T/D
0.6 M_T
Rotor

Figure 3-11. Low Throat Mach Number Configurations.

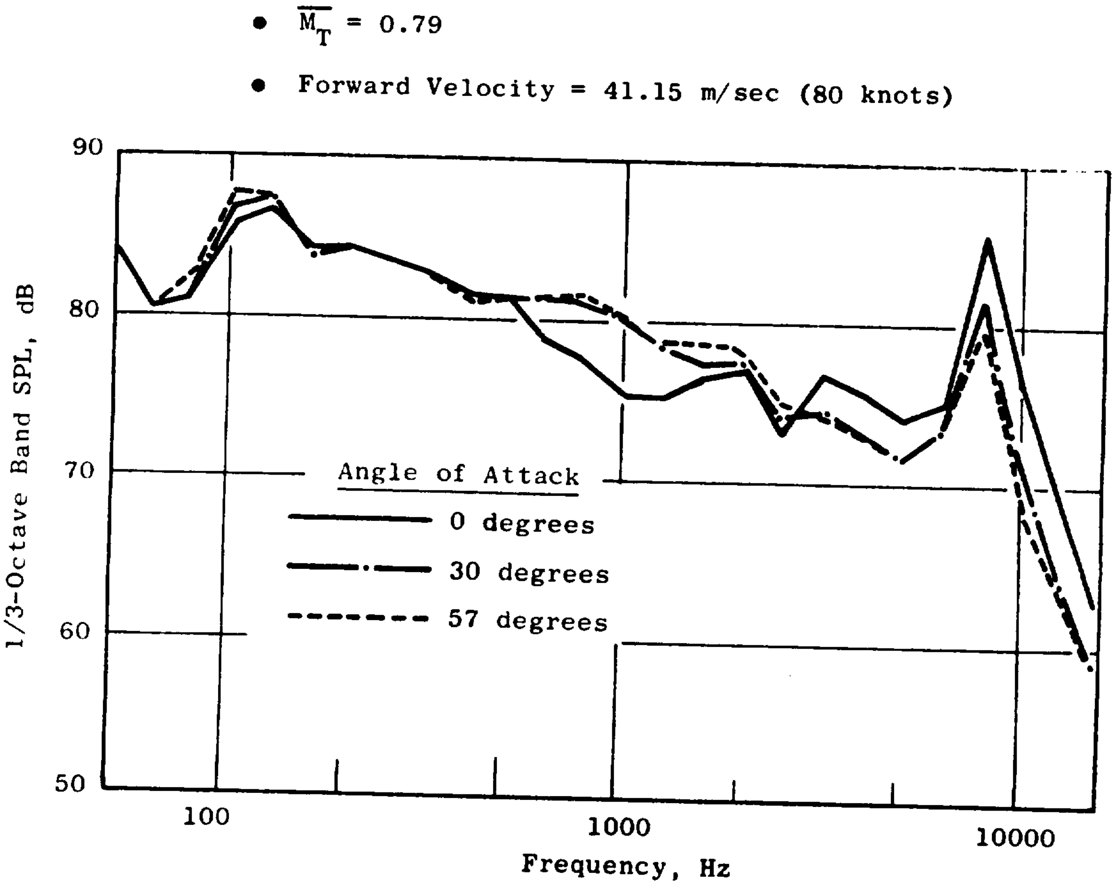

Figure 3-12. Effect of Angle of Attack on Acceleration Suppression.

6. Flow noise floor definition
7. Treated vane row
8. Treated duct curvature

Figure 3-13 shows the Noy-weighted aft fan noise spectrum. Due to the low blade passing frequency (1000 Hz), the fan second and third harmonics lie in the heaviest Noy-weighted region and, thus, are more critical to PNdB reduction. This also results in a requirement for very broadband suppression to obtain 14.5 PNdB total suppression.

Cold-flow duct test results, shown in Figure 3-14, had shown an interaction or phasing effect when treatment panels were arranged with varying thickness. The suppression obtained was greater than that expected from the summation of the individual panel suppressions. The concept was investigated using 50.8 cm (20 in.) diameter low tip speed fan (NASA Rotor 55) in the General Electric Anechoic Chamber. These tests were started in October 1974. Representative data, presented in Figure 3-15, also show wide bandwidth suppression for the varying treatment thickness design. Testing with the phased wall treatment was also conducted using an acoustic splitter. Results of these tests are currently being evaluated.

Rotor OGV treatment was applied to the UTW engine to reduce the blade passing frequency (BPF) tone since the aft duct treatment was designed to reduce the higher frequencies. This type of treatment was also tested on the 50.8 cm (20 in.) diameter fan and showed broadband suppression as well as tone reduction. Test results are presented in Figure 3-16. No benefit had been taken in the engine noise predictions for this broadband suppression. Additional tests and analyses are planned to determine if the rotor-OGV treatment is just as effective when used in combination with a heavily treated aft duct.

Due to the relatively thin nacelle wall utilized on the UTW engine, thick treatment panels cannot be applied to some regions, particularly in the nozzle flap hinge line area. A potential way to increase effective treatment depth is to slant the honeycomb cells so that the cell depth is longer than the radial depth. Results from tests with this type of honeycomb have shown the slant cell to be equivalent to the standard honeycomb of the same depth as the slant cell length. These results are shown in Figure 3-17. The 3.81 cm (1.5 in.) standard treatment and the 3.81 cm (1.5 in.) slant cell treatment are equivalent. Slant cell treatment will be applied to the engine where appropriate.

Flow noise generated by air passing over the treated surfaces, splitter, and support struts represents a floor which limits the amount of suppression attainable in the aft duct. The 50.8 cm (20 in.) Rotor 55 was tested with a nominal and open nozzle to vary duct Mach number for a configuration having an acoustic splitter. These results are shown on Figure 3-18. For a change in Mach number from 0.465 to 0.515, aft suppression did not vary, indicating a noise floor had not been reached at 0.515 Mach number. These

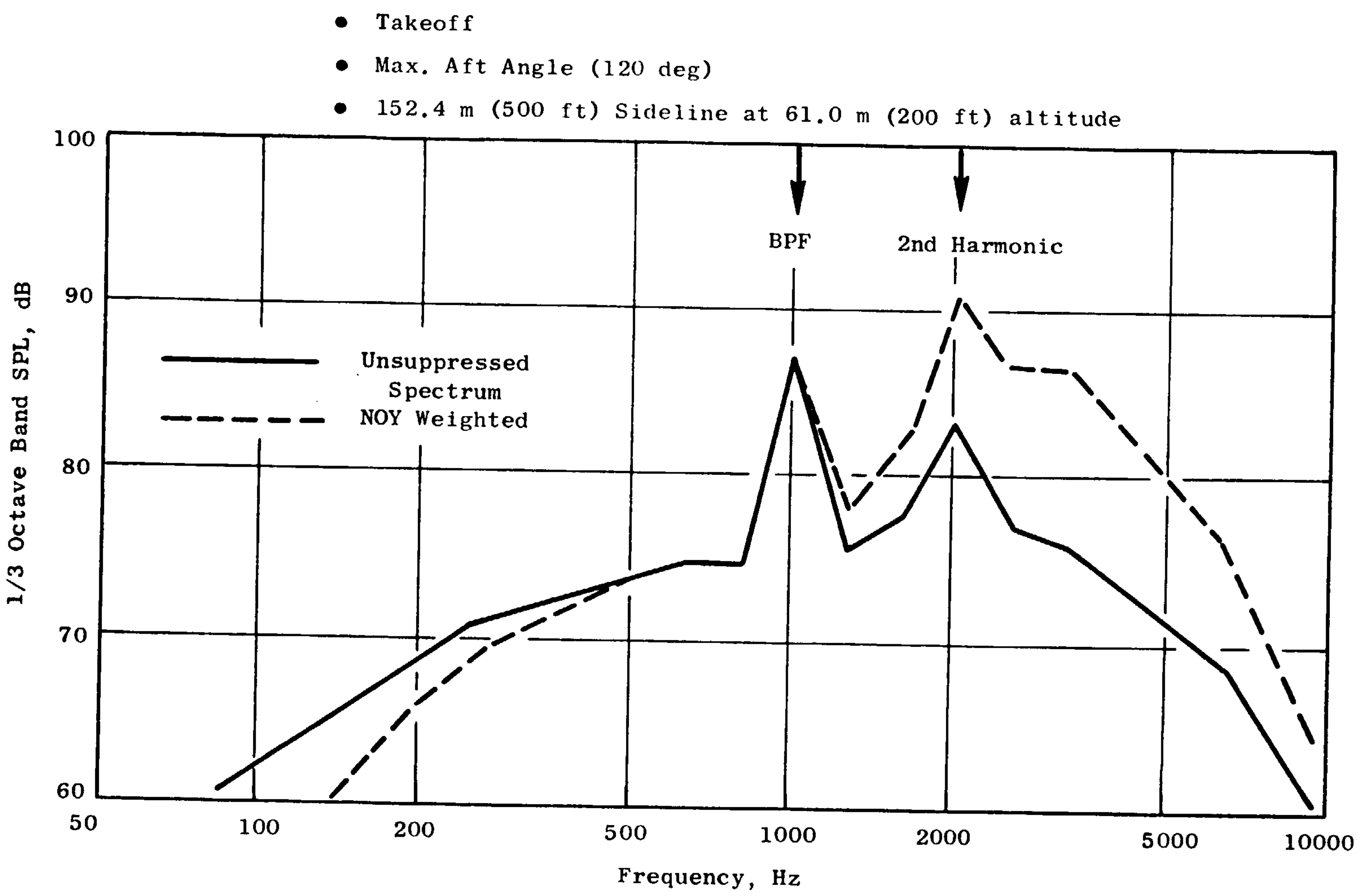

Figure 3-13. UTW Fan Spectra.

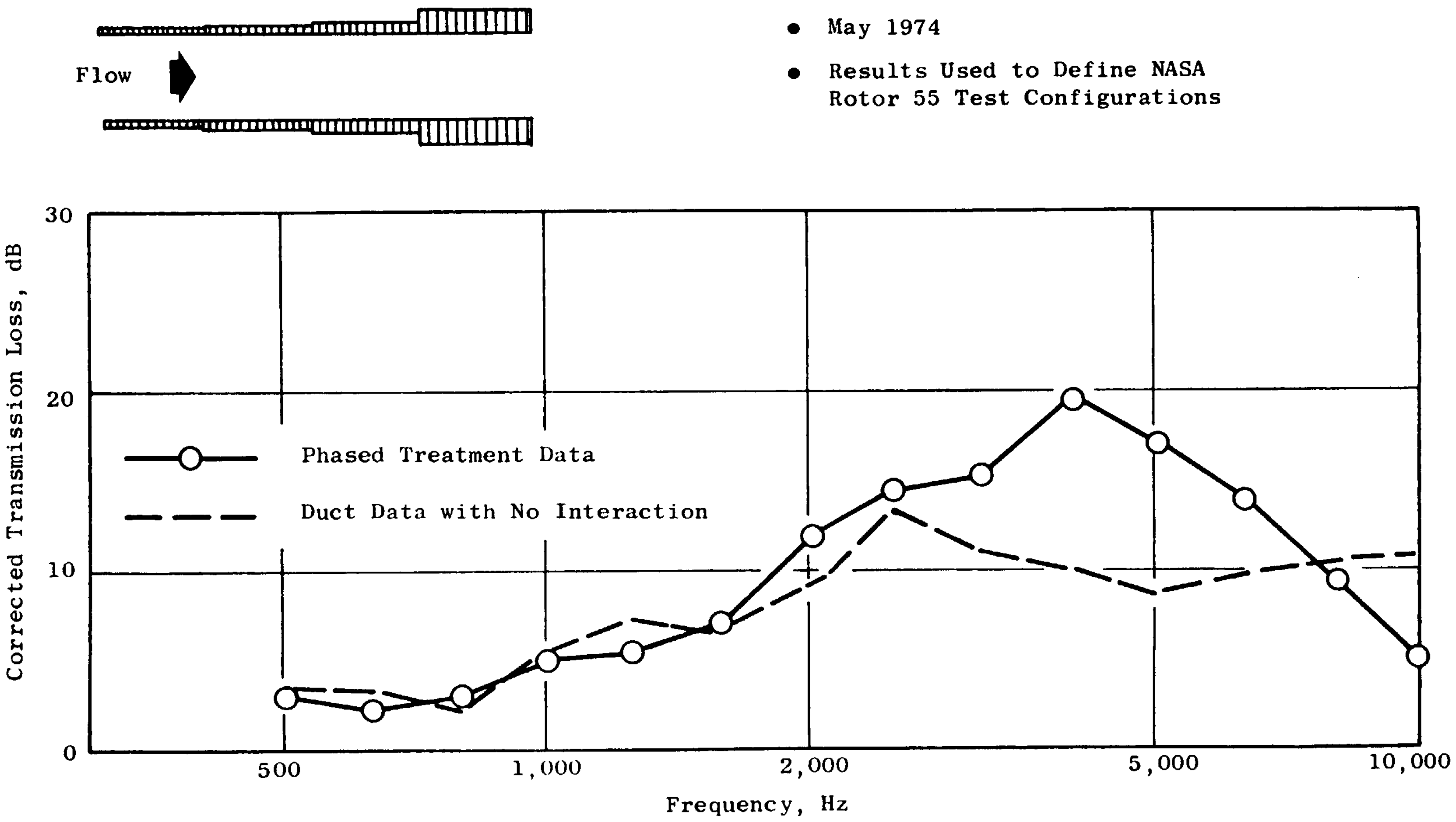

- May 1974
- Results Used to Define NASA Rotor 55 Test Configurations

Figure 3-14. Cold Flow Duct Test Results.

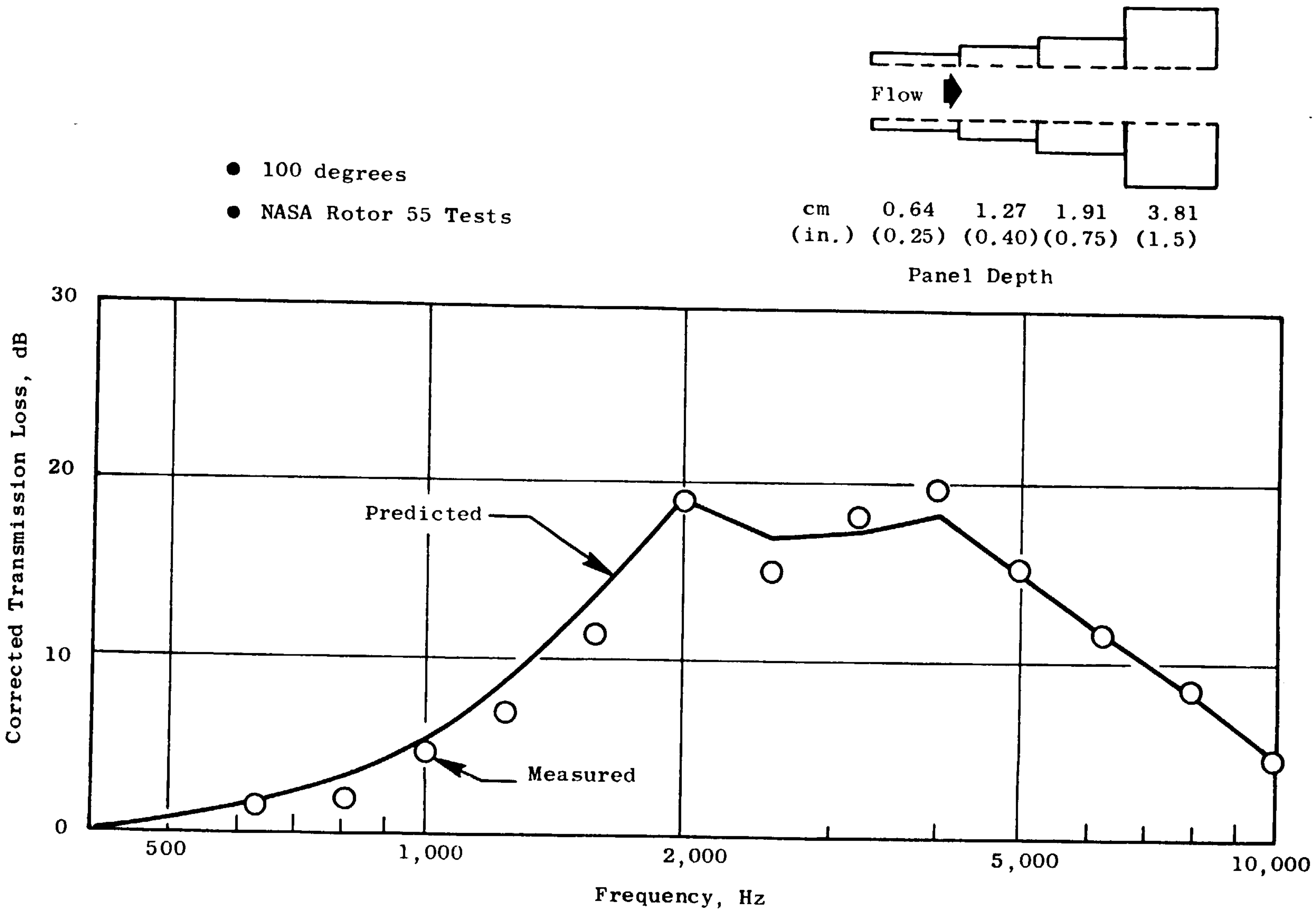

Figure 3-15. Phased Treatment Suppression.

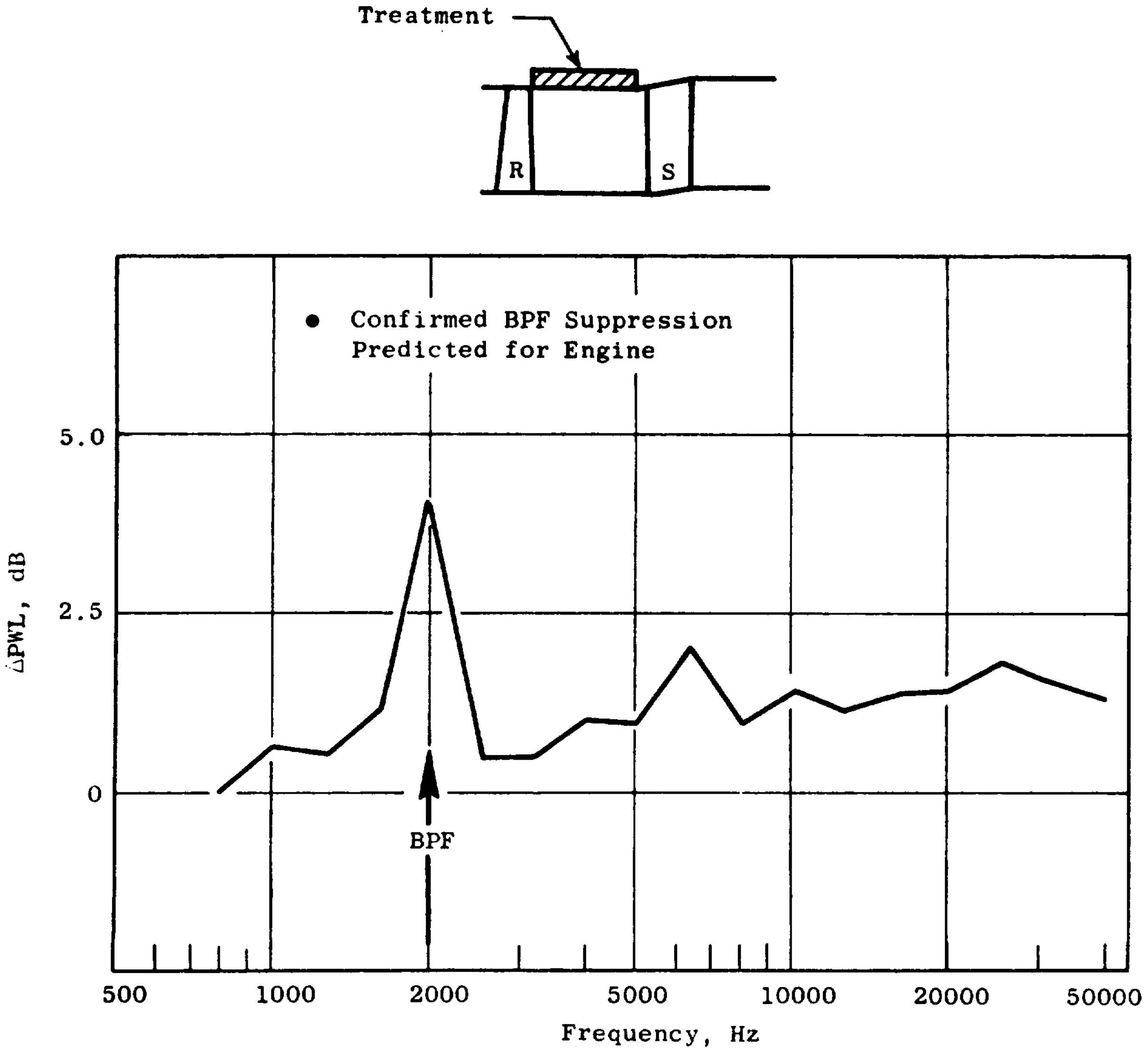

Figure 3-16. Rotor, OGV Treatment Suppression.

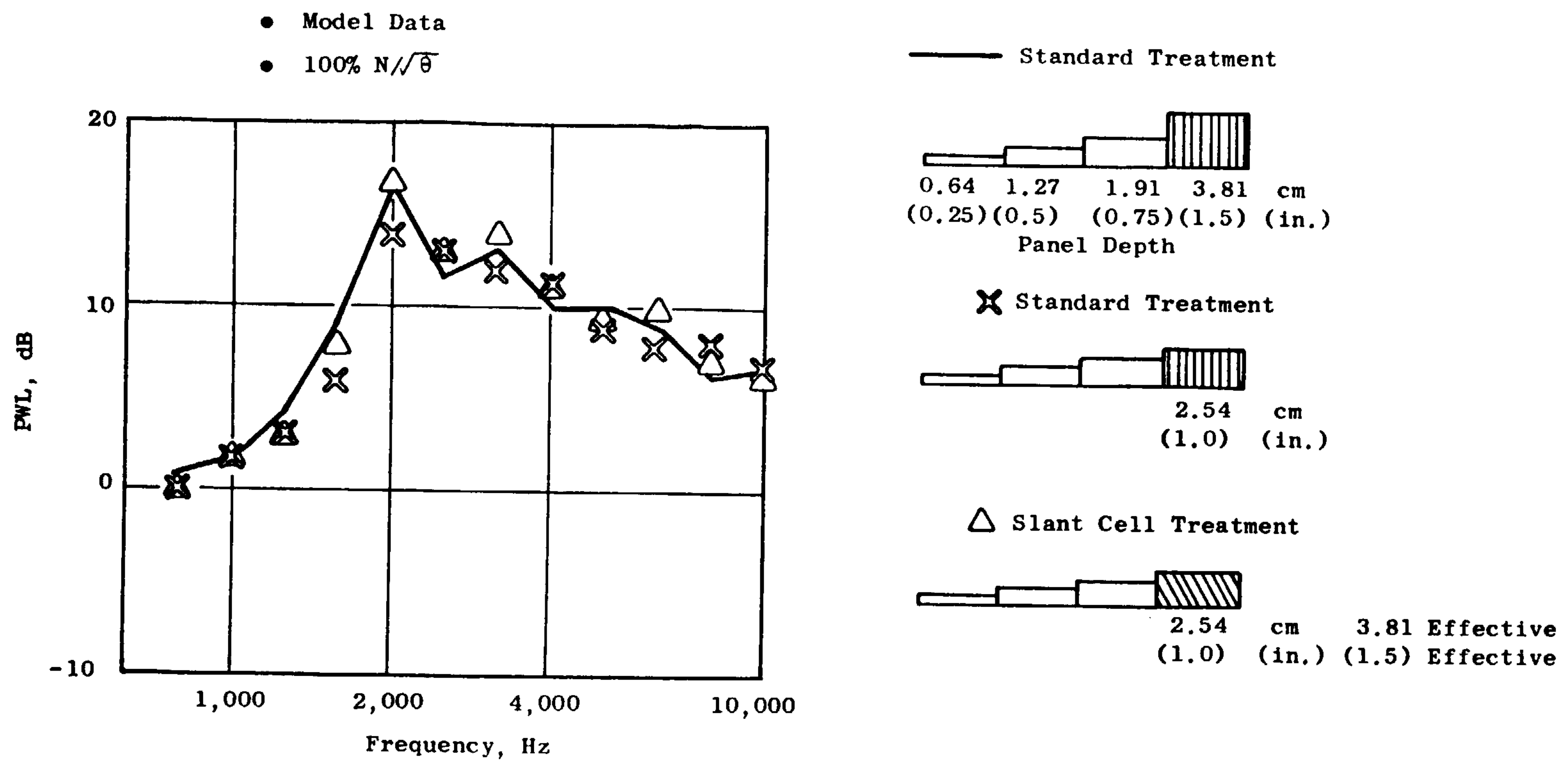

Figure 3-17. Slant Cell Treatment Suppression Results.

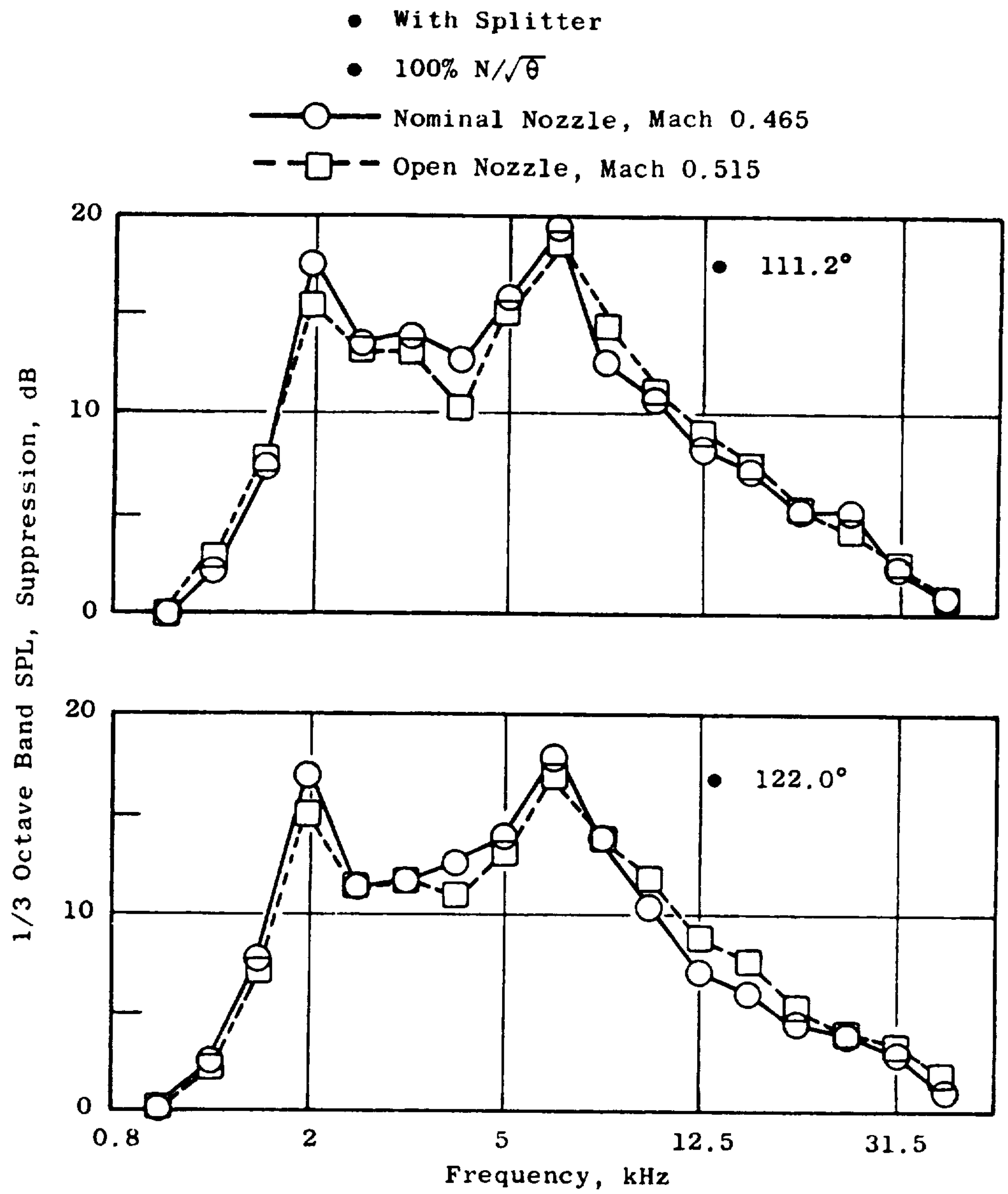

Figure 3-18. Flow Noise Effects.

data will be compared with flow noise prediction methods used for the engine design. The engine aft duct flow lines were selected to provide an average Mach number of 0.47, and, based on these test data, the selected Mach number would be acceptable.

The vane-blade ratio for the UTW engine had been selected as 1.83 in an attempt to reduce second harmonic noise as opposed to the standard procedure of reducing the BPF. Several vane-blade ratios were tested on Rotor 55 to evaluate the theory of second harmonic reduction. All tests were conducted at a spacing of 1.5 rotor chords to simulate the engine configuration. Results, shown in Figure 3-19, did not show any significant change in second harmonic noise from a vane-blade ratio of 0.73 to 2.1. This lack of reduction may be due to the large rotor-stator spacing which will reduce the rotor-stator interaction noise. These tests will be repeated at 0.5 chord spacing to evaluate the effect with a more dominant rotor-stator noise level. The engine vane-blade ratio was left at 1.83 for the following two reasons: (1) no advantage could be established for increasing it to benefit fundamental tone noise generation since the BPF is in a low Noy-weighted region, and (2) under in-flight conditions, the rotor-stator noise may be more predominant and the second harmonic reduction more beneficial. The latter will be evaluated in more detail.

3.5.3 Core Exhaust Design

Two types of core treatment have been selected for development: (1) side branch resonator, Figure 3-20, and (2) stacked SDOF treatment, Figure 3-21.

The side branch resonator design had never been tested on a combustor noise suppressor; therefore, cold flow tests were made to check the theoretical design procedure. Figure 3-22 shows results of the tests versus the predicted suppression. The favorable agreement indicated a resonator could be designed to provide the desired suppression. Both types have been selected for further development using a hot jet facility.

Prediction of low frequency combustor noise had been based on data correlations from various engine tests. To check these predictions, core noise measurements were obtained on an F101 engine. Figure 3-23 shows the test configuration and the location of an acoustic probe in the core nozzle. Farfield measurements were also obtained during the test. Figure 3-24 presents a comparison of farfield levels as a function of jet velocity or engine power setting. At higher power settings, jet noise is the dominant source at 400 Hz, but as power is reduced, the jet noise decays at a V^9 rate and the combustor noise becomes dominant. This is indicated by the break or flattening of the predicted total noise. The data follow the prediction trend, thus indicating that the predictions at least are not overpredicting the combustor noise. Other sources may be influencing the 400 Hz level in the farfield; therefore, the absolute level is not significant. Probe data which are not influenced by other sources, also agreed well with the predicted levels (Figure 3-25) on an absolute level basis.

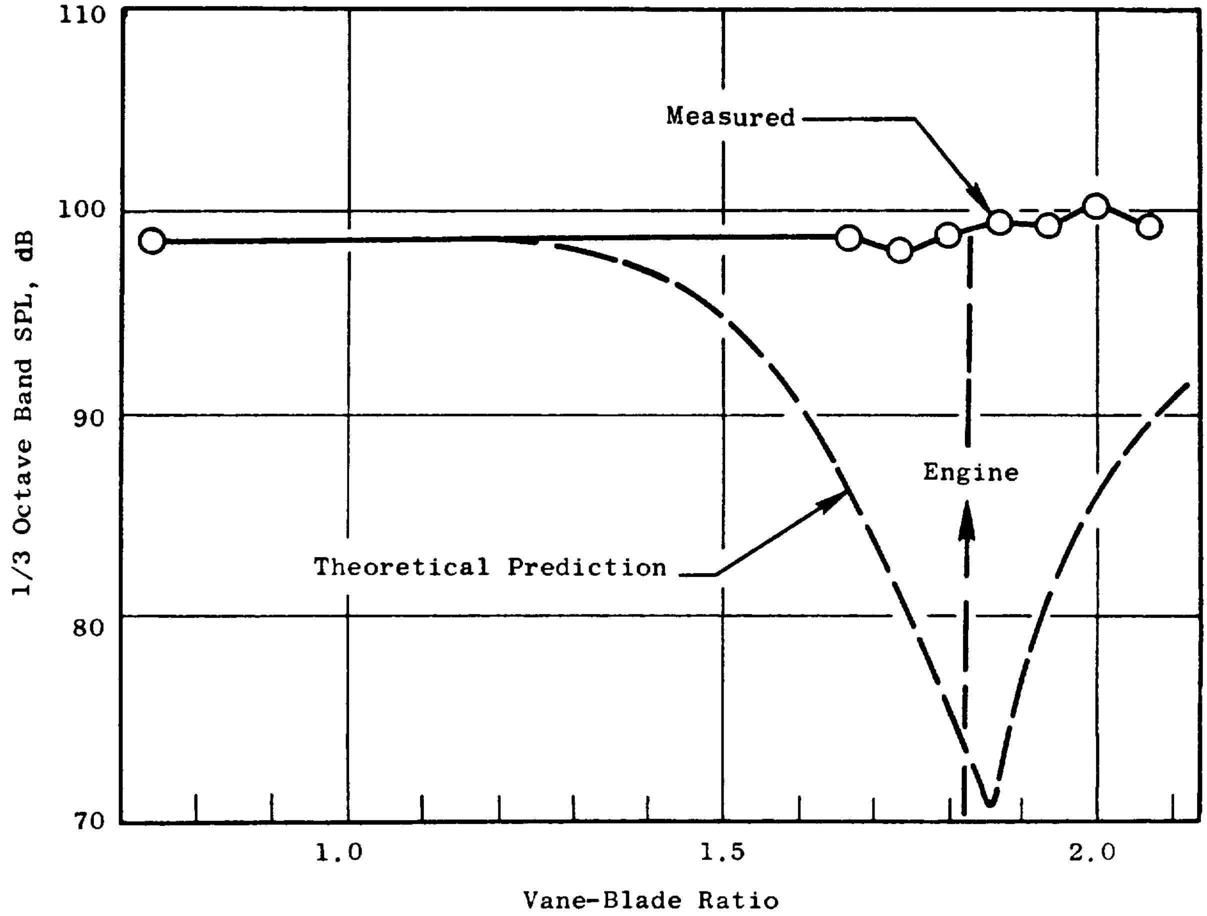

- Engine V/B Ratio Selected at 1.83
- 118° Acoustic Angle
- $100\%\ N/\sqrt{\theta}$
- 4000 Hz

Figure 3-19. Effect of Vane-Blade Ratio on Rotor 55 Second Harmonic.

- Configuration 1

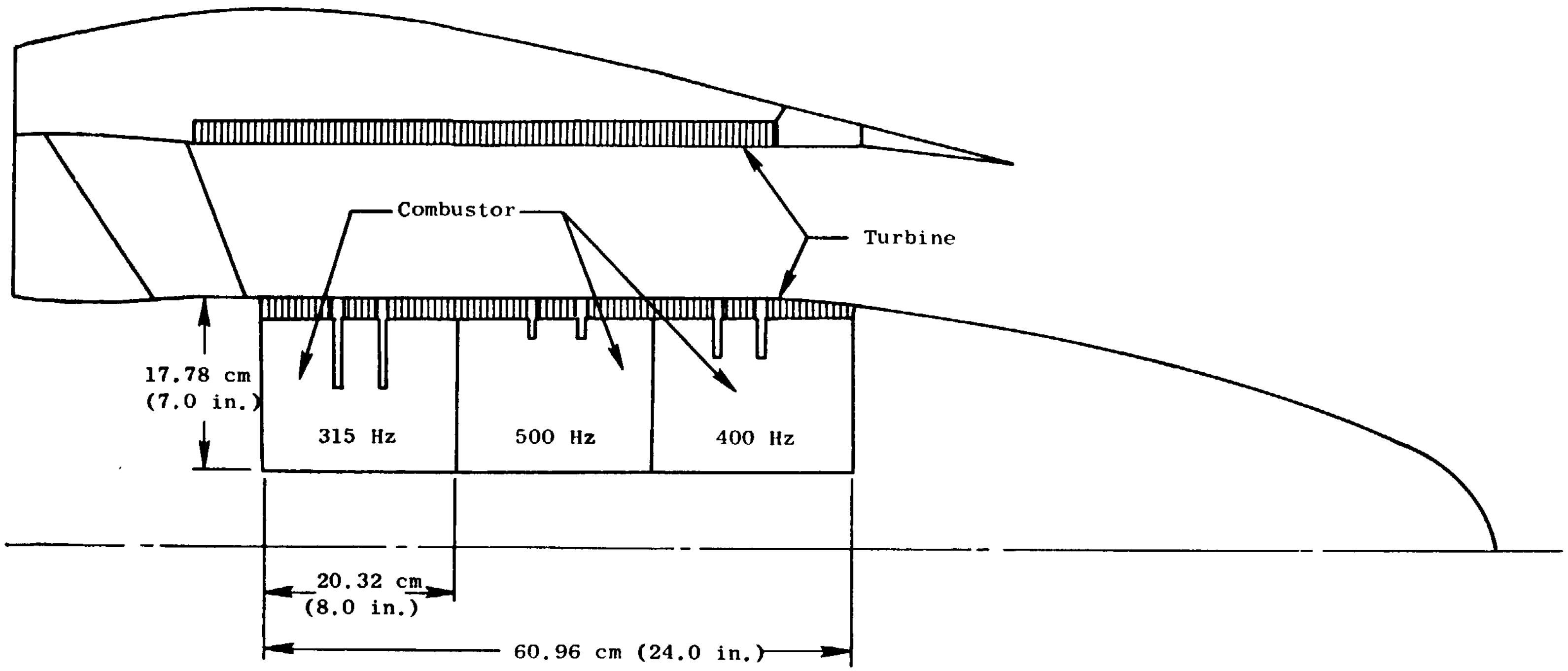
Combustor
Turbine
17.78 cm
(7.0 in.)
315 Hz
500 Hz
400 Hz
20.32 cm
(8.0 in.)
60.96 cm (24.0 in.)

Figure 3-20. UTW Side-Branch Resonator Treatment Configuration.

- Configuration 2

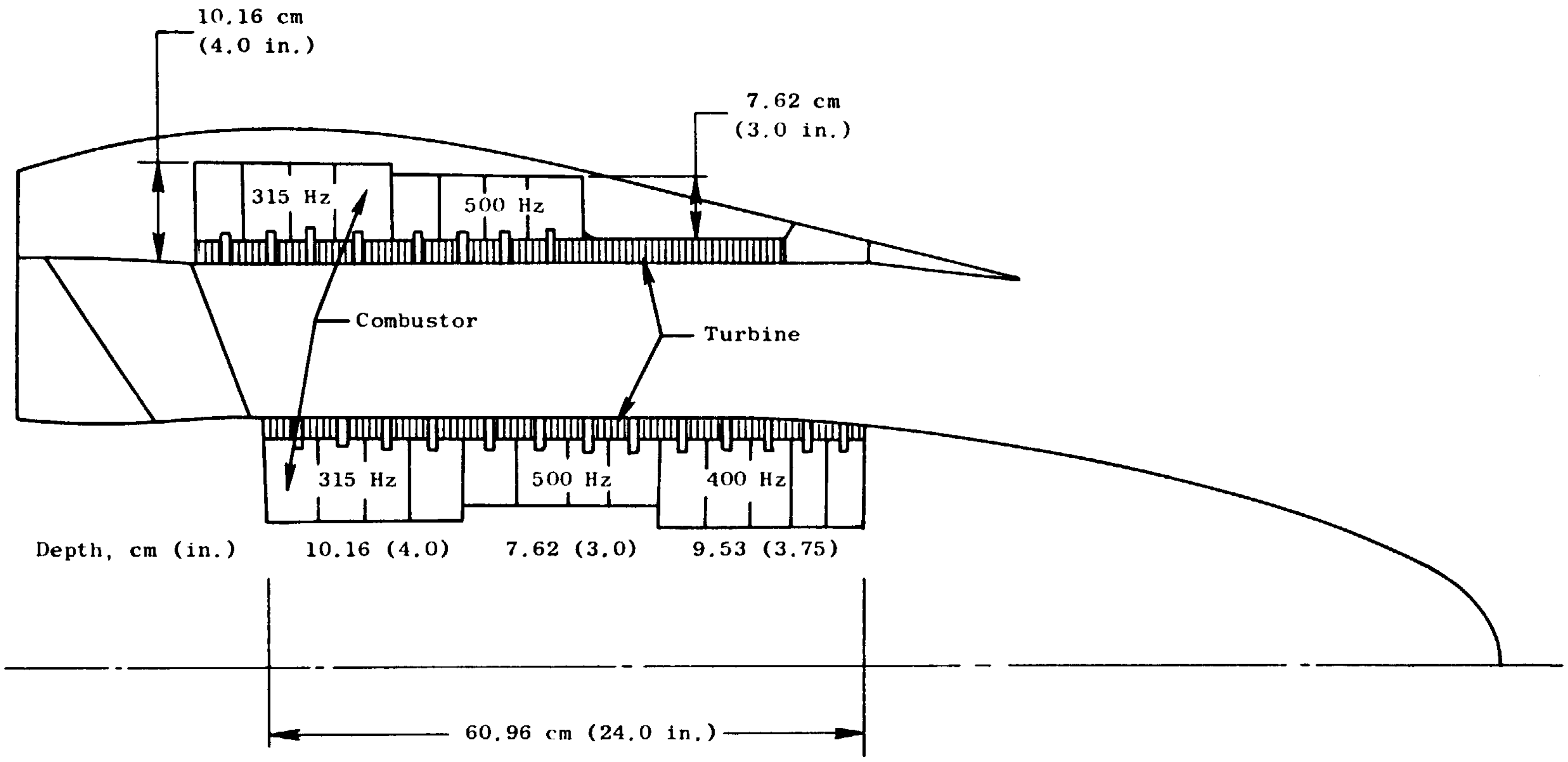
10.16 cm
(4.0 in.)
7.62 cm
(3.0 in.)
315 Hz
500 Hz
Combustor
Turbine
315 Hz
500 Hz
400 Hz
Depth, cm (in.)
10.16 (4.0)
7.62 (3.0)
9.53 (3.75)
60.96 cm (24.0 in.)

Figure 3-21. UTW Core Stacked SDOF Treatment Configuration.

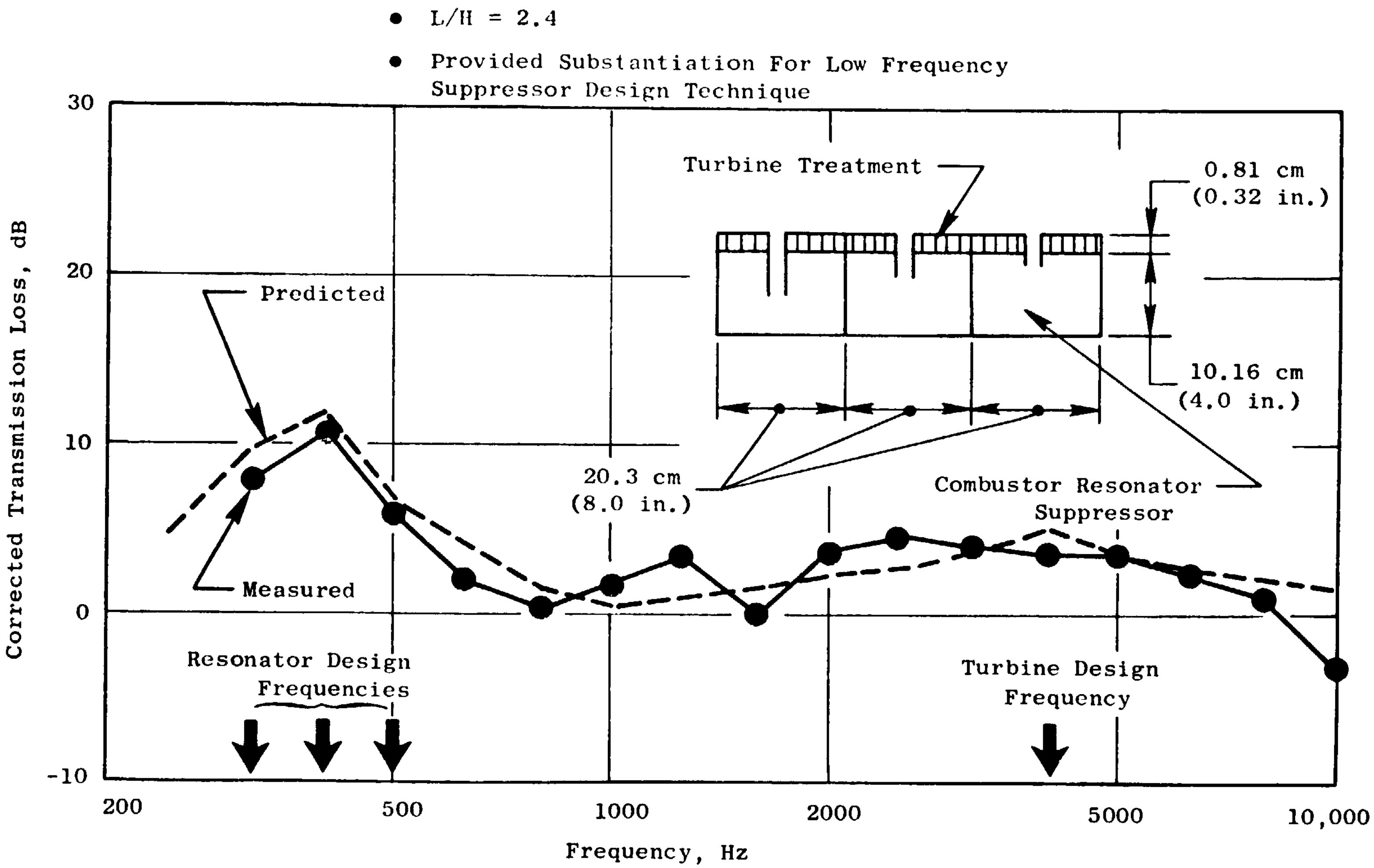

- L/H = 2.4
- Provided Substantiation For Low Frequency Suppressor Design Technique

Figure 3-22. Core Suppressor Cold Flow Duct Tests.

F101 CORE NOISE MEASUREMENT

- CORRELATED WITH ENGINE COMBUSTOR NOISE PREDICTIONS
- DATA ANALYSIS IN PROGRESS

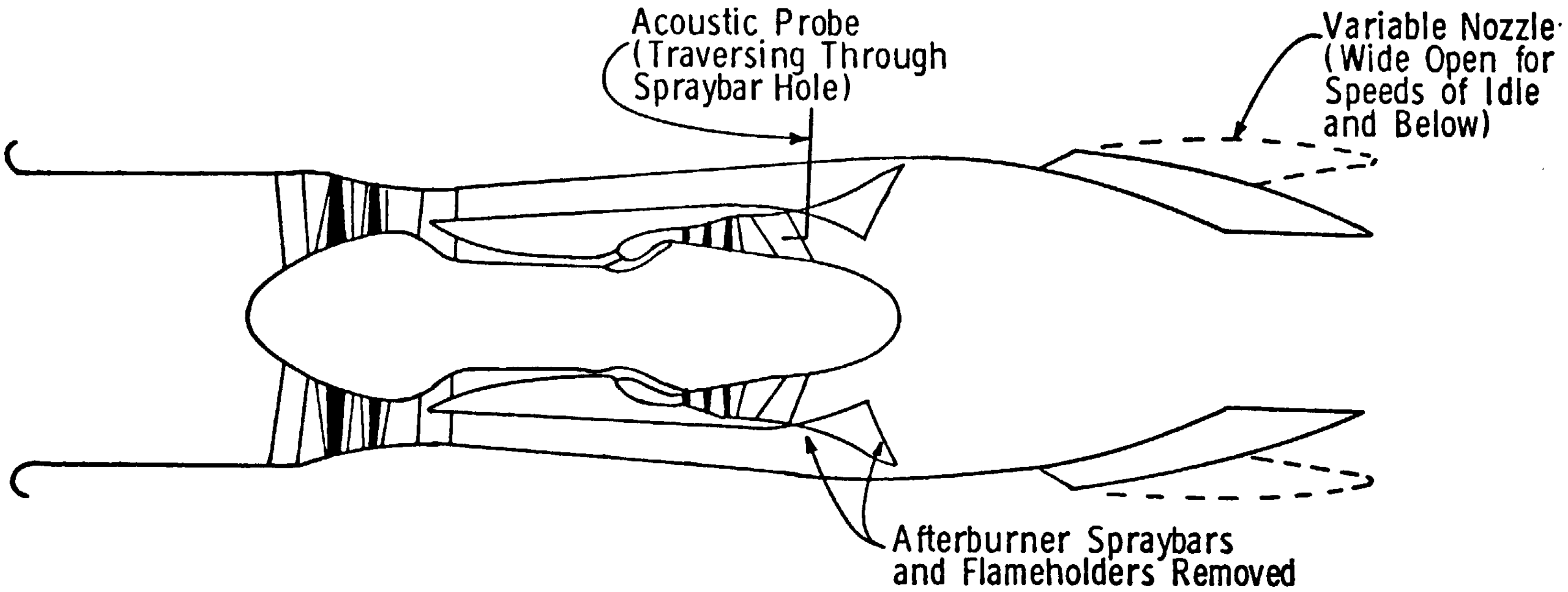
Acoustic Probe
(Traversing Through
Spraybar Hole)
Variable Nozzle
(Wide Open for
Speeds of Idle
and Below)
Afterburner Spraybars
and Flameholders Removed

Figure 3 -23. F101 Core Noise Measurement.

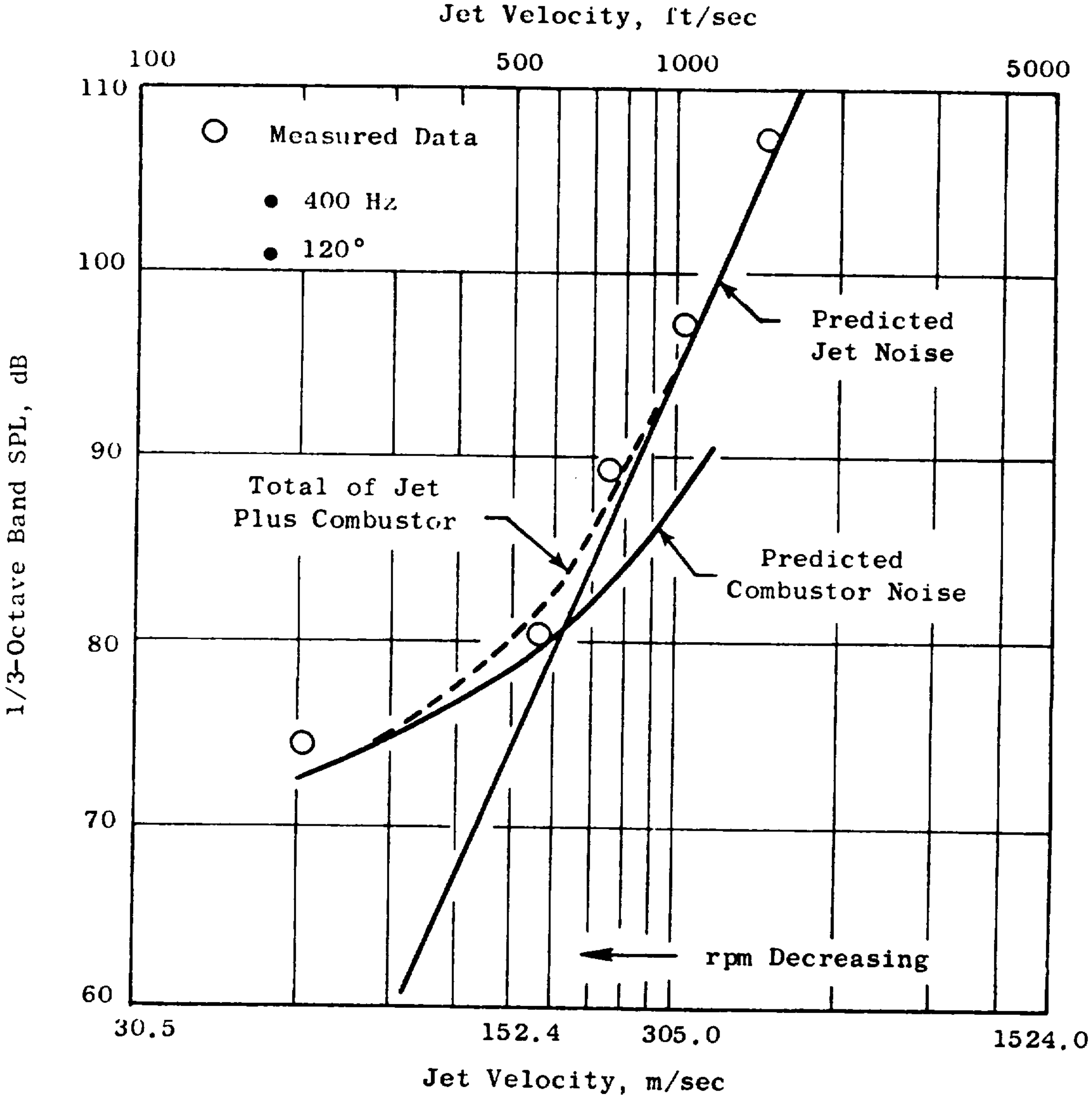

Figure 3-24. Farfield Core Noise Measurements Vs. Predictions.

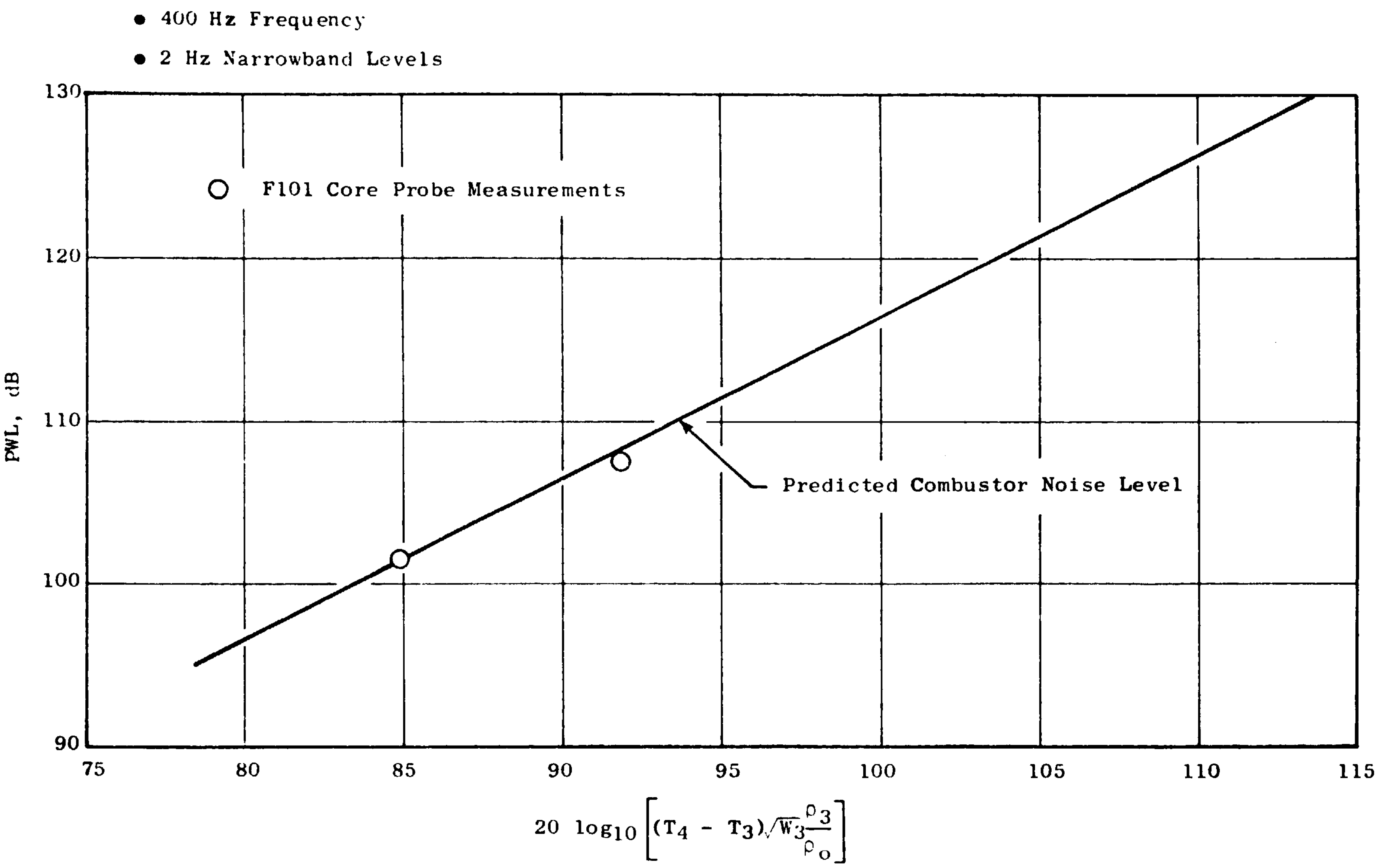

Figure 3-25. Probe Measured Vs. Predicted Combustor Noise.

Based on these data it was concluded the predicted levels were acceptable.

3.6 SYSTEM NOISE LEVELS

The primary constituents in the acoustic design are:

- Fan inlet noise
- Fan exhaust noise
- Core noise

Each has a significant development program defined to arrive at the design objectives. The levels for these three noise sources involve both unsuppressed noise estimates and suppression estimates. If either or both are different than the current evaluation this will have an impact on the system EPNdB.

Figure 3-26 is a carpet plot showing variations in the suppression level for fan inlet and fan exhaust noise. The variation in suppression shown in the figure can also be interpreted as a variation in the unsuppressed levels with constant suppression. The UTW design can tolerate small increases in both source estimates and still meet the goal. For example, using Figure 3-26 with current core suppression estimates, the engine noise goal of 95 EPNdB can be achieved even if the inlet level were increased 3 PNdB and the exhaust 2 PNdB.

Figure 3-27 shows the footprint or contour plot for the UTW aircraft/propulsion system. The approach footprint is slightly larger than takeoff due to the larger noise directly under the aircraft with the flaps extended. On a sideline basis, the takeoff noise is louder. The total 90 EPNdB footprint area is only 20.195 km^2 (499 acres).

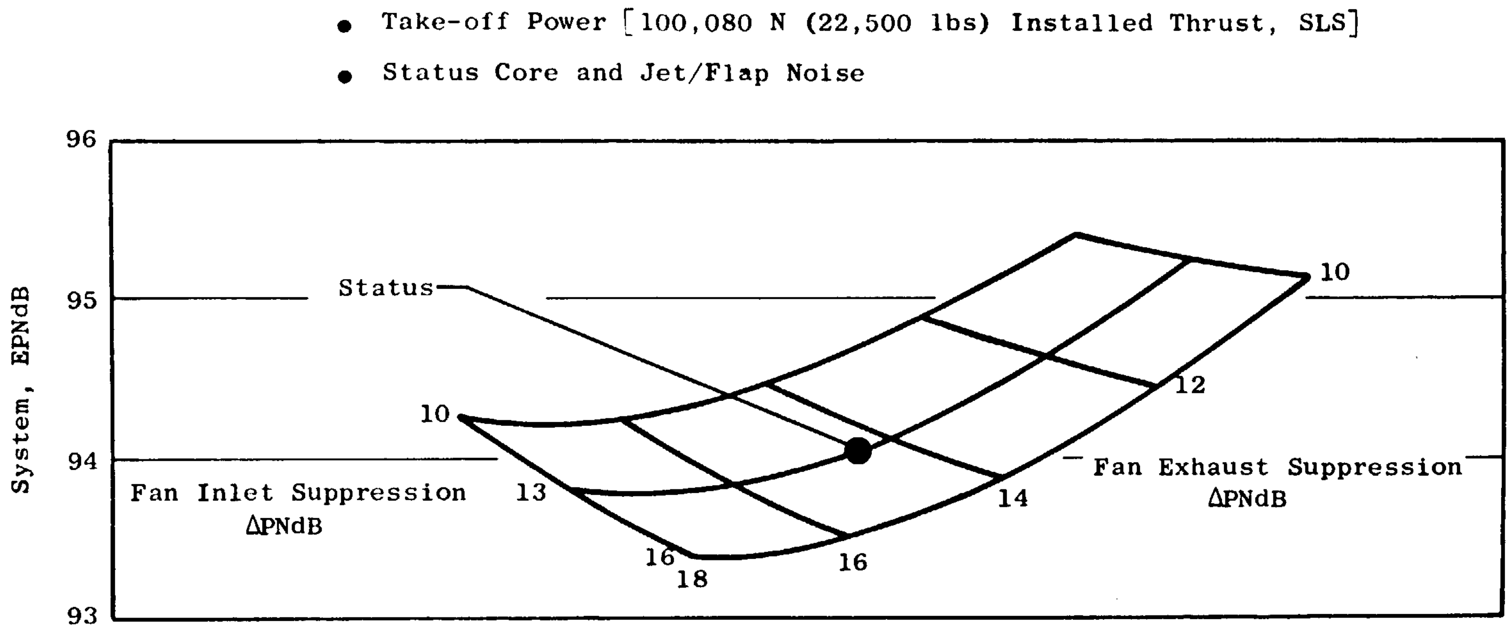

Figure 3-26. Effect of Constituent Suppression on UTW System Noise.

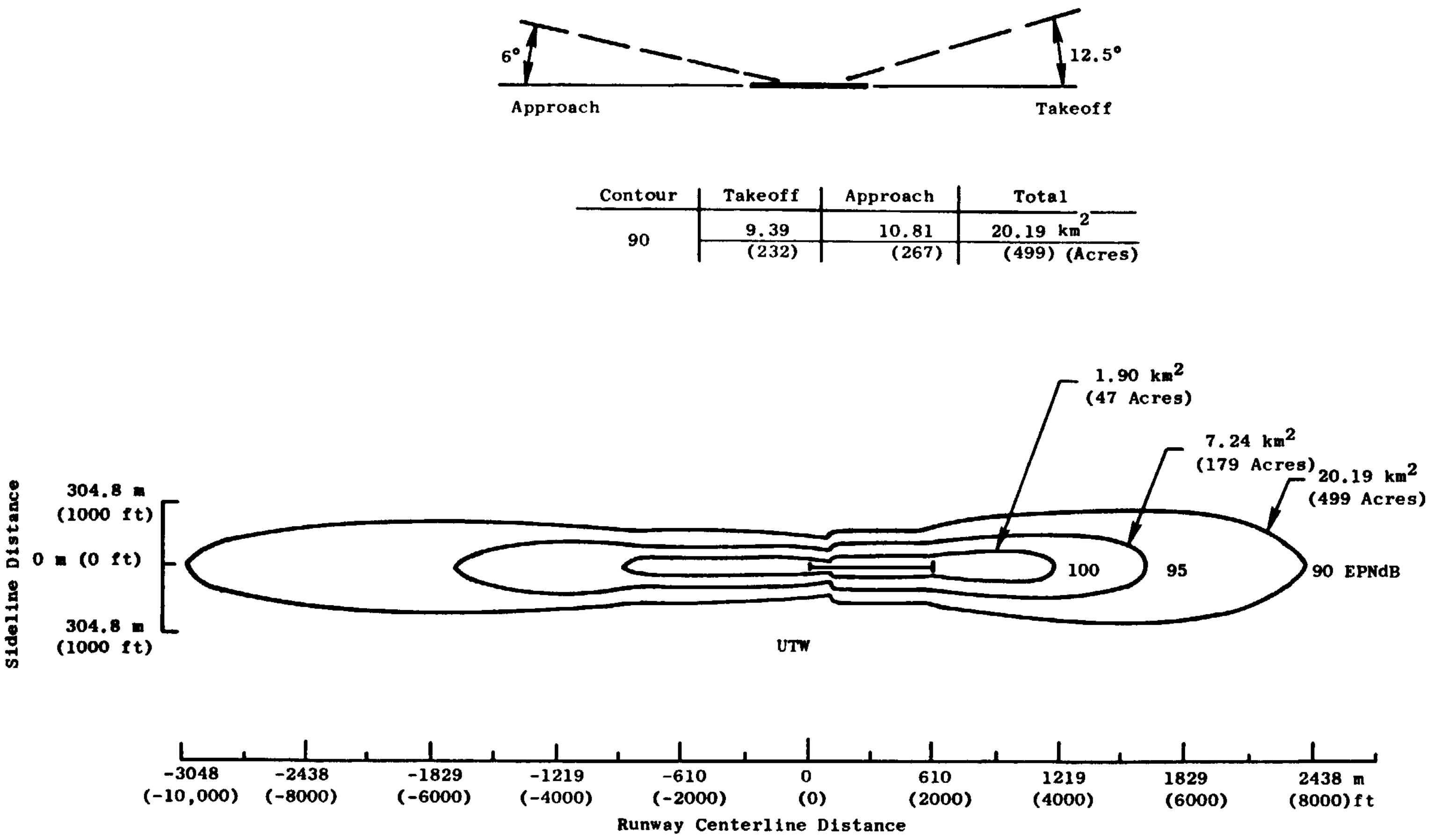

Contour	Takeoff	Approach	Total
90	9.39 (232)	10.81 (267)	20.19 km^2 (499) (Acres)

Figure 3-27. UTW Approach and Takeoff EPNdB Contours.

SECTION 4.0

EMISSIONS CONTROL

4.1 SUMMARY

The objective of the UTW combustor design program was to select a clean combustion system for the UTW engine based on available components and combustion technology being developed under another concurrent component development and technology program.

The F101 PFRT combustor originally selected for the UTW engine is an advanced combustor design that has demonstrated excellent performance characteristics and favorable pollutant emissions characteristics in development tests of the F101 and CFM56 engines. A consideration in the original selection of the PFRT configuration was the determination that design and development schedules and hardware availability of the F101 PV combustor were incompatible with the current UTW engine development program. Subsequent to the decision to use the F101 PFRT combustor design in the UTW engine, a detailed full annular component test of the PFRT combustor was conducted at QCSEE UTW engine operating conditions. Results of this component test revealed that, at the UTW sea level take-off condition, its smoke levels were higher than predicted levels and that visible smoke emissions would probably exist in the separated-flow UTW engine at high power operating conditions. These high smoke levels resulted from a greater than expected sensitivity to combustor fuel-air ratio. The combustor fuel-air ratios at the high power operating conditions of the UTW engine are considerably higher than those at F101 engine operating conditions.

Meanwhile, excellent progress has been made, as a part of CFM56 engine development efforts, in the design and development of a version of the F101 PV combustor design with excellent performance characteristics and generally more favorable pollutant emissions characteristics than those of the F101 PFRT combustor design. Based on this progress and the more rapid availability of PV combustor hardware than was anticipated, a modified version of the F101 PV combustor was recently selected for use in the UTW engine development program.

Prediction of C_xH_y, CO, NO_x, and smoke emission levels have been prepared for the UTW engine based on recent test data from combustor component evaluations of the F101 PV combustor configuration selected for use in the UTW engine. These estimates indicate the UTW engine will meet the 1979 standards for smoke and NO_x emissions. Because of the relatively low cycle pressure ratio of the UTW engine, however, its predicted C_xH_y and CO emissions levels will still exceed the applicable standards for these emissions. Thus, methods of reducing the levels of these two emissions categories are currently being investigated. Several approaches for obtaining these reductions in the UTW engine have been identified based on the results of emissions control technology development programs currently underway at General Electric, including the NASA Experimental Clean Combustor Program. These approaches involve modifications of the operating conditions within the combustor at engine idle power, since virtually all of the C_xH_y and CO emissions are produced at this engine operating mode. These approaches are:

- Compressor discharge bleed air extraction at idle
- Circumferential sector fuel staging at idle
- Flat pitching the fan at idle, permitting higher core engine speeds to achieve higher combustor inlet temperatures and pressures.

All of these operational approaches appear to be suitable for use in the UTW engine without compromising any other combustor performance requirements. Suitable combinations of these approaches are expected to provide significant reductions in CO-C_xH_y emission levels. However, the resulting CO-C_xH_y emission levels are still expected to exceed the program goal for these emission categories.

Development tests of the F101 PFRT combustor conducted at the QCSEE UTW operating conditions have demonstrated that both circumferential sector fuel staging and compressor discharge bleed air extraction do result in significant reductions in CO and C_xH_y at idle. Based on these test results, the QCSEE UTW engine will use sector fuel staging at idle since this approach was found to provide greater CO and C_xH_y reductions.

Although the PV combustor will be used in the UTW engine tests, additional work is under consideration which would involve applying advanced emission reduction technology from the NASA-GE Clean Combustor program to develop a new Double-Annular Dome Combustor for QCSEE. This combustor development will be conducted in a sector test rig and will concentrate on reducing idle emmissions to meet the program goals. This technology can then be applied to a new annular combustor design for the QCSEE UTW engine which would be expected to more nearly approach the program goals.

4.2 EXHAUST EMISSIONS DESIGN GOALS

The target maximum emissions levels to be demonstrated with the UTW engine are the Environmental Protection Agency (EPA) defined emissions standards, which become effective January 1, 1979, for Class T2 aircraft turbine engines. Engines in this EPA-defined category are all engines with a rated thrust of 35,580 N (8,000 lb) or greater. These standards set maximum limits on the quantities of C_xH_y, CO, NO_x, and smoke emissions that can be discharged by engines.

The Class T2 engine standards in the three categories of gaseous emissions are shown in Table 4-I. The standards are defined in terms of pounds of emission per 1000 pound thrust hours for a prescribed takeoff-landing

Table 4-I. EPA Gaseous Emissions Standards for Class T2 Engines.

Gaseous Emissions (C_x, CO, and NO_x)	
● Earliest effective date - January 1, 1979	
● Firm standards for engines newly manufactured on or after 1-1-79 (Pounds per 1000 pound thrust - hours per cycle)	
C_xH_y	0.8
CO	4.3
NO_x	3.0

Table 4-II. EPA Gaseous Emissions Standards - Turbojets and Turbofans.

- Prescribed cycle for Class T2 engines:

Mode	% Power	Time (Minutes)
Taxi-Idle	Ground Idle	19.0
Takeoff	100	0.7
Climbout	85	2.2
Approach	30	4.0
Taxi-Idle	Ground Idle	7.0

mission cycle. This prescribed cycle is shown in Table 4-II. The intent of these standards is to limit the quantities of these exhaust constituents that can be discharged within and around airports.

The smoke standards are expressed in terms of the SAE ARP 1179 Smoke Number. The maximum allowable smoke number is dependent on rated engine thrust, as shown in Figure 4-1. For the UTW engine, the smoke number standard is 25. Also shown in Figure 4-1 are the standards for some other General Electric commercial transport aircraft engines.

4.3 SELECTED COMBUSTOR DESIGN

Based on the results of the F101 PFRT/QCSEE UTW component development tests, which indicated that visible smoke emissions would probably exist for this separated exhaust flow engine, the PFRT combustor was considered unacceptable for the UTW engine application. Currently, development efforts are underway, as part of other engine programs to develop further an improved F101 PV combustor configuration. A version of this PV combustor design was selected for use in the UTW engine. A cross section of this selected combustor is shown in Figure 4-2. This UTW engine combustor selection was based on smoke and emissions test data obtained in component and engine tests with this combustor design. These tests showed that the PV configuration provided generally better performance than that of the PFRT configuration, particularly, much lower smoke emission levels. Based on these findings and the rapid availability of hardware through rework and modification of existing PFRT combustors, this change was found to be an effective one, especially since the PV combustor design is aerodynamically and functionally quite similar to the PFRT combustor design. Therefore, the overall performance characteristics of the two combustors are expected to be quite similar. Also, their size and overall geometry are the same.

The F101 PV combustor is an advanced, short-length configuration which features the use of a unique airblast-type fuel introduction and atomization design approach. The main features of this central fuel injection combustor dome design are illustrated in Figure 4-3. In the PV combustor design, the dome is comprised of 20 carbureting swirl cups. Fuel is supplied to each of these swirl cups at low pressure by means of a simple, multiported fuel injector. The carbureting swirl cups have two stages through which air is introduced, as is shown in Figure 4-3. In the first stage (primary), air is introduced through uniformly spaced airblast injection ports, the exits of which are located near the introduction points of the low pressure fuel injection ports. Thus, fuel is introduced downstream of the flow areas that meter airflow into the primary combustion zone (dome) of the combustor. The airblast jets impinge tangentially on the fuel as it is ejected from individual ports transporting it to the swirl cup venturi, where centrifugal forces of the rotating primary airstream produce a thin uniform rotating fuel film at the trailing edge of the venturi. To assist in mixing between the primary airblast jets and the low pressure fuel jets, a small amount of air is introduced through the fuel injector shroud. A portion of this latter high energy air exits coaxially with the fuel, thus energizing the

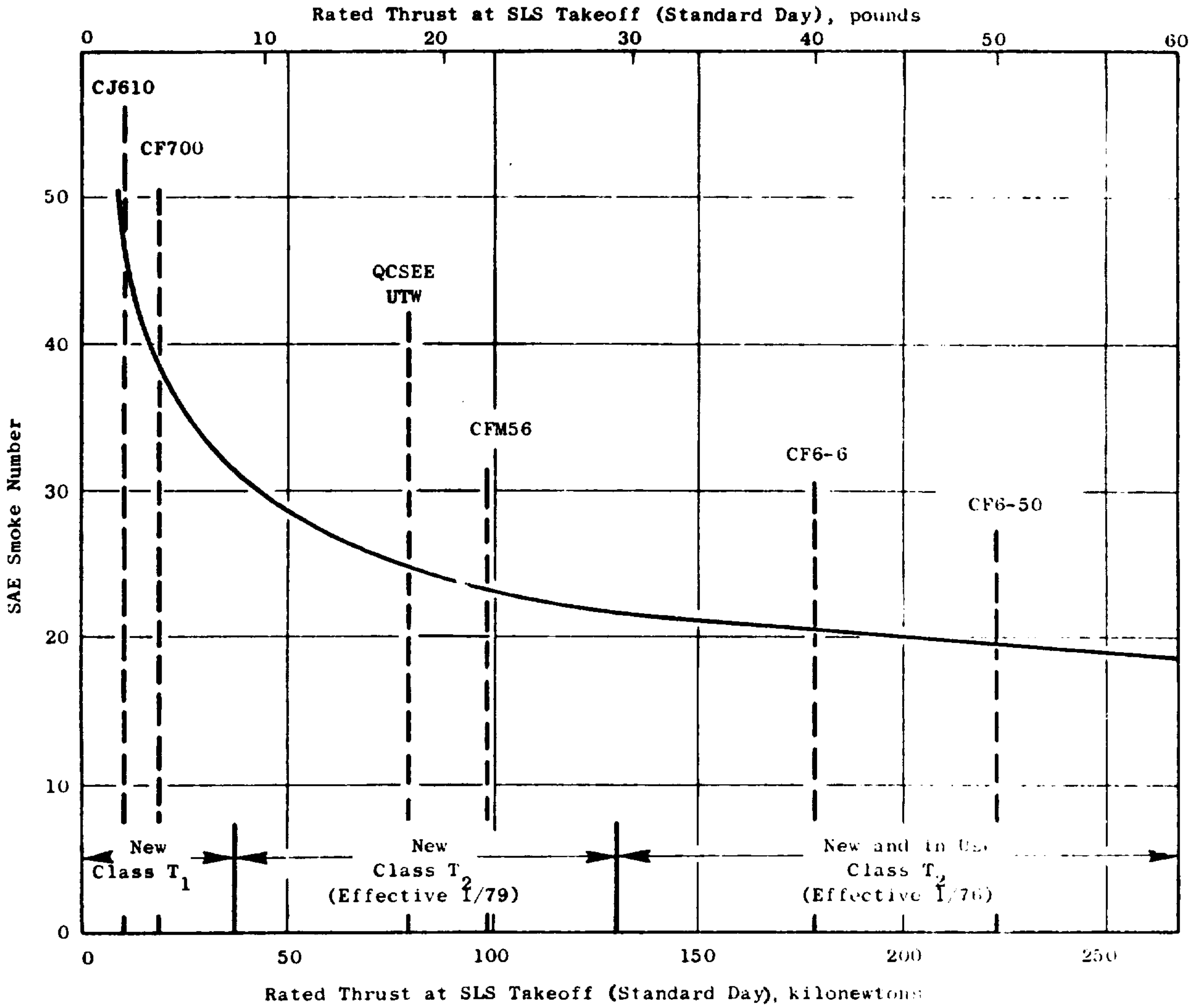

Figure 4-1. EPA Smoke Emission Standards.

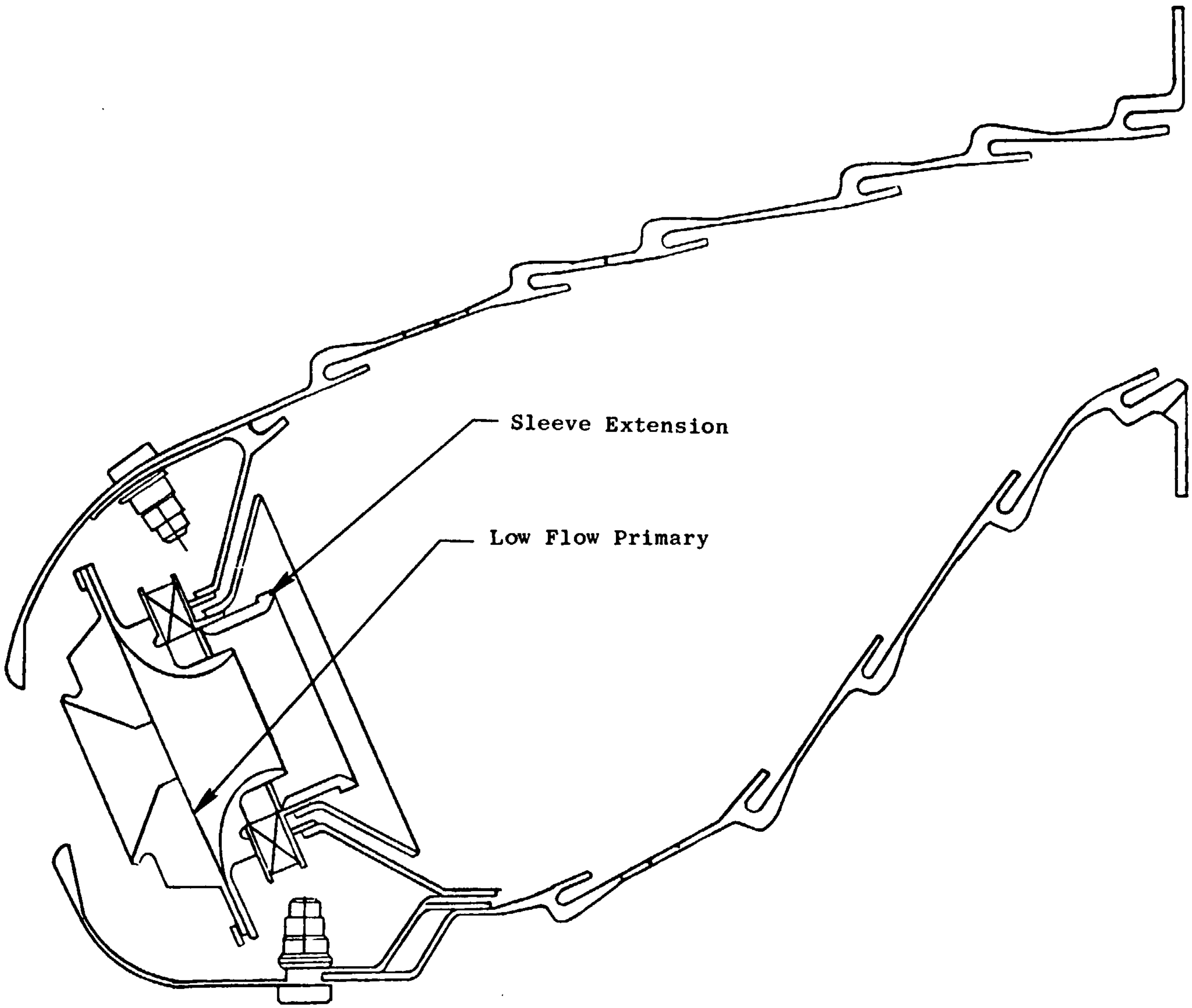
Sleeve Extension
Low Flow Primary

Figure 4-2. F101 PV Combustor.

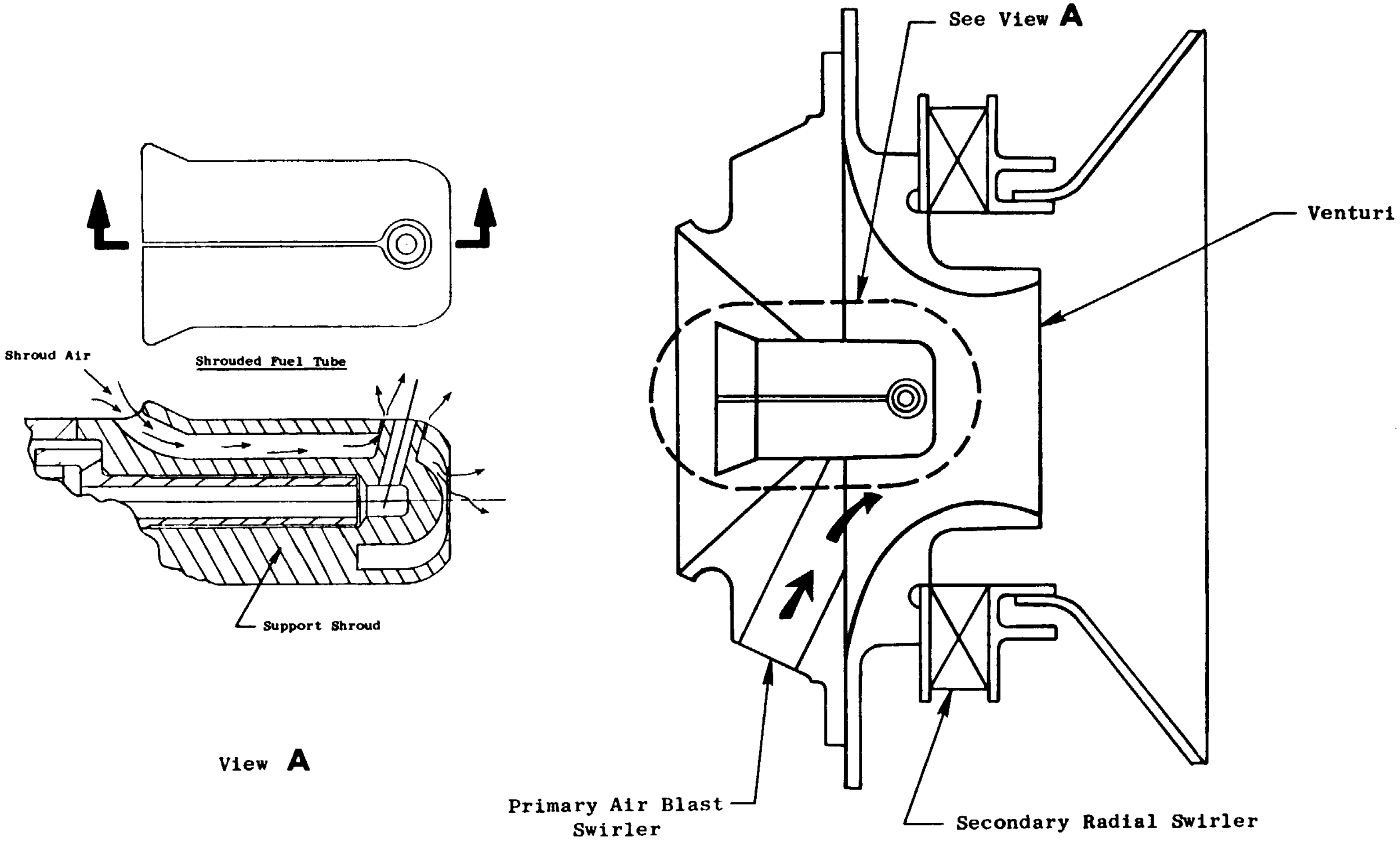
Shroud Air
Shrouded Fuel Tube
Support Shroud
View A
See View A
Venturi
Primary Air Blast Swirler
Secondary Radial Swirler

Figure 4-3. F101 PV Air Blast Carburetor and Low Pressure Fuel Injector.

fuel in a radial direction to provide the desired mixing between the fuel and primary air stream. In addition to the shroud air surrounding the fuel jets, a small portion of the shroud air sweeps the tip of the fuel injector. Both air films serve the additional function of preventing fuel wetting of the injector surfaces, thus preventing any potential carbon buildup which might deteriorate the injector performance.

The secondary air swirler introduces air which rotates in a direction opposite to that of air and fuel mixture exiting from the primary swirler. Fuel leaving the downstream edge of the primary cup venturi enters the shear region created by the mixing boundaries of the counter-rotation flows and the high aerodynamic shear stress imposed on the fuel produces very fine atomization and highly effective fuel-air mixing over wide ranges of combustor operating conditions. With these atomization and mixing capabilities, very short-length combustor designs are possible.

The uniform and symmetric introduction of fuel and air in this design, as opposed to that obtained in the PFRT design which has unsymmetric single-source fuel introduction, produces improved atomization and more uniform fuel and air mixtures in the dome which, in turn, result in its low smoke emissions characteristics.

A feature recently introduced into the PV combustor design is a sleeve in the secondary swirler passage and a low flow primary swirler, as shown in Figure 4-2. The addition of this sleeve results in significant reductions in CO and C_xH_y emissions levels at idle conditions (based on CFM56 combustor component and engine tests) while maintaining the low smoke characteristics already demonstrated in engine and component tests of the original F101 PV design. The basic function of the sleeve is to enhance mixing of the primary and secondary streams at the shear region, and to prevent fuel from coalescing on the dome surfaces and later becoming entrapped in the combustor liner cooling films, which would allow the fuel to escape as unreacted fuel. Reductions in CO and C_xH_y demonstrated with this improved PV design are shown in Figure 4-4.

A test was conducted to evaluate the performance of this modified PV combustor at simulated UTW operating conditions. Of primary interest were the combustor exit circumferential temperature characteristics and ground start ignition. The measured exit temperature profile is compared in Figure 4-5 with the F101 objective levels. As shown in the figure, the measured pattern factor for this combustor is higher than the objective level. Analyses show, however, that since the combustor inlet temperatures of the UTW engine at takeoff conditions are considerably lower than those of the F101 engine, the resulting lower turbine nozzle cooling air temperatures result in adequate temperature margin (approximately 367 K/200° F) for the turbine nozzle vanes at the higher pattern factor.

Ignition data were obtained at conditions simulating a range of engine motoring speeds to determine the light-off characteristics of the selected combustor design. Results of this test shown in Table 4-III indicate that satisfactory ground start ignition will be obtained at core engine motoring speeds exceeding 2700 rpm at standard day conditions.

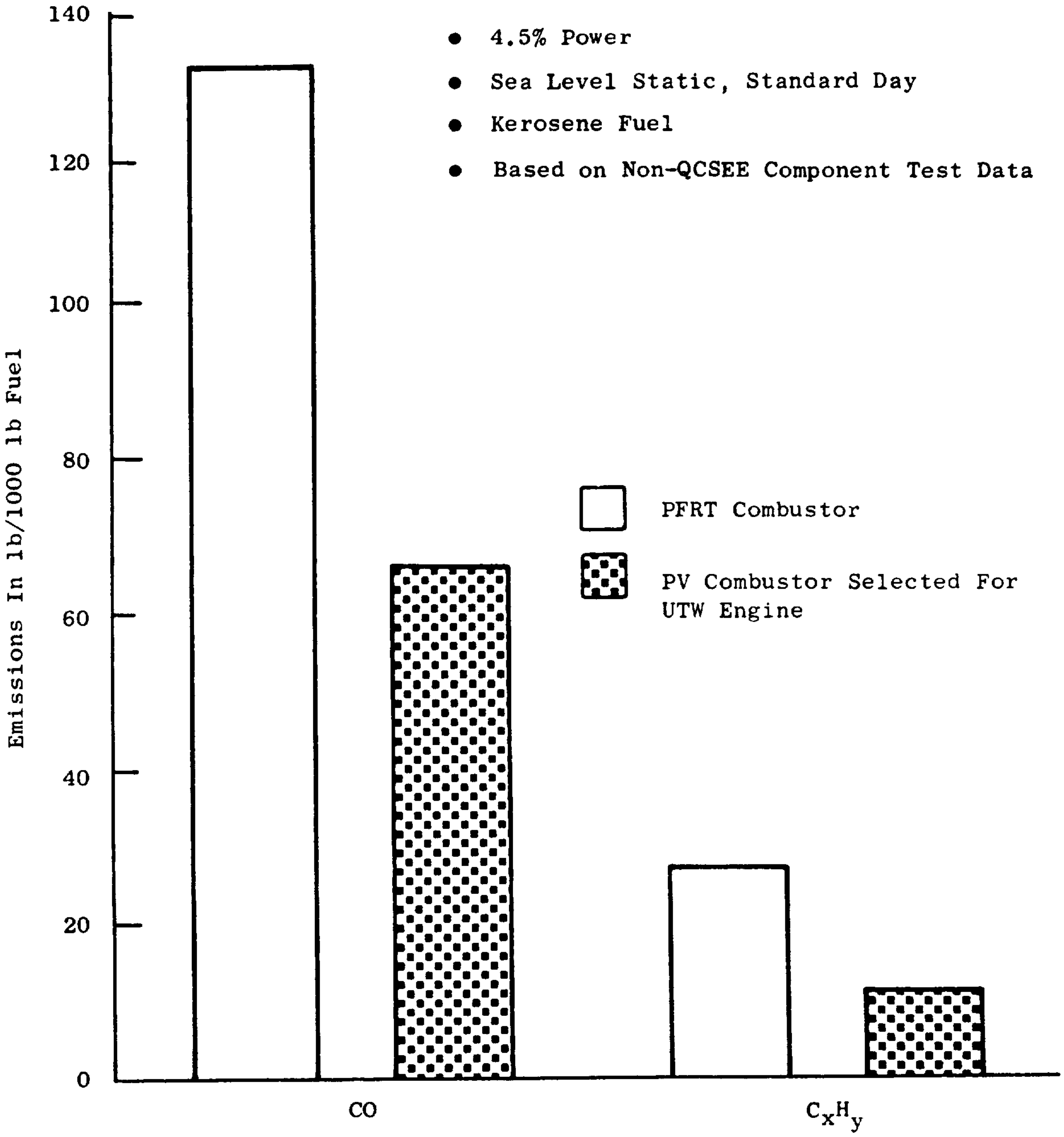

Figure 4-4. Comparison of CO and C_xH_y Emissions of the PFRT Combustor and Selected F101 PV Combustor at UTW Ground Idle Conditions.

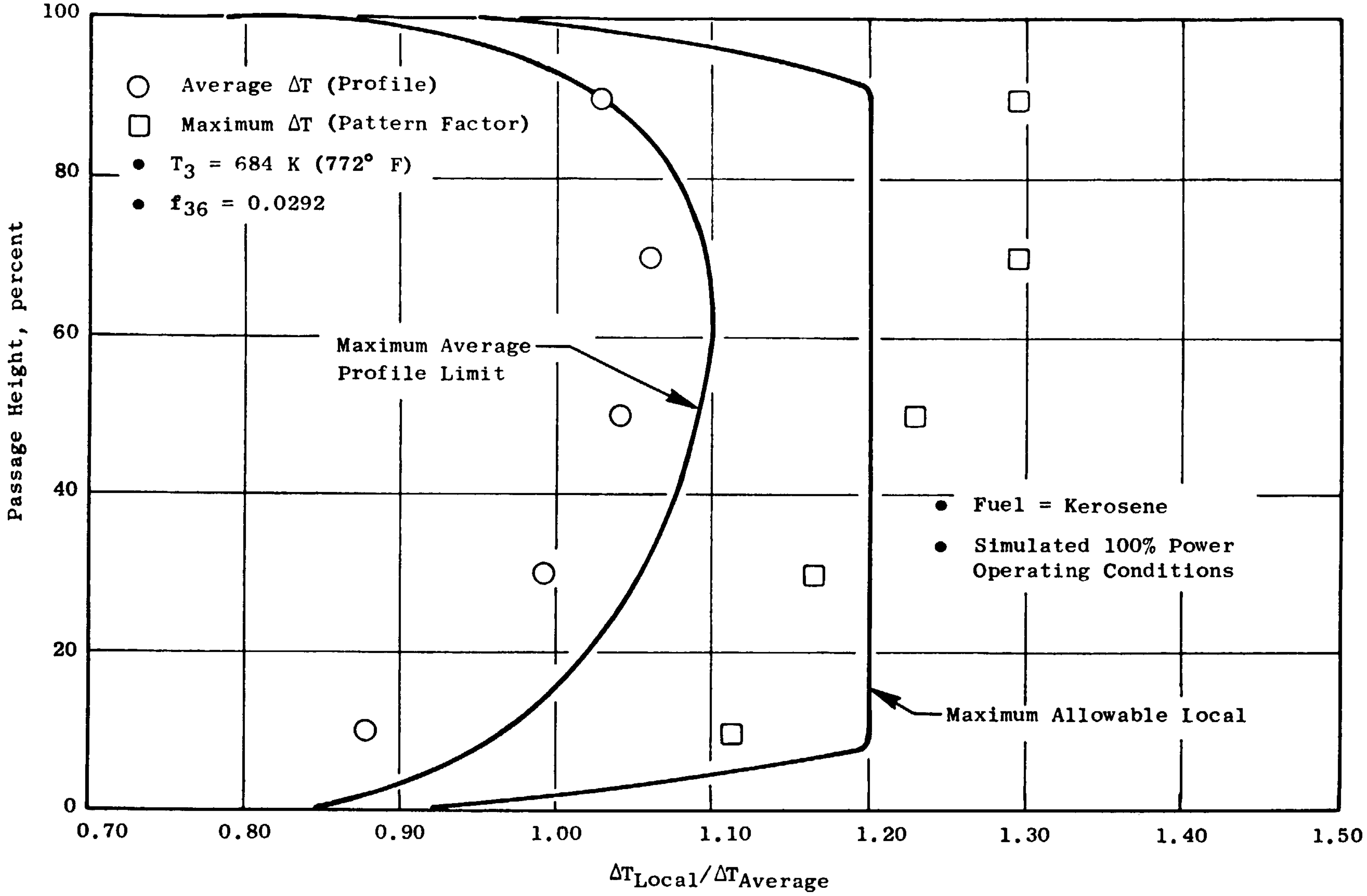

Figure 4-5. Exit Temperature Characteristics of QCSEE UTW Engine Equipped with Modified PV Combustor.

Table 4-III. Ignition Test Results.

Core Engine Motoring Speed rpm	Measured Ignition Fuel/Air Ratio	Core Engine Fuel/Air Ratio (Based on 300 pph minimum fuel flow)
2500	0.034	0.030
3000	0.0210	0.024
3500	0.015	0.0220
4000	0.015	0.0220

Based on test results and related analysis, the modified PV combustor has been judged satisfactory for UTW engine application.

4.4 PREDICTED UTW ENGINE EMISSIONS CHARACTERISTICS WITH SELECTED VERSION OF F101 PV COMBUSTOR

4.4.1 Smoke Emissions

Estimates of the smoke emissions levels of the UTW engine have been made based on data obtained in recent component and engine tests of a similar PV combustor. As shown in Figure 4-6 the UTW engine when equipped with the PV combustor is predicted to have a peak smoke emission level which satisfies the applicable EPA standard with margin. The smoke emission levels of other General Electric commercial aircraft engines are also shown for comparison.

4.4.2 Gaseous Emissions

Estimates of gaseous emissions characteristics of the UTW engine have also been made with the use of test data from component tests of the selected PV combustor. Results of the tests of this new combustor showed significant reductions in CO and C_xH_y emissions levels at idle conditions. Combustor operating conditions in the UTW engine are different from those simulated in the component test because of engine cycle pressure ratio differences. The measured component test emissions indices were therefore adjusted to the combustor operating conditions of the UTW engine at various engine operating modes of interest. Basically, these adjustments involve use of corrections, developed at General Electric, of the emissions indices for the effects of combustor inlet air temperature and pressure. When estimating emissions for the UTW engine, variable-pitch fan capability of the UTW engine may result in different core engine operating conditions depending on the particular fan pitch setting selected. Thus, combustor inlet conditions may vary for

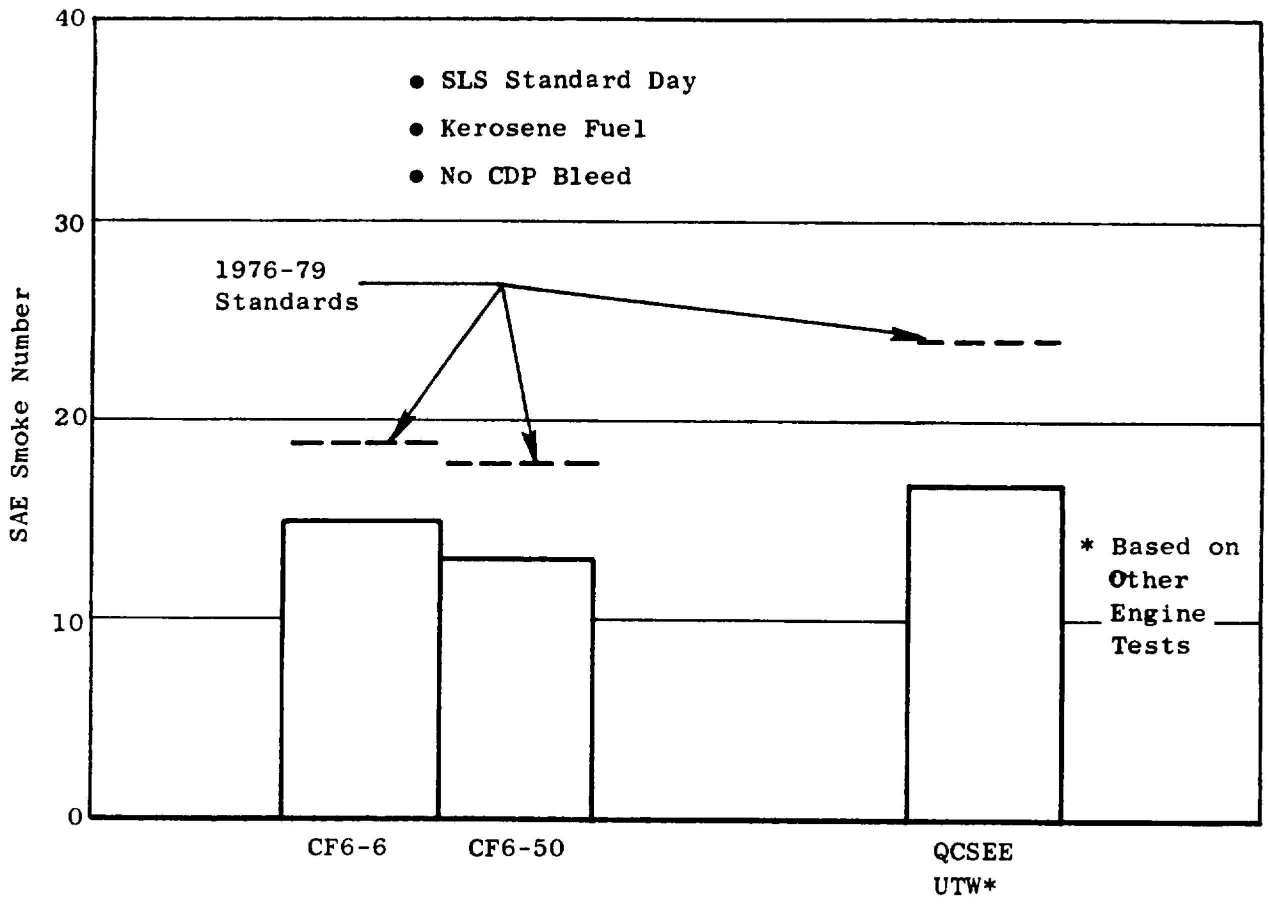

Figure 4-6. Peak Smoke Emission Characteristics of GE-AEG Class T2 Engines.

the same thrust conditions depending on the combination of fan and core thrust selected. The resulting emissions estimates for two such operating modes are shown in Figure 4-7.

Using estimated emissions indices for the UTW engine, the emissions levels in terms of the EPA-defined parameter can be calculated. Copies of computer summary sheets showing these calculations for the UTW engine based on component test results are presented as Tables 4-IV and 4-V. Comparisons of these calculated emissions levels with EPA standards are presented in Table 4-VI for C_xH_y, CO, and NO_x emissions. As shown, the UTW engine is expected to meet the NO_x emission standard when operating with constant fan blade pitch angle. However, even with the improved CO and C_xH_y emissions provided by the PV combustor design, further reductions in the C_xH_y and CO emissions levels of the UTW engine are required to meet the EPA requirements.

Relative to other turbofan engine combustors, the emissions characteristics of this F101 PV combustor are generally quite favorable as is indicated by comparative emissions level data presented in Figures 4-8, 4-9, and 4-10. At the same combustor inlet air operating conditions, its C_xH_y and NO_x emissions levels are significantly lower than those of other modern combustors. However, in the UTW engine application, its CO and C_xH_y emissions levels in terms of the EPA takeoff-landing mission parameter cycle are well in excess of prescribed standards because of adverse combustor operating conditions that prevail at ground idle. These adverse operating conditions are associated with the comparatively low cycle pressure ratio of the UTW experimental engine. This low cycle pressure does, however, result in somewhat lower NO_x emissions levels than those of other modern combustors, as is shown in Figure 4-9.

The differences in combustor operating conditions (which are the primary cause of the differences in emissions levels) between a low pressure ratio engine like the UTW and a high pressure ratio engine are shown in Table 4-VII. The specific effects of combustor operating conditions (primarily inlet temperature and pressure) on the CO and C_xH_y emissions indices of the selected F101 PV combustor are shown in Figure 4-11. The higher C_xH_y and CO emissions indices associated with the UTW engine result in proportionately higher calculated mission cycle EPA parameters for this engine compared to those of the other engine. To meet the applicable CO and C_xH_y emissions standards, as defined by the EPA, emissions indices at idle of about 20 and 4 grams per kilogram of fuel, respectively, are required. These target emissions indices and the estimated UTW engine emissions indices are presented in the form of combustion efficiency values in Figure 4-12. As shown, an improvement of about 1.5 percent in combustion efficiency at idle is required to obtain the emissions indices necessary to meet the EPA goals.

4.5 PERTINENT EMISSIONS REDUCTIONS DESIGN TECHNOLOGY

The CO and C_xH_y emissions are, of course, products of inefficient combustion. As illustrated in Figure 4-7, these emissions are primarily produced at idle and other lower power operating conditions. The higher

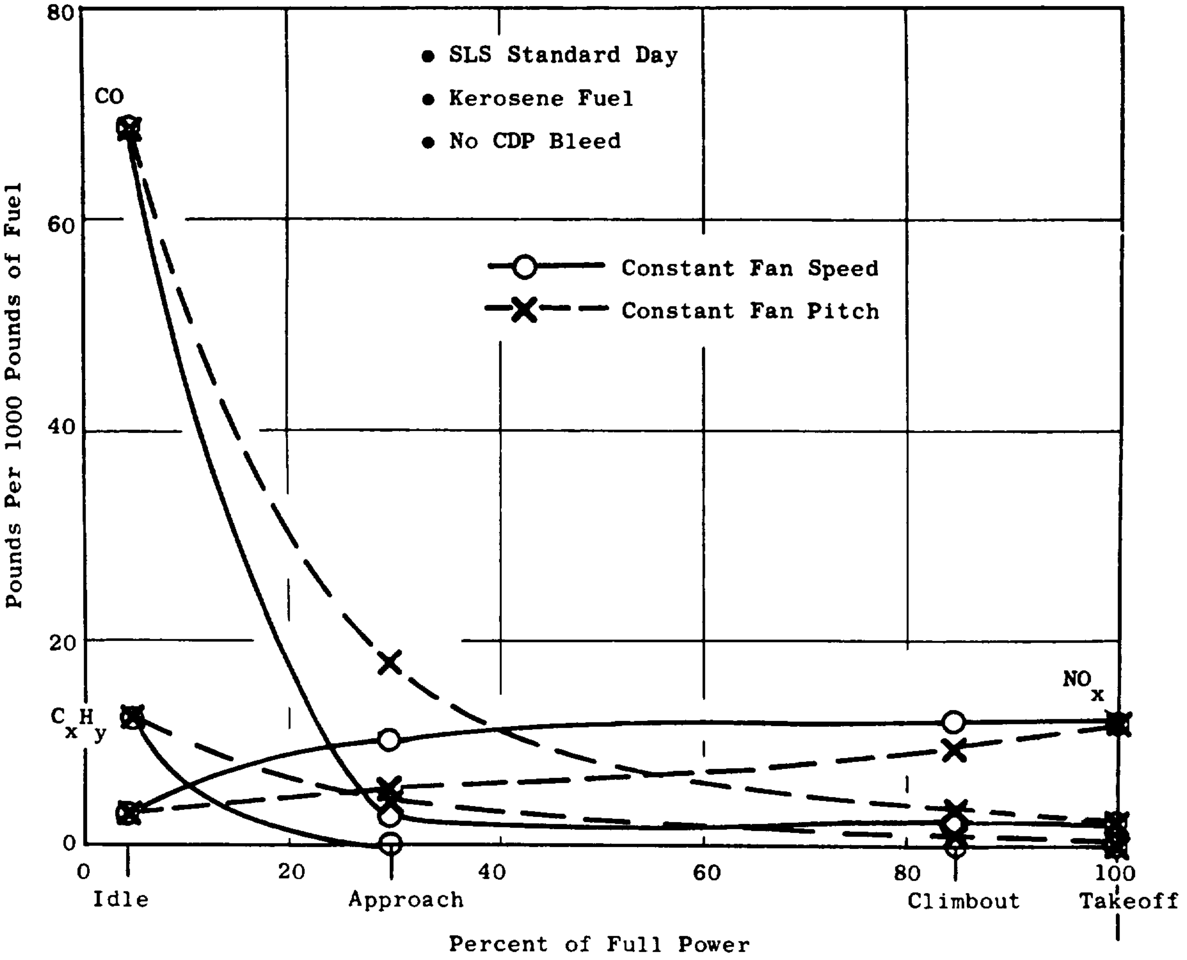

Figure 4-7. Estimated Gaseous Exhaust Characteristics of QCSEE UTW Engine Based on CFM56 Component Test Data.

Table 4-IV. Emissions Calculations Using Prescribed EPA Landing-Takeoff Cycle (Constant Fan Pitch).

Date: 2/11/76
Engine Performance Source: QCSEE UTW Constant Fan Pitch SLS/Standard Day
Emissions Data Source: Cell A3, Run 156 (Adj. to QCSEE Cycle Condition)
Fuel Type: JP-5
Engine Class: T_2

		EPA Cycle Condition		
	Idle	Approach	Climb	Takeoff
Engine Parameters				
Time, minutes	26.00	4.00	2.20	0.70
Percent Power	4.50	30.00	85.00	100.00
Thrust, lb	783	5221	14792	17402
Fuel Flow, pph	646	1612	4469	5582
SFC, pph/lb Thrust	0.8250	0.3088	0.3021	0.3208
Thrust-hours	339.30	348.05	542.36	203.02
Emissions Parameters				
Carbon Monoxide				
lb/1000 lb Fuel	65.000	17.000	4.000	2.500
lb/hour	41.990	27.404	17.876	13.955
lb	18.196	1.827	0.655	0.163
percent of total lb	87.308	8.766	3.145	0.781
Hydrocarbons				
lb/1000 lb Fuel	9.500	4.000	0.100	0.100
lb/hour	6.137	6.448	0.447	0.558
lb	2.659	0.430	0.016	0.007
percent of total lb	85.452	13.813	0.527	0.209
Oxides of Nitrogen				
lb/1000 lb Fuel	2.200	5.500	9.600	10.300
lb/hour	1.421	8.866	42.902	57.495
lb	0.616	0.591	1.573	0.671
percent of total lb	17.847	17.129	45.586	19.438

		EPA Parameter	
Summary		(lb Emission/1000 lb Thrust-hr-Cycle)	
	Calculated Level	1979 Standard	% Reduction Required
Carbon Monoxide	14.55	4.30	70.44
Hydrocarbons	2.17	0.80	63.17
Oxides of Nitrogen	2.41	3.00	0

Table 4-V. Emissions Calculations Using Prescribed EPA Landing-Takeoff Cycle (Constant Fan Speed).

Date: 2/11/76
Engine Performance Source: QCSEE UTW Constant Fan Speed SLS/Standard Day
Emissions Data Source: Cell A3, Run 156 (Adj. to QCSEE Cycle Condition)
Fuel Type: JP-5
Engine Class: T_2

		EPA Cycle Condition		
	Idle	Approach	Climb	Takeoff
Engine Parameters				
Time, minutes	26.00	4.00	2.20	0.70
Percent Power	4.50	30.00	85.00	100.00
Thrust, lb	783	5221	14792	17402
Fuel Flow, pph	646	3320	4777	5582
SFC, pph/lb Thrust	0.8250	0.6359	0.3230	0.3208
Thrust-hours	339.30	348.04	542.36	203.02
Emissions Parameters				
Carbon Monoxide				
lb/1000 lb Fuel	65.000	5.000	3.000	2.500
lb/hour	41.990	16.600	14.331	13.955
lb	18.196	1.107	0.525	0.163
percent of total lb	91.021	5.536	2.629	0.814
Hydrocarbons				
lb/1000 lb Fuel	9.500	0.100	0.100	0.100
lb/hour	6.137	0.332	0.478	0.558
lb	2.659	0.022	0.018	0.007
percent of total lb	98.294	0.818	0.647	0.241
Oxides of Nitrogen				
lb/1000 lb Fuel	2.200	8.300	9.600	10.300
lb/hour	1.421	27.556	45.859	57.495
lb	0.616	1.837	1.682	0.671
percent of total lb	12.816	38.231	34.993	13.959

Summary	EPA Parameter (1b Emission/1000 lb Thrust-hr-Cycle)		
	Calculated Level	1979 Standard	% Reduction Required
Carbon Monoxide	13.95	4.30	69.13
Hydrocarbons	1.89	0.80	57.64
Oxides of Nitrogen	3.35	3.00	10.55

Table 4-VI. Predicted QCSEE UTW Engine Emissions Characteristics.

- Based on non-QCSEE Component Test
- 4.5% Power at Idle
- No CDP Bleed

Emission		1979 Standard*	With Selected F101 PV Combustor	
			Constant Fan Pitch	Constant Fan Speed
C_xH_y	Pounds per 1000 Pound Thrust-Hours Per Cycle	0.8	2.2	1.9
CO		4.3	14.5	14.0
NO_x		3.0	2.4	3.3
Smoke (SAE SN)		25	18	18

*As numerically and dimensionally expressed by the EPA.

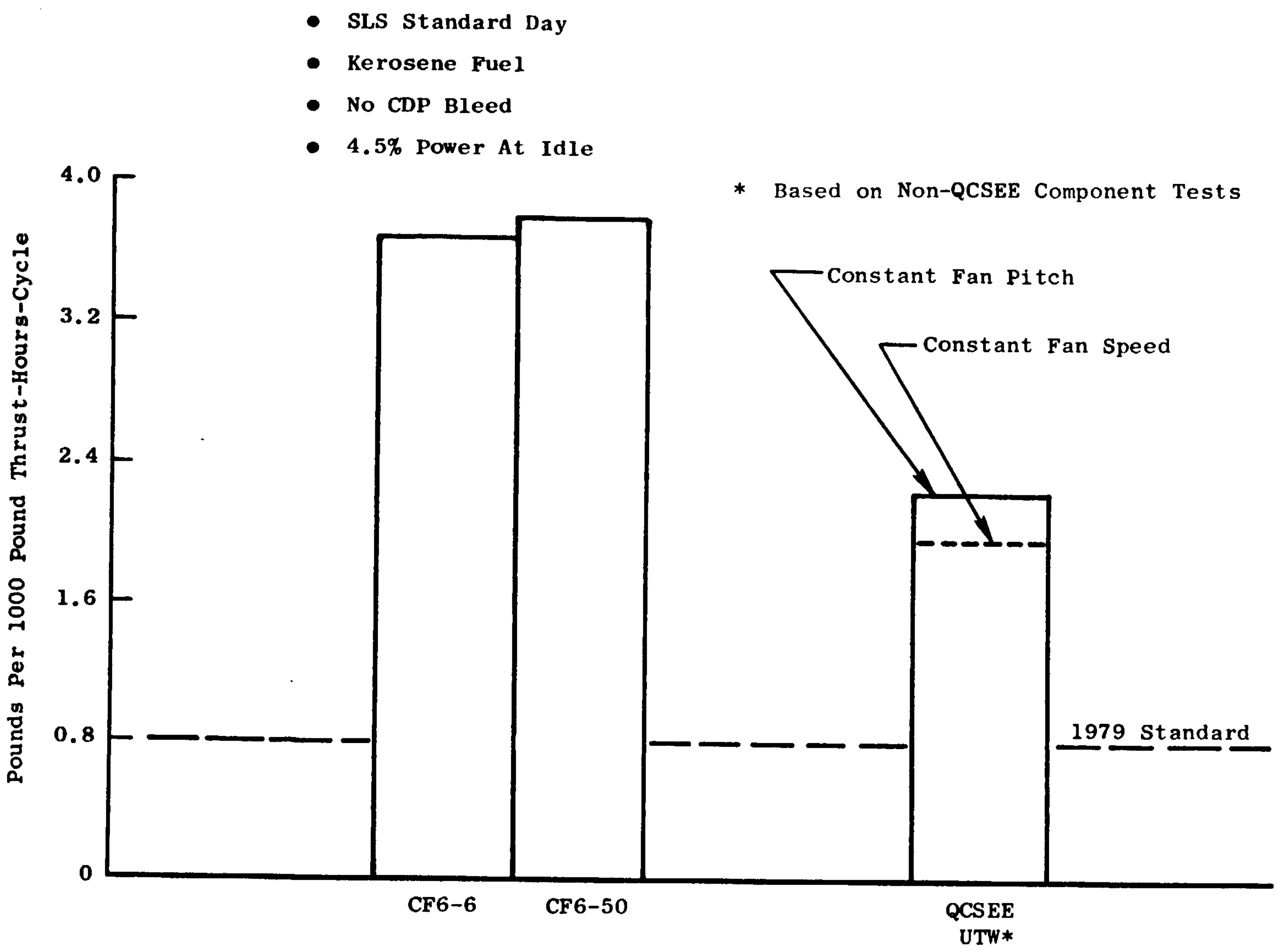

Figure 4-8. C_xH_y Emissions Characteristics of AEG Commercial Engines (Class T2).

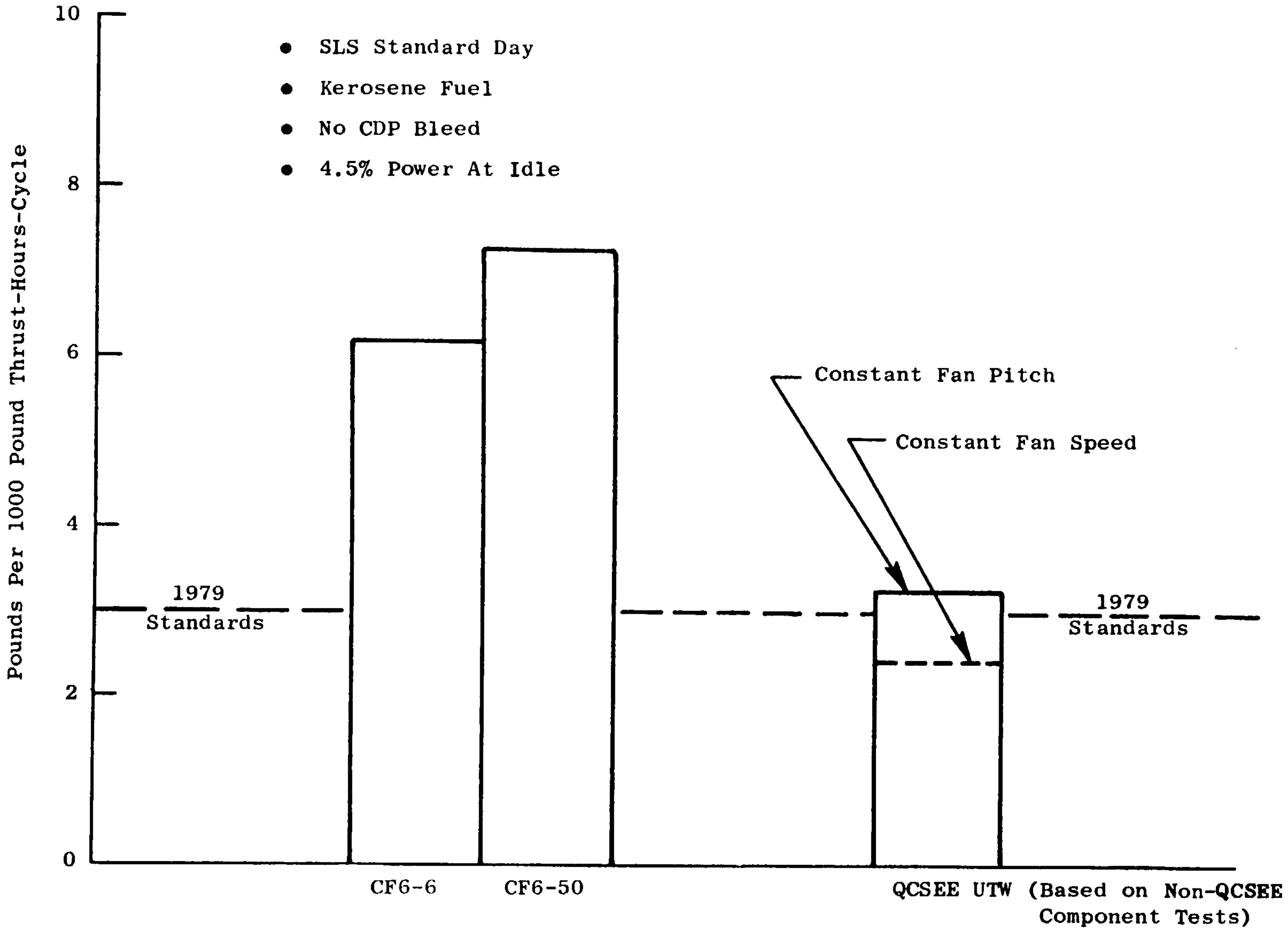

Figure 4-9. NO_x Emissions Characteristics of AEG Commercial Engines (Class T2).

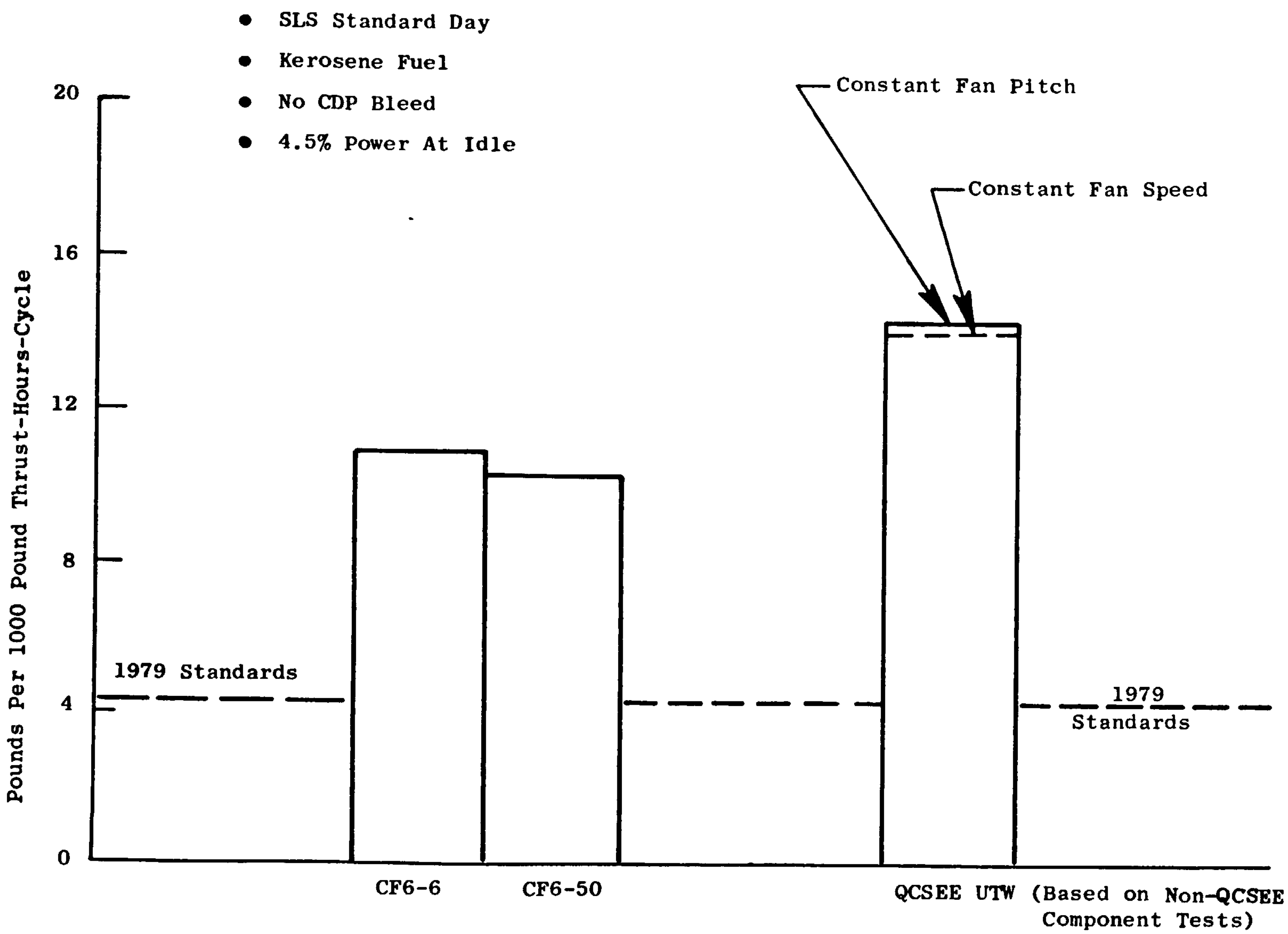

Figure 4-10. CO Emissions Characteristics of AEG Commercial Engines (Class T2).

Table 4-VII. Comparison of Operating Conditions of UTW and a Higher Pressure Ratio Engine at Ground Idle and Takeoff.

	UTW Engine	Higher Pressure Ratio Engine
• Standard Day Ground Idle		
Combustor airflow, kg/s (pps)	4.99 (11)	7.39 (16.3)
Combustor inlet air temperature, ° C (° F)	132.2 (270)	163.9 (327)
Combustor inlet air pressure, kN/m^2 (psia)	227.5 (33)	324.1 (47)
Combustor fuel-air ratio	0.0175	0.0160
• Standard Day Takeoff		
Combustor airflow, kg/s (pps)	24.2 (53.4)	40.6 (89.4)
Combustor inlet air temperature, ° C (° F)	410.6 (771)	509.4 (949)
Combustor inlet air pressure, kN/m^2 (psia)	1434 (208)	2455 (356)
Combustor fuel-air ratio	0.0294	0.0234

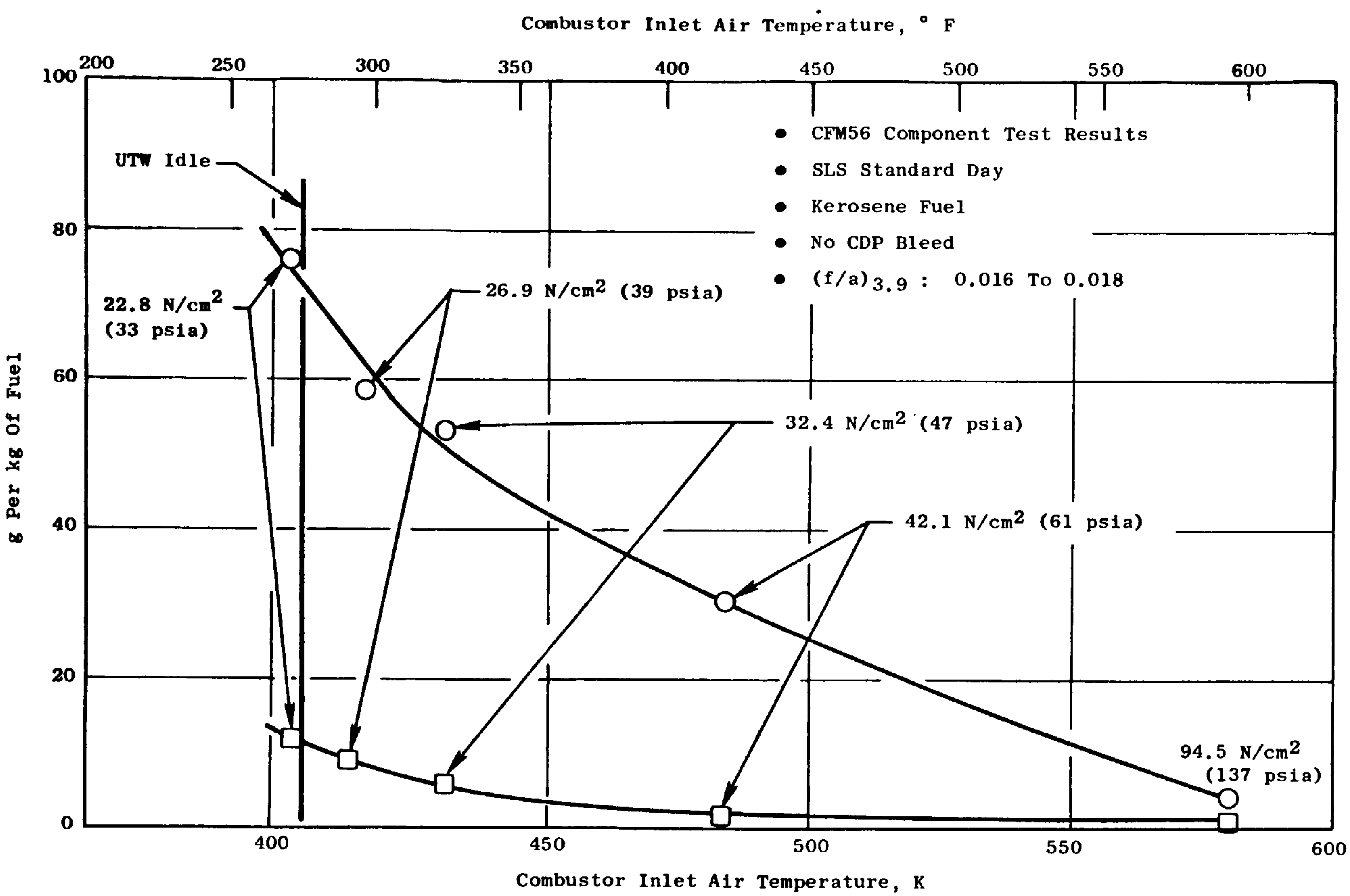

Figure 4-11. CO and C_xH_y Emissions Characteristics of Selected F101 PV Engine Combustor.

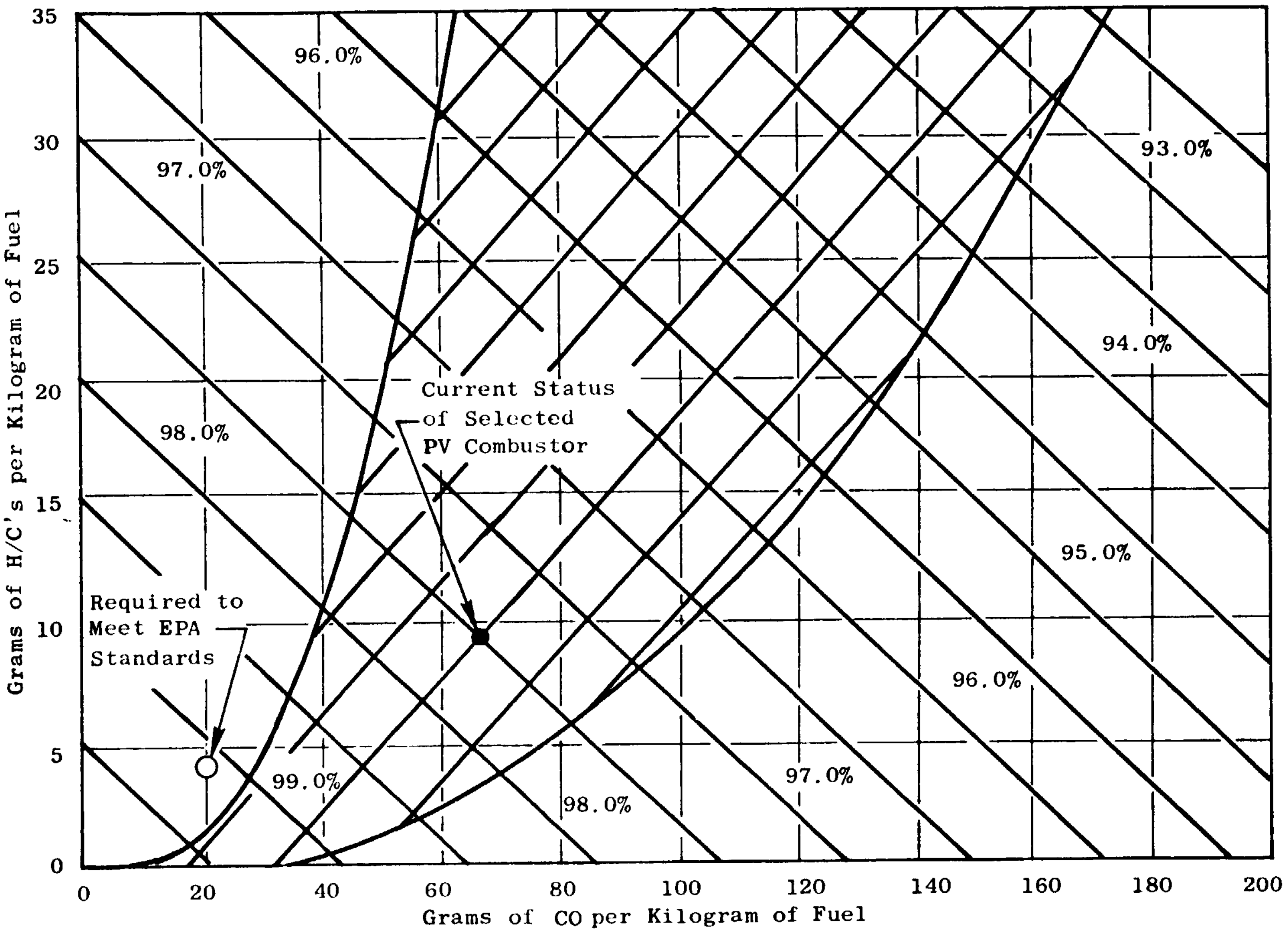

Figure 4-12. Relationships Between CO and H/C's Emissions and Combustion Efficiency.

emissions at these operating conditions generally occur because the combustion efficiencies of most present day engines at these low engine power operating conditions are not optimum, typically falling in the 90 to 96 percent range. At higher engine power settings, combustion efficiency levels of most engines are generally well in excess of 99 percent and, therefore, virtually all of the fuel is converted to the ideal combustion products, carbon dioxide, and water. The reduced combustion efficiency performance of most existing aircraft turbine engines at idle and other low engine power operating conditions is due to adverse combustor operating conditions that normally prevail at such engine operating conditions. At low engine power settings, the combustor inlet air temperature and pressure levels are relatively low, the overall combustor fuel-air ratios are generally low, and the quality of fuel atomization and its distribution within the primary combustion zone is usually poor because of the low fuel and airflows. In any given engine, the combustor operating conditions rapidly improve as the engine power setting is increased above idle power levels and, accordingly, its combustion efficiency performance is quickly increased to near-optimum levels.

To meet the CO and C_xH_y emissions standards defined by the EPA for Class T2 aircraft engines, higher combustion efficiency values at ground idle operating conditions are required. For example, in the case of the UTW engine, CO and C_xH_y emissions levels of about 20 and 4 grams per kilogram of fuel, respectively, are required at idle to meet the EPA standards. This combination of emissions levels is equivalent to a combustion efficiency value of 99 percent. Thus, significant improvements in combustion efficiency performance levels at ground idle operating conditions are required to meet these EPA standards.

Based on combustion chemical kinetics considerations, these required improvements in combustion efficiency at idle appear to be obtainable in engine combustors, providing that improved control of the various processes which occur in the primary combustion zones of the combustors can be attained at idle operating conditions. CO is formed in combustors as a result of combustion of near-stoichiometric or over-stoichiometric fuel-air mixtures in the primary zone, because it is a thermochemical equilibrium product resulting from the combustion of such mixtures. Even in combustors designed to have relatively lean primary zone fuel-air mixtures at all operating conditions, relatively rich mixtures generally exist locally within the primary zone since the fuel-air mixing process is not instantaneous. Considerable amounts of CO can be generated as a result of combustion of these localized rich primary zone mixtures. At idle, any CO that is so generated is not rapidly consumed and can escape from the combustion zones of the combustor. Therefore, to obtain low CO emissions levels at idle operating conditions in any given combustor, very precise control of the equivalence ratios in the primary combustion zone and in the dilution zone immediately downstream, and of the associated residence times in these zones is essential.

Unlike CO, the C_xH_y emissions are not thermochemical equilibrium combustion products. Moreover, combustion chemical kinetics data show that vaporized hydrocarbons, and any partially oxidized hydrocarbons, are consumed much more rapidly than CO. Thus, as long as these constituents reside in a flame zone for even a very brief time period, they are largely consumed. One of the products of this consumption process may be CO, depending on the flame zone stoichiometry and other factors. Thus, at idle operating conditions, relatively low C_xH_y emissions levels should be obtainable, based on these combustion chemical kinetics considerations, providing that the fuel is properly vaporized and mixed to some degree with air within the primary combustion zone. In any given combustor, the primary causes of this category of idle power emissions appear to be associated with its fuel injection characteristics. In particular, coarse fuel atomization may result in large numbers of large fuel droplets which can escape from the primary zone before they are fully vaporized. In many present-day combustors, the fuel atomization quality tends to be relatively coarse at low engine power operating conditions because of the low fuel flows associated with these engine operating conditions. Also, the fuel spray pattern of a given combustor may be such that some of the fuel is directed into the relatively cold air streams used to cool the combustor liners and other parts. At idle, any fuel that is so entrained by these cooling air streams tends to be carried out of the primary combustion zones as unreacted fuel. Accordingly, to obtain reduced C_xH_y emissions levels as well as low CO emission levels, very effective fuel atomization at idle is an important need. The effective atomization is needed both to facilitate rapid and satisfactorily controlled fuel-air mixing in the primary combustion zone and to prevent fuel droplets from escaping from the primary zone.

At General Electric, investigations to identify and develop means of reducing CO and C_xH_y emissions levels at idle by providing improved fuel atomization and improved control of the primary combustion zone fuel-air ratios at idle have been underway for the past several years. For the most part, these investigations have been primarily conducted with CF6 engine combustors, which have already developed low smoke emission characteristics. A major objective of these annular combustor development investigations has, therefore, been to retain these already developed low smoke emission characteristics. One of the major development programs of this kind currently underway is the NASA Experimental Clean Combustor Program. To date, some promising methods of obtaining significant reductions in the CO and C_xH_y emissions levels of these combustors have been identified.

One relatively simple means of obtaining more optimum primary zone fuel-air ratios at idle, without adversely affecting combustion performance characteristics at high power operating conditions, is to extract and dump overboard increased amounts of compressor discharge airflow. This approach results in increased fuel-air ratios throughout the combustor. Tests were conducted of CF6-6 engines, in which various amounts of compressor discharge airflow were extracted. The results (Figure 4-13) illustrate the beneficial effects of increasing the primary combustion zone fuel-air ratio, at a constant fuel flow rate. The use of increased bleed air extraction also results in small, but beneficial, increases in primary zone gas residence time, which are the result of the lower air mass flows through the combustor. Significant CO and C_xH_y emissions levels reductions were obtained in these investigations. Since many advanced engines have provisions for extracting

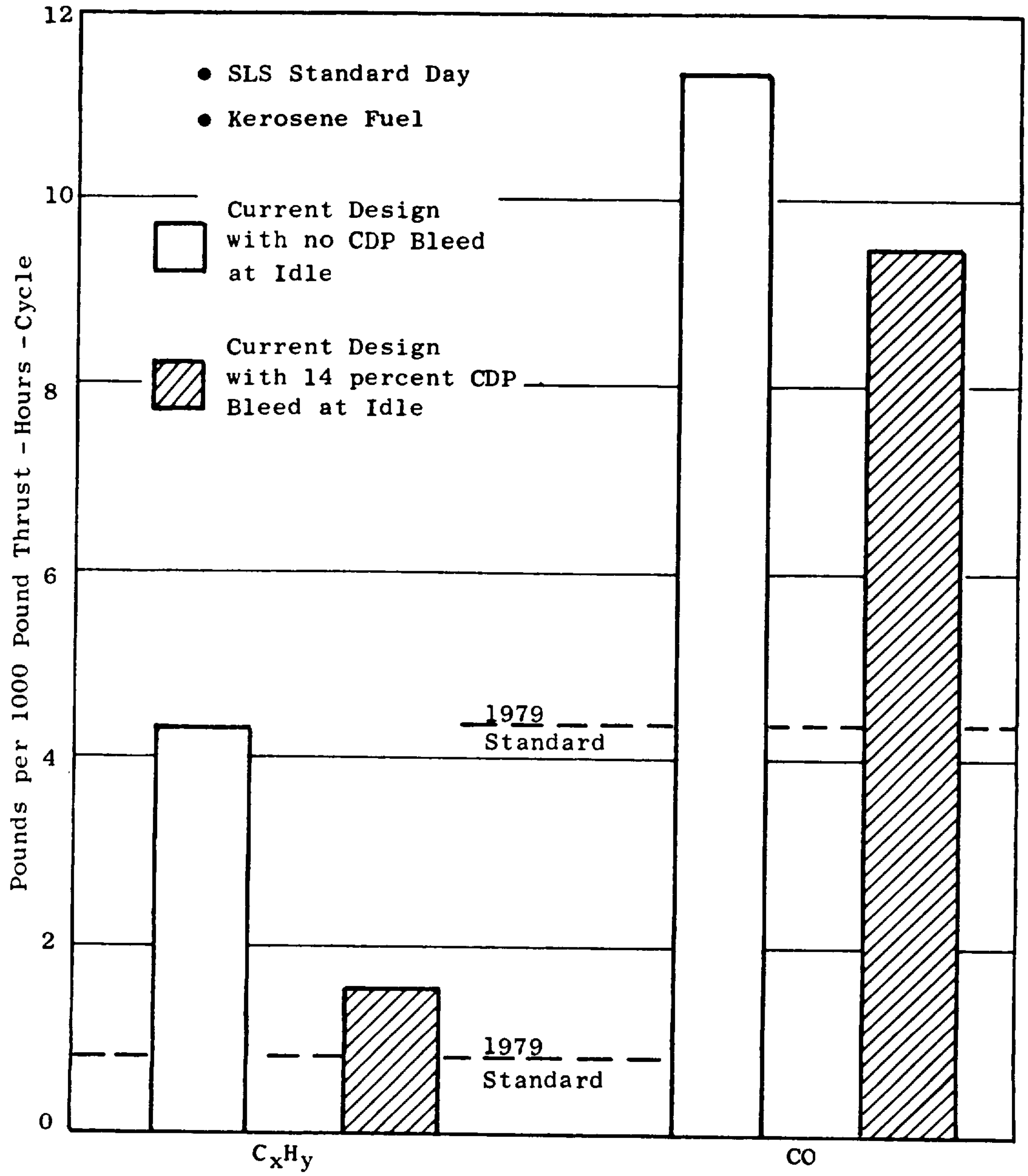

Figure 4-13. C_xH_y and CO Reductions in CF6-6 Engine with Increased CDP Bleed Air Extraction.

large amounts of compressor discharge airflow, this concept appears to offer some promise. In terms of the calculated CO and C_xH_y EPA parameters, however, its effectiveness is offset somewhat if the resulting fuel flow at idle increases rapidly as the degree of bleed air extraction is increased.

Still another means of obtaining the higher primary zone fuel-air ratios is to use fuel injection staging techniques at idle operating conditions. In this type of approach, fuel is valved to only selected fuel nozzles, or fuel injectors, instead of to the full complement of nozzles. This approach results in higher primary zone fuel-air ratios in the portions of the combustor annulus where fuel is concentrated. Various forms of such fuel injection staging can be considered, depending on the nature of the combustor design. Some fuel injection staging techniques that can be conveniently used in conventional annular combustors are illustrated in Figure 4-14. Tests of these fuel staging approaches have been conducted with CF6-50 and other higher pressure ratio engines.

As shown in Figures 4-15 and 4-16, the use of circumferential sector staging, in which fuel was supplied to groups of adjacent nozzles, was found to be highly effective; with this type of staging, enrichened fuel/air mixtures in the fueled zones are obtained, and at the same time, the number of boundaries between fueled and nonfueled regions are minimized. Circumferential fuel staging of this kind, thus, appears to be an attractive approach for use at idle to obtain reduced CO and C_xH_y emissions levels. Further studies are underway to assess the practicality and suitability of applying this approach in advanced engines.

Based on results obtained to date, it appears that significant reductions in CO and C_xH_y idle emissions levels of advanced combustors can be obtained by approaches involving primary zone stoichiometry control. In general, these approaches can be used without adversely affecting either combustion performance or smoke and NO_x emission characteristics at high engine power operating conditions. In some instances, use of these approaches can be accompanied by small increases in NO_x emissions at low engine power operating conditions, but NO_x emissions levels at these engine operating conditions are still quite low.

4.6 PREDICTED UTW EMISSIONS CHARACTERISTICS - WITH ADDED EMISSIONS CONTROL FEATURES

Based on the above described results, the following C_xH_y and CO emissions reductions techniques have been selected for possible use in the UTW engine:

- Sector fuel staging - at idle.
- Increased core engine speed to increase combustor inlet air temperature and pressure and its fuel-air ratio. If this approach were used, the idle engine thrust would be maintained at the required low level (4.5% of rated thrust) by flat-pitching the variable-pitch fan.

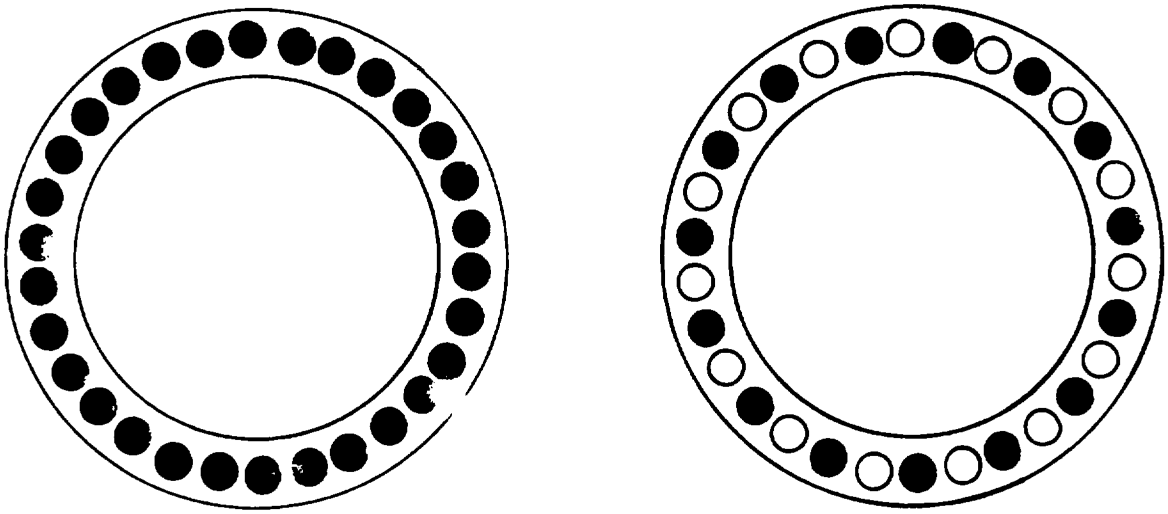

All Nozzles Fueled

Alternate Nozzles Fueled

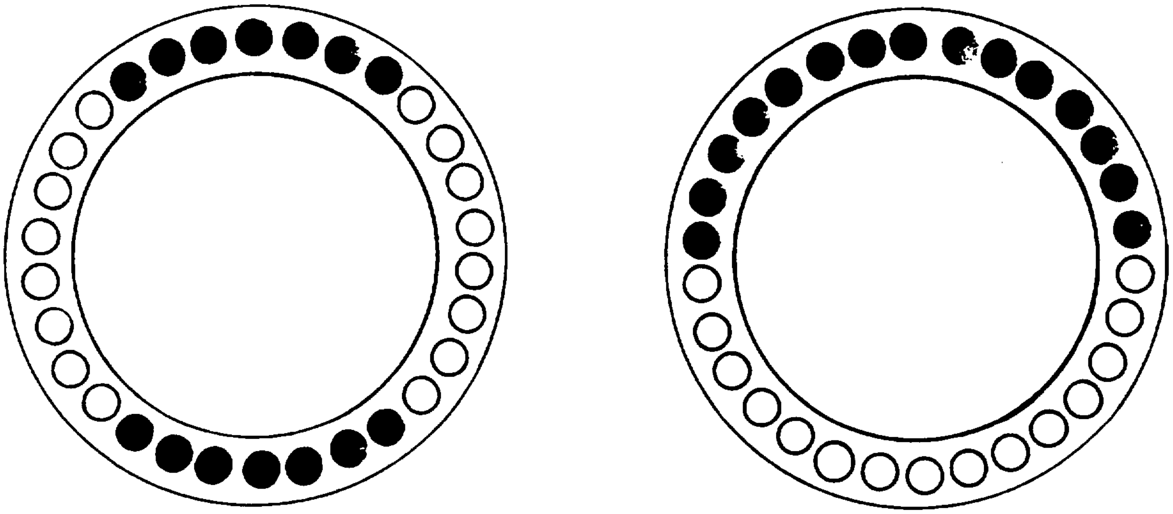

Opposing Sectors Fueled

Single Sector Fueled

Figure 4-14. Fuel Staging Methods at Idle in the CF6 Engine.

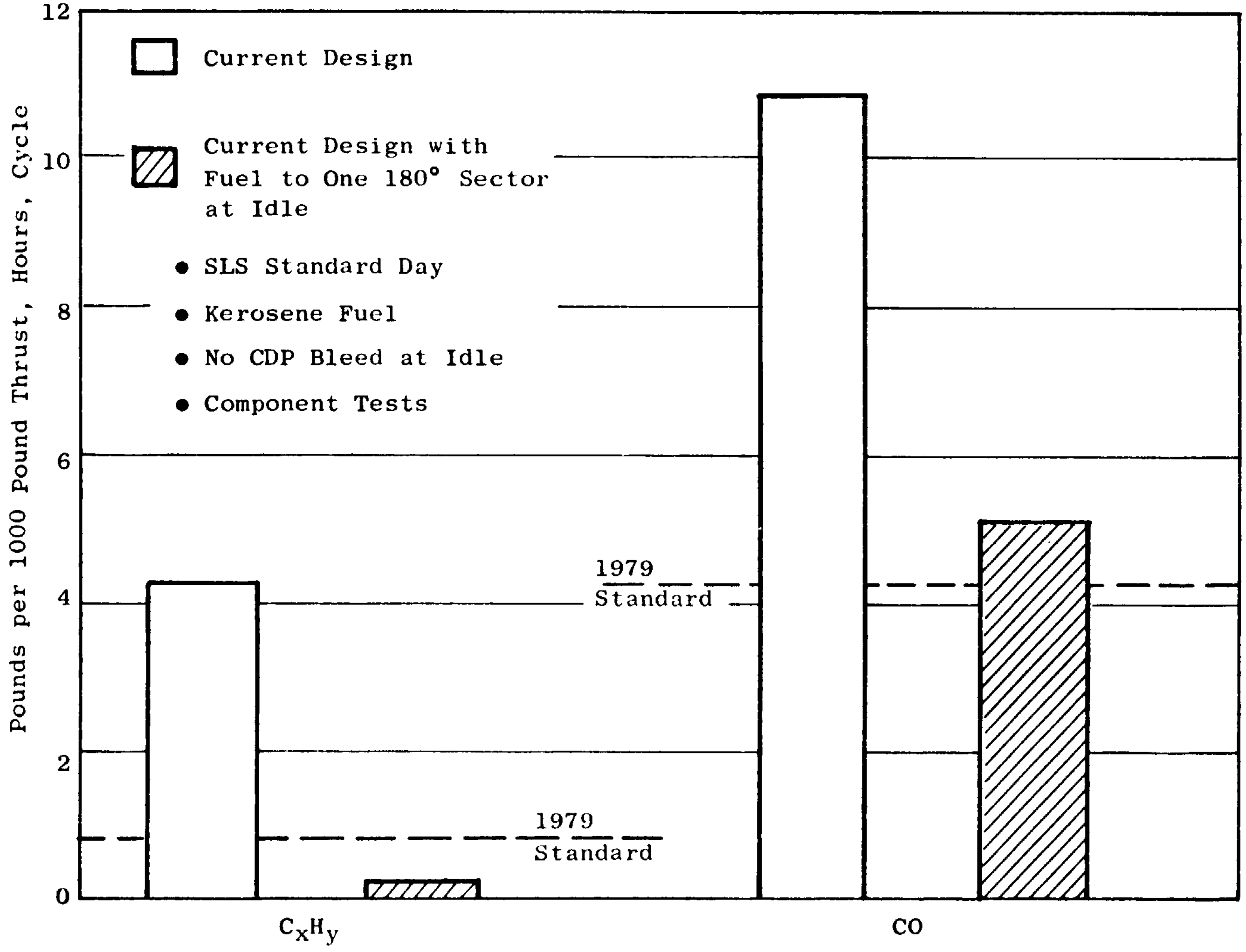

Figure 4-15. C_xH_y and CO Reductions In a CF6-50 Engine Combustor.

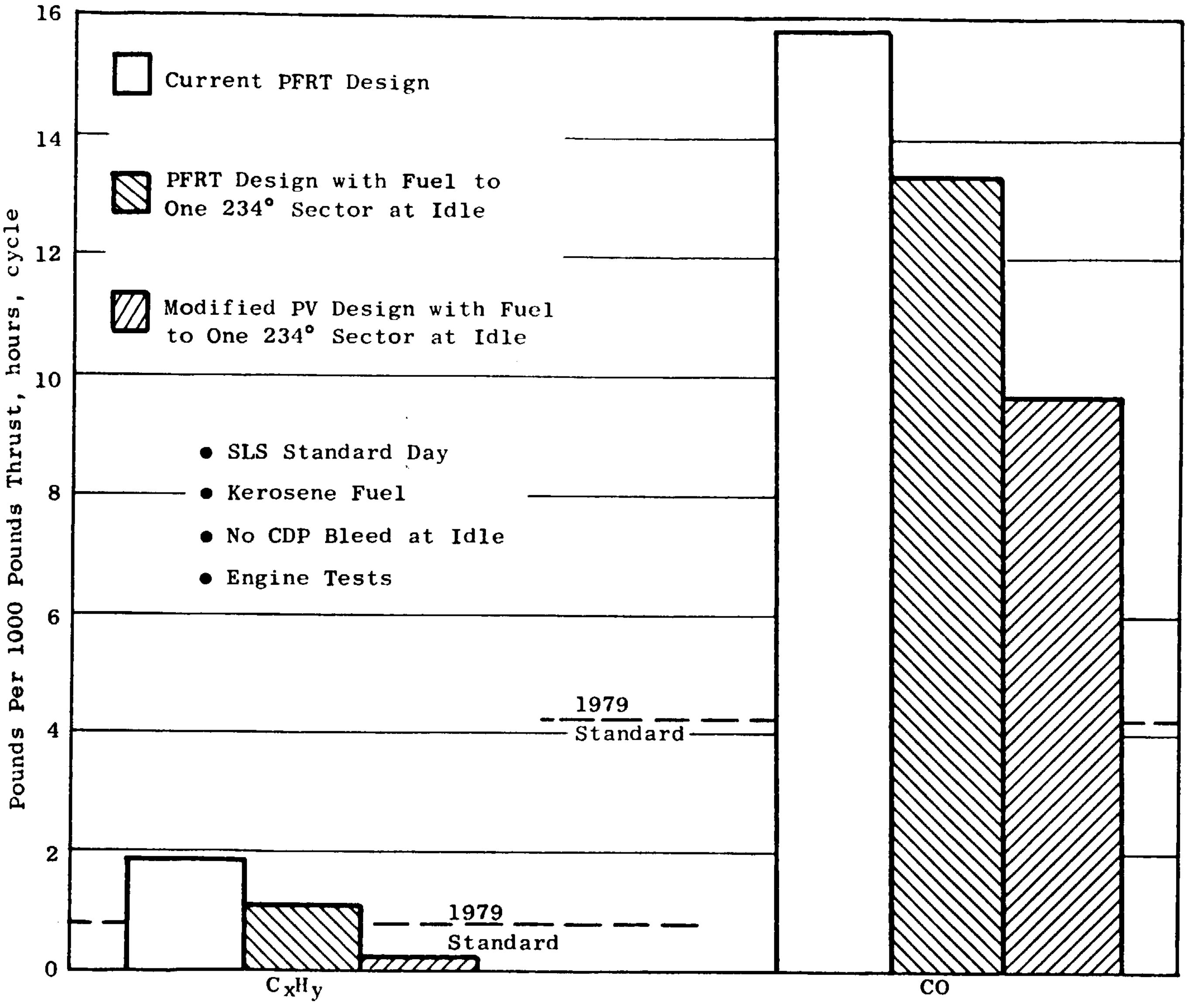

Figure 4-16. C_xH_y and CO Reductions in Higher Pressure Ratio Engine Equipped with a PFRT and a PV Combustor.

Estimates have been made of emissions characteristics of the UTW engine with use of sector fuel staging at idle. These estimates are based on results of component tests of the selected F101 PV combustor. As shown in Table 4-VIII, the predicted CO and C_xH_y emission levels for the UTW are still above the prescribed 1979 standard for all engine operating modes.

Flat pitching, or closing the variable-pitch fan blades, results in increased core engine speed with accompanying increases in combustor inlet temperature and pressure, as shown in Figure 4-17. Significant reductions in C_xH_y and CO emissions levels are obtained at these higher core speeds with the more favorable combustor inlet conditions that exist. These improvements in idle emissions levels were initially expected to result in C_xH_y and CO emissions levels which would satisfy the EPA standards when used in conjunction with sectorized burning. However, in flat pitching the fan to obtain increased core speeds, higher fuel flows are required to maintain the core engine at the higher speed conditions. This increased fuel flow at ground idle is a significant factor in calculations to determine the EPA-defined emissions level parameter.

This calculation, as illustrated below for the UTW engine at idle, is the product of pertinent emissions index (EI) and corresponding fuel flow divided by a constant work output for the entire mission cycle described in Table 4-II.

$$\text{EPA Emission Level} = \frac{(\text{EI} \times W_f *0.28)\ \text{Idle}}{1.4328}$$

$$\left(\frac{\frac{\text{lb Emission}}{\text{lb Fuel}} \times \frac{\text{lb fuel}}{\text{hr}} \times \text{Hour}}{\text{Total 1000 Pound Thrust -- hours for cycle}} \right)$$

Estimates of the effects of flat pitching the fan on CO idle emissions and core engine fuel flow and the resulting EPA-defined parameter are shown in Figure 4-18, in terms of the anticipated increase in combustor inlet temperature. As shown, the CO emission index is reduced significantly as combustor inlet temperature is increased. However, the accompanying core engine fuel flow is increased at nearly the same rate. The overall effect of these two variables is to limit the reduction in EPA-defined parameters for CO by only about one-half of the reduction in CO emission index.

In addition, at the increased core speed conditions and associated higher combustor inlet air temperature and pressure levels, NO_x emissions levels are also increased at the ground idle condition. The increase in NO_x emissions attributed to higher combustor inlet temperature at idle would be expected to have little impact on the calculated EPA parameter for this emissions category since the contribution at low power settings is usually very small compared to contributions at higher power operating conditions.

Table 4-VIII. Predicted UTW Engine Emissions Characteristics.

- Based on non-QCSEE Component Test Data with the Selected F101 PV Combustor.
- 4.5% Power at Idle
- No CDP Bleed
- Kerosene Fuel

Emission		1979 Standard	Combustor as is		With Sector Burning at Idle	
			Constant Fan Speed	Constant Fan Pitch	Constant Fan Speed	Constant Fan Pitch
CO	(Pounds per 1000 Pound Thrust-Hours per Cycle)	4.3	14.0	14.5	12.0	12.6
C_xH_y		0.8	1.9	2.2	0.9	0.9
NO_x		3.0	3.3	2.4	3.3	2.4
Smoke (SAE SN)		24	18	18	18	18

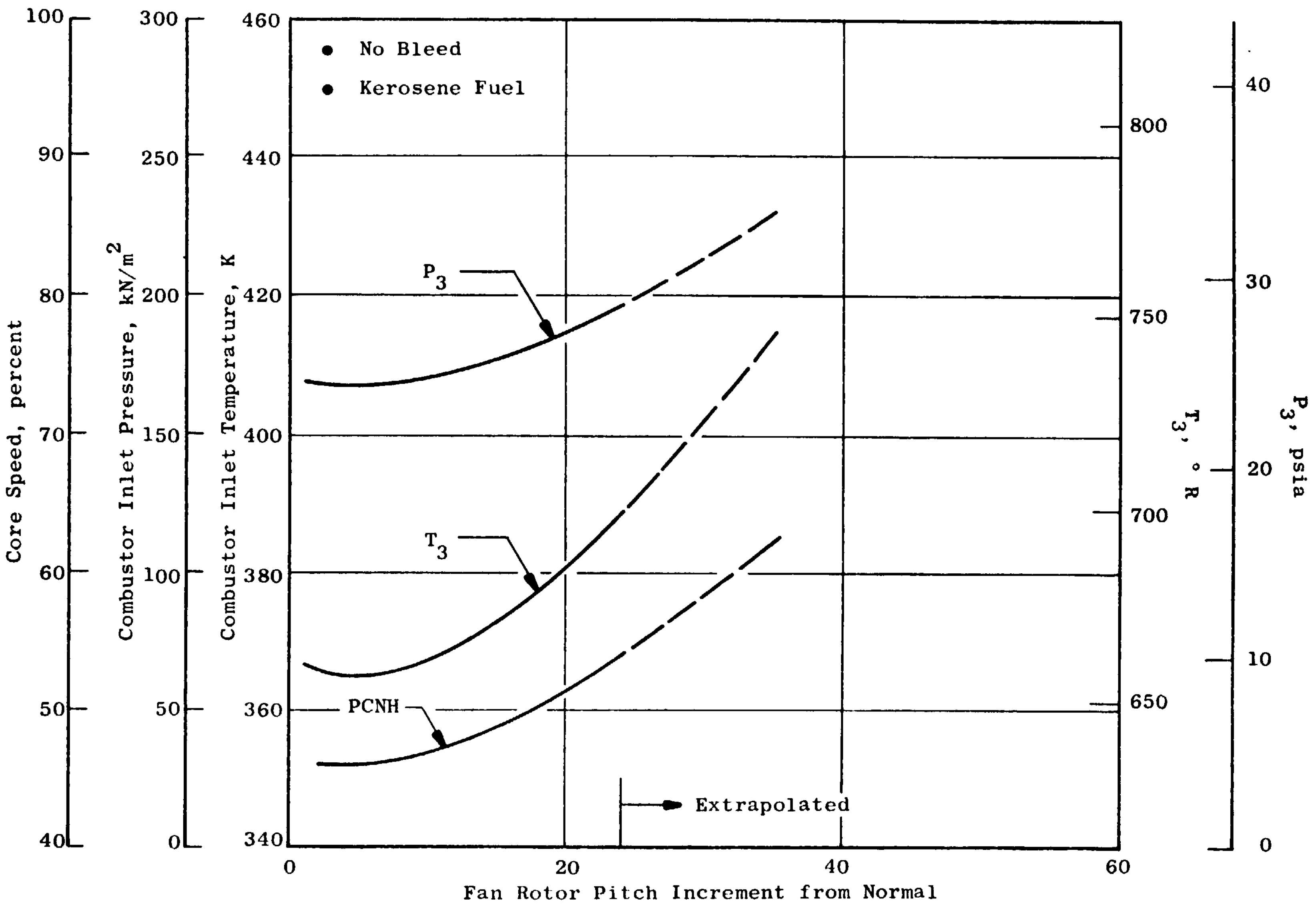

Figure 4-17. Characteristics of UTW Combustor Inlet Conditions with Increased Flat Pitching of Variable Fan.

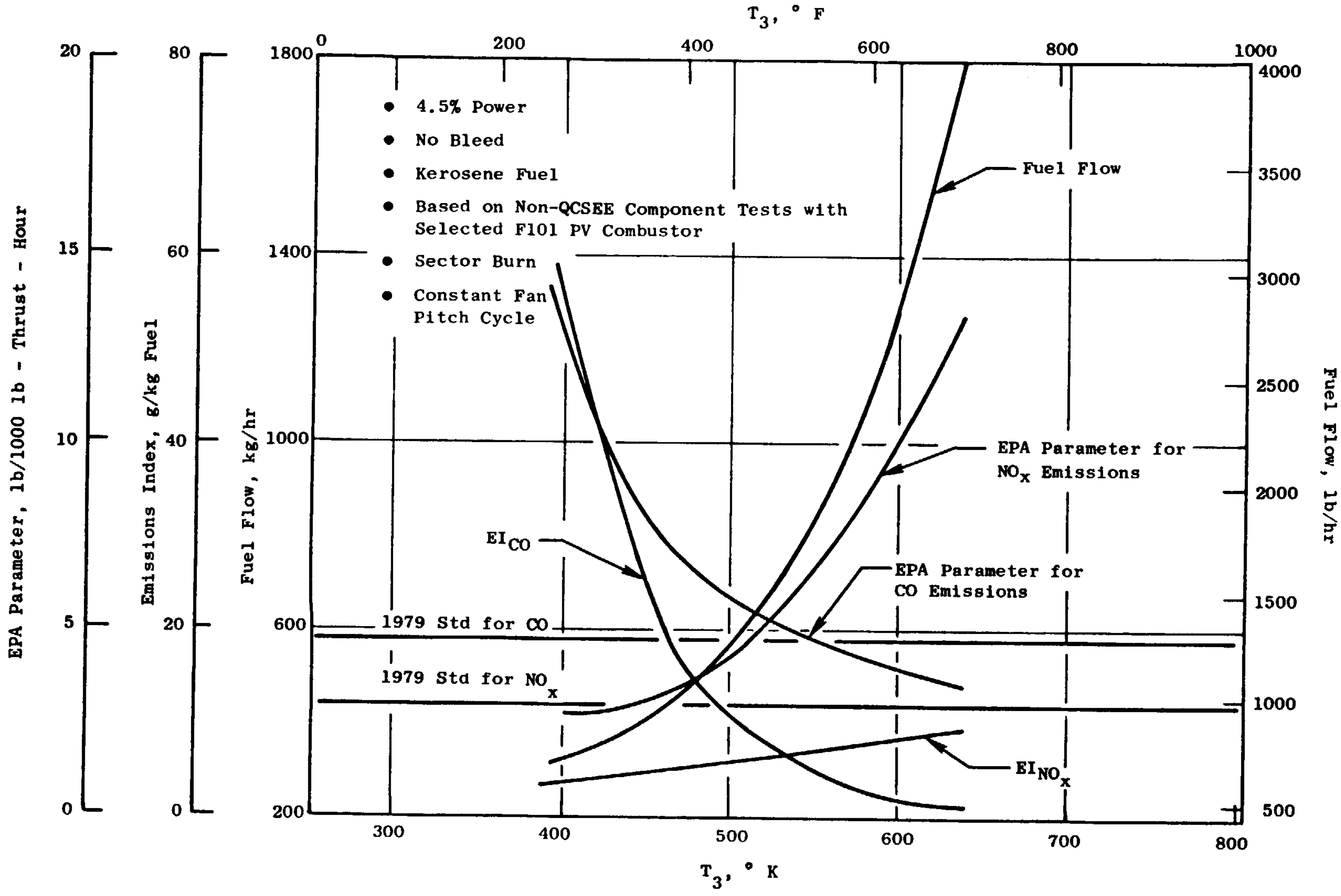

Figure 4-18. Idle Emisssions Characteristics of UTW with Increased Combustor Inlet Temperature for Increased Fan Flat Pitching.

However, the increased fuel flow in conjunction with the increased NO_x emissions attributable to the higher idle combustor inlet temperatures results in a calculated EPA NO_x emissions parameter that would exceed the EPA standard, as shown in Figure 4-18.

These estimates were based on the UTW engine variable-pitch fan operating at projected conditions which far exceed known performance characteristics of the current variable-pitch fan design. Consideration for the approach of flat pitching of the fan with its accompanying diminished potential for CO emissions reduction and increased NO_x emissions, when related to the EPA-defined requirements, appears less attractive than originally anticipated based on these estimates. Final evaluation of this technique for idle emissions reduction will require a more complete definition of the variable-pitch fan performance and/or evaluation during UTW engine tests. Additional effort is under consideration which would involve applying the advanced emission reduction technology developed in NASA-GE Clean Combustor program to a double annular combustor design for QCSEE. This new design would be developed in a sector test program concentrating on reducing idle emissions to meet the program goals.

SECTION 5.0

ENGINE CYCLE AND PERFORMANCE

5.1 SUMMARY

The QCSEE UTW engine cycle was defined to meet requirements of a short-haul aircraft with externally blown flaps incorporating engines mounted under the wing. The engine has a separated-flow cycle, utilizing a single-stage, variable-pitch, gear-driven fan. Objective thrust levels are 81,400 N (18,300 lb) thrust uninstalled at sea level static, and 17,800 N (4,000 lb) thrust uninstalled at cruise, Mach 0.8, 9144 m (30,000 ft). Design cycle and performance data are presented for these flight conditions as well as for the noise rating conditions, 41.2 m/sec, 61.0 m (80 knots, 200 ft) sideline. Predicted fan performance maps are shown for significant flight conditions.

5.2 CYCLE SELECTION CRITERIA

Primary constraints on the QCSEE engine cycle include low-noise and low-exhaust emissions. The particular cycle defined under this program was also selected to allow usage of several major propulsion system components in common with the QCSEE over-the-wing engine. These components include;

- Inlet
- Fan frame
- Fan bypass duct
- Core engine
- Low pressure turbine
- Turbine frame

An inlet throat Mach number of 0.79 is required at maximum power at the noise rating condition [41.2 m/sec, 61.0 m (80 knots, 200 ft) sideline], thus establishing the airflow at that flight condition. Ram recovery characteristics of the selected inlet are shown in Figure 5-1. In Figure 5-2, the corrected airflow characteristics are shown as a function of flight Mach number. Also shown is the inlet throat Mach number for 406 kg/sec (894 lb/sec) corrected airflow, selected as the design value at all flight conditions for control mode purposes.

Performance objectives are summarized in Table 5-I. As shown in the table, the engine has an uninstalled thrust at takeoff of 81,400 N (18,300 lb). At cruise, the thrust is 17,800 N (4000 lb).

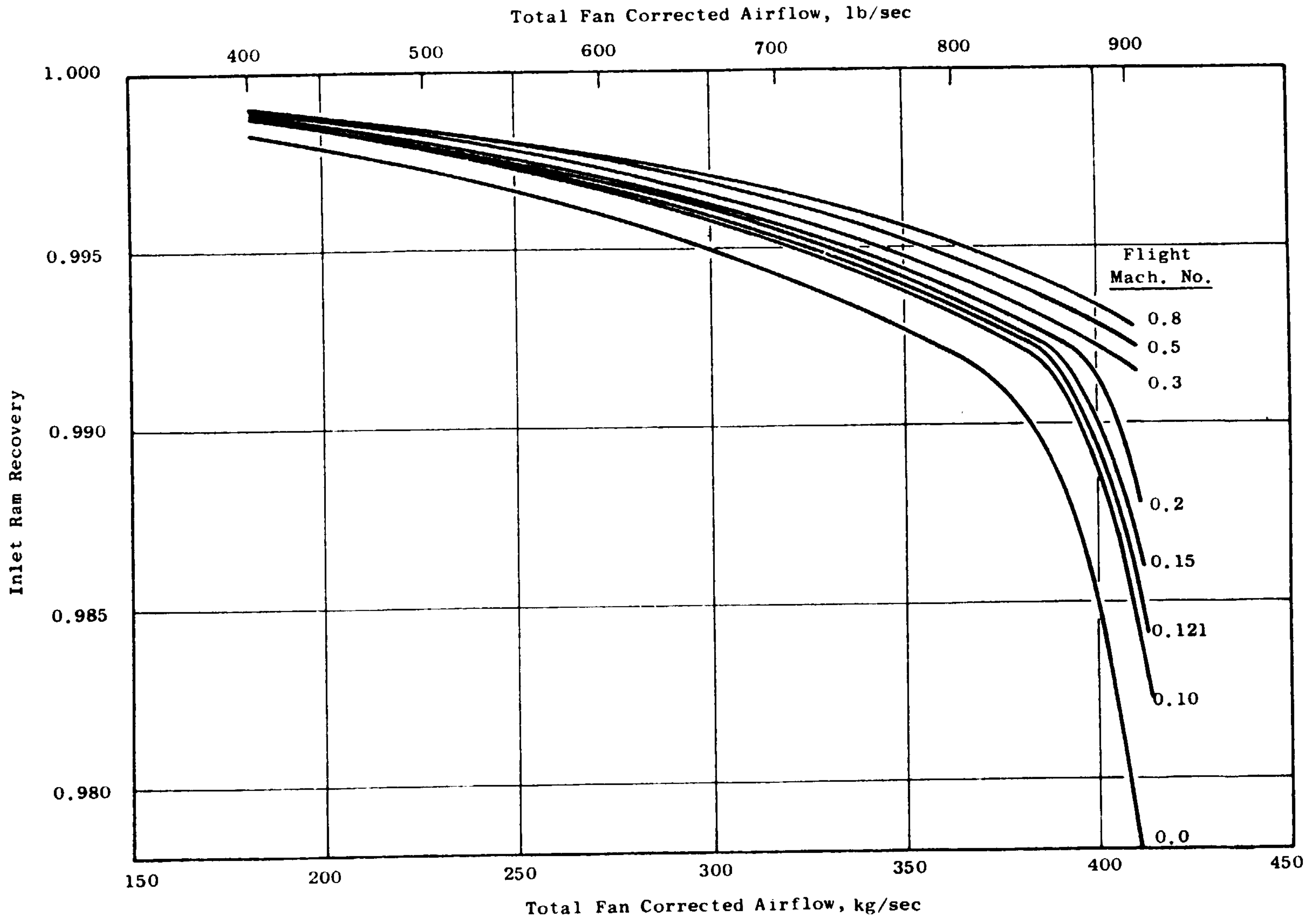

Figure 5-1. QCSEE Inlet Ram Recovery Characteristics.

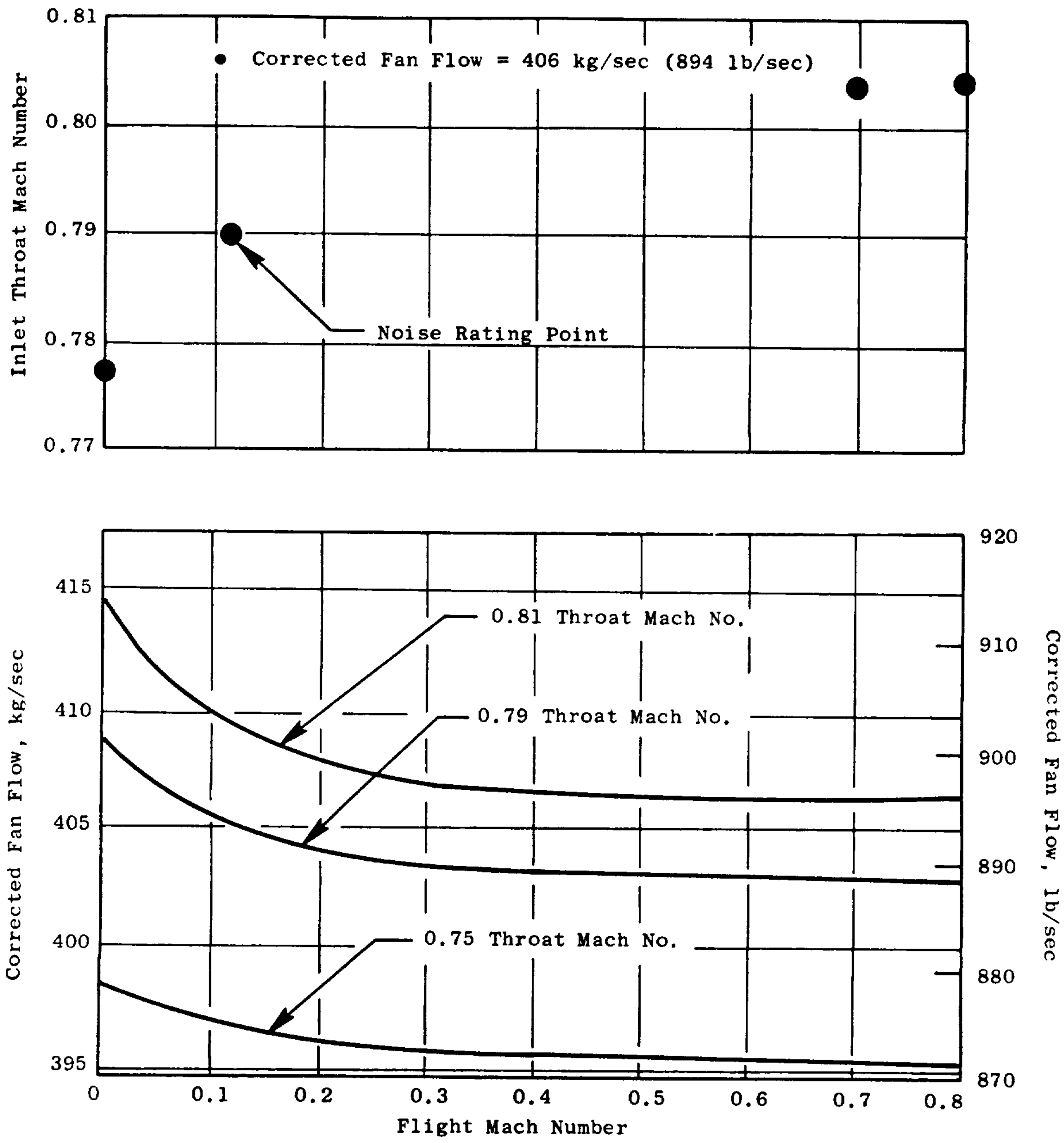

Figure 5-2. QCSEE Inlet Characteristics.

Table 5-I. UTW Engine Performance Objectives.

Takeoff, SLS, 305 K (90° F) Day		
Uninstalled net thrust,(1) N (lb)	81400	(18300)
Uninstalled SFC, kg/Ns (lb/hr/lb)	9.6x10-6	(0.34)
Turbine rotor inlet temperature, K (° F) (maximum)	1611	(2400)
Bypass ratio (approximate)	11.8	
Cycle pressure ratio (approximate)	13.7	
Installed net thrust,(1) N (lb)	77400	(17400)
Takeoff, SLS, Standard Day		
Uninstalled net thrust,(1) N (lb)	81400	(18300)
Uninstalled SFC, kg/Ns (lb/hr/lb)	9.3x10-6	(0.33)
Turbine rotor inlet temperature, K (° F) (maximum)	1533	(2300)
Cruise, Mach 0.8, 9144 m (30000 feet), Standard Day		
Uninstalled net thrust,(1) N (lb)	17800	(4000)
Reverse Thrust		
35% of static takeoff thrust N (lb) (minimum)	28491	(6405)

(1) No bleed or power extraction

The experimental engine is based on utilization of PFRT F101 core engine and low pressure turbine components. The fan is gear driven with the gear ratio selected to match the available LP turbine; the gear ratio is 2.4648. The fan has a corrected tip speed limit at takeoff of 290 m/sec (950 ft/sec).

Reverse thrust capability is achieved by rotating the fan rotor blades so that air is pumped through the fan in the reverse direction to normal flow. The objective reverse thrust level, as shown in Table 5-I, is 35 percent of static takeoff thrust.

5.3 ENGINE AND SYSTEM PERFORMANCE

The UTW propulsion system incorporates a single-stage, variable-pitch, gear-driven fan. The fan and core streams exhaust through separate exhaust nozzles, with the fan nozzle being variable, PFRT level F101 core engine components are utilized. The cycle provides 81,400 N (18,300 lb) thrust uninstalled, at sea level static conditions, flat rated to a 305 K (90° F) day. Installed, with effects of inlet ram recovery and scrubbing drags allowed for, the thrust level is 77,400 N (17,400 lb) at sea level static. At Mach 0.8, 9144 m (30,000 ft) flight condition, the maximum thrust level uninstalled is 17,800 N (4000 lb).

The performance of the UTW experimental engine has been revised from that shown in the preliminary design report (Reference 1). Major factors contributing to the revision include:

- Variable-pitch fan performance logic incorporated into the cycle deck.
- Core performance revised to represent current demonstrated PFRT levels.
- At the 0.8 Mach, 9144 m (30,000 ft) cruise condition, allowance was made for possible flow separation in the turbine frame.

The fan map representations used for the preliminary design were based on estimates at specific takeoff and cruise flight conditions. Following these preliminary studies, the cycle deck was modified to incorporate fan map logic based on a fundamental stage characteristic approach. Pitch change effects are accomplished by transforms from a nominal base characteristic which is a function of speed. This approach has been verified by experimental data, which collapse on a nominal characteristic when adjusted for pitch angle. The characteristic can also be defined from basic data used to generate predicted maps.

The predicted UTW experimental engine base map at nominal pitch setting (0 degrees) is shown in Figure 5-3. At takeoff, the fan pitch is set open 0.99 degree from nominal (Figure 5-4). This pitch setting results from the requirement to produce the objective thrust level in conjunction with the fan corrected tip speed limit of 290 m/sec (950 ft/sec), matching inlet design flow 406 kg/sec (894 lb/sec), and the constraint that pressure ratio be minimized to aid acoustic goals. If airflow was increased to reduce fan pressure ratio, the fan efficiency would decrease and turbine inlet temperature would exceed objective levels. A reduction in flow would have the disadvantage of a higher pressure ratio required to maintain thrust. A SLS operating line at a constant pitch angle and fan exhaust nozzle area is included on the fan map in Figure 5-4. The operating line will change when the variable fan nozzle capability is used to maintain constant or high flows at the reduced thrust levels for acoustic purposes. This is indicated by the dotted operating line.

Predicted fan performance at the Mach 0.7, 7620 m (25,000 ft) cruise condition is shown in Figure 5-5. At this condition, flow is set to the design level, 406 kg/sec (894 lb/sec) and pitch angle and fan speed selected to provide 10 percent cruise stall margin. The operating line is based on constant pitch with fan nozzle area set at the maximum cruise value at this flight condition. Differences in sfc were found to be negligible when alternative pitch angle and/or area schedules were investigated for part power operation.

Parasitic and cooling flows for the UTW engine cycle are shown in Figure 5-6.

Internal cycle parameters and performance for the experimental engine are shown in Table 5-II (see cycle nomenclature Table 5-III and station designations Figures 5-7 and 5-8).

The first three columns in Table 5-III show sea level static takeoff conditions corresponding to the objective levels presented in Table 5-I. The installed data (Column 3) include effects of inlet ram recovery and the following drag terms:

- Fan Flow Scrubbing Loss along the Core Casing
- Fan Flow Scrubbing on the Engine Portion of the Pylon
- Core Flow Scrubbing on the Center Plug

Cruise performance at 0.8 Mach, 9144 m (30,000 ft) is shown in Table 5-II, Column 4, uninstalled, and Column 5, installed. An uninstalled thrust of 17,800 N (4000 lb) is the objective level as identified in Table 5-I. At this flight condition, there is a possibility that flow separation may occur in the turbine frame. It is estimated that this would result in frame losses anywhere from two to five times the unseparated loss levels. A factor of 3.5 was applied in generating the cycle values shown in Table 5-II, at this flight condition only. At flight Mach number 0.7 and below, the combination

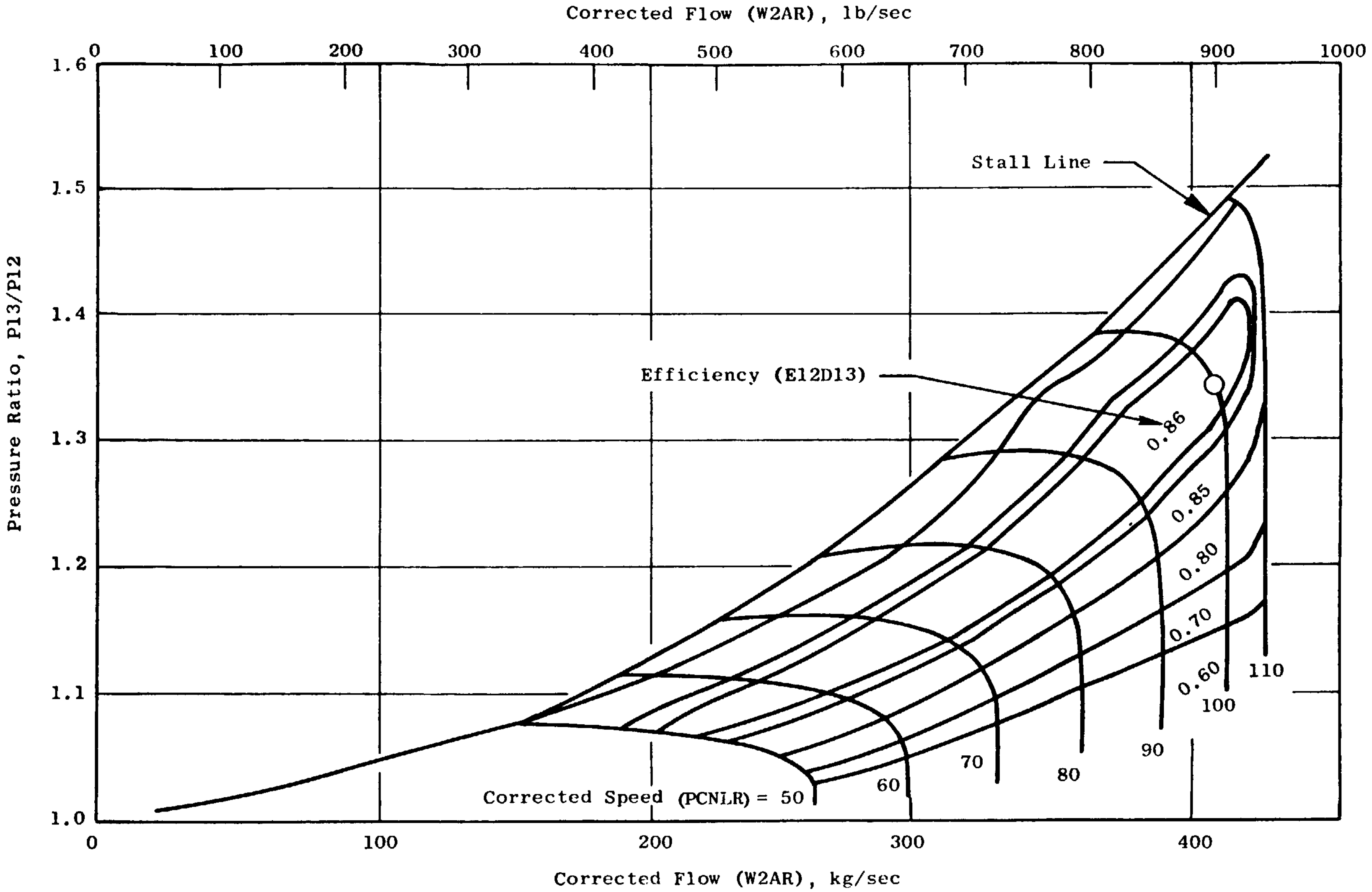

Figure 5-3. Predicted Fan Performance, Nominal Pitch.

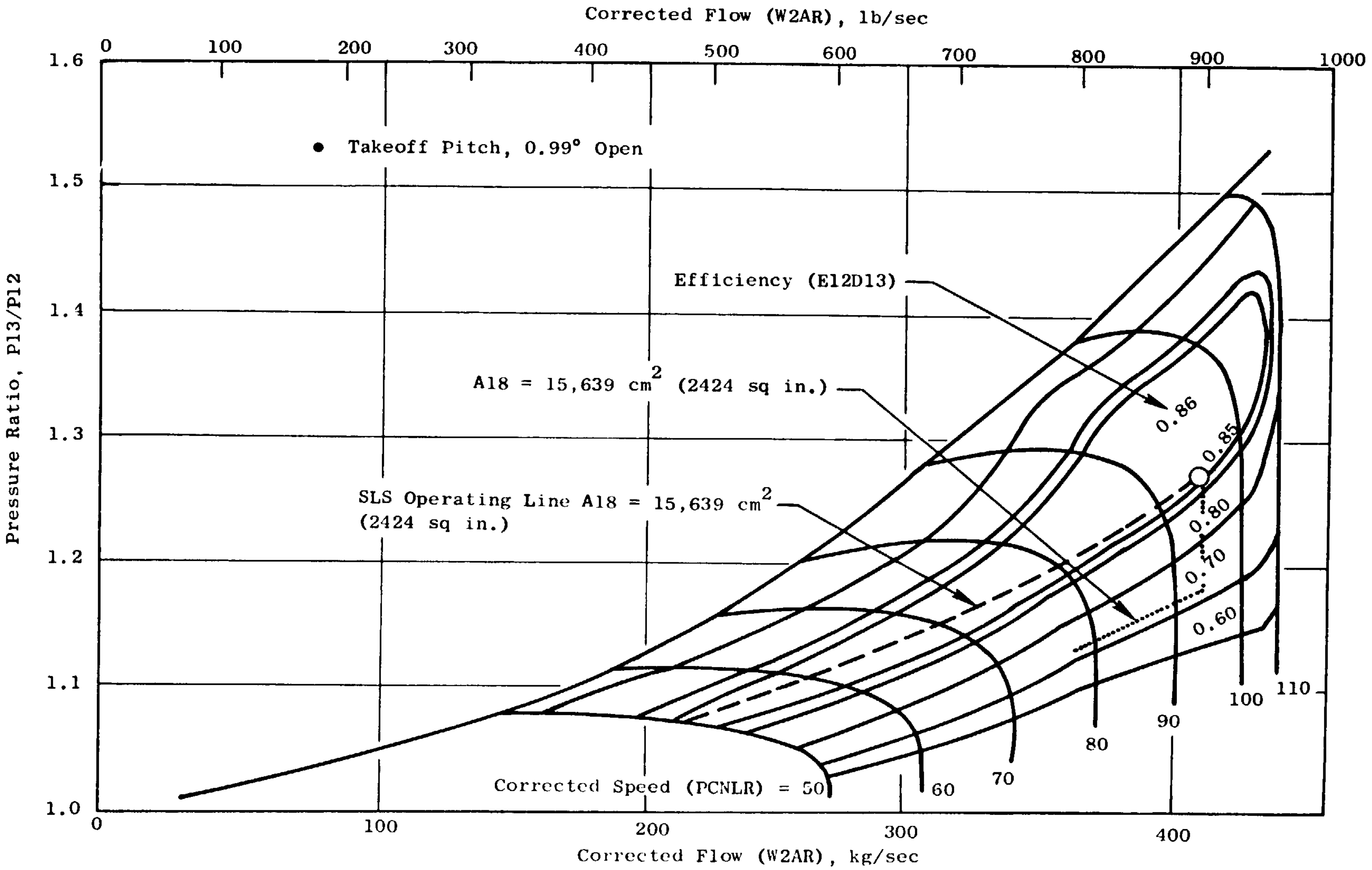

Figure 5-4. Predicted Fan Performance, Takeoff Pitch.

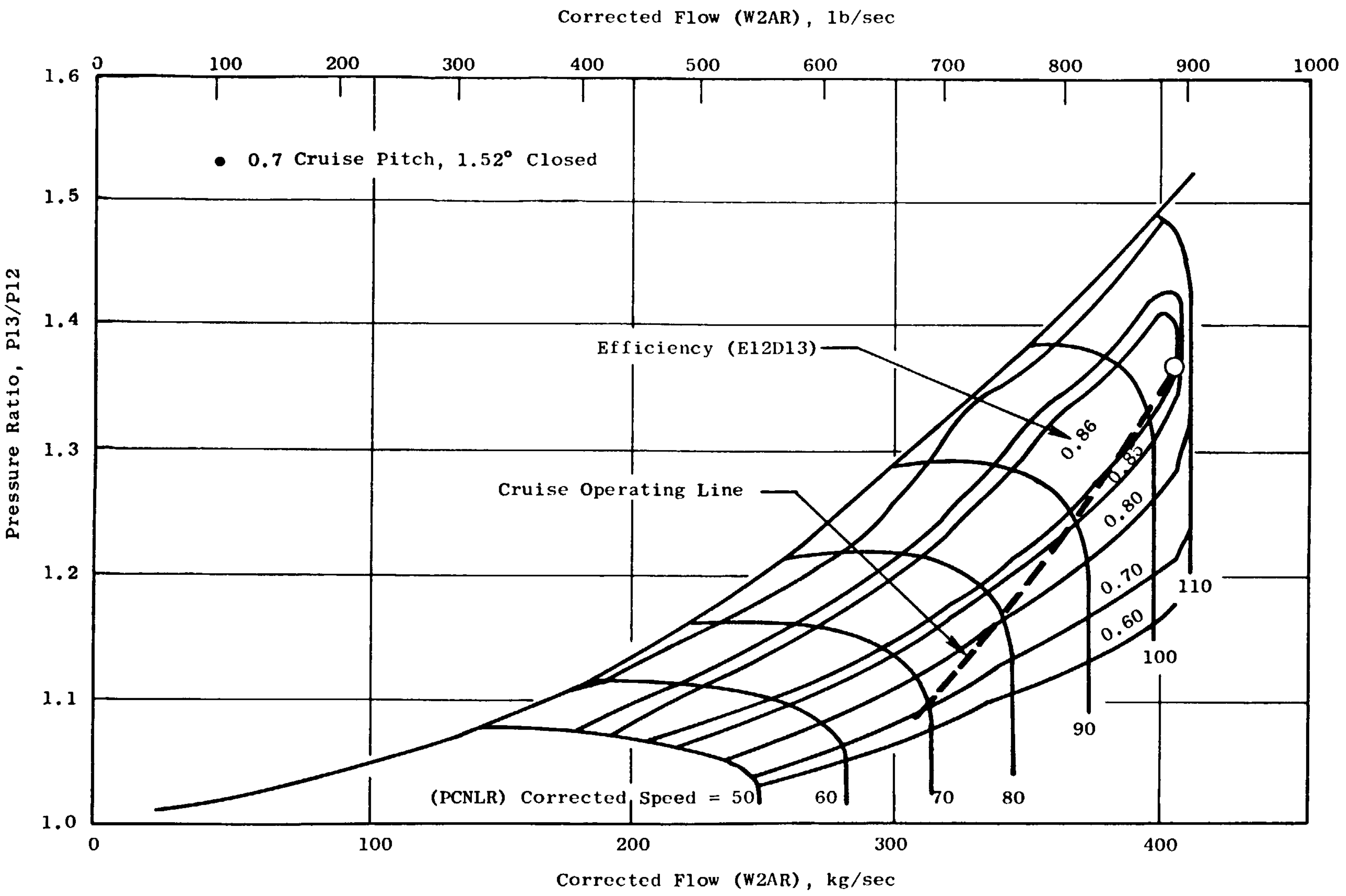

Figure 5-5. Predicted Fan Performance, Cruise Pitch.

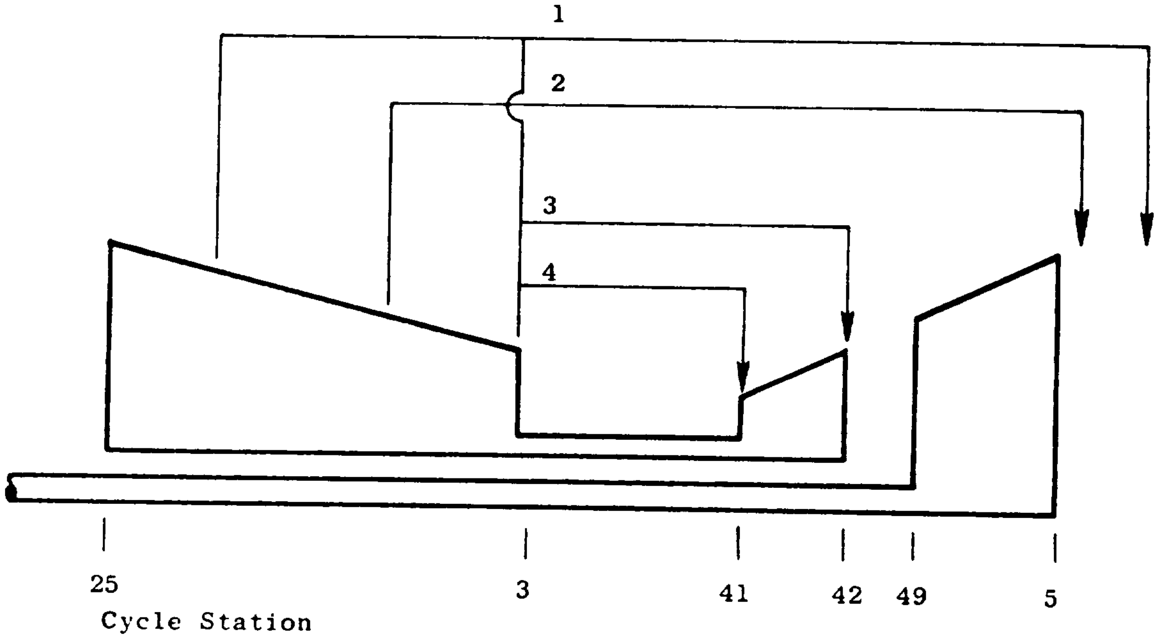

		Source	Sink	Quantity (% of W_{25})
1	Balance Piston, LP Shaft and Rear Bearing Cooling	Stage 3 & CDP	LP Discharge	2.11
2	LP Turbine Rotor Discharge and Dovetail Cooling, LP Turbine Nozzle Vane and Band Cooling	Stage 5	LP Discharge	1.84
3	CDP Seal Leakage, HP Turbine Rotor Cooling	CDP	HP Discharge	5.46
4	HP Nozzle Vane & Band Cooling (Nonchargeable)	CDP	HP Rotor Inlet	11.0

Figure 5-6. Cooling Flow Schematic.

Table 5-II. Experimental Engine Performance.

Parameter	Case Number												
	1	2	3	4	5	6	7	8	9	10	11	12	13
Rating	T/O	T/O	T/O	MXCR	MXCR	MXCR	MXCR	T/O	APP	APP	APP	REV	REV
ALT	0	0	0	30000	30000	25000	25000	200	200	200	200	0	0
XM	0	0	0	0.8	0.8	0.7	0.7	0.121	0.121	0.121	0.121	0	0
DTAMB	+31	0	+31	+18	+18	+18	+18	0	0	0	0	+31	+31
FN	18300(1)	18300(1)	17400(2)	4000(1)	3797(2)	4690(1)	4533(2)	14316(2)	9308(2)	9306(2)	9305(2)	-5265(2)	-6407(2)
SFC	0.320	0.309	0.335	0.759	0.782	0.699	0.718	0.394	0.454	0.485	0.489	0.685	0.584
BPR	12.09	12.17	12.00	11.14	11.23	11.36	11.36	12.14	11.41	13.14	13.79	7.84	9.41
PAMB	14.696	14.696	14.696	4.364	4.364	5.454	5.454	14.590	14.590	14.590	14.590	14.696	14.696
XM11	---	---	0.788	---	0.803	---	0.803	0.790	0.548	0.708	0.790	---	---
T1A	549.67	518.67	549.67	484.92	484.92	491.56	491.56	519.48	519.48	519.48	519.48	549.67	549.67
P1A	14.696	14.696	14.431	6.657	6.610	7.568	7.514	14.557	14.662	14.621	14.557	14.696	14.696
P12Q11	1.0	1.0	0.982	1.0	0.993	1.0	0.993	0.988	0.995	0.992	0.988	0.992	0.989
XNL	3157	3048	3157	3408	3408	3340	3336	3068	3068	3068	3068	3408	2979
PCNLR	91.53	93.95	94.53	108.7	108.7	105.8	105.6	94.50	94.50	94.50	94.50	102.1	89.19
W2AR	891.0	894.0	894.0	894.0	894.0	894.0	894.0	894.0	735.6	852.4	894.0	444.7	538.7
W2A	868.4	894.0	852.8	418.8	415.8	472.9	469.5	884.7	733.4	847.4	884.8	428.7	517.7
P13Q12	1.268	1.268	1.272	1.380	1.373	1.366	1.366	1.269	1.172	1.143	1.141	1.171	1.148
E12D13	0.859	0.864	0.861	0.837	0.834	0.855	0.856	0.861	0.660	0.596	0.611	0.500	0.510
P21Q2	1.181	1.181	1.184	1.247	1.252	1.248	1.248	1.182	1.116	1.096	1.095	---	---
E2D21	0.764	0.768	0.768	0.755	0.752	0.771	0.772	0.766	0.595	0.537	0.546	---	---
ROPDEG	-0.926	-1.140	-0.985	1.834	1.836	1.535	1.519	-0.944	6.202	1.225	-0.624	83.00	-95.00
W15	802.1	826.1	787.2	384.3	381.9	434.7	431.5	817.4	674.3	787.5	825.0	380.2	468.0
T15	594.6	560.9	595.0	541.0	540.2	545.4	545.3	562.0	556.1	553.4	552.1	600.3	593.0
P15	18.63	18.64	18.35	9.19	9.07	10.34	10.27	18.47	17.18	16.70	16.60	17.07	16.69
P18Q15	0.990	0.990	0.990	0.991	0.991	0.991	0.991	0.990	0.992	0.988	0.987	1.00	1.00
P18	18.44	18.44	18.17	9.11	8.99	10.25	10.17	18.28	17.05	16.51	16.38	17.07	16.69
A18	2500	2500	2547	1876	1888	1901	1902	2504	2504	3300	3573	1558	1968
AF18	2424	2423	2469	1845	1856	1862	1862	2427	2431	3205	3471	1527	1928
V19	669.5	650.7	648.1	1041.1	1040.3	1039.6	1033.9	649.0	539.5	479.9	464.2	549.9	505.0
FG19	16607	16626	15779	13197	12998	13976	13799	16407	11250	11687	11845	-6114	-7292
T25	584.7	551.7	585.1	528.5	527.8	533.4	533.3	552.7	547.4	545.3	544.6	549.7	549.7
P25	17.05	17.05	16.78	8.24	8.15	9.30	9.23	16.90	16.16	15.71	15.58	13.50	13.39
P25Q21	0.982	0.982	0.982	0.985	0.984	0.984	0.984	0.982	0.987	0.980	0.977	0.926	0.921
T49	2232.7	2124.6	2244.9	2183.6	2171.3	2149.3	2149.4	2132.7	1924.7	1988.2	2000.0	1976.6	1990.5
P48	53.97	53.78	53.51	27.97	27.47	30.69	30.47	53.45	44.58	45.91	45.99	37.97	38.49
E48D5	0.906	0.905	0.905	0.904	0.904	0.902	0.902	0.905	0.916	0.914	0.914	0.910	0.916
P48Q5	3.231	3.223	3.215	4.192	4.183	4.169	4.156	3.227	2.799	2.880	2.887	2.422	2.450
XNL48	7781	7512	7781	8400	8400	8233	8221	7562	7562	7562	7562	8400	7342
P55Q5	0.994	0.994	0.994	0.912	0.918	0.972	0.974	0.994	0.996	0.996	0.996	0.997	0.997
P8Q5	0.983	0.983	0.983	0.890	0.897	0.953	0.955	0.983	0.988	0.987	0.987	0.992	0.991
W8	67.98	69.47	67.21	35.36	34.82	39.17	38.88	63.91	60.25	61.16	61.10	49.50	50.78
T8	1715.8	1629.3	1727.5	1586.7	1577.6	1563.3	1564.4	1635.2	1509.2	1552.4	1561.3	1603.6	1609.1
P8	16.42	16.40	16.36	5.94	5.89	7.02	7.00	16.29	15.74	15.74	15.73	15.55	15.57
A8	541	541	541	541	541	541	541	541	541	541	541	541	541
AE8	514	514	518	500	499	491	490	514	523	538	541	513	519
V9	603.2	779.0	793.4	1270.9	1250.6	1145.8	1140.8	780.3	624.2	633.3	632.1	554.4	563.6
FG9	1692	1677	1653	1393	1350	1391	1375	18073	12416	12888	13042	850	887
FRAM	0	0	0	10589	10514	10677	10600	3713	3078	3556	3713	0	0

(1) Uninstalled

(2) Installed

Table 5-III. Separated-Flow Turbofan Nomenclature.

ALT	Altitude, feet
XM	Flight Mach Number
DTAMB	Temperature Increment from Standard Day Ambient Temperature, ° R
FN	Net Thrust, lb
SFC	Specific Fuel Consumption, lb/hr/lb
BPR	Bypass Ratio
PAMB	Ambient Pressure, psia
XM11	Engine Inlet Throat Mach Number
T1A	Fan Inlet Total Temperature, ° R
P1A	Fan Inlet Total Pressure, psia
P12Q11	Inlet Duct Pressure Ratio
XNL	Fan Physical Speed, rpm
PCNLR	Fan Corrected Speed, %
W2AR	Engine Inlet Total Corrected Flow, lb/sec
W2A	Engine Inlet Total Flow, lb/sec
P13Q12	Fan Bypass Pressure Ratio
E12D13	Fan Bypass Adiabatic Efficiency
P21Q2	Fan Hub Pressure Ratio
E2D21	Fan Hub Adiabatic Efficiency
ROPDEG	Fan Rotor Pitch Angle, degrees
W15	Bypass Duct Inlet Total Flow, lb/sec
T15	Bypass Duct Inlet Total Temperature, ° R
P15	Bypass Duct Inlet Total Pressure, psia
P18Q15	Bypass Duct Pressure Ratio
P18	Bypass Duct Jet Nozzle Throat Total Pressure, psia
A18	Bypass Duct Jet Nozzle Throat Actual Area, sq in.
AE18	Bypass Duct Jet Nozzle Throat Effective Area, sq in.
V19	Bypass Duct Jet Nozzle Exit Velocity, ft/sec
FG19	Bypass Stream Gross Thrust, lb
T25	Fan Hub Discharge Total Temperature, ° R
P25	Fan Hub Discharge Total Pressure, psia
P25Q21	Intercompressor Transition Duct Pressure Ratio
XNH	HP Compressor Physical Speed, rpm
PCNHR	HP Compressor Corrected Speed, %

Table 5-III. Separated Flow Turbofan Nomenclature (Concluded).

W25R	HP Compressor Corrected Inlet Airflow, lb/sec
W25	HP Compressor Inlet Airflow, lb/sec
P3Q25	HP Compressor Pressure Ratio
E25D3	HP Compressor Adiabatic Efficiency
P3Q2	Overall Cycle Pressure Ratio
T3	HP Compressor Discharge Total Temperature, ° R
P3	HP Compressor Discharge Total Pressure, psia
P4Q3	Combustor Pressure Ratio
E36D4	Main Combustion Efficiency
T4	HP Turbine 1st Stage Nozzle Inlet Total Temperature, ° R
W41	HP Turbine Rotor Inlet Gas Flow, lb/sec
T41	HP Turbine Rotor Inlet Total Temperature, ° R
E4D42	HP Turbine Adiabatic Efficiency
P4Q42	HP Turbine Pressure Ratio
T42	HP Turbine Discharge Total Temperature, ° R
W49	LP Turbine Rotor Inlet Total Gas Flow, lb/sec
T49	LP Turbine Rotor Inlet Total Temperature, ° R
P49	LP Turbine Inlet Total Pressure, psia
E48D5	LP Turbine Adiabatic Efficiency
P48Q5	LP Turbine Pressure Ratio
XNL48	LP Turbine Physical Speed, rpm
P55Q5	LP Turbine Frame Pressure Ratio
P8Q5	Primary Exhaust Duct Pressure Ratio
W8	Primary Jet Nozzle Throat Total Gas Flow, lb/sec
T8	Primary Jet Nozzle Throat Total Temperature, ° R
P8	Primary Jet Nozzle Throat Total Pressure, psia
A8	Primary Jet Nozzle Throat Actual Area, sq in.
AE8	Primary Jet Nozzle Throat Effective Area, sq in.
V9	Primary Jet Nozzle Exit Velocity, ft/sec
FG9	Primary Stream Gross Thrust, lb
FRAM	Ram Drag, lb

Note: In reverse mode the fan cycle stations are assumed consistent with direction of flow so that function of engine component is reversed (i.e., engine bypass duct exit is cycle Station 1, engine inlet throat is cycle Station 18).

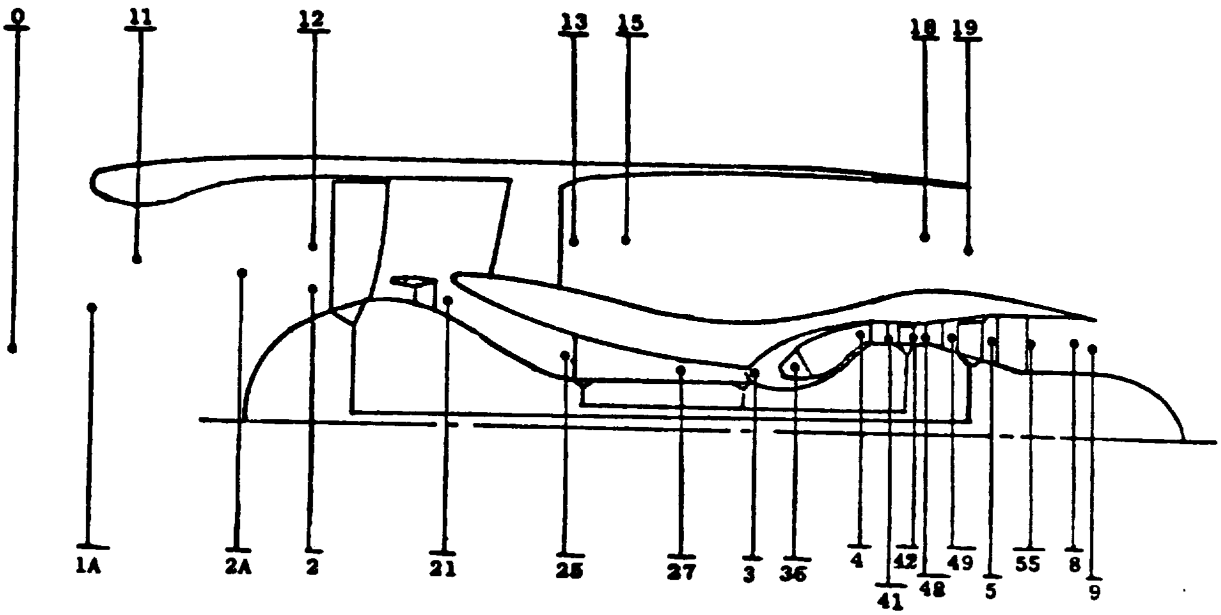

STATION	DESCRIPTION
0	Free Stream Air Conditions
1A	Total Nacelle Inlet
11	Inlet Throat
2A	Total Fan Front Face
2	Fan Hub Inlet
21	Fan Hub Discharge
25	HP Compressor Inlet
27	HP Compressor 5th Stage (Stator Exit)
3	HP Compressor Discharge (Stator Exit)
36	Combustor Inlet
4	Combustor Discharge (HP Turbine Vane Inlet)
41	HP Turbine Rotor Inlet
42	HP Turbine Discharge
48	LP Turbine Vane Inlet
49	LP Turbine Rotor Inlet
5	LP Turbine Discharge
55	LP Turbine Frame Discharge
8	Primary Exhaust Nozzle Throat
9	Primary Exhaust Nozzle Discharge
12	Fan Tip Inlet
13	Fan Tip Discharge
15	Bypass Duct Inlet
18	Bypass Exhaust Nozzle Throat
19	Bypass Exhaust Nozzle Discharge

Figure 5-7. Station Designations - Forward Thrust Mode.

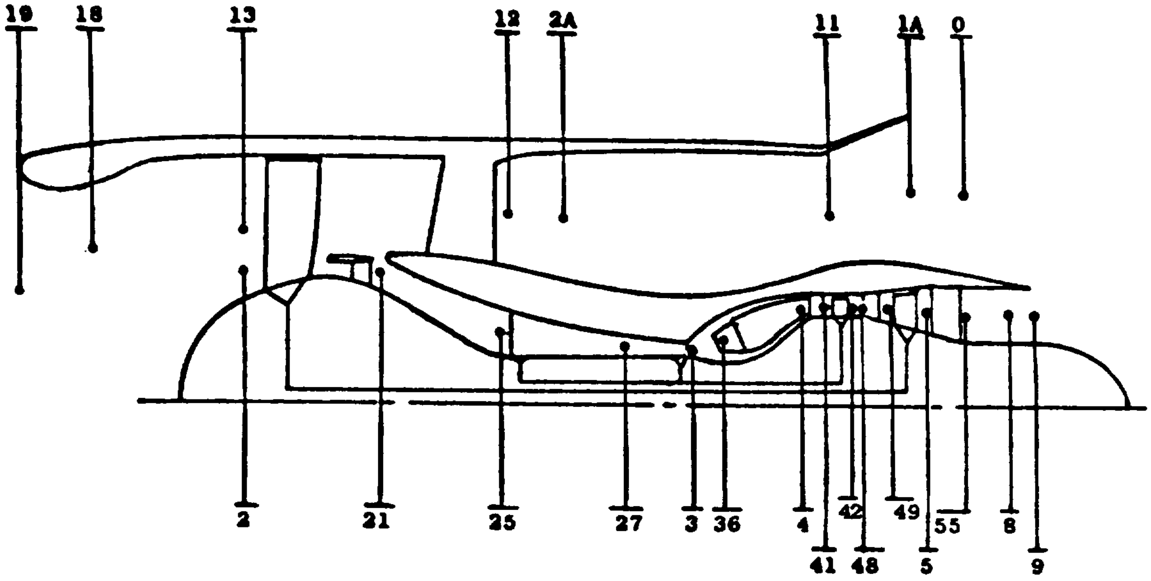

STATION	DESIGNATION
0	Free Stream Air Conditions
1A	Total Nacelle Inlet
11	Inlet Throat
2A	Total Fan Front Face
2	Fan Hub Inlet
21	Fan Hub Discharge
25	HP Compressor Inlet
27	HP Compressor 5th Stage (Stator Exit)
3	HP Compressor Discharge (Stator Exit)
36	Combustor Inlet
4	Combustor Discharge (HP Turbine Vane Inlet)
41	HP Turbine Rotor Inlet
42	HP Turbine Discharge
48	LP Turbine Vane Inlet
49	LP Turbine Rotor Inlet
5	LP Turbine Discharge
55	LP Turbine Frame Discharge
8	Primary Exhaust Nozzle Throat
9	Primary Exhaust Nozzle Discharge
12	Fan Tip Inlet
13	Fan Tip Discharge
18	Bypass Exhaust Nozzle Throat
19	Bypass Exhaust Nozzle Discharge

Figure 5-8. Station Designations - Reverse Thrust Mode.

of turbine exit swirl and Mach Number is much less likely to induce separation, and no additional factor on frame loss is applied at these conditions.

Possible modifications to the turbine frame flowpath were investigated to reduce the possibility of flow separation, but the velocity distribution in the frame could not be altered significantly, and a complete redesign of the frame was beyond the program scope. Since a flight version of the engine would not be restricted to use of an existing turbine frame, the separation problem only arises at this extreme operating condition on the experimental engine. To evaluate effects of this possible flow condition, extended loss representations were incorporated in the cycle. These representations were used only at the 0.8, 9114 m (30,000 ft) condition. At lower Mach flight conditions, there was no significant difference between the revised representation and the base frame loss assumptions.

In Columns 6 and 7 of Table 5-II are shown performance parameters at 0.7 Mach number, 7620 m (25,000 ft) which has developed as the cruise condition of principal interest in aircraft studies.

At the approach flight condition 41.2 m/sec, 61.0 m (80 knots, 200 ft), maximum power is established at 406 kg/sec (894 lb/sec) corrected fan flow resulting in an inlet throat Mach number of 0.79. Performance at this condition is shown in Column 8 of Table 5-II. Approach thrust is assumed to be 65% of the maximum (takeoff) thrust at this flight condition.

Alternative engine operating modes during approach are shown in Columns 9 through 11. The conditions shown in Column 9 are for the fan exhaust area (A18) and fan tip speed set to the takeoff values. This condition produces the best sfc, but also results in the lowest core speed, thus, penalizing engine acceleration time.

In Column 10 is shown performance with the fan nozzle opened up to 2.129 m^2 (3300 $in.^2$). In this position, the exit area is larger than the hingeline area and the nozzle acts as a diffuser. At this condition, the core speed is increased 139 rpm over the value at takeoff fan nozzle area.

Approach performance with the inlet throat Mach number set to 0.79 is shown in Column 11. The fan nozzle is opened to 2.323 m^2 (3573 $in.^2$). Engine operation at this condition may not be feasible, since the fan nozzle may not be able to diffuse to this large an area. It is planned to investigate specific capabilities during experimental engine testing.

The effects of these alternative approach settings on engine operating characteristics are shown in Figure 5-9. Inlet throat Mach number shows an increasing trend as A18 is increased. Fan nozzle exit velocity increases while core exit velocity decreases with increasing A18. As previously noted, core speed increases as area increases. Also included in Figure 5-9 for comparison are the corresponding characteristics with fan pitch angle fixed (instead of fan tip speed).

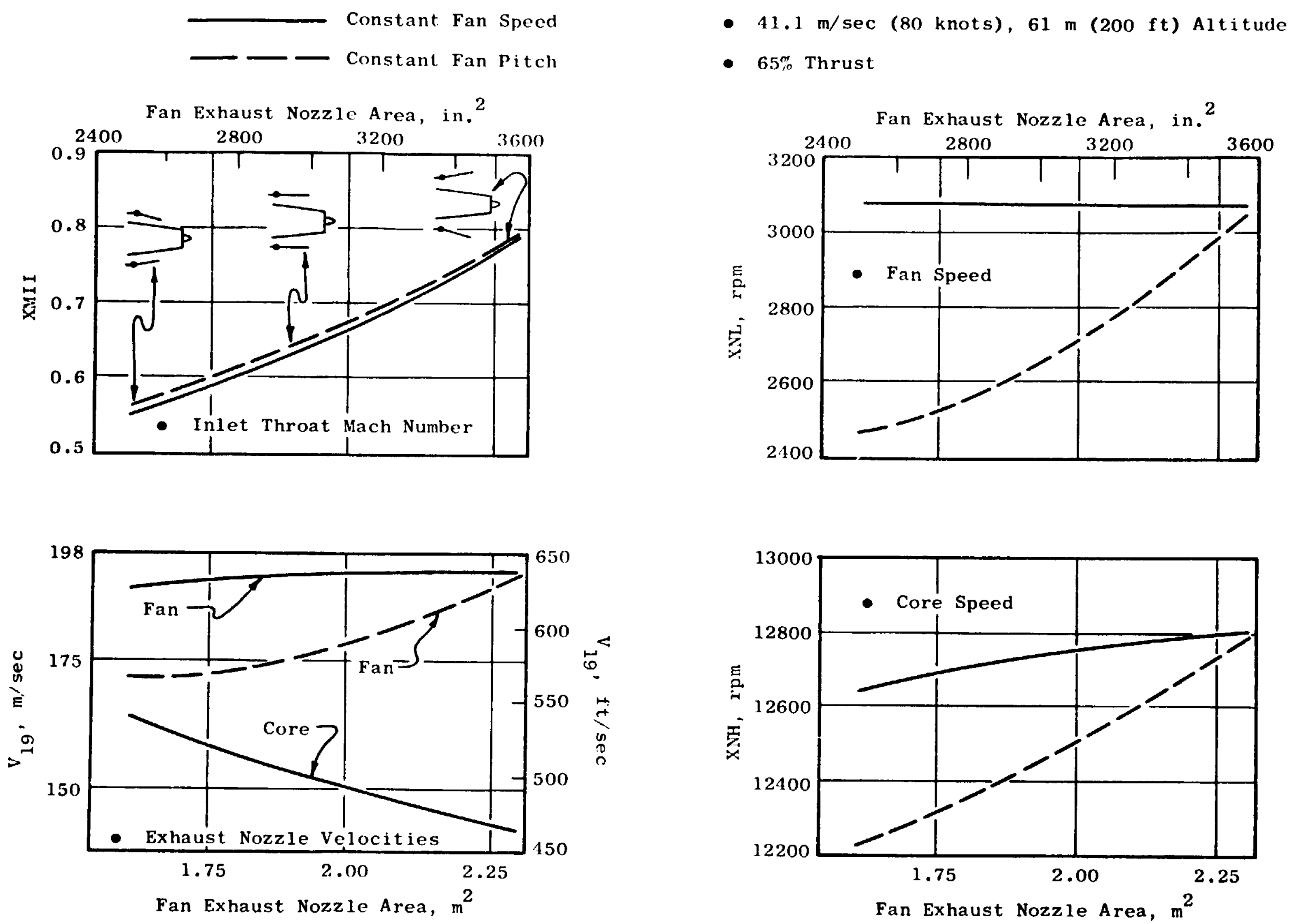

Figure 5-9. UTW Operating Characteristics During Approach.

Reverse mode internal cycle parameters and performance are shown in Table 5-II, Columns 12 and 13 for reverse through flat pitch and reverse through fan stall, respectively. Reverse through flat pitch results in poorer fan aerodynamic performance, and based on predicted fan characteristics, the 35 percent reverse thrust objective cannot be achieved with the flat pitch setting. The predicted maximum thrust with flat pitch (83° closed from nominal) is shown in Table 5-II for operation at limiting LP turbine speed, 8400 rpm.

Rotation of the rotor blades through fan stall results in better aerodynamic performance. Predictions show that the reverse objective of 35 percent can be attained at 89 percent corrected speed with stall pitch setting (95° open from nominal pitch).

SECTION 6.0

FAN AERODYNAMIC DESIGN

6.1 SUMMARY

An under-the-wing (UTW) and an over-the-wing (OTW) fan rotor will be built and tested as part of the NASA QCSEE Program. The UTW fan is a geared variable-pitch design with 18 composite fan blades. This concept, which includes full reverse thrust capability, is expected to offer significant advantages to a high-bypass fan system including:

- Lighter weight through the use of composite fan blades and by eliminating the heavy, large diameter thrust reverser
- Faster thrust response
- Improved off-design sfc
- Reduced off-design noise generation

At the major operating conditions of takeoff and maximum cruise, a corrected flow of 405.5 kg/sec (894 lbm/sec) was selected for both fans which enables common inlet hardware to yield the desired 0.79 average throat Mach number at the critical takeoff noise measurement condition. The aerodynamic design bypass pressure ratio is 1.34 for the UTW and 1.36 for the OTW which is intermediate between the takeoff and maximum cruise power settings. Takeoff pressure ratios are 1.27 for the UTW and 1.34 for the OTW. The takeoff corrected tip speeds are 289 m/sec (950 ft/sec) for the UTW and 354 m/sec (1162 ft/sec) for the OTW. These pressure ratios and speeds were selected on the basis of minimum noise within the constraints of adequate stall margin and core engine supercharging.

The UTW fan was designed to permit rotation of the blades into the reverse thrust mode of operation through both flat pitch (like a propeller) and stall pitch directions. The flowpath has been contoured to maintain tight blade tip and hub clearances throughout the blade actuation range.

The vane-frame, which is common to both engines, performs the dual function of an outlet guide vane for the bypass flow and a frame support for the engine components and nacelle. The UTW island configuration was selected specifically for reverse thrust mode of operation.

Design practices and rotor material selections are consistent with flight-designed fan rotors for both the UTW and the OTW. This includes consideration for fan LCF life and for such FAA flight requirements as burst speed margin and bird strike capability. All rotor components for the UTW fan rotor are of a flight weight design.

6.2 UTW FAN AERODYNAMIC DESIGN

6.2.1 Operating Requirements

Major operating requirements for the under-the-wing (UTW) fan (Figure 6-1) are takeoff, where noise and thrust are of primary importance, and maximum cruise, where economy and thrust are of primary importance. At takeoff a low fan pressure ratio of 1.27 was selected to minimize the velocity of the bypass stream at nozzle exit. A corrected flow of 405.5 kg/sec (894 lbm/sec) at this pressure ratio yields the required engine thrust. The inlet throat is sized at this condition for an average Mach number of 0.79 to minimize the forward propagation of fan noise. This sizing of the inlet throat prohibits higher corrected flow at altitude cruise. Required maximum cruise thrust is obtained by raising the fan pressure ratio to 1.39. The aerodynamic design point was selected at an intermediate condition which is a pressure ratio of 1.34 and a corrected flow of 408 kg/sec (900 lb/sec). Table 6-I summarizes the key parameters for these three conditions.

Table 6-I. UTW Variable-Pitch Fan Design Requirements.

Parameter	Design Point	Takeoff	Maximum Cruise
Total fan flow	408 kg/sec (900 lb/sec)	405.5 kg/sec (894 lb/sec)	405.5 kg/sec (894 lb/sec)
Pressure ratio - bypass flow	1.34	1.27	1.39
Pressure ratio - core flow	1.23	1.20	1.21
Bypass ratio	11.3	11.8	11.4
Pitch setting	Nominal	Open 2°	Closed 2°
Corrected tip speed	306 m/sec (1005 ft/sec	289 m/sec (950 ft/sec)	324 m/sec (1063 ft/sec)

6.2.2 Basic Design Features

A cross section of the selected UTW fan configuration is shown in Figure 6-2. There are 18 variable-pitch composite rotor blades. The solidity of the blades is 0.95 at the OD and 0.98 at the ID. The chord is linear with radius. This permits rotation of the blades into the reverse thrust mode of operation through both the flat pitch and the stall pitch directions. The spherical casing radius over the rotor tip provides good blade tip clearances throughout the range of blade pitch angle settings.

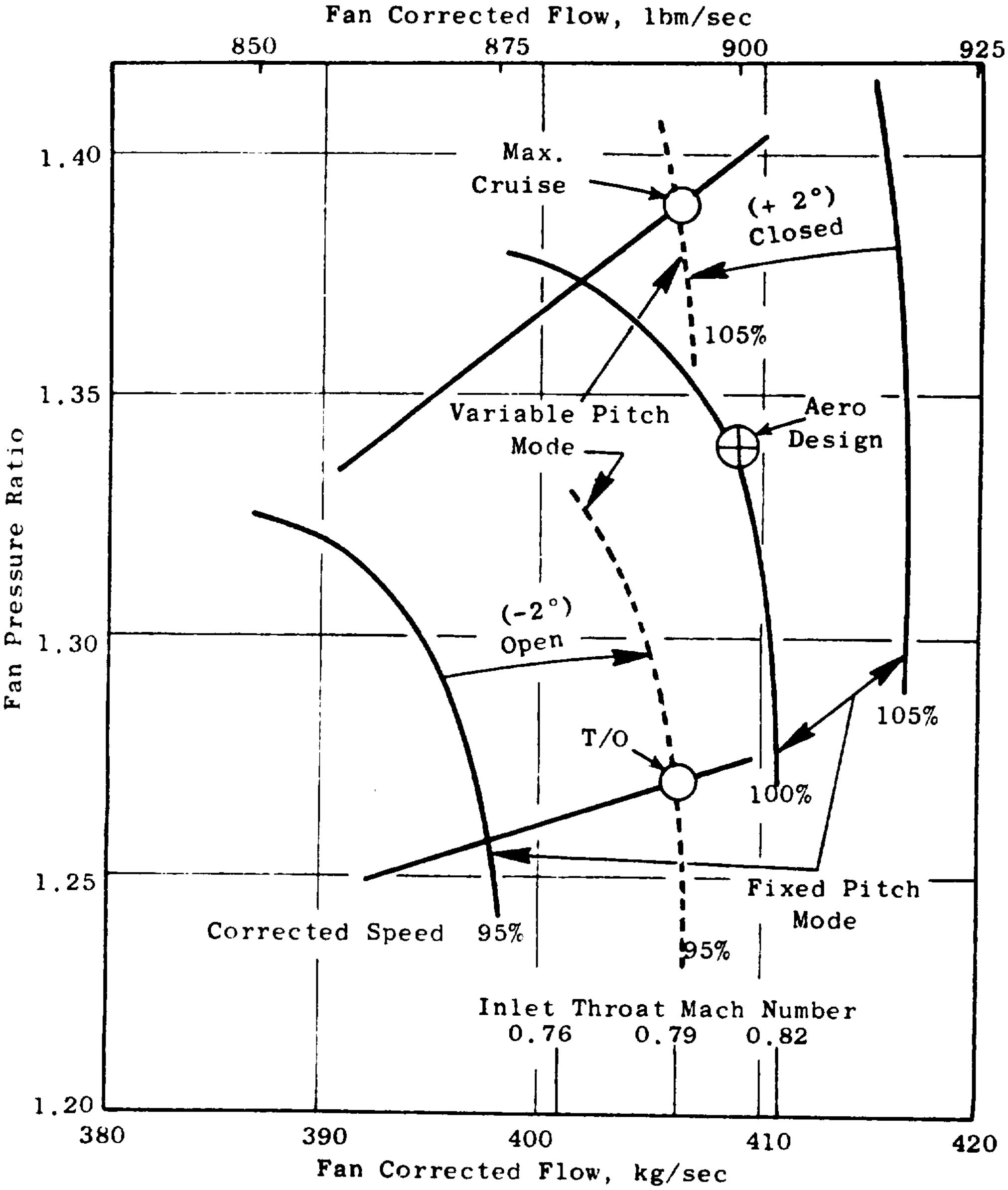

Figure 6-1. UTW Variable-Pitch Fan Design Requirements.

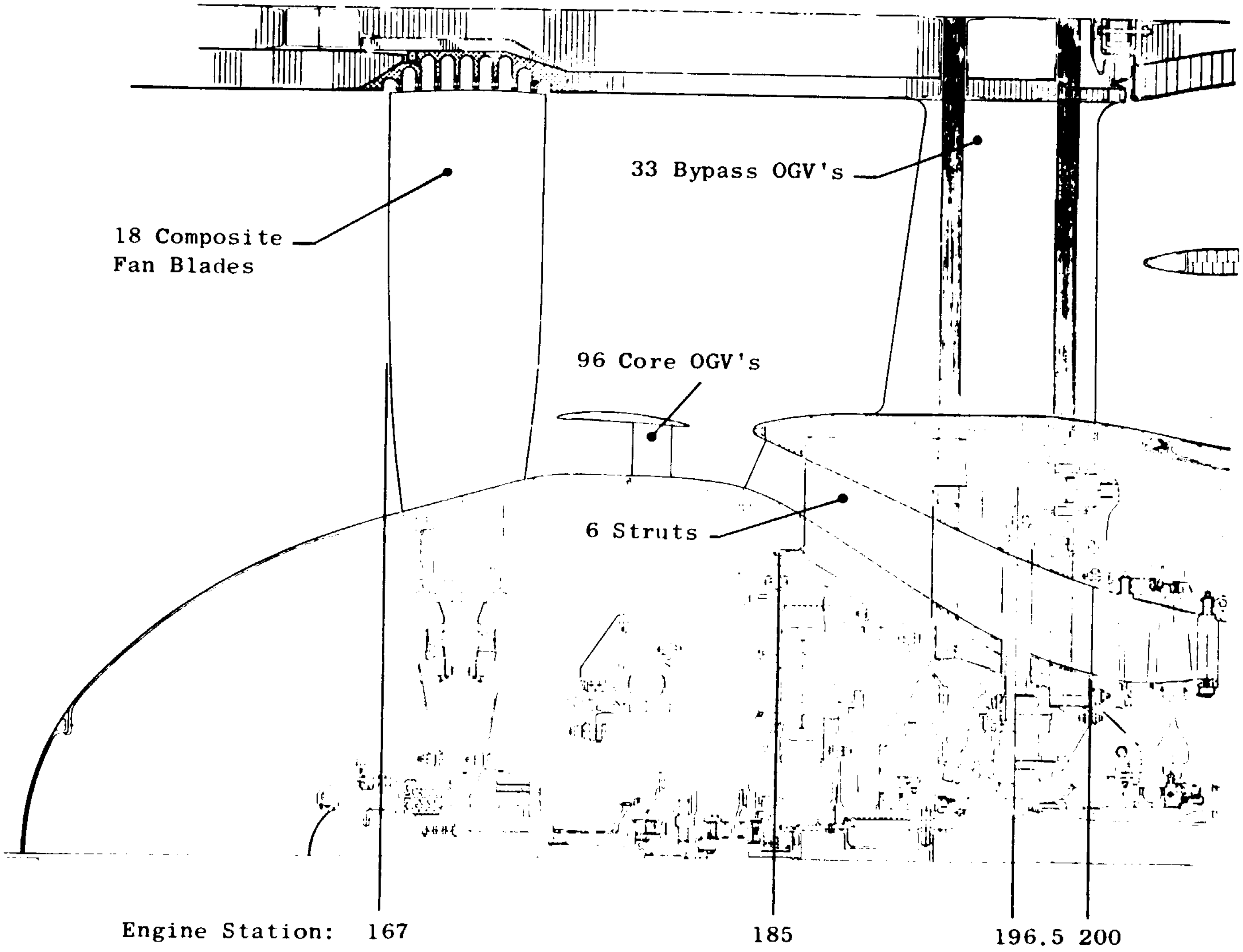
18 Composite Fan Blades
33 Bypass OGV's
96 Core OGV's
6 Struts
Engine Station: 167
185
196.5
200

Figure 6-2. Cross Section of UTW Variable-Pitch Fan.

Circumferential grooved casing treatment is incorporated over the rotor tip to improve stall margin. Stall margins are significant because a minimum fan tip speed was selected to minimize noise generation. The circumferential grooved casing treatment type was selected since this type of treatment improves stall margin and has shown negligible adverse impact on overall fan efficiency. An additional benefit of the casing treatment is to reduce material bulk over the blade tip, for a given clearance, which will reduce severity of an inadvertent blade rub as might be encountered during a bird strike.

The vane-frame is positioned at an axial distance downstream of the rotor trailing edge equal to 1.5 true rotor tip chords. The vanes are nonaxisymmetric in that five vane geometries, each with a different camber and stagger, are employed around the annulus. This nonaxisymmetric geometry is required to conform the vane-frame downstream flow field to the geometry of the plyon, which protrudes forward into the vane-frame, and simultaneously maintain a condition of minimum circumferential static pressure distortion upstream of the vane-frame. There are 33 vanes in the vane-frame which yields a vane-blade ratio of 1.83. Immediately following the rotor, in the hub region, is an annular ring or island. The 96 OGV's for the fan hub, or core portion flow, are in the annular space between the under side of the island and the hub. A full circumference axial gap separates the island trailing edge from the splitter leading edge. The splitter divides the flow into the bypass portion and core portion. There are six struts in the gooseneck which guide the fan hub flow into the core compressor.

The island configuration was selected specifically to permit the attainment of a high hub supercharging pressure ratio for forward pitch operation without causing a large core flow induction pressure drop during reverse pitch operation. In the forward mode of operation, a vortex sheet is shed from the trailing edge of the island in the form of a swirl angle discontinuity since most of the swirl in the flow under the island is removed by the core OGV. Total pressure on top of the island differs from that under the island only by the losses in the core OGV, hence the Mach numbers of the two streams are nearly the same. The General Electric CF6-6 fan incorporates a similar island configuration, except that the bypass OGV's are on top of the island and there is no swirl in the bypass flow at the island trailing edge. A vortex sheet is shed from the trailing edge of this island configuration also. This vortex sheet is in the form of a velocity magnitude discontinuity. The swirl angle is zero both on top of and under the island but the total pressures differ by the work input in the tip region of the 1/4 stage. Numerically, strength of the QCSEE UTW island shed vortex is approximately the same as the strength of the CF6-6 island shed vortex. Orientation of vortex vectors are rotated approximately 70°, however.

6.2.3 Reverse Flow

A major feature of the UTW fan is its ability to change the direction of fan thrust by reversing the direction of flow through the fan. This flow reversal affects the pressure level into the core engine (and, hence, the core engine's ability to produce power) in two ways. First, there is the direct loss of fan hub supercharging pressure; and second, there is the loss associated with inducting flow into the core engine such as the recoveries of the exlet, vane frame, turn around the splitter leading edge, core OGV's, and gooseneck struts. The hub supercharging pressure loss is obviously related to the magnitude of the design (forward mode) fan hub pressure ratio, but flow losses are also related to this magnitude. When operating in the reverse thrust mode, camber on the core OGV's is in the wrong direction and high hub supercharging in forward operation increases the camber of both bypass and core OGV's. Concern over this matter because of relatively high hub pressure ratio of the UTW fan was the primary reason for selecting the island approach. The major advantage to this configuration is that flow can enter the core compressor duct through the axial gap between the island and splitter and thereby avoid the problem of adversely oriented camber on the core OGV's. The swirling flow must still, of course, pass through the six axially oriented struts in the core inlet gooseneck. Relatively, this path for the flow is much less restrictive. A second benefit is that bluntness of the splitter leading edge, compared to the island leading edge (which would be the splitter leading edge if the axial gap were filled), is conducive to minimizing losses associated with reversing the axial component of the core portion flow from its forward direction in the bypass duct to its aft direction in the core transition duct.

Reverse fan thrust can be achieved by rotating the blades through the flat pitch (like a propeller) or stall pitch directions. Rotation of the blades into the reverse thrust condition puts a constraint on selection of blade solidity. This depends primarily on the direction in which the blades are rotated and the blade twist. The constraint is on those blade sections which pass through a tangential orientation, e.g., the leading edge of each blade must be able to pass the trailing edge of the adjacent blade, or physical interference will result. Therefore, those sections must have a solidity less than unity.

Figure 6-3 shows a tip and hub section of two adjacent blades in nominal, reverse through stall, and reverse through flat pitch orientations. The 45° tip stagger for both reverse through flat and reverse through stall was selected based on experimental reverse thrust performance. For blade rotation through the flat pitch direction, the entire blade span is constrained to a solidity less than one. For rotation through the stall pitch direction, the outer portion of the blade is not constrained. However, because of the 44° twist in the blade, the chord of the hub region cannot be increased significantly without interference. The assumed orientation of the tip section would have to be in error on the order of 5° before significant hub region chord increase could be accommodated. Even if a hub region chord increase could be accommodated, a significant

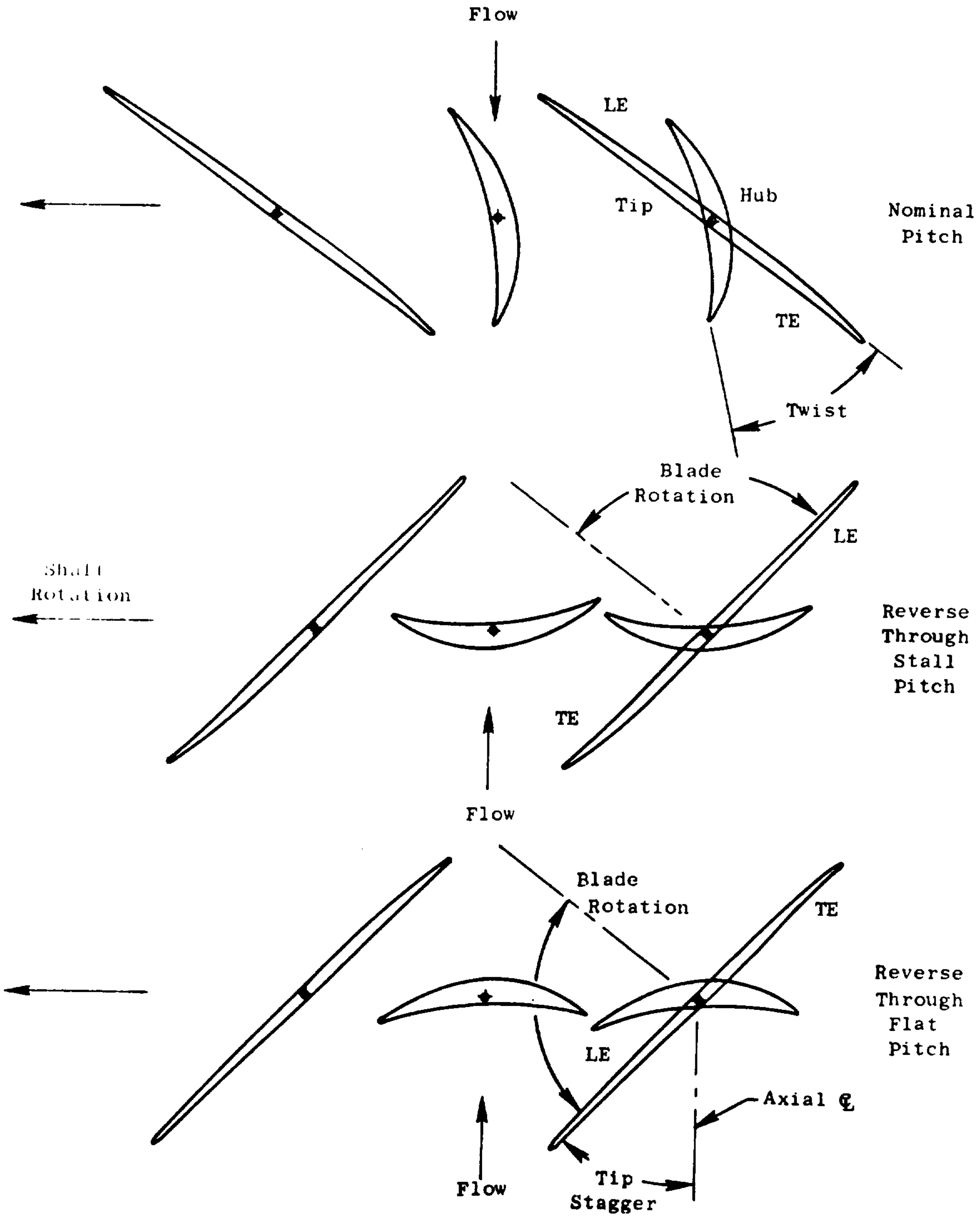
Flow
LE
Hub
Tip
Nominal Pitch
TE
Twist
Blade Rotation
LE
Shaft Rotation
Reverse Through Stall Pitch
TE
Flow
Blade Rotation
TE
Reverse Through Flat Pitch
LE
Axial ℄
Tip Stagger
Flow

Figure 6-3. UTW Fan Blade Geometry at Different Pitch Angle Settings.

increase in supercharging potential is probably not available because the implied increase in blade twist would probably cause a physical interference.

It was therefore concluded that a hub solidity less than unity was a design requirement for reverse through stall pitch rather than a compromise to permit reverse through flat pitch.

6.2.4 Performance Representation with Variable Pitch

The variable-pitch feature of the UTW fan adds a third independent variable to the representation of fan performance in that, in addition to normal independent variables of speed and operating line, the blade pitch angle is also required. It has been found, however, that experimental stage characteristics at different rotor pitch angle settings can be collapsed into a nearly universal characteristic applicable for all blade angle settings. The method used to collapse the characteristics was to deduce rotor incidence and deviation angle from the test data and then calculate performance of the stage at nominal blade angle with the rotor operating at this incidence and deviation angle and the test efficiency. A separate correlation of aerodynamic loading is used to identify a stall limit, as the collapsing technique breaks down due to the change in aerodynamic loading inherent in the transformation. Figure 6-4 shows the stage characteristics assumed for the UTW fan at 100% corrected speed for a range of pitch angles.

In the reverse flow mode of operation a similar, but simplified, form of the universal characteristic approach is used to represent fan performance. The same collapsing technique is incorporated to include the effect of blade angle setting.

6.2.5 Detailed Configuration Design

The corrected tip speed at the aerodynamic design point was selected at 306 m/sec (1005 ft/sec). This selection is a compromise for design purposes between 289 m/sec (950 ft/sec) at takeoff and 324 m/sec (1063 ft/sec) at maximum cruise. The objective design point adiabatic efficiency is 88% for the bypass portion and 78% for the core portion. A stall margin of 16% is projected at takeoff. This stall margin is provided at minimum tip speed by incorporating circumferential grooved casing treatment over the rotor tip. Minimum tip speed is important because of the favorable impact of low tip speed on fan generated noise, fan efficiency in the transonic region, and mechanical design of the variable-pitch system. An inlet radius ratio of 0.44 balances the desire to minimize fan diameter within the physical constraints of the variable-pitch mechanism and gear box and good fan hub supercharging for the core engine. A fan inlet flow per annulus area of 199 kg/sec-m^2 (40.8 lb/sec-ft^2) at the design point results in a tip diameter of 1.803 m (71.0 in.).

The standard General Electric axisymmetric flow computation procedure was employed in calculating the velocity diagrams. Several calculation

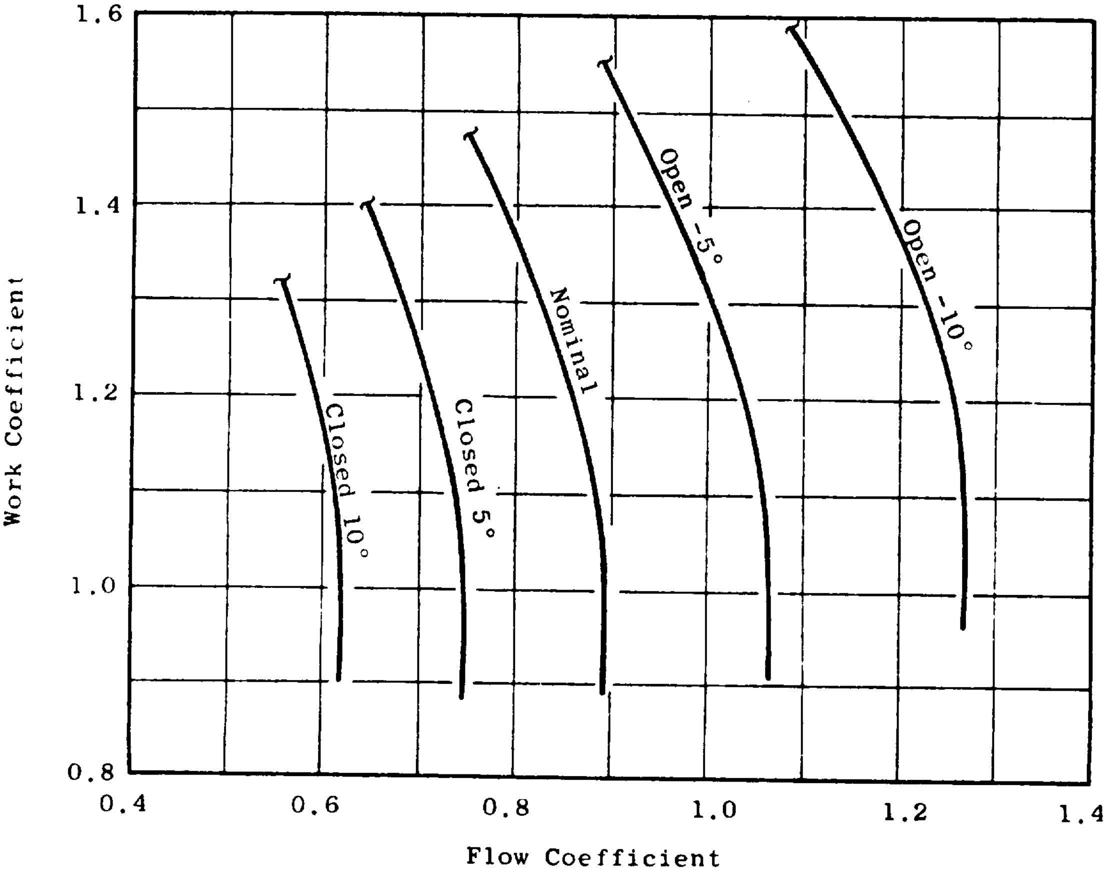

Figure 6-4. UTW Fan Stage Characteristics at 100% Speed for Various Pitch Settings.

stations were included internal to the rotor blade to improve overall accuracy of the solution in this region. The physical island geometry is represented in the calculations. Forward of the island and in the axial space between the island and the splitter, calculation stations span the radial distance from OD to ID. Within the axial space of the island, calculation stations span the radial distance between the OD and topside of the island and between the underside of the island and hub contour. In the bypass and core inlet ducts, calculation stations are also included. At each calculation station effective area coefficients consistent with established design practice were assumed.

A special constraint is necessary in the aerodynamic design of the island geometry in that a smooth flow of Kutta condition must be satisfied at the trailing edge of the island. The technique employed in this design was to specify a calculation station at the axial location of the island trailing edge which spanned the total flowpath height from OD to ID. Using this technique, a continuous radial distribution of static pressure results which was assumed to be consistent with matching the Kutta condition. The radial location of the island stream function at this calculation station was determined and upstream geometry of the island was then adjusted to provide a smooth continuous contour blending into this point. Iteration was obviously necessary because of interaction of the assumed geometry with the calculated radial location of the island stream function. Convergence was found to be quite rapid. An artificial radial displacement was incorporated between the island upper surface streamline and island lower surface streamline in order to avoid problems in calculating the streamline curvatures. This displacement was assumed equal to island thickness at the trailing edge and was smoothly blended to zero at an axial distance of approximately 10 edge thicknesses downstream.

The design radial distribution of rotor total pressure ratio is shown in Figure 6-5. This distribution is consistent with a stage average pressure ratio of 1.34 in the bypass region. Despite lower than average pressure ratio in the hub region, it has been maximized to the extent possible subject to the constraint of acceptable rotor diffusion factors so as to provide maximum core engine supercharging. A stage average pressure ratio of 1.23 results at the core OGV exit. The radial distribution of rotor efficiency assumed for the design is shown in Figure 6-6. The assumption of efficiency, rather than total pressure loss coefficient, is a General Electric design practice for rotors of this type. This distribution was based on measured results from similar configurations with adjustments to account for recognized differences. Radial distribution of rotor diffusion factor which results from these assumptions is shown in Figure 6-7. The moderately high diffusion factor in the tip region of the blade, where stall generally initiates, confirm the need for casing treatment to obtain adequate margin. Radial distributions of rotor relative Mach number and air angle are shown in Figures 6-8 and 6-9, respectively.

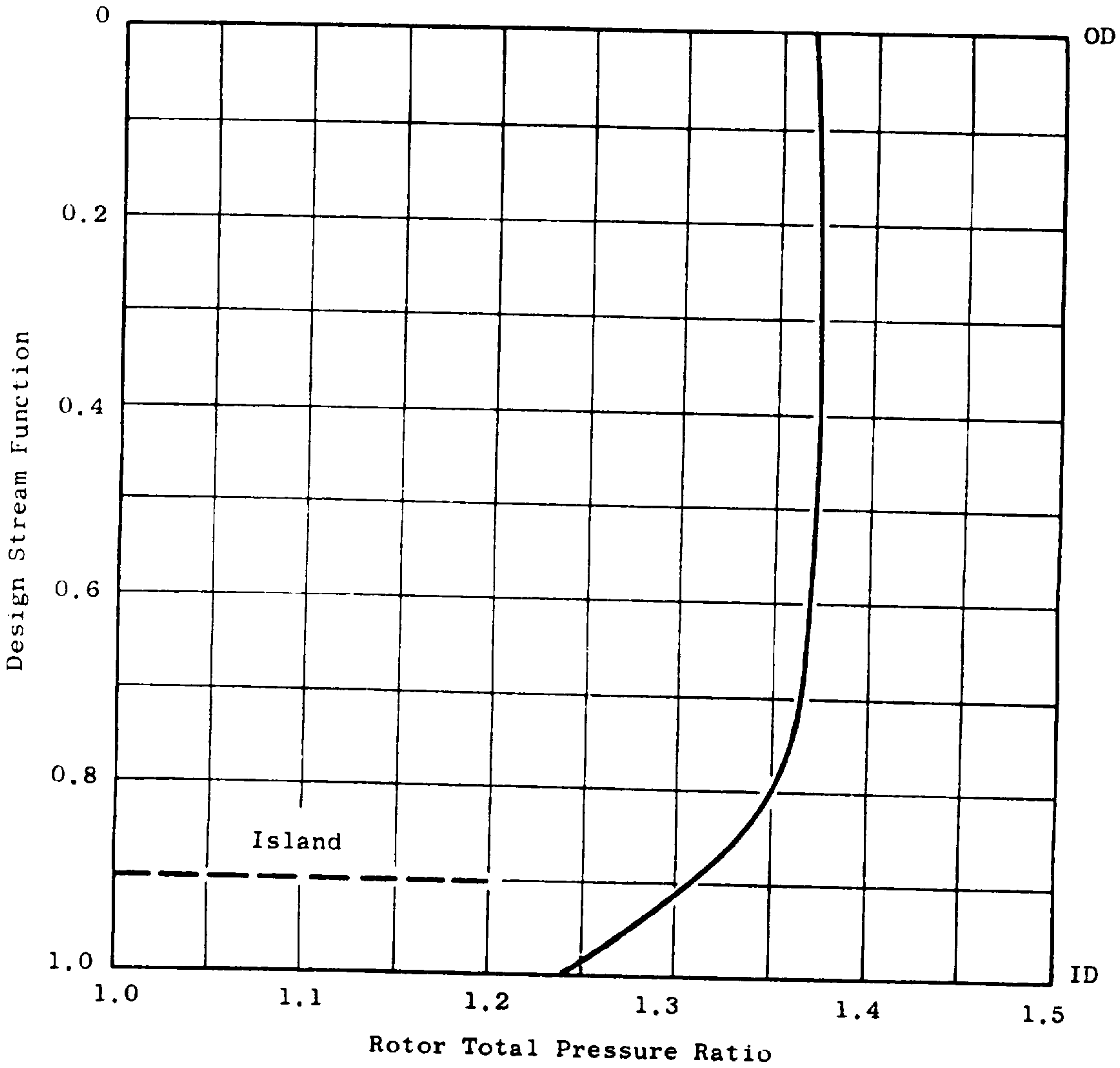

Figure 6-5. Radial Distribution of Rotor Total Pressure Ratio.

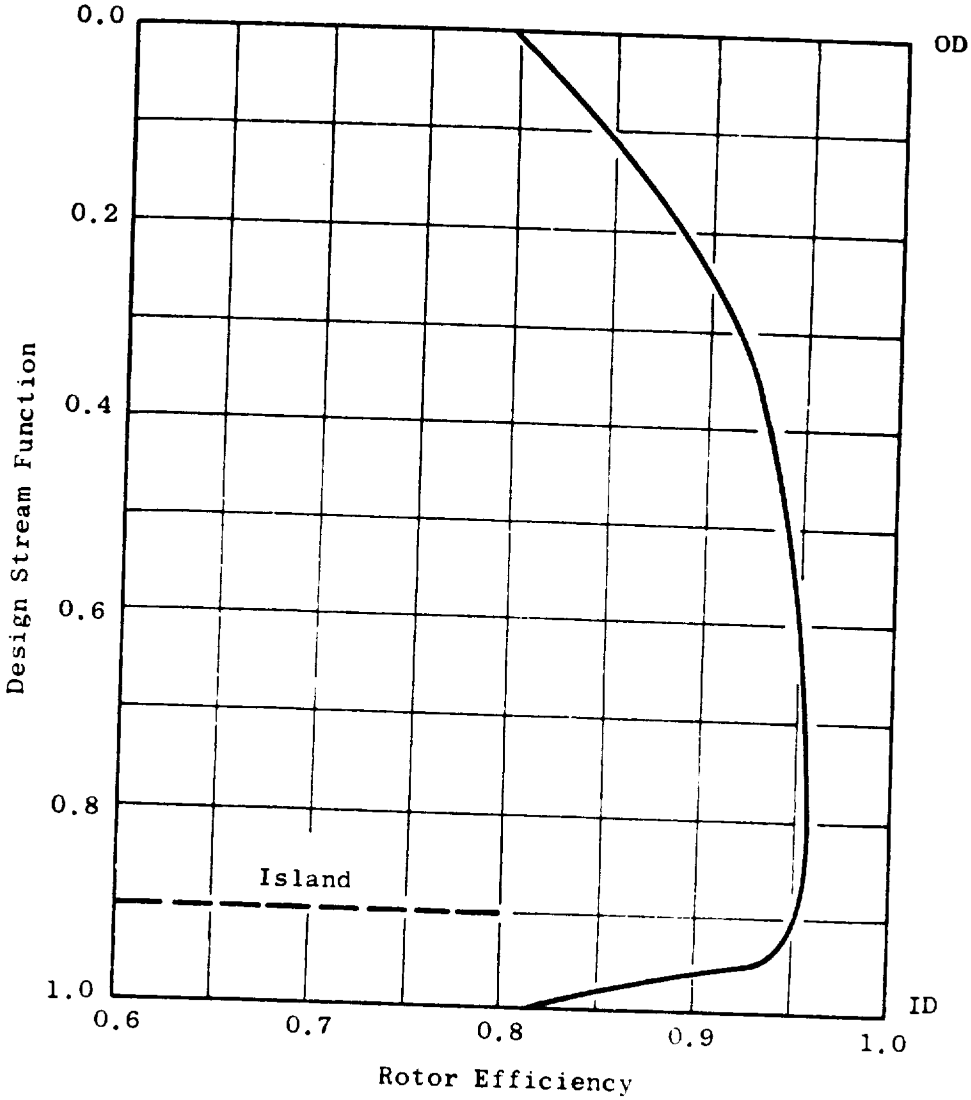

Figure 6-6. Radial Distribution of Rotor Efficiency.

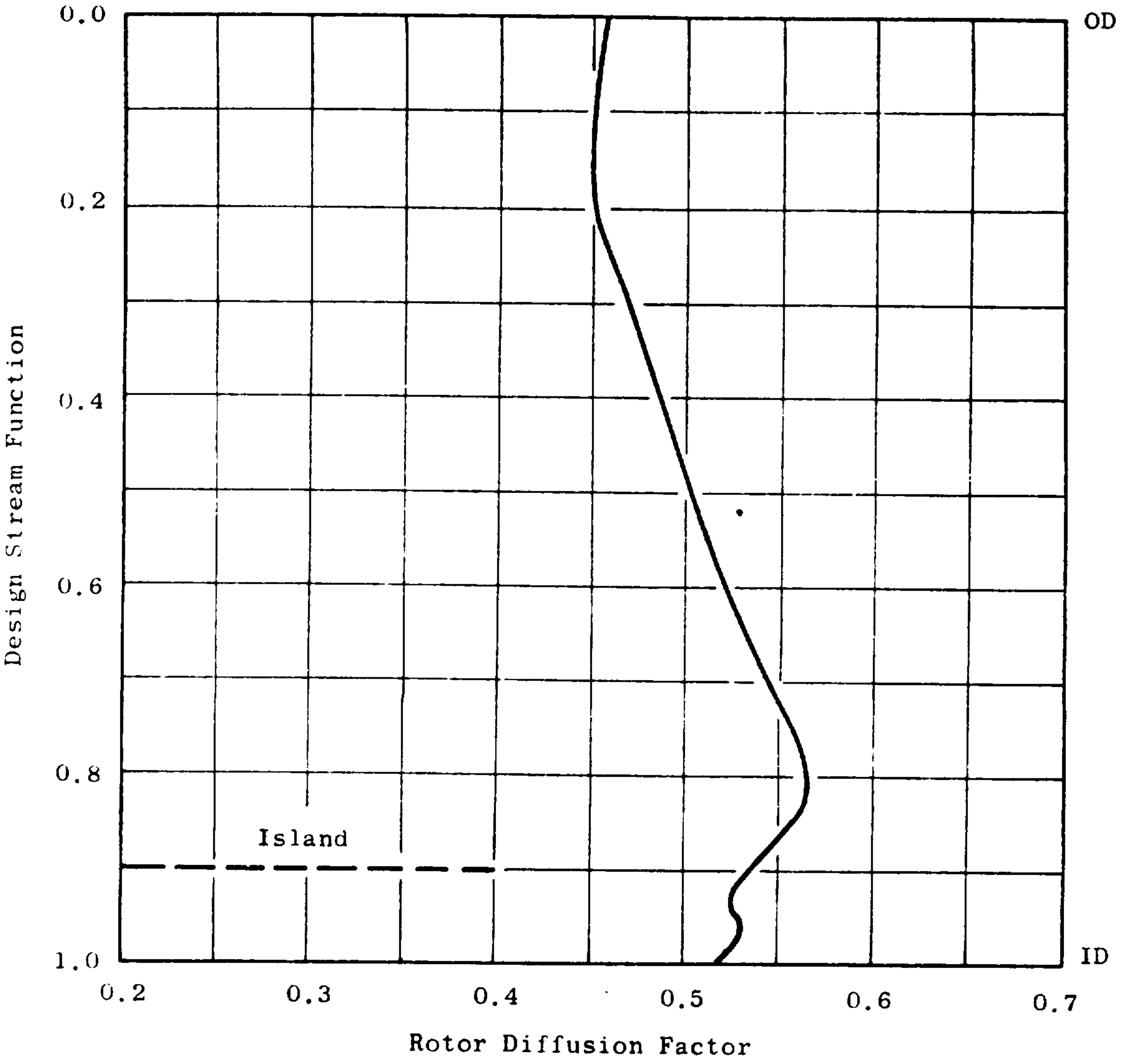

Figure 6-7. Radial Distribution of Rotor Diffusion Factor.

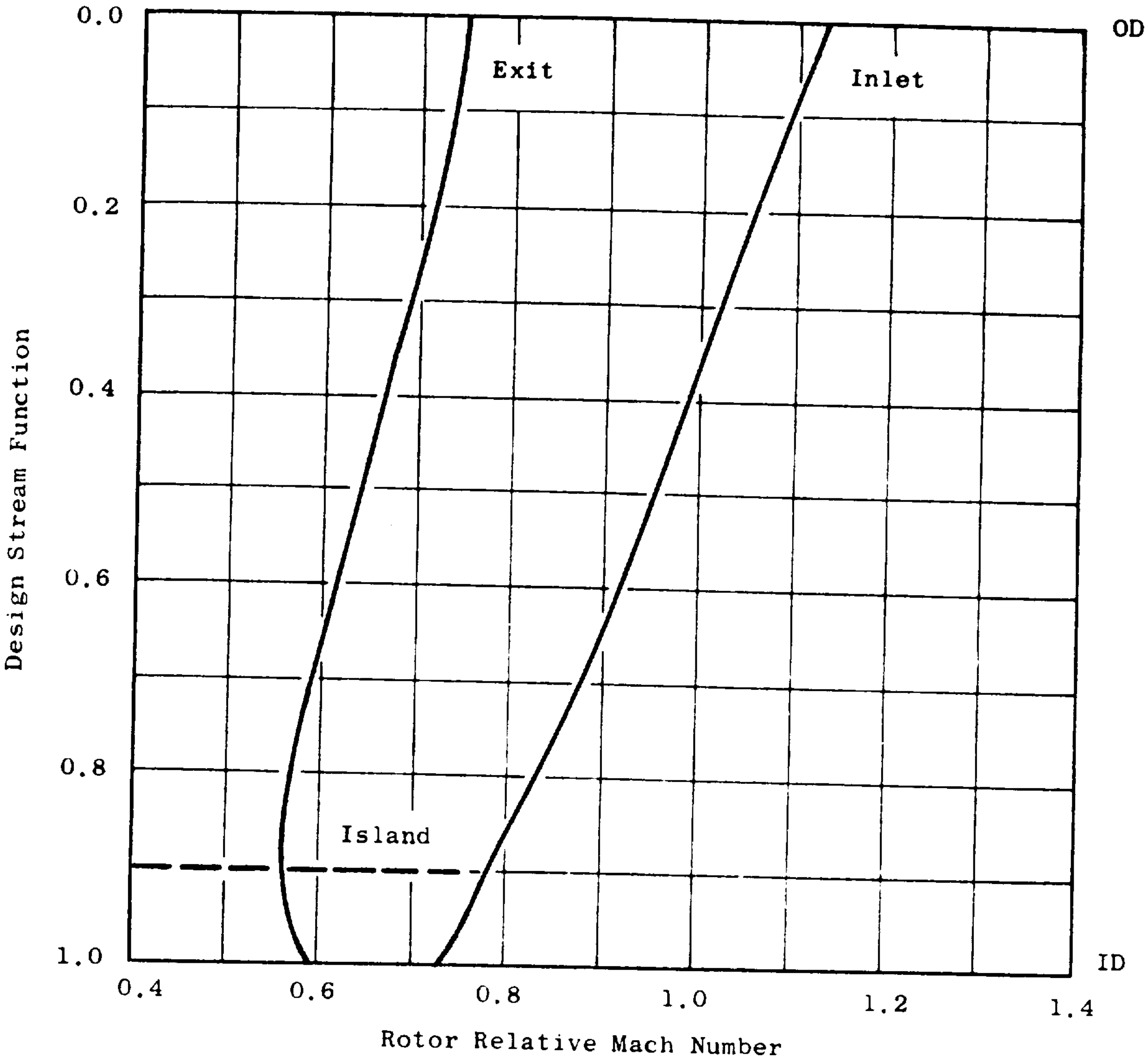

Figure 6-8. Radial Distribution of Rotor Relative Mach Numbers.

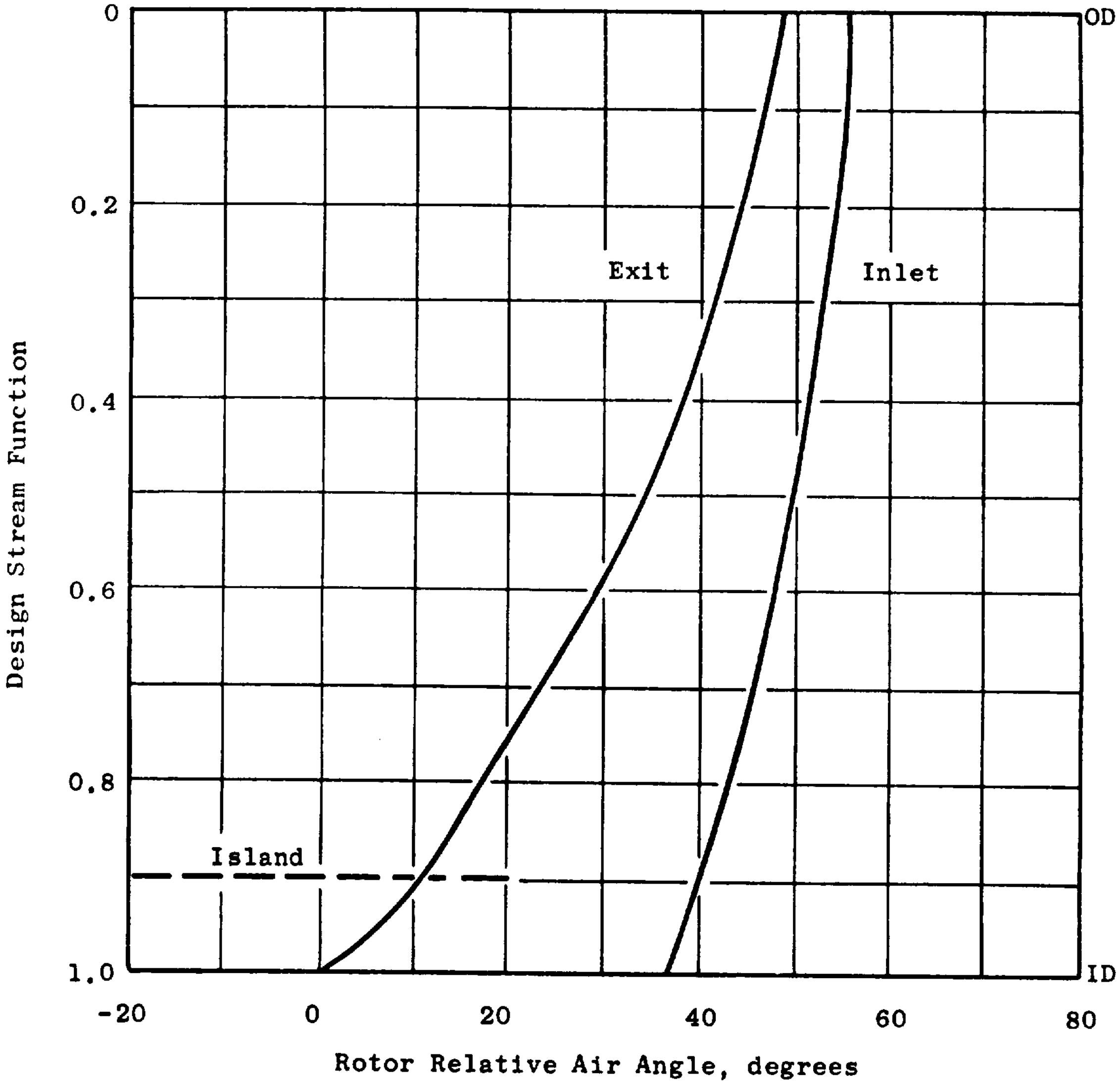

Figure 6-9. Radial Distribution of Rotor Relative Air Angles.

The assumed radial distribution of total-pressure-loss coefficient for the core portion OGV is shown in Figure 6-10. The relatively high level (∿0.2) particularly in the ID region, is in recognition of the very high bypass ratio of the UTW engine and, accordingly, the small size of the core OGV compared to the rotor. The annulus height of the core OGV is approximately one-half of the rotor staggered spacing, a significant dimension when analyzing secondary flow phenomena. It is anticipated that the core OGV will be influenced by rotor secondary flow over the entire annulus height. The diffusion factor, Mach number and air angle radial distributions which result from the design assumptions are also shown in Figure 6-10. An average swirl of 0.104 radian (6°) is retained in the fluid at exit from the core OGV. This was done to lower its aerodynamic loading and the magnitude of the vortex sheet shed from the island. The transition duct (core inlet) struts (6) are cambered to accept this swirl and remove it prior to entrance into the core engine.

A tabulation of significant blade element parameters for the UTW design is presented in Table 6-II.

6.2.6 Rotor Blade Design

Detailed layout procedures employed in design of the fan blade generally parallel established design procedures. In the tip region of the blade, where inlet relative flow is supersonic, the uncovered portion of the suction surface was set to ensure that maximum flow passing capacity is consistent with the design flow requirement. Incidence angles in the tip region were selected according to transonic blade design practice which has yielded good overall performance for previous design. In the hub region, where inlet flow is subsonic, incidence angles were selected from NASA cascade data correlations.

The blade trailing edge angle was established by the deviation angle which was obtained from Carter's Rule applied to the camber of an equivalent two-dimensional cascade with an additive empirical adjustment, X. This adjustment is derived from aerodynamic design and performance synthesis for this general type of rotor. Incidence and deviation angles and the empirical adjustment angle employed in the design are shown in Figure 6-11.

Over the entire blade span, the minimum passage area, or throat, must be sufficient to pass the design flow including allowances for boundary layer, losses, and flow nonuniformities. In the transonic and supersonic region, the smallest throat area, consistent with permitting design flow to pass, is desirable since this minimizes overexpansions on the suction surface. A further consideration was to minimize disturbances to the flow along the forward portion of the suction surface to minimize forward propagating waves that might provide an additional noise source. Design experience guided the degree to which each of these desires was applied to individual section layouts. The percent throat margin, percentage by which the ratio of the effective throat area to the capture area exceeds

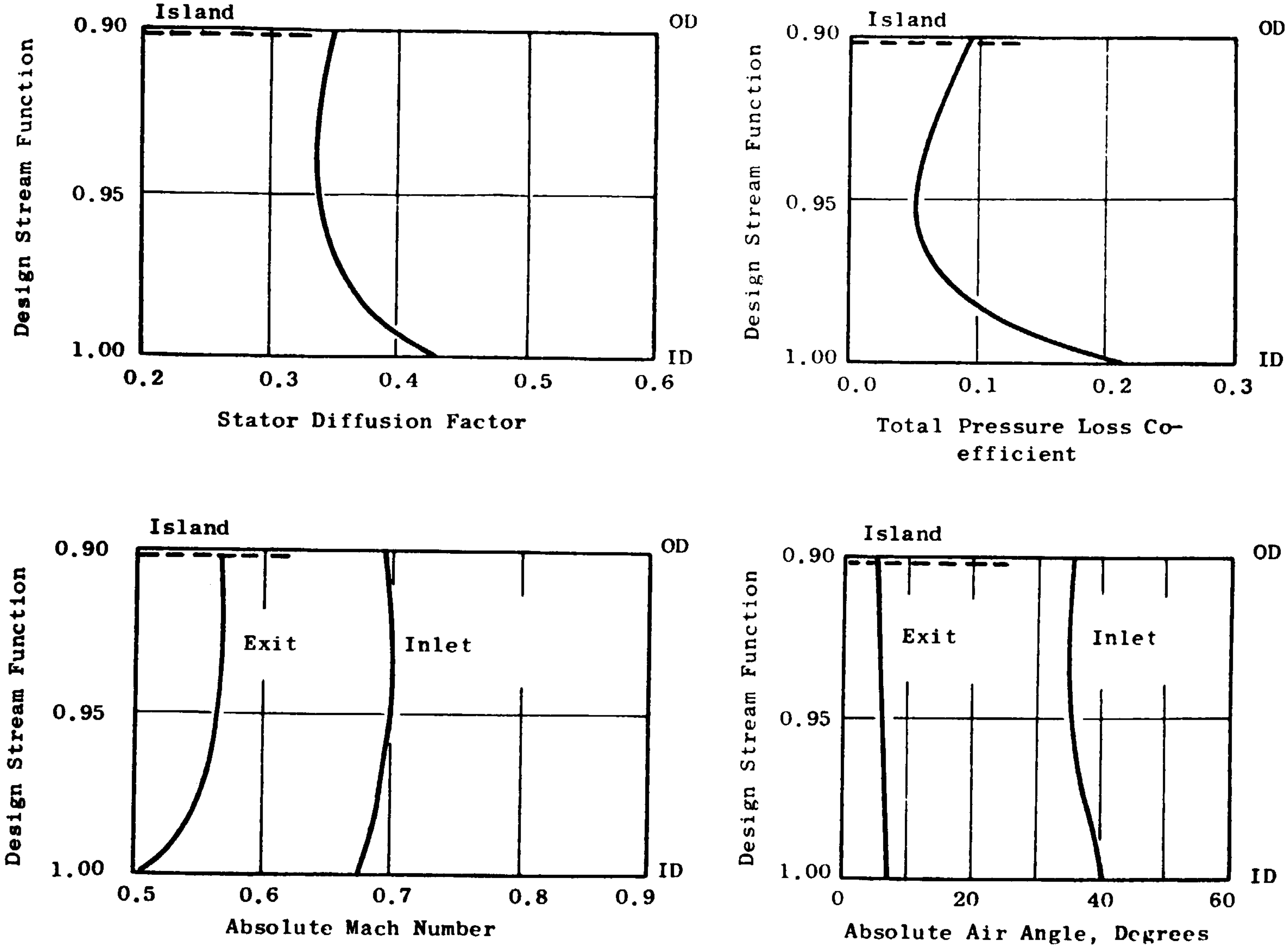

Figure 6-10. Radial Distribution of Design Parameters for Core OGV.

Table 6-II. Design Blade Element Parameters for QCSEE UTW Fan.

NOMENCLATURE FOR TABULATION

HEADING	IDENTIFICATION	METRIC UNITS
GENERAL		
SL	STREAMLINE NUMBER	-
PSI	STREAM FUNCTION	-
RADIUS	STREAMLINE RADIUS	CM.
% IMM	PERCENT IMMERSION FROM OUTER WALL	%
Z	AXIAL DIMENSION	CM.
BLKAGE	ANNULUS BLOCKAGE FACTOR	-
FLOW	WEIGHT FLOW	KG/SEC
ANGLES AND MACH NUMBERS		
PHI	MERIDIONAL FLOW ANGLE	DEG.
ALPHA	ABSOLUTE FLOW ANGLE =ARCTAN (CU/CZ)	DEG.
BETA	RELATIVE FLOW ANGLE =ARCTAN (-WU/CZ)	DEG.
M-ABS	ABSOLUTE MACH NUMBER	-
M-REL	RELATIVE MACH NUMBER	-
VELOCITIES		
C	ABSOLUTE VELOCITY	M/SEC
W	RELATIVE VELOCITY	M/SEC
CZ	AXIAL VELOCITY	M/SEC
U	BLADE SPEED	M/SEC
CU	TANGENTIAL COMPONENT OF C	M/SEC
WU	TANGENTIAL COMPONENT OF W	M/SEC
FLUID PROPERTIES		
PT	ABSOLUTE TOTAL PRESSURE	N/SQ.CM.
TT	ABSOLUTE TOTAL TEMPERATURE	DEG-K
TT-REL	RELATIVE TOTAL TEMPERATURE	DEG-K
PS	STATIC PRESSURE	N/SQ.CM.
TS	STATIC TEMPERATURE	DEG-K
RHO	STATIC DENSITY	KG/CU.METER
EFF	CUMULATIVE ADIABATIC EFFICIENCY REFERENCED TO PTI, TTI	-
PTI	INLET ABSOLUTE TOTAL PRESSURE	N/SQ.CM.
TTI	INLET ABSOLUTE TOTAL TEMPERATURE	DEG-K
AERODYNAMIC BLADING PARAMETERS		
TPLC	TOTAL PRESSURE LOSS COEFFICIENT	-
PR-ROW	TOTAL PRESSURE RATIO ACROSS BLADE ROW	-
DEL-T	TOTAL TEMPERATURE RISE ACROSS ROTOR	DEG-K
D	DIFFUSION FACTOR	-
DP/Q	STATIC PRESSURE RISE COEFFICIENT	-
CZ/CZ	AXIAL VELOCITY RATIO ACROSS BLADE ROW	-
SOLDTY	SOLIDITY	-
R-AVG	AVERAGE STREAMLINE RADIUS ACROSS BLADE ROW	CM.
F-TAN	TANGENTIAL BLADE FORCE PER UNIT BLADE LENGTH	N/CM
F-AXL	AXIAL BLADE FORCE PER UNIT BLADE LENGTH	N/CM
F-COEF	FLOW COEFFICIENT =CZ1/U1	-
T-COEF	WORK COEFFICIENT =(2*G*J*CP*DEL-T)/(U2*U2)	-

Table 6-II. Design Blade Element Parameters for QCSEE UTW Fan (Continued).

```
                                      STATION    1.00000     Z    423.926830   ROTOR     INLET                          METRIC UNITS

SL    PSI      RADIUS   % IMM     PHI     ALPHA     BETA   M-ABS  M-REL      C        W       CZ       U          CU      WU      SL
 1  0.        90.1702    0.      0.        0.      56.03  0.630  1.128   206.4    369.4   206.4   306.3        0.    -306.3    1
 2  0.1000    86.5671    7.2     2.31      0.      55.35  0.620  1.091   203.5    357.6   203.3   294.1        0.    -294.1    2
 3  0.2500    80.7672   18.7     3.55      0.      53.97  0.609  1.034   199.9    339.5   199.5   274.4        0.    -274.4    3
 4  0.4000    74.5029   31.2     5.45      0.      51.68  0.612  0.985   201.0    323.2   200.1   253.1        0.    -253.1    4
 5  0.6900    60.5384   59.1    10.26      0.      46.06  0.614  0.877   201.4    287.8   198.2   205.7        0.    -205.7    5
 6  0.8000    54.2263   71.7    12.60      0.      43.31  0.610  0.829   200.3    272.1   195.4   184.2        0.    -184.2    6
 7  0.9420    44.6160   90.8    15.73      0.      38.32  0.607  0.762   199.3    250.3   191.8   151.6        0.    -151.6    7
 8  0.9610    43.1564   93.7    15.97      0.      37.39  0.608  0.754   199.5    247.6   191.8   146.6        0.    -146.6    8
 9  0.9810    41.5660   96.9    16.09      0.      36.24  0.611  0.747   200.5    245.2   192.7   141.2        0.    -141.2    9
10  1.0000    40.0051  100.0    15.80      0.      34.85  0.619  0.745   202.9    244.2   195.2   135.9        0.    -135.9   10

SL    PSI      RADIUS     PT        TT      TT-REL       PS       TS       RHO      PT/PTI   TT/TTI      EFF     BLKAGE        SL
 1  0.        90.1702   10.132    288.16   334.86     7.755   266.97  1.01199    1.0000  1.00000             0.98000        1
 2  0.1000    86.5671   10.132    288.16   331.20     7.816   267.56  1.01763    1.0000  1.00000             0.98000        2
 3  0.2500    80.7672   10.132    288.16   325.63     7.888   268.27  1.02437    1.0000  1.00000             0.98000        3
 4  0.4000    74.5029   10.132    288.16   320.04     7.867   268.06  1.02239    1.0000  1.00000             0.98000        4
 5  0.6900    60.5384   10.132    288.16   309.21     7.858   267.97  1.02157    1.0000  1.00000             0.98000        5
 6  0.8000    54.2263   10.132    288.16   305.05     7.881   268.20  1.02374    1.0000  1.00000             0.98000        6
 7  0.9420    44.6160   10.132    288.16   299.59     7.902   268.40  1.02565    1.0000  1.00000             0.98000        7
 8  0.9610    43.1564   10.132    288.16   298.86     7.897   268.35  1.02517    1.0000  1.00000             0.98000        8
 9  0.9810    41.5660   10.132    288.16   298.08     7.876   268.15  1.02326    1.0000  1.00000             0.98000        9
10  1.0000    40.0051   10.132    288.16   297.35     7.828   267.68  1.01876    1.0000  1.00000             0.98000       10

                                                MASS AVERAGED VALUES
  PT/PTI    1.0000    EFF              PT    10.132    TT    288.16    TT/TTI    1.00000    CZ    198.76
                  CORR. FLOW    408.233     CORR. RPM    3244.1      CORR. U-TIP    306.3

                                              PTI       10.132
                                              TTI      288.161
                                              GAMMA     1.4000
```

Table 6-II. Design Blade Element Parameters for QCSEE UTW Fan (Continued).

STATION 1.50000 Z 142.722866 ROTOR EXIT

METRIC UNITS

SL	PSI	RADIUS	% IMM	PHI	ALPHA	BETA	M-ABS	M-REL	C	W	CZ	U	CU	WU	SL
1	0.	90.1702	0.	-4.54	33.17	49.01	0.584	0.745	203.3	259.2	169.8	306.3	111.0	-195.3	1
2	0.1000	86.6954	7.7	-0.84	32.05	46.75	0.593	0.734	205.7	254.5	174.4	294.5	109.2	-185.3	2
3	0.2500	81.2467	19.8	0.37	32.12	43.62	0.597	0.698	206.2	241.2	174.6	276.0	109.6	-166.4	3
4	0.4000	75.4725	32.6	1.42	32.90	38.71	0.612	0.659	210.9	226.9	177.0	256.4	114.5	-141.9	4
5	0.6900	62.8425	60.6	4.66	35.64	23.96	0.663	0.590	220.7	201.7	183.8	213.5	131.8	-81.7	5
6	0.8000	57.3360	72.8	7.83	37.25	16.97	0.678	0.566	231.0	192.8	182.8	194.8	139.0	-55.8	6
7	0.9420	48.9809	91.4	8.21	35.96	8.89	0.695	0.572	234.7	192.9	188.7	166.4	136.9	-29.5	7
8	0.9610	47.7524	94.1	8.14	36.60	6.58	0.703	0.570	237.0	192.2	189.0	162.2	140.4	-21.8	8
9	0.9810	46.4111	97.1	8.34	36.88	4.04	0.719	0.579	241.8	194.6	192.1	157.7	144.1	-13.6	9
10	1.0000	45.0952	100.0	8.74	37.02	1.53	0.738	0.592	247.6	198.6	196.2	153.2	148.0	-5.2	10

SL	PSI	RADIUS	PT	TT	TT-REL	PS	TS	RHO	PT/PTI	TT/TTI	EFF	BLKAGE	SL
1	0.	90.1702	13.861	322.00	334.86	11.002	301.44	1.27154	1.3680	1.11743	0.7975	0.96000	1
2	0.1000	86.6954	13.871	320.17	331.33	10.931	299.10	1.27319	1.3690	1.11107	0.8453	0.96000	2
3	0.2500	81.2467	13.891	318.28	326.08	10.919	297.12	1.28026	1.3710	1.10451	0.9027	0.96000	3
4	0.4000	75.4725	13.902	317.39	320.88	10.794	295.25	1.27358	1.3720	1.10143	0.9324	0.96000	4
5	0.6900	62.8425	13.820	316.17	310.84	10.287	290.59	1.23329	1.3640	1.09719	0.9542	0.96000	5
6	0.8000	57.3360	13.678	315.11	307.04	10.050	288.55	1.21340	1.3500	1.09352	0.9572	0.96000	6
7	0.9420	48.9809	13.000	310.83	301.94	9.411	283.43	1.15674	1.2830	1.07868	0.9379	0.96000	7
8	0.9610	47.7524	12.848	310.83	301.26	9.237	282.87	1.13762	1.2680	1.07868	0.8921	0.96000	8
9	0.9810	46.4111	12.706	310.78	300.53	9.007	281.68	1.11396	1.2540	1.07849	0.8512	0.96000	9
10	1.0000	45.0952	12.564	310.72	299.84	8.751	280.22	1.08799	1.2400	1.07829	0.8096	0.96000	10

SL	PSI	TPLC	PR-ROW	DEL-T	D	DP/Q	CZ/CZ	SOLDTY	R-AVG	F-TAN	F-AXL	F-COEF	T-COEF	SL
1	0.	0.13242	1.3680	33.84	0.456	0.346	0.823	0.9500	90.1702	1294.99	1412.76	0.674	0.725	1
2	0.1000	0.10102	1.3690	32.01	0.449	0.359	0.858	0.9506	86.6313	1235.64	1369.50	0.691	0.741	2
3	0.2500	0.06502	1.3710	30.12	0.460	0.396	0.875	0.9522	81.0070	1157.63	1281.33	0.727	0.794	3
4	0.4000	0.04720	1.3720	29.23	0.485	0.433	0.885	0.9541	74.9877	1124.84	1154.99	0.790	0.893	4
5	0.6900	0.03651	1.3640	28.01	0.542	0.475	0.928	0.9595	61.6904	1062.73	827.95	0.964	1.235	5
6	0.8000	0.03600	1.3500	26.95	0.564	0.483	0.935	0.9628	55.7812	996.37	670.86	1.061	1.427	6
7	0.9420	0.05069	1.2830	22.67	0.524	0.407	0.984	0.9701	46.7985	809.62	425.88	1.265	1.645	7
8	0.9610	0.08938	1.2680	22.67	0.530	0.371	0.986	0.9716	45.4544	800.34	367.47	1.308	1.731	8
9	0.9810	0.12430	1.2540	22.62	0.525	0.320	0.997	0.9735	43.9885	793.93	309.81	1.364	1.828	9
10	1.0000	0.15903	1.2400	22.56	0.516	0.265	1.005	0.9757	42.5502	790.72	252.33	1.436	1.932	10

MASS AVERAGED VALUES

PT/PTI 1.3539 EFF 0.9123 PT 13.718 TT 316.72 TT/TTI 1.09911 CZ 179.20 ROW PT2/PT1 1.3539

CORR. FLOW 316.116 CORR. RPM 3094.3

Table 6-II. Design Blade Element Parameters for QCSEE UTW Fan (Continued).

```
                              STATION    1.70000     Z   453.263893    CORE   OGV   INLET                          METRIC UNITS

SL    PSI     RADIUS   % IMM     PHI     ALPHA    BETA   M-ABS   M-REL      C        W       CZ       U        CU       WU     SL
 1  0.9021   51.5672    0.      -3.00    35.39   11.23   0.700   0.582    236.6    196.7    192.7    175.2    136.9    -38.3    1
 2  0.9420   49.1659   37.8     -2.42    35.51    9.04   0.700   0.579    236.1    195.2    192.6    167.0    136.4    -30.7    2
 3  0.9610   47.9546   56.9     -2.21    36.64    7.00   0.694   0.562    234.4    189.5    188.0    162.9    139.8    -23.1    3
 4  0.9810   46.5999   78.2     -2.02    38.20    4.63   0.687   0.542    232.2    183.1    182.4    158.3    143.5    -14.8    4
 5  1.0000   45.2146  100.0     -2.41    40.48    2.00   0.672   0.512    227.4    173.2    172.9    155.6    147.6     -6.0    5

SL    PSI     RADIUS     PT        TT      TT-REL      PS       TS       RHO      PT/PTI   TT/TTI     EFF     BLKAGE          SL
 1  0.9021   51.5672   13.188    312.04    303.43     9.506   284.17   1.16539   1.3016   1.08285   0.9440   0.96000          1
 2  0.9420   49.1659   13.000    310.83    302.05     9.372   285.09   1.15334   1.2830   1.07868   0.9379   0.96000          2
 3  0.9610   47.9546   12.846    310.83    301.37     9.308   285.49   1.14382   1.2680   1.07868   0.8921   0.96000          3
 4  0.9810   46.5999   12.706    310.78    300.63     9.264   283.95   1.13657   1.2540   1.07849   0.8512   0.96000          4
 5  1.0000   45.2146   12.564    310.72    299.90     9.283   284.98   1.13476   1.2400   1.07829   0.8096   0.96000          5

                                                 MASS AVERAGED VALUES
 PT/PTI    1.2737    EFF  0.9009    PT   12.906   TT    311.06    TT/TTI  1.07945    CZ    187.63
                         CORR. FLOW     32.600      CORR. RPM   3122.4
```

Table 6-II. Design Blade Element Parameters for QCSEE UTW Fan (Continued).

```
                              STATION    1.90000     Z    457.835899    CORE    OGV    EXIT                        METRIC UNITS

SL    PSI     RADIUS   % IMM     PHI     ALPHA    BETA   M-ABS  M-REL      C        W       CZ       U        CU      WU    SL
 1  0.9021   51.3259    0.      -3.02     4.97   39.75  0.555  0.719    190.8    247.1    189.6    174.4    10.5  -157.8    1
 2  0.9420   48.9771   37.9     -2.92     5.77   37.65  0.560  0.703    191.9    241.0    190.7    166.4    19.3  -147.1    2
 3  0.9610   47.8116   56.8     -2.11     6.16   36.98  0.553  0.689    189.9    236.3    188.7    162.4    20.4  -142.1    3
 4  0.9810   46.5110   77.8     -1.45     6.56   36.85  0.555  0.665    184.0    228.4    182.8    158.0    21.0  -137.0    4
 5  1.0000   45.1359  100.0     -1.46     6.97   38.76  0.484  0.616    167.0    212.6    165.7    153.3    20.3  -133.1    5

SL    PSI     RADIUS      PT        TT      TT-REL      PS       TS      RHO      PT/PTI   TT/TTI     EFF    BLKAGE        SL
 1  0.9021   51.3259   12.861    312.04    324.30   10.432   293.92  1.23643   1.2693  1.08285  0.8510  0.94000         1
 2  0.9420   48.9771   12.809    310.83    321.42   10.355   292.51  1.23328   1.2641  1.07868  0.8803  0.94000         2
 3  0.9610   47.8116   12.650    310.83    320.67   10.273   292.89  1.22192   1.2484  1.07868  0.8319  0.94000         3
 4  0.9810   46.5110   12.370    310.78    319.90   10.177   293.92  1.20618   1.2208  1.07849  0.7473  0.94000         4
 5  1.0000   45.1359   11.849    310.72    319.33   10.097   296.84  1.16504   1.1694  1.07829  0.5842  0.94000         5

SL    PSI      TPLC    PR-ROW   DEL-T      D     DP/Q   CZ/CZ   SOLDTY   R-AVG     F-TAN     F-AXL   F-COEF T-COEF     SL
 1  0.9021  0.06864  0.9752             0.371  0.251  0.985  1.4411  51.4465   848.85   278.81                        1
 2  0.9420  0.05267  0.9853             0.352  0.271  0.990  1.5087  49.0715   783.90   290.48                        2
 3  0.9610  0.05590  0.9846             0.355  0.273  1.003  1.5436  47.8831   760.28   294.76                        3
 4  0.9810  0.09782  0.9735             0.374  0.265  1.002  1.5647  46.5555   727.85   269.35                        4
 5  1.0000  0.21766  0.9451             0.436  0.248  0.958  1.6445  45.1753   673.89   193.28                        5

                                                 MASS AVERAGED VALUES
 PT/PTI    1.2440    EFF  0.8101    PT    12.605   TT    311.06   TT/TTI  1.07945    CZ    185.95    ROW PT2/PT1  0.9766
                          CORR. FLOW    33.380     CORR. RPM   3122.4
```

Table 6-II. Design Blade Element Parameters for QCSEE UTW Fan (Continued).

STATION 11.50000 Z 482.600948 BYPASS OGV INLET METRIC UNITS

SL	PSI	RADIUS	% IMM	PHI	ALPHA	BETA	M-ABS	M-REL	C	W	CZ	U	CU	WU	SL
1	0.	90.1702	0.	0.	31.07	46.68	0.620	0.775	215.1	268.5	184.2	306.3	111.0	-195.3	1
2	0.1000	86.8359	9.0	0.31	30.18	44.78	0.628	0.765	216.8	264.1	187.4	295.0	109.0	-186.0	2
3	0.2500	81.6850	22.8	0.76	29.72	41.41	0.640	0.741	220.0	254.7	191.0	277.5	109.0	-168.5	3
4	0.4000	76.2516	37.4	1.23	30.45	37.07	0.653	0.705	223.7	241.7	192.6	259.0	113.4	-145.7	4
5	0.6900	64.3910	69.3	2.05	33.51	24.89	0.684	0.629	235.1	214.3	194.3	218.7	126.6	-90.1	5
6	0.8000	59.2058	83.3	1.78	34.71	18.89	0.696	0.605	236.5	205.5	194.4	201.1	134.6	-66.5	6
7	0.9021	53.8026	97.6	0.25	34.67	15.20	0.681	0.580	230.7	196.6	189.7	182.8	131.2	-51.5	7
8	0.9022	53.7973	97.8	0.24	4.19	37.01	0.652	0.614	221.5	276.7	221.0	182.8	16.2	-166.6	8
9	0.9184	52.9921	100.0	0.	4.44	36.50	0.650	0.806	220.8	273.9	220.1	180.0	17.1	-162.9	9

SL	PSI	RADIUS	PT	TT	TT-REL	PS	TS	RHO	PT/PTI	TT/TTI	EFF	BLKAGE	SL
1	0.	90.1702	13.861	322.00	334.86	10.692	298.96	1.24581	1.3680	1.11743	0.7975	0.95000	1
2	0.1000	86.8359	13.871	320.17	331.47	10.636	296.77	1.24852	1.3690	1.11107	0.8453	0.95000	2
3	0.2500	81.6850	13.891	318.28	326.48	10.548	294.20	1.24903	1.3710	1.10451	0.9027	0.95000	3
4	0.4000	76.2516	13.902	317.39	321.56	10.443	292.46	1.24368	1.3720	1.10143	0.9324	0.95000	4
5	0.6900	64.3910	13.820	316.17	311.98	10.107	289.13	1.21781	1.3640	1.09719	0.9542	0.95000	5
6	0.8000	59.2058	13.676	315.11	308.29	9.895	287.27	1.20002	1.3500	1.09352	0.9572	0.95000	6
7	0.9021	53.8026	13.188	312.04	304.79	9.669	285.55	1.17957	1.3016	1.08285	0.9440	0.95000	7
8	0.9022	53.7973	12.861	312.04	325.72	9.669	287.61	1.17113	1.2693	1.08285	0.8510	0.95000	8
9	0.9184	52.9921	12.840	311.54	324.61	9.667	287.28	1.17232	1.2672	1.08115	0.8626	0.95000	9

MASS AVERAGED VALUES

PT/PTI 1.3610 EFF 0.9124 PT 13.791 TT 317.24 TT/TTI 1.10090 CZ 192.06

CORR. FLOW 289.029 CORR. RPM 3091.8

Table 6-II. Design Blade Element Parameters for QCSEE UTW Fan (Continued).

STATION 11.90000 Z 508.000999 BYPASS OGV EXIT

METRIC UNITS

SL	PSI	RADIUS	% IMM	PHI	ALPHA	BETA	M-ABS	M-REL	C	W	CZ	U	CU	WU	SL
1	0.	90.1702*	0.	0.	0.	59.31	0.519	1.017	181.8	356.2	181.8	306.3	0.	-306.3	1
2	0.1000	86.8872	8.8	-0.25	0.	57.62	0.537	1.002	187.2	349.5	187.2	295.2	0.	-295.2	2
3	0.2500	81.8571	22.4	-0.21	0.	55.87	0.542	0.967	188.5	335.9	188.5	278.1	0.	-278.1	3
4	0.4000	76.5508	36.6	-0.07	0.	54.06	0.543	0.926	188.5	321.2	188.5	260.1	0.	-260.1	4
5	0.6900	64.9958	67.7	0.44	0.	49.98	0.535	0.832	185.4	288.3	185.4	220.8	0.	-220.8	5
6	0.8000	59.9231	81.4	0.93	0.	48.39	0.522	0.786	180.8	272.3	180.8	203.6	0.	-203.6	6
7	0.9021	54.2126	96.7	0.15	0.	50.58	0.436	0.686	151.4	238.4	151.4	184.2	0.	-184.2	7
8	0.9022	54.2056	96.7	0.13	0.	53.24	0.394	0.659	137.6	229.9	137.6	184.1	0.	-184.1	8
9	0.9184	52.9921*	100.0	0.	0.	54.09	0.374	0.637	130.4	222.3	130.4	180.0	0.	-180.0	9

SL	PSI	RADIUS	PT	TT	TT-REL	PS	TS	RHO	PT/PTI	TT/TTI	EFF	BLKAGE	SL
1	0.	90.1702	13.515	322.00	368.70	11.248	305.55	1.28250	1.3338	1.11743	0.7304	0.94000	1
2	0.1000	86.8872	13.691	320.17	363.53	11.254	302.73	1.29509	1.3512	1.11107	0.8086	0.94000	2
3	0.2500	81.8571	13.766	318.28	356.76	11.271	300.60	1.30618	1.3586	1.10451	0.8756	0.94000	3
4	0.4000	76.5508	13.791	317.39	351.05	11.283	299.70	1.31152	1.3610	1.10143	0.9077	0.94000	4
5	0.6900	64.9958	13.696	316.17	340.43	11.272	299.05	1.31310	1.3517	1.09719	0.9252	0.94000	5
6	0.8000	59.9231	13.528	315.11	335.74	11.236	298.84	1.30990	1.3351	1.09352	0.9204	0.94000	6
7	0.9021	54.2126	12.766	312.04	328.92	11.206	300.63	1.29858	1.2599	1.08285	0.8236	0.94000	7
8	0.9022	54.2056	12.475	312.04	328.91	11.206	302.62	1.29005	1.2312	1.08285	0.7390	0.94000	8
9	0.9184	52.9921	12.339	311.54	327.67	11.206	303.09	1.28800	1.2178	1.08115	0.7136	0.94000	9

SL	PSI	TPLC	PR-ROW	DEL-T	D	DP/Q	CZ/CZ	SOLDTY	R-AVG	F-TAN	F-AXL	F-COEF	T-COEF	SL
1	0.	0.10933	0.9750		0.366	0.176	0.987	1.2233	90.1702	1374.50	285.46			1
2	0.1000	0.05574	0.9870		0.330	0.191	0.999	1.2974	86.8615	1339.12	334.45			2
3	0.2500	0.03740	0.9910		0.317	0.216	0.987	1.4236	81.7700	1283.06	341.47			3
4	0.4000	0.03216	0.9920		0.318	0.243	0.978	1.5750	76.4012	1252.39	355.51			4
5	0.6900	0.03350	0.9910		0.342	0.314	0.955	1.9934	64.6934	1185.91	392.18			5
6	0.8000	0.03978	0.9890		0.362	0.354	0.930	2.2278	59.5644	1119.04	389.13			6
7	0.9021	0.11991	0.9680		0.454	0.437	0.798	2.5745	54.0076	884.81	265.87			7
8	0.9022	0.12085	0.9700		0.393	0.482	0.623	2.5761	54.0015	113.20	-42.19			8
9	0.9184	0.15785	0.9610		0.423	0.485	0.592	2.8676	52.9921	114.76	-64.87			9

MASS AVERAGED VALUES

PT/PTI 1.3445 EFF 0.8748 PT 13.623 TT 317.24 TT/TTI 1.10090 CZ 183.37 ROW PT2/PT1 0.9879

CORR. FLOW 292.580 CORR. RPM 3091.8

* Bypass OGV Exit Tip and Hub Radii Listed in this Table were Changed to 90.2843 cm and 52.2986 cm, Respectively, After the Aero Design was Completed in Order to Improve Transition of the Fan Flowpath into the Bypass Exhaust Duct Contours. The Impact of These Changes on OGV Blade Element Parameters was Estimated to be Small, and the Design Data were not Recomputed.

Table 6-II. Design Blade Element Parameters for QCSEE UTW Fan (Continued).

NOMENCLATURE FOR TABULATION

HEADING	IDENTIFICATION	ENGLISH UNITS
GENERAL		
SL	STREAMLINE NUMBER	-
PSI	STREAM FUNCTION	-
RADIUS	STREAMLINE RADIUS	IN.
% IMM	PERCENT IMMERSION FROM OUTER WALL	%
Z	AXIAL DIMENSION	IN.
BLKAGE	ANNULUS BLOCKAGE FACTOR	-
FLOW	WEIGHT FLOW	LBM/SEC
ANGLES AND MACH NUMBERS		
PHI	MERIDIONAL FLOW ANGLE	DEG.
ALPHA	ABSOLUTE FLOW ANGLE =ARCTAN (CU/CZ)	DEG.
BETA	RELATIVE FLOW ANGLE =ARCTAN (-WU/CZ)	DEG.
M-ABS	ABSOLUTE MACH NUMBER	-
M-REL	RELATIVE MACH NUMBER	-
VELOCITIES		
C	ABSOLUTE VELOCITY	FT/SEC
W	RELATIVE VELOCITY	FT/SEC
CZ	AXIAL VELOCITY	FT/SEC
U	BLADE SPEED	FT/SEC
CU	TANGENTIAL COMPONENT OF C	FT/SEC
WU	TANGENTIAL COMPONENT OF W	FT/SEC
FLUID PROPERTIES		
PT	ABSOLUTE TOTAL PRESSURE	LBF/SQ.IN.
TT	ABSOLUTE TOTAL TEMPERATURE	DEG-R
TT-REL	RELATIVE TOTAL TEMPERATURE	DEG-R
PS	STATIC PRESSURE	LBF/SQ.IN.
TS	STATIC TEMPERATURE	DEG-R
RHO	STATIC DENSITY	LBM/CU.FT.
EFF	CUMULATIVE ADIABATIC EFFICIENCY REFERENCED TO PTI, TTI	-
PTI	INLET ABSOLUTE TOTAL PRESSURE	LBF/SQ.IN.
TTI	INLET ABSOLUTE TOTAL TEMPERATURE	DEG-R
AERODYNAMIC BLADING PARAMETERS		
TPLC	TOTAL PRESSURE LOSS COEFFICIENT	-
PR-ROW	TOTAL PRESSURE RATIO ACROSS BLADE ROW	-
DEL-T	TOTAL TEMPERATURE RISE ACROSS ROTOR	DEG-R
D	DIFFUSION FACTOR	-
DP/Q	STATIC PRESSURE RISE COEFFICIENT	-
CZ/CZ	AXIAL VELOCITY RATIO ACROSS BLADE ROW	-
SOLDTY	SOLIDITY	-
R-AVG	AVERAGE STREAMLINE RADIUS ACROSS BLADE ROW	IN.
F-TAN	TANGENTIAL BLADE FORCE PER UNIT BLADE LENGTH	LBF/IN
F-AXL	AXIAL BLADE FORCE PER UNIT BLADE LENGTH	LBF/IN
F-COEF	FLOW COEFFICIENT =CZ1/U1	-
T-COEF	WORK COEFFICIENT =(2*G*J*CP*DEL-T)/(U2*U2)	-

Table 6-II. Design Blade Element Parameters for QCSEE UTW Fan (Continued).

```
                          STATION   1.00000   Z   166.900000   ROTOR   INLET                          ENGLISH UNITS

SL   PSI     RADIUS   % IMM    PHI    ALPHA   BETA   M-ABS  M-REL     C       W       CZ      U         CU     WU      SL
 1  0.       35.5000    0.      0.     0.     56.03  0.630  1.128   677.1  1211.8   677.1  1005.0     0.  -1005.0    1
 2  0.1000   34.0815    7.2    2.51    0.     55.35  0.620  1.091   667.5  1173.2   667.0   964.8     0.   -964.8    2
 3  0.2500   31.7981   18.7    3.55    0.     53.97  0.609  1.034   655.9  1113.8   654.7   900.2     0.   -900.2    3
 4  0.4000   29.3318   31.2    5.45    0.     51.68  0.612  0.985   659.4  1060.3   656.4   830.4     0.   -830.4    4
 5  0.6900   25.8340   59.1   10.26    0.     46.06  0.614  0.877   660.8   944.4   650.2   674.7     0.   -674.7    5
 6  0.8000   21.3489   71.7   12.60    0.     43.31  0.610  0.829   657.0   892.7   641.2   604.4     0.   -604.4    6
 7  0.9420   17.5653   90.8   15.73    0.     38.32  0.607  0.762   653.7   821.4   629.2   497.3     0.   -497.3    7
 8  0.9610   16.9907   93.7   15.97    0.     37.39  0.608  0.754   654.6   812.3   629.3   481.0     0.   -481.0    8
 9  0.9810   16.3645   96.9   16.09    0.     36.24  0.611  0.747   657.8   804.6   632.1   463.3     0.   -463.3    9
10  1.0000   15.7500  100.0   15.80    0.     34.85  0.619  0.745   665.6   801.1   640.4   445.9     0.   -445.9   10

SL   PSI     RADIUS     PT       TT     TT-REL     PS       TS       RHO     PT/PTI   TT/TTI    EFF   BLKAGE     SL
 1  0.       35.5000  14.696  518.69  602.75   11.248  480.54  0.06318  1.0000  1.00000        0.98000     1
 2  0.1000   34.0815  14.696  518.69  596.17   11.336  481.61  0.06353  1.0000  1.00000        0.98000     2
 3  0.2500   31.7981  14.696  518.69  586.13   11.441  482.88  0.06395  1.0000  1.00000        0.98000     3
 4  0.4000   29.3318  14.696  518.69  576.08   11.410  482.51  0.06383  1.0000  1.00000        0.98000     4
 5  0.6900   25.8340  14.696  518.69  556.58   11.397  482.35  0.06378  1.0000  1.00000        0.98000     5
 6  0.8000   21.3489  14.696  518.69  549.09   11.431  482.76  0.06391  1.0000  1.00000        0.98000     6
 7  0.9420   17.5653  14.696  518.69  539.27   11.461  483.12  0.06403  1.0000  1.00000        0.98000     7
 8  0.9610   16.9907  14.696  518.69  537.95   11.453  483.03  0.06400  1.0000  1.00000        0.98000     8
 9  0.9810   16.3645  14.696  518.69  536.55   11.424  482.67  0.06388  1.0000  1.00000        0.98000     9
10  1.0000   15.7500  14.696  518.69  535.24   11.353  481.82  0.06360  1.0000  1.00000        0.98000    10

                                          MASS AVERAGED VALUES
  PT/PTI   1.0000   EFF            PT   14.696   TT   518.69   TT/TTI  1.00000   CZ   652.10
                       CORR. FLOW   900.000     CORR. RPM   3244.1     CORR. U-TIP  1005.0

                                                PTI      14.696
                                                TTI     518.690
                                                GAMMA    1.4000
```

Table 6-II. Design Blade Element Parameters for QCSEE UTW Fan (Continued).

STATION 1.50000 Z 174.299999 ROTOR EXIT

ENGLISH UNITS

SL	PSI	RADIUS	% IMM	PHI	ALPHA	BETA	M-ABS	M-REL	C	W	CZ	U	CU	WU	SL
1	0.	35.5000	0.	-4.54	33.17	49.01	0.584	0.745	666.9	850.3	557.0	1005.0	364.1	-640.9	1
2	0.1000	34.1320	7.7	-0.84	32.05	46.75	0.593	0.734	675.0	634.9	572.0	966.3	358.2	-608.1	2
3	0.2500	31.9868	19.8	0.37	32.12	43.62	0.597	0.693	676.5	791.4	572.9	905.5	359.7	-545.9	3
4	0.4000	29.7135	32.6	1.42	32.90	38.71	0.612	0.659	691.9	744.5	580.8	841.2	375.7	-465.4	4
5	0.6900	24.7411	60.6	4.66	35.64	23.96	0.663	0.590	743.7	661.8	605.1	700.4	432.4	-268.0	5
6	0.8000	22.5732	72.8	7.83	37.25	16.97	0.678	0.566	758.0	632.5	599.8	639.0	456.1	-183.0	6
7	0.9420	19.2838	91.4	8.21	35.96	8.89	0.695	0.572	769.9	632.8	619.0	545.9	449.1	-96.8	7
8	0.9610	18.8001	94.1	8.14	36.60	6.58	0.703	0.570	777.6	630.6	620.2	532.2	460.7	-71.6	8
9	0.9810	18.2720	97.1	8.44	36.88	4.04	0.719	0.579	793.3	638.6	630.3	517.3	472.8	-44.5	9
10	1.0000	17.7540	100.0	8.74	37.02	1.53	0.738	0.592	812.2	651.4	643.6	502.6	485.4	-17.2	10

SL	PSI	RADIUS	PT	TT	TT-REL	PS	TS	RHO	PT/PTI	TT/TTI	EFF	BLKAGE	SL
1	0.	35.5000	20.104	579.60	602.75	15.958	542.58	0.07938	1.3680	1.11743	0.7975	0.96000	1
2	0.1000	34.1320	20.119	576.30	596.40	15.854	538.38	0.07949	1.3690	1.11107	0.8455	0.96000	2
3	0.2500	31.9868	20.148	572.90	586.94	15.837	534.82	0.07995	1.3710	1.10451	0.9027	0.96000	3
4	0.4000	29.7135	20.163	571.30	577.58	15.655	531.45	0.07951	1.3720	1.10143	0.9324	0.96000	4
5	0.6900	24.7411	20.045	569.10	559.52	14.921	523.06	0.07699	1.3640	1.09719	0.9542	0.96000	5
6	0.8000	22.5732	19.839	567.20	552.68	14.577	519.39	0.07575	1.3500	1.09352	0.9572	0.96000	6
7	0.9420	19.2838	18.655	559.50	543.49	13.649	510.17	0.07221	1.2830	1.07868	0.9379	0.96000	7
8	0.9610	18.8001	18.634	559.50	542.26	13.398	509.17	0.07102	1.2680	1.07868	0.8921	0.96000	8
9	0.9810	18.2720	18.429	559.40	540.96	13.064	507.02	0.06954	1.2540	1.07849	0.8512	0.96000	9
10	1.0000	17.7540	18.223	559.30	539.71	12.693	504.40	0.06792	1.2400	1.07829	0.8096	0.96000	10

SL	PSI	TPLC	PR-ROW	DEL-T	D	DP/Q	CZ/CZ	SOLDTY	R-AVG	F-TAN	F-AXL	F-COEF	T-COEF	SL
1	0.	0.13242	1.3680	60.91	0.456	0.346	0.823	0.9500	35.5000	739.46	806.71	0.674	0.725	1
2	0.1000	0.10102	1.3690	57.61	0.449	0.359	0.858	0.9506	34.1067	705.58	782.01	0.691	0.741	2
3	0.2500	0.06502	1.3710	54.21	0.460	0.396	0.875	0.9522	31.8924	661.03	731.66	0.727	0.794	3
4	0.4000	0.04720	1.3720	52.61	0.485	0.433	0.885	0.9541	29.5227	642.31	659.52	0.790	0.893	4
5	0.6900	0.03651	1.3640	50.41	0.542	0.475	0.928	0.9595	24.2875	606.84	472.77	0.964	1.235	5
6	0.8000	0.03600	1.3500	48.51	0.564	0.483	0.935	0.9628	21.9610	568.95	383.07	1.061	1.427	6
7	0.9420	0.05069	1.2830	40.81	0.524	0.407	0.984	0.9701	18.4246	462.31	243.18	1.265	1.645	7
8	0.9610	0.08938	1.2680	40.81	0.530	0.371	0.986	0.9716	17.8954	457.01	209.83	1.308	1.731	8
9	0.9810	0.12430	1.2540	40.71	0.525	0.320	0.997	0.9735	17.3163	453.35	176.91	1.364	1.828	9
10	1.0000	0.15903	1.2400	40.61	0.516	0.265	1.005	0.9757	16.7520	451.51	144.09	1.436	1.932	10

MASS AVERAGED VALUES

PT/PTI 1.3539 EFF 0.9123 PT 19.897 TT 570.10 TT/TTI 1.09911 CZ 587.93 ROW PT2/PT1 1.3539

CORR. FLOW 696.917 CORR. RPM 3094.3

Table 6-II. Design Blade Element Parameters for QCSEE UTW Fan (Continued).

STATION 1.70000 Z 178.450001 CORE OGV INLET

ENGLISH UNITS

SL	PSI	RADIUS	X IMM	PHI	ALPHA	BETA	M-ABS	M-REL	C	W	CZ	U	CU	WU	SL
1	0.9021	20.3020	0.	-3.00	35.39	11.25	0.700	0.582	776.3	645.4	632.2	574.7	449.2	-125.5	1
2	0.9420	19.3566	37.8	-2.42	35.31	9.04	0.700	0.579	774.6	640.3	631.7	548.0	447.4	-100.6	2
3	0.9610	18.8797	56.9	-2.21	36.64	7.00	0.694	0.562	769.0	621.9	616.8	534.5	458.7	-75.8	3
4	0.9810	18.3464	78.2	-2.02	38.20	4.63	0.687	0.542	761.7	600.7	598.3	519.4	470.9	-48.5	4
5	1.0000	17.8010	100.0	-2.41	40.48	2.00	0.672	0.512	746.2	568.2	567.3	503.9	484.1	-19.8	5

SL	PSI	RADIUS	PT	TT	TT-REL	PS	TS	RHO	PT/PT1	TT/TT1	EFF	BLKAGE	SL
1	0.9021	20.3020	19.128	561.66	546.18	13.788	511.51	0.07276	1.3016	1.08285	0.9440	0.96000	1
2	0.9420	19.3566	18.855	559.50	543.68	13.593	509.56	0.07200	1.2830	1.07868	0.9379	0.96000	2
3	0.9610	18.8797	18.634	559.50	542.47	13.500	510.28	0.07141	1.2680	1.07868	0.8921	0.96000	3
4	0.9810	18.3464	18.429	559.40	541.14	13.436	511.11	0.07096	1.2540	1.07849	0.8512	0.96000	4
5	1.0000	17.8010	18.223	559.30	539.83	13.463	512.96	0.07084	1.2400	1.07829	0.8096	0.96000	5

MASS AVERAGED VALUES

PT/PT1 1.2737 EFF 0.9009 PT 18.719 TT 559.90 TT/TT1 1.07945 CZ 616.24
CORR. FLOW 71.870 CORR. RPM 3122.4

Table 6-II. Design Blade Element Parameters for QCSEE UTW Fan (Continued).

```
                              STATION    1.90000    Z   180.250000    CORE   OGV   EXIT                          ENGLISH UNITS

SL    PSI     RADIUS   % IMM     PHI     ALPHA    BETA   M-ABS   M-REL      C        W       CZ       U        CU      WU     SL
 1  0.9021  20.2070     0.      -3.02     4.97   39.75   0.555   0.719    626.0    810.6    622.8    572.1    54.2  -517.9    1
 2  0.9420  19.2823    37.9     -2.92     5.77   37.65   0.560   0.703    629.5    790.7    625.5    545.9    63.2  -482.6    2
 3  0.9610  18.8234    56.8     -2.11     6.16   36.98   0.553   0.689    622.9    775.1    618.9    532.9    66.8  -466.1    3
 4  0.9810  18.3114    77.8     -1.45     6.56   36.85   0.535   0.665    603.7    749.5    599.6    518.4    69.0  -449.4    4
 5  1.0000  17.7700   100.0     -1.46     6.97   38.76   0.484   0.616    548.0    697.5    543.8    503.1    66.5  -436.6    5

SL    PSI     RADIUS     PT        TT      TT-REL     PS       TS       RHO     PT/PTI   TT/TTI    EFF    BLKAGE          SL
 1  0.9021  20.2070   18.653    561.66   583.74   15.130   529.05   0.07719   1.2693  1.08285  0.8510  0.94000           1
 2  0.9420  19.2823   18.578    559.50   578.55   15.019   526.52   0.07699   1.2641  1.07868  0.8803  0.94000           2
 3  0.9610  18.8234   18.347    559.50   577.21   14.900   527.20   0.07628   1.2484  1.07868  0.8319  0.94000           3
 4  0.9810  18.3114   17.941    559.40   575.82   14.760   529.06   0.07550   1.2206  1.07849  0.7473  0.94000           4
 5  1.0000  17.7700   17.186    559.30   574.80   14.645   534.31   0.07398   1.1694  1.07829  0.5842  0.94000           5

SL    PSI      TPLC    PR-ROW    DEL-I     D     DP/Q    CZ/CZ   SOLDTY    R-AVG      F-TAN      F-AXL    F-COEF T-COEF   SL
 1  0.9021  0.08884   0.9752            0.371   0.251   0.985   1.4411   20.2545    484.71     159.20                    1
 2  0.9420  0.05267   0.9853            0.352   0.271   0.990   1.5087   19.3195    447.62     165.87                    2
 3  0.9610  0.05590   0.9846            0.355   0.273   1.003   1.5436   18.8516    434.13     168.52                    3
 4  0.9810  0.09782   0.9735            0.374   0.265   1.002   1.5647   18.3269    415.62     155.81                    4
 5  1.0000  0.21766   0.9431            0.436   0.248   0.956   1.6445   17.7855    384.81     110.37                    5

                                               MASS AVERAGED VALUES
 PT/PTI   1.2440   EFF  0.8101   PT   18.281   TT   559.90   TT/TTI  1.07945   CZ   610.07   ROW PT2/PT1  0.9766
                     CORR. FLOW    73.589    CORR. RPM   3122.4
```

Table 6-II. Design Blade Element Parameters for QCSEE UTW Fan (Continued).

STATION 11.50000 Z 190.000000 BYPASS OGV INLET ENGLISH UNITS

SL	PSI	RADIUS	% IMM	PHI	ALPHA	BETA	M-ABS	M-REL	C	W	CZ	U	CU	WU	SL
1	0.	35.5000	0.	0.	31.07	46.68	0.620	0.775	705.6	880.9	604.4	1005.0	364.1	-640.9	1
2	0.1000	34.1873	9.0	0.31	30.18	44.78	0.628	0.765	711.4	866.3	614.9	967.8	357.6	-610.2	2
3	0.2500	32.1586	22.8	0.76	29.72	41.41	0.640	0.741	721.6	835.6	626.7	910.4	357.7	-552.7	3
4	0.4000	30.0202	37.4	1.23	30.45	37.07	0.653	0.705	734.0	793.0	632.7	849.9	371.9	-478.0	4
5	0.6900	25.3507	69.3	2.05	33.51	24.89	0.684	0.629	764.7	703.0	637.4	717.7	422.0	-295.7	5
6	0.8000	23.3093	83.3	1.78	34.71	18.89	0.696	0.605	776.0	674.3	637.7	659.9	441.7	-218.2	6
7	0.9021	21.1821	97.8	0.25	34.67	15.20	0.681	0.580	756.8	645.0	622.4	599.7	430.6	-169.1	7
8	0.9022	21.1800	97.8	0.24	4.19	37.01	0.652	0.814	726.9	907.9	724.9	599.6	53.0	-546.6	8
9	0.9184	20.8630	100.0	0.	4.44	36.50	0.650	0.806	724.4	898.5	722.2	590.6	56.1	-534.5	9

SL	PSI	RADIUS	PT	TT	TT-REL	PS	TS	RHO	PT/PTI	TT/TTI	EFF	BLKAGE	SL
1	0.	35.5000	20.104	579.60	602.75	15.507	538.16	0.07778	1.3680	1.11743	0.7975	0.95000	1
2	0.1000	34.1873	20.119	576.30	596.65	15.426	534.18	0.07794	1.3690	1.11107	0.8453	0.95000	2
3	0.2500	32.1586	20.148	572.90	587.67	15.299	529.56	0.07798	1.3710	1.10451	0.9027	0.95000	3
4	0.4000	30.0202	20.163	571.30	578.80	15.147	526.46	0.07766	1.3720	1.10143	0.9324	0.95000	4
5	0.6900	25.3507	20.045	569.10	561.56	14.659	520.43	0.07603	1.3640	1.09719	0.9542	0.95000	5
6	0.8000	23.3093	19.839	567.20	554.93	14.352	517.09	0.07492	1.3500	1.09352	0.9572	0.95000	6
7	0.9021	21.1821	19.128	561.66	548.62	14.023	513.99	0.07364	1.3016	1.08285	0.9440	0.95000	7
8	0.9022	21.1800	18.653	561.66	586.29	14.023	517.69	0.07311	1.2693	1.08285	0.8510	0.95000	8
9	0.9184	20.8630	18.623	560.78	584.30	14.022	517.11	0.07319	1.2672	1.08115	0.8626	0.95000	9

MASS AVERAGED VALUES

PT/PTI 1.3610 EFF 0.9124 PT 20.002 TT 571.03 TT/TTI 1.10090 CZ 630.13

CORR. FLOW 637.200 CORR. RPM 3091.8

Table 6-II. Design Blade Element Parameters for QCSEE UTW Fan (Concluded).

STATION 11.90000 Z 200.000000 BYPASS OGV EXIT ENGLISH UNITS

SL	PSI	RADIUS	% IMM	PHI	ALPHA	BETA	M-ABS	M-REL	C	W	CZ	U	CU	WU	SL
1	0.	35.5000*	0.	0.	0.	59.31	0.519	1.017	596.5	1160.7	596.5	1005.0	0.	-1005.0	1
2	0.1000	34.2075	6.8	-0.23	0.	57.62	0.537	1.002	614.1	1146.7	614.1	968.4	0.	-968.4	2
3	0.2500	32.2271	22.4	-0.21	0.	55.87	0.542	0.967	618.4	1102.2	618.4	912.3	0.	-912.3	3
4	0.4000	30.1381	36.6	-0.07	0.	54.06	0.543	0.926	616.5	1055.8	616.5	853.2	0.	-853.2	4
5	0.6900	25.5889	67.7	0.44	0.	49.98	0.535	0.832	608.4	946.0	608.4	724.4	0.	-724.4	5
6	0.8000	23.5917	81.4	0.93	0.	48.39	0.522	0.786	595.3	893.3	595.2	667.9	0.	-667.9	6
7	0.9021	21.3435	96.7	0.13	0.	50.58	0.456	0.686	496.7	782.1	496.6	604.2	0.	-604.2	7
8	0.9022	21.3407	96.7	0.13	0.	53.24	0.394	0.659	451.3	754.1	451.3	604.2	0.	-604.2	8
9	0.9184	20.8630*	100.0	0.	0.	54.09	0.374	0.637	427.7	729.2	427.7	590.6	0.	-590.6	9

SL	PSI	RADIUS	PT	TT	TT-REL	PS	TS	RHO	PT/PT1	TT/TT1	EFF	BLKAGE	SL
1	0.	35.5000	19.601	579.60	663.66	16.315	549.99	0.08007	1.3538	1.11743	0.7504	0.94000	1
2	0.1000	34.2075	19.857	576.30	654.35	16.323	544.91	0.08085	1.3512	1.11107	0.8086	0.94000	2
3	0.2500	32.2271	19.967	572.90	642.18	16.347	541.07	0.08154	1.3586	1.10451	0.8756	0.94000	3
4	0.4000	30.1381	20.002	571.30	631.88	16.364	539.46	0.08168	1.3610	1.10145	0.9077	0.94000	4
5	0.6900	25.5889	19.865	569.10	612.76	16.349	538.29	0.08198	1.3517	1.09719	0.9252	0.94000	5
6	0.8000	23.5917	19.621	567.20	604.32	16.297	537.91	0.08178	1.3351	1.09352	0.9204	0.94000	6
7	0.9021	21.3435	18.510	561.66	592.05	16.253	541.13	0.08107	1.2599	1.08265	0.8256	0.94000	7
8	0.9022	21.3407	18.094	561.66	592.04	16.253	544.71	0.08054	1.2312	1.06285	0.7390	0.94000	8
9	0.9184	20.8630	17.896	560.78	589.81	16.253	545.55	0.08041	1.2176	1.08115	0.7136	0.94000	9

SL	PSI	TPLC	PR-RUN	DEF-I	D	DP/Q	CZ/CZ	SOLDTY	R-AVG	F-TAN	F-AXL	F-COEF	T-COEF	SL
1	0.	0.10933	0.9750		0.366	0.176	0.987	1.2233	35.5000	784.87	163.01			1
2	0.1000	0.05574	0.9870		0.330	0.191	0.999	1.2974	34.1974	764.66	190.98			2
3	0.2500	0.03740	0.9910		0.317	0.216	0.987	1.4236	32.1929	732.65	194.99			3
4	0.4000	0.03216	0.9920		0.318	0.243	0.976	1.5750	30.0792	715.14	203.00			4
5	0.6900	0.03350	0.9910		0.342	0.314	0.955	1.9934	25.4698	677.16	223.94			5
6	0.8000	0.03978	0.9890		0.362	0.354	0.930	2.2276	23.4505	638.99	222.20			6
7	0.9021	0.11991	0.9680		0.454	0.437	0.798	2.5745	21.2628	505.24	151.81			7
8	0.9022	0.12085	0.9700		0.393	0.482	0.623	2.5761	21.2604	64.64	-24.09			8
9	0.9184	0.15785	0.9610		0.423	0.485	0.592	2.8676	20.8630	65.53	-37.04			9

MASS AVERAGED VALUES

PT/PT1 1.3445 EFF 0.8748 PT 19.759 TT 571.03 TT/TT1 1.10090 CZ 601.60 ROW PT2/PT1 0.9879
CORR. FLOW 645.028 CORR. RPM 3091.8

* Bypass OGV Exit Tip and Hub Radii Listed in this Table were Changed to 35.5450 in. and 20.5900 in. Respectively, After the Aero Design was Completed in Order to Improve Transition of the Fan Flowpath into the Bypass Exhaust Duct Contours. The Impact of These Changes on OGV Blade Element Parameters was Estimated to be Small, and the Design Data were not Recomputed.

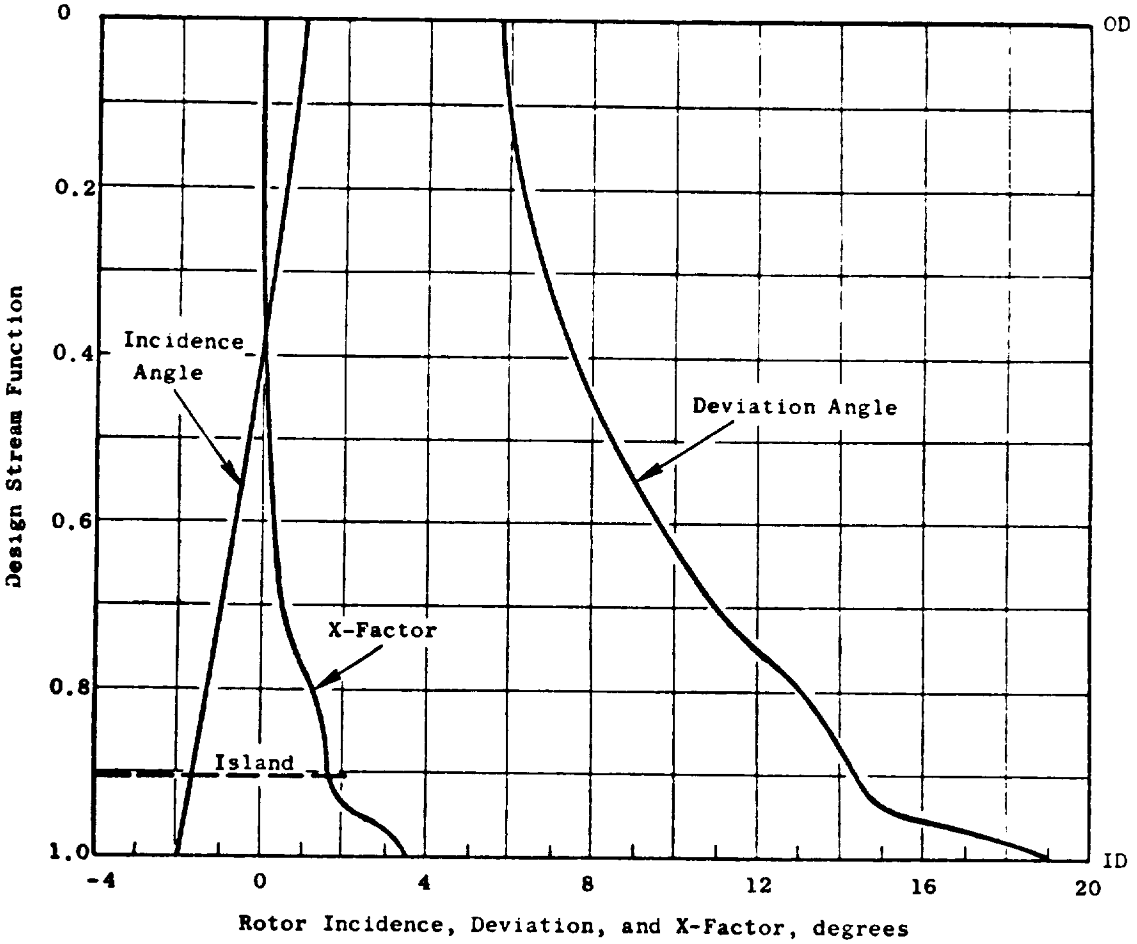

Figure 6-11. Rotor Incidence, Deviation, and Empirical Adjustment Angles.

the critical area ratio, is shown in Figure 6-12. Values employed are generally consistent with past experience. The blade shapes that result are generally similar to multiple circular arc sections in the tip region, with a small percentage of overall camber occurring in the forward portion. In the hub region, blade shapes are similar to double circular arc sections.

Figure 6-13 shows plane sections of the blade at several radial locations. Table 6-III is a tabulation of the fan rotor blade coordinates (in inches) for the sections shown in this figure. The coordinate center is at the stacking axis. Figure 6-14 shows the resulting camber and stagger angle radial distributions. The radial thickness distributions employed, which were dictated primarily by aeromechanical considerations, are shown in Figure 6-15.

The 0.13 thickness-to-chord ratio at the hub is larger than conventional practice because of composite blade requirements and a small performance penalty will result. The additional profile loss created by this thickness, however, is believed smaller than the system penalties associated with altering the configuration (such as reduction in the tip chord or a reduction in blade number) to reduce the hub thickness-to-chord ratio to 0.10, a value more representative of past experience.

6.2.7 Core OGV Design

A moderately low aspect ratio of 1.3 was selected for the core portion OGV to provide a rugged mechanical system. This selection was in recognition of the potentially severe aeromechanical environment (i.e., large rotor wakes) of the core OGV because of its small size in relationship to that of the rotor blade. A solidity at the ID of 1.65 was selected to yield reasonable levels of diffusion factor, Figure 6-10. The number of vanes which result is 96. Radial distribution of total pressure loss coefficient, diffusion factor, Mach number, and air angle are presented in Figure 6-10.

Profiles for the core portion OGV are a modified NASA 65-series thickness distribution on a circular-arc meanline. The incidence angle over the outer portion of the span was selected from a correlation of NASA low-speed cascade data. Locally, in the ID region, the incidence angle was reduced 0.07 radian (4°). This local reduction in incidence was in recognition of traverse data results on other high-bypass fan configurations which show core stator inlet air angles several degrees higher than the axisymmetric calculated values. The deviation angle was obtained from Carter's Rule as was described for the rotor blade, but no empirical adjustment was made. The resulting incidence and deviation angles and throat margin are shown in Figure 6-16. The throat area for the selected geometry was checked to ensure sufficient margin to pass the design flow. The minimum margin relative to the critical contraction ratio was 6%, which is sufficient to avoid choke. Resulting geometric parameters for the core OGV are presented in Figure 6-17. Figure 6-18 is a cylindrical section of the core OGV at the pitch line radius. A tabulation of the coordinates for this core OGV is given in Table 6-IV.

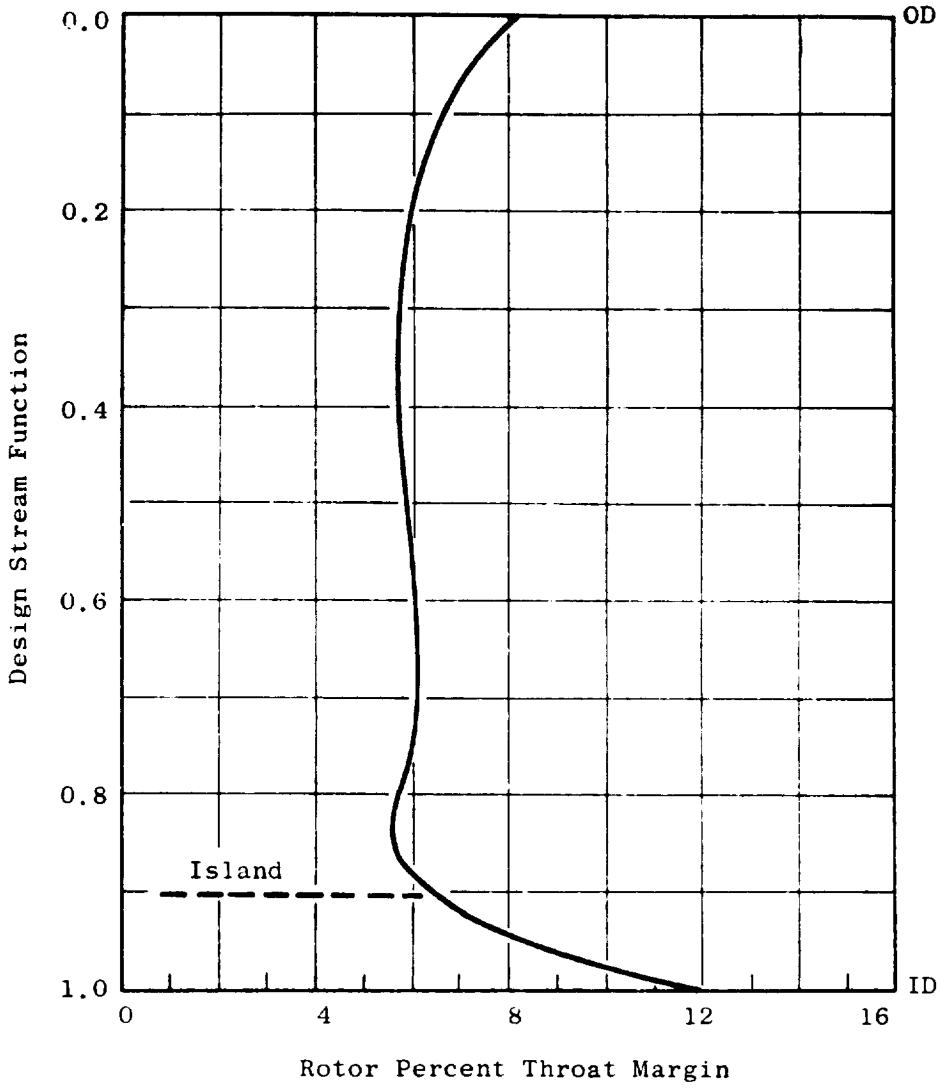

Figure 6-12. Rotor Throat Margin Distribution.

Section	Radius (cm)	Radius (in.)
1	85.8	33.8
2	76.2	30.0
3	66.8	26.3
4	57.2	22.5
5	47.7	18.8

Tip L.E. Radius = 90.2 cm (35.5 in.)
Hub L.E. Radius = 40.1 cm (15.8 in.)

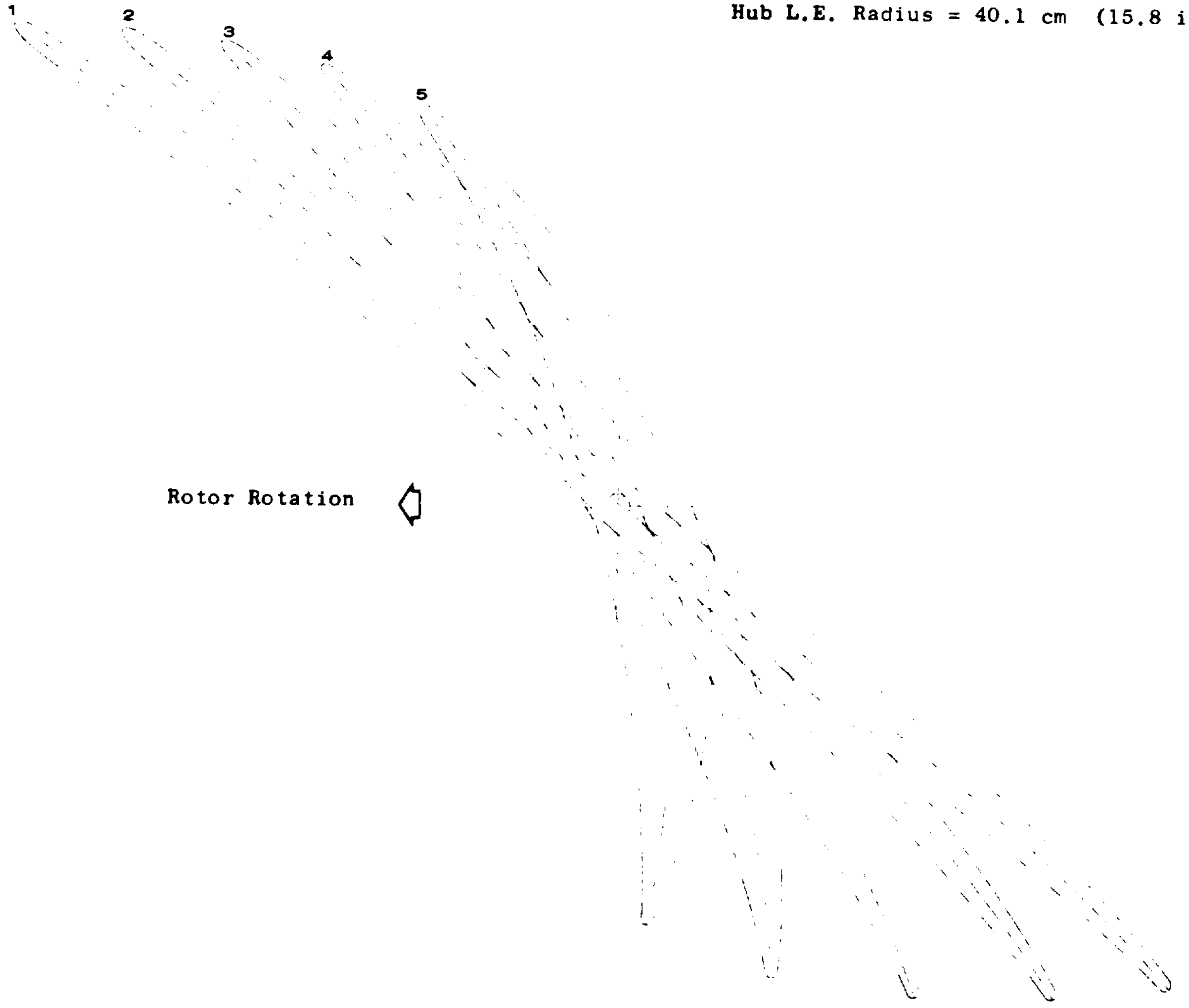
1
2
3
4
5
Rotor Rotation

Figure 6-13. UTW Fan Rotor Blade Plane Sections.

Table 6-III. UTW Fan Rotor Blade Coordinates.

SECTION 1 RADIUS 85.8 cm (33.8 in.)

Convex		Concave	
X (Axial)	Y	X (Axial)	Y
-3,57088	-4,59391	-3,57088	-4,59391
-3,58047	-4,57843	-3,55304	-4,59755
-3,58149	-4,55132	-3,52725	-4,58914
-3,57322	-4,51309	-3,49418	-4,56819
-3,55468	-4,46442	-3,45477	-4,53407
-3,52497	-4,40594	-3,40985	-4,48620
-3,48372	-4,33791	-3,35965	-4,42440
-3,43173	-4,25976	-3,30327	-4,34931
-3,28197	-4,03998	-3,14552	-4,13796
-3,10837	-3,78879	-2,96199	-3,89548
-2,93466	-3,54118	-2,77855	-3,65661
-2,76085	-3,29697	-2,59523	-3,42110
-2,58691	-3,05594	-2,41203	-3,18870
-2,41283	-2,81788	-2,22897	-2,95911
-2,23861	-2,58255	-2,04606	-2,73207
-2,02933	-2,30343	-1,82678	-2,46255
-1,81981	-2,02749	-1,60773	-2,19574
-1,61005	-1,75422	-1,38893	-1,93102
-1,40004	-1,48309	-1,17038	-1,66776
-1,18976	-1,21357	-0,95209	-1,40535
-0,97919	-0,94512	-0,73410	-1,14321
-0,76830	-0,67730	-0,51643	-0,88090
-0,55706	-0,40974	-0,29910	-0,61801
-0,34544	-0,14216	-0,08216	-0,35428
-0,13341	0,12568	0,13438	-0,08948
0,07905	0,39390	0,35048	0,17649
0,29200	0,66258	0,56610	0,44367
0,50541	0,93165	0,78125	0,71187
0,71939	1,20090	0,99583	0,98088
0,93446	1,46953	1,20933	1,25060
1,15118	1,73661	1,42117	1,52080
1,36959	2,00127	1,63132	1,79057
1,58962	2,26258	1,83985	2,05873
1,81122	2,51919	2,04682	2,32380
2,03423	2,76958	2,25237	2,58435
2,25847	3,01244	2,45670	2,83912
2,48369	3,24657	2,66004	3,08697
2,70963	3,47109	2,86266	3,32710
2,93604	3,68531	3,06482	3,55877
3,16264	3,88877	3,26679	3,78150
3,35143	4,04988	3,43513	3,95992
3,50232	4,17313	3,56998	4,09777
3,53436	4,18426	3,58462	4,13010
3,57185	4,16733	3,57185	4,16733

Table 6-III. UTW Fan Rotor Blade Coordinates (Continued).

SECTION 2 RADIUS 76.2 cm (30.0 in.)

Convex		Concave	
X (Axial)	Y	X (Axial)	Y
-3.53096	-3.78711	-3.53096	-3.78711
-3.53951	-3.77219	-3.51429	-3.79124
-3.53964	-3.74671	-3.48973	-3.78440
-3.53068	-3.71117	-3.45787	-3.76615
-3.51173	-3.66625	-3.41950	-3.73590
-3.48194	-3.61259	-3.37527	-3.69315
-3.44093	-3.55049	-3.32533	-3.63779
-3.38936	-3.47944	-3.26875	-3.57053
-3.23593	-3.27533	-3.10711	-3.37975
-3.06179	-3.05086	-2.92182	-3.16812
-2.88750	-2.83311	-2.73667	-2.96328
-2.71310	-2.62119	-2.55163	-2.76416
-2.53857	-2.41421	-2.36672	-2.56974
-2.36391	-2.21141	-2.18195	-2.37919
-2.18911	-2.01213	-1.99731	-2.19170
-1.97915	-1.77680	-1.77595	-1.96984
-1.76893	-1.54478	-1.55484	-1.75039
-1.55840	-1.31538	-1.33404	-1.53261
-1.34752	-1.08803	-1.11360	-1.31584
-1.13622	-0.86234	-0.89358	-1.09966
-0.92445	-0.63802	-0.67403	-0.88369
-0.71217	-0.41484	-0.45498	-0.66769
-0.49933	-0.19267	-0.23650	-0.45148
-0.28588	0.02855	-0.01862	-0.23502
-0.07178	0.24883	0.19860	-0.01830
0.14300	0.46807	0.41515	0.19855
0.35854	0.68608	0.63093	0.41533
0.57513	0.90231	0.84567	0.63193
0.79303	1.11612	1.05909	0.84814
1.01230	1.32693	1.27115	1.06331
1.23284	1.53411	1.48193	1.27675
1.45459	1.73698	1.69151	1.48777
1.67745	1.93487	1.89997	1.69568
1.90130	2.12710	2.10745	1.89976
2.12599	2.31301	2.31408	2.09936
2.35136	2.49202	2.52003	2.29388
2.57722	2.66361	2.72549	2.48276
2.80339	2.82735	2.93065	2.66553
3.02965	2.98287	3.13571	2.84173
3.25581	3.12995	3.34088	3.01103
3.44407	3.24594	3.51206	3.14659
3.59086	3.33233	3.64598	3.24884
3.62375	3.33841	3.66485	3.27823
3.65778	3.31641	3.65778	3.31641

Table 6-III. UTW Fan Rotor Blade Coordinates (Continued).

SECTION 3 RADIUS 66.9 cm (26.3 in.)

Convex		Concave	
X (Axial)	Y	X (Axial)	Y
-3,44902	-3,03130	-3,44902	-3,03130
-3,45631	-3,01728	-3,43399	-3,03624
-3,45564	-2,99433	-3,41140	-3,03192
-3,44652	-2,96289	-3,38170	-3,01797
-3,42827	-2,92354	-3,34544	-2,99392
-3,40027	-2,87680	-3,30309	-2,95936
-3,36226	-2,82288	-3,25468	-2,91428
-3,31482	-2,76130	-3,19940	-2,85937
-3,15984	-2,56706	-3,02637	-2,68941
-2,99245	-2,36411	-2,83784	-2,51105
-2,82463	-2,16755	-2,64974	-2,33963
-2,65638	-1,97693	-2,46207	-2,17435
-2,48767	-1,79173	-2,27486	-2,01442
-2,31848	-1,61151	-2,08814	-1,85914
-2,14878	-1,43584	-1,90191	-1,70781
-1,94447	-1,23052	-1,67912	-1,53056
-1,73937	-1,03059	-1,45712	-1,35712
-1,53340	-0,83559	-1,23598	-1,18674
-1,32651	-0,64513	-1,01577	-1,01875
-1,11859	-0,45896	-0,79658	-0,85271
-0,90958	-0,27691	-0,57850	-0,68827
-0,69938	-0,09890	-0,36159	-0,52522
-0,48796	0,07507	-0,14590	-0,36339
-0,27532	0,24498	0,06856	-0,20265
-0,06144	0,41083	0,28178	-0,04291
0,15371	0,57254	0,49373	0,11595
0,37024	0,73003	0,70431	0,27396
0,58823	0,88309	0,91342	0,43096
0,80777	1,03142	1,12098	0,58671
1,02884	1,17467	1,32702	0,74066
1,25131	1,31237	1,53166	0,89227
1,47503	1,44402	1,73504	1,04101
1,69984	1,56905	1,93733	1,18636
1,92553	1,68698	2,13875	1,32781
2,15181	1,79732	2,33957	1,46492
2,37838	1,89976	2,54010	1,59735
2,60492	1,99412	2,74067	1,72484
2,83111	2,08047	2,94158	1,84731
3,05681	2,15904	3,14299	1,96460
3,28185	2,22986	3,34505	2,07641
3,46864	2,28300	3,51417	2,16531
3,61268	2,32088	3,64570	2,23165
3,64345	2,31843	3,66807	2,25485
3,66937	2,29101	3,66937	2,29101

Table 6-III. UTW Fan Rotor Blade Coordinates (Continued).

SECTION 4 RADIUS 57.2 cm (22.5 in.)

Convex		Concave	
X (Axial)	Y	X (Axial)	Y
-3,27656	-2,27702	-3,27656	-2,27702
-3,28322	-2,26279	-3,26204	-2,28303
-3,28186	-2,24050	-3,23980	-2,28070
-3,27207	-2,21053	-3,21017	-2,26971
-3,25332	-2,17341	-3,17355	-2,24967
-3,22513	-2,12958	-3,13024	-2,22029
-3,18733	-2,07922	-3,08018	-2,18164
-3,14041	-2,02184	-3,02260	-2,13446
-3,00531	-1,86253	-2,86579	-2,00785
-2,84845	-1,68435	-2,68165	-1,86527
-2,69081	-1,51211	-2,49829	-1,72907
-2,53231	-1,34548	-2,31578	-1,59863
-2,37289	-1,18419	-2,13420	-1,47341
-2,21244	-1,02809	-1,95364	-1,35305
-2,05092	-0,87713	-1,77416	-1,23720
-1,85563	-0,70271	-1,56025	-1,10369
-1,65868	-0,53560	-1,34800	-0,97568
-1,46005	-0,37578	-1,13742	-0,85268
-1,25975	-0,22324	-0,92852	-0,73420
-1,05776	-0,07797	-0,72130	-0,61984
-0,85414	0,06003	-0,51571	-0,50917
-0,64895	0,19075	-0,31170	-0,40182
-0,44225	0,31420	-0,10920	-0,29746
-0,23413	0,43043	0,09188	-0,19578
-0,02466	0,53944	0,29162	-0,09654
0,18612	0,64122	0,49005	0,00047
0,39814	0,73569	0,68723	0,09543
0,61134	0,82282	0,88324	0,18838
0,82557	0,90254	1,07821	0,27929
1,04070	0,97480	1,27229	0,36809
1,25652	1,03950	1,46567	0,45467
1,47281	1,09659	1,65858	0,53892
1,68933	1,14604	1,85126	0,62070
1,90583	1,18789	2,04397	0,69984
2,12215	1,22220	2,23685	0,77609
2,33818	1,24891	2,43003	0,84904
2,55368	1,26786	2,62373	0,91817
2,76842	1,27875	2,81820	0,98277
2,98190	1,28127	3,01392	1,04212
3,19369	1,27534	3,21134	1,09559
3,36866	1,26400	3,37737	1,13521
3,50345	1,25130	3,50742	1,16266
3,52868	1,24005	3,53283	1,17756
3,54352	1,20850	3,54352	1,20850

Table 6-III. UTW Fan Rotor Blade Coordinates (Concluded).

SECTION 5 RADIUS 44.7 cm (18.8 in.)

Convex		Concave	
X (Axial)	Y	X (Axial)	Y
-2,99111	-1,53332	-2,99111	-1,53332
-2,99661	-1,51937	-2,97778	-1,54019
-2,99415	-1,49848	-2,95672	-1,53986
-2,98342	-1,47101	-2,92817	-1,53206
-2,96398	-1,43741	-2,89242	-1,51649
-2,93547	-1,39809	-2,84966	-1,49292
-2,89777	-1,35321	-2,79978	-1,46149
-2,85128	-1,30229	-2,74206	-1,42298
-2,74618	-1,19129	-2,62085	-1,34350
-2,60488	-1,04793	-2,45456	-1,23970
-2,46249	-0,91015	-2,28934	-1,14224
-2,31901	-0,77783	-2,12523	-1,05062
-2,17438	-0,65084	-1,96226	-0,96435
-2,02861	-0,52907	-1,80043	-0,88293
-1,88167	-0,41240	-1,63979	-0,80592
-1,70357	-0,27903	-1,44876	-0,71897
-1,52347	-0,15302	-1,25975	-0,63765
-1,34115	-0,03456	-1,07296	-0,56178
-1,15662	0,07596	-0,88837	-0,49114
-0,97013	0,17822	-0,70574	-0,42527
-0,78186	0,27207	-0,52490	-0,36372
-0,59214	0,35744	-0,34551	-0,30593
-0,40109	0,43439	-0,16744	-0,25140
-0,20852	0,50299	0,00911	-0,19998
-0,01449	0,56305	0,18419	-0,15156
0,18120	0,61427	0,35762	-0,10623
0,37827	0,65609	0,52966	-0,06403
0,57603	0,68809	0,70102	-0,02487
0,77398	0,71018	0,87218	0,01129
0,97134	0,72250	1,04394	0,04463
1,16778	0,72543	1,21662	0,07529
1,36313	0,71937	1,39038	0,10335
1,55717	0,70473	1,56546	0,12878
1,74974	0,68192	1,74201	0,15152
1,94060	0,65140	1,92026	0,17148
2,12950	0,61378	2,10047	0,18861
2,31654	0,56974	2,28255	0,20292
2,50190	0,51979	2,46631	0,21426
2,68565	0,46433	2,65167	0,22235
2,86787	0,40358	2,83857	0,22666
3,01856	0,34896	2,99548	0,22686
3,13513	0,30368	3,10630	0,22470
3,15489	0,28737	3,13939	0,22758
3,16082	0,25675	3,16082	0,25675

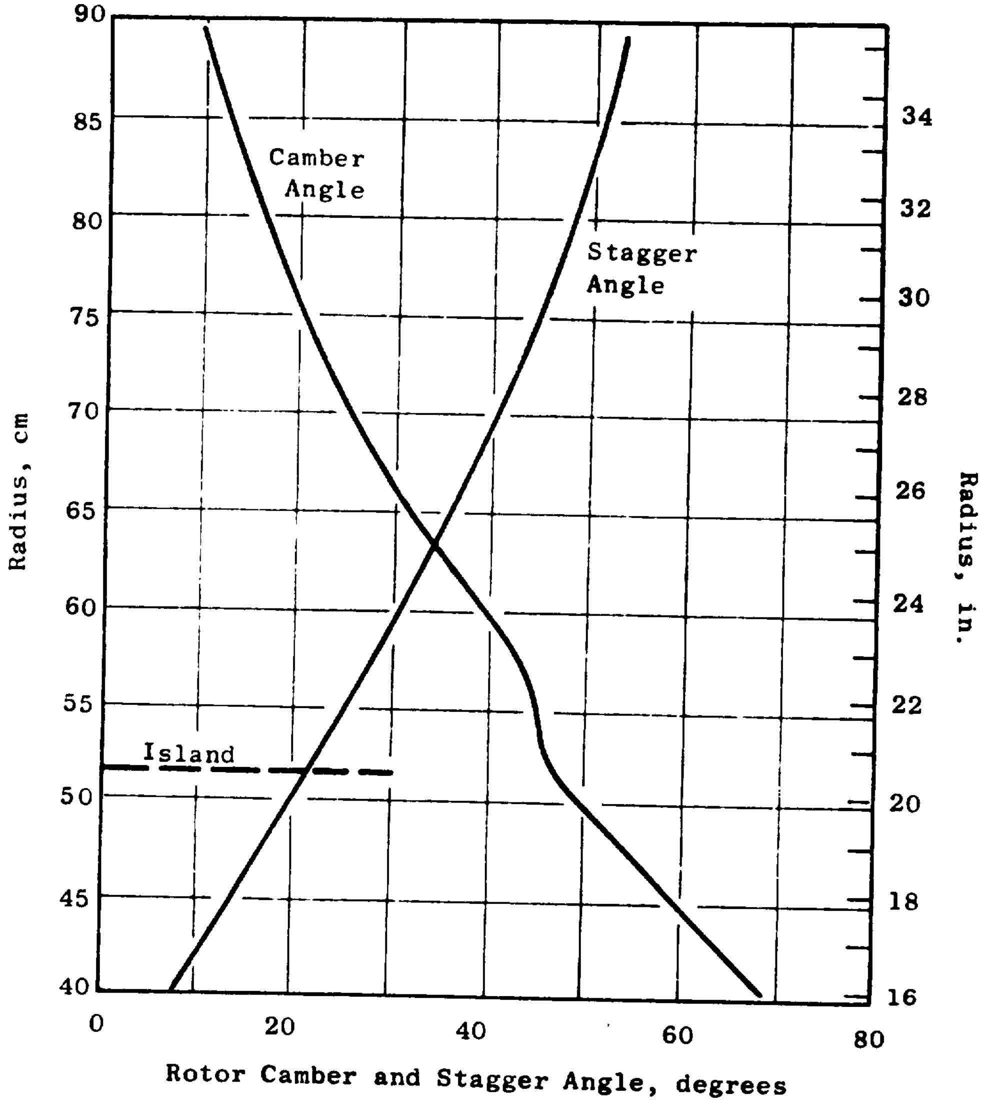

Figure 6-14. UTW Fan Rotor Camber and Stagger Angle Radial Distribution.

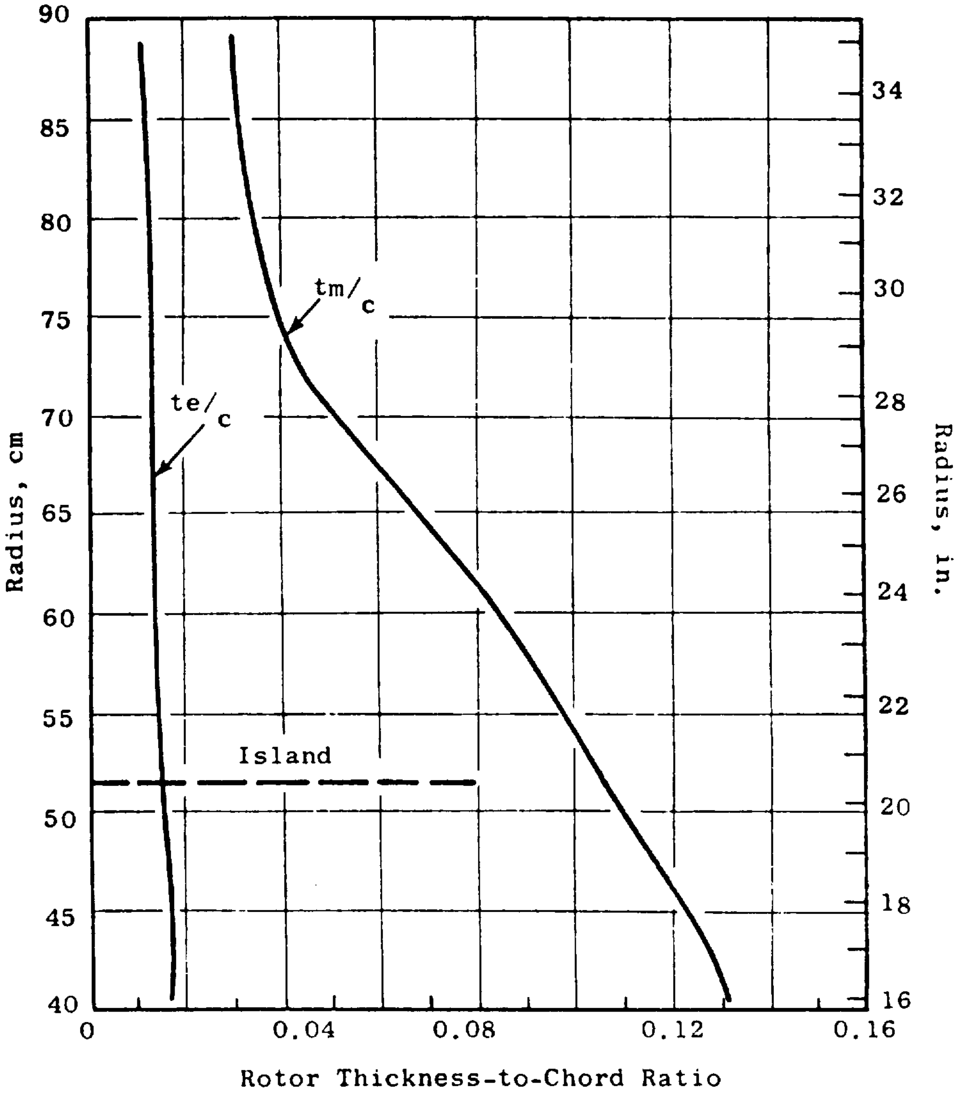

Figure 6-15. Rotor Thickness Distributions.

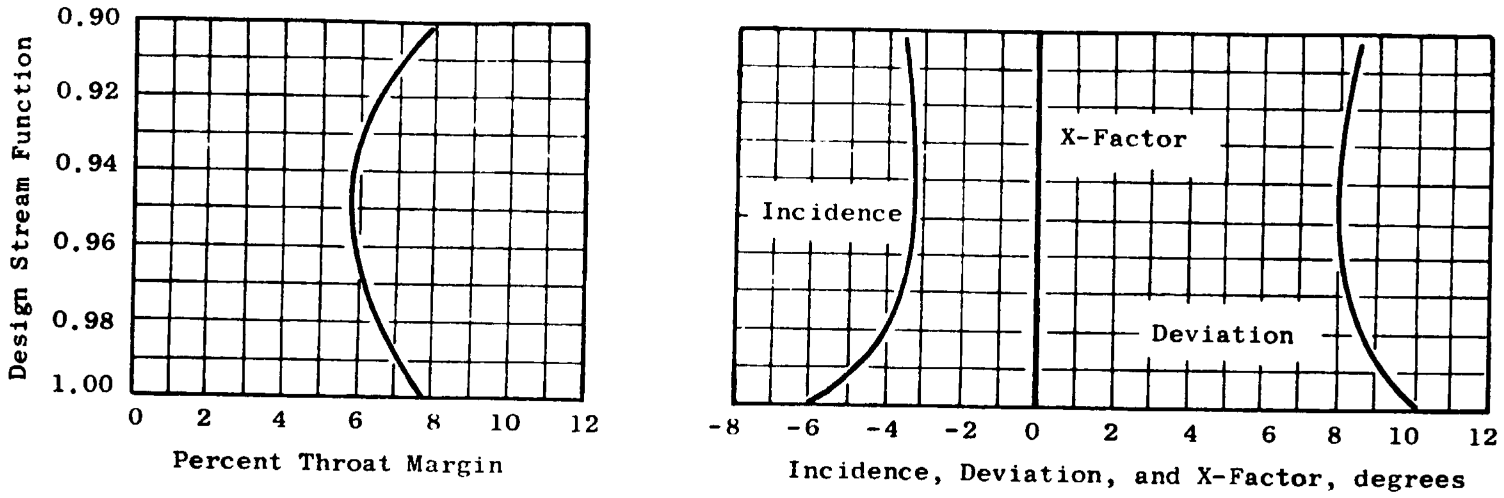

Figure 6-16. Core OGV Aerodynamic Design Characteristics.

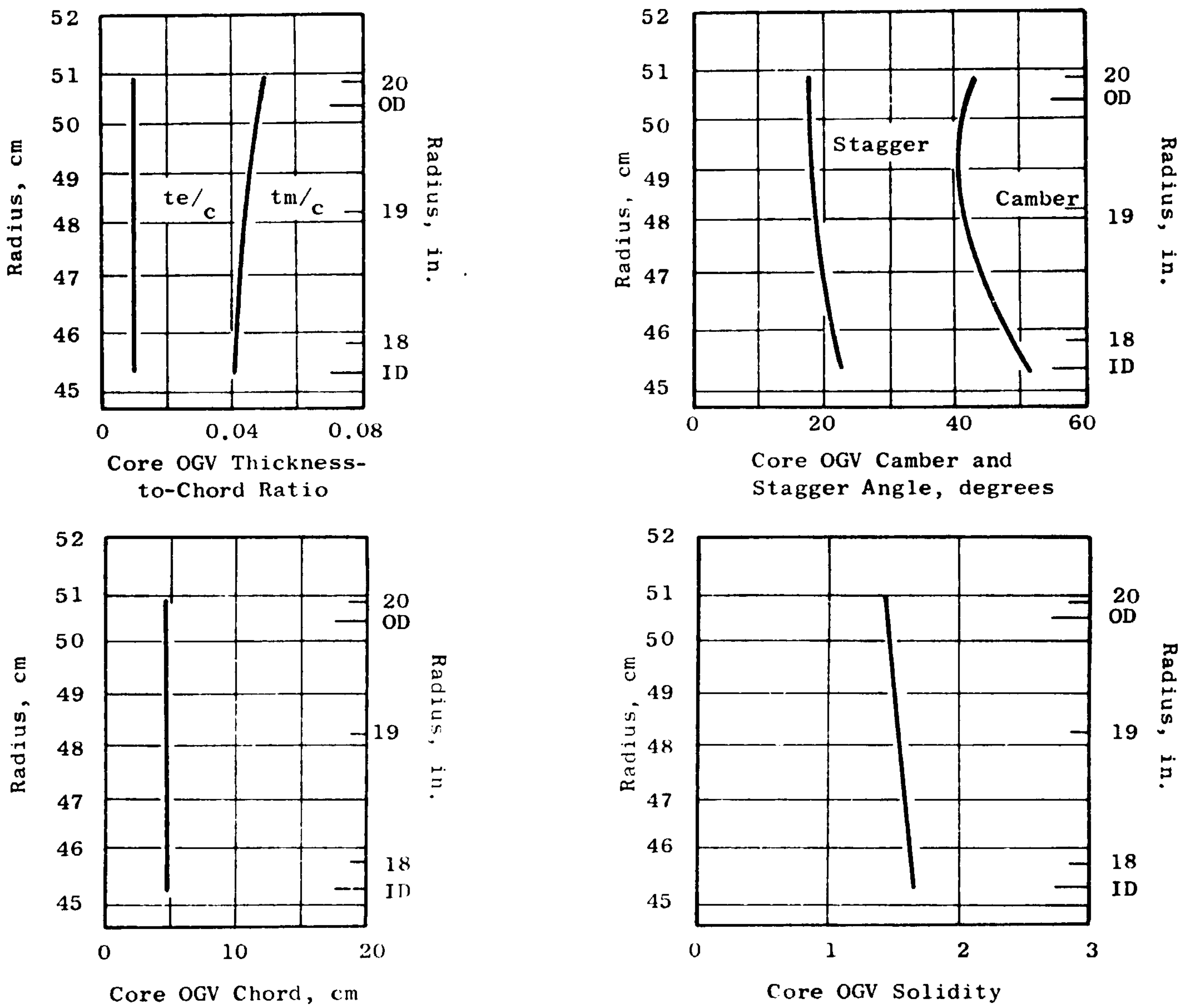

Figure 6-17. Core OGV Geometry Parameters.

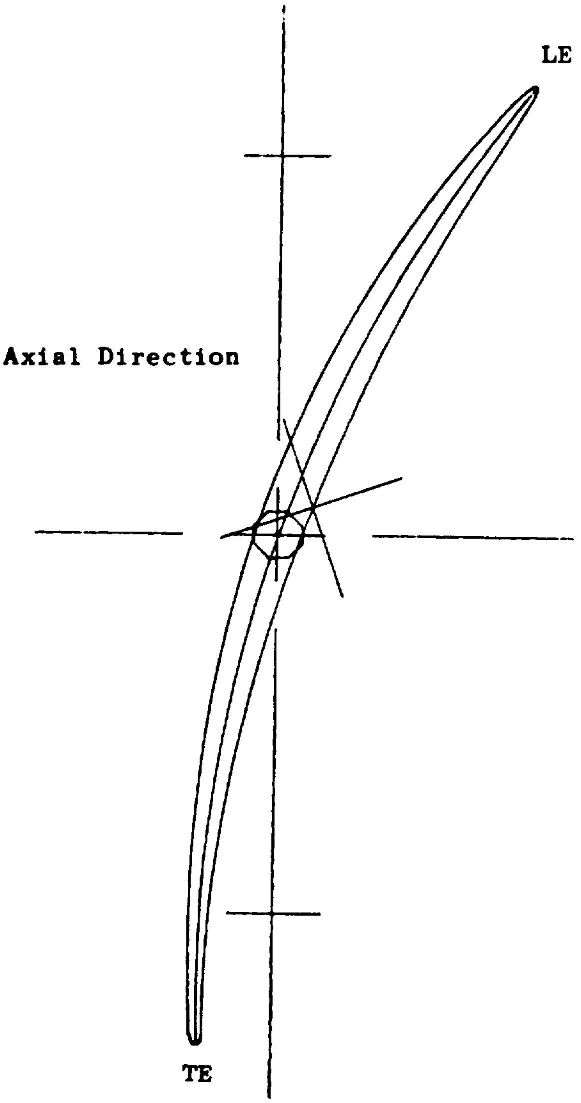
LE
Axial Direction
TE

Figure 6-18. Cylindrical Section of Core OGV at the Pitch Line Radius.

Table 6-IV. UTW Fan Core OGV Coordinates at the Pitch Line Radius.

Convex		Concave	
X (Axial)	Y	X (Axial)	Y
-0,842769	0,477539	-0.842769	0,477539
-0,842102	0,478085	-0,843193	0,476788
-0,841193	0,478426	-0.843371	0,475831
-0,840041	0,478562	-0,843303	0,474671
-0,838648	0,478489	-0,842988	0.473308
-0,837016	0,478207	-0,842422	0,471747
-0,835148	0,477713	-0.841604	0,469990
-0,833043	0,477005	-0.840531	0,468041
-0,830706	0,476081	-0.839199	0,465902
-0,825930	0,473879	-0.836147	0.461586
-0,816825	0,468976	-0.829578	0,453512
-0,795126	0,455609	-0.811971	0,434780
-0,752668	0,428386	-0,775318	0,399261
-0,710699	0,401338	-0.737917	0,365474
-0,668893	0,374802	-0,698908	0,333049
-0,585404	0,323526	-0,619675	0,271892
-0,501676	0,274929	-0,538221	0,215193
-0,417507	0,229049	-0,454815	0.162726
-0,332770	0,185866	-0.369635	0,114358
-0,247368	0,149345	-0.282819	0,070005
-0,161246	0,107397	-0.194455	0,029661
-0,074357	0,071905	-0.104611	-0,006617
0,013395	0,038873	-0.013395	-0,038873
0,102065	0,008204	0.079131	-0,067022
0,191787	-0,019959	0.172840	-0,091196
0,282669	-0,045471	0.267634	-0.111499
0,374803	-0,068200	0.363446	-0,128002
0,468270	-0,087992	0.460225	-0,140766
0,563146	-0,104640	0.557937	-0,149878
0,659491	-0,117933	0,656574	-0,155395
0,757358	-0,127551	0,756149	-0,157452
0,856774	-0,133069	0.856712	-0,156245
0,876843	-0,133602	0,876951	-0,155667
0,896972	-0,133921	0,897236	-0,154995
0,917161	-0,134016	0,917569	-0,154238
0,937408	-0,133872	0.937951	-0,153407
0,948266	-0,133695	0.948850	-0,152936
0,954694	-0,136013	0.955078	-0,150279
0,958048	-0,142994	0,958048	-0,142994

6.2.8 Transition Duct Strut Design

The transition duct flowpath is shown in Figure 6-19. The ratio of duct exit to duct inlet flow area is 1.02. There are six struts in the transition duct which are aerodynamically configured to remove the 0.105 radian (6° of swirl left in the air by the core OGV's and to house the structural spokes of the composite wheels, see Figure 6-2). In addition, at engine station 196.5 (Figure 6-2), the 6 and 12 o'clock strut positions must house radial accessory drive shafts. The number of struts and axial position of the strut trailing edge were selected identical with the F101 engine to minimize unknowns in the operation of the core engine system. Axial position and thickness requirements of the composite wheel spokes were dictated by mechanical considerations. The axial location of the strut leading edge at the OD was determined by its proximity to the splitter leading edge. At the OD flowpath, the strut leading edge is 17.8 mm (0.7 in.) forward of the wheel spoke. A relatively blunt strut leading edge results from the 26.7 mm (1.05 in.) wheel spoke thickness requirement. The wheel spoke is radial. The axial lean of the strut leading edge provides relief from the LE bluntness at lower radii and makes the LE approximately normal to the incoming flow. Since the inlet Mach number in the OD region is less than 0.5 and the boundary layer along the outer wall initiates at the splitter LE, no significant aerodynamic penalty was assessed because of the bluntness. A NASA 65-series thickness distribution was selected for the basic profile thickness which was modified for the special considerations required in this design. The strut thickness is the same for all radii aft of the forward wheel spoke LE (Figure 6-19) to facilitate fabrication. A cylindrical cut cross section showing the nominal strut geometry at three radii is shown in Figure 6-20. The thickness distribution for the 6 and 12 o'clock struts was modified for the envelope of the radial drive shaft. Cylindrical cut cross sections of these struts are also shown in Figure 6-20. The forward 40% chord of these modified sections is identical to that of the nominal strut geometry. Aft of the forward wheel spoke LE, the strut thickness is the same for all radii. The core engine has demonstrated operation in the presence of a similar thick strut in the F101 application without duress.

6.2.9 Vane-Frame (Fan Bypass OGV) Design

The vane-frame performs the dual function of an outlet guide vane for the bypass flow and a frame support for the engine components and nacelle. It is a common piece of hardware for both the UTW and OTW engine fans. It is integrated with the pylon which houses the radial drive shaft at engine station 196.5 (see Figure 6-2), houses the engine mount at approximately engine station 210, provides an interface between the propulsion system with the aircraft system, and houses the forward thrust links. The vane-frame furthermore acts as an inlet guide vane for the UTW fan when in the reverse mode of operation.

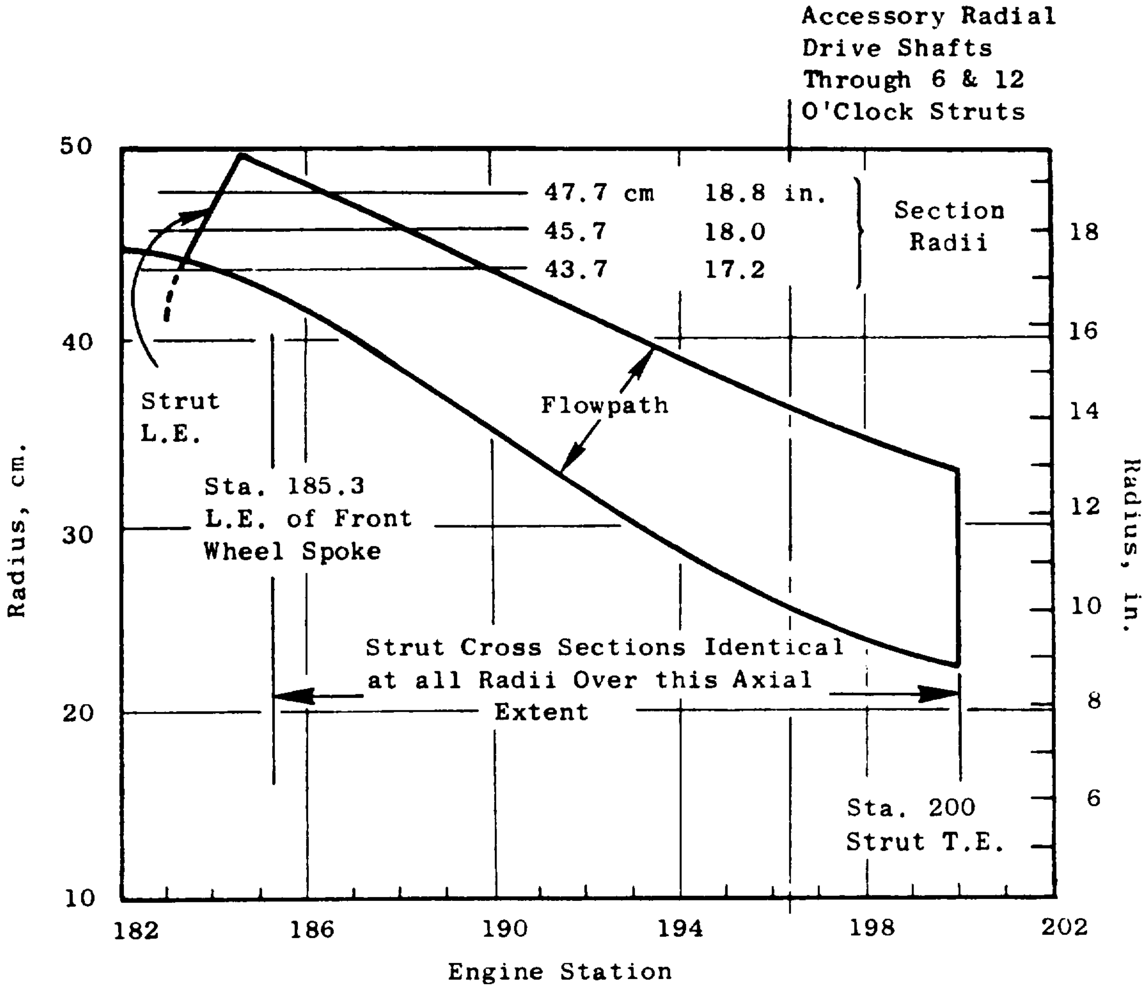

Figure 6-19. Transition Duct Flowpath.

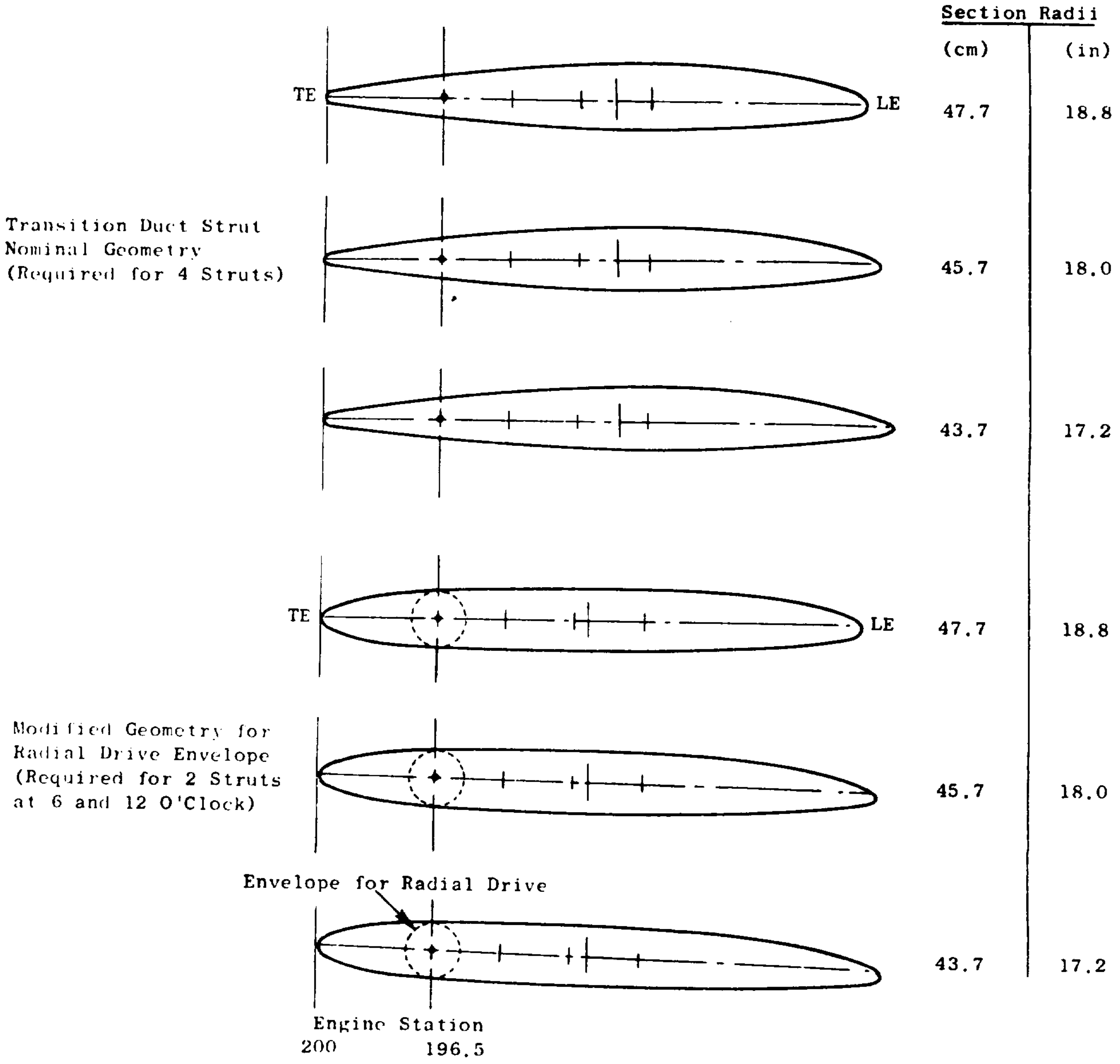
Section Radii
(cm)
(in)
TE
LE
47.7
18.8
Transition Duct Strut
Nominal Geometry
(Required for 4 Struts)
45.7
18.0
43.7
17.2
TE
LE
47.7
18.8
Modified Geometry for
Radial Drive Envelope
(Required for 2 Struts
at 6 and 12 O'Clock)
45.7
18.0
Envelope for Radial Drive
43.7
17.2
Engine Station
200
196.5

Figure 6-20. Nominal and Modified Transition Duct Strut Cylindrical Sections.

A conventional OGV system turns the incoming flow to axial. Housing requirements of the pylon dictate a geometry which requires the OGV's to underturn approximately 0.174 radian (10°) on one side and to overturn approximately 0.174 radian (10°) on the other side. The vanes must be tailored to downstream vector diagrams which conform to the natural flow field around the pylon to avoid creating velocity distortions in the upstream flow. Ideally, each vane would be individually tailored. To avoid excessive costs, however, five vane geometry groups were selected as adequate.

The Mach number and air angle at inlet to the vane-frame (fan bypass OGV) are shown in Figure 6-21 for both the UTW and OTW fans. In the outer portion of the bypass duct annulus, the larger air angle in the UTW environment results in a less negative incidence angle than for the OTW environment. Mach number in the outer portion of the annulus is also higher in the UTW environment. When selecting incidence angles, a higher Mach number environment naturally leads to the desire to select a less negative incidence angle. The amount by which the incidence angle would naturally be increased due to the higher Mach number UTW environment is approximately equal to the increase in inlet air angle of the UTW environment. In the inner portion of the annulus, the inlet Mach number and air angle are higher for the OTW environment. The natural increase in incidence angle desired because of the higher Mach number is approximately the same as increase in the inlet air angle. As a result of these considerations, no significant aerodynamic performance penalty is assessed to using common hardware for both the UTW and OTW fans.

Locally, near the bypass duct ID, there is a discontinuity in the aerodynamic invironment of the UTW configuration. This discontinuity represents that portion of the flow which passes under the island but bypasses the splitter. The calculation ignored mixing across the vortex sheet. In design of the vane geometry, no special considerations were incorporated because of this discontinuity since it is believed that in a real fluid the mixing process will greatly diminish the vortex strength.

The vane chord at the OD was selected largely by the mechanical requirement of axial spacing between the composite frame spokes. At the ID, the vane leading edge was lengthened primarily to obtain an aerodynamically reasonable leading edge fairing on the pylon compatible with envelope requirements of the radial drive shaft. The ID region is significantly more restrictive in this regard because of choking considerations, particularly for the OTW environment, with the reduced circumferential spacing between vanes. The solidity resulting from 33 vanes, an acoustic requirement, was acceptable for an aerodynamic loading viewpoint as shown in Figure 6-22. The two diffusion factor curves are a result of the two aerodynamic environments, UTW and OTW, to which the common vane-frame geometry is exposed. The thickness is a modified NASA 65-series distribution. Maximum-thickness- and trailing-edge-thickness-to-chord ratios of 0.08 and 0.02, respectively, were selected at the OD. The same maximum thickness and trailing edge thickness were used at all other radii which results in maximum-thickness- and trailing-edge-thickness-to-chord ratios of 0.064 and 0.016, respectively, at the ID.

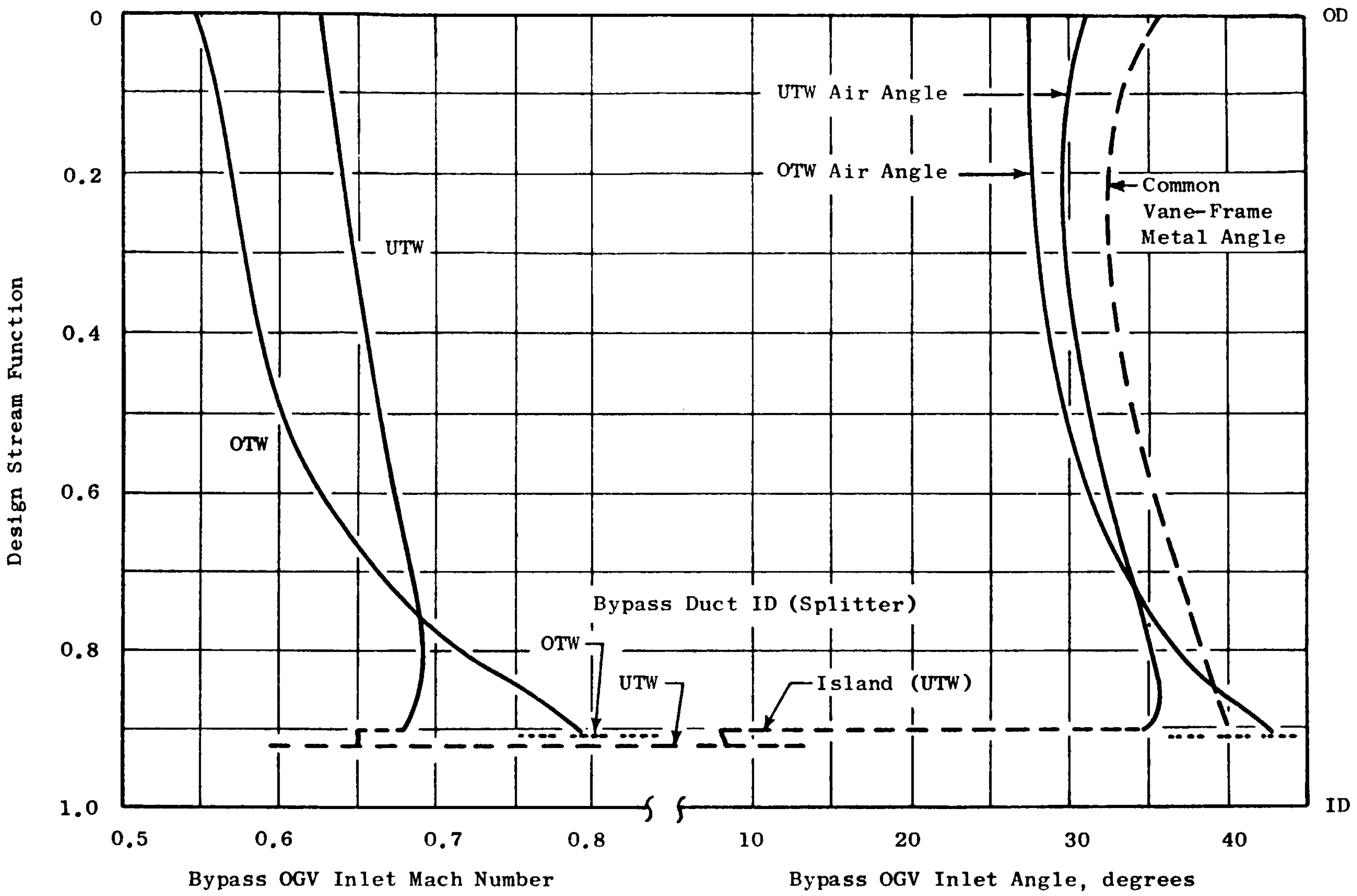

Figure 6-21. Vane-Frame (Fan Bypass OGV) Aerodynamic Environment.

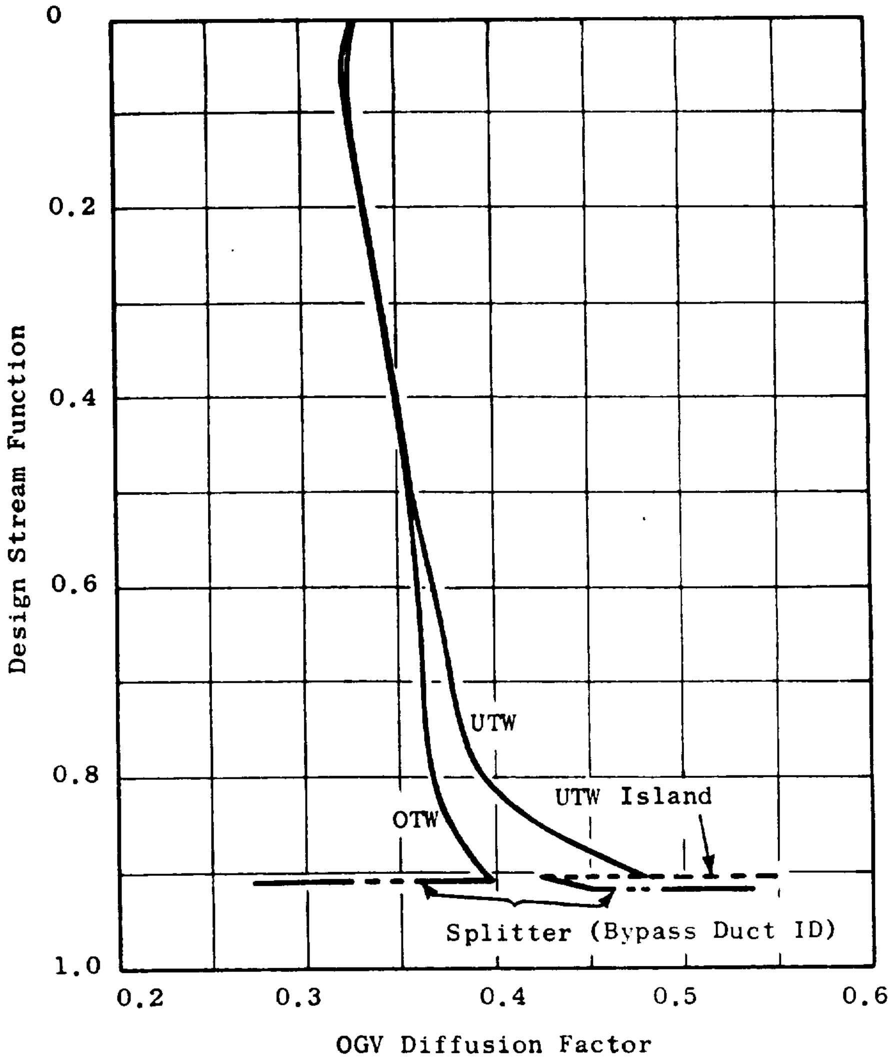

Figure 6-22. Vane-Frame (Fan Bypass OGV) Diffusion Factor for Nominal Vanes.

As a guide in the selection of the overall vector diagram requirements of the vane-frame, a circumferential analysis of an approximate vane geometry including the pylon, was performed. This analysis indicated, for uniform flow at vane inlet, that the vane discharge Mach number was approximately constant circumferentially and that the discharge air angle was nearly linear circumferentially between the pylon wall angles. Figure 6-23, an unwrapped cross section at the ID, shows the flowfield calculated by this analysis. The specific design criteria selected for the layout of the five vane geometry groups was to change the average discharge vector diagram with zero swirl to vector diagrams with ± 5° of swirl and ±10° of swirl.

The meanline shapes for each of the five vane groups vary. For the vane group which overturns the flow by +10° the meanline is approximately a circular arc. As a result of passage area distribution and choking considerations, the meanline shape employed in the forward 25% chord region of this vane group was retained for the other four groups.

The incidence angle for all vane groups was the same and was selected for the group with the highest camber. A correlation of NASA low-speed cascade data was the starting point for the incidence selection. Over the outer portion of the vane, where the inlet Mach number is lower, the incidence angles were slanted to the low side of the correlation. This was done in consideration of the reverse thrust mode of operation for the UTW fan. In this mode, the OGV's impart a swirl counter to the direction of rotor rotation. Additional vane leading edge camber tends to increase the counterswirl and therefore increase the pumping capacity of the fan in reverse. In the inner portion of the vane, the incidence angles are higher than suggested by the correlation because of the higher inlet Mach number. Also, in the reverse mode of operation, this reduction in vane leading edge camber in the ID region reduces the swirl for that portion of the fluid which enters the core engine and tends to reduce its pressure drop.

The deviation angle for each of the five vane groups was calculated from Carter's Rule as described for the rotor. The portion of the meanline aft of the 25% chord point approximates a circular arc blending between the front circular arc and the required trailing edge angle. For the vane group which underturns the flow by 10°, the aft portion of the blade has little camber. Figure 6-24 shows an unwrapped cross section at the ID of two of the 10° over-cambered vanes and two of the 10° under-cambered vanes adjacent to the pylon. Note that spacing between the pylon and the first under-cambered vane is 50% larger than average. This increased spacing was required to open the passage internal area, relative to the capture area, to retrieve the area blocked by the radial drive shaft envelope requirements.

Table 6-V gives the detailed coordinate data for the two vane geometries and the pylon leading edge geometry shown in Figure 6-24. The coordinate data for the nominal vane geometry at three radial locations are also given in this table. The vane coordinate data are in inches.

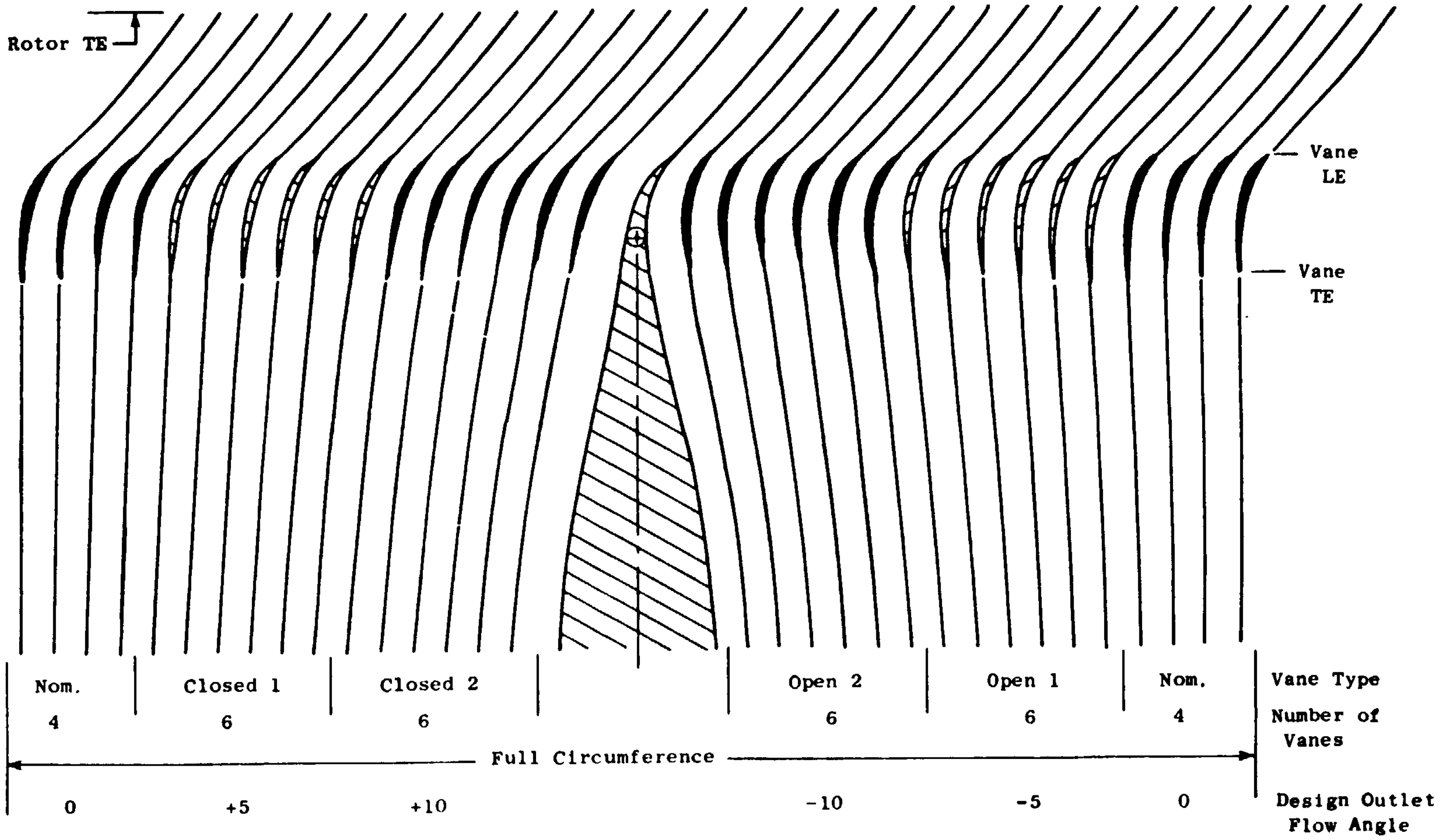
Rotor TE
Vane LE
Vane TE
Nom.
4
0
Closed 1
6
+5
Closed 2
6
+10
Open 2
6
-10
Open 1
6
-5
Nom.
4
0
Full Circumference
Vane Type
Number of Vanes
Design Outlet Flow Angle

Figure 6-23. Vane-Frame (Fan Bypass OGV) Unwrapped Section at ID.

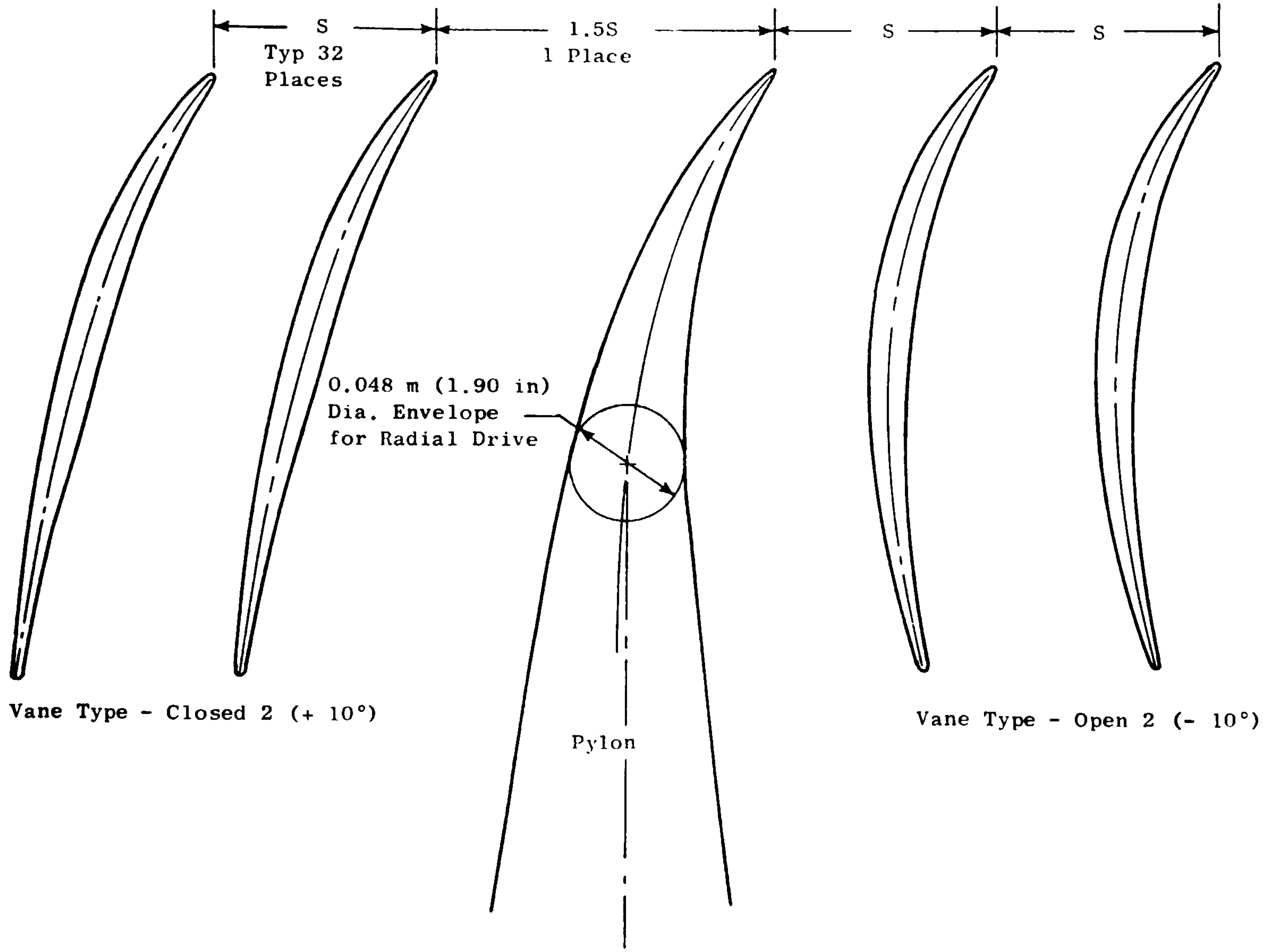
S
Typ 32
Places
1.5S
1 Place
S
S
0.048 m (1.90 in)
Dia. Envelope
for Radial Drive
Pylon
Vane Type - Closed 2 (+ 10°)
Vane Type - Open 2 (- 10°)

Figure 6-24. Vane-Frame (Fan Bypass OGV) Unwrapped Section at ID - Detail Near Pylon LE Fairing.

Table 6-V. Vane-Frame (Fan Bypass OGV) Coordinates.

Vane Type: Closed 2
Radius 53.0 cm (20.86 in.)

Convex		Concave	
X (Axial)	Y	X (Axial)	Y
-6.48210	2.34116	-6.48210	2.34116
-6.48759	2.32790	-6.47014	2.34917
-6.48654	2.30949	-6.45181	2.35181
-6.47875	2.28616	-6.42730	2.34886
-6.46396	2.25823	-6.39677	2.34011
-6.44206	2.22584	-6.36025	2.32555
-6.41331	2.18867	-6.31735	2.30561
-6.29919	2.05618	-6.16591	2.22947
-6.07119	1.83449	-5.89480	2.07990
-5.83097	1.63835	-5.63592	1.92961
-5.58939	1.45347	-5.37839	1.79199
-5.34632	1.27982	-5.12236	1.66526
-5.10018	1.11977	-4.86939	1.54502
-4.85192	0.97171	-4.61855	1.43098
-4.60258	0.83339	-4.36878	1.32361
-4.30233	0.67897	-4.07011	1.20263
-4.00106	0.53619	-3.77245	1.08890
-3.69886	0.40428	-3.47572	0.98129
-3.39590	0.28251	-3.17976	0.87882
-3.09242	0.16986	-2.88431	0.78108
-2.78889	0.06546	-2.58892	0.68742
-2.48547	-0.03115	-2.29341	0.59624
-2.18202	-0.12056	-1.99793	0.50613
-1.87857	-0.20389	-1.70246	0.41663
-1.57498	-0.28229	-1.40712	0.32765
-1.27110	-0.35637	-1.11208	0.23941
-0.96707	-0.42655	-0.81718	0.15212
-0.66307	-0.49346	-0.52225	0.06612
-0.35916	-0.55754	-0.22724	-0.01841
-0.05521	-0.61845	0.06774	-0.10206
0.24894	-0.67585	0.36251	-0.18531
0.55329	-0.73002	0.65709	-0.26774
0.85774	-0.78128	0.95157	-0.34873
1.16223	-0.82964	1.24600	-0.42780
1.46682	-0.87488	1.54034	-0.50454
1.77161	-0.91602	1.83448	-0.57877
2.07653	-0.95211	2.12848	-0.65013
2.38133	-0.98311	2.42260	-0.71727
2.68567	-1.00936	2.71719	-0.77845
2.98924	-1.03206	3.01255	-0.83151
3.24155	-1.04887	3.25934	-0.86832
3.41111	-1.05853	3.42574	-0.88974
3.46658	-1.04155	3.47884	-0.91753
3.50000	-0.98095	3.50000	-0.98095

Table 6-V. Vane-Frame (Fan Bypass OGV) Coordinates (Continued).

Vane Type: Pylon Leading Edge
Radius 53.0 cm (20.86 in.)

Convex		Concave	
X (Axial)	Y	X (Axial)	Y
-6,48132	2,39154	-6,48132	2,39154
-6,48473	2,38081	-6,47148	2,39700
-6,48161	2,36491	-6,45525	2,39712
-6,47179	2,34406	-6,43279	2,39173
-6,45509	2,31849	-6,40420	2,38068
-6,43144	2,28828	-6,36944	2,36404
-6,40114	2,25305	-6,32808	2,34232
-6,28510	2,12434	-6,17848	2,26374
-6,06174	1,89820	-5,90277	2,12120
-5,82801	1,69438	-5,63744	1,98182
-5,58938	1,50620	-5,37700	1,85097
-5,35069	1,32592	-5,11662	1,73488
-5,11131	1,15379	-4,85694	1,63146
-4,86999	0,99135	-4,59920	1,53737
-4,62695	0,83784	-4,34317	1,45194
-4,33354	0,66380	-4,03770	1,36062
-4,03838	0,49997	-3,73397	1,28070
-3,74142	0,34566	-3,43206	1,21133
-3,44249	0,20051	-3,13211	1,15184
-3,14194	0,06430	-2,83378	1,10152
-2,84029	-0,06372	-2,53655	1,05974
-2,53811	-0,18441	-2,23985	1,02584
-2,23601	-0,29875	-1,94307	0,99894
-1,93375	-0,40770	-1,64646	0,97830
-1,63088	-0,51145	-1,35045	0,96310
-1,32713	-0,60978	-1,05531	0,95241
-1,02219	-0,70205	-0,76138	0,94519
-0,71617	-0,78789	-0,46851	0,94075
-0,40945	-0,86865	-0,17635	0,94005
-0,10190	-0,94573	0,11497	0,94418
0,20685	-1,01906	0,40510	0,95304
0,51627	-1,08827	0,69456	0,96621
0,82574	-1,15361	0,98398	0,98345
1,13505	-1,21546	1,27354	1,00450
1,44405	-1,27381	1,56343	1,02871
1,73876	-1,32623	2,14355	1,08453
2,03355	-1,37574	2,44720	1,11734
3.50000	-1.64800	3.50000	1.20800

Table 6-V. Vane-Frame (Fan Bypass OGV) Coordinates (Continued).

Vane Type: Open 2
Radius 53.0 cm (20.86 in.)

Convex		Concave	
X (Axial)	Y	X (Axial)	Y
-6,48210	2,34116	-6.48210	2,34116
-6,48759	2,32791	-6,47013	2,34918
-6,48653	2,30950	-6,45180	2,35183
-6,47873	2,28619	-6,42726	2,34891
-6,46391	2,25830	-6,39669	2,34021
-6,44195	2,22597	-6,36008	2,32574
-6,41309	2,18893	-6,31705	2,30598
-6,29837	2,05743	-6,16673	2,23191
-6,06881	1,84013	-5,89719	2,08881
-5,82663	1,65165	-5,64026	1,94846
-5,58259	1,47746	-5,38519	1,82404
-5,33663	1,31730	-5,13205	1,71340
-5,08740	1,17343	-4,88217	1,61171
-4,83591	1,04408	-4,63456	1,51847
-4,58317	0,92682	-4,38819	1,43400
-4,27866	0,80069	-4,09378	1,34319
-3,97293	0,68941	-3,80058	1,26249
-3,66610	0,59230	-3,50849	1,19083
-3,35833	0,50871	-3,21733	1,12737
-3,04985	0,43788	-2,92688	1,07194
-2,74105	0,37917	-2,63676	1,02425
-2,43218	0,33258	-2,34670	0,98319
-2,12344	0,29797	-2,05652	0,94770
-1,81511	0,27447	-1,76592	0,91756
-1,50737	0,26103	-1,47473	0,89269
-1,20033	0,25681	-1,18284	0,87302
-0,89392	0,26100	-0,89033	0,85854
-0,58804	0,27293	-0,59728	0,84962
-0,28271	0,29217	-0,30369	0,84652
0,02205	0,31915	-0,00952	0,84873
0,32598	0,35420	0,28547	0,85578
0,62892	0,39664	0,58146	0,86776
0,93104	0,44568	0,87827	0,88487
1,23245	0,50099	1,17578	0,90731
1,53315	0,56243	1,47401	0,93516
1,83305	0,63035	1,77304	0,96799
2,13206	0,70496	2,07295	1,00552
2,43030	0,78549	2,37364	1,04842
2,72800	0,87086	2,67486	1,09772
3,02565	0,95941	2,97614	1,15510
3,27398	1,03479	3,22691	1,20994
3,44400	1,08772	3,39850	1,25063
3,49006	1,12517	3,45780	1,24339
3,50000	1,19138	3,50000	1,19138

Table 6-V. Vane-Frame (Fan Bypass OGV) Coordinates (Continued).

Vane Type: Nominal
Radius 53.0 cm (20.86 in.)

Convex		Concave	
X (Axial)	Y	X (Axial)	Y
-6,48210	2,34116	-6,48210	2,34116
-6,48759	2,32791	-6,47013	2,34918
-6,48654	2,30949	-6,45181	2,35182
-6,47874	2,28617	-6,42729	2,34888
-6,46394	2,25825	-6,39675	2,34014
-6,44203	2,22588	-6,36020	2,32561
-6,41324	2,18874	-6,31726	2,30572
-6,29896	2,05654	-6,16614	2,23018
-6,07054	1,83608	-5,89545	2,08244
-5,82980	1,64205	-5,63708	1,93498
-5,58753	1,46015	-5,38025	1,80119
-5,34355	1,29036	-5,12513	1,67933
-5,09631	1,13518	-4,87326	1,56502
-4,84677	0,99309	-4,62370	1,45801
-4,59597	0,86190	-4,37539	1,35882
-4.29378	0,71764	-4,07866	1,24915
-3,99047	0,58679	-3,78304	1,14834
-3,68627	0,46852	-3,48832	1,05511
-3.38139	0,36194	-3,19426	0,96836
-3,07616	0,26589	-2,90057	0,88755
-2,77084	0,17937	-2,60697	0,81205
-2,46549	0,10210	-2,31339	0,74054
-2,16009	0,03377	-2,01986	0,67182
-1,85478	-0,02657	-1,72625	0,60556
-1,54964	-0,07997	-1,43246	0,54168
-1,24470	-0,12720	-1,13847	0,48014
-0,93983	-0,16894	-0,84442	0,42105
-0,63494	-0,20568	-0,55038	0,36497
-0,33012	-0,23761	-0,25628	0,31230
-0,02535	-0,26417	0.03788	0,26268
0,27916	-0,28484	0,33230	0,21567
0,58316	-0,30022	0,62722	0,17134
0,88725	-0,31091	0,92205	0,13018
1,19188	-0,31606	1,21636	0,09358
1,49640	-0,31452	1.51076	0,06272
1,80035	-0,30547	1,80573	0,03755
2,10352	-0,28852	2,10149	0,01793
2,40575	-0,26457	2,39819	0,00441
2,70721	-0,23490	2,69565	-0,00204
3,00816	-0,20101	2,99363	0,00047
3,25869	-0,17029	3,24220	0,01049
3,42732	-0,14778	3.40980	0,02082
3,47856	-0,12068	3,46729	0,00351
3,50000	-0,05474	3.50000	-0,05474

Table 6-V. Vane-Frame (Fan Bypass OGV) Coordinates (Continued).

Vane Type: Nominal
Radius 69.8 cm (27.48 in.)

Convex		Concave	
X (Axial)	Y	X (Axial)	Y
-5,58734	1,85159	-5,58734	1,85159
-5,59204	1,83581	-5,57482	1,86239
-5,58888	1,81511	-5,55459	1,86805
-5,57767	1,78979	-5,52679	1,86834
-5,55820	1,76017	-5,49156	1,86305
-5,53036	1,72642	-5,44892	1,85215
-5,49435	1,68825	-5,39858	1,83610
-5,41795	1,61418	-5,30236	1,80216
-5,20924	1,44123	-5,05671	1,70308
-4,99074	1,28915	-4,82084	1,59775
-4,77087	1,14424	-4,58634	1,49967
-4,54950	1,00677	-4,35334	1,40820
-4,32535	0,87963	-4,12313	1,32006
-4,09911	0,76188	-3,89500	1,23567
-3,87166	0,65193	-3,66808	1,15607
-3,59755	0,52960	-3,39695	1,06657
-3,32237	0,41733	-3,12689	0,98287
-3,04629	0,31473	-2,85773	0,90412
-2,76943	0,22135	-2,58935	0,82965
-2,49196	0,13645	-2,32158	0,75933
-2,21403	0,05948	-2,05428	0,69304
-1,93557	-0,00932	-1,78749	0,62999
-1,65657	-0,06966	-1,52125	0,56948
-1,37718	-0,12194	-1,25540	0,51166
-1,09766	-0,16670	-0,98968	0,45683
-0,81820	-0,20440	-0,72390	0,40517
-0,53899	-0,23556	-0,45787	0,35687
-0,26019	-0,26089	-0,19143	0,31220
0,01826	-0,28092	0,07536	0,27132
0,29653	-0,29522	0,34234	0,23382
0,57458	-0,30326	0,60952	0,19928
0,85232	-0,30529	0,87702	0,16812
1,12961	-0,30174	1,14497	0,14089
1,40634	-0,29289	1,41349	0,11784
1,68247	-0,27890	1,68260	0,09902
1,95797	-0,25944	1,95234	0,08396
2,23282	-0,23433	2,22272	0,07231
2,50703	-0,20433	2,49376	0,06473
2,78065	-0,17056	2,76537	0,06229
3,05389	-0,13473	3,03738	0,06670
3,28146	-0,10422	3,26418	0,07653
3,42738	-0,08386	3,40977	0,08530
3,47882	-0,05633	3,46701	0,06804
3,50000	0,00941	3,50000	0,00941

Table 6-V. Vane-Frame (Fan Bypass OGV) Coordinates (Concluded).

Vane Type: Nominal
Radius 90.1 cm (35.5 in.)

Convex		Concave	
X (Axial)	Y	X (Axial)	Y
-4.49480	1.64519	-4.49480	1.64519
-4.50141	1.62777	-4.48003	1.65611
-4.49961	1.60423	-4.45704	1.66064
-4.48913	1.57488	-4.42603	1.65851
-4.46969	1.54012	-4.38719	1.64946
-4.44110	1.50020	-4.34056	1.63344
-4.40352	1.45490	-4.28574	1.61098
-4.36001	1.40641	-4.22984	1.58666
-4.17865	1.23208	-4.01147	1.48459
-3.98730	1.08043	-3.80307	1.38218
-3.79412	0.93890	-3.59652	1.28894
-3.59889	0.80698	-3.39201	1.20396
-3.40085	0.68675	-3.19030	1.12394
-3.20110	0.57686	-2.99032	1.04840
-3.00038	0.47518	-2.79129	0.97765
-2.75845	0.36283	-2.55353	0.89860
-2.51543	0.26034	-2.31686	0.82511
-2.27133	0.16734	-2.08128	0.75648
-2.02632	0.08355	-1.84660	0.69213
-1.78065	0.00833	-1.61258	0.63195
-1.53453	-0.05889	-1.37902	0.57580
-1.28796	-0.11786	-1.14590	0.52287
-1.04094	-0.16833	-0.91323	0.47240
-0.79365	-0.21078	-0.68083	0.42448
-0.54628	-0.24579	-0.44852	0.37939
-0.29894	-0.27378	-0.21617	0.33741
-0.05184	-0.29518	0.01642	0.29879
0.19482	-0.31062	0.24945	0.26389
0.44100	-0.32059	0.48296	0.23289
0.68673	-0.32477	0.71691	0.20524
0.93213	-0.32276	0.95120	0.18045
1.17721	-0.31479	1.18580	0.15901
1.42173	-0.30120	1.42098	0.14150
1.66547	-0.28239	1.65692	0.12812
1.90844	-0.25863	1.89364	0.11880
2.15059	-0.22976	2.13118	0.11295
2.39198	-0.19569	2.36947	0.11011
2.63272	-0.15716	2.60842	0.11097
2.87313	-0.11508	2.84770	0.11677
3.11356	-0.07029	3.08696	0.13000
3.31347	-0.03164	3.28679	0.14794
3.43200	-0.00838	3.40618	0.16054
3.48205	0.02185	3.46416	0.14584
3.50000	0.08854	3.50000	0.08854

Radial distributions of camber and stagger for the nominal and two extreme vane geometries are shown in Figure 6-25. Radial distributions of chord and solidity for the nominal vane are shown in Figure 6-26. The design held the leading and trailing edge axial projection common for all five groups which results in slightly different chord lengths for the other four vane types.

6.2.10 Fan Performance Based on Scale Model Tests

Aerodynamic performance data in forward and reverse thrust modes were obtained from a 50.8 cm (20-inch) diameter scale model of the UTW engine fan. This simulator had ajustable-pitch rotor blades, allowing forward fan performance to be measured at the design stagger angle ($\beta_F = 0°$) and with the blades opened 5° and closed 5° from the design forward value. Complete results of these tests are described by Giffin, et al.* and key results relating to the adequacy of the fan design for use in the UTW engine are presented in this section.

Sufficient data were obtained to define the fan bypass and core flow performance maps at each forward stagger angle. The three bypass stream maps were curve-fit using a technique that allowed the stagger angle to be used as a parameter along with the usual parameters of speed and throttle area. This permitted convenient prediction of fan performance at a given stagger angle by interpolation within the group of maps based upon test data. A universal characteristic approach was tried as a means of unifying the data obtained at different rotor angle settings in forward thrust, but was not as successful as the curve-fit interpolation method. The curve-fit method was in excellent agreement with the test data with respect to pressure ratio versus flow and speed and generally fit the efficiency data within one point.

The fan bypass performance map for the design forward stagger angle is shown in Figure 6-27, scaled to UTW engine size from the curve fit model of the 50.8 cm (20 inch) scale-model test data at this setting angle. The aero design point is indicated on this figure, and comparison with the 100% corrected speed line shows that at design speed the fan demonstrated the design flow but was low in pressure rise. This is believed to be due to the rotor deviation angles being larger than assumed during the design process. Along a fixed-area operating line through the aero design point, the fan achieved a pressure ratio of 1.30 and a scaled flow of 386 kg/sec (851 lbm/sec) at design speed and nominal stagger angle. These values are, respectively, 3.0% and 5.5% less than the objectives.

---

* Giffin, R.G.; McFalls, R.A.; and Beacher, B.F.; "Aerodynamic and Aeromechanical Performance of a 50.8 cm (20 inch) dia. 1.34 PR Variable Pitch Fan with Core Flow," NASA CR-135017.

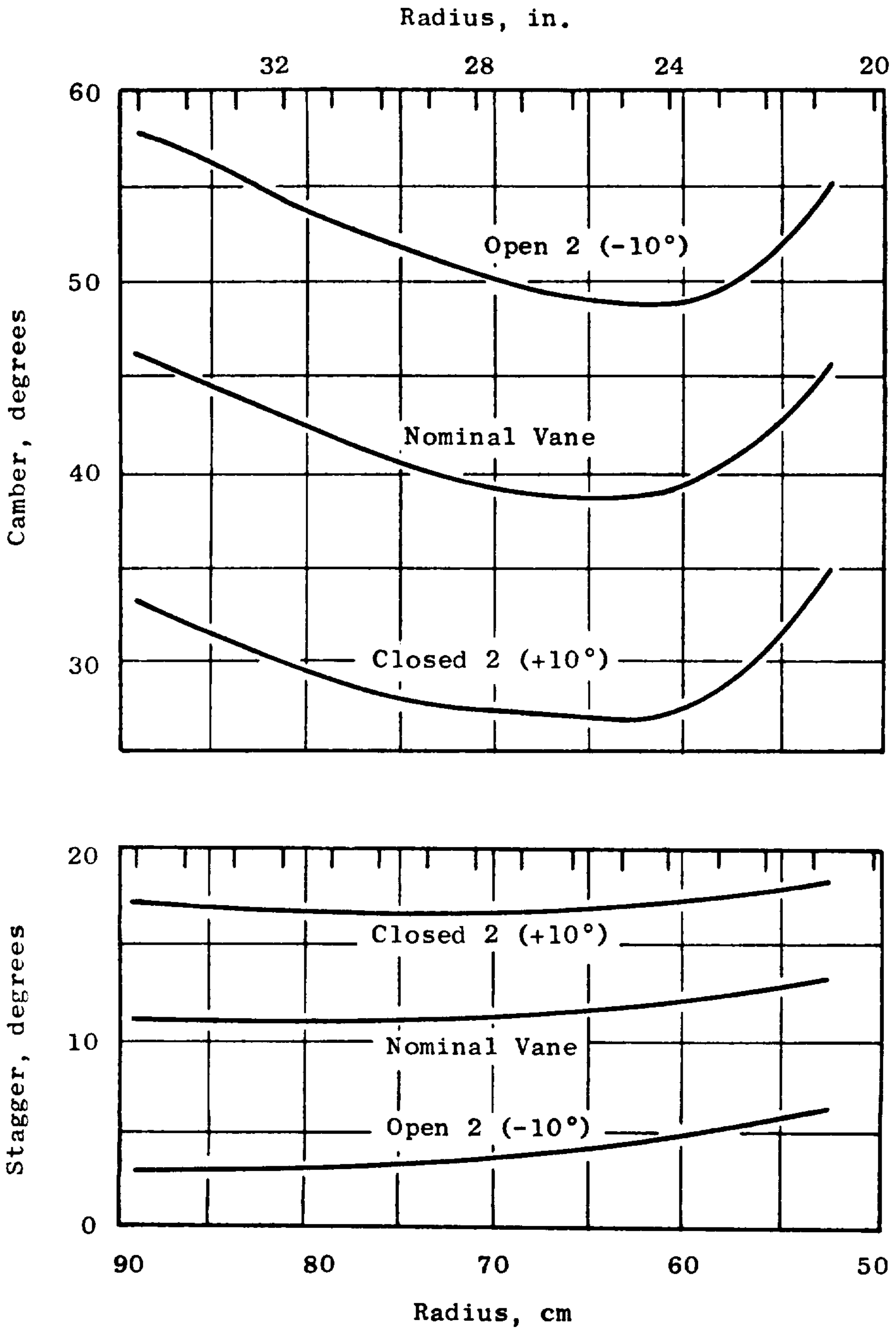

Figure 6-25. Vane-Frame (Fan Bypass OGV) Stagger and Camber Distributions.

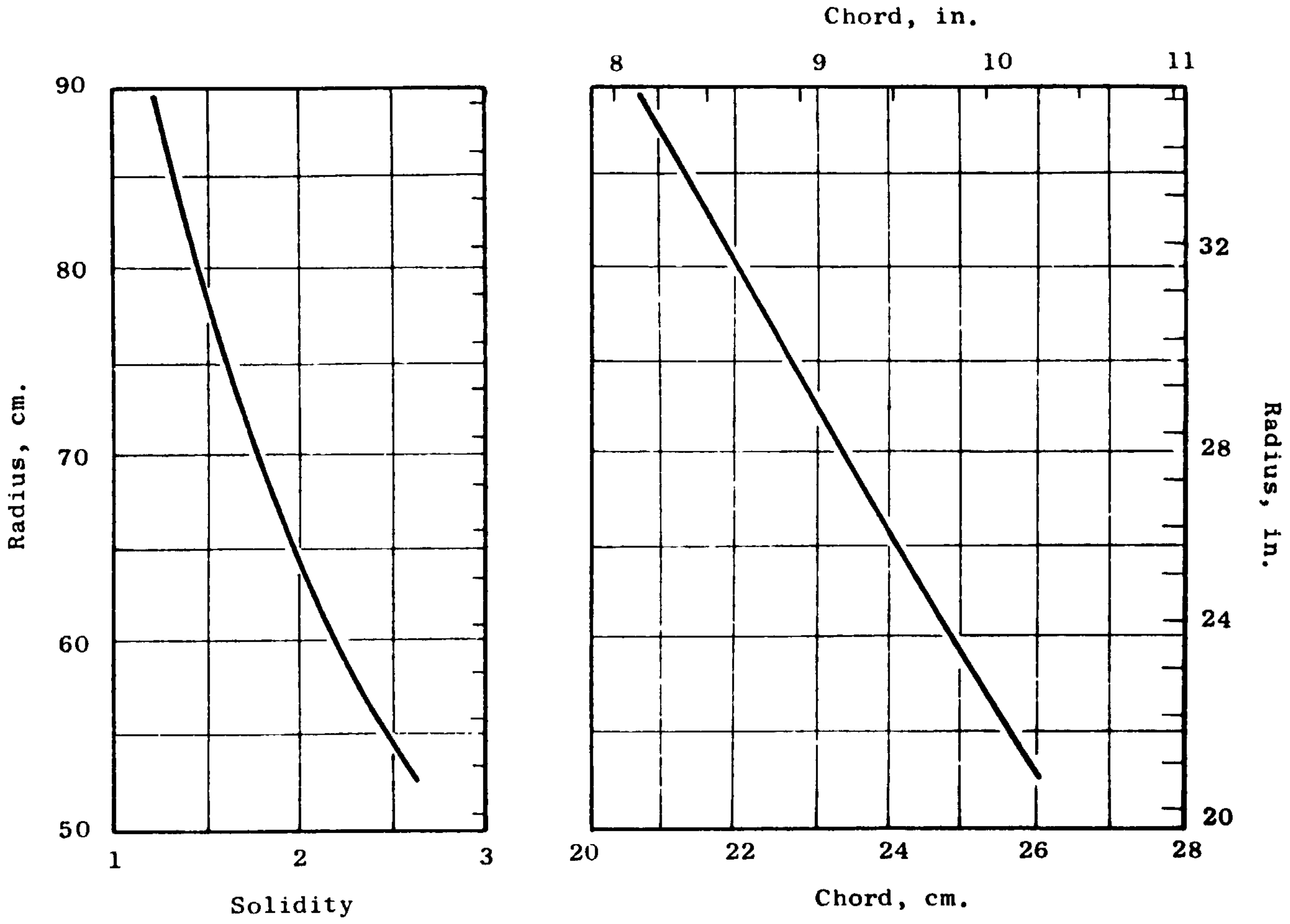

Figure 6-26. Vane-Frame (Fan Bypass OGV) Solidity and Chord Distributions.

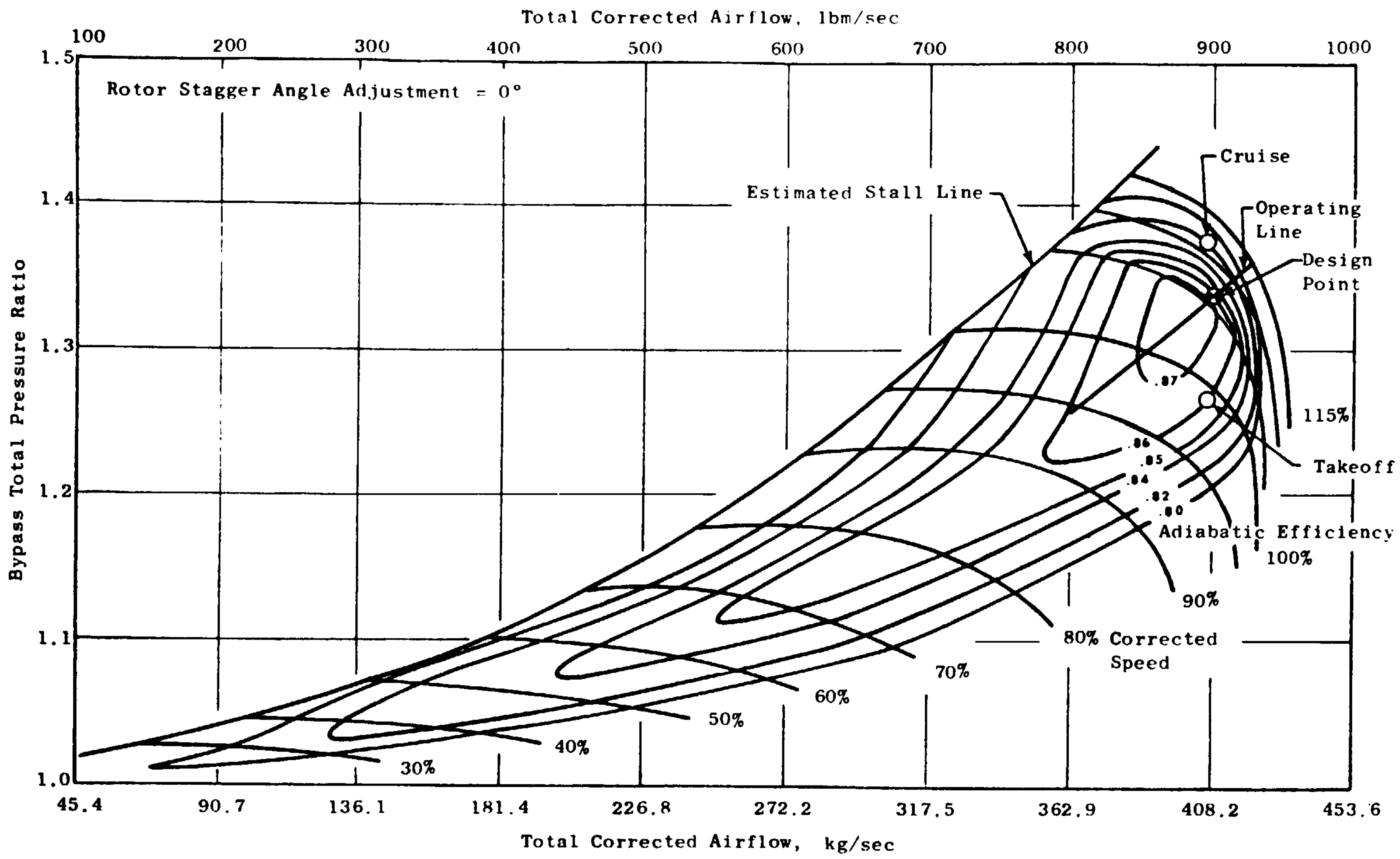

Figure 6-27. Fan Bypass Stream Performance Map at Design Rotor Stagger Setting.

The fan aero design point, however, was selected simply as an intermediate point between the two critical engine operating conditions at takeoff and maximum cruise power settings; it is fan flow and pressure ratio at these conditions that must be met in order for the engine to meet its thrust goals. The variable-pitch rotor and variable-area bypass stream exhaust nozzle features of the UTW fan allow these objectives to be met even though the design point was not achieved. In particular, the variable-pitch feature results in better overall engine system operating characteristics than would have been possible if changing only fan speed and nozzle area were used to reach these fan operating conditions.

Figure 6-28 shows the estimated fan bypass performance map at the maximum cruise condition. In this case, the flow of 405.5 kg/sec (894 lbm/sec) and pressure ratio of 1.38 required to achieve the thrust goal are achieved at a corrected speed of 109% and a stagger angle adjustment of -1.4° (open). Estimated efficiency at this condition is 0.811, about the same as would be obtained at nominal stagger by running the fan at 112% speed. The lower-speed, open-stagger setting was selected in order to limit the high Mach inlet throat Mach number (0.79) by maintaining a constant airflow (894 lbm/sec) at the highest possible pressure ratio for cruise, and to stay below a physical speed limitation on the fan drive turbine.

Similarly, the estimated takeoff condition fan performance map (Figure 6-29) shows that for a fan stagger angle adjustment of -3° (open), the required fan flow of 405.5 kg/sec (894 lbm/sec) and pressure ratio of 1.27 are achieved at 95% corrected speed and an efficiency of 0.833. This efficiency is lower than the value of 0.86 achieved at 100% speed and nominal stagger angle, but the lower fan speed is needed to reduce engine takeoff noise to objective levels.

To describe estimated full-scale engine performance, the fan hub performance data from the simulator fan tests were expressed in the form of modifying factors applied to the bypass stream performance maps. The fan hub pressure ratio is found as a function of bypass stream pressure ratio, as shown in Figure 6-30. This curve is an average of numerous data points at various throttle settings, rotor stagger angles, and speeds for the assumed bypass ratio schedule used in the simulator fan tests. In general, the fan hub pressure ratio at a given bypass pressure ratio slightly exceeds the objectives, assuring that the core engine will be adequately supercharged by the fan. Fan hub efficiency is related to bypass stream efficiency according to the relationship shown in Figure 6-31. Along a reference constant-throttle-area operating line passing somewhat below the design point, having a throttle area parameter of 1.34, the hub efficiency is a function of corrected fan speed. At a given corrected speed, the hub efficiency varies from its value at the reference operating line according to the variation in throttle area. These curves also are composites of a large number of data points. As mentioned by Giffin, et al., the fan hub efficiency exceeded the objective value at design speed with the nominal rotor pitch setting.

Performance in the reverse thrust mode of operation was determined for several rotor angle settings during the 50.8 cm (20 in.) scale model fan

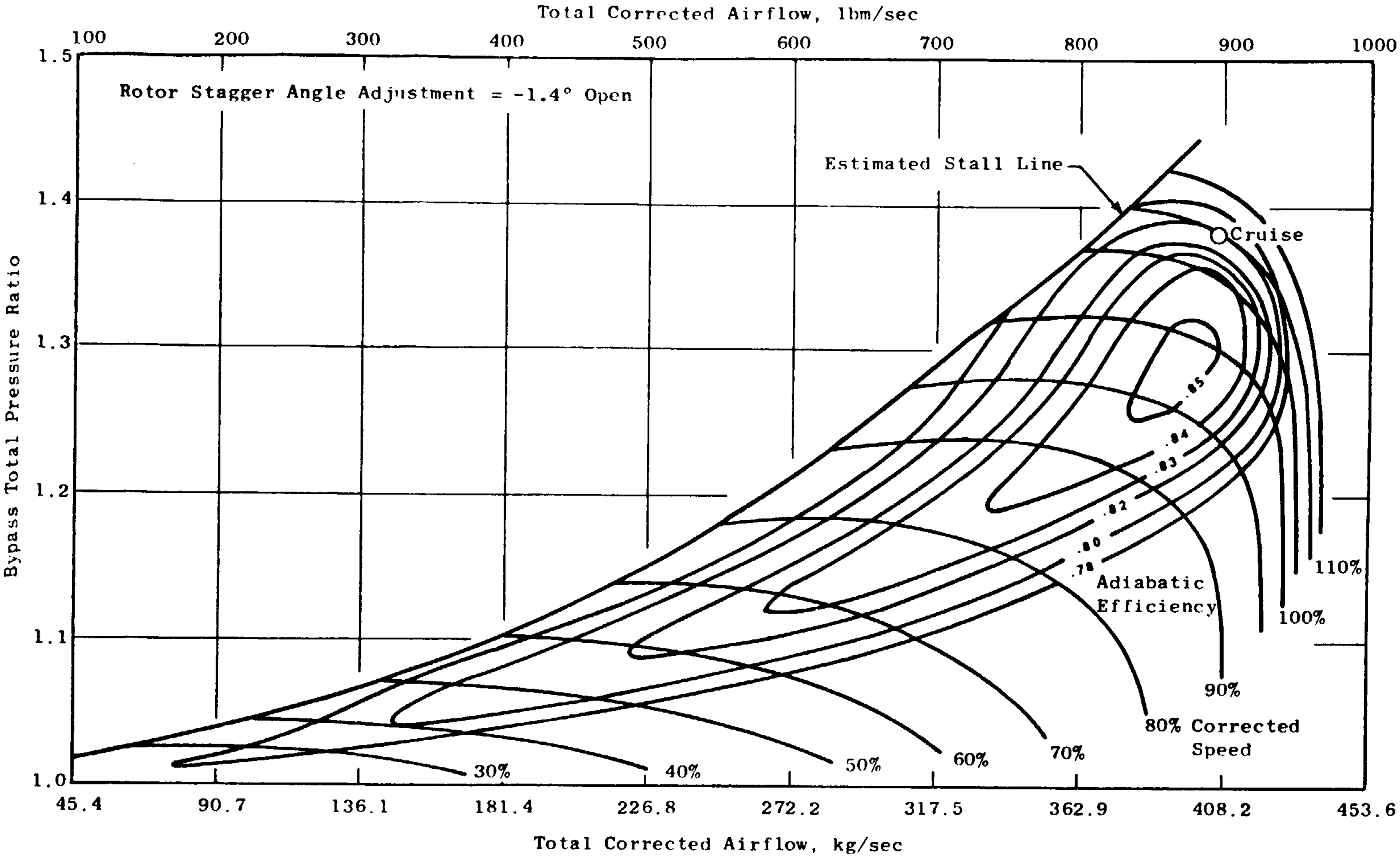

Figure 6-28. Fan Bypass Stream Performance at Estimated Cruise Rotor Stagger Setting.

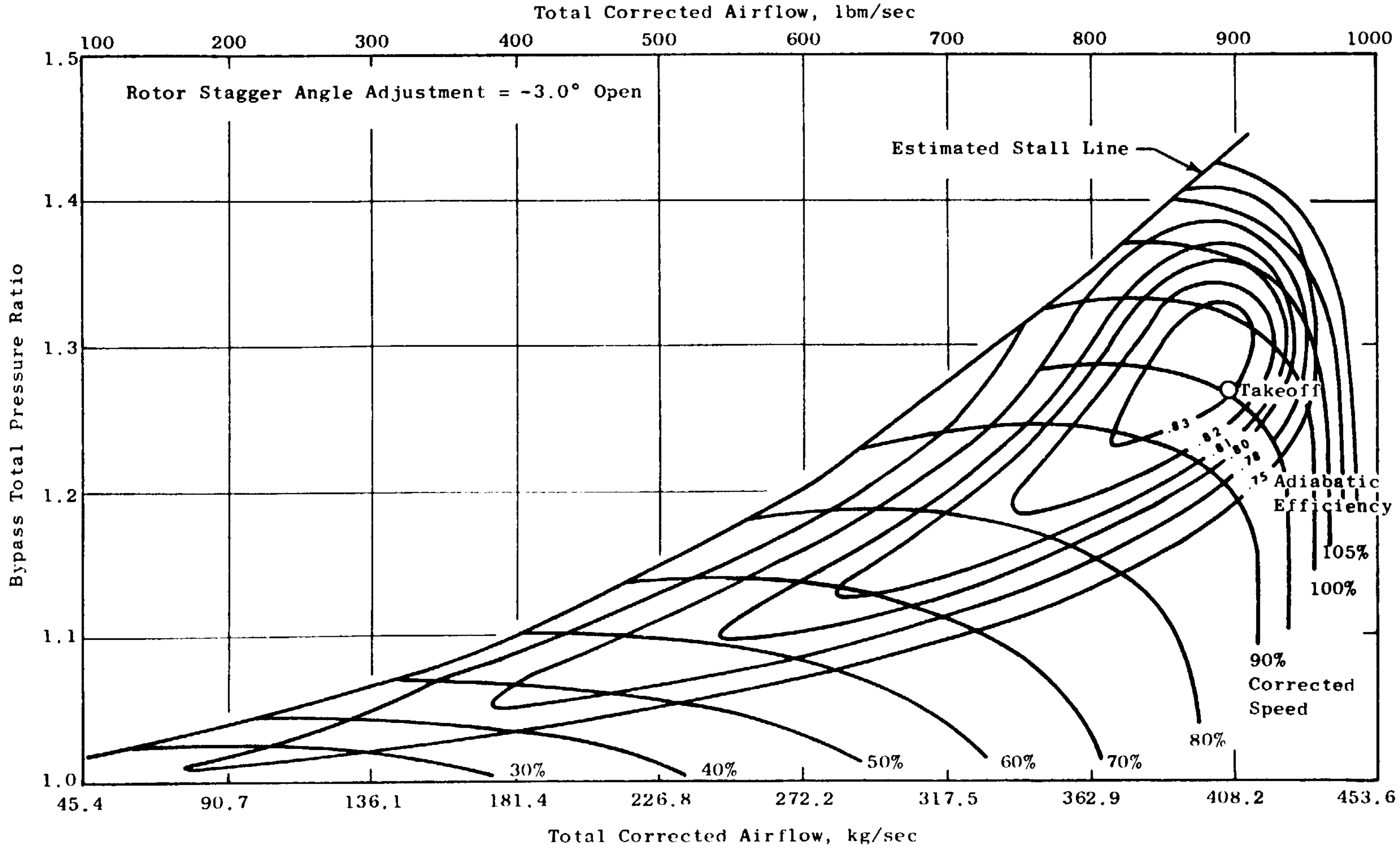

Figure 6-29. Fan Bypass Stream Performance Map at Estimated Takeoff Rotor Stagger Setting.

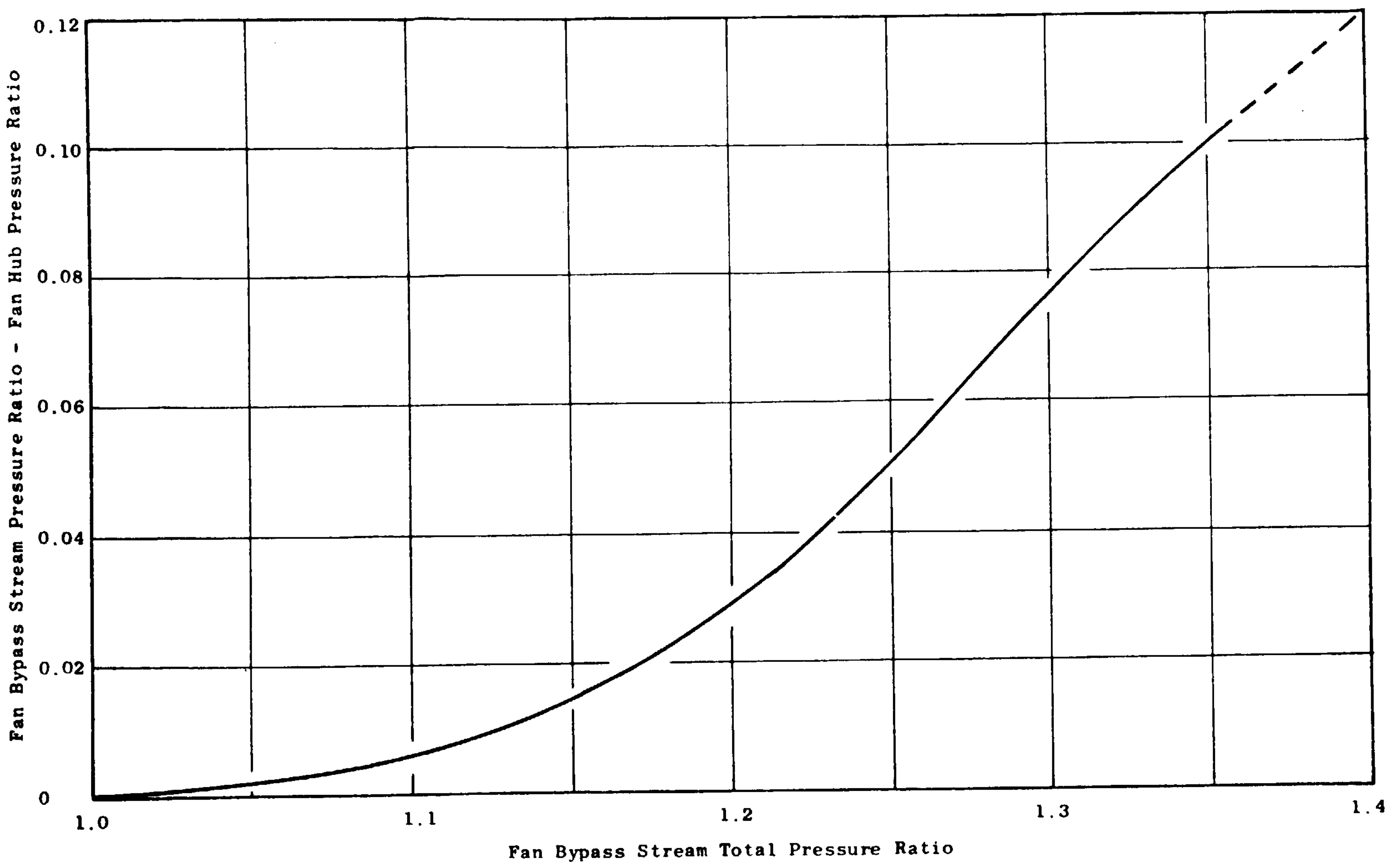

Figure 6-30. Fan Hub Pressure Ratio Correlation (Forward Mode).

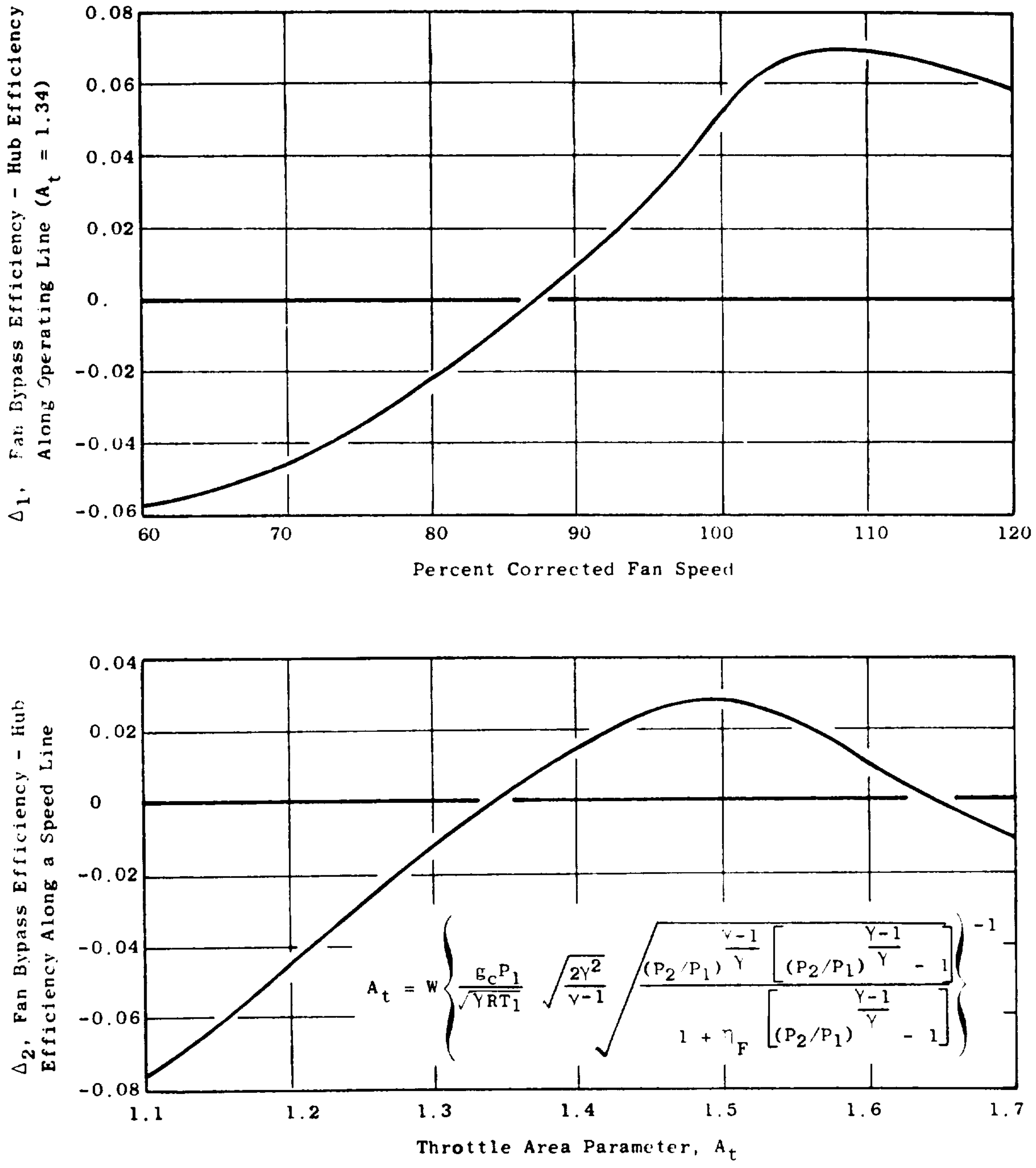

$$A_t = W\left\{\frac{g_c P_1}{\sqrt{\gamma R T_1}}\sqrt{\frac{2\gamma^2}{\gamma-1}}\sqrt{\frac{(P_2/P_1)^{\frac{\gamma-1}{\gamma}}\left[(P_2/P_1)^{\frac{\gamma-1}{\gamma}}-1\right]}{1+\eta_F\left[(P_2/P_1)^{\frac{\gamma-1}{\gamma}}-1\right]}}\right\}^{-1}$$

W = **Total Fan Corrected Airflow**

P_1, T_1 = **Fan Inlet Total Pressure and Temperature**

P_2/P_1 = **Fan Bypass Pressure Ratio**

η_F = **Fan Bypass Adiabatic Efficiency**

Fan Hub Efficiency = $\eta_H = \eta_F - \Delta_1 - \Delta_2$

Figure 6-31. Fan Hub Efficiency Correlation (Forward Mode).

tests, and is discussed in detail by Giffin, et al. Pressure ratio and efficiency data are shown in Figure 6-32, plotted versus rotor corrected flow in the 50.8 cm (20 in.) scale model size. In UTW engine size, the resulting trends of gross corrected fan reverse thrust versus fan corrected speed are shown in Figure 6-33. The general conclusion from these data is that reverse thrust objectives can be met with the rotor blades reversed through stall pitch, but probably not when reversed through flat pitch. Engine system cycle analysis, however, is required to evaluate effects of bypass duct/core engine inlet duct recoveries on available core engine power and achievable fan speed before determining the best pitch angle setting for reverse thrust.

The test data recorded in reverse thrust mode were expressed in terms of a universal stage characteristic. A work coefficient, defined in Figure 6-34, was calculated involving a correction for rotor stagger angle variations such that this coefficient represents the work input that would have been produced if the rotor had always been set at a nominal stagger angle rather than at the angle for the particular data point. Similarly, a flow coefficient, defined in Figure 6-34, was calculated to represent the flow that would have been passed at the nominal rotor angle setting, for the same incidence as the actual test data point. Two such characteristics were actually obtained, one for reverse through stall pitch and one for reverse through flat pitch. The stagger angle settings used as normalizing values were -100° and +73° for reverse through stall pitch and flat pitch, respectively. The resulting characteristic curves are shown in Figure 6-34, while the trends of efficiency versus speed and stagger angle used to represent the reverse mode data are shown in Figure 6-35.

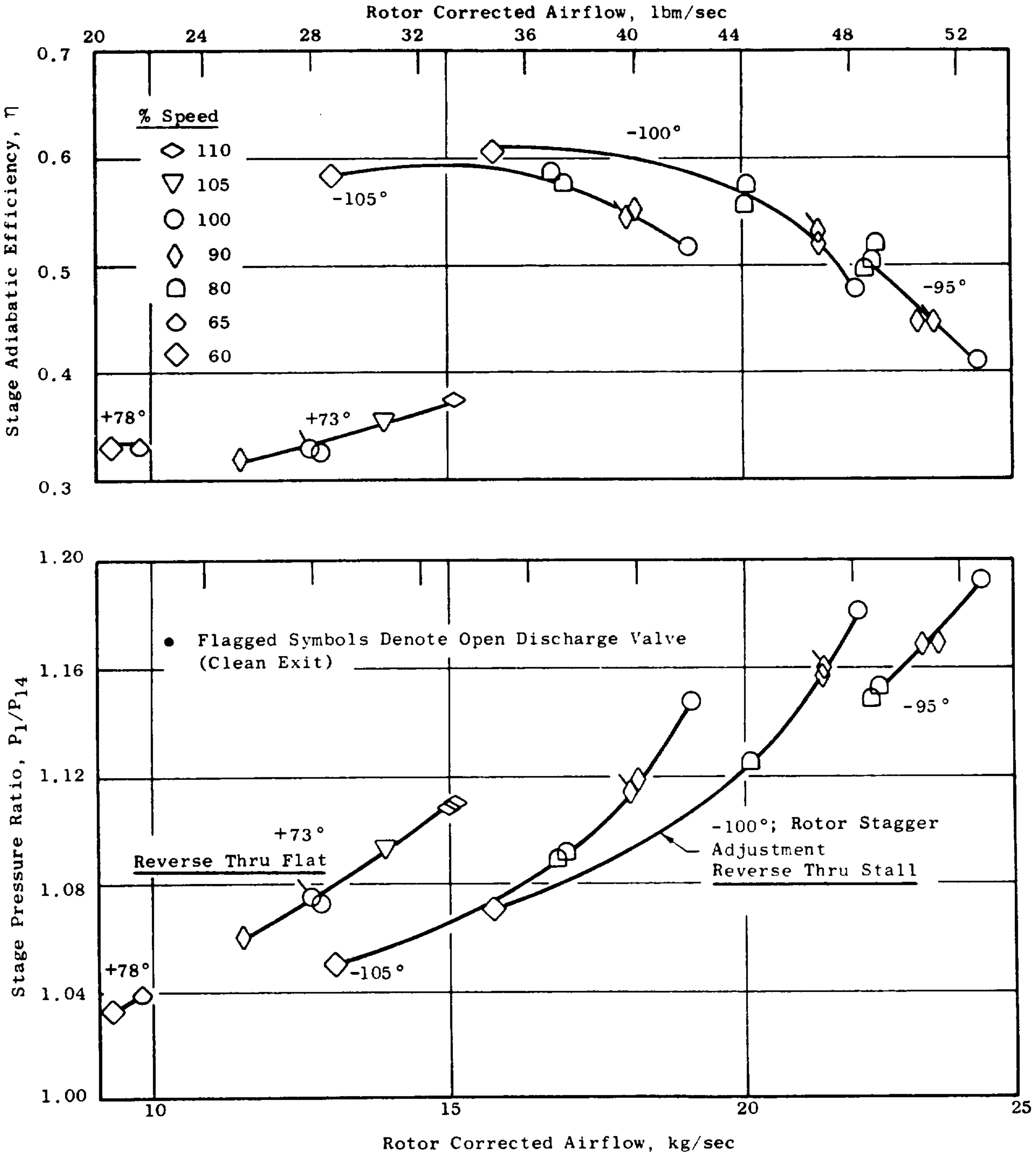

Figure 6-32. Reverse Mode Fan Performance.

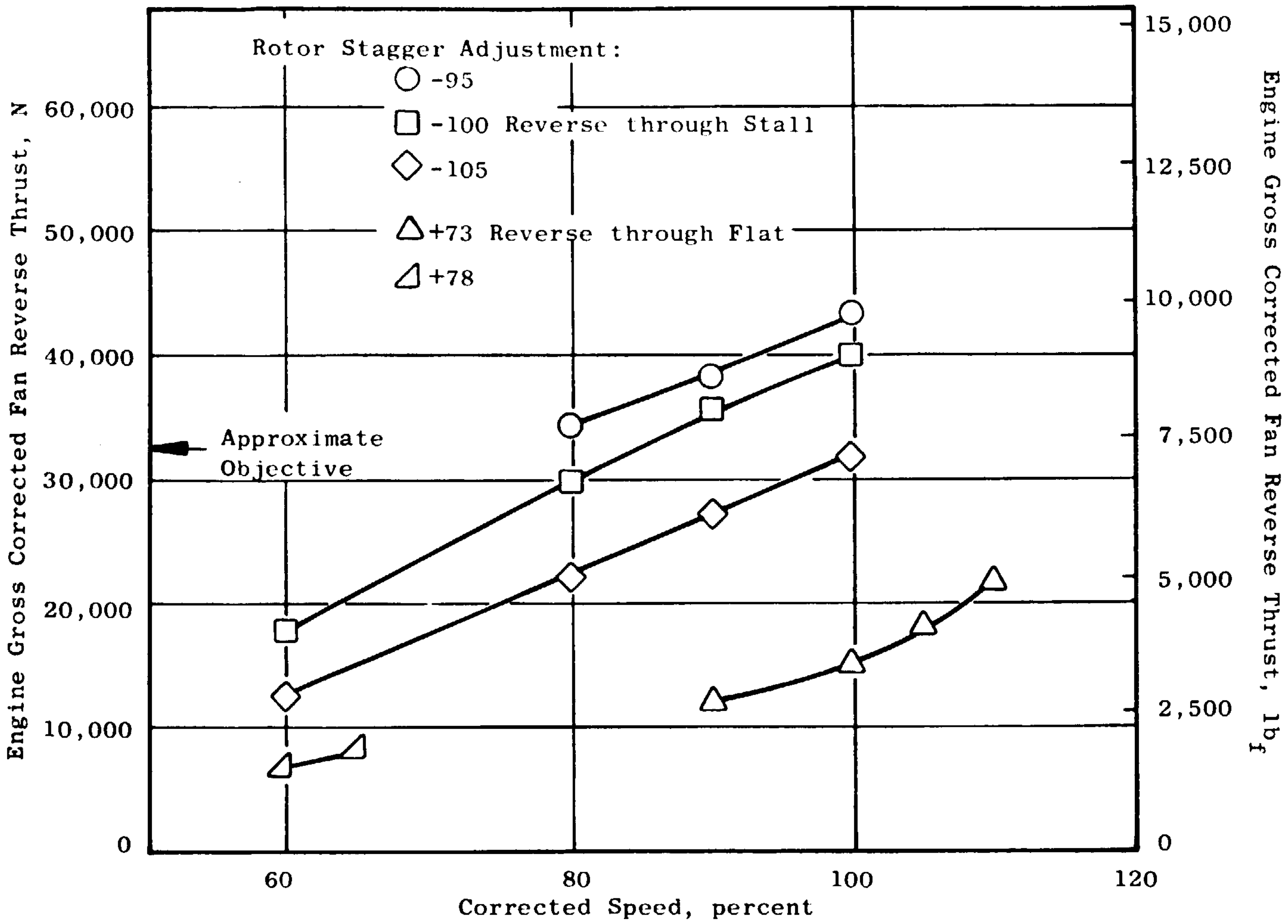

Figure 6-33. UTW Fan Scale Model Gross Reverse Thrust, Scaled to Engine Size.

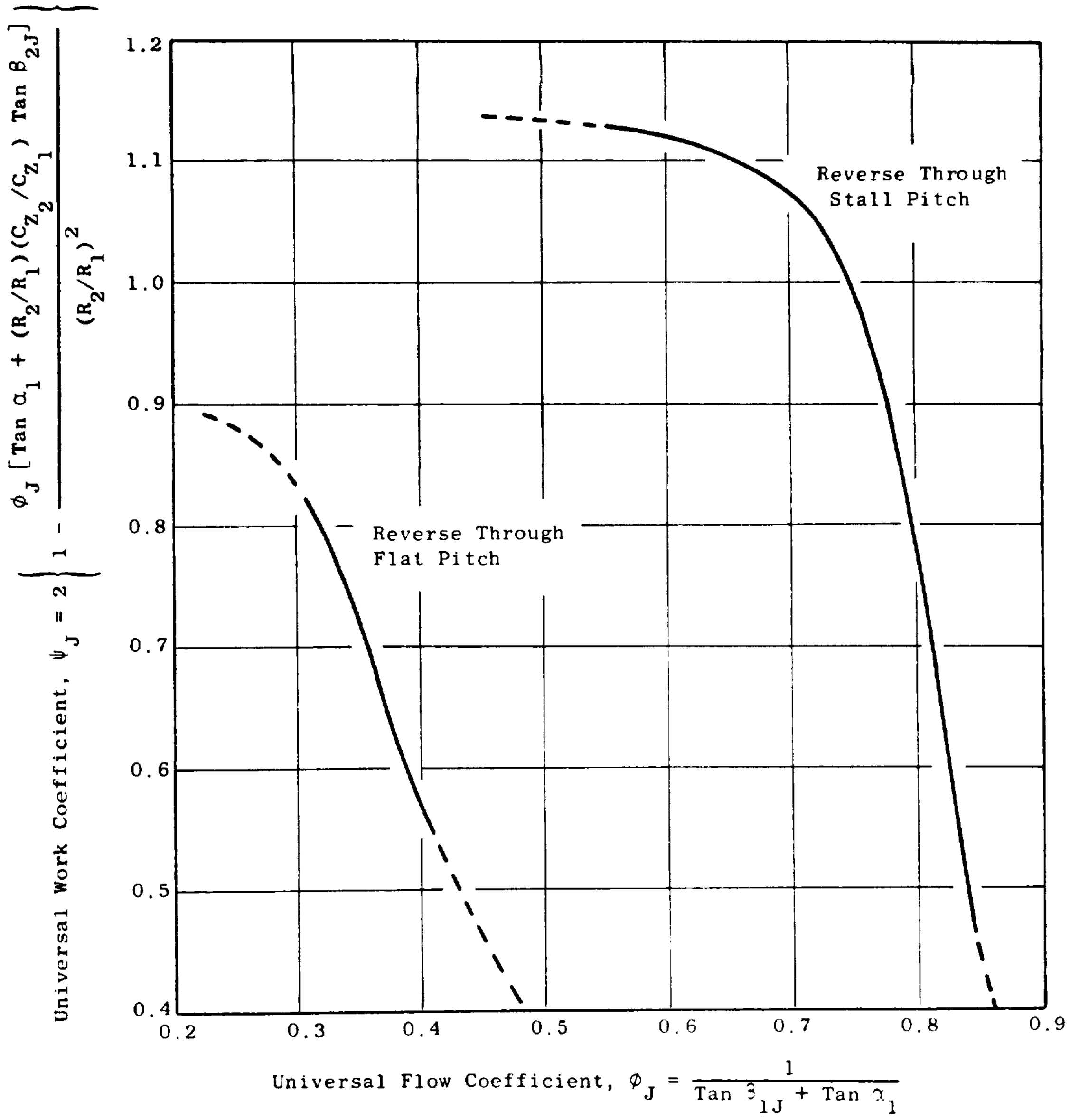

P_{Norm} = Normalizing Value of Rotor Stagger Angle Setting
P = Rotor Stagger Angle
β_1 = Rotor Inlet Relative Air Angle
α_1 = Rotor Inlet Absolute Air Angle
$\beta_{1J} = \beta_1 + P - P_{Norm}$; $\alpha_{1J} = \alpha_1 + P - P_{Norm}$
C_{Z_2}/C_{Z_1} = Axial Velocity Ratio Across the Rotor
R_2/R_1 = Radius Ratio Across the Rotor

Figure 6-34. UTW Fan Reverse Mode Universal Characteristics.

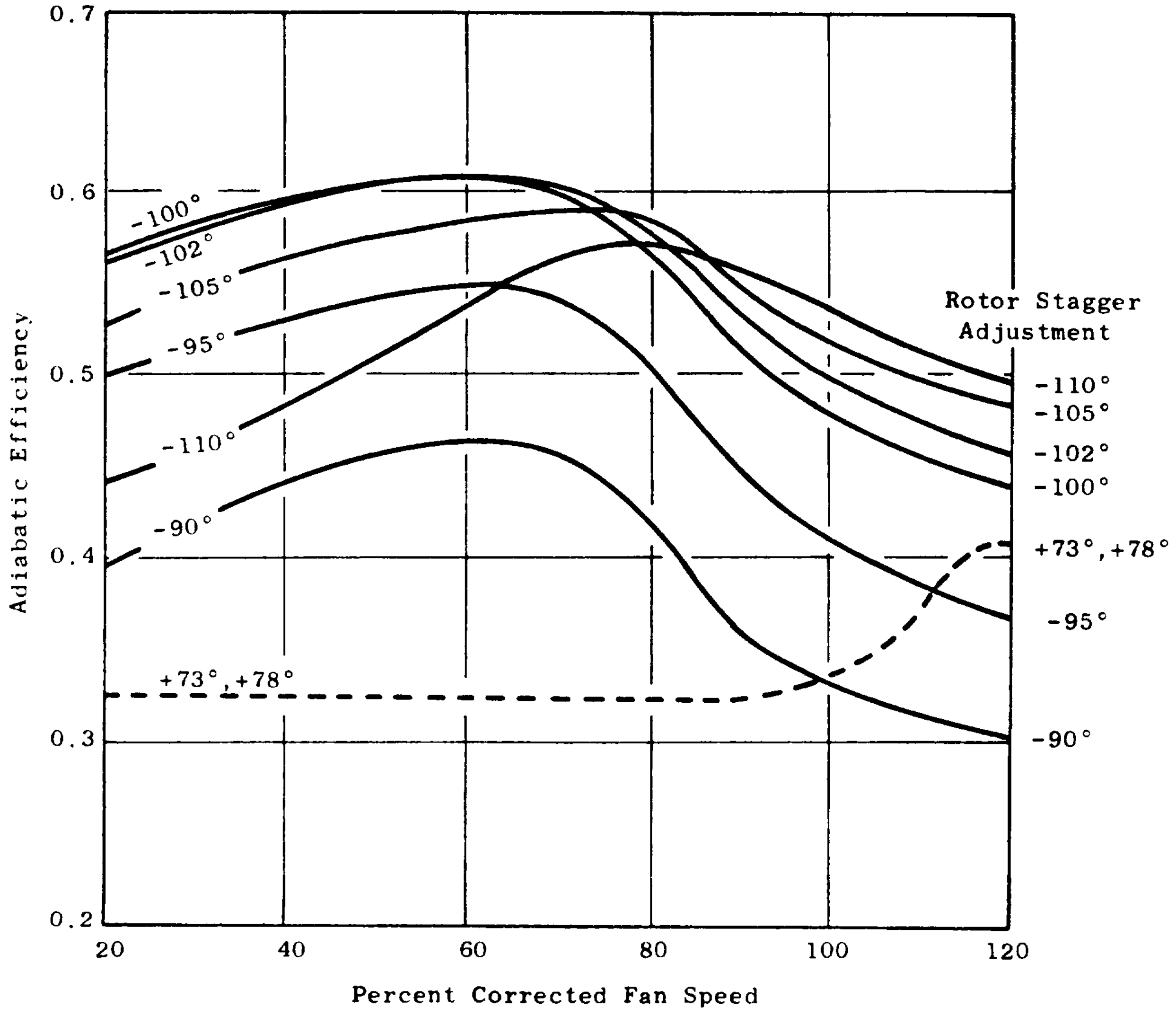

Figure 6-35. UTW Fan Reverse Mode Adiabatic Efficiency.

SECTION 7.0

VARIABLE-PITCH FAN ACTUATION SYSTEMS

7.1 SUMMARY

Because of the complexity of the design necessary to achieve variable-pitch fan actuation, two actuation systems are being developed as a part of the UTW experimental engine program. The cam/harmonic drive actuation system, illustrated in Figure 7-1, is being developed by the Hamilton Standard Division of United Technology Corporation under subcontract to the General Electric Company. A hydraulic motor, which is a part of the beta regulator module mounted in the core cowl area, provides rotary mechanical input to the differential gear train through a flexible drive shaft which passes through the main reduction gear support. The rotary motion is then transmitted through a no-back, harmonic drive, rotating cam, and cam follower arms to the blade trunnion.

The overall gear ratio from the blades to the flexible shaft is 773/1, with most of the ratio (201/1) provided by the harmonic drive. This permits the low torque power transmission elements between the beta regulator and the harmonic drive to be designed for high speed, low weight, and improved blade angle accuracy.

The planetary differential gear train provides a 5/1 ratio, and is utilized to cross the rotating boundary of the fan. The function of the bidirectional, spring-type no-back is to lock the fan blades in position in the absence of a pitch change command.

Two LVDT's, located in the beta regulator unit and driven by hydraulic motor output, provide a blade angle feedback to the engine digital control system.

Utilization of a flexible drive shaft permits the LVDT's and hydraulic motor to be remotely located in an engine area which permits ease of inspection and component replacement. Detail design of the Hamilton Standard actuation system has been completed and approved by GE and NASA.

The ball spline actuation system shown in Figure 7-2 is being developed by General Electric. A hydraulic motor located on the fan center-line drives a ball screw actuator through a differential gear and no-back. Linear motion of the ball nut of the ball screw causes the sleeve (middle member) of a ball spline to translate in a fore or aft direction. The ball spline is a double acting member with helical ball tracks between the translating sleeve and inner member and straight ball tracks between the sleeve and the outer ball spline member. The inner member is attached to the aft ring gear while the outer member is attached to the forward ring gear. Translation of the ball spline sleeve fore and aft drives the two ring gears in

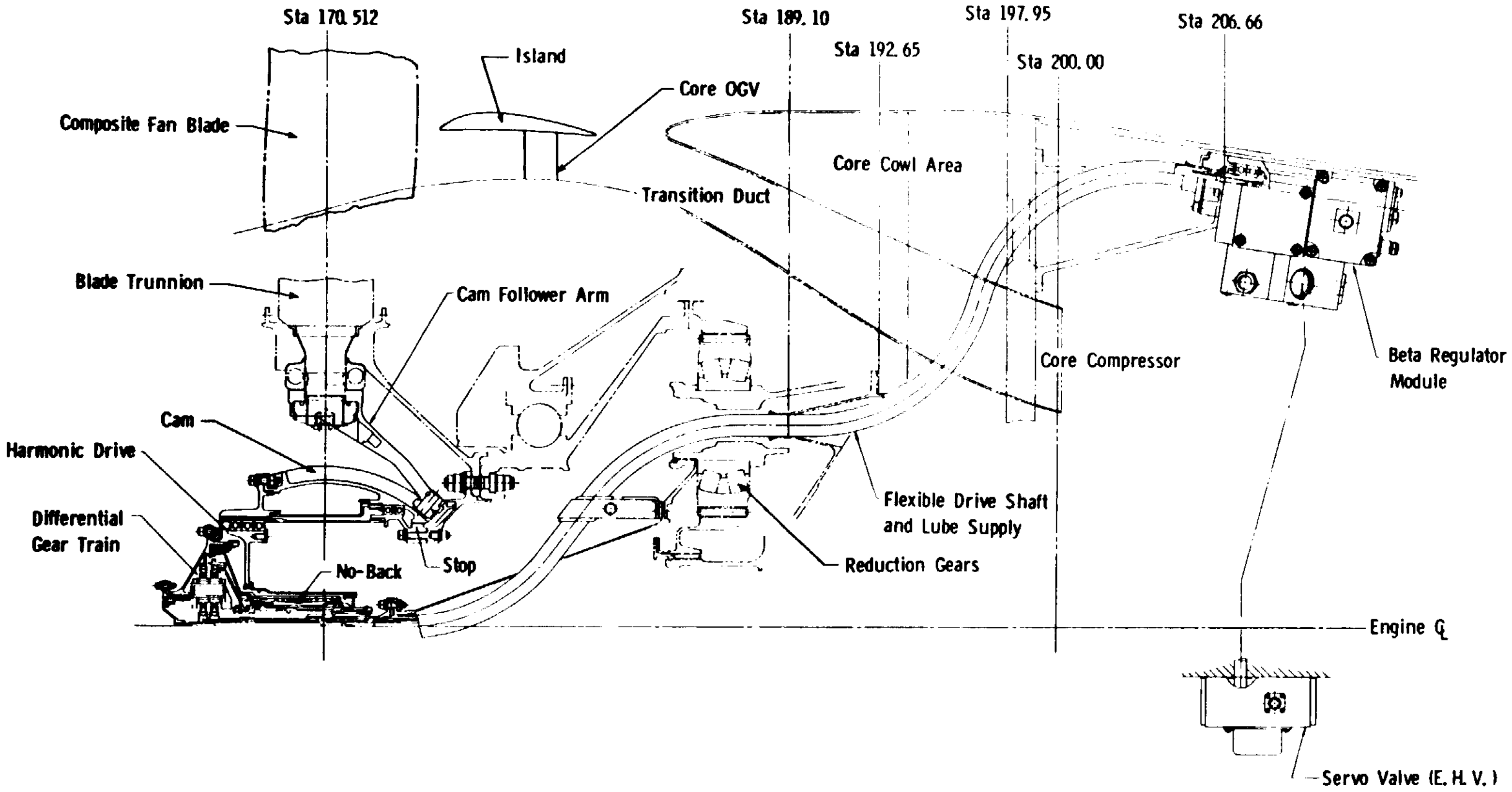
Sta 170.512
Sta 189.10
Sta 192.65
Sta 197.95
Sta 200.00
Sta 206.66
Island
Core OGV
Composite Fan Blade
Core Cowl Area
Transition Duct
Blade Trunnion
Cam Follower Arm
Core Compressor
Beta Regulator Module
Cam
Harmonic Drive
Differential Gear Train
Flexible Drive Shaft and Lube Supply
No-Back
Stop
Reduction Gears
Engine ℄
Servo Valve (E.H.V.)

Figure 7-1. Hamilton Standard Cam-Harmonic Drive Actuator System.

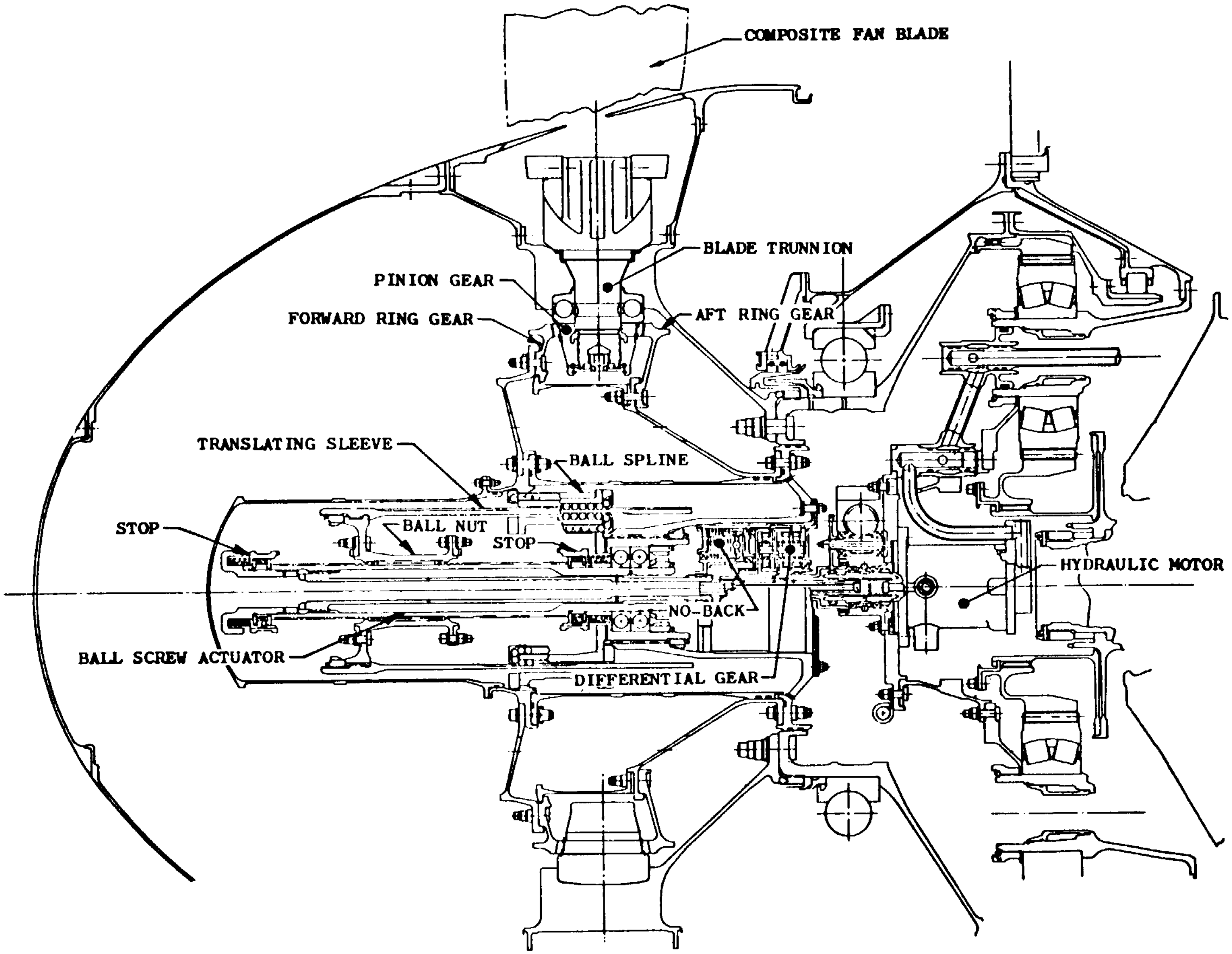
COMPOSITE FAN BLADE
BLADE TRUNNION
PINION GEAR
FORWARD RING GEAR
AFT RING GEAR
TRANSLATING SLEEVE
BALL SPLINE
STOP
BALL NUT
STOP
HYDRAULIC MOTOR
NO-BACK
BALL SCREW ACTUATOR
DIFFERENTIAL GEAR

Figure 7-2. General Electric Ball Spline Actuator System.

tangentially opposite directions. The ring gears in turn are mated to 18 pinion gears that are splined to the corresponding fan blade trunnion.

Gear ratio between the hydraulic motor and the fan blade is 479/1. Two LVDT's driven by the hydraulic motor provide a blade angle feedback to the engine digital control system.

This actuation system is an improved version of a proven ball spline actuation system utilized in previous General Electric variable-pitch fan test vehicles. Detail design of this system has been completed and approved by NASA.

7.2 DESIGN REQUIREMENTS AND CRITERIA

The GE and HS variable-pitch fan systems are designed to meet specified flight engine and experimental engine requirements, including resistance to bird strikes. These requirements are defined in detail in GE Specification M50TF1635-S1. A life requirement of 36,000 hours (48,000 mission cycles) was specified for all component parts, with the exception of bearings and standard nonreusable parts, when the actuation system was operated in accordance with the conditions specified in the Mission Duty Cycle presented in Figure 7-3. The mechanisms were designed for no replacement of parts (including bearings and nonreusable parts) at intervals of less than 9000 hours.

Both variable-pitch systems, including retention bearings, must also meet the duty cycle requirements of the experimental UTW engine, defined as follows:

EXPERIMENTAL ENGINE DUTY CYCLE

Item	Fan Speed, (rpm)	Time, (hours)
1	3447	0.3
2	3347	1
3	3157	181
4	2841	500
5	2368	1000
6	947	1000

The above operation is assumed to occur on a 90° F day. The actuation system must be capable of operation at any of the above conditions. For the experimental engines the system operation capability should also be consistent with the following:

- Item 1
  No actuation required

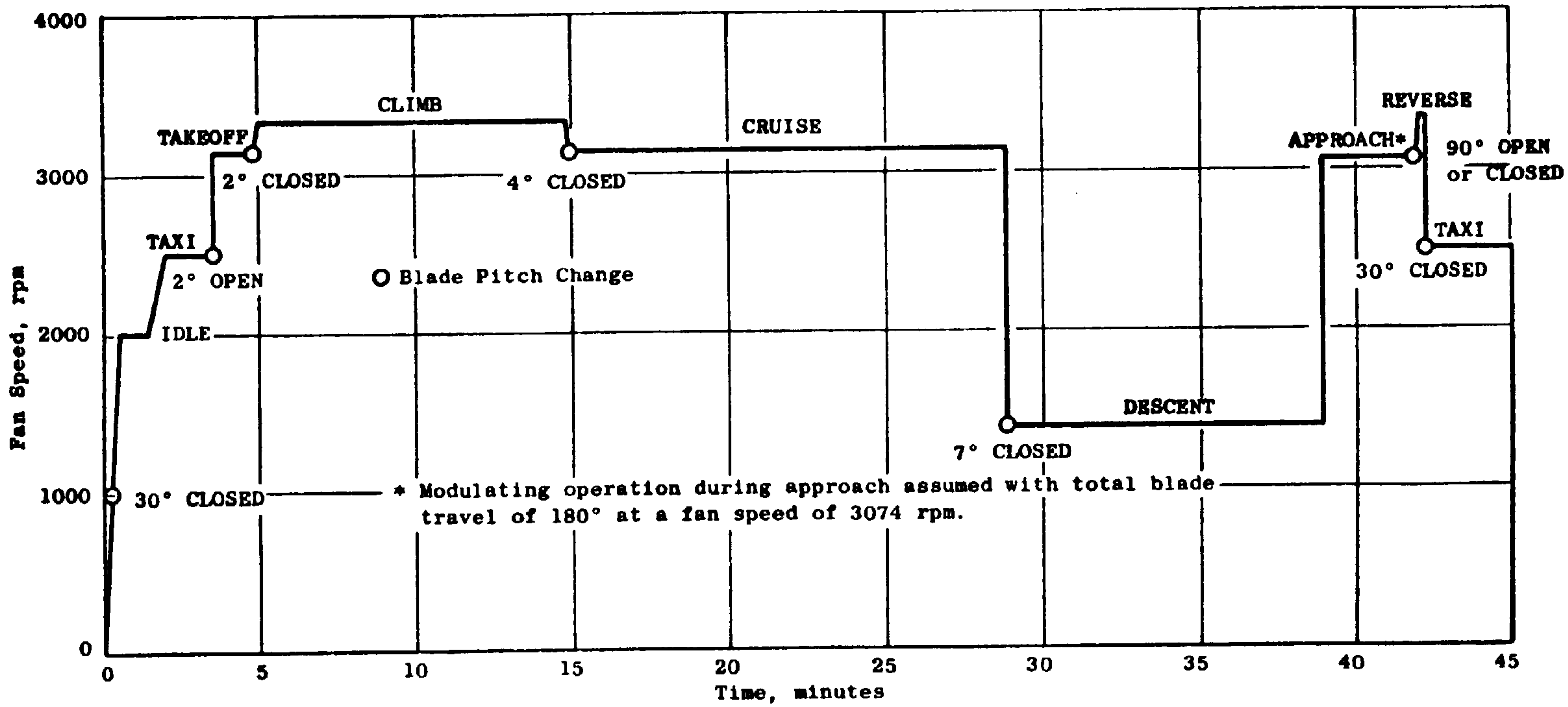

Figure 7-3. UTW Mission Duty Cycle.

- Item 2
  10 blade actuations at 5 minute intervals in the range of operation from 5° open to 5° closed.

- Item 3
  500 total blade actuations from forward to reverse through flat pitch and stall pitch

  1000 blade actuations at 5 minute intervals in the range of operation from 5° open to 10° closed

- Item 4
  10,000 blade actuations in 5° increments from 5° open to 30° closed.

Specific blade-torque, speed, and accuracy design requirements are shown in Table 7-I.

Figure 7-4 is a plot of the expected blade twisting moments in the operating range. The designs are also based on consideration of the following aircraft flight requirements:

- Following foreign object ingestion, the dynamic pitch change mechanism must be capable of 10 additional cycles at maximum torque and actuation rate.

- The system must be capable of withstanding 20 g vibratory and should not impose over 5 g vibratory on the engine.

- The system must be capable of operation after exposure to fluids conventionally used by Airlines such as "Skydrol Type" hydraulic fluids, methylene chloride, and butyl cellasolve.

7.3 HAMILTON STANDARD CAM-HARMONIC DRIVE VARIABLE-PITCH ACTUATION SYSTEM

7.3.1 System Description

The Hamilton Standard variable-pitch actuator system is shown in Figure 7-1. An electrical input command signal from the digital control to the electro-hydraulic servovalve (EHV) directs high pressure oil to a hydraulic motor in the beta regulator. This provides rotary mechanical input to the actuator differential gear train through a flexible drive shaft. Rotary motion is then transmitted through a no-back, harmonic drive, rotating cam and cam follower arms to the blade trunnions. Since there is a fixed mechanical relationship between hydraulic motor rotation and blade angle, two LVDT's driven by the hydraulic motor output shaft provide a blade angle feedback signal to the digital control to close the control loop and null the input signal when the blades reach the commanded position.

Overall gear ratio from the blades to the drive shaft is 773/1 with most of the ratio (201/1) taken near the blades in the harmonic drive. This permits the low-torque power transmission elements between the beta

Table 7-I. Variable-Pitch System Design Requirements.

	Normal Range	Extreme Range
Fan Speed, rpm	0 - 3326	3450 Without Actuation
Blade Twisting Torque(1)	See Figure 7-2	1692 N-m (15,000 lb-in.)(2)
Blade Overturning Moments		22,600 N-m (200,000 lb-in.)(2)
Centrifugal Load for Blade and Dovetail Only	15,196 kg (33,500 lb) (at 3200 rpm)	Must Not Burst at 4432 rpm (141% of T/O rpm)
Average Actuation Rate	135°/sec	
Actuation Jogging at Blades	0.5° Steps Min	
Feedback Signal Accuracy	±0.25° Blade Position	
Flight Maneuver Forces(3)	Per Mil-E-5007C (12/30/65) Par. 3.14 Except Precession Rate Shall be One Radian per sec Max.	

---

(1) Friction must be included over and above this data

(2) FAA Advisory Circular AC 33-1b, 4/22/70 (Bird Strike Torque)

(3) Polar moment of inertia of blades = 1273 kN-cm^2 ($44{,}376\ \text{lb-in.}^2$)

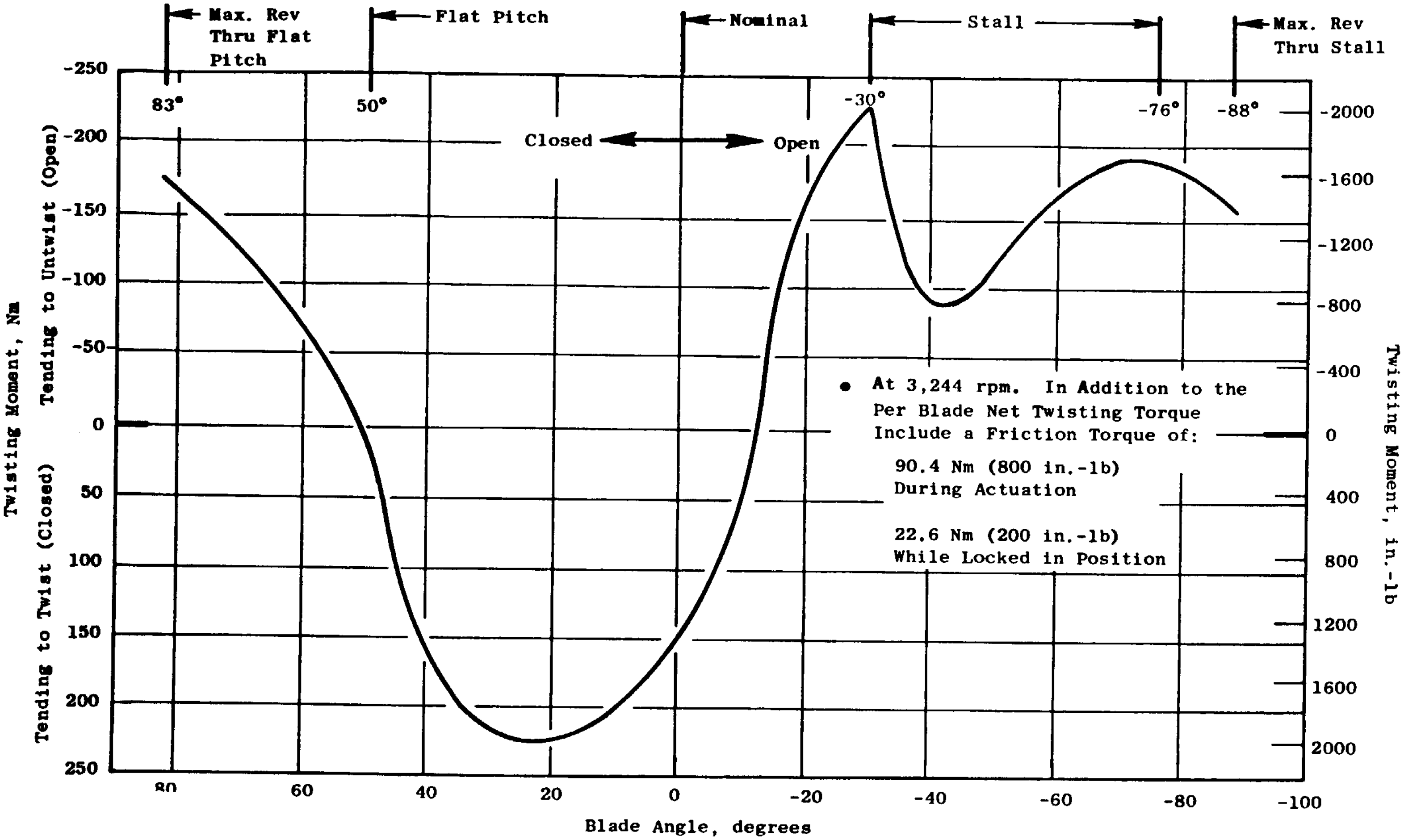

- At 3,244 rpm. In Addition to the Per Blade Net Twisting Torque Include a Friction Torque of:

  90.4 Nm (800 in.-lb) During Actuation

  22.6 Nm (200 in.-lb) While Locked in Position

Figure 7-4. Net per Blade Twisting Torque at 3244 rpm, SLS Standard Day.

regulator and the harmonic drive to be designed for low weight and improved blade angle accuracy.

Mechanical pitch change command and blade angle feedback functions are provided by the beta regulator module which is remotely mounted in a readily accessible area of the engine core cowling. A simplified schematic of the beta regulator is shown in Figure 7-5. A blade angle change command from the engine control to the EHV mounted in the accessory section, causes movement of the servovalve to direct supply oil to either the open- or closed-pitch ports of the hydraulic motor. The hydraulic motor output shaft drives the flexible shaft to change blade angle and drives two LVDT's through a worm gear and screw to provide an electrically redundant blade position feedback. Electrical limit switches are provided to cut off the command signal to the EHV if a blade angle is commanded beyond the maximum operating range. Pressure relief valves across the hydraulic motor ports limit input pressure to 3000 psi during rapid accelerations of the actuator system.

The rotary output of the beta regulator is transmitted to the actuator differential gear train through a flexible drive shaft passing through the engine reduction gearing. The shaft core is encased in a flexible Teflon-lined casing supported in a rigid conduit mounted on the engine reduction gear support. Continuous engine lubrication oil flow is directed through the casing from the beta regulator end to lubricate the flexible shaft and the actuator components.

A planetary differential gear train is utilized to cross the rotating boundary of the fan. The differential gearing is a conventional 5/1 ratio phase difference type that utilizes a grounded sun gear fixed to the engine static structure, an input sun gear driven by the flexible shaft, three pairs of planet gears on a bearing supported cage, a reference speed ring gear fixed to the fan disk, and an output ring gear driving the no-back input. With no pitch-change input, the output ring gear rotates at fan speed. Rotation of the input sun gear during pitch change causes the output ring gear to either advance or recede with respect to the fan speed. This change in output is the input to the no-back. The differential gears and bearings are lubricated by oil directed outward centrifugally from the sun gear shafts.

A bidirectional spring clutch or "no-back" is provided between the differential gearing and the harmonic drive to maintain the set blade angle position in the absence of a pitch change command. This device consists of a self-energizing steel spring which is in contact with the inner surface of a fixed housing, the input and output shafts, and the necessary couplings and bearings. When holding a fixed blade angle, the blade loads are transmitted to ground (housing) through the spring. When the input acts against opposing blade loads (raising the load), the spring slides in the housing and reacts no blade loading. When the input acts against aiding blade loads (lowering the load), the input releases the spring at the commanded pitch rate and the blade load energy is dissipated in frictional heat

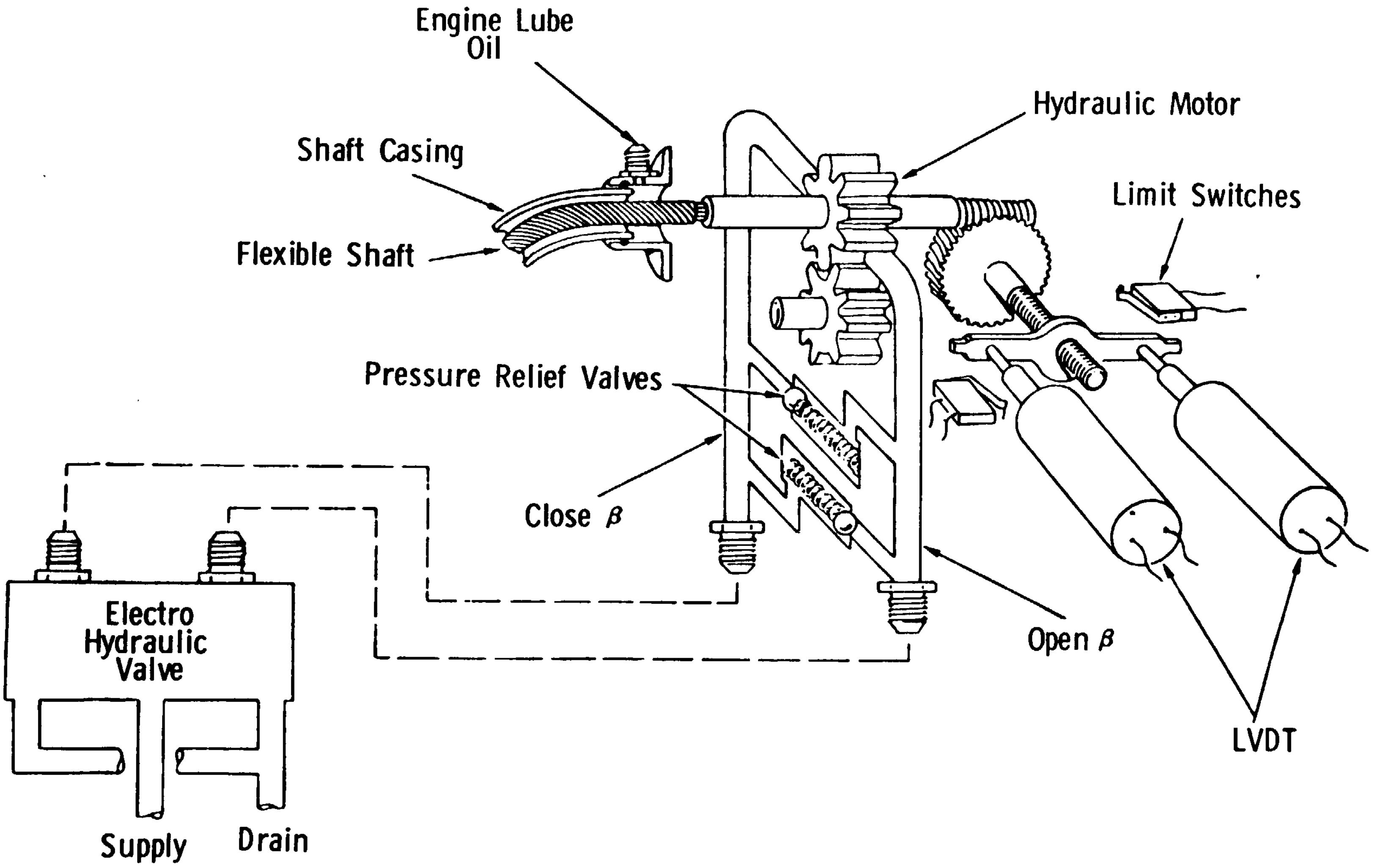
Engine Lube Oil
Shaft Casing
Flexible Shaft
Hydraulic Motor
Limit Switches
Pressure Relief Valves
Close β
Open β
LVDT
Electro Hydraulic Valve
Supply
Drain

Figure 7-5. Beta Regulator Schematic.

between the spring and housing. Due to the short duty cycle, the total heat rise is low and is contained within the no-back. Lubrication oil flows continually through the no-back and is supplied centrifugally from the sun gear shafts.

No-back housing torque is reacted by a disk-type torque limiter brake. The no-back is a high-gain locking device capable of locking more than 11.3 Mcm-N (million in.-lb) of torque at high friction coefficients, and the torque limiter limits no-back torque to acceptable structural limits during rapid pitch change decelerations. The brake disks are lubricated by oil supplied centrifugally from the differential gearing.

Harmonic drive provides the primary gear reduction for the mechanical actuator and increases the input torque to the level required to change blade pitch. Four basic elements are incorporated in this high-ratio (201:1) mechanical transmission of 0.57 Mcm-N (50,000 in.-lb) output. They are: (1) a three-lobed harmonic-shaped wave generator input plug for symmetrical loading, (2) a triplex split inner race ball bearing set for high radial stiffness, (3) a flexible spline (flex spline) to convert from the harmonic lobe shape to a grounded circular shape with minimum frictional losses, and (4) a stiff circular output spline which drives the blade pitch cam.

The thin-race ball bearings are pressed on the three-lobed wave generator plug and assume the three-lobe harmonic shape. Spline teeth on the outside diameter of the flex spline mesh with spline teeth on the inside diameter of the circular spline at the three lobe locations. Circular splines on the other end of the flex spline ground it to the fan disk. Due to a three-tooth difference in number of teeth between the circular spline and flex spline (603 - 600 = 3), one revolution of the wave generator input rotates the circular spline output 3/603 or 1/201 of a revolution.

Lubrication oil for the harmonic bearings and splines is supplied centrifugally from the differential gearing and no-back.

The cam and follower arms convert output rotation of the harmonic drive to fan blade angle change. Titanium follower arms, splined and clamped to the blade trunnions, engage individual cam slots in the spherical cam surface through cam rollers to synchronize the blades and sum the blade torques. The radial axis defined by the roller and cam track centerlines always intersects the fan axis of rotation at the same point similar to the apex point of a bevel gear mesh.

Cam support is provided by a preloaded duplex bearing set mounted on a support ring attached to the fan mounting flange for accurate balance control. Lubrication oil from the harmonic drive lubes the bearing set and is returned centrifugally to the engine scavenge area. A single dynamic oil seal with centrifugal venting precludes a dynamic pressure head.

Fixed mechanical stop lugs between the cam and cam support ring restrict the blades to 7° overtravel at each end of the maximum operating range.

The component speed/torque relationships are summarized in Table 7-II. Data presented are for 31,866 cm-N (2820 in.-lb) blade twisting moment at a blade pitch angle of +22° (closed) at 3244 fan rpm and 135 degrees/sec pitch change rate.

7.3.2 Component Design

Trunnion Arm and Roller

The trunnion arms and rollers shown in Figure 7-6, produce a counterweight effect which balances a portion of the blade twisting moment to reduce system power requirements. A steel cam roller is attached to each titanium arm by a steel pin pressed and cross-pinned to the arm lug. The arm is shot peened and coated with dry film lubricant to inhibit fretting at the trunnion spline and retention bearing. A thin chrome plating is applied to the roller and pin for corrosion protection and to provide a hard bearing surface for the roller bushing. Fibriloid woven Teflon bushing and thrust washers are bonded to the roller to provide a low friction bearing requiring no additional lubrication.

The arm is designed basically for minimum deflection with the critical stresses occurring in the roller pin lug area. Centrifugal loading, F_c, produces arm bending and the roller/cam normal load, F_R, produces transverse and longitudinal bending, axial force and torsion in the arm. Maximum arm loads occur when the fan blades are closed 7° ($\beta = +7°$) from the nominal blade position at 3347 rpm. At this condition, the maximum operating roller load, F_R = 3114 N (700 lb) at 25,199 cm-N (2230 in.-lb) blade torque, acts at $\theta = 32°$ (Figure 7-6). F_R is equal to 19,349 N (4350 lb) at the blade bird strike torque of 169,500 cm-N (15,000 in.-lb). Moment distribution due to F_c is shown in Figure 7-7.

Maximum bending stress occurs in Section B-B (Figure 7-6) at point D ($K_e = 1.0$). The resulting stress levels are shown in Table 7-III. Maximum arm deflections are specified at the roller, and were obtained by graphical integration of M/EI over the arm length. Results are presented in Table 7-IV. F_c at 3347 rpm and F_R equal to 3114 N (700 lb) are the maximum arm loads. The cam slot height has been designed to preserve adequate roller engagement for these radial deflections in addition to fan disk deflections and tolerances. Transverse arm deflections are accommodated within the ±0.25 β accuracy required. Stress coat tests of a trunnion arm model were conducted early in the program. Within the range of accuracy to be expected from this type of test good agreement was obtained between the test results and the calculated stresses.

Table 7-II. Component Operating Characteristics.

	Speed, rpm	Gear Ratio	Efficiency, %	Operating Torque	
				cm-N	in.-lb
Blade	22.5	-	-	28,815	2550*
Harmonic Output	17.3	0.97	0.94	568,390	50,300
Harmonic Input	3477	201/1	0.75	3774	334
Differential Input	17,385	5/1	0.98	768	68
Flex Shaft Input	17,385	-	0.90	859	76
Hydraulic Motors (2)	14,490	0.833	0.99	1040	92

This condition requires 1739 cm^3/sec (27.6 gpm) at 1517 N/cm^2 (2200 psi) delta P at the motors.

---

*Blade torque includes 3051 cm-N (270 in.-lb) counterweight effect of trunnion arm.

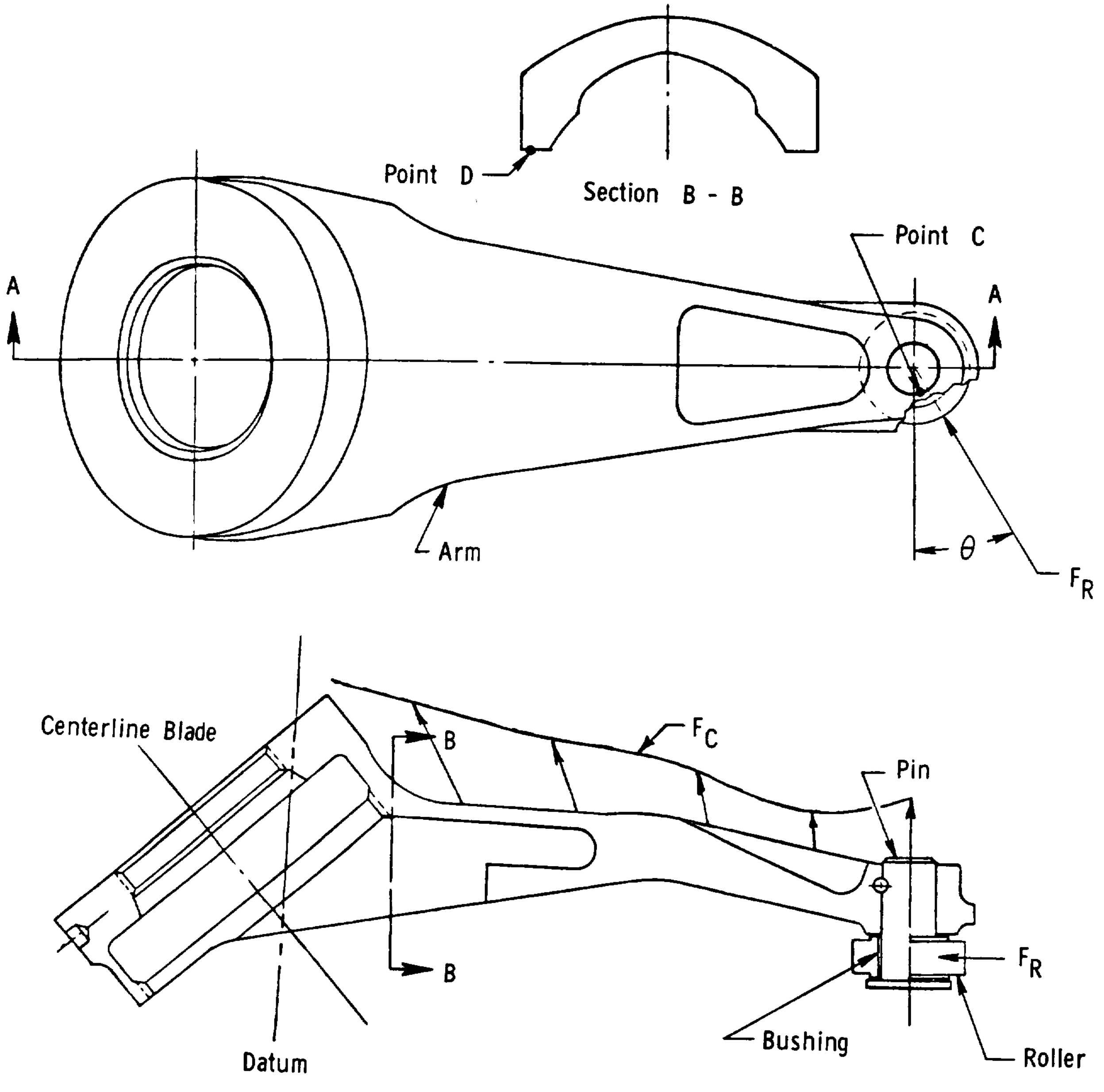
Point D
Section B - B
Point C
A
A
Arm
θ
F_R
Centerline Blade
B
F_C
Pin
B
F_R
Bushing
Roller
Datum
Section A - A

Figure 7-6. Blade Trunnion Arm and Roller.

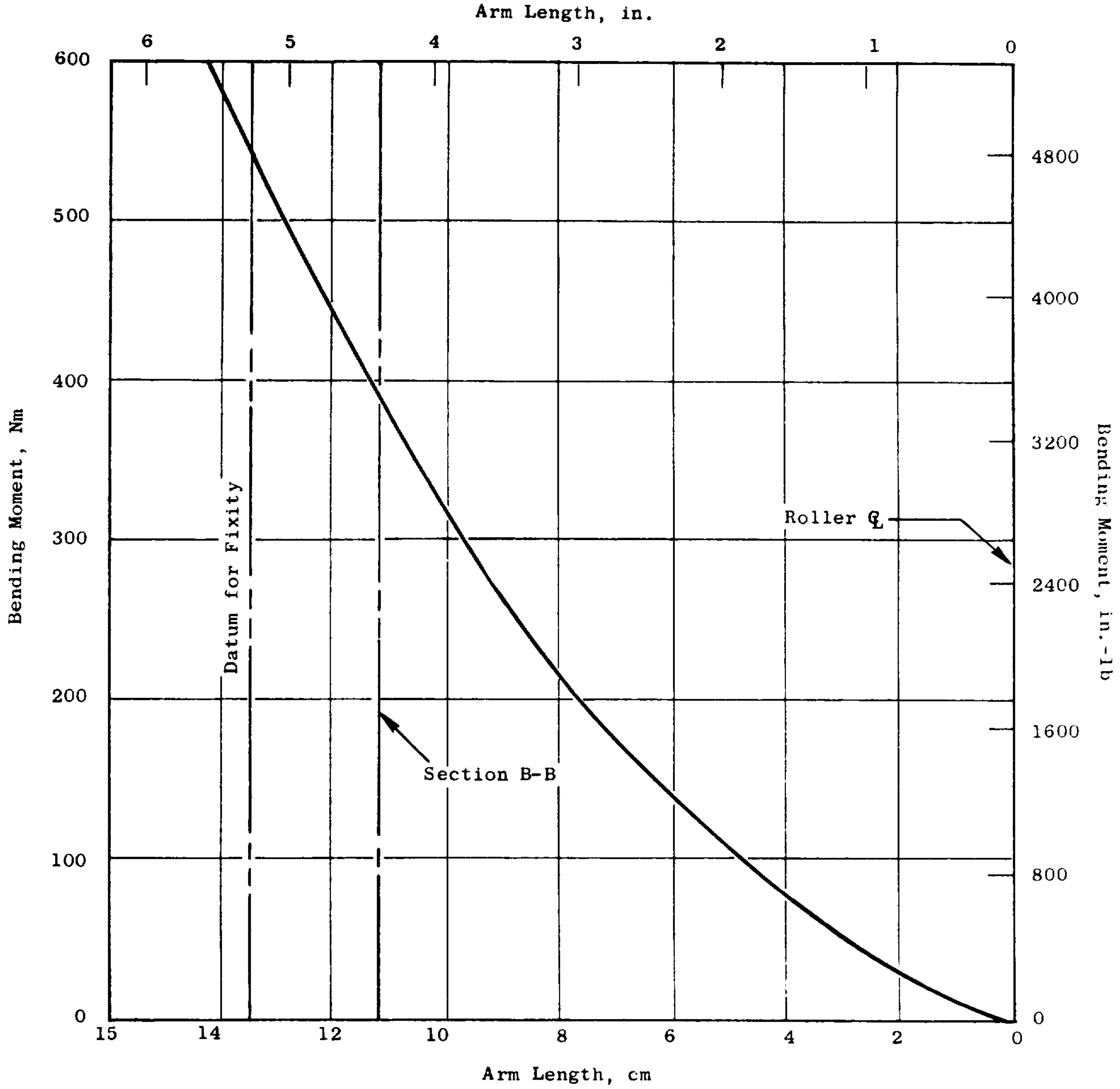

Figure 7-7. Trunnion Arm Bending Moment Distribution from Centrifugal Force at 3347 rpm.

The roller, roller bushing, and roller pin stresses were evaluated under cyclic loading conditions. Two load cases (Figure 7-8) were considered. Load Case No. 1 represents roller loading during approach modulation over a 5° blade pitch angle range. A total of 864,000 cycles are required to meet the specification requirements. Load Case No. 2 represents roller loading for the full blade pitch angle range during reverse through stall. A total of 48,000 reverse cycles plus the 864,000 cycles for approach modulation are required to meet the full system life.

Evaluation results based on these requirements show a roller contact stress of 146,174 N/cm^2 (212,000 psi) versus an allowable stress of 151,690 N/cm^2 (220,000 psi). The maximum bushing compressive stress is 3448 N/cm^2 (5000 psi) versus an allowable stress of 27,580 N/cm^2 (40,000 psi) based on vendor quoted maximum allowable stresses for Fibriloid. Bushing compressive stress due to bird strike is 21,375 N/cm^2 (31,000 psi) versus an allowable stress of 68,950 N/cm^2 (100,000 psi). Stress in the roller pin with bird strike is 95,151 N/cm^2 (138,000 psi) versus an allowable stress of 95,841 N/cm^2 (139,000 psi). The bearing stress at the trunnion arm pin socket during bird strike is 85,705 N/cm^2 (124,300 psi) versus an allowable stress of 122,042 N/cm^2 (177,000 psi). Combined axial and bending stress in the lug at Point C (Figure 7-6) during bird strike is 75,845 N/cm^2 (110,000 psi) versus a minimum ultimate stress of 81,361 N/cm^2 (118,000 psi). At normal operating conditions the allowable number of cycles far exceeds the required cycles.

Cam Assembly (Figure 7-9)

The spherical cam slots engage the trunnion arm rollers and are contoured to obtain a variable torque ratio. This permits the blade/cam ratio to be tailored to the blade torque curve to reduce system power requirements. The cam is made of M250 maraging steel heat treated after machining to 48-52 R_c hardness. Wall thickness between cam slots varies with stroke, and material is removed where possible to reduce weight. A Dow Corning 3400A molybdenum disulfide coating is applied all over the cam for track lubrication and corrosion protection.

The roller load normal to the cam track has a component tangent to the cam about the axis of rotation which develops the cam torque reacted by the harmonic drive output, which is bolted and splined to the forward end of the cam. The axial component of the roller load is reacted by the preloaded duplex cam support bearing set. Support for the cam and bearings is provided by a forward steel cone attached through a bolted face spline to a titanium adapter cone mounted on the disk mounting bolts. A face spline joint is used to provide accurate centering of the parts for balance control coupled with ease of disassembly for maintenance. Eighteen 1/4-inch steel bolts preload the joint against separation under maximum operating loads and temperature.

Primary stresses in the cam are contact stress and localized slot wall bending stress due to roller load. Stress and deflection were determined

Table 7-III. Trunnion Arm Stresses.

Load	Stress	Required Cycles	Allowable Cycles
F_c	17169 N/cm^2 (24,900 psi)		
F_R = 3114 N (700 lb)	6895 N/cm^2 (10,000 psi)		
F_c + (F_R = 3114 N (700 lb)	0 to 24,064 N/cm^2 (34,900 psi) 12,032 ± 12,032 (17,450 ± 17450)	10^5	10^8
F_c + (F_R = 19349 N (4350 lb)	54,471 N/cm^2 (79,000 psi)	1	Min. UTS = 81,361 N/cm^2 (118,000 psi)

Table 7-IV. Trunnion Arm Deflections.

Load	Deflection at Roller	Direction
F_c	0.123 cm (0.0485 in.)	Radially outward from fan axis of rotation.
F_R	0.005 cm (0.002 in.)	Radially inward from fan axis of rotation.
F_R	0.023 cm (0.0092 in.)	Transverse to arm axis.

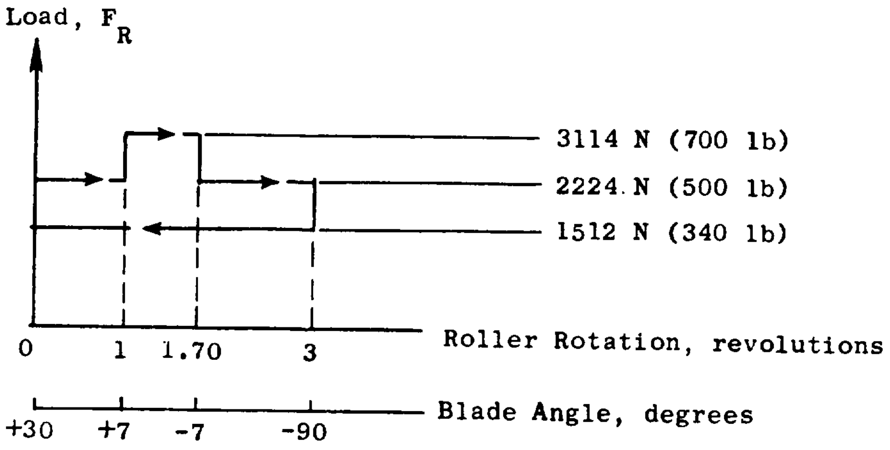

Load Case No. 2
Reverse Through Stall

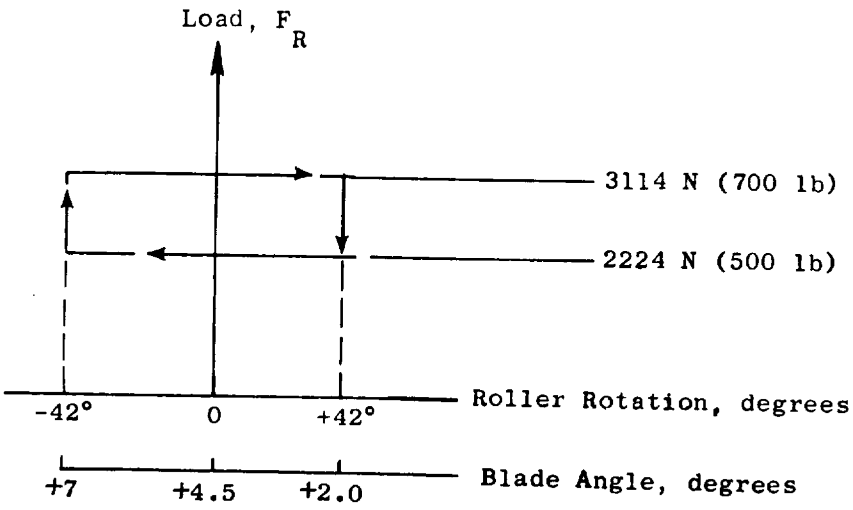

Load Case No. 1
Approach Modulation

Figure 7-8. Roller Cyclic Load Conditions.

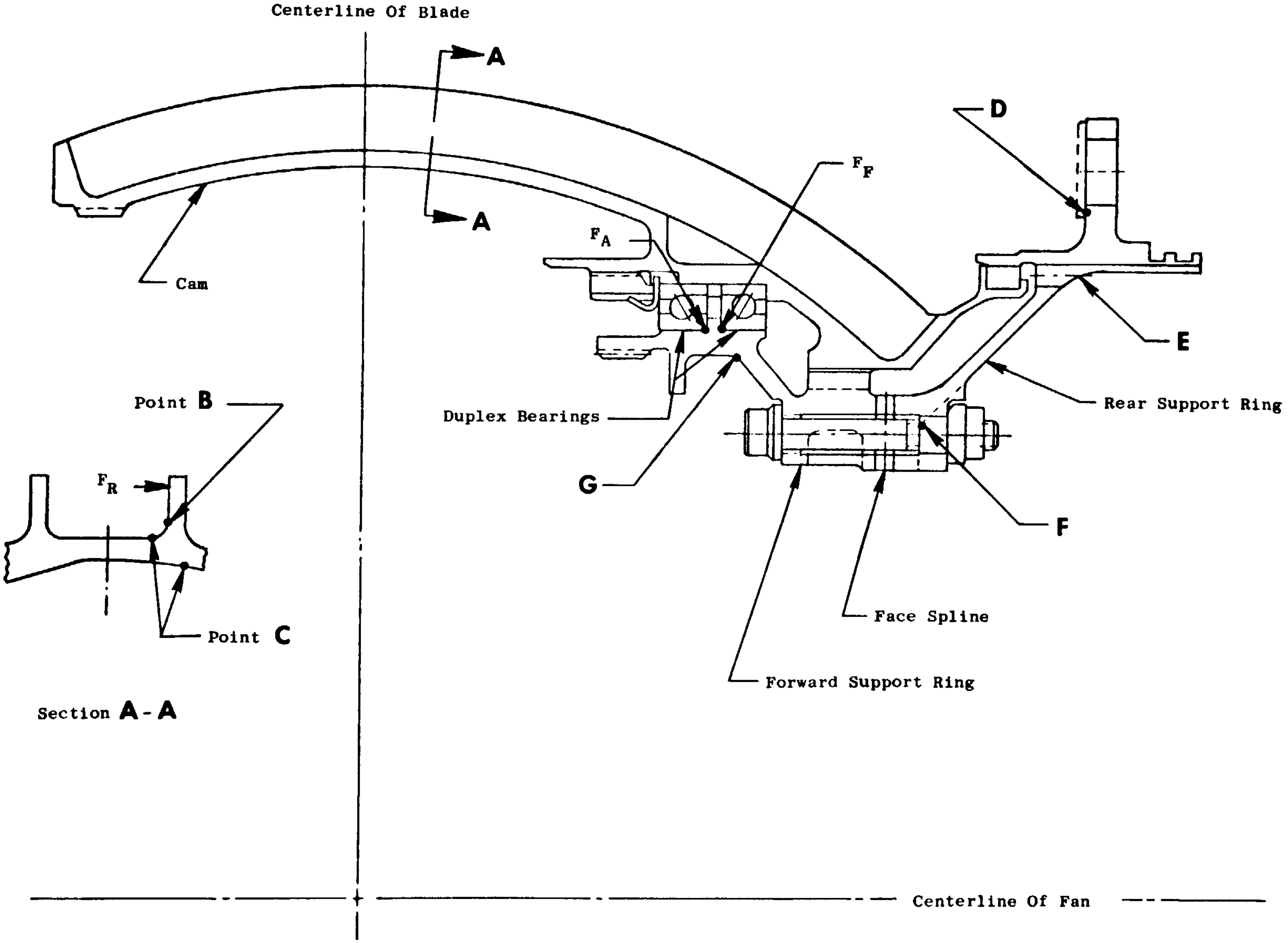
Centerline Of Blade
A
A
Cam
F_A
F_F
D
E
Rear Support Ring
Duplex Bearings
G
F
Face Spline
Forward Support Ring
Point B
F_R
Point C
Section A-A
Centerline Of Fan

Figure 7-9. Cam Assembly.

in the support rings by a computer shell program. Stresses were maximum at the cone-to-flange junctures and ring stiffness was designed to maintain roll deflections under the duplex bearings within acceptable limits.

Maximum cam stress occurs in the cam slot wall, subjected to the roller load. The highest load occurs at Section A-A (Figure 7-9) resulting in a roller contact stress at the load, and a maximum wall bending stress in the wall fillet radius at Point B.

Evaluation of contact stresses under cyclic load conditions indicated that at the resulting stress conditions the total number of required cycles was 24% of the allowable cycles. Under bird strike conditions, the contact stress in the cam wall reaches a level of 364,400 N/cm^2 (528,500 psi) versus an allowable minimum bearing ultimate strength of 258,563 N/cm^2 (375,000 psi). This indicates that local brinelling will occur which is considered acceptable for bird-strike.

Analysis of the bending stress at Point B (Figure 7-9) indicates that at the resulting stress conditions the summation of required cycles is 13.7% of the total number of allowable cycles. Bird strike results in a stress at Point B of 159,275 N/cm^2 (231,000 psi) versus a minimum ultimate strength of 162,033 N/cm^2 (235,000 psi). The bird strike stress includes a factor of 1.4 representing material plastic flow.

Cam Support Housing

The cam support housing is shown as a part of the cam assembly (Figure 7-9). Maximum loads on the housing are cam thrust loads of 31,136 N (7000 lb) aft and 48,038 N (10,800 lb) forward acting through the 30° contact angle duplex bearings. The resultant loads, F_A = 62,272 N (14,000 lb) and F_F = 96,077 N (21,600 lb), act around the housing periphery at the bearing mounting sections. Combined axial bending and torsional stresses at key housing points, D, E, F, and G, are presented in Table 7-V. Stress at Point D is based on forward load, F_F, only since the flange receives backing from the mating engine flange for aft loads. Stresses at the remaining points are based on reversed loading.

The critical bousing deflection is radial deflection at the support bearings. The maximum radial deflection is ΔR = 0.0033 cm (0.0013 in.) as a result of load, F_F = 96,077 N (21,600 lb). The allowable ΔR required to maintain an acceptable contact angle under load is 0.0038 cm (0.0015 in.).

Harmonic Drive

A cross section of the harmonic drive component is shown in Figure 7-10. A three-lobe harmonic drive was selected for this design instead of a two-lobe configuration because the three-lobe unit is inherently stiffer radially, and is lighter due to more uniform load distribution. More

Table 7-V. Cam Support Housing Stresses.

Stress Location(1)	Stress		K_t	Required Cycles	Allowable Cycles
	N/cm^2	psi			
D	11,997 ± 11,997	17,400 ± 17,400	1.0	0.48×10^5	10^6 (2)
E	690 ± 12,825	1,000 ± 18,600	3.0	0.48×10^5	10^8
F	1,379 ± 13,997	2,000 ± 20,300	1.45	0.48×10^5	10^8
G	3,965 ± 27,028	5,750 ± 39,200	1.34	0.48×10^5	10^8

(1) Reference Figure 7-9.

(2) Allowable cycles at point D are based on acceptable stresses including possible fretting under the washer face.

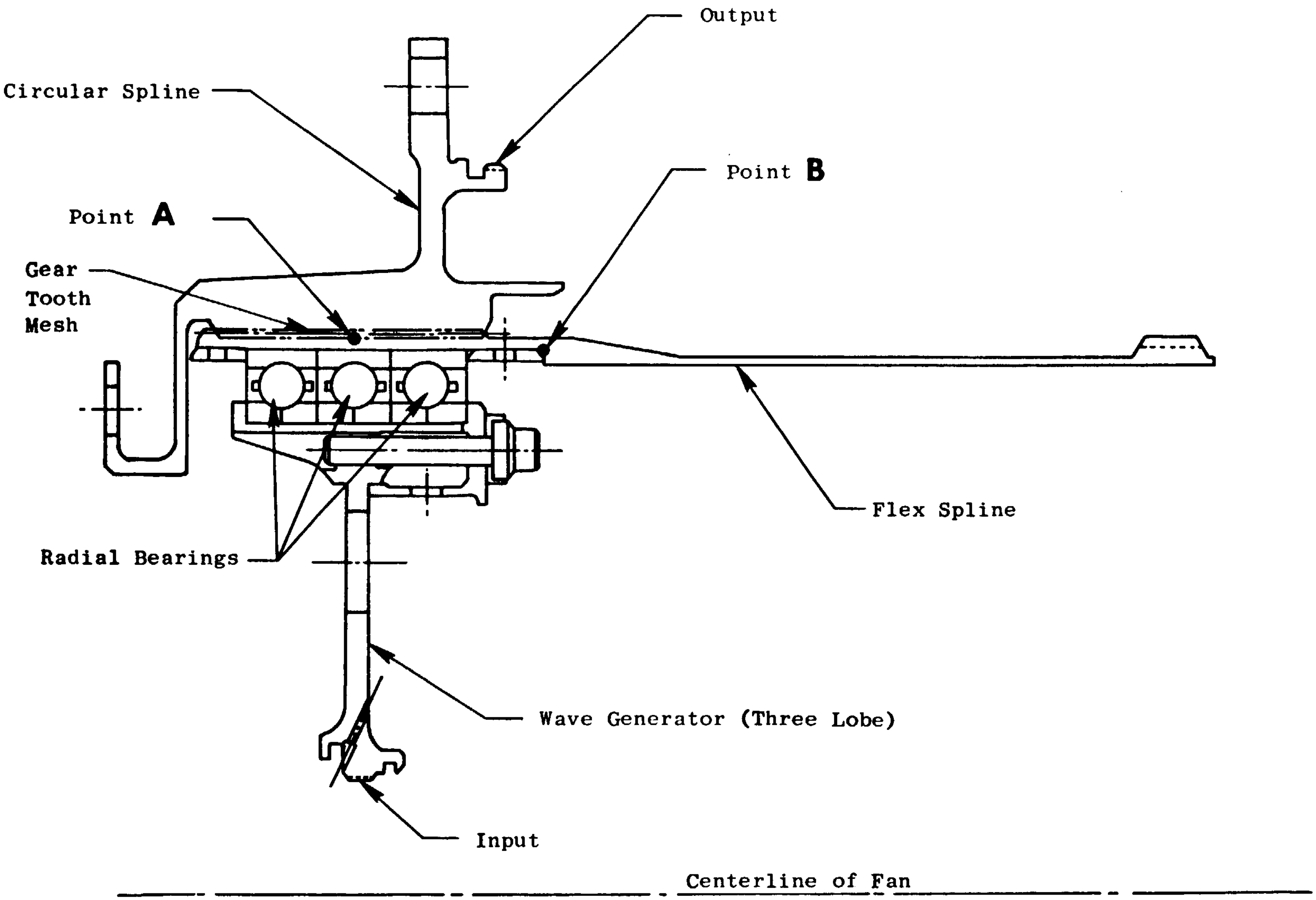
Output
Circular Spline
Point B
Point A
Gear
Tooth
Mesh
Flex Spline
Radial Bearings
Wave Generator (Three Lobe)
Input
Centerline of Fan

Figure 7-10. Harmonic Drive.

effective radial support and centering of parts is possible with three lobes and should result in improved balancing capability. Except for the flex spline and bearing races, the harmonic drive components are designed for high radial stiffness. This minimizes radial deflection under load at the harmonic tooth mesh to maintain safe tooth stresses under operating loads and to increase the ratcheting capacity of the unit. Ratcheting can occur if radial and tangential deflections at the tooth mesh are sufficiently high to permit tooth tip-to-tip interference between the flex and circular spline teeth. For maximum assurance, a ratcheting capacity of three times the maximum operated torque or 1,695,000 cm-N (150,000 in.-lb), has been designed into this harmonic drive by the addition of 2.3 kg (5 lb) of additional weight. All clearances, tolerances, deflections, and thermal effects that affect tooth meshing under load were considered in the design.

A computer shell program was utilized to arrive at a balanced stiffness design for the circular spline and wave generator. A computer program was developed to solve for the tooth load distribution at the three lobe meshes taking into account bearing radial stiffness along with the other members. This program has become a valuable tool for determining deflections and tooth meshing paths in addition to load distribution. Loads and deflections from this program were used in the computer shell program to determine deflections and stresses over the entire flex spline length. The maximum stress is at the root of the flex spline teeth.

A triplex ball bearing set is used in the harmonic drive for maximum radial stiffness. Three bearings of smaller cross section support the flex spline over the full tooth length and the smaller balls result in more uniform radial support. The inner race is split to permit a solid one-piece cage to be used. The solid steel cage is silver plated and rides on the inner race at the three lobe points. Ball pockets are designed to accept the full ball excursion and speed variations in traversing the harmonic path. The bearing outer race thickness was designed based on flexing stress and overhang bending stress transverse to the ball path.

No practical analysis has been found that would permit an accurate evaluation of bearing skidding, but reasonable safeguards have been used in the bearing design to reduce the tendency for ball skidding and to improve life if skidding occurs. The bearing material is M50 steel, vacuum induction melted with vacuum arc remelting. Ball race finish is held to 15.25 x 10^{-6} cm (6 x 10^{-6} in.) with 127 x 10^{-6} cm (50 x 10^{-6} in.) waviness control. Control on internal clearance, OD, and bore tolerances is held closer than specified for ABEC-7 bearings. All thermal and centrifugal effects on clearances and fits have been considered. Contact angle on the inner races and conformity are such that the contact pattern is always on the race for loads based on harmonic output torque in excess of maximum operating torque. Bearing life was calculated for the bearing set using A.B. Jones' "Rolling Element" program with a load distribution factor between bearings of 1.45. A curve of B_{10} life versus harmonic output torque was plotted and used with the mission torque requirements to determine bearing life as a function of cubic mean mission torque. The resulting bearing life values are discussed later.

The harmonic drive design and operating characteristics are summarized in Table 7-VI. Shown in Table 7-VII are the radial deflections at the tooth mesh and loss of "d" for the maximum design operating torque and design nonratcheting torque, where "d" is defined as the cam rise of the wave generator from minor to major axis. The value of "d" for this unit is 0.109 cm (0.043 in.). Radial deflections reduce tooth engagement directly while loss in "d" is listed only to show that an empirical harmonic design rule is satisfied. The rule states that loss in "d" under maximum operating torque shall be less than 10 percent. This rule and the 10 percent value are based on experience obtained by United Shoe Machinery.

For the normal operating thermal environment of hot oil inside and cold air outside the harmonic drive, thermal radial deflection at the tooth mesh is 0.00434 cm (0.00171 in.) into mesh for 383 K (230° F) oil and 244 K (-20° F) air. For a transient thermal inversion condition of 268 K (23° F) oil and 328 K (130° F) air, the radial tooth deflection is 0.00185 cm (0.00073 in.) out of mesh. A minimum engagement of 0.0505 cm (0.0199 in.) is used for tooth bearing stress calculations for life requirements. Results are presented in Table 7-VIII.

The maximum flex spline stresses occur at the spline root, Point "A", and the shoulder fillet at Point "B" (Reference Figure 7-10). Stress at "A" is combined tooth bending stress due to 1601 N (360 lb) maximum tooth load and member hoop and bending stress due to forced harmonic deflection. Stresses at "B" are hoop and axial due to the forced deflection. These stresses are summarized in Table 7-IX.

The critical torsional buckling shear stress for the flex spline is 29,097 N/cm^2 (42,200 psi). Torsional shear stress at nonratcheting torque of 1,695,000 cm-N (150,000 in.-lb) is 23,926 N/cm^2 (34,700 psi). The torsional shear stress margin is 22%. Torsional natural frequency of the flex spline is 3880 cps or 233,000 cpm.

Stresses in the wave generator and circular spline are not critical since they are designed for radial stiffness. The gyroscopic moment (M_{GYRO}) of the wave generator and bearing inner races at 3350 fan rpm and 4500 input rpm (7850 rpm total) at a precession rate of 1 rad/sec is 1695 cm-N (150 in.-lb). This moment is reacted by the bearings with a negligible effect on life.

No-Back

A cross section of the bidirection spring clutch (no-back) is shown in Figure 7-11. The self-energizing no-back spring locks blade torque in either direction by locking the harmonic drive input to output. Minimum holding torque capacity is 19,210 cm-N (1700 in.-lb) at a minimum coefficient of friction of 0.06. Maximum torque capacity is 27,120 cm-N (2400 in.-lb) as limited by the torque limiter brake. Since the load per coil varies exponentially with the number of coils and friction coefficient, the

Table 7-VI. Harmonic Drive - Design and Operating Characteristics.

Max. Output Torque:	565,000 cm-N (50,000 in.-lb) Normal 1,695,000 cm-N (150,000 in.-lb) Nonratchet
Min. Input rpm:	2800 @ Maximum Normal Output Torque 4500 @ No-Load
Reduction Ratio:	201/1
Min. Torque Efficiency:	70% @ 2870 rpm and Maximum Normal Output Torque
No. Wave Generator Lobes:	3
No. Circular Spline Teeth:	603
No. Flex Spline Teeth:	600
Tooth Pressure Angle:	20°
Torsional Stiffness:	40° Max. Input Rot. @ Maximum Normal Output Torque
Max. Operating "K" Value:	76
Circular Spline Pitch Diameter:	22.098 cm (8.700 in.)

Item	Material	Heat Transfer	Surface Treatment
Circular Spline	AMS 6415	32 - 38 R_c	Cad Plate (External)
Flex Spline	AMS 6414 (CEVM)	40 - 44 R_c	Peened and Black Oxide
Wave Generator	AMS 6415	36 - 40 R_c	
Bearings	M-50		

Table 7-VII. Harmonic Drive - Radial Deflection at Tooth Mesh and Loss of "d"(1).

Item	MAX. DESIGN OPERATING TORQUE				DESIGN NON-RATCHETING TORQUE			
	565,000 cm-N (50,000 in. lb)				1,695,000 cm-N (150,000 in. lb)			
	Loss in "d"		Radial Deflection		Loss in "d"		Radial Deflection	
	cm	in.	cm	in.	cm	in.	cm	in.
Circular Spline	0.00338	0.00133	0.00257	0.00101	0.01016	0.00400	0.00767	0.00302
Bearing	0.00376	0.00148	0.00376	0.00148	0.00660	0.00260	0.00660	0.00260
Plug Ring	0.00163	0.00064	0.00137	0.00054	0.00485	0.00191	0.00406	0.00160
Plug Overhang	0.00028	0.00011	0.00025	0.00010	0.00086	0.00034	0.00076	0.00030
	0.00905	0.00356	0.00795	0.00313	0.02247	0.00885	0.01909	0.00754
% Loss In "d"	8.18	8.18			20.3	20.3		

(1) "d" is cam rise of the wave generator from minor to major axis.

Table 7-VIII. Harmonic Drive Flex Spline/Circular Spline Tooth-Bearing Stress.

Tooth Load at Maximum Normal Output Torque	Stress	Required Cycles	Allowable Stress
1601 N (360 lb)	7585 N/cm^2 (11,000 psi)	1 x 10^6	7929 N/cm^2 (11,500 psi)

Table 7-IX. Flex Spline Stresses.

Location*	Stress Type	K_t	Stress		Required Cycles	Allowable Stress @ 10^8 Cycles	
			N/cm^2	psi		N/cm^2	psi
A	Combined	1.75	9584±29,855	13,900±43,300	10^8	9584±32,047	13,900±47,000
B	Hoop	1.0	-1076±17,582	-1560±25,500	10^8	-1076±35,165	-1560±51,000
C	Axial	1.93	-4723±14,066	-6850±20,400	10^8	-4723±35,165	-6850±51,000

*Reference Figure 7-10.

Table 7-X. No-Back Design Characteristics.

Max. Normal Holding Torque:	2825 cm-N (250 in.-lb)
Max. Dynamic Holding Torque:	27120 cm-N (2400 in.-lb)
Max. Input Torque, Aiding Load:	181 cm-N (16 in.-lb)
Max. Input Torque, Operating Load:	4068 cm-N (360 in.-lb)
Max. Dynamic Input Torque:	9605 cm-N (850 in.-lb)
Max. rpm, Aiding Load:	4500
Min. rpm, Max Opposing Load:	2800
Spring Drag Torque Tare:	181 cm-N (16 in.-lb)

Item	Material	Heat Treat	Surface Treatment
Housing	AMS 6415	40-44 R_c	Chrome Oxide Bore
Spring	AMS 6415	40-44 R_c	
Energizers	AMS 6415	40-44 R_c	
Quills	AMS 6415	40-44 R_c	
Support Ring	AMS 6415	40-44 R_c	Silver Plated Journals 0.0005 - 0.0010 cm (0.0002 - 0.0004 in.) thick

center coils react less load than the end coils and are, therefore, smaller in cross section to conserve weight. The housing bore is coated with a chrome oxide flame-sprayed coating which experience has shown to provide a durable, low-wear friction surface when lowering an aiding load. Holes in the housing at the spring running surface are used to prevent a hydrodynamic film from forming which could delay dynamic spring engagement.

Since the no-back is bidirectional, both the input from the differential and the output to the harmonic drive must be capable of acting torsionally on both ends of the spring. This is accomplished with input and output quill shafts splined to both ends of the spring and to each other. All splines are designed with sufficient gaps between teeth to permit the relative motion of the splined members required to engage and disengage the no-back spring under all conditions of load, tolerances, deflections, and temperature. All parts in the no-back are steel and the quill shafts are supported on silver-plated journal bearings. The primary design criteria for the various no-back parts are: low hoop deflection in the housing, compressive stress in the spring coils, torsional shear stress in the quills, and spline bearing stress. The no-back design characteristics are presented in Table 7-X.

Torque Limiter Brake

The torque limiter brake, shown in Figure 7-12, is a disk-type brake which grounds the no-back housing to the harmonic output through the differential gear housing. Disks with four rubbing surfaces are loaded axially by an adjustment nut acting against a Belleville-type spring to set the brake slip torque. The brake disk surfaces incorporate radial grooves for continuous lubrication.

The slip torque range is from 19210 to 27120 cm-N (1700 to 2400 in.-lb). The coefficient of friction range is from 0.08 to 0.113 (total). Disk pressure will be set at 290 N/cm^2 (420 psi) at assembly. Expected maximum temperature is 506 K (450° F). Selected materials are as follows:

Item	Material	Heat Treat	
Housing	HS463 (6Al-4V) Ti	Annealed 30-39 R_c	Peen Splines, Ni Plate 0.0003 - 0.0005 thick.
No-Back Support	AMS 6415 Gylon Ex 38*	40-44 R_c	Silver-plate journal dia., 0.0002-0.0004 thick.
Brake Disks	On AMS 6415	32-38 R_c	

---

* Gylon is a Teflon-base brake material heavily impregnated with a ceramic material for good thermal stability. It has a close range of static to dynamic friction coefficients in MIL-L-23699 fluid. The material operates in clutches up to 533 K (500° F) and 345 N/cm^2 (500 psi) disk pressure.

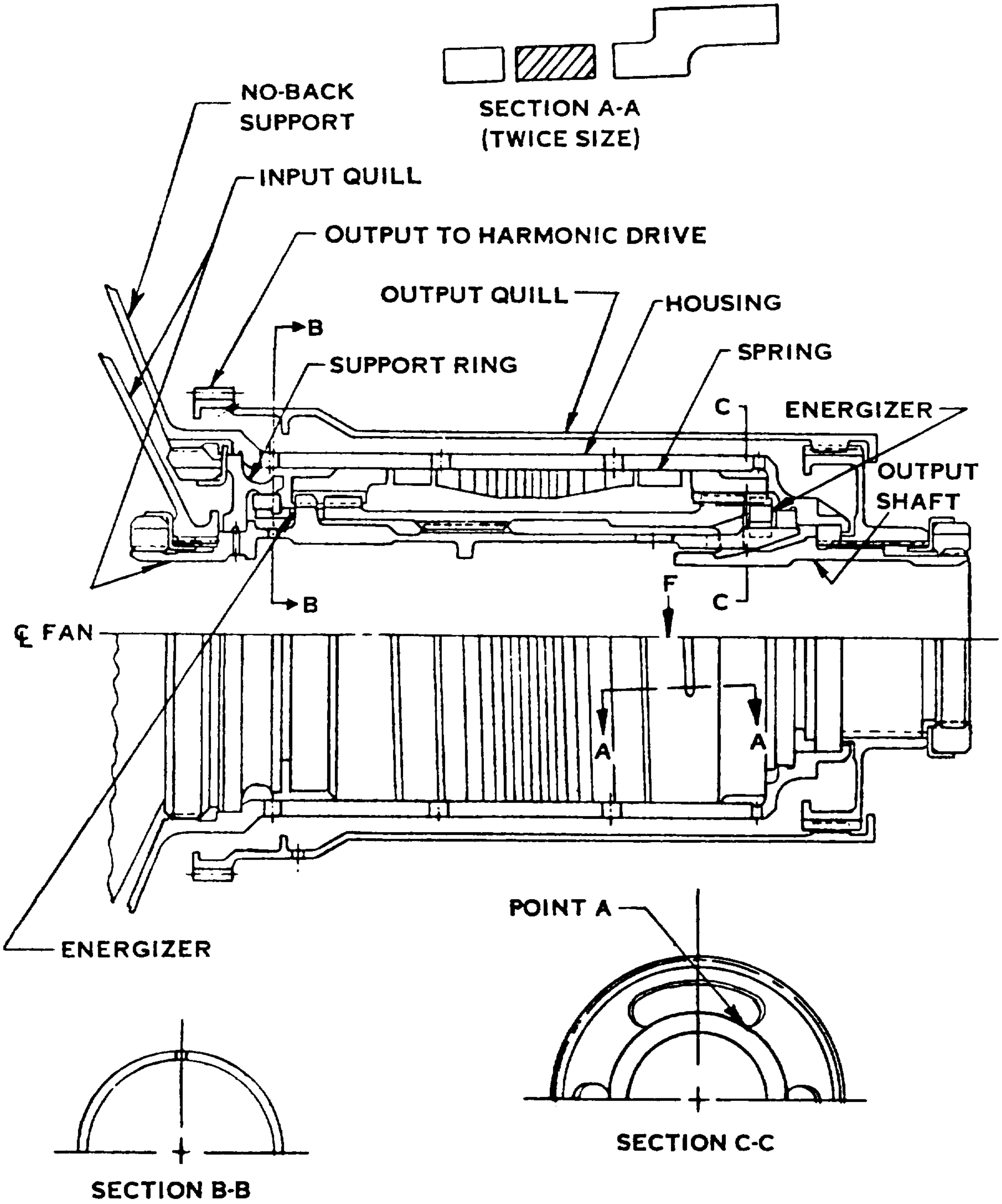
SECTION A-A
(TWICE SIZE)
NO-BACK SUPPORT
INPUT QUILL
OUTPUT TO HARMONIC DRIVE
OUTPUT QUILL
HOUSING
B
SUPPORT RING
SPRING
C
ENERGIZER
OUTPUT SHAFT
F
B
C
℄ FAN
A
A
ENERGIZER
POINT A
SECTION B-B
SECTION C-C

Figure 7-11. No-Back.

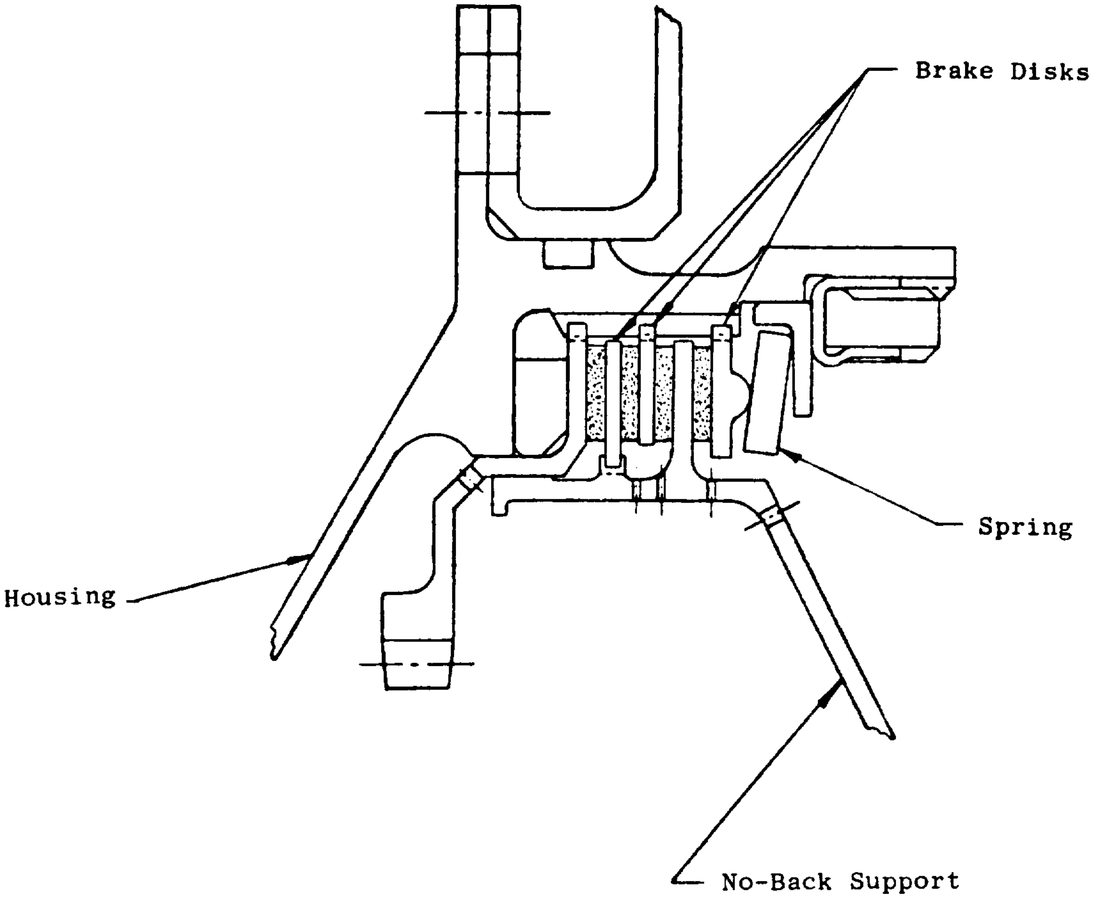
Brake Disks
Spring
Housing
No-Back Support

Scale: 2/1

Figure 7-12. Torque Limiter Brake.

Differential Gearing

The differential gear assembly is shown in Figure 7-13. The gears are made from AMS 6263 (AISI 9315, CEVM) steel and are carburized and ground. They are designed for infinite life at maximum operating torque. The sun gears form a floating mesh with three planet gears for equal load sharing. Sun gear shafts are sized for acceptable torsional shear stress. Ring gears are designed with sufficient tooth backing material to maintain low radial ring deflections. Planet gears are mounted on caged needle bearings running on case-hardened steel shafts in the planet cage.

A one-piece titanium planet cage is supported on a preloaded duplex ball bearing set mounted in the differential housing. This housing is closely centered on the harmonic output flange and bolted in place. The planet cage incorporates fore and aft rings tied together by integral cross beams located between planets. Pitch change torque on the gearing imposes bending on the cross beams from opposing torques in the end rings. Bending deflection is maintained within acceptable limits of angularity for the planet gear bearings. The lug stresses around the planet shafts were analyzed in much the same manner as the trunnion arm roller pin lugs.

Maximum dynamic input torque to the gears is 1921 cm-N (170 in.-lb) and maximum input rpm is 21,100. The minimum estimated torque efficiency is 98%. A summary of gear geometry and design characteristics is presented in Table 7-XI.

Flexible Drive Shaft

The flexible drive shaft assembly, shown in Figure 7-14, consists of a 0.953 cm (0.375 in.) diameter bidirectional flexible core running in a flexible Teflon-lined steel braided casing in a rigid-steel conduit. The core fittings are swaged to the core. A continuous 9.45 cm^3/sec (0.6 qt/min) lubrication flow passes between the core and casing to reduce wear. Bend radii are limited to 17.78 cm (7 in.) minimum. Fittings for "O" ring sealing are swaged to each end of the casing to seal in the lube flow. Identical splined drive fittings are swaged to each end of the flexible core.

Maximum dynamic (start-up) torque is 1921 cm-N (170 in.-lb), versus a yield torque capacity of 2825 cm-N (250 in.-lb). Maximum shaft speed is 21,100 rpm and the estimated minimum torque efficiency is 85%. Minimum torsional stiffness is 723 cm-N/rad (64 in.-lb/rad).

Fatigue capacity of flex shafts is dependent upon wire strand wear which in turn depends upon the number of revolutions, bend radius, number of bends, and lubrication. Fatigue capacity will be determined by tests which monitor wear (torsional stiffness).

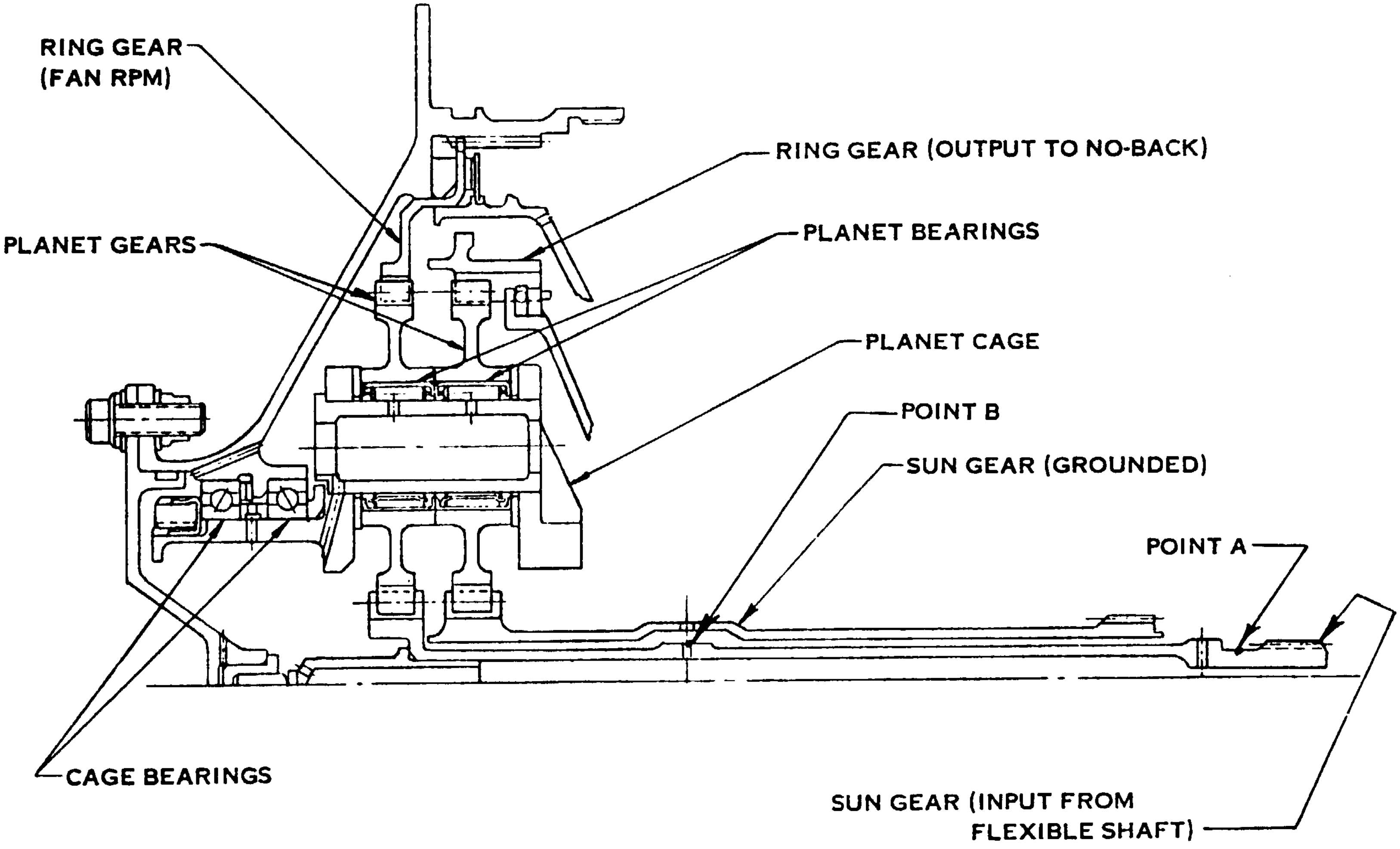
RING GEAR (FAN RPM)
RING GEAR (OUTPUT TO NO-BACK)
PLANET GEARS
PLANET BEARINGS
PLANET CAGE
POINT B
SUN GEAR (GROUNDED)
POINT A
CAGE BEARINGS
SUN GEAR (INPUT FROM FLEXIBLE SHAFT)

Figure 7-13. Differential Gear Assembly.

Table 7-XI. Differential Gear Data.

(Gear Ratio = 5:1)

	Sun	Planets (3)	Ring
No. Teeth	15	30	75
Dia. Pitch	16	16	16
Pressure Angle	22° 30'	22° 30'	22° 30'
Pitch Dia.	2.381 cm (0.9375 in.)	4.763 cm (1.8750 in.)	11.906 cm (4.6875 in.)
Min. Axial Engagement	0.559 cm (0.220 in.)	0.559 cm (220 in.) & 0.457 cm (180 in.)	0.457 cm (0.180 in.)
Min. Face Width	0.635 cm (0.250 in.)	0.635 cm (0.250 in.)	0.457 cm (0.180 in.)
Torque Condition	1921 cm-N (170 in.-lb)	3842 cm-N (340 in.-lb)	9605 cm-N (850 in.-lb)
Tang. Tooth Load	538 N (121 lb)	538 N (121 lb)	538 N (121 lb)
Dynamic Load	854 N (192 lb)	854 N (192 lb)	854 N (192 lb)
Dynamic Hertz	140,406 N/cm^2 (203,635 psi)	140,406 N/cm^2 (203,635 psi)	69,422 N/cm^2 (100,685 psi
Dynamic Bending	30,890 N/cm^2 (44,800 psi)	33,875 N/cm^2 (49,130 psi)	30,683 N/cm^2 (44,500 psi)
Static Hertz	111,461 N/cm^2 (161,655 psi)	111,461 N/cm^2 (161,655 psi)	111,461 N/cm^2 (79,930 psi)
Static Bending	19,465 N/cm^2 (28,230 psi)	21,347 N/cm^2 (30,960 psi)	19,337 N/cm^2 (28,045 psi)
Required Dynamic Cycles	3×10^6	5×10^5	1.8×10^6
Allow Dynamic Hertz	155,138 N/cm^2 (225,000 psi)	155,138 N/cm^2 (225,000 psi)	155,138 N/cm^2 (225,000 psi)
Allow Dynamic Bending	31,028 N/cm^2 (45,000 psi)	34,475 N/cm^2 (50,000 psi)	31,028 N/cm^2 (45,000 psi)
Gear Separating Loads	222 N (50 lb)	222 N (50 lb)	222 N (50 lb)

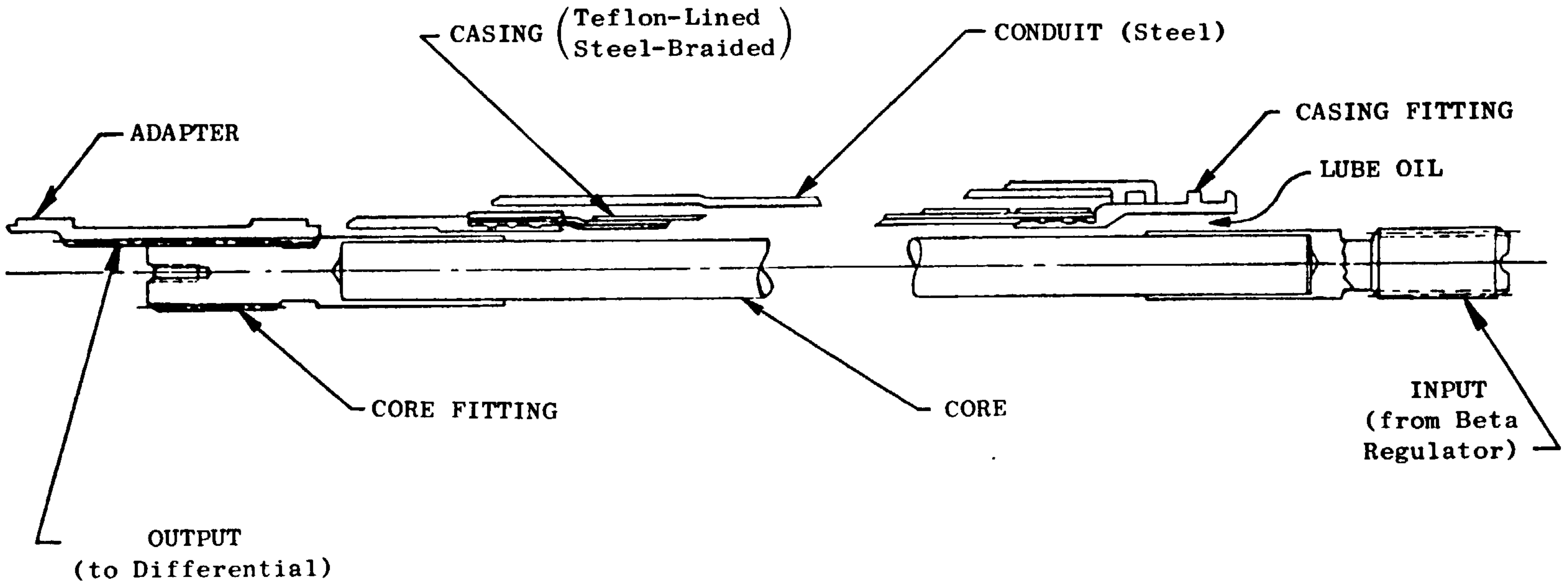
CASING (Teflon-Lined Steel-Braided)
CONDUIT (Steel)
ADAPTER
CASING FITTING
LUBE OIL
CORE FITTING
CORE
INPUT (from Beta Regulator)
OUTPUT (to Differential)

Figure 7-14. Flexible Shaft.

Beta Regulator

The test beta regulator, illustrated pictorially in Figure 7-5 and shown in cross section in Figures 7-15 and 7-16, is designed with two standard gear-type hydraulic motors driving a common output gear through a bevel gear mesh. The bevel gear ratio is 1.2, providing an increase in speed from the hydraulic motor to the flexible shaft. A flight-regulator would use a single positive displacement gear motor driving the output shaft directly. The standard hydraulic motors have 4.965 cm^3/rev (0.303 in.^{3}/rev) displacement each and have been modified for side porting. A feedback worm shaft is driven directly by the output shaft and drives a translating screw (0.375-16 UNJC-3A thread) through a 19:1 helical gear mesh. The screw is lapped for low axial play and translates parallel-mounted LVDT cores through a common yoke. Average LVDT feedback sensitivity is 0.0200 cm/deg (0.00788 in./deg). The estimated feedback loop accuracy, expressed in terms of fan blade angle, is defined in Table 7-XII.

Table 7-XII. Feedback Loop Accuracy In Terms of Fan Blade Angle.

	Thermal Effects 344° K±50° K(160° F±90° F)	Backlash	Linearity
Feedback Shaft			
Axial	±0.002°	±0.008°	
Rotation	0.000	±0.001°	
Gear/Screw Interface	0.000	±0.025°	
LVDT Core Position			
LVDT Electrical	±0.106°	0.000	±0.118° (full stroke)
	±0.108°	±0.034°	±0.118°

The combined full stroke feedback loop accuracy is ±0.260° for ±50° K (±90° F). The backlash of the gear screw interface (±0.025) can be eliminated through use of a preload spring. Also the linearity error (±0.118°) can be reduced approximately 50% by programming compensation into the digital control.

The mechanical blade angle error is ±0.240° which includes ±0.124° for the deflection between the no-back and the blades, ±0.081° for the backlash from the Beta regulator to the no-back and ±0.035° for the deflection from the Beta regulator to the no-back.

The feedback worm shaft has a hexagonal end which can be used to rotate the regulator output shaft manually to change pitch for rigging or trouble-shooting. A limit switch mounted adjacent to the feedback screw

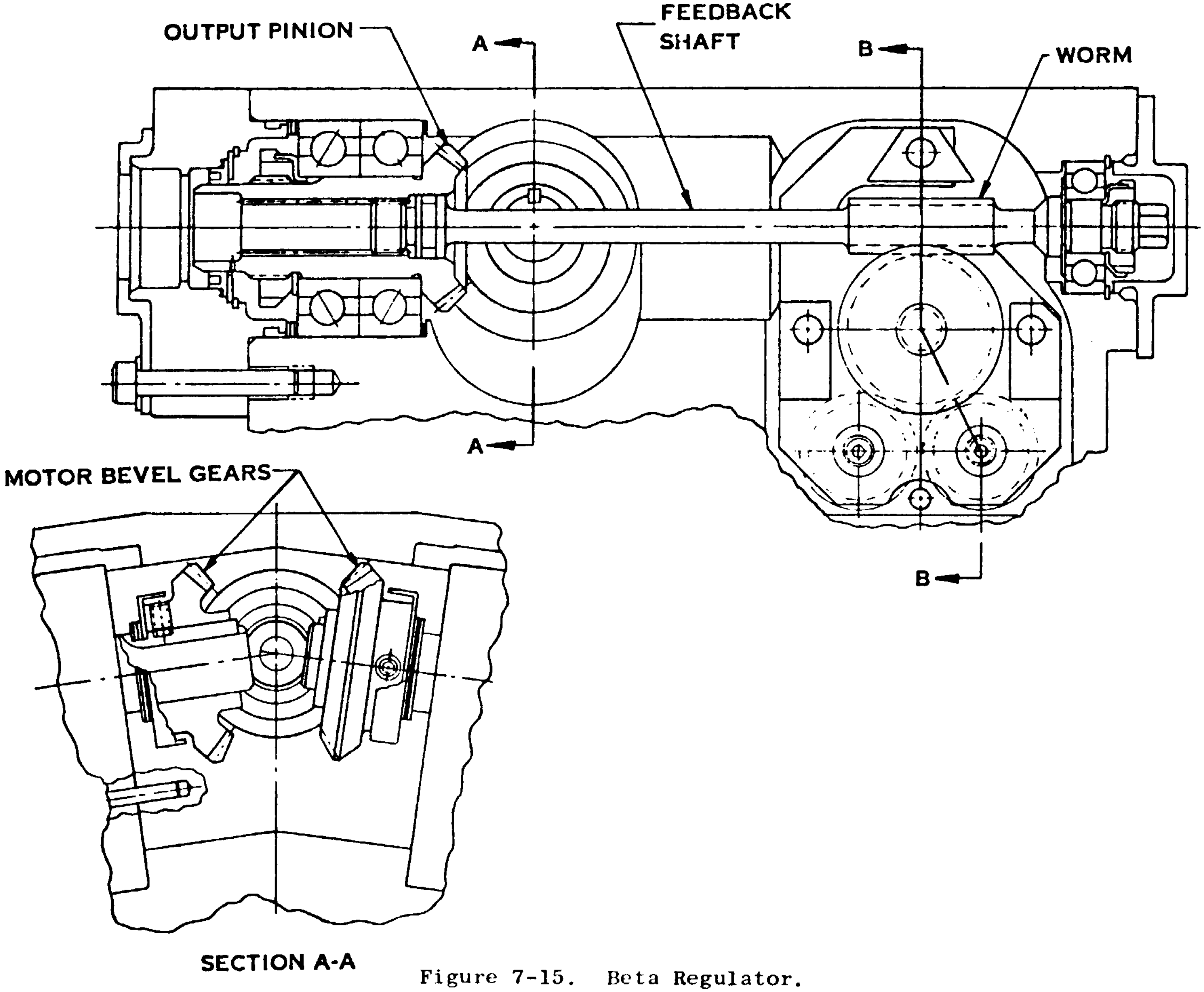
OUTPUT PINION
A
FEEDBACK SHAFT
B
WORM
A
MOTOR BEVEL GEARS
B
SECTION A-A

Figure 7-15. Beta Regulator.

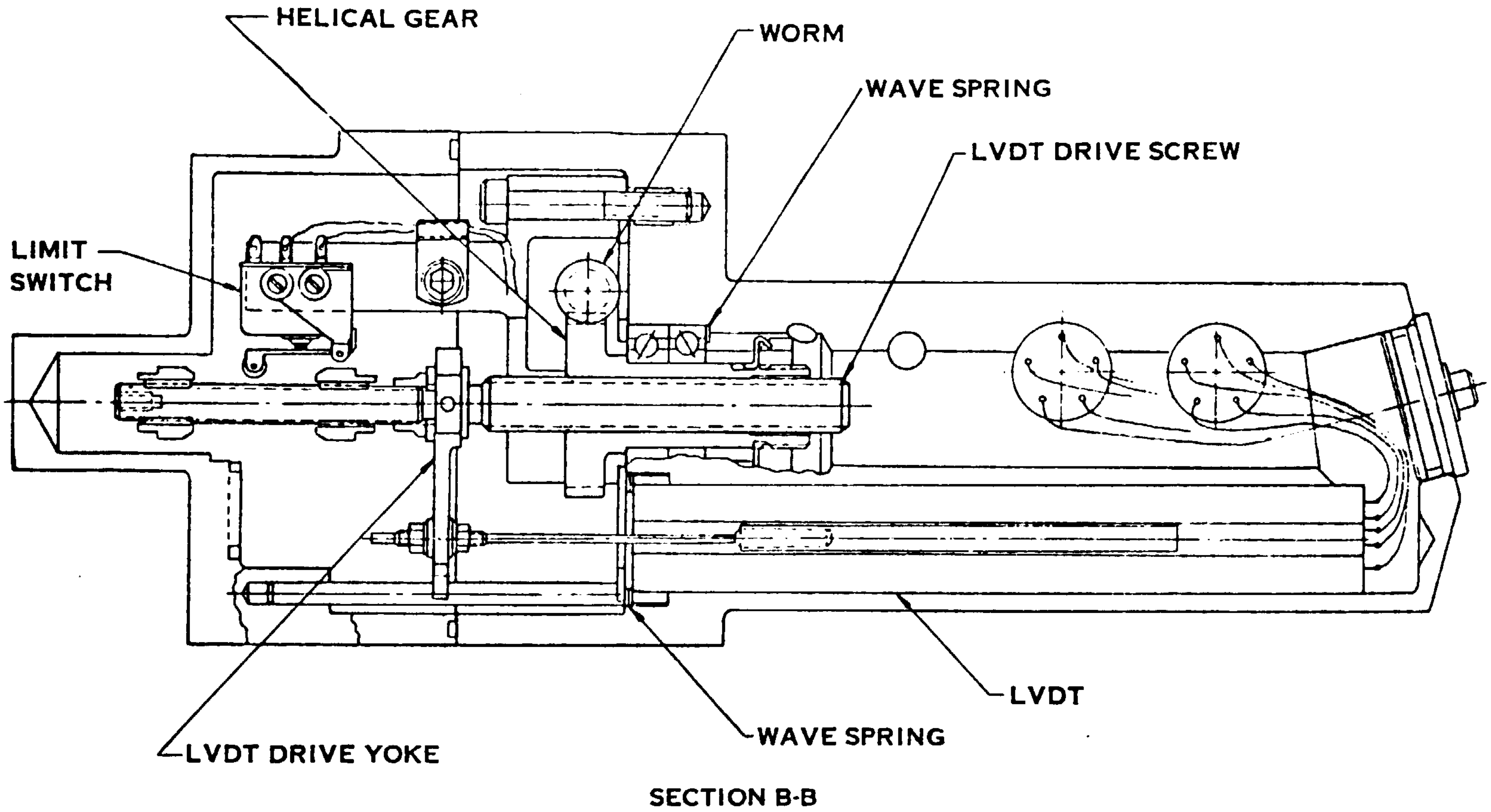
HELICAL GEAR
WORM
WAVE SPRING
LVDT DRIVE SCREW
LIMIT SWITCH
LVDT
WAVE SPRING
LVDT DRIVE YOKE
SECTION B-B

Figure 7-16. Beta Regulator.

extension is actuated by adjustable cam nuts on the extension at preset blade angles. The switch cuts off the electrical signal to the EHV, returning it to the null position and terminating pitch change. Setting of the switch cams would normally be just outside of the normal operating range to prevent the mechanical stops from engaging at full rate from a hard-over input beyond the operating range.

The beta regulator has three electrical connectors: two for LVDT's and one for the limit switch; and three hydraulic connections: fluid pressure ports to open and closed pitch and a drain port. A vent hole connects the beta regulator housing cavity to the flexible shaft conduit which is vented to the engine reduction gear section.

Output torque of the beta regulator is 0 cm-N (0 in.-lb) at 965 N/cm^2 (1400 psi) ΔP at no load, and 1582 cm-N (140 in.-lb) at 2069 N/cm^2 (3000 psi) ΔP at maximum load. Maximum output rpm (at no load) is 21,100.

Hydraulic motor speed/torque characteristics are shown in Figure 7-17 and speed/flow characteristics in Figure 7-18. Maximum operating motor ΔP is 2069 N/cm^2 (2000 psi) at maximum load and the minimum ΔP is 965 N/cm^2 (1400 psi) at no load. Maximum flow to the motors is 2268 cm^3/sec (36 gal/min) at 17,600 motor rpm and 965 N/cm^2 (1400 psi). The motors are manufactured by Ackley Corp, Clackamas Oregon and are modified by Hamilton Standard per P/N 763469-1.

Electro-Hydraulic Servovalve

The electro-hydraulic servovalve will be remotely located from the beta regulator in the engine pylon. The selected servovalve is a standard ABEX Corporation Model No. 425. Design characteristics of the servovalve include a 2758 N/cm^2 (4000 psi) maximum supply pressure, and rated flows of 1575 cm^3/sec (25 gpm) with a 690 N/cm^2 (1000 psi) ΔP, and 2728 cm^3/sec (43 gpm) with a 2069 N/cm^3 (3000 psi) ΔP.

Bearings

Design summaries for the cam support duplex bearings, harmonic drive triplex bearings, differential gear planet cage support bearings, and the differential gear planet roller bearings are presented in Table 7-XIII.

7.3.3 Actuator System Lubrication

Because the actuator duty cycle is short and high flows are not required for cooling, lubrication flow requirements are low. Low flows provide sufficient lubrication of parts and reduce torque losses in the system due to windage. The lubrication schematic, Figure 7-19, shows the lubrication flow paths and pressures for the actuator system. A total flow

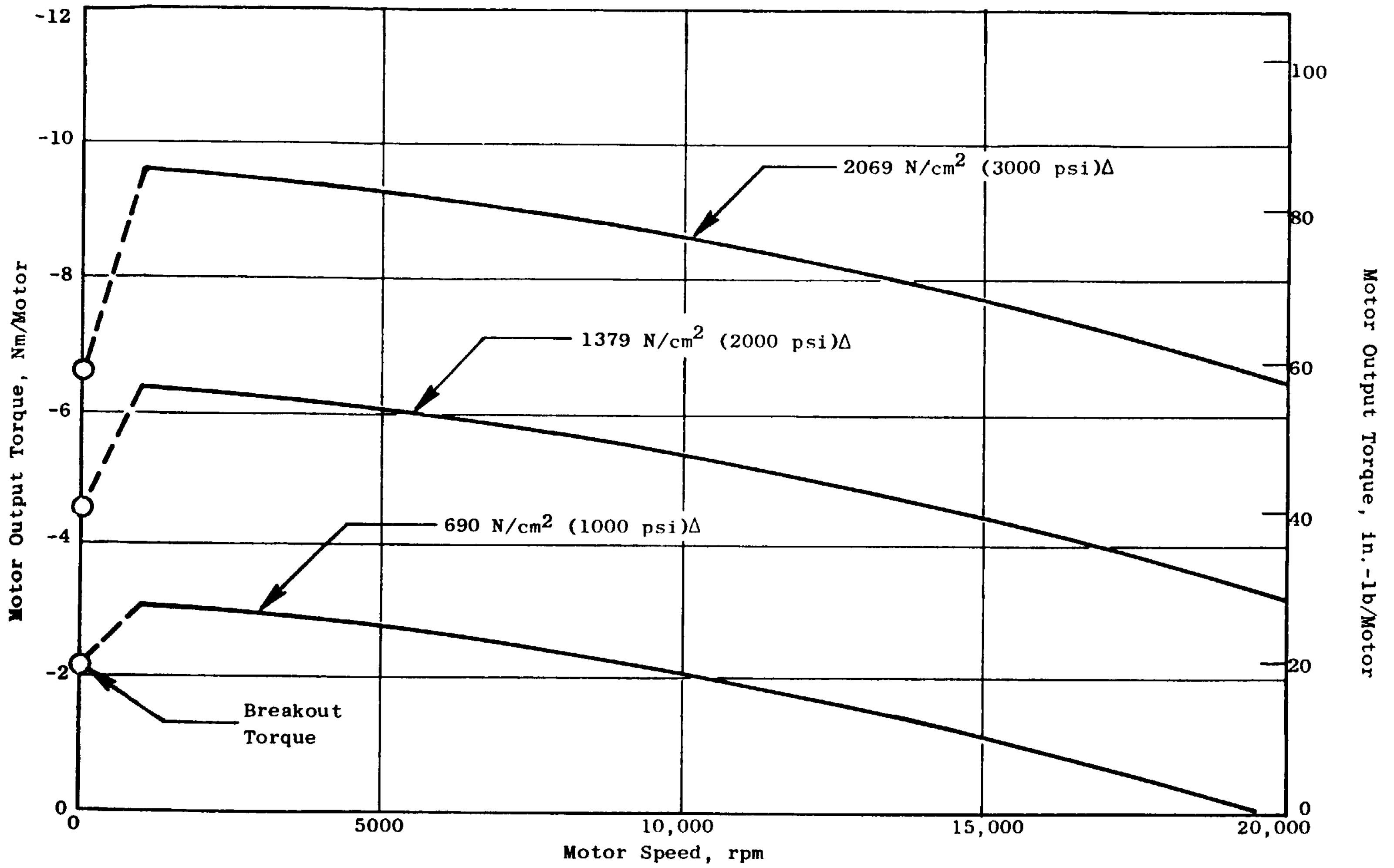

Figure 7-17. Beta Regulator - Hydraulic Motor Torque/Speed Performance.

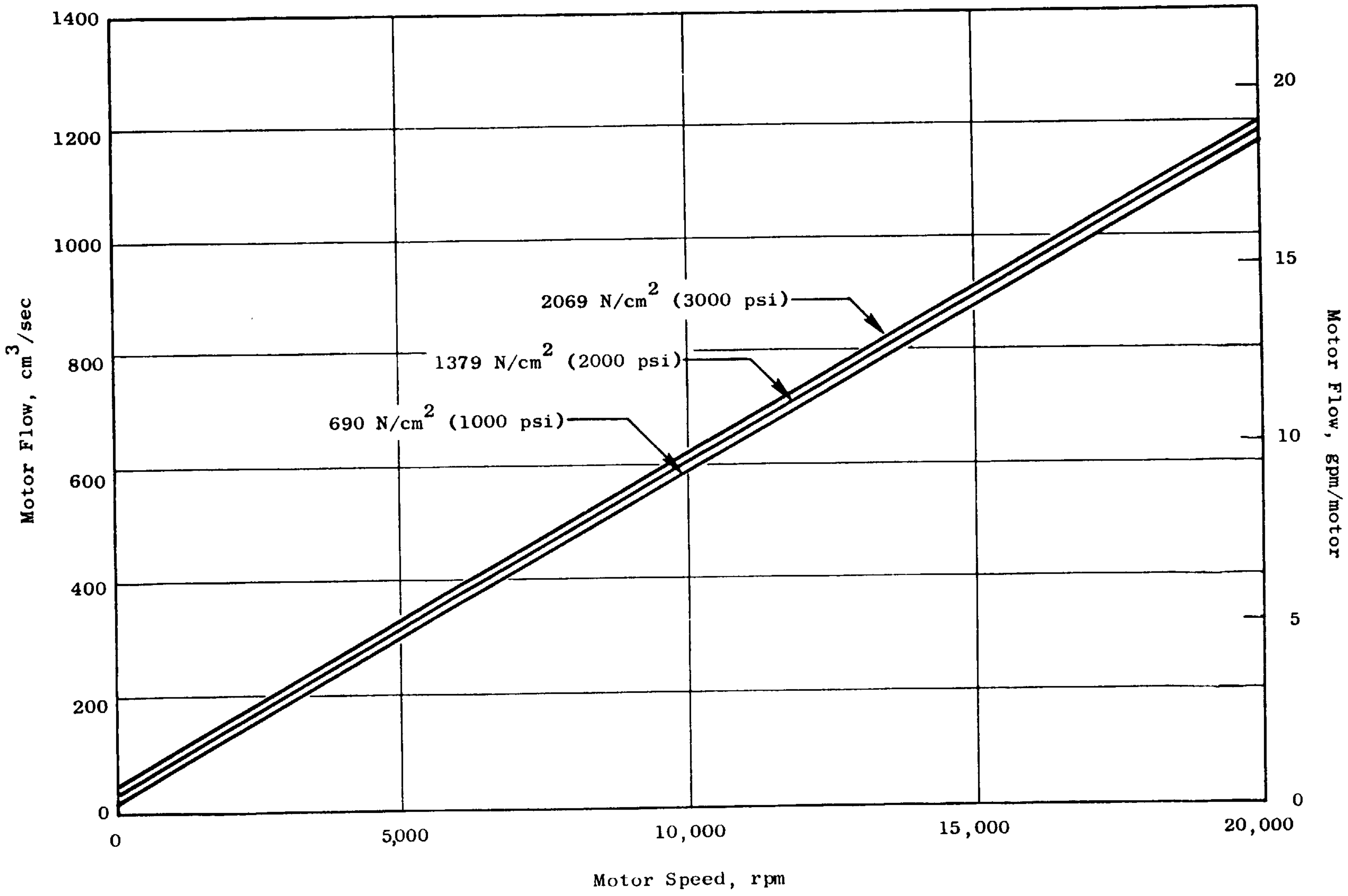

Figure 7-18. Beta Regulator - Hydraulic Motor Flow/Speed Performance.

Table 7-XIII. Bearing Data.

Bearing Item	Cam Support	Harmonic Drive	Planet Cage	Planets
Type	Duplex	Split Inner Race	Duplex	Roller
Bore	22.86 cm (9.00 in.)	19.46 cm (7.66 in.)	5.080 cm (2.00 in.)	1.429 cm (0.5625 in.)
No. Balls	106	66	36	Torrington J-97 Bearing
Ball Diameter	0.4763 cm (0.1875 in.)	0.7144 cm (0.28125 in.)	0.3175 cm (0.125 in.)	
Contact Angle	30°	30°	30°	Radial
Dynamic Capacity	N.A.	N.A.	4181 N (940 lb) For 1 x 10^6 Rev.	3336 N (750 lb) for 1 x 10^6 Rev.
Load Share Factor	1.0	1.45	1.0	1.2
Cage Type, Material	One-Piece Bronze Silver Plated	One-Piece Steel Silver Plated	One-Piece Bronze Silver Plated	Steel
Mean Load	32,470 N (7300 lb)	N.A.	200 N (45 lb)	273.6 N (61.5 lb)
Mean rpm	17.2	3450	1544	1164
B_{10} Life (Bearing Hours)	286	112	53,000	50,000
B_{10} Life (Aircraft Hours)	197,017	77,140	53,000	50,000
Required Life (Aircraft Hours)	36,000	36,000	36,000	36,000
MTBR (Aircraft Hours)	1,970,170	771,380	530,000	500,000

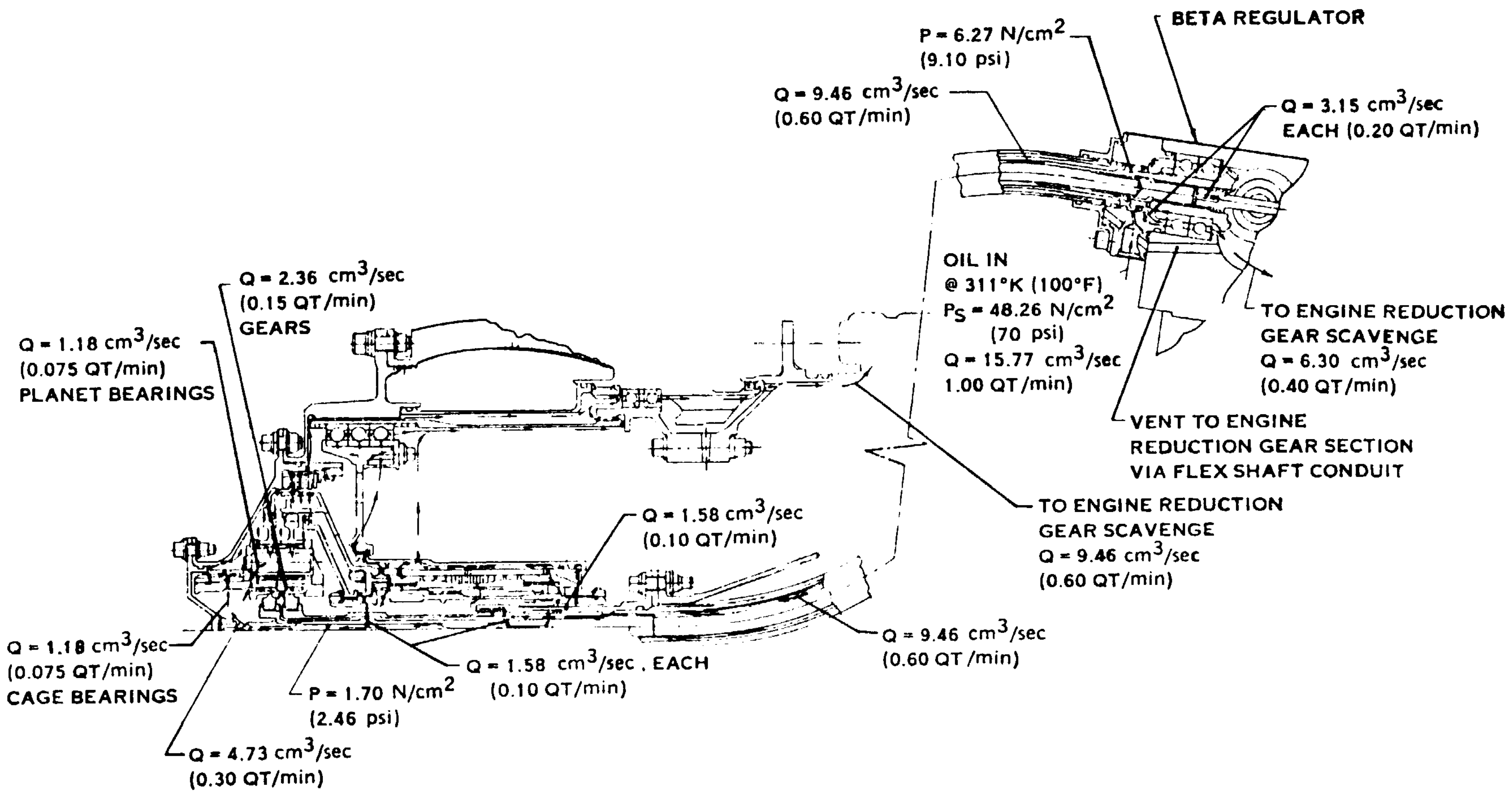
BETA REGULATOR
P = 6.27 N/cm^2 (9.10 psi)
Q = 9.46 cm^3/sec (0.60 QT/min)
Q = 3.15 cm^3/sec EACH (0.20 QT/min)
OIL IN @ 311°K (100°F) P_S = 48.26 N/cm^2 (70 psi) Q = 15.77 cm^3/sec 1.00 QT/min)
TO ENGINE REDUCTION GEAR SCAVENGE Q = 6.30 cm^3/sec (0.40 QT/min)
VENT TO ENGINE REDUCTION GEAR SECTION VIA FLEX SHAFT CONDUIT
TO ENGINE REDUCTION GEAR SCAVENGE Q = 9.46 cm^3/sec (0.60 QT/min)
Q = 2.36 cm^3/sec (0.15 QT/min) GEARS
Q = 1.18 cm^3/sec (0.075 QT/min) PLANET BEARINGS
Q = 1.58 cm^3/sec (0.10 QT/min)
Q = 1.18 cm^3/sec (0.075 QT/min) CAGE BEARINGS
Q = 9.46 cm^3/sec (0.60 QT /min)
Q = 1.58 cm^3/sec , EACH (0.10 QT/min)
P = 1.70 N/cm^2 (2.46 psi)
Q = 4.73 cm^3/sec (0.30 QT/min)

Figure 7-19. Lubrication Schematic.

of 13.39 cm^3/sec (0.85 qt/min) is taken from the engine lube system by an orifice at the beta regulator output shaft cover. 3.94 cm^3/sec (0.25 qt/min) is directed through an orifice to lubricate the beta regulator output bearings and the remaining 9.45 cm^3/sec (0.60 qt/min) is directed through the flexible shaft casing to lubricate the shaft core and actuator parts.

After leaving the flexible shaft casing, fluid passes through the shaft spline and is metered under pressure from four orifices inside the sun gear drive coupling and shafts. The first three orifices distributes 1.58 cm^3/sec (0.10 qt/min) each through the sun gear splines, no-back journal bearings, quill splines, and spring.

The fourth orifice directs the remaining 4.73 cm^3/sec (0.30 qt/min) flow inside the differential planet cage which distributes the fluid centrifugally to lubricate the cage bearings, planet bearings, and planet gears. This fluid passes centrifugally outward through the brake disks to the forward end of the harmonic drive.

Fluid from the no-back is directed centrifugally outward on both sides of the harmonic drive. The fluid on the forward side of the harmonic drive passes through the lobed flex spline and aft through the cam support bearings to return to the main reduction gear scavenge area through holes in the cam and cam support. Fluid on the aft side of the harmonic drive is directed aft along the flex spline to lubricate the circular ground spline and exit through the duplex cam bearings. The dynamic cam seal is centrifugally vented by the exit holes to preclude a pressure head on the seal. The triplex bearings are oil-mist lubricated.

Beta regulator gears, feedback drive, and bearings are lubricated by oil mist formed by fluid sprayed under pressure from the hydraulic motors against the bevel gear teeth.

7.3.4 Blade Pitch Angle Range

The following summarizes the maximum design blade pitch angle operating range capability based on the current actuation/rotor system:

Reverse Through Stall

Mechanical Stops:	+37°30' closed to -105° open
Electrical Stops:	+31° closed to -98° open

Reverse Through Flat Pitch

Mechanical Stops:	-23° open to +98°30' closed
Electrical Stops:	-16° open to +91°30' closed

For engine test, the blades may be reindexed to provide additional open or closed operating range capability. However, at any index setting the maximum blade pitch angle operating range remains the same.

7.3.5 Actuation System Weight

The component and overall system weights for the flight engine system based on final design analysis are summarized in Table 7-XIV. Also shown are weight adders to the experimental engine hardware to reduce development risk and cost. The 5.53 kg (12.2 lb) addition to the beta regulator and electro-hydraulic servovalve is to take advantage of low cost existing components. The 4.54 kg (10 lb) adder to the overall system weight leaves out specific final component machining operations, such as final tailoring of the cam slot walls, and includes the substitution of steel for titanium for certain parts, such as the front cover assembly, to reduce manufacturing cost. The design of the harmonic has not been optimized on the basis of weight in order to minimize risks. This results in a 2.27 kg (5 lb) weight penalty for the experimental engine. As shown, the weights of the flight weight and experimental engine actuation systems are 40.28 kg (88.8 lb) and 52.62 kg (116.0 lb), respectively.

7.4 GENERAL ELECTRIC BALL SPLINE VARIABLE-PITCH ACTUATION SYSTEM

7.4.1 System Description

The General Electric ball spline actuation system is shown in cross section in Figure 7-2, and is illustrated pictorially (except for the drive system) in Figure 7-20. A functional system schematic is also presented in Figure 7-21. The actuation system functions in the following manner.

Pinion bevel gears attached to each of the 18 fan blade trunnions are rotated by the motion of two counteracting master ring gears. The pinion bevel gears are attached to the trunnions by accurately positioned fine pitch splines, which allow for proper synchronizing with the two ring bevel gears. The fine pitch splines also permit reindexing of the blades to vary the open and closed blade angle limits for engine thrust reversal through both stall and through flat pitch. Use of two ring gears permits load sharing, and also adds redundancy to the system. An axial tie member in the area of the pinions prevents separation of the two ring gears. Overall gear ratio of the pinion bevel gear/ring gear mesh is designed to achieve the maximum gear capacity within the space available between any two blades. A shim is provided to ensure proper tooth meshing.

The ring gears are rotated by a ball spline driven by a rigid translating sleeve. The forward ring gear is driven by the outer (straight) portion of the ball spline while the aft ring gear is driven by the inner (helical) portion of the ball spline. As shown in Figure 7-2, both ring gears are easily removed at their bolted flange joints for modular assembly and disassembly of the actuator.

Table 7-XIV. Hamilton Standard Actuation System.

Flight Weight Design

Item	Weight kg	Weight lb
Arms & Rollers	7.67	16.9
Cam, Stops, Support	14.88	32.8
Harmonic Drive	7.39	16.3
No-Back	1.77	3.9
Differential Gear	2.54	5.6
Flexible Shaft & Housing	1.72	3.8
Beta Regulator	4.31	9.5
Total	40.28	88.8

Test System Weight Adders

Item	kg	lb
Harmonic Risk Reduction	2.27	5.0
Beta Regulator	5.53	12.2
Weight Increase for Cost Reduction	4.54	10.0
Total Weight Adders	12.34	27.2
Final Weight of Experimental Engine Actuation System	52.62	116.0

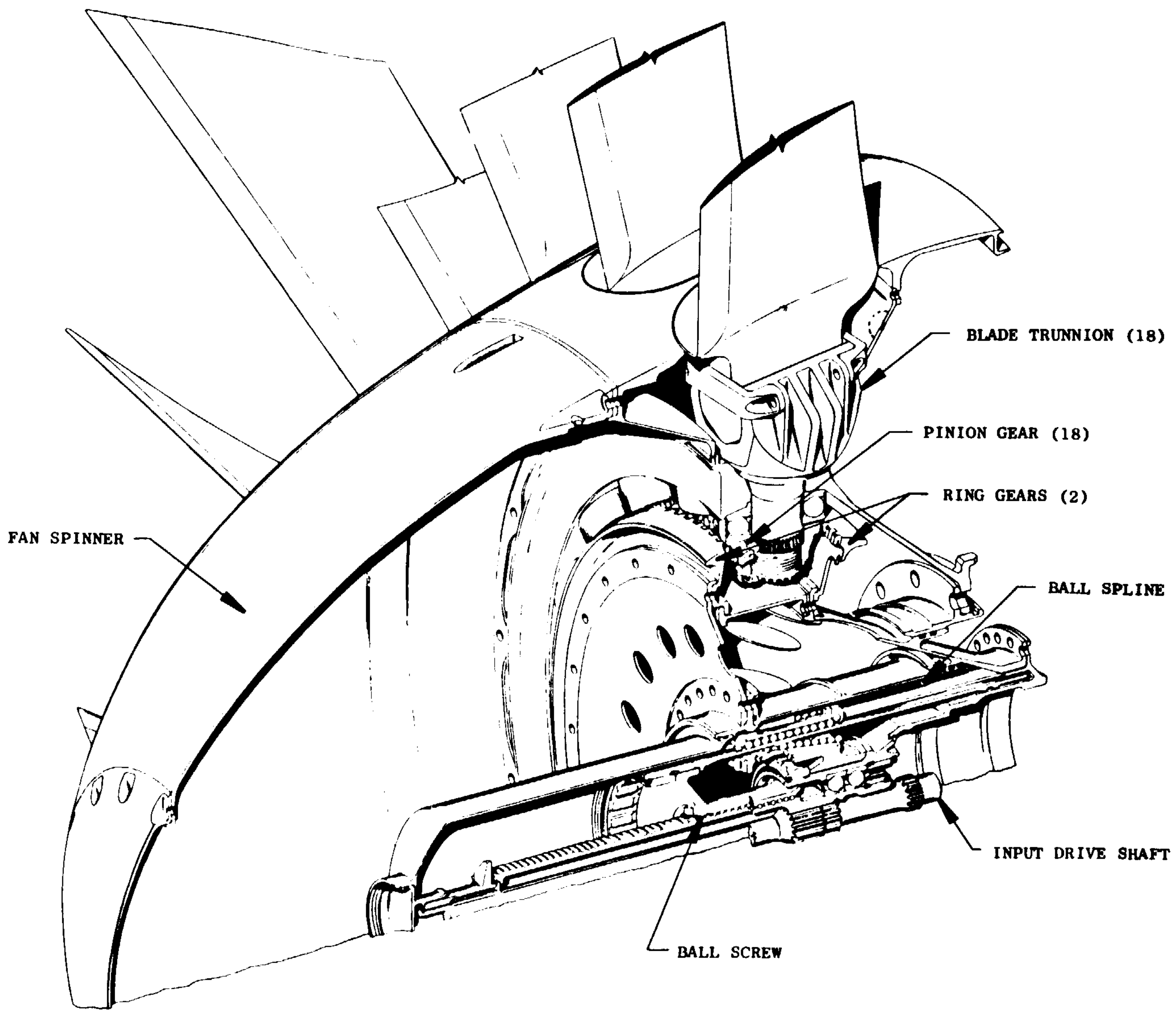
BLADE TRUNNION (18)
PINION GEAR (18)
RING GEARS (2)
FAN SPINNER
BALL SPLINE
INPUT DRIVE SHAFT
BALL SCREW

Figure 7-20. GE Ball Spline Actuation System.

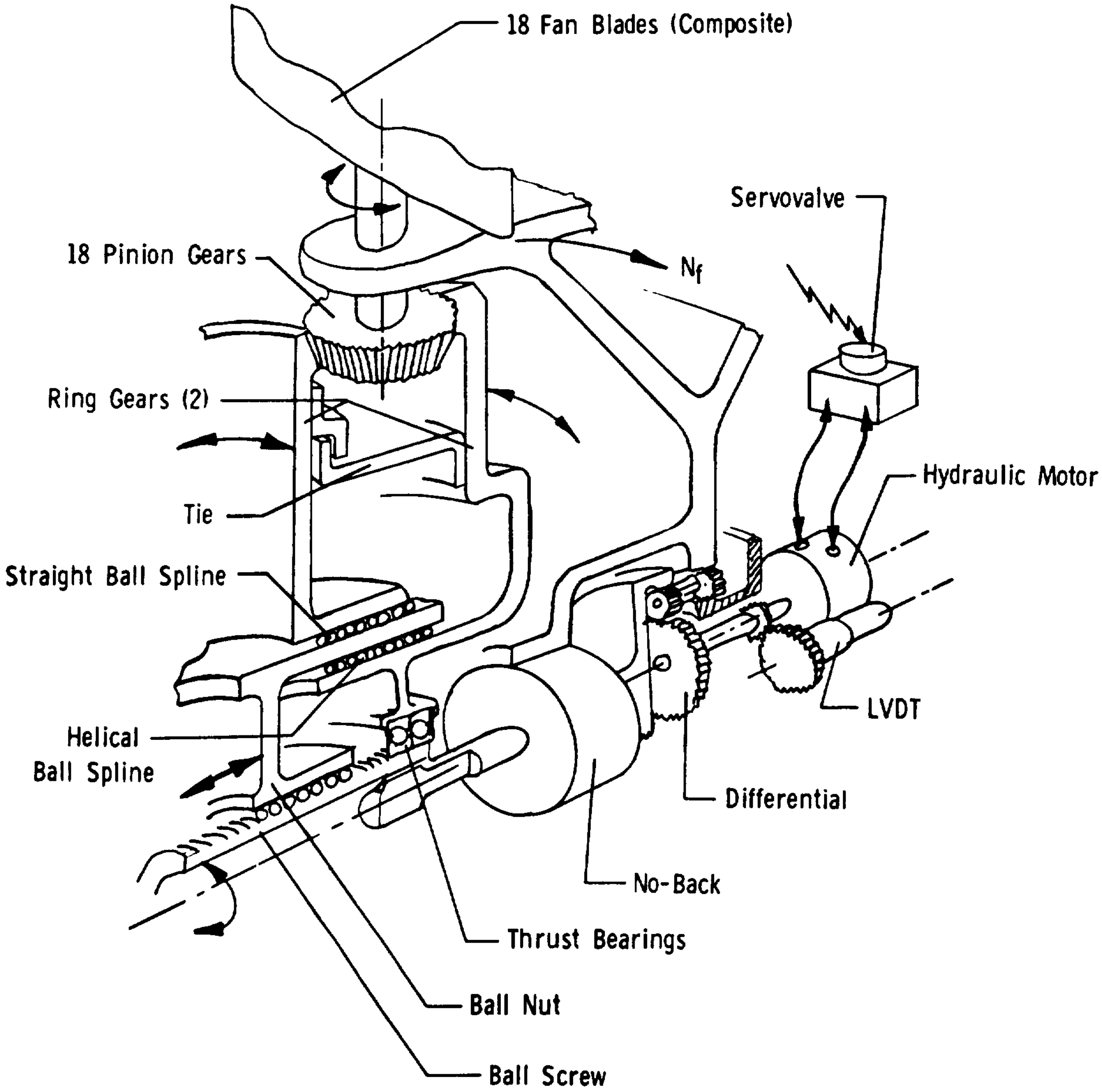
18 Fan Blades (Composite)
Servovalve
18 Pinion Gears
N_f
Ring Gears (2)
Hydraulic Motor
Tie
Straight Ball Spline
LVDT
Helical Ball Spline
Differential
No-Back
Thrust Bearings
Ball Nut
Ball Screw

Figure 7-21. GE Ball Spline Variable-Pitch Mechanism Schematic.

The rigid translating sleeve of the ball spline is driven by a ball screw through a stroke of 15.49 cm (6.10 in.) to achieve a blade rotation of 135°. The balls of the ball spline ride in a continuous path made up of a loaded track and a return guide. The return guides are tubes located out of the load zone. Loaded tracks and return guides are connected by end return caps. These end caps permit easy replacement of the balls during servicing.

Helical ball tracks between the inner and middle members of the ball spline generate a maximum axial load during normal operation of approximately 108.6 kN (24,398 lb). As illustrated in Figure 7-21, these axial loads are reacted from the middle member into the ball screw through a ball nut. Ball screw thrust loads are transmitted back into the inner member through a set of precision ground M50 duplex thrust ball bearings. Thus, all high actuator axial loads are close looped on a small diameter within the actuator. This close coupling of high axial loads was instrumental in achieving a low weight for a flight system.

As shown in Figure 7-2 and illustrated in Figure 7-21, power to drive the ball screw is provided by a hydraulic motor, acting through a gear differential. A ball/ramp-type no-back is included between the differential gear and the ball screw to allow torque to be transmitted only in one direction. Axial dynamic stops at each end of the ball screw (Figure 7-2) limit actuator travel.

A summary of the actuator design speed (rpm) and load characteristics is presented in Figure 7-22.

7.4.2 Component Design

Bevel Gears

As shown in Figure 7-2, torque generated by the ball spline is transferred radially outward through cones to the forward and aft ring gears. These ring bevel gears synchronize and drive the 18-blade pinion bevel gears. Transmitting torque from the ball spline through two gear meshes into each pinion gear minimizes the actuator requirements and provides redundancy in the event of excessive blade impact twisting loads.

Geometry of the mating pinion and ring gear teeth is defined in Figure 7-23. Pinion gear tooth design loads and stress data are presented in Table 7-XV. Allowable stress for the condition of maximum operating torque is based on GE design practice for maximum continuous operating bending and compressive stresses. For the bird strike condition (FOD impact load), the allowable bending stress is based on GE design practice for impact loading of gear teeth. Gear tooth stresses in the ring gears would be essentially the same as those shown for the pinion gears.

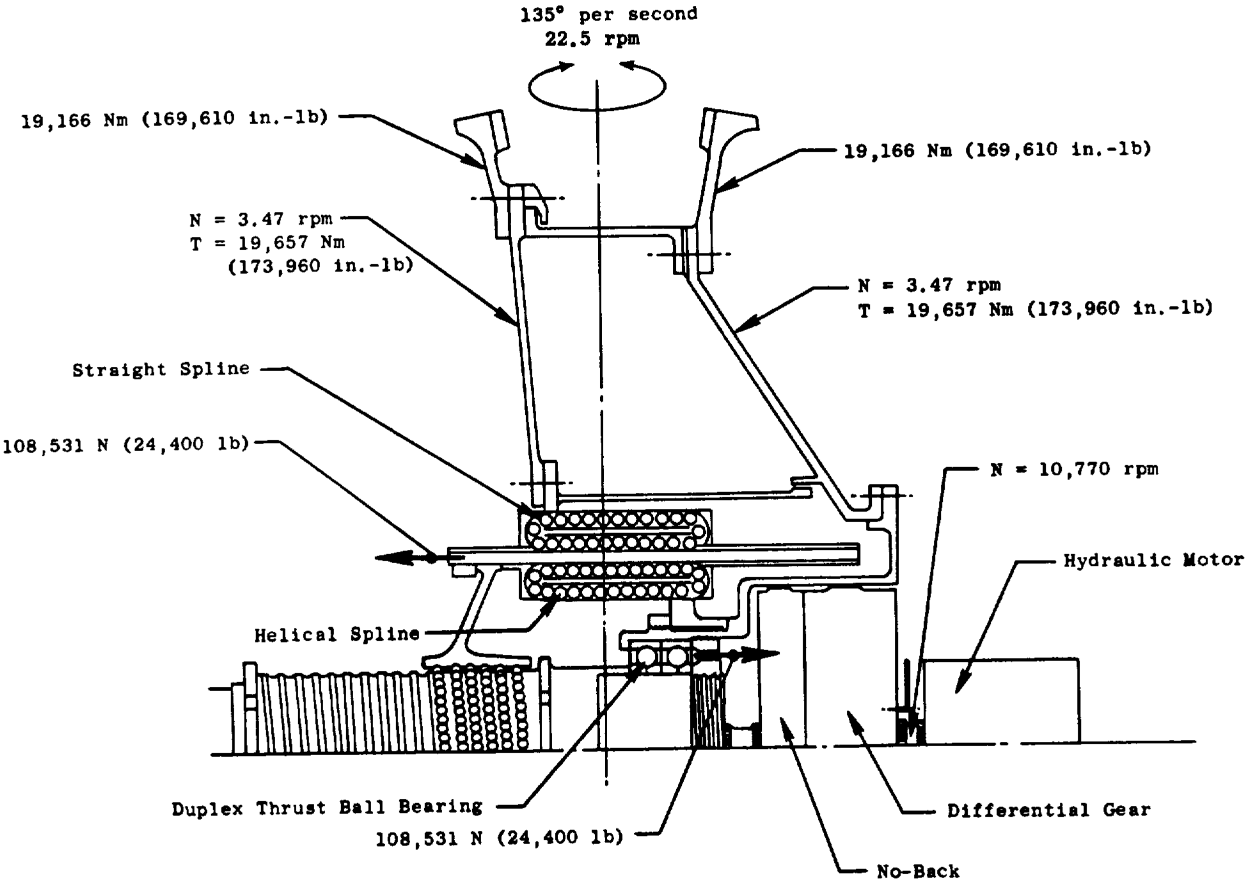

135° per second
22.5 rpm
19,166 Nm (169,610 in.-lb)
19,166 Nm (169,610 in.-lb)
N = 3.47 rpm
T = 19,657 Nm
(173,960 in.-lb)
N = 3.47 rpm
T = 19,657 Nm (173,960 in.-lb)
Straight Spline
108,531 N (24,400 lb)
N = 10,770 rpm
Hydraulic Motor
Helical Spline
Duplex Thrust Ball Bearing
108,531 N (24,400 lb)
Differential Gear
No-Back

- Per Blade Torque = 318.8 Nm (2821 in.-lb)
- Total Torque At Blades = 5738 Nm (50,778 in.-lb)
- System Efficiency = 66.1%
- System Gear Ratio = 478.68
- Torque At Motor = 18.1 Nm (160.5 in.-lb)

Figure 7-22. Actuator Design Speed and Load Characteristics.

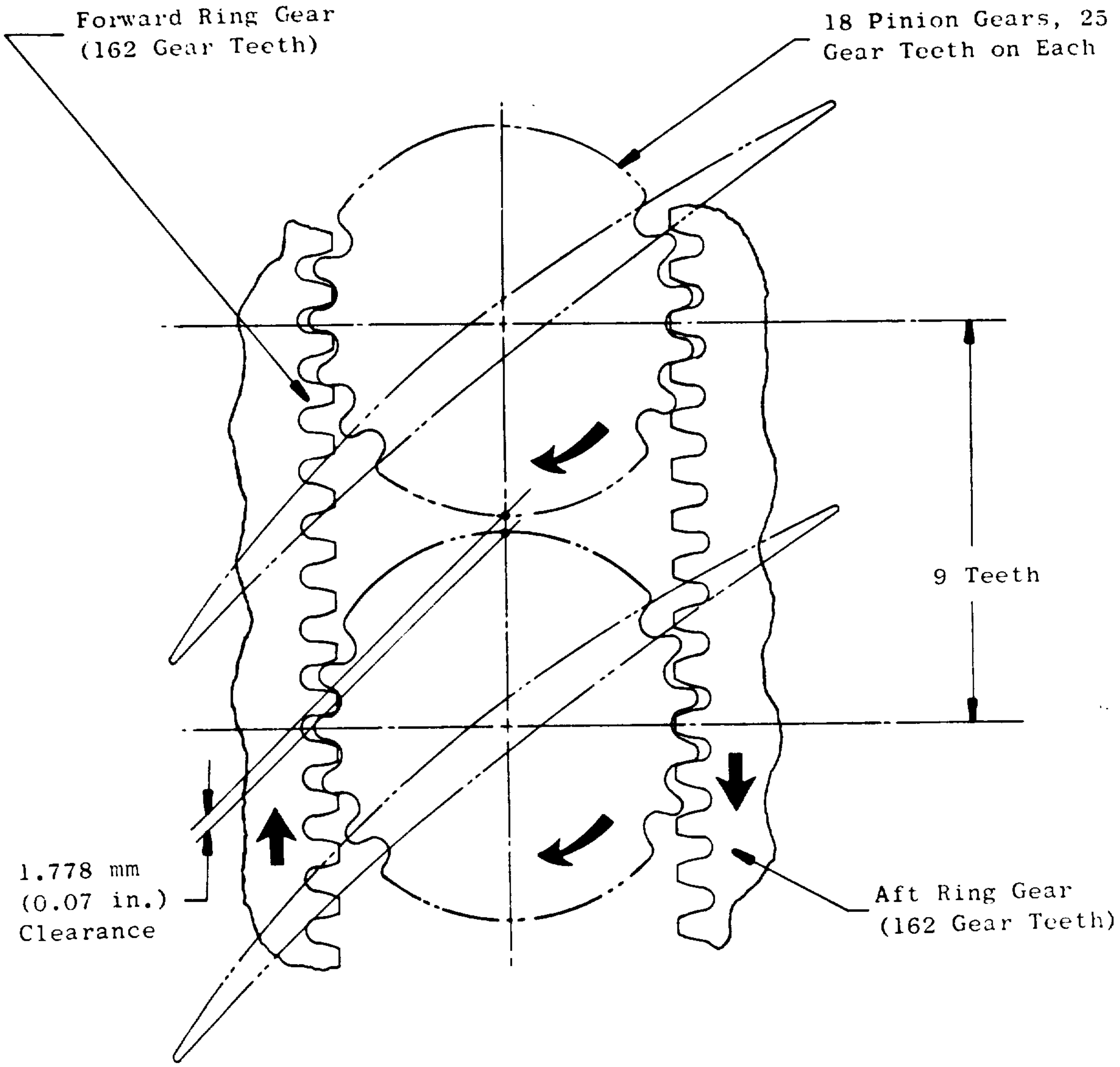
Forward Ring Gear
(162 Gear Teeth)
18 Pinion Gears, 25 Gear Teeth on Each
9 Teeth
1.778 mm
(0.07 in.)
Clearance
Aft Ring Gear
(162 Gear Teeth)

- Gear Ratio = 6.4800
- Diameter Pitch = 21.7025 cm (8.5443 in.)
- Face Width = 1.143 cm (0.450 in.)
- Pressure Angle = 20°
- Tooth Type = Zerol
- Material = AISI 9310

Figure 7-23. Bevel Gear Geometry.

Table 7-XV. Pinion Gear Teeth Design Data.

	Maximum Operating Loads and Stresses (Per Mesh)		Allowable Stresses	
	Condition of Maximum Operating Torque	Bird Strike Condition*	Condition of Maximum Operating Torque	**Bird Strike Condition***
Design **Loads**	15,933 cm-N (1410 in.-lb)	84,750 cm-N (7500 in.-lb)	---	---
Bending Stress	**23,443 N/cm^2 (34,000 psi)**	99,978 N/cm^2 (145,000 psi)	33,786 N/cm^2 (49,000 psi)	**103,425 N/cm^2 (150,000 psi)**
Compressive Stress	**157,206 N/cm^2 (228,000 psi)**	---	172,375 N/cm^2 (250,000 psi)	---

---

*Bird strike condition is assumed to be an equivalent torque on two adjacent blades of 169,500 cm-N (15,000 in.-lb) each.

Pinion deflection and rotation is governed by the amount of fan rotor disk radial growth and in-plane rotational movement, and, thus, the forward and aft ring gears were designed to accommodate these motions over a wide range of fan operating conditions. Also, since the pinion deflection and rotation is of a relative large magnitude and, therefore, by itself yields a great amount of backlash at high fan rotor speeds, the ring gears were designed to be very stiff members to prevent any additional backlash contribution from their relative deflections, which are presented in Figures 7-24 and 7-25. The matching of pinion and ring gear deflections and rotations to produce a proper tooth contact pattern at high gear loadings and minimization of backlash yielded moderately low resultant gear web stresses as compared to the gear material strength. The stresses, as shown in Figures 7-26 and 7-27, are representative of the most severe loading conditions only; for a typical nominal operating condition the stresses are lower and, as a result of the range and magnitude of loading, no fatigue problems are incurred with this gear design. All stress numbers presented are effective stresses; calculated using von Mises-Hencky failure criterion and compared directly with the yield strength to obtain margins of safety.

Axial Support Link

As shown in Figure 7-2, the axial support link ties the forward and aft ring gears together providing a close-coupled load path for reacting the ring gear separating loads. Resultant effective stresses, calculated using von Mises-Hencky failure criterion, are presented in Figure 7-28 for conditions of maximum gear torque and bird strike. The residual torque shown for the load conditions is a resultant of the ring gear thrust bearing efficiency discussed below.

Ring Gear-Sliding Thrust Bearing

Since there is relative motion between the forward ring gear and the aft ring gear, a sliding thrust bearing is provided at the forward ring gear and axial support link interface. Bearing design loads equivalent to gear separating loads for maximum operating torque and bird strike are presented in Figure 7-29. Also shown in the same figure is the available friction test data for Fibriloid. The test data were used for the most severe conditions of low loads and low temperatures to arrive at a coefficient of friction for the bearing of 0.087 which, in conjunction with the maximum design loading, yields a bearing efficiency of 0.975. Also shown in Figure 7-29 is the calculated maximum bearing axial load of approximately 42,585 N (9574 lb) which can be compared on a load/area basis with the wear test data of 0.00381 cm (0.0015 in.) resulting from 100,000 cycles of load/area equivalent to 27,580 N/cm^2 (40,000 psi) and subjected to a temperature of 436 K (325° F). Consideration has also been given to the use of Karon as a substitute or prime material to be used for this bearing application, since component testing has shown that the Karon yields both coefficients of friction and resistance to wear of equivalent magnitude to that of the Fibriloid.

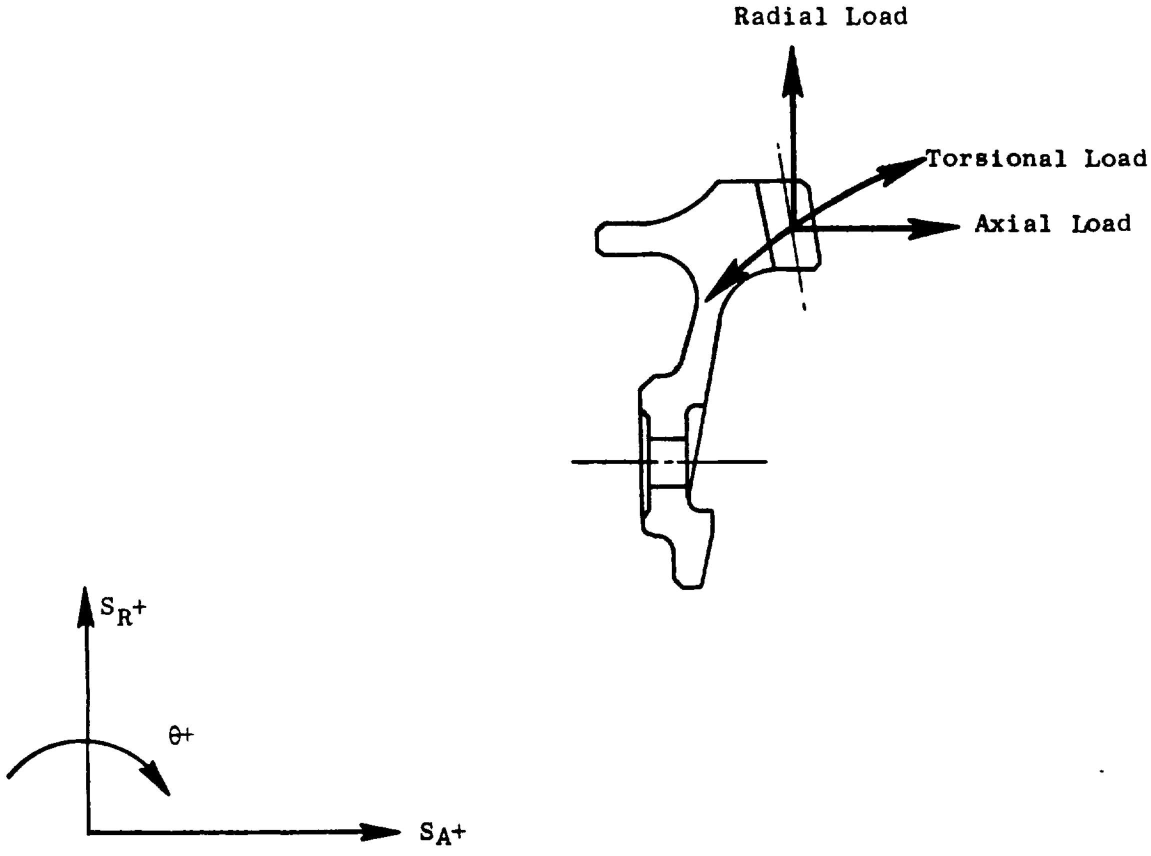
Radial Load
Torsional Load
Axial Load
S_R+
θ+
S_A+

Gear Mesh Deflection

	Centrifugal	Maximum Torque
S_R	0.00518 cm (0.00204 in.)	0.0142 cm (0.00558 in.)
S_A	-0.00340 cm (-0.00134 in.)	-0.0251 cm (-0.0099 in.)
θ	-0.00060 Radians	-0.0067 Radians

Figure 7-24. Forward Ring Gear Deflections.

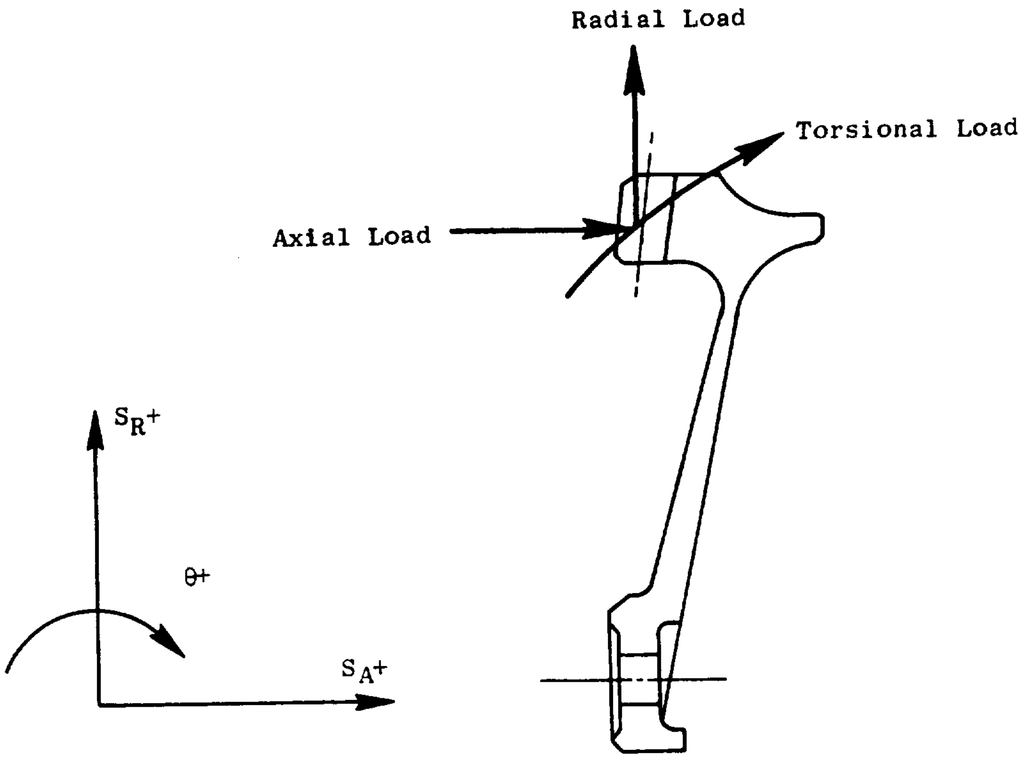
Radial Load
Torsional Load
Axial Load
S_R+
θ+
S_A+

Gear Mesh Deflections

	Centrifugal	Maximum Torque
S_R	0.00376 cm (0.00148 in.)	0.0094 cm (0.0037 in.)
S_A	-0.00551 cm (-0.00217 in.)	0.0290 cm (0.0114 in.)
θ	-0.00057 Radians	0.0074 Radians

Figure 7-25. Aft Ring Gear Deflections.

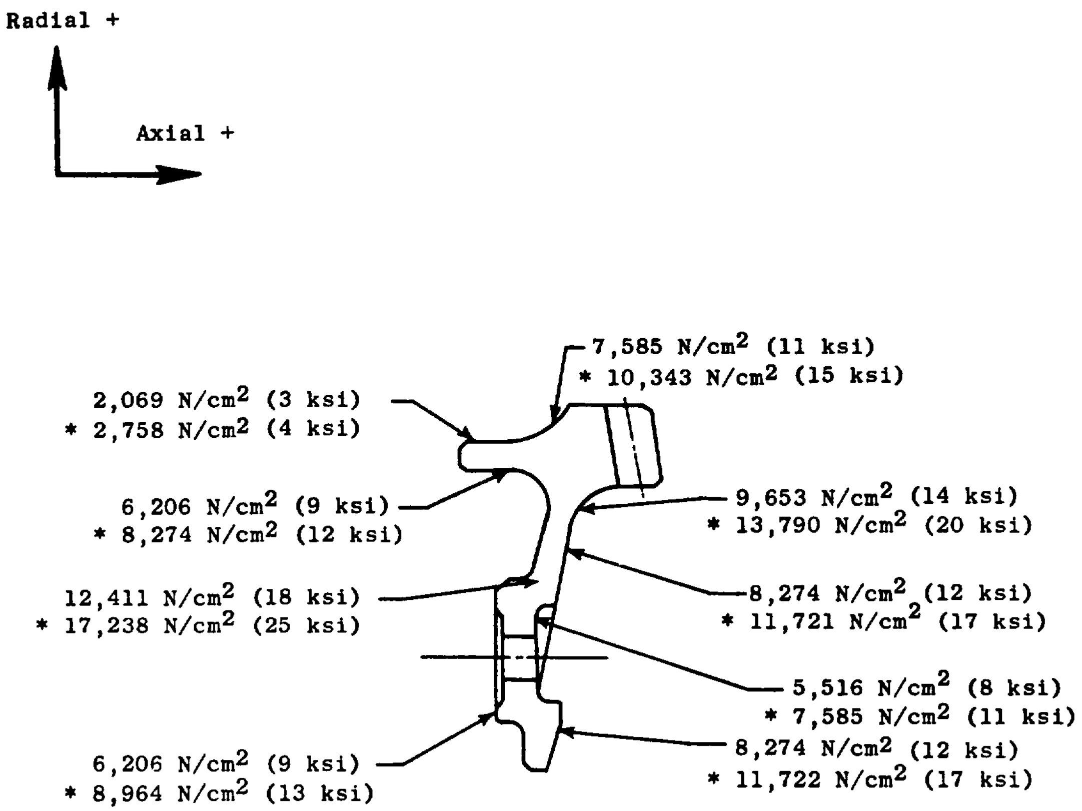
Radial +
Axial +
7,585 N/cm2 (11 ksi)
* 10,343 N/cm2 (15 ksi)
2,069 N/cm2 (3 ksi)
* 2,758 N/cm2 (4 ksi)
6,206 N/cm2 (9 ksi)
* 8,274 N/cm2 (12 ksi)
9,653 N/cm2 (14 ksi)
* 13,790 N/cm2 (20 ksi)
12,411 N/cm2 (18 ksi)
* 17,238 N/cm2 (25 ksi)
8,274 N/cm2 (12 ksi)
* 11,721 N/cm2 (17 ksi)
5,516 N/cm2 (8 ksi)
* 7,585 N/cm2 (11 ksi)
8,274 N/cm2 (12 ksi)
* 11,722 N/cm2 (17 ksi)
6,206 N/cm2 (9 ksi)
* 8,964 N/cm2 (13 ksi)

- Loading

	Maximum Torque	* Bird Strike (FOD Impact Load)
Torque	± 19,166 Nm (± 169,610 in.-lb)	± 27,509 Nm (± 243,440 in.-lb)
Axial	- 29,668 N (- 6,670 lb)	- 42,585 N (- 9,574 lb)
Radial	4,893 N (1,100 lb)	7019 N (1,578 lb)
Speed	3,200 rpm	3,200 rpm

- Material = AISI 9310, 0.2 Yield Strength, S_Y = 95,151 N/cm^2 (138 ksi)

Figure 7-26. Forward Ring Gear Design Loads and Stresses.

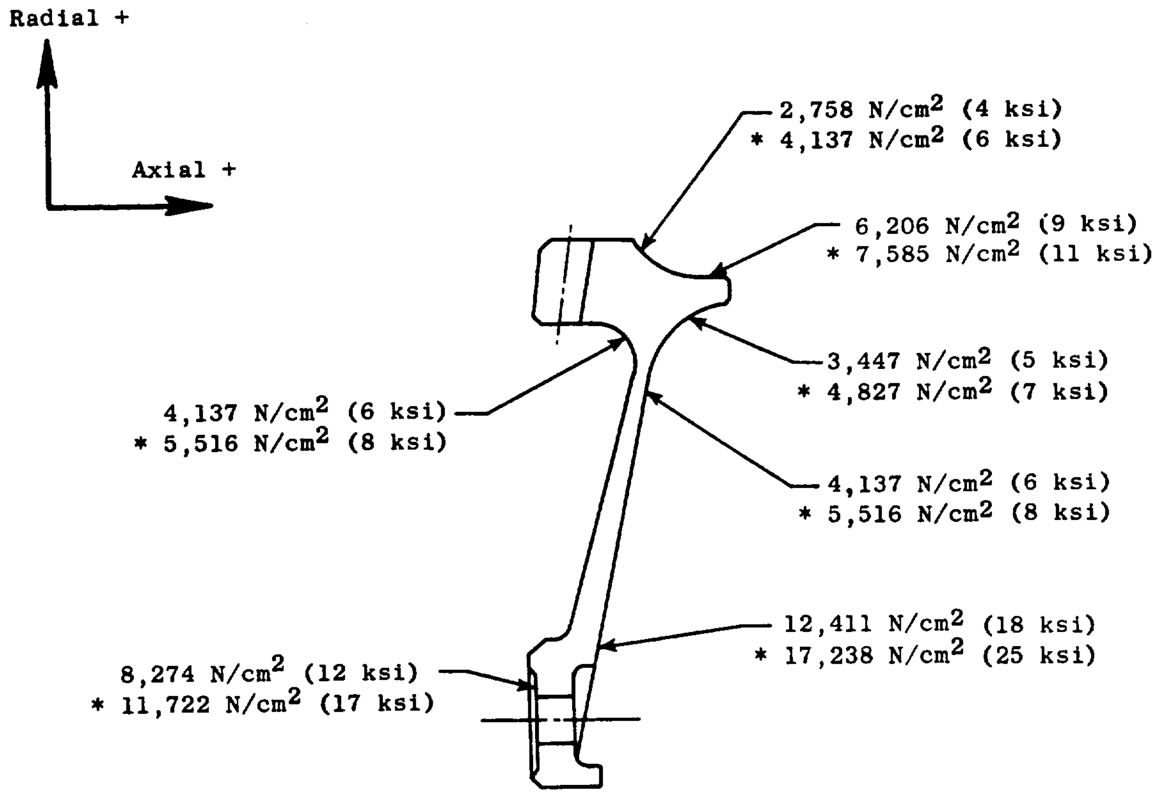
Radial +
Axial +
2,758 N/cm^2 (4 ksi)
* 4,137 N/cm^2 (6 ksi)
6,206 N/cm^2 (9 ksi)
* 7,585 N/cm^2 (11 ksi)
3,447 N/cm^2 (5 ksi)
* 4,827 N/cm^2 (7 ksi)
4,137 N/cm^2 (6 ksi)
* 5,516 N/cm^2 (8 ksi)
4,137 N/cm^2 (6 ksi)
* 5,516 N/cm^2 (8 ksi)
12,411 N/cm^2 (18 ksi)
* 17,238 N/cm^2 (25 ksi)
8,274 N/cm^2 (12 ksi)
* 11,722 N/cm^2 (17 ksi)

- Loading

	Maximum Torque	* Bird Strike (FOD Impact Load)
Torque	± 19,166 Nm (± 169,610 in.-lb)	± 27,509 Nm (± 243, 440 in.-lb)
Axial	29,668 N (6,670 lb)	42,585 N (9,574 lb)
Radial	4,893 N (1,100 lb)	7,019 N (1,578 lb)
Speed	3,200 rpm	3,200 rpm

- Material = AISI 9310, S_Y = 95,151 N/cm^2 (138 ksi)

Figure 7-27. Aft Ring Gear Design Loads and Stresses.

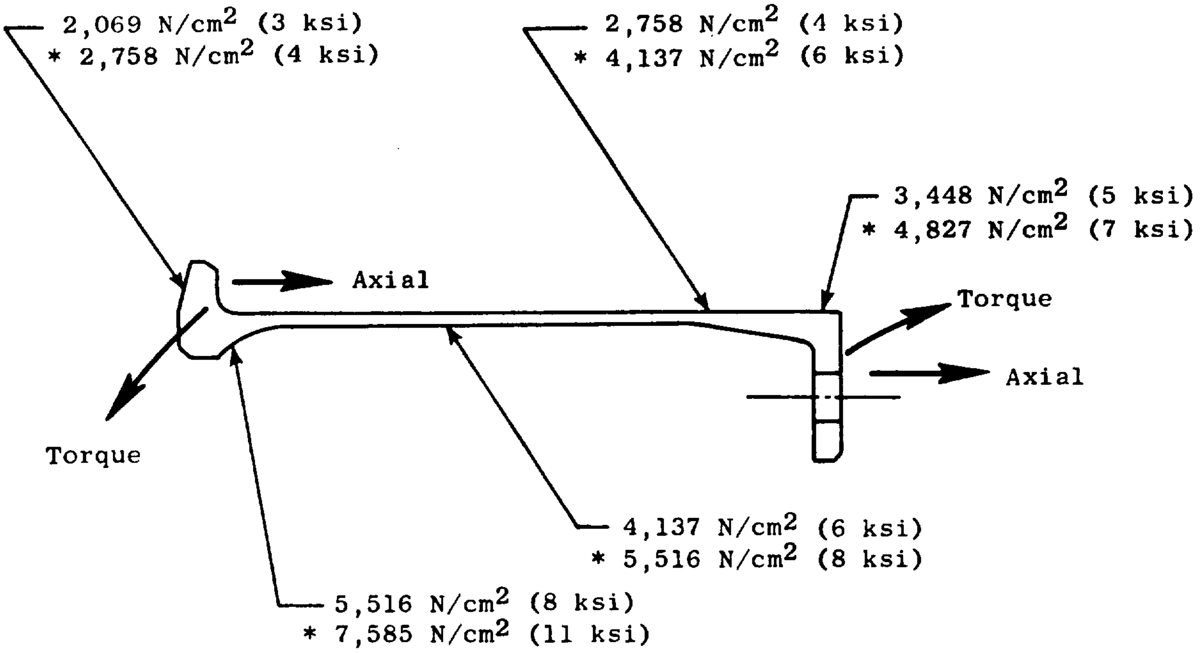
2,069 N/cm^2 (3 ksi)
* 2,758 N/cm^2 (4 ksi)
2,758 N/cm^2 (4 ksi)
* 4,137 N/cm^2 (6 ksi)
3,448 N/cm^2 (5 ksi)
* 4,827 N/cm^2 (7 ksi)
Axial
Torque
Torque
Axial
4,137 N/cm^2 (6 ksi)
* 5,516 N/cm^2 (8 ksi)
5,516 N/cm^2 (8 ksi)
* 7,585 N/cm^2 (11 ksi)

• Loading	Maximum Torque	* Bird Strike (FOD Impact Load)
Torque	491 Nm (4,349 in.-lb)	705 Nm (6,242 in.-lb)
Axial	29,668 N (6,670 lb)	42,585 N (9,574 lb)
Speed	3200 rpm	3200 rpm

- Material = Ti 6-4, 0.02 Yield Strength, S_Y= 66,881 N/cm^2 (97 ksi) at 328 K (130° F)

Note: Assumed Torque From Loss in Bearing (2.5%)

Figure 7-28. Axial Support Link Design Loads and Stresses.

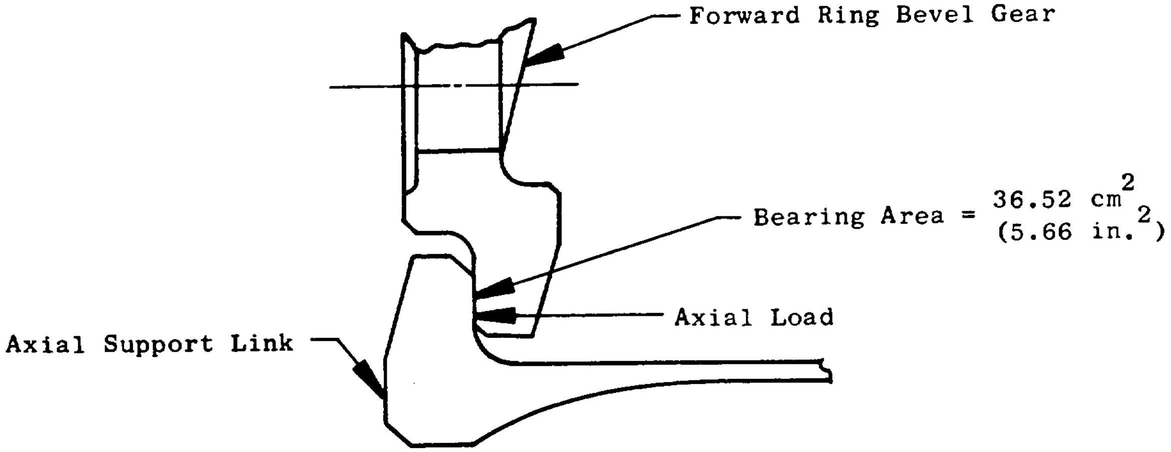
Forward Ring Bevel Gear
Bearing Area = 36.52 cm^2 (5.66 in.^{2})
Axial Load
Axial Support Link

- Loading:

	Maximum Torque	Bird Strike (FOD Impact)
Axial Load	29,668 N (6670 lb)	42,585 N (9574 lb)
Load/Area	829 N/cm^2 (1202 psi)	1189 N/cm^2 (1725 psi)

- Material = Fibriloid or Karon
- Test Data:

  Load/Area = 27,580 N/cm^2 (40,000 psi) at 436 K (325° F)
  Wear = 0.0381 mm (0.0015 inch) for 100,000 Cycles

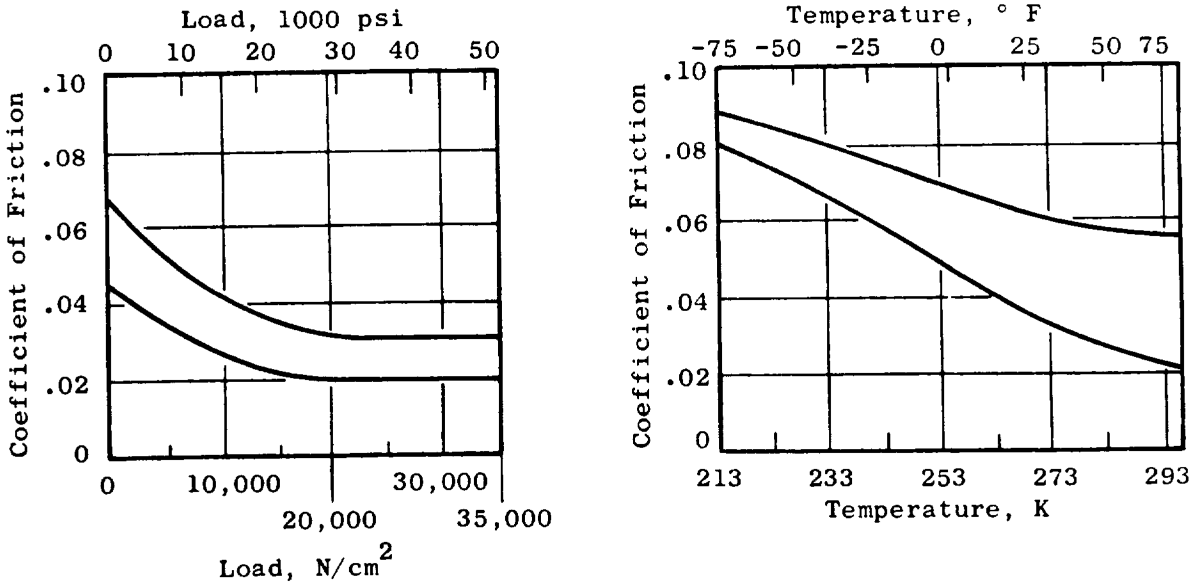
FIBRILOID — Friction Versus Load FIBRILOID — Friction Versus Temperature

Figure 7-29. Ring Gear Sliding Thrust Bearing Design Loads.

Ring Gear Drive Cones

Torque is transmitted to the ring gears from the ball spline through forward and aft drive cones attached to the outer and inner diameter ball spline members, respectively. The majority of load on these drive cones is the torque developed at the ring gears and the torque required to overcome friction in the ring gear sliding thrust bearing. The loads and resultant stresses (von Mises-Hencky effective stresses) for the conditions of maximum operating torque and bird strike (FOD impact loading) are presented in Figures 7-30 and 7-31. As shown, overall stress levels are low with the exception of the area around the access holes, these holes being required for modular removal of actuation and fan rotor disk. In these regions, high stress levels are encountered due to the combination of large meridional, hoop and torsional stress concentration factors. It is to be noted that the stresses are compared to 0.02% yield strength values and not 0.2%; the higher yield strength (0.2%) would produce 15% higher margins of safety.

Ball Spline

The ball spline included in the UTW actuation system is a scaled version of a proven design used in two previous General Electric variable-pitch fan blade test vehicles. As shown in Figure 7-32, the ball spline is basically a three piece configuration, consisting of the outer and inner diameter members whose motion is tangentially opposite, and the fore and aft translating midmember. There are 12 recirculating linear ball tracks between the outer and middle member and 12 recirculating helical tracks between the middle and inner members. Each of the circuits contains 144 active balls, 0.635 cm (0.25 in.) in diameter.

Maximum normal operating design torque of the ball spline is 19,659 m-N (174,000 in.-lb). Maximum steady state capacity is 23,391 m-N (207,000 in.-lb), providing a 19% design margin. Under bird strike (FOD impact) conditions, the ball spline is subjected to a restraining torque of 27,459 m-N (243,400 in.-lb), providing a 45% design margin.

To meet 36,000 hours of engine life, a total linear travel of 2.581×10^6 cm (1.016×10^6 in.) based on the mission duty cycle shown in Figure 7-3 is required. This includes an allowance of 180° of blade angle travel for modulation during approach for each flight cycle. The calculated design life in total linear travel based on the cubic mean torque load and the torque capacity of the ball spline is 1.270×10^6 cm (0.50×10^6 in.). The capacity of the ball spline is determined from design criteria developed by Saginaw Steering Gear, Saginaw, Michigan. This indicates that the balls will only have to be changed once during the life time of the engine. This exceeds the 9000 hours replaceable parts requirement by a factor of two. If the blades are fixed in position during approach, the life of the ball spline exceeds the total 36,000 hour engine life requirement.

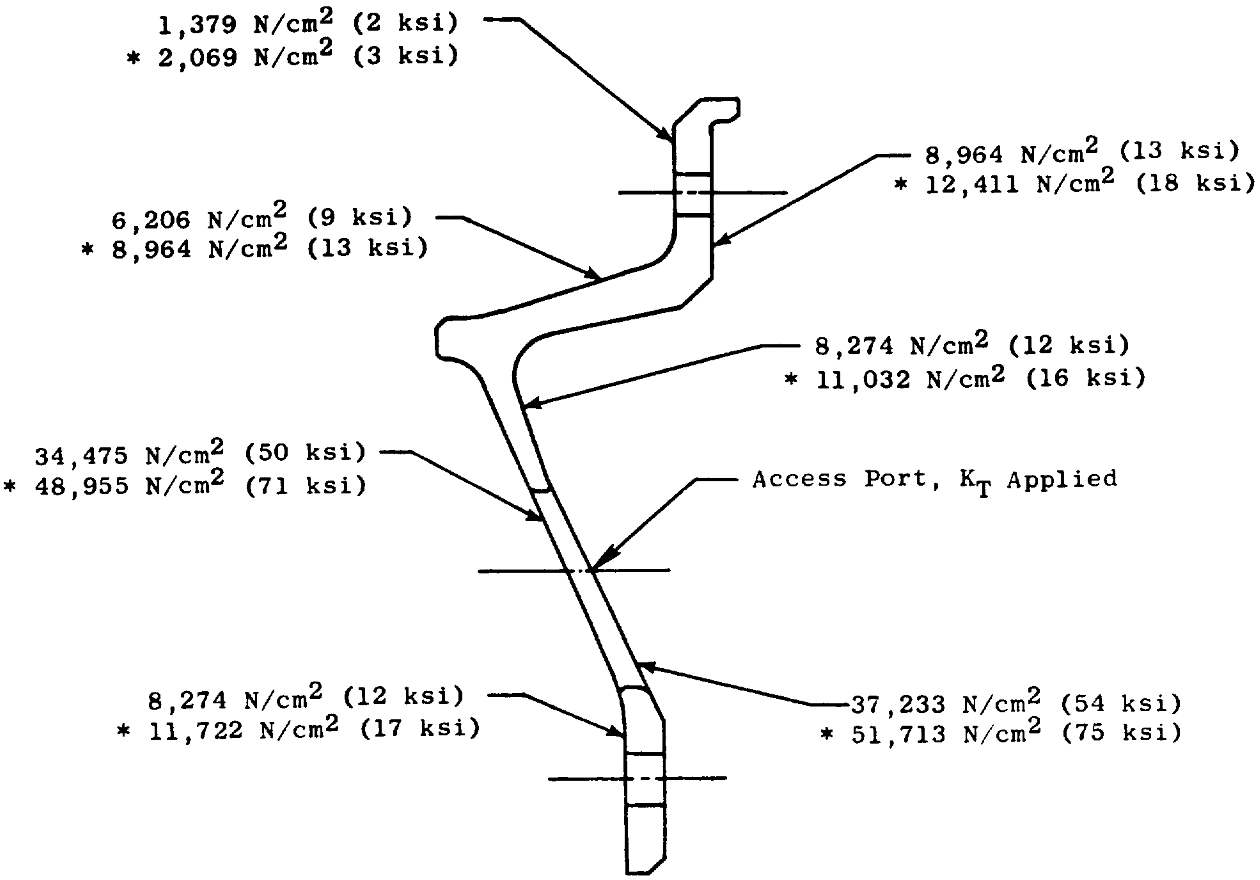
1,379 N/cm^2 (2 ksi)
* 2,069 N/cm^2 (3 ksi)
8,964 N/cm^2 (13 ksi)
* 12,411 N/cm^2 (18 ksi)
6,206 N/cm^2 (9 ksi)
* 8,964 N/cm^2 (13 ksi)
8,274 N/cm^2 (12 ksi)
* 11,032 N/cm^2 (16 ksi)
34,475 N/cm^2 (50 ksi)
* 48,955 N/cm^2 (71 ksi)
Access Port, K_T Applied
8,274 N/cm^2 (12 ksi)
* 11,722 N/cm^2 (17 ksi)
37,233 N/cm^2 (54 ksi)
* 51,713 N/cm^2 (75 ksi)

- Loading

	Maximum Torque	* Bird Strike (FOD Impact Loads)
Torque	19,657 Nm (173,960 in.-lb)	27,509 Nm (243,440 in.-lb)
Speed	3,200 rpm	3,200 rpm

- Material = Ti 6-4, 0.02% Yield Strength, S_Y = 66,881 N/cm^2 (97 ksi) at 328 K (130° F)

Note: Assumed Bird Strike Torque Has No Gear or Bearing Losses.

- $K_{T_{Meridional}} = 3.0$
- $K_{T_{Hoop}} = 3.0$
- $K_{T_{Shear}} = 4.86$

Figure 7-30. Forward Drive Cone Design Loads and Stresses.

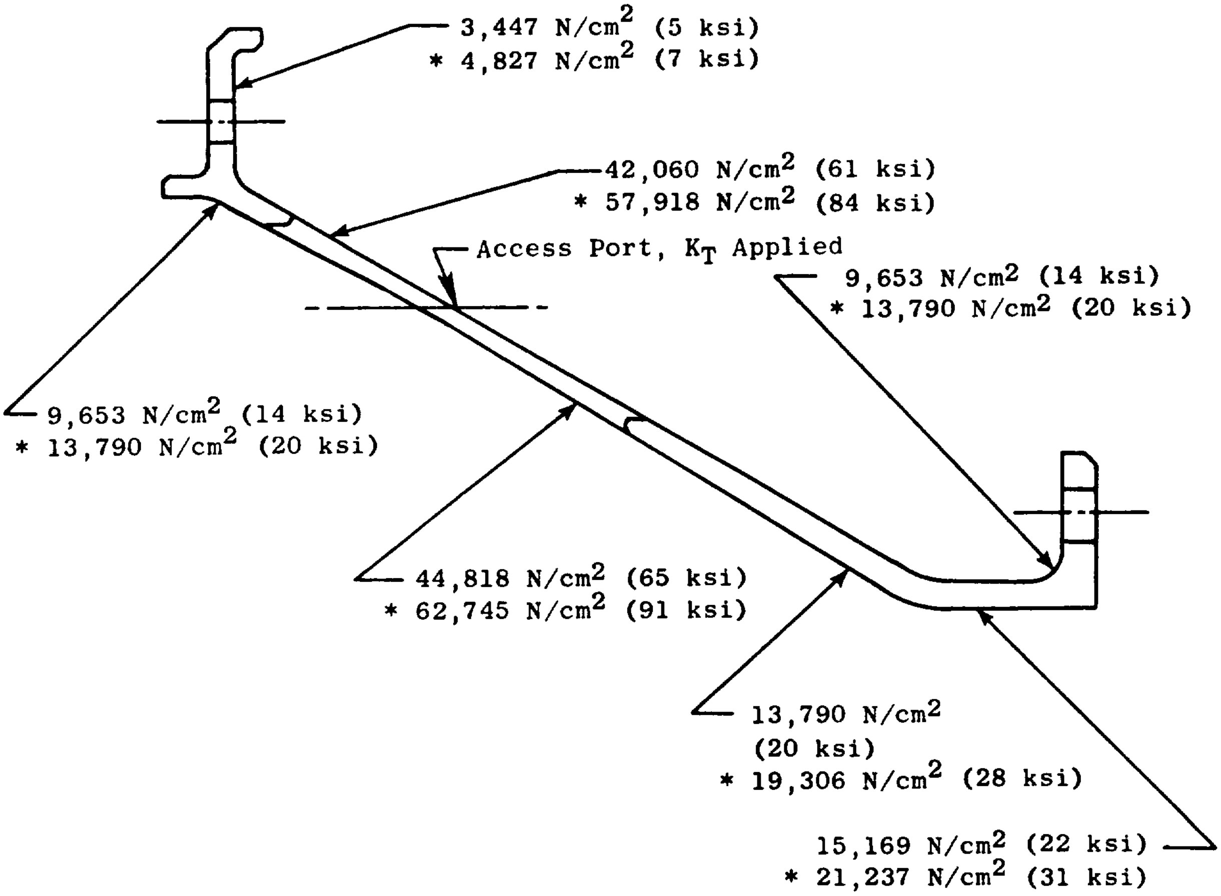
3,447 N/cm^2 (5 ksi)
* 4,827 N/cm^2 (7 ksi)
42,060 N/cm^2 (61 ksi)
* 57,918 N/cm^2 (84 ksi)
Access Port, K_T Applied
9,653 N/cm^2 (14 ksi)
* 13,790 N/cm^2 (20 ksi)
9,653 N/cm^2 (14 ksi)
* 13,790 N/cm^2 (20 ksi)
44,818 N/cm^2 (65 ksi)
* 62,745 N/cm^2 (91 ksi)
13,790 N/cm^2 (20 ksi)
* 19,306 N/cm^2 (28 ksi)
15,169 N/cm^2 (22 ksi)
* 21,237 N/cm^2 (31 ksi)

- Loading	Maximum Torque	* Bird Strike (FOD Impact Load)
Torque	19,657 Nm (173,960 in.-lb)	27,509 Nm (243,440 in.-lb)
Speed	3,200 rpm	3,200 rpm

- Material = Ti 6-4, 0.02% Yield Strength, S_Y = 66,881 N/cm^2 (97 ksi) at 328 K (130° F)

Note: Assumed Bird Strike Torque Has No Gear or Bearing Losses.

- $K_{T_{Meridional}} = 3.0$
- $K_{T_{Hoop}} = 3.0$
- $K_{T_{Shear}} = 4.86$

Figure 7-31. Aft Drive Cone Design Loads and Stresses.

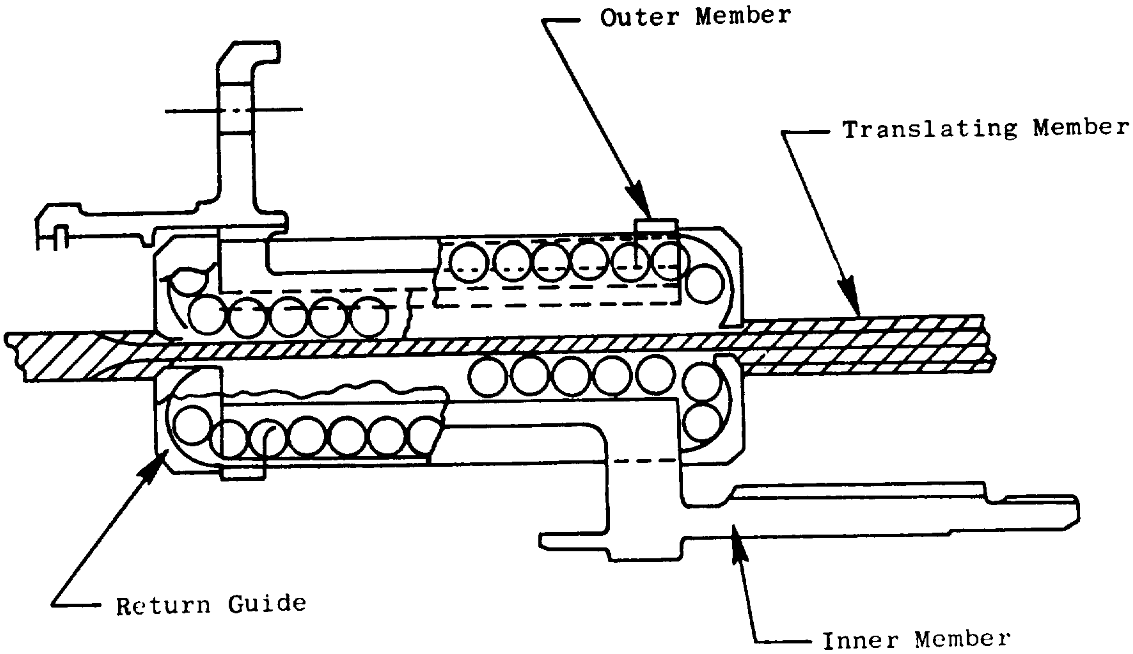
Outer Member
Translating Member
Return Guide
Inner Member

Figure 7-32. Ball Spline.

Design loads and corresponding stresses for the outer, mid, and inner members of the ball spline are presented in Figures 7-33, 7-34, and 7-35, respectively.

Ball Screw Assembly

The ball screw, shown in Figures 7-2 and 7-36, is splined to the output shaft of the no-back. Rotation of the ball screw translates the ball nut along the axis of the engine. The ball nut, in turn, provides axial translation of the ball spline middle member.

The ball screw has a 5.08 cm (2.00 in.) pitch diameter with a 0.47 cm (0.185 in.) thread lead, and contains 12 ball circuits having 1.5 turns per circuit.

Previous General Electric variable-pitch fan test vehicles used hydraulic pistons to provide the axial translation required for the ball spline midmember. Application of a ball screw in the UTW system design permitted a reduction in the overall diameter of the ball spline.

To meet the 9000 hour maintainability requirement for bearings and nonreusable parts, based on the mission duty cycle of Figure 7-3, a total linear travel of 0.645×10^6 cm (0.254×10^6 in.) is required. This includes an allowance of 180° of blade travel for modulation during approach for each flight cycle. The calculated design life in total linear travel based on the cubic mean axial load and the axial load capacity of the ball screw is 0.685×10^6 cm (0.270×10^6 in.) which meets the design requirement. The axial load capacity is based on design criteria developed by Saginaw Steering Gear, Saginaw Michigan. If the blades are fixed in position during approach, the life of the ball screw exceeds the total 36,000 hour engine life requirement. Under bird strike (FOD impact) conditions, the ball screw is subjected to an estimated axial load of 129,090 N (29,022 lb). The static axial load capacity of the ball screw is 429,517 N (96,564 lb) which is 3.33 times calculated requirement.

Design loads and resulting stresses for the ball screw and ball nut are presented in Figures 7-37 and 7-38, respectively.

Ball Screw Thrust Bearing

The ball screw duplex thrust ball bearings, shown in Figure 7-2, react the ball nut and ball spline axial load. Design data for the bearing is presented in Figure 7-39. Bearing races are (assembled and) flush ground (by the bearing vendor) to maximize load sharing capability. Bidirectional load sharing is also improved by close matching of the contact angles. Although additional bearing race shoulder height was required to accommodate the high thrust loads, there is still sufficient radial space for an adequate cage cross section.

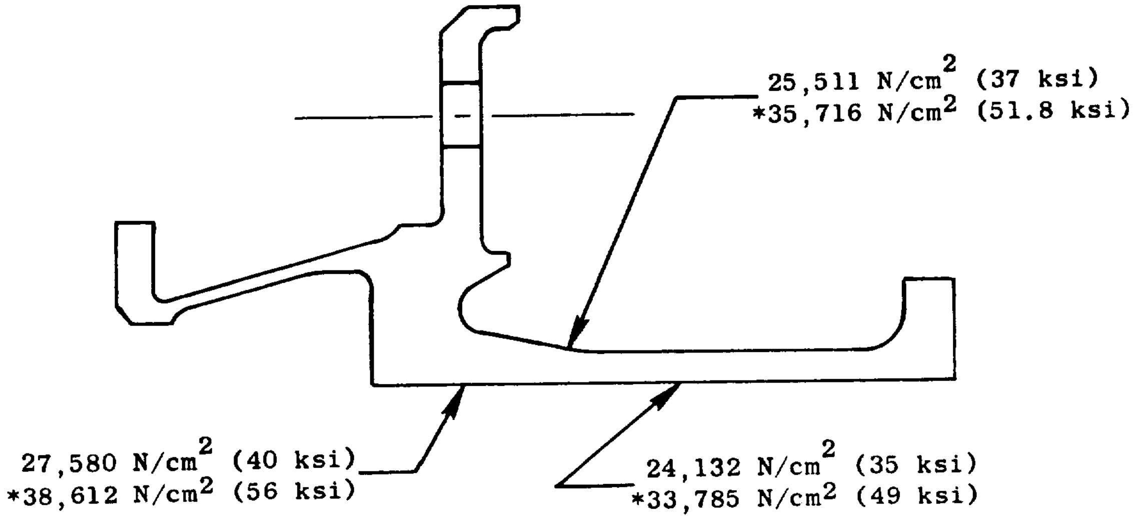
25,511 N/cm^2 (37 ksi)
*35,716 N/cm^2 (51.8 ksi)
27,580 N/cm^2 (40 ksi)
*38,612 N/cm^2 (56 ksi)
24,132 N/cm^2 (35 ksi)
*33,785 N/cm^2 (49 ksi)

- Loading

  Max. Torque 19,657 Nm (173,960 in.-lb)

  *Bird Strike 27,509 Nm (243,440 in.-lb)

  Speed 3,200 rpm

- Material

  AISI 9310; $S_Y = 95,840$ N/cm^2 (139 ksi)

Figure 7-33. Ball Spline Outer Diameter Member Design Loads and Stresses.

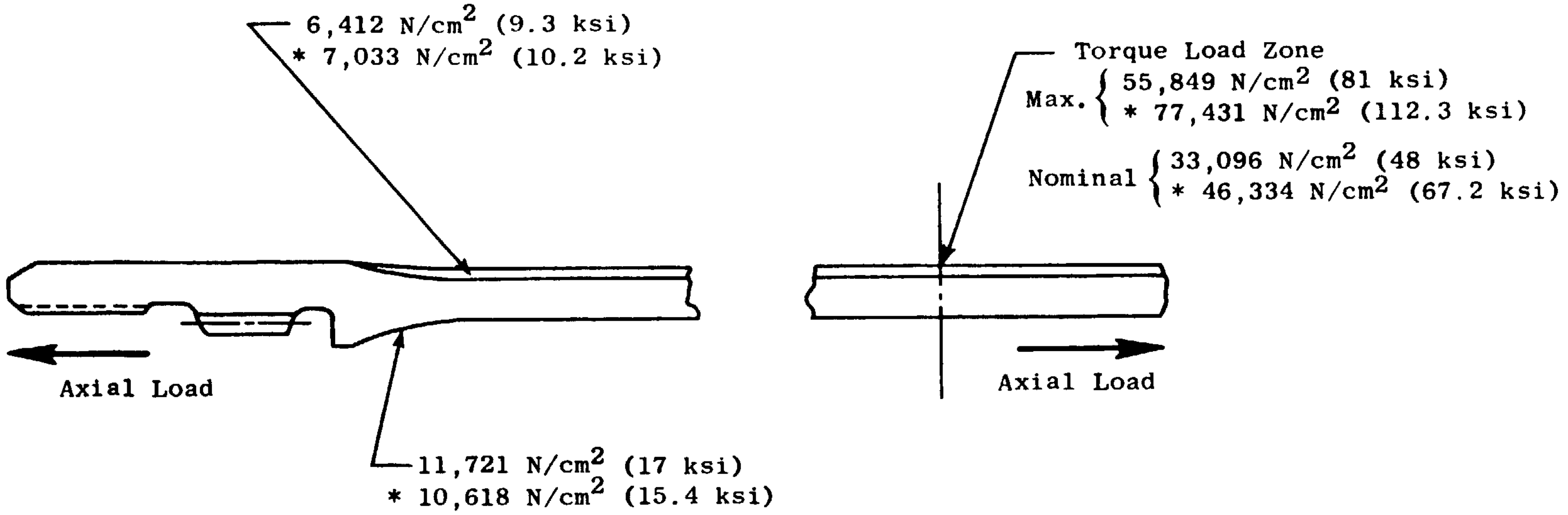

6,412 N/cm² (9.3 ksi)
* 7,033 N/cm² (10.2 ksi)
Torque Load Zone
Max. { 55,849 N/cm² (81 ksi)
* 77,431 N/cm² (112.3 ksi)
Nominal { 33,096 N/cm² (48 ksi)
* 46,334 N/cm² (67.2 ksi)
Axial Load
Axial Load
11,721 N/cm² (17 ksi)
* 10,618 N/cm² (15.4 ksi)

- **Loading**

  Maximum Torque 19,657 Nm (173,960 in.-lb) Between Outer Diameter and Inner Diameter Members Only

  Maximum Axial Load 108,531 N (24,400 lb)

  *** Bird Strike Axial Load 129,090 N (29,022 lb)**

  Speed = 3,200 rpm

- **Material = AISI 9310, S_Y = 95,840 N/cm^2 (139 ksi)**

Figure 7-34. Ball Spline Midmember Design Loads and Stresses.

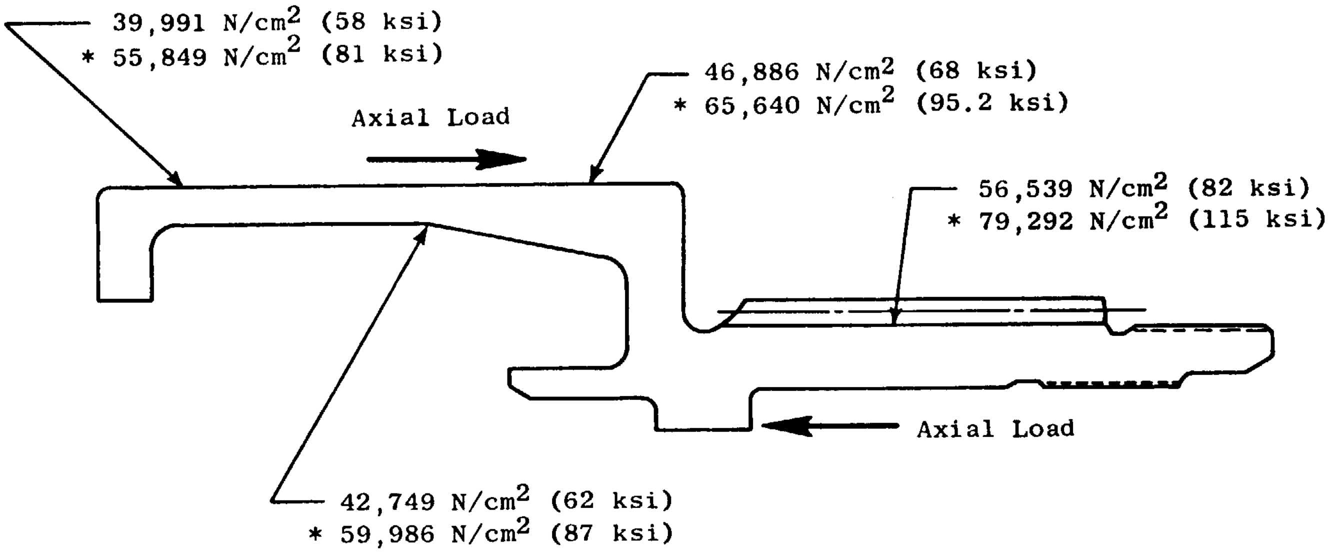
39,991 N/cm^2 (58 ksi)
* 55,849 N/cm^2 (81 ksi)
Axial Load
46,886 N/cm^2 (68 ksi)
* 65,640 N/cm^2 (95.2 ksi)
56,539 N/cm^2 (82 ksi)
* 79,292 N/cm^2 (115 ksi)
Axial Load
42,749 N/cm^2 (62 ksi)
* 59,986 N/cm^2 (87 ksi)

• Loading	Maximum Torque	* Bird Strike (FOD Impact Load)
Torque	19,657 Nm (173,960 in.-lb)	27,509 Nm (243,440 in.-lb)
Axial	108,531 N (24,400 lb)	129,090 N (29,022 lb)
Speed	3,200 rpm	3,200 rpm

- Material = AISI 9310, S_Y = 95,840 N/cm^2 (139 ksi)

Figure 7-35. Ball Spline Inner Diameter Member Design Loads and Stresses.

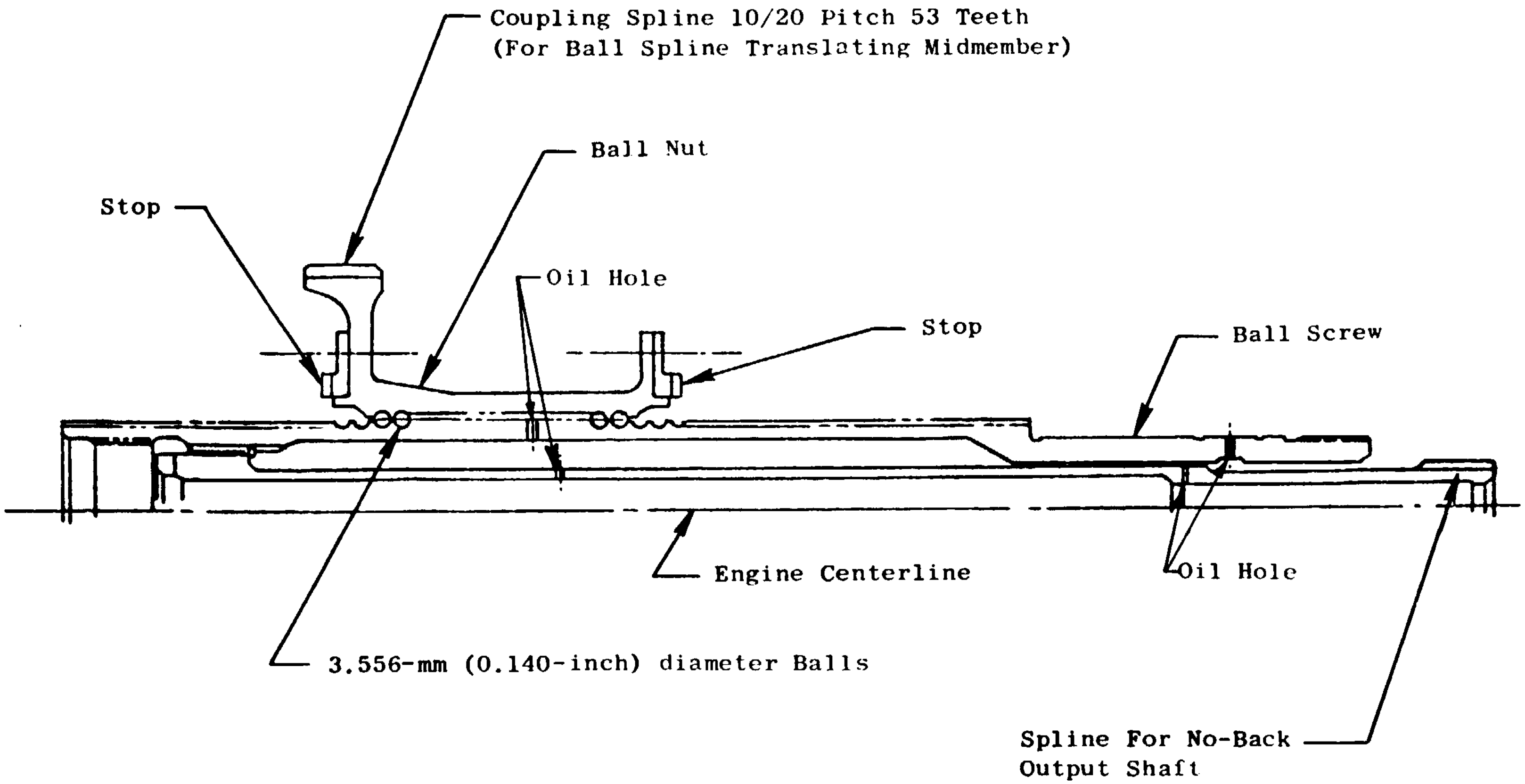
Coupling Spline 10/20 Pitch 53 Teeth
(For Ball Spline Translating Midmember)
Ball Nut
Stop
Oil Hole
Stop
Ball Screw
Engine Centerline
Oil Hole
3.556-mm (0.140-inch) diameter Balls
Spline For No-Back
Output Shaft

Figure 7-36. Ball Screw Assembly.

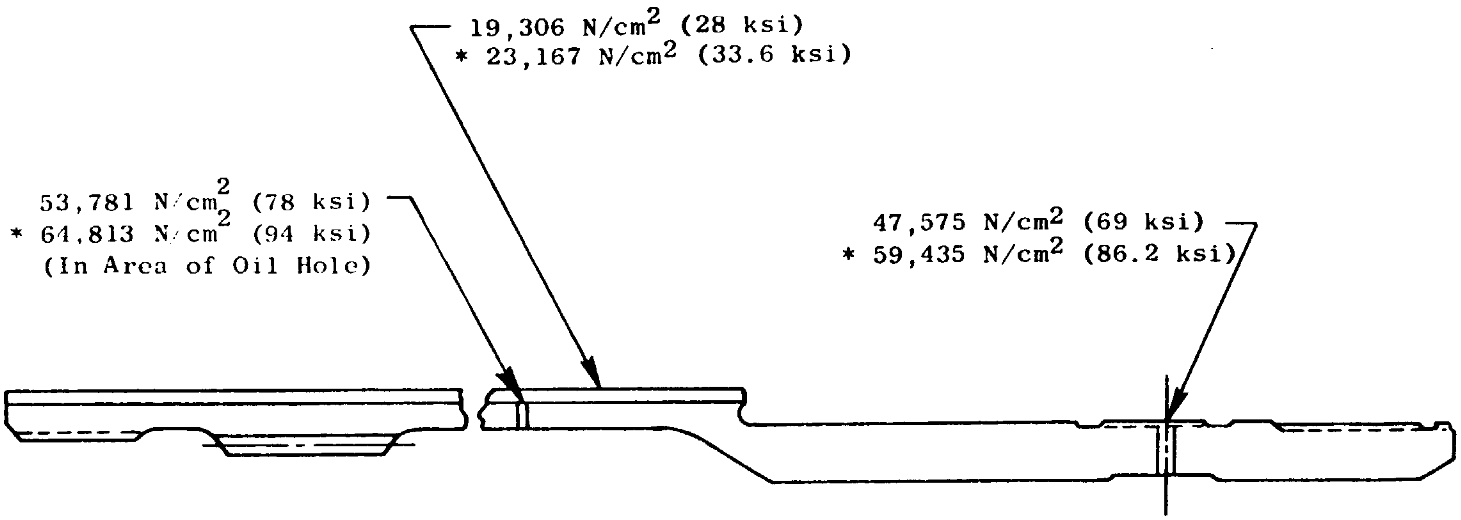
19,306 N/cm2 (28 ksi)
* 23,167 N/cm2 (33.6 ksi)
53,781 N/cm2 (78 ksi)
* 64,813 N/cm2 (94 ksi)
(In Area of Oil Hole)
47,575 N/cm2 (69 ksi)
* 59,435 N/cm2 (86.2 ksi)

• Loading:	Maximum Torque	* Bird Strike (FOD Impact Load)
Torque	88.2 Nm (780.9 in.-lb)	96.6 Nm (854.5 in.-lb)
Axial Load	108,531 N (24,400 lb)	129,090 N (29,022 lb)
Speed	3,200 rpm	3,200 rpm

- Material = AISI 9310, S_Y = 95,840 N/cm^2 (139 ksi)

Figure 7-37. Ball Screw.

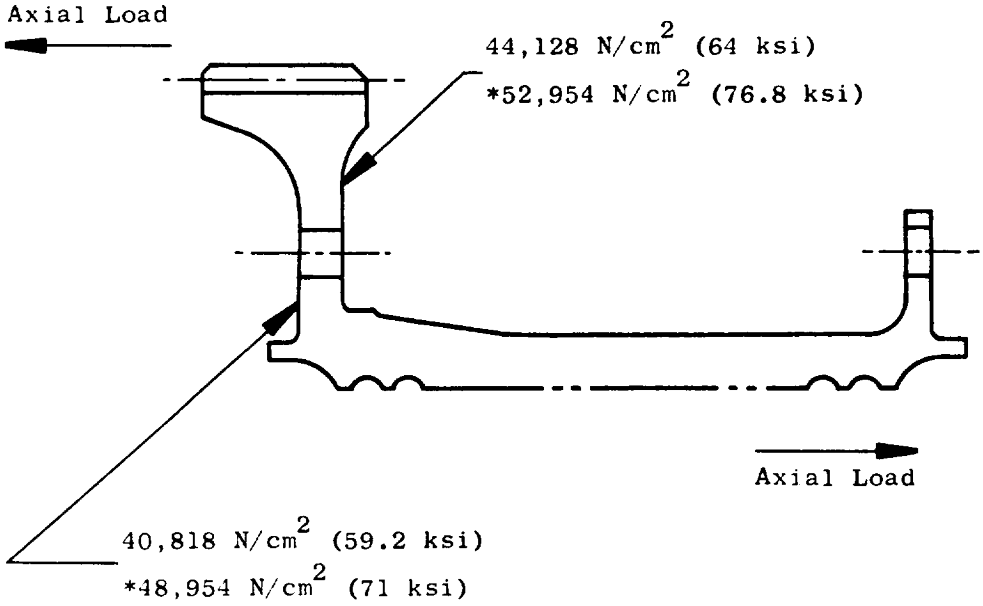
Axial Load
44,128 N/cm^2 (64 ksi)
*52,954 N/cm^2 (76.8 ksi)
Axial Load
40,818 N/cm^2 (59.2 ksi)
*48,954 N/cm^2 (71 ksi)

- Loading

  Maximum Axial Load 108,531 N (24,400 lb)
  *Bird Strike Axial Load 129,090 N (29,022 lb)
  Speed 3200 rpm

- Material

  AISI 9310; S_Y = 95,840 N/cm^2 (139 ksi)

Figure 7-38. Ball Nut.

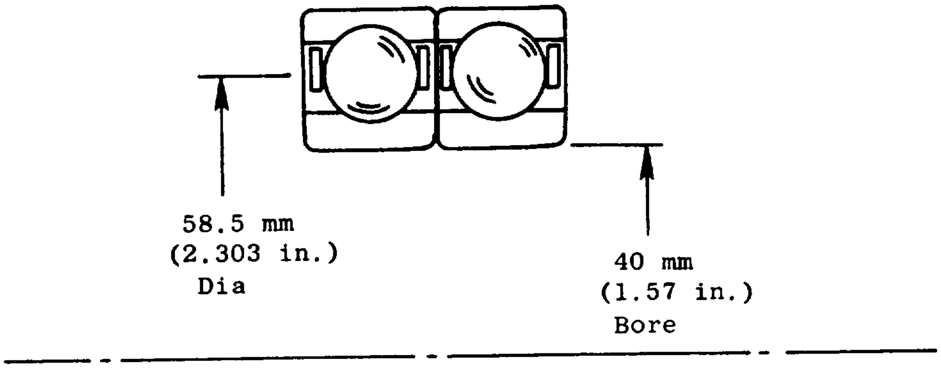
58.5 mm
(2.303 in.)
Dia
40 mm
(1.57 in.)
Bore

- 12 X 12.7-mm (0.5-in.)-Diameter Balls per Row
- Cubic Mean Thrust Load = 55,026 N (12,371 lb)
- Calculated B_{10} Life/Required B_{10} Life*
  78 Hours/46 Hours

* Required Life Shown is for 48,000 Missions with Modulation on Approach.

Figure 7-39. Ball Screw Thrust Ball Bearing.

As shown in Figure 7-39, the calculated bearing B_{10} life is considerably in excess of the required B_{10} life to satisfy the full 48,000 engine mission cycles.

Dynamic Stops

As shown in Figure 7-2, axial dynamic stops are included at each end of the ball screw travel. These stops are designed to absorb the full dynamic load transmitted by the ball nut in the event of a system failure.

The forward axial dynamic stop configuration is shown in Figure 7-40. The stops consist of Belleville springs, keyed disks, and torsional jaws. Similar jaws, located on each end of the ball nut, engage the stops and drive one half of the disks with respect to their mating faces. This design dissipates energy for one full turn of the ball screw before hard axial stops engage and prevent further actuation. Upon disengagement of the jaws, return springs reposition the stops in their original axial location.

High Speed Power System

The high speed power system consists of the hydraulic motor, an LVDT feedback system coupled to the motor, a differential gear, and a no-back. The motor, differential gear and no-back are shown in the actuation system cross section (Figure 7-2). This high speed power system has been designed and developed by Curtiss-Wright (Caldwell N.J.) under subcontract to the General Electric Company.

Hydraulic Motor - The hydraulic motor selected for the GE actuation system is an existing flight weight design currently used on the Lockheed L1011 aircraft for wing flap actuation. The hydraulic motor configuration and basic design characteristics are presented in Figure 7-41. Utilizing the maximum per blade twisting torque during actuation of 31,870 cm-N (2821 in.-lb) and working through the established gear ratios utilizing an estimated "worst" system efficiency, the hydraulic motor must provide a maximum input torque of 18.13 m-N (160.5 in.-lb). The hydraulic motor torque versus speed characteristics are shown in Figure 7-42.

LVDT Feedback Mechanism - The feedback mechanism, shown in Figure 7-43 uses two linear variable differential transformers (LVDT's) to sense fan blade angle. Rotation of the hydraulic motor output shaft is geared down and mechanically linked to an internally threaded shaft through a spur and worm gear combination. Rotation of the worm gear and mating sleeve shaft causes a mating externally threaded member to translate back and forth along its axis. Attached to each end of this translating member is the magnetic core of an LVDT.

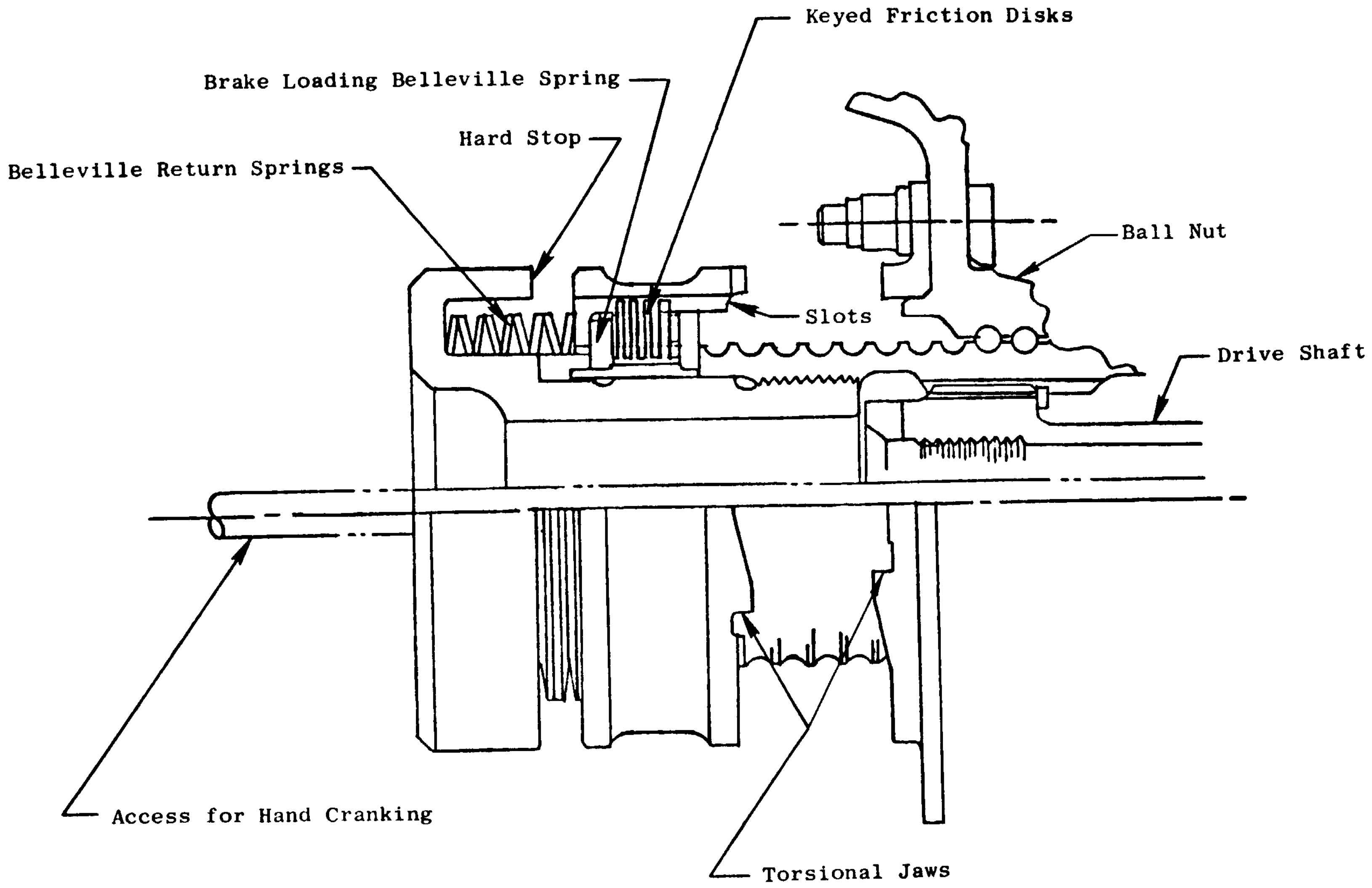
Keyed Friction Disks
Brake Loading Belleville Spring
Hard Stop
Belleville Return Springs
Ball Nut
Slots
Drive Shaft
Access for Hand Cranking
Torsional Jaws

Figure 7-40. Axial Dynamic Stop (Forward).

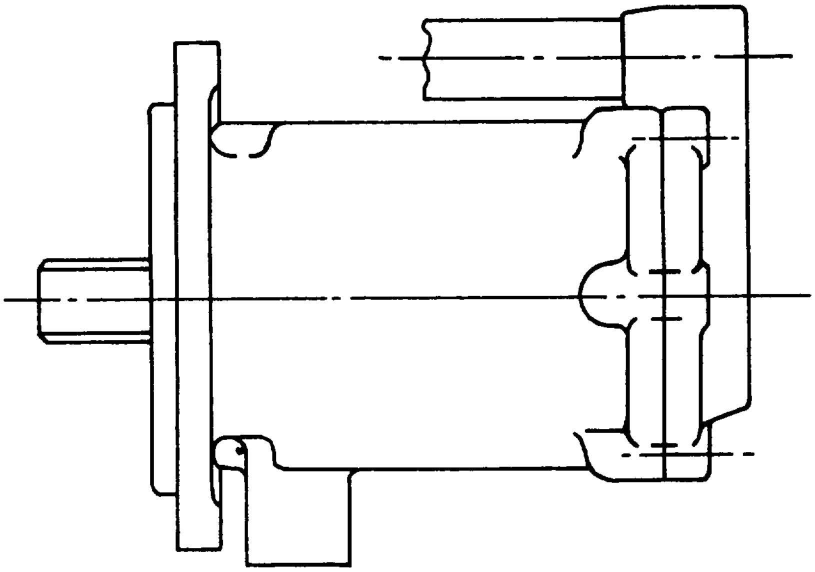

- Vickers Model MS3-044-3 Fixed-Displacement 7.201 cm^3/rev (0.44 $in.^3$/rev) Multiple Piston (7) Hydraulic Motor
- Stall Torque = 20.34 Nm (180 in.-lb) at 2,379 N/cm^2 (3,450 psi)
- Torque = 19.89 Nm (176 in.-lb) at 10,000 rpm at 2,068 N/cm^2 (3,000 psi)
- Flow = 1,298 cm^3/sec (20.6 gpm) at 10,000 rpm

Figure 7-41. Hydraulic Motor.

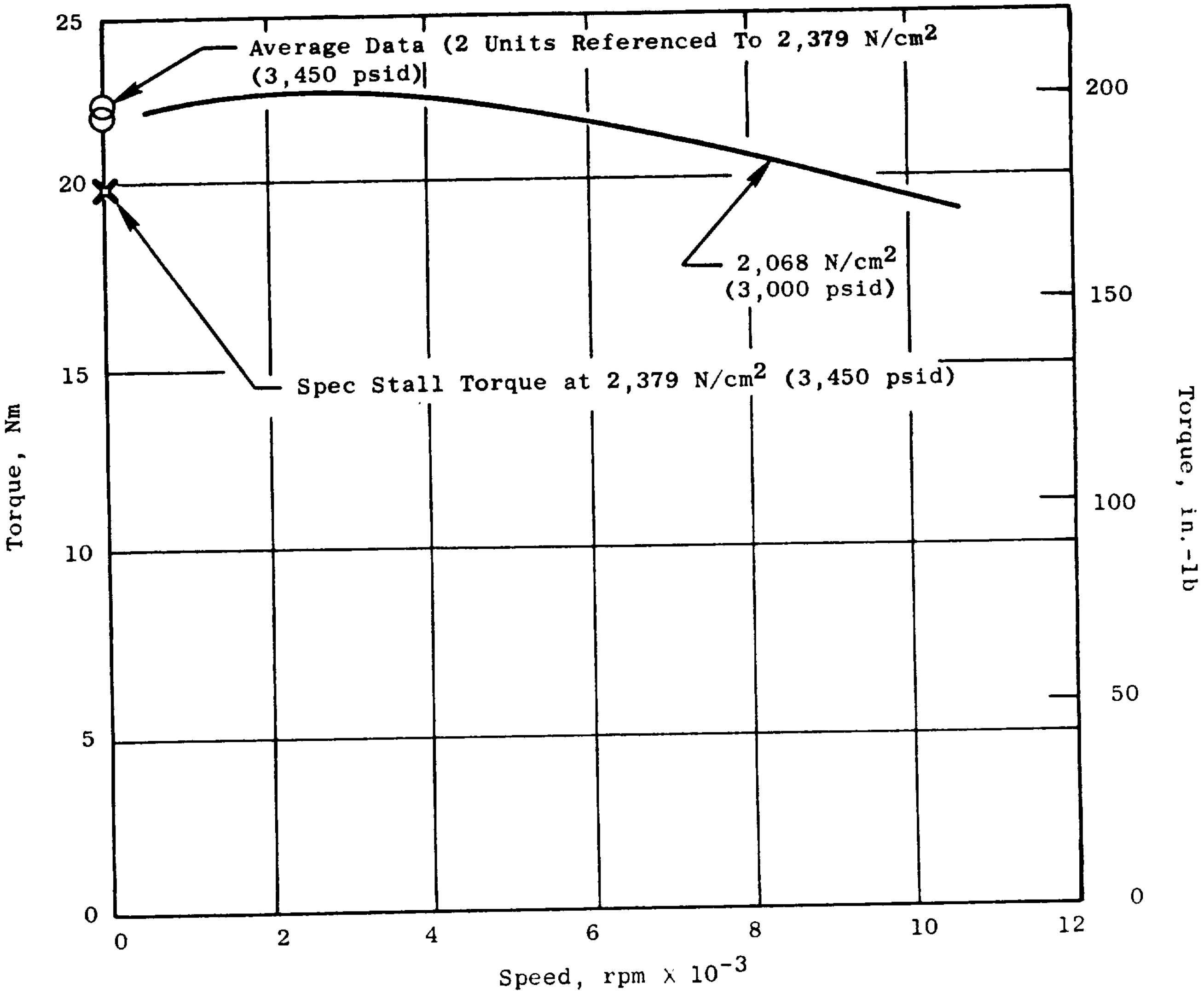

Figure 7-42. Hydraulic Motor Characteristics-Torque Versus Speed.

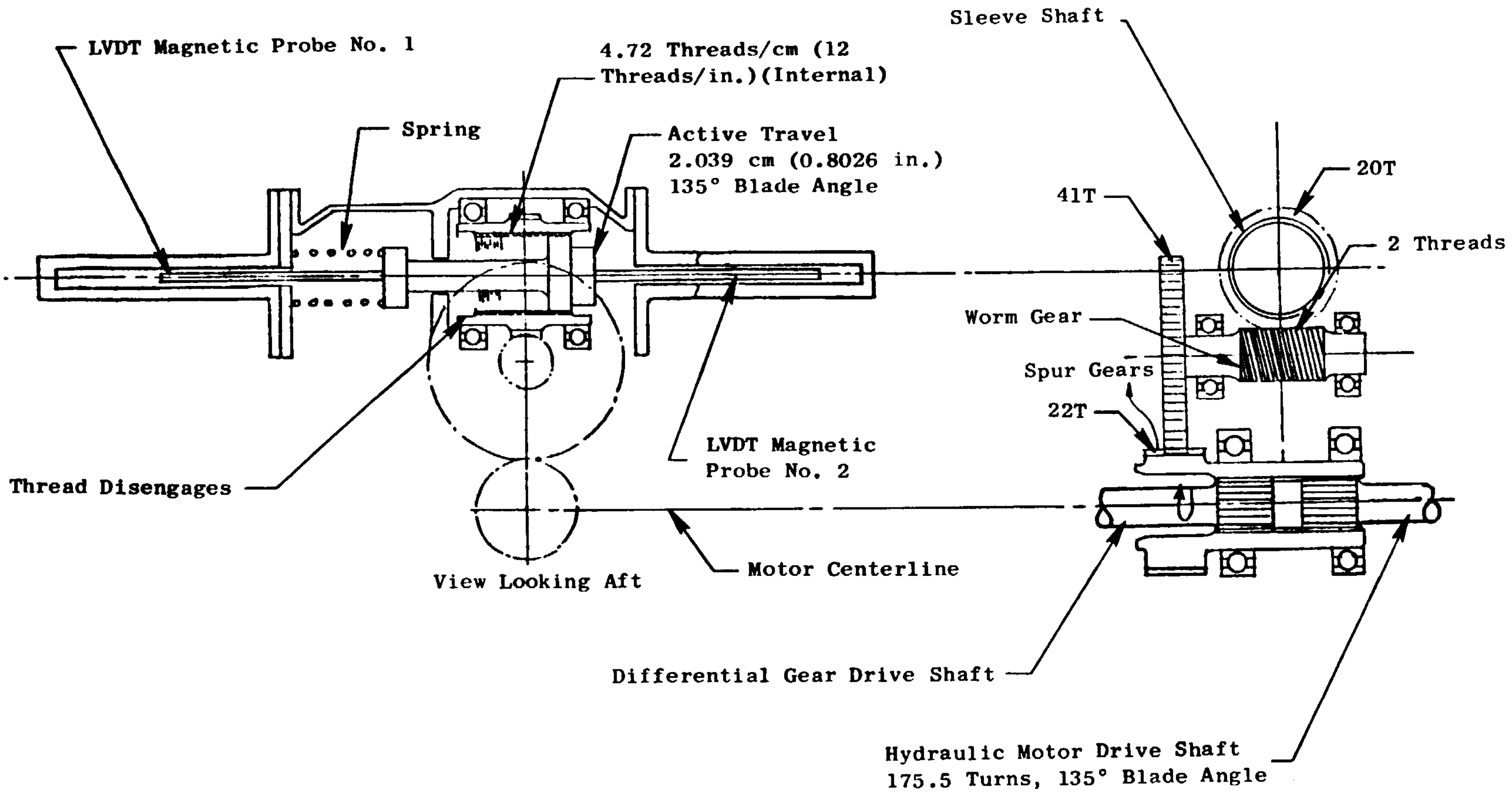
LVDT Magnetic Probe No. 1
Spring
4.72 Threads/cm (12 Threads/in.)(Internal)
Active Travel
2.039 cm (0.8026 in.)
135° Blade Angle
Sleeve Shaft
41T
20T
2 Threads
Worm Gear
Spur Gears
22T
LVDT Magnetic Probe No. 2
Thread Disengages
View Looking Aft
Motor Centerline
Differential Gear Drive Shaft
Hydraulic Motor Drive Shaft
175.5 Turns, 135° Blade Angle

Figure 7-43. LVDT Drive Schematic.

Translation of the magnetic core of the LVDT produces an a-c output voltage which is proportional to displacement. These transducers are constructed of one primary coil and two secondary coils. An alternating current is fed through the primary winding. The magnetic core couples the primary and secondary coils by conducting the alternating field inside the coils. When the core is in the center position, an equal portion of the core extends into each of the secondary coils and affects an equal coupling between the primary coil and each secondary coil. An alternating voltage of equal magnitude is induced in the secondary coils. With the secondary coils connected in series opposed, the output is close to zero. As the core is moved to either side, the coupling between the primary and one secondary coil is increased while the coupling between the primary and the other secondary is decreased. A larger alternating voltage is then induced in one secondary coil and the output voltage is the difference between the two voltages.

Differential and No-Back - The differential and no-back, shown in Figure 7-44, are the drive system connection between the hydraulic motor and the actuator assembly. This modular package attaches to the actuator and rotates at fan speed. Differential gearing connects the hydraulic motor output shaft to the rotating no-back and results in a gear reduction of 5.44:1. Differential movement is transmitted through the no-back in either direction of rotation. The no-back, however, prevents imposed blade torque from back driving the system.

The no-back design is a ball-ramp-type configuration similar to the Curtiss-Wright design currently being used on the F-111 aircraft trailing edge flap system. The differential gear is similar to designs used previously in Curtiss-Wright turboprop pitch-change mechanisms.

Common gears are used in all three stages of the differential gear. Coupling drive splines are designed to accommodate estimated misalignment during operation. The number of gear teeth and materials for the gears, gear bearings, and no-back disks are as follows:

N_T (SUN) = 27 N_T (PLANET) = 18 N_T (RING) = 63

Gear Material: H-11 through Hard (R_C 56-59)

Bearing Material: 52100

No-Back Disks: AISI 1095 with Sintered Bronze

As shown in Figure 7-44, provision is made along the engine center-line to hand crank the actuation system by removing the fan spinner cap and the cap bolted to the forward drive cone.

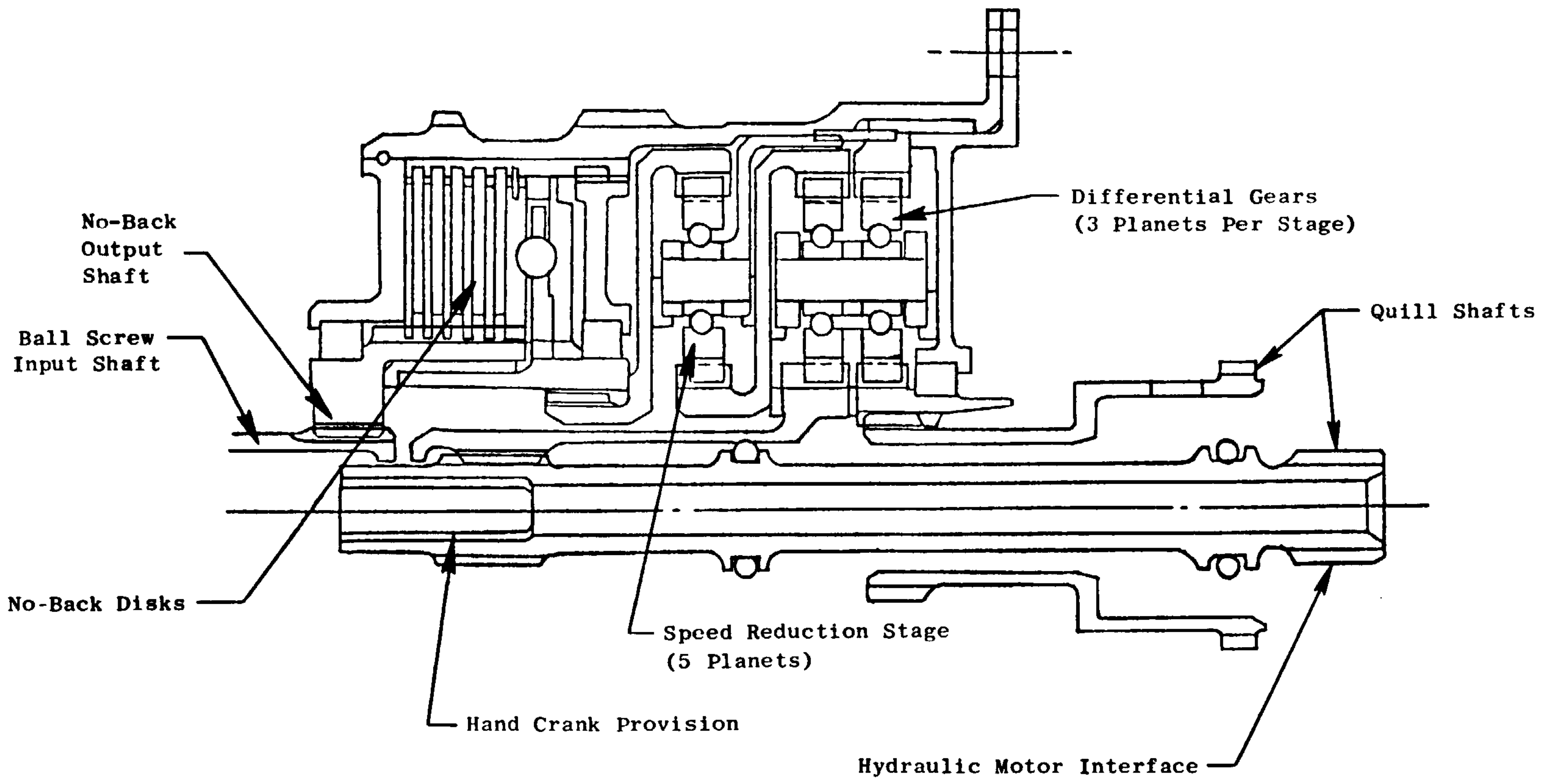
No-Back Output Shaft
Ball Screw Input Shaft
No-Back Disks
Differential Gears (3 Planets Per Stage)
Quill Shafts
Speed Reduction Stage (5 Planets)
Hand Crank Provision
Hydraulic Motor Interface

Figure 7-44. Differential and No-Back.

7.4.3 Lubrication System

A schematic showing the actuator lubrication system is presented in Figure 7-45. As shown, lube oil from the engine lube system is supplied through the stationary hydraulic motor housing. A system of sleeves and dams centrifugally directs the lubricant to the critical areas of the actuator. The oil is then centrifuged outward and drains back to the sump along the outer actuator wall. All seals are designed so that no dynamic head of oil is in contact with the seal interfaces. The total actuator lubrication oil flow is 47.25 cm^3/sec (0.75 gal/min).

7.4.4 Maximum Blade Pitch Angle Actuation Range

The maximum blade angle range, assuming the actuator stroke is defined as the distance between the dynamic stops just starting to engage, is 130.6°, representing 14.99 cm (5.90 in.) of stroke. To prevent touching stops and to allow for tolerances, only 14.48 cm (5.70 in.) stroke (126.1°) will be considered as the normal operating blade angle actuation range.

With the actuator set up to go from the nominal blade setting angle to reverse through stall, there is capability to go to -116.0° (open) and +10.1° (closed). By indexing pinion teeth (100.8°) when setting up to go to reverse through flat pitch, there is capability to go to -15.2° (open) and +110.9° (closed).

The actuation system is designed to permit an increase in the maximum open or closed positions for either reverse through flat pitch or reverse through stall simply by reindexing the blade pinions with respect to the ring gears.

7.4.5 Actuation System Weight

The weight of the experimental engine actuation system is 69.05 kg (152 lb) and is tabulated by various components in Table 7-XVI. Weight of the hydraulic motor support, LVDT drive, servovalve and no-back/differential gear assembly would be reduced for the flight type configuration. The approximate weight of a flight type system would be 62.2 kg (137 lb). Further reductions in weight may be realized by optimizing the ball screw and spline stroke.

7.4.6 Design Blade Angle Setting Accuracy

The calculated mechanical blade angle error based on the system backlash is ±0.446° which includes the items shown in Table 7-XVII. These calculations are based on worst stackup conditions.

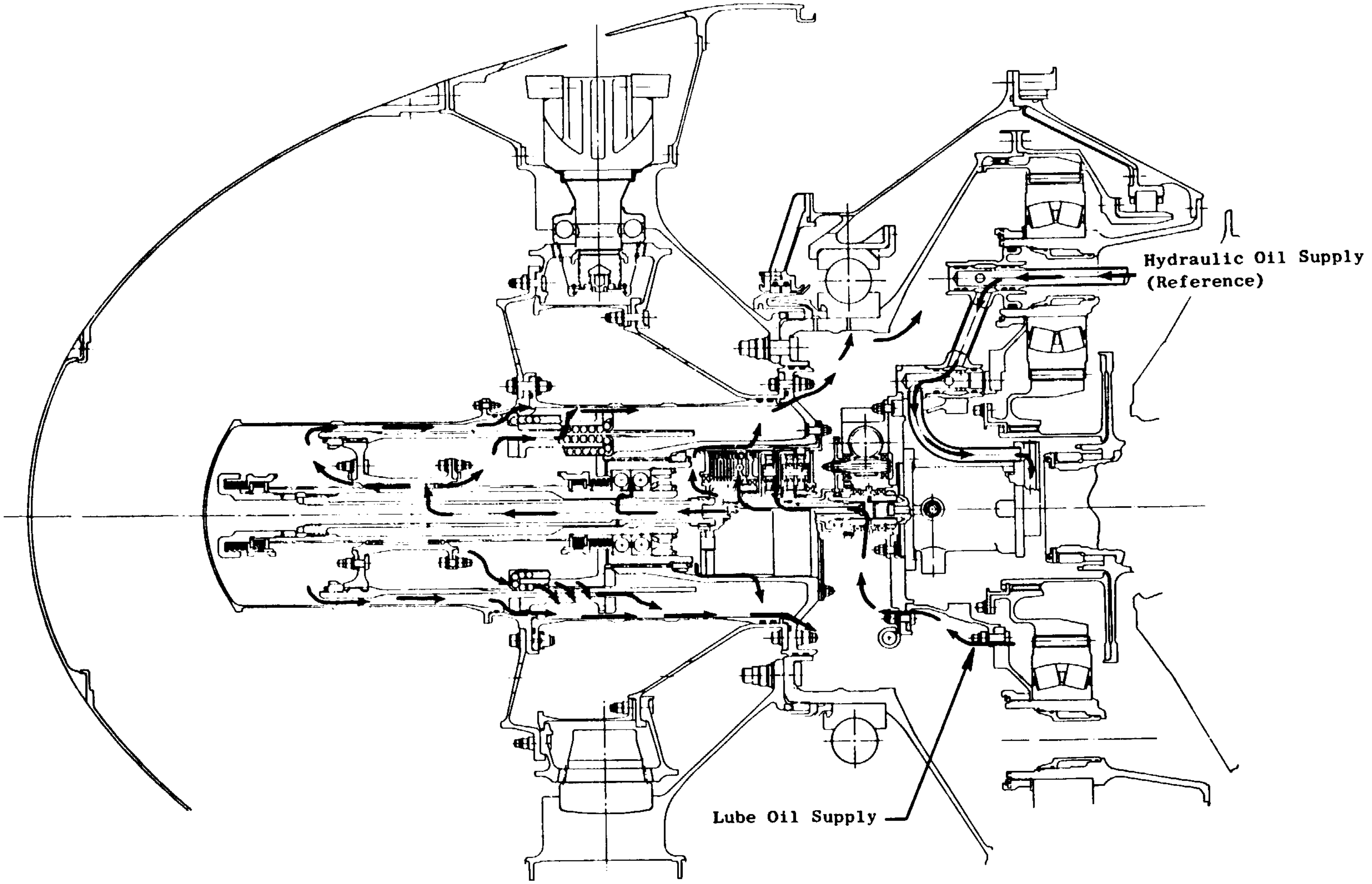
Hydraulic Oil Supply (Reference)
Lube Oil Supply

Figure 7-45. Actuation Lubrication System.

Table 7-XVI. Experimental Engine Actuation System Weights.

Component	Weight			
	kg		lb	
Pinion Gears		4.65		10.25
Actuator		46.72		103.00
Ring Gears	15.84		34.92	
Ball Spline and Translating Member	16.00		35.27	
Ball Screw, Thrust Bearing, and Ball Nut	5.11		11.27	
Drive Sleeve	3.28		7.22	
Cover, Miscellaneous	6.49		14.32	
Differential, No-Back, and Motor		7.25		15.98
Miscellaneous		10.43		23.00
Total		69.05		152.23

Table 7-XVII. Mechanical System Backlash in Terms of Fan Blade Angle.

	Mechanical Backlash
Ball Spline	±0.203°
Ball Screw	0.022°
Thrust Bearing	0.120°
No-back Play	0.084°
LVDT Drive Train	0.013
Involute Splines	0.004
	±0.446

SECTION 8.0

FAN ROTOR MECHANICAL DESIGN

8.1 SUMMARY

The UTW fan rotor illustrated in Figure 8-1 is a variable-pitch design that offers full reverse thrust capability. The design includes 18 composite fan blades fabricated from a hybrid combination of Kevlar-49, Type AS graphite, boron, and S-glass fibers in a PR288 epoxy resin matrix. The blades incorporate a metal leading edge to provide FOD and erosion protection. Solidity of the blade airfoil is 0.95 at the OD and 0.98 at the ID which permits rotation of the blades into the reverse thrust mode of operation through both the flat pitch and the stall pitch directions. A spherical casing radius and a spherical blade tip provide good blade tip clearances throughout the range of blade pitch angle settings.

Each blade is attached to a rotor trunnion at the blade's root. The trunnions are retained by the disk. Retainer straps, attached to the trunnion, lock the blade in axial position and resist trunnion opening deflections under blade centrifugal loading.

Centrifugal force of each blade and trunnion is carried by a single-row ball thrust bearing. This bearing has a full complement of balls to reduce the per-ball loading. The race has a much higher conformance than is standard for thrust bearings because of its highly loaded, intermittently actuated environment. The bearing is grease lubricated, with a cup shield completely covering the upper race and most of the lower race, preventing the grease from leaking out under high radial "g" loads. This concept was successfully demonstrated on General Electric's reverse-pitch fan. Fail-safe lubrication is accomplished by a tungsten disulfide coating applied to the balls and races. Under the planned loading, this coated bearing is capable of operating 9000 engine hours after loss of lubricant with only a slight increase in coefficient of friction and negligible wear. Secondary and vibratory loads from the trunnion are resisted by dry thrust and journal bearings located at the OD of the fan disk.

In a concept similar to that used on the CF6-50 fan, balance weights are accessible in the fan spinner, and field balance of the fan is possible without removing the spinner. Ease of maintenance has also been considered in the design of the other rotor components. After removal of the rotor spinner and the forward retaining straps, the blades can be individually removed and replaced without disassembly of the blade trunnion. Access holes in the flange of the aft rotating flowpath permit bolt removal to allow removal of the fan rotor, blade actuator, and the reduction gear as a complete subassembly.

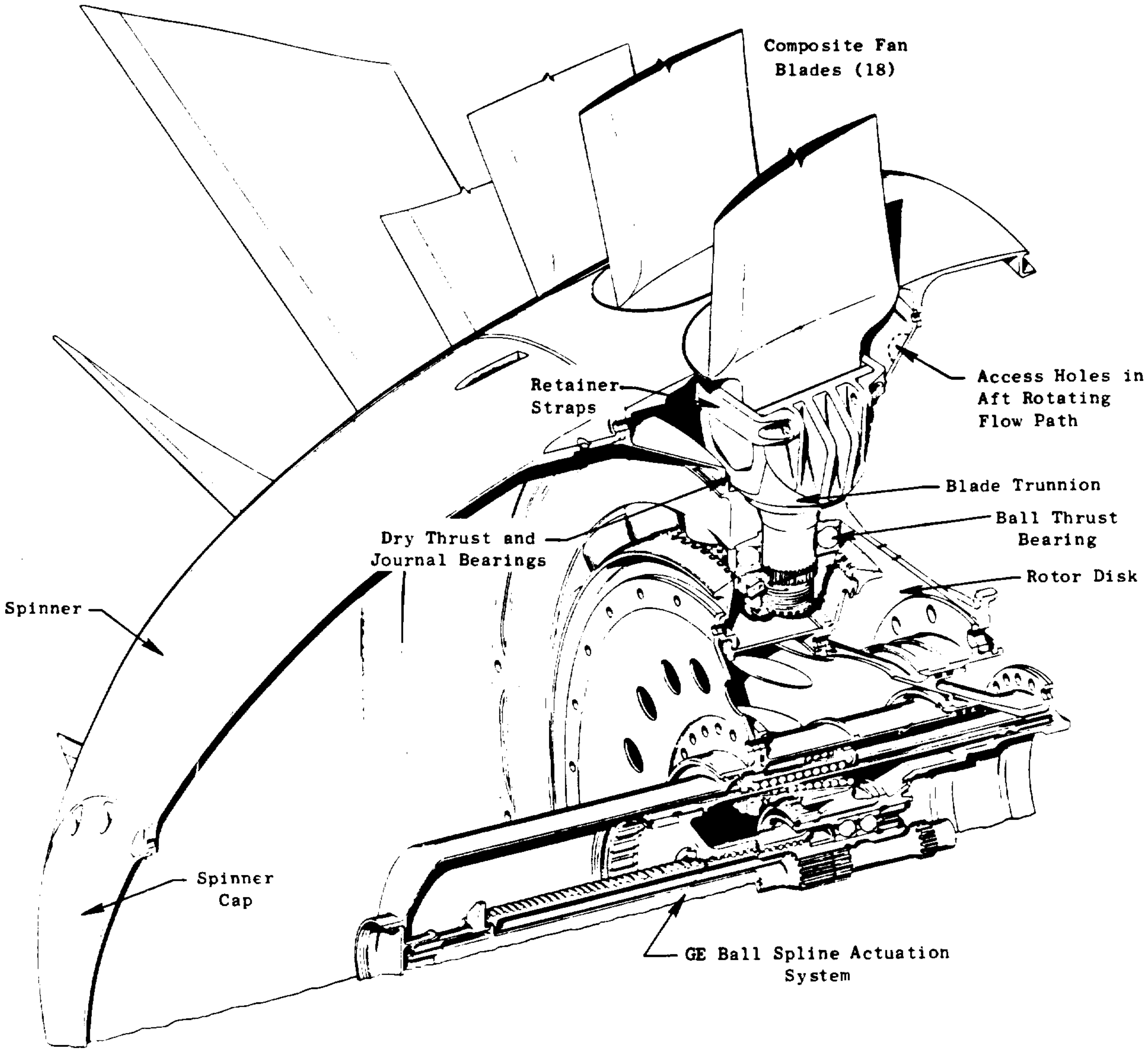
Composite Fan Blades (18)
Access Holes in Aft Rotating Flow Path
Retainer Straps
Blade Trunnion
Ball Thrust Bearing
Dry Thrust and Journal Bearings
Rotor Disk
Spinner
Spinner Cap
GE Ball Spline Actuation System

Figure 8-1. UTW Fan Rotor Configuration.

All UTW fan rotor components are of flight-weight design. Rotor material selections were made to satisfy life requirements with minimum weight. Normal flight engine design practices, including consideration of LCF life and FAA flight requirements such as burst speed margin and bird strike capability, have been adhered to in the rotor design.

8.2 COMPOSITE FAN BLADES

8.2.1 Design Requirements

Design requirements for the UTW composite fan blade were established to provide realistic long-life operation in a flight engine. Major design requirements are listed as follows:

- Design Mechanical Speeds
  - 100% mechanical design - 3244 rpm
  - 100% SLS hot-day takeoff - 3143 rpm
  - Maximum steady-state duty cycle speed - 3326 rpm
  - Maximum design overspeed - 3614 rpm
  - Maximum burst speed - 4700 rpm
- Design Life and Cycles
  - 36,000 hours
  - 48,000 cycles (based on a 45-minute mission)
  - 1000 ground check-out cycles, full power
- Mechanical Design Requirements
  - Blade is capable of operation from flat pitch through stall pitch.
  - Blades are individually replaceable without major teardown.
  - Blade untwist has been factored into airfoil configuration.
  - Stresses are within allowable stress range diagram, with sufficient vibratory margin.
  - First flexural frequency crosses 2/rev above flight idle and below takeoff and climb engine speeds.

- First flexural frequency has greater than 15% margin over 1/rev at 115% speed.
- Blade nickel leading edge protection has been kept within aero airfoil limits.

Of these mechanical design requirements, the first is of prime importance. Successful operation of the experimental engine depends on having a rugged blade which can withstand reverse pitch operation and other inlet disturbances including crosswind testing. Initially the design requirements included provisions for satisfying FAA specifications for FOD resistance. However, during testing of preliminary blades it was found that the blade FOD capability was less than desired and FOD requirements were dropped pending further developments on other NASA and related programs.

8.2.2 Basic Design Features

The UTW composite blade is illustrated in Figure 8-2. Design features of the blade are described in the following paragraphs.

Aerodynamic Blade Parameters

A summary of the aero blade parameters is presented in Table 8-I. Detailed blade aerodynamic design characteristics, including blade chord, maximum thickness, stagger angle, and camber are presented in Section 6.0, "Fan Aerodynamic Design." The blade length, thickness, and twist geometries are similar to composite blades which have undergone extensive development and proof testing on other programs.

Blade Configuration

Finished configuration of the fan blade is shown in Figure 8-3 and consists of a molded composite blade and a molded composite platform. The molded blade is shown in Figure 8-4. The platform is described in a subsequent section.

The blade molded configuration consists of a solid composite airfoil and a straight bell-shaped composite dovetail. The molded blade leading edge is slightly reduced in thickness along the entire span to allow for a nickel plate over wire mesh protection. The dovetail is undercut at the leading edge and trailing edge to reduce local stresses and to permit better transitioning of the cambered airfoil section into the straight dovetail.

Airfoil definition is described by 15 radially spaced airfoil cross sections which are stacked on a common axis. These are shown along with some details of the blade cross sections in Figure 8-5. Each section location corresponds to the like-designated elevation defined on the blade, Figure 8-3. The dotted portion of the leading edge defines the aero profile and the solid inner portion describes the molded composite cross section. Only a

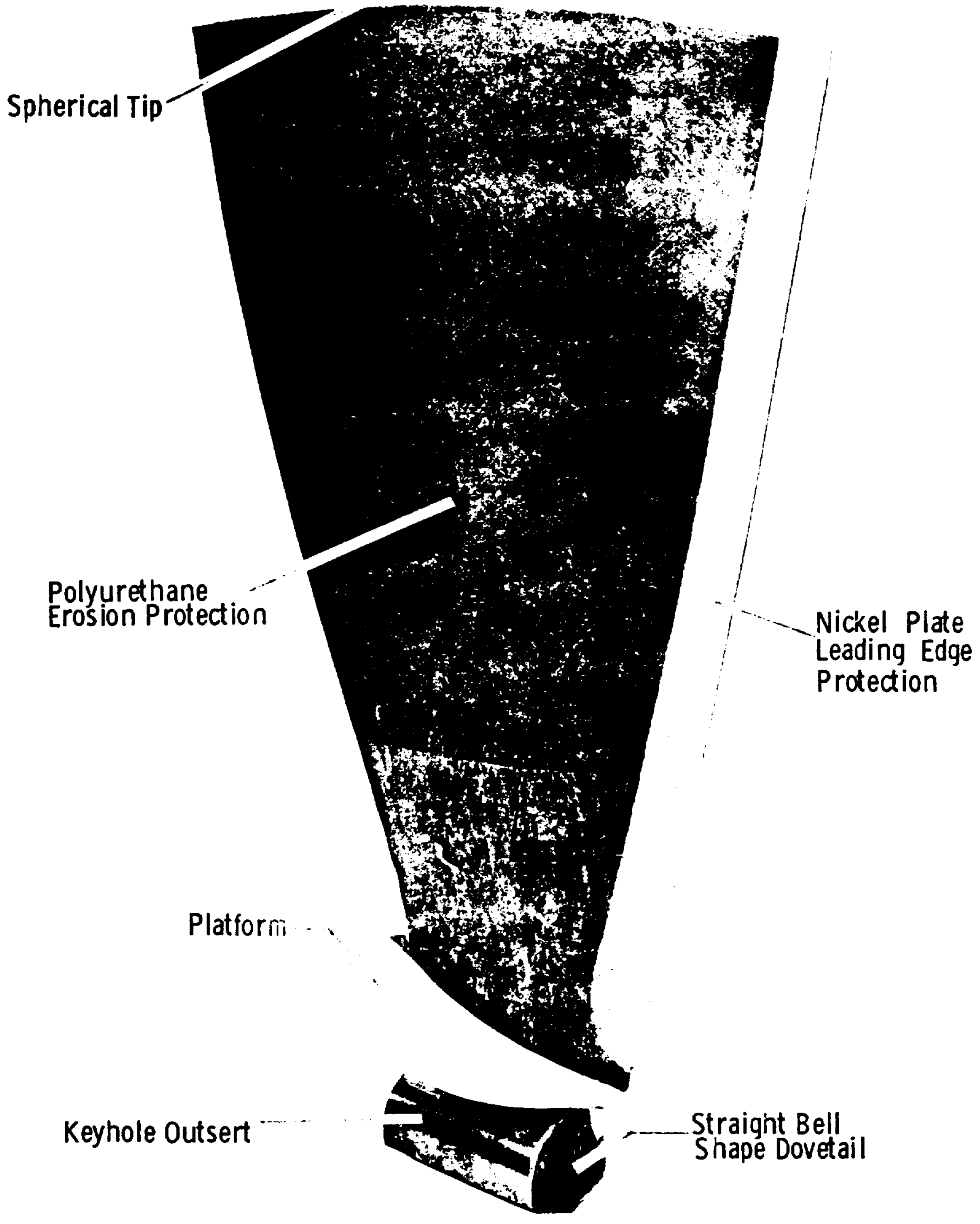
Spherical Tip
Polyurethane Erosion Protection
Nickel Plate Leading Edge Protection
Platform
Keyhole Outsert
Straight Bell Shape Dovetail

Figure 8-2. UTW Composite Fan Blade and Platform.

Table 8-I. UTW Composite Fan Blade Design Summary.

Aero Definition	
Tip Speed	306 m/sec (1005 ft/sec)
Tip Diameter	180 cm (71 in.)
Radius Ratio	0.44
Number of Blades	18
Bypass Pressure Ratio	1.27 Takeoff
Aspect Ratio	2.11
Tip Chord	30.3 cm (11.91 in.)
Root Chord	14.8 cm (5.82 in.)
T_M Root	1.92 cm (0.76 in.)
T_M Tip	0.91 cm (0.36 in.)
Root Camber	66.2°
Total Twist	44°
Solidity	
Tip	0.95
Root	0.98
Angle Change from Forward to Reverse	
Through Flat Pitch	85°
Through Stall	95°

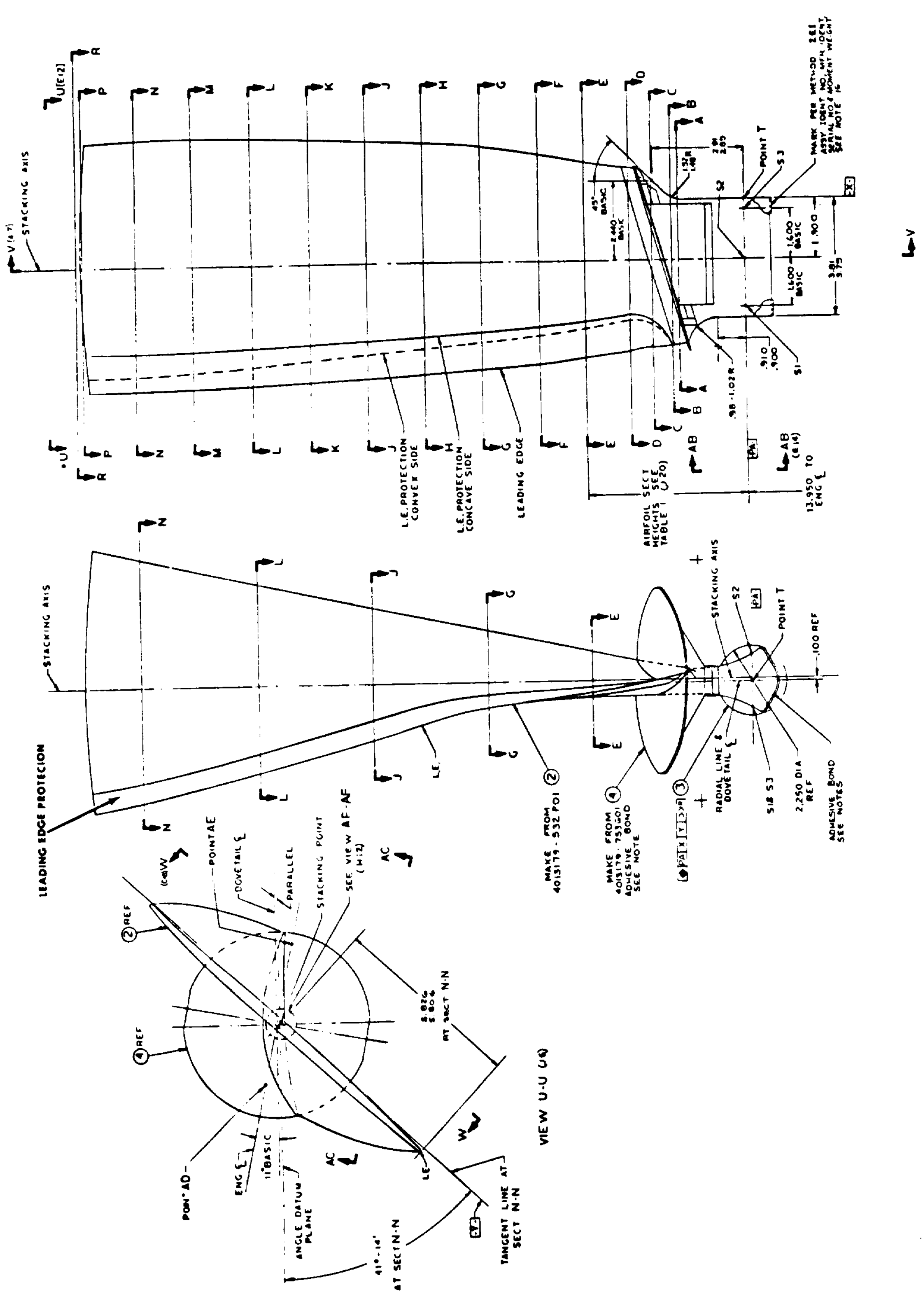
STACKING AXIS
V (H7)
U (E12)
A
B
C
D
E
F
G
H
J
K
L
M
N
P
R
AB
AB (E14)
45° BASIC
2.440 BASIC
1.52 1.48
2.91 2.89
POINT T
S3
S2
S1
MARK PER METHOD 281 ASSY IDENT NO, MFR IDENT SERIAL NO & MOMENT WEIGHT SEE NOTE 16
X
1.600 BASIC
1.900
3.81 3.75
.910 .900
.98-1.02R
PA
L.E. PROTECTION CONVEX SIDE
L.E. PROTECTION CONCAVE SIDE
LEADING EDGE
AIRFOIL SECT HEIGHTS SEE TABLE I (J20)
12.950 TO ENG ℄
LEADING EDGE PROTECTION
LE
MAKE FROM 4013179-532 P01
②
MAKE FROM 4013179-753G01 ADHESIVE BOND SEE NOTE
④
③
RADIAL LINE & DOVETAIL ℄
S1 & S3
2.250 DIA REF
ADHESIVE BOND SEE NOTES
.100 REF
POINT AE
DOVETAIL ℄
PARALLEL
STACKING POINT
SEE VIEW AF-AF (H12)
AC
W
② REF
④ REF
8.826 8.806 AT SECT N-N
VIEW U-U (J6)
POINT AD
ENG ℄
11° BASIC
ANGLE DATUM PLANE
41°-14' AT SECT N-N
TANGENT LINE AT SECT N-N

Figure 8-3. UTW Composite Fan Blade.

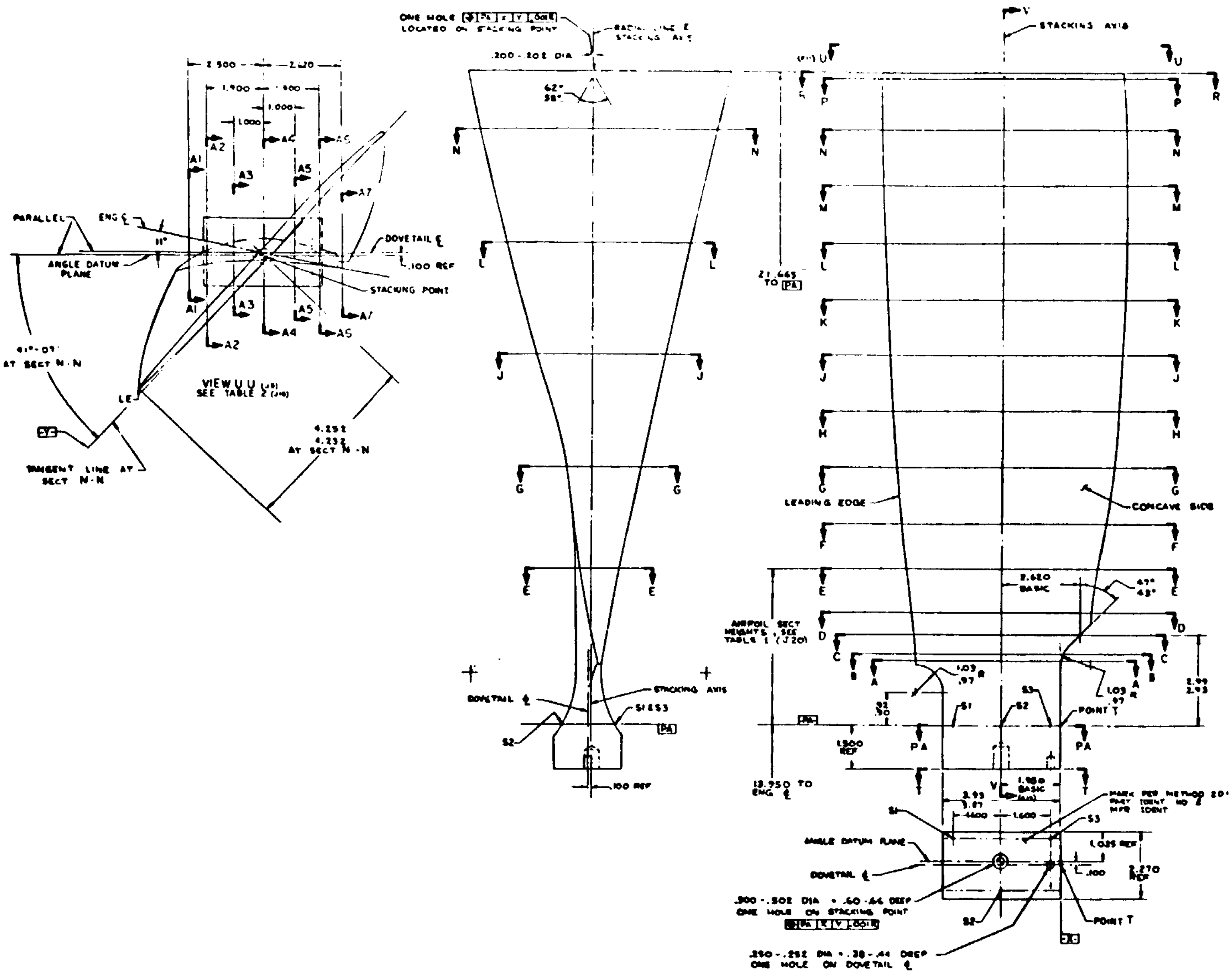

ONE HOLE ⊕ PA X V .001 Ⓡ LOCATED ON STACKING POINT
.200 - .202 DIA
RADIAL LINE ℄ STACKING AXIS
62°
58°
STACKING AXIS
V
U
R
P
N
M
L
K
J
H
G
F
E
D
C
B
A
PA
21.665 TO PA
LEADING EDGE
CONCAVE SIDE
2.620 BASIC
47°
43°
AIRFOIL SECT HEIGHTS, SEE TABLE 1 (J20)
1.03 R
.97
S1
S2
S3
POINT T
.92
.90
2.99
2.93
1.500 REF
13.950 TO ENG ℄
1.980 BASIC
2.93
2.87
1.600
MARK PER METHOD 201 PART IDENT NO & MFR IDENT
1.025 REF
.100
2.270 REF
ANGLE DATUM PLANE
DOVETAIL ℄
.500 - .502 DIA × .60 - .66 DEEP ONE HOLE ON STACKING POINT
⊕ PA K V .001 Ⓡ
.250 - .252 DIA × .38 - .44 DEEP ONE HOLE ON DOVETAIL ℄
STACKING AXIS
S1 & S3
.100 REF
2.500
2.620
1.900
1.000
A1
A2
A3
A4
A5
A7
PARALLEL
ENG ℄
11°
DOVETAIL ℄
.100 REF
STACKING POINT
41°-09'
AT SECT N-N
LE
VIEW U U (J8)
SEE TABLE 2 (J10)
4.252
4.232
AT SECT N-N
TANGENT LINE AT SECT N-N

Figure 8-4. Molded Fan Blade.

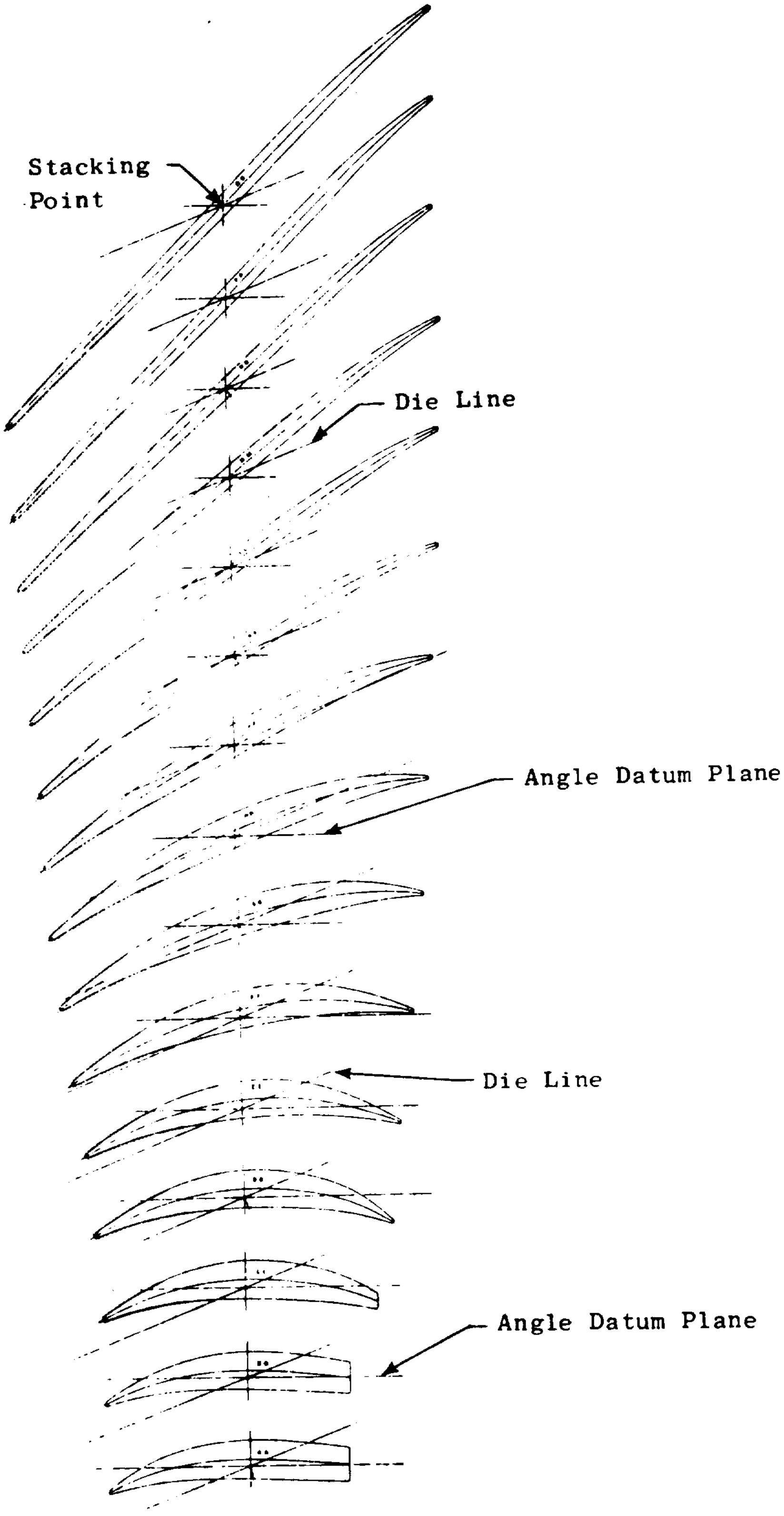
Stacking Point
Die Line
Angle Datum Plane
Die Line
Angle Datum Plane

Figure 8-5. Blade Airfoil Sections.

portion of the lowest three sections extend above the flowpath. The aft portion of these sections lie below the platform, and therefore do not need to correspond with aero defined profiles. Erosion and small FOD protection of the basic organic composite material blade consists of nickel plating on stainless steel wire mesh which is bonded onto the molded blade and is applied to the leading edge portion of the blade. The details of the blade leading edge protection are shown on the finished blade drawing (Figure 8-3).

Radial sections through the molded blade are shown in Figure 8-6. Sections correspond to the like-designated locations on the molded blade. The dovetail axial centerline is offset from the stacking axis by 0.254 cm (0.1 in.) to provide a smooth airfoil-to-dovetail transition.

Material Selection/Blade Layup Configuration

Material selection and ply arrangement for the UTW hybrid composite blade are based on previous development efforts conducted by General Electric and sponsored by NASA under Contract NAS3-16777 and development effort conducted during the preliminary design phase of the QCSEE program. These efforts led to the selection of a combination of fibers in a single blade to provide the proper frequency responses to satisfy STOL engine conditions. Figure 8-7 shows the general ply shapes, layup arrangement, fiber orientations, and material in each ply of the blade. Figure 8-8 is a trimetric view of the general arrangement of the plies in the blade. The flex root surface plies in the lower region of the blade contain S-glass fibers. These plies, being near the surface and having relatively low bending stiffness and high tensile strength, provide higher strain-to-failure characteristics, thereby, allowing the blade to absorb large bird impact loading without the classic root failure that usually accompanies brittle composite materials. Torsional stiffening plies in the airfoil region of the blade are oriented at ± 45° to provide the shear modulus required for a high first torsional frequency. These plies contain boron toward the outer surfaces of the blade and graphite in the inner regions. Plies of Kevlar-49 are interspersed throughout the blade with the majority of them being oriented with their fibers in the longitudinal direction of the blade. Several of the Kevlar plies in the tip region of the blade are oriented at 90° to the longitudinal axis to provide chordwise strength and stiffness to the blade.

The resin system being used in this program is a product of the 3M Company and is designated as PR288. This is a resin system that has proven satisfactory for the needs of advanced composite blading. Some of its unique characteristics in the prepreg form are:

- Has constant processing characteristics
- Can be prepregged with many different fibers including hybrids
- Uniform prepreg thickness and resin content control

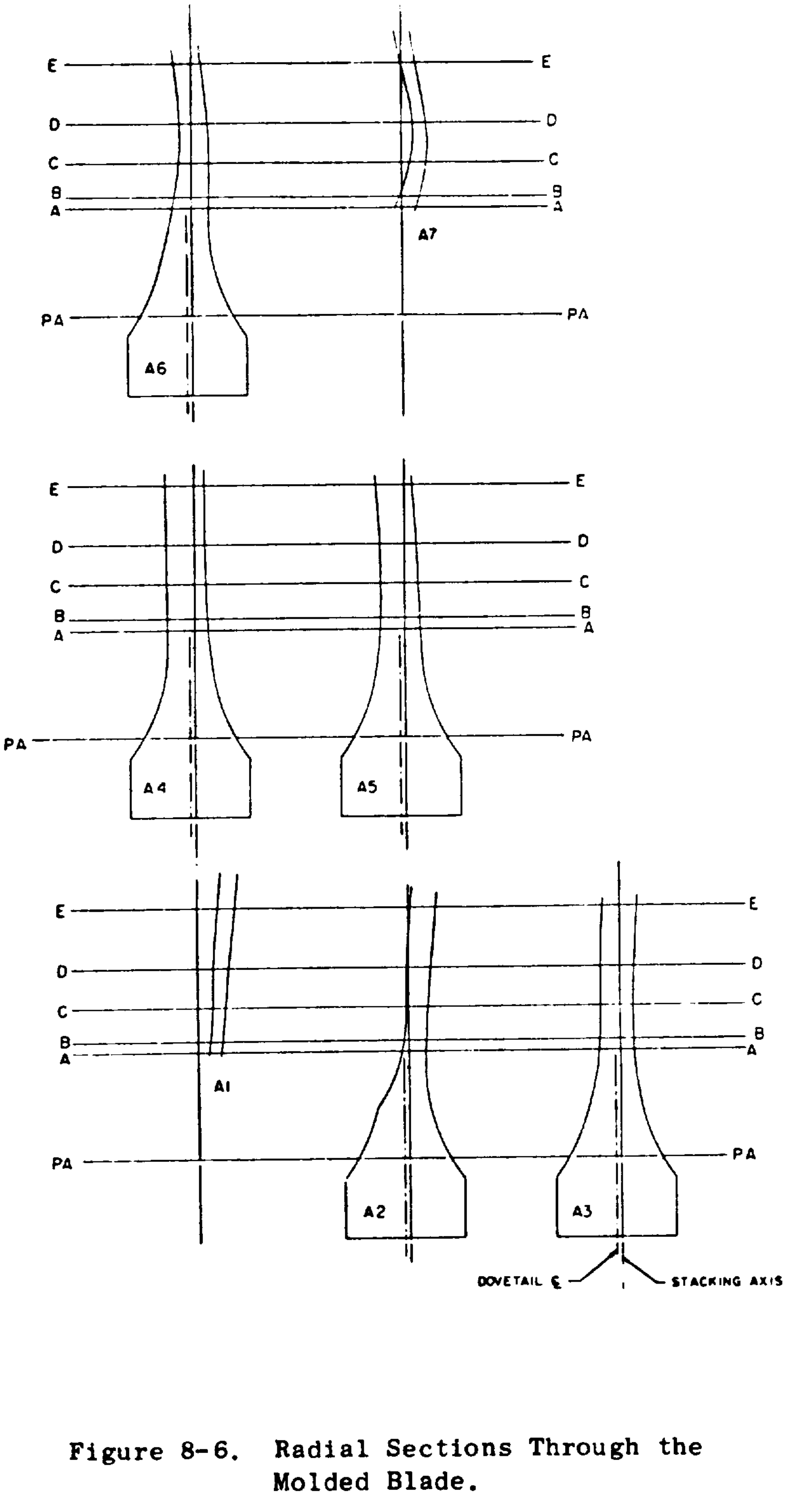

E
D
C
B
A
PA
A6
A7
A4
A5
A1
A2
A3
DOVETAIL ℄
STACKING AXIS

Figure 8-6. Radial Sections Through the Molded Blade.

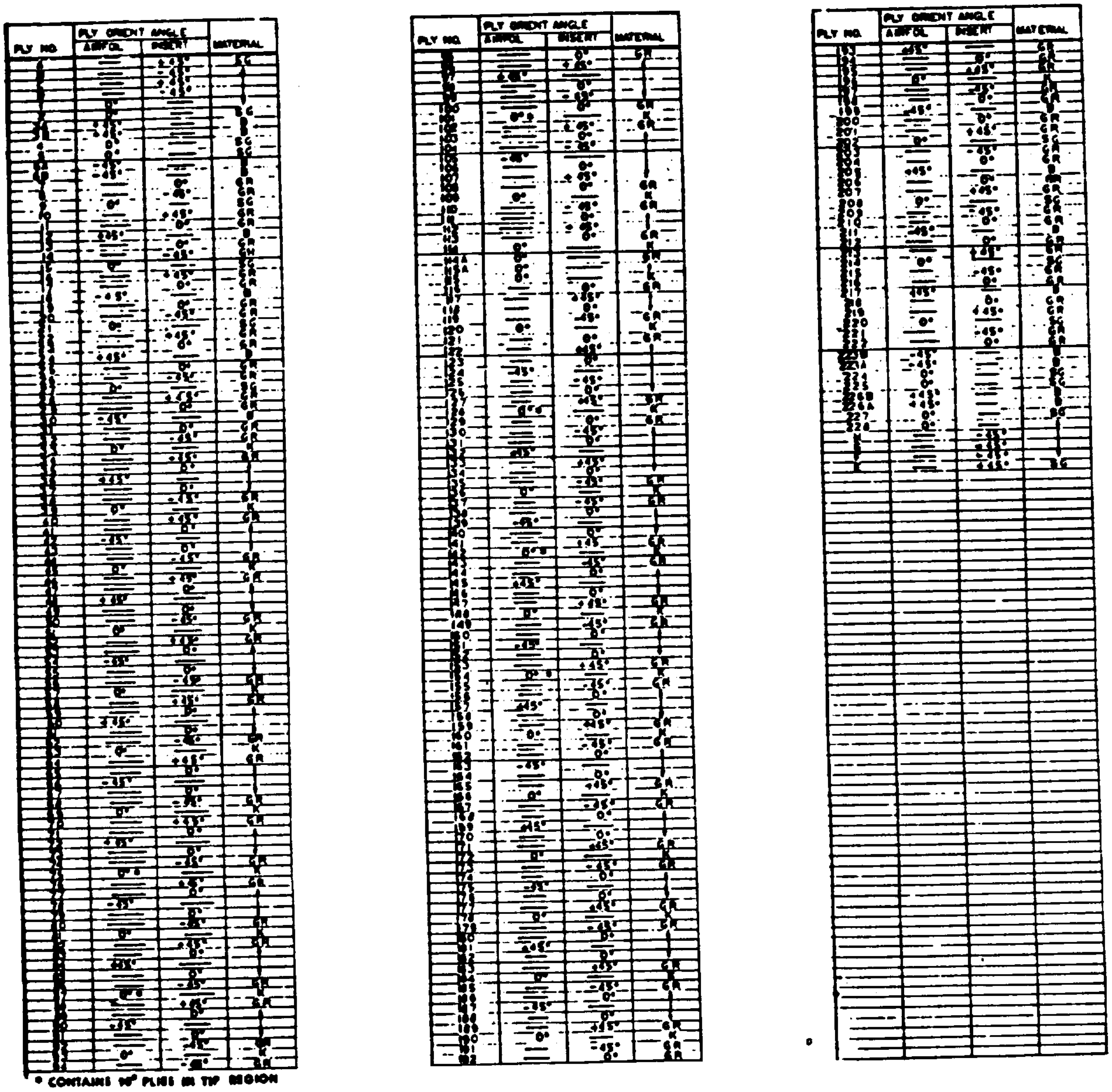
PLY NO.
PLY ORIENT ANGLE
AIRFOIL
INSERT
MATERIAL
* CONTAINS 90° PLIES IN TIP REGION

Figure 8-7. Ply Layup

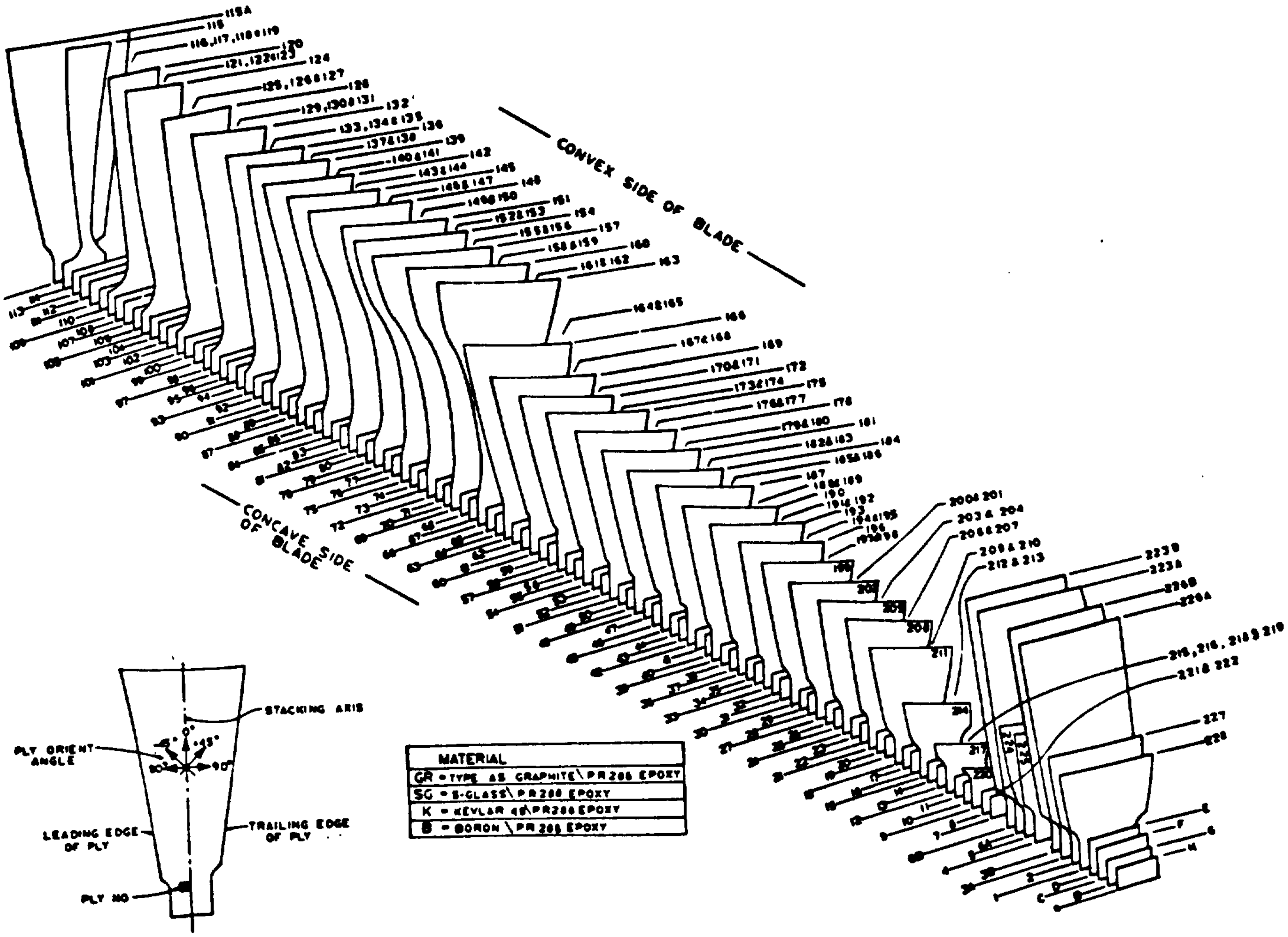

CONVEX SIDE OF BLADE
CONCAVE SIDE OF BLADE
STACKING AXIS
PLY ORIENT ANGLE
0°
-45°
+45°
90°
90°
LEADING EDGE OF PLY
TRAILING EDGE OF PLY
PLY NO
MATERIAL
GR = TYPE AS GRAPHITE\PR 286 EPOXY
SG = S-GLASS\PR 286 EPOXY
K = KEVLAR 49\PR286 EPOXY
B = BORON\PR 286 EPOXY
119A
115
116,117,118&119
120
121,122&123
124
125,126&127
128
129,130&131
132
133,134&135
136
137&138
139
140&141
142
143&144
145
146&147
148
149&150
151
152&153
154
155&156
157
158&159
160
161&162
163
164&165
166
167&168
169
170&171
172
173&174
175
176&177
178
179&180
181
182&183
184
185&186
187
188&189
190
191&192
193
194&195
196
197&198
200&201
203&204
205&207
208&210
212&213
223B
223A
226B
226A
215,216,218&219
221&222
227
228
E
F
G
H
C
D
B
A

Figure 8-7. Material Arrangement.

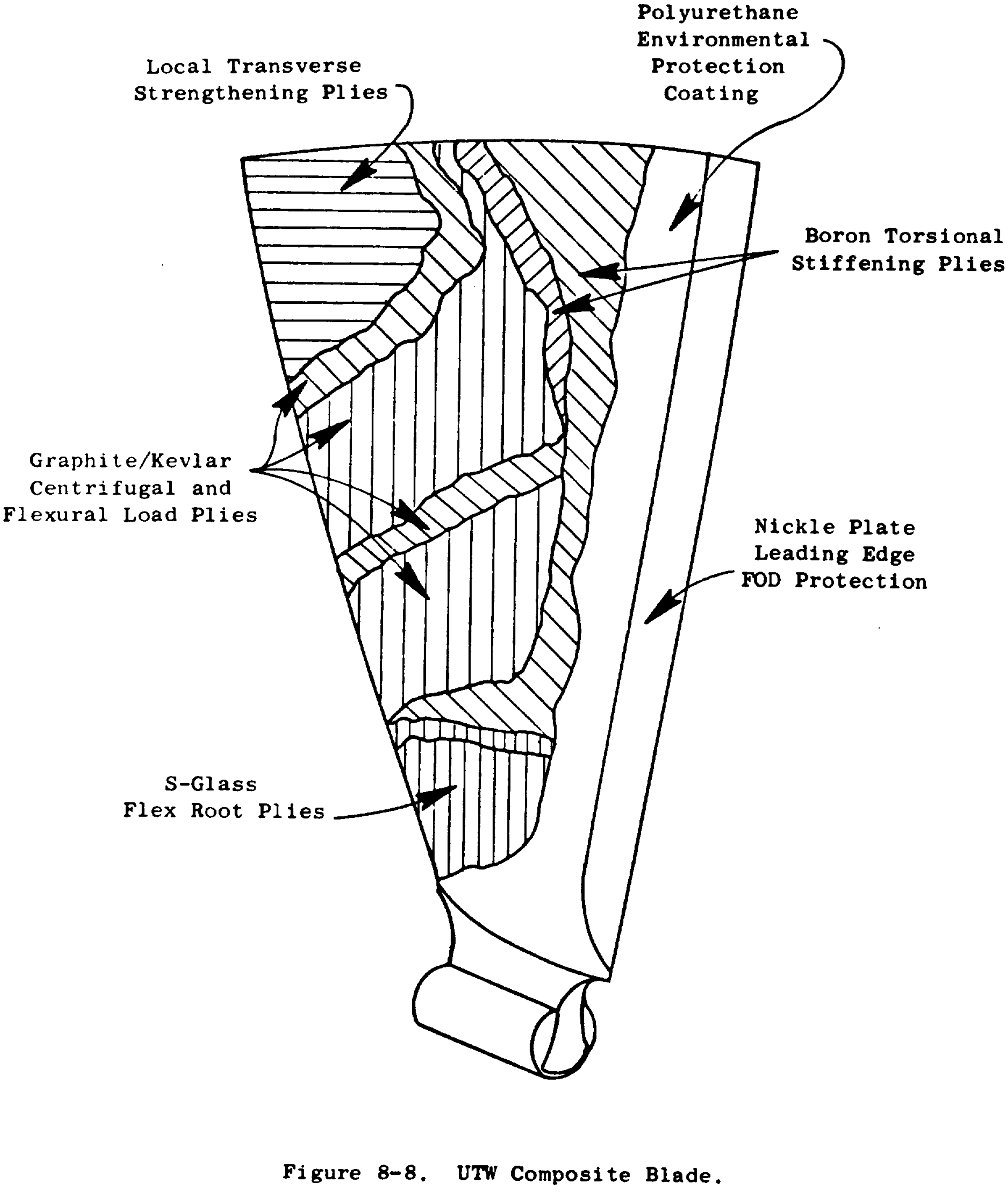
Local Transverse Strengthening Plies
Polyurethane Environmental Protection Coating
Boron Torsional Stiffening Plies
Graphite/Kevlar Centrifugal and Flexural Load Plies
Nickle Plate Leading Edge FOD Protection
S-Glass Flex Root Plies

Figure 8-8. UTW Composite Blade.

Typical properties of the PR288/AS prepreg are shown in Table 8-II. Material properties for several fiber composite prepregs are shown in Table 8-III.

Dovetail Design

The dovetail design for the composite fan blade consists of a straight bell-shaped dovetail with a 8.89 cm (3-1/2 in.) radius. The bell-shaped dovetail design reflects many years of development efforts to achieve an efficient dovetail configuration having both high static pull strength and good fatigue strength. All airfoil plies extend continuously down into the dovetail and are interspersed with insert plies which act to fill out the enlarged cross section. This can be seen in Figure 8-9 where a radial section of the blade root and dovetail prior to dovetail machining is shown. The final dovetail is shown in Figure 8-6.

Platform Design

The QCSEE UTW engine incorporates a variable-pitch fan. The blade variable-pitch operation requires a circular opening through the spinner and hub to permit airfoil clearance in the different blade position rotations, either actuated in the flat pitch or stall direction. To maintain reasonable actuation forces and blade dovetail stresses, the centrifugal loading on each blade platform and dovetail is required to be kept to a minimum. This requires a lightweight design. Therefore, composite platforms in addition to composite blades are necessary. The following paragraphs summarize the design requirements and description of the platform.

The platform design selected for the QCSEE UTW blade satisfies several requirements including (1) lightweight - less than 0.16 kg (0.35 lb), (2) a structural stress margin of safety of 2 at 3326 rpm to provide for positive margin at the design burst condition of 4700 rpm, (3) a fail-safe design in the event the platform-to-blade bond becomes ineffective, and (4) a low radial deflection, less than 0.05 cm (0.020 in.), at tip of platform overhang. In addition, the circular opening required for blade rotation is filled by the platform. The platform is attached to the blade and contoured to match closely the spinner and hub which make up the fan inner aerodynamic contours and provide a smooth inner flowpath. The platform is also designed to avoid interference with adjacent blades and adjacent platforms during variable-pitch blade turning.

Structurally the platform is a varing width tapered beam cantilevered from the blade root. It consists of honeycomb core stabilized by upper and lower graphite/epoxy face sheets which are simultaneously molded and bonded onto the blade using a co-curing process. The result is a one piece platform design. With structural plies extending around the blade root leading and trailing edge undercuts, the single-piece design has the inherent capability of being retained even with a complete loss of the blade-to-platform adhesive bond. This satisfies the fail safe requirements.

Table 8-II. PR288/AS Prepreg Properties.

Property	PR288/AS
Supplier	3M
Process	Film - Continuous Tape
Cure Schedule	2.5 hr at 129° C (265° F)
Postcure Schedule	4 hr at 135° C (275° F)
Flexural Strength	
Room Temperature	193 kN/cm^2 (280 ksi)
121° C (250° F)	138 kN/cm^2 (200 ksi)
Elastic Modulus	
Room Temperature	11.9 kN/cm^2 (17.2 ksi)
121° C (250° F)	11.6 kN/cm^2 (16.8 ksi)
Short Beam Shear	
Room Temperature	9.0 kN/cm^2 (13.0 ksi)
121° C (250° F)	5.2 kN/cm^2 (7.5 ksi)
Charpy Impact	8.0 m-N (6.0 ft-lb)
Fiber Volume, %	59.8
Specific Gravity, g/cm^3	1.58
Void Content, %	0.0

Table 8-III. Composite Material Properties.

	PR288 AS-Graphite	PR288 Boron	PR288 S-Glass	PR288 Kevlar 49
Fiber volume, Percent	60	55	60	60
Elastic Modulus, MN (10^6 psi) (0° Orientation)	11.9 (17.2)	20.0 (29.0)	5.9 (8.5)	7.6 (11.0)
Elastic Modulus, MN (10^6 psi) (90° Orientation)	1.1 (1.6)	1.2 (1.8)	0.8 (1.1)	0.6 (0.8)
Elastic Modulus, MN (10^6 psi) (0/22/0/-22 Orientation)	9.5 (13.8)	11.7 (17.0)	4.7 (6.8)	5.9 (8.6)
Shear Modulus, MN (10^6 psi) (0/22/0/-22)	1.1 (1.6)	1.9 (2.7)	0.6 (0.9)	0.6 (0.93)
Poisson's Ratio (0/22/0/-22)	0.65	0.97	0.39	0.90
Density, G/cm^3 (lb/in^3)	1.5 (0.056)	1.9 (0.070)	2.0 (0.072)	1.4 (0.050)
Tensile Strength, kN/cm^2 (ksi) (0°)	138 (200)	138 (200)	138+ (200+)	138 (200)
Tensile Strength, kN/cm^2 (ksi) (0/22/0/-22)	95 (138)	95 (138)	95+ (138)	95 (138)
Flex Strength, kN/cm^2 (ksi) (0°)	193 (280)	---	---	62 (90)
Flex Strength, kN/cm^2 (ksi) (0/22/0/-22)	168 (244)	---	172 (250)	59 (85)
Shear Strength, kN/cm^2 (ksi) (0°)	9.0 (13.0)	7.6 (11.0)	8.1 (11.8)	3.4-7 (5-10)
Charpy Impact, m-N (ft-lb) (±10°)	8 (6)	10 (7.5)	47 (35)	23 (17)

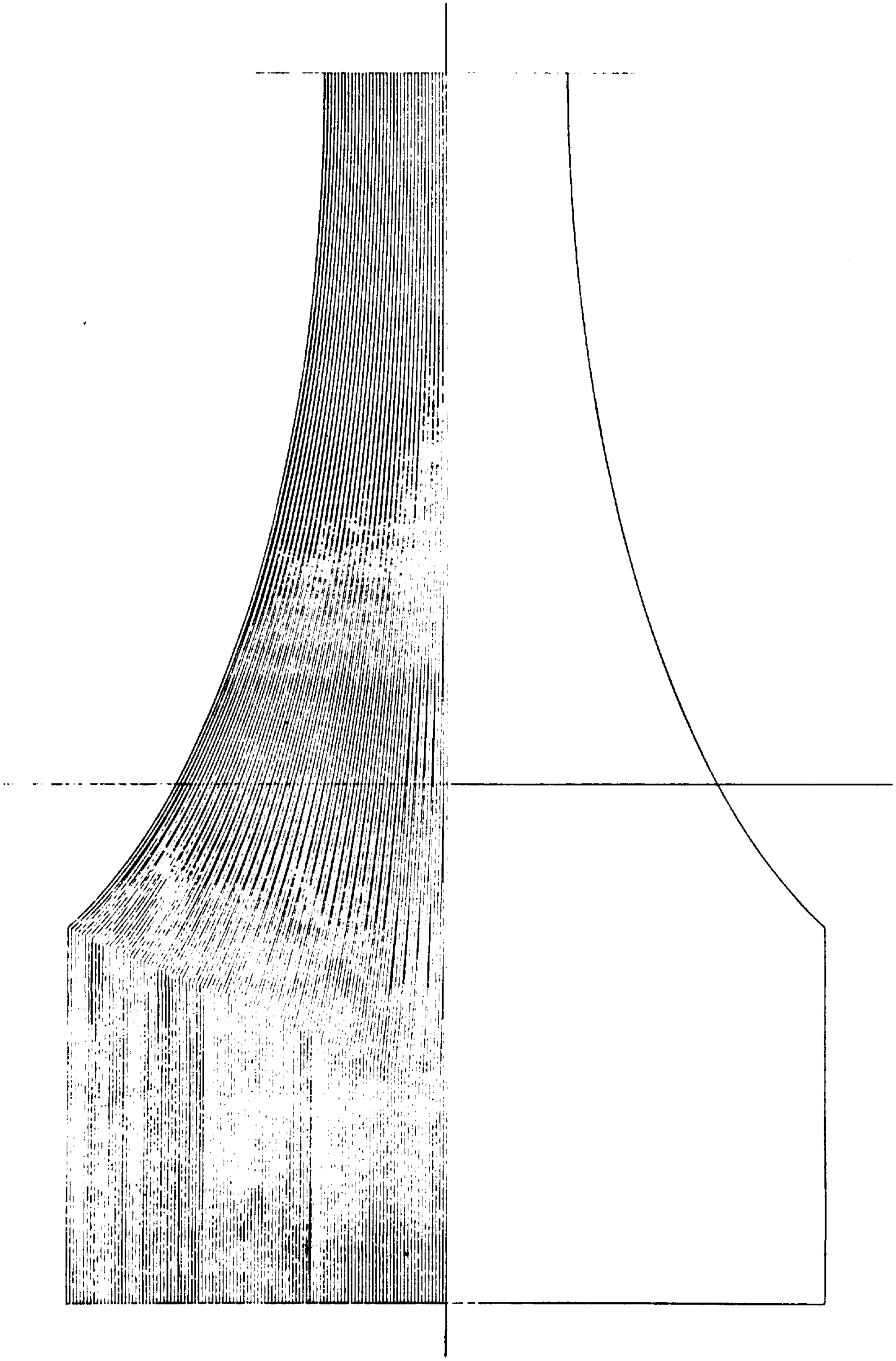

Figure 8-9. Dovetail Molded Section.

Figure 8-3 shows the final platform on the blade, while Figure 8-10 is a schematic showing the platform details.

8.2.3 Design Analysis

Blade Stress and Deflection Analysis

The blade stress analysis was performed using the 3-D finite element computer program "PARA-TAMP-EIG". This program is a parametric, 3-D, finite element eigenvalue and thermal stress computer program. The program accounts for the inertia forces of rotation and vibration. Account is taken of the stiffening effect of rotation. The program gives directly the lowest eight modes, stresses, and frequencies for a specified speed of rotation. In addition, it gives deflections and stresses at any given operating rpm. The material properties are 3-D anisotropic. Thermal stresses are also computed.

The finite element model used for the blade analysis was generated to geometrically represent the blade design, without platform, as shown in Figure 8-6.

A number of computer runs were made to provide steady-state stresses under centrifugal and pressure loading conditions and vibratory (eigenvalue/eigenvector) relative stresses at zero and speed conditions assuming the blade dovetail to be fixed at the radial cross section corresponding to the PA plane as defined in Figure 8-6. The steady-state results at 3326 rpm (the blade duty cycle steady-state speed) show that the highest tensile stresses exist in the airfoil-to-dovetail transition region slightly above the leading edge undercut. The highest calculated tensile stress is 15,490 N/cm^2 (22,460 psi). The highest compressive stress is 3790 N/cm^2 (5,500 psi) at the corresponding trailing edge location. The highest calculated shear stress is 3400 N/cm^2 (4930 psi) in the region of the leading edge overhang. The material minimum tensile, compressive, and shear strengths are 58,600 N/cm^2 (85,000 psi), 17,240 N/cm^2 (25,000 psi), and 4,480 N/cm^2 (6,500 psi), providing margins of safety of 2.7, 3.5, and 0.3, respectively. The shear strength safety of margin at the leading edge undercut region is expected to be improved by the addition of the platform which will share in carrying the shear loads to the dovetail. Figure 8-11 shows a plot of stresses as a function of blade span length while Figures 8-12, 8-13, and 8-14 show stress maps for the concave and convex blade faces for radial stress, chordwise stress, and interlaminar shear stress, respectively. Figure 8-15 is a plot of blade deflection and twist as a function of span length. Figures 8-16, 8-17, and 8-18 show relative radial stresses over the blade for the first three vibratory modes. These maps of relative radial stresses under vibratory conditions show the changes in stress locations for the different vibratory modes.

Blade vibratory strengths as determined from specimens and preliminary QCSEE blade testing are shown on the stress range diagram in Figure 8-19. The anticipated maximum vibratory stress is 11 ksi single amplitude on the basis of testing on other engine programs. For the steady-state conditions

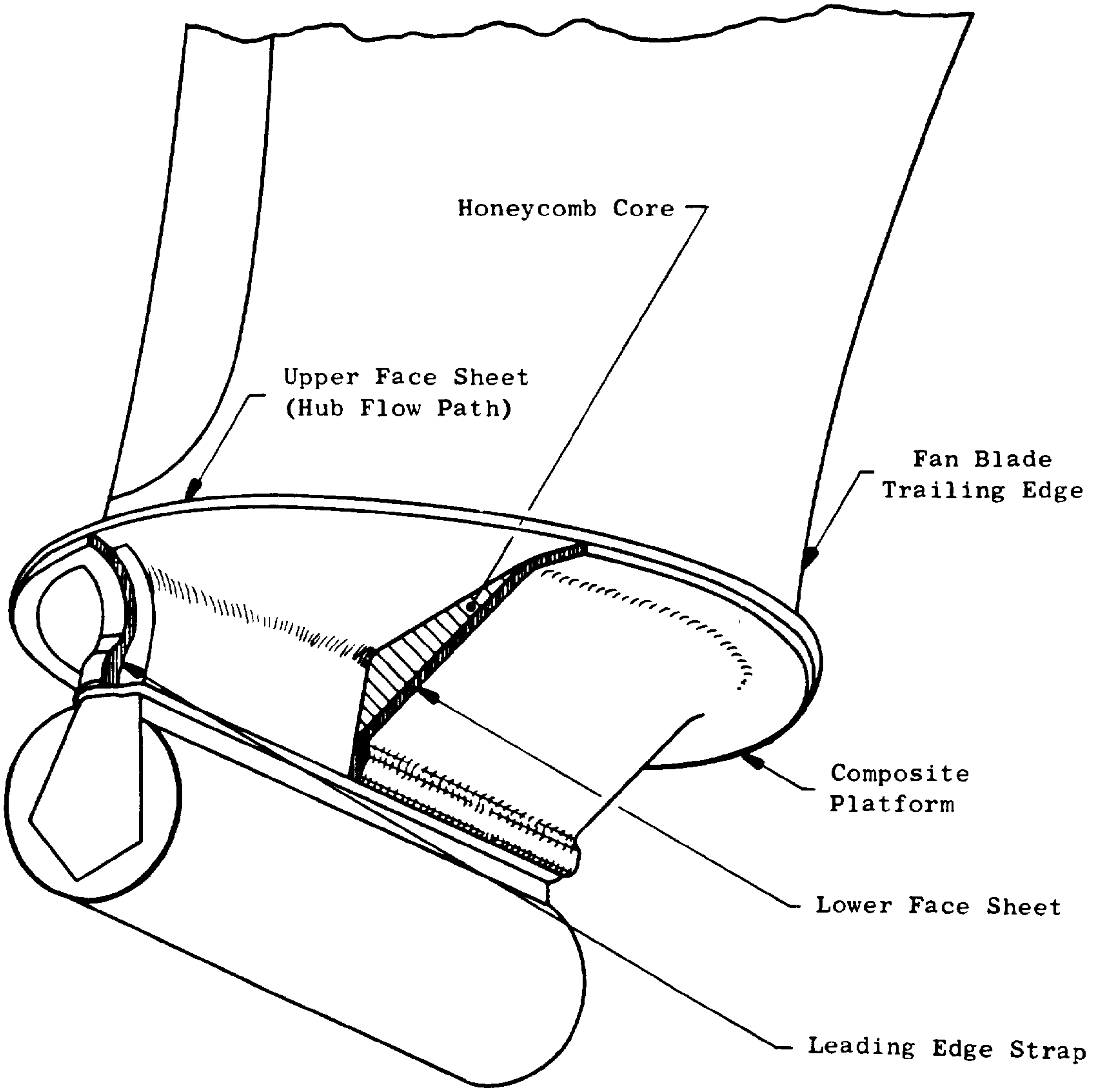
Honeycomb Core
Upper Face Sheet
(Hub Flow Path)
Fan Blade
Trailing Edge
Composite
Platform
Lower Face Sheet
Leading Edge Strap

Figure 8-10. Platform Design.

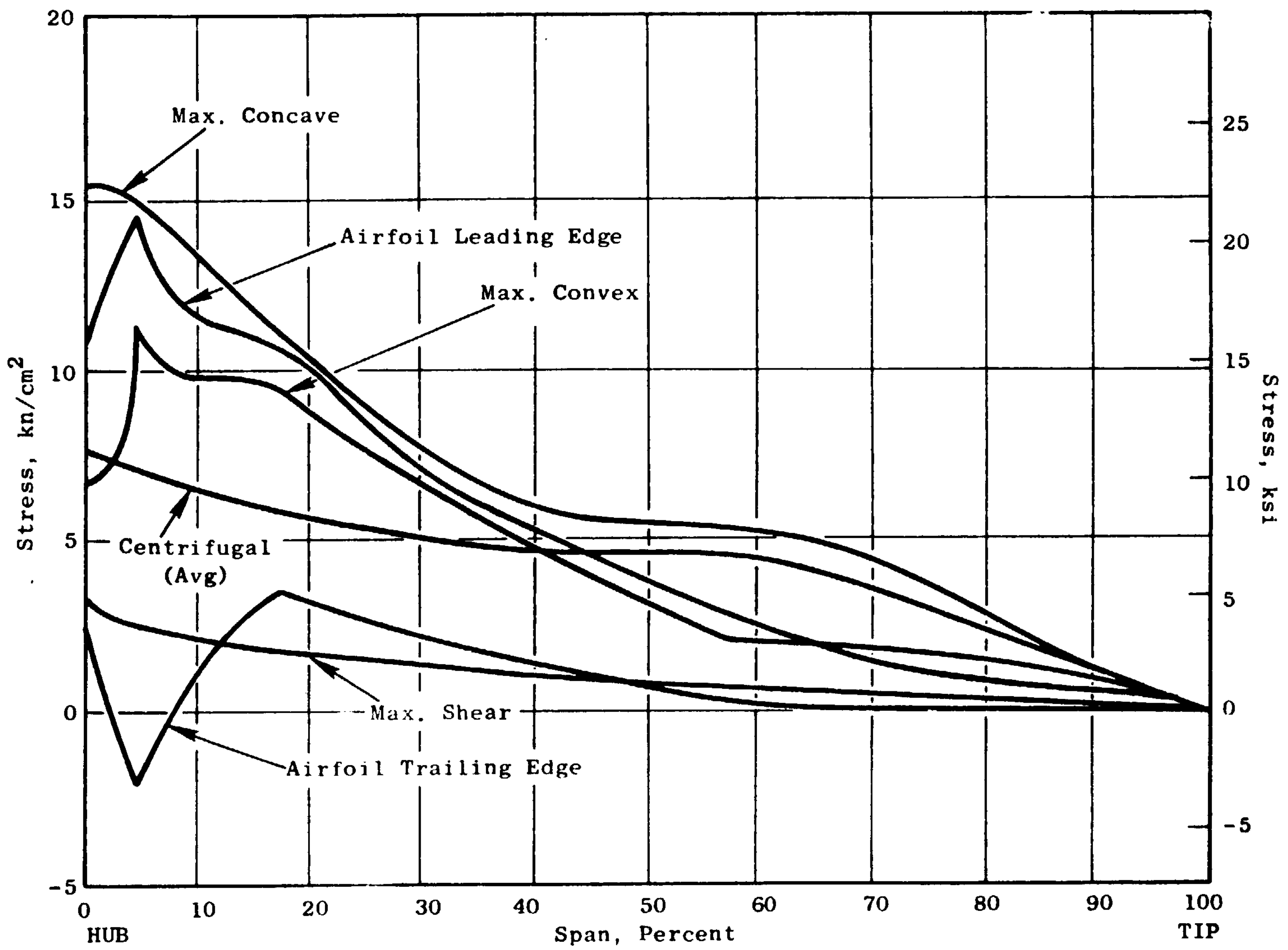

Figure 8-11. UTW Blade Resultant Radial Stress - 3326 rpm.

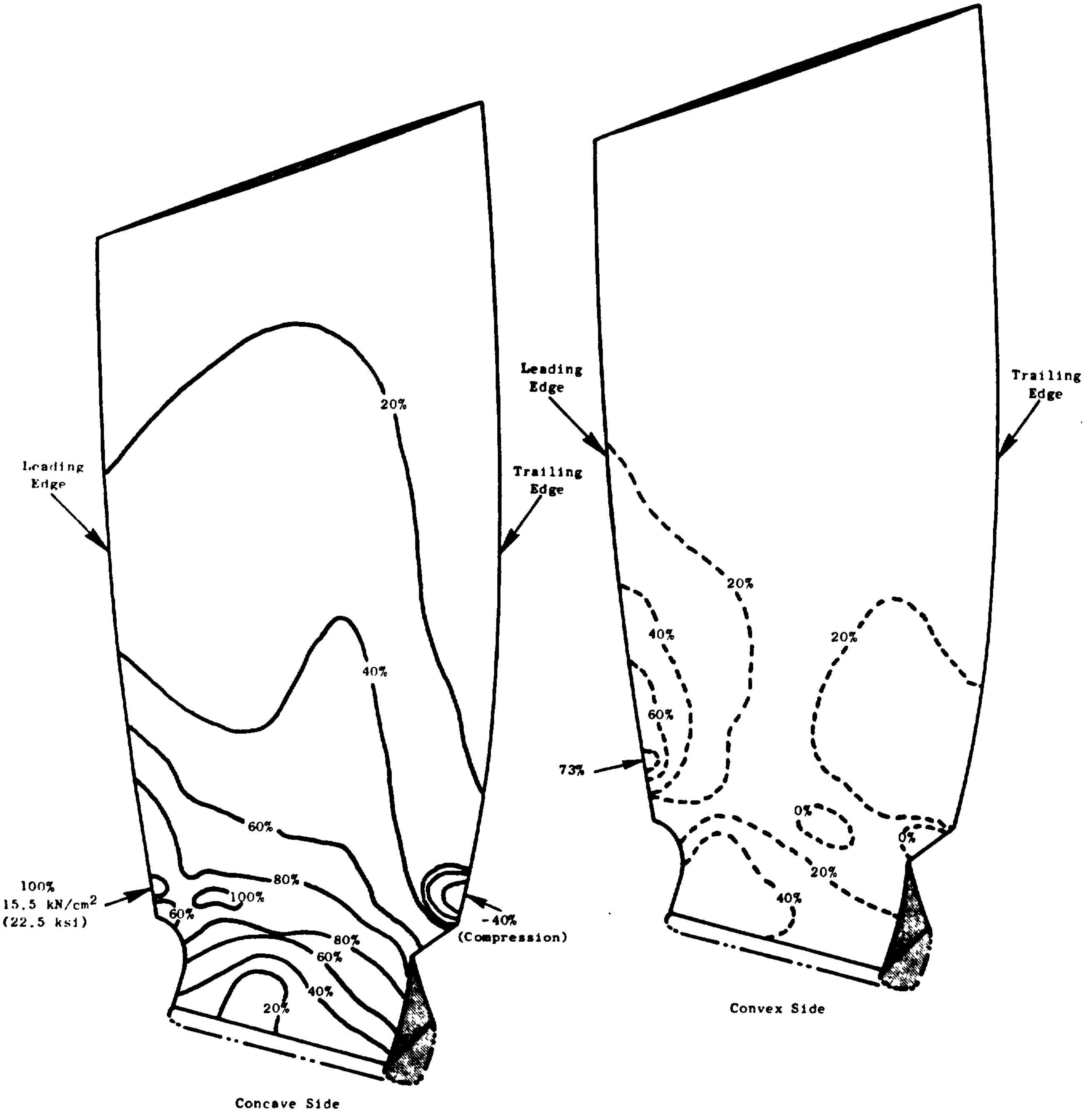
Leading Edge
Trailing Edge
20%
40%
60%
80%
100%
100%
15.5 kN/cm²
(22.5 ksi)
60%
80%
60%
40%
20%
-40%
(Compression)
Concave Side
Leading Edge
Trailing Edge
20%
40%
20%
60%
73%
0%
0%
20%
40%
Convex Side

Figure 8-12. Calculated Blade Radial Stress.

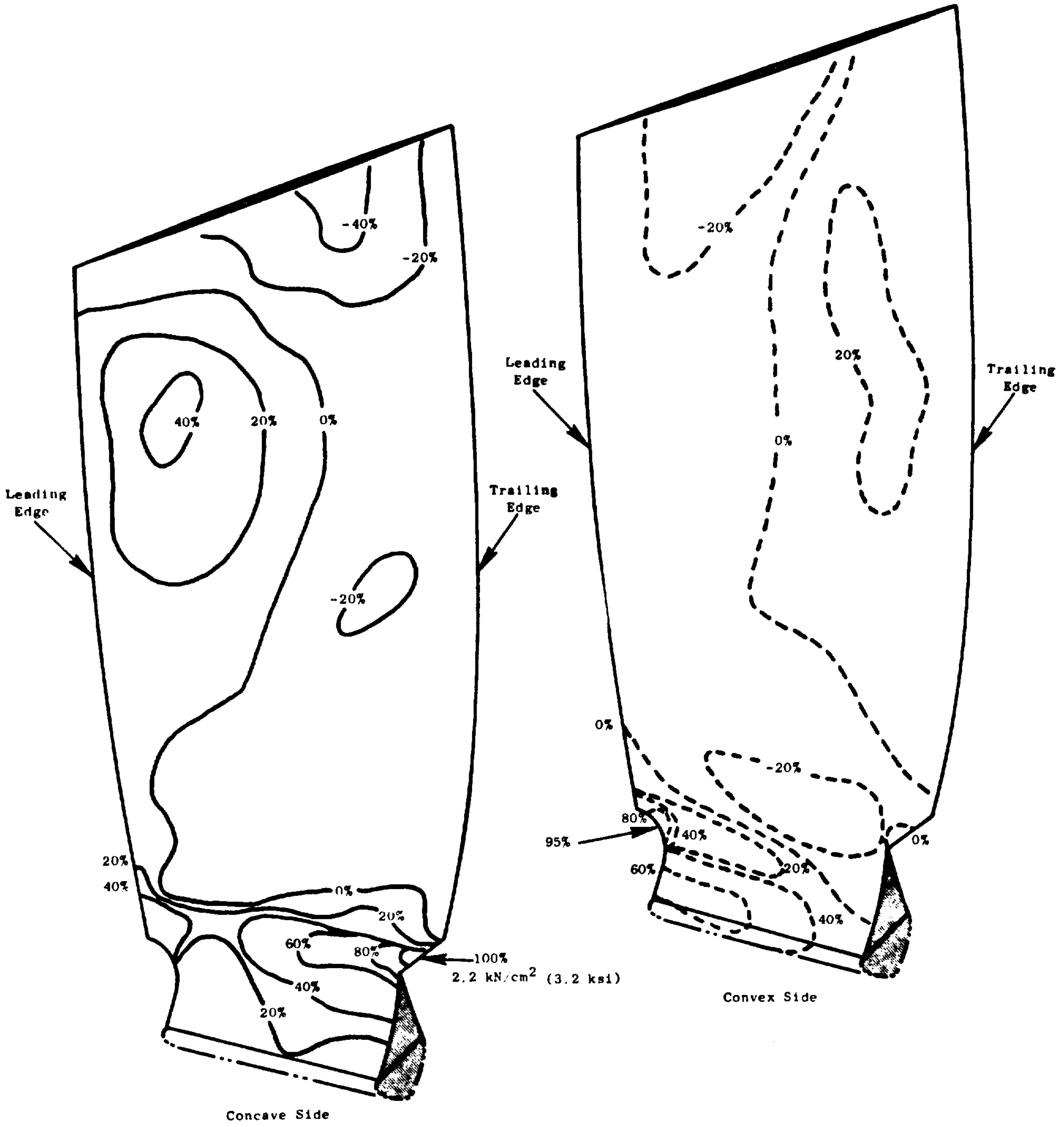
Leading Edge
Trailing Edge
-40%
-20%
40%
20%
0%
-20%
20%
40%
0%
20%
60%
80%
100%
2.2 kN/cm² (3.2 ksi)
40%
20%
Leading Edge
Trailing Edge
-20%
20%
0%
0%
-20%
80%
95%
40%
60%
20%
40%
0%

Concave Side

Convex Side

Figure 8-13. Calculated Blade Chordal Stress.

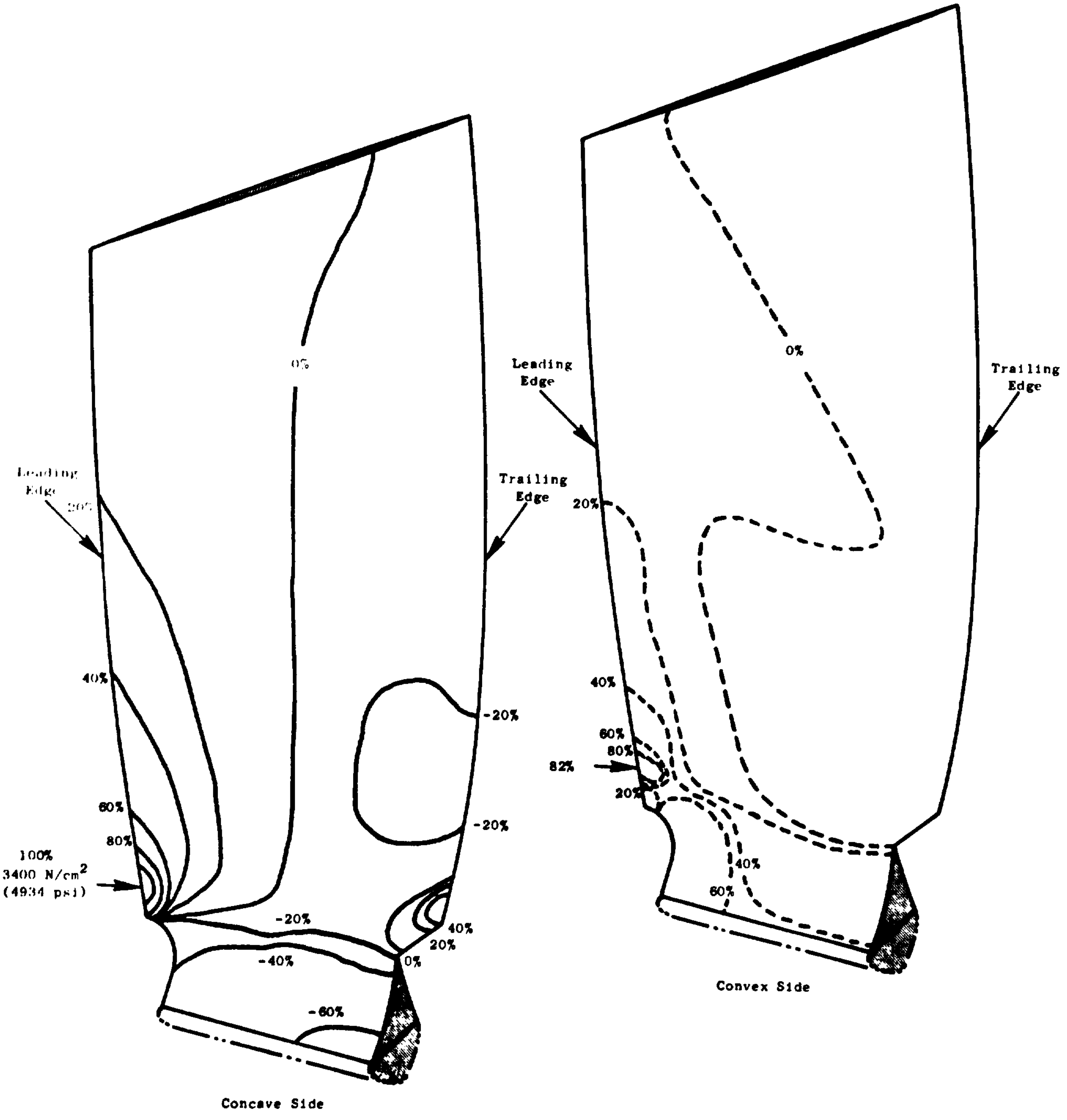
0%
Leading Edge
20%
Trailing Edge
40%
-20%
-20%
60%
80%
100%
3400 N/cm^2
(4934 psi)
-20%
40%
20%
-40%
0%
-60%
0%
Leading Edge
Trailing Edge
20%
40%
60%
80%
82%
20%
40%
60%

Concave Side

Convex Side

Figure 8-14. Calculated Blade Interlaminar Shear Stress.

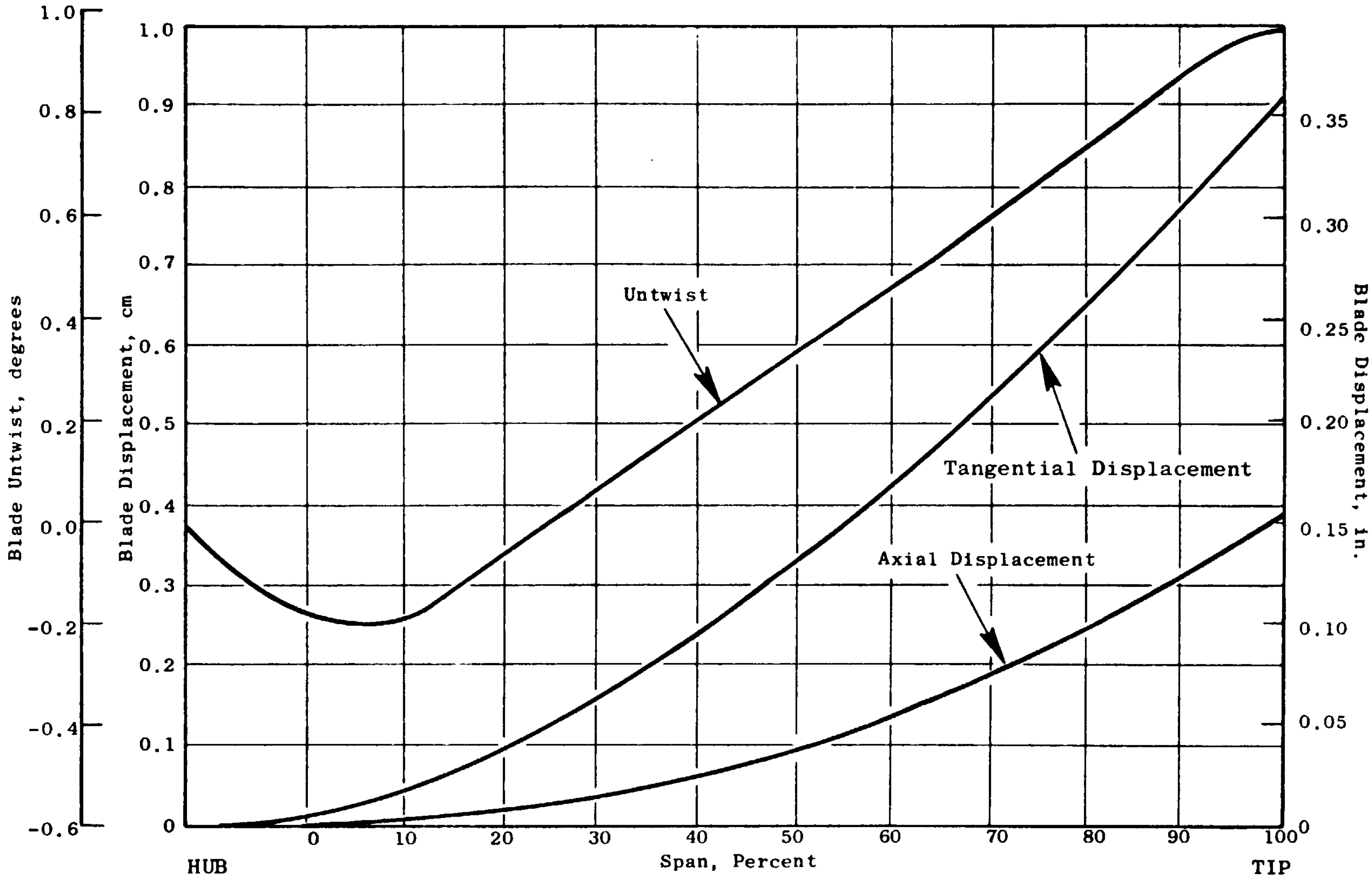

Figure 8-15. UTW Blade Displacements and Twist.

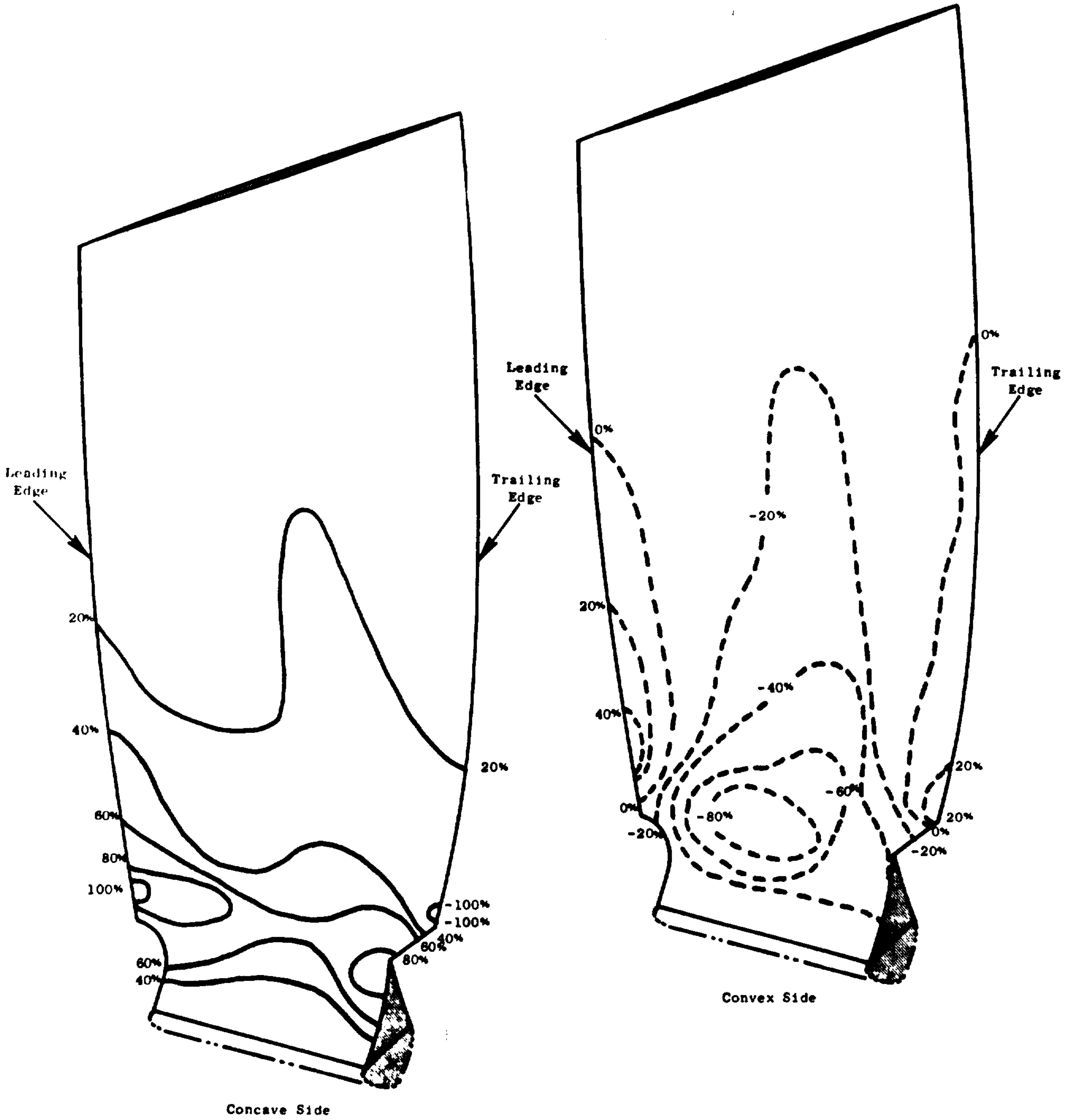
Leading Edge
Trailing Edge
20%
40%
60%
80%
100%
60%
40%
20%
-100%
-100%
40%
80%
80%
Concave Side
Leading Edge
Trailing Edge
0%
0%
20%
40%
0%
-20%
-20%
-40%
-60%
-80%
20%
20%
0%
-20%
Convex Side

Figure 8-16. Calculated Blade Relative Radial Stresses for First Flexural Mode.

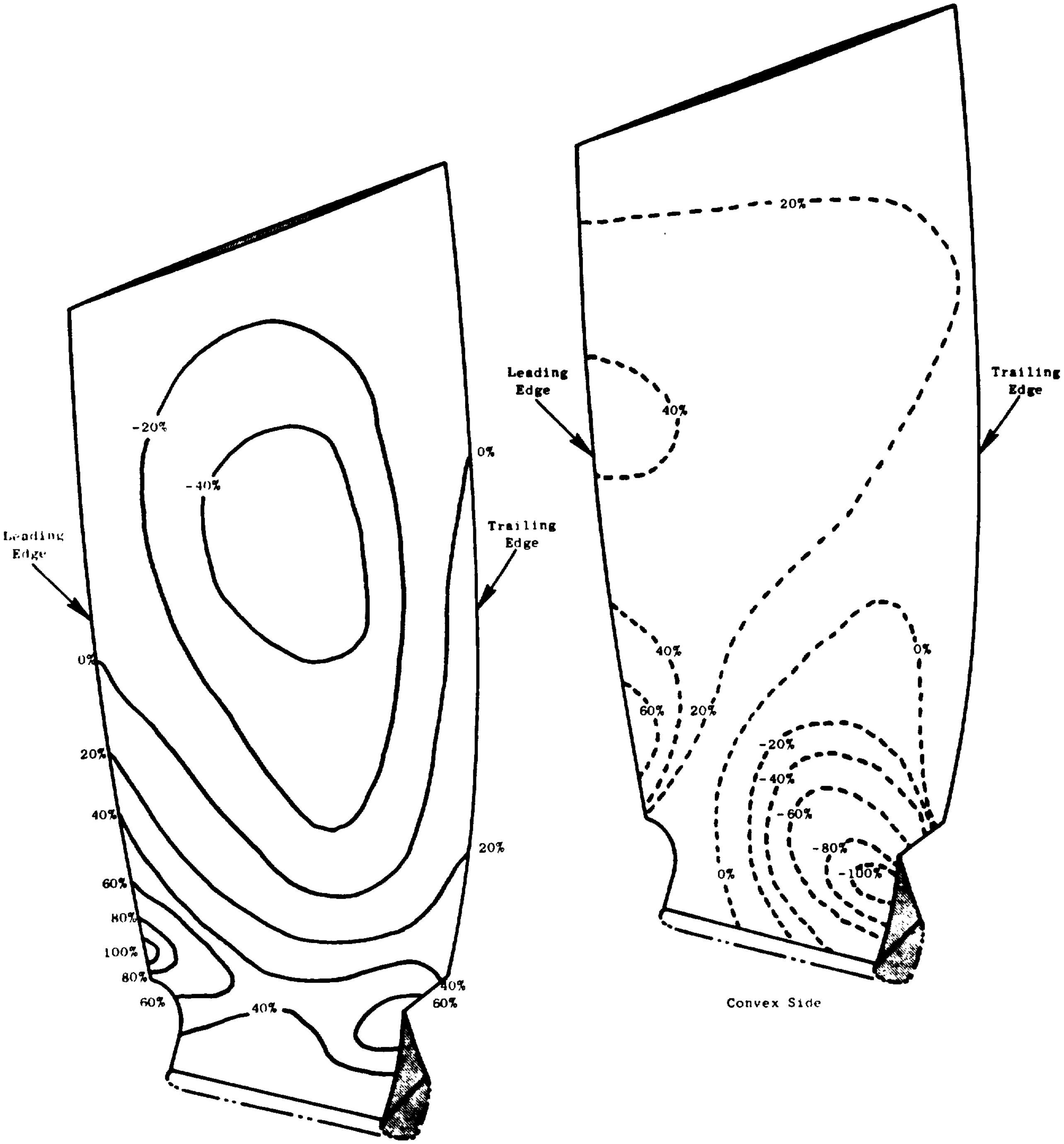

Leading Edge
-20%
-40%
0%
Trailing Edge
0%
20%
40%
60%
80%
100%
80%
60%
40%
20%
40%
60%
20%
Leading Edge
40%
Trailing Edge
40%
0%
60%
20%
-20%
-40%
-60%
-80%
-100%
0%

Concave Side

Convex Side

Figure 8-17. Calculated Blade Relative Radial Stresses for Second Flexural Mode.

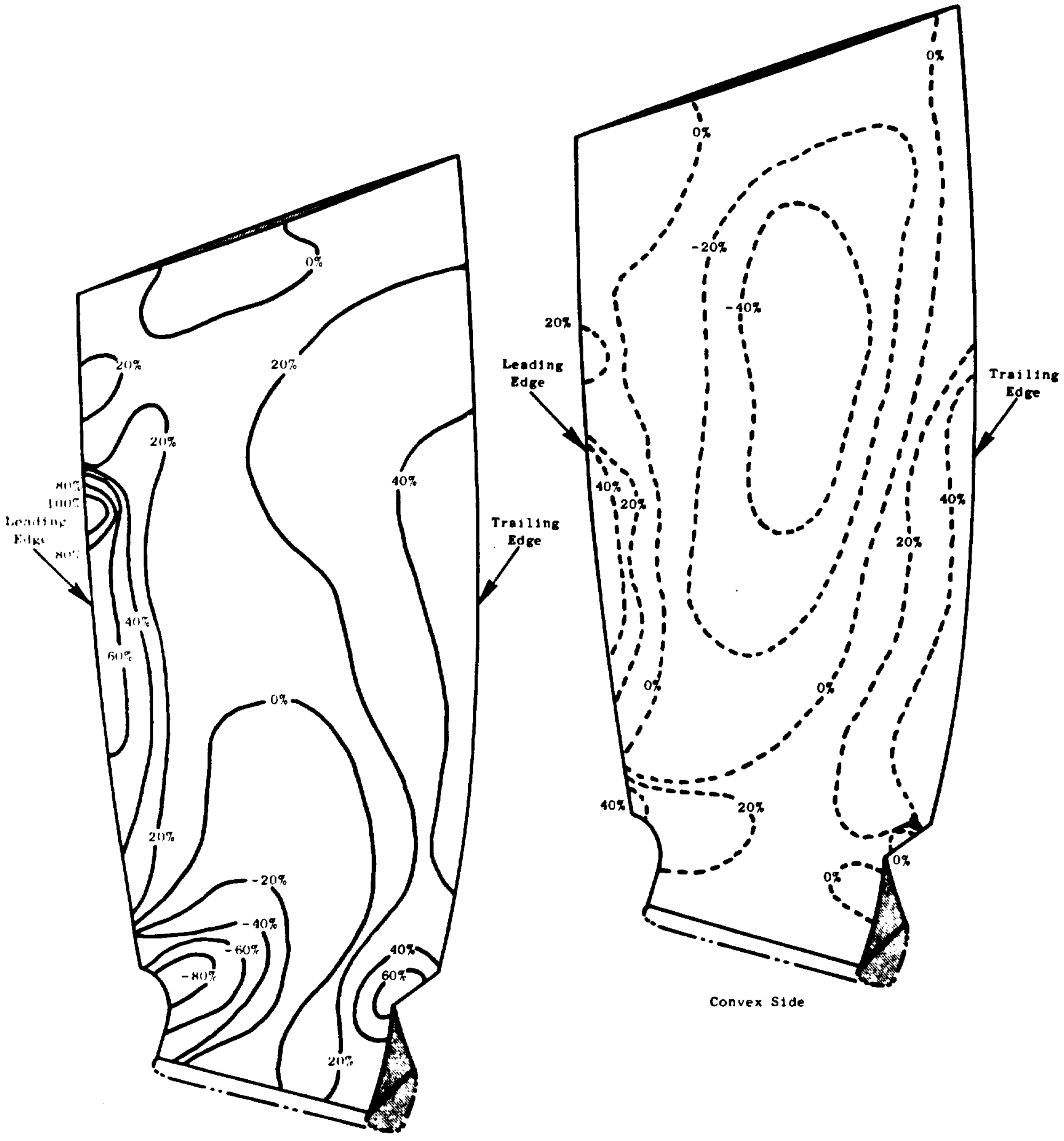
0%
20%
20%
20%
80%
100%
Leading Edge
80%
40%
Trailing Edge
40%
60%
0%
20%
-20%
-40%
-60%
-80%
40%
60%
20%
Concave Side
0%
0%
-20%
-40%
20%
Leading Edge
Trailing Edge
40%
20%
40%
20%
0%
0%
40%
20%
0%
0%
Convex Side

Figure 8-18. Calculated Blade Relative Radial Stresses for First Torsional Mode.

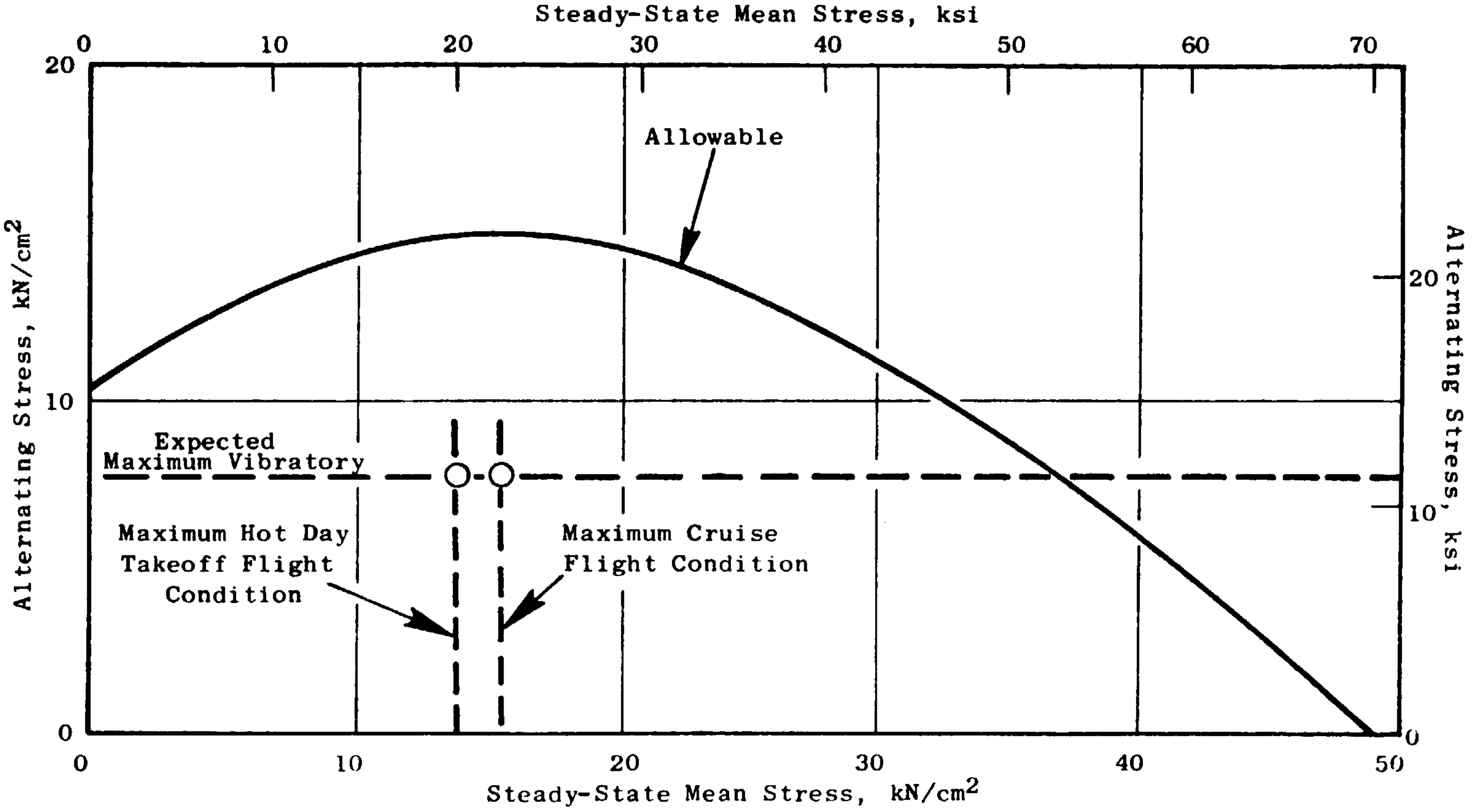

Figure 8-19. Allowable Stress Range Diagram - Blade Radial Stress.

shown, that of a hot day takeoff and maximum standard day cruise, the combination of steady-state mean stress and expected maximum vibratory stress results in an acceptable blade life.

The blade composite dovetail stresses were determined using the radial load distribution from the above blade analysis and experimental data from previous 2-D dovetail specimens and blade testing. Maximum dovetail crushing stress is calculated to be 15,290 N/cm^2 (22,180 psi) and maximum dovetail calculated shear stress is 4760 N/cm^2 (6900 psi) at a blade speed of 3326 rpm. The allowable dovetail crushing and shear strengths are 55,160 N/cm^2 (80,000 psi) and 16,550 N/cm^2 (24,000 psi), respectively, showing adequate static strength margins of safety in each case. These strengths were further verified by two blade-dovetail pull tests which demonstrated corresponding minimum crushing and shear strengths of 56,750 N/cm^2 (82,300 psi) and 17,650 N/cm^2 (25,600 psi), respectively. It is expected that these strengths would actually be higher since the test load reached the capability of the loading fixture without dovetail failure.

The dovetail vibratory strengths were projected from previous composite experimental data and the QCSEE dovetail static strength data. Figure 8-20 shows the allowable stress range diagram for dovetail crushing and Figure 8-21 shows the allowable stress range diagram for dovetail shear. The anticipated maximum single-amplitude vibratory stresses are 5580 N/cm^2 (8100 psi) in crushing and 2340 N/cm^2 (3400 psi) in shear and are based on the anticipated maximum blade radial vibratory stresses. For the steady-state conditions shown, that of hot day takeoff and maximum cruise, the combination of steady-state mean stress and expected maximum vibratory stress results in an acceptable dovetail life.

Platform Stress and Vibration Analysis

The analytical approach used in evaluating the platform was to calculate the stresses and mechanical frequencies using simple conservative models of unit width cross sections representing the platform design. The stresses were calculated for the platform operating in the 5259 "g" centrifugal force field resulting from 100% speed operation at 3326 rpm. Positive margin at a 41% overspeed condition of 4700 rpm is met by maintaining a margin of safety, MS = 2, at 3326 rpm. As a further precaution to guard against a possible material property loss from the planned manufacturing co-curing process, only 70% of the published material allowable is used.

Figure 8-22 shows a cross section of the platform. Since the outer face sheet (location 5 flowpath surface, Figure 8-22) is an eccentric compressively loaded sheet operating in a centrifugal force field producing lateral loading, and is stabilized by the honeycomb bond, it has been investigated for its beam-column capability. It is designed to be adequate even with a partial loss of honeycomb bond. For correlation with the analysis and to investigate various alternate design features, typical platform sections have been manufactured and tested. The testing has supported the analytical findings and, at location 3, has identified the load-carrying capability to be greater

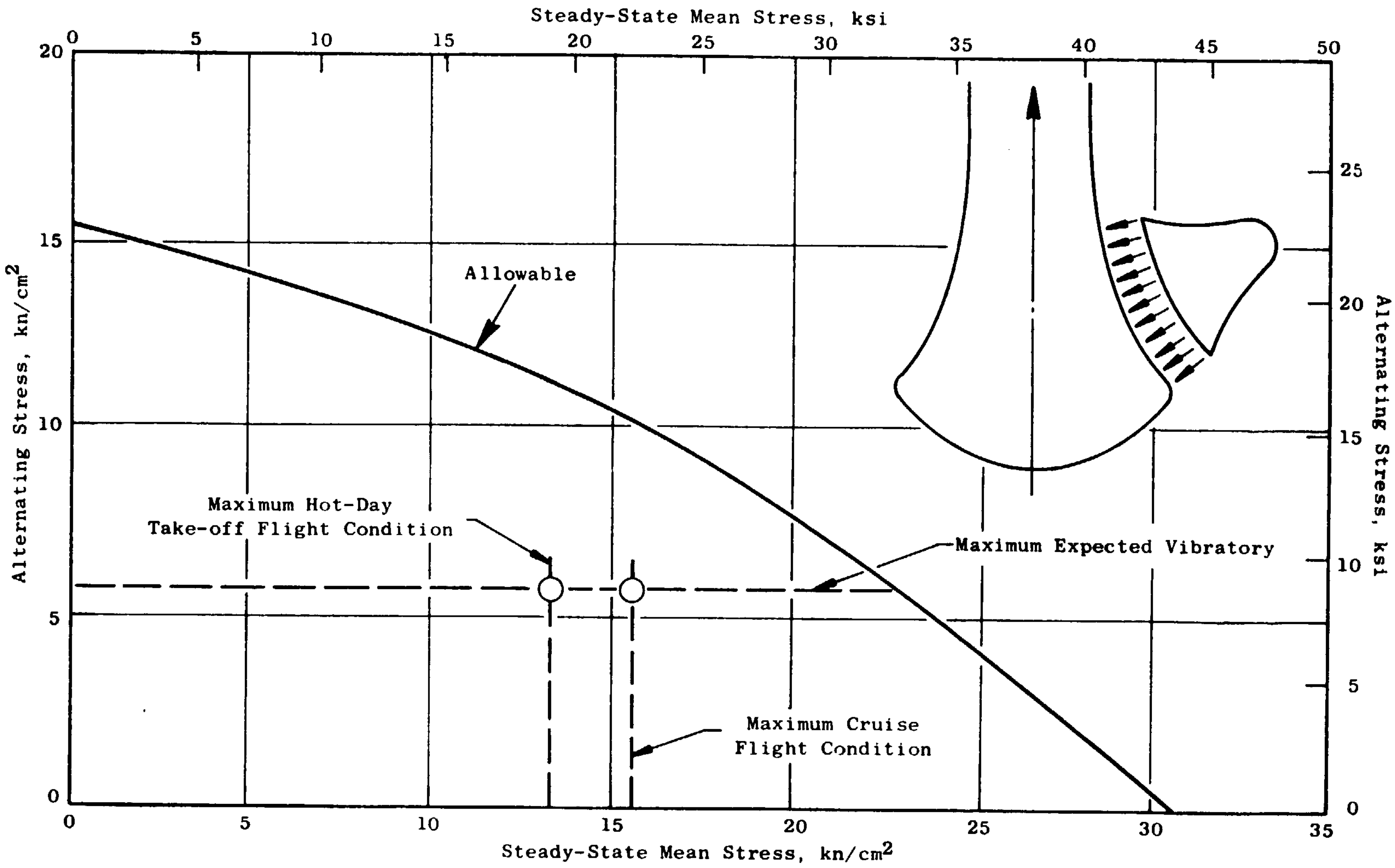

Figure 8-20. Allowable Stress Range Diagram - Blade Radial Stress.

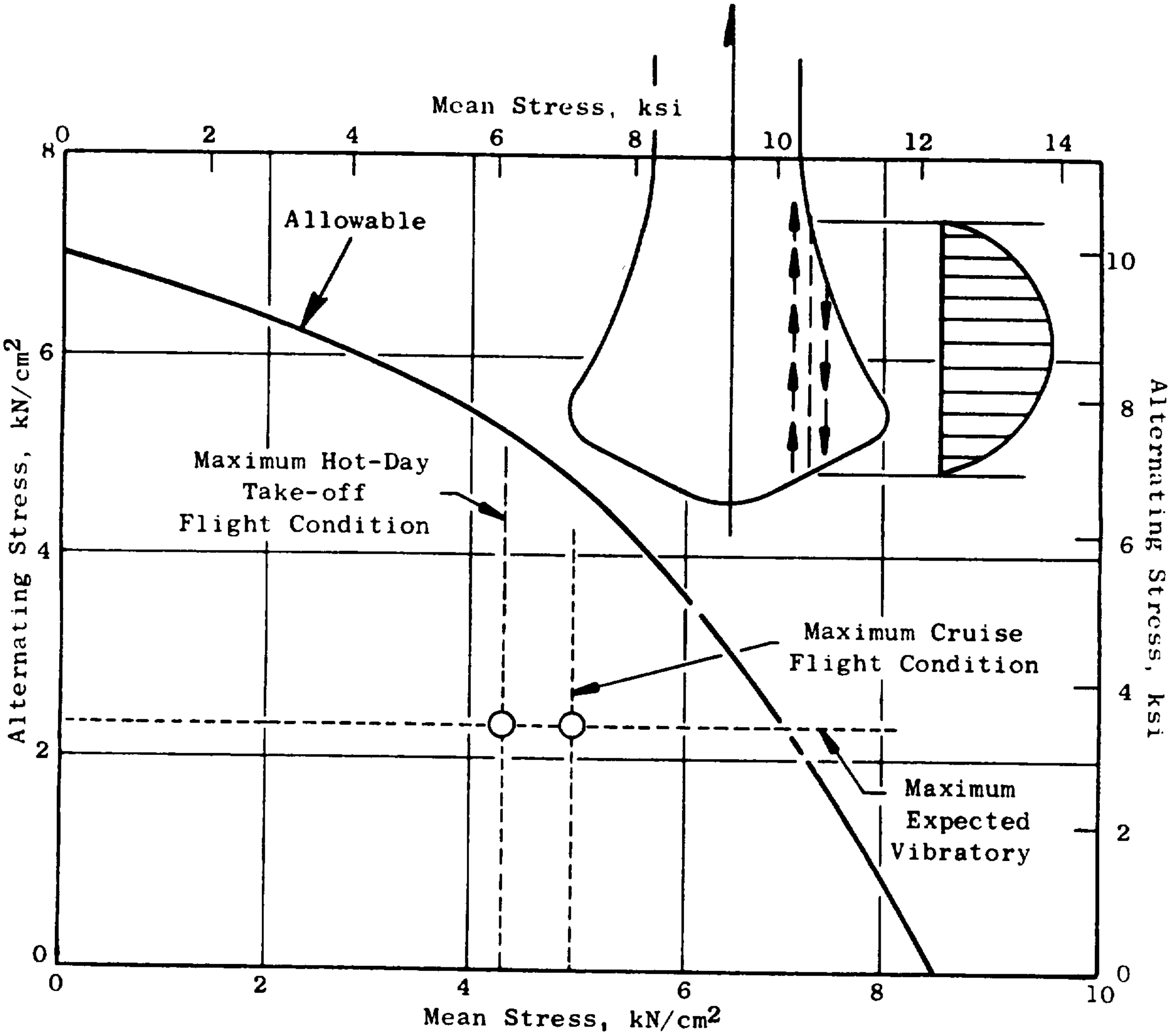

Figure 8-21. Allowable Stress Range Diagram - Dovetail Shear Stress.

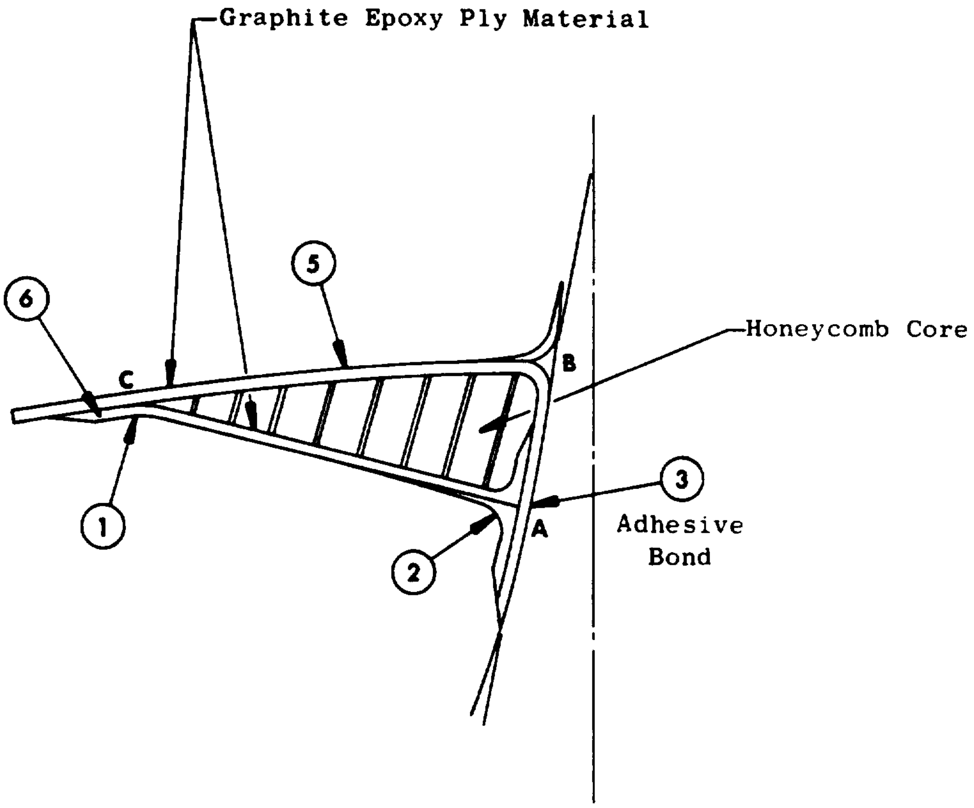
Graphite Epoxy Ply Material
6
5
C
B
Honeycomb Core
1
2
3
A
Adhesive Bond

Figure 8-22. Platform Cross Section.

than 490 N/cm (280 lb/in.) normal to the blade centerline. This has allowed a MS = 2 at location 3 to be identified by test where an otherwise difficult analysis would be required to identify the maximum stress.

A stress and margin of safety summary is presented in Table 8-IV for six points of interest.

The platform is modeled and the vibratory characteristics are investigated from three points of view. First, the platform is considered cantilevered from the blade. Second, as a member running from fore to aft, it is considered free from the blade to flex in a free-free (floating) condition, and in the tangential direction (still free from the blade), it is considered to be cantilevered from the leading and trailing edge straps. Third, the upper face sheet with a partial loss of the honeycomb bond is considered. The first natural frequency for these various models is tabulated in Table 8-V.

The platform is stiffer than any of the models used to calculate the first natural frequency. Therefore, the platform's first natural frequency is higher than those calculated and will be above the excitation frequencies of the blade.

The platform weight at less than 0.16 kg (0.35 lb) is composed of 20% honeycomb, 10% adhesive, and 70% graphite/epoxy composite.

The platform is fabricated in one piece which is simultaneously molded and bonded onto the composite blade using a co-curing process. The upper face sheet or flowpath contour is controlled by a hard die fitted around the blade. The graphite/epoxy upper face sheet is layed-up on the contour formed by the die and blade root surface. A contoured aluminum honeycomb core is next put in place followed by the lower face sheet layed-up on the honeycomb core. The layed-up assembly is then put into a vacuum bag and the entire assembly is co-cured onto the blade. The result is a one-piece platform design. The outer contour of the platform overhang is then trimmed to final dimensions.

Blade Vibration Analysis

Blade "instability" or "limit cycle vibration" can be a problem on fans. It is characterized by a high amplitude vibration in a single mode (normally the first flexural or torsional mode) at a nonintegral per-rev frequency. Because of the nonlinearity in the aerodynamics involved, it has resisted practical solutions by solely theoretical means. Accordingly, General Electric has adopted a semiempirical "reduced velocity parameter" approach for limit cycle avoidance. Reduced velocity parameter, V_R, gives a measure of a blade's stability against self-excited vibration. This parameter is defined as:

$$V_R = \frac{W}{bf_t}$$

Table 8-IV. Platform Stresses and Margins of Safety.

Location of Interest	Description and Type of Stress	Stress kN/cm^2 (ksi)	Margin of Safety
1	Flexural Stress in Overhang up to 2.5 cm (1 inch) with Additional Single Thickness Overhang up to 1 cm (0.400 inch)	$\sigma \leq 16.5$ (24)	> 2.0
2	Tensile Stress in Lower Face Sheet	$\sigma \leq 13.8$ (20)	> 2.2
3	Tensile Stress Capability at this Location Is Correlated with Test Results	--	> 2.0
4 Not Shown	Tensile Stress in Leading Edge Strap	$\sigma \geq 13.8$ (20)	> 2.0
5	Combined Compression and Flexural Stress in Upper Face Sheet	$\sigma \leq 24$ (35)	> 2.0
6	Shear Stress between Upper and Lower Face Sheets	$\tau > 0.05$ (0.07)	> 2.1

Table 8-V. Platform Natural Frequencies.

Models Considered	First Natural Frequency
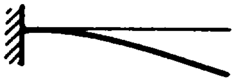 Cantilever (Platform)	$f_1 > 5000$ Hz
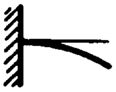 Cantilever (Platform Overhang)	$f_1 > 2000$ Hz
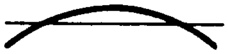 Free-Free (Platform)	$f_1 > 8000$ Hz
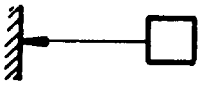 Cantilevered Mass (End Straps Supporting a Free Platform)	$f_1 > 1500$ Hz
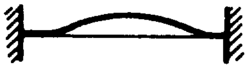 Clamped Beam (Face Sheet Partial Loss of H/C Bond)	$f_1 > 1500$ Hz

where:

b = 1/2 chord at 5/6 span, m

W = average air velocity relative to the blade over the outer third of the span, m/sec

f_t = first torsional frequency at design rpm, rad/sec.

The basic criterion used for setting the design of the UTW composite blade was the requirement of having a reduced velocity parameter in the range of 1.3 to 1.4. This allowable range is based on previous testing of a variety of fan configurations in combination with the specific aerodynamic design of the UTW blade. The 18-blade design using a hybrid of boron, graphite, and Kevlar material was selected to provide the desired aeromechanical requirements. The operating and stall characteristics of this blade are presented in Figure 8-23 in terms of reduced velocity versus incidence angle. This shows the capability of reaching full rotation stall prior to encountering blade instability.

The Campbell diagram for the UTW blade assembled in the trunnion and disk is shown in Figure 8-24. The coupled frequency of the blade-trunnion assembly, as plotted here, is somewhat lower than the individual blade frequencies due to the flexibility of the supporting trunnion and disk. The expected first flexural frequencies at 2/rev crossover is shown to be at 67% speed. This is above the engine flight idle speed and below the normal operating speed for takeoff, climb, and maximum cruise flight conditions; it is therefore considered a transient point in the flight mission and not subject to continuous steady-state conditions. Blade excitation stresses at 2/rev crossover will be monitored during engine testing. Blade pitch and speed changes will be employed should the stress levels become excessive.

The margin for first flexural frequency over 1/rev at 115% speed is approximately 50%, and the margin for first flexural frequency below 2/rev at 100% speed is approximately 13%.

The second flexural mode crosses several per/rev lines in the operating speed range. Each of these crossings represent a potential for forced resonances, however, it takes considerably more energy to drive the higher vibration frequencies, such as second flex, and no problems are anticipated.

The first torsional frequency 6/rev crossover is at approximately 83% speed with the 100% speed frequency margin being approximately 6% over 5/rev. Since the excitation forces should be small at the higher order crossovers, no vibratory problems are anticipated during normal engine operating conditions.

Blade Impact Analysis

In addition to the need to satisfy flutter requirements, resistance to bird impact is also of major importance. Flight engine QCSEE blades must be

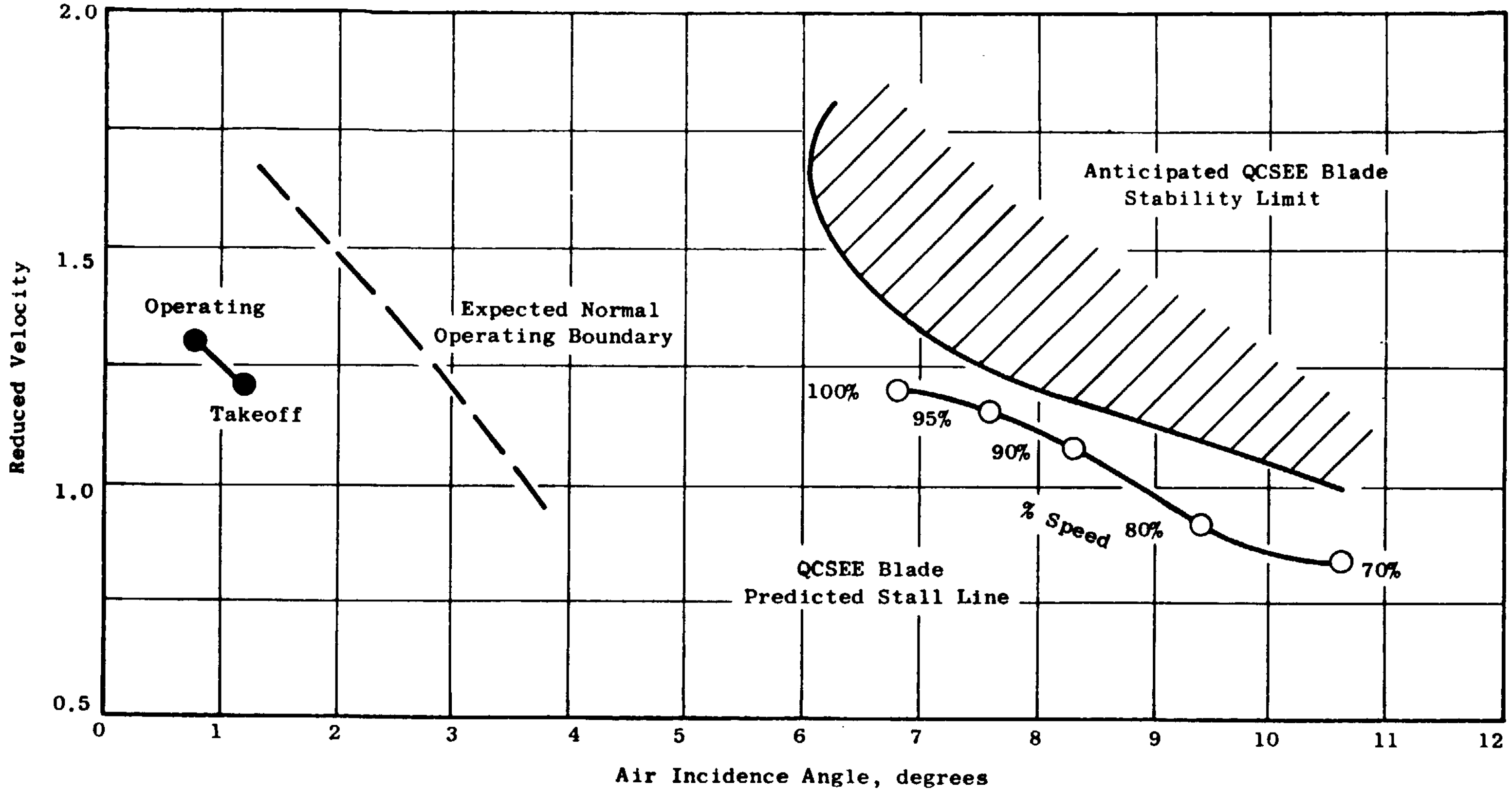

Figure 8-23. Limit Cycle Boundaries.

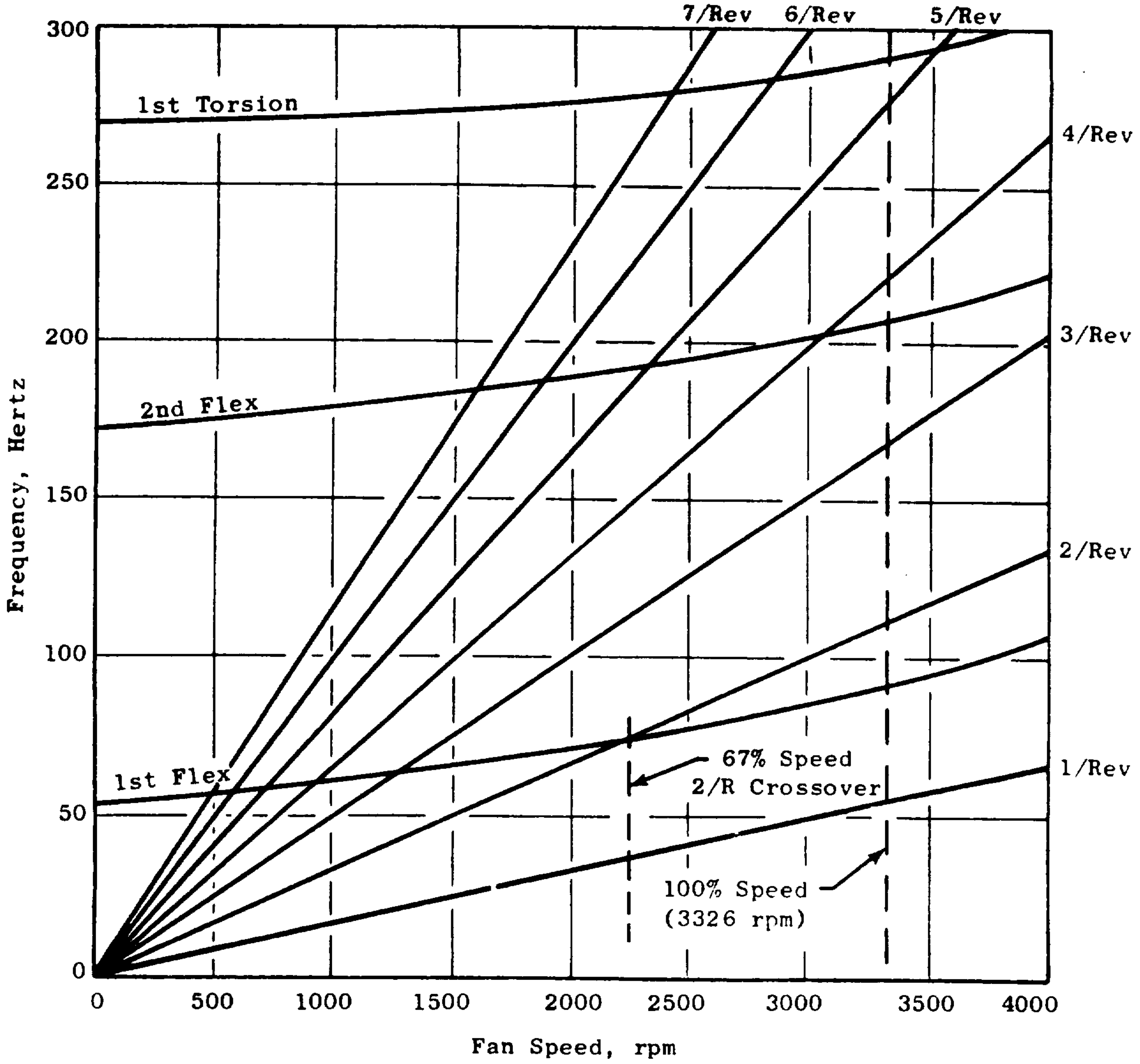

Figure 8-24. Campbell Diagram - UTW Composite Blade.

capable of absorbing the impact of 16, 0.085 kg (3 oz) birds (starlings); 8, 0.68 kg (1.5 lb) birds (pigeons); and a 1.8 kg (4 lb) bird in order to satisfy FAA specifications. The objectives are to sustain little or no damage during starling ingestion, be able to maintain 75% engine thrust following pigeon ingestion, and be able to have a safe engine shutdown with all damage being contained within the engine casing following ingestion of a 1.8 kg (4 lb) bird.

Two different damage modes require consideration in the design. The first is a brittle root-type fracture which can result in the blade breaking off close to the dovetail, and the second is local damage which can result in airflow delamination and loss of material.

The projected elimination of root failures during large bird impact in the QCSEE blade has been achieved. The necessary flexibility and strain-to-failure capability has been built into the blade root through the use of hybrid materials. The dovetail design provides for energy dissipation through centrifugal recovery and increase in friction energy. Figure 8-25 illustrates the magnitude of energy that has to be absorbed by the blade at the root, tip, and pitch for the spectrum of relative bird velocities for a 1.8 kg (4 lb) bird. This shows that the most vulnerable condition and blade impact location is during climb at approximately 91.4 m/sec (300 ft/sec) and at the blade 50% span location, respectively. The predicted gross impact capability of the QCSEE blade is shown in Figure 8-26. This shows the advantages of the QCSEE dovetail attachment and the use of hybrid materials over the previous fixed-root solid-graphite-type blade. Figure 8-27 shows a plot of the calculated projectile normal momentum for a 0.68 kg (1.5 lb) bird at the blade 50% and 75% span locations as a function of airplane speed.

Weight

The weight of the composite blade was computed using the final blade configuration as shown in Figure 8-6. The resulting weight breakdown is as follows (Table 8-VI).

Table 8-VI. Composite Fan Blade Weight Breakdown.

	Weight	
	kg	lb
Composite Airfoil	1.74	3.83
Leading Edge Protection	.20	.45
Polyurethane Coating	.07	.15
Platform and Adhesive Bond	.15	.34
Dovetail	.47	1.03
Total Weight	2.63	5.80

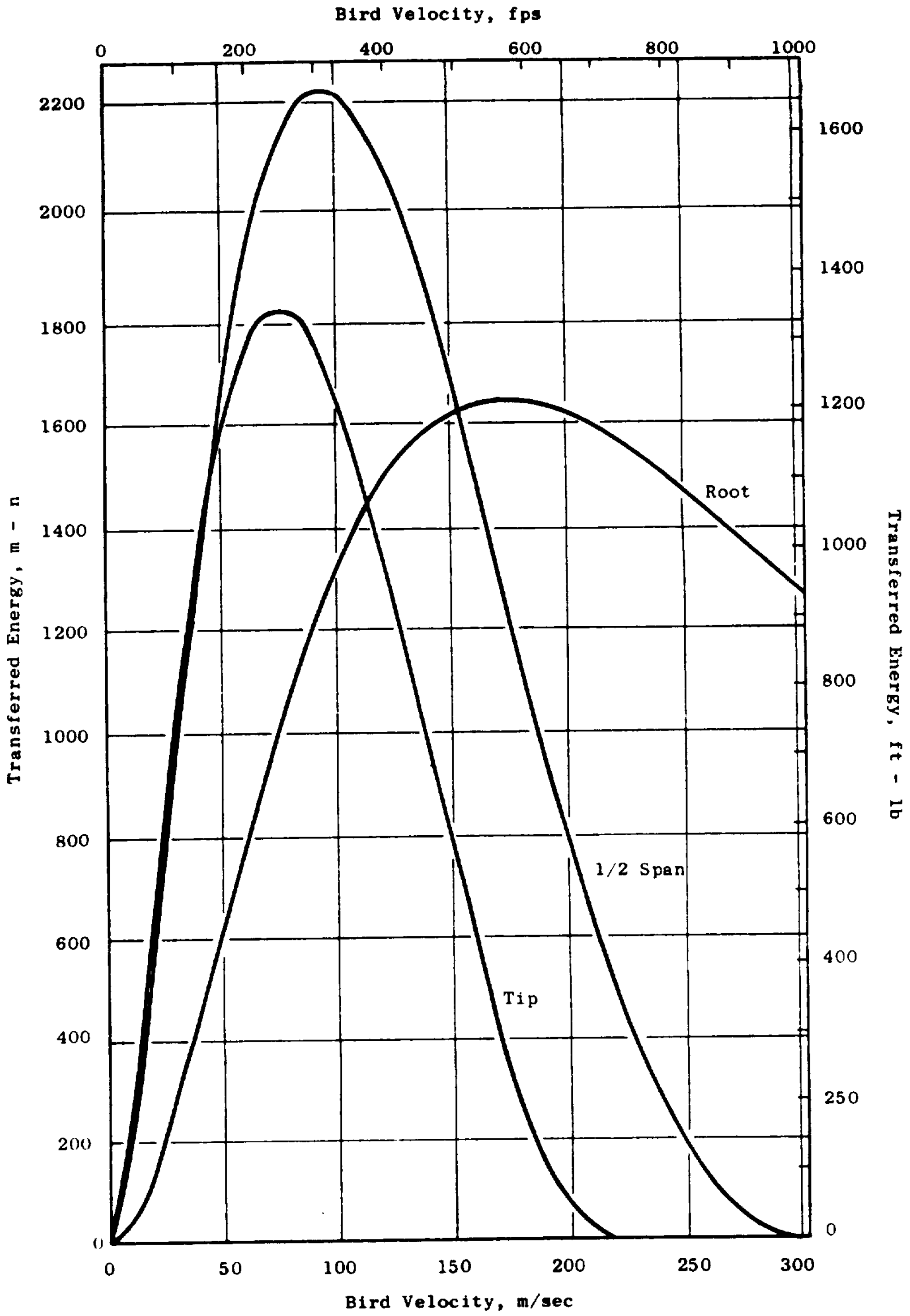

Figure 8-25. UTW Blade Transferred Impact Energy for a 1.81 kg (4 lb) Bird.

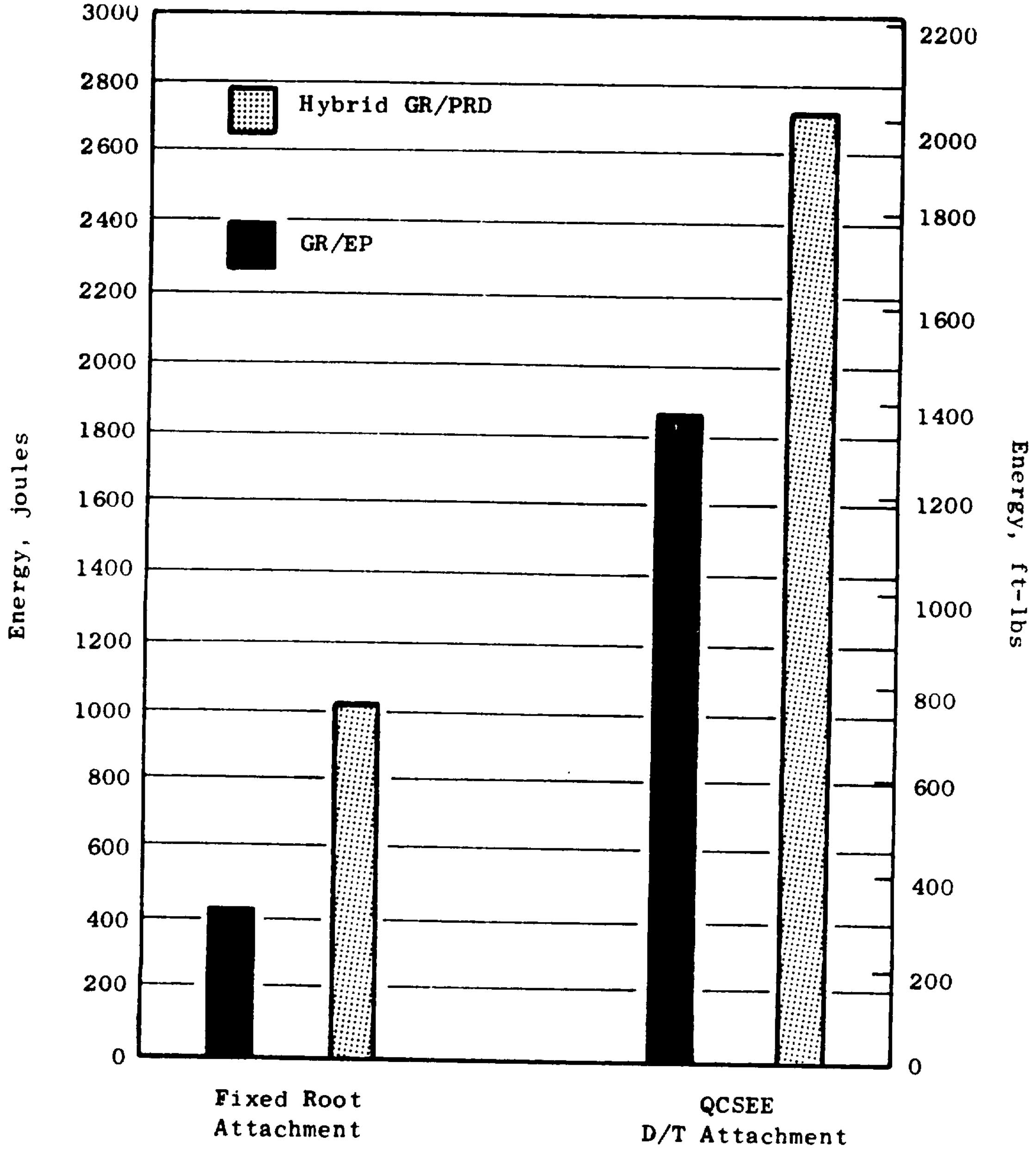

Figure 8-26. Composite Blade Predicted Gross Impact Capability.

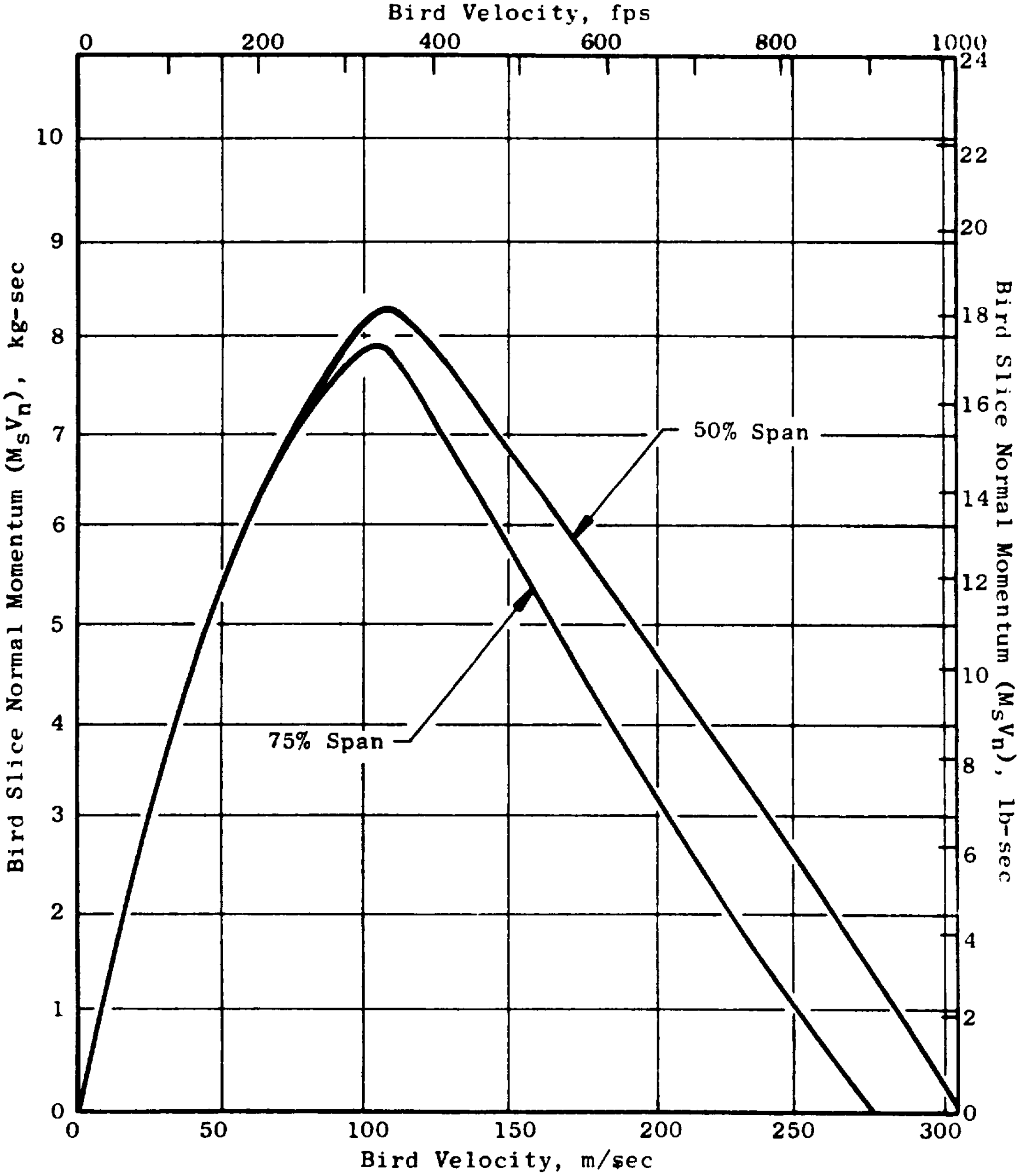

Figure 8-27. UTW Blade Impact Momentum for a 0.68 kg (1.50 lb) Bird.

8.3 FAN DISK

The UTW fan disk is a single-piece-machined 6Al-4V titanium ring forging designed for a commercial life in excess of 36,000 hours. This disk is shown in Figure 8-28. Eighteen radial holes pierce the disk ring to provide for blade support trunnions which retain the fan blades. An integral cone on the aft side of the disk connects the disk to the fan stub shaft through a bolted flange. The disk cone is contoured to alleviate low-cycle fatigue (LCF) problems generated by the forward and aft cycles of thrust generated during engine operation. Flanges on the outside of the disk rim provide attachment planes for the spinner and forward and aft flowpath adapter cones.

The inside of the disk rim is a turned, modified spherical blade bearing seating surface for the blade retention bearing (Figure 8-29). This results in a low-cost, lightweight disk design with a uniformly stressed rim. Blade thrust bearings have mating spherical seats and are mounted as shown in Figure 8-29. The bearing seating surface is not machined perfectly spherical but is designed to become spherical under operating loads. A spherical copper shim is included between the disk and the bearing, although at the pressure loadings expected beneath the bearing, fretting is not expected to be a problem.

The UTW fan disk design loads and stress data are shown in Table 8-VII for both the GE and Hamilton Standard actuators. Resulting actual and allowable stresses on the rotor configuration are shown in Figure 8-30, based on the Hamilton Standard variable-pitch fan actuation system loads. As shown in the figure, the final design provides adequate margin of safety at all critical stress locations.

8.4 BLADE SUPPORT BEARING

The blade support bearing (Figure 8-28) has a full complement of balls to reduce the per-ball loading. Bearing race conformance is relatively high (51%) to achieve the required bearing fatigue life in its highly loaded environment. All surfaces on this bearing will be coated with a tungsten disulfide film. Tests on previous General Electric variable-pitch fan bearings have shown this coating provides enough lubrication to enable the bearing to safely operate for 9000 flight hours in the event of a loss-of-grease situation.

The blade support thrust bearing configuration is illustrated in Figure 8-31. Shields attached to the outer race create a centrifugal "cup" which prevents the grease from leaking out in the high centrifugal field when the engine is running. Grease will not leak from the clearance gaps at the bottom of the shields when the engine is not operating due to the high viscosity of the grease, provided oil separation from the grease soaping agent does not occur. General Electric has conducted centrifuge tests on various greases to determine separation tendencies and has selected one which has little tendency to separate under prolonged periods of high "g" loads.

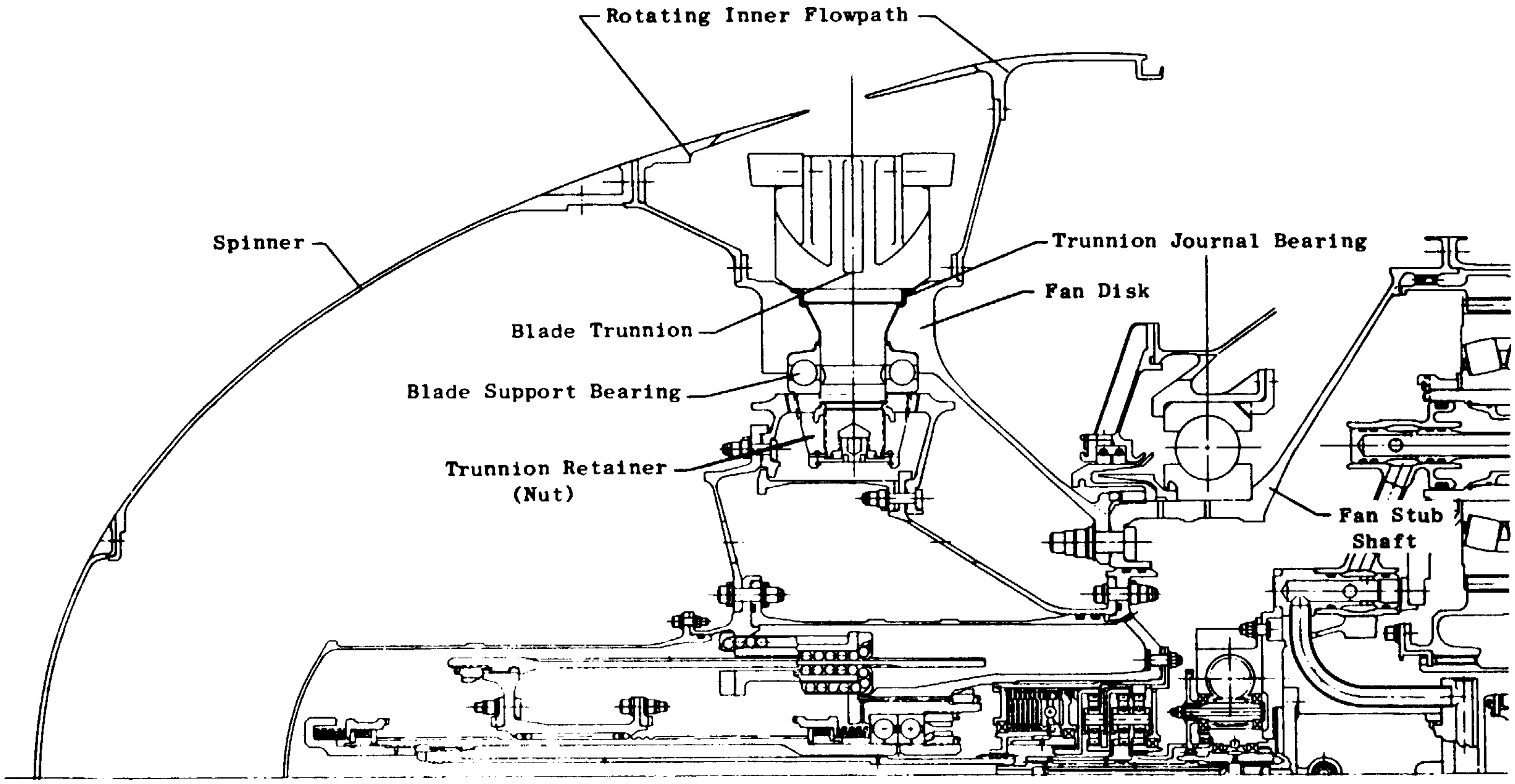
Rotating Inner Flowpath
Spinner
Trunnion Journal Bearing
Fan Disk
Blade Trunnion
Blade Support Bearing
Trunnion Retainer (Nut)
Fan Stub Shaft

Figure 8-28. Fan Rotor.

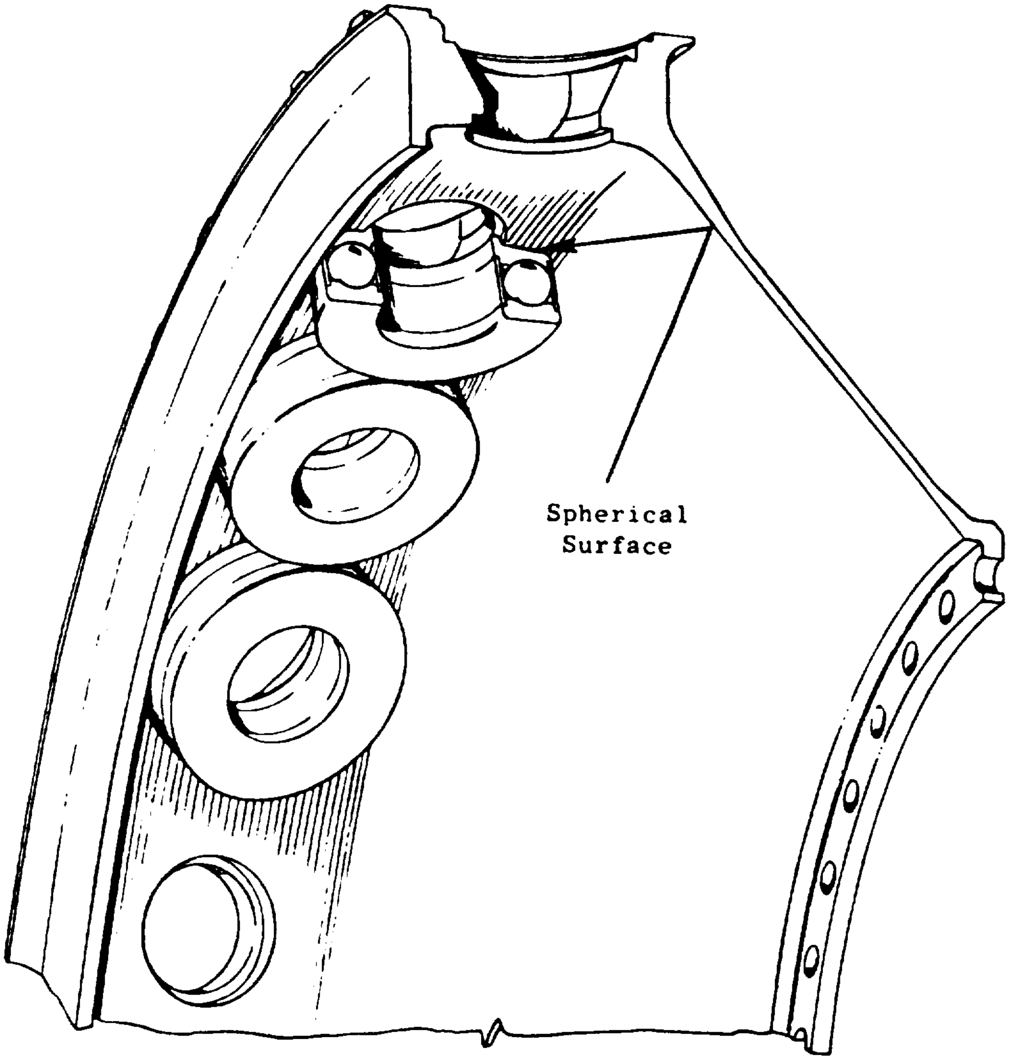
Spherical
Surface

Figure 8-29. Bearing and Disk Seat.

Table 8-VII. Fan Disk Design Data.

All Loads and Stresses Calculated at 3326 RPM

Attachment Load		
With GE Pinion Gear	327,718 N/Blade	(73,674 lb/Blade)
With HS Lever Arm	337,829 N/Blade	(73,947 lb/Blade)
Average Rim Stress (GE)	35.577×10^7 N/m^2	(51,600 psi)
(HS)	38.299×10^7 N/m^2	(55,446 psi)
Burst Speed		4928 rpm)
LCF Life of Disk With -3 Material Properties		48,000 Cycles
LCF Life of Disk With 0.01 × 0.03 Initial Defect		16,000 Cycles

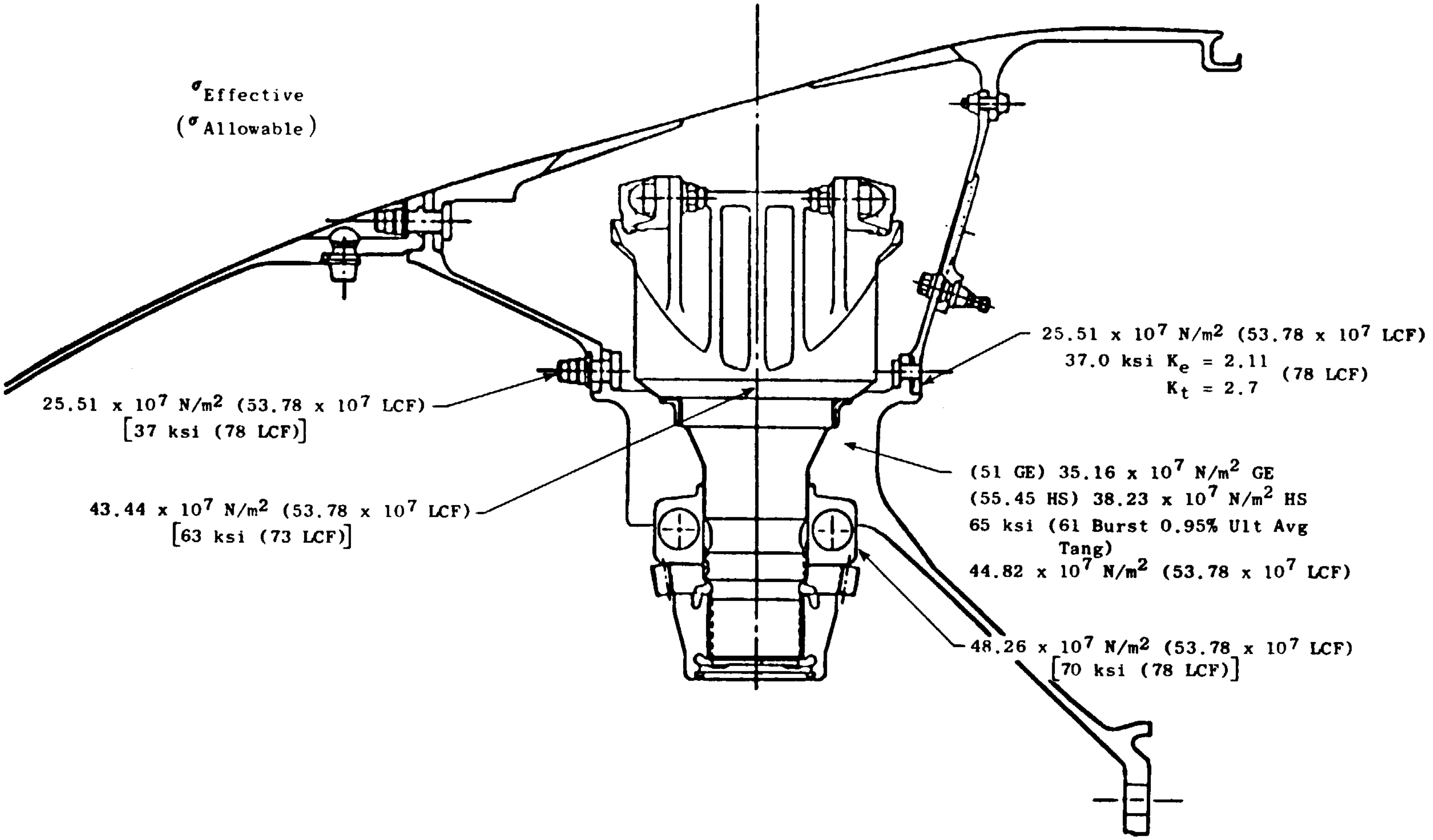
$\sigma_{Effective}$
($\sigma_{Allowable}$)
25.51×10^7 N/m^2 (53.78×10^7 LCF)
[37 ksi (78 LCF)]
43.44×10^7 N/m^2 (53.78×10^7 LCF)
[63 ksi (73 LCF)]
25.51×10^7 N/m^2 (53.78×10^7 LCF)
37.0 ksi $K_e = 2.11$ (78 LCF)
$K_t = 2.7$
(51 GE) 35.16×10^7 N/m^2 GE
(55.45 HS) 38.23×10^7 N/m^2 HS
65 ksi (61 Burst 0.95% Ult Avg Tang)
44.82×10^7 N/m^2 (53.78×10^7 LCF)
48.26×10^7 N/m^2 (53.78×10^7 LCF)
[70 ksi (78 LCF)]

Figure 8-30. Fan Disk Stresses with Hamilton-Standard Actuator.

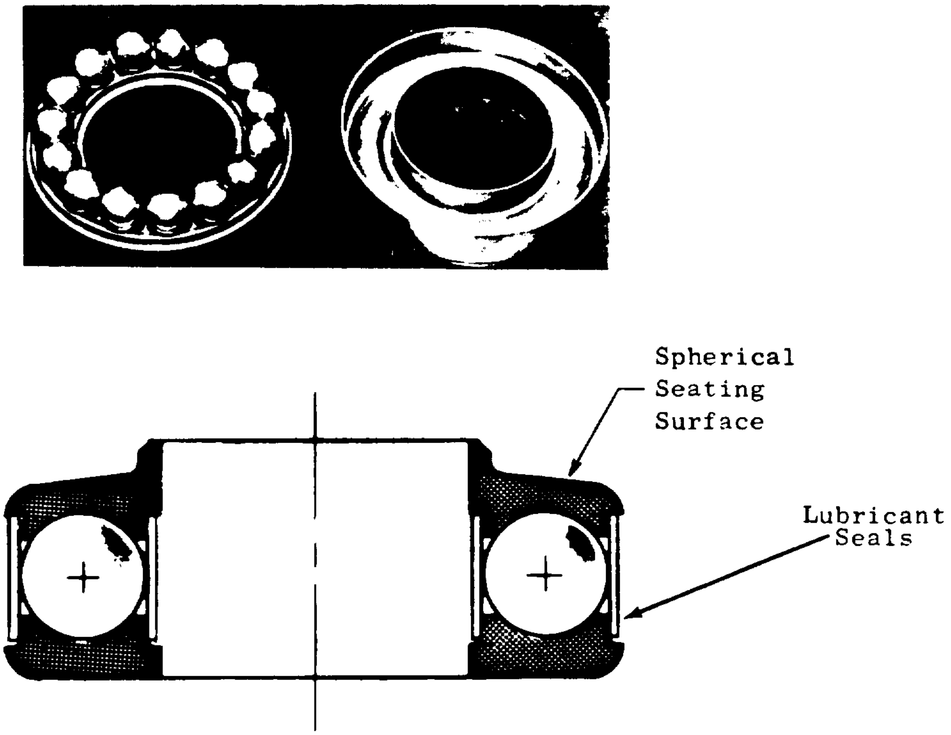
Spherical Seating Surface
Lubricant Seals

- Single Row Ball Thrust Bearing
- Full Complement of Balls (12)
- High Conformance (51%)
- Separable Races
- Lubricant Seals

Figure 8-31. Blade Thrust Bearing.

Design criteria peculiar to variable-pitch blade support bearings were developed and applied to the design of this bearing. Unique design criteria used in designing the QCSEE UTW bearing are as follows:

1. The blade support bearing system B10 life should be 9000 flight hours. This requires an individual bearing B10 life of over 13 times the system B10 life. The need for this stringent requirement is based on the statistical problem of a multibearing (18) system in a multi-engine (4) aircraft.

2. Blade support bearings will not be dependent upon the grease lubricant to obtain 9000 hours between overhauls. This restriction ensures that failure will not occur due to loss of bearing grease. In addition to normal bearing design criteria, the following requirements must also be met, or by definition, failure is said to occur:

   a. An apparent coefficient of friction at the pitch diameter less than 0.01. This allows the blade actuator to be designed to a maximum capacity with assurance that it will not be overloaded because of worn bearings.

   b. Bearing wear less than the bearing preload [approximately 0.00508 cm (0.002) total wear]. This definition provides a simple method for condition monitoring without rotor disassembly.

3. Ball or race fracture must not occur under the maximum possible bird impact loads. The actuation system of an 18-bladed fan is sufficiently powerful to cause secondary damage upon seizure of any one of the individual bearings. Ball fracture, a potential cause of such seizure, must be eliminated as a potential problem.

4. Bearing life calculations are based on the mission/duty cycle as shown in Table 8-VIII. Blade angle and cyclic amplitude data correspond to information presented in Figure 7-3. A total blade modulation of 180° per mission (in 2° increments) is assumed during aircraft approach for bearing life analysis.

The upper surface of the top bearing race is a spherical surface which is designed in conjunction with the disk bearing seat to minimize transmission of warping stress to the race under operating conditions. This spherical mating surface will be coated with an antifretting coating to ensure that loss of LCF life of the fan disk will not occur.

Bearing loads and life predictions are given in Table 8-IX. As indicated in Table 8-VIII, the number of bearing cycles during 9000 hours of engine operation is approximately 12 times greater when modulation during approach is assumed than without modulation. As shown in Table 8-IX the

Table 8-VIII. UTW Blade Support Bearing, Operating Conditions of Mission Duty Cycle.

Action	N	F		α	Δα	Cycles/Mission
	rpm	N	lb			
Ignition-Taxi	1,000	29,358	(6,600)	30° Closed	0°	1/4
Taxi-T/O	2,400	169,032	(38,000)	2° Closed	32	1/4
T/O-Climb	3,143	290,024	(65,200)	2° Closed	4	1/4
Climb-Cruise	3,143	290,024	(65,200)	4° Closed	2	1/4
Cruise-Descent	1,400	57,382	(12,900)	7° Closed	3	1/4
Approach	3,074	277,569	(69,400)	180° Mod.	±2	22-1/2
Approach-Reverse	3,074	277,569	(62,400)	90° Closed	90	1/4
Reverse-Taxi	2,400	169,032	(38,000)	30° Closed	60	1/4
Shutdown	1,000	29,358	(6,600)	30° Closed	0	1/4
					Total	24-1/2 Cycles/Mission

α - Blade angle setting relative to nominal (design) position
Δα - Blade angle cyclic amplitude

Total Cycles for 9,000 Engine Hours:
With 180° Modulation:
(24.5 Cycles/Mission) (60/45 Missions/Hours) (9,000 Hours) 294,000 Cycles

Without Modulation:
(2.0 Cycles/Mission) (60/45 Missions/Hour) (9,000 Hours) 24,000 Cycles

Table 8-IX. UTW Blade Support Bearing Loads and Life Predictions.

Geometry	
Number of balls	12
Ball Diameter	1.588 cm (0.625 IN)
Bearing Diameter	6.147 cm (2.420 IN)
Conformance	0.51
Material	AISI 52100

Capacity	Without Modulation	With Modulation For Approach
Dynamic Capacity	121,875 N (27,400 lb)	121,875 N (27,400 lb)
Static Capacity	298,016 N (67,000 lb)	288,016 N (67,000 lb)
Mean Effective Rotating Load	151,721 N (34,110 lb)	89,672 N (20,160 lb)
Material Factor	3	3
Bearing System Life In Engine Operating Hours (B_{10})	43,245 Hrs	17,100 Hrs. (GE) 15,300 Hrs. (HS)

bearing B10 system life in terms of engine operating hours exceeds the 9000-hour TBO requirement when modulation during approach is assumed, and exceeds the total engine life requirement of 36,000 hours if blade modulation during approach is not required.

8.5 BLADE TRUNNION

Blade trunnions mechanically tie the composite fan blades to the fan disk through the blade support bearing. They also provide an attachment point through which torque can be applied by the blade actuator to change the pitch of the blades. The QCSEE UTW blade retention trunnion is shown in Figure 8-32.

The entire blade support system is designed to withstand the maximum possible loads which can be transmitted into it by the blades without blade failure. This includes not only the trunnion but all of its mating components. This ensures that in the event of extensive foreign object damage only small composite fan blade pieces will be broken off and secondary engine damage will be minimized.

Fan blades slide into the dovetail slots on top of the trunnion and are retained by shouldered straps. Marage 250 is used for the straps because of its very high strength. The dovetail slot will be protected by an anti-fretting coating applied to the blade dovetails. Two plasma sprayed coatings, one plated coating, and a chemical conversion coating are presently being considered for this wear coating.

The trunnion is machined from single forgings of 6Al-4V titanium. This material was selected based on its natural corrosion resistance, low density, and high strength. Titanium also allows relatively large diameter threads to be rolled by more conventional capacity thread rolling equipment on the trunnion end (per Mil-S-8879) for the trunnion retainer. This rolling procedure has been used on the titanium trunnions of previous General Electric variable-pitch fans and produces above average properties in this critical region. Critical trunnion stresses are shown on the drawing in Figure 8-33. All stresses fall within the allowable limits with an adequate margin of safety.

Each trunnion is held in the hole of the disk by a silver-plated threaded steel retainer. A stress summary for this trunnion retainer (nut) is presented in Table 8-X. This retainer can be torqued to preload the blade support bearing and is locked by a redundant locking system. Either a pinion gear for the GE actuation system or a lever arm for the Hamilton Standard System is captured on the trunnion between the trunnion retainer and the blade support bearing [see Figures 8-34 (GE) and 8-35 (HS)]. Torque to change the blade pitch is carried through this device into mating splines just above the trunnion threads.

Outer sliding bearings support the top of the trunnion. The outer sleeve sliding bearing and axial thrust seating surfaces will be a very high

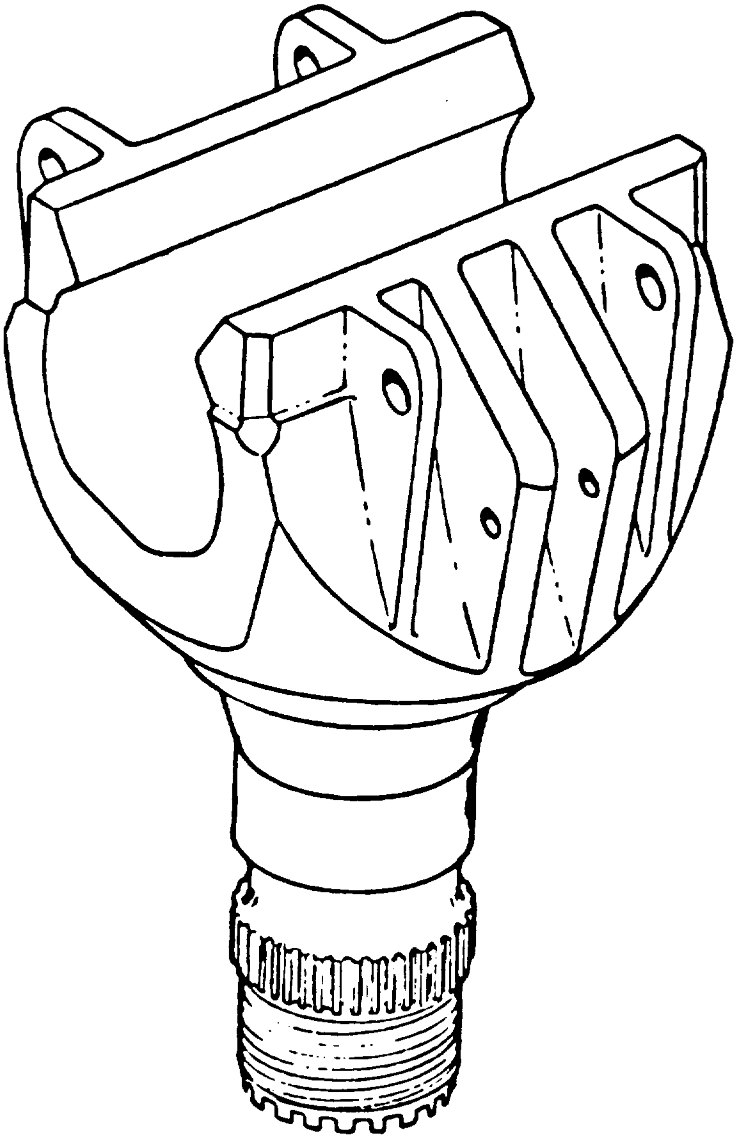

Figure 8-32. Blade Trunnion.

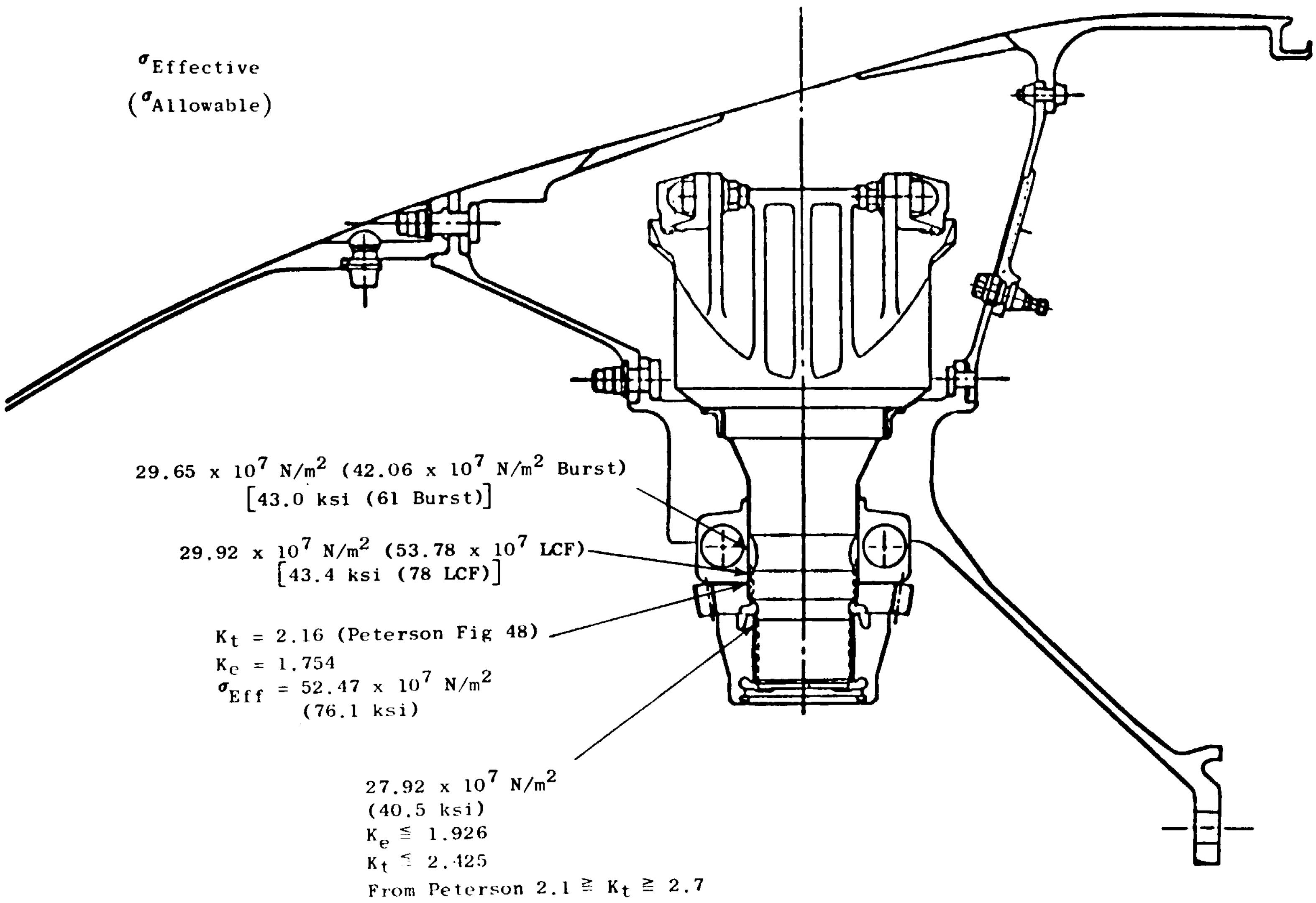
$\sigma_{Effective}$
($\sigma_{Allowable}$)
29.65×10^7 N/m^2 (42.06×10^7 N/m^2 Burst)
[43.0 ksi (61 Burst)]
29.92×10^7 N/m^2 (53.78×10^7 LCF)
[43.4 ksi (78 LCF)]
K_t = 2.16 (Peterson Fig 48)
K_e = 1.754
σ_{Eff} = 52.47×10^7 N/m^2
(76.1 ksi)
27.92×10^7 N/m^2
(40.5 ksi)
$K_e \leqq 1.926$
$K_t \leqq 2.425$
From Peterson $2.1 \geqq K_t \geqq 2.7$

Figure 8-33. UTW Blade Trunnion Stresses.

Table 8-X. Trunnion Retainer (Nut).

Load - 306,912 N (69,000 lb) at 3326 rpm

Stress Summary -

	Calculated	Allowable
Hoop Stress	18,158 N/cm^2 (26,335 psi)	67,571 N/cm^2 (98,000 psi) (LCF)
Shear Stress on Threads	23,074 N/cm^2 (33,465 psi)	38,612 N/cm^2 (56,000 psi) (LCF)
Bearing Design Criteria	16,096 N/cm^2 (23,345 psi)	27,580 N/cm^2 (40,000 psi) (Fretting)

Limiting Design Criteria - Local Retainer Stresses Due to Ring Roll

- Threat Stresses in Trunnion

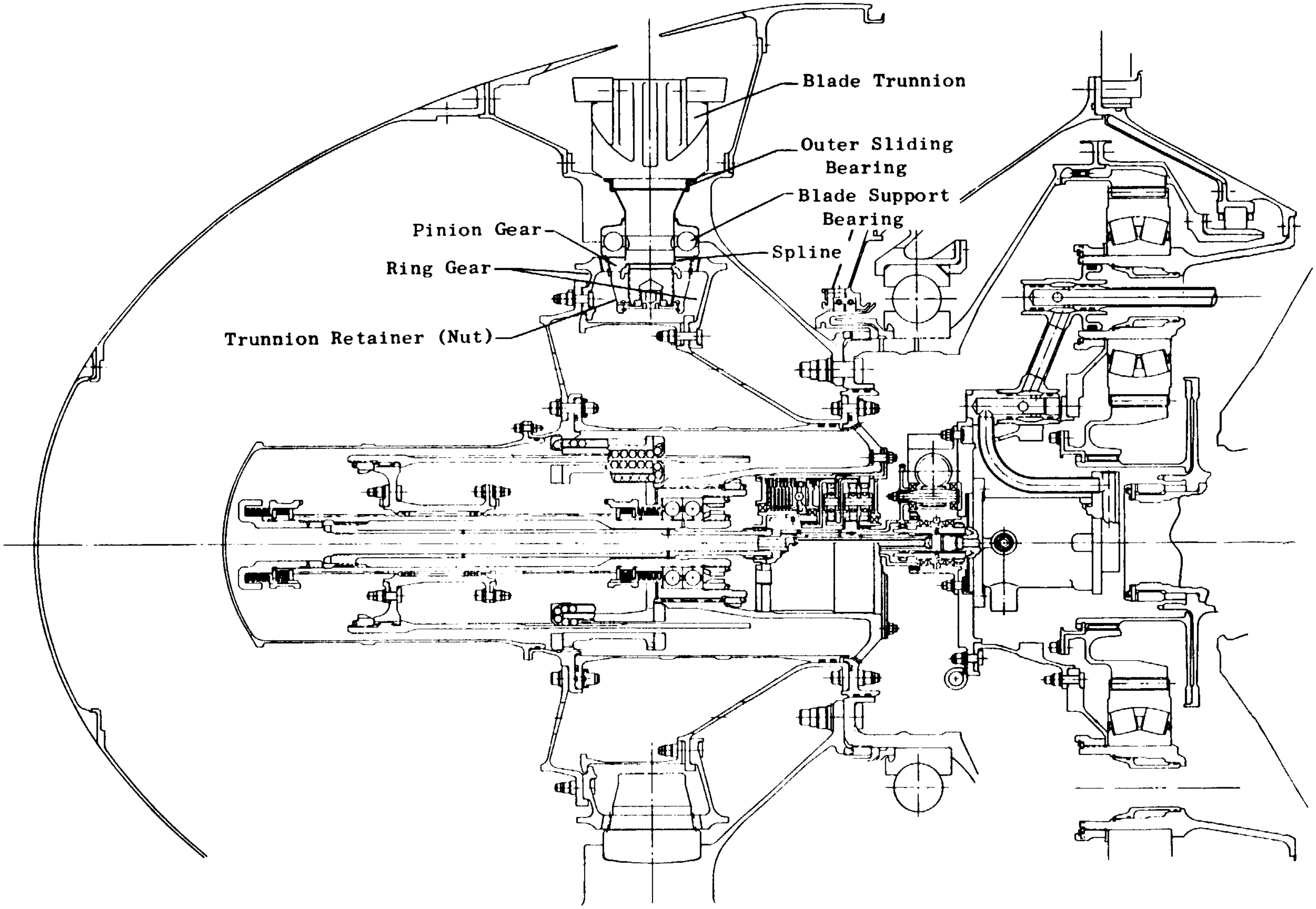
Blade Trunnion
Outer Sliding Bearing
Blade Support Bearing
Spline
Pinion Gear
Ring Gear
Trunnion Retainer (Nut)

Figure 8-34. GE Ball Spline Actuation System.

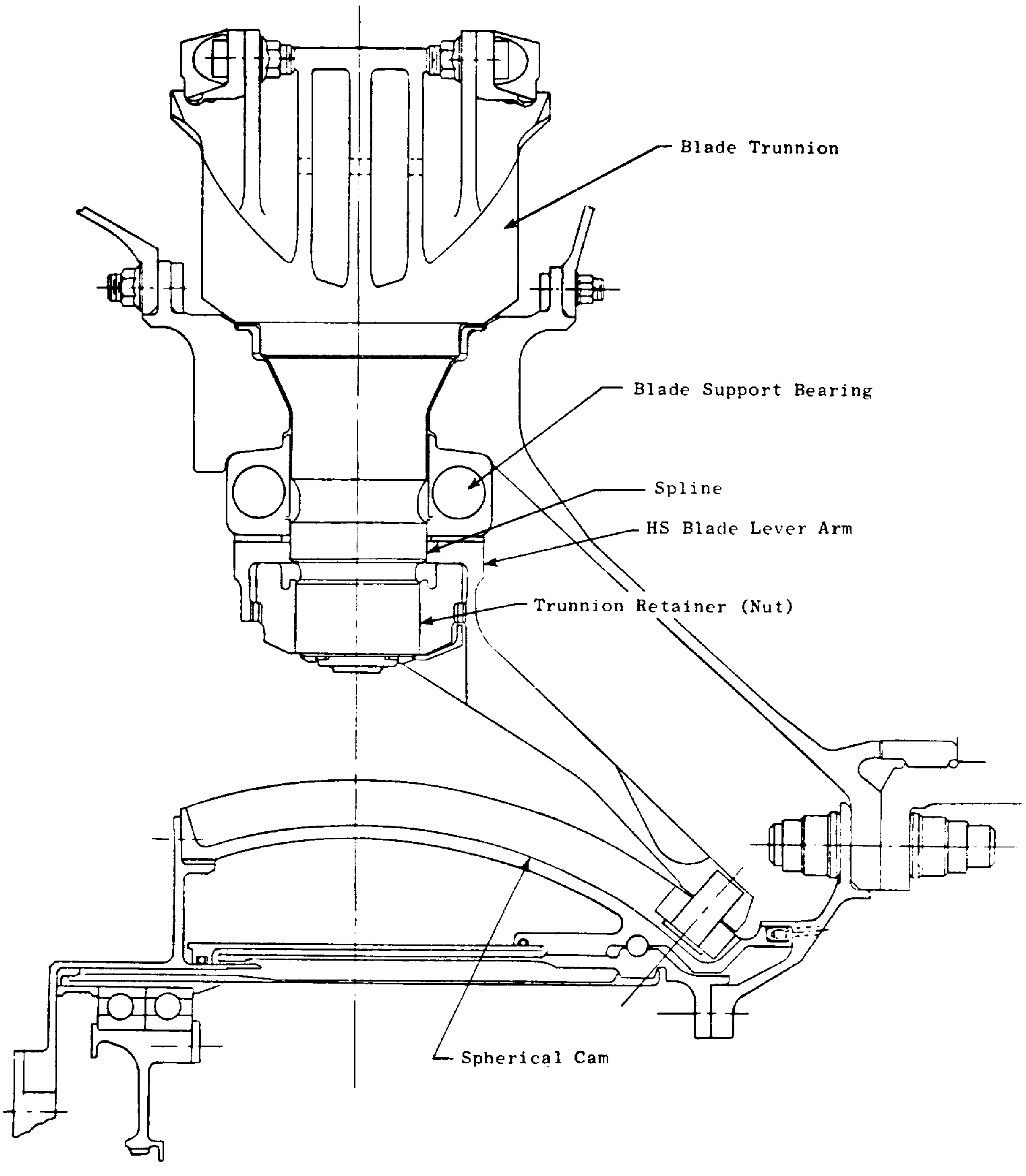
Blade Trunnion
Blade Support Bearing
Spline
HS Blade Lever Arm
Trunnion Retainer (Nut)
Spherical Cam

Figure 8-35. Hamilton-Standard Variable Pitch Interface.

capacity bearing of Nomex and Teflon fibers or apolyimode. This bearing seats inside the disk and can easily tolerate the circumferential strain of the disk. The high capacity of this bearing, compared to conventional ball bearings, enables it to easily withstand anticipated vibratory and bird impact loads. The outer bearing has resistance to all oils, fuels, and solvents which might normally come in contact with engine parts.

8.6 FAN SPINNER

The UTW fan has both a rotating forward spinner and flowpath adapters as shown in Figures 8-1 and 8-28. These parts attach to flanges on the fan disk. Both fore and aft rotating flowpath adapters are scalloped where they meet to provide round holes for the blade platforms. Together they provide the inner flowpath for the fan. The spinner and flowpath adapters are fabricated from 6061 Aluminum. This material has good section stiffness-to-weight and has the good welded properties needed for fabricating development hardware.

The forward spinner also has a spinner cap for inspection and access to the interior of the fan assembly and the slipring hardware. After removal of the fan spinner, all of the rotating hardware and sump regions forward of the fan frame are easily accessible. Blades may be individually replaced and the blade actuator or the actuator and disk assembly may be removed as a package. This permits removal of the fan disk assembly, blade actuator, and main reduction gear as a complete module.

Radial fan balance screw bosses are provided in the spinner. This will permit field balance of the engine without removal of the spinner. The concept has been developed and used successfully on General Electric's CF6-50 engine.

The aft flowpath adapter continues the inner flowpath back to the fan core OGV's. A flow discourager seal inhibits air recirculation at this point. There are access holes in the flange of the aft spinner which, with the forward spinner removed, permit access to the fan frame flange which retains the main reduction gear. Critical spinner and adapter stresses are shown in Figure 8-36. As shown, all stresses fall well within the allowable limits.

8.7 FAN ATTACHMENT HARDWARE

All bolted joints in the fan rotor use Inco 718 bolts and dry film lubricant coated A286 nuts. The main rotor joint to the fan stub shaft is held with 18 MP159 1.27 cm (1/2 in.) - 20 bolts. MP159 was chosen for its high strength. Bolt preload has been set to assure that total torque in the joint can be carried in friction. A summary of the disk cone flange bolts design characteristics is presented in Table 8-XI.

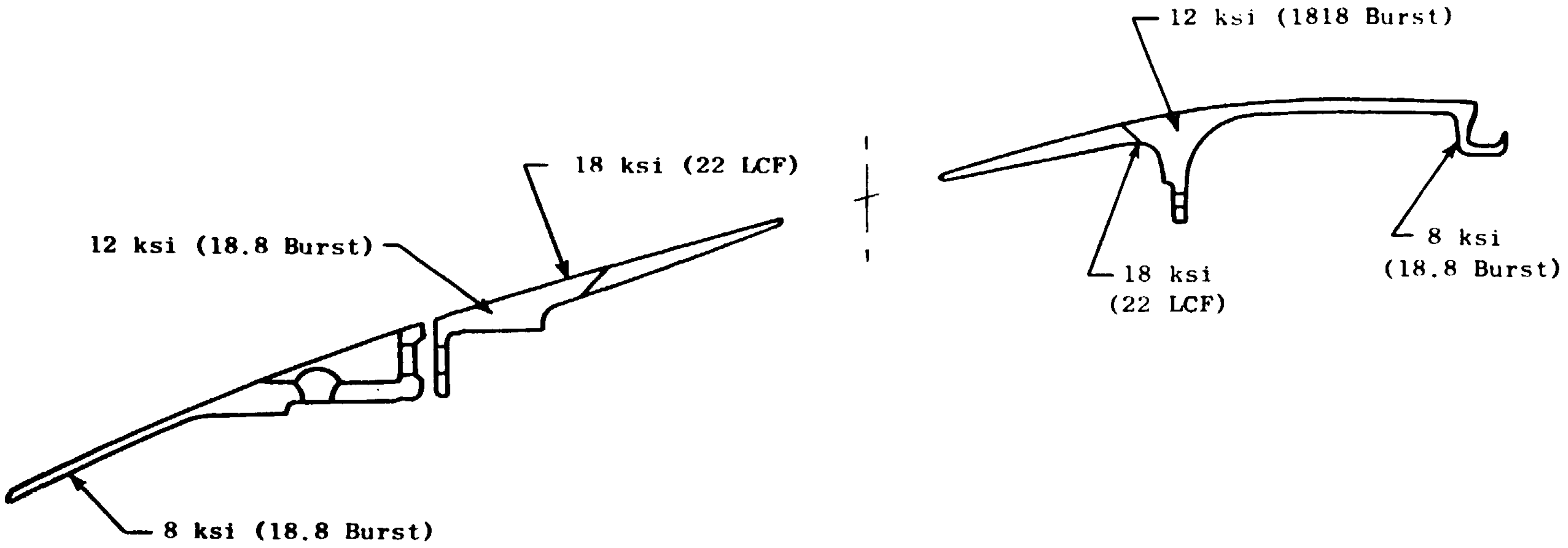
12 ksi (1818 Burst)
18 ksi (22 LCF)
12 ksi (18.8 Burst)
8 ksi (18.8 Burst)
18 ksi
(22 LCF)
8 ksi
(18.8 Burst)

Material 6061 T6 Aluminum

Limiting Criteria-Deflection Matching with Blade

$\sigma_{Effective}$
$(\sigma_{Allowable})$

Figure 8-36. Fan Flowpath Adapters.

Table 8-XI. **Disk Cone Flange Bolts.**

- Number 18 bolts
- Size - 1.27 cm (1/2 in.) - 20
- Material - MP159
- Torque 217-271 mN (160 - 200 ft-lb)
- Min. Preload - 82,288 N (18,500 lb) per bolt
- Total Preload - 146.8 kN (33,000 lb)
- Percent Torque Carried By Friction -125% At = 0.15
- Bladeout (5 blades) Stress 64,124 N/cm^2 (93,000 psi)
- Min. Preload Stress in bolts - 76,672 N/cm^2 (111,200 psi)

SECTION 9.0

FAN FRAME MECHANICAL DESIGN

9.1 SUMMARY

The UTW fan frame is a flight weight, integrated design constructed of advanced composite materials. Design integration is achieved by combining the functions of the fan stator vanes, fan outer casing, and fan frame into one unitized structure, as shown in Figure 9-1. This approach saves considerable duplication of structure, resulting in a significantly lighter weight design. This unitized approach is particularly suited to the use of composite materials since these materials are more efficient when employed in large bonded structures rather than small structures which must be bolted together.

The composite material system selected as the basic material for the frame is Type AS graphite fiber in Hercule's 3501 epoxy resin matrix. This material was selected based on the rather extensive data base for the material, its good mechanical properties, cost, and its ready availability.

The frame was analyzed using a finite element digital computer program. This program was run a number of times using different material property inputs for the various elements in order to arrive at practical thickness and ply orientations to achieve a final design that met all strength and stiffness requirements for all of the critical conditions. Using this information, the detail design of each of the individual parts of the frame was completed and released. On the basis of these designs, the tooling required to fabricate the various component parts of the frame was designed.

The composite design concepts used for the frame are essentially those which were developed for, and demonstrated by, the F101 simulated composite front frame shown in Figure 9-2. The basic concept consists of "wheels" in which the inner, mid, and outer rings and the spokes are fabricated as a one-piece integral structure. Two or more of the wheels are then joined together by flowpath panels to form the basic frame. This concept, as applied to the QCSEE fan frame, is shown in Figures 9-3 and 9-4. Its primary advantage is that the major circumferential load-carrying structure (the ring or hubs of the wheels) are integrally bonded structures rather than separate structures which must transfer load by means of bolted joints.

To verify the structural integrity of the critical joint areas, a subcomponent test program is now being carried out and partial results are reported herein. In addition, an element test program was conducted to verify predicted mechanical properties for specific orientations required for the frame.

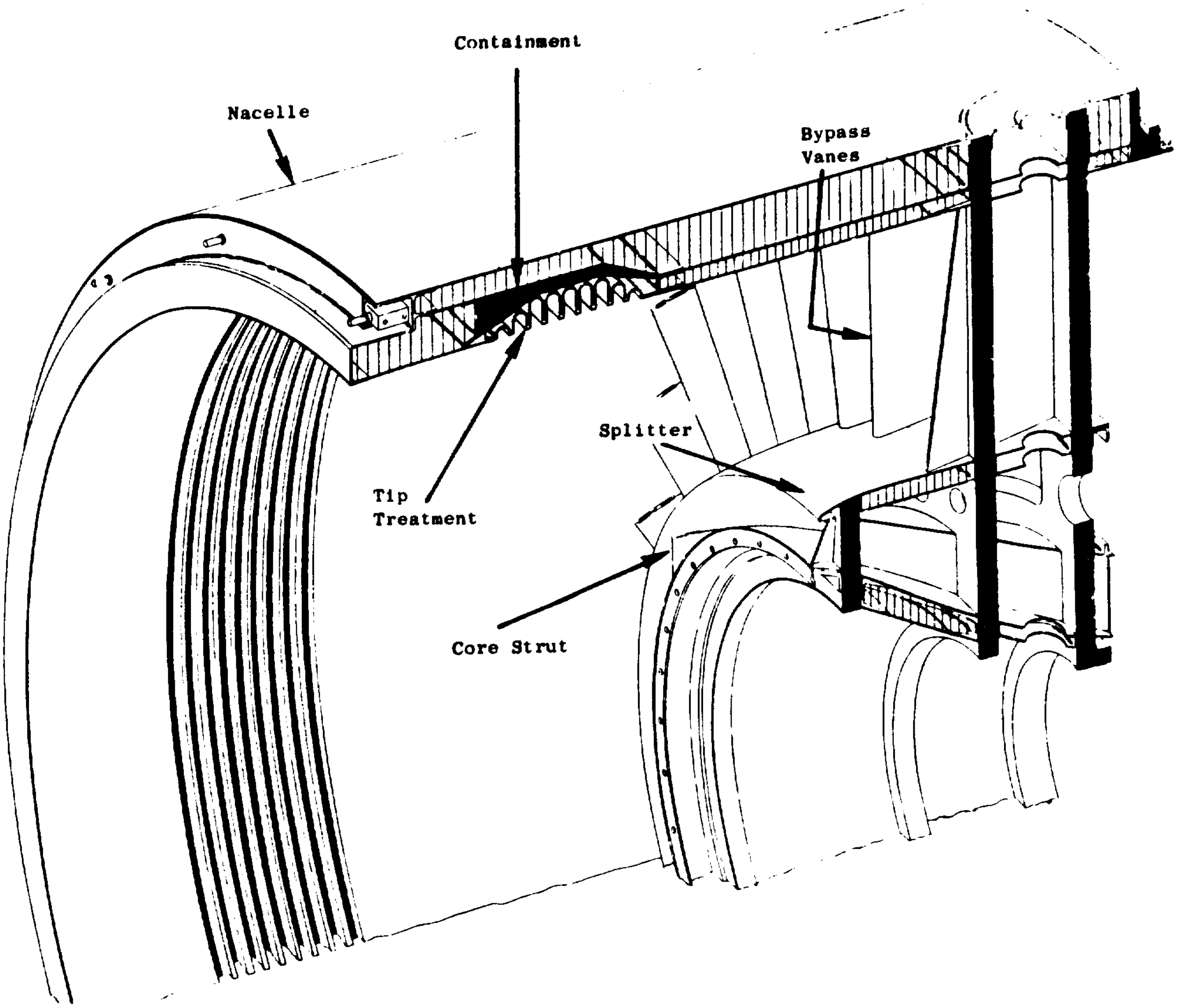
Containment
Nacelle
Bypass
Vanes
Splitter
Tip
Treatment
Core Strut

Figure 9-1. OTW Fan Frame.

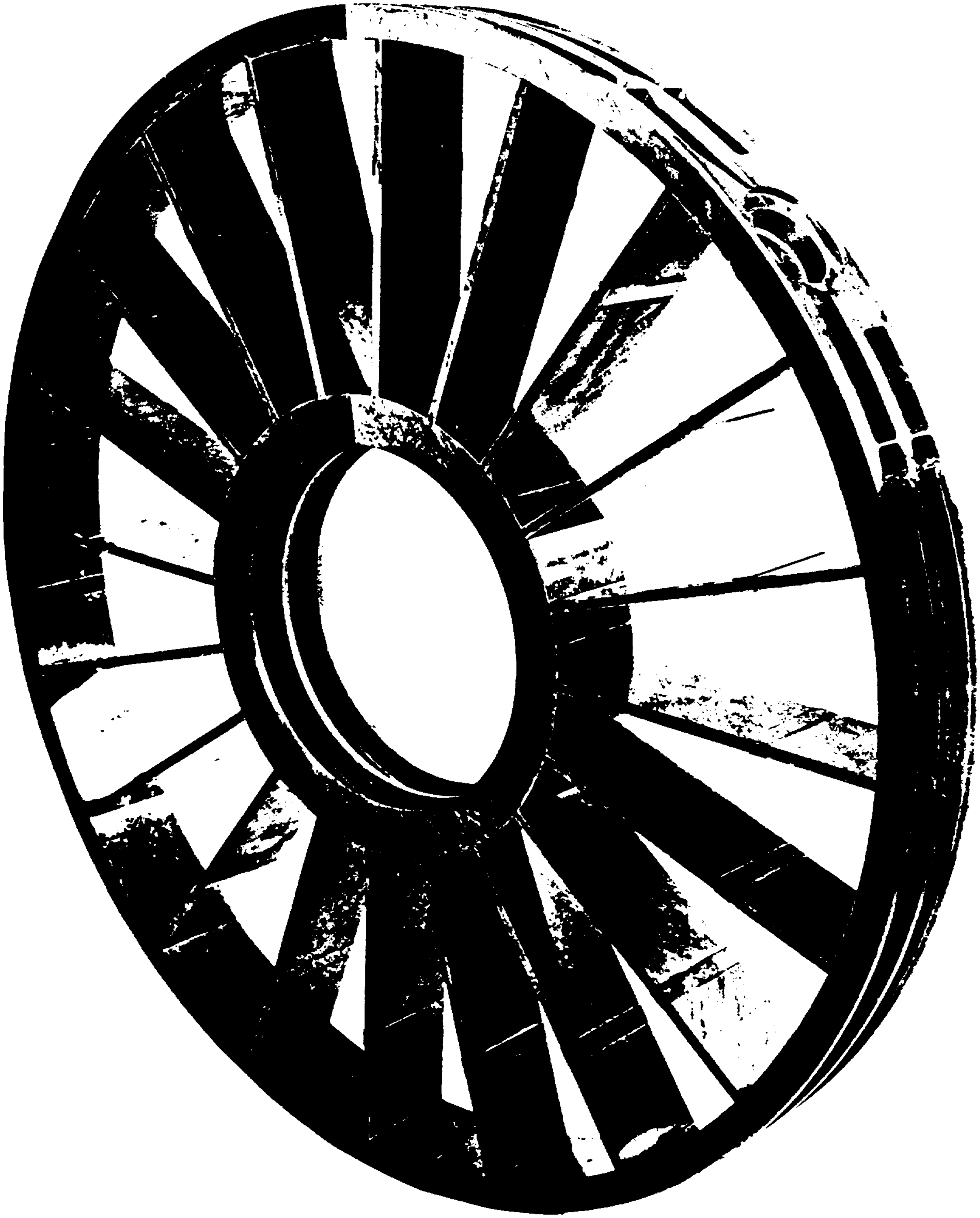

Figure 9-2. Simulated Composite Frame.

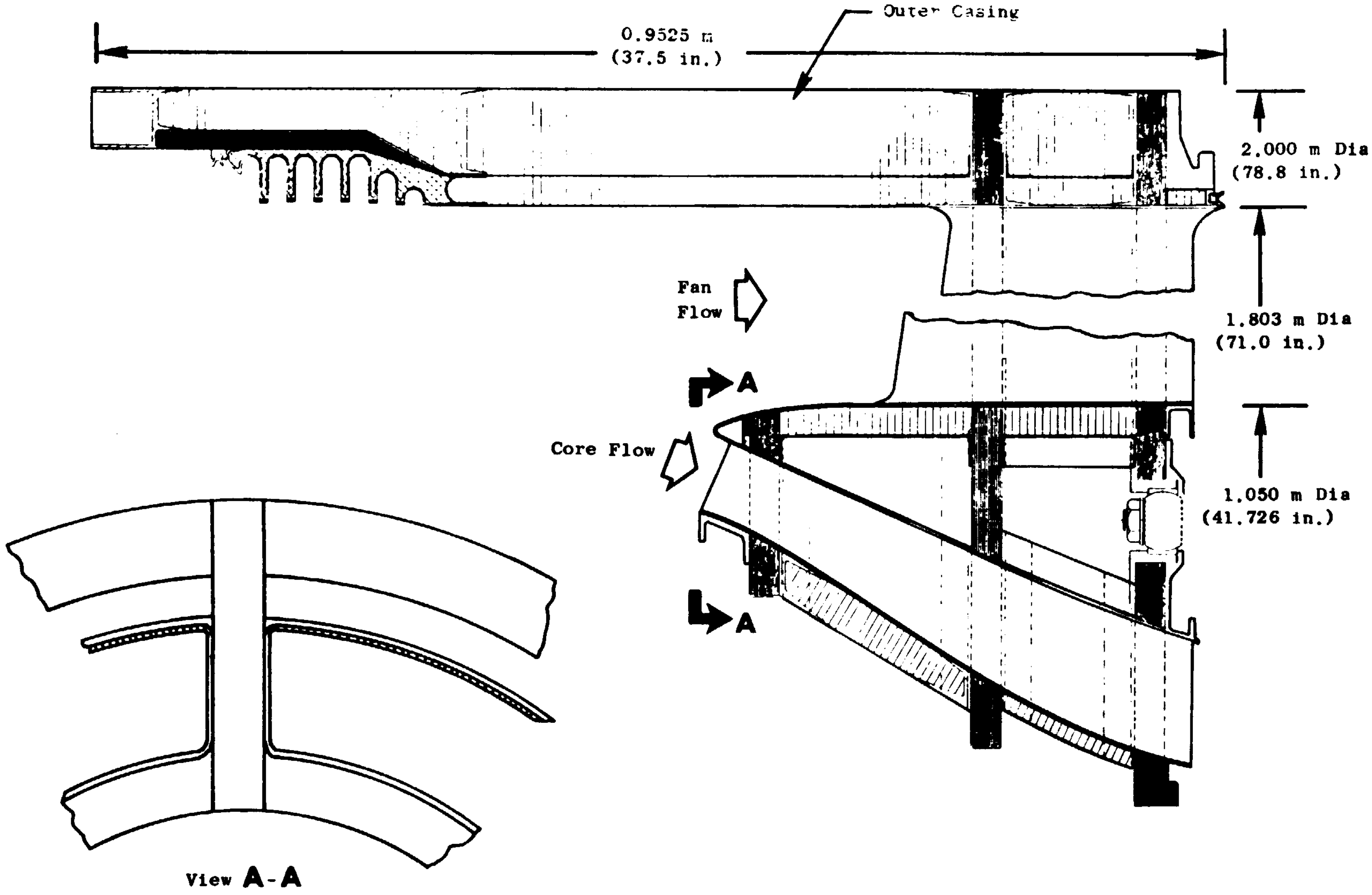
Outer Casing
0.9525 m
(37.5 in.)
2.000 m Dia
(78.8 in.)
Fan
Flow
1.803 m Dia
(71.0 in.)
A
Core Flow
1.050 m Dia
(41.726 in.)
A
View A-A

Figure 9-3. QCSEE Composite Frame.

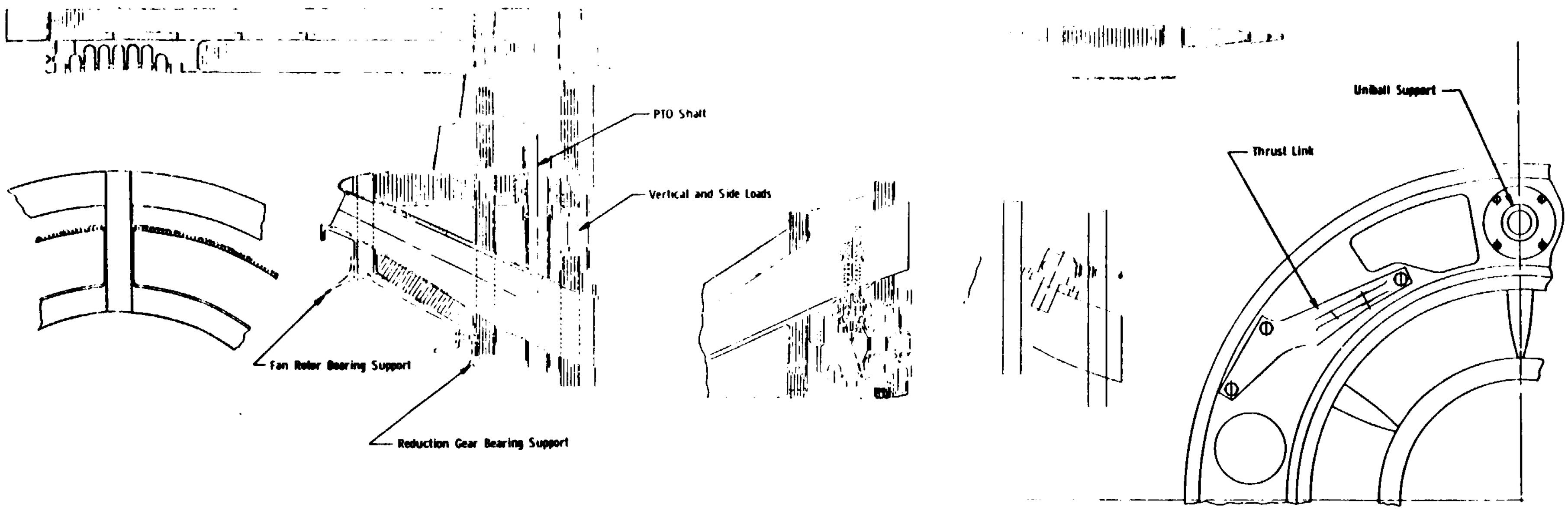
PTO Shaft
Vertical and Side Loads
Fan Rotor Bearing Support
Reduction Gear Bearing Support
Thrust Link
Uniball Support

Figure 9-4. Frame Assembly.

9.2 DESIGN REQUIREMENTS

9.2.1 Loads

In addition to the normal range and combination of steady-state pressure, thermal, thrust, and torque loads, the engine has been designed to withstand the loads defined in Table 9-I. Table 9-II summarizes the engine bearing loads on the frame for 1/g down, 1 radian/sec, and one composite fan blade-out conditions for the UTW composite frame. Air loading on the bypass vanes is shown in Figure 9-5.

9.3 STRUCTURAL DESCRIPTION

The UTW frame is an all composite, static structure formed from integration of several separate structures. As seen in Figure 9-1, the outer casing of the frame is an integration of the nacelle with the frame outer shell. This casing provides part of the external nacelle flow lines as well as the internal fan flow lines. Fan blade tip treatment and containment are provided by the grooved and Kevlar-filled structures integrated into the forward portion of the outer casing. Positioning of the fan and core engine relative to the integral nacelle/outer casing is provided by 33 bypass vanes which also serve as structural supports and provide flow turning of the fan flow discharge. The hub of the frame is connected to the frame splitter through six equally spaced struts. The inner shell of the outer casing, the bypass duct and core duct surfaces of the frame splitter, and the pressure faces of the bypass vanes are perforated to provide acoustic suppression within the frame structure. Flow turning of the fan flow into the core is provided by an independent set of outlet metallic guide vanes (DGV) attached to the forward flange of the frame hub. The OGV design is a brazed and machined fabrication. The vanes are supported at the hub through brazed joints into a machined inner casing which is bolted to the fan frame. Both island and stator vane air loads are transmitted through this inner casing to the fan frame. The assembly of this region is shown in Figure 9-6.

The composite frame mechanical design provides the normal penetrations (oil lines, shafts, etc.) and accessory mounting pads generally required of frame components. It also accommodates firewall-type protection between component parts and any fuel or lubricant. This additional objective required that all lube-carrying frame passages be metallically lined and sealed.

Oil containment has been achieved by closing all strut ends and forming the sump wall at the frame hub. Major interfaces for all penetrations into the fan sump area will be achieved by forming local bosses at all penetration points. These penetrations include oil in, oil scavenge, PTO shaft, fan speed sensor, fan VP drive mechanisms, seal drain lines, and the scavenge pump drive shaft, as shown in Figures 9-7, 9-8, and 9-9. Provisions are also made for the $T_{2.5}$ temperature sensor, six total pressure and temperature rakes, and several static pressure taps.

Table 9-I. QCSEE Engine Loads.

Limit Loads

For anyone of the following load conditions, all stresses shall remain within the material elastic limits.

Condition I:	(Flight and Landing) - See load diagram, Figure 2-2.
Condition II:	(Gust Load) - An equivalent load from a 51.44 m/sec (100 knot) crosswind acting at any angle within a plane 1.5708 radians (90 degrees) to the axis of the engine, zero-to-minimum thrust.
Condition III:	(Side Load) - A 4g side load combined with 1/3 the equivalent load as defined in Condition II, zero-to-maximum thrust.

Ultimate Loads

The engine shall not separate from the aircraft when subjected to Conditions IV, V, and VI and for static loads equivalent to 1.5 times the loads specified as limit loads in metal parts, and 3.0 times the loads specified as limit loads in composite parts.

Condition IV:	(Flight-Engine Seizure) - The seizure loads are due to the fan and engine basic gas generator decelerating from maximum to zero engine speed in one second.
Condition V:	(Crash Load) - The crash load is defined as 10g forward, 2.25g side, and 4.5g down at maximum thrust or up to zero thrust.
Condition VI:	(5 blades out) - The engine shall be capable of withstanding unbalance loads caused by the loss of five adjacent fan blades at maximum rpm (composite blades only).

Table 9-II. Frame Radial Bearing Loads.

Condition	Radial Bearing Load	
1 G Down	Newtons	Pounds
Bearing No.		
1	3,425	770
2	1.099	247
3	364	82
4	823	185
1 Radian/Sec		
Bearing No.		
1	27,397	6,159
2	27,397	6,159
3	1,699	382
4	9,559	2,149
1 Fan Blade Out		
Bearing No.		
1	175,468	39,447
2	144,295	32,439
3	16,182	3,638
4	32,494	7,305

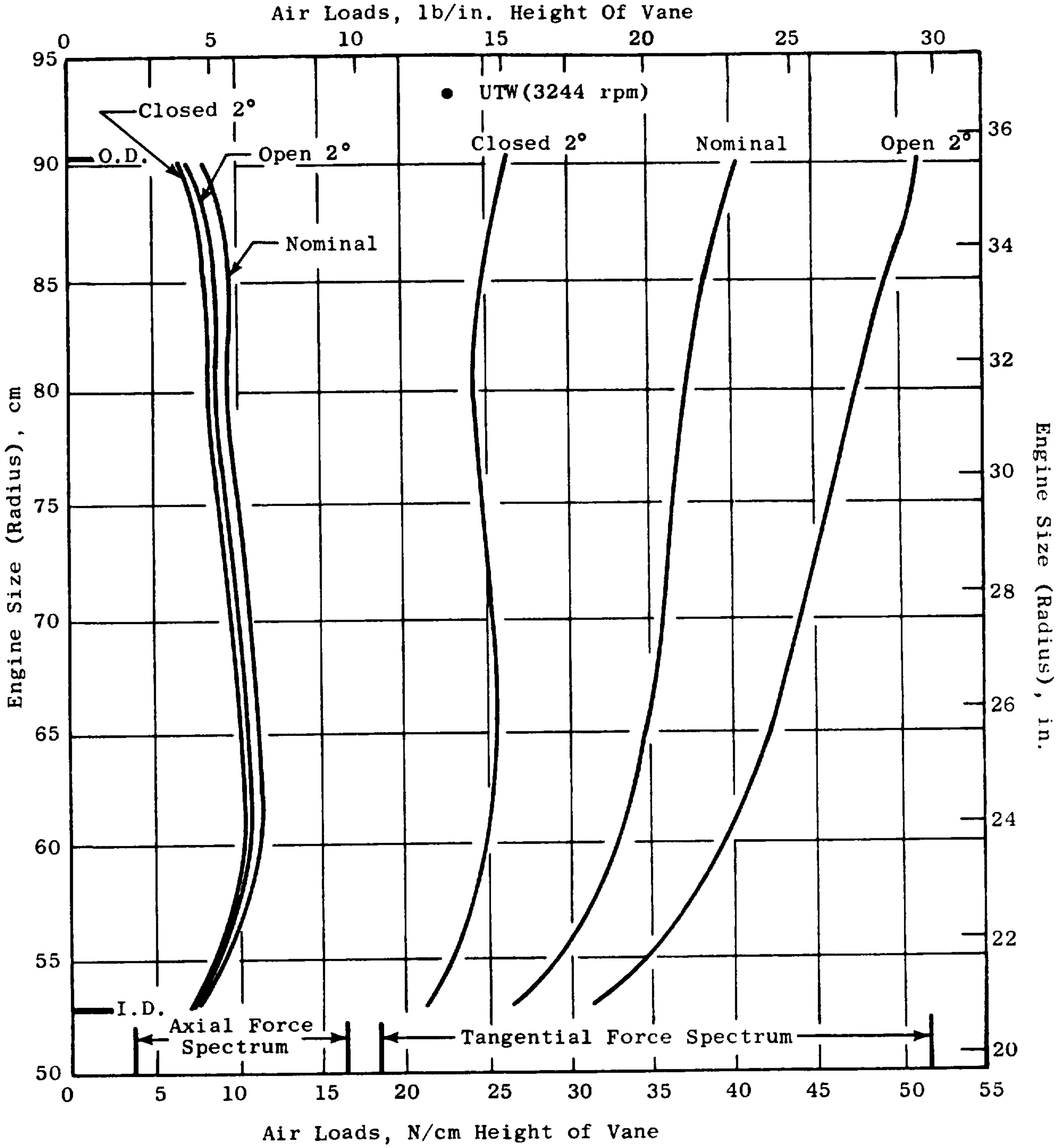

Figure 9-5. QCSEE Fan Design Bypass OGV/Frame Aero Design Air Loads - Closed 2°, Open 2°, and Nominal Vanes.

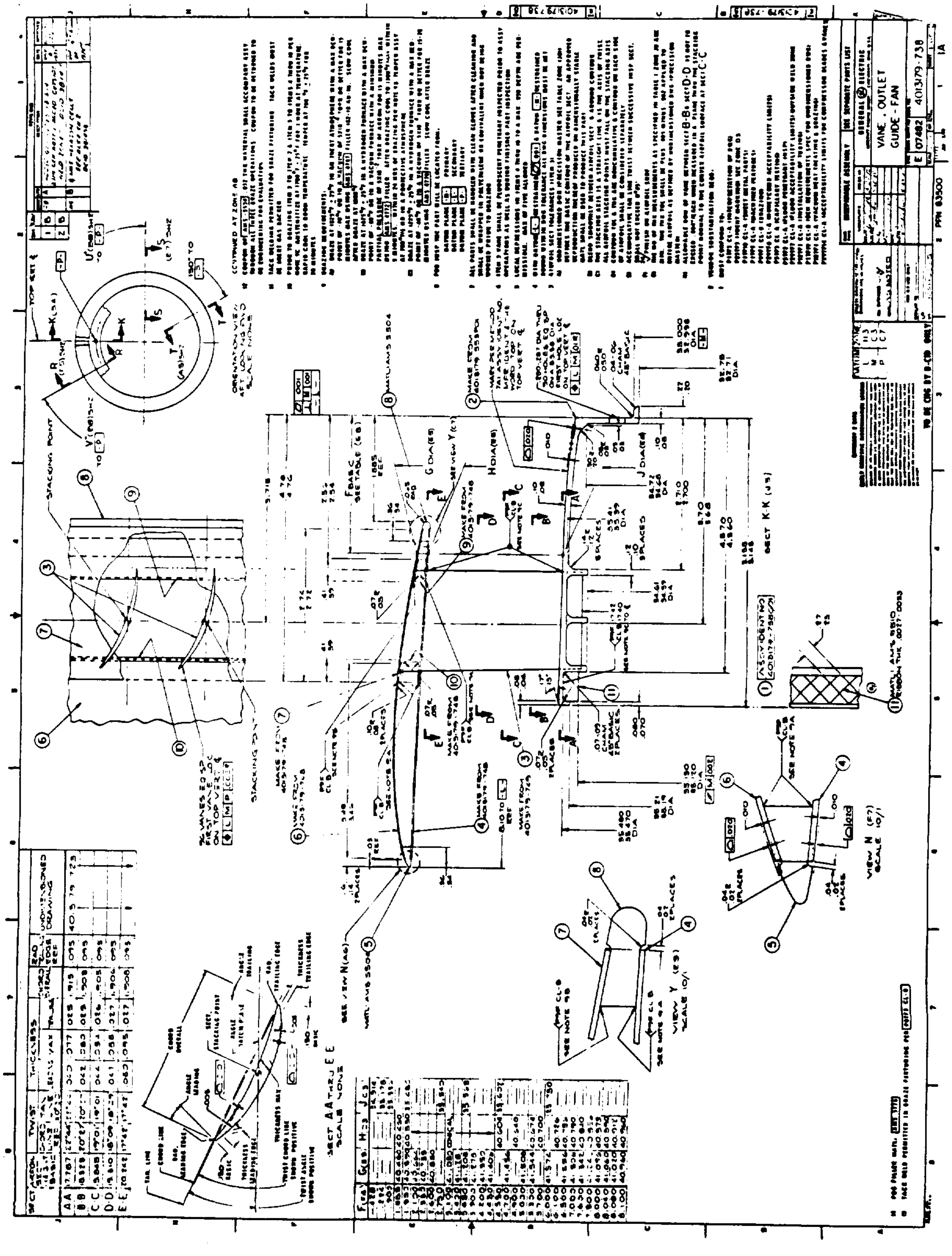
VANE, OUTLET
GUIDE - FAN
4013179-738
GENERAL ELECTRIC
SECT K-K
VIEW N
VIEW Y
SECT AA THRU EE
STACKING POINT
ORIENTATION VIEW
AFT LOOKING FWD

Figure 9-6. Fan Core OGV Assembly.

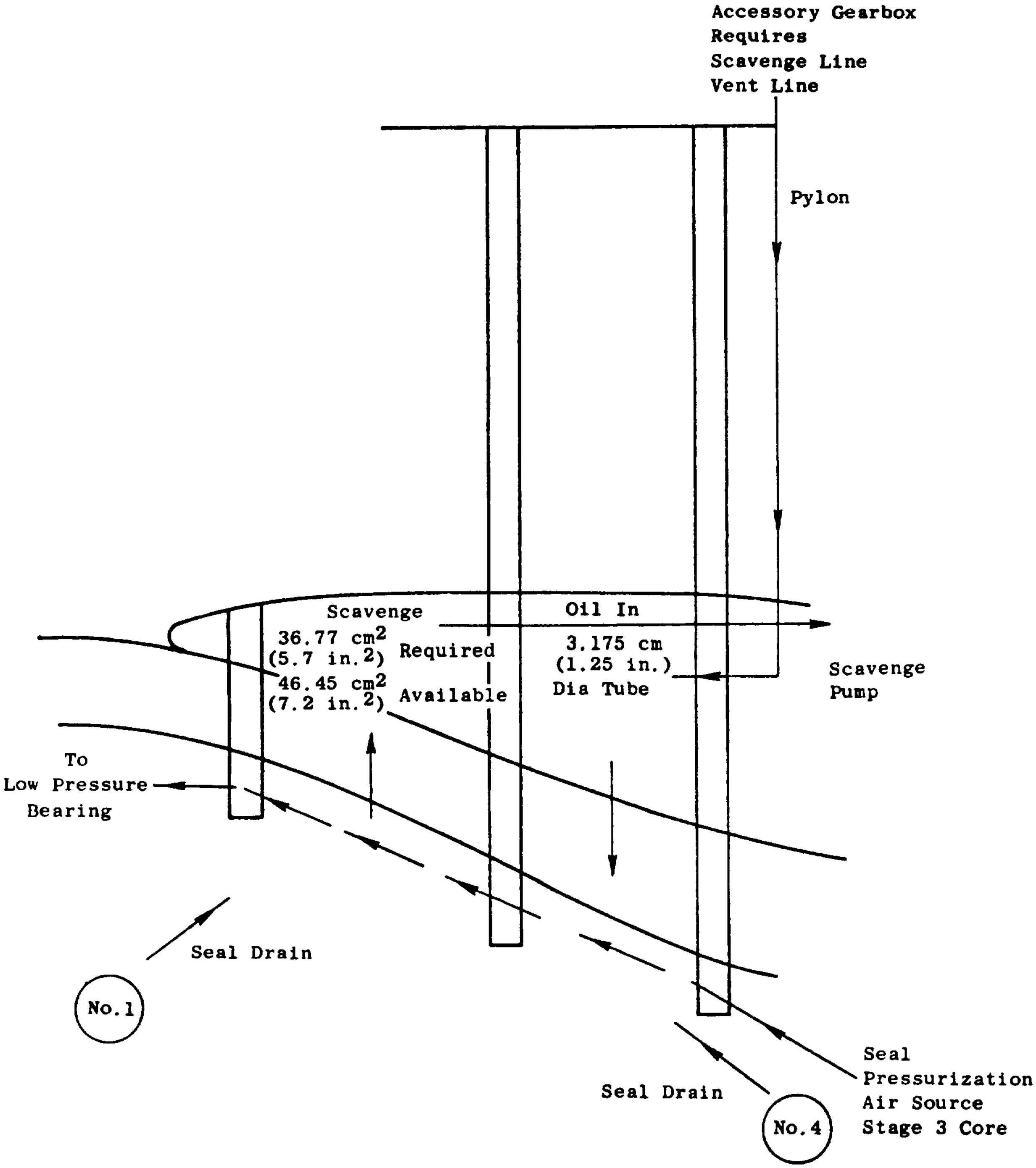
Accessory Gearbox
Requires
Scavenge Line
Vent Line
Pylon
Scavenge
Oil In
36.77 cm^2
(5.7 in.^{2})
Required
46.45 cm^2
(7.2 in.^{2})
Available
3.175 cm
(1.25 in.)
Dia Tube
Scavenge
Pump
To
Low Pressure
Bearing
Seal Drain
No. 1
Seal Drain
No. 4
Seal
Pressurization
Air Source
Stage 3 Core

Figure 9-7. Fan Frame Service Areas.

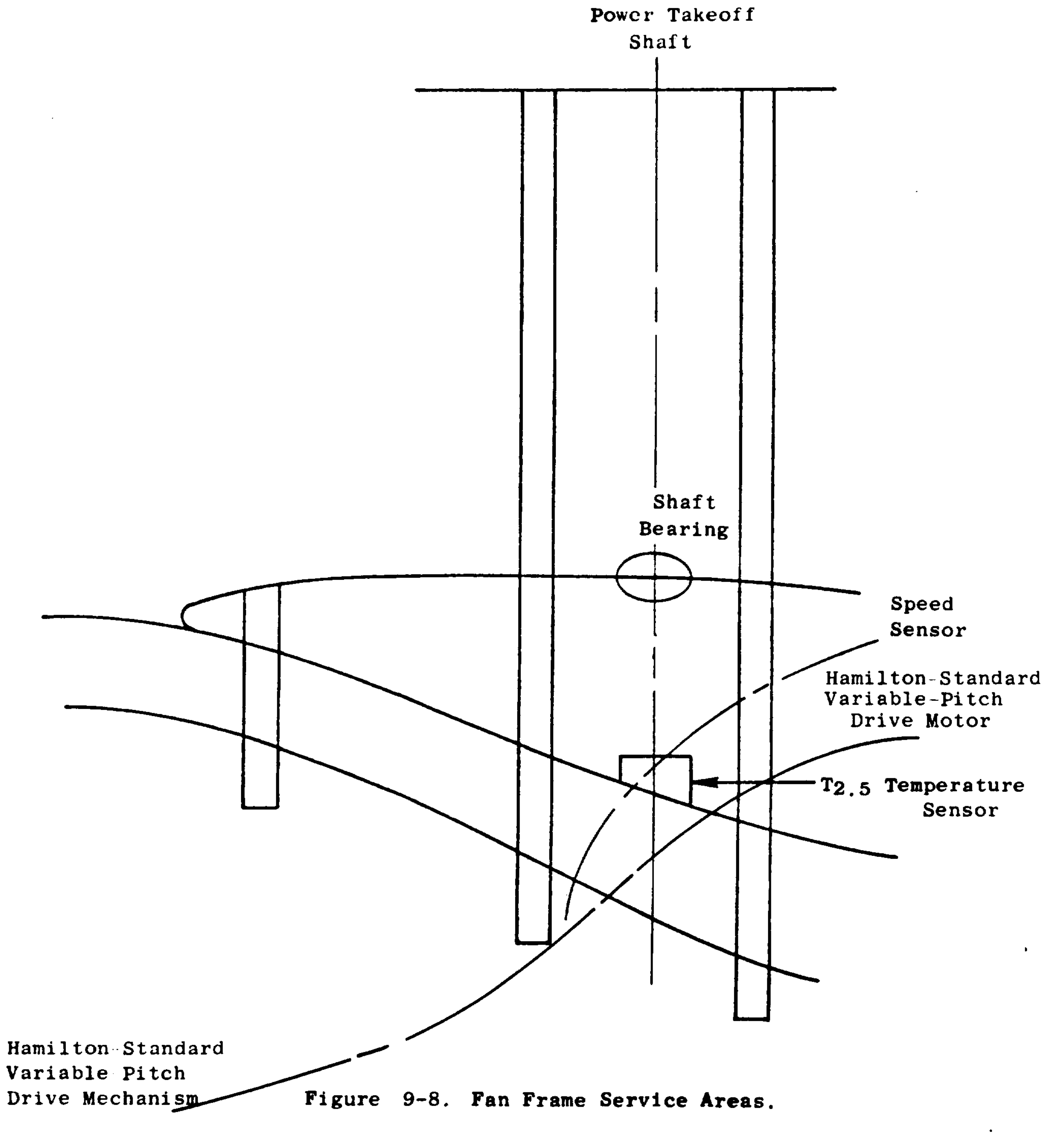
Power Takeoff
Shaft
Shaft
Bearing
Speed
Sensor
Hamilton-Standard
Variable-Pitch
Drive Motor
$T_{2.5}$ Temperature
Sensor
Hamilton-Standard
Variable Pitch
Drive Mechanism

Figure 9-8. Fan Frame Service Areas.

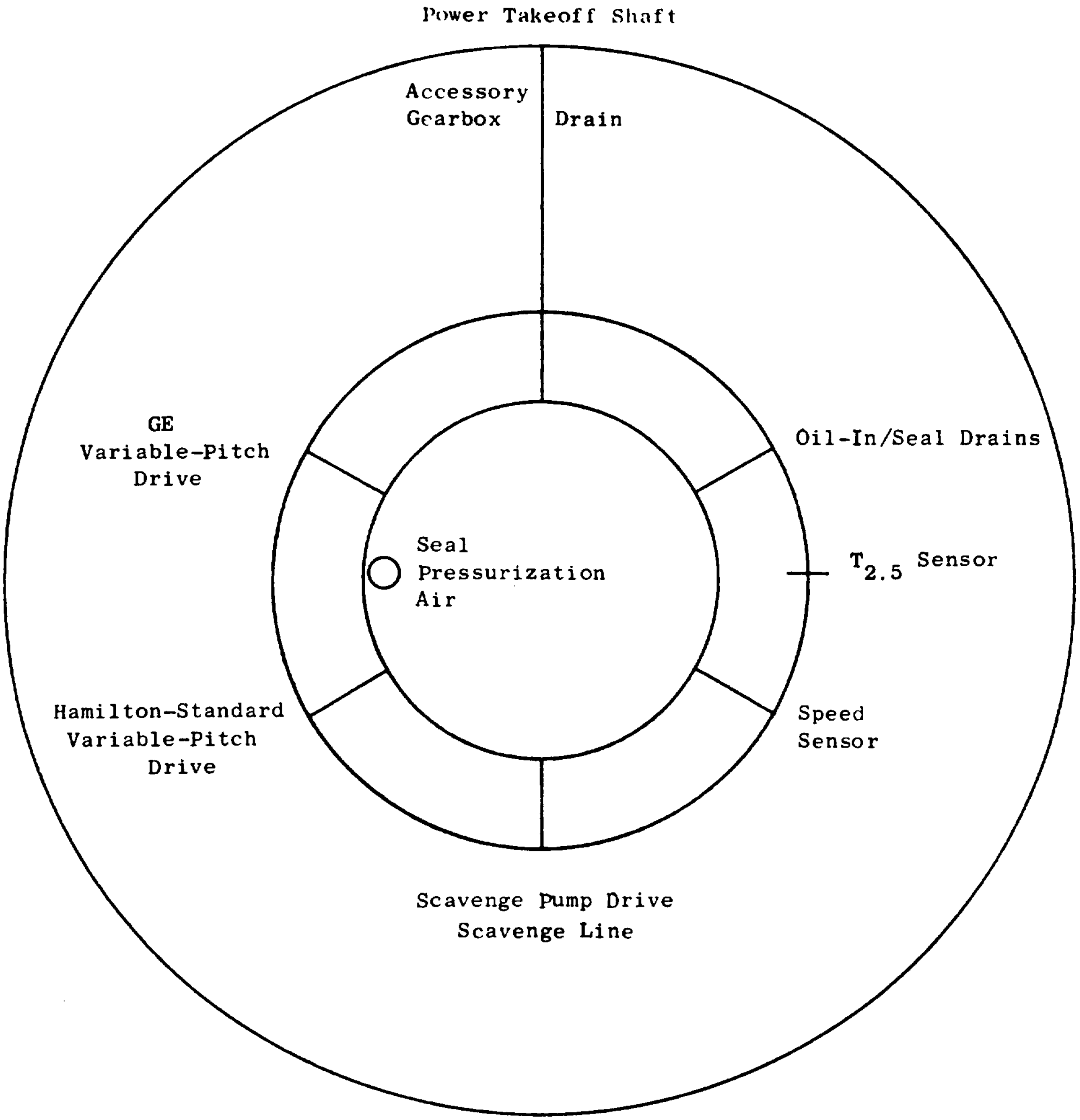
Power Takeoff Shaft
Accessory Gearbox
Drain
GE Variable-Pitch Drive
Oil-In/Seal Drains
Seal Pressurization Air
$T_{2.5}$ Sensor
Hamilton-Standard Variable-Pitch Drive
Speed Sensor
Scavenge Pump Drive
Scavenge Line

Figure 9-9. Fan Frame Service Areas (Forward Looking Aft).

Fan frame fabrication will be tailored to include the numerous penetration lines at specified steps in the manufacturing cycle. The lines are welded sheet metal and machined ring with local bosses at each O-ring to support the required clamping force. The scavenge tube and the other penetration lines are welded sheet metal or formed tubing fabricated with the required end connections for the O-ring seals.

Since the composite frame hub forms the sump wall, original plan was to have a 360° metal liner to protect the composite material from exposure to the hot sump oil; however, a series of exposure tests showed that the composite material suffered no degradation when exposed to hot oil. Supporting test data are presented in Section 9.7. As a result of these tests, the liner was eliminated.

9.4 STRUCTURAL FUNCTIONS

The QCSEE frame is required to perform the following major structural and aerodynamic functions:

- Provides the main engine forward attachment points for thrust, vertical, and side loads sustained during flight and ground handling
- Supports the fan thrust bearing
- Supports the fan radial load bearing
- Supports the variable-pitch system
- Supports the reduction gear
- Supports the compressor thrust bearing
- Supports the inlet
- Supports the aft outer and aft inner fan cowl
- Supports the core compressor at the forward casing flange
- Supports the fan hub outlet guide vanes
- Provides the mounting position for the accessory gearbox

Attachment points for all of the above structures are shown in Figure 9-10.

9.5 STRUCTURAL CONCEPT

The overall structural concept used in the frame consists of three basic elements (i.e., structural wheels, shear panels, and reinforcing flanges)

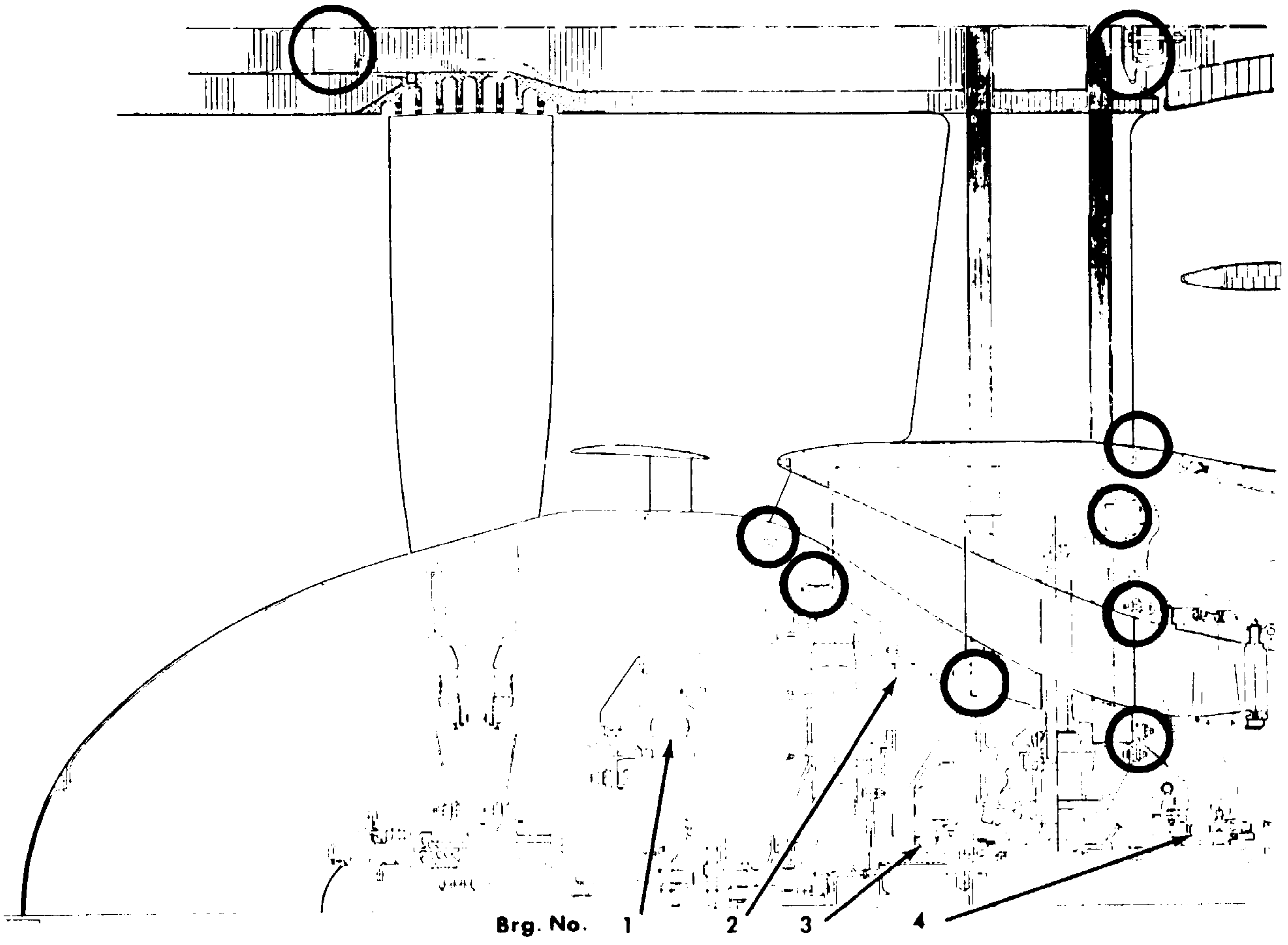

Figure 9-10. Composite Frame.

with each element designed to perform specific load-carrying functions. The large wheel-like structures are joined together with shear panels which form the bypass and core flowpaths. The frame is then locally reinforced with flanges in the outer casing splitter and hub areas as needed.

The structural wheel satisfies several load transfer requirements. First, it transfers tensile and compressive radial loads through the struts from one casing ring to another. Second, it transfers both normal and bending ring loads throughout the ring structure. Third, it transfers any forward overturning bending moments that exist in the strut from one casing shell to another. As an example of this type of structure, the detail drawing of the UTW frame mid-wheel is shown in Figure 9-11.

The shear panels are bonded to the four sides of each wheel cavity and serve as the basic load-carrying members between wheels. The panels perform the following functions. Transfer shear forces between wheels imposed on the frame by a forward overturning bending moment. Transfer radial tensile and compressive forces between casings imposed on the struts by a tangential bending moment. Transfer axial tensile and compressive forces between wheels. Serve as the airflow surfaces within the frame cavities.

Examples of these types of panels are presented in Figures 9-12 and 9-13 which show the nominal bypass vane and the core strut skin, respectively.

The reinforcing flanges located at either end of each strut or vane perform two basic load-carrying functions: first, they transfer tangential bending moments out of the struts and into the forward and aft rings, and second, they transfer tensile and compressive axial loads between wheels.

For the UTW composite frame design, analyses have shown that a three-wheel frame concept is adequate to carry all imposed loads. The forward wheel is a flat-spoked wheel comprised of splitter ring, a hub ring, and six spokes. The middle and aft wheels are flat-spoked wheels consisting of an outer casing ring, splitter ring, hub ring, six spokes integrally connecting the hub and the splitter rings, and 33 spokes integrally connecting the outer casing and the splitter rings. The shear panels are bonded to the interior of each wheel cavity, and the panels form the airflow surfaces. "L" flanges are bonded to the inner and outer rings and flowpath panels. This structural concept not only provides a frame with highly efficient joints, but also results in a structure which should facilitate fabrication and repair. Structural soundness is enhanced by transferring loads by bonding in many small increments rather than in a few large increments.

Metal engine mount parts and metal brackets are attached to the composite by bonding and mechanical fastening. The aft splitter ring contains three engine-mount attachment points. The first attachment point is located at the 0° (12 o'clock) position on the aft splitter ring and consists of a metal uniball which supports vertical and side loads. At 45° down from either side of the metal uniball, are metal brackets which support all

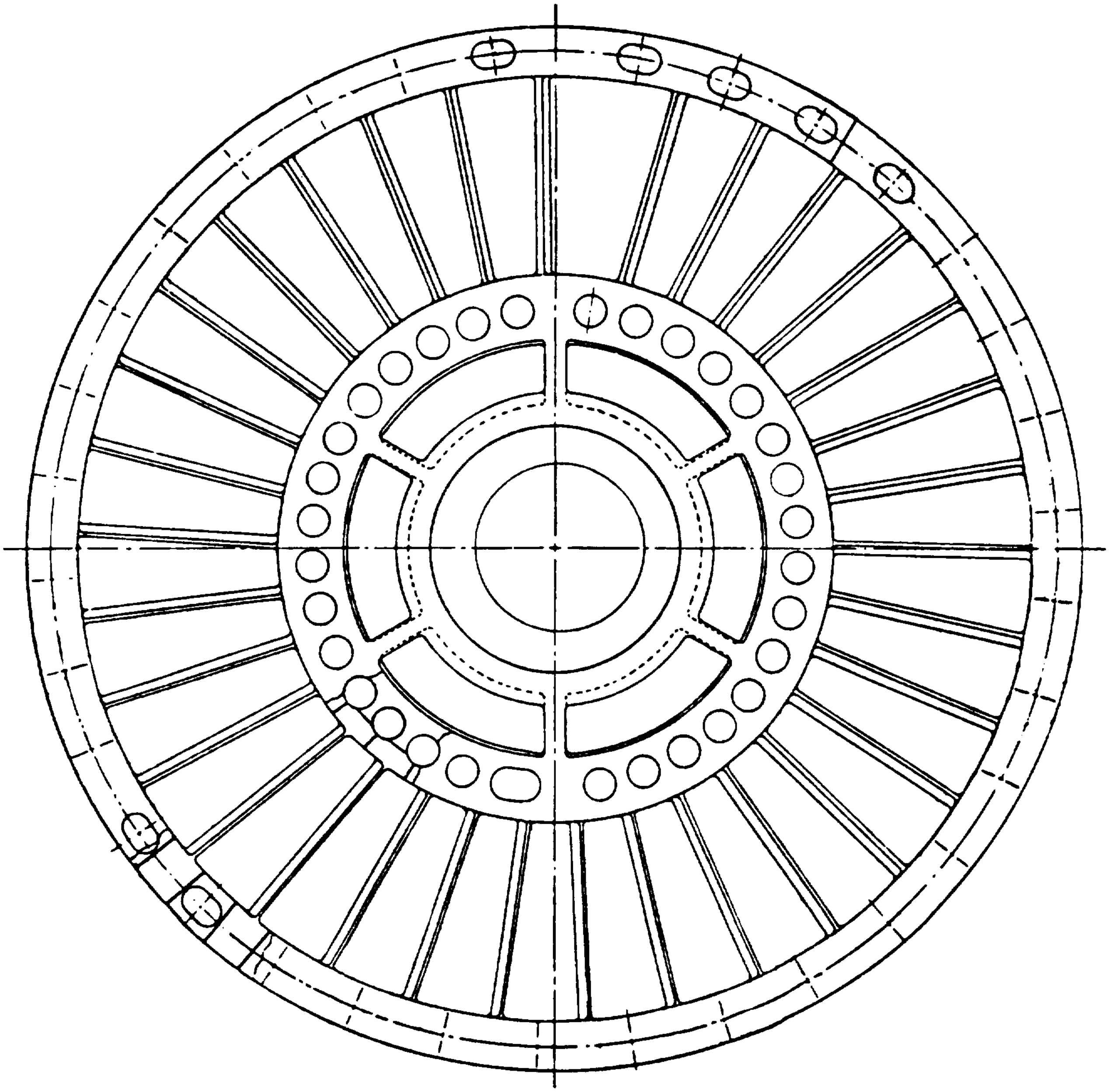

Figure 9-11. UTW Frame Midwheel.

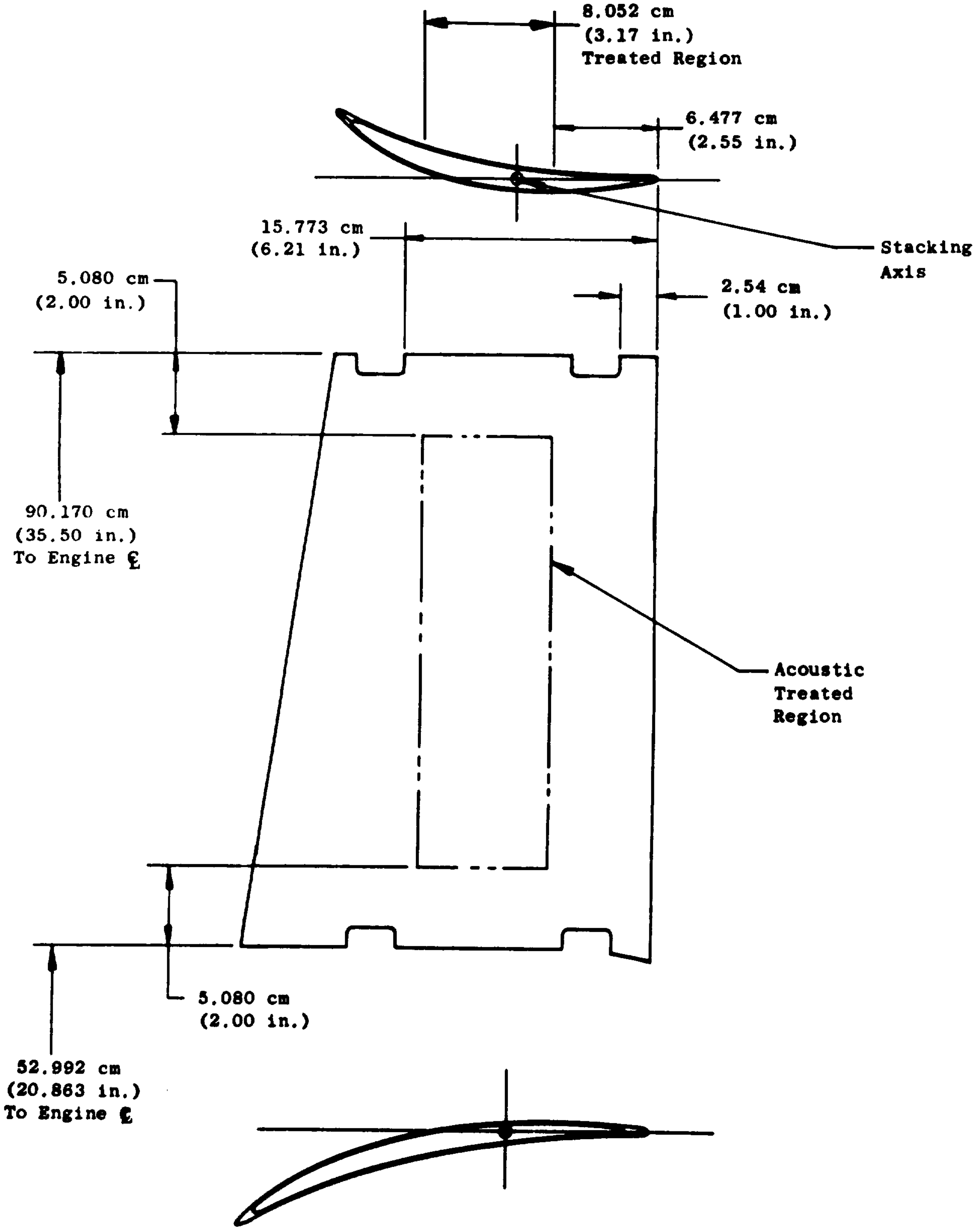
8.052 cm
(3.17 in.)
Treated Region
6.477 cm
(2.55 in.)
15.773 cm
(6.21 in.)
Stacking
Axis
5.080 cm
(2.00 in.)
2.54 cm
(1.00 in.)
90.170 cm
(35.50 in.)
To Engine ℄
Acoustic
Treated
Region
5.080 cm
(2.00 in.)
52.992 cm
(20.863 in.)
To Engine ℄

Figure 9-12. Nominal Bypass Vane Skin.

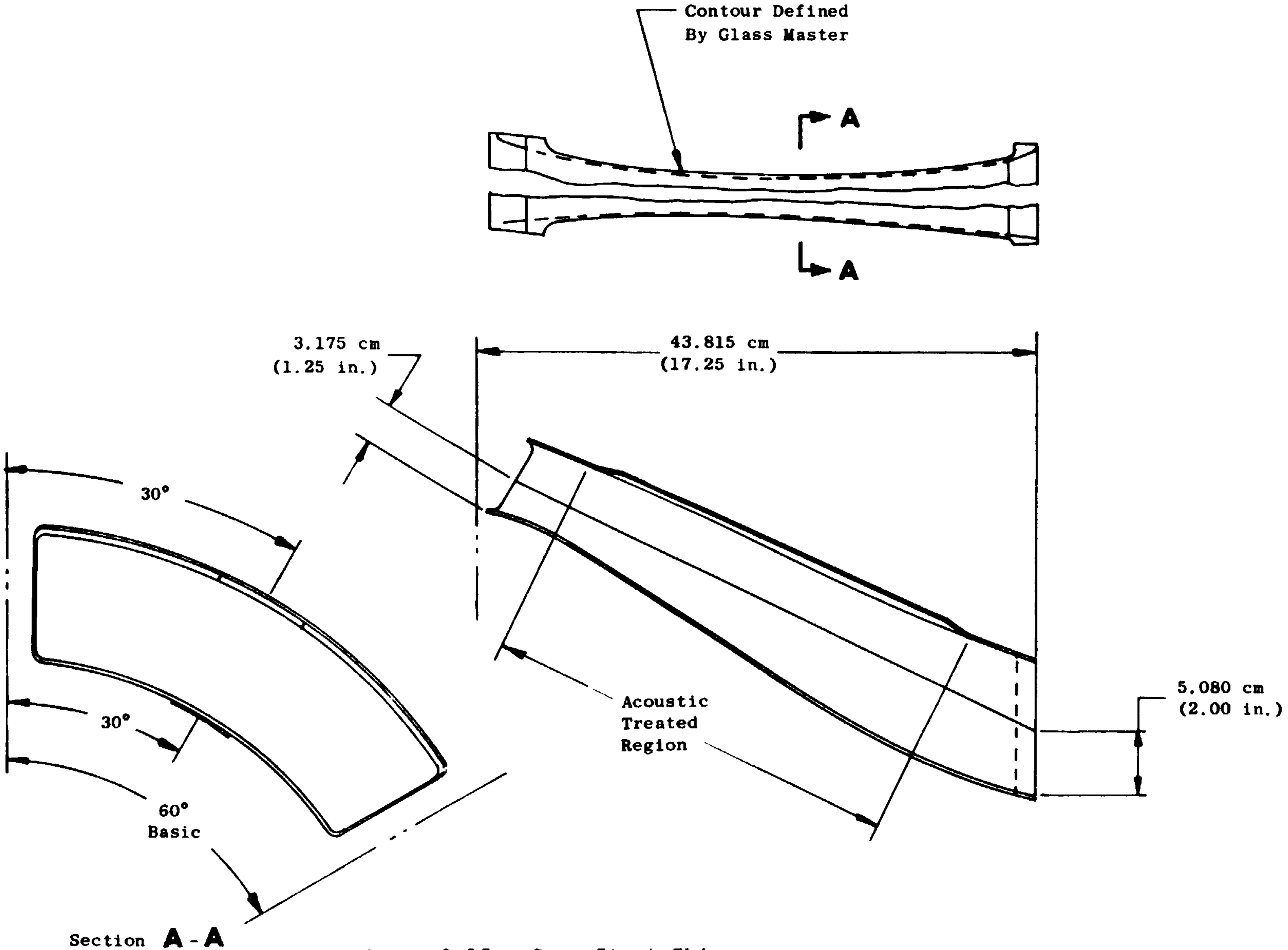
Contour Defined
By Glass Master
A
A
3.175 cm
(1.25 in.)
43.815 cm
(17.25 in.)
30°
30°
60°
Basic
Acoustic
Treated
Region
5.080 cm
(2.00 in.)
Section A-A

Figure 9-13. Core Strut Skin.

thrust loads of the engine (see Figure 9-4). The inner hub of the frame has flanges for attachment of fan rotor bearing supports, stationary reduction gear bearing supports, the low pressure turbine shaft forward bearing support, and the core rotor forward bearing support.

The nacelle and fan casing are integral with the frame from the bypass vanes forward to the inlet. The high strength and stiffness in the frame provide the necessary nacelle support and also support the stator, radial drive gearbox, and other equipment. The entire wall thickness of the fan case and nacelle is utilized to provide fan shroud stiffness and to support the blade containment member. The full-depth honeycomb is lighter and less expensive to fabricate compared to the conventional double structure. The joints normally required in a metal frame design are minimized, which reduces weight, tooling, and fabrication costs. This concept is particularly well-suited to composite materials due to their low density and easy "bondability." Slotted tip treatment and a small area of frangible honeycomb are provided over the fan blade. The blade FOD containment provisions consist of unimpregnated Kevlar-49 wrap, located in a cavity on the outside of the tip treatment structure. This material is kept in place by a closure of the cavity after the Kevlar is installed. Although this material has never been used for this particular application, it is now being successfully used in ballistic armor and has high promise as a very efficient containment material. The actual demonstration of containment using this concept is, however, not a part of the QCSEE program. A detailed view of the design is shown in Figure 9-14.

In addition to its structural functions, the frame also contains integral acoustic treatment as indicated by the cross-hatched areas in Figure 9-15. All sound treatment in the frame is 10% open area. The holes are 0.159 cm (0.0625 in.) in diameter and are produced by numerically controlled laser drilling.

9.6 DESIGN ANALYSIS

The integral load distribution for the frame was determined using a finite element computer program which represented the frame structure as a combination of curved beams, straight beams, and plates, all capable of having orthotropic material properties.

In the core region of the frame, the struts were modeled as three straight beams (representing the spokes of the wheels) connected to curved beams in the hub and splitter region (rims of the wheels), all tied together by plates representing the flowpath and splitter walls. The fan flowpath area was represented by radial beams representing the bypass vanes (wheel spokes and flowpath panels were lumped together and appropriate section properties used for these pseudo beams) tied to plates representing the outer casing forward to the inlet. Appropriate structure was also included to represent the mount structure and the compressor case back to the turbine frame; although this structure is not shown in the accompanying figures. The basic mathematical model is shown, superimposed on the frame trimetric in Figure 9-16. Computer generated views of the model are shown in Figures 9-17 and 9-18.

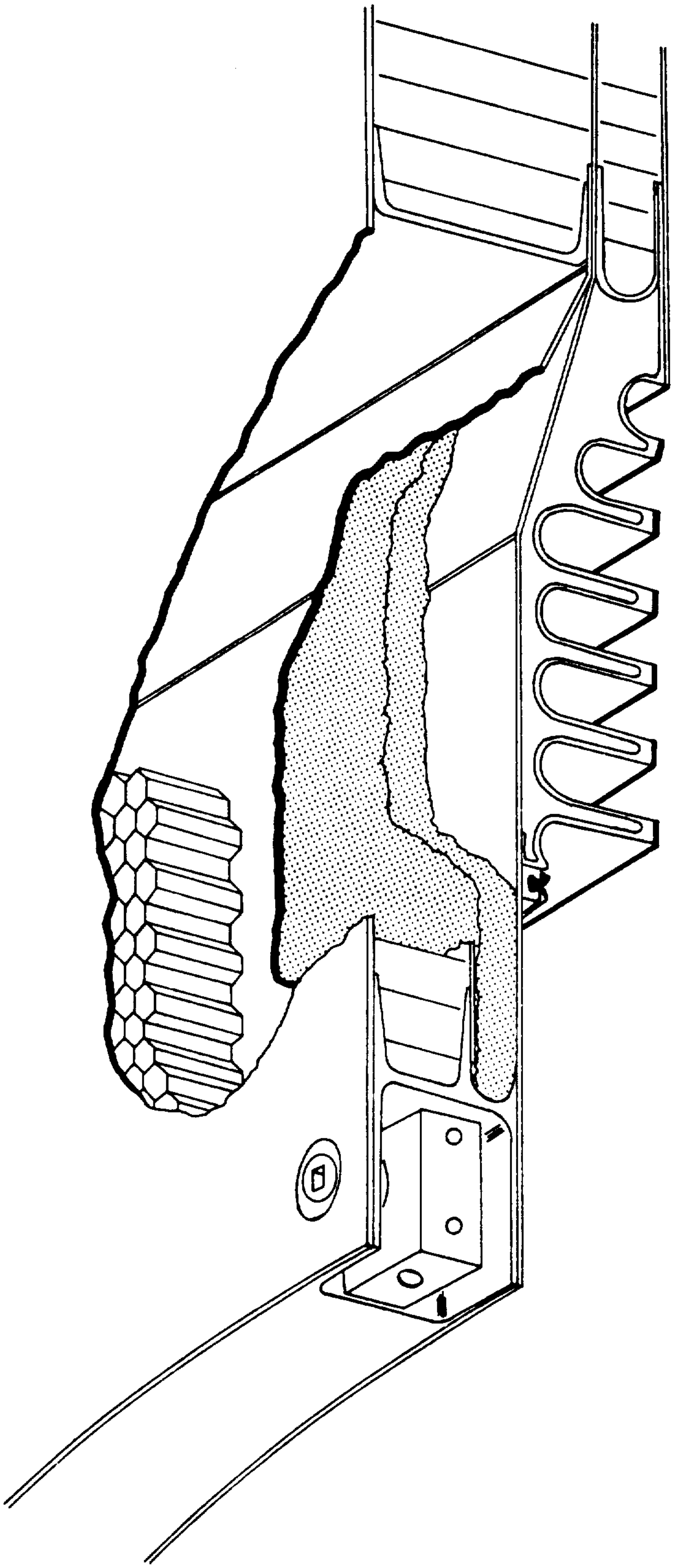

Figure 9-14. Fan Blade Containment Ring.

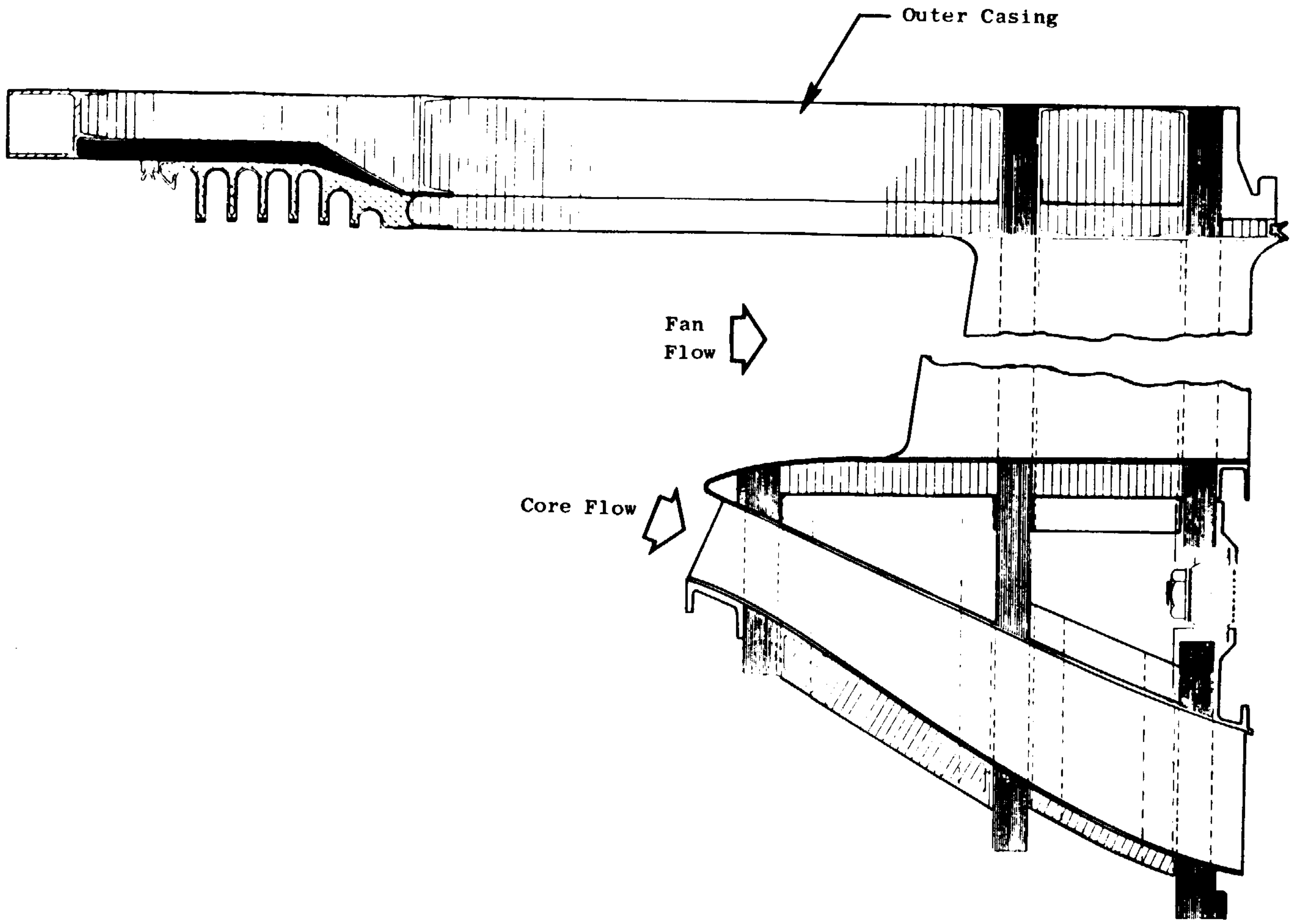
Outer Casing
Fan Flow
Core Flow

Figure 9-15. Fan Frame Acoustic Treated Areas.

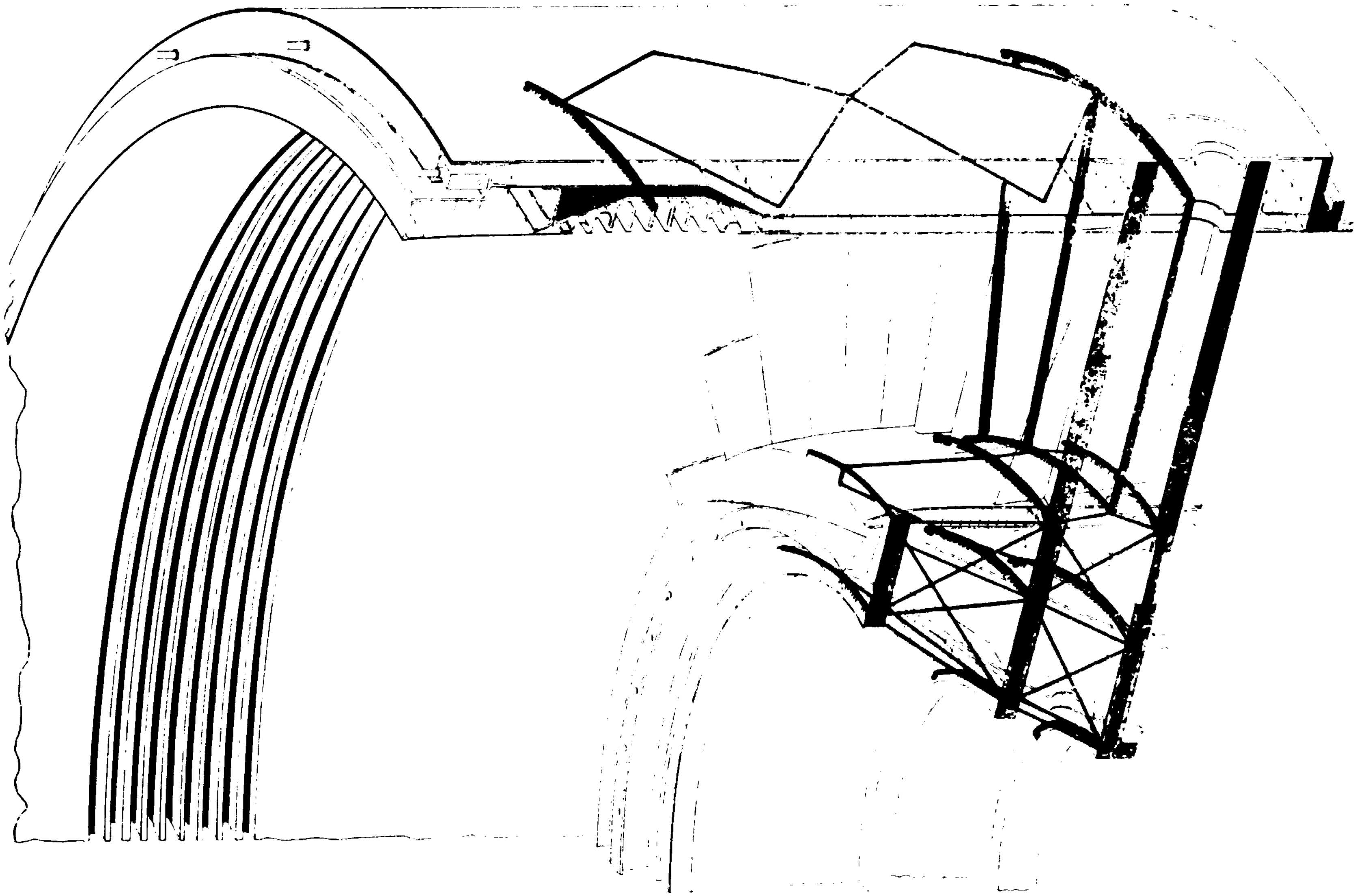

Figure 9-16. Computer Analytical Model of Composite Frame.

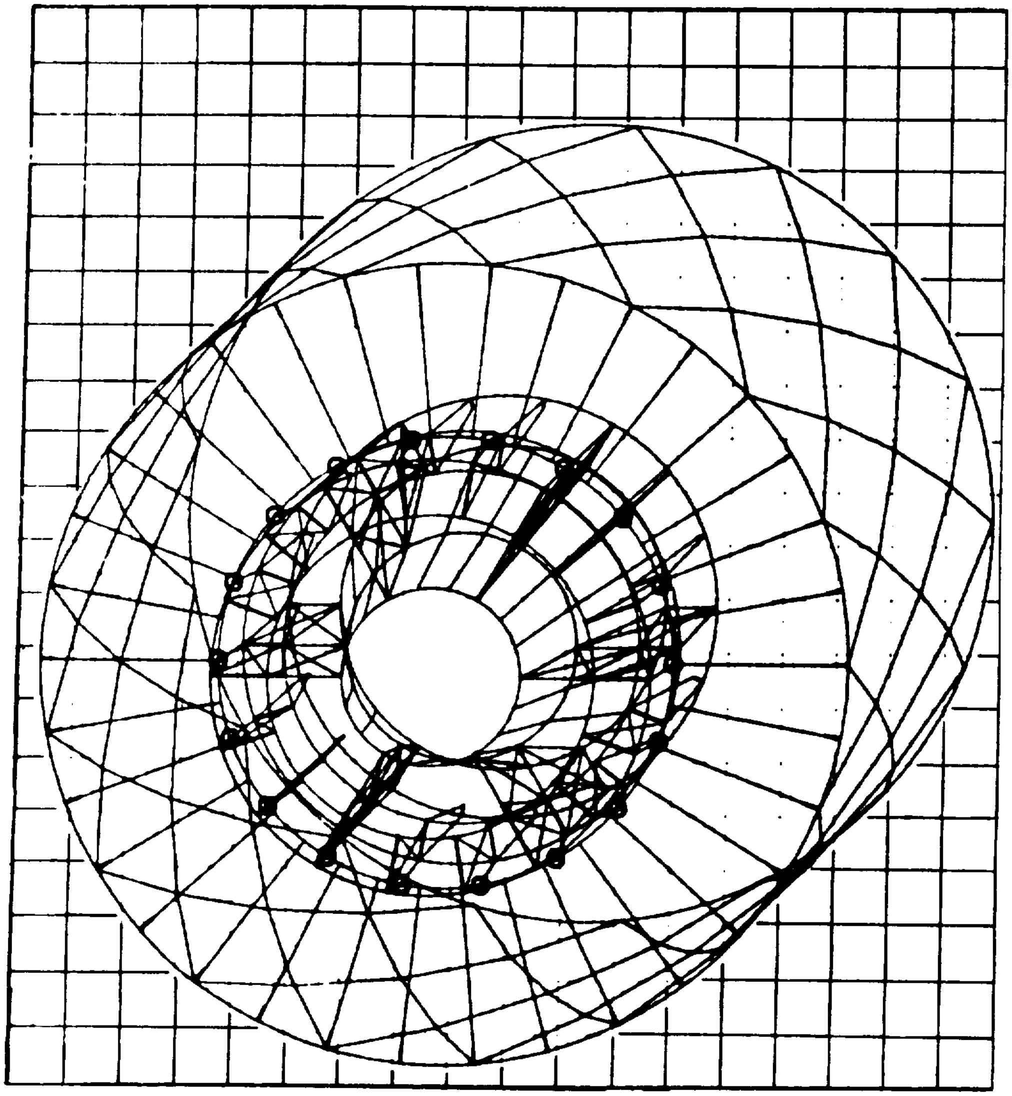

Figure 9-17. Computer-Generated 3-Dimensional Finite Element Model - Composite Frame.

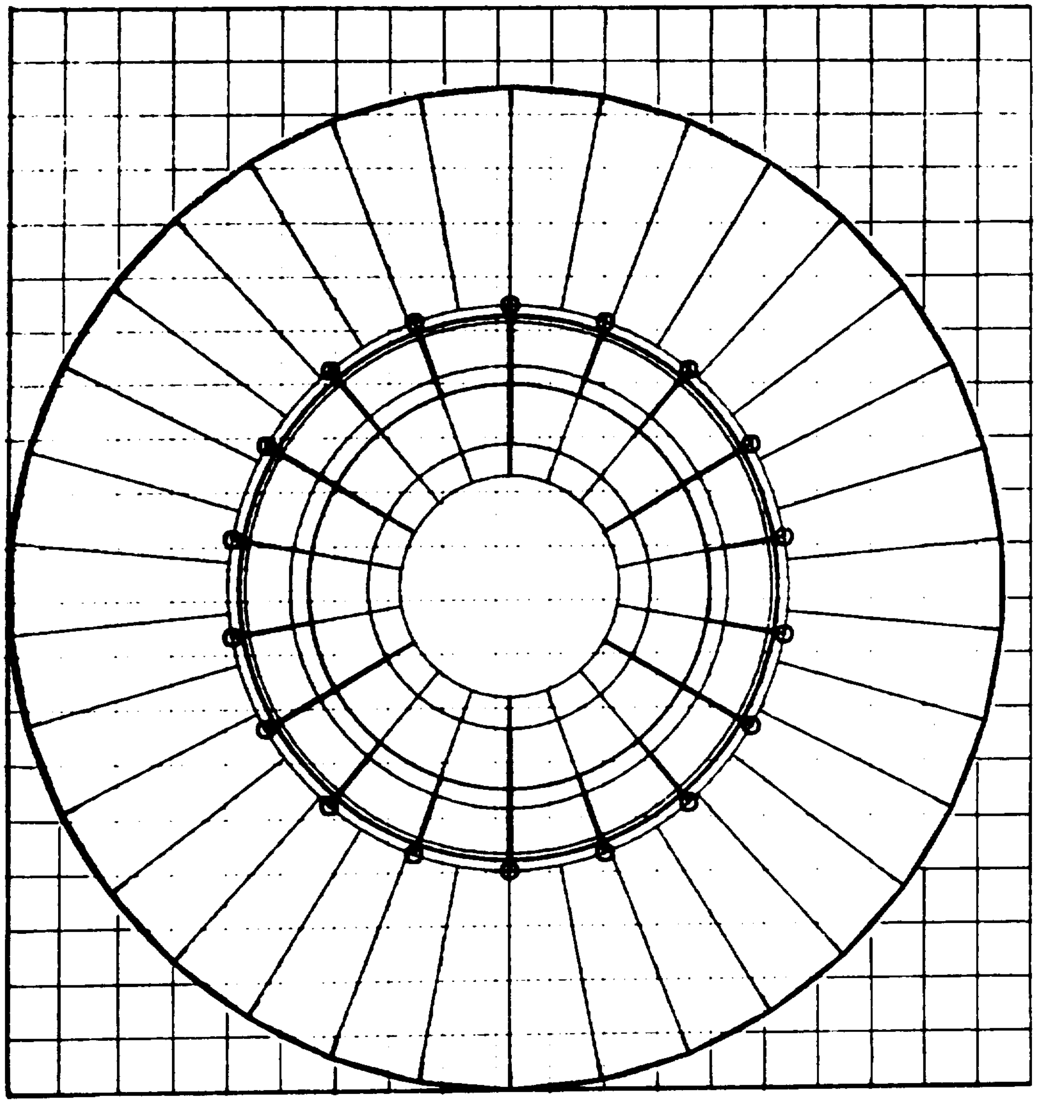

Figure 9-18. Computer-Generated End View Finite Element Model - Composite Frame.

A number of iterations were made on thicknesses and orientations of the various constituent elements of the mathematical model to arrive at an efficient structure which would satisfy the most severe loading conditions. The frame structure, in conjunction with the engine mounts, must withstand the maneuver loads as imposed by the conditions defined in Table 9-I. The frame must withstand these loads and maintain structural integrity without permanent deformation. In addition, this structure must be capable of transmitting mount loads equivalent to 3.0 times the worst possible combination of maneuver loads without experiencing collapsing, even though the member may acquire permanent deformation. All ultimate load conditions are calculated under a room temperature environment. Investigation of the mission requirements yielded two critical loading cases.

The first case is Condition II (gust loading). Design conditions require the frame to withstand three times the loads of a 51.44 m/sec (100 knot) crosswind acting at any angle within a plane perpendicular to the axis of the engine at zero-to-maximum thrust. This condition sized the outer nacelle shell and bypass vanes.

The second case is Condition VI (five-blade-out condition) which requires the frame to withstand the unbalance load resulting from a five composite blade-out condition on the fan rotor which causes a dynamic, 1/rev radial load on the No. 1 bearing support. This condition sized the core struts, hub, and splitter.

The final sizing for all the major frame structure is shown in Table 9-III, which gives both thicknesses and material configuration. The internal loads, stresses, and deflections associated with this configuration were computed by the finite element computer program. The critical stresses, along with the predicted allowables, for the major structural members are shown in Table 9-IV. The allowables are taken from the Advanced Composites Design Guide. A comparison of these predicted allowables with coupon test data is presented in Section 9.7. The critical bond stresses calculated from the computer model output are shown in Table 9-V. The maximum radial deflection of the fan casing over the fan was 0.086 cm (0.034 in.). Running clearance is 0.254 cm (0.1 in.).

9.6.1 Thermal Analysis

Due to the low thermal coefficient of expansion that is characteristic of graphite/epoxy composites, an analysis of the critical interface areas, where metal structure is attached to composite structure and subjected to thermal changes, was performed. The only areas where this occurs to any significant extent is in the hub region where the titanium bearing cones are bolted to the composite rings and are subjected to a ΔT of 366 K (200° F). Applying the entire $\alpha\Delta T$ stress to the composite structure results in the stresses shown in Table 9-VI. This table also shows the summation of the static stress and the thermal stress versus the allowable stress. As can be seen, the thermal stresses are relatively low and had little or no effect on the sizing of the composite structure.

Table 9-III. Geometry of Composite Frame Components.

Material: Type AS Graphite/3501 Epoxy

Item	Thickness		Layup Configuration			0° Datum
	cm	inches	0°	± 45°	90°	
Forward "Wheel"	2.54	1.000	50%	20%	30%	Radial
Middle "Wheel"	2.87	1.130	30%	20%	50%	Radial
Aft "Wheel"	2.87	1.130	30%	20%	50%	Radial
Nacelle Panel	0.089	0.035	28.5%	57%	14.5%	Axial
Bypass Vane Panel	0.127	0.050	40%	40%	20%	Radial
Bypass Vane Spoke	2.54	1.000	80%	20%	0%	Radial
Bypass Vane Outer Ring	2.54	1.000	30%	20%	50%	Radial
Core Vane Panel	0.203	0.080	25%	50%	25%	Axial
	0.254	0.100	40%	40%	20%	Axial

Table 9-IV. Frame Component Stresses.

Load Condition	Location	Calculated Stress, N/cm^2 (psi)	Mode(1)	Direction(2)	Stress Allowable N/cm^2 (psi)	Temperature K (° F)
Ground Test	Forward "Wheel" Hub Ring	17,906 (25,970)	T	C	42,749 (62,000)	406 (270)
5 Airfoils Out	Forward "Wheel" Hub Ring	37,233 (54,000)	T	C	42,749 (62,000)	406 (270)
Ground Test	Forward "Wheel" Spoke	19,805 (28,724)	C	R	65,503 (95,000)	294 (70)
5 Airfoils Out	Forward "Wheel" Spoke	53,574 (77,700)	C	R	65,503 (95,000)	294 (70)
Ground Test	Bypass Vane Panel	4,208 (6,103)	C	R	57,229 (83,000)	294 (70)
Critical Flight	Bypass Vane Panel	40,921 (59,349)	T	R	57,229 (83,000)	294 (70)
Ground Test	Bypass Vane Spoke	2,742 (3,977)	C	R	93,083 (135,000)	294 (70)
Critical Flight	Bypass Vane Spoke	34,938 (50,671)	C	R	93,083 (135,000)	294 (70)
5 Airfoils Out	Core Panel	8,599 (12,471)	S	-	17,238 (25,000)	294 (70)
Ground Test	Nacelle Panel	2,803 (4,065)	T	A	27,580 (40,000)	294 (70)
Critical Flight	Nacelle Panel	12,699 (18,417)	T	A	27,580 (40,000)	294 (70)

(1) T - Tension; C - Compression; S - Shear
(2) C - Circumferential; R - Radial; A - Axial

Table 9-V. Bond Shear Stresses.

Load Case No.(1)	Location	Design Stress(2)		Allowable Stress	
		N/cm^2	psi	N/cm^2	psi
2	Vane/Splitter	605	878	1034	1500
6	Panel/O.R. Fwd "Wheel"	748	1085	1034	1500
6	Panel/Spoke Fwd "Wheel"	806	1169	1034	1500
6	Panel/I.R. Fwd "Wheel"	481	698	1034	1500

(1) Case 2 - 154.33 m/sec^2 (100 knot) crosswind gust load + max maneuver
Case 6 - 5 composite blade out + max maneuver.

(2) Design stress - 3 x actual for flight and actual for emergency conditions.

Table 9-VI. Effect of Different Thermal Coefficients.

Ring	Thermal Coefficient Graphite Epoxy Ring cm/cm/° K x 10^{-6} (in./in./° F x 10^{-6})	Bearing Number	Thermal Coefficient Bearing - Ti6-4 cm/cm/° K x 10^{-6} (in./in./° F x 10^{-6})	Thermal Stress N/cm^2 (psi)	Static Ring Stress N/cm^2 (psi)	Total Stress N/cm^2 (psi)	Allowable Stress N/cm^2 (psi)
Forward Hub	4.5 (2.5)	1a, 1b	8.46 (4.7)	2069 (3000)	37233 (54000)	39302 (57000)	42749 (62000)
Mid Hub	2.34 (1.3)	2	8.46 (4.7)	4827 (7000)	20685 (30000)	25512 (37000)	59987 (87000)
Aft Hub	2.34 (1.3)	3	8.46 (4.7)	4827 (7000)	13790 (20000)	18617 (27000)	59987 (87000)

9.6.2 Dynamic Analysis

Since the fan stator vanes are an integral part of the fan frame a dynamic analysis was performed to determine the relationship of the vane first flexural frequency to fan speed for the critical 18 per revolution (18 blade) excitation. The first flexural frequency of the composite vane was estimated by making an empirical correction to a theoretically calculated value. This correction was determined by actually measuring the frequency response of a very similar vane in the composite simulated F101 front frame which was available as a result of a previous program. This measured value was compared to the theoretical value for this vane and the correction factor thus obtained. Using this method, the first flexural frequency of all five of the UTW bypass vane configurations was obtained. These show up as a band in Figure 9-19, which shows the lowest first flexural frequency crossing the 18/rev line at 115% of the maximum normal fan speed. It was concluded from this analysis that the vane first flexural response to the critical 18/rev pressure pulse was outside the engine operating range.

9.6.3 Weight Analysis

A weight analysis was performed based on the structure described in Section 9.3 and the sizing determined from the structural analysis. Results of this analysis are shown in Table 9-VII. These weights do not, however, include the weight of instrumentation or auxiliary items, even though they will become an integral part of the frame.

9.7 SUPPORTING DATA

The composite frame must attach to (and be detachable from) various structures at a large number of locations. Also, the composite frame employs a large number of structural joints that are integrally bonded rather than mechanically fastened together. Component tests were conducted using specimens and subcomponents representative of various critical areas of the frame to verify the effect of geometry, fiber orientation, and environmental exposure on the allowable design stress levels in these specific components.

9.7.1 Element Test Program

The material properties used in the design and analysis of the composite fan frame were taken from the Advanced Composites Design Guide, third edition. A limited element test program was conducted to verify that the processing techniques to be used on the frame would produce adequate results, and also to provide a check on the data obtained from the Design Guide.

The test program is summarized in Table 9-VIII. Four critical areas of the frame were selected and preliminary material configurations were defined. Since the purpose of the test program was to verify the processing techniques, and not to produce specific design data, it was not necessary to delay the test program until the final material configurations were determined.

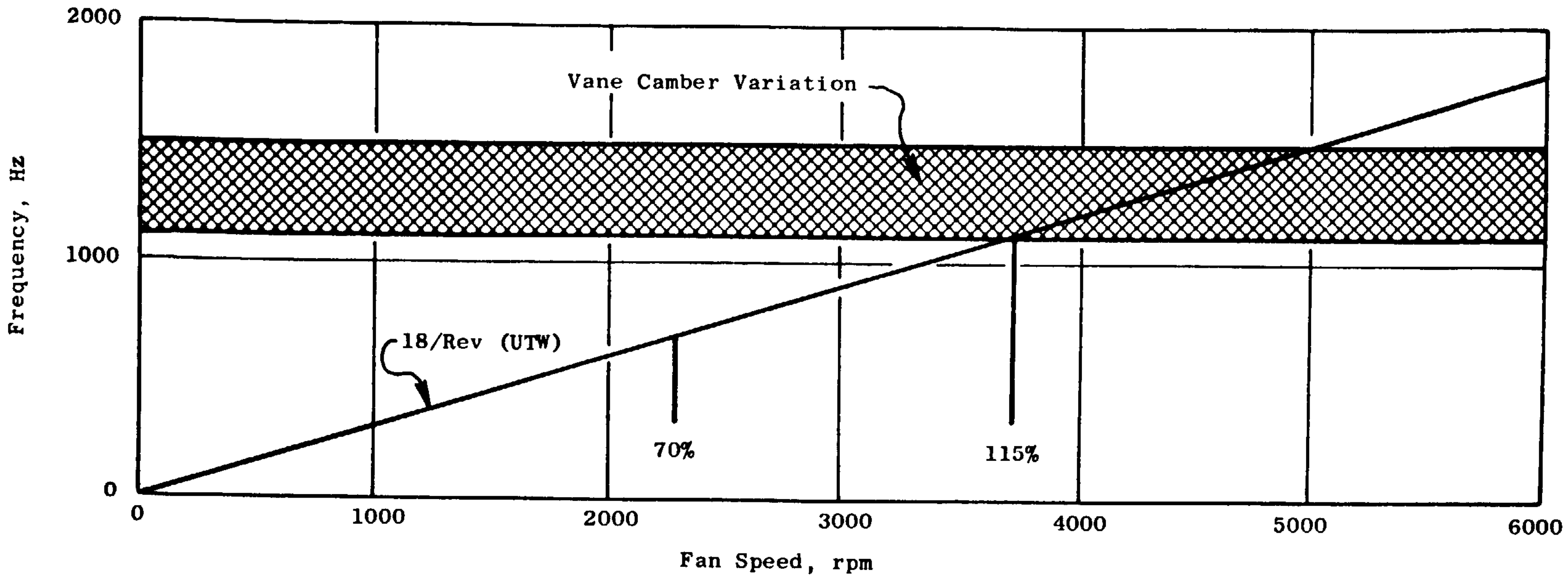

Figure 9-19. First Flexural Mode of Composite Frame Bypass Vanes.

Table 9-VII. Composite Frame Weight Breakdown.

	Weight	
	kg	lb
Composite "Wheels," Rings, and Panels	120.2	265
Honeycomb	13.2	29
Composite Reinforcing Flanges	21.8	48
Adhesive	4.5	10
Inlet Flange	8.6	19
Sump Shield	2.7	6
Containment	20.9	46
TOTAL WEIGHT	191.9	423
Mounts	10.4	23

Table 9-VIII. Test Specimen Configurations.

Serial Identification	General Configuration Representation	Material	0° Datum	Test Dir.	Test Temp.	Test Mode (2)									
						IITRI (3) Tensile	Sandwich Beam Tensile	Sandwich Beam Compression	Rail Shear (Flat Panel)	Rail Shear (Sandwich Panel)	Interlaminar Shear	Bolt Hole Bearing	Bolt Hole Shear-Out	Bolt Hole Net Tension	Clamping
101	Outer Nacelle Shell	Boron-Graphite/ Epoxy	Axial	0°	R.T.	X	X	X	X	X					
				90°	R.T.	X	X	X	X	X					
102	Bypass Vane Panels	Graphite/Epoxy	Radial	0°	R.T.	X	X	X	X						
				90°	R.T.	X		X	X						
		Graphite/Epoxy (10% Open Area)		0°	R.T.	X	X	X	X	X					
103	Bypass Spoke	Boron-Graphite/ Epoxy (1)	Radial	0°	R.T.	X		X			X				
104	Forward Core Spoke and Rings	Graphite/Epoxy	Radial	0°	R.T.	X	X	X	X		X	X	X	X	
				0°	406 K (270° F)	X		X				X	X	X	X
				90°	R.T.	X		X	X		X	X	X	X	
				90°	406 K (270° F)	X		X				X	X	X	

(1) 0° Plys - Boron
± 45° and 90° plys are graphite

(2) Each test mode consists of 3 replicates

(3) IITRI - Illinois Institute of Technology Research Institute

The test results for the tension, compression, shear, and bolt hole testing are shown in Tables 9-IX through 9-XII. Configurations 101 and 102, as defined in Table 9-IX, were relatively thin (<0.127 cm/0.050 in.) and several tab failures occurred during the IITRI (Illinois Institute of Technology Research Institute) type tensile testing. Comparable sandwich beam tests indicated that the tensile values obtained from the tests in which tab failures occurred were not representative. Configurations 103 and 104 were relatively thick (<0.254 cm/0.100 in.) and sandwich beam data could not be obtained due to shear failure of the core-to-face bond, as indicated in Tables 9-IX and 9-X. The only test value in the program that was significantly below predicted was the zero degree orientation at room temperature test of Configuration 104. Other tests of this configuration [90° orientation at 405 K (270° F)] were considerably above predicted strength, indicating that the results for zero degrees orientation at room temperature were not valid. Based on these data, it was concluded that it was reasonable and valid to use information obtained from the Design Guide for the design and analysis of the frame.

To evaluate the effect of acoustic treatment holes in the vane skins, IITRI tensile tests were run using a 10% open area pattern of holes. The gross tensile strength was 29,600 N/cm^2 (43,000 psi) and the net tensile strength was 37,700 N/cm^2 (54,700 psi) compared to a baseline (no holes) value of 53,900 N/cm^2 (78,200 psi) as shown in Table 9-IX. This gives a stress concentration factor of 1.43. This information was taken into account in the stress analysis of the bypass vanes. The same stress concentration was assumed for the acoustically treated outer casing.

9.7.2 Fluid Exposure Tests

Two series of tests were run to evaluate the effect of evaluated temperature exposure to aircraft fluids. The first series of tests evaluated the exposure to "Skydrol 500C." The exposure conditions were selected based on that expected in the UTW engine installation where any exposure of the graphite/epoxy will be of an intermittent nature which will leave residual fluid on the composite material. The specific composite material system tested was the type AS graphite fiber in Hercules' 3501 epoxy resin matrix.

The degradation due to exposure was measured as changes in the compression and tension values of the exposed material. The composite material was molded and fabricated into individual test specimens. The tension specimens were of the IITRI type, while the compression specimens were modified ASTMD 695-69 specimens. The specimens, except for the control specimens, were exposed to "Skydrol 500C" hydraulic fluid for five minutes at 355 K (180° F) followed by an oven exposure (without wiping or drying the specimens) at 355 K (180° F) for time periods ranging from zero to 15 days. Ultimate strength values were then obtained from the specimens.

The results of these tests are shown in Figure 9-20. Although there is some test scatter, it appears that the material system tested was not degraded by the exposure.

Table 9-IX. Tensile Test Results.

Basic Material - Graphite/Epoxy

Serial Identification	Laminate Configuration % Fiber at			Load Direction (degrees)	Temperature K (° F)	Predicted Stress N/cm^2 (psi)	Avg. Test Results		Average % Difference
	0°	45°	90°				IITRI(4) N/cm^2 (psi)	Sandwich Beam N/cm^2 (psi)	
101	14(1)	57	29	0	Room Temperature	23305 (33800)	23395 (34800)	24408 (35400)	+4
				90	Room Temperature	39439 (57200)	32682 (47400)(2)	40405 (58600)	+2
102	40	40	20	0	Room Temperature	56539 (82000)	53919 (78200)	51575 (74800)	-7
				90	Room Temperature	37923 (55000)	27856 (40400)(2)	--- ---	--- ---
103	80(1)	20	0	0	Room Temperature	93083 (135000)	94875 (137600)	--- ---	+2
104	50	20	30	0	Room Temperature	64124 (93000)	51023 (74000)	(3)	-20
				0	406 (270)	59987 (87000)	69364 (100600)	--- ---	+16
				90	Room Temperature	44128 (64000)	51988 (75400)	--- ---	+18
				90	406 (270)	42060 (61000)	63020 (91400)	--- ---	+50

(1) Boron/epoxy

(2) Tab failures

(3) Excessive beam deflection failed core-to-face bond

(4) IITRI - Illinois Institute of Technology Research Institute

Table 9-X. Compression Test Results.

Sandwich Beam Tests

Serial Identification	Load Direction	Temperature K (° F)	Predicted Stress		Test Results		% Difference
			N/cm^2	psi	N/cm^2	psi	
101	0	Room Temperature	39370	57100	43645	63300	+11
	90	Room Temperature	40749	59100	37026	53700	- 9
102	0	Room Temperature	56539	82000	54195	78600	- 4
	90	Room Temperature	30338	44000	29580	42900	- 3
103	0	Room Temperature	144795	21000	*	---	---
104	0	Room Temperature	65503	95000	*	---	---
	0	406 (270)	48265	70000	*	---	---
	90	Room Temperature	43439	63000	*	---	---
	90	406 (270)	33786	49000	*	---	---

*Laminate did not fail - aluminum-to-honeycomb core bond failure.

Table 9-XI. Shear Test Results.

All Tests at Room Temperature

Serial Identification	Load Direction (degrees)	In Plane (Rail) Shear					Interlaminar (Short Beam) Shear Test Results	
		Predicted/Stress		Actual/		% Difference		
		N/cm^2	psi	N/cm^2	psi		N/cm^2	psi
101 (Laminated)	0 90	16203 16203	23500(1) 23500(1)	13928 18065	20200 26200	-14 +11	--- ---	--- ---
101 (Sandwich)	0 90	19306 19306	28000 28000	24133 24133	35000 35000	+28 +28	--- ---	--- ---
102 (Laminated)	0 90	17238 17238	25000 25000	19651 18410	28500 26700	+14 + 7	--- ---	--- ---
103	---	---	---	---	---	---	8964	13000
104 (Laminated)	0 90	10687 10687	15500 15500	9860 16962	14300(2) 24600	- 8 +59	5033 6343	7300 9200

(1) Buckling.

(2) Load deformation curve stepped at this value. Final failure at 17,376 N/cm^2 (25,200 psi).

Table 9-XII. Bolt Hole Test Results.

All Tests Done on Serial Number 104 Type Laminates

Temperature* K (° F)	Load Direction (degrees)	Bearing Stress		Net Tension Stress		K	Shear Out Stress	
		N/cm^2	psi	N/cm^2	psi		N/cm^2	psi
Room Temperature	0	48058	69700	42266	61300	1.2	18823	27300
Room Temperature	90	48265	70000	43439	63000	1.2	19030	27600
406 (270)*	0	53505	77600	43576	63200	1.6	16272	23600
406 (270)*	90	55160	80000	39370	57100	1.6	16617	24100

*Include S.I. Units

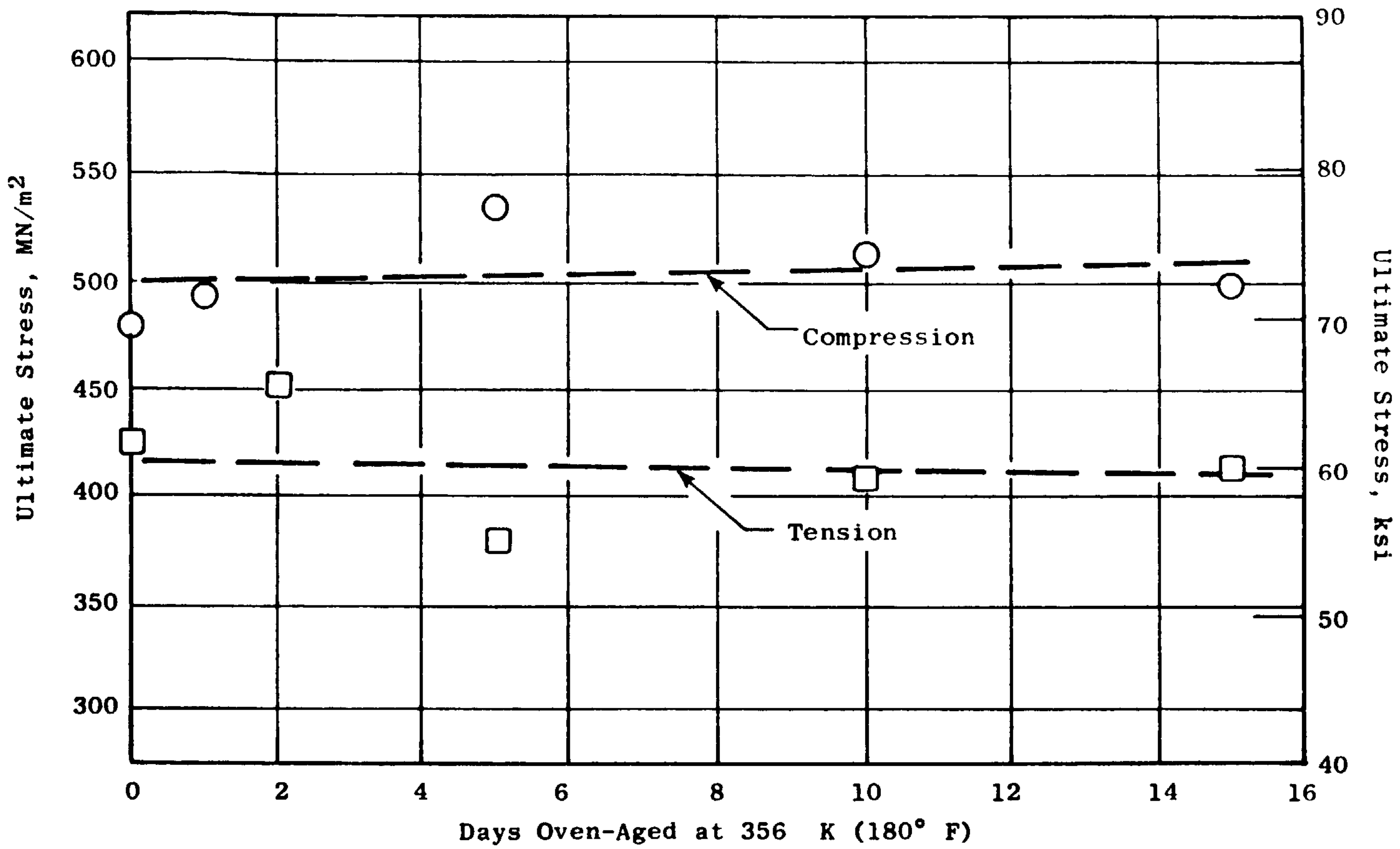

Figure 9-20. Graphite/Epoxy AS 3501 Exposed to Skydrol 500C for 5 Minutes at 356 K (180° F), Tested at 356 K (180° F).

Another series of tests was made to determine if the hot sump oil could be in direct contact with the composite frame without causing degradation in the composite material properties. The primary purpose of these tests was to determine if a metal oil shield was required in the sump region.

Tensile test specimens (IITRI) were fabricated using the AS/3501 graphite epoxy system. The layup pattern was (45°, 0°, -45°, -45°, 90°, 45°, 45°, 90°, -45°, -45°, 0°, and 45°) which is representative of the composite sandwich facing in the sump region, which would be in contact with the hot oil. Several of the specimens were coated with different coatings to see if they would provide any additional protection to the bare composite. The coatings used were Nubulan, Valspar, and Metlbond 328 adhesive. The specimens were soaked in hot MIL-L-23699 oil for one week at an oil temperature of 422 K (300° F). The specimens were then tested to failure at 405 K (270° F). In addition to the oil exposure specimens, several unexposed specimens were tested at 405 K (270° F) after 30 minutes in 422 K (300° F) air and several after one week in 422 K (300° F) air. The resulting test data are shown in Table 9-XIII. The predicted unexposed tensile strength, as obtained from the Design Guide for these specimens is 31,700 N/cm^2 (46,000 psi) at 405 K (270° F). Based on these data, it was concluded that there was no degradation of the bare graphite/epoxy due to exposure to hot MIL-L-23699 oil, and neither the oil shield nor the protective coatings are required.

9.7.3 Subcomponent Tests

Since one of the most critical areas of composite structures is the joining of the individually molded pieces, either by bonding or mechanically fastening, the critical joint areas of the UTW fan frame will be individually tested prior to the final frame assembly. This series of subcomponent tests is outlined in Figure 9-21 and listed in Table 9-XIV. The average results of these tests are shown in Table 9-XV along with the analytically predicted values and the values actually required by the frame design. As can be seen, the test results show that the specimens more than meet the requirements in all cases.

Table 9-XIII. Exposure Evaluation - MIL-L-23699.

Specimens		Exposure Environment	Coating	Stress	
				N/cm^2	psi
A		422 K (300 F) air for 30 min	None	32,173	46,661
B		422 K (300 F) air for 1 week	None	33,103	48,010
C	Set 1	422 K (300 F) oil for 1 week	None	31,758	46,060
C	Set 2	422 K (300 F) oil for 1 week	None	33,269	48,251
D		422 K (300 F) oil for 1 week	Nubulan	33,765	48,970
E		422 K (300 F) oil for 1 week	Valspar	30,283	43,920
F		422 K (300 F) oil for 1 week	Metlbond	32,949	47,787

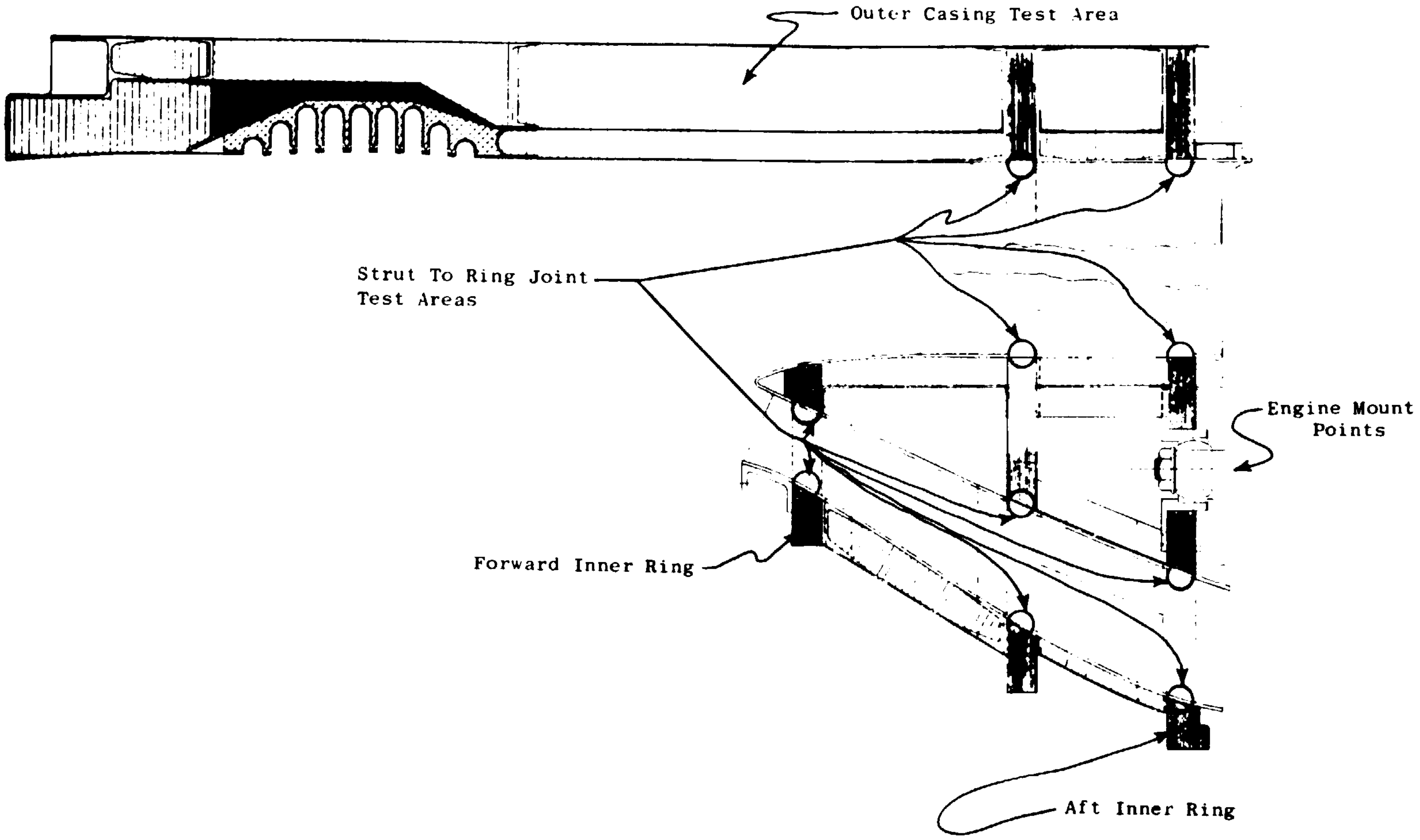
Outer Casing Test Area
Strut To Ring Joint Test Areas
Engine Mount Points
Forward Inner Ring
Aft Inner Ring

Figure 9-21. Frame Subcomponent Test Areas.

Table 9-XIV. Composite Frame Subcomponents Test Plan Summary.

Test Specimen Configuration	Test Temperature	Test Mode	No. of Replicates (Tests)
Ring structures			
Forward inner ring	Room temperature	Bend - I.D. tension	2
Forward inner ring	Room temperature	Bend - I.D. comp.	2
Aft inner ring	Room temperature	Bend - I.D. tension	2
Aft inner ring	406 K (270° F)	Bend - I.D. tension	2
Aft inner ring	Room temperature	Bend - I.D. comp.	2
Aft inner ring	406 K (270° F)	Bend - I.D. comp.	2
Strut-to-ring joints			
Core vane forward	Room temperature	Spoke tension	2
Core vane mid	Room temperature	Spoke tension	2
Core vane aft	Room temperature	Spoke tension	2
Core vane aft	406 K (270° F)	Spoke tension	2
Fan vane forward	Room temperature	Spoke tension	2
Fan vane aft	Room temperature	Spoke tension	2
Maximum moment joint	Room temperature	Spoke bending	2
Engine mount attachment			
Uniball attachment	Room temperature	Radial load	1
Uniball attachment	406 K (270° F)	Radial load	1
Thrust link attachment	Room temperature	Axial load	1
Thrust link attachment	406 K (270° F)	Axial load	
Outer casing			
Honeycomb sandwich panel	Room temperature	Bend - I.D. tension	2
Honeycomb sandwich panel	Room temperature	Bend - I.D. comp.	2
Inlet-to-frame attachment	Room temperature	Tension	1
Core Cowl Extension to Frame Joint	406 K (270° F)	Tension	1
Frame to Outer Cowl Door Joint	Room Temperature	Tension	1

Table 9-XV. Subcomponent Test Results.

Test Specimen Configuration	Test Temperature	Test Mode	Required for Safe Design	Average Failure Loads	
				Predicted	Test Average
Ring Structures					
Forward Inner Ring	Room Temperature	Bend - ID Tension	48,590 cmN	257,640 cmN	300,580 cmN/26,600 in.-lb
Forward Inner Ring	Room Temperature	Bend - ID Comp.	18,080 cmN	298,320 cmN	427,140 cmN/37,800 in.-lb
Aft Inner Ring	Room Temperature	Bend - ID Tension	59,100 cmN	354,140 cmN	297,472 cmN/26,325 in.-lb
Aft Inner Ring	406 K (270° F)	Bend - ID Tension	59,100 cmN	354,140 cmN	312,083 cmN/27,618 in.-lb
Aft Inner Ring	Room Temperature	Bend - ID Comp.	59,100 cmN	442,734 cmN	498,330 cmN/44,100 in.-lb
Aft Inner Ring	406 K (270° F)	Bend - ID Comp.	59,100 cmN	442,734 cmN	419,303 cmN/45,956 in.-lb
Strut-to-Ring Joints					
Core Vane Forward	Room Temperature	Spoke Tension	177,920 N	273,552 N	245,530 N/55,200 lb
Core Vane Mid	Room Temperature	Spoke Tension	213,950 N	269,550 N	298,016 N/67,000 lb
Core Vane Aft	Room Temperature	Spoke Tension	20,016 N	114,314 N	105,418 N/23,700 lb
Core Vane Aft	406 K (270° F)	Spoke Tension	20,016 N	--	123,210 N/27,700 lb
Fan Vane Forward	Room Temperature	Spoke Tension	34,660 N	153,130 N	105,868 N/23,800 lb
Fan Vane Aft	Room Temperature	Spoke Tension	42,667 N	108,092 N	71,172 N/16,000 lb
Maximum Moment Joint	Room Temperature	Spoke Bending	128,820 cmN	160,460 cmN	164,980 cmN/14,600 in.-lb
Engine Mount Attachment					
Uniball Attachment	Room Temperature	Radial Load		230,435 N	253,015 N/56,880 lb
Uniball Attachment	406 K (270° F)	Radial Load		--	207,732 N/46,700 lb
Thrust Link Attachment	Room Temperature	Axial Load	111,206 N	182,377 N	120,102 N/27,000 lb
Outer Casing					
Honeycomb Sandwich Panel	Room Temperature	Bend - ID Tension	23,906 N/cm^2	31,164 N/cm^2	31,268 N/cm^2/45,350 psi
Honeycomb Sandwich Panel	Room Temperature	Bend - ID Comp.	23,906 N/cm^2	31,164 N/cm^2	36,236 N/cm^2/52,555 psi
Inlet-to-Frame Attachment	Room Temperature	Tension	9,341 N	28,800 N	28,636 N/6,438 lb
Core Cowl Extension to Frame Joint	406 K (270° F)	Tension	297.7 N/cm	774 N/cm	788 N/cm/450 lb/in.
Frame to Outer Cowl Door Joint	Room Temperature	Tension	446.5 N/cm	630.4 N/cm	446.5 N/cm/255 lb/in.

SECTION 10.0

REDUCTION GEAR DESIGN

10.1 SUMMARY

A reduction gear is utilized in the UTW engine to provide a decrease in rotational speed between the low pressure turbine and fan rotor. Application of the reduction gear permits the low tip speed fan to be driven by a two-stage F101 low pressure turbine. As shown in Figure 10-1 the main reduction gear, located in the forward engine sump region, has a gear ratio of 2.465, reducing the low pressure turbine speed from 7781 to 3157 rpm for the fan. Design power to be transmitted by the reduction gears is 9885 kw (13,256 hp).

The main reduction gear is being designed and developed by the Curtiss-Wright Corporation, Wood-Ridge, New Jersey. The design is based on application of technology developed by Curtiss-Wright for the reduction gear set of the YT49 turboprop engine.

The UTW gear set is arranged in an epicyclic star configuration. The low pressure power turbine drives a sun gear which drives a ring gear through a set of six star gears. These star gears are mounted on spherical roller bearings which are, in turn, mounted on a fixed carrier. This arrangement provides the required gear ratio and results in a compact lightweight design.

Design gear stresses have been maintained within industry-approved limits for the flight design. Somewhat higher stresses will be encountered during a limited part of the experimental testing. This higher stress level only occurs during fan mapping and is within limits previously found acceptable by both Curtiss-Wright and General Electric. Gear scoring will be prevented by controlling inlet oil temperature and oil flows. Contact ratio of the gears is maintained at a value of 2, further reducing stress since two gears are always in contact and sharing the load. This high contact ratio also reduces vibration and noise.

A bearing test program was conducted to ensure satisfactory star gear spherical roller bearing operation prior to testing in the gearbox. Results indicated the selected bearing design with reduced radial clearances would meet the requirements of the UTW experimental engine.

Back-to-back rig tests of two UTW reduction gear units are planned for the fourth quarter of 1975 to substantiate the design prior to engine test. Calculated design objective gear efficiency is 99.2% at 100% speed and 100% power, 9885 kw (13,256 hp).

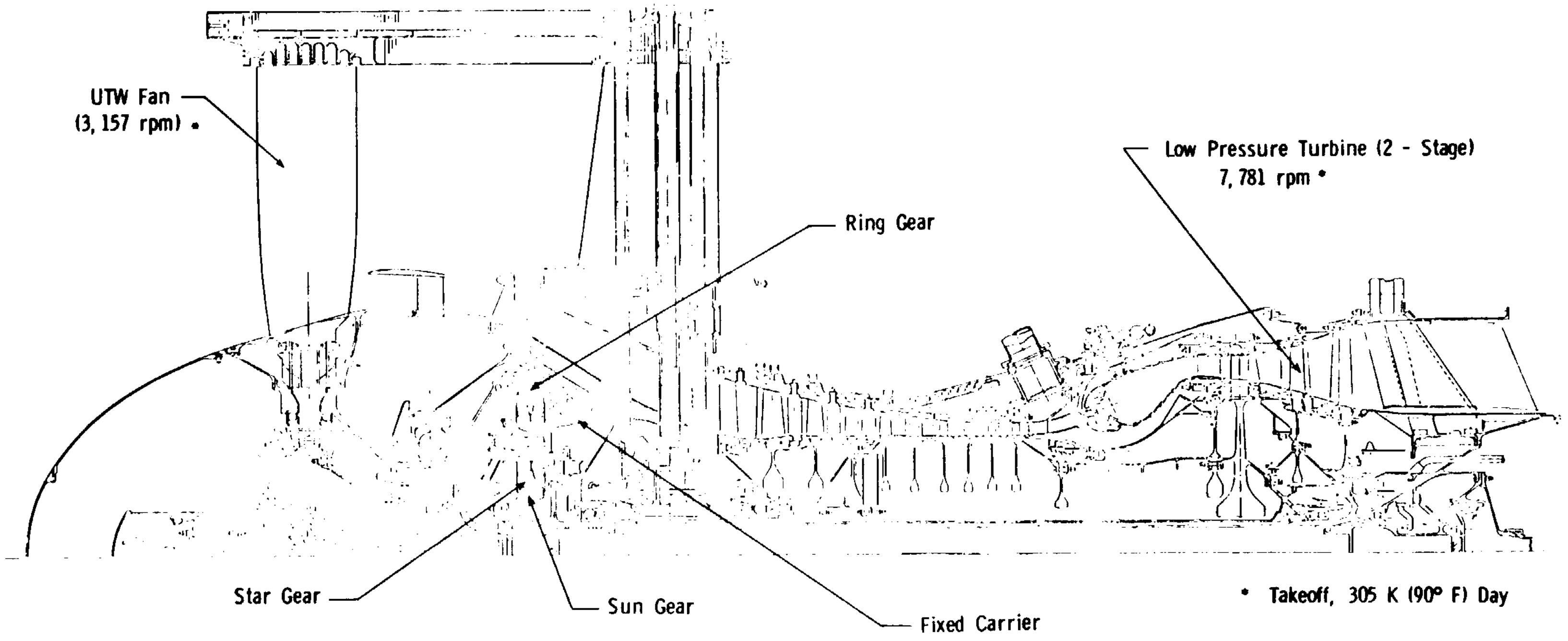
UTW Fan
(3, 157 rpm) •
Low Pressure Turbine (2 - Stage)
7, 781 rpm *
Ring Gear
Star Gear
Sun Gear
Fixed Carrier

* Takeoff, 305 K (90° F) Day

• Gear Ratio = 2.465

Figure 10-1. UTW Engine Low Pressure Rotor Configuration.

10.2 DESIGN REQUIREMENTS

The UTW main reduction gear unit was designed to meet the following general requirements:

- 36,000 hours life
- 6,000 hours time between overhaul (TBO)
- 6,000 hours minimum bearing B1 life
- Flight weight design
- Minimum noise
- Mil-L-23699 or Mil-L-7808 oil
- Minimum efficiency of 99.2% (100% speed, 100% power)

The gear set has been designed to satisfy the above requirements in accordance with the flight duty cycle specified in Section 2.0 of this report. The resulting design was then checked for satisfactory operation in the experimental engine ground test cycle.

A common set of engine/reduction gear interfaces was established for the UTW and OTW main reduction gears to permit commonality of the engine interface components (fan frame, engine bearings, shafting, etc.) between the UTW and OTW engines.

10.3 DESIGN DESCRIPTION

The UTW reduction gear is an epicyclic star gear arrangement. As illustrated in Figure 10-2, the star arrangement uses a concentric external-tooth sun gear and internal-tooth ring gear with a set of idlers (star gears) between them. The star gears, which are mounted by spherical roller bearings on a fixed support (star gear carrier), distribute the load to many teeth in both the input sun gear and output ring gear members. Power input to the unit is transmitted from the low pressure turbine through a flexible coupling to the sun gear. Output power to the fan is transmitted from the ring gear through a spline and cone shaft to the fan disk shaft. Design and configuration details are presented in Table 10-I.

10.4 DESIGN APPROACH

The selected UTW epicyclic star gear arrangement is very similar to the first stage of the YT49-W-1 reduction gear unit shown in Figure 10-3, which was developed for the Curtiss-Wright YT49 turboprop engine. The YT49 engine was designed, built, and tested during the mid 1950's. Listed below is a summary of the YT49 engine testing:

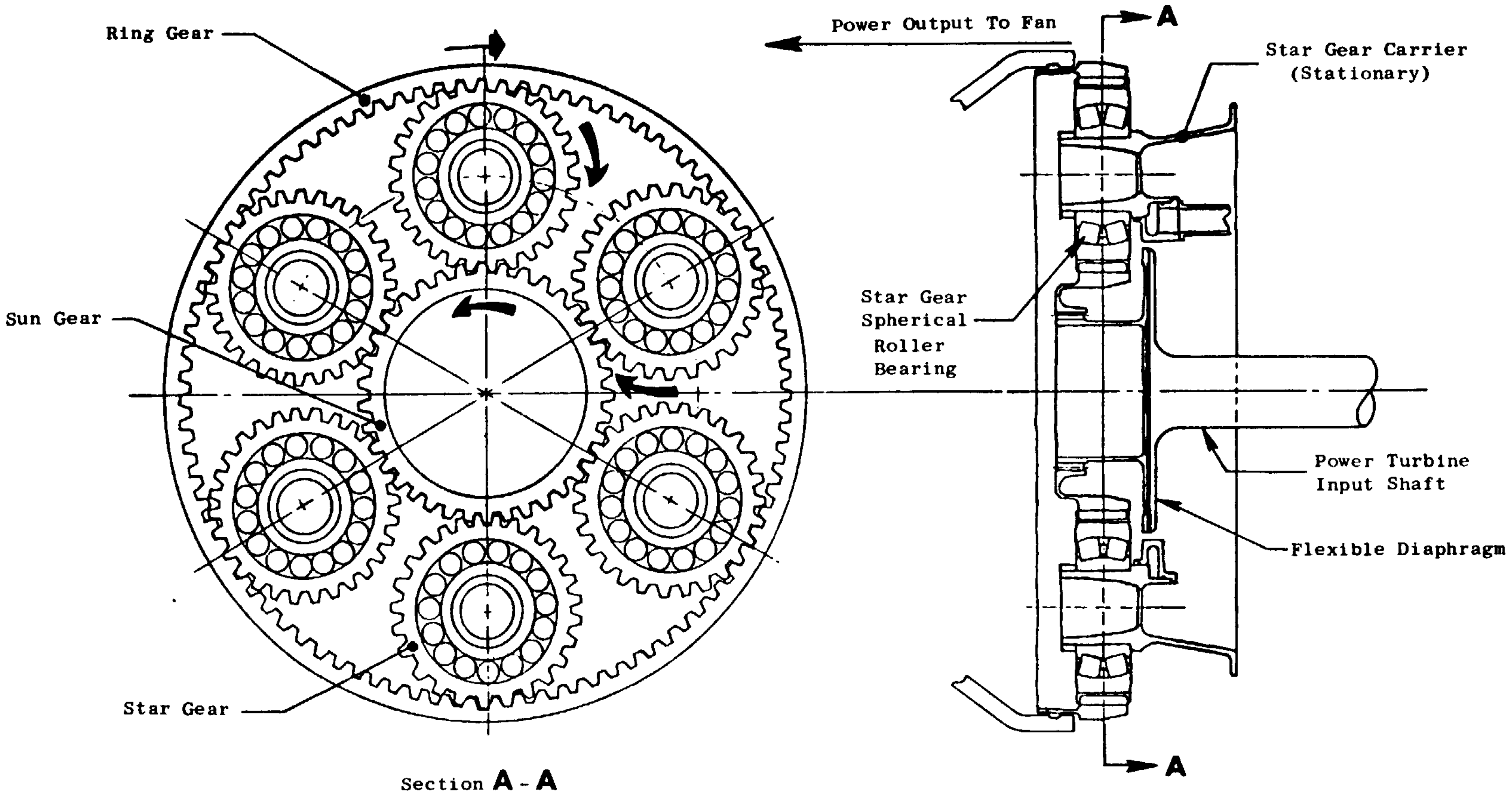
Ring Gear
Sun Gear
Star Gear
Section A-A
Power Output To Fan
A
A
Star Gear Carrier (Stationary)
Star Gear Spherical Roller Bearing
Power Turbine Input Shaft
Flexible Diaphragm

Figure 10-2. Main Reduction Gear Configuration.

Table 10-I. UTW Reduction Gear Design Details.

[Takeoff, 306 K (90° F) Day]
(100% Power, 100% Speed)

Gear Ratio	2.465
Turbine Power	9889 kw (13,256 hp)
Turbine Speed	7747 rpm
Gear Pitch Line Velocity	97.1 m/sec (19,117 ft/min)
Star Gear Speed	10,577 rpm
Bearing Load	33,925 N (7627 lb)
Number of Stars	6
Number of Gear Teeth	
Sun Gear	71
Star Gear	52
Ring Gear	175
Hunting	Yes
Nonfactoring	Yes

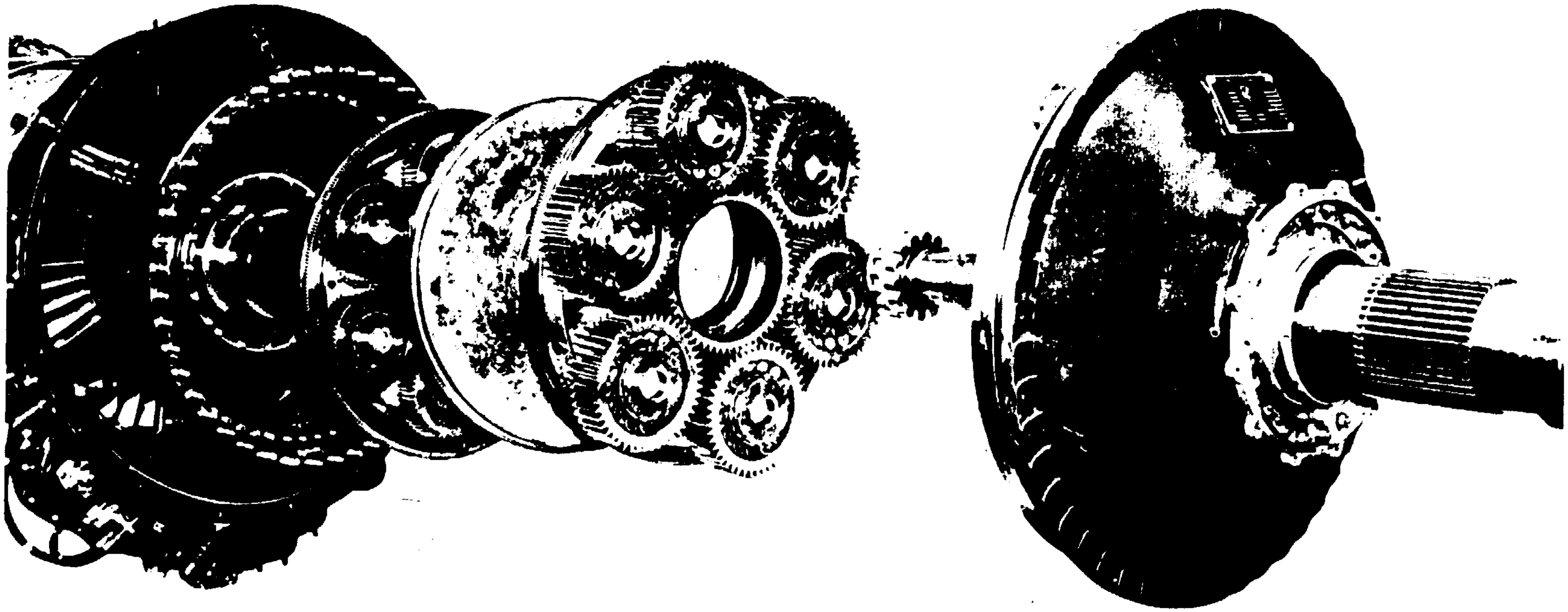

Figure 10-3. Curtiss-Wright YT49-W-1 Reduction Gear.

Bench Tests	290 hours
Factory Engine Tests	1960 hours
Flight Test in B17 and B47 Flight Test Beds	150 hours

A comparison of the principal design features of the UTW and YT49 (1st stage) gear sets is presented in Table 10-II. As shown, the design differences are relatively small.

Table 10-II. Comparison of UTW and YT49 (1st Stage) Reduction Gear Data.

	UTW	YT49
Turbine Power	9802 kw (13,145 hp)	7457 kw (10,000 hp)
Gear Ratio	2.465	2.672
Sun Gear rpm	7782	8000
Star Gear rpm	10,689	9574
Ring Gear rpm	3157	2994
Output Torque	29,641 m-N (21,895 ft-lb)	23,777 m-N (17,535 ft-lb)
Gear Contact Ratio (min.)	1.98	~1.6
Bearing DN x 10^{-6}	0.74	0.72

A star gear arrangement is the only epicyclic gear train capable of providing the selected UTW reduction gear ratio. In a star gear system, the star gears distribute the load to many teeth in both the sun gear and ring gear members. This feature greatly reduces the face width required for each gear. Also, the star gears rotate about a fixed axis, unlike planetary gears which rotate about a sun gear as well as their own axis. This feature eliminates the centrifugal field created by rotation about the sun gear, allowing the star gears to utilize lighter bearings than a corresponding planetary gear arrangement.

Specific design approach features of the UTW reduction gear unit are as follows:

- Flexibility - Both the input and output members of the system are flexibly mounted to prevent engine deflections from influencing gear operation.

- Controlled Gear Deflections - Rims of the sun and ring gears are contoured so that their deflections match the deflection in the star gears.
- Self-Aligning Star Gears - Double-row spherical roller bearings are used to permit the star gears to align themselves with the sun and ring gears and thereby minimize the effects of carrier deflections. The bearing outer race is integral with the star gear to obtain maximum bearing capacity in minimum space.
- Nonfactoring Hunting Teeth - This combination of numbers of teeth results in minimum vibration, low noise, and long life.
- Modular Concept - Can be installed and removed as a unit.

In addition to hunting teeth, the design approach includes the following low noise features:

- Precision AGMA Quality 13 gears
- Contact ratio of 2
- Diametral Pitch = 7.5321
- 21° pressure angle
- Modified involute at tip and root

10.5 DESIGN ANALYSIS AND RESULTS

10.5.1 Design Conditions

The detail design of the UTW reduction gear has been conducted in accordance with the operating condition defined in Table 10-III for the Flight Engine Cycle. Upon completion of the design the stresses were evaluated at operating conditions established by the experimental engine duty cycle (Table 10-IV). Results indicated that although the stress levels were highest during the fan mapping portion of the experimental engine cycle, they fell within operating limits previously found to be acceptable by both Curtiss-Wright and General Electric.

Table 10-III. Reduction Gear Detail Design, Flight Cycle.

Condition	Power %	Speed %	Time %	Oil-In Temperature K	Oil-In Temperature ° F
Start	0	0-30	1.11	--	--
Idle	10	66.81	6.89	363	194
Takeoff	100	100	2.71	366	200
Climb	85.15	102.99	22.22	369	205
Cruise	68.92	102.99	31.11	383	230
Descent	3.27	34.489	22.22	403	266
Approach	61.23	97.805	6.67	370	207
Reverse	62.46	109.672	0.18	364	195
Idle	10	66.81	6.89	363	194

100% Fan Power = 9781 kw (13,116 hp)

100% Fan Speed = 329 rad/sec (3,143 rpm)

10.5.2 Materials

Table 10-V lists the materials used in the UTW gear set. The gear materials are the same as those utilized in the YT49 reduction gear design.

10.5.3 Reduction Gear Geometry

Final UTW reduction gear geometry details are summarized in Table 10-VI. Without exception all resulting design details are consistent with good reduction gear design practice based on the experience of both Curtiss-Wright and General Electric.

10.5.4 Stress Analysis

The stress analysis approach and results are summarized in Figures 10-4, 10-5, and 10-6 for the sun, star, and ring gears, respectively. Conventional compressive and bending stress levels presented in the figures were calculated using the American Gear Manufacturers Association (AGMA) recommended procedure. Also shown in the figures are allowable compressive and bending stress levels based on AGMA and Curtiss-Wright experience. As shown, the calculated stresses fall well within the limits set by AGMA for infinite life.

Table 10-IV. Reduction Gear Detail Design, Experimental Engine Cycle.

Hours	% Time	% Turbine Speed	% Turbine Power
1	0.04	105	100
1	0.04	100	140
15	0.56	100	130
15	0.56	100	110
150	5.59	100	100
500	18.64	90	80
1000	37.28	75	50
1000	37.28	30	10

100% Turbine Power = 9885 kw (13,256 hp)

100% Turbine Power = 811 rad/sec (7,747 rpm)

Table 10-V. Gear Set Materials.

• Sun Gear	AMS 6265 - Carburized - silver plate
• Star Gear (with integral bearing outer race)	AMS 6265 - Carburized - shot peen, black oxide
• Ring Gear	AMS 6470 - Nitrided
• Carrier Support	AMS 6415 - RC3236
• Bearing	
- Inner Race	AMS 6490 - CEVM M-50
- Rollers	AMS 6490 - CEVM M-50
- Cage (Steel)	AMS 6414 - Silver Plated

Table 10-VI. Reduction Gear Geometry.

	Sun Gear	Star Gears	Ring Gear
No. of Teeth	71	52	175
Diametral Pitch	7.5321	7.5321	7.5321
Pressure Angle	21°	21°	21°
Pitch Diameter	239.4 mm (9.4263 in.)	175.4 mm (6.9038 in.)	590.1 mm (23.2339 in.)
Center Distance	207.4 mm (8.165 in.)	207.4 mm (8.165 in.)	
Base Diameter	233.5 mm (8.8002 in.)	163.7 mm (6.4452 in.)	550.9 mm (21.6907 in.)
Tooth Thickness at P.D.	5.2464 mm (.2067 in.)	5.3467 mm (.2105 in.)	5.2484 mm (.2066 in.)
Backlash	.102-.152 mm (.004-.006 in.)	.102-.152 mm (.004-.006 in.)	.177-.203 mm (.005-.008 in.)
Root Radius	1.17 mm min. (.046 in. min.)	1.35 mm min. (.053 in. min.)	.89 mm min. (.035 in. min.)
Contact Ratio (no edge break)	2.127	2.118	
Gear Face Width	47.1 mm (1.856 in.)	51.5 mm (2.03 in.)	45.9 mm (1.806 in.)

In addition to the conventional gear tooth compressive and bending stresses, an attempt was made to combine the bending stresses with the rim stresses. Referring to Figure 10-4 for the sun gear, rim stresses were calculated at three circumferential locations: Stations I, II, and III. The sun gear teeth are in mesh with the star gear teeth at Stations I and II, but out of mesh at Station III. The tooth bending stress, ±27,854 N/cm^2 (±40,398 psi), was directly added to the rim stress at Stations I and II to determine the combined stress. It should be noted that this represents a conservative approach, since the maximum rim and bending stresses actually do not occur at the same location. As shown in Figure 10-4, the maximum positive, 42,715 N/cm^2 (61,951 psi), and negative, 28,620 N/cm^2 (41,509 psi), combined stresses occur at Stations I and II. These two numbers were then used to define the alternating stress, 35,668 N/cm^2 (51,730 psi), and the steady-state stress, 7047 N/cm^2 (10,221 psi), plotted on the Goodman diagram. As shown, the resulting stress condition falls within the limit line for infinite life. The same procedure was used to substantiate the star gear (Figure 10-5) and the ring gear (Figure 10-6) designs.

10.5.5 Design Oil Flow Rates

The design oil flow rates based on the flight cycle conditions are presented in Table 10-VII. Oil inlet temperatures were defined by General Electric on the basis of overall engine heat balance studies. The maximum

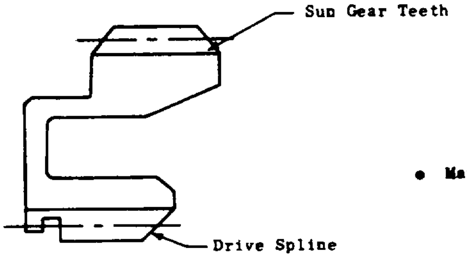

- **Material:** AMS 6265 Case Carburized Steel

Combined Rim and Gear Stresses

Station	I (Loaded Tension)	II (Compression)	III (Out-of-Mesh)
Rim Stress Incl SCF, N/cm^2 (psi)	14,861 (21,553)	-766.4 (-1,111.5)	17,351 (25,165)
Combined Stress, N/cm^2 (psi)	42,715 (61,951)	-28,620 (-41,509)	17,351 (25,165)

Conventional Gear Stresses

	Compressive Stress, N/cm^2 (psi)
Flight	92,423 (134,044)
AGMA	102,570 (148,760)
C-W	110,320 (160,000)

	Bending Stress
Flight	27,854 (40,398)
AGMA	38,693 (55,250)
C-W	41,370 (60,000)

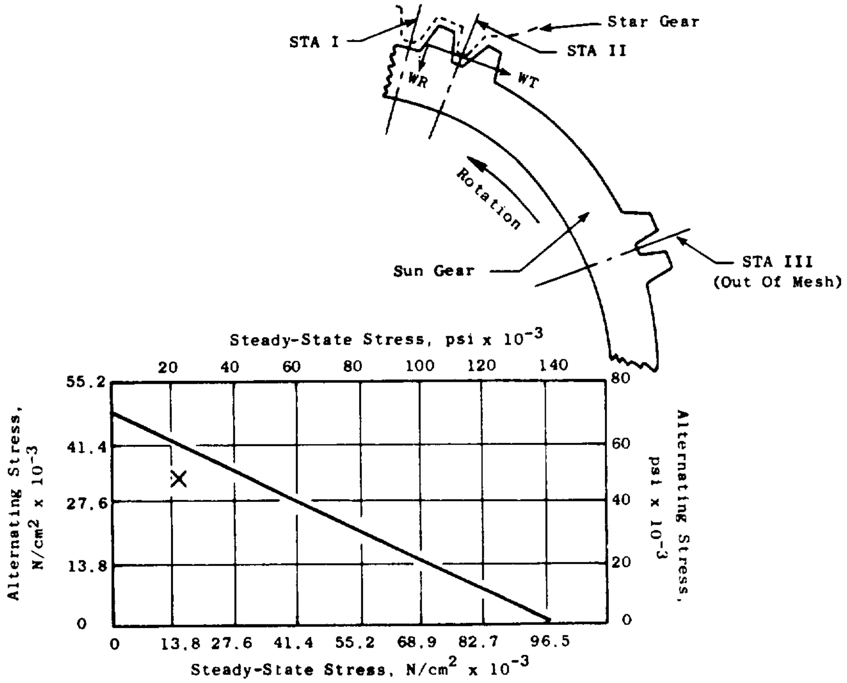

Figure 10-4. Sun Gear Stresses.

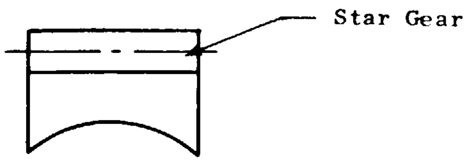

- Material: AMS 6265 Case Carburized Steel

Combined Rim and Gear Stresses

Station	I (Loaded Tension)	II (Compression)
Rim Stresses Incl SCF, N/cm^2 (psi)	9,315 (13,510)	-1,440 (-2,088)
Combined Stress, N/cm^2 (psi)	36,243 (52,564)	-28,367 (-41,142)

Conventional Gear Stresses

	Compressive Stress, N/cm^2 (psi)
Flight	92,423 (134,044)
AGMA	102,570 (148,760)
C-W	110,320 (160,000)

	Bending Stress
Flight	21,618 (31,350)
AGMA	26,928 (39,054)
C-W	38,693 (56,117)

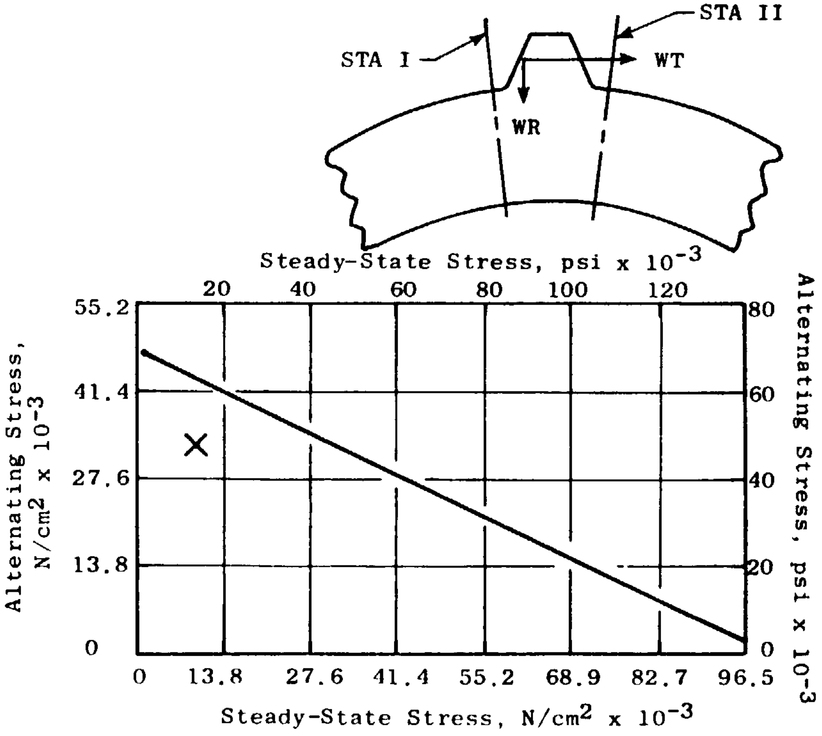

Figure 10-5. Star Gear Stresses.

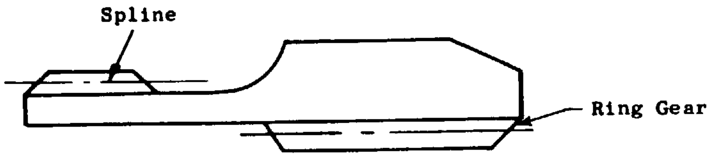

- **Material: AMS 6470 Nitralloy**

Combined Rim and Gear Stresses

Station	I (Loaded Tension)	II (Compression)	III (Out-of-Mesh)
Rim Stress Incl SCF, N/cm^2 (psi)	5,081 (7,369))	-11,516 (-16,702)	32,065 (46,504)
Combined Stress, N/cm^2 (psi)	27,028 (39,199)	-33,463 (-48,532)	32,065 (46,504)

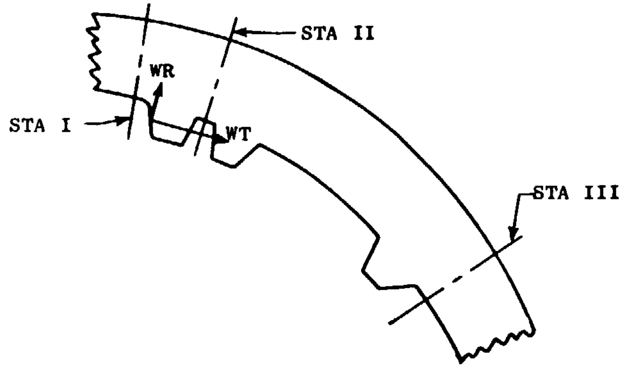

Conventional Gear Stresses

	Compressive Stress, N/cm^2 (psi)
Flight	59,755 (86,664)
AGMA	102,570 (148,760)
C-W	110,320 (160,000)

	Bending Stress
Flight	21,947 (31,830)
AGMA	32,888 (47,699)
C-W	41,370 (60,000)

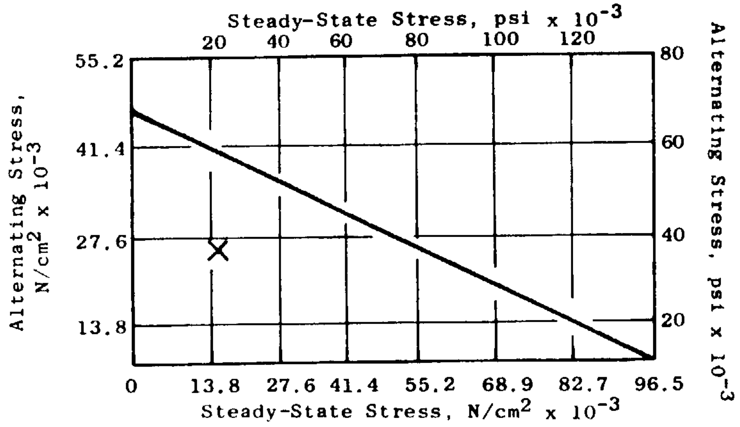

Figure 10-6. Ring Gear Stresses.

Table 10-VII. Reduction Gear Oil Flow Rates (Flight Cycle).

Condition	Total Star Brg Flow		Flow to Gears (Spray Bars)		Total Oil Flow		Temp., Oil-In		Brg Outer Race Temp.	
	cm^3/sec	gal/min	cm^3/sec	gal/min	cm^3/sec	gal/min	K	° F	K	° F
Idle	379	6.00	673	10.66	1052	16.66	363	194	385	234
Takeoff	502	7.95	887*	14.067*	1389	22.02	366	200	407	273
Climb	493	7.82	896	14.199	1389	22.02	369	205	410	279
Cruise	490*	7.77*	898	14.231	1388	22.00	383	230	422*	300*
Descent	397	6.30	706	11.196	1104	17.50	403	266	410	273
Approach	464	7.35	858	13.595	1322	20.95	370	207	409	276
Reverse	481	7.62	878	13.924	1359	21.54	364	195	410	278
Idle	379	6.00	673	10.66	1052	16.66	363	194	385	234

*Controlling Condition

limit for the bearing outer race temperature was established at 422 K (300° F). As shown, the calculated maximum bearing outer race temperature occurs at the cruise operating condition. Available oil pressure at any given operating condition is a function of the core engine speed. The required bearing oil flow at the cruise condition, together with the oil supply pressure, established the bearing oil flow orifice control size. The controlling operating condition for oil flow to the gears based on gear scoring criteria is cruise. With the bearing and gear oil orifice control sizes set, the resulting total oil flows at each operating condition were established. The engine will be capable of providing flow rates significantly higher than the design values, should component or engine tests indicate increased oil flow rates are desirable.

10.5.6 Reduction Gear Efficiency

Overall reduction gear efficiency is determined by calculating losses for the spherical roller bearings, gear mesh, and for churning and windage. These losses are presented in Table 10-VIII. As shown, at takeoff the estimated gearbox efficiency is 99.3%, which is slightly above the objective level (99.2%). It should be noted that roughly half the losses are in the gears, while the bearings, churning, and windage make up the balance.

10.5.7 Heat Rejection

Total heat generated due to the losses in the gears, and the effect of this heat on the temperature of the oil supplied to the gears for the flight cycle is shown in Table 10-IX. The resulting bulk oil temperatures do not exceed the capabilities of either MIL-L-7808 or MIL-L-23699.

10.5.8 Gear Scoring

Tabulated in Table 10-X are gear scoring index data based on the AGMA method of analysis. A maximum scoring index of 422 K (300° F) was used in the design. Although AGMA scoring data indicate this falls within the medium risk range, both General Electric and Curtiss-Wright experience indicate that scoring does not occur in high quality gearing at this scoring index. During the experimental engine ground test program, the oil inlet temperature to the gears will be maintained at a low level to minimize any risk of scoring. As shown in the table, the calculated maximum value of the AGMA gear scoring index occurs at the cruise operating condition.

10.5.9 Star Gear Bearing

The selected star gear bearing configuration is illustrated in Figure 10-7. Bearing design features include:

- Double-row spherical roller bearing

Table 10-VIII. Reduction Gear Efficiency.

(Flight Cycle)

Power Loss

Condition	Spherical Bearing		Gear Mesh		Churn & Windage		Total		Overall Efficiency %
	kw	hp	kw	hp	kw	hp	kw	hp	
Idle	6.22	8.34	3.36	4.51	0.71	0.947	10.29	13.80	98.96
Takeoff	14.36	19.26	36.58	49.05	18.38	24.65	69.32	92.96	99.30*
Climb	14.33	19.22	30.31	40.64	16.06	21.54	60.70	81.40	99.28
Cruise	13.31	17.85	25.21	33.81	13.49	18.09	52.01	69.75	99.24
Descent	1.90	2.55	1.33	1.78	0.05	0.063	3.27	4.39	98.99
Approach	12.76	17.11	21.79	29.22	10.46	14.03	45.01	60.36	99.26
Reverse	15.82	21.21	20.99	28.15	12.91	17.31	49.72	66.67	99.19
Idle	6.22	8.34	3.36	4.51	0.71	0.947	10.29	13.80	98.96

*Spec 99.20%

Table 10-IX. Reduction Gear Heat Rejection. (Flight Cycle)

Condition	Total Loss		Delta Rise in Bulk Oil Temp.		Oil-In Temp.		Bulk Oil Temp.	
	kw	Btu/min	K	° F	K	° F	K	° F
Idle	10.28	585	4.92	8.85	363	194	368	203
Takeoff	69.24	3940	25.22	45.39	366	200	391	245
Climb	60.63	3450	22.17	39.90	369	205	391	245
Cruise	52.01	2960	19.38	34.89	383	230	403	265
Descent	3.27	186	1.57	2.82	403	266	405	269
Approach	44.99	2560	17.10	30.78	370	207	387	238
Reverse	49.70	2828	18.43	33.18	364	195	382	228
Idle	10.28	585	4.92	8.85	363	194	368	203

Table 10-X. Reduction Gear Scoring Index. (Flight Cycle)

Condition	Oil-in Temp.		AGMA T		AGMA Scoring Index	
	K	° F	K	° F	K	° F
Idle	363	194	10.15	18.27	373	212
Takeoff	367	200	51.58	92.84	418	293
Climb	369	205	45.48	81.86	415	287
Cruise	383	230	38.73	69.71	422*	300*
Descent	403	266	5.17	9.30	408	275
Approach	371	207	35.91	64.63	407	272
Reverse	364	195	35.41	63.74	399	259
Idle	363	194	10.15	18.27	373	212

*Controlling Condition

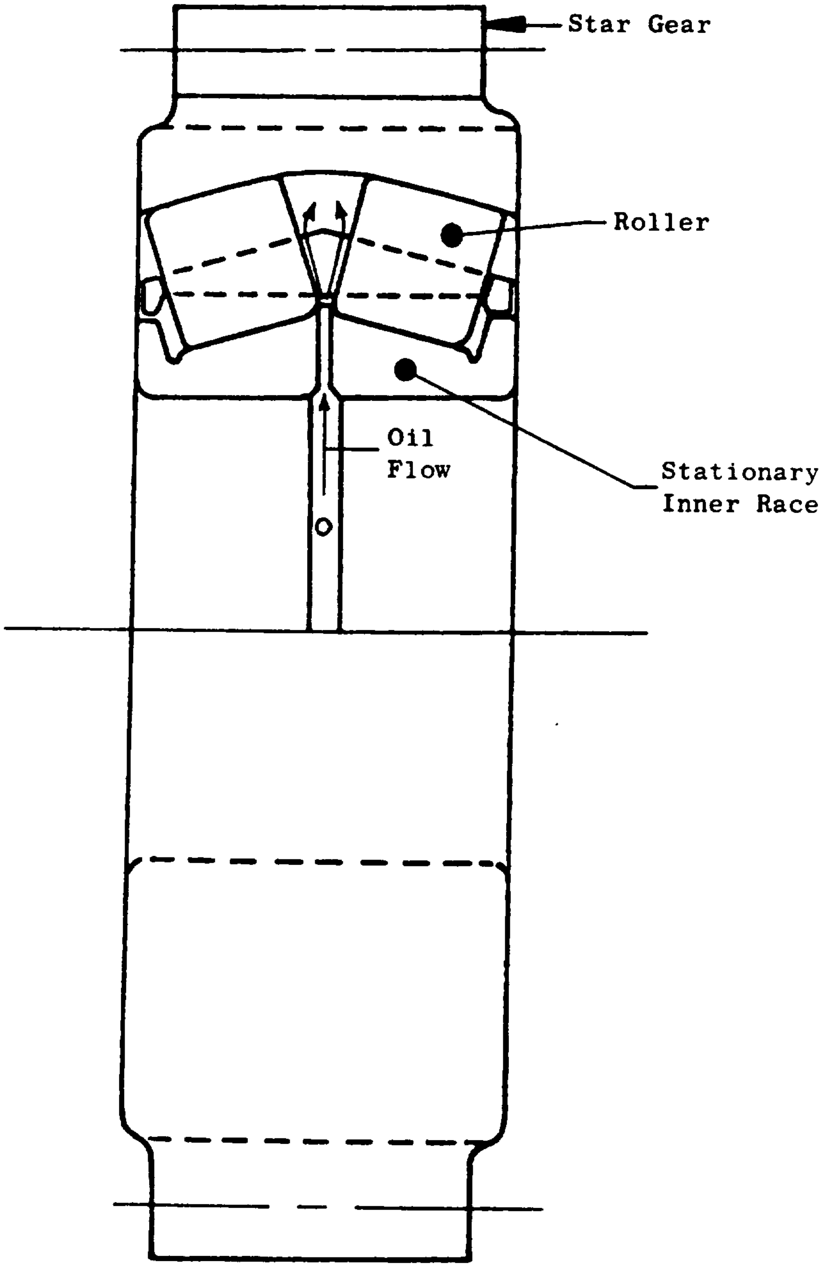
Star Gear
Roller
Oil Flow
Stationary Inner Race

Figure 10-7. Star Gear Spherical Roller Bearing.

- Integral star gear and outer race
- "Conventional" inner race, roller, and cage
- Oil feed through center of inner race

This spherical roller bearing was chosen as the prime candidate based on past experience with similar bearings in the Curtiss-Wright YT49 turboprop engine first-stage reduction gears and the recommendations by the SKF Bearing Corporation.

Table 10-XI shows the average loads and speed used to determine the bearing B_1 life. The results indicate that the bearings can meet requirements of both the flight and experimental duty cycle.

Table 10-XI. Star Gear Bearing Life Prediction.

Flight Cycle	
Cubic Mean Load	23,886 N (5370 lb)
Mean Speed	8141 rpm
B1 Life	6319 hr
Experimental Engine Cycle	
Cubic Mean Load	25,189 N (5663 lb)
Mean Speed	6827 rpm
B1 Life	6313 hr

10.5.10 Weight

The weights of the reduction gear components and the overall gear weight for the UTW experimental engine are presented in Table 10-XII.

10.6 COMPONENT TEST PROGRAMS

10.6.1 Star Gear Bearing Tests

From the start of the QCSEE program the star gear bearing has been considered as the most critical reduction gear element. This is particularly true for the OTW engine where the bearing speeds are much higher than those of the UTW engine. To ensure successful operation of the bearings, a component test program was conducted by Curtiss-Wright. A schematic of the bearing test rig is shown in Figure 10-8, and a photograph of the rig is presented in Figure 10-9. The bearing tested was an available SKF bearing very

Table 10-XII. Reduction Gear Weight Summary.

	kg	lb
Sun Gear Assembly	8.96	19.75
Ring Gear	13.80	30.43
Star Nuts	1.49	3.28
Carrier Support	23.94	52.78
Star Gear - Bearing Assemblies (6)	40.62	89.54
Starwasher	0.11	0.25
Oil Manifold	1.09	2.40
Spray Bars (Gears)	0.88	1.95
Total	90.89	200.38

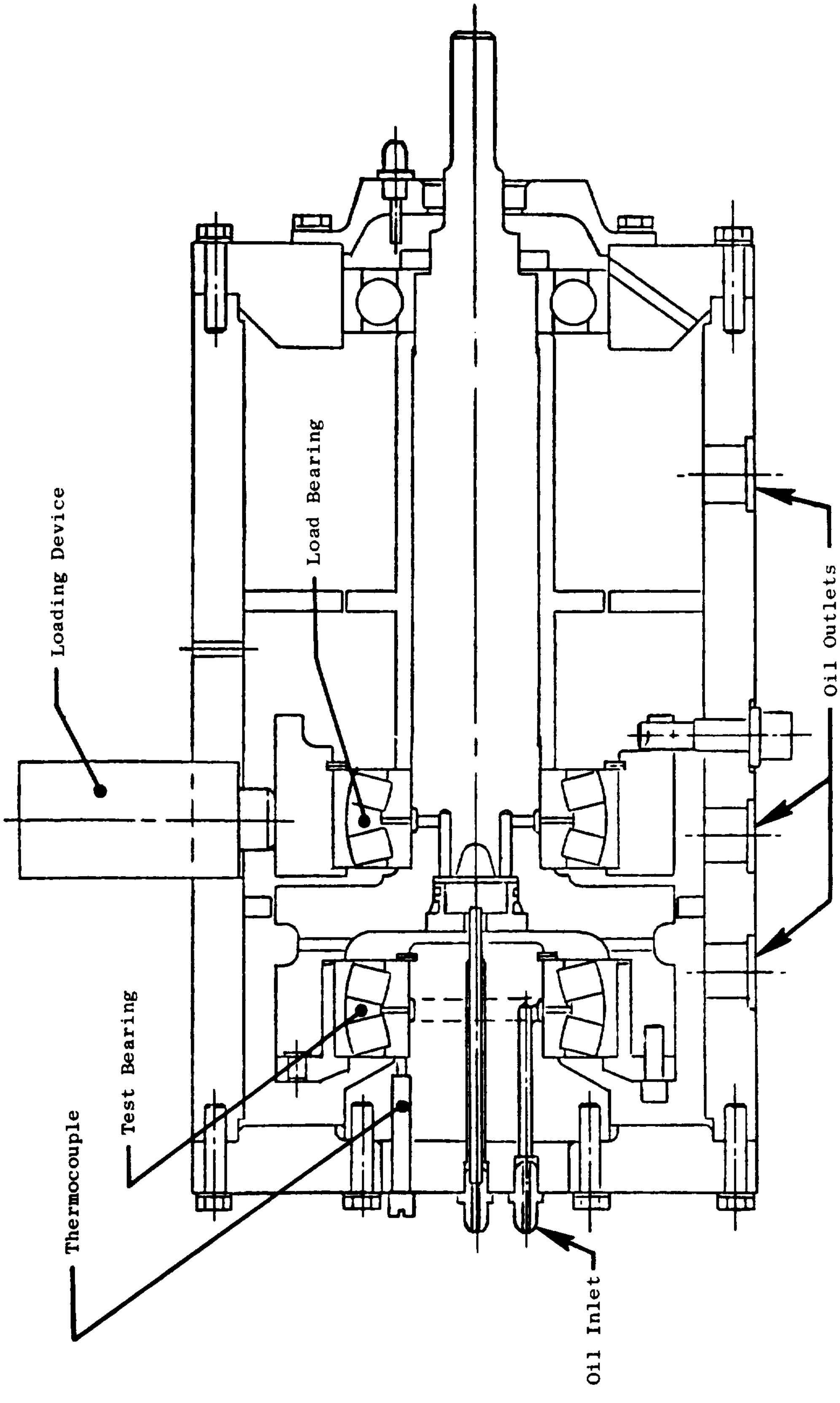
Loading Device
Load Bearing
Oil Outlets
Test Bearing
Thermocouple
Oil Inlet

Figure 10-8. Bearing Test Rig Schematic.

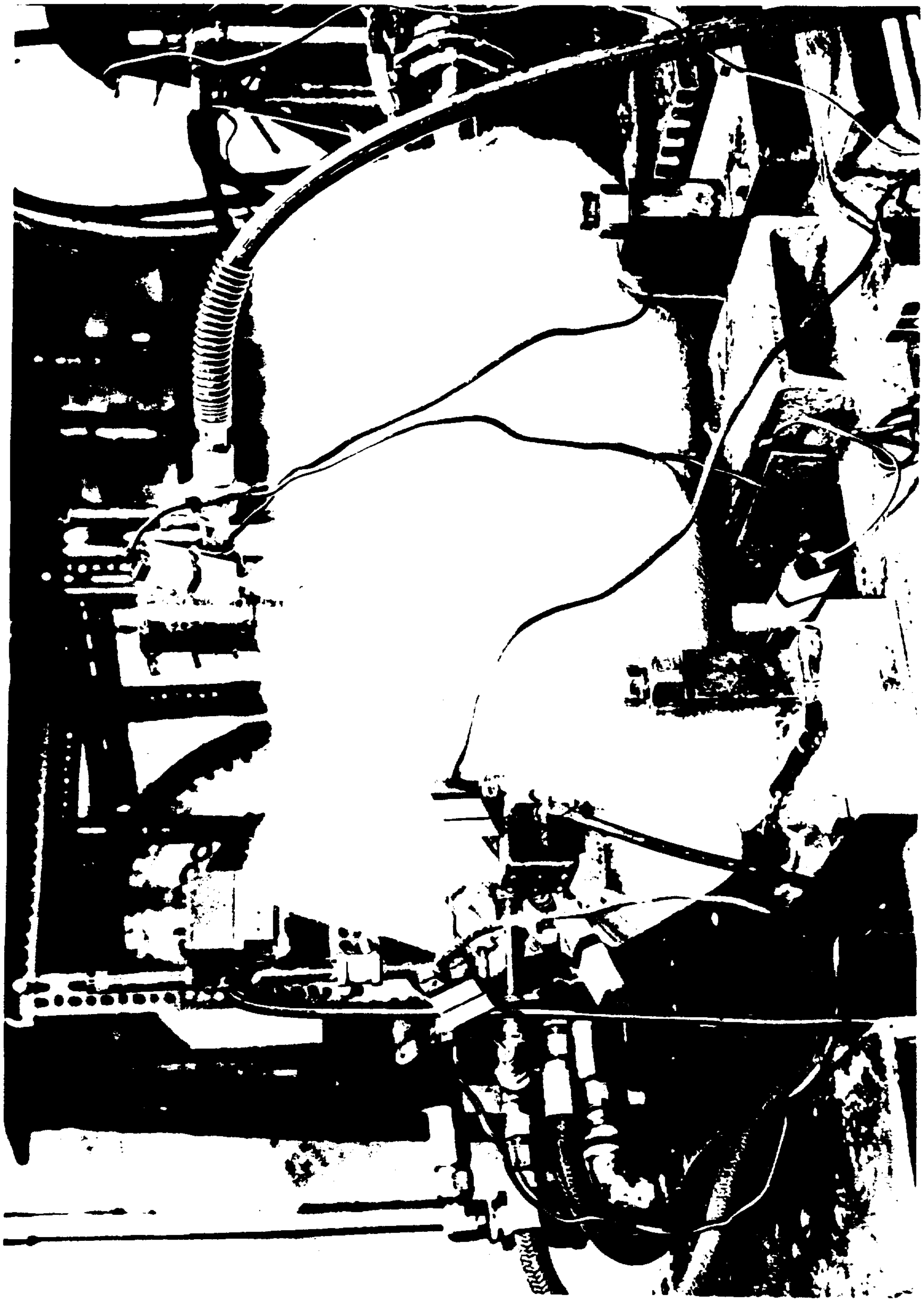

Figure 10-9. Bearing Test Rig.

similar in design, but slightly larger than the UTW bearing, and slightly smaller than the OTW bearing. Tests were conducted to simulate the more severe OTW operating conditions. The test results are summarized in Table 10-XIII. As shown, skidding was encountered at low power, high speed conditions during the first test. Evaluation of the data indicated that the large bearing clearance and a low oil flow rate resulted in the skidding problem. The clearance was reduced, and the tests were extended to cover all critical engine operating modes. No further problems were encountered. Based on these test results, it has been concluded that the selected UTW bearing design will perform satisfactorily during the engine test program. Detailed Bearing Test results are reported in NASA CR-134890, Main Reduction Gears Bearing Development Program Final Report.

10.6.2 Reduction Gear Back-To-Back Test

Back-to-back tests of the UTW reduction gear are planned during the fourth quarter of 1975. A schematic of the test rig is presented in Figure 10-10. As shown in the figure, two reduction gear units will be run back to back. Simulated loads will be applied by hydraulic cylinders at the torque plates. With this type of test setup, the input power requirement is only that required to overcome the losses in the system, which is only 2 to 3% of the design power transmission level of a single gear unit.

As indicated in Figure 10-10, the engine fan tail shaft geometry and scavenge system will be simulated on the test gear set side of the rig. During the rig tests the reduction gear power levels, speeds, and oil-in temperatures will be simulated over the range of flight cycle operating conditions. Objective of the test is to verify operating characteristics, including oil flow, heat rejection, efficiency, gear tooth pattern, adequacy of gear lubrication (absence of scoring), and bearing performance. Satisfactory completion of these tests will provide the necessary confidence in the reduction gear design prior to engine test.

Table 10-XIII. Star Gear Bearing Test Results.

SKF 22313 Double-Row Spherical Roller Bearing

Test No.	Test Conditions						Simulated Engine Test Conditions	Test Results
	Clearance		Oil-in Temp.		Oil Flow			
	cm	inches	K	° F	kg/min.	lb/min.		
1	.0178	0.007	356	180	2.99 - 4.99	6.6-11.0	Full Range	Skidding at Low-Power, High-Speed Conditions.
2	.0064	0.0025	358	185	3.99 - 4.99	8.8-11.0	TO and Climb	OK
3	.0064	0.0025	358	185	4.49	9.9	Cruise and Approach	OK
4	.0064	0.0025	358	185	3.99	8.8	Idle Descent	OK
5	.0064	0.0025	358	185	2.49	5.5	SLS Idle	OK

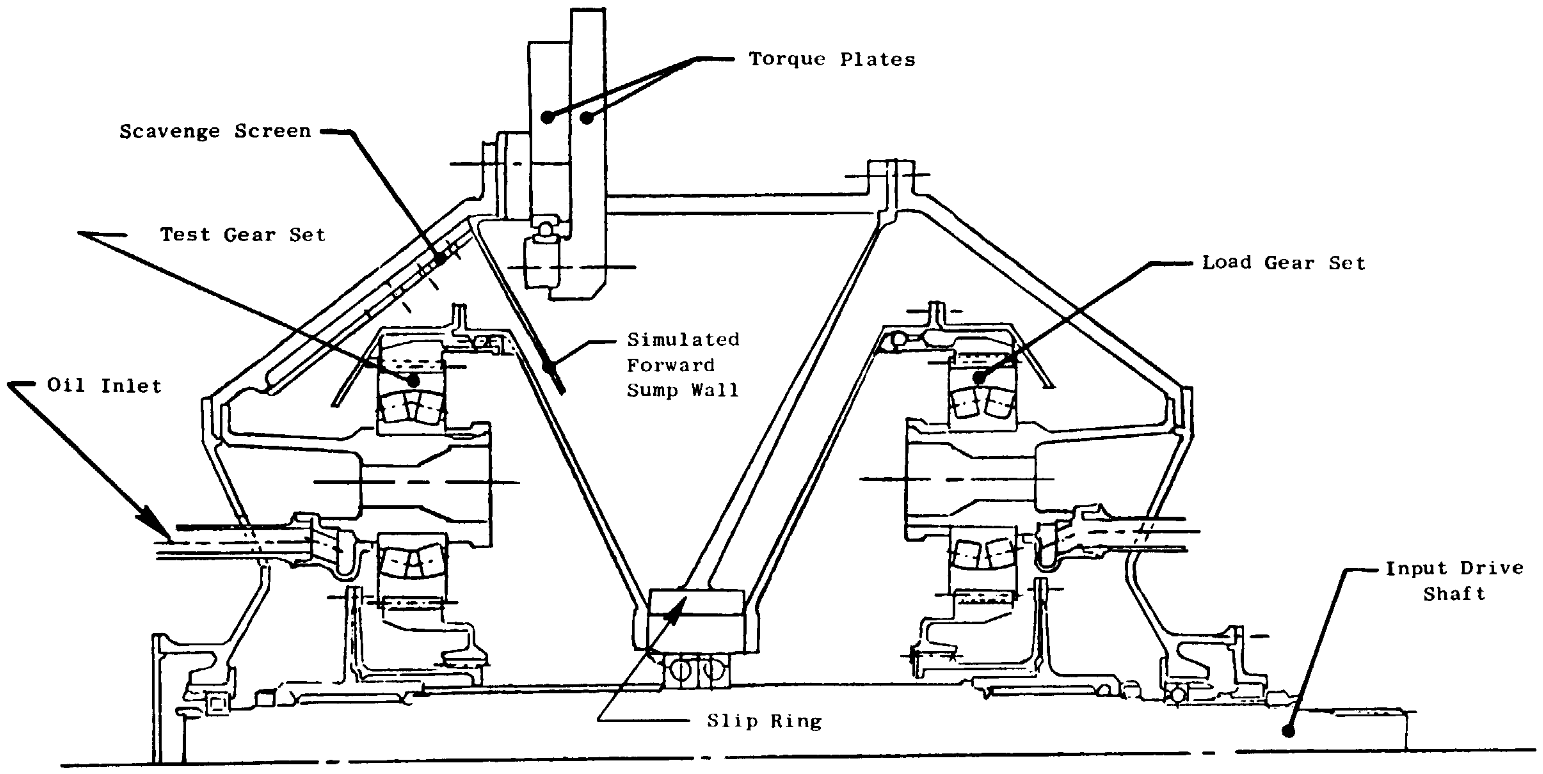
Torque Plates
Scavenge Screen
Test Gear Set
Load Gear Set
Oil Inlet
Simulated
Forward
Sump Wall
Input Drive
Shaft
Slip Ring

Figure 10-10. Main Reduction Gear Test Rig Schematic (Back-to-Back Test).

SECTION 11.0

ENGINE CORE AND LOW PRESSURE TURBINE DESIGN

11.1 SUMMARY

To minimize development risk and expense in the QCSEE program, the F101 core and low pressure turbine were selected. Moreover, to capitalize on the advanced state of development of these components, the qualified PFRT, or YF101, design was specified insofar as practical. Several exceptions to this approach exist. The following components are different from the PFRT configuration:

1. Accessory Drive Gear Mount
2. Compressor IGV Inner Flowpath
3. Compressor Stator Actuator and Feedback
4. Compressor First Stage Rotor Blade Airfoil
5. Combustor
6. HP Turbine Diaphragm Area
7. LP Turbine Diaphragm Area
8. LP Turbine No. 2 Blade
9. Turbine Frame
10. Balance Piston Arrangement
11. PV HP Turbine Shrouds
12. Warm Bridge HP Turbine Blade

11.2 DESIGN REQUIREMENTS

The F101 core and low pressure turbine were proposed for the QCSEE engines, because, in addition to providing desirable cycle and thrust size, this core engine employs suitable advanced technology components.

A major consideration in the detail core selection has been the desire to retain as much "qualified" hardware as practical. Therefore, the PFRT configuration has been specified in all areas except those discussed in the following paragraphs.

11.3 ENGINE CORE MODIFICATIONS

The following specific deviations from the PFRT configuration are planned for the UTW engine.

11.3.1 Accessory Drive Gear Mount

The F101 internal accessory drive bevel gears are mounted in a 17-4PH steel casting. This casting is bolted to the aft inner flange of the fan frame. Because of the higher bypass ratio of the UTW engine, the aft ring of the composite frame interferes with this gear mount casting. The solution to this problem was to reverse the casting and bolt it to the forward ring of the frame as shown in Figure 11-1.

In addition, the UTW experimental engine will have two radial drive shafts; one driving the top-mounted accessories and another driving the scavenge pump, located in the lower core cowl region. This requirement can be readily satisfied by using two sets of bevel gears and two support castings in each engine. (The casting occupies less than 180° of the mounting flange.)

11.3.2 Compressor IGV Inner Flowpath

The F101 inner flowpath in the IGV region is shown as a heavy line in Figure 11-2. Because of the higher bypass ratio and lower fan exit radius ratio in the UTW engine, difficulty was encountered in fairing into this flowpath contour from the fan frame with acceptable aerodynamic flow lines. Therefore, a modification was made to the inner ring of the inlet guide vane as shown in the figure.

11.3.3 Compressor Stator Actuator

The F101 compressor has been developed to optimize efficiency and flow at reduced corrected speeds, as required by its higher Mach number mixed mission. For use in the UTW engine, a higher airflow is desired, consistent with existing rpm and T4 limits. Operation at greater than 100% corrected speed would result in a severe compressor efficiency loss.

Fortunately, as a part of the F101 compressor development, various other stator schedules have been tested. One of the demonstrated schedules delivers significantly higher corrected flow at high corrected speeds, which meets the UTW requirements.

The UTW stator schedule is shown in terms of IGV setting angle versus corrected core speed in Figure 11-3.

Increased vane travel is required to achieve the higher airflow, necessitating several minor modifications in the actuator and linkages.

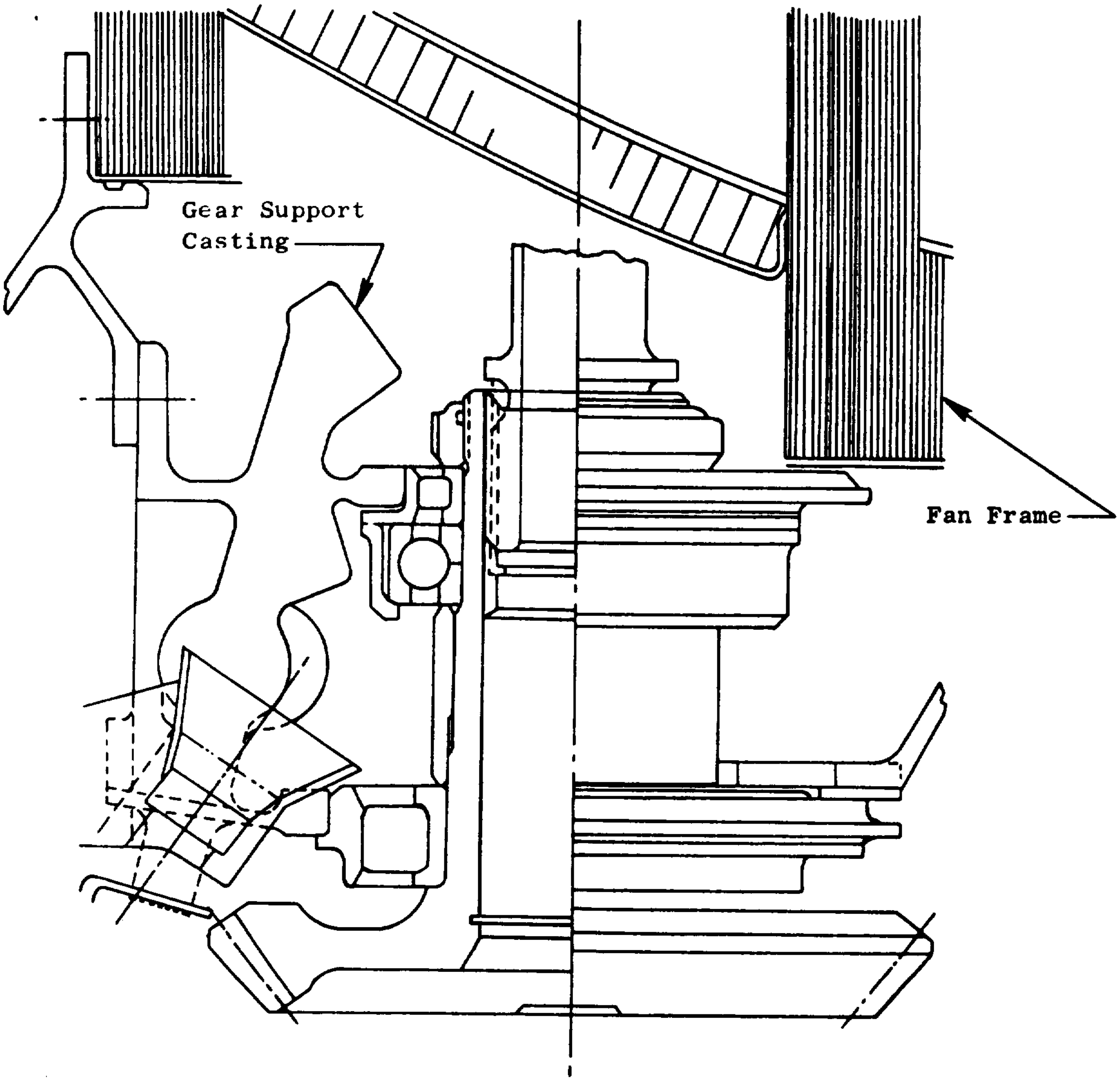
Gear Support Casting
Fan Frame

Figure 11-1. Accessory Drive Gear Mount.

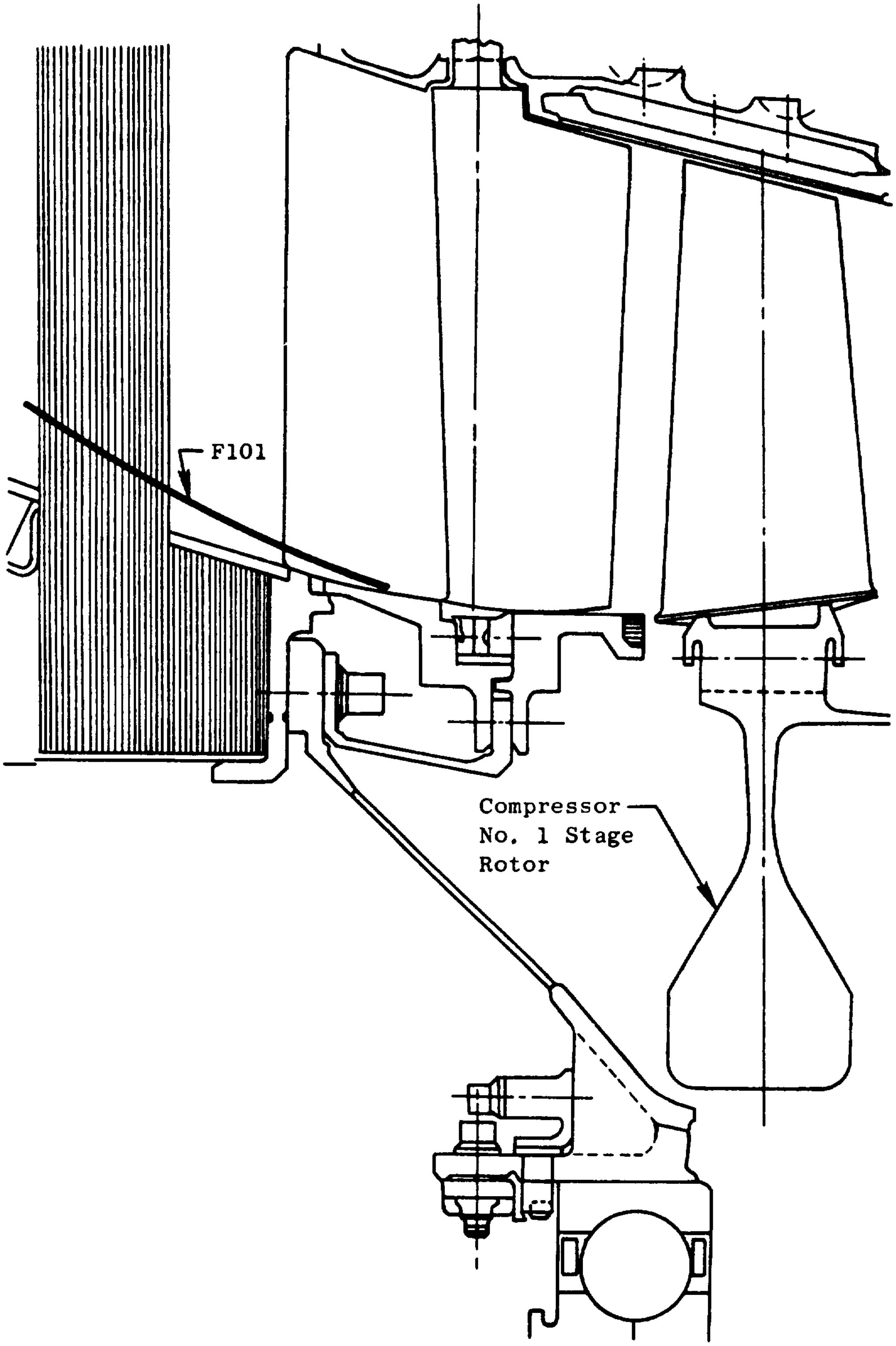
F101
Compressor No. 1 Stage Rotor

Figure 11-2. Compressor IGV Inner Flowpath.

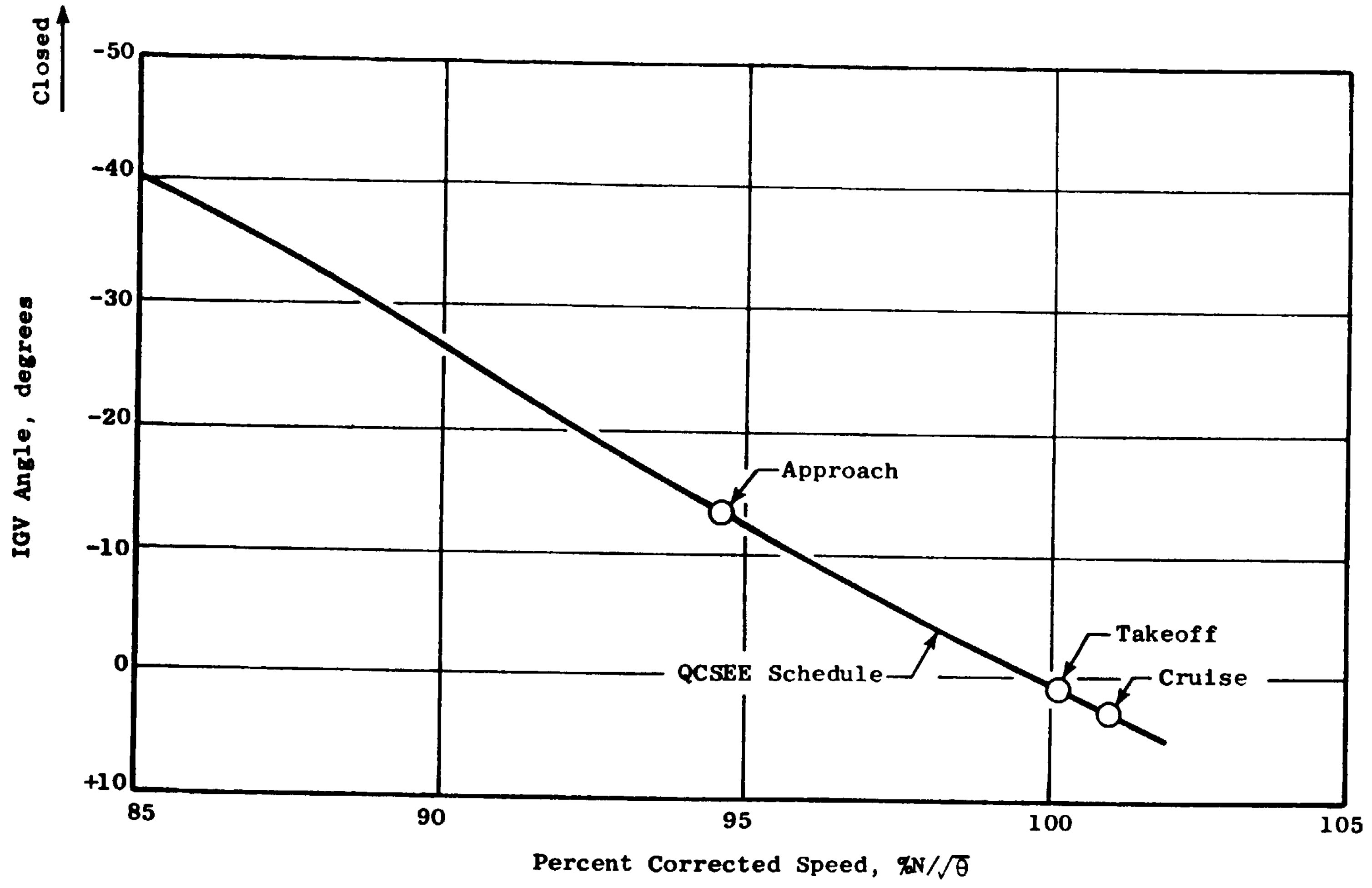

Figure 11-3. UTW Compressor Stator Schedule.

1. The vane actuator stroke must be increased from 7.747 cm (3.05 in.) to 9.627 cm (3.79 in.).

2. A new Stage 3 bellcrank must be provided.

3. The rod end of the Stage 3 linkage must be shortened about 0.127 cm (0.050 in.).

4. Bolts and nuts in the actuation assembly bellcranks must be replaced with flathead pins to permit them to pass between the actuation support members.

5. In the F101 engine, compressor stator angle is fed back to the control by means of a splined shaft. This shaft is too short for use in the UTW engine and will be replaced by a flex cable leading from the bellcrank, through the pylon to the control.

11.3.4 Compressor First Stage Rotor Blade Airfoil

To increase Stage 1 Rotor Blade aero-elastic margins, the F101 QT airfoil has been selected for the UTW engine.

Figure 11-4 shows the UTW engine frequency margin provided for takeoff operation as a function of ambient temperature on the day of testing. Also shown are the other limits that would come into play only during fan mapping with elevated operating lines. Rotor speed limits will be set to ensure adequate frequency margin at all ambient temperatures. All first stage rotor blades will be frequency screened to determine these limits.

11.3.5 Combustor

Since the UTW engine operates at a considerably higher takeoff fuel/air ratio than the F101 engine, the PFRT combustor would be expected to produce visible smoke at high power settings. Recent testing of a central injector combustor, similar to that which is currently planned for the F101 PV engine, has demonstrated that this design produces lower pollutant levels as well as no visible smoke. The PV combustor, described in detail in Section 4.0, has, therefore, been selected for the UTW engine.

Target emissions levels for the QCSEE Program are the EPA-defined 1979 emissions standards for class T2 aircraft engines. Current predictions indicate that the UTW engine will meet NO_x and smoke requirements; however, due to its low idle pressure ratio, its C_xH_y and CO emissions levels will exceed the standard. Consequently methods such as sector burning, compressor bleed, and flat pitchline of the fan will be employed at idle to reduce these emissions to the lowest practical level.

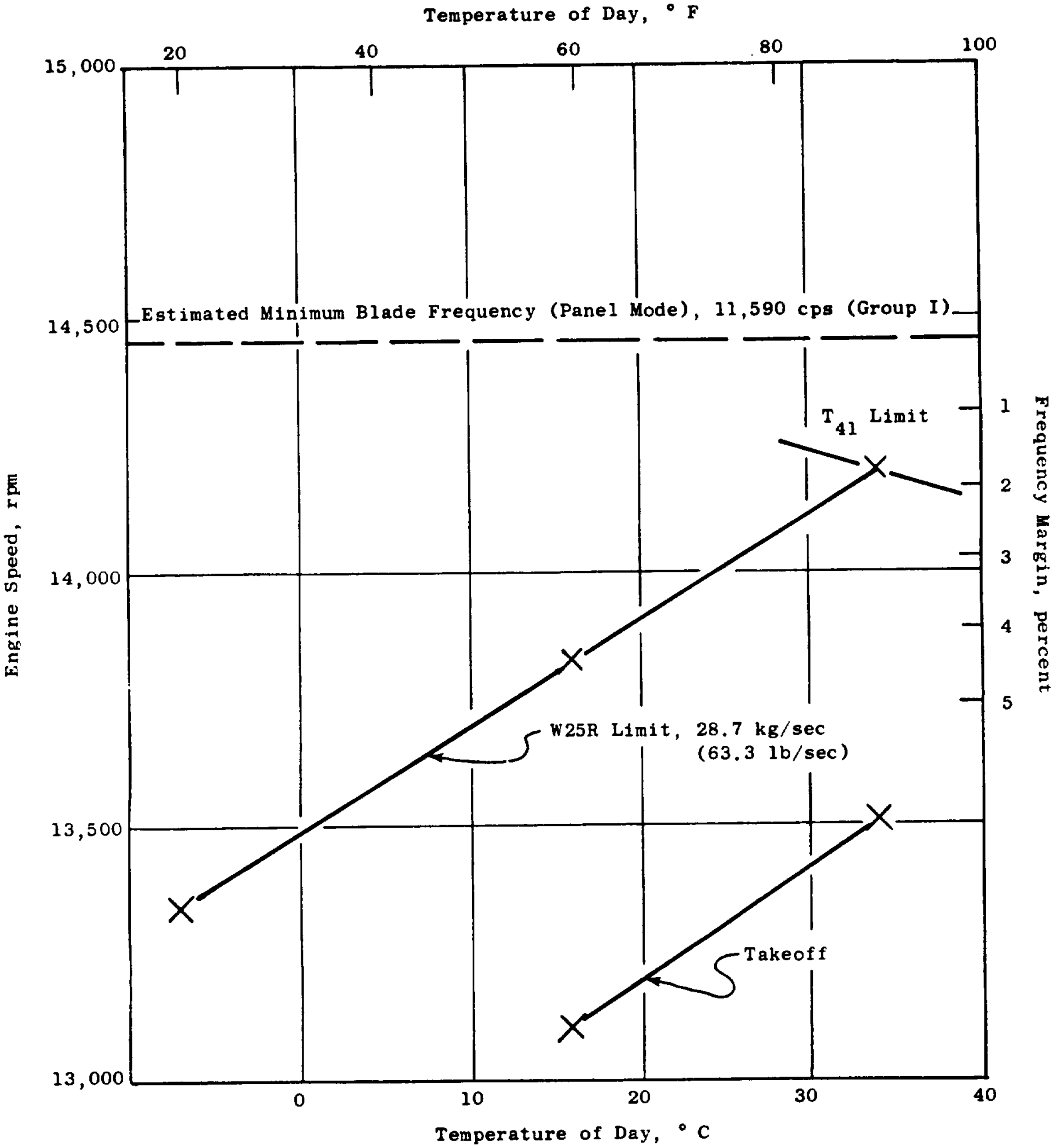

Figure 11-4. UTW Engine Frequency Margin, Takeoff.

11.3.6 HP Turbine Diaphragm Area

Figure 11-5 shows the compressor characteristic selected for the UTW engine. Because of the reduced cycle pressure ratio of the UTW engine compared to the F101 cycle, both the HP and LP turbine effective areas require adjustment to satisfy turbine flow function requirements.

By increasing the HP turbine effective area by 5% and decreasing the LP turbine effective area by 5%, the compressor can be made to operate at a more favorable point.

The means for adjusting turbine area is to rotate the vanes slightly to open or close the throat dimension. Figure 11-6 illustrates the degree of rotation needed for a 5% increase in HP turbine area. This will be accomplished by rotating the tool used to EDM the vane slots in the bands. Modified inspection fixtures are also required.

11.3.7 LP Turbine Diaphragm

In the case of the LP turbine, 5% reduction of area is accomplished by similar means. In either case the change in throat dimension (Do) is less than 0.05 cm (0.020 in.). Figure 11-7 illustrates this adjustment in the LPT stage one diaphragm.

11.3.8 Low Pressure Turbine Second Stage Blade

In the UTW engine, the higher energy extraction of the LP turbine results in an increase in exit swirl, which will be removed by using longer straightening vanes in the turbine frame. However, to minimize the required turning in these vanes, and to provide more predictable angles of attack on the vanes, it was deemed advisable to incorporate a QT second-stage LPT blade.

11.3.9 Turbine Frame

Modifications to the F101 turbine frame to extract greater swirl and to adapt the frame structurally to meet the UTW requirements are described in detail in Sections 11.4 and 11.5.

11.3.10 Balance Piston

Introduction of a reduction gear between the low pressure turbine and the fan of the UTW engine effectively cuts the load path normally used to balance fan plus LPT rotor net thrust force. Therefore, the rear sump area will be modified to incorporate a pneumatic piston to balance part of the turbine rotor thrust. The design of the balance piston is discussed in detail in Section 12.5.

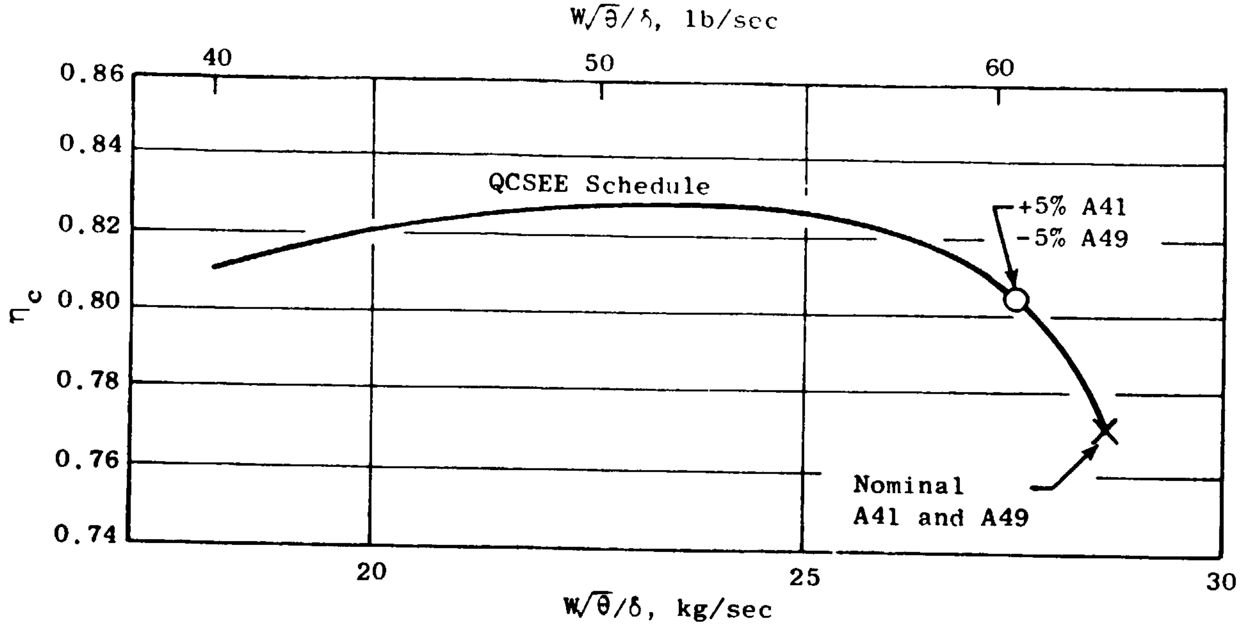

Figure 11-5. Compressor Characteristics.

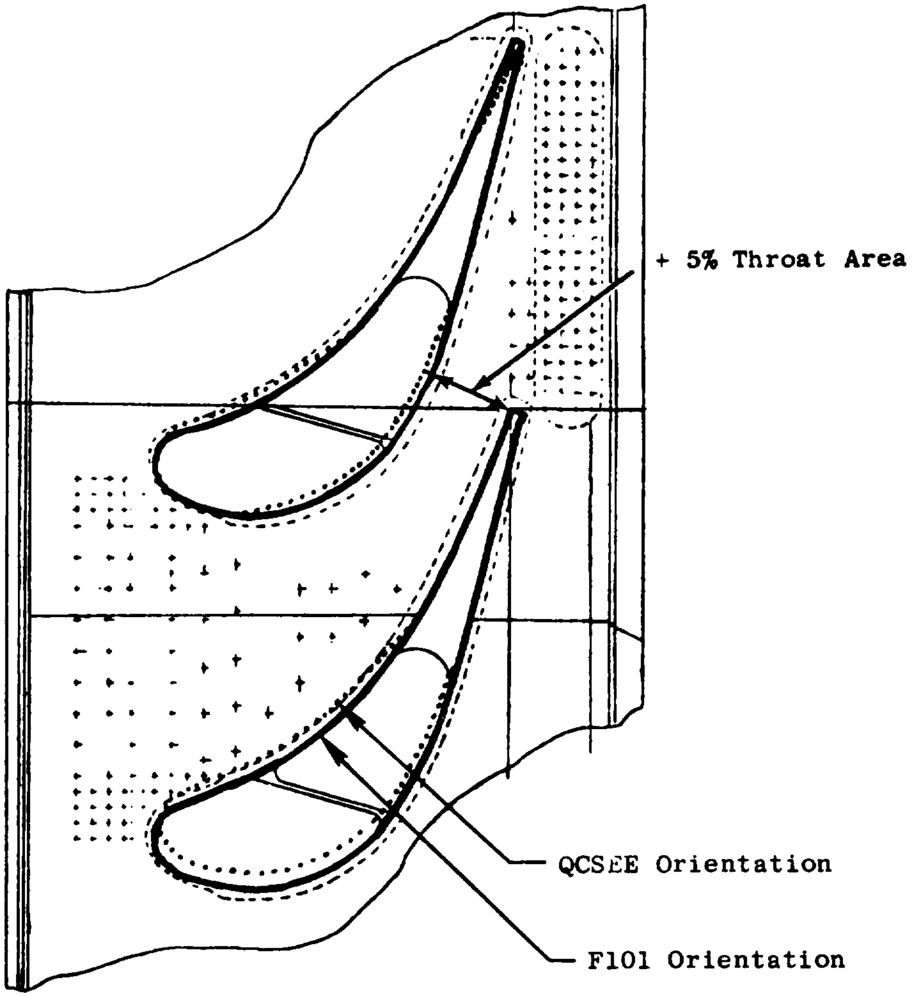
+ 5% Throat Area
QCSEE Orientation
F101 Orientation

Figure 11-6. High Pressure Turbine Stator Assembly.

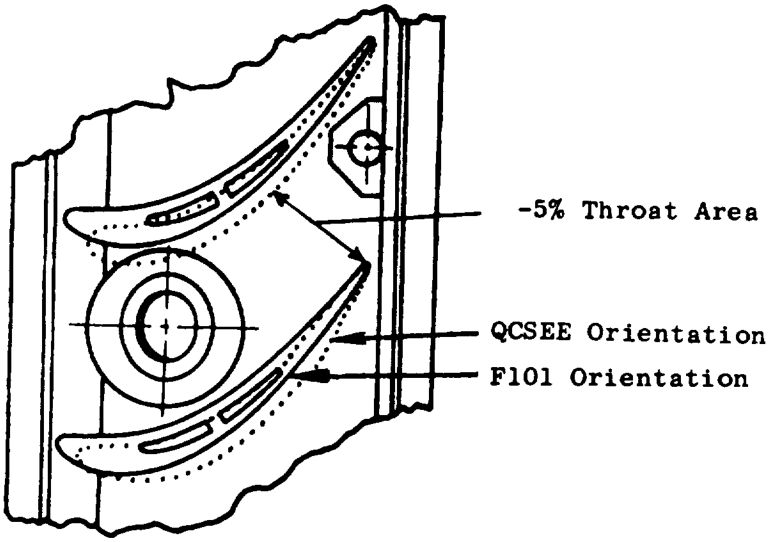
-5% Throat Area
QCSEE Orientation
F101 Orientation

Figure 11-7. Low Pressure Turbine Stage 1 Stator Assembly.

11.3.11 PV Turbine Shrouds

The stationary shrouds at the tips of the high pressure turbine blades consist of Poroloy rub pads welded to structural support segments. Some shroud failures have occurred in F101 PFRT engines wherein the Poroloy pads crack and small pieces break out. Although no secondary damage has been observed, an improved shroud design has been released for the F101 PV engine. This design uses a coarser wire in the Poroloy, a revised layup pattern, and additional support points. Since the shroud is fully interchangeable with the PFRT design, it has been specified for the UTW core.

11.3.12 Warm Bridge HP Turbine Blade

Another change being introduced in the F101 PV engine is the warm bridge turbine blade. This design employs serpentine cooling air passages with leading edge film discharge and trailing edge pin-fin cooling, in place of the impingement insert design used in the PFRT blade. Test experience has indicated a much superior endurance life with the warm bridge blade. The blades can be substituted in the same disk; however, minor modifications are required in the retainers to adjust axial blade clamping, and in the cooling air inducer to increase airflow 1/2% of W25. These changes have been specified for the UTW engine.

11.4 LOW PRESSURE TURBINE FRAME AERODYNAMIC DESIGN

11.4.1 Introduction

The UTW low pressure turbine is a slight modification of the F101 low pressure turbine operating at an increased pressure ratio. The increased turbine exhaust swirl necessitated a modification to the present F101 frame/OGV aerodynamic geometry. The frame/OGV was redesigned for low noise and low loss characteristics.

A single frame configuration has been designed to satisfy the requirements of both the UTW and OTW engines. Frame design modifications related to OTW engine requirements are therefore included in the following discussion.

11.4.2 Design

Design Point Selection

Turbine operating point for the frame/OGV aerodynamic design was selected to avoid off-design modes where separation and consequent core noise can occur at critical engine operating points. Based on initial cycle data turbine off-design vector diagram studies were made at significant QCSEE operating points using the Multi-Sector NASA Turbine Computer Program (TCP). A summary of results is shown in Table 11-I. The OTW takeoff condition was

Table 11-I. Low Pressure Turbine Operating Point Data.

Engine Condition	UTW			OTW		
	TO	APPR	Max. Cruise(1)	TO	APPR	Max. Cruise(1)
$\frac{\Delta h}{T} \sim$ Btu/lb° R	0.063	0.055	0.073	0.066	0.056	0.066
$\frac{\Delta h}{T} \sim$ J/g ° K	0.264	0.230	0.306	0.277	0.235	0.277
$\frac{N}{\sqrt{T}} \sim$ rpm/$\sqrt{°\ R}$	165	180	176	164	152	162
$\frac{N}{\sqrt{T}} \sim$ rpm/$\sqrt{°\ K}$	221	241	236	220	204	217
$\Psi = \frac{\Delta Vu}{u}/2$	1.04	0.76	1.05	1.10	1.10	1.12
Swirl (degrees)	25.8	8.2	33.5	29.6	24.1	29.9
Mach Number	0.47	0.34	0.68	0.53 ⬆ Design Point	0.40	0.52

(1) Alt/Mach Number = 600 m/0.7 (20,000 ft/0.7)

chosen as the design point since this case represented the highest turbine exhaust swirl and Mach number conditions (excluding maximum cruise points). Subsequent cycle data indicated somewhat higher swirl points, but the OTW takeoff case shown was still considered to be a reasonable design condition.

Axisymmetric Analysis and Flowpath Modification

Axisymmetric analysis of the frame/OGV was done using the CAFD computer program. This calculation accounts for streamline slope and curvature as well as lean and sweep effects. The analysis was set up with many intrablade calculation stations in order to analyze endwall Mach number distributions. First, the F101 frame flowpath with an additional 2.54 cm (1 in.) of axial width in the OGV was analyzed. Based on the results of this analysis, a modified flowpath was selected which was considered an aerodynamic improvement (with reduced diffusion) and also satisfied frame mechanical design and exhaust system requirements. This flowpath is shown in Figure 11-8.

The results of the axisymmetric analysis are shown in Figure 11-9. Plotted versus radial height at the OGV inlet are the gas angle, OGV design angle, and inlet absolute Mach number. Also shown is the absolute Mach number distributions on the inner and outer walls through the OGV. The NASA diffusion factors associated with this flowpath are:

$D_{Root} = 0.316$

$D_{Pitch} = 0.440$

$D_{Tip} = 0.183$

Vane Modification

The vane modification involved adding 2.54 cm (1 in.) of axial width to the present F101 OGV to remove the additional swirl. The change was made entirely in the false nose extension with the strut and aft strut extension remaining unchanged. Three vane sections at approximate root, pitch, and tip locations were designed and analyzed using both the CASC and CABIS programs. The CABIS (Cascade Analysis due to Beuckner, Isay, and Schnacker) program is an incompressible analysis while CASC (Cascade Analysis by Streamline Curvature) gives a compressible solution which accounts for radius change and streamtube thickness variation. The CASC Mach number distribution for the pitch section is given in Figure 11-10 for two different false nose extensions. Figure 11-10 shows that if the nose extension was designed to attach to the strut, as it presently does in the F101, there would be a distinct "bump" on the pressure surface. A smooth pressure surface was designed as shown and both configurations were analyzed with CASC. The resulting Mach number distributions clearly indicate the effect of the bump. Consultation with experienced OGV designers indicated only a small decrement in performance associated with this. However, it was decided (with Mechanical Design concurrence) to modify the OGV smoothly as shown. CASC Mach number distributions

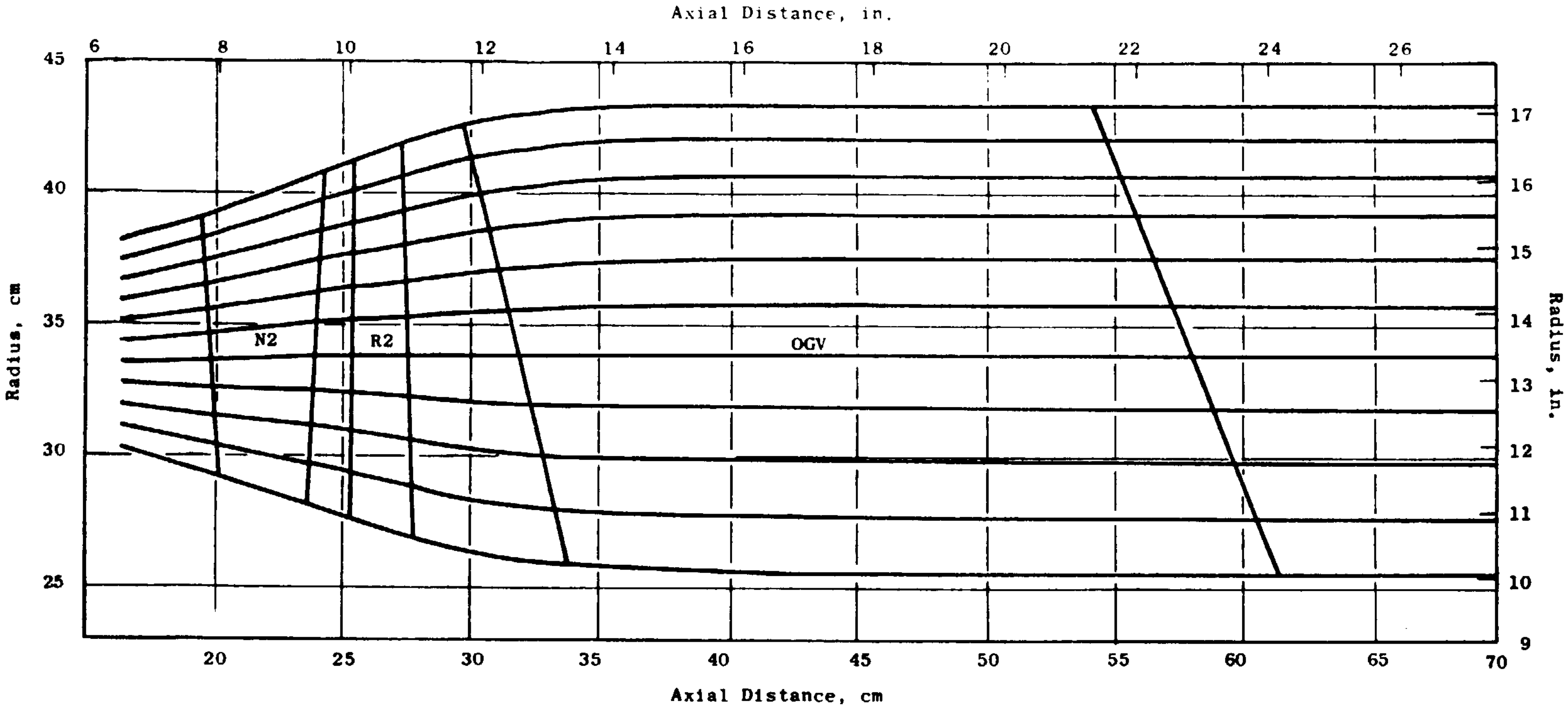

Figure 11-8. QCSEE OGV/Frame Flowpath.

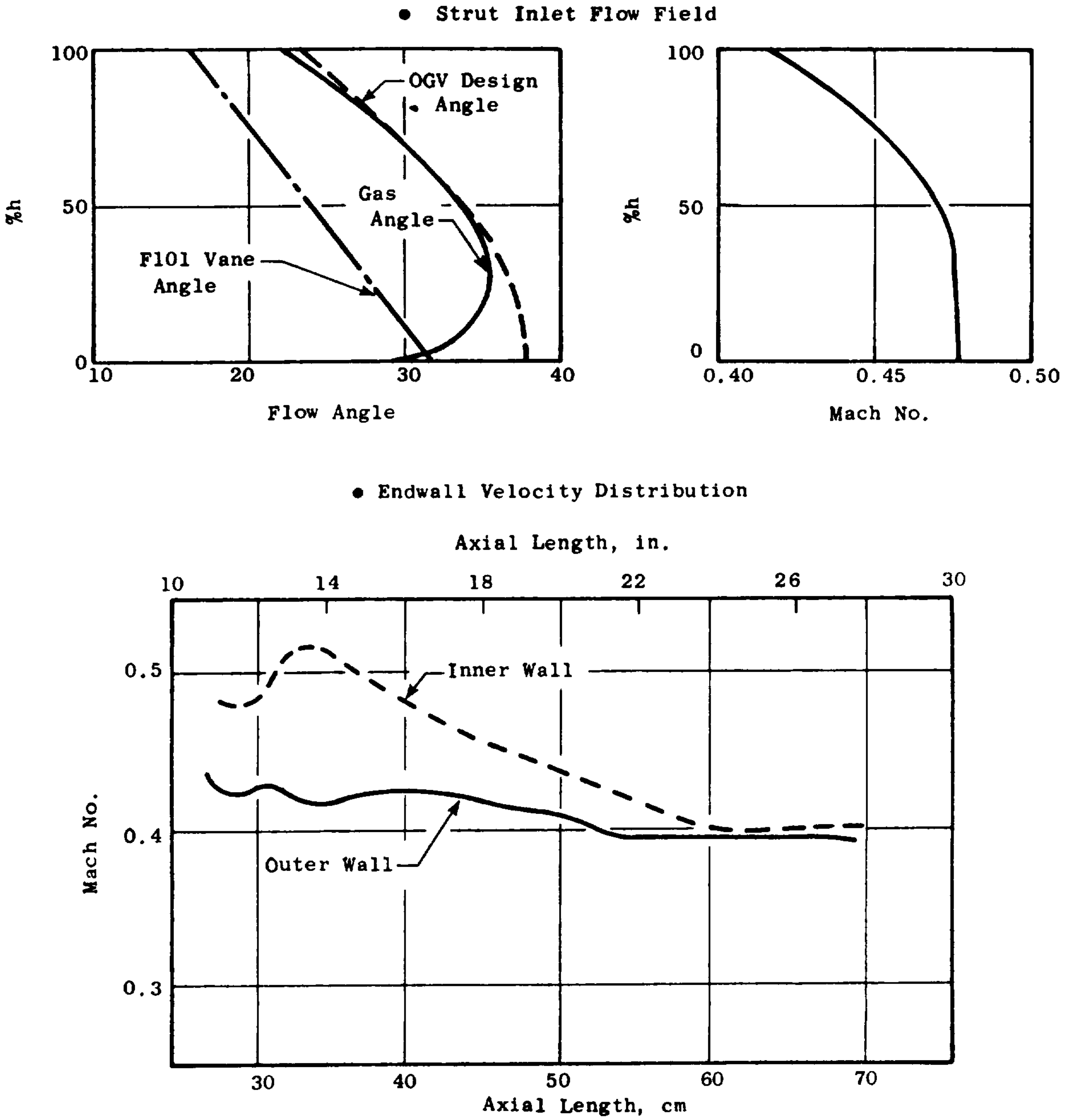

Figure 11-9. QCSEE Turbine Frame Axisymmetric Flow Analysis.

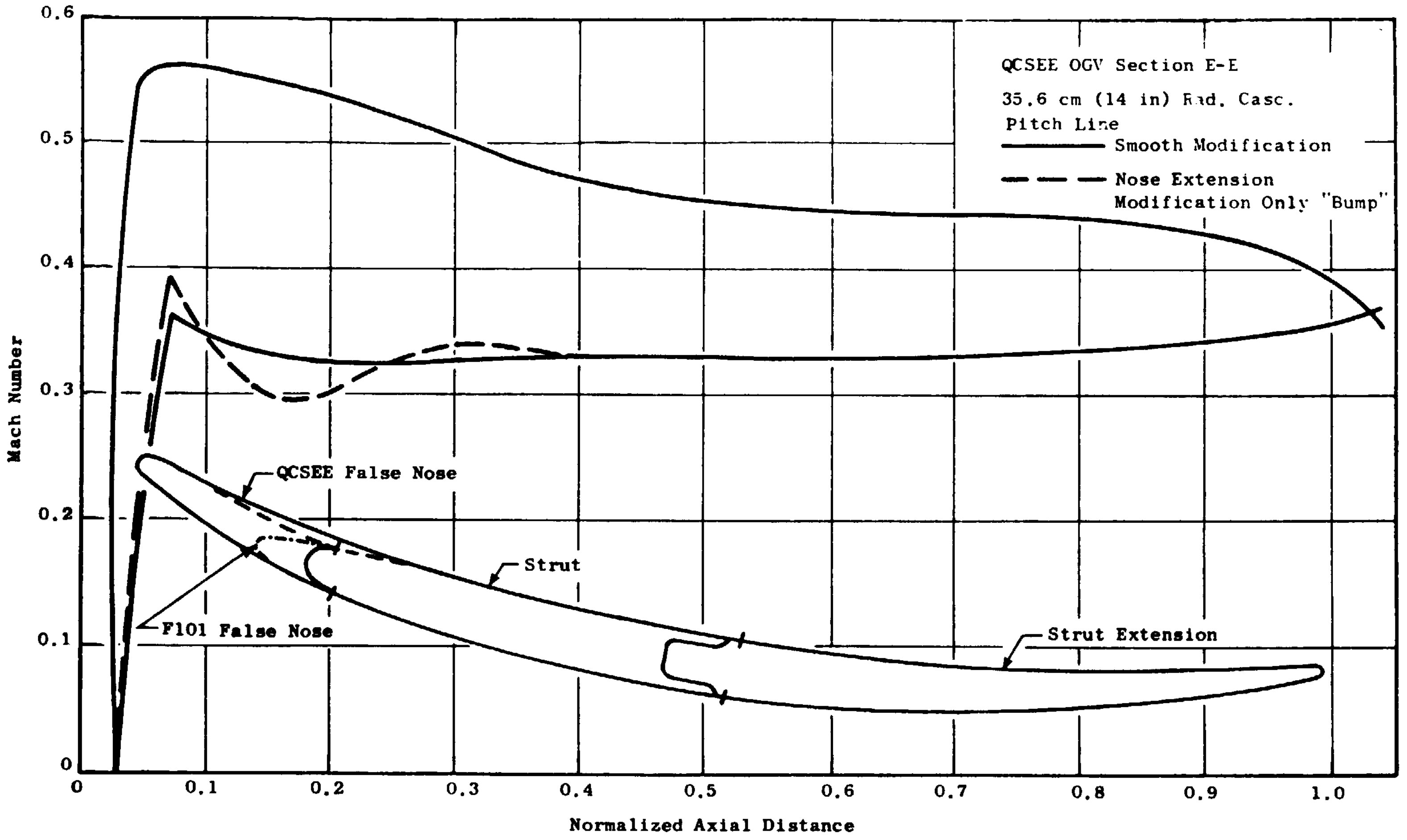

Figure 11-10. QCSEE Vane Modification.

for the root and tip are shown in Figures 11-11 and 11-12. Other intermediate sections were designed to yield a smooth stack-up.

11.4.3 Off-Design Study

Based on revised cycle data, an off-design study was undertaken to evaluate the OGV performance at several significant operating points. Vector diagram for the low pressure turbine operating at the takeoff, approach and maximum cruise points for both the UTW and OTW engines were calculated with the TCP program. A summary of these results is shown in Table 11-II. Axisymmetric analyses for the OTW takeoff case (design point) and the UTW approach and maximum cruise points (representing extremes in operation) were made using the CAFD program. These results are shown in Figure 11-13.

Plotted versus radial height at OGV inlet are the gas angle, OGV design angle, and Mach number. Also shown are the absolute Mach number distributions on the inner and outer walls through the OGV for the UTW approach and maximum cruise positions. Root, pitch, and tip vane surface Mach number distributions for these cycle points were obtained using the CASC program. These are shown in Figures 11-14, 11-15, and 11-16. At the OTW takeoff point, the Mach number distributions are satisfactory. The distributions at the UTW approach point (negative incidence) show higher pressure side diffusion but separation is considered unlikely and performance should be good. However, at the UTW maximum cruise point (high inlet Mach number and positive incidence), the CASC results show very high suction surface Mach numbers at the leading edge with subsequent large diffusion and likely separation. Some performance loss will result at this operating point.

In order to reduce the likelihood of suction surface separation at the UTW maximum cruise point, several approaches were taken. First, an attempt was made at increasing the chord of the OGV by increasing the length of the false nose. For a 1.27 cm (0.5 in.) increase in axial width at the pitchline, Vmax/V2 dropped from 2.46 to 2.29, and the peak suction surface Mach number dropped from 0.98 to 0.91. Due to cost considerations, this redesign was dropped in favor of reducing A8 at the UTW maximum cruise point which will lower the OGV inlet Mach number and angle. However, results for this change were somewhat disappointing because, while the peak suction surface Mach number was decreased from 0.98 to 0.89, Vmax/V2 was only decreased from 2.46 to 2.40.

Since it was apparent that separation off the OGV probably could not be avoided at the UTW maximum cruise point, estimates were made of the magnitude of losses associated with separation and the effects on engine performance were evaluated. At the extreme UTW maximum cruise point (30K/0.8 M), the OGV loss, expressed as the loss in total pressure normalized by the OGV inlet pressure head, $(P_{T1}-P_{T2})/(P_{T1}-P_{S1})$, was estimated to be 0.12. With this loss, objective maximum cruise thrust could still be achieved without exceeding any normal engine operating limits.

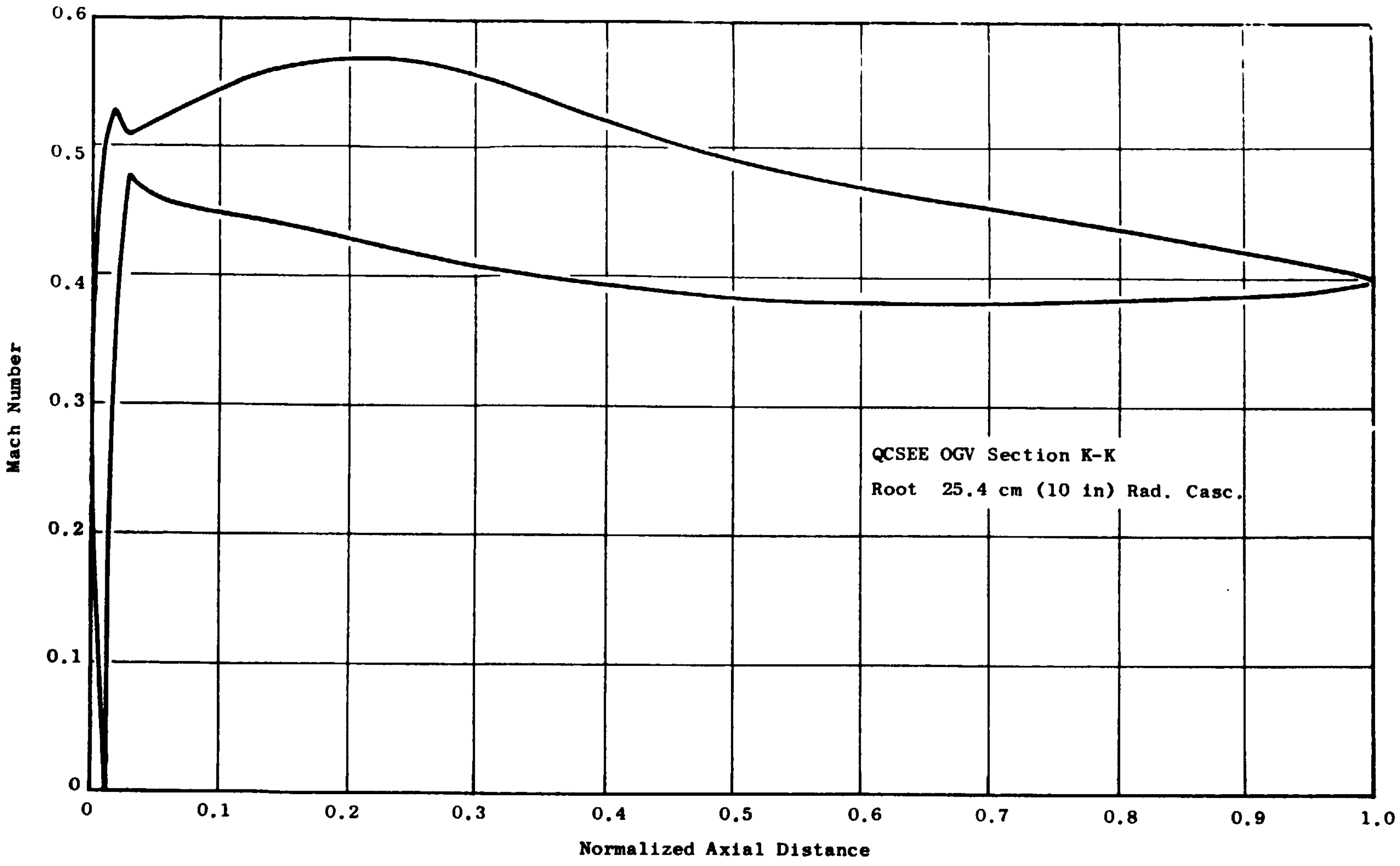

Figure 11-11. CASC Mach Number Distributions.

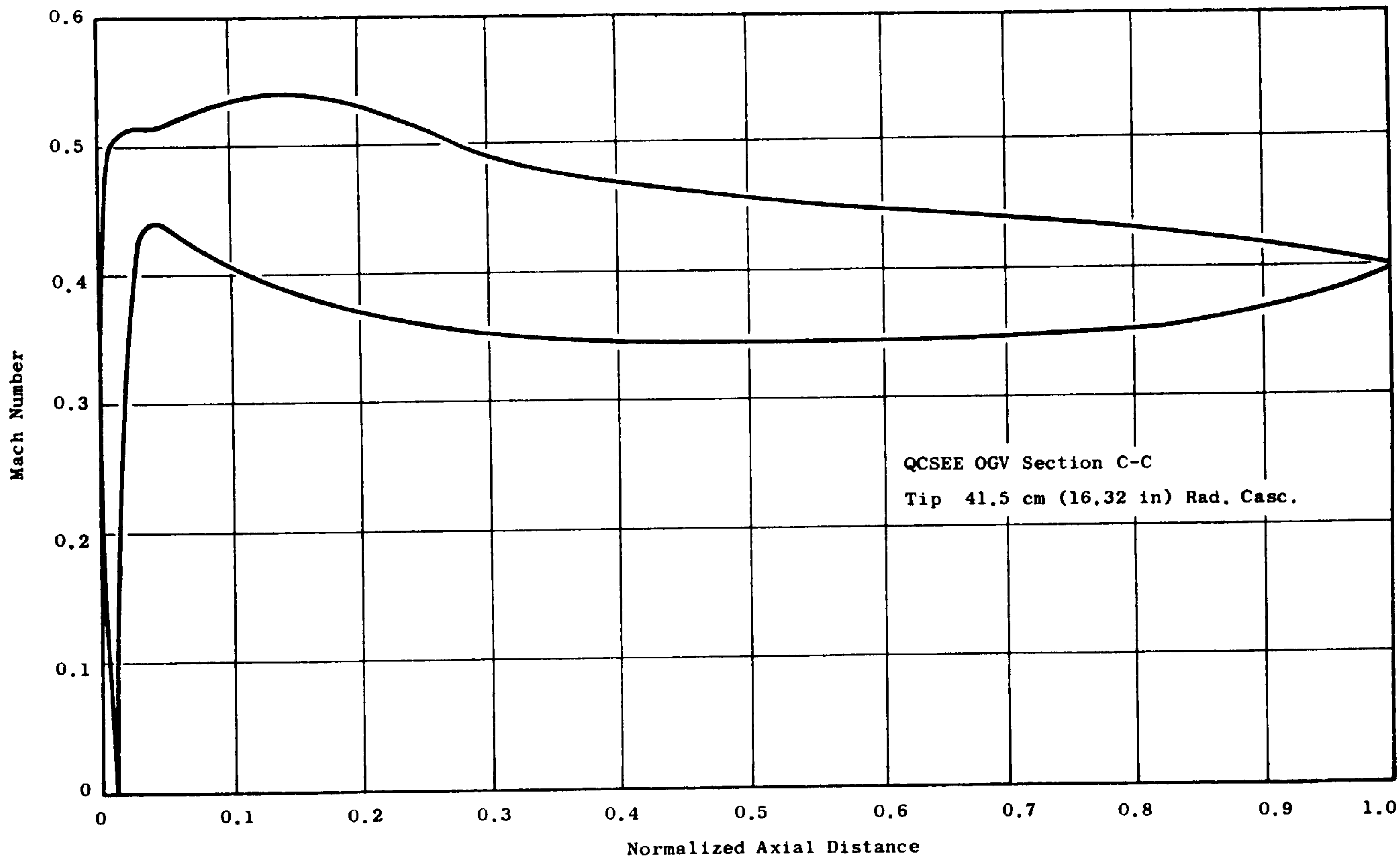

Figure 11-12. CASC Mach Number Distributions.

Table 11-II. Fan Turbine Operating Point Data.

Engine Condition	UTW			OTW		
	T/O	Approach$^{(1)}$	Max. Cruise$^{(2)}$	T/O	Approach$^{(1)}$	Max. Cruise$^{(3)}$
$\frac{\Delta h}{T}$ ~ Btu/lb° R	0.063	0.057	0.075	0.067	0.055	0.067
$\frac{\Delta h}{T}$ ~ J/g ° K	0.264	0.239	0.314	0.281	0.230	0.281
$\frac{N}{\sqrt{T}}$ ~ rpm/$\sqrt{° R}$	164	172	177	164	148	161
$\frac{N}{\sqrt{T}}$ ~ rpm/$\sqrt{° K}$	220	231	237	220	199	216
$\psi = \frac{\Delta Vu}{u} /2$	1.05	0.86	1.07	1.11	1.13	1.17
Swirl (degrees)	27.1	15.1	34.5	31.5	24.8	33.3
Mach Number	0.48	0.37	0.79	0.56	0.39	0.59
				▲ Design Point		

(1) Alt/Mach = 61 m/0.121 (200 ft/0.121)
(2) Alt/Mach = 7620 m/0.7 (25,000 ft/0.7)
(3) Alt/Mach = 9144 m/0.8 (30,000 ft/0.8)

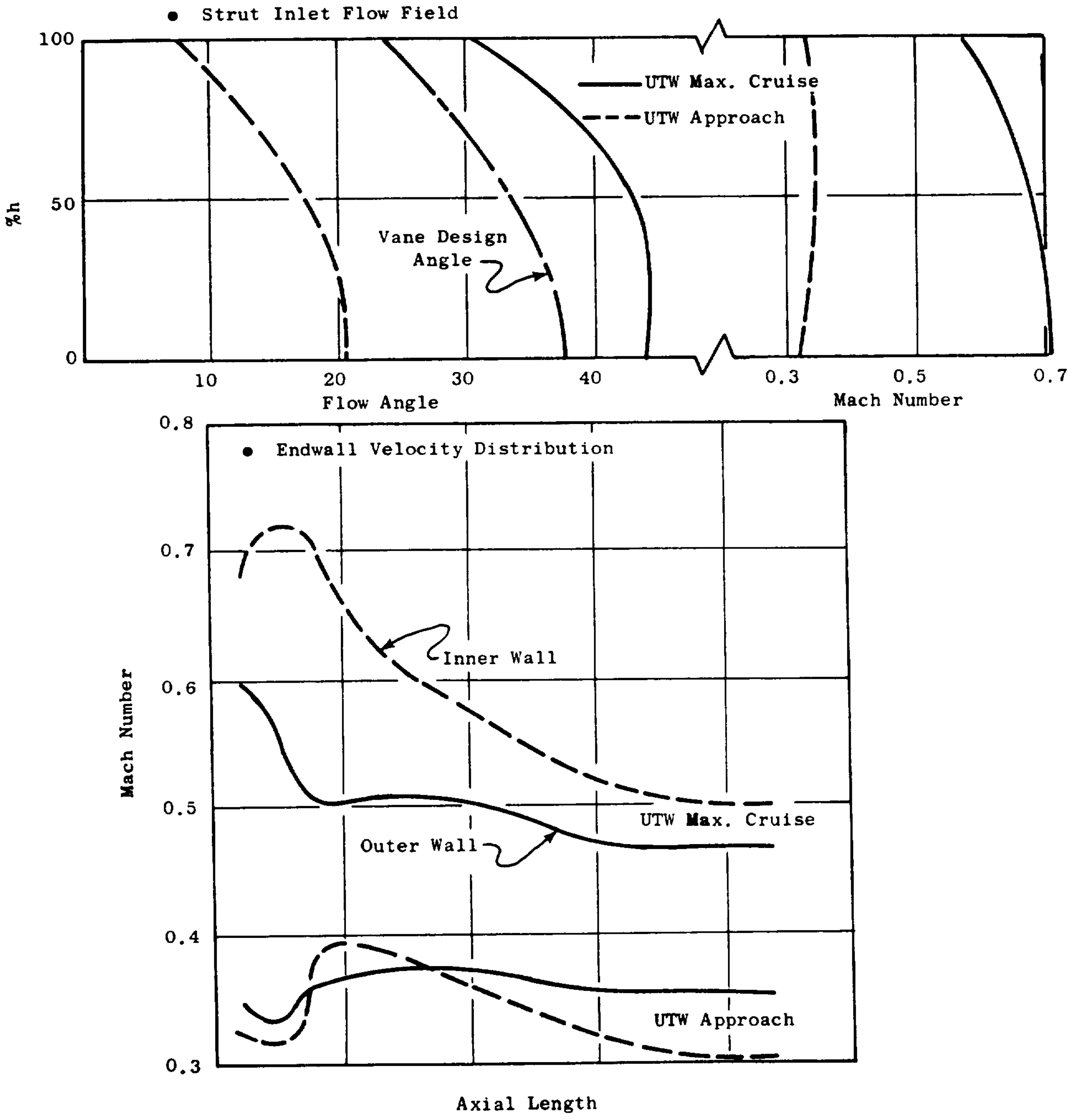

Figure 11-13. Turbine Frame Axisymmetric Flow Analysis.

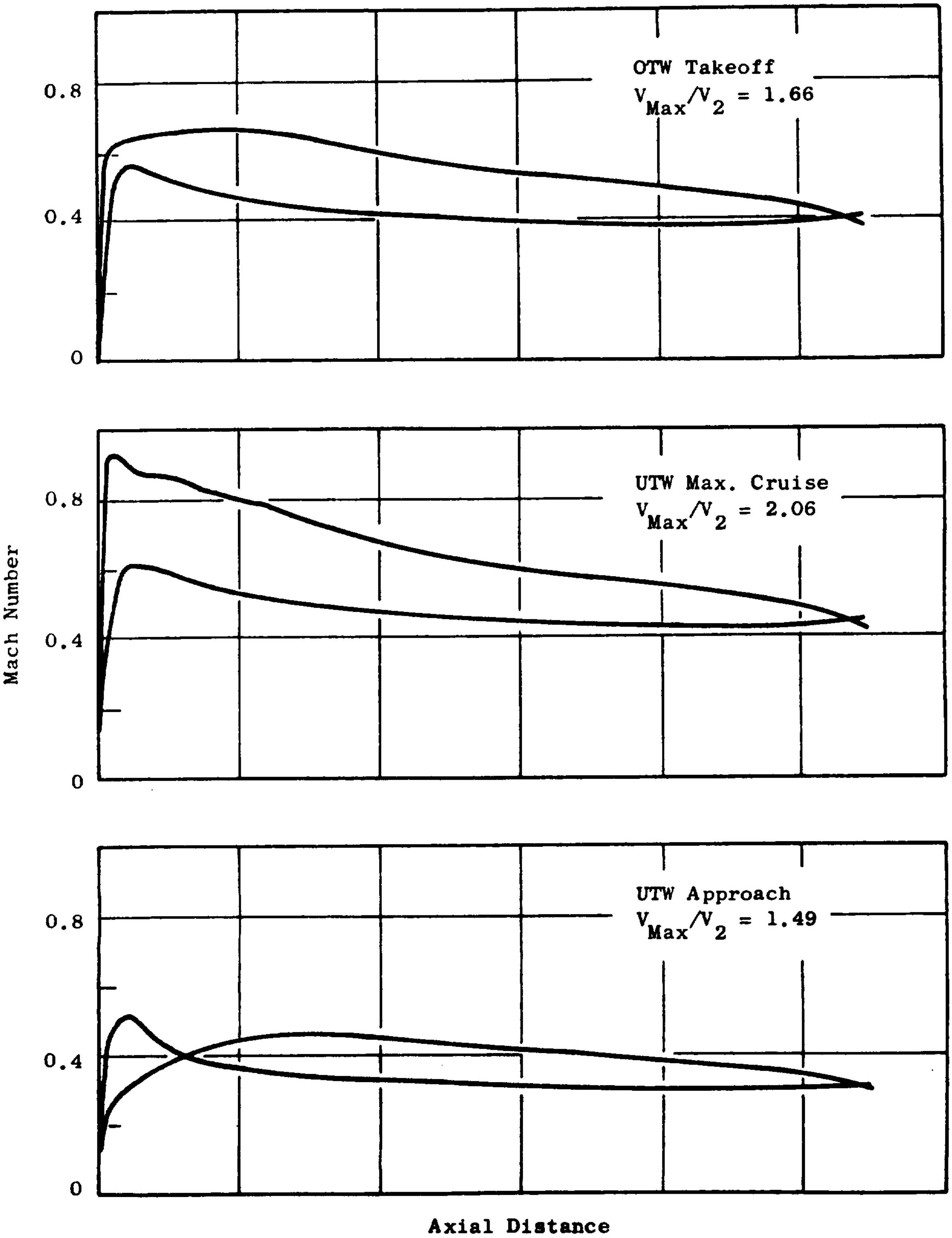

Figure 11-14. Off-Design Study, CASC Results, Root Section.

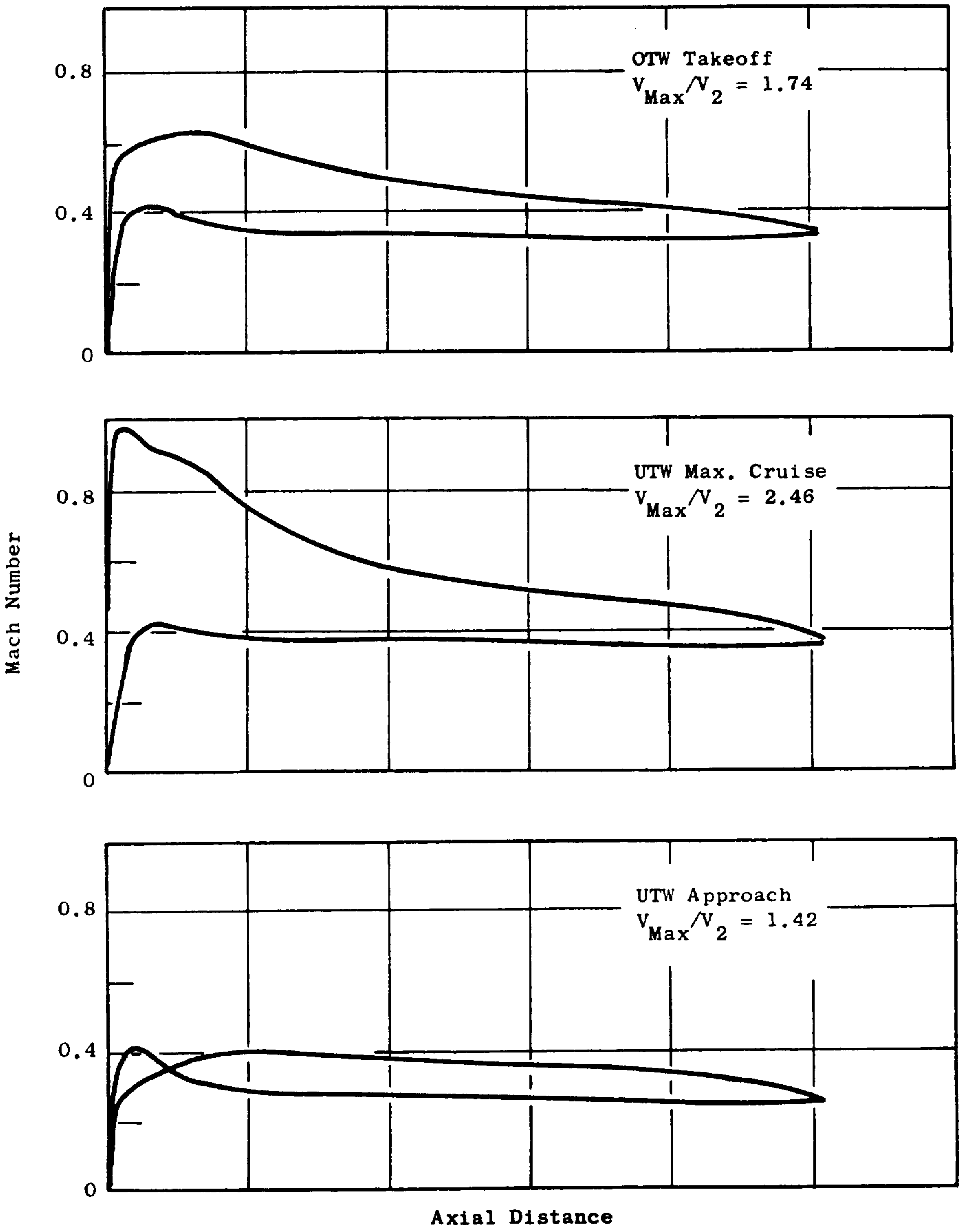

Figure 11-15. Off-Design Study, CASC Results, Pitch Section.

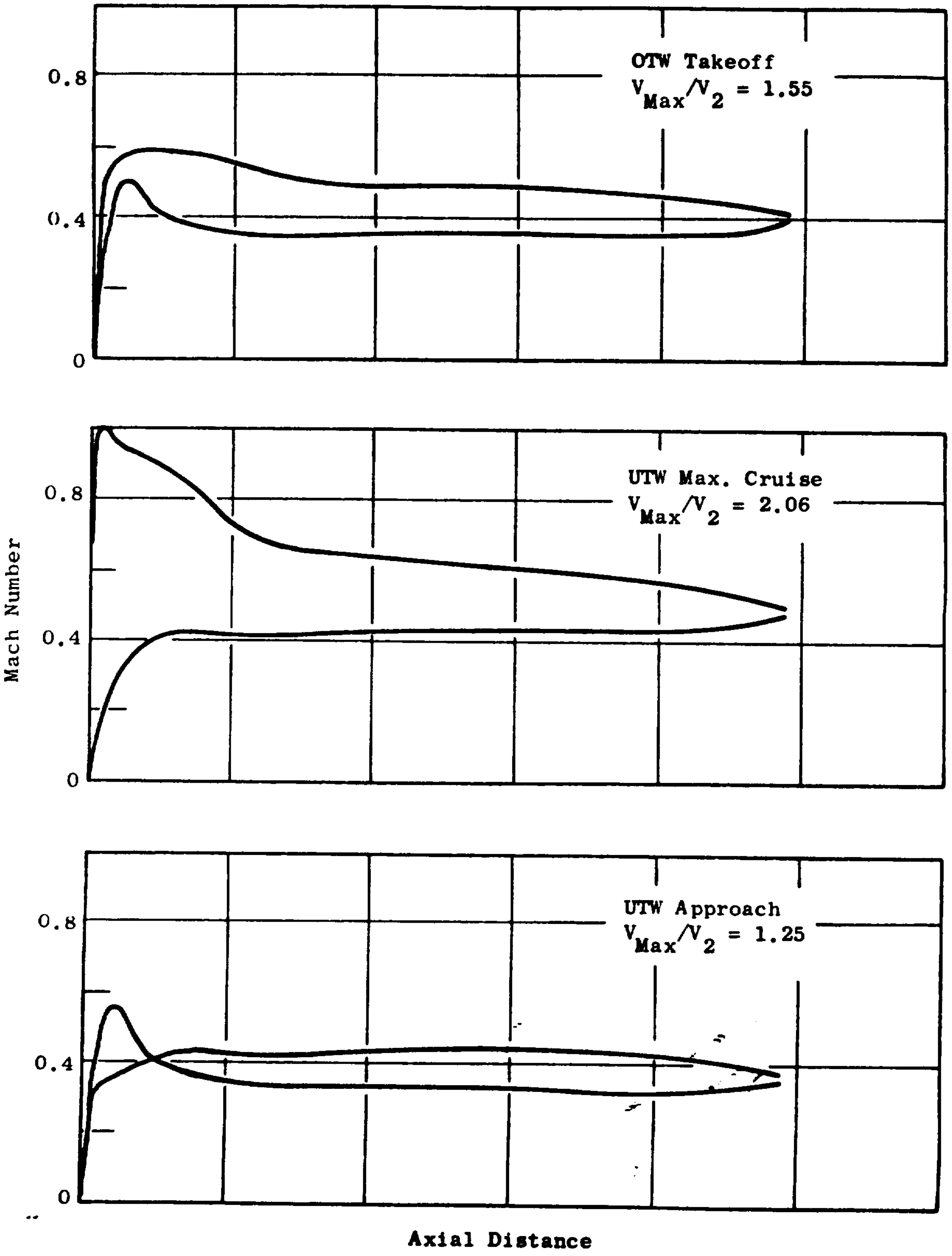

Figure 11-16. Off-Design Study, CASC Results, Tip Section.

11.5 LOW PRESSURE TURBINE FRAME MECHANICAL DESIGN

11.5.1 Summary

The turbine frame used in the UTW engine is a modification of the F101 turbine frame. Figure 11-17 illustrates the major design features, and Table 11-III summarizes the differences from the F101 frame.

11.5.2 Design Requirements

In addition to the maneuver loads shown in Section 2.0, the following specific design criteria were established:

	Stress
Max. maneuver loads at operating temperatures	<0.2% Y.S.
1-1/2 times max. maneuver loads at operating temp	<UTS
Blade-out loads at operating temp	Maintain Engine Support
1-1/2 times buckling loads at operating temp	<0.2% Y.S.
Transient thermal plus 1 g load	<0.2% Y.S.
4 g vibratory load	<Goodman Diagram

In conjunction with the above limit loads, the primary gas temperature profile used for frame analysis is shown in Figure 11-18.

11.5.3 Design Description

The UTW turbine frame consists of an outer frame casing, 14 aerodynamic vane/struts, flow path liners, and a hub structure. The outer frame structure includes the outer ring, which contains the three link support for engine mounting, and the outer case. Figure 11-19 is a schematic of UTW engine mounting system.

Since the UTW pylon and short bypass duct necessitate a top-mounted frame configuration, a three-link system has been employed. These links take vertical and side loads and rolling moments.

Since the three-link configuration concentrates the mount reactions at the top of the frame, the outer ring section properties must be increased. This results in a larger ring section as shown in Figure 11-20. Details of the revised outer ring are shown in Figure 11-21.

In addition to engine mounting provisions, the outer frame casing extends aft from the turbine casing to support the core exhaust nozzle.

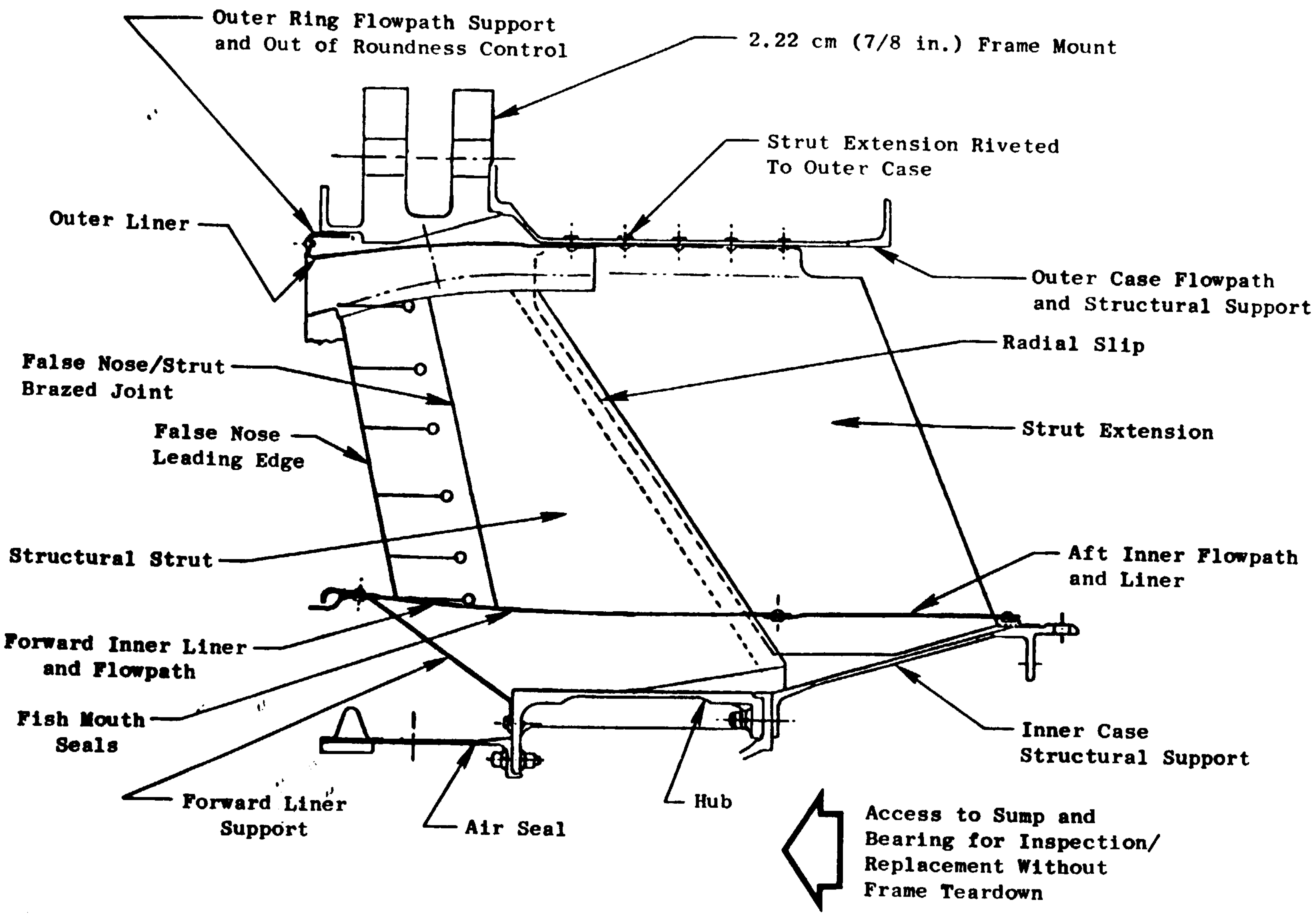
Outer Ring Flowpath Support
and Out of Roundness Control
2.22 cm (7/8 in.) Frame Mount
Strut Extension Riveted
To Outer Case
Outer Liner
Outer Case Flowpath
and Structural Support
False Nose/Strut
Brazed Joint
Radial Slip
False Nose
Leading Edge
Strut Extension
Structural Strut
Aft Inner Flowpath
and Liner
Forward Inner Liner
and Flowpath
Fish Mouth
Seals
Inner Case
Structural Support
Forward Liner
Support
Air Seal
Hub
Access to Sump and
Bearing for Inspection/
Replacement Without
Frame Teardown

Figure 11-17. Turbine Frame Assembly Features.

Table 11-III. Summary of Design Changes.

Item	Change	Reason
Vane/Strut	Extended forward fairing	Remove additional swirl
Outer Ring	Larger cross section	Change mounting system to accommodate pylon
Flowpath Liners	Recontour	Improve aero flowpath
Outer Casing	New structural part	Support exhaust nozzle
Inner Casing	Thicken and added flanges	Support centerbody

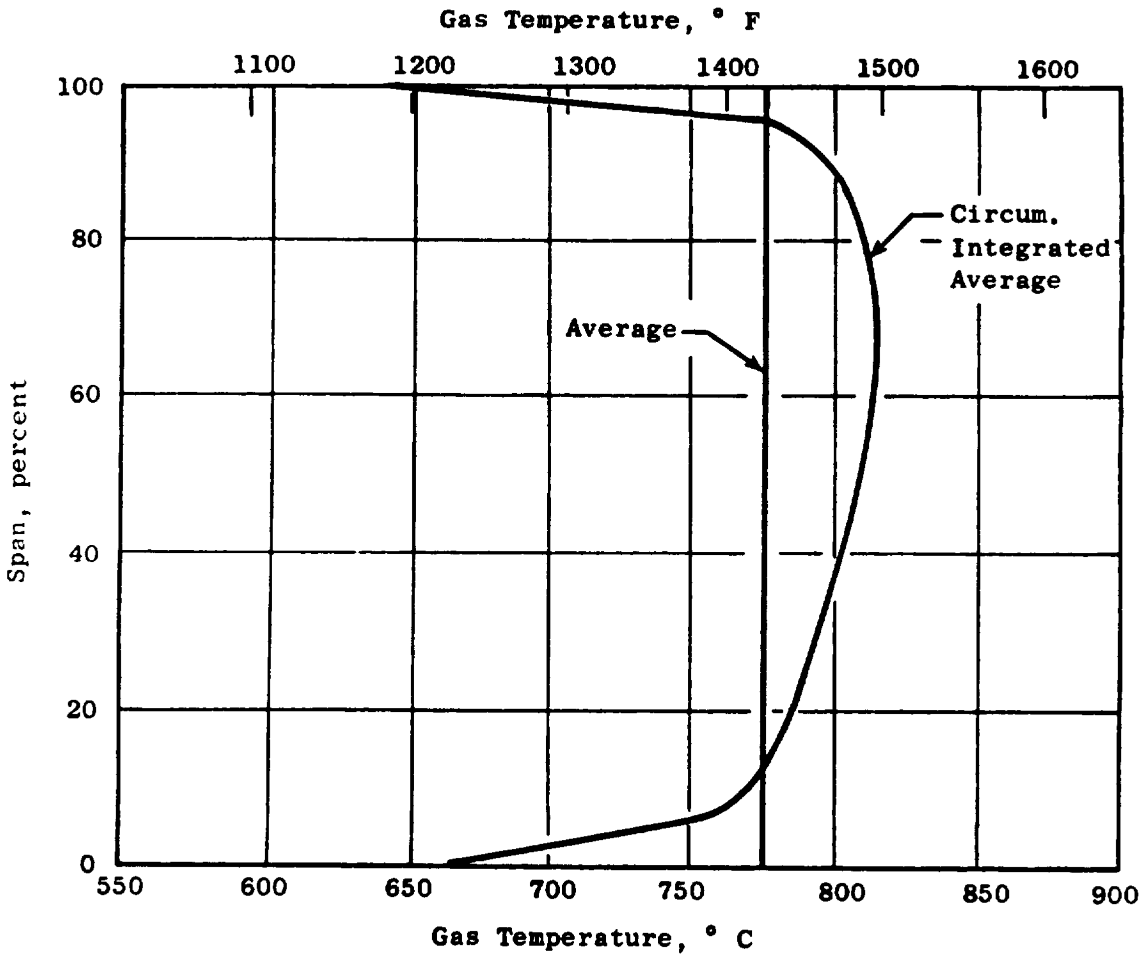

Figure 11-18. Turbine Exit Gas Profile.

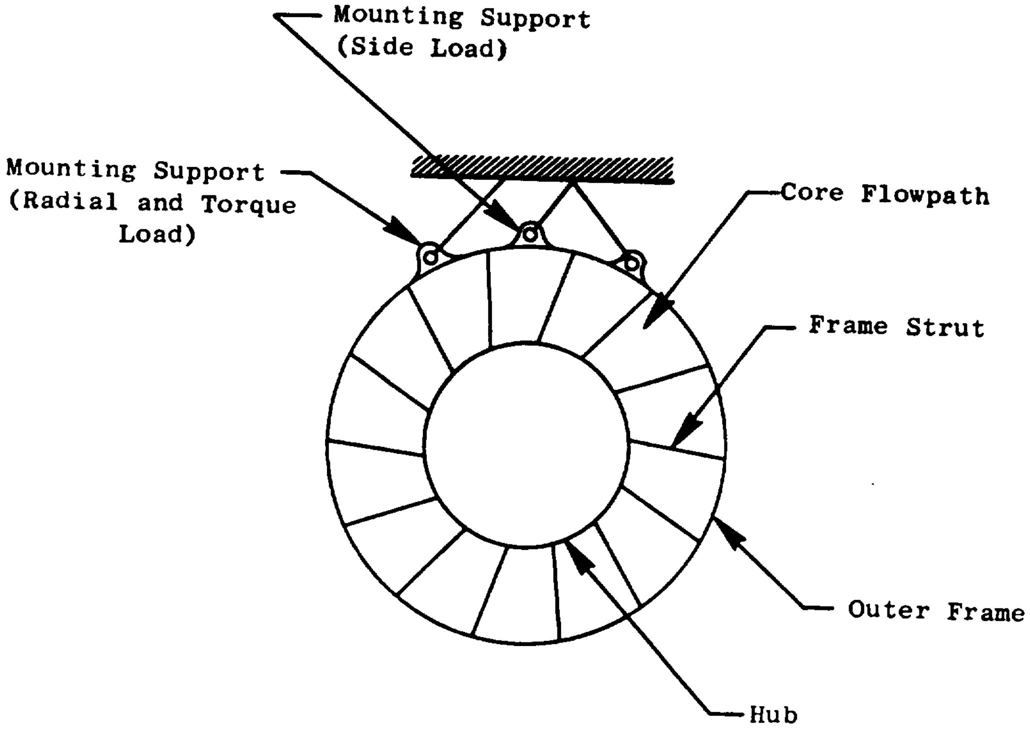
Mounting Support
(Side Load)
Mounting Support
(Radial and Torque
Load)
Core Flowpath
Frame Strut
Outer Frame
Hub

Figure 11-19. Rear Mount System.

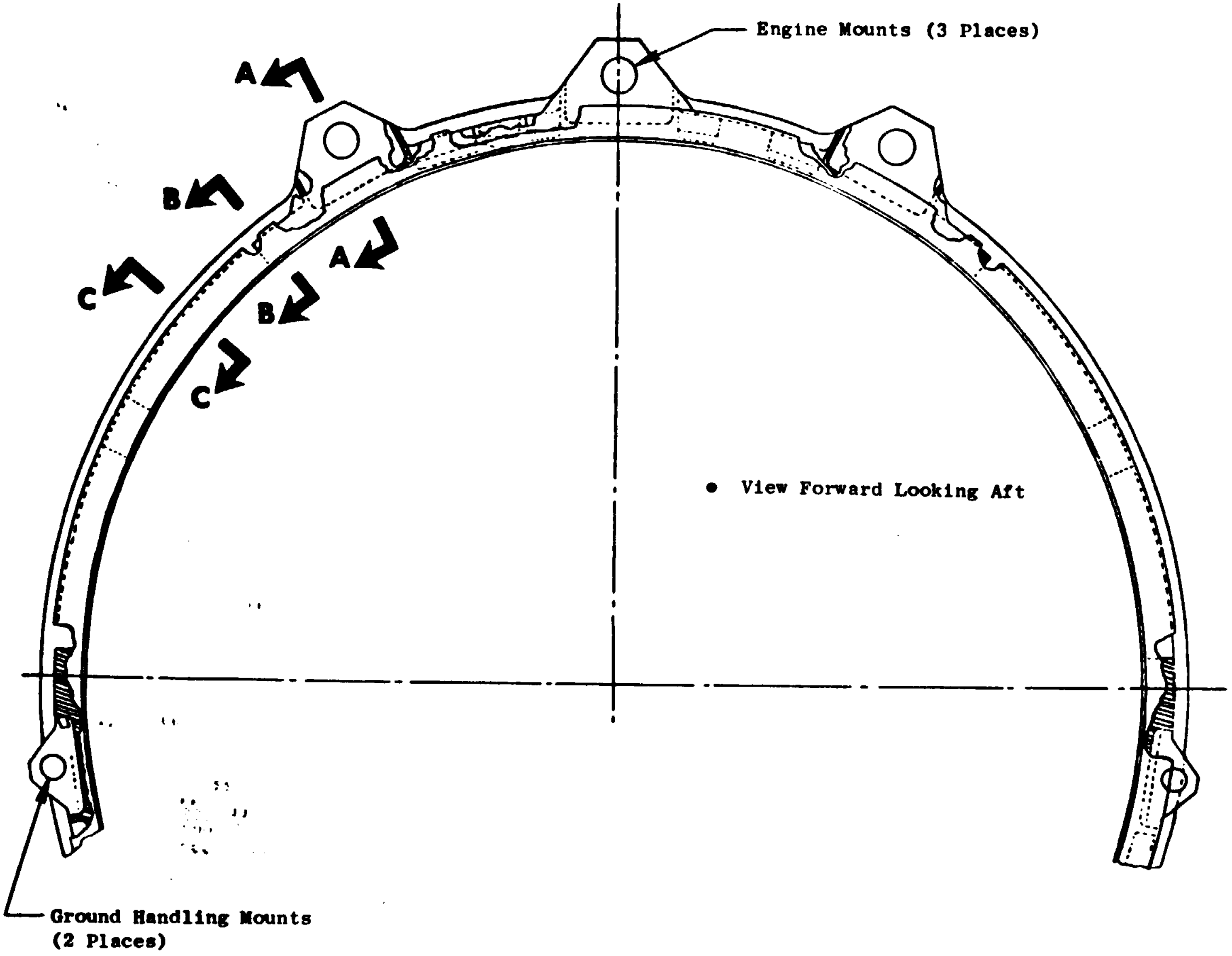
Engine Mounts (3 Places)
A
A
B
B
C
C
• View Forward Looking Aft
Ground Handling Mounts
(2 Places)

Figure 11-20. Outer Ring Support.

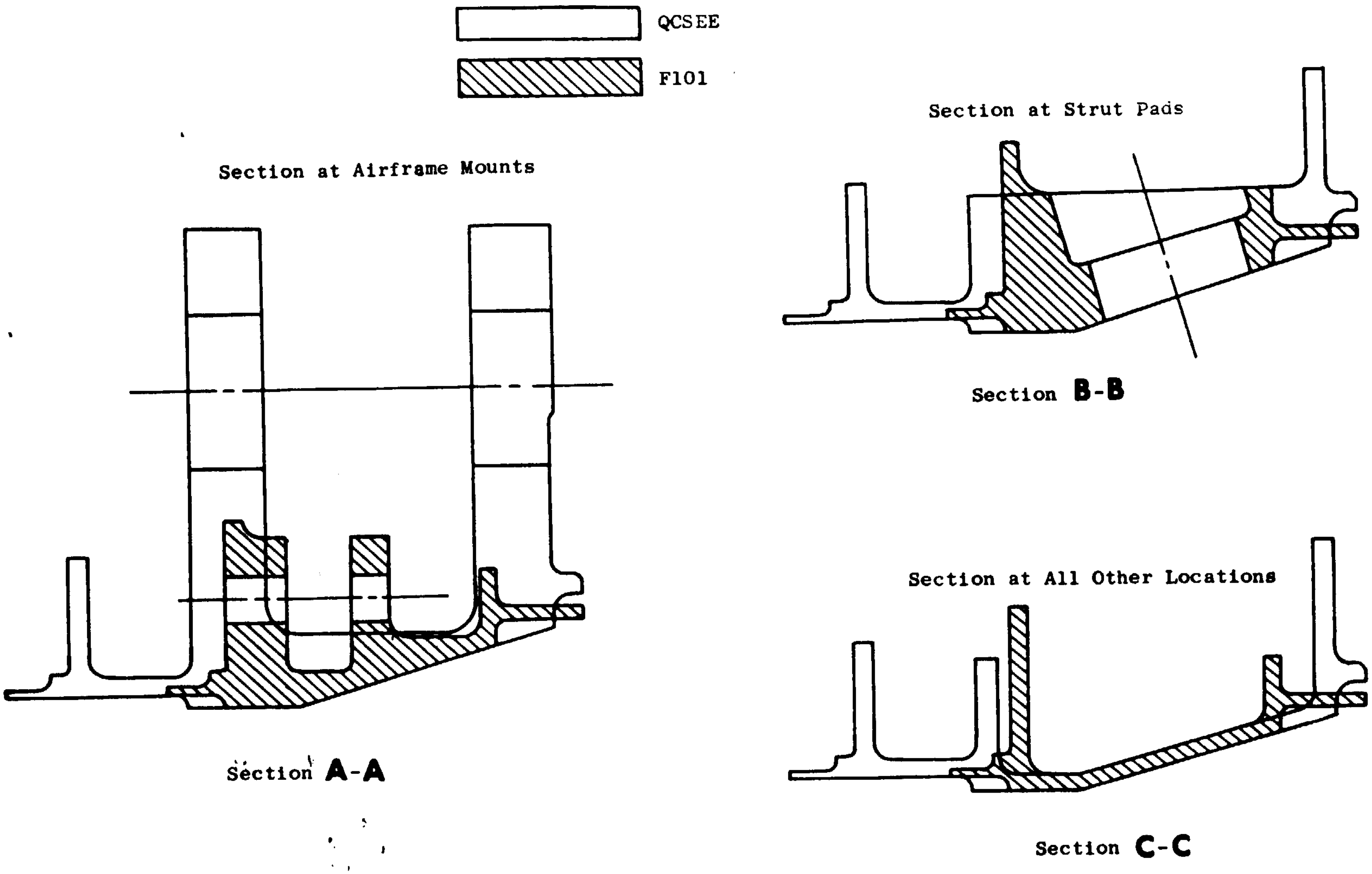
QCSEE
F101
Section at Airframe Mounts
Section A-A
Section at Strut Pads
Section B-B
Section at All Other Locations
Section C-C

Figure 11-21. QCSEE and F101 Mounting System.

In order to axially straighten the exhaust gas, greater turning must be provided through the 14 vane/struts. These vane/struts are assemblies consisting of a central structural section with leading and trailing edge fairings having the cross section shown in Figure 11-22. The fairings are nonload-carrying members with the leading edge fairing sawcut at intervals to relieve thermal stress. The leading edge fairings are modified to accept the higher turbine exit swirl in the UTW engine.

Bearing loads are transferred through the central structural portion of the struts. The inner ends of the struts are bolted to the hub through foot pad extensions. The outer ends are assembled to the outer ring through uniball connections designed to carry loads (but not moments) into the frame.

The rear fairings act as vane trailing edges and are attached to the central strut section by slip joints, providing for thermal expansion. The outer ends of the rear fairings are riveted to the casing and the inner ends are supported by pin joints.

As shown in Figure 11-17, a cast hub forms the inner structural member of the frame. It is composed of forward and aft flanges connected by a shear cylinder. Additional stability is provided by 14 gussets connected to the forward and aft flanges. Mounted off of the forward flange are the forward liner support stability and inner turbine seals, while the aft flange supports the bearing and sump housing and the nozzle centerbody.

Inner and outer flowpath liners are contoured to provide a smooth aerodynamic passage from the turbine to the exhaust nozzle and centerbody. In addition, the liners protect the hub from contact with the hot gas, allowing improved thermal matching with the outer structure.

The inner liner is formed in segments between struts. The liner is supported along its axial length at three axial stations as shown in Figure 11-17. The outer liner is segmented between struts also, but forms a separate continuous part behind the struts. The outer liner is supported from the outer casing and outer ring flowpath support. The liners are fabricated from Hastelloy-X material.

The space between the flowpath liners and structural struts is purged by turbine rotor cooling air. To minimize losses from purge air reentering the gas stream, a fish-mouth seal is brazed to the strut along the inner flowpath as shown in Figure 11-23. The purge air reenters the gas stream aft of the strut extension.

11.5.4 Design Analysis

An analytical model representing the turbine frame system was developed. The GE computer program "MASS" was used to determine loads, stresses, and deflections. The model consisted of plates in the form of rectangles and squares. These geometric sections were joined to form the cylindrical and conical surfaces of revolution. The struts were modeled as beams with variations of section properties along their length. The outer mount ring was

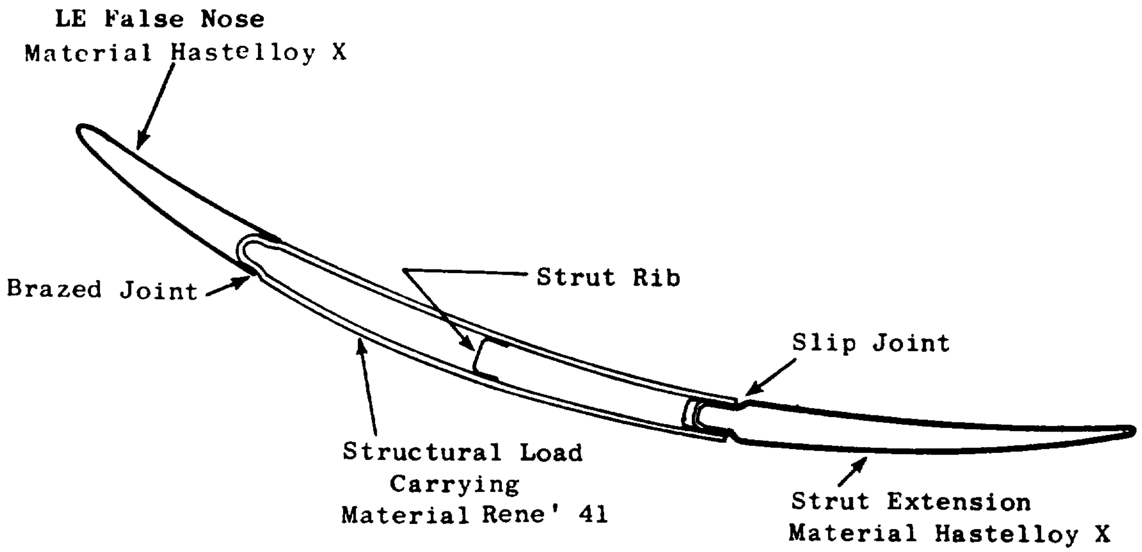
LE False Nose
Material Hastelloy X
Brazed Joint
Strut Rib
Slip Joint
Structural Load Carrying Material Rene' 41
Strut Extension Material Hastelloy X

Figure 11-22. Turbine Frame Strut, Cross Section.

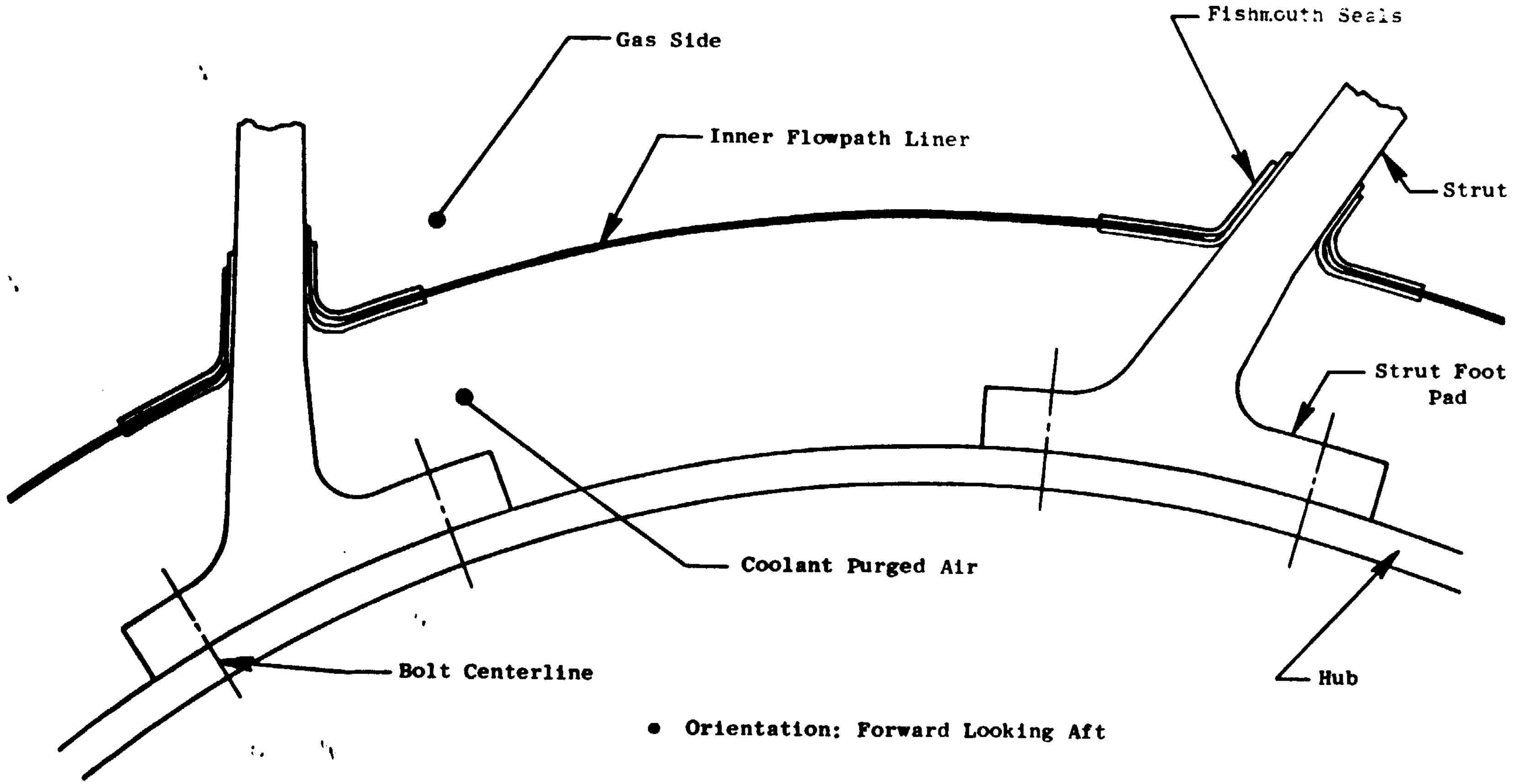
Gas Side
Inner Flowpath Liner
Fishmouth Seals
Strut
Strut Foot Pad
Coolant Purged Air
Bolt Centerline
Hub

• Orientation: Forward Looking Aft

Figure 11-23. Turbine Frame Strut Fishmouth Seal, Forward Looking Aft.

modeled as curved beams. Variation of physical properties along the circumference was included in the analysis.

The forward and aft hub flanges were modeled as curved beams and connected to the shear cylinder which is modeled as curved plates. The axial gussets in the hub were connected to the hub flanges and to the shear cylinder plates. The outer strut ends were connected to the outer ring mount using a boundary condition that allows rotation with no moment transfer to the mount. The three locations at the outer mount system connect to ground through uniballs.

Results of the analysis were as follows:

Steady-State Plus 10 g Landing at Temperature

Loading and stresses are shown in Figure 11-24. Table 11-IV summarizes the maximum effective stresses for the various components. All parts meet the design criteria under this loading condition.

Strut Buckling

This condition was based on establishing the transient time under which the maximum strut combined stress due to compression and bending would occur. This was based on a 50-second excursion from start to maximum sea level thrust based on the temperature shown in Figure 11-25. The strut weld joint was found to be the most critical element, as defined in Figure 11-26. Interaction between the strut longitudinal compression and bending determined the effective buckling stress. The allowable stress in compression and bending established the margin of safety of 1.56.

Transient plus 1 g Load

Using the 50-second transient condition, the effective stresses and loads are presented in Figure 11-27. Table 11-V summarizes the maximum effective stresses for the components, together with the resulting margins of safety. Maximum steady state plus 4 g vibratory are the combined loads existing under normal operating conditions. The Campbell diagrams shown in Figures 11-28 and 11-29 reflect these combined loads for the hub and struts. Maximum combined loads under temperature for the struts were found to be at the inner strut weld line. Stress concentration factors (K_T) have been applied to the vibratory stress.

Pin Reaction and Link Attachment

Inco 718 mounting pins, 2.22 cm (7/8 in.) in diameter, have been selected for the UTW rear mount. Pin load reactions for the blade-out condition are shown in Table 11-VI. Table 11-VII reflects the pin mount loads due to maneuvers. The frame loads shown in Table 11-VIII reflect the UTW unit loadings. As can be seen from the tables, the pin diameter was controlled by the blade-out condition.

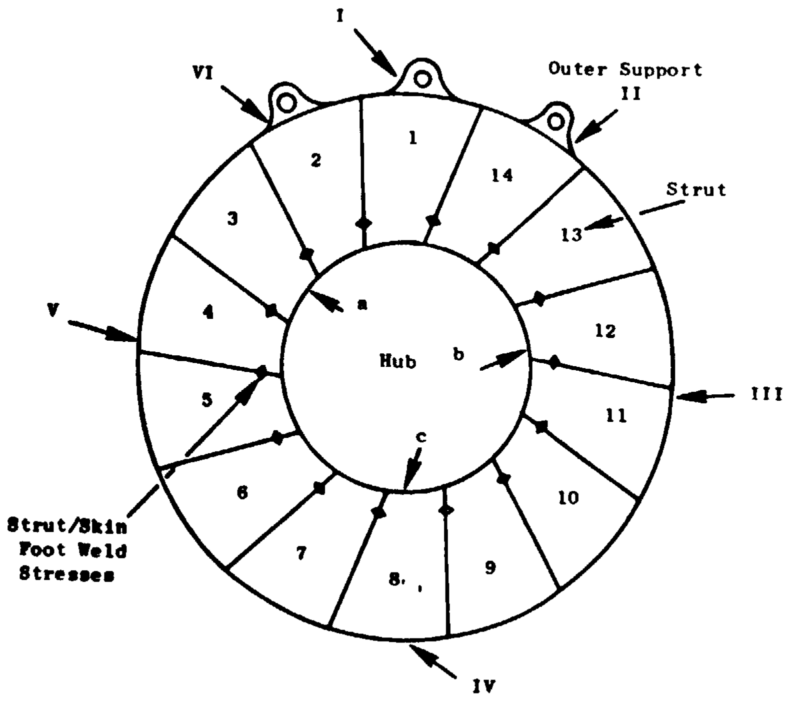
I
VI
Outer Support
II
Strut
1
2
3
4
5
6
7
8
9
10
11
12
13
14
Hub
a
b
c
V
III
IV
Strut/Skin
Foot Weld
Stresses

Note: Frame Orientation is Forward Looking Aft

Note. Max. Hub Moment/Stresses Occur at the Aft Hub Flange for this Condition.

Strut	Loads		Stresses	
	N	lb	kn/cm^2	ksi
1	17100	3845	13.6	19.7
2	18200	4098	4.4	6.4
3	20600	4636	6.2	8.9
4	1170	263	13.1	19.0
5	3380	762	14.2	20.6
6	4640	1044	13.1	18.9
7	5850	1318	11.1	16.1
8	6640	1492	12.9	18.7
9	6600	1484	11.2	16.2
10	6350	1437	15.4	22.3
11	3560	800	6.1	8.8
12	2940	660	16.0	23.2
13	-1510	-339	22.6	32.8
14	18500	4158	15.8	22.8
Outer Support				
I	14000	1239	15.5	22.4
II	75300	6659	49.4	71.5
III	-	-	4.3	6.2
IV	4950	437	10.0	14.5
V	-	-	8.0	11.6
VI	71900	6352	46.7	67.8
Hub	Moment			
	kNm	lb in.		
a	3.27	2893	18.0	26.0
b	3.22	2848	18.0	26.0
c	1.02	901	6.7	9.7

Figure 11-24. Turbine Frame Stresses and Loads - Max. Sea Level Steady State plus 10 G Landing.

Table 11-IV. Turbine Frame Maneuver Stresses, Maximum Steady-State Plus 10 G Down Loading.

Item	Material	Eff. Stress/ys† $kN/cm^2/kN/cm^2$ (ksi/ksi)	Ult. Eff. Stress/ Ult. Stress‡ $kN/cm^2/kN/cm^2$ (ksi/ksi)	**MS†** 0.2% ys	**MS‡** Ult.
Hub	**Cast IN 718**	17.9/53 (26/77)	24.1/66.2 (35/96)	1.96	1.74
Outer Support	**Forge IN 718**	49.3/81.4 (71.5/118)	89.5/124.1 (130/180)	0.65	0.38
Strut Foot/ Skin Weld	**Cast René 41**	22.6/58.5 (32.8/85)	31.3/63.5 (45.2/92)	1.35	1.03

† 0.2% yield strength at temperature

‡ ● Ultimate stress is (1.5 X mech.) + thermal
● Ultimate strength at temperature

$$MS = \frac{\sigma_{all}}{\sigma_{eff}} - 1$$

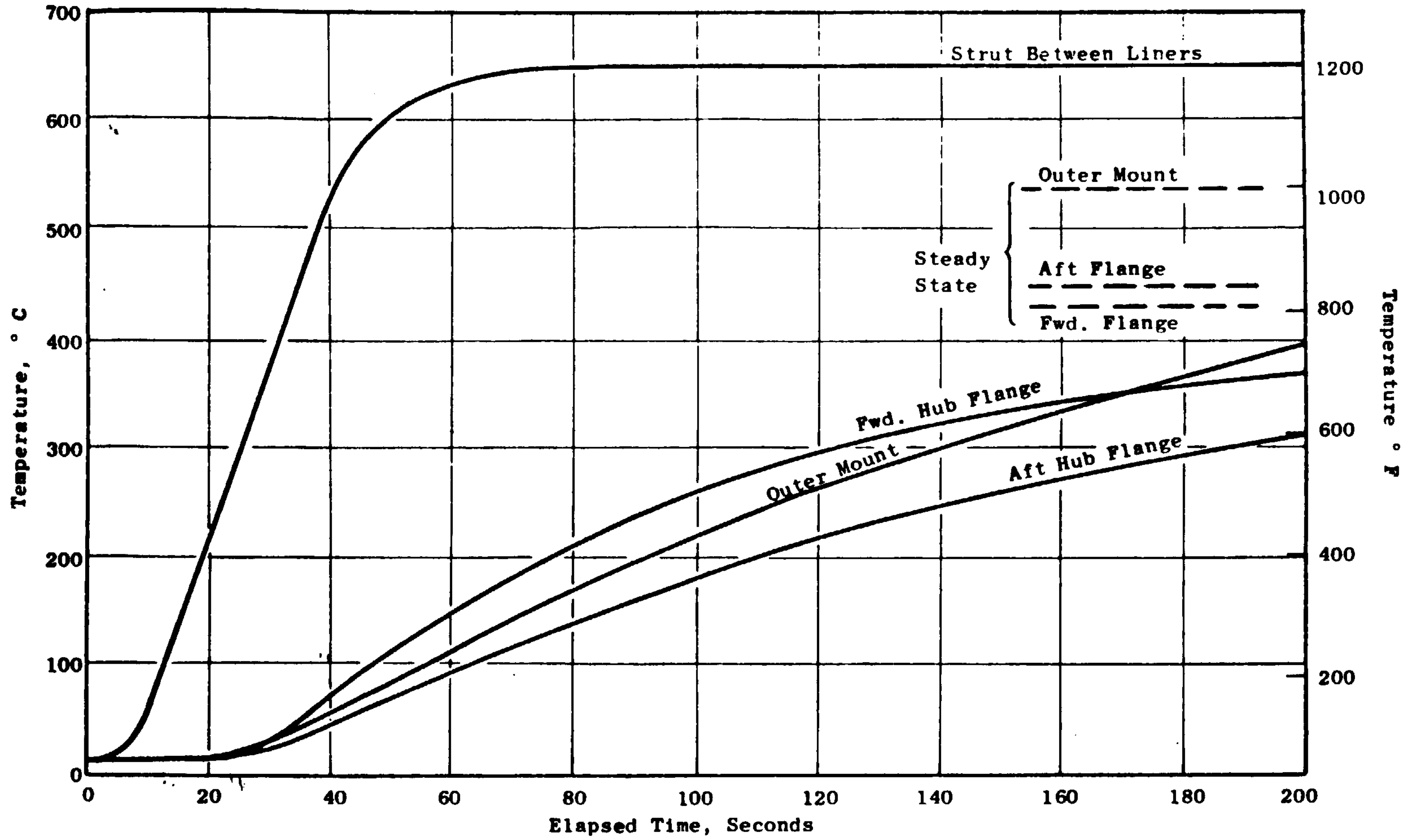

Figure 11-25. Turbine Frame Transient Average Temperatures for Start to Maximum Sea Level.

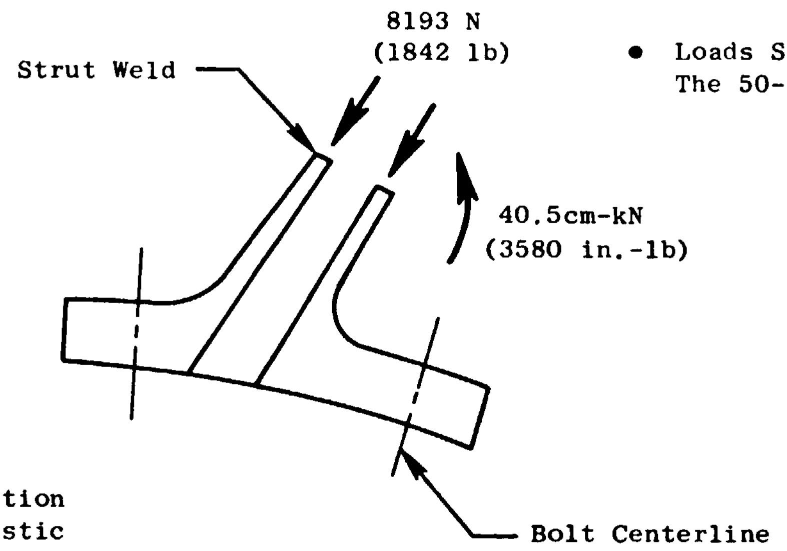
Strut Weld
8193 N
(1842 lb)
40.5cm-kN
(3580 in.-lb)
Bolt Centerline

- Loads Shown Are At The 50-Second Transient Condition

$$\frac{L_{eff}}{L_{act}} \approx 1.20$$

Assume Elliptical Section Analysis Indicate Elastic Buckling Due To Compression

Compression and Bending Interaction

$$R_c + R_b \leqq 1$$

$$R_c + R_b = 0.391$$

$$MS = \frac{1}{R_c + R_b} - 1 = 1.56$$

Buckling Meets Criteria of ≧ 0.5

Where $R_c = \frac{\sigma_{comp}}{\sigma_{all}}$

$$R_b = \frac{\sigma_{bend}}{\sigma_{all}}$$

Figure 11-26. Turbine Frame Strut Buckling.

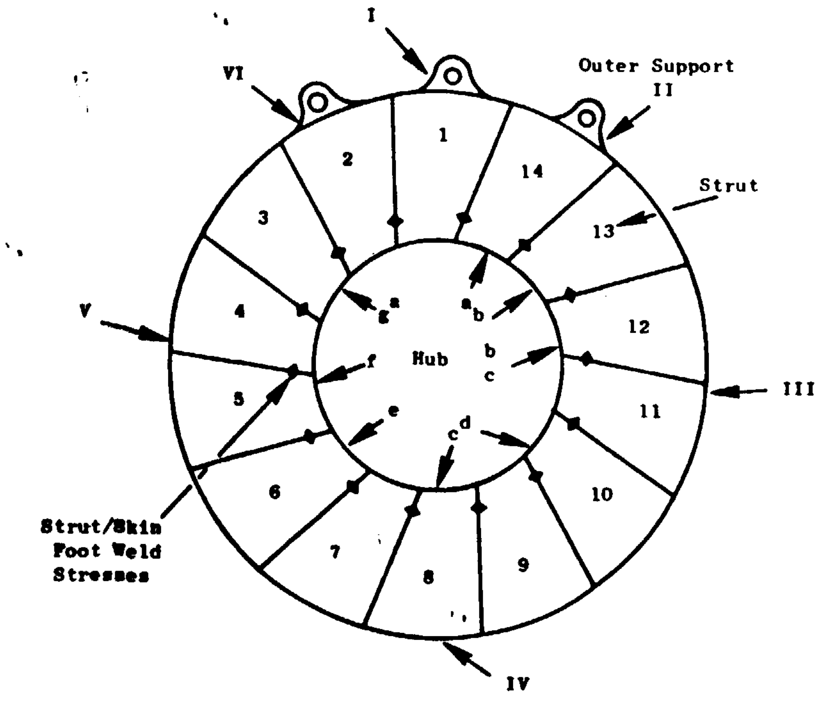
I
VI
Outer Support
II
Strut
V
III
IV
Strut/Skin
Foot Weld
Stresses
Hub
1
2
3
4
5
6
7
8
9
10
11
12
13
14
a
b
c
d
e
f
g

Note: Frame Orientation is Forward Looking Aft

* Max. Hub Moment/Stresses Occur at the Forward Flange for this Condition

Strut	Loads		Stresses	
	N	lb	kN/cm^2	ksi
1	-6085	-1368	30.2	43.7
2	-6032	-1356	29.7	44.0
3	-5764	-1296	30.7	44.5
4	-7460	-1677	31.1	45.0
5	-7264	-1633	30.9	44.7
6	-7028	-1580	30.8	44.6
7	-6912	-1554	30.8	44.6
8	-6872	-1545	30.8	44.6
9	-6899	-1551	30.9	44.7
10	-7273	-1635	30.9	44.7
11	-6828	-1535	30.7	44.5
12	-8193	-1842	31.2	45.1
13	-7513	-1689	30.2	43.7
14	-6041	-1358	30.1	43.6
Outer Support				
I	18553	4171	5.9	8.60
II	19359	4352	5.1	7.33
III	18290	4112	8.1	11.70
IV	17246	3877	6.2	9.03
V	17388	3909	6.3	9.12
	Moment			
Hub	kNm	lb in.		
a	5.62	4974	17.8	25.7
b	5.70	5042	18.3	26.6
c	5.97	5282	19.1	27.7
d	5.70	5043	18.5	26.8
e	5.81	5139	18.6	26.9
f	5.92	5239	18.6	26.9
g	5.75	5090	17.8	25.7

Figure 11-27. Turbine Frame Stresses and Loads - 50 Second Transient plus 1 G Load.

Table 11-V. Turbine Frame Stresses Thermal Loading and 1 G Engine Loading, Start to Maximum Sideline Thrust.

Component	Material	Temp, ° C (° F)	Stress/LCF Strength (1000 Cycles) kN/cm^2/kN/cm^2 (ksi/ksi)	K_t	% LCF Used at Transient Stress	Effective Stress, kN/cm^2 (ksi)	Buckling (Comb. Bend Plus Comp. Ratios)
Hub	**IN 718 Cast**	116 (240)	14.8/87.6 (21.4/127)	1.6	< 1	18.5 (26.9)	---
Outer Support	**IN 718 Forge**	88 (190)	5.4/151.7 (7.9/220)	1.35	< 1	8.1 (11.7)	---
Strut Skin	**René 41 Sheet**	621 (1150)	20.2/84.1 (29.3/122)	1	< 1	40.6 (58.6)	---
Strut Skin/ Foot Weld	**René 41 Cast**	316 (600)	34.7/51.7 (50/75)	2.2	10.5	30.7 (45.1)	0.391†
Strut Foot	**René 41 Cast**	288 (550)	28.7/51.7 (37.3/75)	1.6	2.2	32.2 (46.7)	---

† The margin of safety for strut buckling is $\frac{1}{.391} - 1 = 1.56$

$$\sigma_{LCF} = \frac{\sigma_{eff} \times K_t}{2}$$

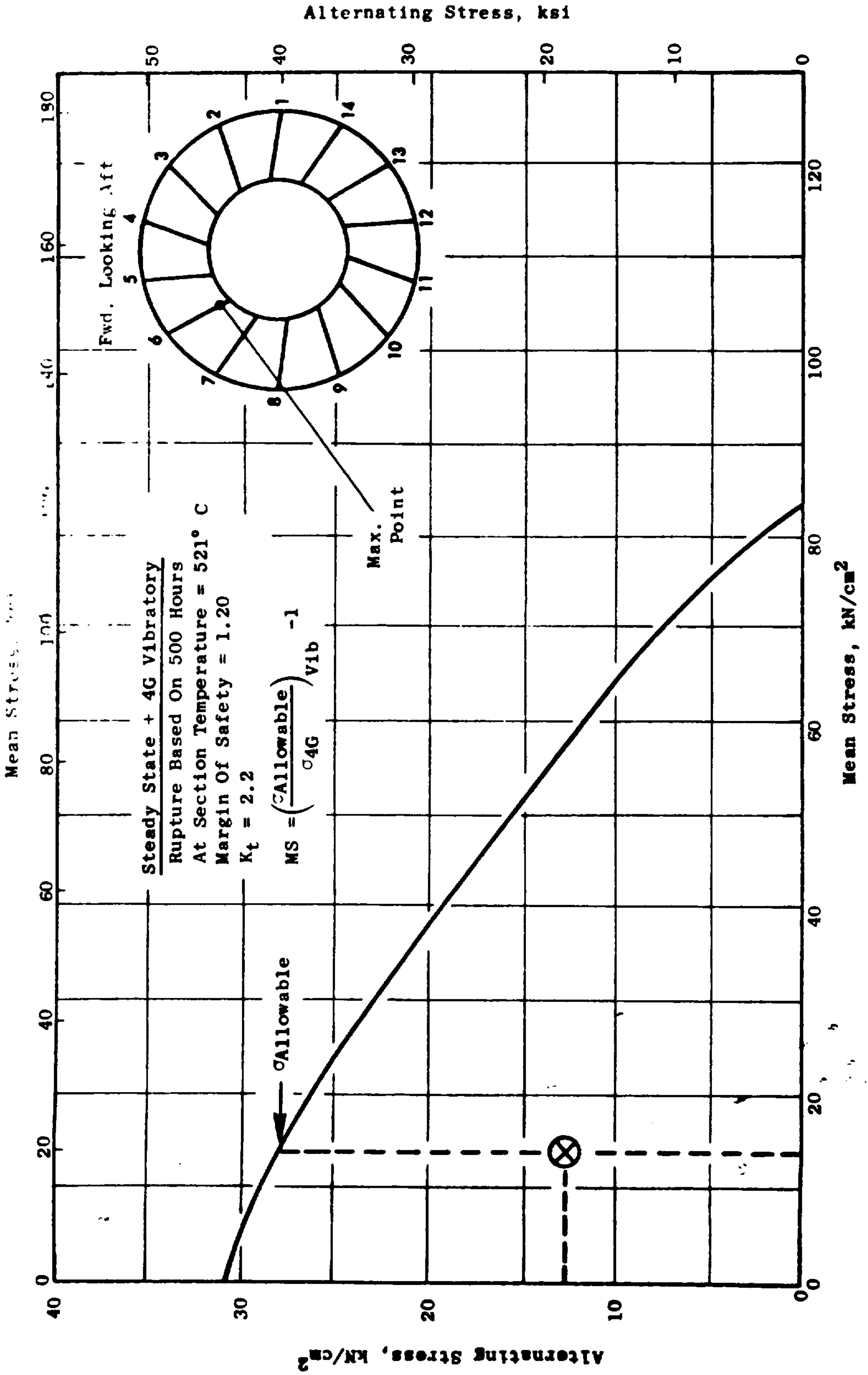

Figure 11-28. Frame Stress Range Diagram - Foot/Skin Weld Line.

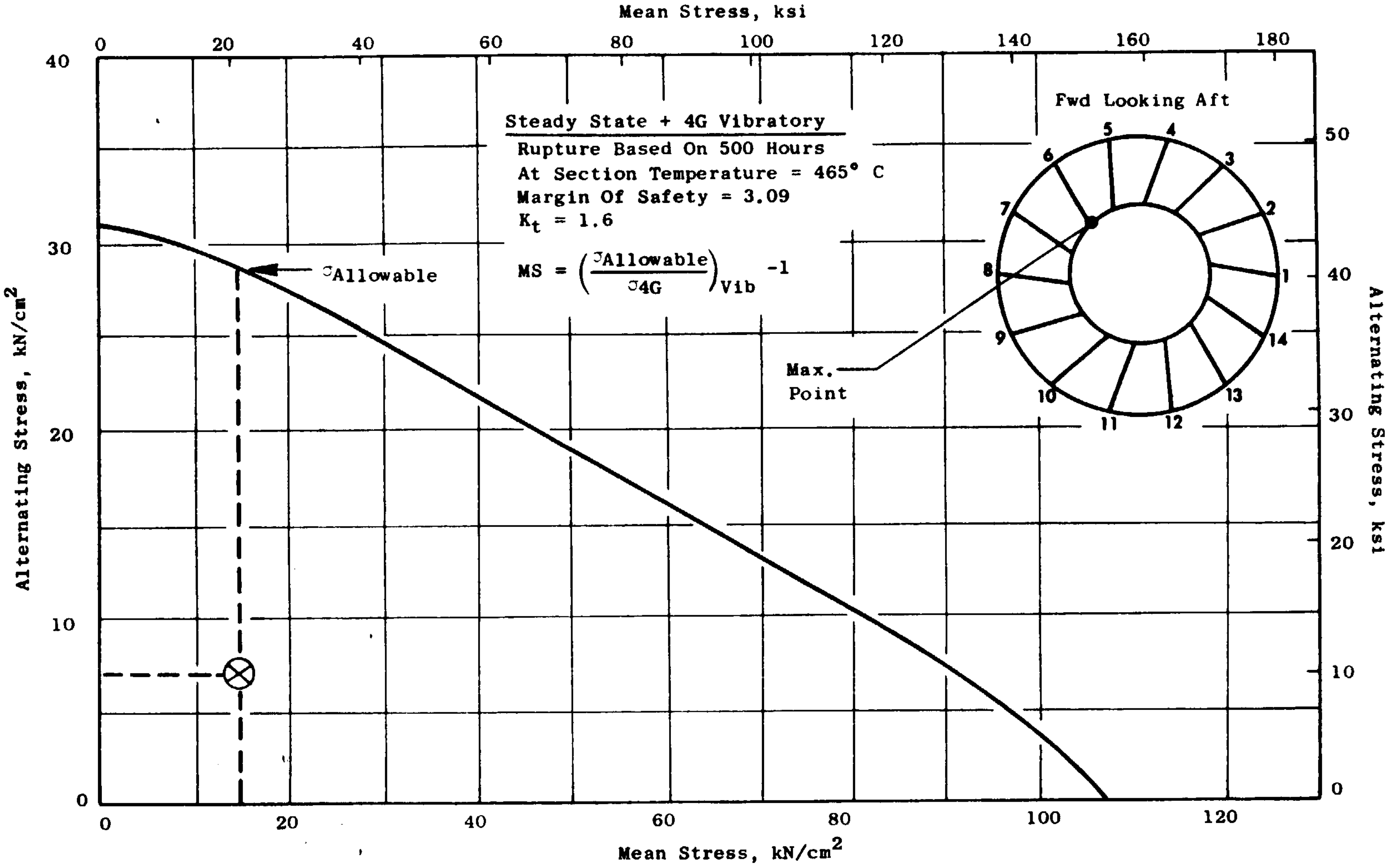

Figure 11-29. Frame Stress Range Diagram - Hub.

Table 11-VI. Turbine Frame Mount Reactions, 2.22 cm (7/8 in.) Pin Mount, 2-1/2 Blades Out.

	Load		Effective Stress		
	N	lb	kN/cm^2	ksi	MS
R_R	124,811	28,060	27.9	40.4	2.84
R_L	124,811	28,060	27.9	40.4	2.84
R_S	152,624	34,313	34.1	49.4	2.14

$$MS = \frac{\sigma_{ult}}{\sigma_{eff}} - 1$$

σ_{ult} = Ultimate strength of Incro 718 bar at 700° K (800° F)

σ_{eff} = Effective stress of 2.22 cm (7/8 in.) pin under double shear

Table 11-VII. Engine Mount Reaction Load Due to Maneuver, 2.22 cm (7/8 in.) Pin Mount.

Maneuver Condition (All Conditions Include 77,397 N, 17400 lb Thrust)	R_L, N (lb)	R_R, N (lb)	R_S, N (lb)
10 G Down, 2 G Side	44,627 (10,033)	55,996 (12,589	62,593 (14,072)
10 G Down, 1.5 G Side, 2 G Fwd	22,876 (5,143)	52,593 (11,824)	46,949 (10,555)
6 G Down, 4 G Side, 2 G Fwd	120,252 (27,035)	81,003 (18,211)	125,203 (28,148)
6 G Down, 4 G Side, 3 G Aft	132,395 (29,765)	68,860 (15,481)	125,203 (28,148)
4 G Side, 4 G Fwd	134,740 (30,292)	66,511 (14,953)	125,203 (28,148)
4 G Side, 3 G Aft	155,740 (34,114)	49,511 (11,131)	125,203 (28,148)

UTW Engine Weight Used in 2070 kg (4,549 lb)

Table 11-VIII. Engine Mount Reaction Loads for 2.22 cm (7/8 in.) Pin.

Manuever	UTW		
	R_L, N (lb)	R_R, N (lb)	S, N (lb)
1 G Down	3225 + (725)	3225 + (725)	--- ---
1 G Side	33787 ± (7596)	16520 ± (3714)	31301 ± (7037)
1 G Aft	2429 + (546)	2433 - (547)	--- ---
1 P Accel	111 ± (25)	107 ± (24)	--- ---
1 P Vel	8509 ∓ (1913)	3981 ± (895)	22640 ± (5090)
1 Y Accel	98 ± (22)	40 ± (9)	254 ± (57)
1 Y Vel	9763 ∓ (2195)	9759 ∓ (2194)	--- ---
1 Thrust (Aft)	9292 + (2089)	9287 + (2088)	---
UTW Engine Weight - 12,063 kg, (4,549 lb)			

Pin Reaction Mounting Lug Design

The mount lug design is based on withstanding the maximum load due to 2-1/2 blade-out and maintaining engine support. Maximum stress levels occur due to tension across the net section. Under this condition the design strength far exceeds the limit imposed by the land. Figure 11-30 shows the blade-out lug stresses.

Blade-Out Load

The turbine frame is designed to withstand the 2-1/2 UTW fan airfoils-out condition, and to maintain engine support. The frame loads under this condition are shown in Figure 11-31. The stresses under a 2-1/2 airfoil-out condition are shown in Figure 11-32. A comparison of the resulting stresses with the ultimate stress levels presented in Table 11-IV indicates that for the 2-1/2 airfoil-out condition the calculated stresses are less than the ultimate. Therefore, based on these analytical results, the frame will meet the established requirements.

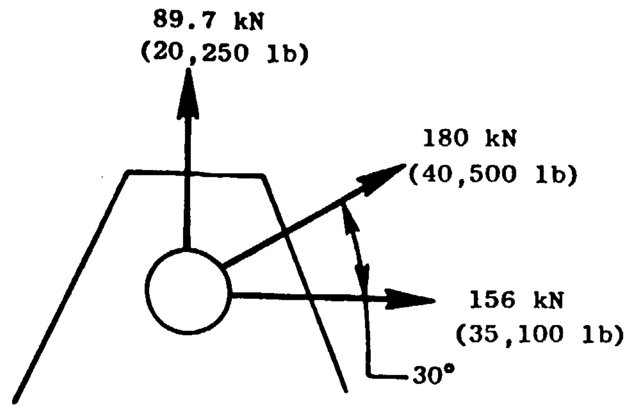
89.7 kN
(20,250 lb)
180 kN
(40,500 lb)
156 kN
(35,100 lb)
30°

Detail **A-A**

- **Design Includes Addition of 15% for Fitting Factor**
- **Shear Tearout Greater than Tension Across Net Section**
- **MS** $= \dfrac{1}{\left(R_a^{1.6} + R_{tr}^{1.6}\right)^{0.625}} - 1$

where: $R_a = \dfrac{P_{\text{Axial Applied}}}{P_{\text{Ult at Temp.}}}$

$R_{tr} = \dfrac{P_{\text{Traverse}}}{P_{\text{Ult at Temp.}}}$

MS = 2.39

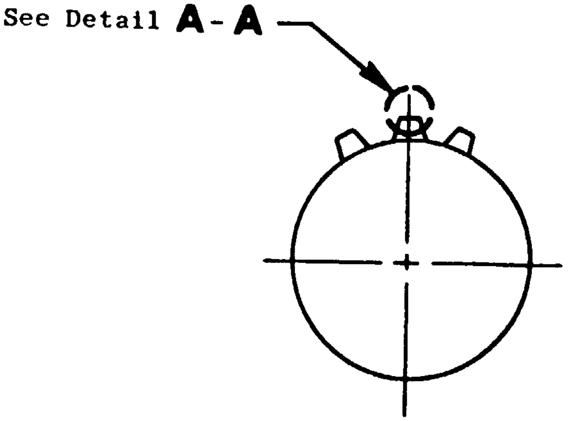
See Detail A - A

UTW 2-1/2 Airfoil Out Load Controls the Lug Design Conditions

Figure 11-30. Turbine Frame Ring Support Lug Analysis.

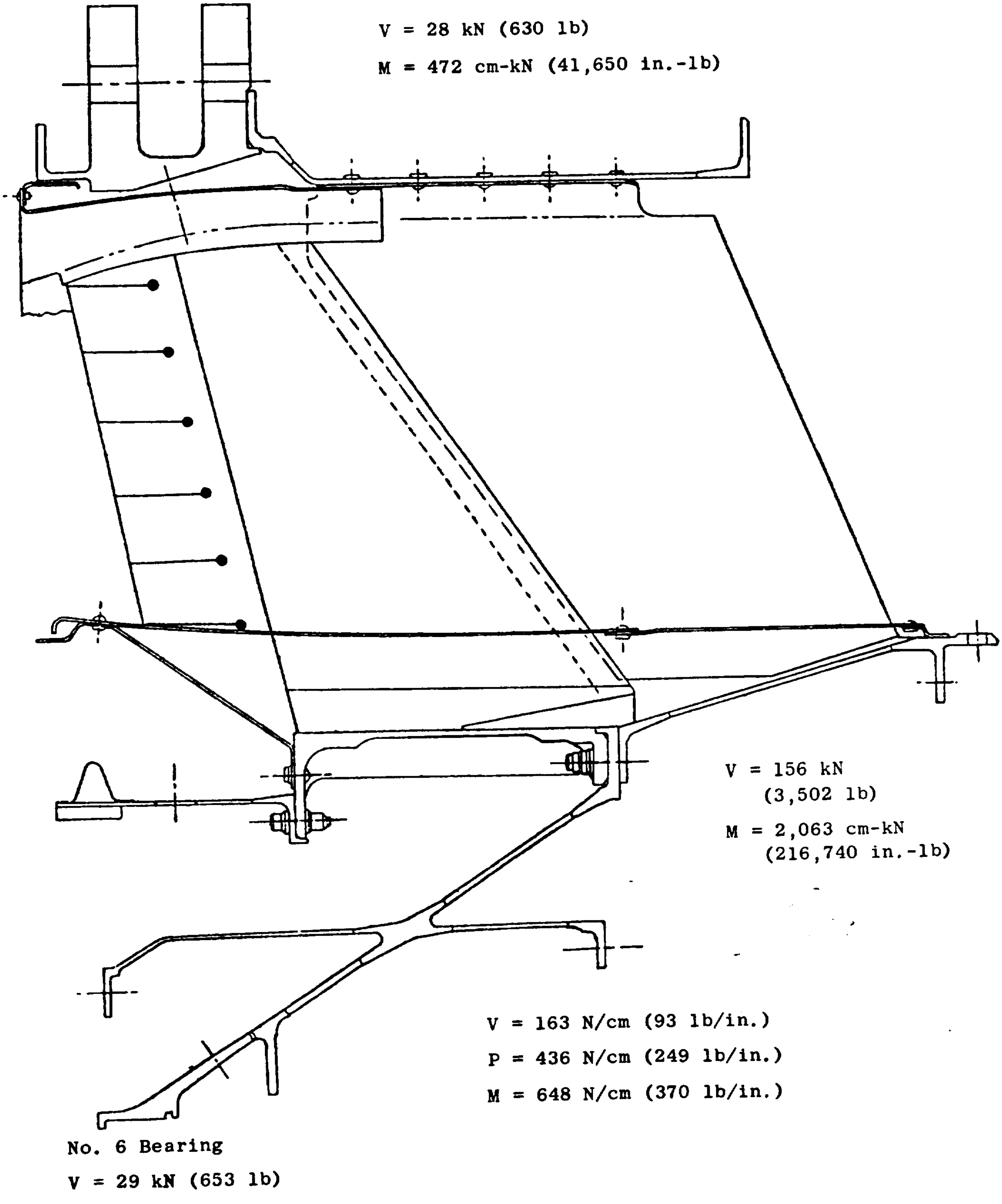
V = 28 kN (630 lb)
M = 472 cm-kN (41,650 in.-lb)
V = 156 kN (3,502 lb)
M = 2,063 cm-kN (216,740 in.-lb)
V = 163 N/cm (93 lb/in.)
P = 436 N/cm (249 lb/in.)
M = 648 N/cm (370 lb/in.)
No. 6 Bearing
V = 29 kN (653 lb)

Figure 11-31. Turbine Frame External Loads for 1 Airfoil Out.

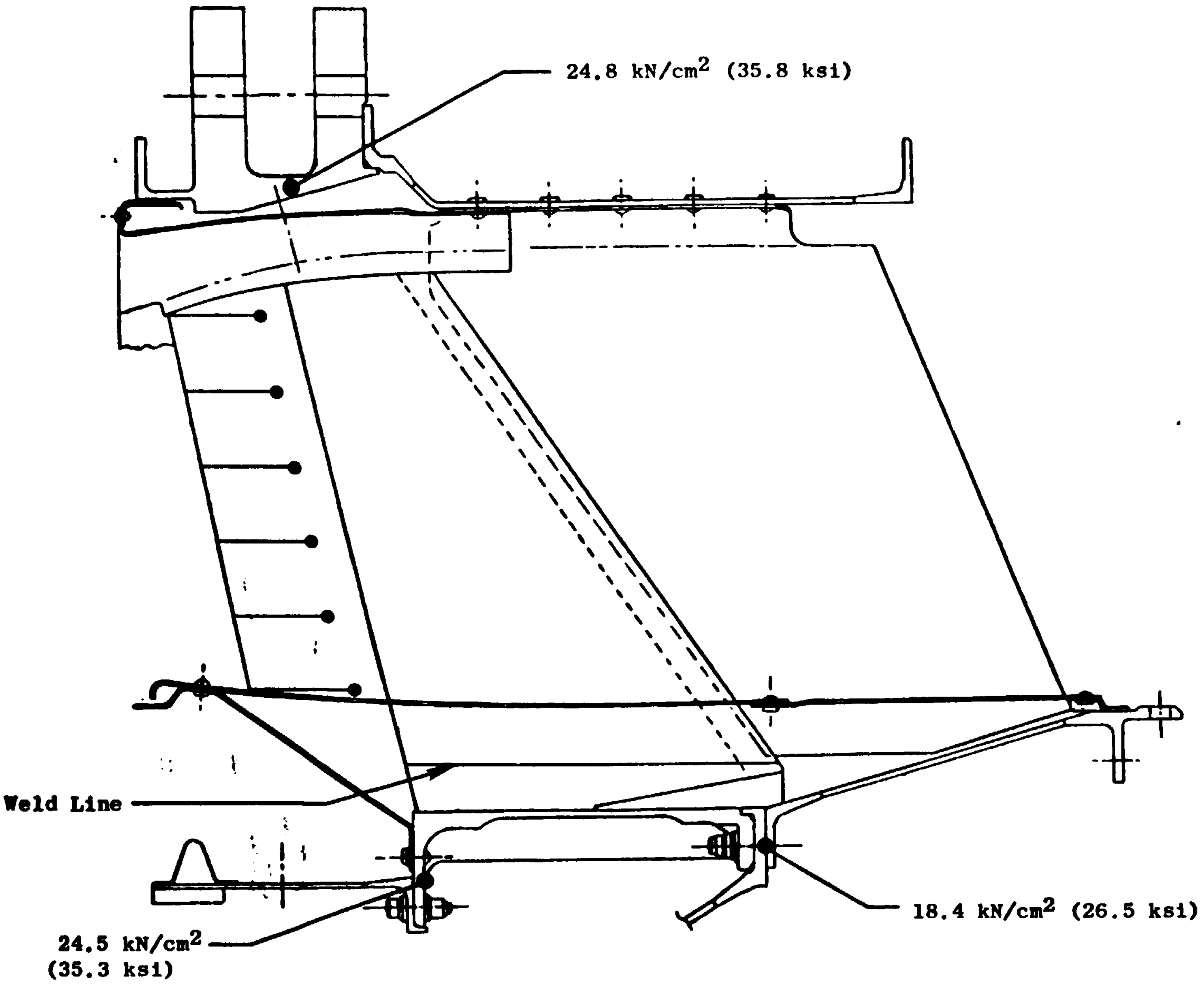
24.8 kN/cm^2 (35.8 ksi)
Weld Line
18.4 kN/cm^2 (26.5 ksi)
24.5 kN/cm^2
(35.3 ksi)

Figure 11-32. QCSEE Turbine Frame (UTW) Stresses Due to 2-1/2 Blade-Out Load.

SECTION 12.0

BEARINGS AND SEALS DESIGN

12.1 SUMMARY

This section summarizes the detail design of the UTW bearings, seals, and accessory drives. The systems described in this section include the sumps, lube oil supply and scavenge, dynamic oil seals, venting and pressurizing systems, pump, oil coolers, filters, deaerators, magnetic chip detectors, static leak check valves, and the lube storage tank. Also included in this discussion is a review of the bearing and accessory lubrication and cooling systems and the rotor thrust balance provisions.

The UTW engine utilizes six main shaft bearings to support the rotating turbomachinery. The short construction of the concentric UTW rotors permits a two-bearing support system for each rotor. The No. 1B and 1R bearings support the fan rotor. The high pressure core rotor is supported by the No. 3 and No. 4 bearings. The No. 2 and No. 5 bearings support the low pressure turbine and power transmission shaft. Both the fan and low pressure turbine shaft are soft coupled to the engine main reduction gear to minimize induced forward sump to provide more precise control of fan and compressor blade clearances.

Application of a main reduction gear between the fan and low pressure turbine requires that the normal axial load "tie" between fan and low pressure turbine components be severed. As a result, the No. 2 thrust bearing must react the full aft load of the turbine without any negating forward thrust from the fan. To reduce the bearing load to an acceptable level, a thrust balance cavity has been added to the rear sump. This cavity uses compressor discharge air to pressurize a balance piston, providing a forward compensating force on the turbine rotor. A high-load-capacity CF6 No. 1 thrust bearing is used in the design to react the fan axial loads.

A top-mounted accessory gearbox is driven from the core by an F101 internal bevel gearset and a long radial drive shaft. An additional F101 internal bevel gearset located in the bottom half of the engine is combined with a short radial shaft and a second bevel gearset located in the core cowl area to drive a vane-type pump that scavenges oil from both the forward and aft sumps. This pump also scavenges the top-mounted accessory gearbox which drains into the forward sump.

The lubrication system is designed on the basis of current dry sump technology utilizing a circulating oil system. Internal engine and gearbox passages are used wherever possible for oil delivery and return. Venting and pressurization functions also make use of internal engine passages when possible. The accessories and tube tank are located in the engine pylon area.

Careful attention has been given to fire-safe design features. Carbon seals are provided for minimal leakage of pressurization air into the sumps. During normal operation these seals also eliminate oil leakage from the sump and thus minimize oil consumption. Oil slingers or windbacks are provided with the objective of preventing coke formation in the moving parts of the seals. Each of the cavities adjacent to the sumps is pressurized with cool air to prevent the inflow of hot gases into the sumps. Adequate oil drains have been provided to remove inadvertent oil leakage and prevent fire damage. There are also no trapped oil pockets within the rotating hardware.

12.2 DESIGN REQUIREMENTS

The UTW engine sump and drive system components are designed to meet the following requirements:

- Design loads for sumps and drives components are derived from the duty cycles defined in Section 2.0. Design life, based on these loads, meets established life requirements.
- Sumps are designed to scavenge at all steady-state attitudes shown in Figure 2.3.
- The design is applicable to future airline use. Where slave hardware is utilized, no compromises have been made that would not permit future adaptability for airline application.
- The system is designed to operate with MIL-L-7808 or MIL-L-23699 oil.
- Gearbox and sumps are vented to areas where temperatures are less than 371° C (700° F).
- The design eliminates any possibility of trapped oil in the rotors.
- Where possible, the experimental engine system has been designed to meet maintainability criteria. Where exceptions occur, due to utilization of existing hardware and components, studies have identified changes ncessary in the flight design to meet maintainability requirements.

12.3 LUBRICATION SYSTEM

The UTW lubrication system contains the following subsystems:

- Oil supply
- Oil scavenge

- Seal pressurization air
- Vent air

A conventional dry sump system similar to that used on other General Electric engines is provided. The lube system schematic is shown in Figures 12.1 and 12.2. The bulk of the system oil supply is retained in the oil tank. Oil is pressure fed to each engine component requiring lubrication and/or cooling, and is removed from the gearbox and rear sump by scavenge pump elements for return to the oil tank.

The entire lubrication system has been designed to ensure that there are no areas where oil can be trapped (i.e., rotors, gearboxes, shafts, etc.) which could be detrimental to the engine. Also, the system has been sized to prevent flooding of sumps and gearboxes during engine shutdowns and to limit excessive lube tank gulping during engine start ups.

12.3.1 Oil Supply System

The oil supply subsystem consists of the oil tank, gearbox-mounted oil supply pump, oil supply filters, static leak check valve, oil supply nozzles, and associated piping.

The basic lube supply system operates in the following manner: MIL-L-23699 oil is supplied by gravity to the inlet of the supply pump at all operating conditions. The oil is then pumped through two parallel-piped, 46-micron oil supply filters to protect the lube nozzles from contaminants. The oil then flows through the static check valve and is distributed to the desired areas in the engine. Presented in Table 12-I are the engine system oil flow requirements.

During engine shutdowns, sump and gearbox flooding are prevented by the static check valve located downstream from the lube supply filters. This valve, along with careful pipe sizing, also prevents lube flooding during engine startups.

To sense oil supply pressure during engine running, a port for a pressure sensor is provided immediately downstream of the static leak check valve. This pressure sensor, along with other pressure readings taken in the sumps and gearbox, provides a ΔP indication across the oil nozzles.

The following special oil supply features have been included in the system design:

- The constant-displacement supply pump has been modified to add a variable bypass orifice to increase engine oil flow.
- Pressure relief bypass valves have been added to the oil supply filter system. These valves open when the pressure across the

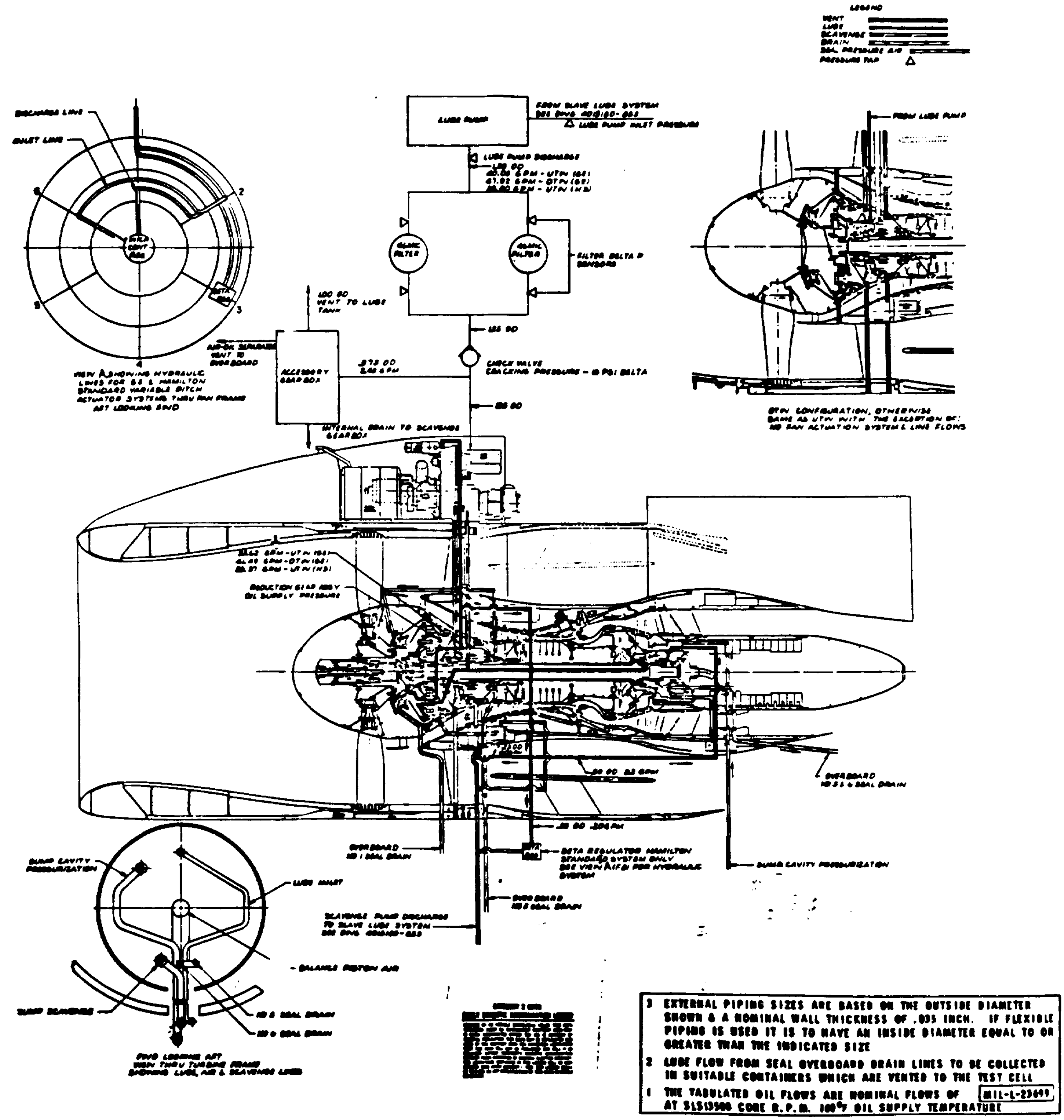
LEGEND
VENT
LUBE
SCAVENGE
DRAIN
SEAL PRESSURE AIR
PRESSURE TAP
LUBE PUMP
FROM SLAVE LUBE SYSTEM
SEE DWG 4013160-833
LUBE PUMP INLET PRESSURE
LUBE PUMP DISCHARGE
.625 OD
40.06 GPM - UTW (GE)
47.92 GPM - OTW (GE)
33.60 GPM - UTW (HS)
MAIN FILTER
MAIN FILTER
FILTER DELTA P SENSORS
.625 OD
CHECK VALVE
CRACKING PRESSURE - 10 PSI DELTA
.625 OD
.500 OD
VENT TO LUBE TANK
AIR-OIL SEPARATOR VENT TO OVERBOARD
ACCESSORY GEAR BOX
.375 OD
2.46 GPM
INTERNAL DRAIN TO SCAVENGE GEARBOX
DISCHARGE LINE
INLET LINE
BETA CONT
BETA REG
1
2
3
4
5
6
VIEW A SHOWING HYDRAULIC LINES FOR GE & HAMILTON STANDARD VARIABLE PITCH ACTUATOR SYSTEMS THRU FAN FRAME AFT LOOKING FWD
FROM LUBE PUMP
OTW CONFIGURATION, OTHERWISE SAME AS UTW WITH THE EXCEPTION OF: NO FAN ACTUATION SYSTEM & LINE FLOWS
REDUCTION GEAR ASSY OIL SUPPLY PRESSURE
.500 OD
.30 OD .32 GPM
OVERBOARD
NO 3 & 4 SEAL DRAIN
.25 OD .20 GPM
OVERBOARD
NO 1 SEAL DRAIN
BETA REGULATOR HAMILTON STANDARD SYSTEM ONLY
SEE VIEW A (FS) FOR HYDRAULIC SYSTEM
SUMP CAVITY PRESSURIZATION
OVERBOARD
NO 2 SEAL DRAIN
SCAVENGE PUMP DISCHARGE TO SLAVE LUBE SYSTEM
SEE DWG 4013160-833
SUMP CAVITY PRESSURIZATION
LUBE INLET
BALANCE PISTON AIR
SUMP SCAVENGE
NO 5 SEAL DRAIN
NO 6 SEAL DRAIN
FWD LOOKING AFT VIEW THRU TURBINE FRAME SHOWING LUBE, AIR & SCAVENGE LINES

3 EXTERNAL PIPING SIZES ARE BASED ON THE OUTSIDE DIAMETER SHOWN & A NOMINAL WALL THICKNESS OF .035 INCH. IF FLEXIBLE PIPING IS USED IT IS TO HAVE AN INSIDE DIAMETER EQUAL TO OR GREATER THAN THE INDICATED SIZE

2 LUBE FLOW FROM SEAL OVERBOARD DRAIN LINES TO BE COLLECTED IN SUITABLE CONTAINERS WHICH ARE VENTED TO THE TEST CELL

1 THE TABULATED OIL FLOWS ARE NOMINAL FLOWS OF MIL-L-23699 AT SLS13500 CORE R.P.M. 100°F OIL SUPPLY TEMPERATURE

Figure 12-1. Engine Lube System Schematic.

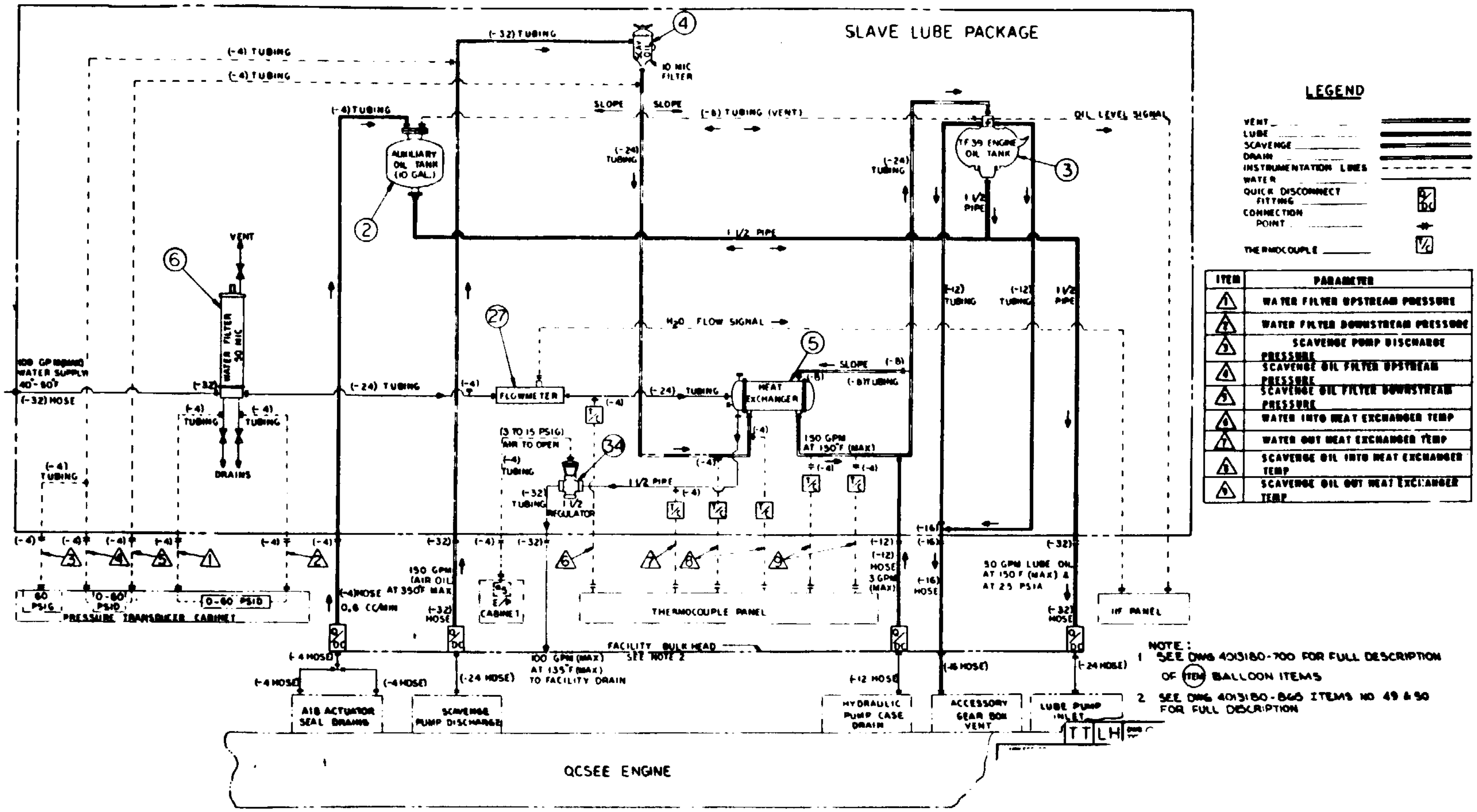
SLAVE LUBE PACKAGE
LEGEND
VENT
LUBE
SCAVENGE
DRAIN
INSTRUMENTATION LINES
WATER
QUICK DISCONNECT FITTING
CONNECTION POINT
THERMOCOUPLE
ITEM
PARAMETER
1 WATER FILTER UPSTREAM PRESSURE
2 WATER FILTER DOWNSTREAM PRESSURE
3 SCAVENGE PUMP DISCHARGE PRESSURE
4 SCAVENGE OIL FILTER UPSTREAM PRESSURE
5 SCAVENGE OIL FILTER DOWNSTREAM PRESSURE
6 WATER INTO HEAT EXCHANGER TEMP
7 WATER OUT HEAT EXCHANGER TEMP
8 SCAVENGE OIL INTO HEAT EXCHANGER TEMP
9 SCAVENGE OIL OUT HEAT EXCHANGER TEMP
(-32) TUBING
10 MIC FILTER
(-4) TUBING
(-4) TUBING
(-4) TUBING
SLOPE
SLOPE
(-8) TUBING (VENT)
OIL LEVEL SIGNAL
AUXILIARY OIL TANK (10 GAL)
(-24) TUBING
(-24) TUBING
TF 39 ENGINE OIL TANK
1 1/2 PIPE
1 1/2 PIPE
VENT
WATER FILTER 30 MIC
DRAINS
100 GPM WATER SUPPLY 40°-60°F
(-32) HOSE
(-32)
(-4) TUBING
(-4) TUBING
(-24) TUBING
(-4)
FLOWMETER
H2O FLOW SIGNAL
(-24) TUBING
HEAT EXCHANGER
SLOPE
(-8)
(-8) TUBING
150 GPM AT 150°F (MAX)
(3 TO 15 PSIG) AIR TO OPEN
(-4) TUBING
(-32) TUBING
1 1/2 REGULATOR
1 1/2 PIPE
(-4)
(-12) TUBING
(-12) TUBING
1 1/2 PIPE
(-4) TUBING
60 PSIG
0-60 PSID
0-60 PSID
PRESSURE TRANSDUCER CABINET
(-4) HOSE 0.8 CC/MIN
150 GPM (AIR OIL) AT 350°F MAX
(-32) HOSE
E/P CABINET
THERMOCOUPLE PANEL
(-12) HOSE 3 GPM (MAX)
(-16) HOSE
50 GPM LUBE OIL AT 150°F (MAX) & AT 25 PSIA
(-32) HOSE
IF PANEL
FACILITY BULK HEAD SEE NOTE 2
100 GPM (MAX) AT 135°F (MAX) TO FACILITY DRAIN
(-4 HOSE)
(-24 HOSE)
(-12 HOSE)
(-16 HOSE)
(-24 HOSE)
A18 ACTUATOR SEAL DRAINS
SCAVENGE PUMP DISCHARGE
HYDRAULIC PUMP CASE DRAIN
ACCESSORY GEAR BOX VENT
LUBE PUMP INLET
QCSEE ENGINE
2
3
4
5
6
27
34

NOTE:
1 SEE DWG 4013180-700 FOR FULL DESCRIPTION OF ITEM BALLOON ITEMS
2 SEE DWG 4013180-860 ITEMS NO 49 & 50 FOR FULL DESCRIPTION

Figure 12-2. Facility Lube System Schematic.

Table 12-I. QCSEE Lube Flows - UTW.

	Cm^3/Sec	GPM
No. 1B Bearing	126	2.00
No. 1 Seal	63	1.00
No. 1R Bearing	94.6	1.50
No. 2 and 3 Bearing	137.5	2.18
No. 3 Seal	14.5	0.23
No. 1 and No. 2 Inlet G/B	148.9	2.36
Accessory Gearbox	156.4	2.48
Scavenge Pump Gearbox	31.5	0.50
V.P. Actuator	47.3	0.75
Main Reduction Gears	1488.7	23.6
No. 4 and No. 5 Bearing	164.0	2.60
No. 6 Seal	37.8	0.60
Rad. Shaft Midspan Bearing	9.5	0.15
	2520.01	39.95

Flows Referenced to 14,460 rpm Core Speed (5977 rpm Pump Speed) filters reaches 27.6 N/cm^2 (40 psid). Thus, if the filters become plugged, full oil flow is always supplied to the engine.

- The static leak valve, which is designed to crack and reseat at 10.3 N/cm^2 (15 psid) has been strategically placed to prevent flowing of engine sumps and gearboxes during shutdown.
- Ten gallon supplementary oil resevoir, which is vented to the oil tank and discharges directly into the line leading to the lube pump inlet. This resevoir is required to accommodate the volumetric expansion and contraction of the air/oil mixture in the large capacity slave lube system components.

Oil supply subsystem components selected for the experimental engine are defined in the following paragraphs:

Oil Tank - A TF39 oil tank (Figure 12-2) has been modified for application in the UTW experimental engine oil supply system. Modifications will include:

- A new vortex generator plate designed to accept two CF6 deaerators to handle increased oil flows.
- Addition of a level sensor similar to one used in the CF6 and F101 tanks.
- Replacement of the TF39 lube supply port by a larger port.
- Replacement of the TF39 filter caps with CF6 caps. A specially marked dip stick also has been provided that permits filling to the 37,850 cm^3 (10 gallon) level. The supplementary reservoir provides an additional 37,850 cm^3 (10 gallon) of capacity.

A cross section of the modified TF39 tank is shown in Figure 12-3.

Lube Supply & Hydraulic Charge Pump- A CF6 engine lube/scavenge pump is utilized in the UTW experimental engine oil supply system. Specific design features including necessary modifications are as follows:

- 5 CF6 scavenge elements manifolded for UTW lube supply
- Lube bypass variable orifice added [2268 cm^3/sec (36 gpm) at 126 cm^3/sec (2 gpm)/turn]
- 276 N/cm^2 (400 psi) lube relief added
- LM2500 tach pad cover and filter bowl plug
- F101 drive spline (to mate with gearbox)
- Hydraulic charge element (CF6 lube) 189 cm^3/sec (3 gpm) steady state, 378 cm^3/sec (6 gpm) transient [remainder of 1134 cm^3/sec (18 gpm) total bypassed].
- Hydraulic relief valve pressure setting of 34.5-44.8 N/cm^2 (50-65 psi) accomplished by changing the spring.

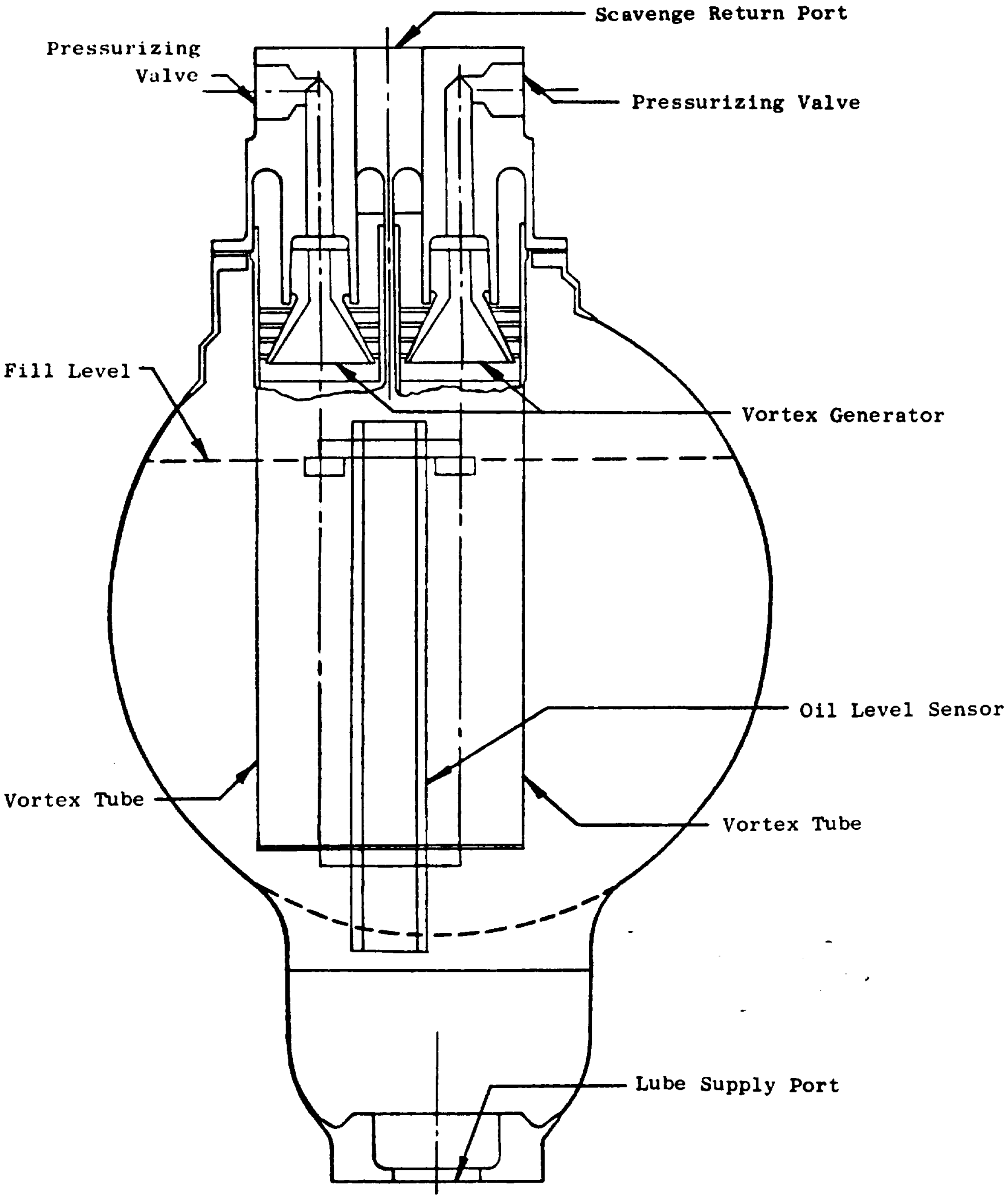
Scavenge Return Port
Pressurizing Valve
Pressurizing Valve
Fill Level
Vortex Generator
Oil Level Sensor
Vortex Tube
Vortex Tube
Lube Supply Port

Figure 12-3. Lube Tank Cross Section.

- Gearcase bolts changed from AN4CH6A to MS9501-12 bolts to increase vibratory capability

- CF6 gask-o-seals, manifold bolts/washers, V-band, and seal.

Figures 12-4, 12-5, and 12-6 show demonstrated pump performance.

Lube Filter - Two CF6 scavenge filters will be connected in parallel and located downstream of the lube pump in the experimental engine oil supply system. Design features include:

- 46μ nom/76μ absolute

- 827 N/cm^2 (1200 psi) proof pressure

- 11.0 N/cm^2 (16 psi) ΔP @ 1512 cm^3/sec (24 gpm), 367 K (200° F)

- 27.6 N/cm^2 (40 psi) minimum bypass ΔP

- 46 cleanable water elements

A cross section of the lube filter is shown in Figure 12-7.

Check Valve - The lube check valve located downstream of the lube filters has the following design features:

- Proof pressure 414 N/cm^2 (600 psig) without leakage or distortion

- Cracking and reseat pressure is 10.3 N/cm^2 (15 psid)

- Capability of operation with lube temperature range of 233 K (-40° F) to 450 K (+ 350° F) for either oils conforming to MIL-L-7808 or MIL-L-23699.

12.3.2 Oil Scavenge Subsystem

The scavenge subsystem consists of a three-element pump, slave filter, slave oil cooler, oil deaerators in the oil tank, and other associated hardware.

The basic scavenge subsystem operates in the following manner: oil in the top-mounted accessory gearbox flows by gravity into the forward sump through drain pipes where it is combined with the forward sump scavenge oil. This combined oil is then scavenged by the bottom-mounted scavenge pump. Oil, which lubricates the scavenge pump drive system, is scavenged by a separate element located within the pump. Aft sump scavenge oil is piped forward to the bottom-mounted scavenge pump and scavenged by a third element. Each element is provided with an inlet screen and magnetic chip detector. The inlet screens catch any debris which is larger than can be

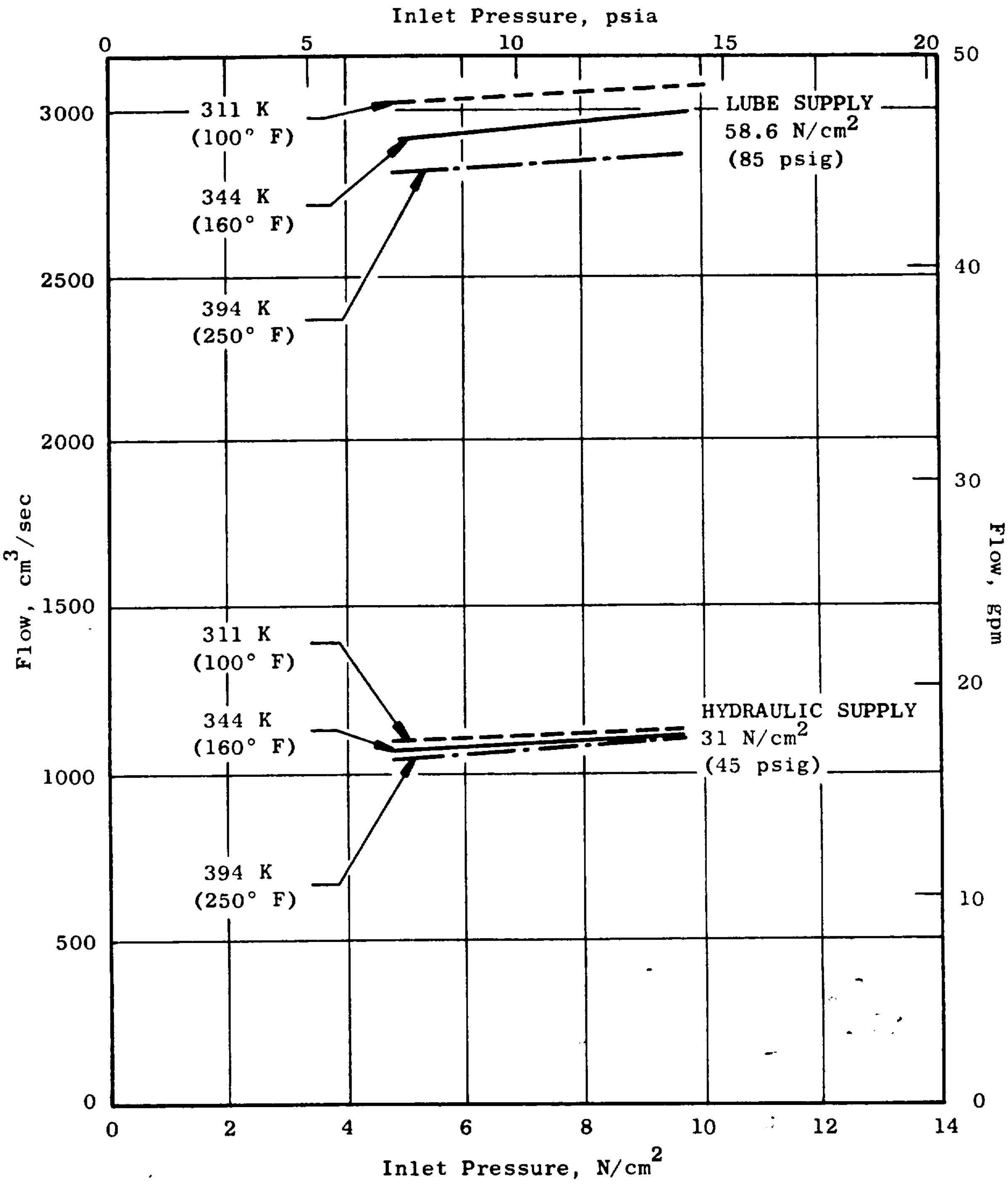

Figure 12-4. Lube Supply Pump Flow Vs. Inlet Pressure at 5977 rpm.

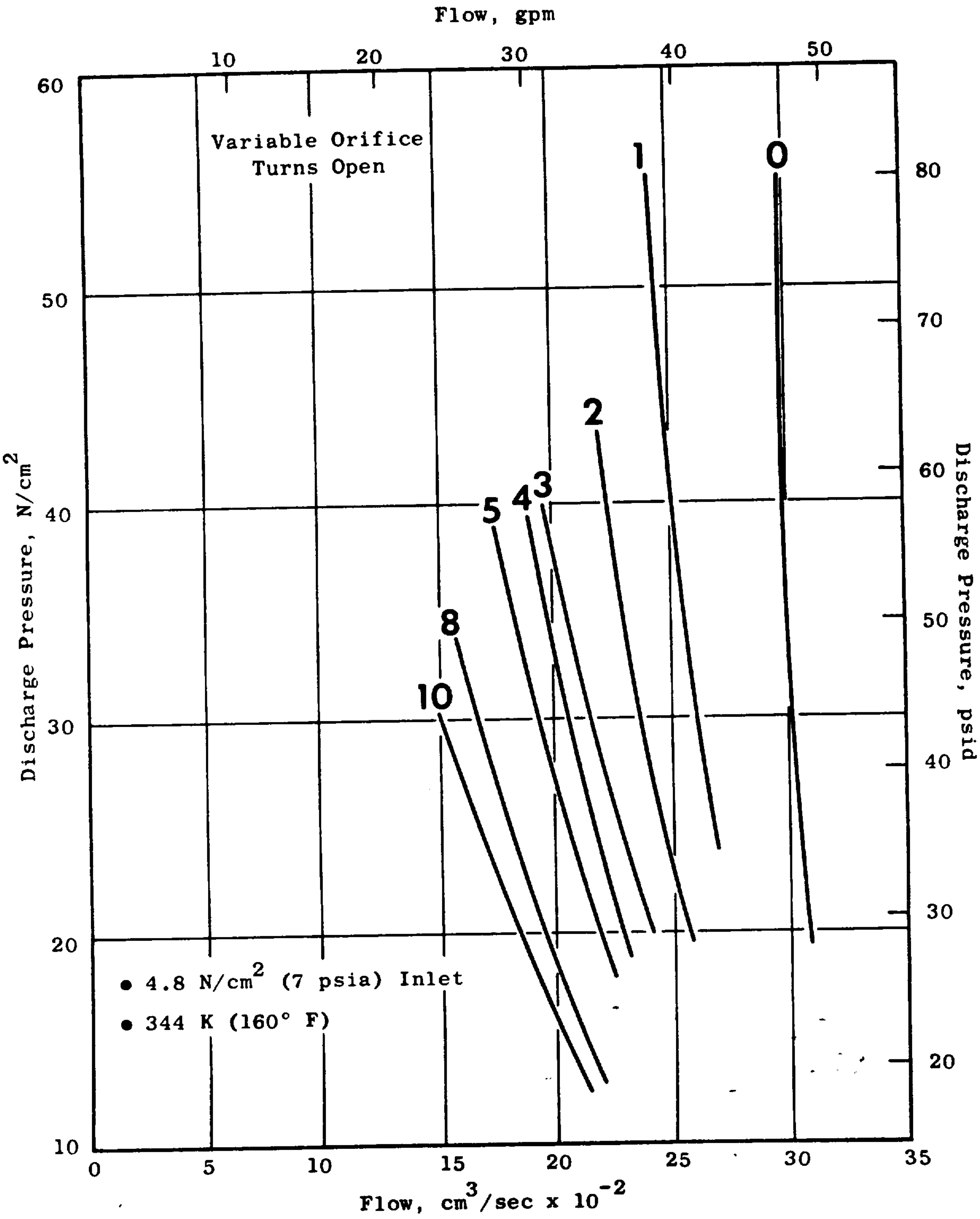

Figure 12-5. Lube Supply Pump Flow Vs. Discharge Pressure at 5977 rpm.

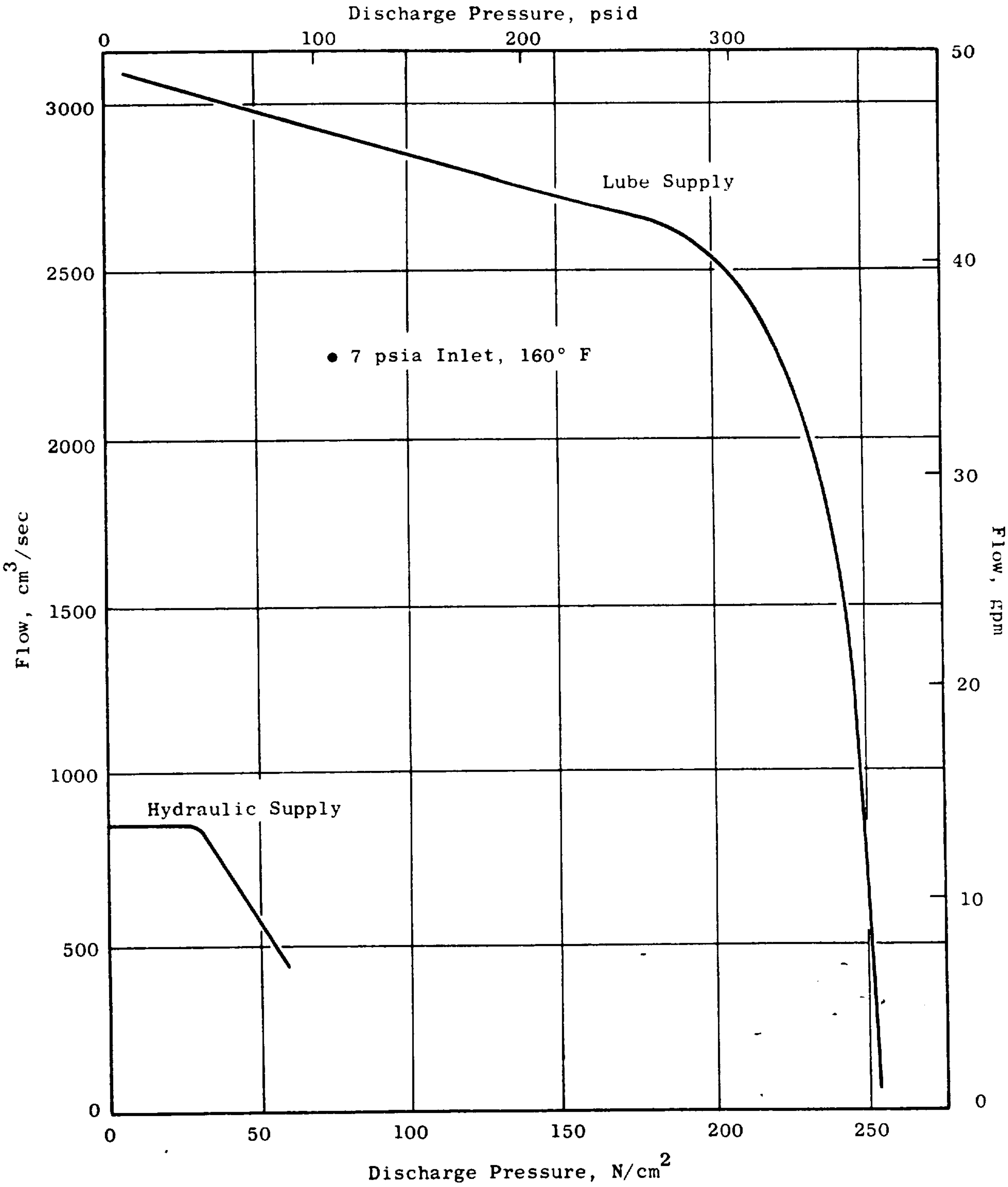

Figure 12-6. Relief Valve Flow Vs. Discharge Pressure at 5977 rpm.

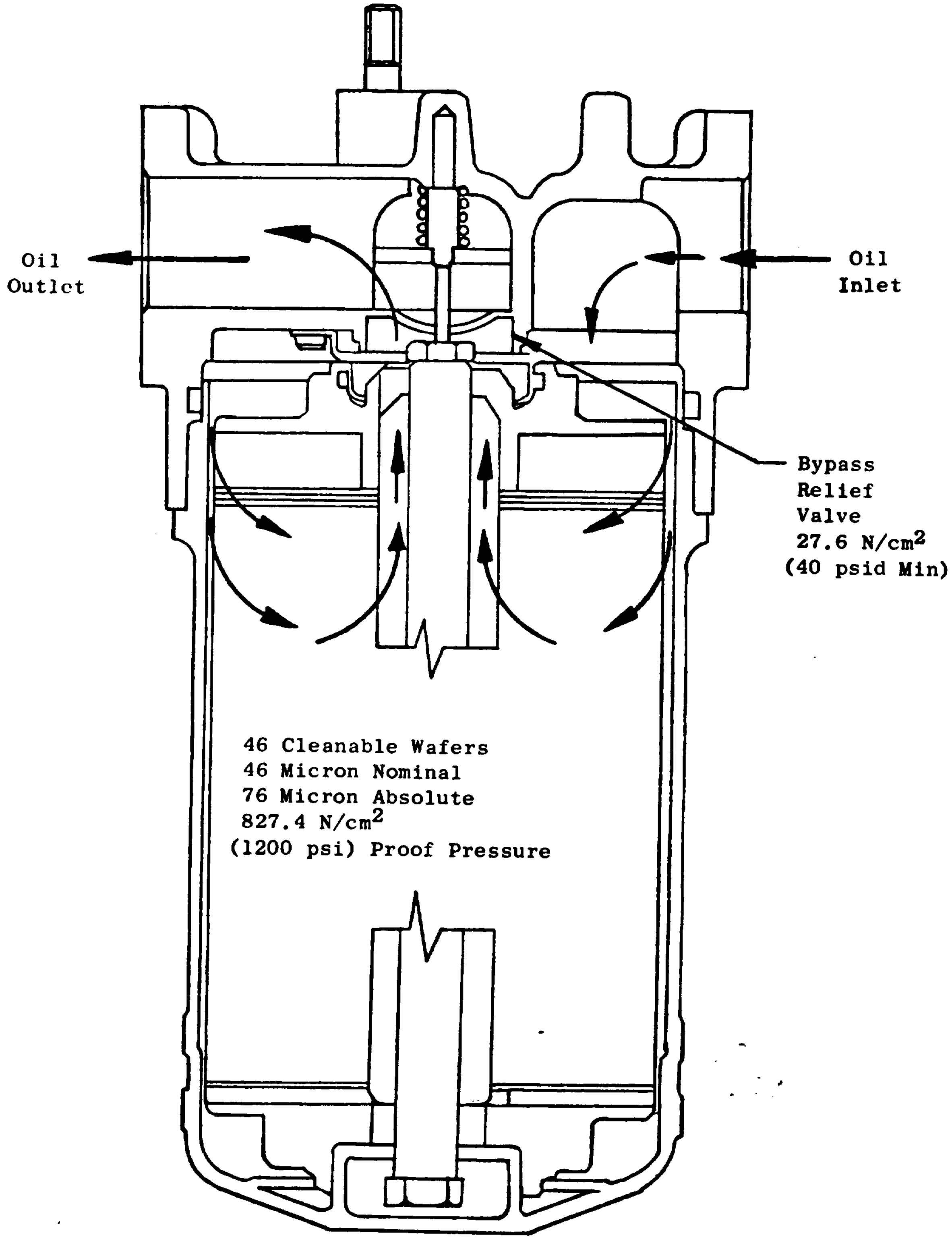
Oil Outlet
Oil Inlet
Bypass Relief Valve 27.6 N/cm^2 (40 psid Min)
46 Cleanable Wafers
46 Micron Nominal
76 Micron Absolute
827.4 N/cm^2
(1200 psi) Proof Pressure

Figure 12-7. Lube Filter.

passed through the pumping element without causing damage or excessive wear. The magnetic chip detectors collect ferrous particles to help condition monitor the sumps and gearbox components. More detailed information is available through spectrographic analysis of collected debris.

Total engine scavenge flow is discharged through a common port and routed through a static check valve internal with the pump into the 10-micron scavenge filter. The oil then flows to the system heat exchanger where the heat load of the main shaft bearings, seals, sump walls, gearboxes, and piping is transferred to the coolant. The oil is then returned to the tank where deaerators remove entrained air and condition the oil for reuse by the supply system.

Special features of the scavenge subsystem include:

- A static check valve in the discharge line to prevent flooding of the sump
- Chip detectors at all scavenge pump inlets for condition monitoring of accessory drives, sumps, and bearings
- A pressure relief bypass valve on the scavenge filter, which opens when the pressure across the filter reaches 27.6 N/cm^2 (40 psi), to ensure continuous flow to the tank
- A service shutoff valve in the filter to minimize oil loss during filter element changes

Major scavenge system component features are summarized in the following paragraphs:

Scavenge Pump - design features of the scavenge pump, shown schematically in Figure 12-8, are as follows:

- Three elements (main, rear sump, gearbox, scavenge) 5166, 473, 126 cm^3/sec (82, 7.5, 2.0 gpm) minimum, respectively
- 9144 m (30,000 ft) altitude design [3.0 N/cm^2 (4.4 psia) inlet]
- Inlet screens and push-turn magnetic plugs at all inlets
- Static leak check valve [1.36 - 2.76 N/cm^2 (2 -- 4 psi) crack]
- Mini-element (gearbox scavenge) is metering element discharging into main inlet to prevent priming problems
- 6700 rpm input (rear and gearbox elements) geared to 2931 rpm for main element

Detail design information for the three scavenge pump elements is presented in Table 12-II. Test results are shown in Figures 12-9 and 12-10.

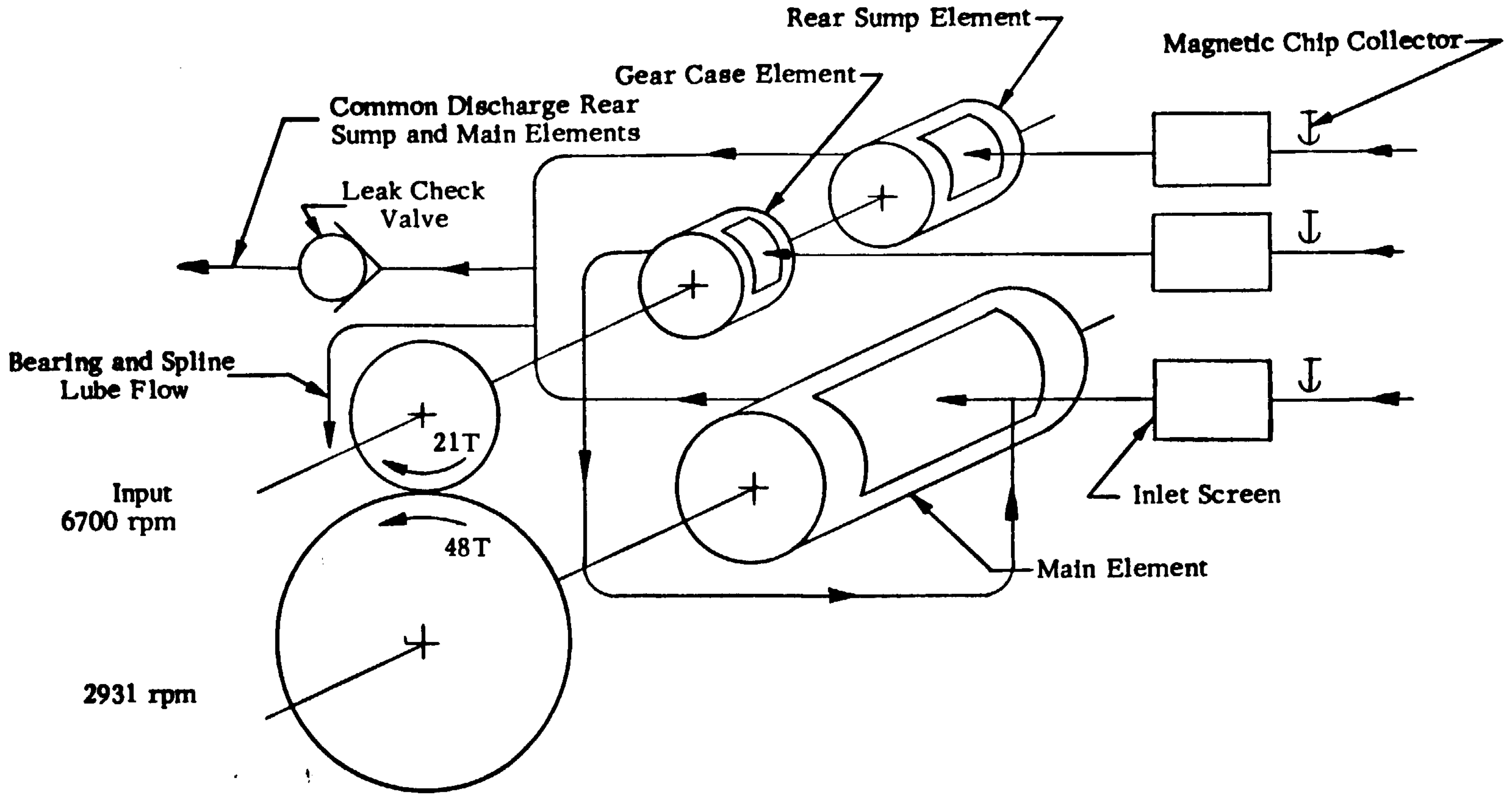

Rear Sump Element
Magnetic Chip Collector
Gear Case Element
Common Discharge Rear
Sump and Main Elements
Leak Check
Valve
Bearing and Spline
Lube Flow
21T
Input
6700 rpm
48T
2931 rpm
Inlet Screen
Main Element

Figure 12-8. QCSEE Scavenge Pump Schematic.

Table 12-II. Scavenge Element Predicted Performance.

	Main	Rear Sump	Gear Case
rpm	2931	6700	6700
Bore Diameter	4.72 cm (1.86 in.)	1.91 cm (0.75 in.)	1.91 cm (0.75 in.)
Element Length	9.65 cm (3.8 in.)	3.25 cm (1.28 in.)	1.17 cm (0.46 in.)
Element L/D	2.04	1.70	0.61
Theoretical Displacement	139.3 cm^3/rev (8.5 $in.^3$)	5.4 cm^3/rev (0.33 $in.^3$)	1.97 cm^3/rev (0.12 $in.^3$)
Theoretical Flow	6804 cm^3/sec (108 gpm)	610 cm^3/sec (9.67 gpm)	213 cm^3/sec (3.53 gpm)
Estimated Flow(1)	6245 cm^3/rev (99 gpm)	540 cm^3/rev (8.7 gpm)	217 cm^3/rev (3.5 gpm)
Estimated Flow(2)	5774 cm^3/sec (93 gpm)	540 cm^3/sec (8.7 gpm)	217 cm^3/sec (3.5 gpm)
Theoretical Cav. Knee	3.41 N/cm^2 (3.5 psia)	1.86 N/cm^2 (2.7 psia)	1.86 N/cm^2 (2.7 psia)
Flow In	2286 cm^3/sec (36.2 gpm)	233 cm^3/sec (3.7 gpm)	32 cm^3/sec (0.50 gpm)
Scavenge Ratio	2.6	2.3	6.8
Bearing P/A Loads	525 N/cm (300 lb/in.)	394 N/cm (225 lb/in.)	3.5 N/cm (2 lb/in.)

---

(1) Sea level, 394 K (250° F)

(2) 9144 m (30,000 ft) altitude, 394 K (250° F), 3.03 N/cm^2 (4.4 psia) inlet

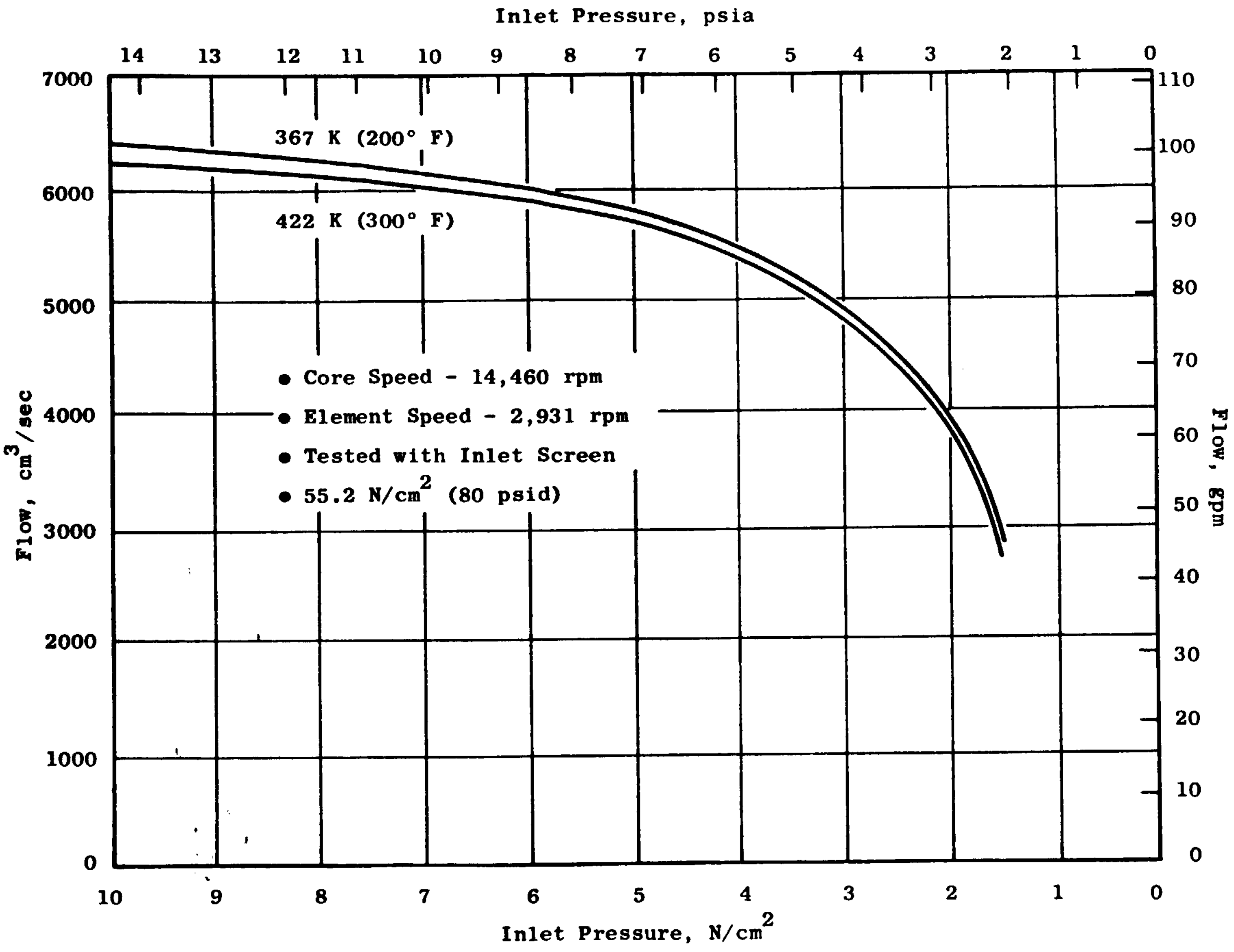

Figure 12-9. Scavenge Pump Main Element Flow Vs. Inlet Pressure.

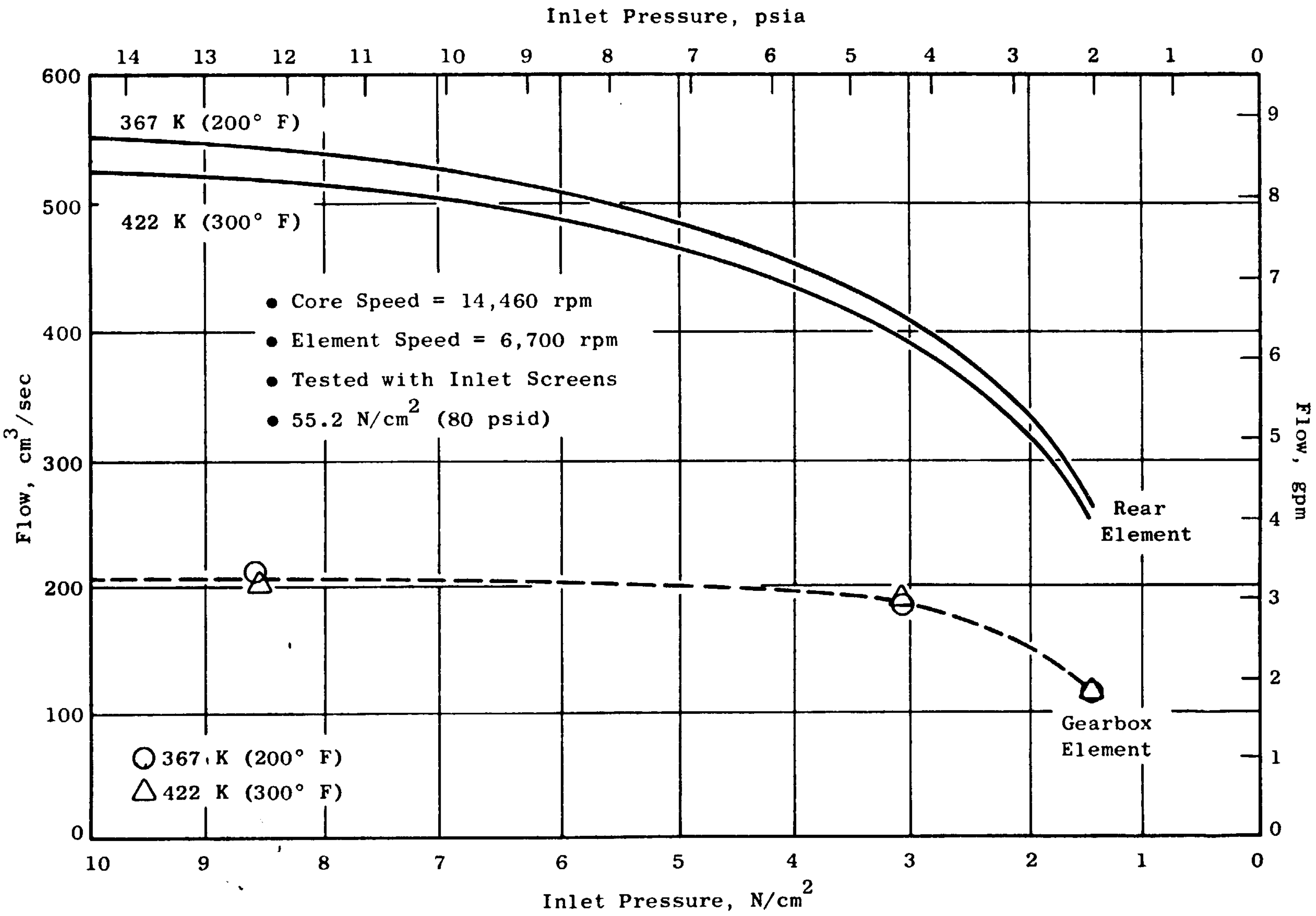

Figure 12-10. Scavenge Pump Gearbox and Rear Element Flows Vs. Inlet Pressure.

Scavenge Filter - specific design characteristics of the slave scavenge filter are:

- Pressure: rated 276 N/cm^2 (400 psi), proof 414 N/cm^2 (600 psi), burst 862 N/cm^2 (1250 psi)
- Temperature range: 233 to 810 K (-40° to +350° F)
- Element collapse pressure: 103 N/cm^2 (150 psid)
- Bypass valve cracking pressure: 34.5 ± 3.4 N/cm^2 (50 ± 5 psid)
- Visual bypass indication: 27.6 ± 3.4 N/cm^2 (40 ± 5 psid)
- Pressure drop at 50 gpm, MIL-L-7808

Housing:	2.07 N/cm^2 (3.0 psi)
Element:	2.07 N/cm^2 (3.0 psi)
Total	4.14 N/cm^2 (6.0 psi)

- Materials: Anodized Aluminum, AISI 1010 Carbon Steel, Epoxy Painted.

12.3.3 Vent Subsystem

Venting of the oil seal pressurization air from the sump cavities is accomplished through the gearbox. The rear sump is vented through the low pressure turbine shaft to the forward sump. The forward sump is vented to the accessory gearbox. The air in the gearbox is vented overboard through a rotating air/oil separator. Air which is separated from the scavenge oil in the lube tanks is returned to the accessory gearbox. This air is required at all conditions to satisfy the scavenge ratio requirements of the scavenge pump.

The vent flow areas have been sized to:

- Maintain the sump internal pressure below outside cycle air pressure.
- Prevent reverse airflow across the oil seals during rapid power reductions
- Continue engine operation
    - with one seal failed from any cause including coking
    - with the remaining seals at their maximum service leakage limit

12.3.4 Flight Engine Thermal Balance

The flight engine lube oil is cooled by transferring heat to the engine fuel as well as bypass fuel which is returned to the fuel tanks. The engine heat balance study showed that, on a 32° C (90° F) day at 100% rated reduction gear power, this type of system will probably provide the required 82° C (180° F) oil needed to maintain 149° C (300° F) maximum gear temperature with 50° C (122° F) fuel inlet temperature. The fuel bypass will absorb the pumping temperature rise. The engine heat loads shown in Table 12-III were determined from the November 1, 1974 QCSEE Technical Requirements and the July 18, 1974 Curtiss Wright Gearing Data. Heat loads from the reduction gearbox, engine hydraulic and lube systems have been calculated for each flight condition and are tabulated in Table 12-IV.

Additional studies, outside the QCSEE work scope, are required to obtain a total system understanding of a recirculating fuel system for future aircraft application. These studies must include fuel cooling, wing tank cooling, flight envelope considerations, and the impact of circulating and storing heated fuel, Utilizing this heat exchanger, Tables 12-V and 12-VI show predicted bearing race and AGMA scoring temperatures for estimated and derated reduction gear efficiency. All temperatures are below the limit of 148.9° C (300° F) of 9310 steel.

12.3.5 Heat Exchanger

A General Electric LM2500 engine lube oil heat exchanger module has been selected as a slave heat exchanger for the UTW experimental engine. This heat exchanger is an all-stainless-steel heat exchanger offering 527, 950 j/sec (30,000 Btu/min) with 6300 cm^3/sec (100 gpm) of 200 K (80° F) water. Oil-side pressure drop of the heat exchanger is less than 6.9 N/cm^2 (10 psi) at 3024 cm^3/sec (48 gpm). Water-side pressure drop is less than 6.9 N/cm^2 (10 psid).

12.3.6 Hydraulic System

The hydraulic system uses the same oil tank as the lube system. Oil is supplied from the oil tank through a boost element on the lube pump to the hydraulic pump. Case drain oil from the hydraulic pump is routed to the tank.

The hydraulic system will include a 10 micron filter at the pump inlet and a magnetic chip detector in the hydraulic system discharge line. The F101 hydraulic pump (which had an integral boost element) did not have sufficient capacity to meet the hydraulic system requirement. A 2961 cm^3/s (47 gpm), 2344 N/cm^2 (3400 psig) pump has been ordered from Abex.

Table 12-III. Heat Study Conditions[*].

Condition	Case No.	Alt.	Flt. Mach No.	Reduction Gear Efficiency %	LPT kw/HP	Fan Speed, %	Core Speed, %
G Idle	112	SL	0	98.96	75.3/101	27.8	50.3
Takeoff	1	SL	0	99.30	9802/13145	97.3	93.3
Climb	301	SL	0.38	99.28	10512/14097	92.0	92.8
Cruise	404	25K	0.7	99.24	5335/8496	102.8	89.8
Descent	503	15K	0.6	98.99	1749/2346	61.2	77.8
Approach	8	200 Ft.	0.12	99.26	6804/9125	95.2	87.4
Reverse	Table III (Thru Stall)	SL	0	99.19	5470/7335	91.8	89.8
Max Fan Torque	928	SL	0	99.30	11804/15830	96.2	92.3

[*] From November 1, 1974 Tech Req. and July 18, 1974 C - W Data Selected on the Basis of Max ATMA Scoring ΔT

Table 12-IV. Predicted Heat Loads and Oil Flows.

Condition	Reduction Gearbox kw/btu/min	Engine Lube kw/btu/min	Engine Hydraulic kw/btu/min	Total Q kw/btu/min	Oil Flow* kg/min/lbs/min
G Idle	0.79/45	4.1/234	1.9/110	6.8/389	73.5/162
Takeoff	68.6/3905	58.7/3343	3.6/205	131.0/7453	127.4/281
Climb	75.7/4307	54.9/3124	3.6/204	134.2/7635	126.5/279
Cruise	48.1/2740	56.0/3189	3.5/198	107.7/6127	122.9/271
Descent	17.7/1005	23.7/1347	3.0/171	44.3/2523	107.9/238
Approach	50.4/2866	47.4/2695	3.4/192	101.1/5753	119.7/264
Reverse	44.3/2521	49.5/2815	3.5/197	97.2/5533	122.9/271
Max Fan Torque	82.6/4703	56.2/3200	3.6/203	142.4/8106	126.1/278

*8.866 × 10^{-4} kg/cm^3 (7.4 lb/gal)

Table 12-V. Predicted Temperatures, 100 gpm [26.7° C (80° F)] Cooling Water.

Condition	AGMA ΔT °C/°F	Bearing Race ΔT °C/°F	Scav. Oil °C/°F	Lube Oil °C/°F	Bearing Race* °C/°F	AGMA Scoring Index* °C/°F
G Idle	-16.1/3	-12.2/10	30/86	27.2/81	32.8/91	28.9/84
Takeoff	33.3/92	22.8/73	67.2/153	37.2/99	77.8/172	88.3/191
Climb	36.7/98	20/68	68.3/155	37.8/100	75.6/168	92.2/198
Cruise	18.3/65	22.2/72	60.6/141	35/95	75/167	71.1/160
Descent	-2.2/28	-1.1/30	42.2/108	30.6/87	47.2/117	46.1/115
Approach	21.1/70	21.1/70	59.4/139	35/95	73.9/165	73.9/165
Reverse	15.6/60	19.4/67	57.2/135	34.4/94	71.7/161	67.8/154
Max Fan Torque	41.1/106	22.8/73	71.1/160	37.8/100	78.3/173	96.7/206

*9310 Steel (148.9° C - 300° F) Limit

Table 12-VI. Derated Reduction Gear Efficiency, 100 gpm [26.7° C (80° F)] Cooling Water.

Condition	Red. Gear Efficiency %	Total Q kw/Btu/Min	Lube Oil °C/°F	Bearing Race* °C/°F	AGMA Scoring Factor* °C/°F
G Idle	96.96	8.3/474	27.2/81	32.8/91	28.9/84
Takeoff	97.30	327.0/18610	52.8/127	93.3/200	103.9/219
Climb	97.28	344.4/19601	54.4/130	92.2/198	108.9/228
Cruise	97.24	234.4/13339	45.6/114	103.3/186	81.7/179
Descent	96.99	79.3/4515	32.8/91	49.4/121	48.3/119
Approach	97.26	237.2/13498	45.6/114	84.4/184	84.4/184
Reverse	97.19	206.6/11759	42.8/109	135.6/176	76.1/169
Max Fan Torque	97.30	378.6/21542	57.2/135	97.8/208	116.1/241
*9310 Steel = 148.9° C (300° F) Limit					

12.3.7 Seal Pressurization Subsystem

Oil leakage can potentially contribute to seal coking and contamination of compressor bleed air, as well as increasing the engine oil consumption. In order to prevent oil leakage, the mainshaft oil seals are pressurized to force air to flow across the seals into the sumps at all operating conditions.

The compressor stage for extraction of seal pressurization-air has been selected to have adequate pressure to prevent the hot engine cycle air from entering the sumps and yet low enough in temperature during higher-Mach-number, hot-day operation to permit the oil seals to meet their required life. Pressurization air is extracted at the hub of the third-stage compressor rotor and routed internally within the engine to both the forward and rear sump oil seals. Air from the hub of the compressor is used because it contains the minimum contamination. For ground idle operation, shop air will be provided to the aft sump to ensure that hot gas will not back-flow into the system. A higher pressure source could be used in a flight engine if required.

Oil seal drains are provided in the forward sump oil seals to remove any seal leakage which could contaminate the compressor. Since these drains carry fluid only in the case of a seal failure, the forward sump seal drains are routed overboard. The aft sump seal drains are routed to the flowpath aft of the low pressure turbine.

12.4 ROTOR THRUST BALANCE

In addition to the loads resulting from flight maneuvers and misalignment, the main shaft bearings of a turbofan engine are subjected to axial loads which are the result of the axial aerodynamic forces on the turbomachinery blading, plus pressure forces on the rotor components. Generally these thrust loads can be minimized by adjusting the radial location of one or more labyrinth seals.

The core engine (high pressure compressor and high pressure turbine) of the F101 uses a conventional method of thrust balancing; i.e., the forward compressor load and aft turbine load are balanced by radially adjusting the labyrinth seals to provide the balancing gas loads. The net axial thrust load is taken at the No. 3 ball bearing.

The rotor thrust balance situation for the low pressure rotor (fan and low pressure turbine) of a geared fan system is quite different from that of a conventional turbofan engine. This is illustrated in Figure 12-11. Loads shown are typical for the takeoff condition of the UTW engine. In the conventional engine, the low pressure midshaft ties the turbine rotor to the fan rotor so that the thrust bearing feels only the difference in thrust between the rotors. The UTW engine has a reduction gear which axially disconnects the fan from the LP turbine. Therefore, each rotor system (fan and LP turbine) must have its own thrust bearing. Figure 12-11 shows schematically the difference between a conventional system and a geared system to support the UTW fan rotor thrust loads. To satisfy these requirements, the UTW fan rotor uses a high-load-capacity ball bearing from the CF6 engine. This bearing is identified as the No. 1 ball bearing in the UTW engine. A balance piston arrangement has been applied to the low pressure turbine rotor to minimize the axial thrust loads on the rotor thrust bearing (No. 2 ball bearing).

Rotor thrust bearing design conditions and loads are discussed for the fan, core, and LP turbine rotor systems in the following paragraphs.

12.4.1 Fan Rotor Balance

Thrust forces considered in determining the axial loads acting on the fan rotor thrust (No. 1B) bearing are identified in Figure 12-12. Results of the analyses, based on the UTW experimental engine duty cycle, are presented in Table 12-VII.

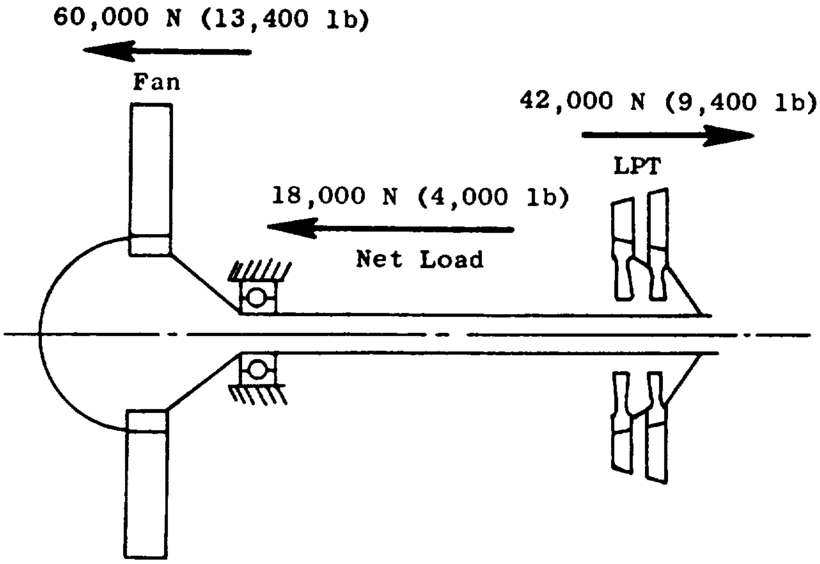
60,000 N (13,400 lb)
Fan
42,000 N (9,400 lb)
LPT
18,000 N (4,000 lb)
Net Load

- Conventional Low Pressure System
  UTW Takeoff Conditions

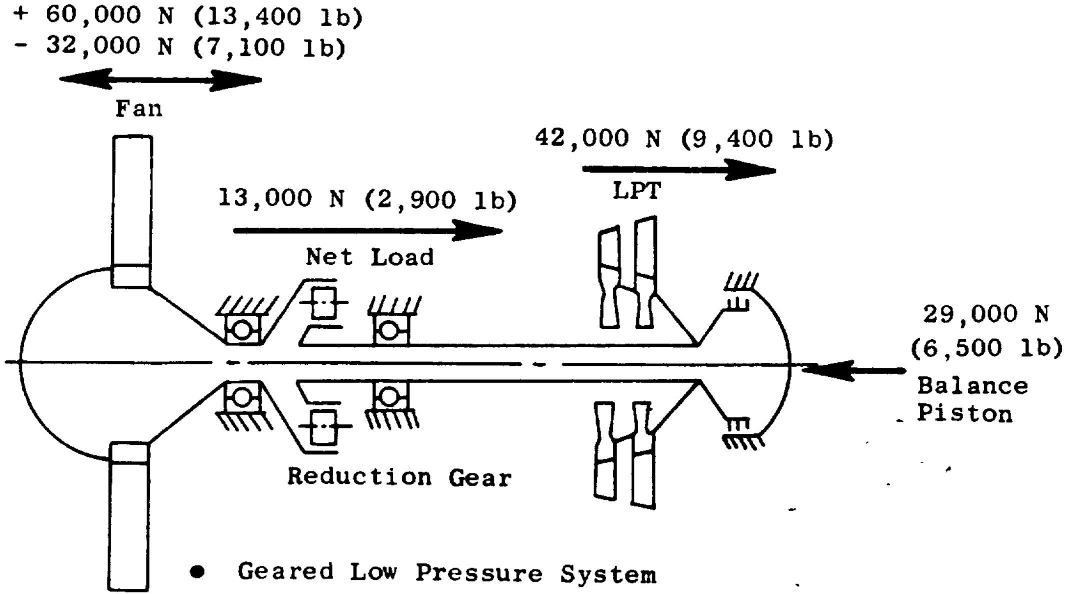
+ 60,000 N (13,400 lb)
- 32,000 N (7,100 lb)
Fan
42,000 N (9,400 lb)
LPT
13,000 N (2,900 lb)
Net Load
29,000 N
(6,500 lb)
Balance
Piston
Reduction Gear

- Geared Low Pressure System
  UTW Takeoff Conditions

Figure 12-11. Schematic of Conventional and Geared LP Drive Systems.

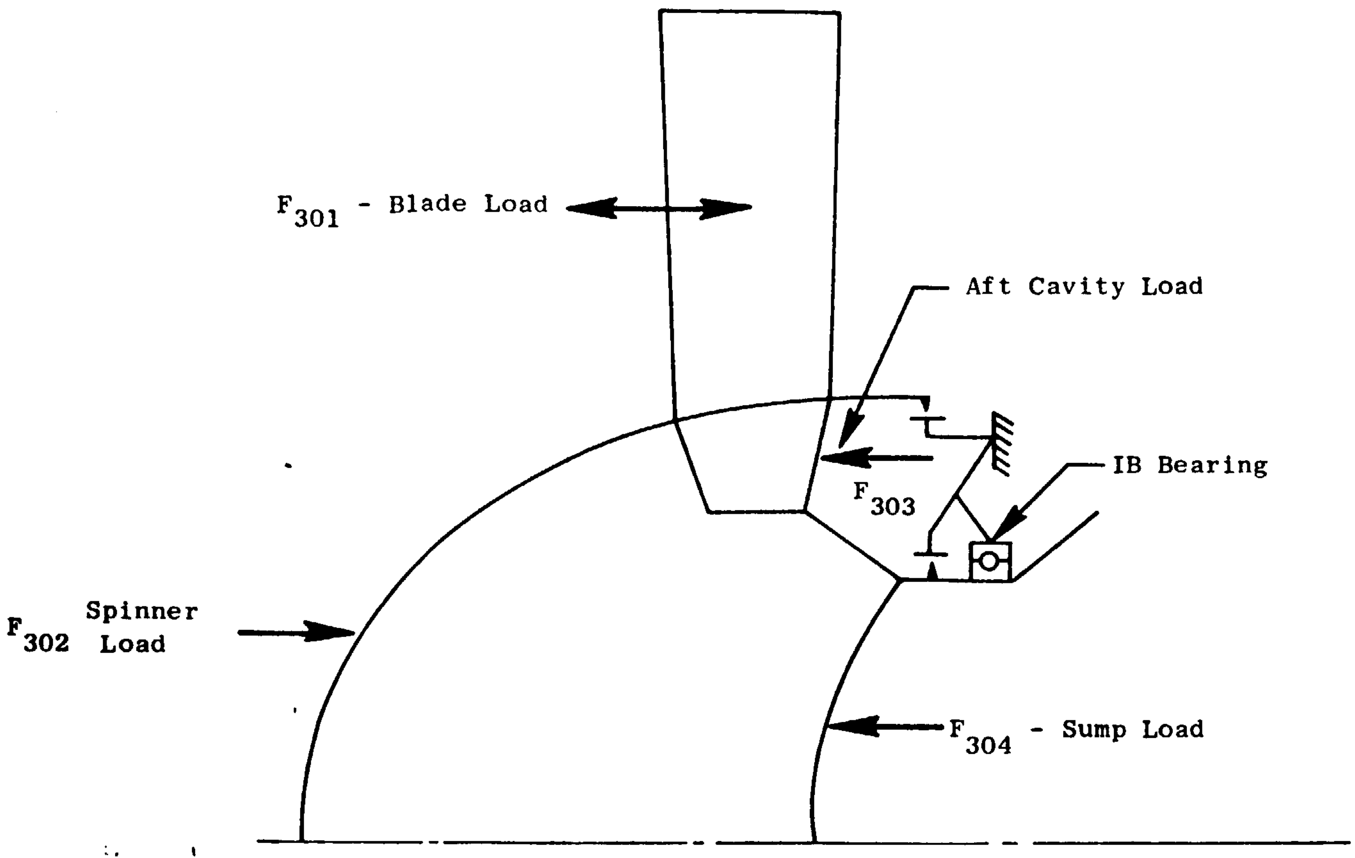
F_{301} - Blade Load
Aft Cavity Load
F_{303}
IB Bearing
F_{302} Spinner Load
F_{304} - Sump Load

$$\text{Net IB Bearing Load} = (F_{301} + F_{303} + F_{304}) - F_{302}$$

Figure 12-12. Fan Thrust Load Vectors.

Table 12-VII. Fan Rotor Thrust (No. 1B) Bearing Axial Loads.

Case No.	Operating Condition	% Time(1)	% N_F	% Fan HP	RPM	kN	lb
962	Forward Thrust	0.04	105	100	3406	+56.5(2)	+12702(2)
928	Forward Thrust	0.60	96.17	121	3120	+69.3	+15587
961	Forward Thrust	0.55	97.31	112	3157	+64.2	+14429
1	Forward Thrust	5.59	97.31	100	3157	+59.7	+13414
963	Forward Thrust	18.64	90	80	2920	+51.9	+11670
964	Forward Thrust	36.51	75	50	2433	+38.5	+ 8645
965	Forward Thrust	36.51	30	2.4	973	+ 4.9	+ 1120
	Reverse (83°) (Through Flat Pitch)	0.78	-	-	3408	-31.5	- 7081
	Reverse (-95°) (Through Stall)	0.78	-	-	2977	-30.8	- 6919

(1) Total operational time = 2682 hours.

(2) Sign convention: (+) forward, (-) aft

The No. 1 bearing cubic mean thrust load for the experimental duty cycle is 39.46 kN (8870 lb). Based on a specific dynamic capacity of 308.7 kN (69,400 lb) and a radial load of 4.003 kN (900 lb), this bearing has a calculated B_{10} life of 25,750 hours. A material life multiplier of 5 was used in this analysis.

12.4.2 Core Engine

High pressure rotor (HP compressor and HP turbine) thrust load vectors considered in the core engine thrust balance analysis are shown in Figure 12-13. The HP rotor thrust (No. 3) bearing net axial loads resulting from these vectors are presented in Table 12-VIII for the UTW experimental engine duty cycle.

The No. 3 bearing cubic mean thrust load for the experimental duty cycle is 5.59 kN (1257 lb). Based on a specific dynamic capacity of 95.99 kN (21,580 lb) and a radial load of 0.89 kN (200 lb), this bearing has a calculated B_{10} life of 20,090 hours. A material life multiplier of 5 was used in this analysis.

12.4.3 Low Pressure Turbine Rotor

Low pressure turbine thrust balance load vectors considered in the rotor thrust balance analysis are shown in Figure 12-14. The turbine aft load is counteracted by the forward-acting balance cavity force. The balance piston seal is located in the aft sump area described in Section 12.5. The net load (aft LP turbine minus forward balance piston) acts on the No. 2 ball bearing. Thrust balance air is supplied from the high pressure compressor 9th stage rotor as shown in Figure 12-15. This compressor discharge (CDP) air is routed through a 5.09 cm (2 inch) pipe to the bottom vertical service strut. The pipe then passes through the strut and connects to the balance piston cavity.

CDP airflows required for the thrust balance cavity are: 0.20 kg/sec (0.45 lb/sec) for a 0.038 cm (0.015 inch) seal clearance. A 0.152 cm (0.060 inch) seal clearance requires 0.63 kg/sec (1.39 lb/sec).

Axial loads resulting from the LP turbine load vectors based on the experimental engine duty cycle are presented in Table 12-IX.

The No. 2 bearing cubic mean thrust load for the experimental duty cycle is 7.55 kN (1698 lb). Based on a specific dynamic capacity of 84.20 kN (18,930 lb) and a radial load of 2.67 kN (600 lb), this bearing has a calculated B_{10} life of 70,150 hours. A material life multiplier of 5 was used in the analysis.

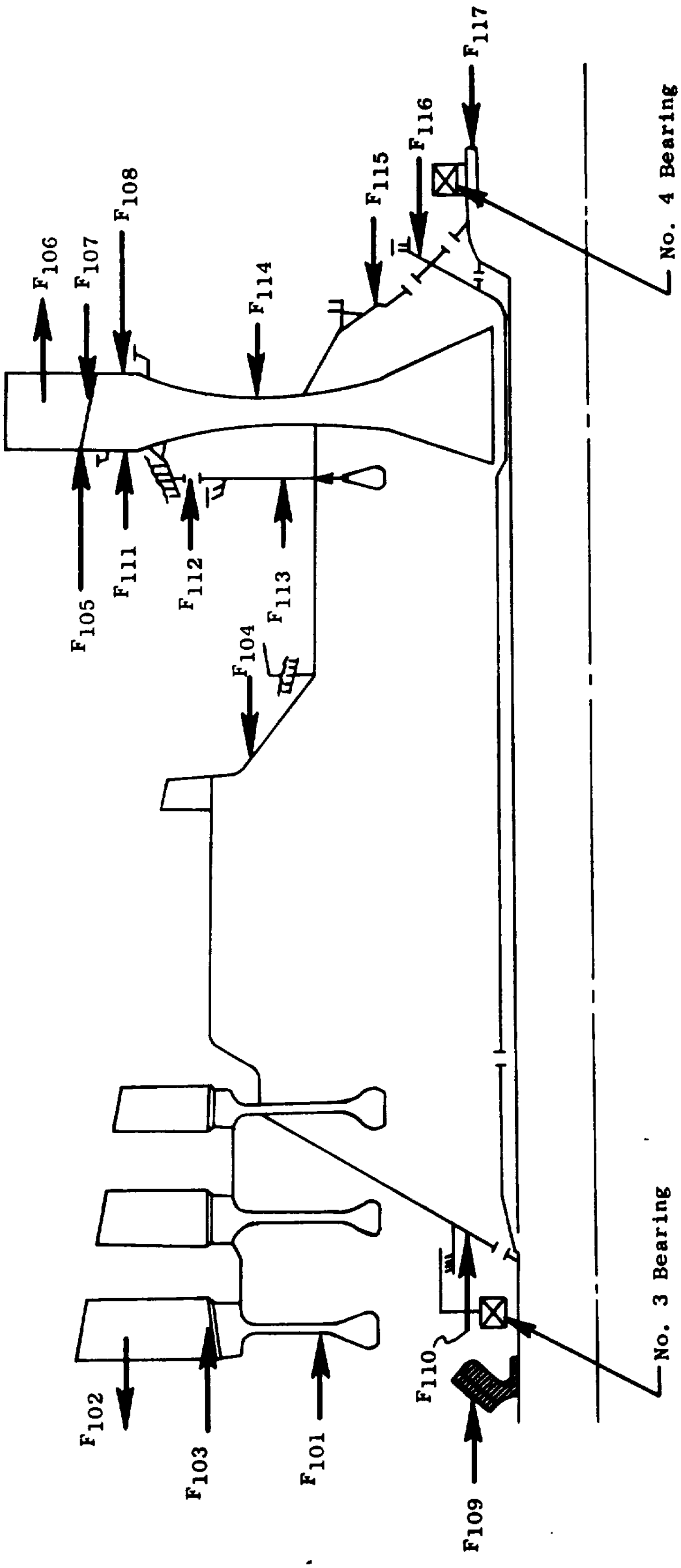
F_{106}
F_{107}
F_{108}
F_{105}
F_{111}
F_{112}
F_{113}
F_{114}
F_{115}
F_{116}
F_{117}
F_{104}
No. 4 Bearing
F_{102}
F_{103}
F_{101}
F_{110}
F_{109}
No. 3 Bearing

Figure 12-13. HP Spool Thrust Load Vectors.

Table 12-VIII. Core Engine Rotor Thrust (No. 3) Bearing Axial Loads.

Case No.	% Time(1)	HP Spool rpm	kN	lb
962	0.04	13576	-3.96(2)	- 890
928	0.60	13347	-6.16	-1385
961	0.55	13780	-5.90	-1326
1	5.59	13493	-5.32	-1197
963	18.64	13141	-4.93	-1108
964	37.29	12508	-6.92	-1555
965	37.29	9282	+1.85	+ 417

(1) Total operational time = 2682 hours.

(2) Sign convention: (+) Forward, (-) Aft.

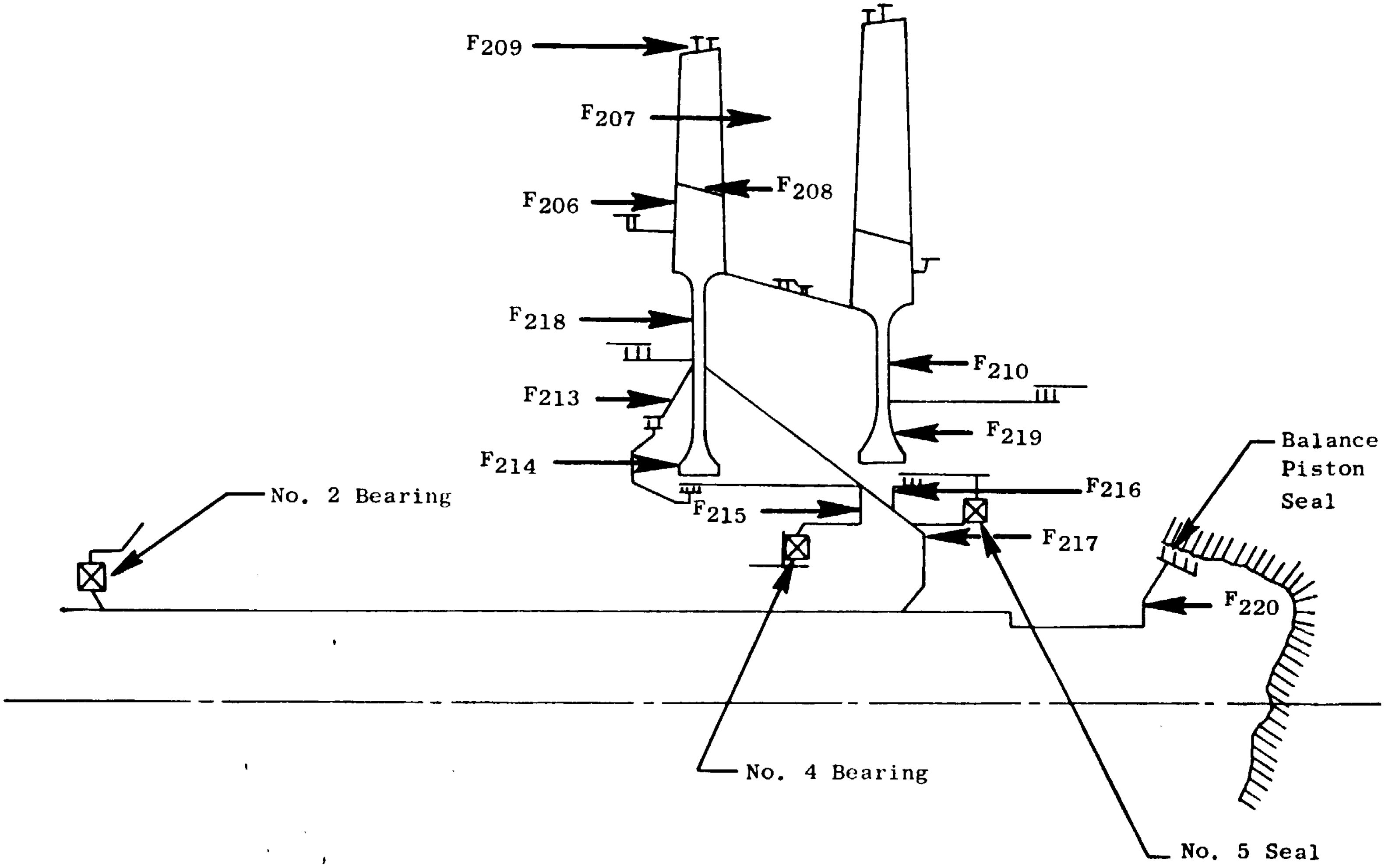
F209
F207
F206
F208
F218
F213
F214
F210
F219
F216
F215
F217
F220
No. 2 Bearing
Balance
Piston
Seal
No. 4 Bearing
No. 5 Seal

Figure 12-14. LP Turbine Thrust Load Vectors.

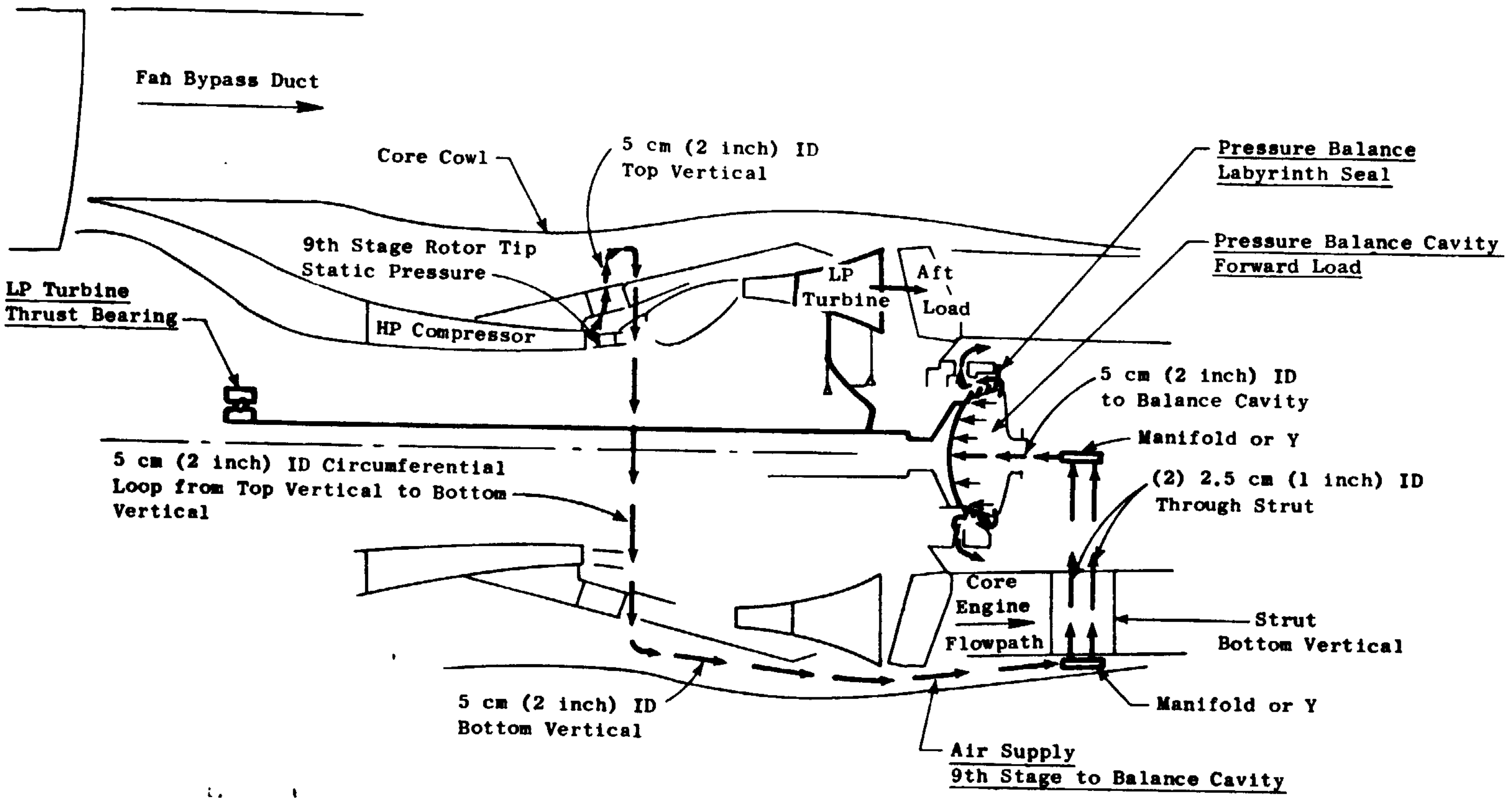

Fan Bypass Duct
Core Cowl
5 cm (2 inch) ID
Top Vertical
Pressure Balance
Labyrinth Seal
Pressure Balance Cavity
Forward Load
9th Stage Rotor Tip
Static Pressure
LP
Turbine
Aft
Load
LP Turbine
Thrust Bearing
HP Compressor
5 cm (2 inch) ID
to Balance Cavity
Manifold or Y
5 cm (2 inch) ID Circumferential
Loop from Top Vertical to Bottom
Vertical
(2) 2.5 cm (1 inch) ID
Through Strut
Core
Engine
Flowpath
Strut
Bottom Vertical
5 cm (2 inch) ID
Bottom Vertical
Manifold or Y
Air Supply
9th Stage to Balance Cavity

Figure 12-15. LP Turbine Thrust Balance System.

Table 12-IX. Low Pressure Turbine Rotor Thrust (No. 2) Bearing Axial Loads.

Case No.	% Time(1)	% N_F	% Fan HP	LP Turbine RPM	kN	lb
962	0.04	105	100	8211	-13.38(2)	-3008(2)
928	0.60	96.17	121	7690	-19.61	-4409
961	0.55	97.31	112	7781	-15.91	-3576
1	5.59	97.31	100	7781	-12.88	-2895
963	18.64	90	80	7196	- 8.02	-1802
964	37.29	75	50	5997	- 1.22	- 275
965	37.29	30	2.4	2399	+ 1.50	+ 337

(1) Total operational time = 2682 hours

(2) Sign conventions: (+) Forward (-) aft.

12.5 BEARINGS, SEALS, AND SUMPS DESIGN

The UTW engine bearing arrangement is shown schematically in Figure 12-16. As shown, the core is supported by a ball thrust bearing (No. 3) located at the forward end of the HP compressor and an intershaft roller bearing (No. 4) located at the HP turbine aft end. The ball thrust bearing, which reacts HP system unbalance thrust loads and radial component loads, is supported by a housing structurally identical to the housing used in the F101 engine. This housing is mounted on the aft inner flange of the composite fan frame. The No. 4 roller bearing, which supports the aft end of the core rotor, is mounted between the HP and LP turbine shafts.

The low pressure system of the UTW engine is supported by four bearings. The main LP turbine shaft is supported by a ball thrust bearing (No. 2) at the forward end and a roller bearing (No. 5) at the aft end. The ball bearing is the same as the F101 fan thrust bearing. This bearing carries the net thrust load of the LP turbine rotor and thrust balance piston, and also a radial load component from the LP shaft. The No. 5 roller bearing, which is identical to the corresponding F101 engine bearing, carries radial loads from the LP shaft and the No. 4 intershaft bearing. Both the No. 2 and No. 5 bearings are supported by housings similar to the corresponding F101 engine housings. The No. 2 bearing housing is mounted to the mid-inner flange of the composite fan frame, and the No. 5 roller bearing support is mounted to the aft end of the turbine frame. The fan rotor is supported by two bearings; a ball thrust bearing (No. 1B) at the forward end, and a roller bearing (No. 1R) at the aft end, the ball thrust bearing carries fan thrust and radial loads. The roller bearing reacts only fan shafting radial loads. Ball bearing support is provided by a housing mounted to the composite fan frame forward flange. The roller bearing housing is mounted to the same forward flange of the composite frame.

A tandem circumferential carbon seal is positioned forward of the No. 1B bearing. It provides a seal between the fan rotor cavity and the forward sump. The No. 3 bearing is sealed from the HP compressor rotor cavity by a face-type carbon seal. The HP turbine rotor cavity is sealed from the aft sump by the No. 4 carbon piston ring seal located forward of the inner shaft bearing. Both the No. 3 and No. 4 seals and their associated parts are identical to F101 hardware. Another tandem circumferential carbon seal is placed between the No. 5 bearing and the balance piston cavity, sealing off the aft sump.

All structures such as shafting, seals, and housings were analyzed using a GE computer program capable of structural analysis with axisymmetric or discrete loading. Stresses were combined using Von Mises failure criteria with appropriate stress concentration factors. All combined stresses, under the most severe design conditions, are below material 0.2% yield properties.

Bolted connections were analyzed using a GE computer program (where applicable) for analyzing bolted flanges. This program includes thermal, centrifugal, torque, and all other flange-type loadings. Bolt materials

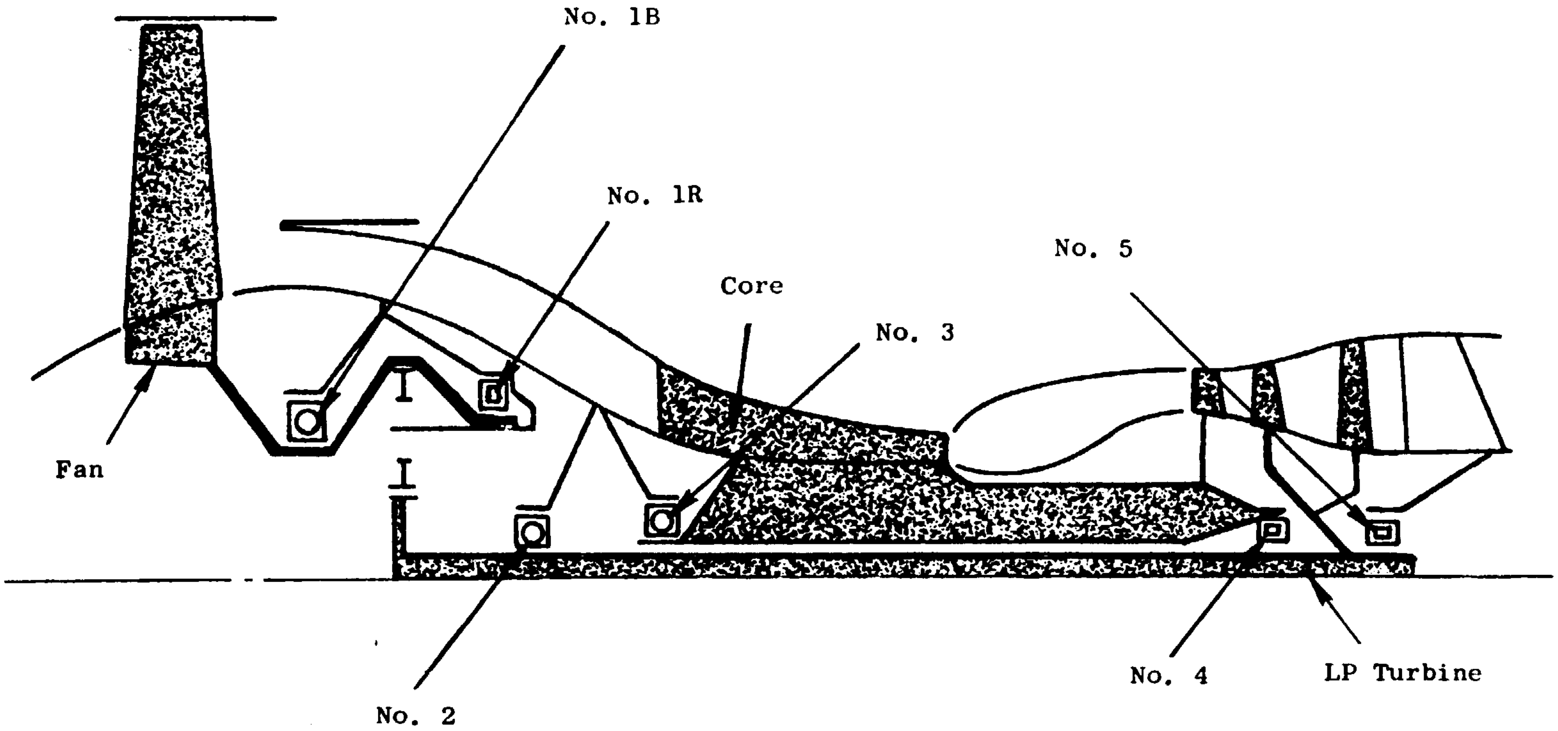
No. 1B
No. 1R
No. 5
Core
No. 3
Fan
No. 2
No. 4
LP Turbine

Figure 12-16. Schematic of UTW Engine Bearing Arrangement.

were selected on the basis of strength and material compatibility with mating structures.

Interface connections were analyzed by evaluating structural component stiffness levels. These stiffness values were calculated using various analytical techniques for required directional loadings, and were then combined with appropriate mating structures to obtain stress resultants.

12.5.1 Forward Sump

The forward sump, shown in Figure 12-17, contains the internal accessory drive bevel gearsets, reduction gears, variable pitch mechanism, the No. 1B and No. 1R fan shaft bearings, the No. 2 LP shaft bearing, the No. 3 HP shaft bearing, and carbon seals forward of the No. 1B bearing and aft of the No. 3 bearing.

The balls and cage of the No. 1B bearing are the same as those used in the CF6 fan bearing. New inner and outer races have been designed to accommodate the common CF6 parts and to provide the necessary support during reverse thrust fan operation. The inner race is mounted on a chrome-plated fan shaft journal and is retained by a spanner nut common to the CF6 design. Lubrication is provided for this bearing by inner race slots and a groove that is positioned over oil holes that penetrate the fan shaft. The holes in the shaft are fed by two oil jets. The outer race is mounted to the forward support housing by a flange that incorporates an anti-rotation device. Both inner and outer races are made of M50 material. The cage is silver-plated AMS 6414 (AISI 4340 steel).

A tandem circumferential carbon seal forward of the No. 1B bearing is mounted in a 400 series stainless steel housing that is detachable from the No. 1B bearing support cone. The carbon rides on a fan shaft runner clamped between the No. 1B inner race and spanner nut. The runner is made from AMS 6322 with the sealing surface chrome plated. The seal is pressurized between the carbons by third stage air and is cooled by oil flowing against the underside of the runner. A seal drain is provided between the carbons to collect any incipient leakage and direct it overboard to prevent core engine contamination. Seal design information is presented in Table 12-X.

Table 12-X. No. 1 Seal Design.

Bore Diameter	39.17 cm (15.42 in.)
Rotational Speed	3400 rpm
Surface Speed	580.2 cm/sec (228 ft/sec)
Delta Pressure	6.21 N/cm^2 (9.0 psid)
Max Supply Air Temp	204.4° C (400° F)
Rubbing Surface Heat Generation	1855 J/sec (105 Btu/min.)
Oil Flow Rate	63.1 cm^3/sec (1 gpm)
Projected Minimum Seal Life	>6200 hrs

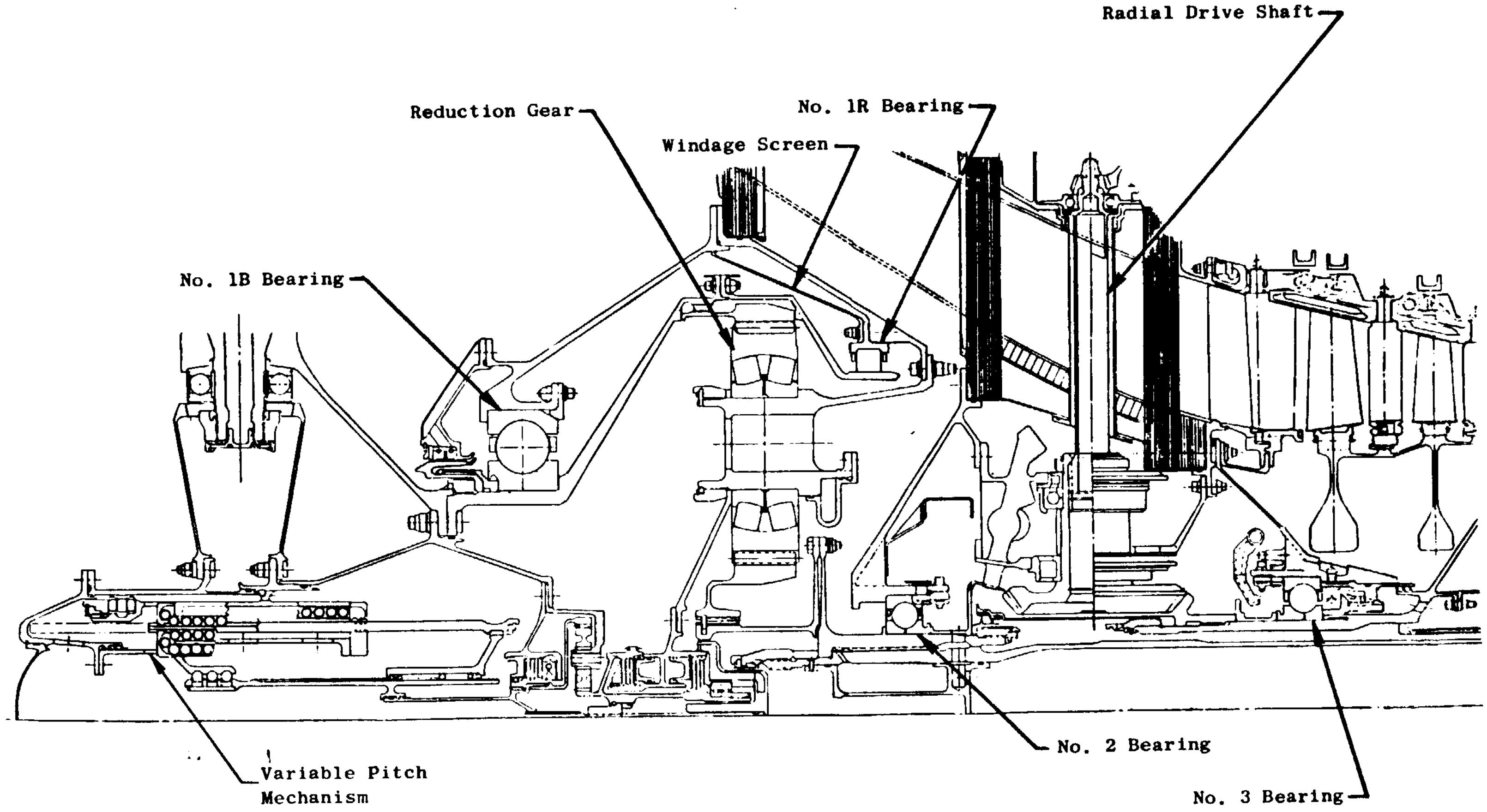
Radial Drive Shaft
Reduction Gear
No. 1R Bearing
Windage Screen
No. 1B Bearing
Variable Pitch Mechanism
No. 2 Bearing
No. 3 Bearing

Figure 12-17. UTW Forward Sump.

The No. 1R bearing has a flanged inner race which is mounted to the aft chrome-plated journal of the fan shaft. Rollers, cage, and outer race are mounted as an assembly to the reduction gear support housing. The bearing is lubricated by two jets mounted 180° apart in the reduction gear support on the aft side of the bearing. The bearing is preloaded with a radial interface to prevent skidding. Bearing race and roller material are AISI 52100. Bearing design information is presented in Table 12-XI.

Table 12-XI. No. 1R Bearing Design.

Bore Diameter	518 mm (20.39 in.)
Rotational Speed	3400 rpm
DN Value	1.76×10^6
No. of Rollers	60
Roller Diameter	18 mm (0.7087 in.)
Fatigue Life Exceeds	2×10^6 hrs

The LP turbine rotor No. 2 ball thrust bearing, which is identical to the corresponding bearing in the F101 engine, is made of M50 material and jet lubricated on both its forward and aft sides. The No. 3 HP rotor ball thrust bearing, identical to the corresponding F101 bearing, also is made of M50 material and jet lubricated on both sides. Oil from the aft jet cools the back face of the No. 3 carbon seal runner.

Fan shafting consists of two sections and is made of 17-4PH steel. The forward section is splined at its outer end to provide a torque connection between it and the main reduction ring gear. This shaft is flanged at the forward end to support the rotor disk. The shafting is supported at the forward end by the No. 1B bearing and at the aft end by the No. 1R bearing.

The outer cone that supports the star gear carrier of the main reduction gear is made of 17-4PH steel. This cone is bolted to the star gear carrier at its aft end, and is mounted to the forward inner ring of the composite frame at the forward end. This cone also supports the forward sump scavenge scoop/screen.

The No. 1B bearing support is made of 17-4PH steel. This housing supports both the No. 1B bearing and the No. 1 tandem carbon seal. Integral piping is incorporated in this housing to supply air to, and to drain leakage oil from, the carbon seal. The housing assembly is mounted to the forward inner ring of the composite frame.

The No. 2 bearing housing utilizes the inner casting from the F101 engine. A new conical shell and outer flange are required to mate with the composite frame. Two F101 internal bevel gear assemblies are mounted from the No. 2 bearing housing. Material for this housing is 6-4 titanium.

The No. 3 bearing housing is identical to that of the F101 with the exception that the extreme outer flange has been modified to accommodate a new fastener for mounting the housing to the aft ring of the composite frame. The housing, which is made from 6-4 titanium, provides support for the No. 3 carbon face seal and various lube jets.

Loading diagrams for the forward sump are presented in Figures 12-18 through 12-21 for both steady-state and blade-out conditions.

Shafting was designed using maximum steady-state stresses combined with maximum blade-out loads. Steady-state loading included torque, centrifugals, thermals, and thrust. The blade-out condition was 2-1/2 composite blades at maximum speed. Stresses in the No. 1B bearing housing were calculated from the resultant radial and axial load components transferred to the housing through the No. 1B bearing.

Star gear loads, as well as No. 1R bearing reactions, are carried by the reduction gear support housing. These loads were combined and used to calculate maximum stresses and deflections in this housing.

A flexible coupling is provided between the LP turbine shaft and the main reduction gear; the coupling is splined at the aft end to the LP turbine shaft and supported by the No. 2 bearing. The forward end is splined to the main reduction sun gear. This coupling is designed to accommodate misalignment between the reduction gears and the LP turbine shaft. The aft coupling section is made of 4340 steel. The forward coupling, which is mated to the reduction gear, is made of AISI 9310. Both the forward and aft sections are bolted together at the OD of the coupling diaphragms. Stresses for this coupling are shown in Figure 12-22.

12.5.2 Aft Sump

The aft sump, shown in Figure 12-23 with maximum steady-state temperatures, contains the No. 4 intershaft roller bearing which supports the aft end of the HP turbine rotor on the LP turbine shaft and the LP turbine shafting which is supported by roller bearing No. 5. The F101 LP turbine shaft has been analyzed and is acceptable for QCSEE.

The aft sump cavity is sealed on the forward end by a carbon piston ring intershaft seal and on the aft end by a tandem circumferential carbon oil seal. A new bearing housing supports the No. 5 bearing, No. 5 seal, No. 6 seal, and the balance piston cavity stationary hardware. An extension of LP turbine shafting is mounted to the aft end of the F101 shaft. This new shaft supports the balance piston four-tooth labyrinth/seal and also carries oil to the No. 4 bearing. Major modifications to the F101 aft sump hardware include the addition of a balance piston and the removal of the F101 aft sump metering/scavenge pump. The No. 4 intershaft roller bearing, which is made of M50 material, is lubricated through holes under the bearing inner race in the LP turbine shaft. The No. 5 bearing, also made of M50 material, is jet lubricated from its aft side.

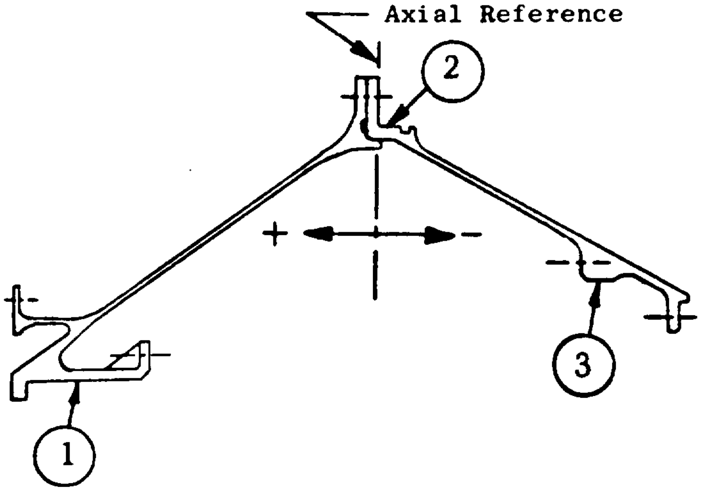

UTW Case 928

Steady State Loading

- Fan Torque 36,117 Nm (319,672 in.-lb)
- Turbine Torque 14,653 Nm (129,695 in.-lb)
- Fan Thrust 94,008 N (21,135 lb)
- Temperature 121° C (250° F)

Deflections

Point	Axial	Radial ↑	Rotational Radians +
1	0.0442 cm (0.0174 in.)	0.0210 cm (0.0082 in.)	-0.0005
2	————	0.0006 cm (0.0002 in.)	————
3	-0.0348 cm (-0.0137 in.)	0.0256 cm (0.0101 in.)	-0.0012

Figure 12-18. Forward Sump Stationary Structure Deflections.

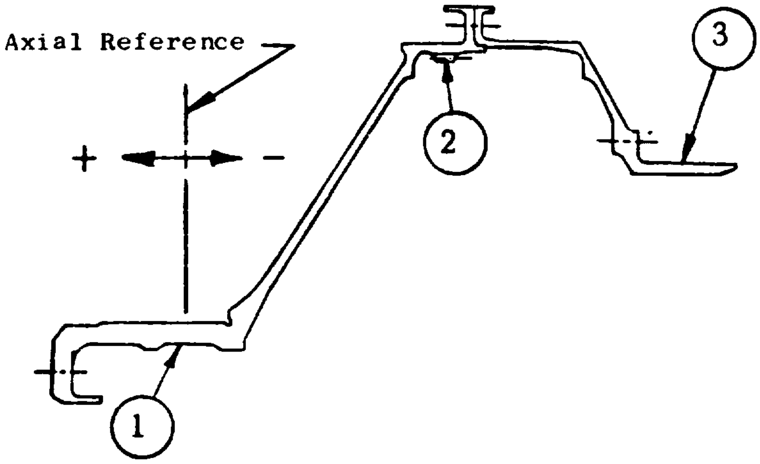

UTW Case 928

Steady-State Loading

● Fan Torque	36,117 Nm (319,672 in.-lb)
● Fan Speed	3,120 rpm
● Fan Thrust	94,008 N (21,135 lb)
● Temperature	121° C (250° F)

	Deflections		
Point	Axial	Radial ↑	Rotational Radians ↷+
1	0	0.0153 cm (0.0060 in.)	0.0003
2	-0.0257 cm (-0.0101 in.)	0.0455 cm (0.0179 in.)	0.0006
3	-0.0401 cm (-0.0158 in.)	0.0197 cm (0.0078 in.)	0.0034

Figure 12-19. Forward Sump Rotating Structure Deflections.

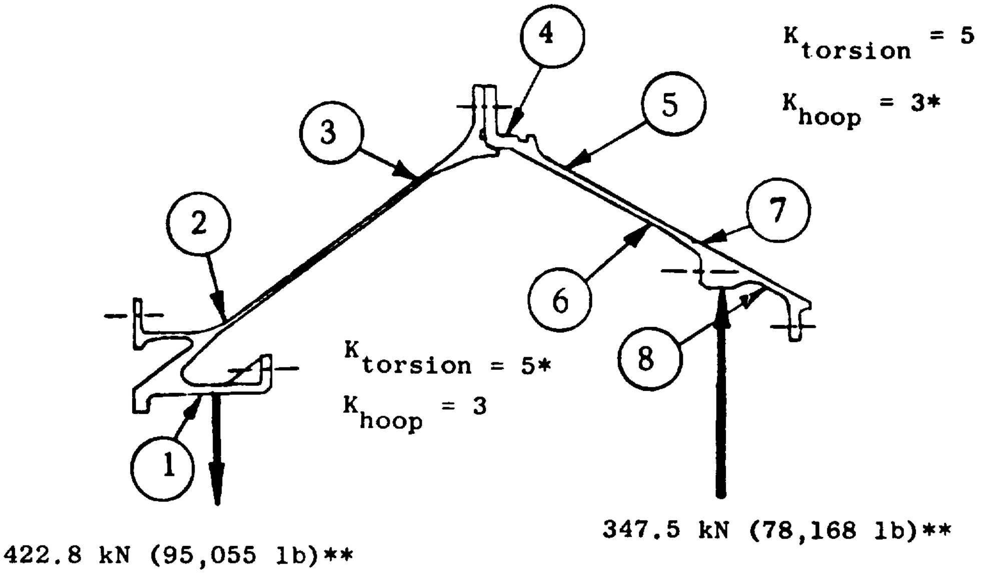
4
$K_{torsion} = 5$
$K_{hoop} = 3$*
3
5
2
7
6
8
$K_{torsion} = 5$*
$K_{hoop} = 3$
1
347.5 kN (78,168 lb)**
422.8 kN (95,055 lb)**

Point	Steady-State Effective Stress kN/cm^2 (ksi)	2-1/2 Composite Blades Out ** Effective Stress kN/cm^2 (ksi)
1	2.62 (3.8)	22.6 (32.8)
2	1.97 (2.9)	46.3 (67.1)
3	27.6 (40.0)	38.0 (55.2)
4	23.5 (34.1)	41.0 (59.4)
5	35.4 (51.4)	58.8 (85.3)
6	34.0 (49.3)	52.9 (76.8)
7	8.34 (12.1)	12.6 (18.3)
8	11.3 (16.5)	18.8 (27.2)

17-4PH Steel - Rc 33/36
Min 0.2% Yield = 82.7 kN/cm^2 at 121° C (120 ksi at 250° F)
Min Ultimate = 95.8 kN/cm^2 at 121° C (139 ksi at 250° F)

* Stress Concentrations Included in Tabulated Stresses

Figure 12-20. Forward Sump Stationary Structure Stresses.

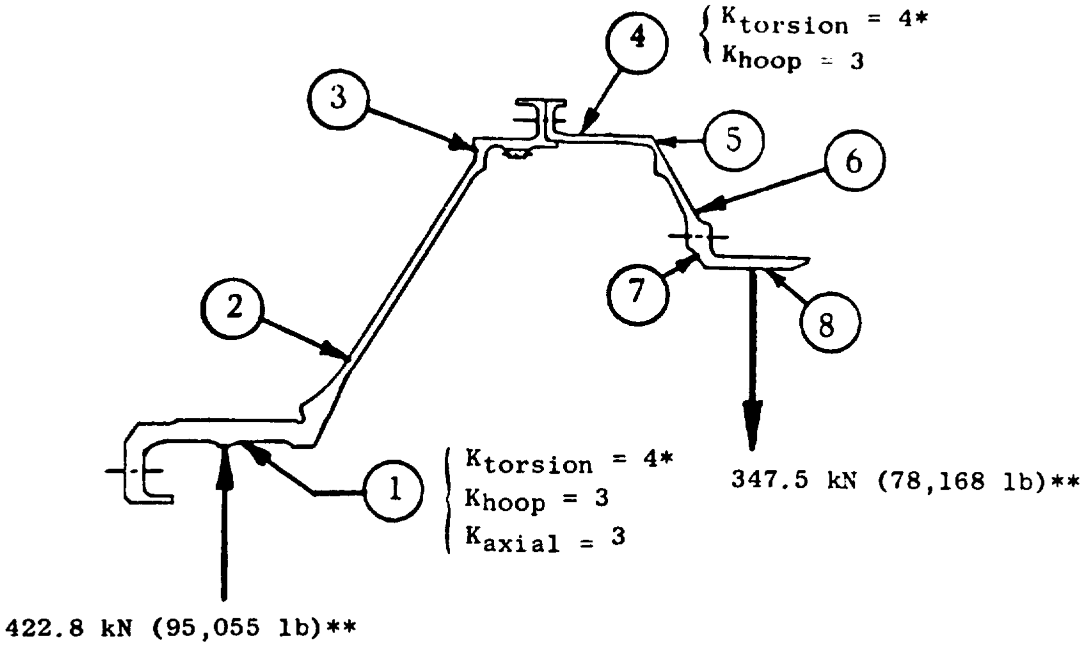

4
$K_{torsion}$ = 4*
K_{hoop} = 3
3
5
6
7
2
8
1
$K_{torsion}$ = 4*
K_{hoop} = 3
K_{axial} = 3
347.5 kN (78,168 lb)**
422.8 kN (95,055 lb)**

Point	Steady-State Effective Stress kN/cm^2 (ksi)	2-1/2 Composite Blades Out ** Effective Stress kN/cm^2 (ksi)
1	9.31 (13.5)	13.7 (19.8)
2	9.9 (14.5)	51.9 (75.4)
3	14.9 (21.6)	18.7 (27.2)
4	13.6 (19.7)	24.3 (35.2)
5	13.3 (19.3)	22.1 (32.2)
6	12.1 (17.6)	21.7 (31.5)
7	27.4 (10.7)	14.7 (21.2)
8	13.2 (19.1)	23.2 (33.6)

17-4PH Steel - Rc 33/36

Min 0.2% Yield = 82.7 kN/cm^2 at 121° C (120 ksi at 250° F)

Min Ultimate = 95.8 kN/cm^2 at 121° C (139 ksi at 250° F)

* Stress Concentrations Included in Tabulated Stresses

Figure 12-21. Forward Sump Rotating Structure Stresses.

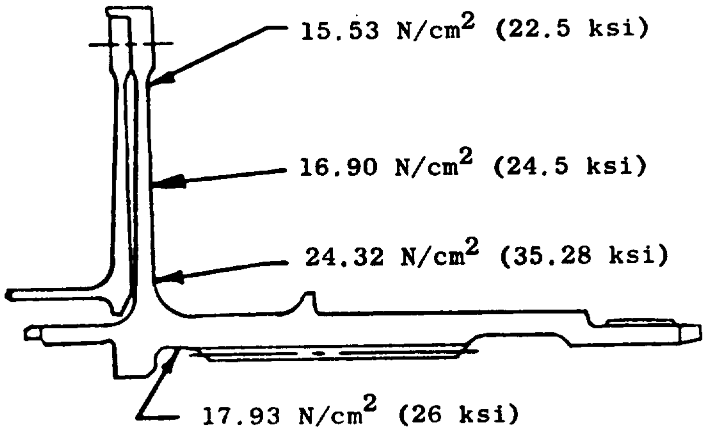
15.53 N/cm^2 (22.5 ksi)
16.90 N/cm^2 (24.5 ksi)
24.32 N/cm^2 (35.28 ksi)
17.93 N/cm^2 (26 ksi)

UTW Case 928

Steady-State Loading

LPT Speed	7,690 rpm
LPT Torque	14,653 Nm (129,695 in.-lb)
Temperature	121° C (250° F)

AISI 4340 Steel

Min. 0.2% Yield = 68.9 kN/cm^2 at 121° C (100 ksi at 250° F)

For a 0.051 cm (0.020 in.) Offset Max. Alternating Stress is 12.4 kN/cm^2 (18 ksi)

Figure 12-22. Flex Coupling Stresses.

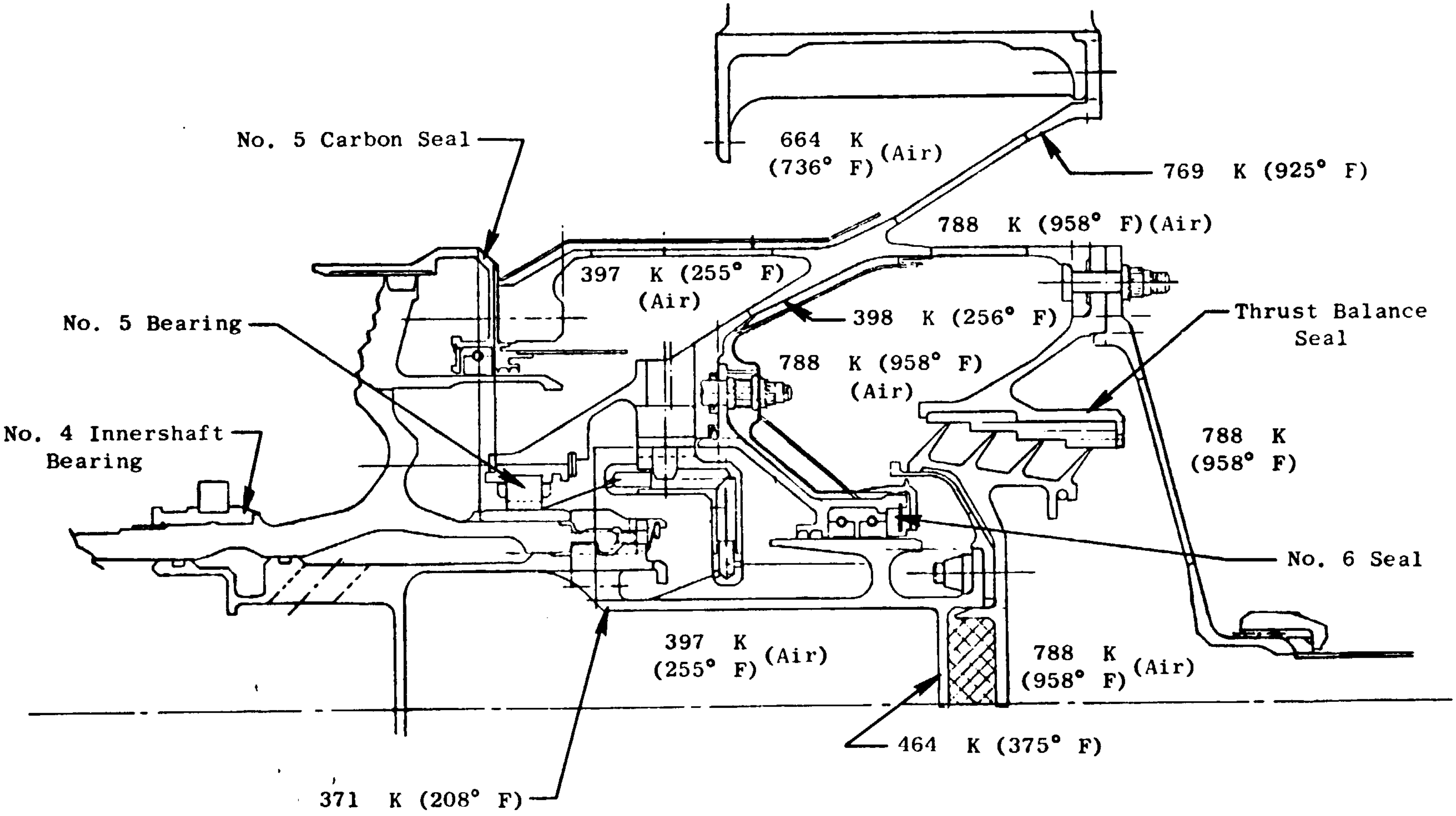
No. 5 Carbon Seal
664 K (736° F) (Air)
769 K (925° F)
788 K (958° F)(Air)
397 K (255° F) (Air)
No. 5 Bearing
398 K (256° F)
Thrust Balance Seal
788 K (958° F) (Air)
No. 4 Innershaft Bearing
788 K (958° F)
No. 6 Seal
397 K (255° F) (Air)
788 K (958° F) (Air)
464 K (375° F)
371 K (208° F)

Figure 12-23. UTW Maximum Steady-State Temperatures.

A tandem carbon seal is located between the No. 5 bearing and the balance piston cavity. The carbons are retained in a small support housing made of Inco 718 and mounted to the No. 5 bearing support cone. The seal runner is made of Inco 718, and coated with tungsten carbide to provide a hard running surface. This runner is integral with the new section of aft shafting and is cooled by oil dispersed from the aft side of the same jet assembly which feeds the No. 4 and No. 5 bearings. Seal design information is presented in Table 12-XII.

Table 12-XII. No. 6 Seal Design.

Bore Diameter	10.4 cm (4.1 in.)
Rotational Speed	8040 rpm
Surface Speed	365.8 cm/sec (144 ft/sec)
Delta Pressure	4.14 N/cm^2 (6 psid)
Max Supply Air Temp	263° C (505° F)
Rubbing Surface Heat Generation	272.6 J/sec (15.5 Btu/min)
Oil Flow Rate	37.9 cm^3/sec (0.6 gpm)
Projected Minimum Seal Life	>10,000 hours

The balance piston cavity is formed by a four-tooth, slant-stepped labyrinth seal made of Inco 718 and bolted to the aft end of the LP turbine shaft extension. Seal nominal diameter is 17.15 cm (6.75 in.). The seal teeth are designed for a one-to-one height-to-pitch ratio. This rotating seal is insulated from the shafting by a combination of insulating material and a metal heat shield. The seal teeth are coated with aluminum oxide to improve their ability to withstand a rub. The stationary rub surface for this seal is made of Hastelloy X abradable 1/32 hex cell honeycomb with a ribbon thickness of 0.0076 cm (0.003 inch). The honeycomb is brazed into an Inco 718 support. This support is mounted to a flange on the No. 5 bearing housing.

The No. 5 bearing, No. 6 seal, and balance piston stationary seal hardware are supported by a new Inco 718 housing which is mounted to the aft end of the turbine frame. This housing also provides a sump cavity with attachments for oil service lines.

All other aft sump hardware such as seals, spacers, and structural shafting are common between the F101 and UTW engines.

Loading diagrams for the aft sump are presented in Figures 12-24 through 12-27 for both steady-state and blade-out conditions.

Maximum stresses for the aft sump were calculated using steady-state operating conditions combined with stresses resulting from 2-1/2 composite blades out. Steady-state loads are not as severe as those in the F101 engine due to reduced UTW horsepower requirements. The No. 5 bearing support housing stresses were calculated including resultant loads from the LP turbine frame assembly.

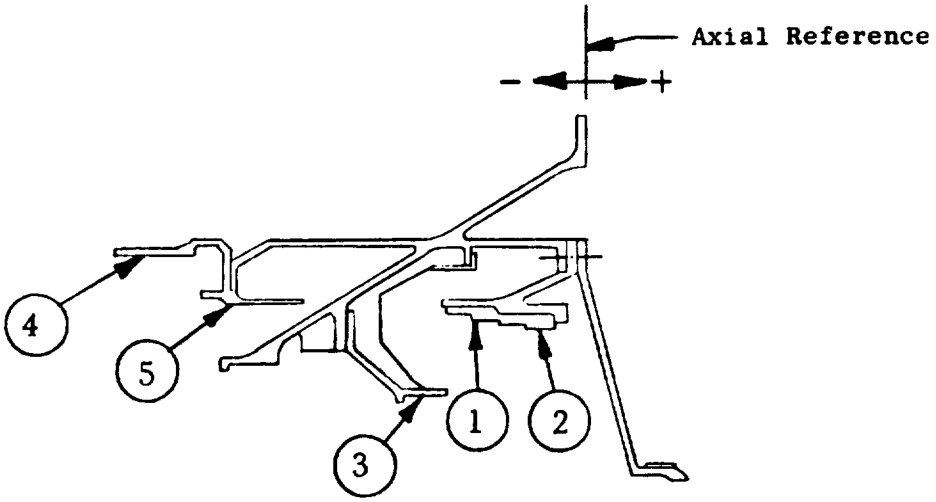

UTW Case 928

Steady-State Loading

Deflections

Point	Axial	Radial ↑+	Rotational Radians ↶+
1	0.0167 cm (0.00658 in.)	0.0622 cm (0.0245 in.)	0.000729
2	0.00574 cm (0.00226 in.)	0.0592 cm (0.0233 in.)	-0.000587
3	0.00299 cm (0.00118 in.)	0.0147 cm (0.0058 in.)	-0.0185
4	-0.0256 cm (-0.0101 in.)	0.0518 cm (0.0204 in.)	0.00039
5	-0.0274 cm (-0.0108 in.)	0.0224 cm (0.0088 in.)	0.00438

Figure 12-24. Aft Sump Stationary Structure Deflections.

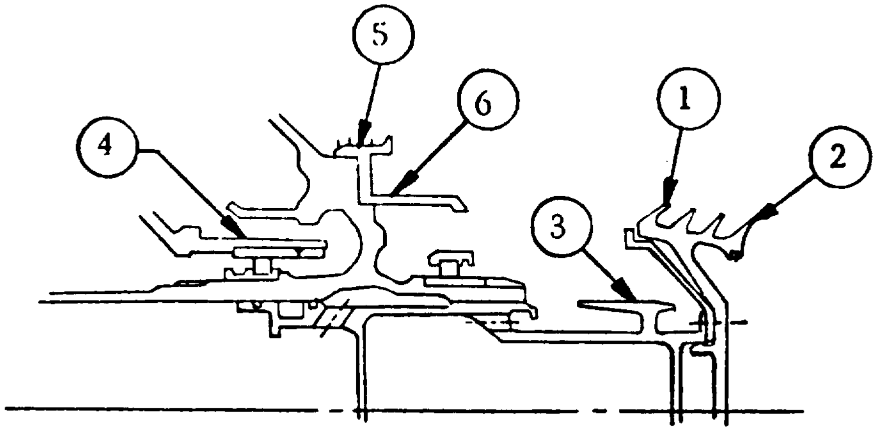

UTW Case 928

Steady-State Loading

- Turbine Speed = 8050 rpm

Deflections

Point	Axial+ →	Radial+ ↑	Rotational Radians ↶+
1	0.0500 cm (0.01969 in.)	0.0592 cm (0.0233 in.)	0.0027
2	0.0749 cm (0.0295 in.)	0.0582 cm (0.0229 in.)	-0.003
3	0.0536 cm (0.0211 in.)	0.0264 cm (0.0104 in.)	0.0039
4	0.0396 cm (0.0156 in.)	0.04541 cm (0.0179 in.)	0.0029
5	0.0671 cm (0.0264 in.)	0.0379 cm (0.0149 in.)	0.0044
6	0.0625 cm (0.0246 in.)	0.01725 cm (0.00679 in.)	0.0036

Figure 12-25. Aft Sump Rotating Structure Deflections.

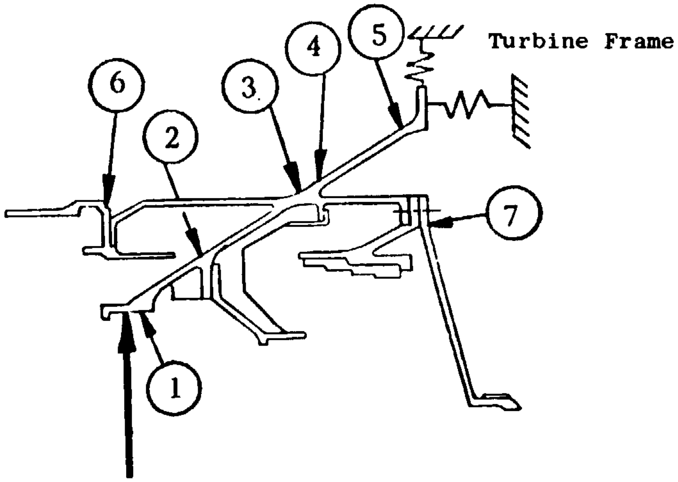

Point	Steady State Effective Stress kN/cm^2 (ksi)	2-1/2 Composite UTW * Blades Out Effective Stress kN/cm^2 (ksi)	Kt**	Temperature ° C (° F)	Min 0.2% Yield kN/cm^2 (ksi)	Min Ultimate kN/cm^2 (ksi)
1	0.43 (0.62)	19.2 (27.8)	--	123° (254°)	97.6 (141.5)	120.0 (174)
2	12.4 (18)	22.2 (32.2)	3.0	139° (283°)	96.9 (140.5)	119.3 (173)
3	6.9 (10)	8.55 (12.4)	--	276° (528°)	93.7 (135.9)	113.8 (165)
4	7.7 (11.2)	22.88 (33.2)	1.6	320° (608°)	87.6 (127)	112.4 (163)
5	7.7 (11.2)	31.7 (46.0)	1.6	495° (925°)	82.0 (119)	105.5 (153)
6	15.2 (22)	6.69 (9.7)	--	276° (528°)	93.7 (135.9)	113.8 (165)
7	6.2 (9)	2.73 (3.96)	--	514° (958°)	89.6 (130)	110.3 (160)

● Material = Inconel 718

** Stress Concentrations Included In Tabulated Stresses.

Figure 12-26. Aft Sump Stationary Structure Stresses.

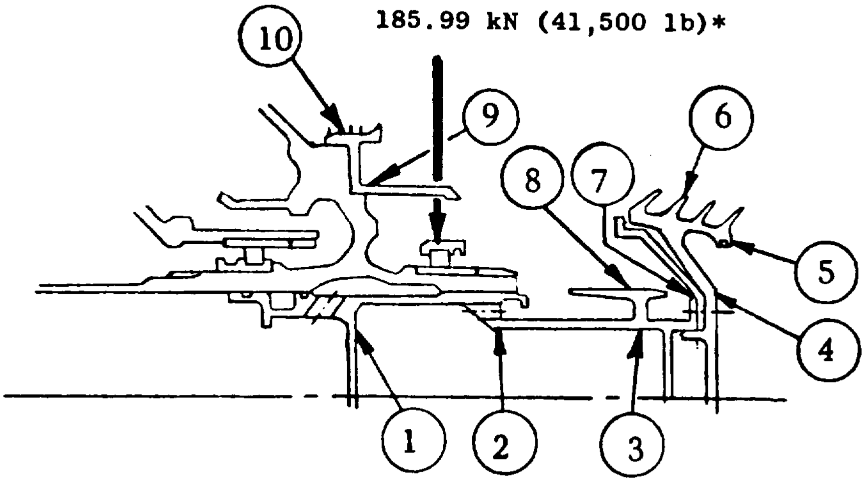

Point	Steady-State Effective Stress kN/cm^2 (ksi)	2-1/2 Composite UTW * Blades Out Effective Stress kN/cm^2 (ksi)
1	47.8 (69.3)	48.3 (70.0)
2	5.04 (7.3)	5.04 (7.3)
3	19.5 (28.3)	19.5 (28.3)
4	43.4 (62.9)	43.3 (62.9)
5	7.5 (10.9)	7.5 (10.9)
6	1.24 (1.8)	1.24 (1.8)
7	28.3 (41.0)	28.3 (41.0)
8	8.83 (12.8)	8.83 (12.8)
9	20.8 (30.1)	20.8 (30.1)
10	37.7 (54.7)	37.7 (54.7)

- Material = Inconel 718
- Minimum 0.2% Yield = 82.0 kN/cm^2 At 495° C (119 ksi At 925° F)
- Minimum Ultimate = 105.5 kN/cm^2 At 495° C (153 ksi At 925° F)

Figure 12-27. Aft Sump Rotating Structure Stresses.

12.6 ACCESSORY DRIVE DESIGN

Engine accessory power is extracted from the core engine shaft through right angle bevel gearing, and transmitted through radial drive shafting to a top-mounted accessory gearbox and to a scavenge pump gearbox mounted in the core cavity area on the bottom vertical. To minimize frontal area projection of the engine, the accessory gearbox is configured to match the width of the pylon strut. Mounted to and driven from the accessory gearbox are the following components:

- Fuel pump and control
- Lube supply pump
- Hydraulic pump
- Control alternator
- Starter

The drive system is shown schematically in Figures 12-28 and 12-29. The internal right angle bevel gearing utilizes two sets of F101 bevel gears. Splined to the main engine shaft is a 47-tooth gear which drives 35-tooth gears mounted in two individual gear housings. Figure 12-30 shows one of these gear housing assemblies. To utilize these gear assemblies, they are rotated about the vertical gear centerline to mount to the aft side of the No. 2 bearing housing instead of just forward of the No. 3 bearing housing, as is the case in the F101 engine. Larger moment loads associated with this system require a support between the fan frame aft flange and the bevel gear housing. The OTW engine design loads are presented in Table 12-XIII. Results indicate that adequate margin exists for the UTW engine test program.

Table 12-XIII. Inlet Gearbox Design Data.

Maximum started torque loads	339 mN (250 ft-lb)
Maximum accessory horsepower	125 kW (167 hp)
Equivalent horsepower (for bearing design)	53 kW (71 hp)
Calculated bearing design life(1)	750,000 hr

---

(1) Based on an M50 material factor of five.

Gears and bearing materials are AISI 9310 and CEVM-M50, respectively, and the housing is investment-cast 17-4PH. The lubrication system is similar to that of the F101 engine with modifications to the internal lube manifold.

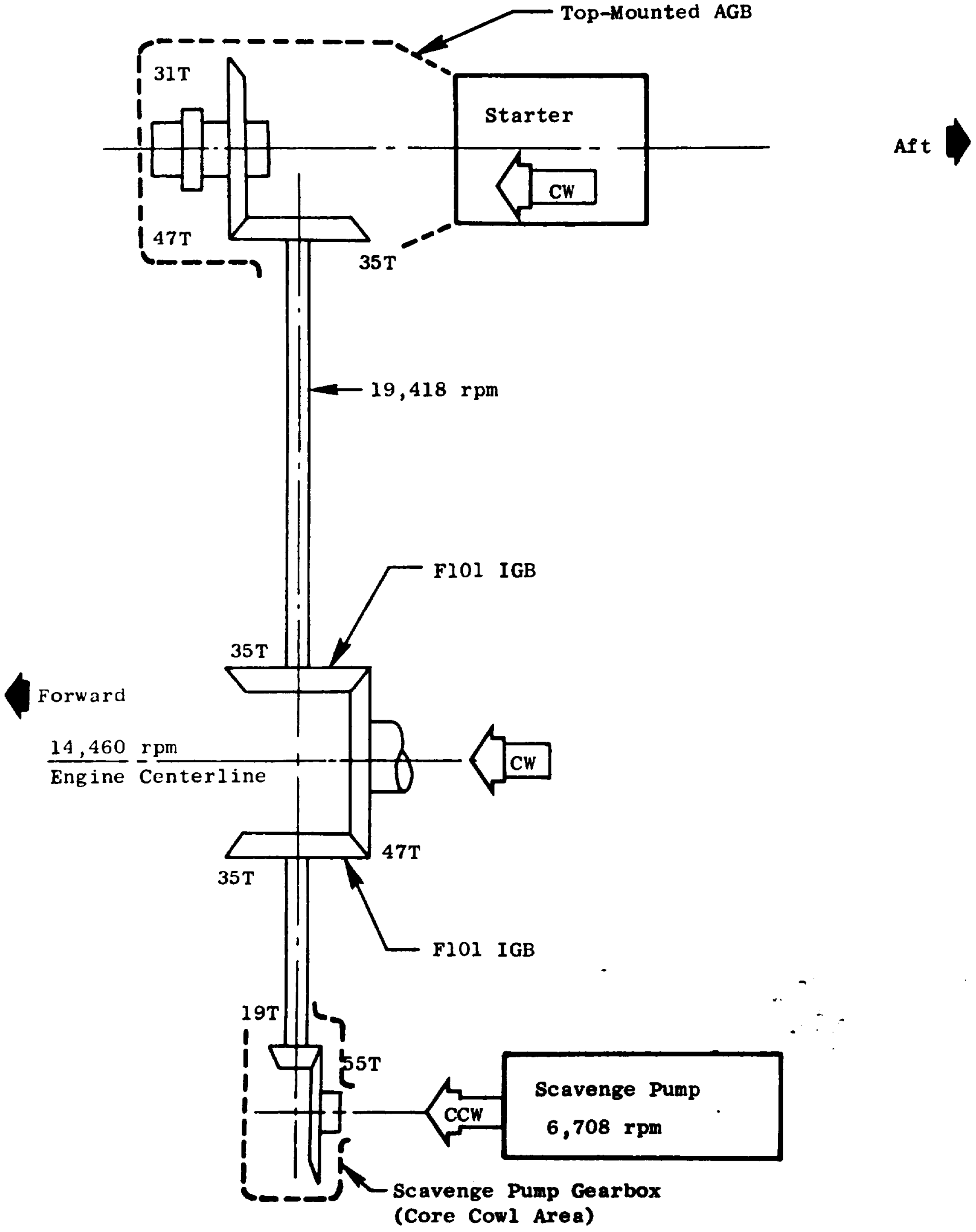
Top-Mounted AGB
31T
47T
35T
Starter
CW
Aft
19,418 rpm
F101 IGB
35T
Forward
14,460 rpm
Engine Centerline
CW
47T
35T
F101 IGB
19T
55T
Scavenge Pump
6,708 rpm
CCW
Scavenge Pump Gearbox
(Core Cowl Area)

Figure 12-28. Accessory Drive System.

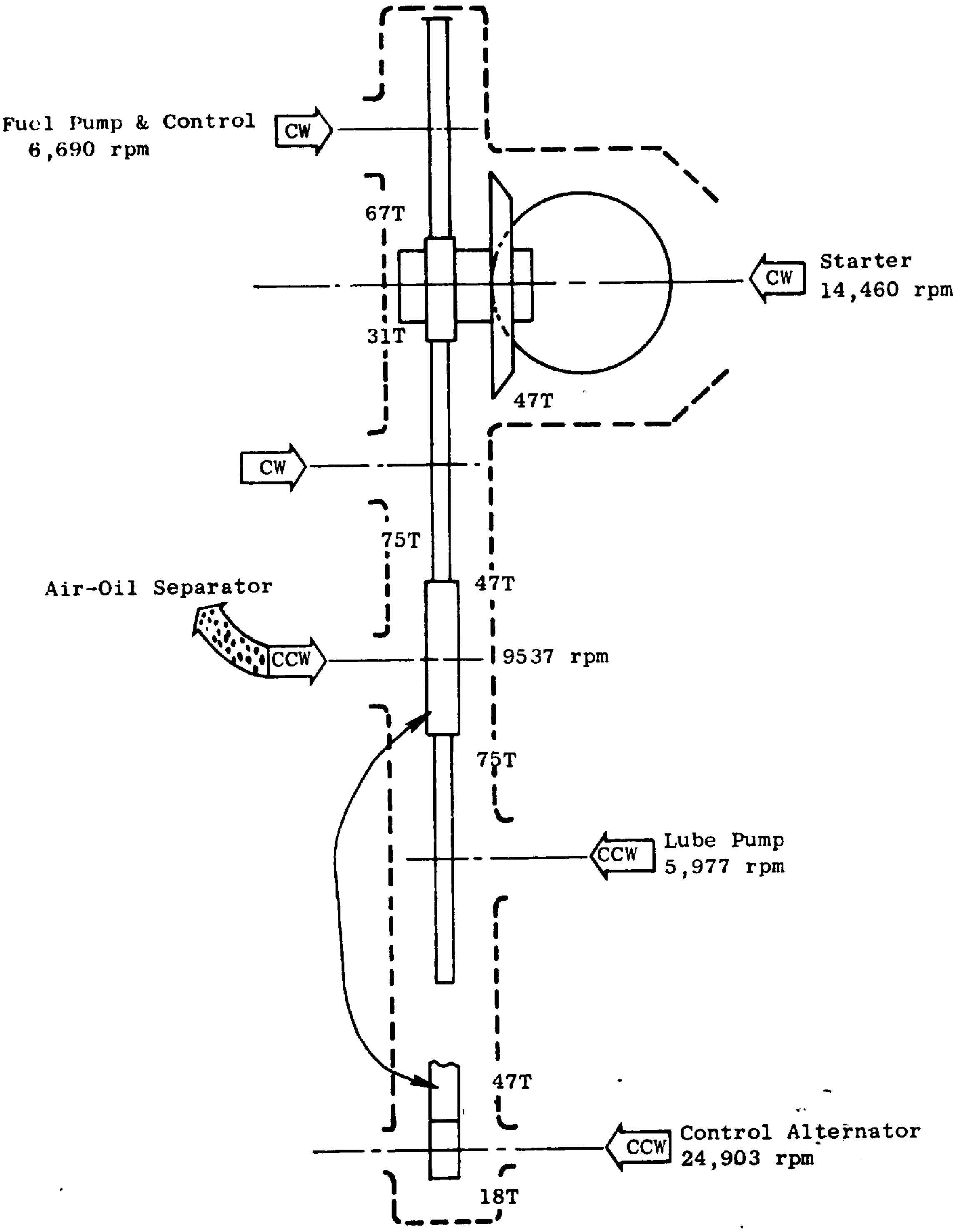
Fuel Pump & Control
6,690 rpm
CW
67T
31T
47T
Starter
14,460 rpm
CW
CW
75T
47T
Air-Oil Separator
CCW
9537 rpm
75T
Lube Pump
5,977 rpm
CCW
47T
Control Alternator
24,903 rpm
CCW
18T

Figure 12-29. Accessory Gearbox System.

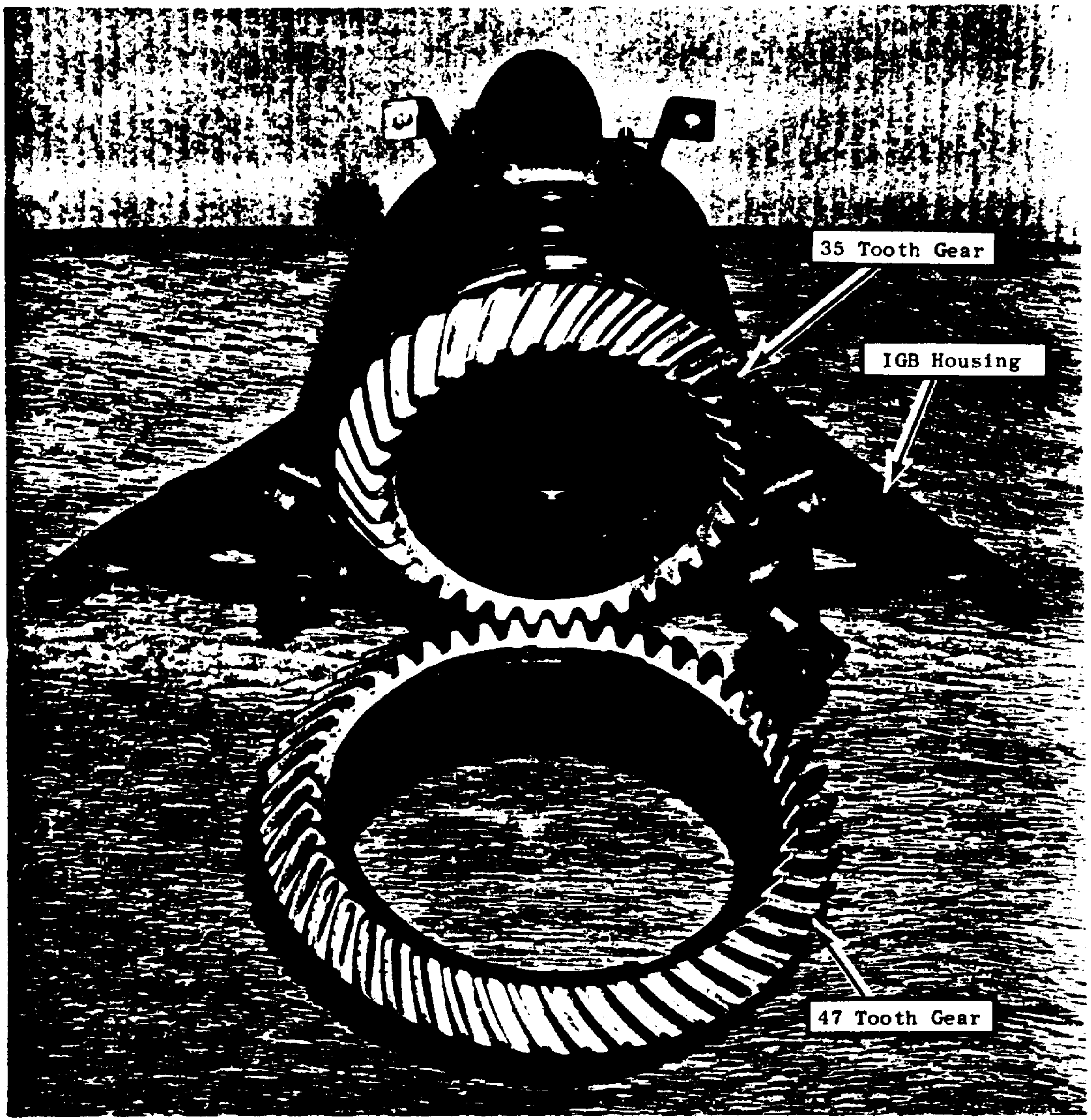
35 Tooth Gear
IGB Housing
47 Tooth Gear

Figure 12-30. Inlet Gearbox Assembly.

The bevel gears driving the bottom-mounted scavenge pump in the experimental engine are lightly loaded. Design optimization is required for the flight configuration. For the flight design, the 35-tooth gears driving the top accessory gearbox and the bottom scavenge pump are mounted in a common housing.

The one-piece radial drive shaft between the internal bevel gear and accessory gearbox has a central support bearing to keep the critical speed approximately 25% above shaft operating speed. The bearing is mounted in a machined housing which is bolted to the aft composite ring of the fan frame. Provisions are made in the top accessory gearbox for access to the radial drive shaft to raise it up approximately 3.81 cm (1.5 in.) so that the internal gearboxes can be removed without removing the top accessory gearbox. The center hole of the shaft is used to vent the sumps to the accessory gearbox. The shaft material is AISI 4340 and the splines are induction hardened.

The shaft between the internal bevel gears and the bottom-mounted scavenge pump gearbox does not require a central support bearing because of its short length.

12.6.1 Accessory Gearbox

A cross section and external view of the top-mounted accessory gearbox are presented in Figures 12-31 and 12-32, respectively.

The accessory gearbox uses F101 bevel gears, spur gears, and bearings. One new bevel gear is required, and it will be made from an F101 forging. The spur and bevel gears are 10 and 7.100 diametral pitch, respectively, and are case-carburized AISI 9310 material. All bearings are CEVM-M50 material. The bearings are assembled in steel liners in the aluminum casing, and all outer races are keyed to prevent rotation.

F101 carbon face seals are used on the rotating gear shafts. Two new "gasko" seals have been designed to seal interfaces between the gearbox main housing and the adapters.

A new cast aluminum (AMS 4217) housing has been designed to fit in front of the pylon. The main casing is a one-piece design utilizing forward and aft adapters. These adapters also are cast aluminum (AMS 4217). These are machined from forged aluminum bars.

Gear and bearing cooling and lubrication are accomplished in a manner similar to other General Electric gearbox designs. The lower bevel gear is shrouded to facilitate scavenging of oil to the forward sump. An air-oil separator attached to the 47-tooth spur gear provides oil separation for the sump vent system before venting overboard. The air-oil separator is the same as that used in F101 MQT vent systems.

Pad	rpm
Starter	14,460
Fuel Pump	6,690
A/O Separator	9,537
Lube Pump	5,977
Alternator	24,903

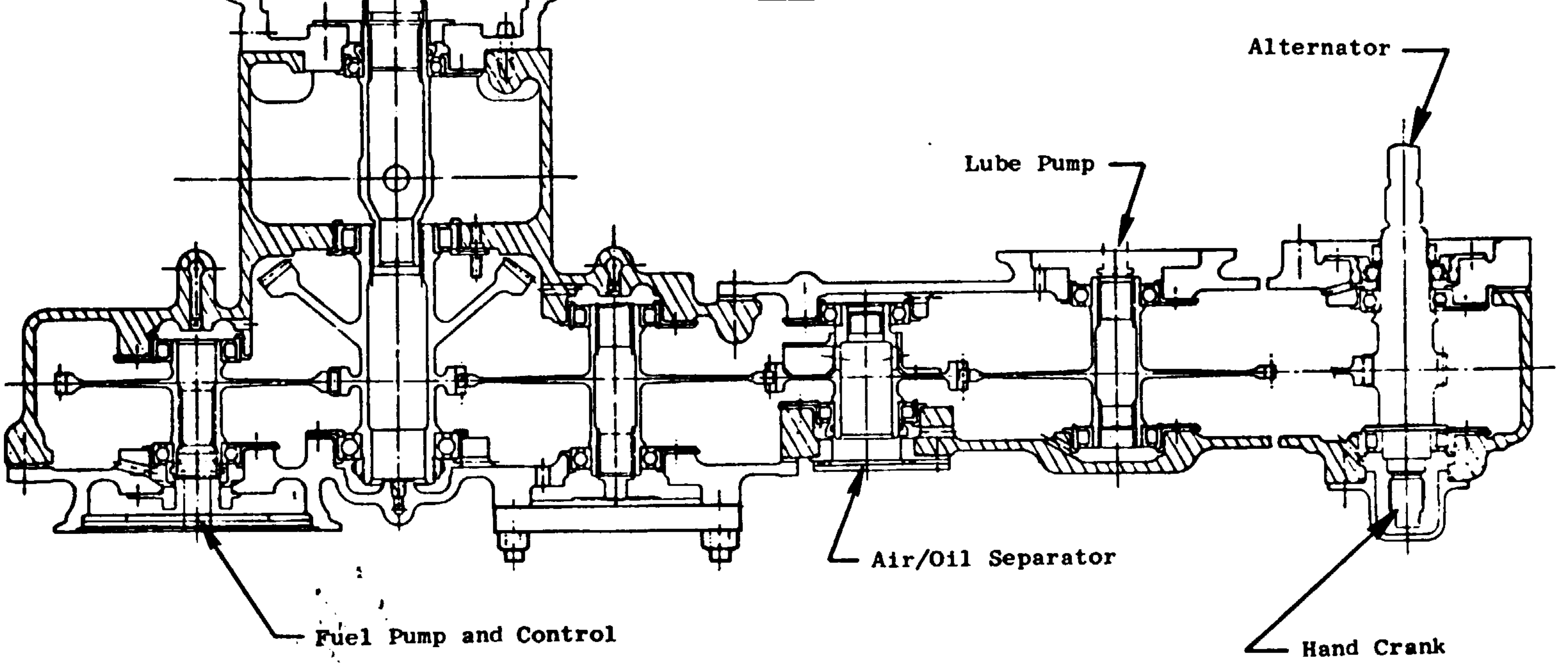
Starter
Alternator
Lube Pump
Air/Oil Separator
Fuel Pump and Control
Hand Crank

Figure 12-31. Accessory Gearbox.

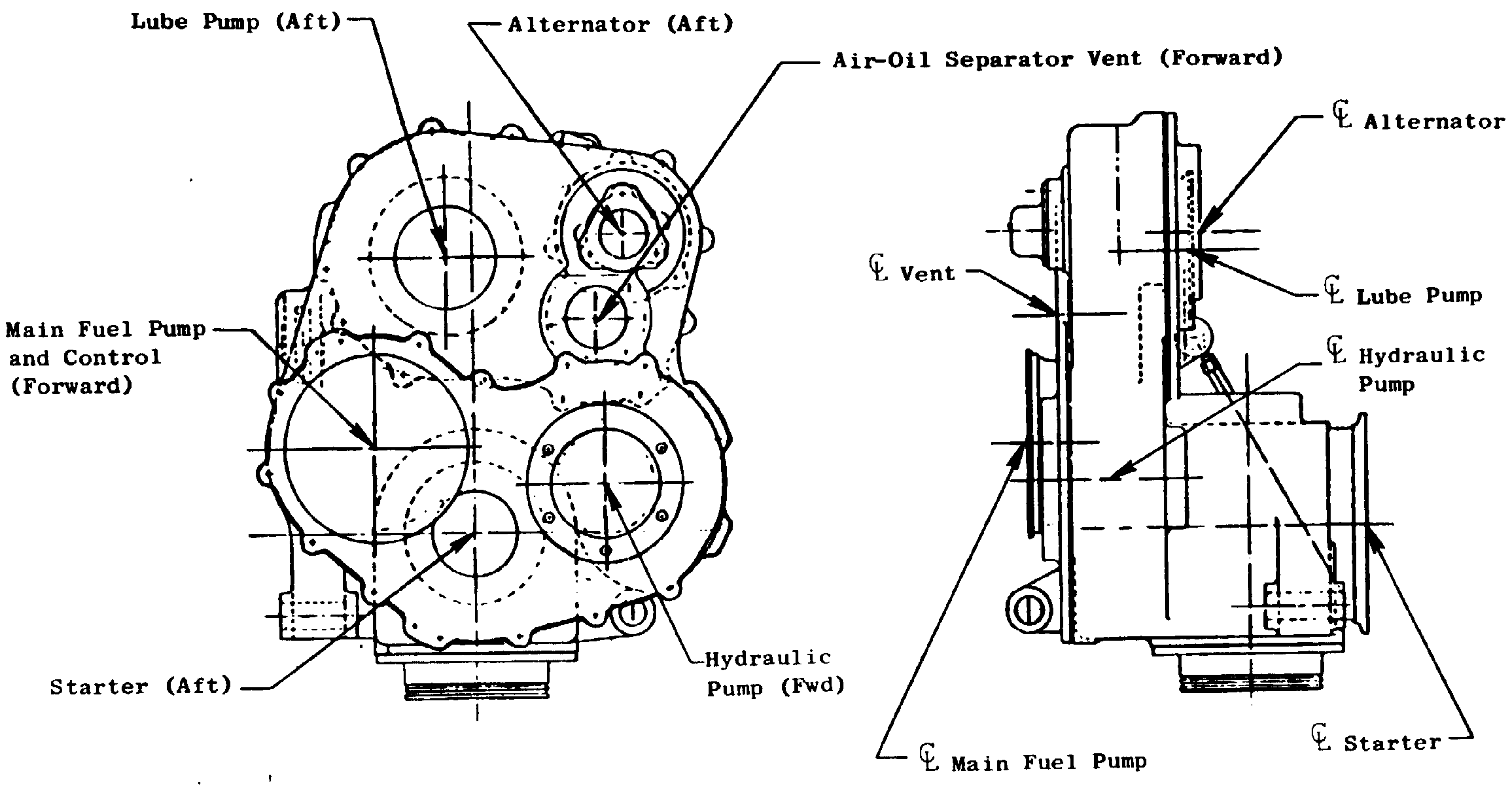
Lube Pump (Aft)
Alternator (Aft)
Air-Oil Separator Vent (Forward)
Main Fuel Pump and Control (Forward)
Starter (Aft)
Hydraulic Pump (Fwd)
℄ Alternator
℄ Vent
℄ Lube Pump
℄ Hydraulic Pump
℄ Main Fuel Pump
℄ Starter

Forward Looking Aft

Figure 12-32. Accessory Gearbox Housing.

The maximum calculated gear tooth bending stress and compressive stress (Hertz) are 27,580 N/cm^2 (40,000 psi) and 113,078 N/cm^2 (164,000 psi), respectively. With applicable factors, the material allows tooth bending and compressive stresses of 33,096 N/cm^2 (48,000 psi) and 137,900 N/cm^2 (200,000 psi), respectively. The lowest calculated bearing life is 58,000 hours which is more than adequate for the UTW engine test program.

The accessory gearbox provides drive pads for the fuel pump/control, lube supply pump, hydraulic pump, control alternator, and starter. Provisions are made to hand crank the drive system through the 18-tooth gear shaft should that be necessary.

The fuel pump/control is the same as that of the F101 with the exception of some modifications in the control area. The lube pump is basically a CF6 lube pump with all its elements manifolded together, and a new quill drive shaft to fit the F101 gear shaft. The control alternator is adapted from the F101 engine.

The starter is based on an existing design modified to be compatible with the QCSEE accessory gearbox. These modifications include:

1. Provisions for a lubricated drive spline with oil being supplied from the accessory gearbox
2. The clutch has been adjusted to be compatible with the minimum engine idle speed
3. The QAD (quick-attach-detach) housing was eliminated from the starter and incorporated into the accessory gearbox.
4. The air inlet flange position has been made adjustable circumferentially

Design features of the starter include a single-stage, radial-inflow turbine wheel, turbine nozzle, compound reduction gearing, pawl and ratchet-type engaging mechanism, and an output shaft splined to mate with the engine drive shaft.

The radial inflow turbine eliminates the need for an air access hole in the main engine mount located aft of the starter.

Shown in Figure 12-33 is the predicted starter torque characteristics at various pressure ratios. Starter torques at pressure ratios greater than 4 to 1 are above the anticipated engine lightoff point. Facility capability up to pressure ratios of approximately 5 to 1 is being provided. The program scope does not allow for optimization of starting time and it is anticipated that start time will be approximately 60 seconds.

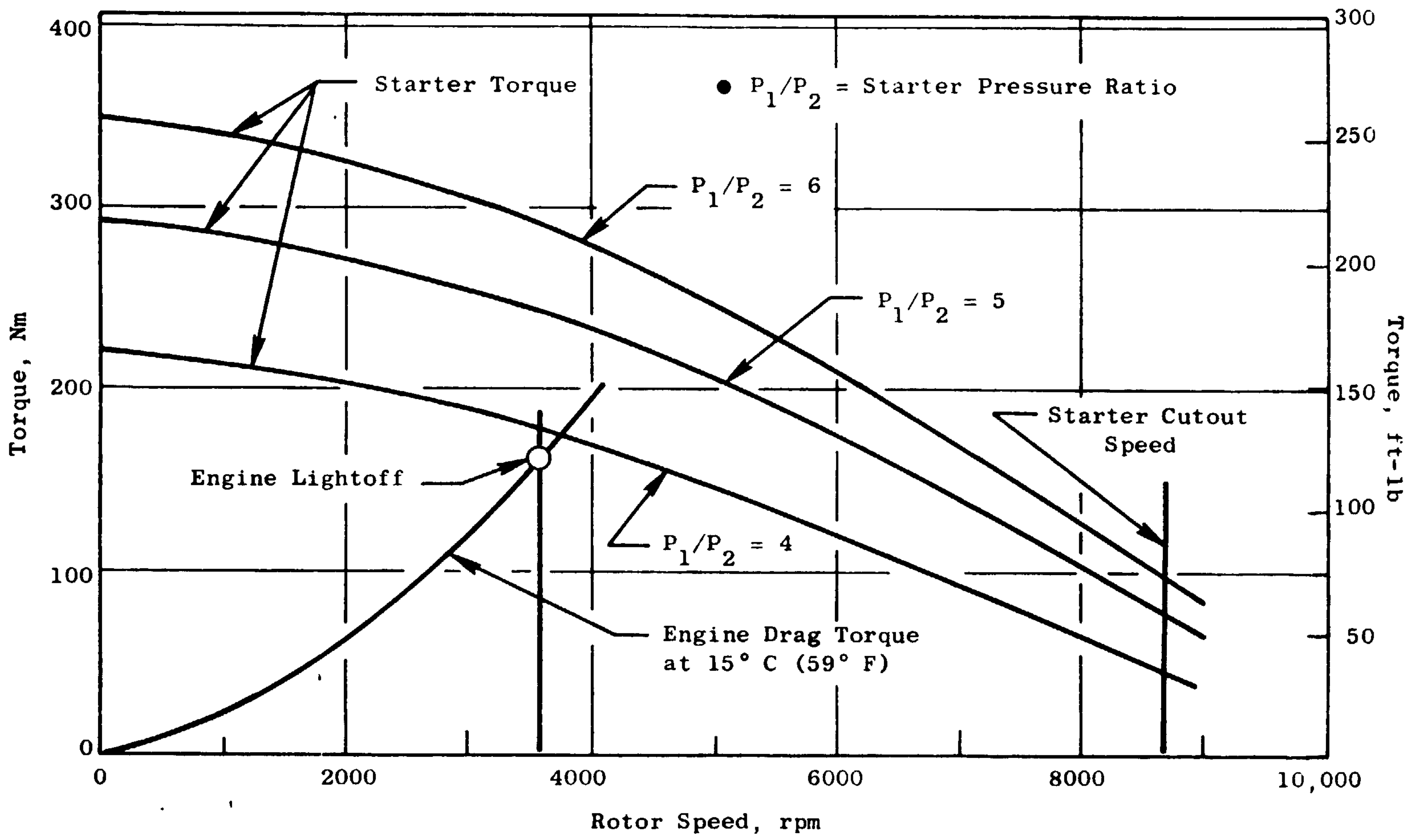

Figure 12-33. Starter Torque Vs. Rotor rpm at Various Starter Pressure Ratios.

12.6.2 Scavenge Pump

As shown in Figure 12-34, a short radial shaft connects the lower internal gearbox to a right-angle drive to power the scavenge pump. This gearbox is located in the core cowl region between the fan frame mid- and aft composite rings. The gears have been selected to reduce the radial shaft speed from 19,418 rpm to the pump input speed of 6708 rpm. Radial access to the gears and shafting is accomplished by a plug in the bottom of the gearbox and an access panel in the fan flowpath liner between adjacent vanes.

The gears are carburized AISI 9310. Basic gear information is as follows:

	Gear Data	
	Pinion	Gear
Number of teeth	19	55
Diametral Pitch	16	16
Pressure angle	20°	20°
Spiral angle	35°	35°

The capacity of this gear set is calculated at 53 kw (71 hp), which greatly exceeds the maximum calculated pump requirements of 6.7 kw (9 hp).

Bearings are CEVM-M50 material. The lowest calculated bearing life of 52,000 hours is more than adequate for the UTW engine.

The housing and mounting adapter are case aluminum (AMS 4217).

The gear mesh and bearings are jet and splash lubricated, respectively, and the horizontal gear is shrouded to facilitate scavenging of the gear casing. Provisions are made to lubricate the pump spline.

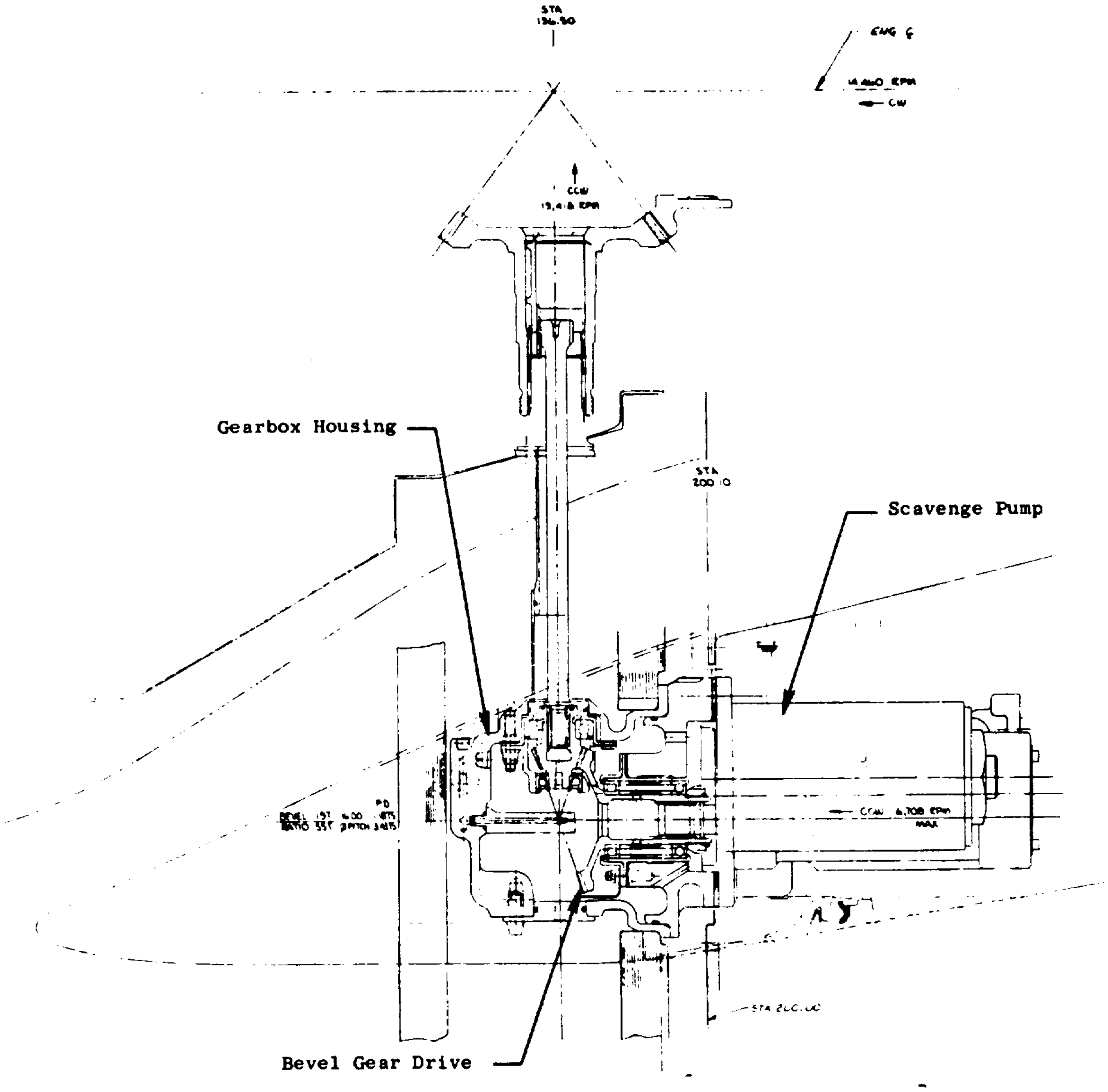
STA 136.50
ENG ℄
14,440 RPM
CW
CCW
13,418 RPM
Gearbox Housing
STA 200.10
Scavenge Pump
PD
BEVEL 19T
RATIO 55T
CCW 6,708 RPM MAX
Bevel Gear Drive

Figure 12-34. Scavenge Pump and Drive System.

SECTION 13.0

CONTROLS AND ACCESSORIES DESIGN

13.1 SUMMARY

The UTW engine control system controls four variables - fuel flow, fan pitch, fan nozzle area, and compressor stator angle - to achieve an optimum balance between thrust, fuel consumption, noise, and exhaust pollution goals.

The design incorporates two basic control components, a modified F101 hydromechanical fuel control and an engine-mounted digital electronic control designed specifically for the QCSEE engines. The latter provides the primary control and limiting of engine variables with the hydromechanical control acting as a backup and providing additional limits.

The system includes both automatic and manual operating modes. The automatic mode provides integrated control of engine variables to allow exploration of steady-state and transient characteristics of the engine when automatically controlled. Several different automatic modes options will be explored. The manual mode and several partial automatic/partial manual modes are provided to allow independent manipulation of controlled variables so that engine characteristics can be completely mapped. In addition, a remote mode is provided in which the system is integrated with a remote digital computer simulating a STOL transport aircraft computer, thus allowing STOL propulsion system investigations to be performed.

The definition of the automatic control mode was made primarily on the basis of a tolerance analysis using a computer program which evaluated many potential modes relative to the accuracy with which they maintain key engine variables when subjected to typical control and engine manufacturing tolerances, sensing tolerances, and hardware deterioration. Scheduling practicality, stability, response, and failure considerations were also factors in choosing the control mode. The primary mode which has been chosen is one in which fuel flow controls engine pressure ratio (compressor discharge pressure/inlet total pressure - a variable related closely to thrust), fan pitch controls fan rpm, and fan nozzle area controls inlet Mach number (a key inlet noise parameter).

The system contains provisions for monitoring and displaying 48 engine and control variables, for detecting certain malfunctions, and for taking corrective action in the event of some critical malfunctions such as fan drive gear failure, high vibration, loss of fan speed signal, and certain digital computation faults. More extensive failure detection and correction capability will be added to the system when it is modified for the OTW engine.

An F101 fuel pump is utilized in the system for supplying engine fuel, for operating servomechanisms in the hydromechanical control, and for providing a source of high pressure fuel for operation of the actuators which position the core compressor stator vanes. A variable-displacement, constant-pressure hydraulic pump supplies fluid for operation of the actuators which position the fan nozzle and the hydraulic motor which drives the variable-pitch actuation mechanisms.

13.2 DESIGN REQUIREMENTS

The control system design is based on a number of requirements, some contractual and some resulting from the nature of the UTW engine designs. The major requirements are described below.

Commponents - General - The system shall utilize existing controls and accessories components as applicable except it shall utilize digital electronics to perform functions not now performed by existing hydromechanical controls.

Digital Control - General - The digital control shall be mounted on the engine and shall interface with a remotely located aircraft computer to provide selectable power management, failure indication, and failure corrective action.

Control Variables - The UTW control system shall control fuel flow, core compressor stator vanes, fan blade pitch, and fan exhaust nozzle area.

Experimental Engine Flexibility - The systems shall include capability for independently manipulating variables so that engine characteristics can be completely explored.

Automatic Control Capability - The systems shall be capable of coordinated control variables so that STOL aircraft propulsion test investigations can be performed with the intent of achieving:

- Thrust control throughout specified flight map with minimum pilot workload
- Fast thrust response

1.0 sec	62 to 95% forward thrust
1.5 sec	Takeoff to maximum reverse thrust

- Specified noise and pollution goals

Engine Protection - The system shall protect the engine from rotor overspeeds, turbine overtemperature, and excessive compressor or fan back pressure.

13.3 ENGINE CONTROL SYSTEM

13.3.1 General Description

The requirements outlined in the previous section established the general structure of the control system, as shown in Figure 13-1. The digital electronic control is the heart of the system and controls the manipulated variables in response to commands representing those which would be received from an aircraft propulsion system computer. The system includes an existing (F101) hydromechanical control as called for in the program requirements. This control includes an electro-hydraulic servovalve through which the digital control maintains primary control of fuel flow. The fuel-operated servomechanisms in the hydromechanical control serve primarily as backup fuel controlling elements and limits although they are the primary controlling elements for the core compressor stators.

In order to achieve the operational flexibility required by the QCSEE program, the commands to the digital electronic control are being introduced through the control room elements shown on Figure 13-2. The interconnect unit, operator panel, and engineering panel are actually peripheral elements of the digital control. They provide means for the engine operators to introduce commands, to switch between available operating modes, to adjust various control constants, and to monitor control and engine data. The remote computer is a separate digital computer system supplied by NASA to represent a typical aircraft computer. The engine digital control is designed to accommodate the digital input/output language of this remote computer.

13.3.2 Automatic Control

General

The control system is designed for automatic modes in which operation of the controlled variables is integrated to respond to input demand signals simulating those which would exist in a STOL transport propulsion system. Studies have been conducted exploring a variety of potential methods for inter-relating the controlled variables.

As a guideline for automatic mode studies, a list of general principles was established with advise from NASA, McDonnell-Douglas, and Boeing. The list is as follows:

1. A mechanical power level link is assumed from the aircraft to the engine to be used as an enable and for backup fuel control only.
2. A digital electrical signal is assumed from the aircraft computer to the engine digital control demanding percent of available thrust.
3. A digital electrical mode signal is assumed from the aircraft computer to the engine digital control to select between available operating modes such as takeoff, climb, cruise, etc.

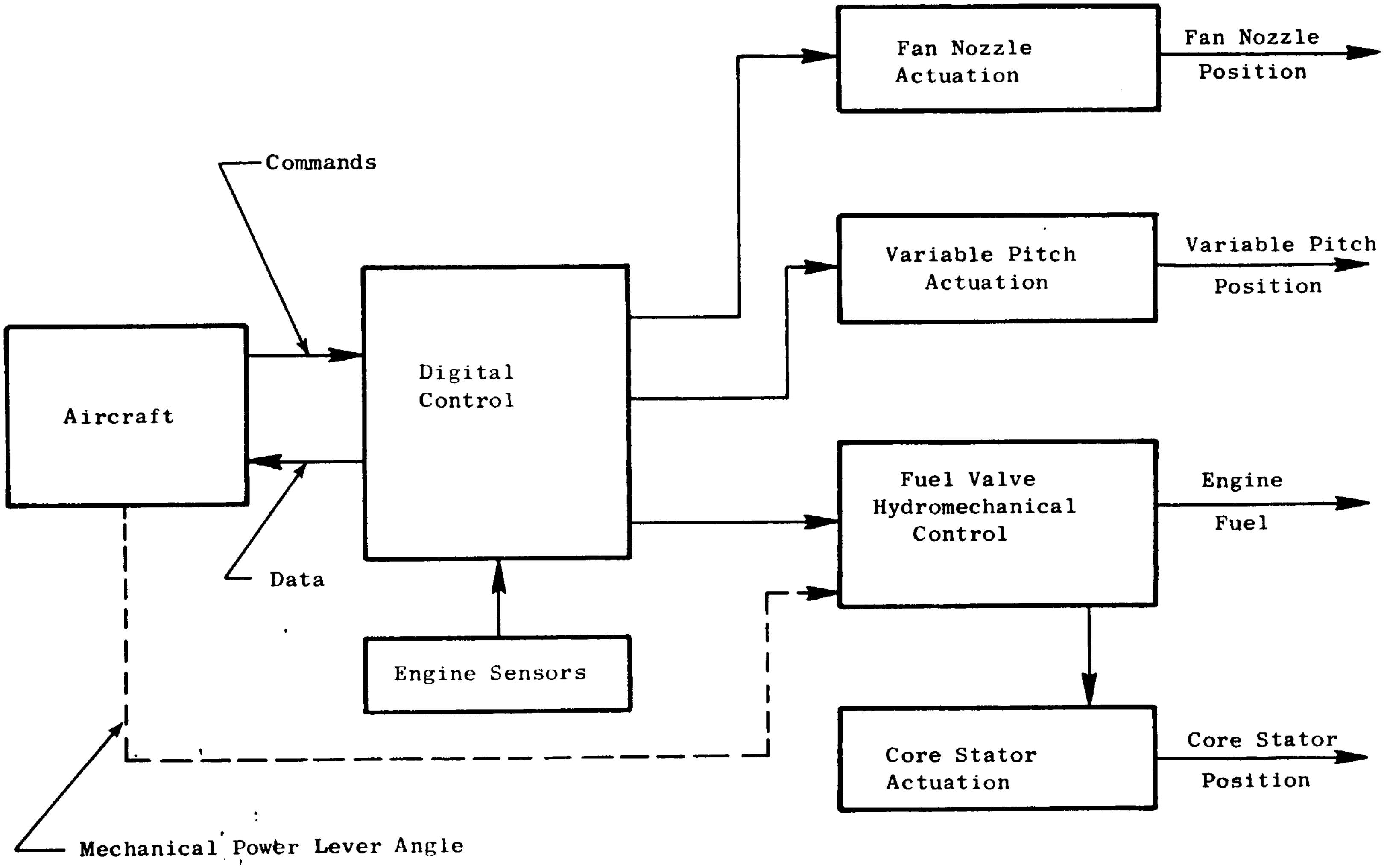
Commands
Aircraft
Digital Control
Data
Engine Sensors
Mechanical Power Lever Angle
Fan Nozzle Actuation
Fan Nozzle Position
Variable Pitch Actuation
Variable Pitch Position
Fuel Valve Hydromechanical Control
Engine Fuel
Core Stator Actuation
Core Stator Position

Figure 13-1. Control System Schematic.

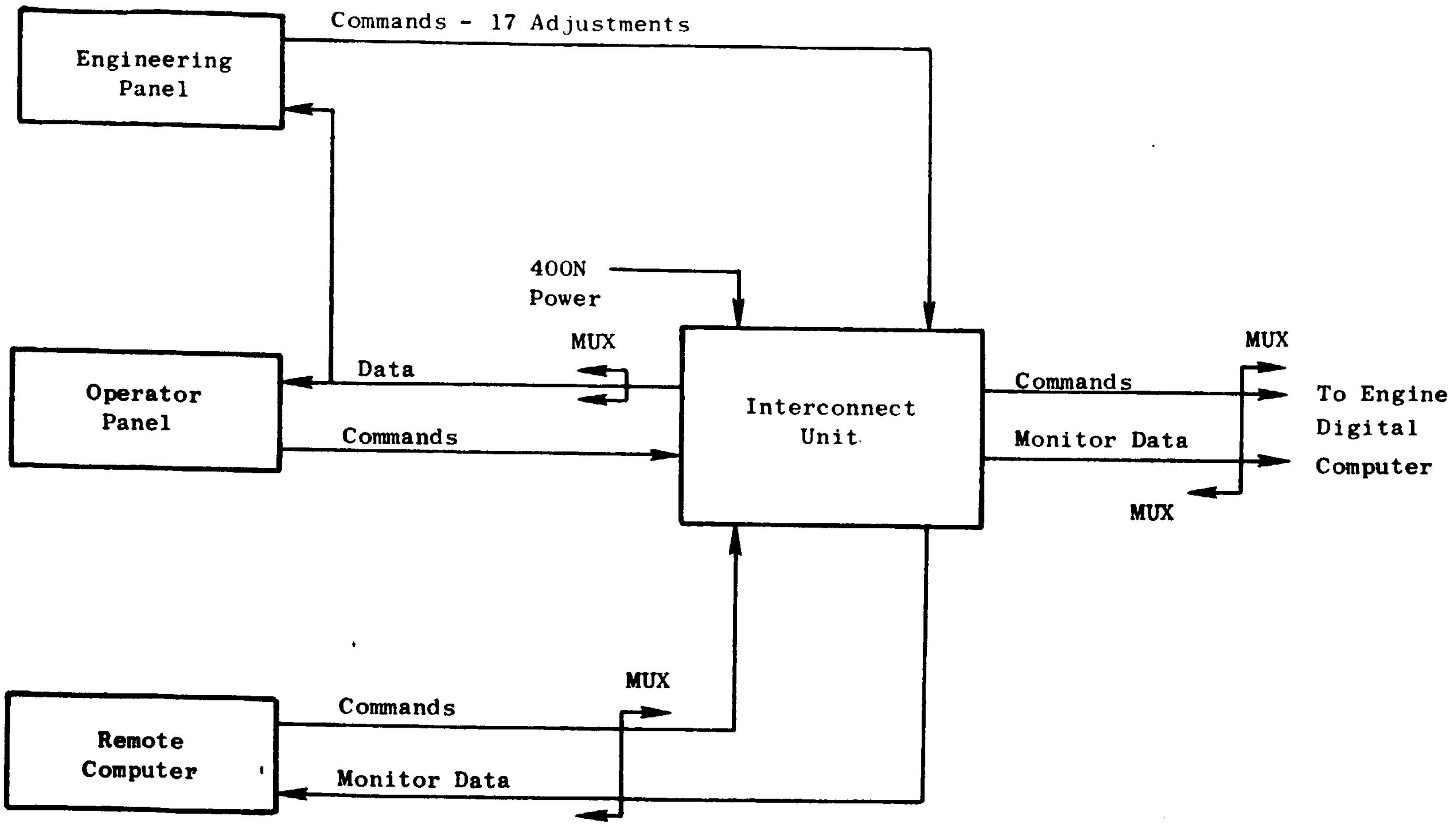
Engineering Panel
Commands - 17 Adjustments
400N Power
MUX
Data
Operator Panel
Commands
Interconnect Unit
Commands
Monitor Data
MUX
To Engine Digital Computer
MUX
MUX
Remote Computer
Commands
Monitor Data

Figure 13-2. Overall Control Room Functional Block Diagram.

4. The engine digital control shall compute maximum available thrust at all flight conditions and shall be capable of setting this thrust or any portion of it as a function of a single aircraft thrust demand signal.

5. The engine control system shall provide selected engine safety limits, protecting against rotor overspeeds, fan or compressor stall, turbine overtemperature, and compressor discharge overpressure.

6. Manual control of thrust via the throttle shall be maintainable within safe limits if the engine digital control and/or aircraft digital control fails.

7. It is desirable that no throttle or thrust demand changes be required during takeoff except in the event of an abort.

8. It shall be an objective that fan pitch shall not change if the engine digital control fails.

9. It shall be an objective that fan nozzle area shall go to the takeoff position in the event of a failure.

10. Detection of engine failure to produce commanded thrust shall be achieved through a combined indication from engine parameters in the engine digital control and a signal shall be transmitted to the aircraft.

Thrust Control Function

One fundamental factor in designing for automatic control is the choice of a thrust control and indication function. This function must be an accurate measure of thrust in the takeoff regime, and must be related to other sensed variables in such a manner that the engine digital control can compute and set maximum available thrust or any portion thereof anywhere in the flight envelope. A list of thrust functions evaluated for the UTW engine is given in Table 13-I.

To determine the thrust setting accuracy of the various potential thrust control functions, tolerance studies were conducted. These studies were made up of a series of cases in which different sets of three independent variables were considered to be controlled by manipulation of fuel flow, fan pitch, and fan nozzle area (it being assumed that the fourth UTW manipulated variable, core variable stators, will be scheduled as a function of core corrected speed as on the F101). One of the independent variables in each case was one of the candidate thrust functions. Each case was run through a computer program which combines typical control and measurement tolerances, engine component tolerances, and engine component deterioration with engine cycle characteristics to define expected variations in important characteristics such as thrust, turbine temperature, stall margins, etc. Typical

Table 13-I. Thrust Functions Evaluated for UTW Control.

Thrust Function	Basic Type
TP1 = P49/PTP	Core Power
TP2 = PS3/PTO	Core Power
TP3 = f(P14/PAMB) x (A18)	Gross Thrust
TP4 = f(P14/PTO) x (A18)	Gross Thrust
TP5 = f(XM11)/(A18)	Gross Thrust
TP6 = f(P14/PTO) x f_2(XM11)	Gross Thrust
TP7 = $K_1 + K_2$ (ΔA18) + K_3 (ΔROPDEG) + f(PCNLR)	Gross Thrust
TP8 = T41C/T1	Core Power
TP9 = PCNHR	Core Power
TP10 = PS3/PS8	Core Power
TP11 = T8/T1	Core Power
TP12 = [(T15 - T1)/T15] x f(XM11)	Fan Power
TP13 = WFM/PTO	Core Power

Note: Nomenclature same as used in cycle and performance section with the following additions:

TP = thrust parameter
PTO = free stream total pressure
T41C = calculated T41
PS3, PS8 = static pressure at respective stations

results of such runs are shown in Table 13-II and the variations used in getting these results in Table 13-III.

The tolerance studies provide a good theoretical basis for initial comparison, separation, and selection of potential thrust control functions. However, additional factors which are not considered during the tolerance study must be explored prior to final thrust parameter selection. Further examination and consideration of the TP12 function, which the tolerance studies showed to be the most accurate, revealed several undesirable characteristics that resulted in its rejection as a thrust parameter candidate on the QCSEE UTW experimental engine. These were: (1) temperature sensing errors introduced by rain and the subsequent heat loss due to water evaporation, (2) failure to meet the objective that changes in engine thrust should be primarily a function of the thrust parameter. An examination of thrust partials associated with the TP12 control modes revealed a significant interaction between the controlled variables; as a result, changes in engine thrust were not primarily a function of changes in the thrust parameter; and (3) concern about the time response requirements for the fan discharge temperature sensor. Achievement of the required engine thrust response would require a rapidly responding temperature sensor which would be difficult to implement when sensor environmental and life requirements are considered.

After further consideration, the thrust function based on fuel flow, measurement was also rejected because it exhibited the same type of interaction between controlled variables as did TP12. Also, even with optimistic sensing accuracy assumption, the parameter was sensitive to engine deterioration factors which resulted in a thrust loss with engine age.

Applying considerations similar to those described in the previous two paragraphs to the other potential thrust functions narrowed the choice to two, TP5 and PS3/PTO. These two were then evaluated further to determine if they were schedulable over a wide range of operating conditions. Using a large amount of engine cycle data, it was determined that both thrust functions can be scheduled as a function of reference fan inlet temperature, actual fan inlet temperature, and free stream total pressure to provide satisfactory scheduling of maximum available thrust throughout the QCSEE flight envelope. The schedules are shown on Figures 13-3 and 13-4. The temperature reference is based on the inlet total temperature-to-inlet total pressure relationship that exists on the normal QCSEE flight path. Cycle data indicate that deviations from this flight path or from standard atmospheric conditions are accommodated satisfactorily by the temperature ratio effects shown on the schedules.

One other factor to be considered in evaluating a potential thrust function is control loop stability when the function is combined with other manipulated variables in an automatic control system. This matter is discussed as a part of the next section.

Table 13-II. Tolerance Study Results.

Variables Controlled 1	Variables Controlled 2	Variables Controlled 3	Thrust P.I.(1)	Variations(2) - % of Point FN	T41	SM12	XM11
			SLS Takeoff				
TP12	A18	ROPDEG	1.34	1.27	2.0	9.2	1.5
TP12	A18	PCNL	1.48	1.43	2.0	5.5	2.0
TP13	A18	PCNL	1.93	1.43	1.1	5.6	2.0
TP5	PCNL	ROPDEG	2.05	1.95	2.6	7.9	2.6
TP5	XM11	PCNL	2.11	1.96	2.2	7.2	1.7
A18	XM11	PCNL	2.12	1.97	2.3	7.4	1.7
TP2	A18	PCNL	2.20	2.00	2.8	7.7	2.7
TP7	A18	PCNL	2.27	2.22	2.9	10.3	2.8
PCNL	A18	ROPDEG	2.39	2.34	2.9	10.4	2.5
P14/PTO	XM11	PCNL	2.44	2.34	2.3	8.1	1.7
TP5	A18	PCNL	2.51	2.36	3.0	9.2	3.3
TP6	PCNL	ROPDEG	2.54	2.44	2.5	8.6	2.6
TP6	XM11	PCNL	2.55	2.45	2.2	8.2	1.7
TP2	XM11	PCNL	3.63	3.38	2.4	10.6	1.7
			Mach 0.7/7.62 km (25,000 ft.), Max Climb Power				
TP12	A18	ROPDEG	3.35	3.3	2.0	10.0	4.2
TP12	M14	PCNL	3.35	3.3	2.0	16.0	8.7
TP12	XM11	PCNL	3.5	3.5	1.9	13.0	2.4
TP12	PCNL	ROPDEG	3.6	3.5	2.0	16.0	6.8
TP13	A18	PCNL	4.5	3.4	1.3	11.0	2.7
P14/PTO	XM11	PCNL	4.7	4.4	2.3	15.0	2.4
TP13	A18	ROPDEG	4.8	3.9	1.4	21.0	3.9
TP13	XM11	PCNL	5.0	3.8	1.3	14.0	2.4
TP2	A18	PCNL	5.4	5.0	2.7	14.0	5.0
TP2	XM11	PCNL	5.6	5.2	2.6	19.0	2.4
TP5	A18	PCNL	5.8	5.4	2.6	15.0	4.5
XM11	A18	PCNL	6.8	6.2	2.6	19.0	2.4
TP5	XM11	PCNL	7.6	7.3	2.9	25.0	2.4

(1) Thrust Performance Indicator = FN variation + 1/2 deterioration effects.

(2) Variations are RSS stack-up of the tolerances and variations listed on Table 13-III.

Note: Nomenclature same as used in cycle and performance section.

Table 13-III. Tolerances and Variations Used.

Control Variables		
	Assumed Tolerances	
Variable	SLS Takeoff	Mach 0.7 7.62 km (25K ft) Max. Climb
PCNLR	0.38	0.61
A18	1.20	1.63
ROPDEG	0.50	0.50
XM11	1.68	2.40
P49/PTO	1.20	2.29
PS3/PTO	1.03	2.22
T41C	1.23	1.61
TP3	7.03	2.76
TP4	3.94	4.68
TP5	1.80	2.29
TP6	2.16	4.47
TP7	2.65	2.78
T41C/T1	1.23	1.61
T49/T1	1.09	1.10
T8/T1	0.95	1.22
PCNHR	0.31	0.33
TP12	2.41	2.49
Wfm/PTO	1.34	2.13
P14/PTO	0.81	2.33

Engine Characteristics	
Characteristic	Variation
Fan Airflow	1.5
Fan Eff.	1.5
Core Airflow	1.0
Core Compr. Eff.	1.0
P4/P3	0.5
Comb. Eff.	0.3
A41	1.0
HP Turb. Eff.	1.0
A49	1.0
LP Turb. Eff.	1.0
P18/P14	0.2
A8	0.5
P56/P5	0.1
Interstage Bld.	1.0
P3 Bld.	1.0
HP Extract.	18.6 kw (25 HP)
Cooling Bld.	0.55
AE11	0.1

Note:

- All are ±% of point unless noted otherwise
- Nomenclature same as used in cycle and performance section.
  PTO = Free stream total pressure

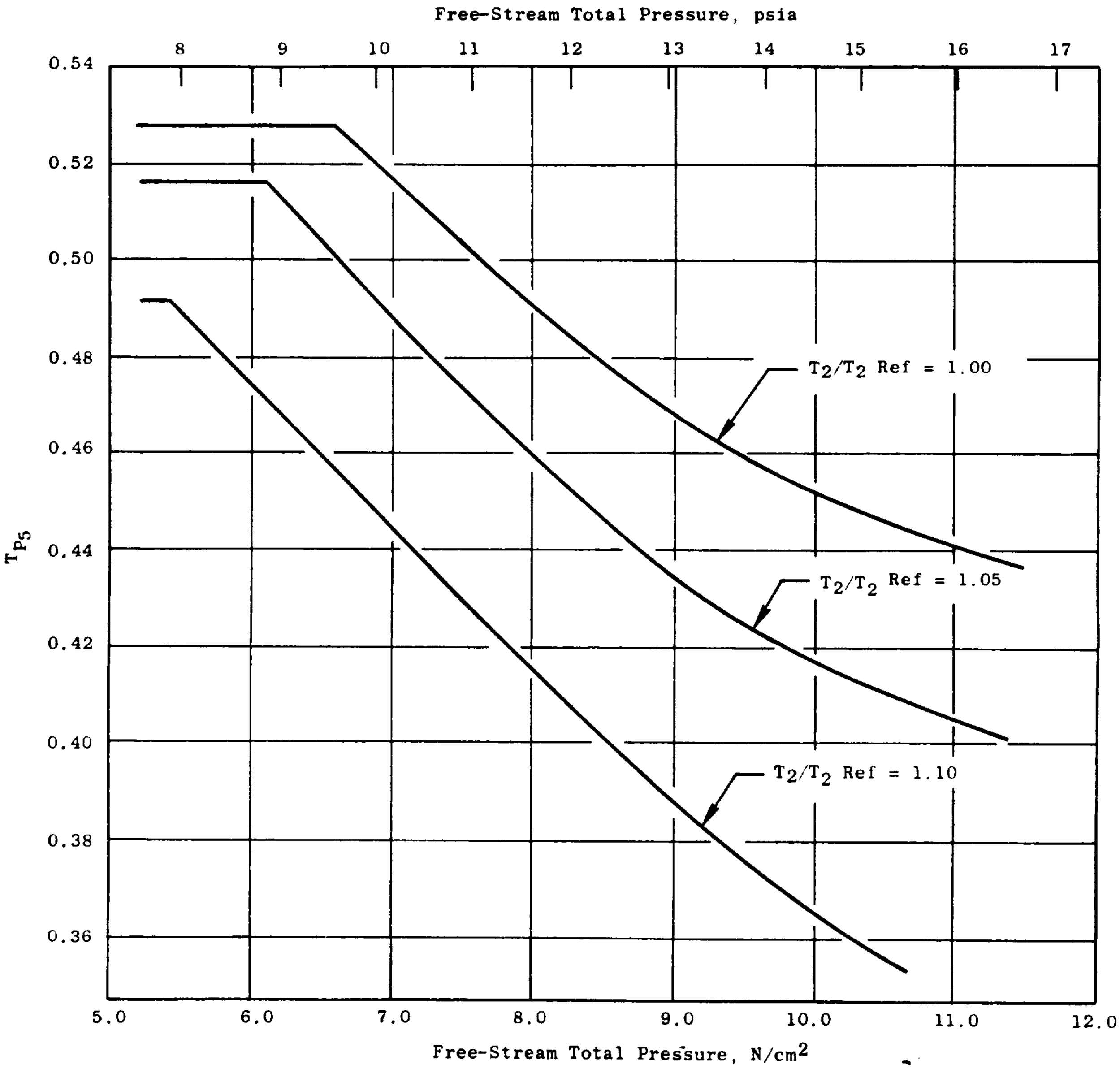

Figure 13-3. Base Schedule for TP5 Maximum Climb Power.

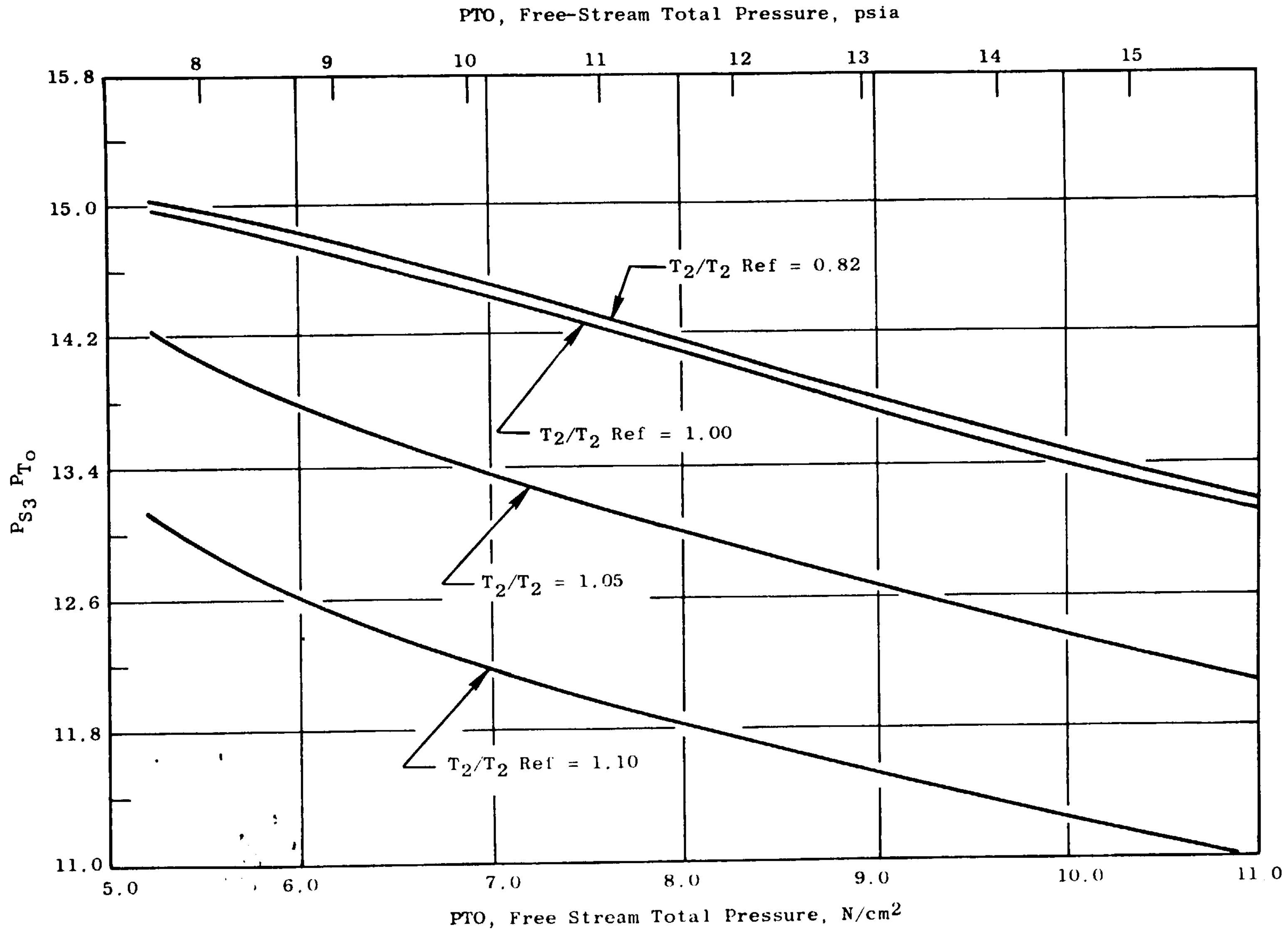

Figure 13-4. Engine Core Pressure Ratio for Maximum Climb Power on Reference Climb Path.

Control Modes

Another task necessary to definition of the automatic control was the identification and evaluation of control modes, that is, the interrelationships between manipulated and controlled variables.

Key operational requirements applicable to establishing automatic control modes at various conditions are:

Takeoff

- Set guaranteed maximum static thrust or percent thereof
- Set inlet throat Mach number (XM11) for optimum noise/performance compromise

Climb

- Set guaranteed maximum installed thrust or percent thereof
- Control inlet Mach number for optimum performance

Cruise

- Attain minimum installed SFC at required thrust level

Descent

- Maintain sufficient core speed for air conditioning and power extraction

Approach

- Fast thrust response at readily controlled level up to guaranteed maximum
- Maximize inlet Mach number and airflow for low noise

Ground Idle

- Minimum thrust
- Minimum exhaust pollution
- Low noise
- RPM sufficient for centrifugal anti-icing

From this listing of requirements, it was concluded that the primary controlled variables in the automatic control mode should be: (1) the thrust function, (2) inlet Mach number, and (3) fan rpm. The problem then to be faced was which of the available manipulated variables should be used to set each of these controlled variables.

One facet of this problem which was investigated was the relative effect of each manipulated variable on each controlled variable with the other manipulated variable held constant. Using engine cycle derivatives, these effects were defined. The data below show the effects on the TP2 thrust function.

		SLS Takeoff	Max. Climb Mach 0.7, 7.62 km (25,000 Feet)
$\frac{\% \Delta TP2}{\% \Delta WF}$	with constant A18 and fan pitch	0.547	0.580
$\frac{\% \Delta TP2}{\% \Delta A18}$	with constant WF and fan pitch	-0.126	-0.233
$\frac{\% \Delta TP2}{\% \Delta pitch}$	with constant WF and A18	0.004	-0.577

Thus fuel flow (WF) definitely has the strongest effect on the thrust function and it was chosen as the thrust control variable subject to stability and transient response evaluation.

Similar data are given below on the two remaining variables.

		SLS Takeoff	Max. Climb Mach 0.7, 7.62 km (25,000 Feet)
$\frac{\% \Delta XM11}{\% \Delta A18}$	with TP2 and pitch constant	0.547	1.198
$\frac{\% \Delta XM11}{\% \Delta pitch}$	with TP2 and A18 constant	0.816	-3.208
$\frac{\% \Delta fan\ rpm}{\% \Delta A18}$	with TP2 and pitch constant	0.557	1.482
$\frac{\% \Delta fan\ rpm}{\% \Delta pitch}$	with TP2 and A18 constant	2.903	5.528

These data show that both fan pitch and nozzle area have adequate influence on XM11 and fan rpm but that pitch has the stronger effect on both. However, another consideration was applied to this choice of variable interrelationships. To minimize noise at reduced thrust levels it is desirable to maintain a high XM11 to as low a thrust as possible. The data plotted on Figure 13-5 show that this can be done by opening A18 as thrust is reduced but that pitch variation alone will not maintain high XM11. Thus it was decided that SM11 would be controlled by modulating A18, and fan speed would be controlled by modulating pitch.

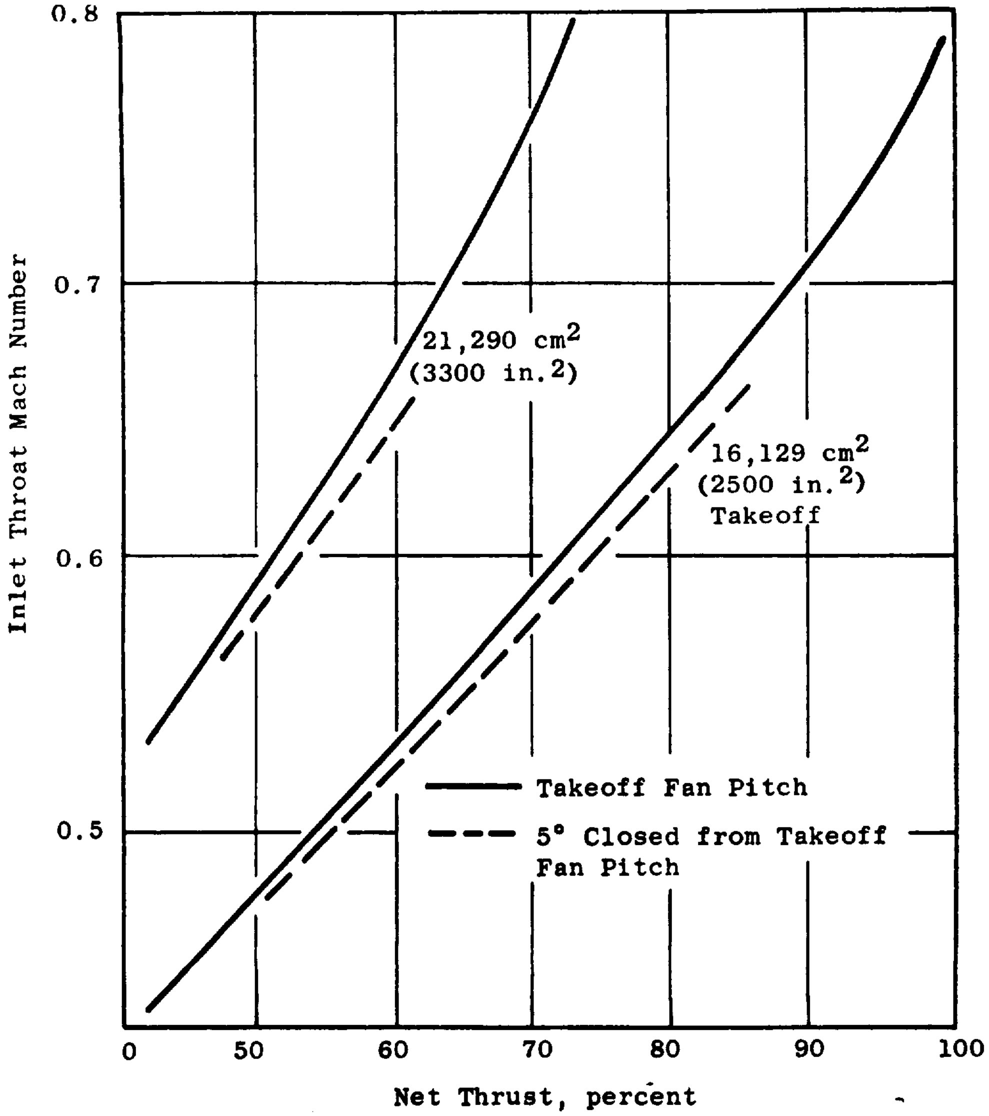

Figure 13-5. Fan Nozzle Effect on Inlet Mach Number.

Once the basic control mode was defined it was integrated into a hybrid computer model of the engine and control system in order to evaluate stability and response characteristics. The control portion of the model included three basic loops which are shown in simplified form on Figures 13-6, 13-7, and 13-8. In the fuel control loop, the thrust function (PS3/PTO in this case) was the primary input to the controller with rpm, temperature (T41), acceleration, and deceleration fuel flow limits applied. In the fan nozzle area loop, inlet Mach number error is the primary controller input with a roof schedule and maximum and minimum area limits applied. The fan pitch loop has fan rpm error (from a power setting generated schedule) as the primary controller input with maximum and minimum limits applied.

Numerical values in the model were set in several ways, some being based on engine limits, some on linear stability analyses, and some on past experience. The model was run and adjustments made as necessary to provide optimum stability. Figure 13-9 shows a typical run made during the stability optimization process in which a power setting disturbance was introduced during steady-state operation and the reaction observed. As a result of this process the model was refined to provide satisfactory steady-state stability.

It should be noted at this point that stability work was done on the model with both of the thrust functions identified in the previous section as prime candidates; i.e., TP5 and PS3/PTO. This work revealed that PS3/PTO is satisfactory from a stability viewpoint but that there are stability problems in the 75 to 85% thrust region with TP5. As a result of this, it was decided that PS3/PTO would be the thrust function in the digital automatic control and that further stability compensation work is necessary to make TP5 suitable.

After the numerical values in the model were refined for optimum stability, the model was run to explore the transient response characteristics of the chosen control mode, particularly at approach conditions where fast response is most important. A typical data trace from one of these runs is shown in Figure 13-10 and summary data from similar runs with minor changes made are shown in Figures 13-11 and 13-12. Figure 13-13 shows that the chosen control mode meets the QCSEE program response goal of one second from 62 to 95% thrust at approach and they also indicate the response improvement over a fixed-pitch fan engine.

This improved response was achieved with the control system programmed to maintain constant fan rpm by varying fan pitch and constant inlet Mach number by varying exhaust area. Since the fan is maintained at 100% speed, the effects of fan rotor inertia on response time have been eliminated. Closing the fan pitch to maintain the speed reduces the fan efficiency which results in keeping the core speed high. Opening the nozzle (done primarily for noise control) also has the same effect. Thus, the effects of the inertia of the engine rotating parts has been minimized resulting in a very rapid response time.

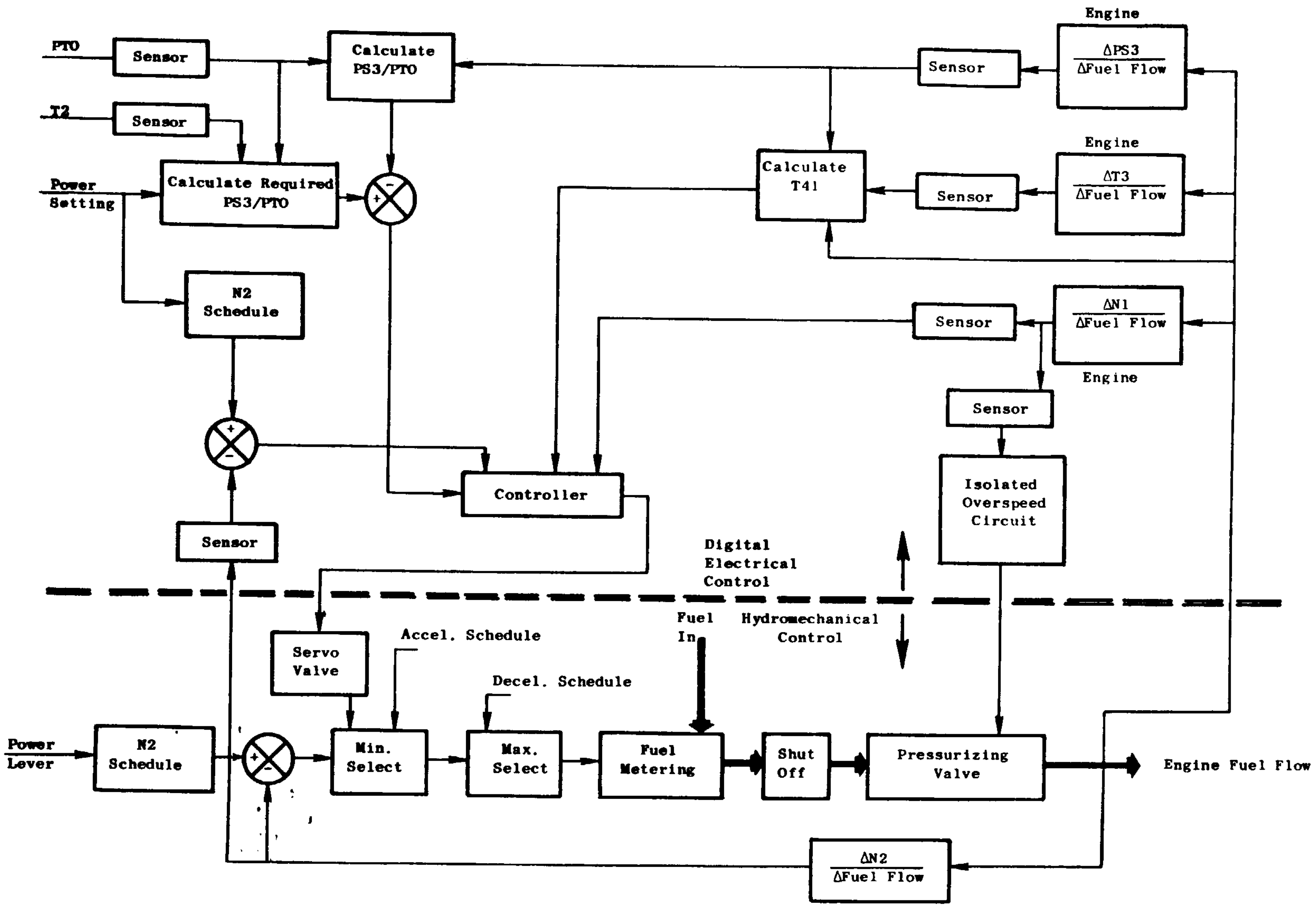
PTO
Sensor
T2
Sensor
Power Setting
Calculate PS3/PTO
Calculate Required PS3/PTO
+
-
N2 Schedule
+
-
Sensor
Controller
Calculate T41
Engine
ΔPS3 / ΔFuel Flow
Sensor
Engine
ΔT3 / ΔFuel Flow
Sensor
ΔN1 / ΔFuel Flow
Engine
Sensor
Sensor
Isolated Overspeed Circuit
Digital Electrical Control
Hydromechanical Control
Fuel In
Servo Valve
Accel. Schedule
Decel. Schedule
Power Lever
N2 Schedule
+
-
Min. Select
Max. Select
Fuel Metering
Shut Off
Pressurizing Valve
Engine Fuel Flow
ΔN2 / ΔFuel Flow

Figure 13-6. Fuel Control Loop.

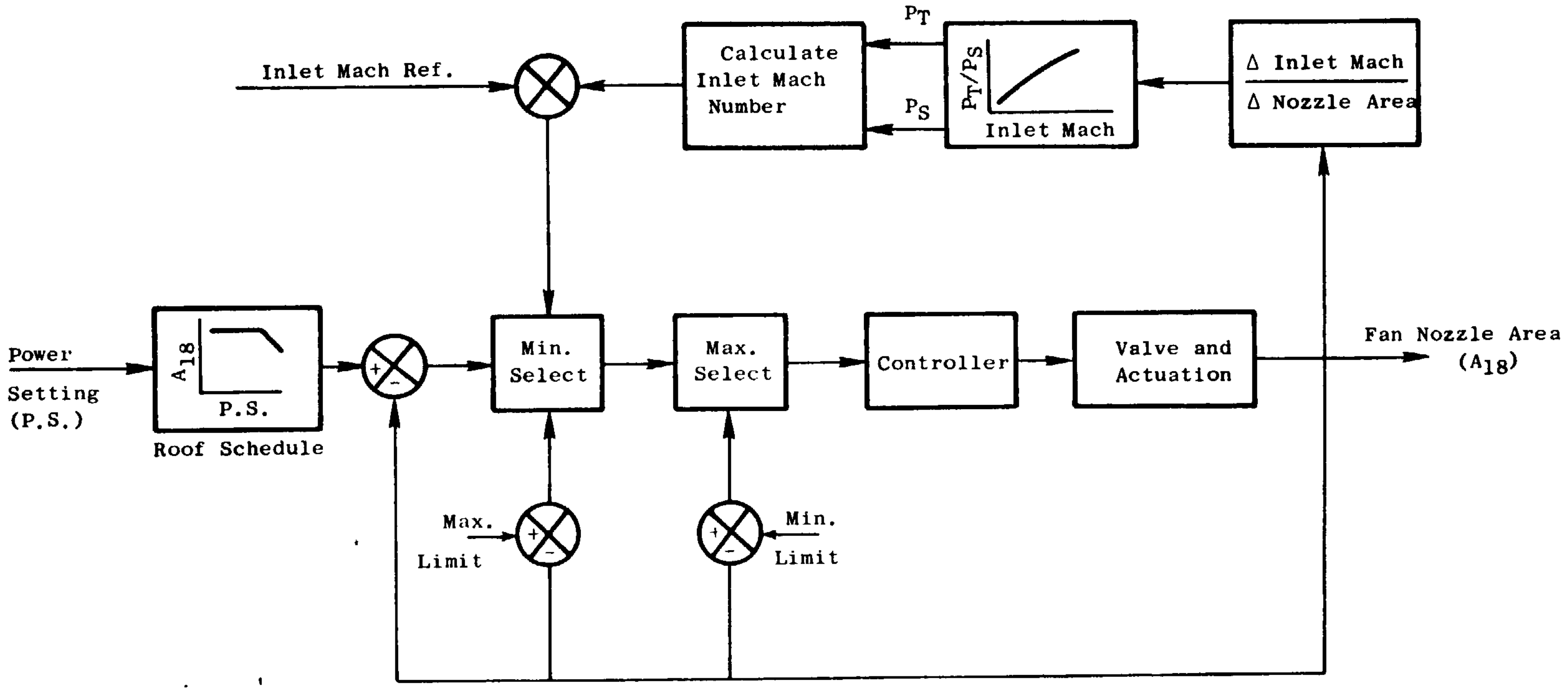
Inlet Mach Ref.
Calculate Inlet Mach Number
P_T
P_S
P_T/P_S
Inlet Mach
Δ Inlet Mach / Δ Nozzle Area
Power Setting (P.S.)
A_{18}
P.S.
Roof Schedule
+
-
Min. Select
Max. Select
Controller
Valve and Actuation
Fan Nozzle Area (A_{18})
Max. Limit
Min. Limit

Figure 13-7. Fan Nozzle Area Control Loop.

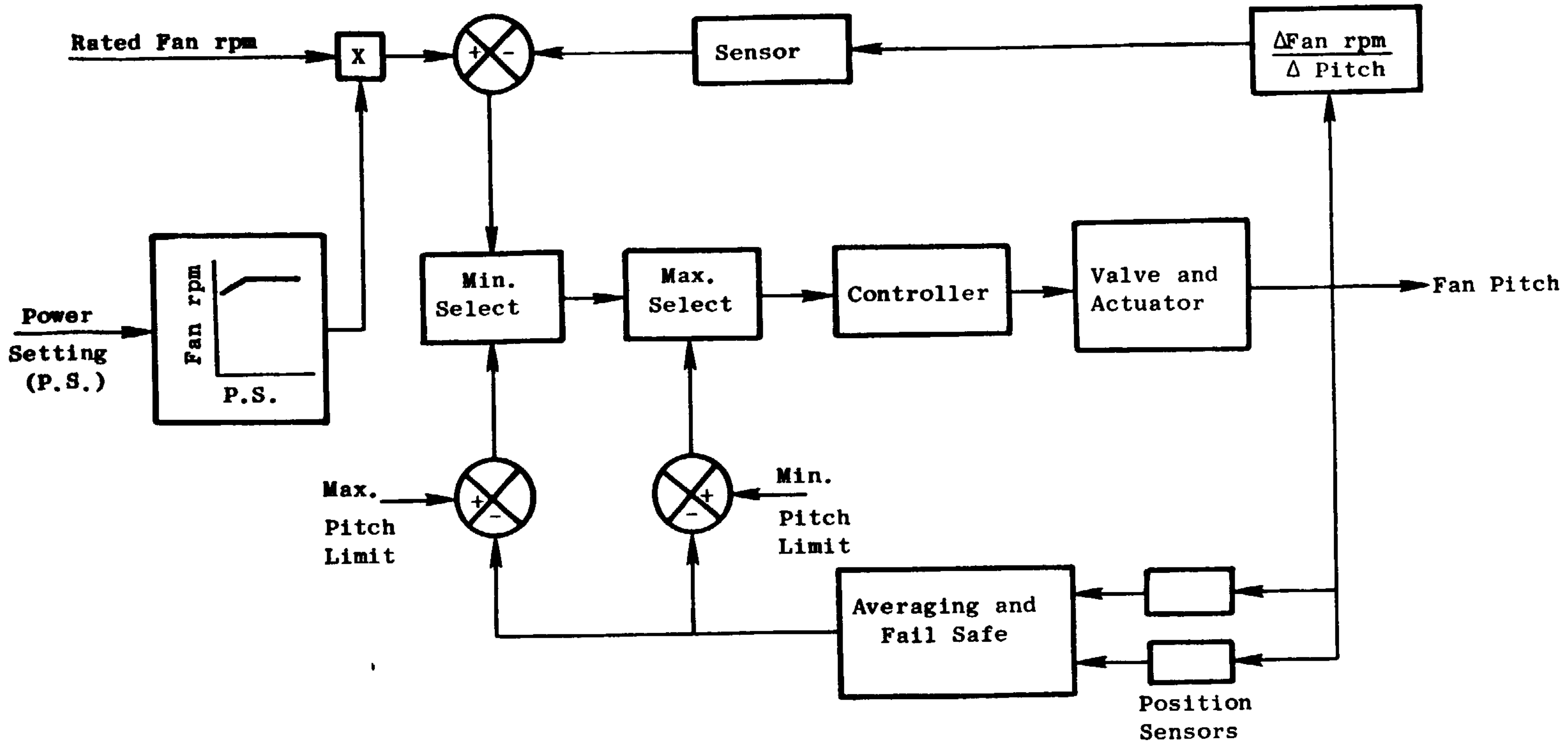
Rated Fan rpm
X
+
-
Sensor
ΔFan rpm / Δ Pitch
Power Setting (P.S.)
Fan rpm
P.S.
Min. Select
Max. Select
Controller
Valve and Actuator
Fan Pitch
Max. Pitch Limit
+
-
+
-
Min. Pitch Limit
Averaging and Fail Safe
Position Sensors

Figure 13-8. Fan Pitch Control Loop.

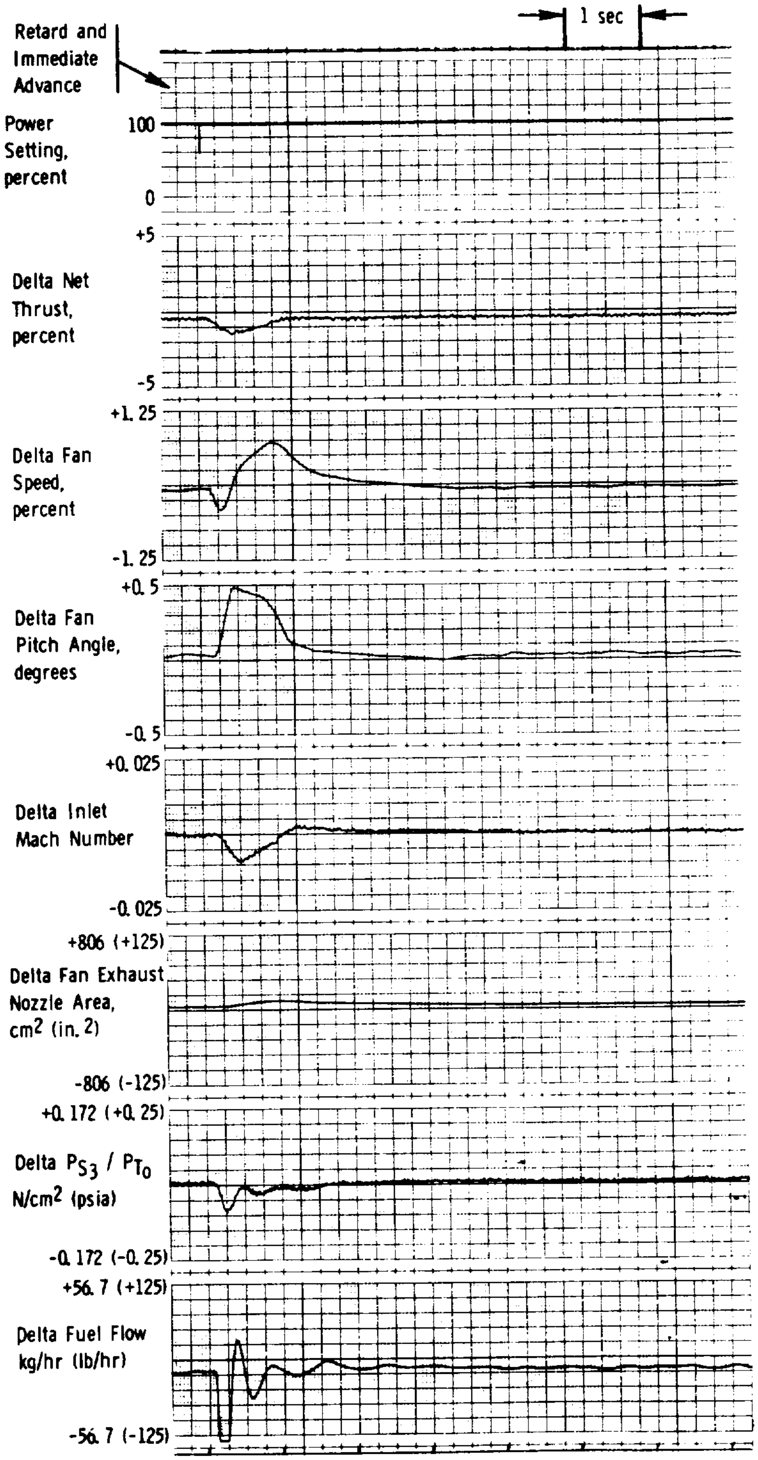

Figure 13-9. UTW Engine 2nd Control System Hunting at Nominal Design Conditions, SLS, Standard Day.

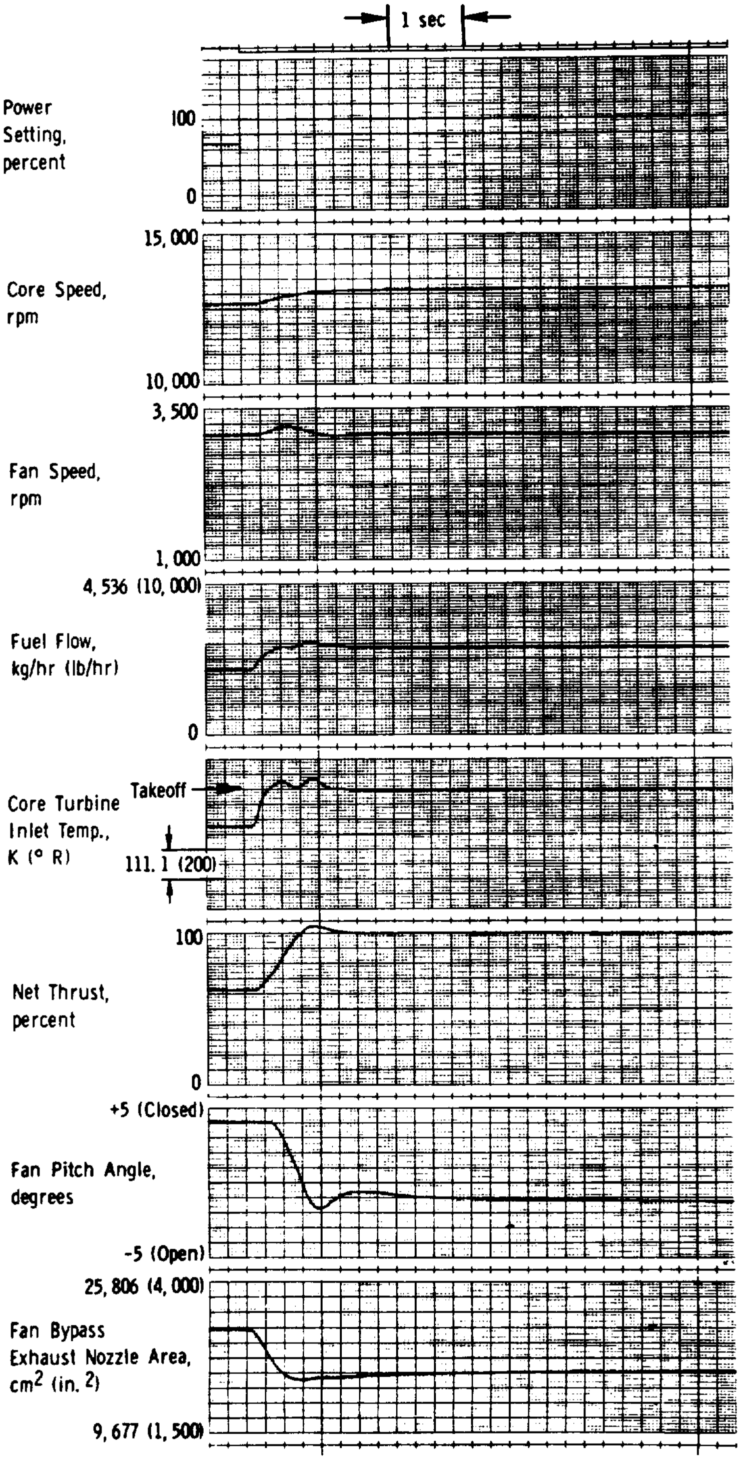

Figure 13-10. UTW Throttle Burst from 62 to 100% Net Thrust at SLS, Standard Day, Zero Bleed.

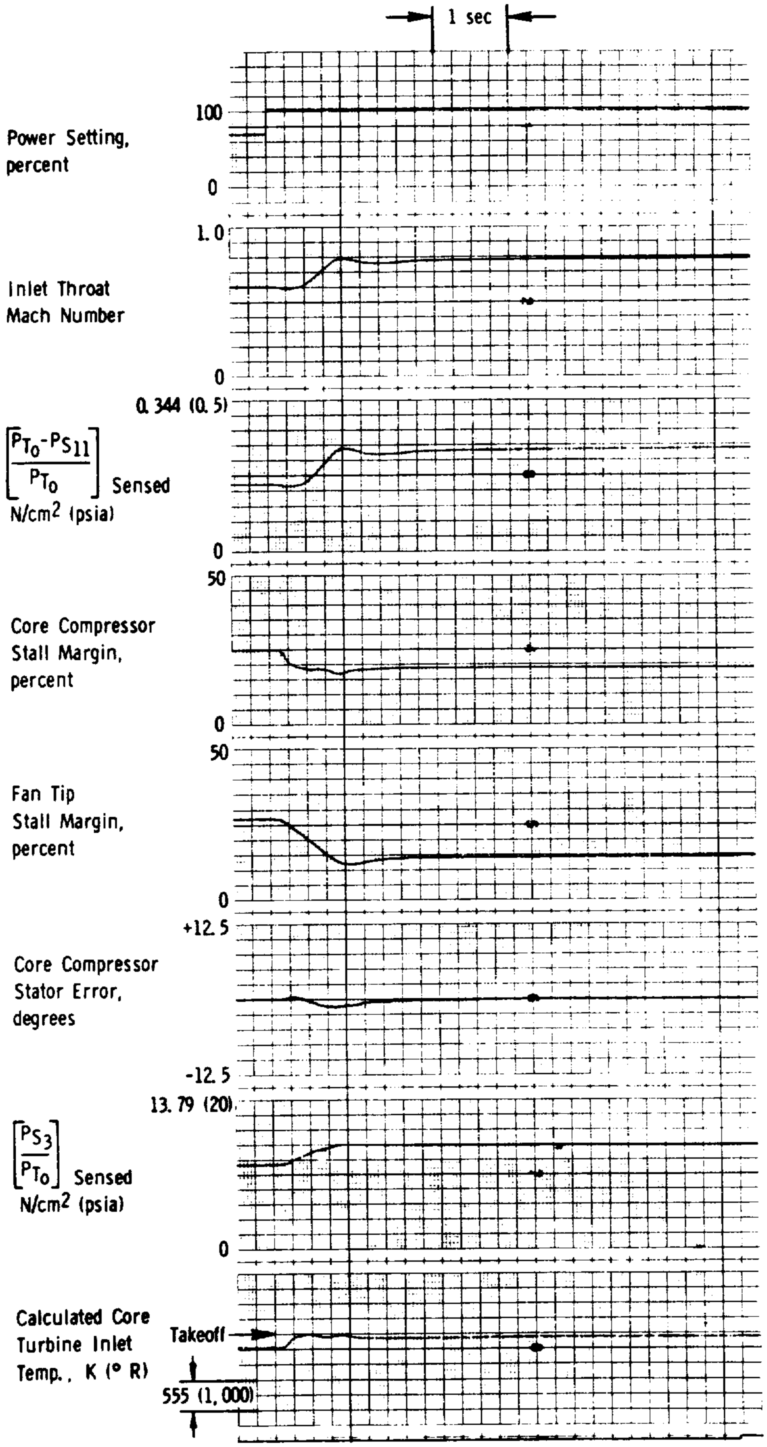

Figure 13-10. UTW Throttle Burst from 62 to 100% Net Thrust at SLS, Standard Day, Zero Bleed (Concluded).

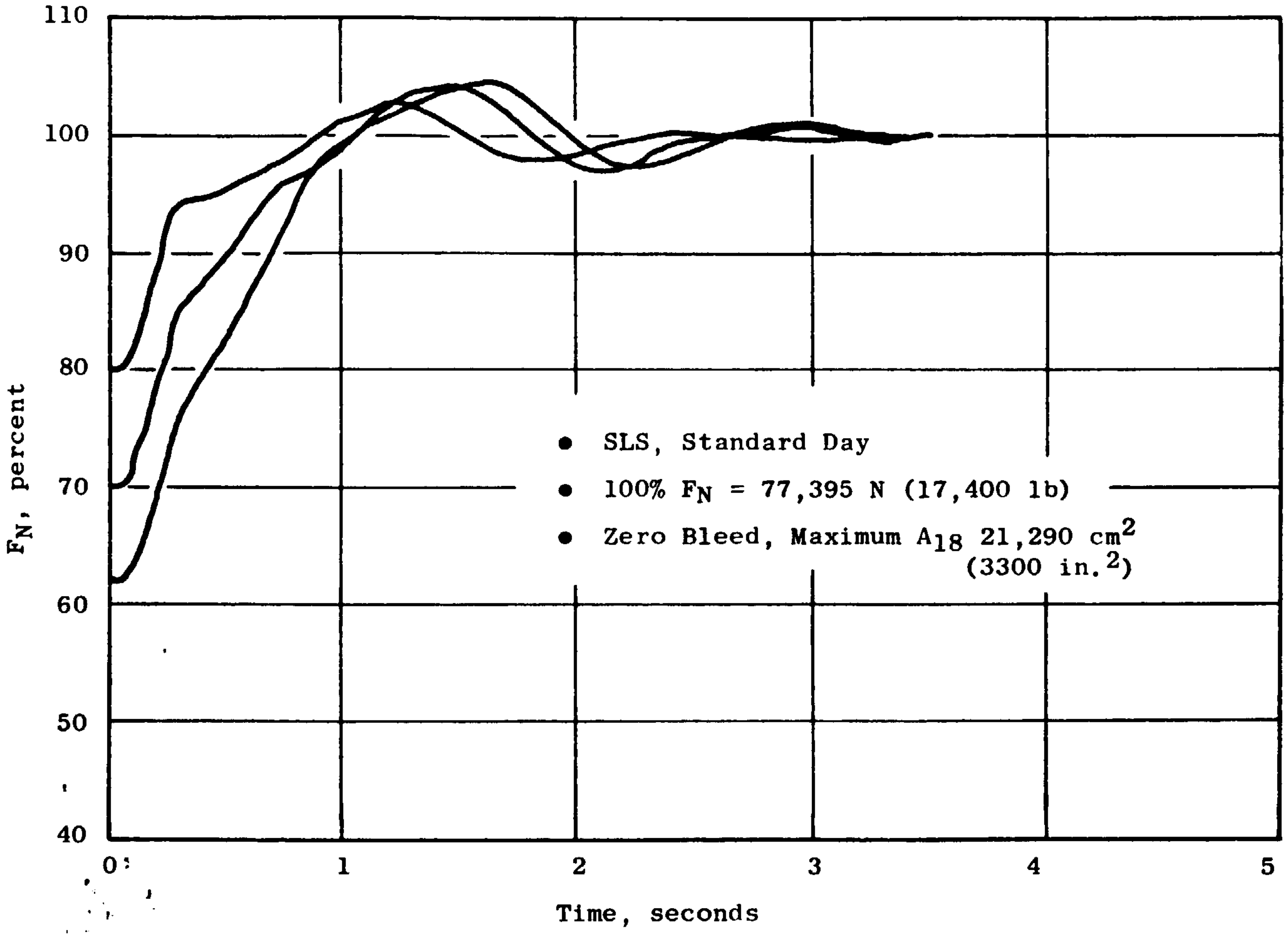

Figure 13-11. Preliminary Performance Constant NIK Control Configuration Percent Net Thrust Versus Time.

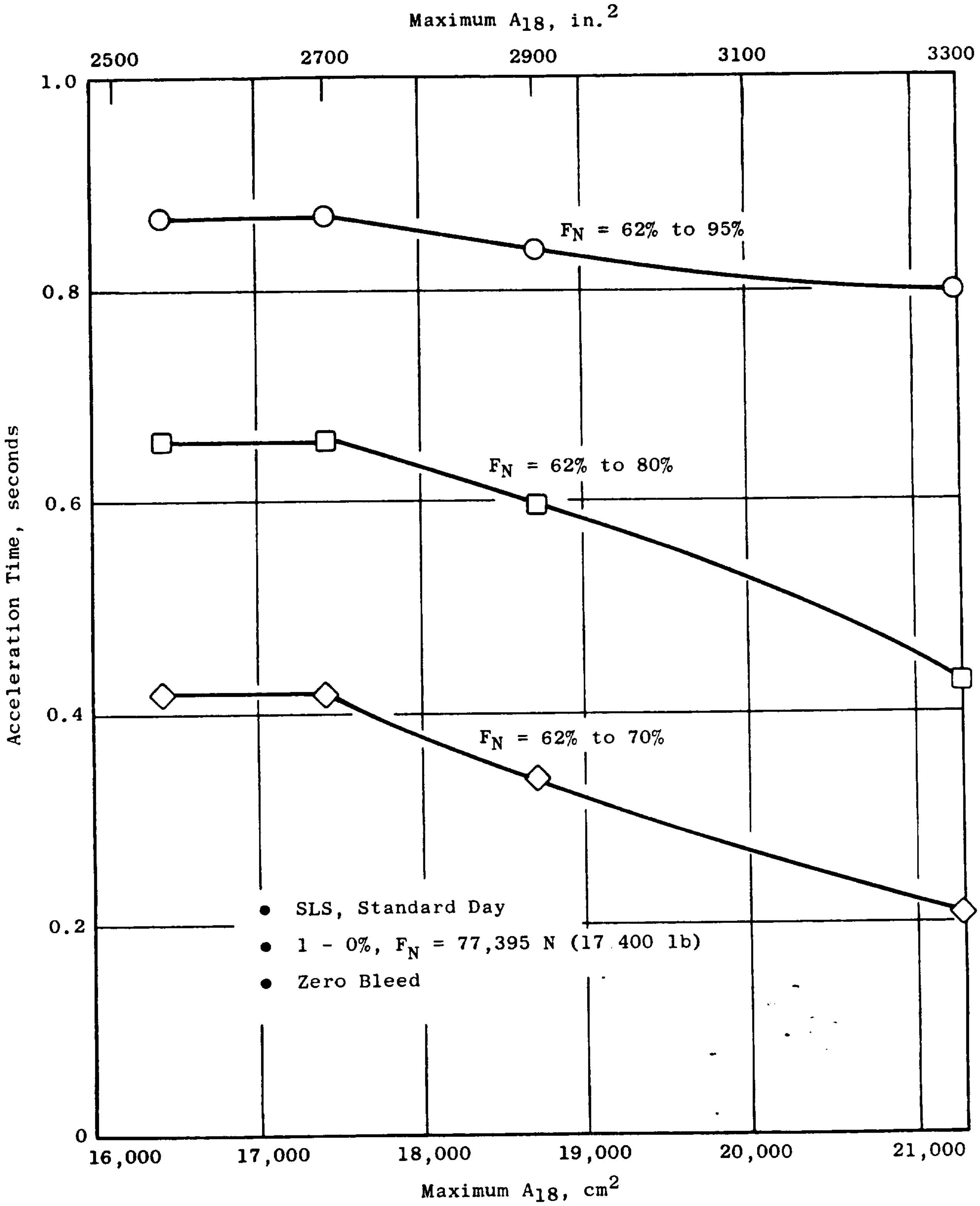

Figure 13-12. Preliminary Performance Constant NIK Control Configuration Acceleration Time Versus Maximum A_{18}.

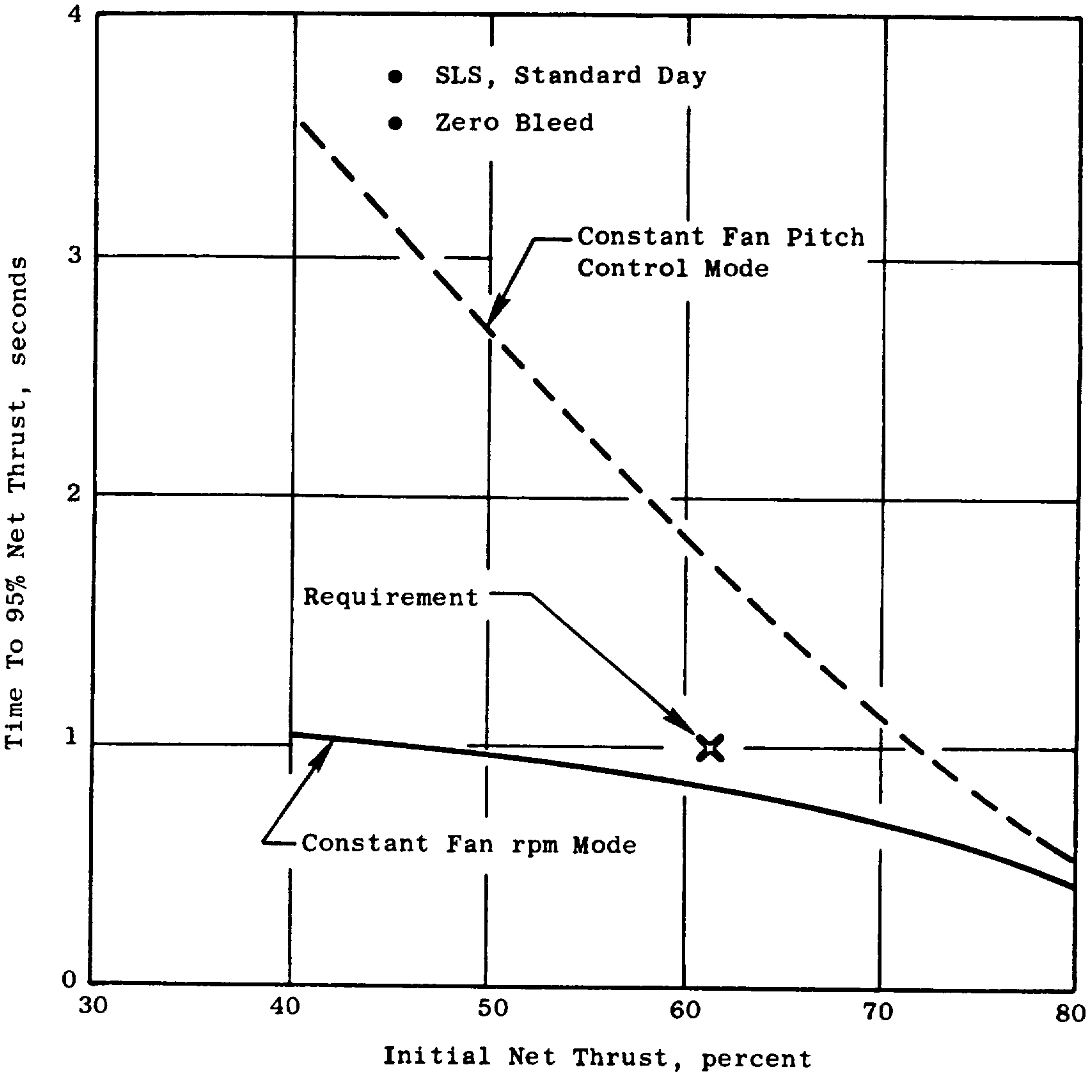

Figure 13-13. Control Model Effect On Transient Response Hybrid Model Data.

To obtain reverse thrust, the fan pitch must be set at the reverse thrust position and the exhaust area opened to the point which provides the optimum angle for reverse air intake. Pitch and area are not modulated in reverse because the range of flight conditions in which reverse thrust will be used is small and there is negligible benefit in such modulation. Thrust variation in reverse is provided in the initial control program in the same manner as on current engines, that is, by manipulating fuel flow to set fan speed as a function of power setting.

Consideration has also been given to cruise operation. For cruise the method of scheduling noted above as optimum for takeoff and approach results in some fuel consumption penalties as shown on Figures 13-14 and 13-15. These data suggest that different scheduling of variables and possibly even a different control mode is desirable at cruise. Further study is being applied to the definition of automatic control in cruise and the results will be introduced later by modifying the digital control program.

Safety Limits

The automatic control includes a number of safety limits which are shown on the functional block diagrams of Figures 13-6 through 13-8. These are listed and briefly described below:

T41 Limit - Turbine inlet gas temperature (T41) is calculated in the digital control from compressor discharge temperature (T3), fuel flow, and compressor discharge pressure, and fuel flow is limited to prevent this calculated T41 from exceeding a predetermined limit.

Acceleration Limit - An acceleration fuel schedule which is a function of core rpm, core compressor inlet temperature, and core compressor discharge pressure is incorporated in the hydromechanical control and fuel flow is prevented from exceeding this schedule. The schedule is designed to provide satisfactory starts and rapid acceleration without core compressor stall or excessive turbine temperature transients.

Deceleration Limit - A deceleration fuel schedule which is a fraction of the acceleration schedule is incorporated in the hydromechanical control, and fuel flow is not allowed to go below this schedule except in the case of operation of the emergency shutdown noted below. This schedule is designed to provide rapid engine deceleration without loss of combustion.

Fan Speed Limit (Normal) - The digital control senses reduction gear input rpm and limits fuel flow to prevent exceeding a predetermined normal fan rpm limit.

Emergency Shutdown - This feature provides complete fuel shutoff in the event that reduction gear input rpm exceeds an absolute maximum limit or if this rpm increases at a rate indicative of fan turbine unload (as would occur with fan or gear failure). All elements of this feature are electrically isolated from the remainder of the system so that it also protects against system faults which might cause fan overspeed.

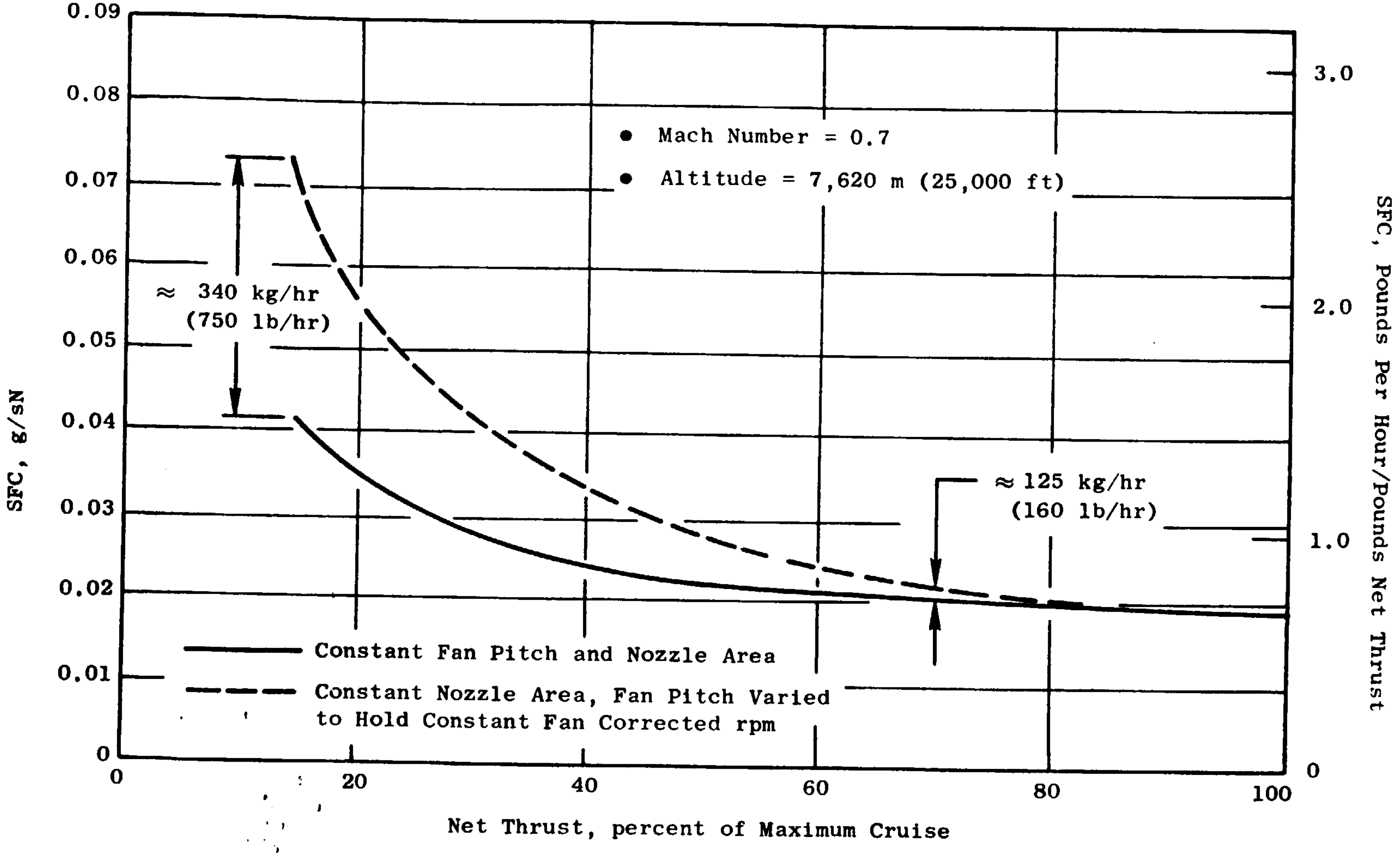

Figure 13-14. Fan Pitch Effect on Cruise SFC.

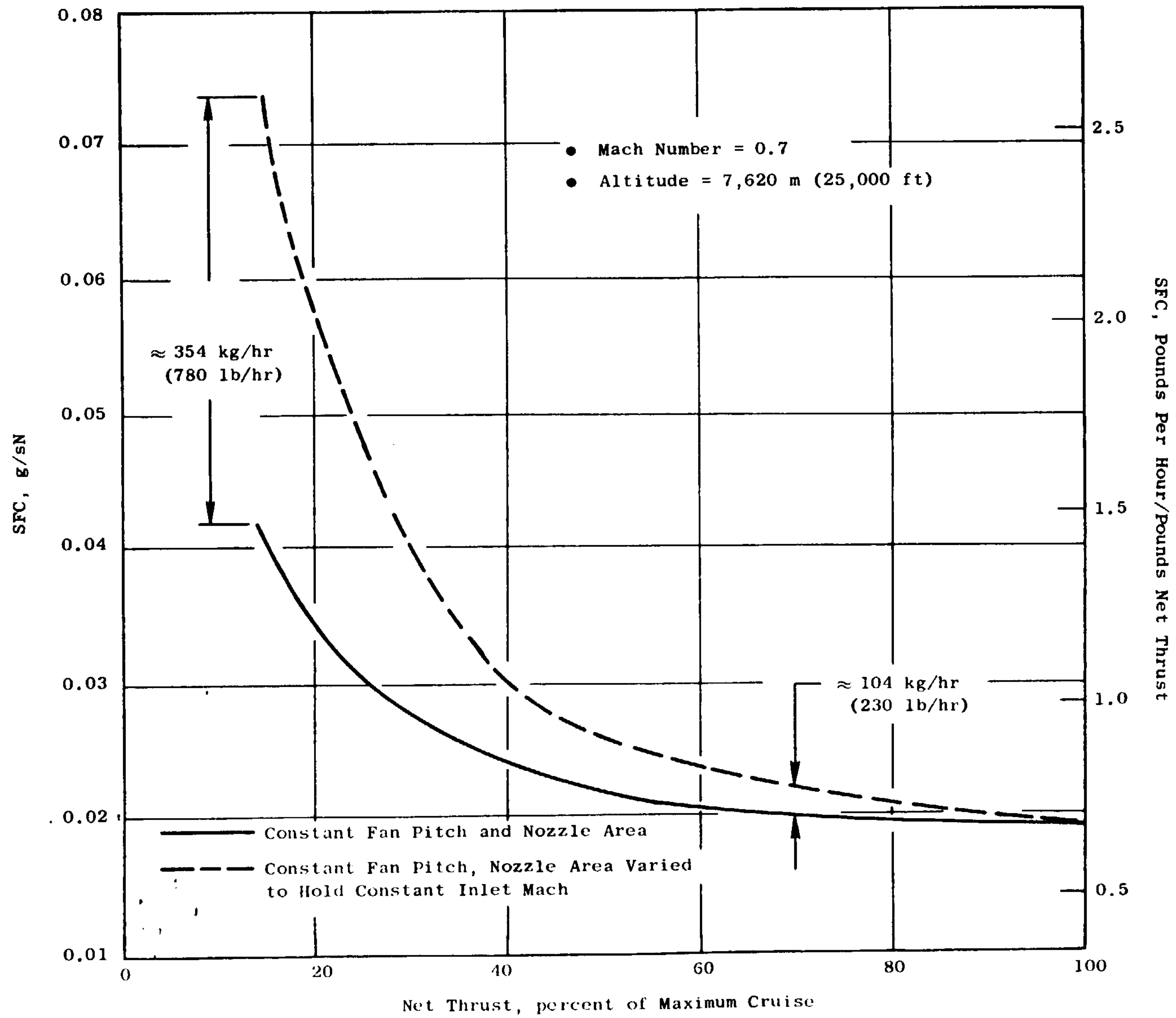

Figure 13-15. Fan Nozzle Effect on Cruise SFC (Mach 0.7, 25,000 ft)

Core Speed Limits - Both the digital and hydromechanical controls sense core speed and provide fuel flow limiting to prevent core overspeed.

Fan Pitch Limits - The fan pitch control loop includes position limits and transient rate limits in both the open and closed directions. The limits will vary depending on mode and are adjustable from the control room.

Fan Nozzle Limits - The fan nozzle control loop includes position limits and transient rate limits in both the open and closed directions. The limits vary depending on mode and are adjustable from the control room.

13.3.3 Manual Control

In addition to automatic control modes, the system also includes a manual control mode and several partially manual modes in which all or some of the manipulated variables can be controlled independently from the control room. The manual modes are provided so that the characteristics of the engine with its variable geometry can be thoroughly explored.

In the all-manual mode, the system operates in response to four basic inputs from the control room, the manual power lever input to the hydromechanical control and three potentiometer inputs to the digital control. The power lever provides backup control of fuel flow through its core engine governor and fuel flow limits. The digital control provides the basic fuel control below the maximum limit in the hydromechanical control to set fan speed as a function of one of the three demand inputs it receives from the control room. The other two demand inputs to the digital control operate fan pitch and fan nozzle position control loops. Thus, in this mode, fan speed, core speed, fan pitch, and fan nozzle area can each be controlled.

In the partially manual modes, one or two of the manipulated variables is under manual control while the others or other are being scheduled and controlled as in the automatic mode.

All of the safety limits described earlier in the automatic control section remain active in the manual and partially manual control modes.

13.3.4 Hydromechanical Control

General Description

The QCSEE hydromechanical control is an F101 main engine control which will contain appropriate modifications applicable to the unique requirements of the QCSEE control system and engine. The control is capable of performing the computation (hydromechanical) and fuel metering necessary to control engine combustor fuel flow and compressor stator vane positioning. Woodward Governor Company is the Vendor source for this control.

The modified F101 Control will perform the following subsystem functions:

- Modulates core engine fuel flow to govern core speed as a backup to the digital control
- Schedules acceleration and deceleration fuel flow limits
- Schedules variable stator vane position
- Provides positive fuel flow shutoff and limits core engine overspeed
- Limits compressor discharge pressure
- Reduces fuel flow in proportion to electrical signals from the digital control as the primary fuel control method
- Provides power lever position intelligence to the digital control
- Provides minimum fuel system pressurization
- Provides fuel flow shutoff to limit fan overspeed in response to electrical control signals from the digital control
- Provides core stator vane reset in response to electrical control signals from the digital control
- Provides electrical metering valve position intelligence to the digital control

Hydromechanical Control Inputs and Outputs

The inputs to and outputs from the hydromechanical control are listed below:

Inputs	Outputs
• Pump discharge fuel flow	• Metered engine fuel flow
• Power lever angle	• Bypass fuel flow
• Core engine drive speed	• Stator vane actuator control pressures
• Compressor discharge static pressure	• Power level electrical position signal
• Core inlet air temperature	
• Core stator actuator position	• Metering valve electrical position signal

Inputs	Outputs
• Electrical fuel flow demand signal	
• Electrical fan overspeed signal	
• Electrical stator reset signal	

Hydromechanical Control Functional Description

A functional block diagram of the hydromechanical control is shown in Figure 13-16.

Fuel flow to the engine is set by controlling the area of the metering valve and maintaining a constant pressure differential across it by means of the bypass valve which returns excess fuel to the fuel return and thence to the fuel pump inlet.

Metering valve area is controlled by the metering valve actuator which is a fuel-operated piston that responds to the output of an electro-hydromechanical computer network within the control. One of the inputs to this network is an electrical signal from the digital control, and, for the UTW engine, this signal will normally be in command of the metering valve. However, the authority of this signal is limited by a core speed governor, an acceleration schedule, and a deceleration schedule.

The core speed governor receives an input demand by means of a 3-D cam that is scheduled as a function of mechanical power lever position and core compressor inlet temperature. This demand is applied to a flyball governor rotated by the core engine rotor through the accessory gearbox and control drive shaft. If the demanded speed and actual speed do not correspond, the governor ports fuel servo pressure toward the metering valve actuator to change fuel flow and thus correct the difference. This pressure will only get through to the actuator, however, if the governor is calling for less fuel flow than either the electrical command from the digital control or the acceleration fuel schedule.

The acceleration fuel schedule is provided by another 3-D cam which is positioned as a function of core engine speed and inlet temperature. The radius of this cam represents the maximum allowable ratio of fuel flow to core compressor discharge pressure (WF/PS3). Through a system of levers, this cam radius, the mechanical position output of a PS3 sensing servo, and the position of the metering valve are combined to provide a schedule upper limit on metering valve position which cannot be exceeded. The deceleration schedule is provided in a similar manner except that it serves as a scheduled lower limit on metering valve position.

Control of the core variable stators is accomplished by generating a stator position demand as a function of core engine speed and inlet temperature, mechanically comparing this to the position of the core stator

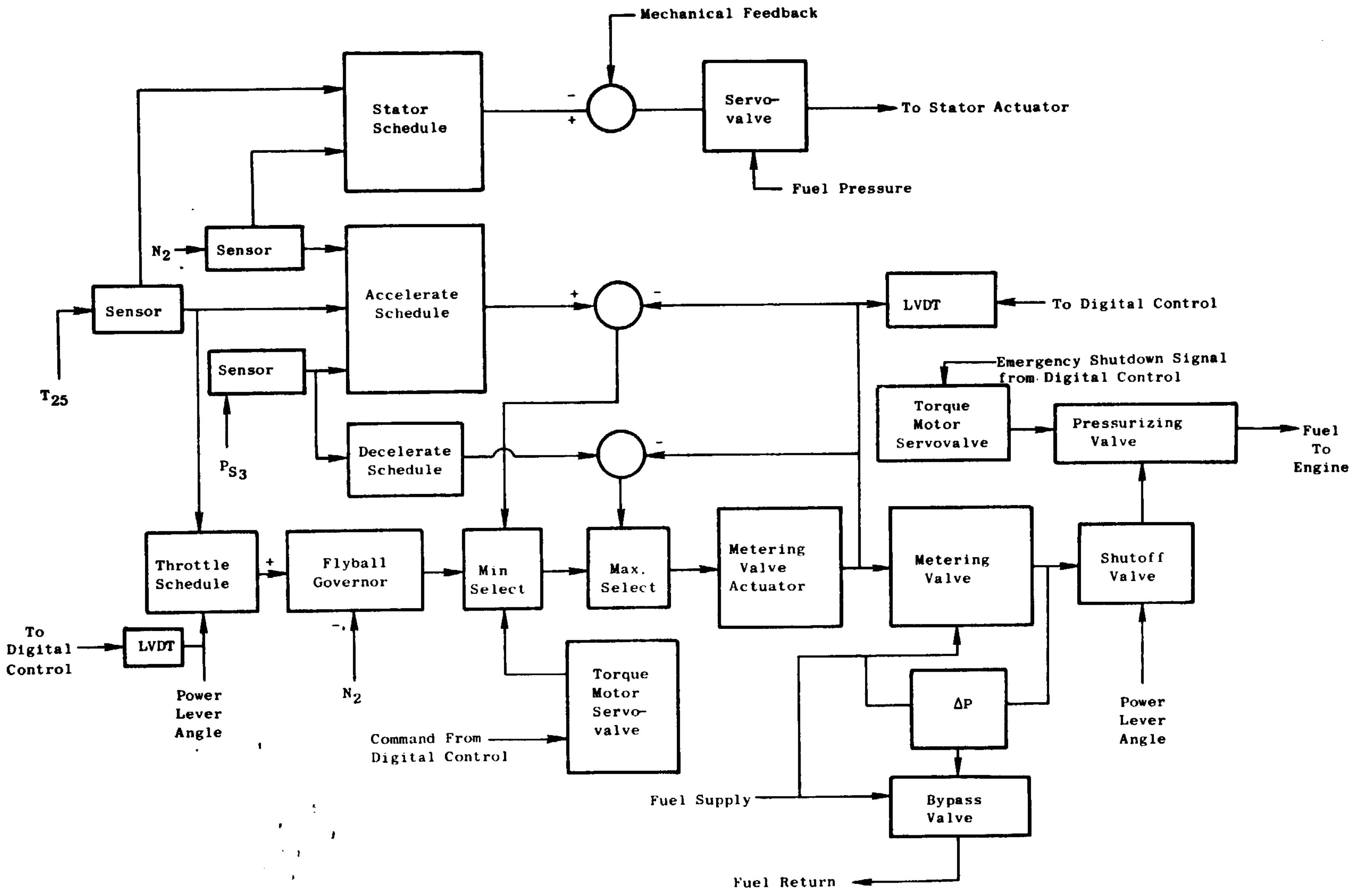
Mechanical Feedback
Stator Schedule
-
+
Servo-valve
To Stator Actuator
Fuel Pressure
N_2
Sensor
Sensor
T_{25}
Accelerate Schedule
+
-
LVDT
To Digital Control
Sensor
P_{S3}
Emergency Shutdown Signal from Digital Control
Torque Motor Servovalve
Pressurizing Valve
Fuel To Engine
Decelerate Schedule
-
Throttle Schedule
+
Flyball Governor
Min Select
Max. Select
Metering Valve Actuator
Metering Valve
Shutoff Valve
To Digital Control
LVDT
Power Lever Angle
-
N_2
Command From Digital Control
Torque Motor Servo-valve
ΔP
Power Lever Angle
Fuel Supply
Bypass Valve
Fuel Return

Figure 13-16. Hydromechanical Control Schematic.

feedback, and applying the results of this comparison to the stator servovalve which ports fuel to the stator actuators as necessary to set the demanded position.

A separate servomechanism remotely located in the core compressor inlet operates in conjunction with elements within the hydromechanical control to set a fuel pressure proportional to compressor inlet temperature thereby sensing this temperature for use in scheduling of variables as noted above.

The control includes two valves downstream from the metering valve, a power-lever-operated shutoff valve and a pressurizing valve which operates to assure adequate fuel pressure at low flow conditions to operate the core stator actuators and other fuel servomechanisms and which also serves as an emergency fuel shutoff valve, closing in response to a fuel servovalve operated by a signal from the digital control.

The hydromechanical control will be mounted on the F101 fuel pump similar to Figure 13-17. The pump is V-band flange mounted to an F101 gearbox pump drive pad. Through shafting is used to provide core speed input to the control drive spline.

13.3.5 Digital Control Subsystem

The digital control subsystem, shown in Figure 13-18, consists of an engine-mounted digital control, and command and monitor peripheral equipment located in the control room.

The digital control performs the computational requirements for the overall engine control system based on the demands received from the command and monitor equipment and other parameters received from engine-mounted sensors. In addition to generating control signals to manipulate fuel flow, fan pitch angle, and fan nozzle area, the digital control transmits engine and control data to the Command and Monitor equipment in the control room.

The command and monitor equipment approximates an aircraft interface in that it provides the command inputs to operate the engine, and the transmission process is the same from a hardware viewpoint as a flight-type system. That is, all command data are transmitted to the digital control in a time-shared digital format over a data link that could be adapted for a flight-type system; however, the command and monitor equipment has a number of added features to provide flexibility in testing an experimental engine. These include several modes of operations, provisions for manually controlling all manipulated variables, selected adjustments inputs to modify steady-state and dynamic characteristics of the control strategy, a fault indication and corrective action program, and a comprehensive control and engine parameter display system.

Fault indication and corrective action is part of the digital control strategy. Five fault tests are performed by the digital control. These are as follows:

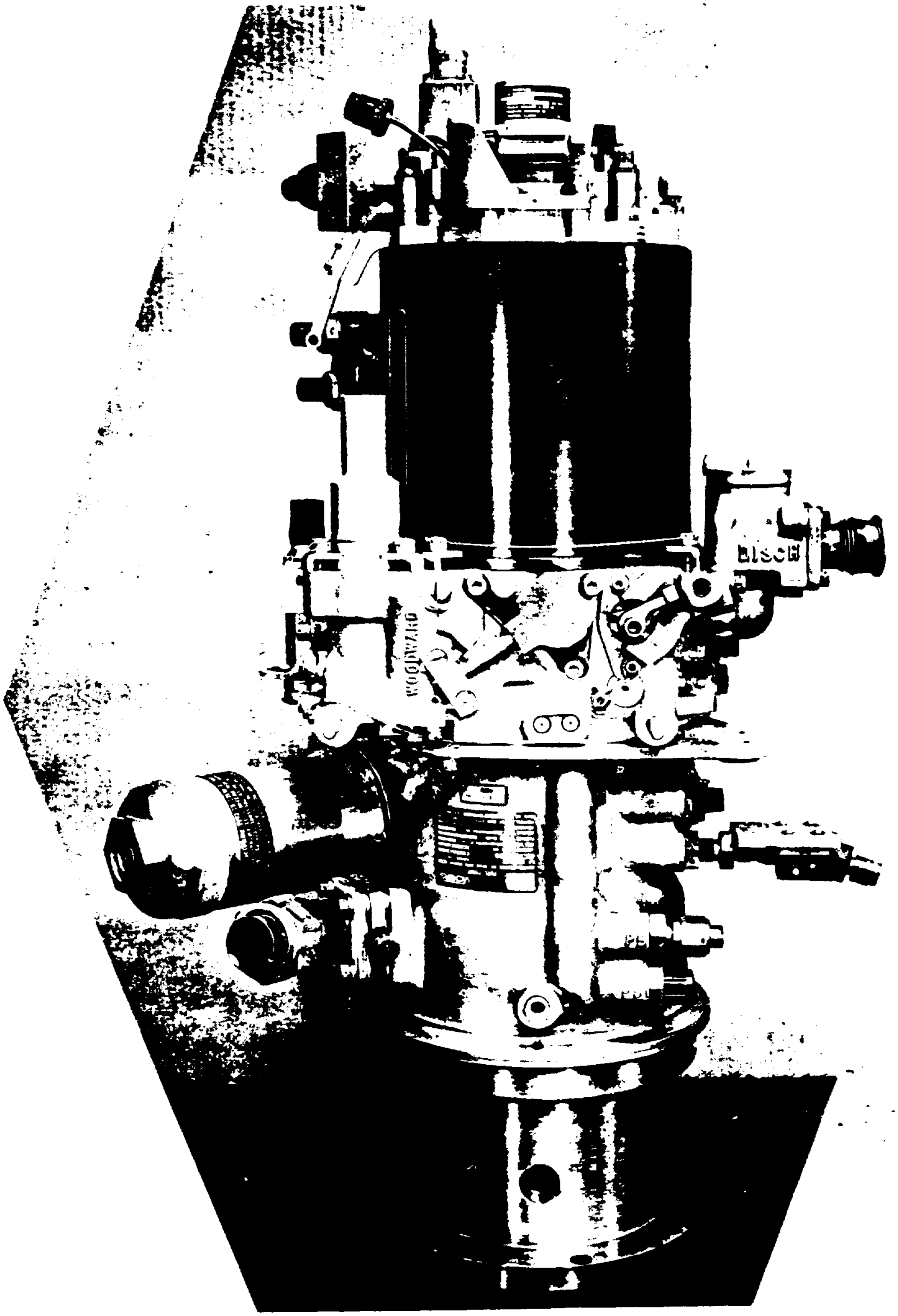

Figure 13-17. F101 Fuel Pump and Control.

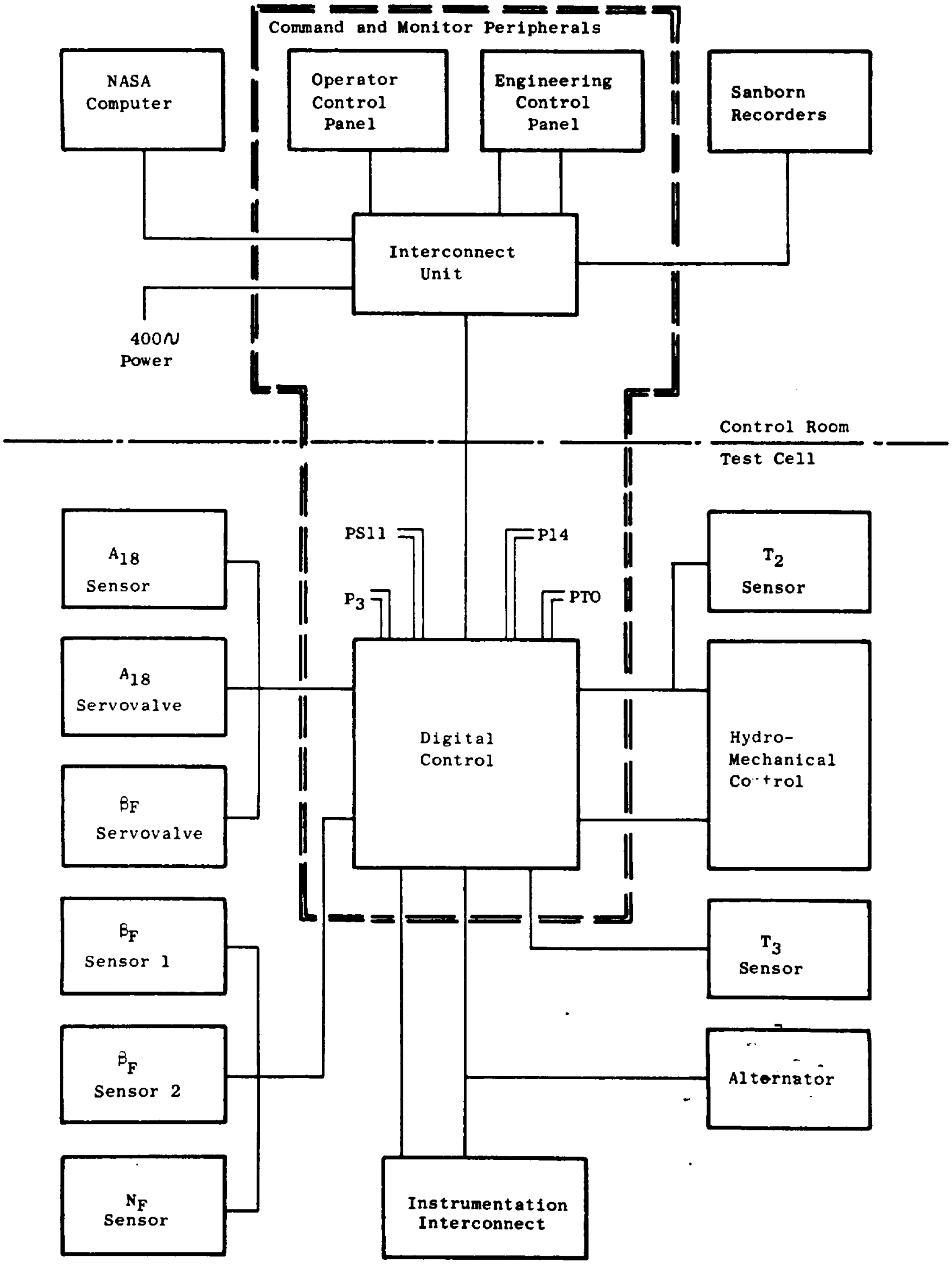
Command and Monitor Peripherals
NASA Computer
Operator Control Panel
Engineering Control Panel
Sanborn Recorders
Interconnect Unit
400∿ Power
Control Room
Test Cell
PS11
P14
P3
PTO
A18 Sensor
A18 Servovalve
βF Servovalve
βF Sensor 1
βF Sensor 2
NF Sensor
Digital Control
T2 Sensor
Hydro-Mechanical Control
T3 Sensor
Alternator
Instrumentation Interconnect

Figure 13-18. Digital Control Subsystem.

1. Digital control fault test to check out the analog-to-digital and digital-to-analog converters and certain portions of the digital control associated with test.

2. Fan speed sensor failure

3. High engine vibration levels

4. Low pressure turbine rotor overspeed

5. Loss of command data link

The corrective action for the first four fault conditions is to reduce or shut down fuel flow, and the corrective action for the last fault condition is to fail (fixed) at the last true inputs. Fault status is part of the monitoring system. If a fault occurs, a fault discrete lights on the operator control panel and the fault condition may be uniquely identified on the engineering control panel.

The following 48 control and engine parameters can be read out from the command and monitor equipment in the control room.

1. Fan nozzle area torque motor current

2. Fan pitch angle torque motor current

3. Fuel control torque motor current

4. Fan nozzle area

5. Fan pitch angle

6. Fuel flow

7. Calculated turbine inlet temperature

8. Inlet Mach number

9. Compressor discharge to inlet pressure ratio

10. Electrical power demand

11. Hydromechanical power lever angle

12. Fan speed

13. Core speed

14. Fuel manifold pressure

15. Compressor stator angle

16. Fuel mode control indication

17. Fan pitch mode control indication

18. Fan nozzle area mode control indication

19. Fault identification

20. Inlet temperature

21. Inlet total pressure

22. Fan discharge to inlet differential pressure

23. Inlet total-to-static differential pressure

24. Compressor discharge pressure

25. Metering valve position

26. Fan pitch angle sensor No. 1 output

27. Fan pitch angle sensor No. 2 output

28. Fan pitch angle demand

29. Nozzle area demand

30. Compressor discharge temperature

31. Compressor stator reset torque motor current

32. Mode control demand input

33. Hydraulic pump discharge pressure

34. Fuel temperature

35. Spare

36. Exhaust gas temperature

37. Engine oil inlet temperature

38. Scavenge oil temperature

39. Engine oil inlet pressure

40. Scavenge oil pressure

41. Fan discharge temperature

42. Low pressure turbine discharge pressure

43. Gearbox interrace bearing temperature

44. Engine horizontal vibration

45. Engine vertical vibration

46. Spare

47. Spare

48. Spare

The above data may be read from a number of stations in the control room. Any one of the 48 parameters may be selected for display on a Binary Coded Decimal readout on the engineering control panel and all parameters are transmitted serially to the remote (NASA) computer in binary form. Parameters 1 through 15 are available for real time analog recording at the interconnect panel and any of the 48 channels may be selected for analog recording a 16 channel. Full parametric readouts of parameters 4, 5, 7 through 10, 12, and 13, are displayed on the operator control panel to aid in the engine operation. In addition, the torque motor currents, items 1 trough 3, are displayed on analog meters on the engineering panel.

Digital Control

The digital control accepts operational input demand and engine parameter information in the form of ac and dc analog signals and digital signals and uses this information to generate engine control signals and engine condition monitoring data. A simplified block diagram of the control is shown in Figure 13-19. The analog signals are conditioned to a standard voltage range and then multiplexed to an analog-to-digital (A/D) converter. The output of the A/D converter is fed to the central precessor unit (CPU) where all necessary calculations are performed. The CPU output is fed into two circuits. One circuit is a multiplexer that sends data out to the aircraft. The other circuit is a digital-to-analog (D/A) converter circuit. The output of the D/A converter is fed to sample and hold circuits and subsequently to the output drive circuits. The drive circuits provide signals to the torque motors that are used to provide engine control. Power to the control is provided by an engine-mounted alternator. The alternator ac signal is converted to the necessary regulated dc voltages.

Digital Control Inputs and Outputs

The QCSEE digital control inputs and outputs listed in Tables 13-IV, 13-V, 13-VI, and 13-VII are described below.

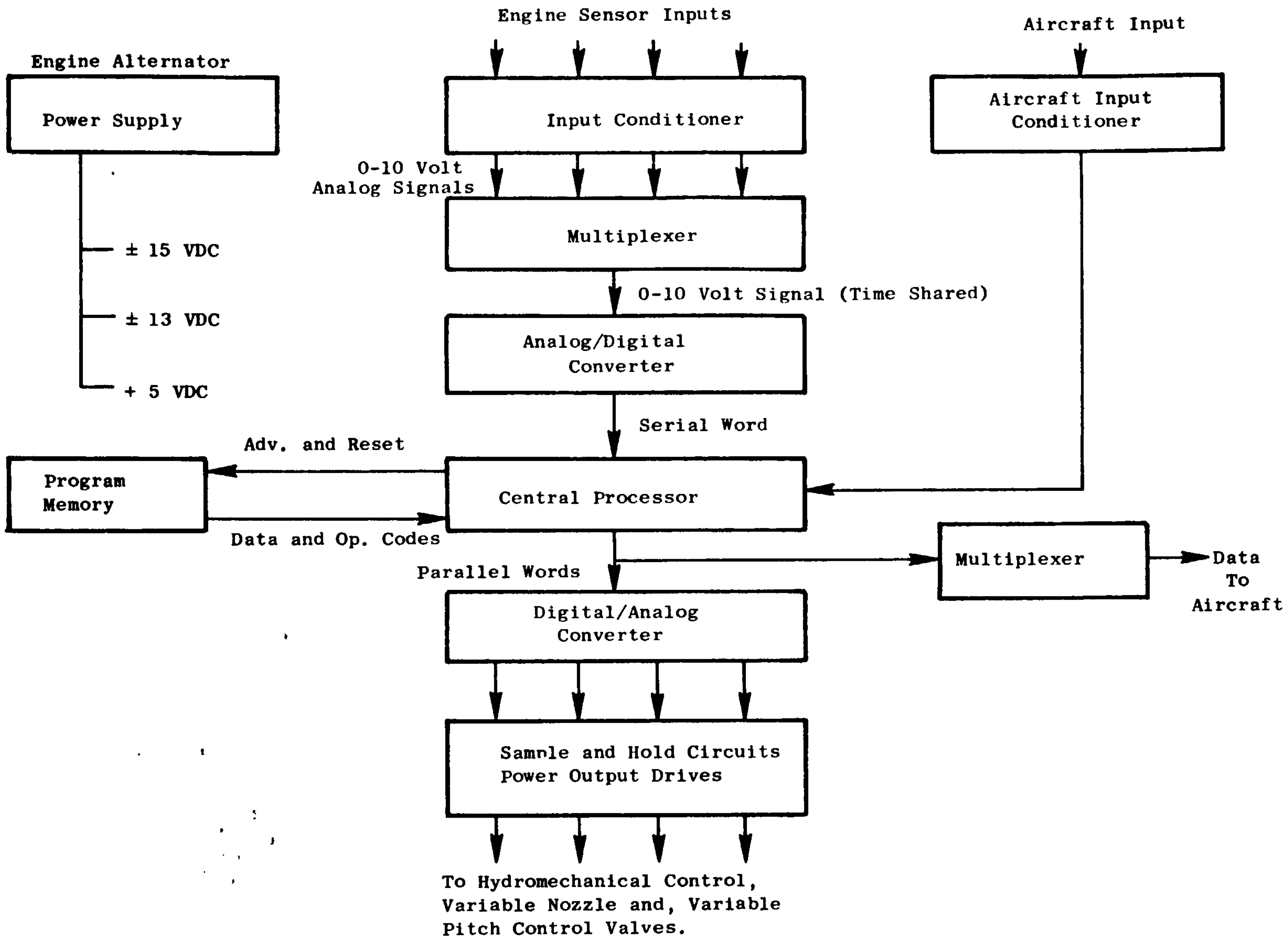
Engine Alternator
Power Supply
± 15 VDC
± 13 VDC
+ 5 VDC
Engine Sensor Inputs
Input Conditioner
0-10 Volt
Analog Signals
Multiplexer
0-10 Volt Signal (Time Shared)
Analog/Digital
Converter
Serial Word
Aircraft Input
Aircraft Input
Conditioner
Adv. and Reset
Program
Memory
Data and Op. Codes
Central Processor
Parallel Words
Multiplexer
Data
To
Aircraft
Digital/Analog
Converter
Samnle and Hold Circuits
Power Output Drives
To Hydromechanical Control,
Variable Nozzle and, Variable
Pitch Control Valves.

Figure 13-19. Digital Control Schematic.

Table 13-IV. Digital Control Instrumentation Input Signals.

(1) Hydraulic Pump Outlet Pressure
(2) Fuel Temperature
(3) Wf Manifold Pressure
(4) EGT
(5) Fuel Flow
(6) Lube Pressure
(7) Lube Scavenge Pressure
(8) Lube Oil Inlet Temperature
(9) Lube Scavenge Oil Temperature
(10) T25
(11) P5 Pressure
(12) Gearbox Inner Race Bearing Temperature
(13) Horizontal Vib
(14) Vertical Vib
(15) Core Stator Position
(16) Spare
(17) Spare
(18) Spare
(19) Spare

Table 13-V. Digital Control Engine Sensor and Transducer Signals.

(1) Power Lever RVDT (Rotary Variable Differential Transformer)
(2) Fuel Metering Valve RVDT
(3) Fan Pitch LVDT (Linear Variable Differential Transformer)
(4) Fan Pitch LVDT
(5) Fan Nozzle LVDT
(6) N_{IT} (LP Turbine rpm No. 1)
(7) N_{IT} (LP Turbine rpm No. 2)
(8) T3 (Compressor Discharge Total Temperature)
(9) T12 (Fan Inlet Total Temperature)
(10) PS3 (Compressor Discharge Static Pressure)
(11) PTO (Engine Inlet Total Pressure)
(12) PTO-PS11 (Inlet Static Pressure)
(13) P14 (Fan Discharge Total Pressure)-PTO

Table 13-VI. Alternator and Digital Signals to Digital Control.

(1) N2 Alternator Winding	
(2) N2 Alternator Winding	
(3) Command Data	Digital Signals - 3 twisted pairs to digital control
(4) Command Sync.	
(5) Command Clock	

Table 13-VII. Digital Control Outputs.

(1) Fuel Metering Valve Torque Motor Current (TMC)	
(2) Fan Nozzle TMC	
(3) Fan Pitch TMC	
(4) Fan Pitch LVDT Excitation	
(5) Fan Pitch LVDT Excitation	
(6) Fuel Metering Valve RVDT Excitation	
(7) Power Lever RVDT Excitation	
(8) Fan Nozzle LVDT Excitation	
(9) Core Stator Reset TMC	
(10) Emergency Shutdown TMC	
(11) Monitor Sync.	Digital Signals - 4 twisted pairs to control room interconnect unit
(12) Monitor Clock	
(13) Monitor Data	
(14) Reset	
(15) T12 Excitation	

Inputs to the digital control consist of four classifications: (1) instrumentation signals, (2) sensor and transducer signals, (3) power signals, and (4) digital signals. Table 13-IV is a list of the instrumentation input signals. These signals are all 0-10 volt levels and the only signal conditioning required is an isolation amplifier in the digital control. Presently there are 15 instrumentation signals being used and there are four spare inputs that may be used if needed.

The sensor signals are shown in Table 13-V and come from various transducers and sensors located on the engine. Some signals are ac and some are dc, and have various voltage ranges. These signals are conditioned to a standard 0-10 volt level in order to be used by the digital control.

The remaining inputs are the alternator signals that provide the power to the digital control and the digital signals that feed digital data to the control. These are listed in Table 13-VI.

The QCSEE digital control outputs are of three types: (1) torque motor drive signals, (2) transducer and sensor excitation signals, and (3) digital signals. Table 13-VII lists these.

Digital Control Functional Description

Input Signal Conditioners

The input signal conditioning circuits are of two types: (1) isolation amplifiers and (2) processing amplifiers. The isolation amplifiers isolate the instrumentation output amplifiers from the control. These amplifiers prevent loading problems.

The signal processing amplifiers differ in design depending on the type of input signal. These consist of demodulating circuits, frequency to dc converters, and straight-gain setting amplifiers. These circuits condition all input signals to a standard 0-10 volt level over the signal range of interest. The proper gains and offsets to accomplish this are set in these amplifiers. The outputs of both isolation amplifiers and processing amplifiers are fed into an analog multiplexer.

Analog Multiplexer

The analog multiplexer circuit consists of three 16-channel multiplexer chips making a total of 48 signals which can be multiplexed. Each channel can be addressed separately depending on the signal needed by the digital control at any particular time. The outputs of the three multiplexer chips are connected together and are fed to a sample and hold circuit. The output of this circuit goes to an A/D converter circuit.

Analog-to-Digital (A/D) Converter

The A/D converter is a 12-bit successive approximation type circuit with a conversion time of 24 microseconds. The input to the A/D converter is a 0-10 volt dc signal and is converted to a digital word that corresponds to the particular voltage at the converter input. For 12 bits, there are 4096 possible words. The output of the A/D converter is fed to a serial digital multiplexer and from there to the central processor unit (CPU).

Central Processor Unit

The CPU along with the program memory form the digital computer of the digital control. This circuit contains the arithmetic logic unit, the control and timing unit, the scratch pad memory, the accumulator, and other logic circuits necessary to carry out all calculations to generate the engine control signals and other functions. This unit accepts the A/D converter signals and the aircraft digital signals via the serial digital multiplexer. A block diagram of the CPU is seen in Figure 13-20. The output of the CPU is fed to a digital multiplexer whose output transmits data to the aircraft. The CPU output also goes to a digital-to-analog converter.

Digital-to-Analog (D/A) Converter

The D/A converter has a 12-bit digital word as an input and the output is one of 4096 possible voltage levels corresponding to the digital input. The output of the D/A is bipolar and will be in the -5 volt to +5 volt range. The D/A output is fed to the output drive circuits.

Output Drive Circuits

The output drive circuits consist of sample and hold circuits and the output circuits needed to power the valves, torque motors, etc. As the digital control performs the programmed calculations, the output of the D/A converter is sampled at the proper time and stored in a sample and hold circuit. This value is held until the next time the program calls for this particular sample and hold circuit to be pulsed and the next value of the calculation to be stored. The output of each sample and hold circuit is fed to a driver amplifier. The outputs of the driver amplifiers are used to actuate the torque motors, and valves that provide engine control.

Other Circuits

Transducer excitation circuits are also provided in the digital control. A 2.048 mHz clock signal is used to generate a 3011 Hz, 20 v p-p sine wave signal. This signal is fed to two transducer driver amplifiers whose outputs are used to provide the excitation voltage for the LVDT's. The 3011 Hz signal is also used as a demodulate reference.

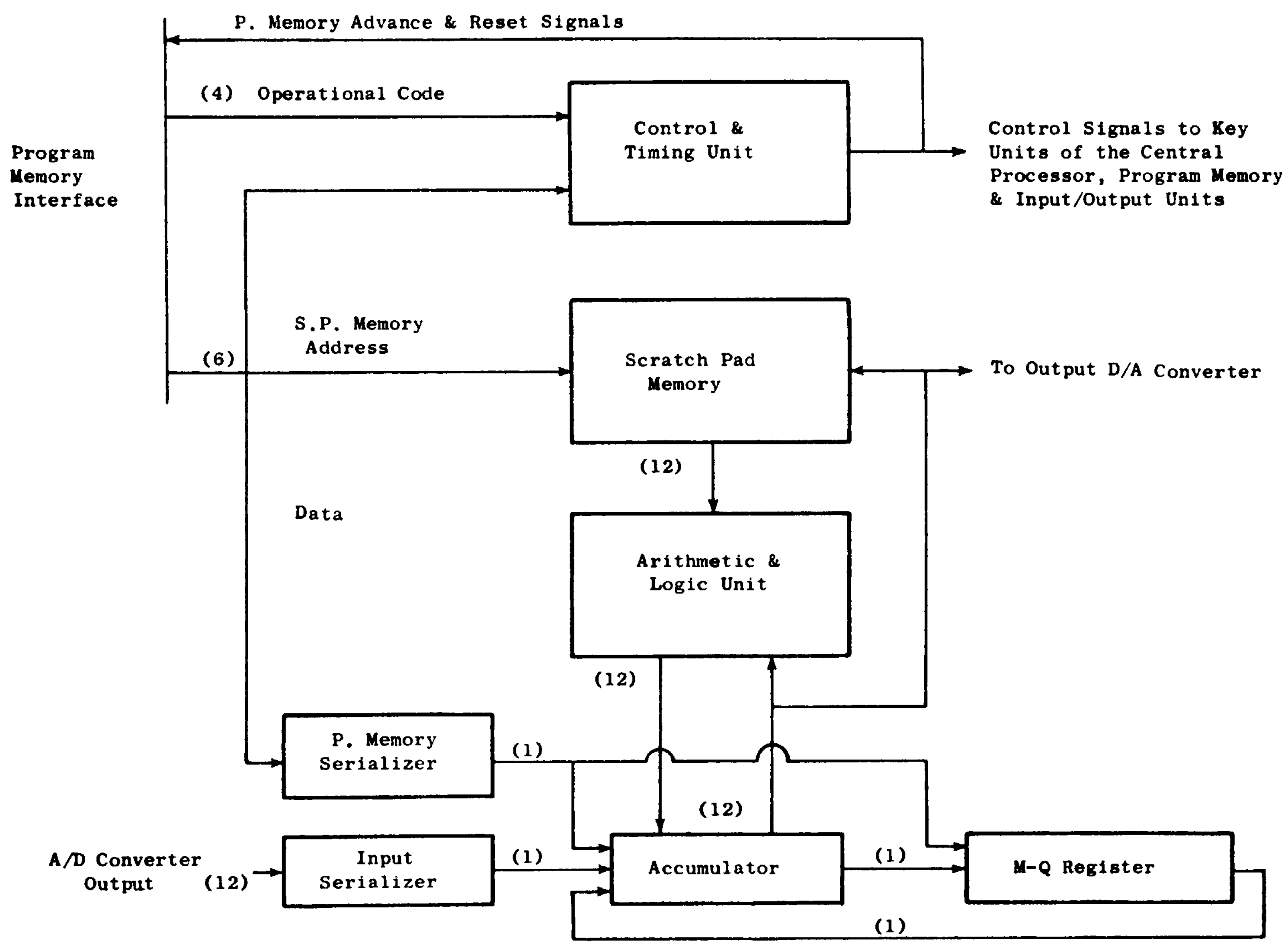
P. Memory Advance & Reset Signals
(4) Operational Code
Program Memory Interface
Control & Timing Unit
Control Signals to Key Units of the Central Processor, Program Memory & Input/Output Units
S.P. Memory Address
(6)
Scratch Pad Memory
To Output D/A Converter
(12)
Data
Arithmetic & Logic Unit
(12)
P. Memory Serializer
(1)
(12)
A/D Converter Output
(12)
Input Serializer
(1)
Accumulator
(1)
M-Q Register
(1)

Figure 13-20. Central Processor Unit.

The emergency shutdown and overspeed circuit performs two functions: (1) detects a failure in the low pressure system through speed rate of change and (2) detects a low pressure turbine overspeed. If either of these conditions exist, a fuel valve is closed to shut down the engine. This circuit is self-contained and has its own power supply.

The QCSEE digital control power supply circuit accepts an AC signal from an engine-mounted alternator and converts it to the desired regulated voltages. There are three supplies: (1) a + and -15 volt supply, (2) a + and -11 volt supply, and (3) a + 5 volt supply.

Mechanical Design

The engine-mounted digital control unit is made up of a chassis which provides mounting and which contains electrical connectors for external communications and a series of individual modules which contain the electrical components and circuits. A sketch of the unit is shown in Figure 13-21.

The mechanical design and packaging approach for the digital control uses designs similar to existing on-engine electrical controls which have been proven on many military engine applications. To achieve the required reliability level, the control mechanical design must consider the unique turbine engine environment. Detail consideration is given to vibratory loads and cyclic temperature effects with respect to materials, mounting, potting, and interconnections. Structural integrity of the electrical components and interconnections is provided by installing the component in module cans which are filled with a resilient potting compound. This approach provides vibration damping. The digital control will be designed to meet the maximum vibration inputs expected from the fan frame. Vibration scans will be made on the complete assembly for the experimental engine. These results will be evaluated in light of past experiences and the brackets on chassis will be modified as required to assure successful on-engine performance.

Heat generated by the electrical components is dissipated by positive conduction and convection. Various thermally conductive materials are used as required to provide a path for transferring the component heat to an air-cooled heat sink system. The cooling air is gathered by an air scoop on the outer surface of the engine nacelle, piped through the digital control and discharged into the air inlet of the engine. The relatively low inlet static pressure in the inlet provides a difference in pressure sufficient to assure adequate airflow in the heat sink. This positive airflow system provides sufficient heat transfer to adequately control the internal temperatures of the digital control. Details on module and chassis construction are presented below.

Electrical analog circuits are mounted to printed circuit boards (PCB's). A typical analog circuit requires two PCB's with copper runs on one or two sides. An anodized aluminum heat sink, which provides the high conductivity heat path to the mounting flange, is bonded to the component side of the

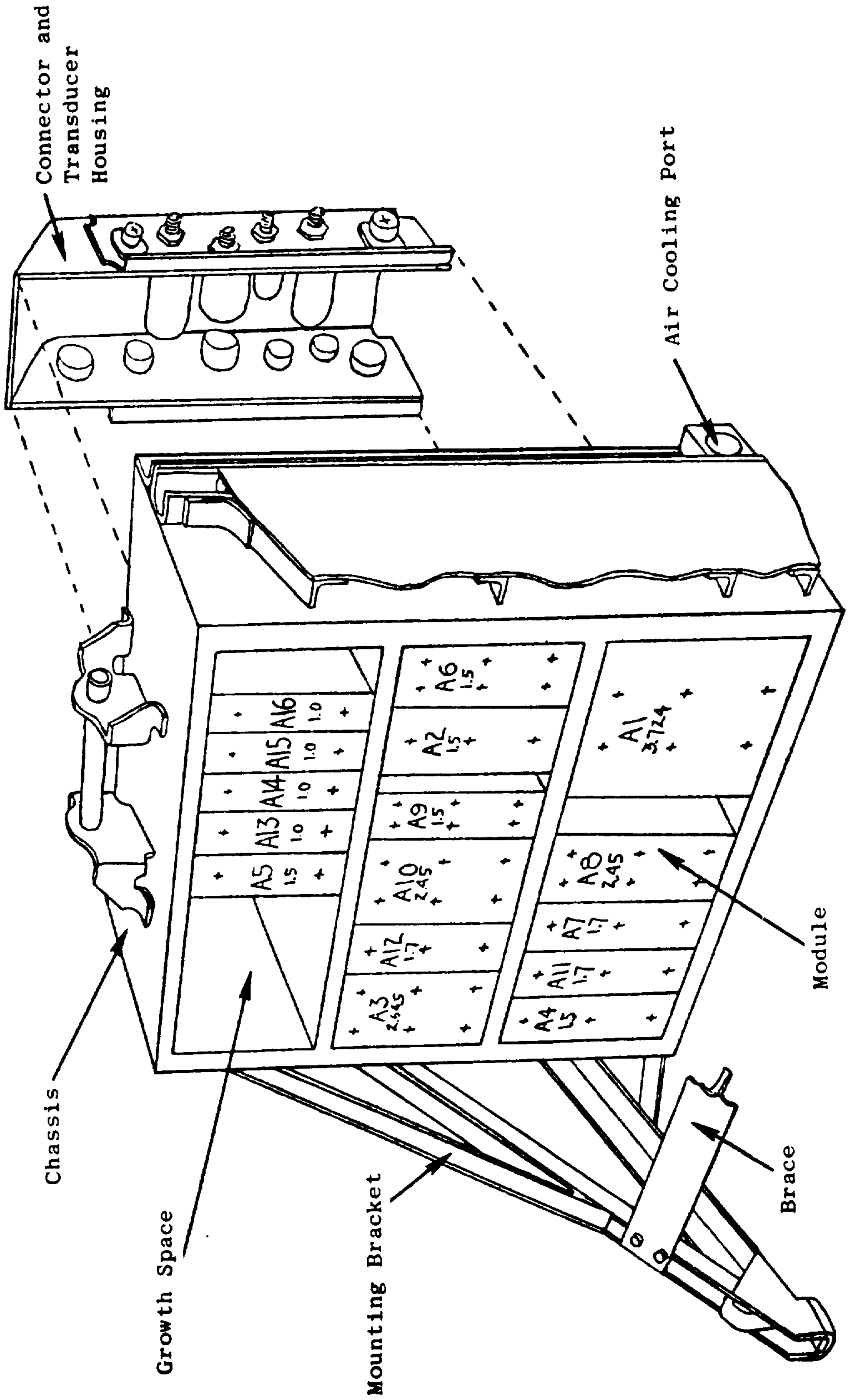
Connector and Transducer Housing
Air Cooling Port
Chassis
Growth Space
Mounting Bracket
Brace
Module
A5 1.5
A13 1.0
A14 1.0
A15 1.0
A16 1.0
A3 2.45
A12 1.7
A10 2.45
A9 1.5
A2 1.5
A6 1.5
A4 1.5
A11 1.7
A7 1.7
A8 2.45
A1 3.724

Figure 13-21. Digital Control.

PCB. The electrical components are mounted so that they rest on the heat sink and their leads protrude through the plated holes. The board assemblies are wave-soldered and then tested for performance. The two-board assemblies are mounted in module cans as shown in Figure 13-22. The can is filled with an RTV potting material to a level covering the upper edge of the PCB's. Hookup wires are attached to the exposed pins at the upper edge of the PCB's and a clear RTV is used to fill the module can. The above potted assembly is called a module. Each module is a functionally discrete portion of the control. It is tested as an individual assembly and is directly interchangeable with a like module should replacement become necessary.

Digital circuits, which use dual in-line package (DIP) components, are mounted on wire-wrapped PCB's. These PCB's have terminal inserts. Interconnections are made by wire-wrapping solid insulated wire as required for a point-to-point wiring arrangement on the inserts.

These wire wraps and the DIP terminal interfaces are soldered to complete the electrical connections. The DIP's for the Central Processor will be mounted on wire-wrapped PCB's also. The remainder of the module assembly for the wire-wrapped PCB's is the same as for the analog modules.

The chassis contains the modules, the connectors, the electrical filters and pressure transducers and is a dip-brazed, aluminum, inseparable assembly. The chassis is supported on each end by a mounting bracket to the fan frame inside of the nacelle. Brackets are strengthened with a "T" sectioned brace between them. One of the connectors is mounted on the electrical filter housing which is needed for electromagnetic compatibility (EMC) purposes. Three of the pressure transducers are mounted on a single manifold which receives the necessary inputs through three pressure ports. The manifold is mounted to a support plate along with two connectors and a self-mounted transducer. Five connectors are mounted on a second support plate. These two connector supports and the filter housing help form the housing on the chassis. Internal to the chassis, two stiffening ribs are used to carry the module loads out to the sides of the chassis. Two flanges, stiffened with gussets, carry the loads from the chassis sides out to the mounting brackets. The transducer and connector mounting system is rugged enough to adequately resist the loads imposed by the electrical cables and the pressure lines. External surfaces of the chassis and covers are anodized to improve their resistance to handling. Chassis surfaces which interface with connectors, modules, transducers, covers, electrical filters, and ground paths are chemically treated to minimize electrical resistance. Iridite and alodine are two acceptable types of treatment. The lower electrical resistance improves the EMC capability. The module mounting surface has finned passages in which the cooling air flows. These passages are located so as to maximize the conductive-convective relationships. The whole heat transfer system is designed to minimize the temperature difference between the cooling air and the electrical components.

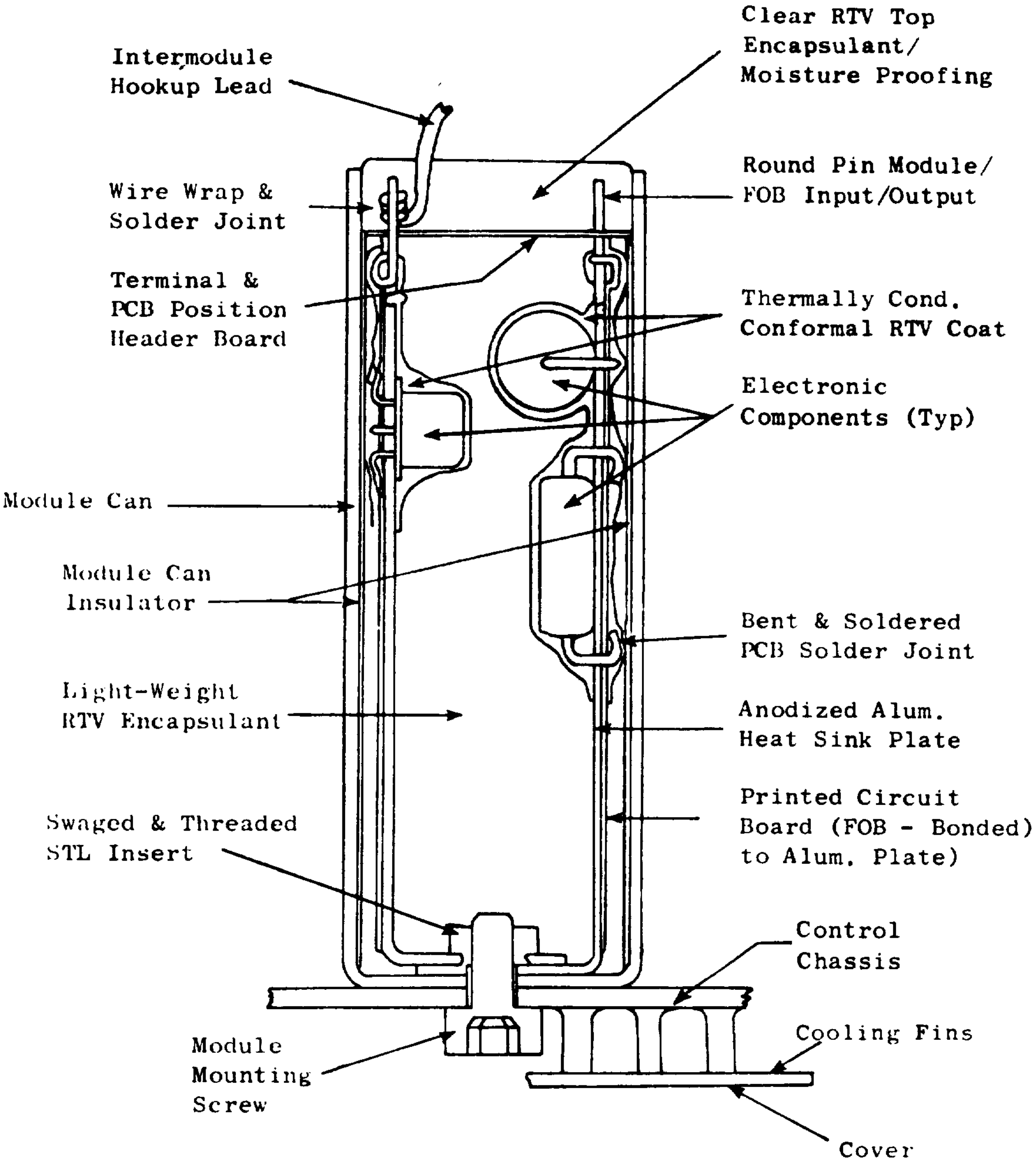
Intermodule Hookup Lead
Clear RTV Top Encapsulant/ Moisture Proofing
Wire Wrap & Solder Joint
Round Pin Module/ FOB Input/Output
Terminal & PCB Position Header Board
Thermally Cond. Conformal RTV Coat
Electronic Components (Typ)
Module Can
Module Can Insulator
Bent & Soldered PCB Solder Joint
Light-Weight RTV Encapsulant
Anodized Alum. Heat Sink Plate
Printed Circuit Board (FOB - Bonded) to Alum. Plate)
Swaged & Threaded STL Insert
Control Chassis
Cooling Fins
Module Mounting Screw
Cover

Figure 13-22. Typical Digital Control Module.

Command and Monitor Peripheral Equipment

An overall function schematic of the command and monitor equipment is shown in Figure 13-23. The interconnect unit processes all the command data received from the operator and engineering control panels and the remote NASA computer and transmits this data to the digital control in a time-shared serial format in a sequence prescribed by the digital control. Engine and control monitor data received from the digital control are processed in the interconnect unit and transmitted to operator control panel, the engineering panel, the remote (NASA) computer, and to instrumentation. The following is a description of the input and output requirements of each of the command and monitor units.

Input and Output

The inputs and outputs to and from the interconnect unit are in the form of digital and analog signals.

Engineering Control Panel

From the Engineering Control Panel to the interconnect unit, analog signals of levels 0 to 10 volts are used to transmit control demand and adjustment information. Mode information is transmitted in a parallel digital manner.

Monitoring information is transmitted in serial digital form from the interconnect unit to the Engineering Control Panel. The information transmitted is converted from binary to binary-coded decimal and one selected word at a time is displayed on a four-decade digital panel meter. Analog signals representing fuel metering, fan nozzle, and fan pitch torque motor currents are transmitted to the Engineering Control Panel and displayed on three analog panel meters (Figure 13-24).

Operator Control Panel

From the operator control panel to the interconnect unit, analog signals (0 to 10 volts) are used to transmit control demand information. Mode information is transmitted in a parallel digital manner. The information transmitted is illustrated on the lower portion of the front panel display of Figure 13-25.

From the interconnect unit to the operator control panel, monitoring information is transmitted serially in a digital manner. The information is scaled by a microprocessor and displayed on nine 4-decade digital panel meters. The information displays are shown on the upper front panel as shown on Figure 13-25.

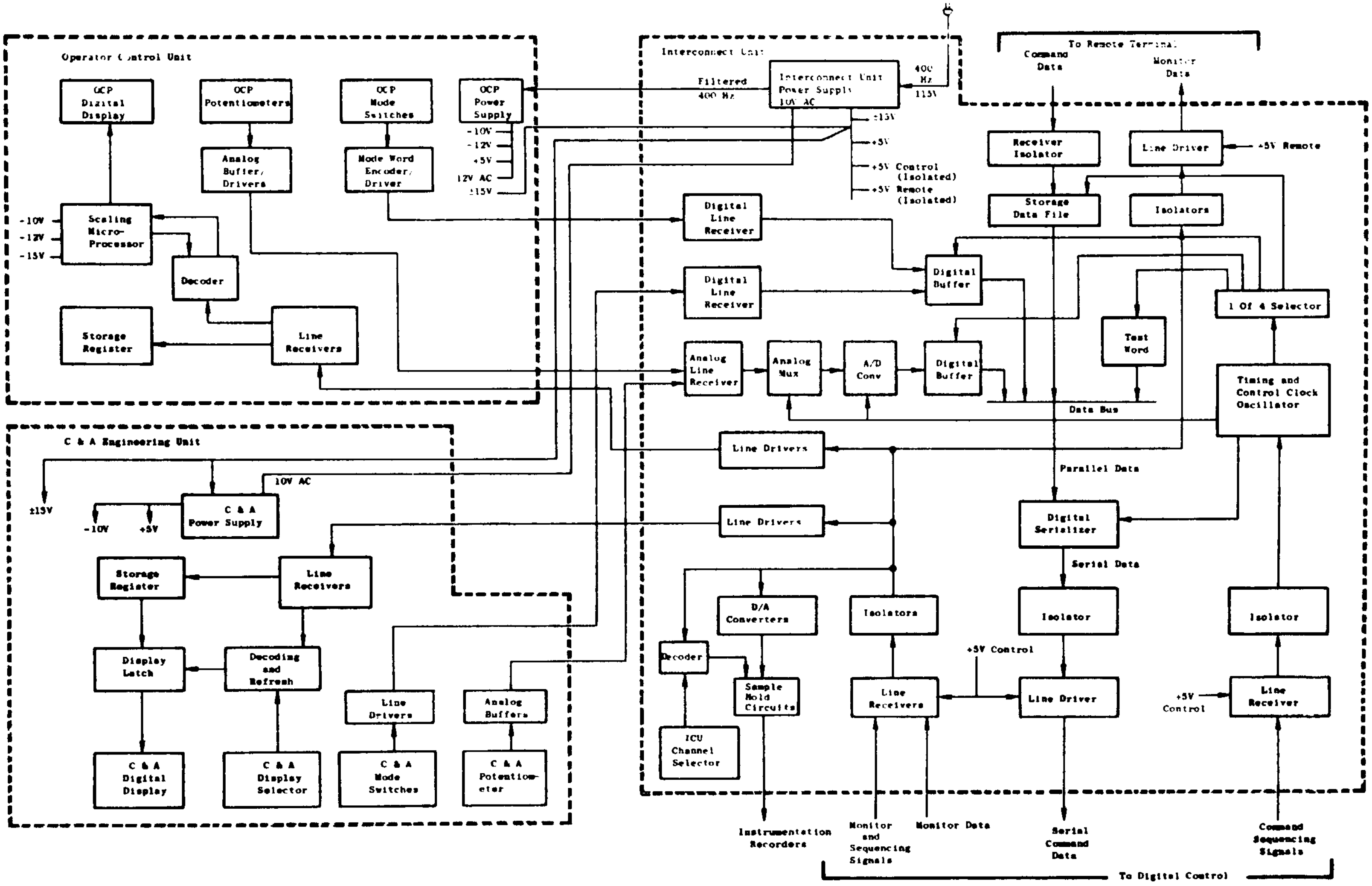
Operator Control Unit
OCP Digital Display
OCP Potentiometers
OCP Mode Switches
OCP Power Supply
-10V
-12V
+5V
12V AC
±15V
Analog Buffer/ Drivers
Mode Word Encoder/ Driver
-10V
-12V
-15V
Scaling Micro-Processor
Decoder
Storage Register
Line Receivers
C & A Engineering Unit
±15V
10V AC
C & A Power Supply
-10V
+5V
Storage Register
Line Receivers
Display Latch
Decoding and Refresh
Line Drivers
Analog Buffers
C & A Digital Display
C & A Display Selector
C & A Mode Switches
C & A Potentiometer
Interconnect Unit
Filtered 400 Hz
Interconnect Unit Power Supply
10V AC
400 Hz
115V
±15V
+5V
+5V Control (Isolated)
+5V Remote (Isolated)
Digital Line Receiver
Digital Line Receiver
Analog Line Receiver
Analog Mux
A/D Conv
Digital Buffer
Digital Buffer
Data Bus
Line Drivers
Line Drivers
D/A Converters
Decoder
Sample Hold Circuits
ICU Channel Selector
Isolators
Line Receivers
To Remote Terminal
Command Data
Monitor Data
Receiver Isolator
Line Driver
+5V Remote
Storage Data File
Isolators
Test Word
1 Of 4 Selector
Timing and Control Clock Oscillator
Parallel Data
Digital Serializer
Serial Data
Isolator
Isolator
+5V Control
Line Driver
+5V Control
Line Receiver
Instrumentation Recorders
Monitor and Sequencing Signals
Monitor Data
Serial Command Data
Command Sequencing Signals
To Digital Control

Figure 13-23. Digital Control Command and Monitor Equipment.

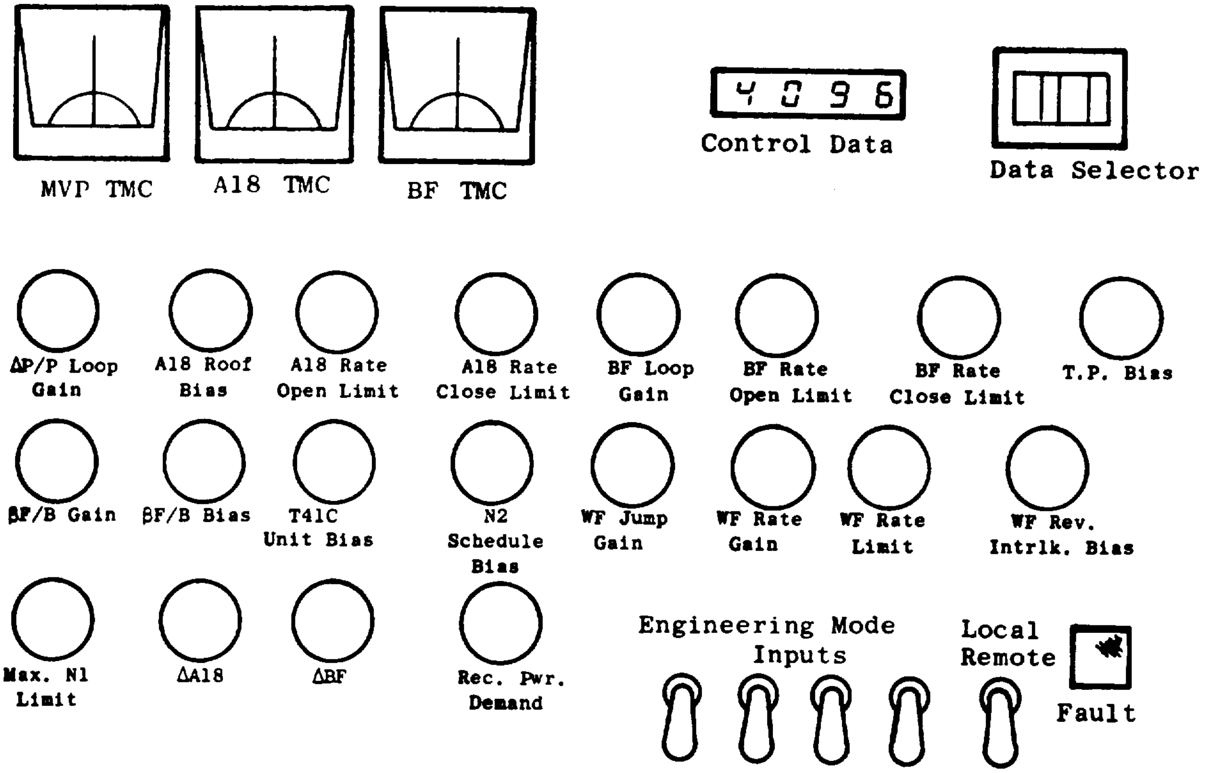
4 0 9 6
Control Data
Data Selector
MVP TMC
A18 TMC
BF TMC
ΔP/P Loop Gain
A18 Roof Bias
A18 Rate Open Limit
A18 Rate Close Limit
BF Loop Gain
BF Rate Open Limit
BF Rate Close Limit
T.P. Bias
βF/B Gain
βF/B Bias
T41C Unit Bias
N2 Schedule Bias
WF Jump Gain
WF Rate Gain
WF Rate Limit
WF Rev. Intrlk. Bias
Max. N1 Limit
ΔA18
ΔBF
Rec. Pwr. Demand
Engineering Mode Inputs
Local
Remote
Fault

Figure 13-24. Engineering Control Panel.

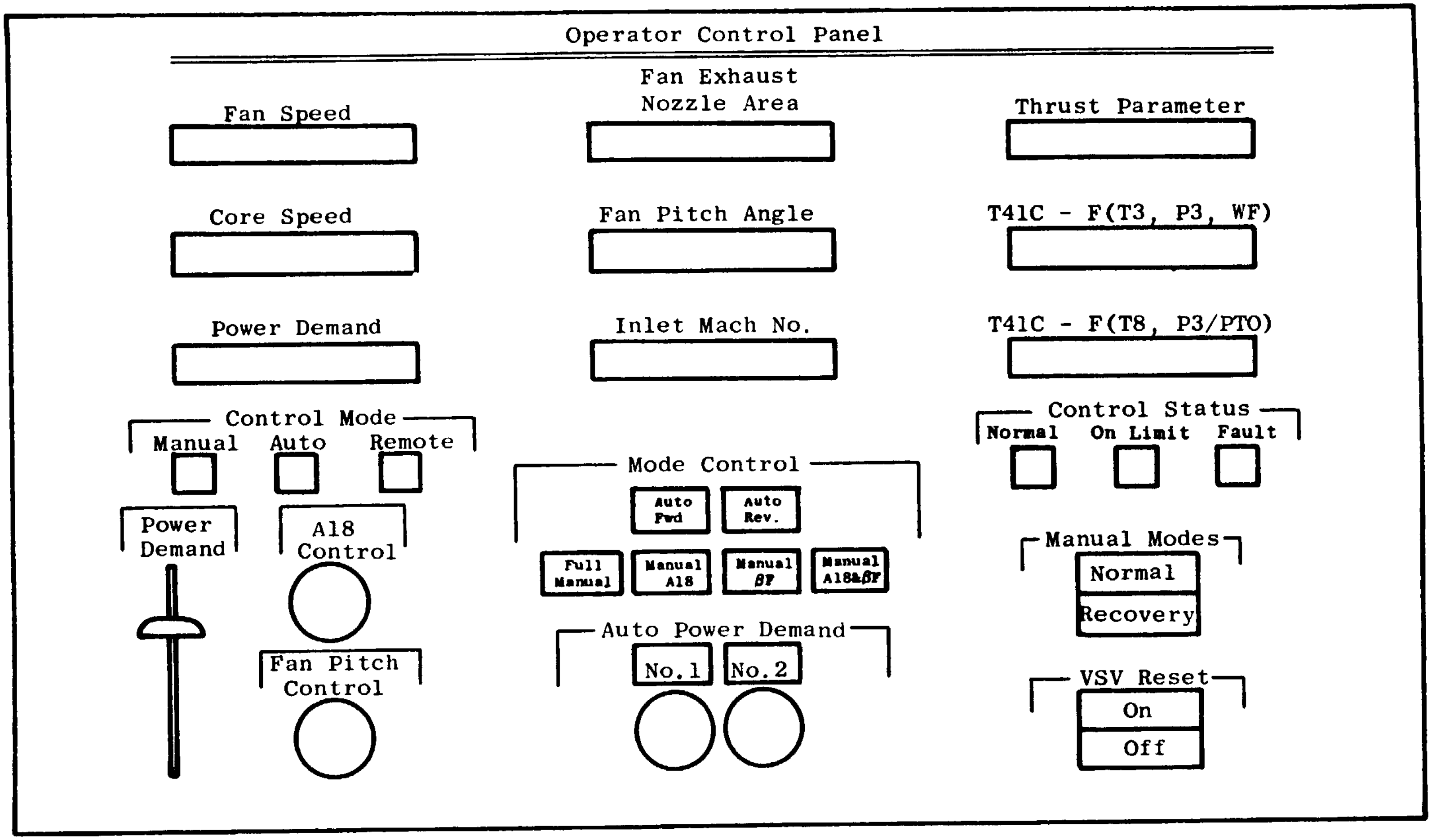
Operator Control Panel
Fan Speed
Core Speed
Power Demand
Fan Exhaust Nozzle Area
Fan Pitch Angle
Inlet Mach No.
Thrust Parameter
T41C - F(T3, P3, WF)
T41C - F(T8, P3/PTO)
Control Mode
Manual
Auto
Remote
Power Demand
A18 Control
Fan Pitch Control
Mode Control
Auto Fwd
Auto Rev.
Full Manual
Manual A18
Manual βF
Manual A18&βF
Auto Power Demand
No.1
No.2
Control Status
Normal
On Limit
Fault
Manual Modes
Normal
Recovery
VSV Reset
On
Off

Figure 13-25. Operator Control Panel.

Remote Terminal Unit

From the Remote NASA Computer to the Interconnect Unit, four 16-bit data words are transmitted serially by bit. These words contain one mode word and three control command words.

From the interconnect unit to the Remote NASA Computer, monitoring information is transmitted serially by bit. The Remote Computer will accept this information and convert it to a form acceptable to the user.

Digital Control

From the interconnect unit to the digital control, all the information gathered from the peripheral units is transmitted to the digital control serially by bit upon demand from the digital control.

From the digital control to the interconnect unit, monitoring information is transmitted serially by bit and distributed to each peripheral unit in a suitable format acceptable to that unit.

Functional Description

Signal Conditioners

All digital signals are transmitted by differential line drivers and received by a differential line receiver over twisted wire pairs. All analog signals transmitted are buffered by low output impedance amplifiers and received by operational amplifiers in a differential configuration.

Analog Multiplexer

The analog multiplexer located in the Interconnect Unit consists of two 16-channel multiplexer chips capable of handling all the analog inputs from the Engineering Control Unit and the Operator Control Unit. Each of the eighteen inputs are capable of being addressed separately in a predetermined sequence at a particular time determined by the digital control. The output of the multiplexer circuit goes to a sample and hold circuit and awaits A/D conversion.

Analog-to-Digital Conversion

All analog signals coming into the Interconnect Unit are converted to a digital word upon command from the digital control just prior to being transmitted to the digital control.

Data Bus

Digital multiplexing at the data bus is accomplished by employing tri-state logic devices to provide inputs to the bus. The three states are high output, low output, and high impedance. Placed in the high impedance state, the devices can be essentially deactivated, while the other two states are used to define logic levels in the transmission mode. All but one of the devices whose outputs are connected to the data bus shown in Figure 13-23 are placed in the high impedance state, and the remaining device will be in the transmission mode. In this manner, a single input to the data bus is made available to the digital serializer as 12-bit parallel data word.

Digital Serializer

The digital serializer is a 12-bit shift register which is parallel loaded upon command. Subsequently, the data is shifted one bit at a time into the transmission system.

Isolators

The isolation of signal and signal grounds is accomplished by means of optical isolators. These devices convert electric signals into light, internally, and then reconvert the light signal back into electrical signals. This process breaks all electrical connection from input to output while maintaining the signal information. The purpose of the isolators is to assure that ground loops, power differences between systems and signal noise are reduced to a minimum.

Power Supply System

The power supply for the peripheral units is derived from a 400 Hz source of 200 volt/amps or more. In the interconnect unit ±15 volts are developed and routed to the Engineering Control Unit and the Operator Control Unit. Analog circuits requiring the use of ±15 volts in any of the three units use this regulated supply.

The +5 volts supply is generated separately and used as a logic supply in each of the three units.

There are two isolated +5 volt logic supplies in the interconnect unit derived specifically to be used in the isolation technique used in this system.

The Operator Control Unit develops -10 v and -12 v for the scaling microprocessor. The +5 volts is developed for a logic supply and the 12 volts ac is used to light the front panel push button switches and indicators.

The Engineering Control Unit develops -10 v to reference the potentiometers. The +5 volts is used as a logic supply while the 10 volts ac is the deriving source as well as the supplier of the one lighted indicator on the front panel. The ± 15 volts is used to derive the -10 volts as well as operating analog circuits.

Other Considerations

The packaging of the Off-Engine Control Peripheral Units consisting of the Operator Control Unit, the Engineering Control Unit, and the Interconnect Unit is designed to operate in a control room environment. Both mechanical and electrical systems are designed for control room use only.

13.4 FUEL DELIVERY SYSTEM

The QCSEE fuel delivery system is primarily based on F101 engine main fuel system components including the hydromechanical control and temperature sensor described in Section 13.3.4. The fuel delivery system includes the following elements:

- Fuel Control (metering section)
- Main Fuel Pump
- Fuel Filter

These elements are interconnected as shown in the schematic of Figure 13-26.

The fuel pump is an unmodified standard F101 main fuel pump. It is a balanced vane design of fixed displacement and contains an integral centrifugal booster stage to charge the vane intakes. Sizing of the fuel delivery system is indicated by the fuel pump characteristics listed in Table 13-VIII.

13.5 VARIABLE-GEOMETRY ACTUATION SYSTEMS

13.5.1 Hydraulic Supply System

Purpose

The hydraulic supply system provides hydraulic motive power to the fan duct nozzle (A18) actuators and fan blade variable-pitch mechanism. The system consists of a hydraulic pump, boost pump element, filters, and magnetic chip detector.

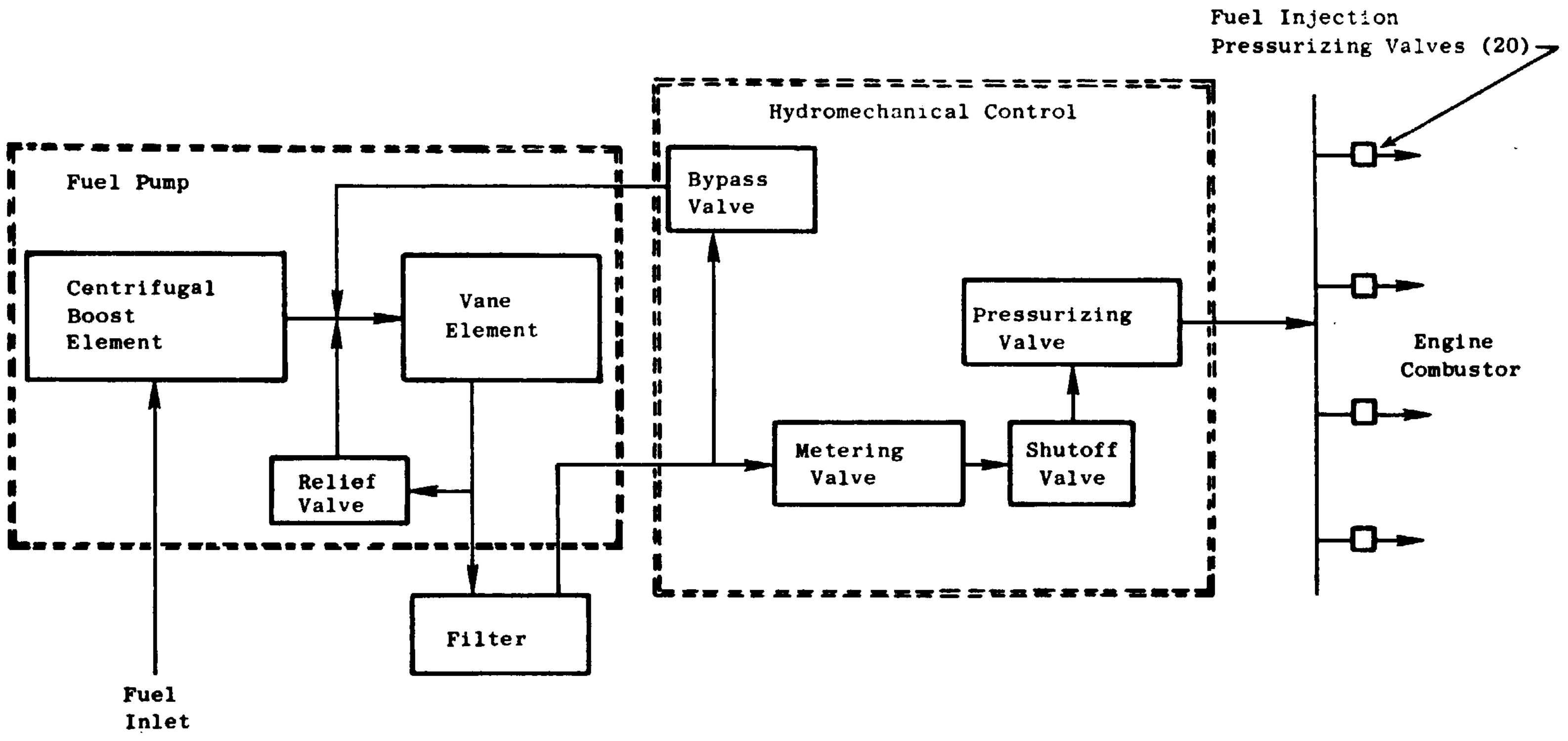
Fuel Injection
Pressurizing Valves (20)
Hydromechanical Control
Fuel Pump
Bypass Valve
Centrifugal Boost Element
Vane Element
Pressurizing Valve
Engine Combustor
Metering Valve
Shutoff Valve
Relief Valve
Filter
Fuel Inlet

Figure 13-26. Fuel Delivery System.

Table 13-VIII. Pump Characteristics (F101 Pump).

	Main Fuel Pump	
	Boost Element	Vane Element
Rated Speed, rpm	6690	6690
Maximum S.S. Speed, rpm	6891	6891
Rated Flow (Delivered Flow @ Service Limit @ Rated Speed)	2.7×10^{-3} m^3/sec (42.8 gpm) @ 107.2° C (225° F)	2.7×10^{-3} m^3/sec (42.8 gpm) @ 107.2° C (225° F)
Rated ΔP @ Rated Flow	2.76×10^5 N/m^2 (40 psi) min.	$\approx 6.65 \times 10^6$ N/m^2 (≈ 9.64 psi)
Power Loss @ Rated Speed	1.49×10^3 w (2 hp) max.	Overall Efficiency = 0.72 @ Design Point

System Description

The system is shown in Figure 13-27. A pressure-compensated hydraulic piston pump is driven by the accessory gearbox and provides varying flow output at constant pressure to servovalves which are part of the fan duct nozzle, or variable-pitch, systems. Pump output flow is determined by the demand from the servovalves, varying from zero at holding condition to maximum during the engine thrust reversal transient. The supply system is sized to provide peak transient flow for simultaneous operation of A18 and variable pitch at 65% core engine speed. Although pump maximum flow capability is proportional to engine speed, the output pressure is constant and virtually independent of speed or flow.

The hydraulic system receives and uses the same oil as the engine lube system. Once the hydraulic system is filled, however, it functions very nearly as an independent closed system. When oil leaves the pump to the servovalves at high pressure, oil is at the same time returning at low pressure from the servovalves. The servovalve incoming flow passes through a 1×10^{-5} m (10 micron) filter which provides servovalve protection from hydraulic pump and engine lube system contaminants.

As the A18 actuators slew from head-end to rod-end position, there is differential displaced volume equal to the volume represented by the actuator 1.89×10^{-4} m^3/sec (3 gpm) which must be made up from the engine lube system oil. Also, it is necessary to provide approximately 1.89×10^{-4} m^3/sec (3 gpm) to the pump during steady-state holding for pump cooling. Both of these functions, makeup and pump cooling, are provided by using an element in the engine lube pump as a makeup and boost pump to the hydraulic pump. A relief valve across the lube pump element acts as a pressure regulator so that the hydraulic pump inlet pressure is sufficiently high to avoid cavitation in the pump piston cavities. Hydraulic pump cooling is provided by virtue of mixing hydraulic oil with lube oil which passes through the engine oil coolers. Incoming hydraulic system makeup and cooling flow is filtered to the 46-micron level in the lube system, which minimizes the capacity required of the fine-micron-rated hydraulic filter. A magnetic chip detector is provided in the line returning hydraulic makeup and cooling flow to the engine lube system so that any ferrous metal contaminant generated in the hydraulic system can be identified.

Hydraulic Pump

The pump slated for use is an ABEX Model AP12V pressure-compensated piston pump. This pump is qualified and in production for the F-111 fighter aircraft and CH53 helicopter applications. The pump, shown in Figure 13-28, is compact in size and weighs 7.7 kg (17 pounds).

The pump has a revolving cylinder barrel which contains nine pistons. By means of a hold-down plate and hydraulically balanced shoes, the pistons are supported on an inclined cam plate which causes them to reciprocate as the barrel revolves. The angle of the cam plate is varied by moving the

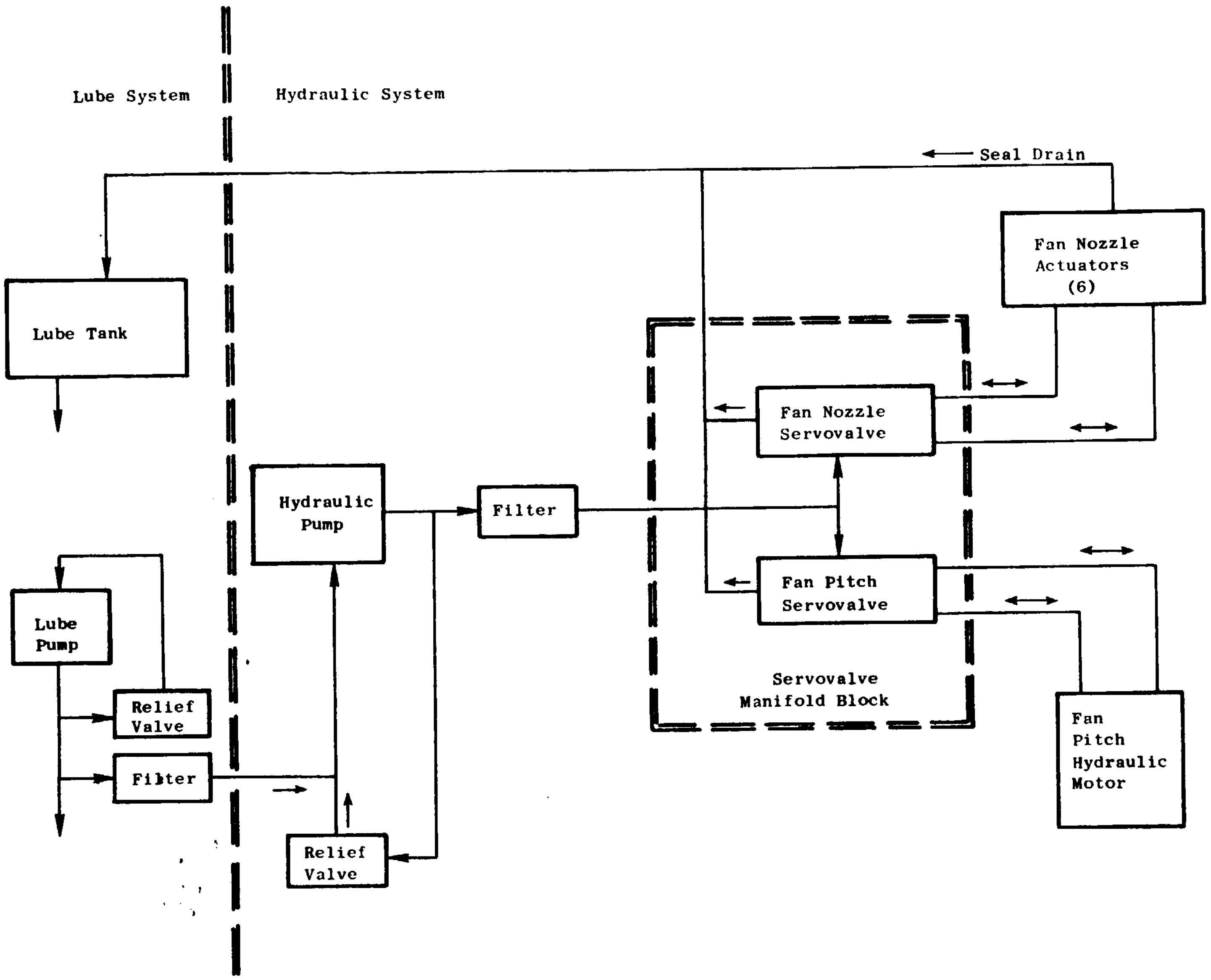
Lube System
Hydraulic System
Seal Drain
Fan Nozzle Actuators (6)
Lube Tank
Fan Nozzle Servovalve
Hydraulic Pump
Filter
Fan Pitch Servovalve
Lube Pump
Relief Valve
Filter
Servovalve Manifold Block
Fan Pitch Hydraulic Motor
Relief Valve

Figure 13-27. Hydraulic System.

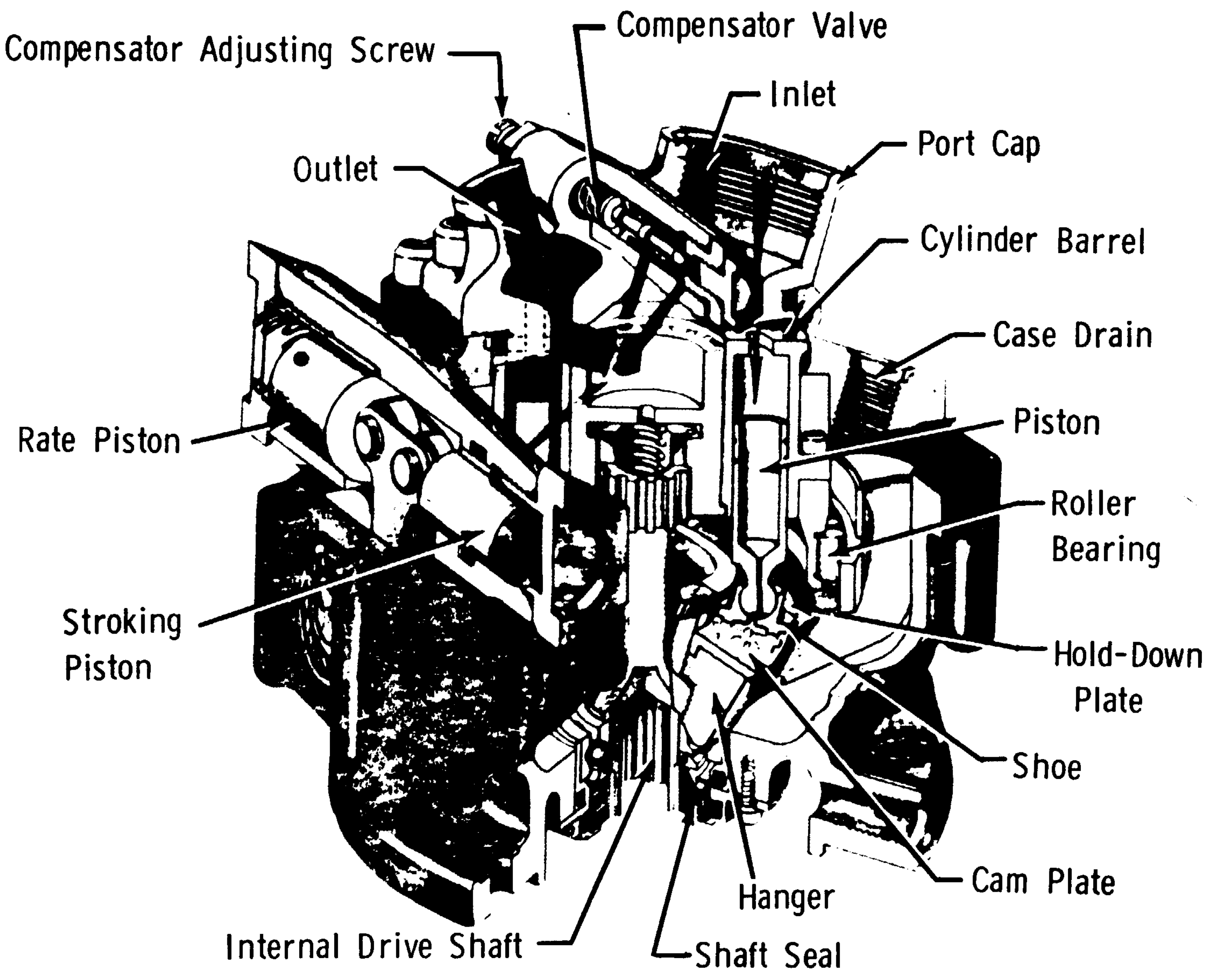
Compensator Adjusting Screw
Compensator Valve
Inlet
Port Cap
Outlet
Cylinder Barrel
Case Drain
Piston
Rate Piston
Roller
Bearing
Stroking
Piston
Hold-Down
Plate
Shoe
Cam Plate
Hanger
Internal Drive Shaft
Shaft Seal

Figure 13-28. Hydraulic Pump.

trunnioned hanger on which it is mounted, thereby changing the displacement of the pump. The hanger, in turn, is controlled by the pressure compensator. Oil passes through the main inlet and then through porting in the end of the cylinder barrel to cylinders from which the pistons are being withdrawn. As the cylinder barrel revolves, these pistons are forced into their bores and discharge high pressure oil through porting in the end of the barrel to the outlet port. The cylinder barrel, supported by a radial bearing, is driven by an internal shaft that passes through the trunnioned hanger.

The pressure compensator regulates the volume delivered in accordance with the demand of the system, thereby maintaining a predetermined pressure. System pressure is directed to a compensating valve with a spool which is held in the closed position by an adjustable spring load. When system pressure exceeds the spring load, it moves the spool to admit system oil into a stroking cylinder. The stroking piston then moves the hanger to a lesser angle, which reduces the volume pumped sufficiently to maintain the desired pressure. When system pressure is less than the compensator spring load, the spring moves the spool to vent oil in the stroking cylinder to the pump case. The stroking piston then retracts and an inherent force assisted by the rate piston spring moves the hanger to a greater angle, increasing the volume pumped.

DESIGN FEATURES

Hydraulic Pump

Speed	5676 rpm (100%)
Output Flow	3.09×10^{-3} m^3/sec (49 gpm) at 100% speed 1.99×10^{-3} m^3/sec (31.5 gpm) at 65% speed
Pressure Rise	2.41×10^7 N/m^2 (3500 psid)
Overall Efficiency	90%
Rated Shaft HP (at 1.99×10^{-3} m^3/sec demand)	4.55×10^4 w (73 hp)
Inlet Oil Temperature	-40° to 123° C (-40° to 250° F) at 100% speed

13.5.2 Fan Nozzle Actuators

Six cylindrical, hydraulic ram actuators are used for fan nozzle actuation as shown in Figure 13-29. Two of the actuators include internal screws which provide synchronization capability, two include internal, electrical position transducers, and two are simple rams. The six actuators are connected in parallel hydraulically and flow to them is controlled by a servovalve which is defined in Section 13.5.3. Mechanical synchronization is provided by the nozzle flaps themselves on each side of the engine (two

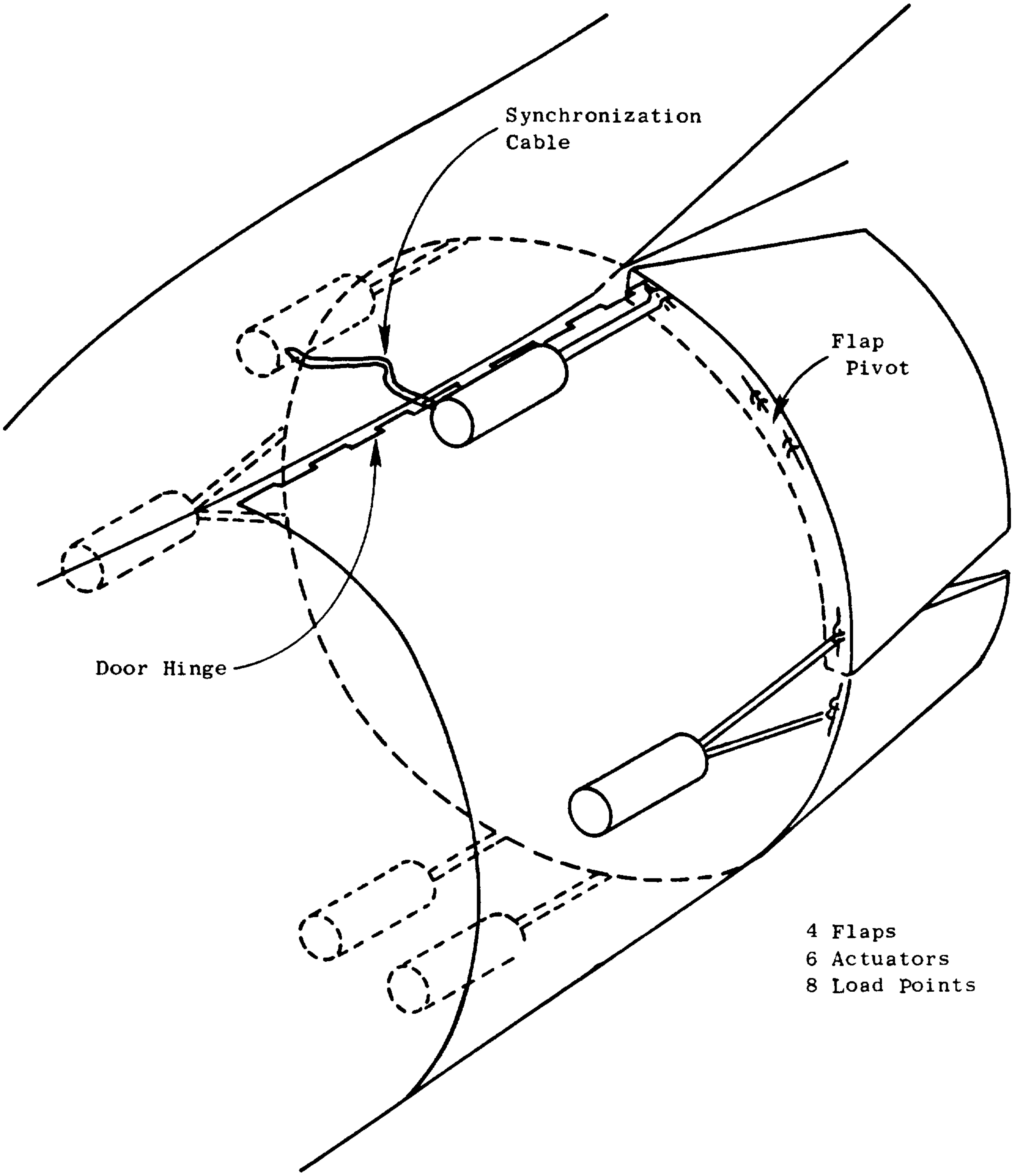
Synchronization Cable
Flap Pivot
Door Hinge
4 Flaps
6 Actuators
8 Load Points

Figure 13-29. Variable Nozzle Actuation Schematic.

flaps on each side) and synchronization between the two sides is provided by a flexible cable connecting the rotary, synchronizing outputs of the center actuator on each side. The center actuators provide the rotary output as shown on Figure 13-30. The ACME nut within the actuator piston causes the internal ACME to rotate (the piston being rotationally restrained at the rod end connection) and this rotation is transmitted through a worm gear to provide the rotary output.

Key design data on the nozzle actuators are listed below:

	Synchronous Actuator	Nonsynchronous Actuator
Design Load (tension-act.)	22,240 N (5,000 lb)	10,675 N (2,400 lb)
Design Load (compression - act.)	10,675 N (2,400 lb)	5338 N (1200 lb)
Stroke	12.7 ± 0.08 cm (5.0 ± 0.03 inch) adjustable to 10.9 cm (4.3 inches) with rod collar in retract direction.	
Head End Area	16.1 cm^2 (2.5 $in.^2$)	10.6 cm^2 (1.65 $in.^2$)
Rod End Area	8.1 cm^2 (1.25 $in.^2$)	4.4 cm^2 (0.83 $in.^2$)

13.5.3 Fan Pitch and Fan Nozzle Servovalves

Hydraulic flow to the fan pitch and fan nozzle actuation is controlled by separate, four-way, electrohydraulic, directional flow control valves mounted on a common manifold block which is mounted on the accessory gearbox. The valves control flow in response to a direct-current electrical signal from the digital control.

A schematic of the valve design is shown on Figure 13-31. The electrical signal is applied to parallel, redundant coils of the flat armature torque motor which applies torque to the jet-pipe causing it to deflect. This deflection unbalances the pressure on the opposite ends of the spool causing it to move until the jet pipe is returned to its center position by the feedback spring, the force of the spring just counteracting the torque generated by the electrical signal. In this manner, spool position is made proportional to the electrical signal current. The position of the spool determines the porting between the high pressure supply from the hydraulic pump (P), the actuation ports (1 and 2), and the low pressure return (R).

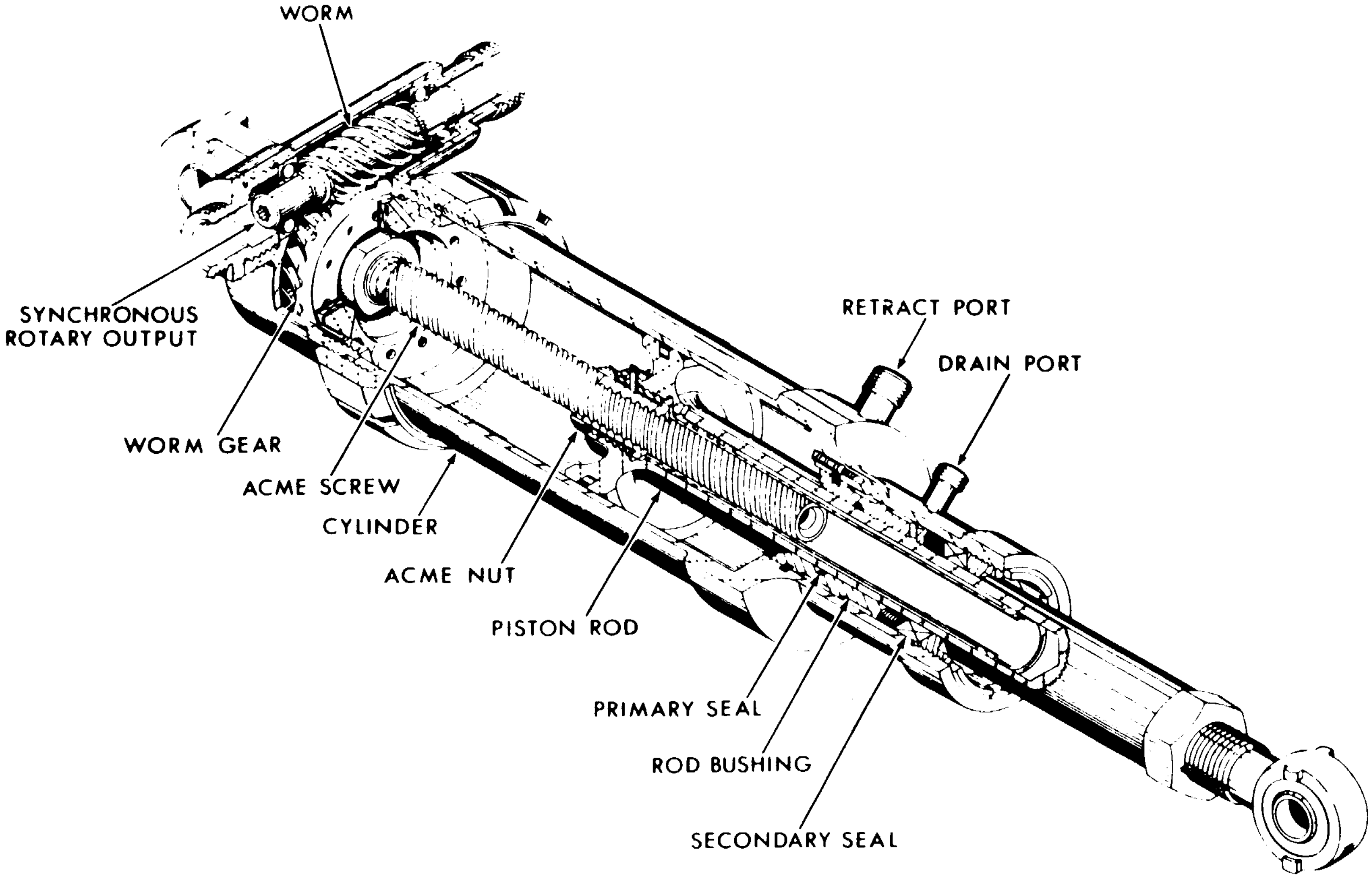
WORM
SYNCHRONOUS ROTARY OUTPUT
WORM GEAR
ACME SCREW
CYLINDER
ACME NUT
PISTON ROD
RETRACT PORT
DRAIN PORT
PRIMARY SEAL
ROD BUSHING
SECONDARY SEAL

Figure 13-30. Exhaust Nozzle Actuator.

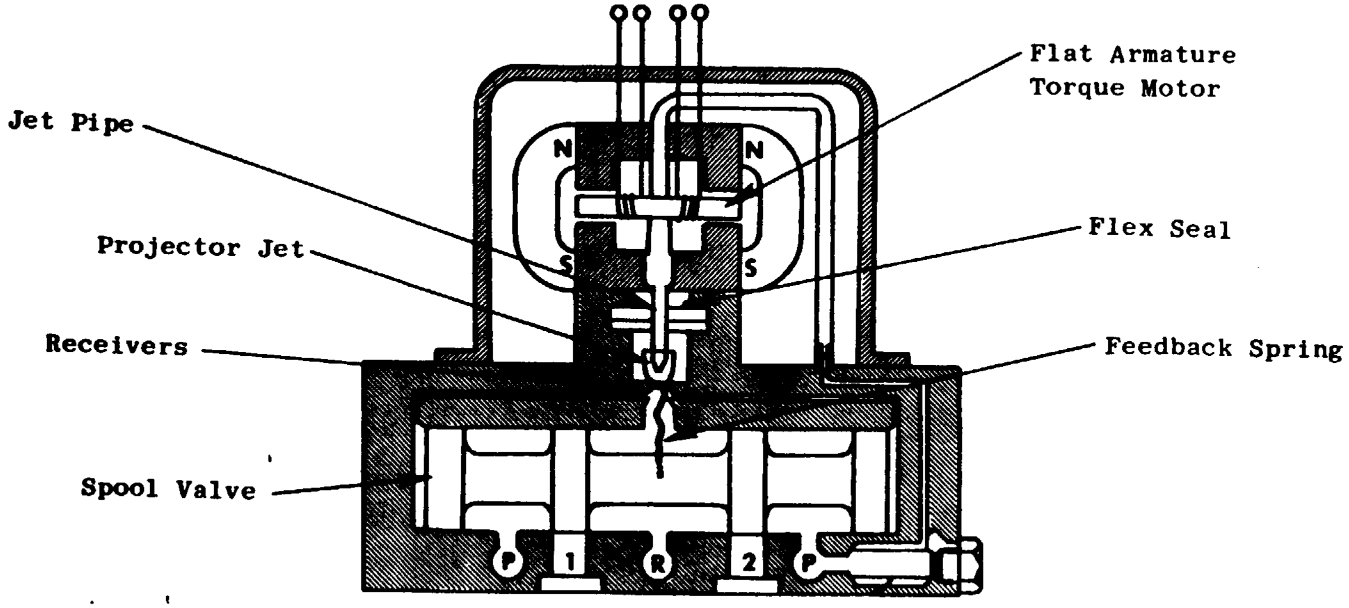
Flat Armature Torque Motor
Jet Pipe
Flex Seal
Projector Jet
Receivers
Feedback Spring
Spool Valve
N
N
S
S
P
1
R
2
P

Figure 13-31. Electrohydraulic Servovalve.

13.5.4 Core Stator Actuation and Feedback

Actuation of the core compressor stators is accomplished by a pair of fuel-operated, ram actuators. Flow to the actuators is controlled by the hydromechanical control.

The actuators are F101 components modified to increase the linear stroke by 5.08×10^{-3} m (0.2 inch). The modification is accomplished by shortening the piston head axial dimension to permit increased retraction when bottomed in the cylinder.

An F101-type core stator feedback cable provides the hydromechanical control with a stator position signal used for closed-loop stator scheduling. The cable is of the linear stroke type consisting of a fixed-length cable and a fixed-length conduit. The conduit provides a stroke path and protection for the cable. Rigging is obtained by adjusting the position of one end of the conduit.

It will be necessary to procure a cable of greater length, but of identical construction, for the QCSEE installation. Routing distance from the core stator feedback crank to the control location in the pylon is longer for the QCSEE installation. The F101 cable presently has sufficient stroke capability to accommodate the 5.08×10^{-3} m (0.2 in.) stroke increase for QCSEE.

13.6 SENSORS

The engine sensors are devices which change the variable to be measured into a form that can be used as an input signal to the engine digital or hydromechanical control or as an input signal to an indicator gage. The sensors include the following:

- Low pressure turbine speed sensor
- Core engine speed sensor (ac generator)
- Fan inlet temperature sensor
- Static pressure and pressure ratio sensors
- Position feedback sensors

13.6.1 Low Pressure Turbine (LPT) Speed Sensor

Purpose

The LPT shaft speed sensor produces two electrical signals that represent the rotational speed of the low pressure turbine shaft. One signal will be used for engine fan speed governing. The other signal will be used to limit the rate of speed change and maximum speed in the event of a loss of fan load, overspeed, or control failure.

Description

The speed sensor is nearly identical to that used on the F101 engine with a magnetic pickup at one end and an electrical connector at the other. The sensor is mounted within the fan frame, the pickup head and supporting tube extending through a fan frame strut to a point aft of the LPT shaft front bearing. The pickup is fixed in close proximity to a flanged ferromagnetic disk having 36 equally spaced teeth machined into the flange, 35 with the same air gap and one with less gap to provide a locating signal for use in rotor balancing.

Operation

The magnetic pickup consists basically of a permanent magnet behind a soft-iron pole piece around which a coil has been wound. The magnetic flux linking the coil is high when a ferrous metal object (tooth) is placed in front of the pole piece and is low with no ferrous metal in front of the pole piece (slot). The generated voltage is proportional to the rate of change of flux in the pole piece, and the frequency of the ac signal is proportional to the speed at which the ferrous material (teeth) passes in front of the pole piece. The wave form of the electrical signal is nearly sinusoidal depending upon the relative width of slots and teeth on the rotating disk and also the width of the piece relative to the slots and teeth. Signal output from the speed sensor is routed to a conditioner device in the digital control which produces a uniform voltage amplitude and wave form at varying speed so that ultimately the conditioned signal is interpreted in terms of frequency rather than voltage amplitude.

13.6.2 Core Engine Speed Sensor

Purpose

An alternating current generator driven by the engine gearbox provides electrical power to the engine digital control. In addition, a signal source is generated which represents core engine speed and is used for engine control and indicating purposes.

Description

The generator is a 12-pole, high-speed, four-winding, alternating current generator. The generator, shown in Figure 13-32, is identical to that used on the F101 engine. The generator rotor is mounted to a drive shaft which is supported by bearings in the accessory gearbox. Each winding on the stator functions as an independent power source with independent leads and pins in a single connector.

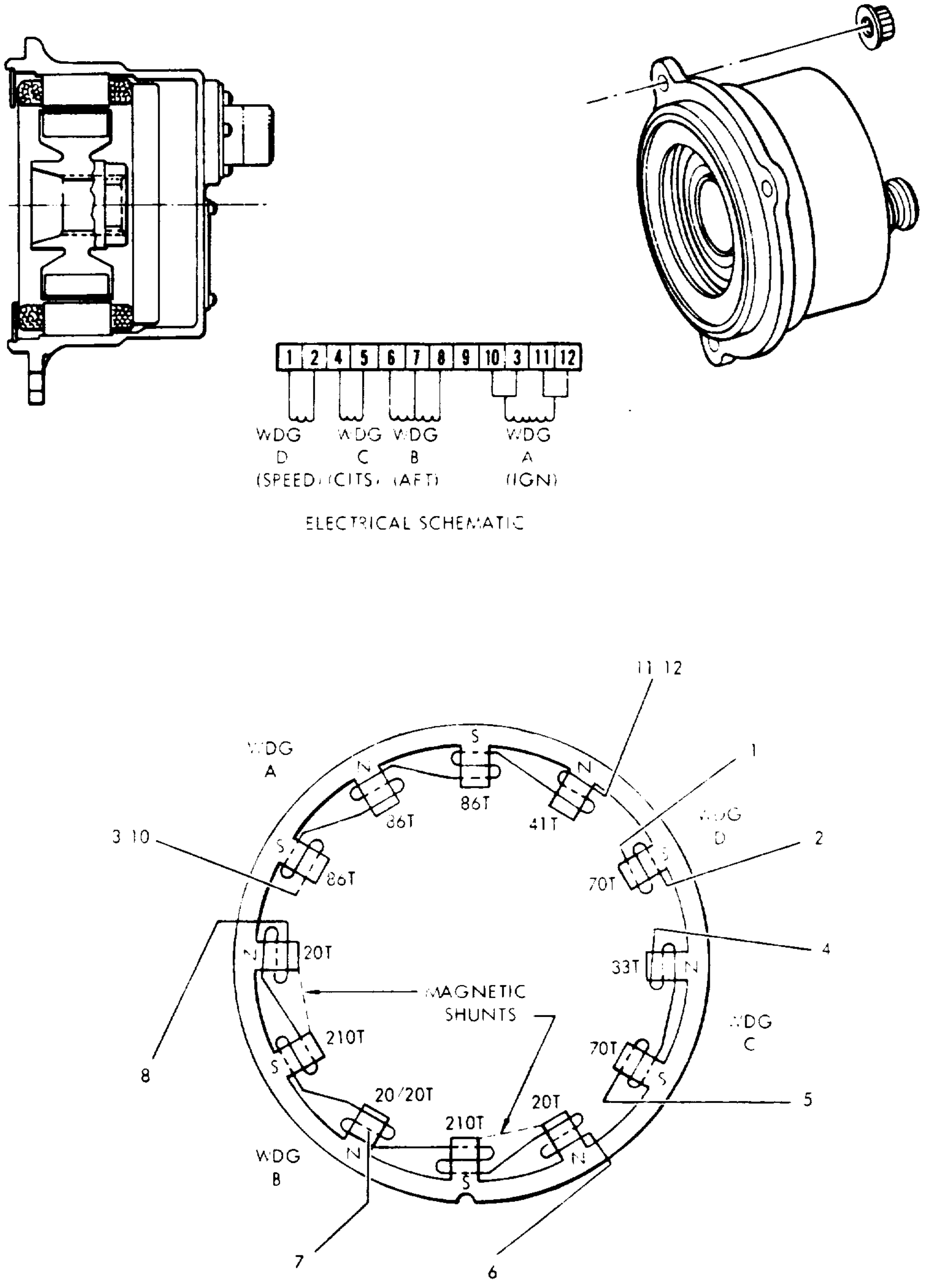
1 2 4 5 6 7 8 9 10 3 11 12
WDG D (SPEED)
WDG C (CITS)
WDG B (AFT)
WDG A (IGN)
ELECTRICAL SCHEMATIC
11 12
WDG A
1
WDG D
2
3 10
S
N
86T
86T
41T
86T
70T
20T
4
33T
MAGNETIC SHUNTS
210T
WDG C
70T
8
5
20/20T
210T
20T
WDG B
7
6

Figure 13-32. Alternating Current Generator.

A shaft seal in the gearbox permits the rotor to run in an essentially dry environment, reducing heat generation and avoiding the possiblity of metallic particle pickup on the Alnico-9 magnetic rotor. The rotor is shielded for retention of the magnetic segments and to provide a smooth, low disk friction surface.

Operation

The frequency of the sinusoidal wave form signal is used as an indication of core engine speed. The drive gear ratio is such that the rotor turns at 24,903 rpm at 100% engine speed which results in a frequency of 2490 Hz.

13.6.3 Fan Inlet Temperature (T12) Sensor

Purpose

The T12 sensor provides the engine control with an electrical signal representing the total temperature of the air entering the fan for use in scheduling and computing within the digital control.

Description

The fan inlet temperature sensor shown in Figure 13-33 is identical to that used on the F101 engine. The sensor is a wire-wound, resistance-type device mounted on and protruding through the front frame into the fan inlet air stream. The sensor consists of a sensing element and housing. The sensing element contains a platinum wire wound on a cylindrical platinum mandrel. The wires are insulated from each other and the mandrel by a ceramic insulant. The element is hermetically sealed in a capped platinum sheath and the connections are potted. The housing is a slotted airfoil which controls airflow so that the sensed temperature is that of the free stream. A series of small holes bleeds off the boundary layer and turns the stream, but not heavier particles, inward toward the sensing element. The boundary layer air is exhausted out the top. Some of the diverted air stream flows through the first slot and carries the lighter liquid contaminants. The remaining portion of the diverted flow goes through the second slot and around the sensing element.

Operation

The T12 sensor operates on the principle that the resistance of the platinum wire is a predictable function of temperature. A constant direct current of 12.5 milliamperes is applied to the sensor coil and the voltage used as an indication of temperature.

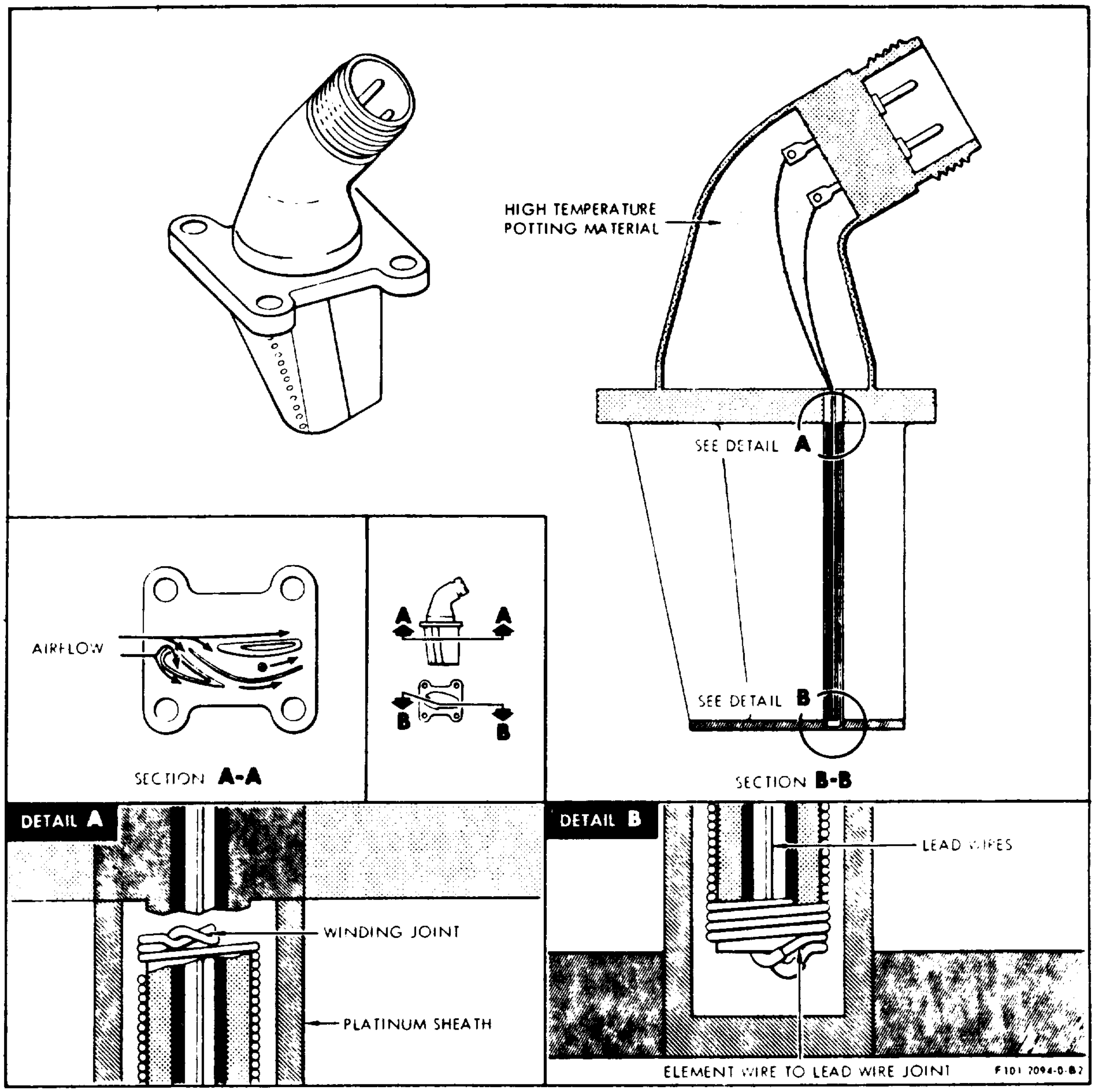
HIGH TEMPERATURE POTTING MATERIAL
SEE DETAIL A
SEE DETAIL B
SECTION B-B
AIRFLOW
SECTION A-A
A
A
B
B
DETAIL A
WINDING JOINT
PLATINUM SHEATH
DETAIL B
LEAD WIRES
ELEMENT WIRE TO LEAD WIRE JOINT
F101 7094-0-82

Figure 13-33. Fan Inlet Temperature (T12) Sensor.

13.6.4 Absolute and Differential Pressure Sensors

Purpose

Fan inlet static pressure (PS11), fan discharge pressure (P14), free-stream total pressure (PTO), and core compressor discharge static pressure (PS3) are sensed and used in the digital control for scheduling and computation. PS3 and PTO are sensed as absolute pressures and (PTO-PS11) and (PT14-PTO) are sensed as differential pressures.

Description

The sensors are thin-film strain gage bridge transducers identical to those used in the F101 engine. A cross section of the sensor is shown in Figure 13-34. The sensors receive their electrical excitation from the control and change the ΔP and static pressure signals to electrical signals. They are located inside the digital control chassis.

In the thin-film resistance strain gage bridge transducer [below 6.89 x 10^5 N/m^2 (100 psia)], the strain member is a cantilever beam which provides a metal substrate on which a ceramic film is deposited for electrical insulation. For higher pressures, a diaphragm is used instead of the cantilever beam. The four strain gage resistors are then vacuum deposited on the insulator. The resistors are electrically connected into a bridge circuit using film-deposited interconnecting leads.

Operating ranges for the sensors are 0 to 206.9 N/cm^2 (0 to 300 psia) for PS3, 0 to 13.8 N/cm^2 (0 to 20 psia) for PTO, and 0 to 8.3 N/cm^2 (0 to 12 psid) for both differential sensors.

Operation

The sensors operate on the principle of a mechanical distortion producing a change in electrical resistance across a strain gage and hence a change in electrical current output from a bridge circuit. Referring to Figure 13-34, pressure is ported to the sensing diaphragm which deflects and drives a linkage pin against the sensing beam. The beam is shaped such that it bends and causes "stretch" on the surface to which the strain gages are attached.

13.6.5 Position Feedback Sensors

Purpose

Rotary and linear variable differential transformer transducers will be used to sense the position of various engine parts and components. These are:

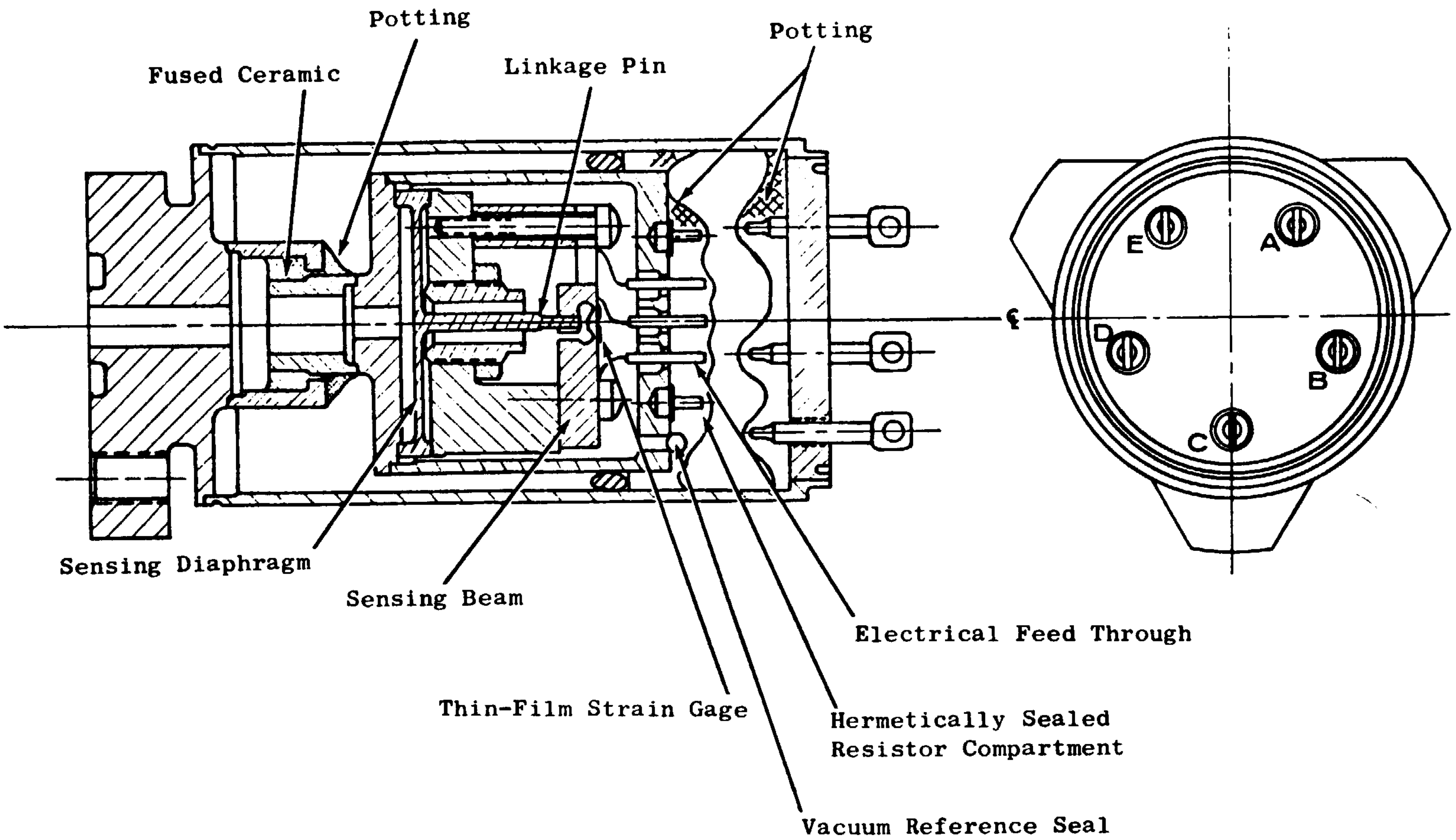
Potting
Fused Ceramic
Linkage Pin
Potting
E
A
D
B
C
℄
Sensing Diaphragm
Sensing Beam
Electrical Feed Through
Thin-Film Strain Gage
Hermetically Sealed
Resistor Compartment
Vacuum Reference Seal

Figure 13-34. Pressure Sensor.

	Type
Fan nozzle (A18) actuators position	LVDT
Power lever position	RVDT
Fuel metering valve position	RVDT
Fan blade pitch angle	LVDT

Description and Operation

The variable differential transformer translates the displacement of a magnetic core into an ac output voltage which is proportional to the displacement. Several different designs are used to obtain specific performance characteristics, but basically, these transducers are constructed of one primary coil and two secondary coils.

An alternate current (6.6 volts rms, 3030 Hz) is fed through the primary winding. The magnetic core couples the primary and secondary coils by conducting the alternating field inside the coils. When the core is in center position, an equal portion of the core extends into each of the secondary coils and affects an equal coupling between the primary and each secondary coil. An alternating voltage of equal magnitude is induced in the secondary coils. With the secondary coils connected in series opposed, the output is close to zero. As the probe is moved to either side, the coupling between the primary and one secondary coil is increased, while the coupling between the primary and the other secondary coil is decreased. A larger voltage is then induced in one secondary coil than in the other, and the output voltage will be the difference between the two voltages.

SECTION 14.0

NACELLE AERODYNAMIC DESIGN

14.1 SUMMARY

The UTW nacelle has been designed as an integrated propulsion system to be compatible with the aircraft wing/pylon relationship representative of the advanced external blown flap (EBF) installation shown in Figure 14-1. This installation is based on the wing nacelle relationship recommended by Douglas Aircraft for a 914 m (3000 ft) runway design.

The nacelle envelopes for the experimental engine and the flight engine are shown in Figure 14-2. The experimental engine is designed for a 610 m (2000 ft) runway aircraft while the flight engine is designed for an aircraft operating out of a 914 m (3000 ft) airfield. Both aircraft have the same maximum 152 m (500 ft) sideline noise goal of 95 EPNdB. The differences between the two are the lesser aft acoustic treatment in the flight engine resulting in the elimination of the exhaust acoustic splitter and the shorter core duct nozzle. The nacelle maximum diameter of 200.2 cm (78.8 inches) is the minimum diameter achievable by a balanced design of aerodynamic internal and external performance and structural requirements. The nacelle external geometry reflects a cruise Mach number design of 0.70 with a drag rise slightly higher than that level. The inlet external geometry and nacelle afterbody and boattailing are designed to achieve minimum drag at the $M_o = 0.70$ point. The aerodynamic design intent of achieving a very low profile integrated engine/nacelle configuration capable of providing high levels of internal performance and low external drag has been accomplished, based on analysis of the data base.

An accelerating inlet with a high throat Mach number and acoustic treatment in the diffuser was selected to meet the engine noise requirements. Design objective in selecting the throat Mach number was to achieve the highest practical Mach number consistent with high levels of inlet performance across the assumed aircraft operating envelope using a fixed-geometry inlet system. The design throat Mach number was selected as $M = 0.79$ based on studies and available inlet data. The inlet was also to be as short as possible, consistent with acoustic treatment needs and required aerodynamic performance at all aircraft/propulsion system operating conditions including operation without internal flow separation at 50° angle of attack at an aircraft speed of 41 m/sec (80 knots) and 90° crosswind at aircraft speeds up to 18 m/sec (35 knots).

Scale model inlet tests of several inlet configurations, conducted in the NASA-Lewis 2.74 x 4.57 m (9 x 15 ft) wind tunnel, resulted in the selection of an inlet geometry capable of meeting all requirements. The selected configuration has a $D_{highlight}$ to D_{throat} ratio of 1.21 and a $D_{highlight}$ to D_{max} ratio of 0.905.

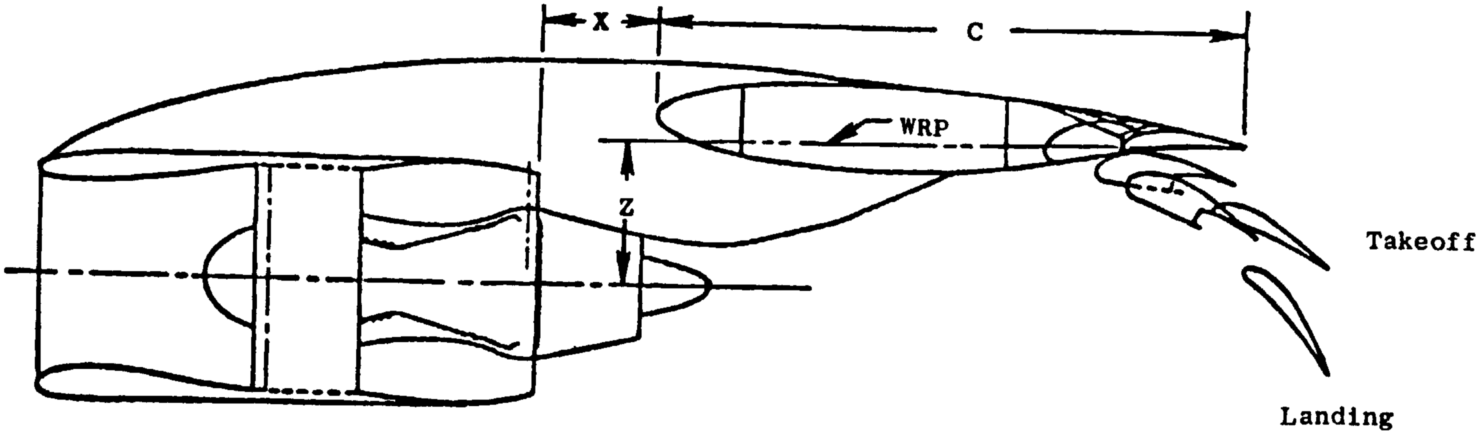
X
C
WRP
Z
Takeoff
Landing

- X/C = 0.20
- Z/C = 0.24
- No Engine Tilt Relative To WRP

Figure 14-1. Engine/Flap Relationship, Inboard Station.

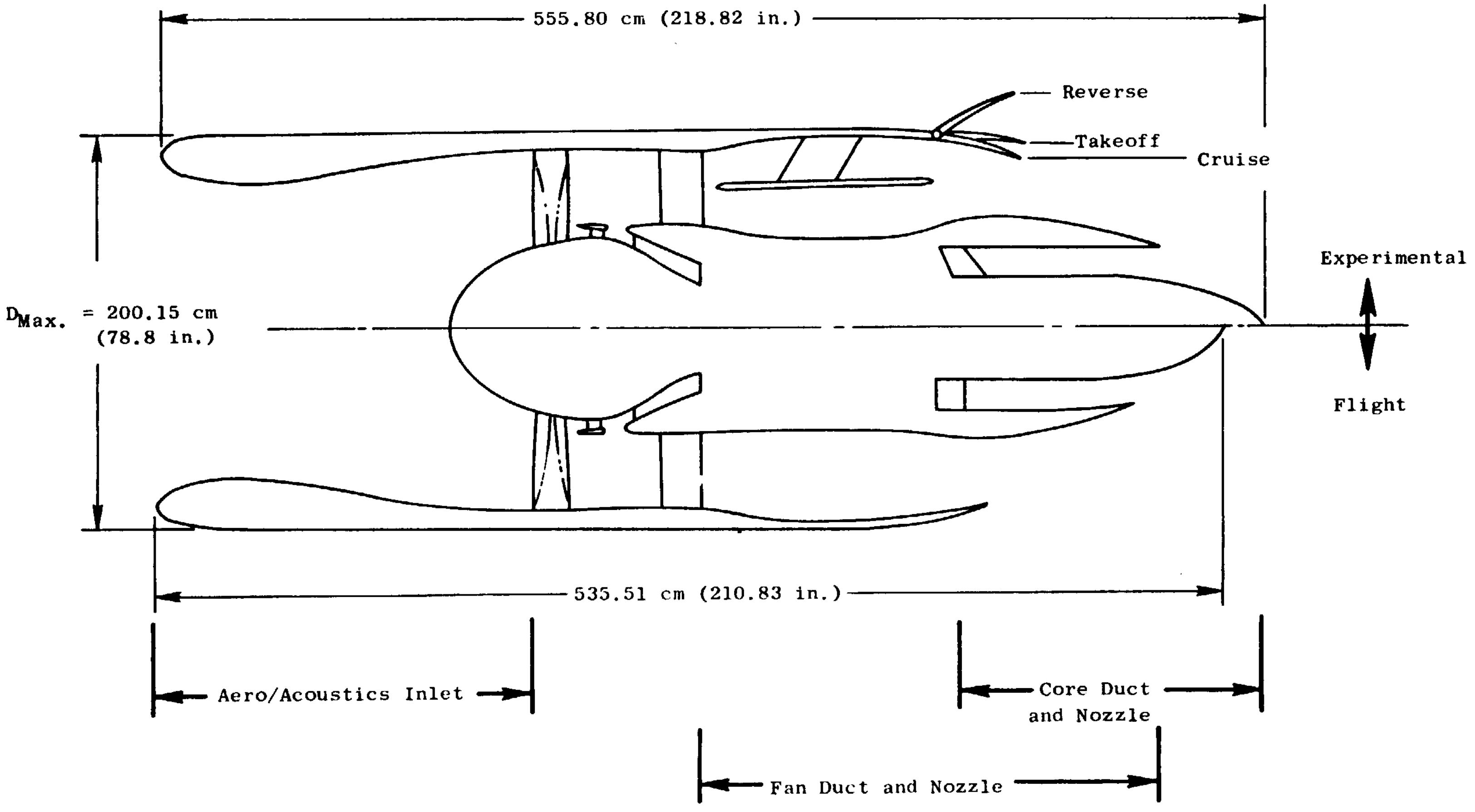
555.80 cm (218.82 in.)
Reverse
Takeoff
Cruise
Experimental
Flight
$D_{Max.}$ = 200.15 cm (78.8 in.)
535.51 cm (210.83 in.)
Aero/Acoustics Inlet
Core Duct and Nozzle
Fan Duct and Nozzle

Figure 14-2. Nacelle Aerodynamic Flowpath.

The fan duct has been designed to accommodate the acoustic splitter of the experimental engine configuration and to operate without internal wall separation with or without the splitter in place, while providing minimum pressure drag.

A variable-geometry fan nozzle was selected to meet the nozzle area requirements at takeoff and cruise engine operating conditions, and to provide the necessary "inlet" geometry during reverse thrust operation.

Scale model tests of the fan duct/fan nozzle configuration in the reverse operating mode were conducted in the NASA-Lewis 2.74 x 4.57 m (9 x 15 ft) wind tunnel to verify and optimize the selected geometry. Results indicated the final selected configuration will provide high levels of recovery and low distortion at ground speeds from 0 to 72 m/sec (140 knots).

14.2 DESIGN REQUIREMENTS

Primary requirements included in the nacelle aerodynamic design of the UTW flight and experimental propulsion systems are:

- Tolerance to aerodynamic distortion expected under operational conditions which include high crosswinds, large angles of attack, and side slip, and still provide good cruise performance. Specific objectives include capability to operate without endangering the aircraft or engine with crosswind velocities up to 18 m/sec (35 knots) at angles from 0° to 90°, and angles-of-attack to 50° with 41.2 m/sec (80 knots) wind velocity.

- Reverse thrust operation without exceeding normal operating limits at forward ground speeds down to 5.1 m/sec (10 knots).

- Accurate representation of the external and internal aerodynamic contours of the flight nacelle in the experimental engine propulsion system configuration.

- Variable-area fan exhaust nozzle capable of satisfying the area requirements at all critical engine operating conditions, including takeoff, cruise, approach, and landing (reverse thrust).

- A nacelle configuration which will permit achievement of the 4.3 installed thrust-to-weight-ratio objective for the flight propulsion system.

14.3 COMPONENT DESIGN

14.3.1 Inlet

The operational requirements for the inlet are consistent with the most advanced STOL EBF aircraft operating envelope (typified by the YC15) as shown in Figure 14-3. The critical operating conditions are at 41 m/sec (80 knots) at 50° angle of attack and 18 m/sec (35 knots) at 90° crosswind. At these conditions the inlet was designed to have no internal flow separation while operating at the design Mach number.

The inlet flow characteristics depart considerably from the conventional CTOL aircraft as shown on Figure 14-4. This plot shows the engine demand percentage maximum corrected flow at the critical flight placard conditions of takeoff, maximum climb, cruise, approach, and reverse. The UTW engine has a throat Mach number of 0.79 at almost all the conditions while the CTOL system has a much lower throat Mach number at takeoff and approach. This characteristic of the UTW engine, due to its variable fan exhaust nozzle and variable-pitch fan blades, enables the propulsion system to achieve significant front end noise attenuation due to the high throat Mach number. In addition, because of the lower throat diameter, a lower inlet external diameter is possible resulting in reduced system weight.

The initial inlet throat Mach number design objective of the UTW inlet was to achieve the highest practical throat Mach number consistent with inlet/engine operation across the assumed aircraft operating envelope using a fixed-inlet system. The practical upper limit is dictated by the inlet recovery characteristic, as shown in Figure 14-5. As shown, large degradation in inlet recovery is encountered at one-dimensional throat Mach numbers in excess of $M = 0.82$, due to effects of radial throat velocity gradient and boundary layer growth along the inlet lip. Consequently, to provide margin for effects such as engine-to-engine flow variations, flow variation due to operational effects on engine tolerances, and inlet-to-inlet throat area variations, a design throat Mach number of 0.79 was selected.

The inlet aerodynamic design requirement was to achieve the high level of recovery at the high throat Mach number with integrated acoustic treatment in the diffuser and in the shortest possible length. The solution to this problem was approached by a team design effort managed by GE with the technical aero inlet data base provided by GE, Douglas, and NASA-Lewis. A scale model inlet program was conducted at the NASA-Lewis 2.74 x 4.57 m (9 x 15 ft) wind tunnel (Reference 1). The scale model installed in the wind tunnel is shown in Figure 14-6. The 30.48 cm (12 in.) diffuser exit diameter model represents a 17% scale model of the engine inlet system. Test data in terms of inlet recovery as a function of angle-of-attack are presented in Figure 14-7 for four different inlet configurations. As shown, two of the configurations exceeded the objectives and two failed to meet the objectives. On the basis of the test results, the 1.21 diameter ratio (D_{HL}/D_{TH}) with an external ratio of 0.905 (D_{HL}/D_{MAX}) was selected as the best overall balanced design for angle of attack, crosswind and cruise operation. In order to allow a cylindrical outer nacelle wall, a D_{HL}/D_{MAX} value of 0.900 was used for the design of the full-scale engine inlet. The wall Mach number distributions

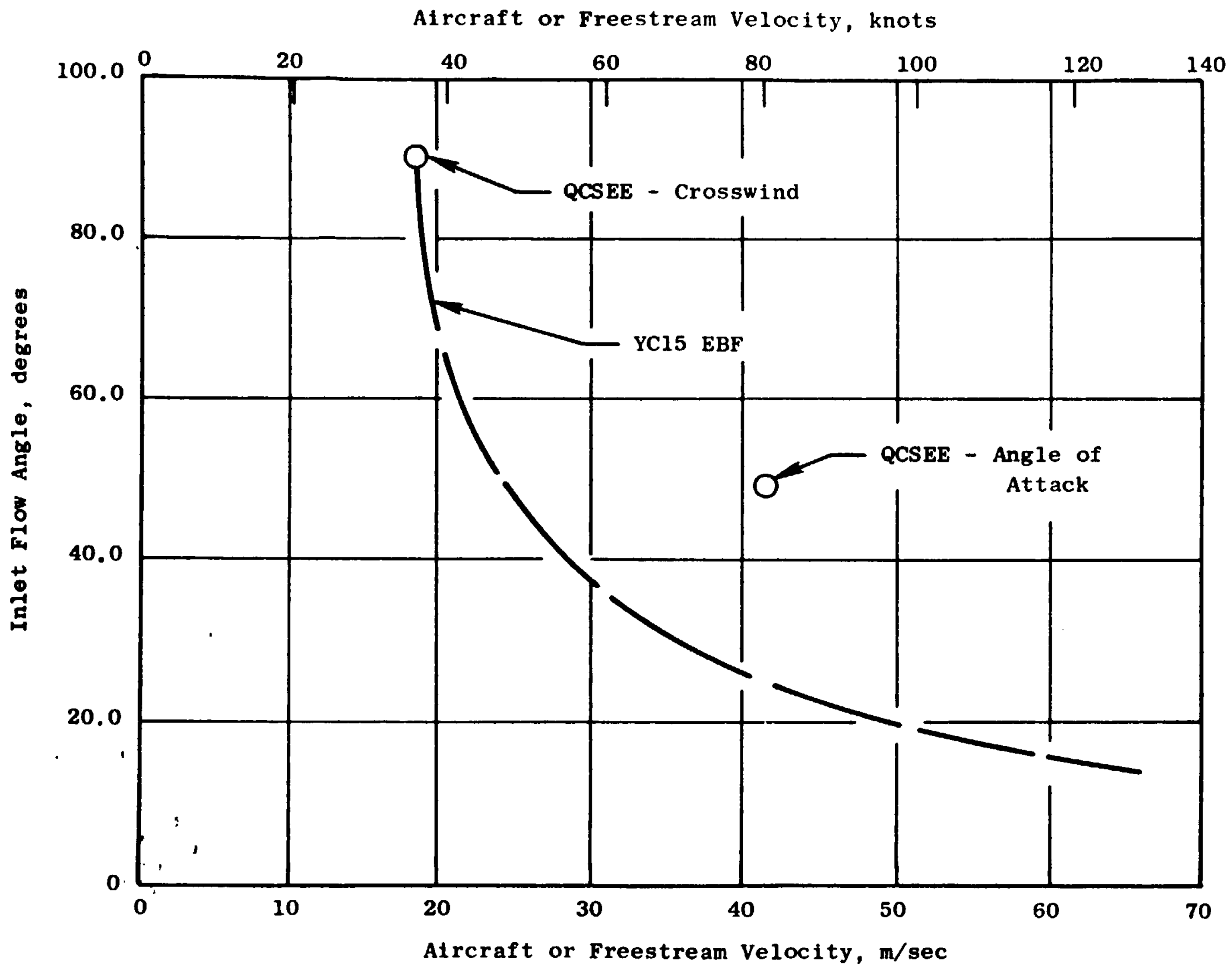

Figure 14-3. STOL Aircraft Design Envelope, YC15 EBF and QCSEE.

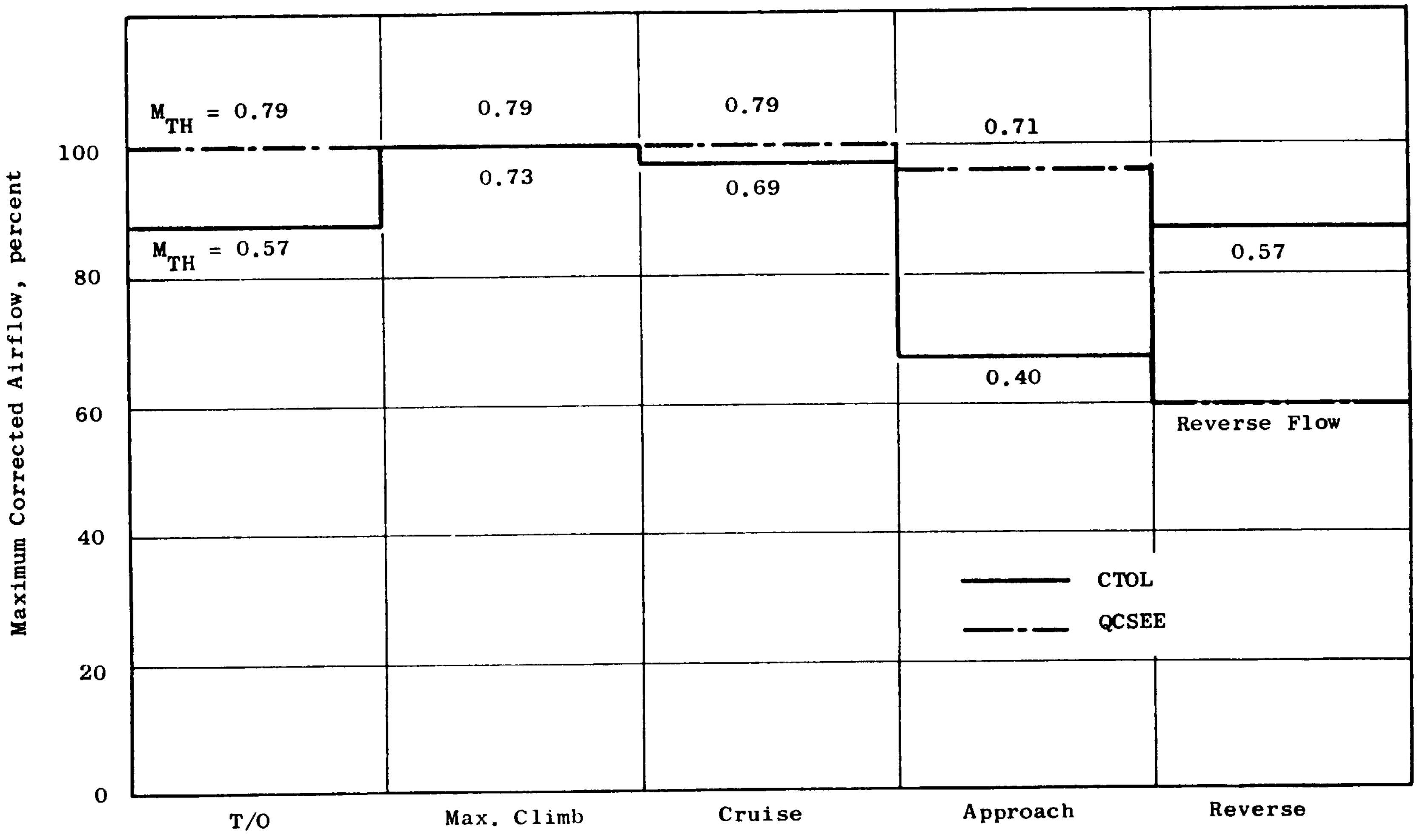

Figure 14-4. Flight Placard Airflow Characteristics for QCSEE and CTOL Aircraft.

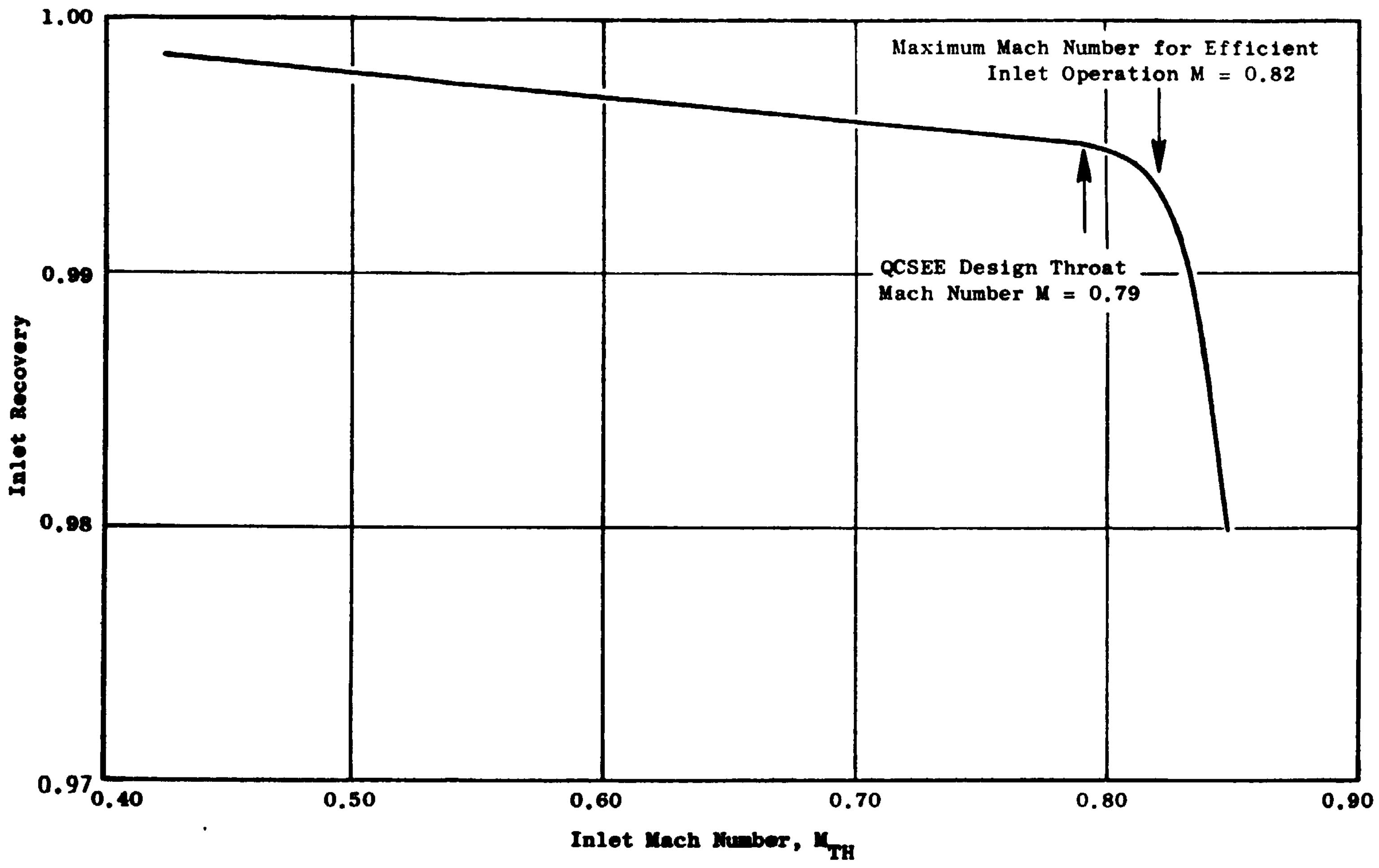

Figure 14-5. Inlet Throat Mach Number Selection.

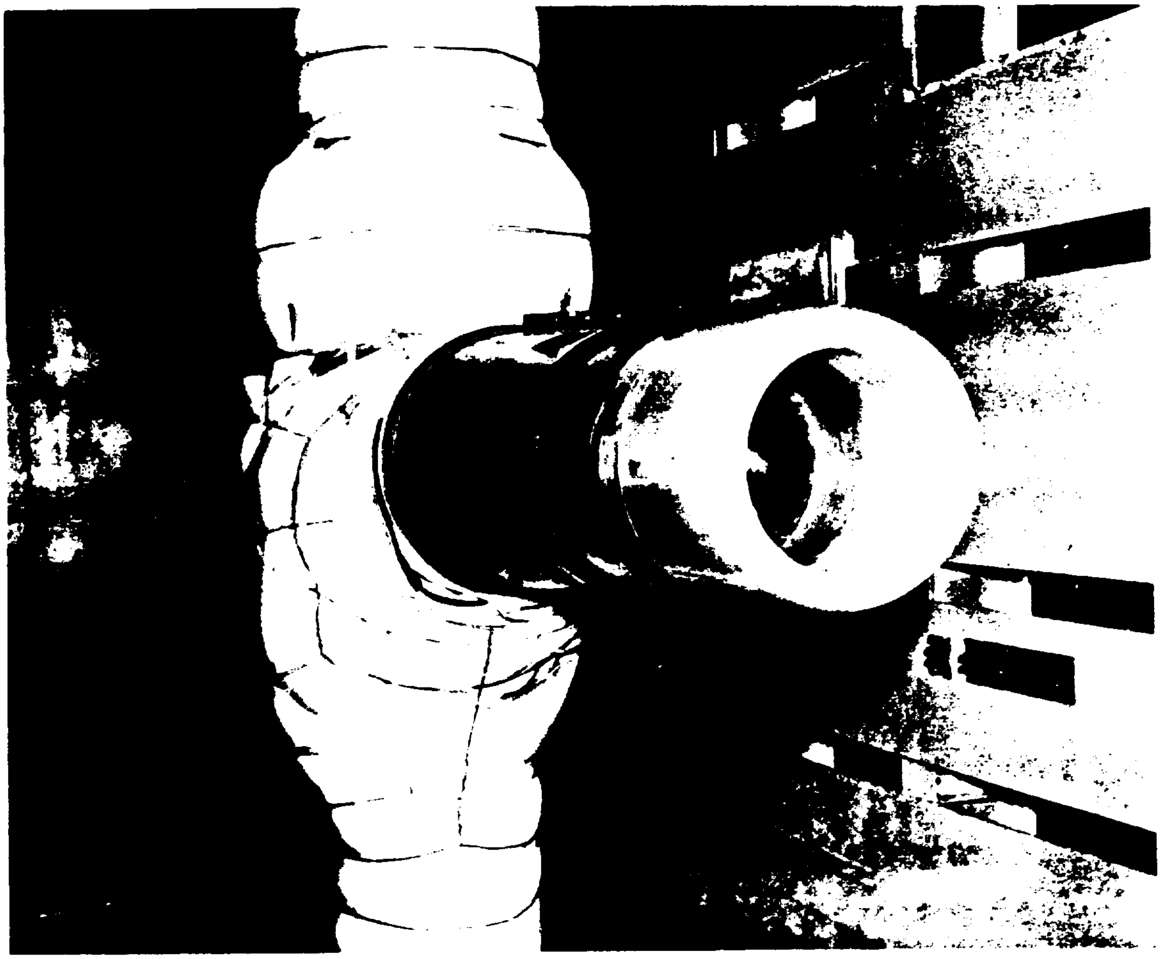

Figure 14-6. 30.5 cm (5.5 in.) Inlet Model in NASA-Lewis 2.7 x 4.6 m (9 x 15 ft) Wind Tunnel.

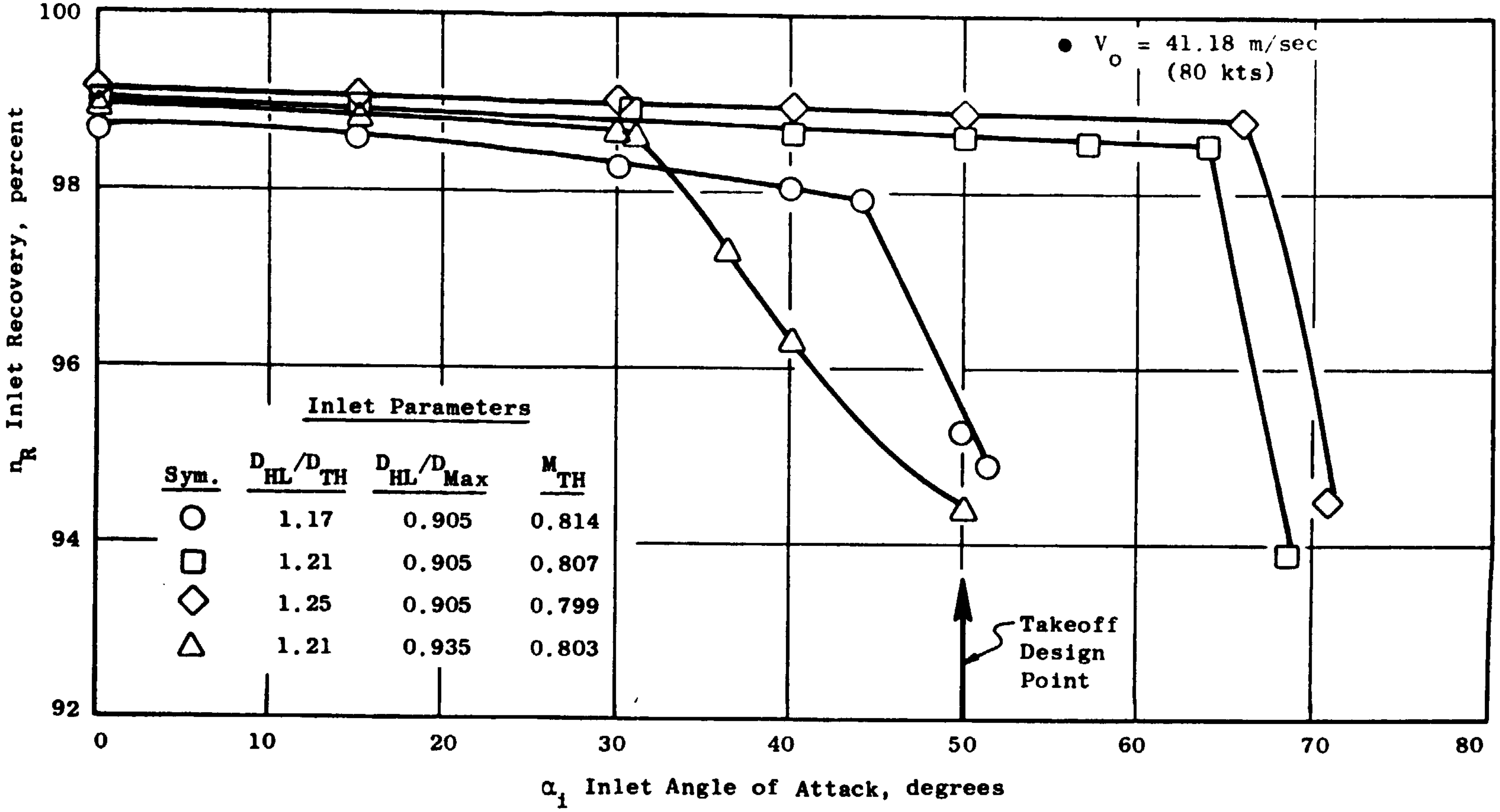

Figure 14-7. Inlet Performance Comparison Versus Angle of Attack.

(calculated from wall static pressure measurements) for the selected inlet at 41.2 m/sec (80 knots), and 0° angle of attack are shown in Figure 14-8; calculated values are compared with analytical results obtained from the Streamtube Curvature (STC) computer program (Reference 2). Test results indicated that the selected configuration achieved all of the design objectives. The final engine inlet geometry which evolved from the 30.48 cm (12 inch) inlet tests is presented in Figure 14-9.

14.3.2 Fan Bypass Duct and Exhaust Nozzle

The internal and external aerodynamic configurations of the experimental engine and "flight" engine fan duct and fan exhaust nozzle components are presented in Figures 14-10 and 14-11, respectively. As shown, the primary differences between the two geometries are the modifications in nacelle length and inner diameter flowpath of the experimental engine necessary to accommodate the 101.6 cm (40 in.) acoustic splitter. The acoustic splitter is required to meet the noise goals established for the experimental engine.

The nozzle flap length for both configurations is 45.7 cm (18 inches). Nacelle boattail angles at maximum thrust, cruise operating condition are 20° and 18° for the experimental and flight configurations, respectively. As indicated in the figures, nacelle fairings are used to cover the externally mounted flap actuators.

The fan duct flow characteristics were analyzed using the Streamtube Curvature (STC) and Stratford & Beavers Boundary Layer (SABBL) computer programs (Reference 2). The experimental engine configuration was analyzed both with the acoustic splitter in place, and with the splitter removed, as will be the case for some engine test conditions. Analytical results indicated that separation will not occur under any engine operating conditions.

The fan duct Mach number distribution for the experimental engine at takeoff power setting is shown in Figure 14-12. As shown in the figure, the local flow Mach number in the region of the splitter is close to the 0.45 Mach number established as an acoustic objective for the flow Mach number over the splitter. Estimated total pressure losses for the fan duct are as follows:

	Takeoff $\% \Delta P_T/P_T$	Cruise $\% \Delta P_T/P_T$
Experimental Engine	1.14	0.99
Flight Engine	0.69	0.60

A variable-geometry exhaust nozzle was selected for the UTW engine to satisfy the fan exit area requirements at all critical engine operating conditions. These include not only the forward mode operating conditions

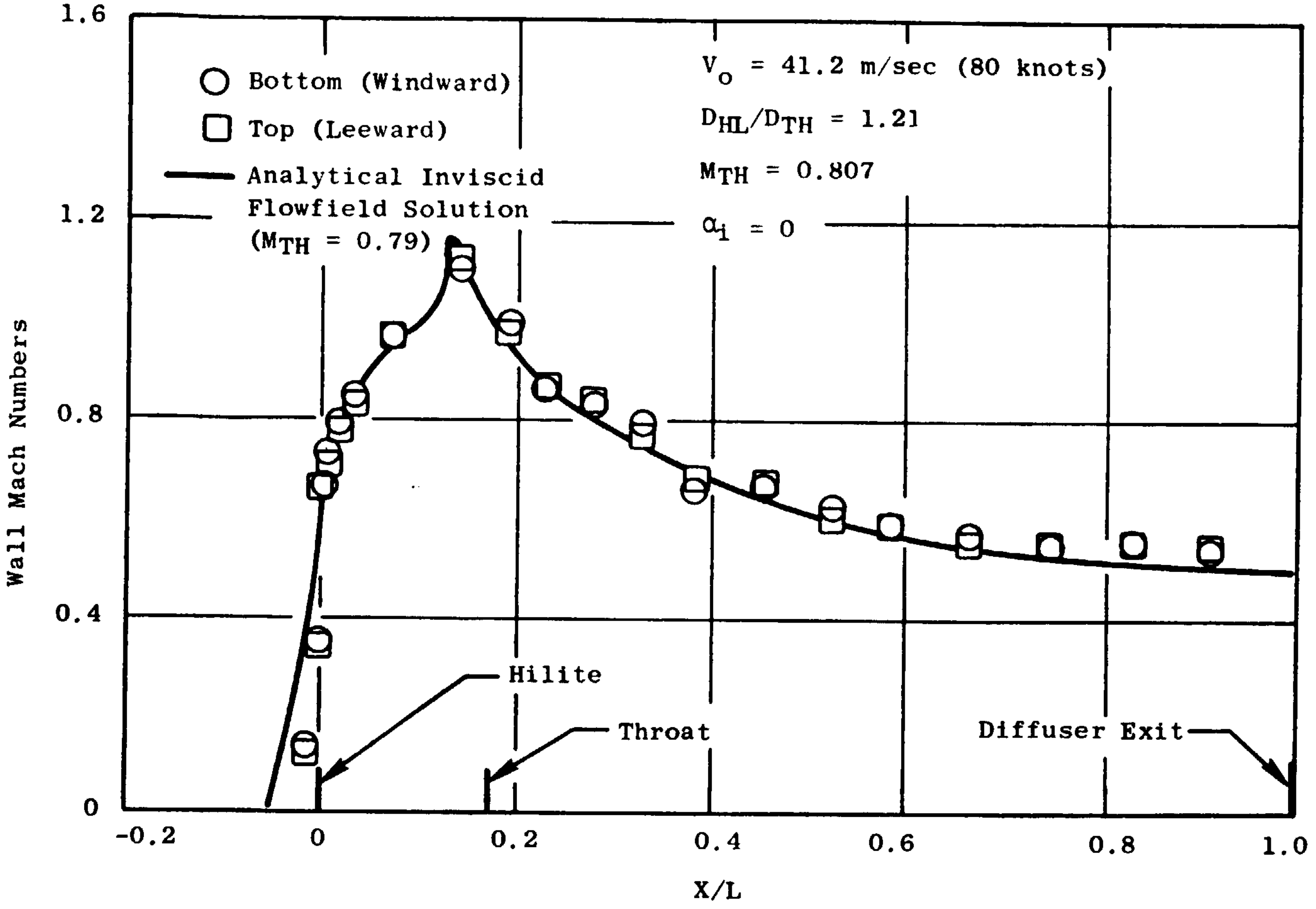

Figure 14-8. 30.48 cm (12 in.) Inlet Wall Mach Number Distributions.

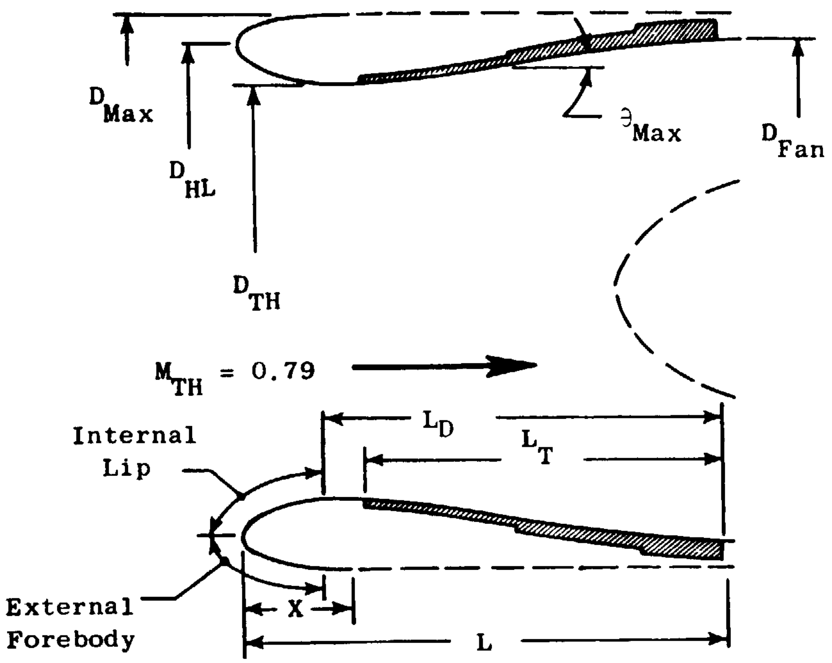

D_{Max}
D_{HL}
D_{TH}
θ_{Max}
D_{Fan}
$M_{TH} = 0.79$
Internal Lip
External Forebody
L_D
L_T
X
L

$L/D_{Fan} = 1.0291$

$D_{HL}/D_{TH} = 1.21$ Symmetrical

$D_{HL}/D_{Max} = 0.900$

$X/D_{Max} = 0.219$

$\theta_{Max} = 8.7°$(At Diffuser Midpoint)

$(D_{Fan}/D_{TH})^2 = 1.466$

$L_T/D_{Fan} = 0.74$

$L_D/D_{Fan} = 0.856$

Internal Lip Contour = 2:1 Ellipse

External Forbody Contour = DAC-1*

Diffuser (L_D) Surface is a Cubic

* The DAC-1 Contour was developed by the Douglas Aircraft Company and is presented in Reference 1.

Figure 14-9. Inlet Aerodynamic Design.

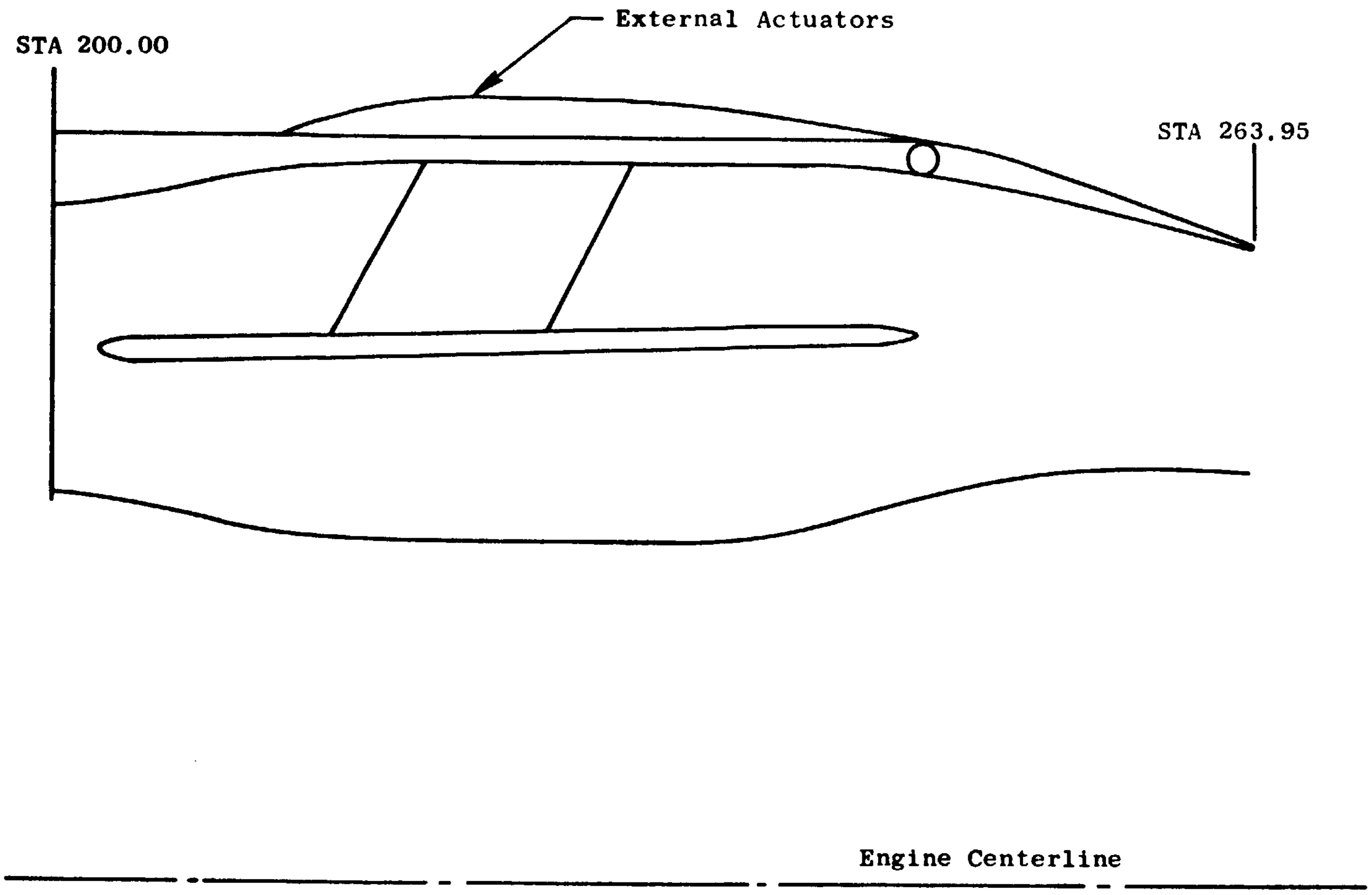
External Actuators
STA 200.00
STA 263.95
Engine Centerline

Figure 14-10. Fan Duct and Nozzle Design Experimental Nacelle.

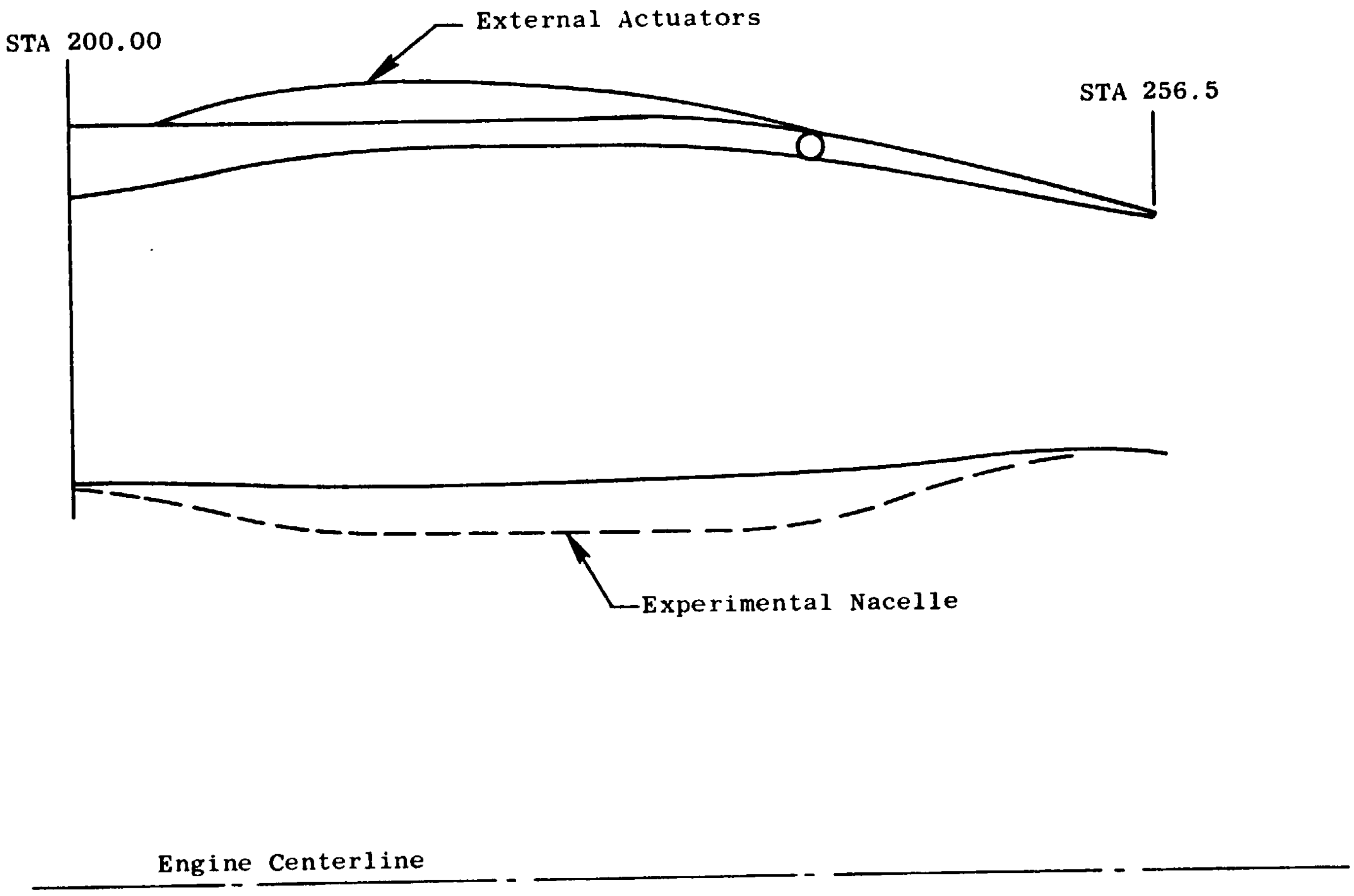
STA 200.00
External Actuators
STA 256.5
Experimental Nacelle
Engine Centerline

Figure 14-11. Fan Duct and Nozzle Design Flight Nacelle.

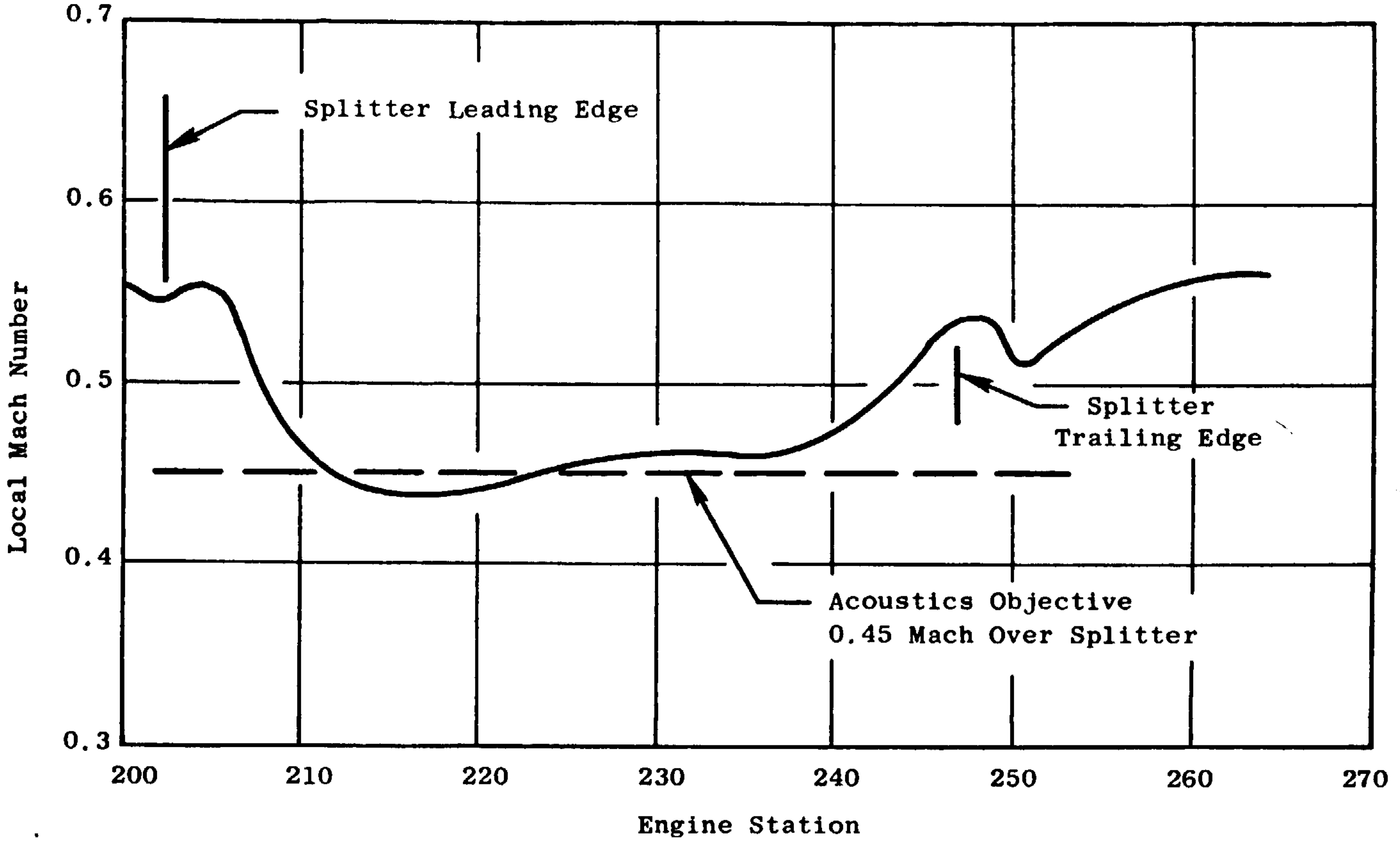

Figure 14-12. Experimental Nacelle Fan Duct Mach Number Distribution, Takeoff Power Boiler Plate and Composite Nacelle.

of takeoff, cruise and approach, but also the reverse mode operation during landing. The fan exhaust nozzle physical areas at these operating conditions based on current cycle considerations are:

	Nozzle Exit Area	
	cm^2	$in.^2$
Takeoff	16,125	2501
Cruise (Max. Thrust)	12,103	1876
Approach	21,290	3300
Reverse	38,710 (Approx.)	6000 (Approx.)

A flare-type nozzle was selected to satisfy these requirements. This inlet/exit (exlet) nozzle was a new aerodynamic development and required experimental investigation to achieve the best installed recovery and lowest distortion for highest systems reverse thrust. This was accomplished in the NASA-Lewis 2.74 x 4.57 m (9 x 15 ft) wind tunnel by a joint GE/NASA-Lewis test program (Reference 3). The model test configuration was a 14.0 cm (5.5 in.) powered fan model. A cross section of the model is shown in Figure 14-13, and a photograph of the model installed in the tunnel is presented in Figure 14-14.

A series of nozzle flares (Figure 14-15) was designed and tested during the model test program. The test range (in terms of flare geometry) in comparison to the baseline design is as follows:

	Test	Design
Flare	25.4 - 55.9 cm (10-22 in.)	45.7 cm (18 in.)
Flare Angle	20° - 36°	28.5°
Flare Area Ratio	1.4 - 1.95	1.7

The flare configurations were experimentally evaluated in terms of pressure recovery and distortion over the range of tunnel velocities from 0 to 66.9 m/sec (130 knots). In addition, the normal takeoff nozzle position was evaluated as a baseline. Test results are shown in Figure 14-16. As shown, the performance levels of all of the flare configurations fall into a narrow band, and the baseline design falls near the best performance level achieved. The baseline design was therefore retained and integrated into the engine design.

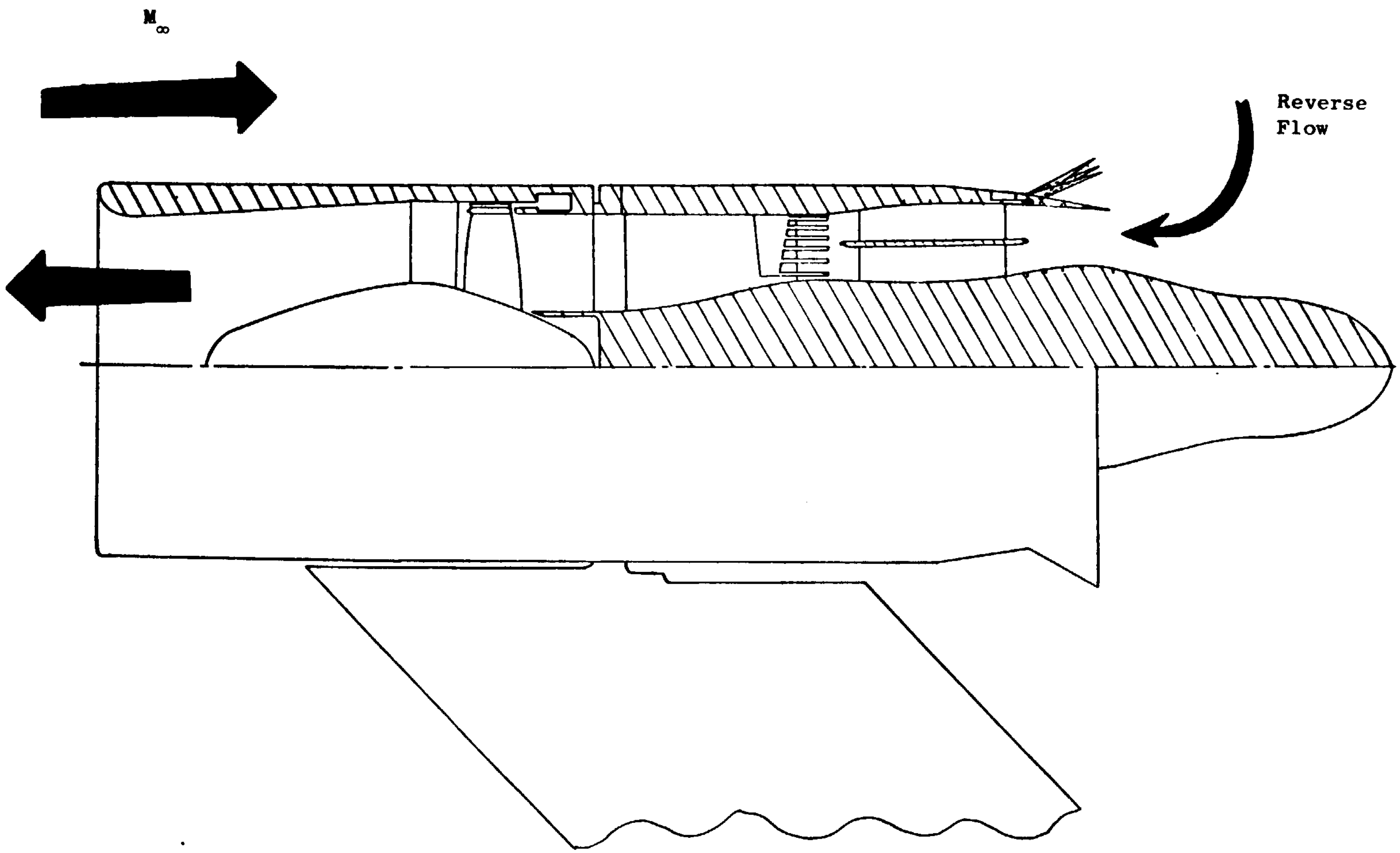
M_∞
Reverse
Flow

Figure 14-13. 14.0 cm (5.5 in.) Exlet Model Typical Tunnel Installation.

NASA
C-74-2718

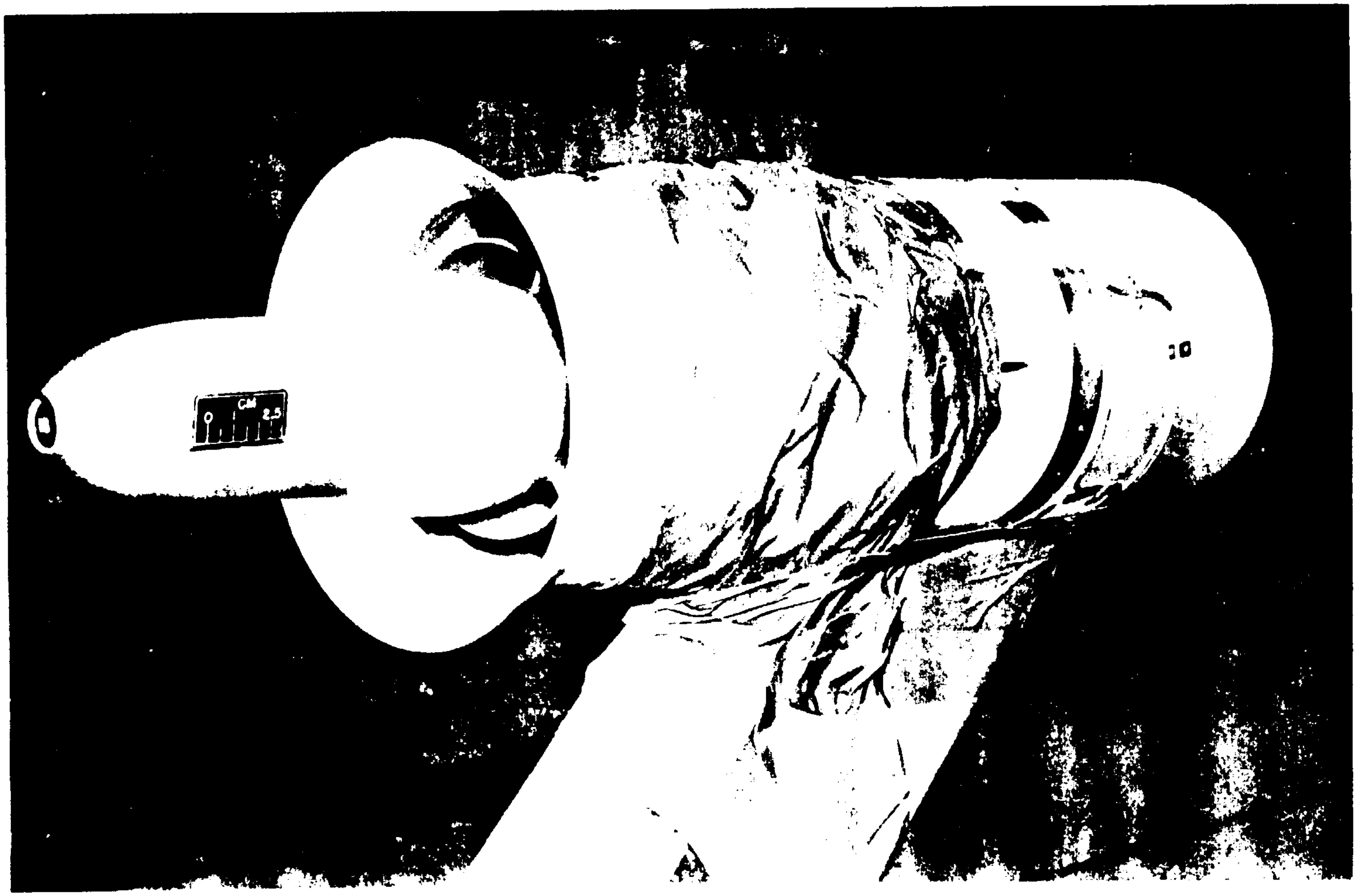

Figure 14-14. 14.0 cm (5.5 in.) Exlet Model in NASA-Lewis 2.7 x 4.7 m (9 x 15 ft) Wind Tunnel.

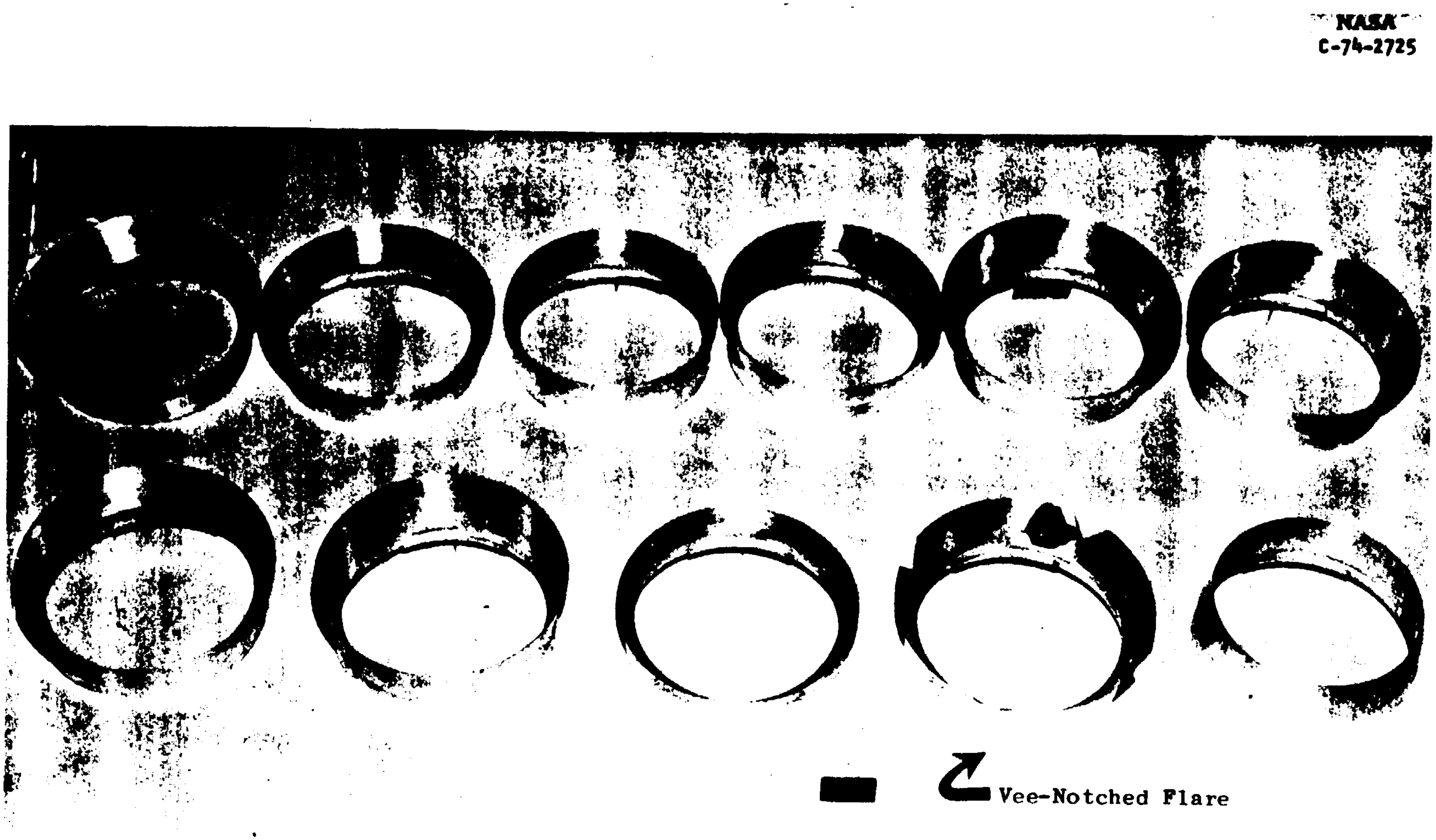
NASA
C-74-2725
Vee-Notched Flare

Figure 14-15. 14.0 cm (5.5 in.) Exlet Model Test Configurations.

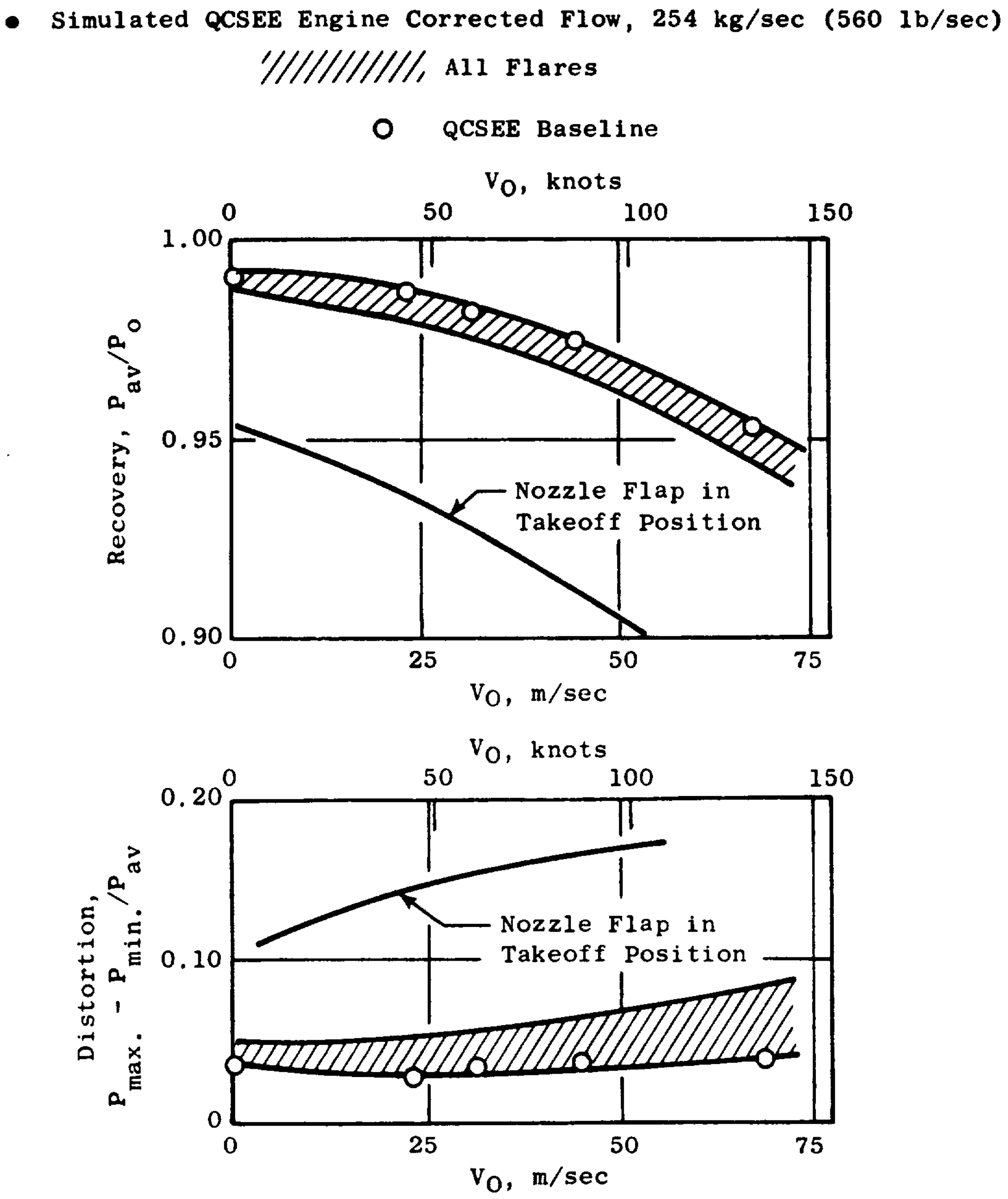

- Simulated QCSEE Engine Corrected Flow, 254 kg/sec (560 lb/sec)

Figure 14-16. Performance Summary - 13.97 cm (5.5 in.) Exlet Tests.

14.3.3 Core Nozzle

The core nozzle is an annular convergent nozzle having a fixed exit (physical) area of 3490 cm^2 (541 $in.^2$). The nozzle duct length is established on the basis of acoustic treatment length requirements and the desired axial separation of the fan and core nozzle exit planes to avoid hot core ingestion during thrust reversal. The experimental engine and flight engine core nozzle configurations are shown in Figure 14-17. As shown, the differences in geometry are due primarily to the elimination of the need for core duct acoustic treatment in the flight engine, and replacement of the experimental engine modified F101 rear frame with a redesigned frame, resulting in a reduced frame strut chord length.

The core nozzle external boattail angles for the experimental and flight engines are 12.5° and 16°, respectively. Estimated core duct pressure losses are as follows:

	Takeoff $\%\Delta P_T/P_T$	Cruise $\%\Delta P_T/P_T$
Experimental Engine	0.89	1.59
Flight Engine	0.75	1.33

14.3.4 Pylon

As discussed in Section 6.0, the internal pylon is an integral part of the fan vane-frame. The pylon configuration is shown in Figure 14-18. As shown, the leading edge section of the pylon houses the radial drive shaft that runs from the core to the top-mounted accessory gear box. The pylon shape from its leading edge to the area of maximum thickness, 40.64 cm (16 in.), was established by fan aerodynamic design considerations to eliminate fan back pressure in the pylon region. The internal (scrubbed by fan flow) pylon closes out with a 12° half angle boattail and extends slightly beyond the core nozzle exit plane.

The external pylon above the nacelle is 50.8 cm (20 in.) wide to accommodate the controls and accessories (C&A) packaging; the 50.8 cm (20 in.) width is blended into the internal pylon by undercutting along the C&A pylon and nacelle interface ahead of the fan nozzle exit plane.

The flight and experimental engine propulsion systems pylons are identical internally; however, the experimental pylon is simplified to better fit the outdoor test facilities. The simplification does not affect the aerodynamic flow characteristics.

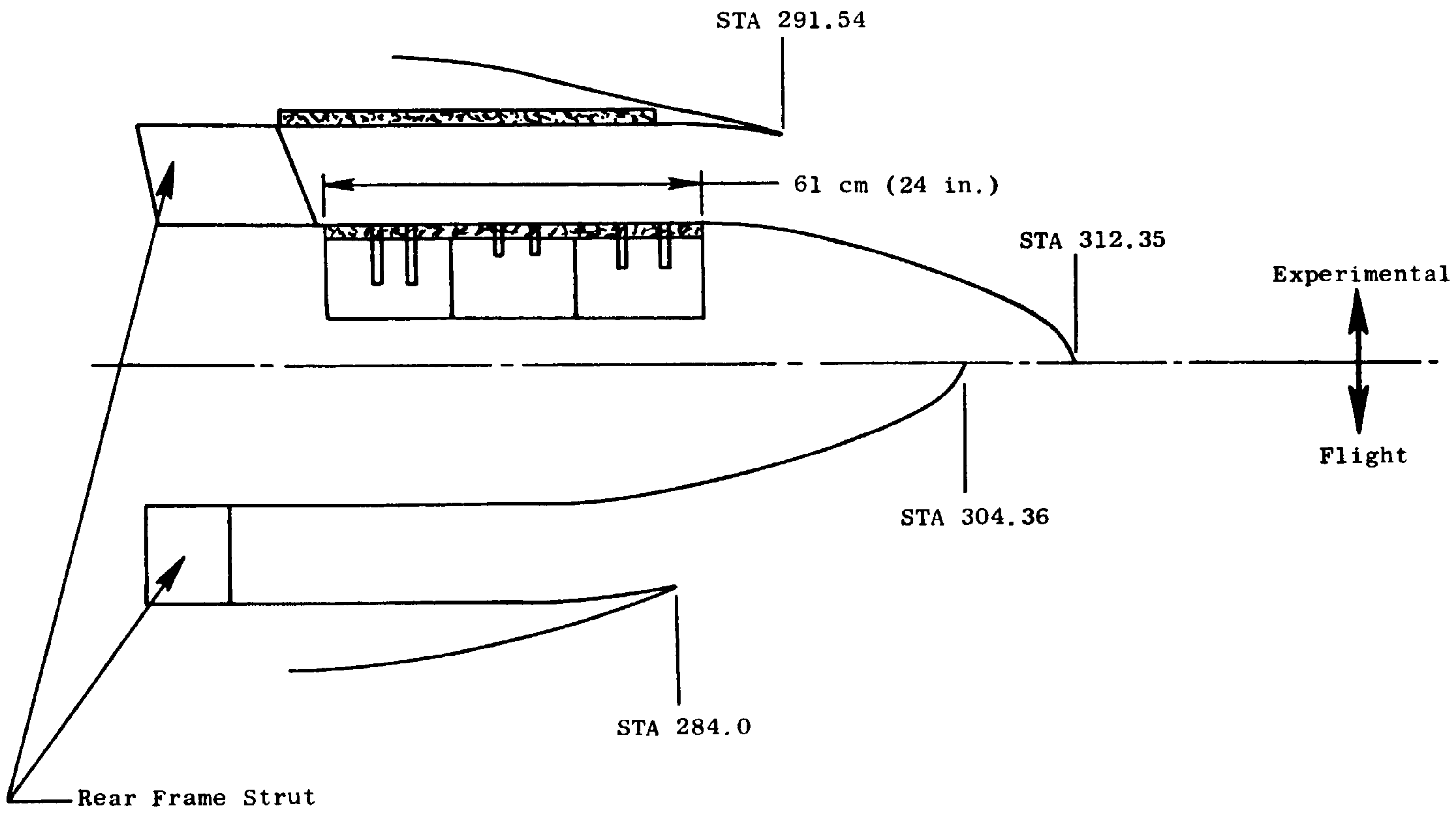
STA 291.54
61 cm (24 in.)
STA 312.35
Experimental
Flight
STA 304.36
STA 284.0
Rear Frame Strut

Figure 14-17. QCSEE UTW Core Nozzle Design.

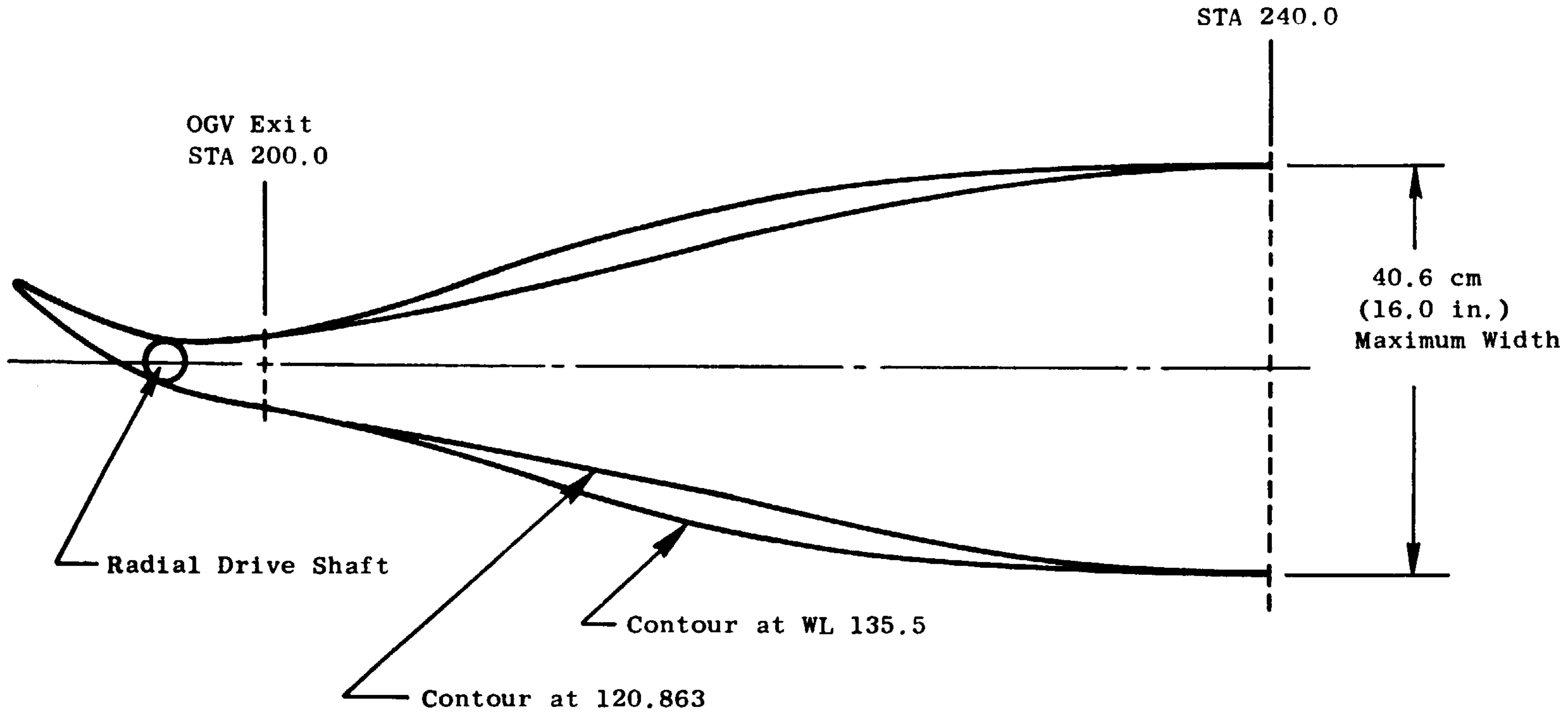
STA 240.0
OGV Exit
STA 200.0
40.6 cm
(16.0 in.)
Maximum Width
Radial Drive Shaft
Contour at WL 135.5
Contour at 120.863

Figure 14-18. Contoured Pylon Nose Section.

14.4 REFERENCES

1. Miller, B.A., et.al., "Effect of Entry-lip Design on Aerodynamics and Acoustics of High-Throat-Mach-Number Inlets for the Quiet, Clean, Short-haul Experimental Engine," TM-X-3222, May 1975, NASA, Cleveland, Ohio.

2. Keith, J.S., Ferguson, D.R., Merkle, C.L., Heck, P.H., and Lahti, D.J., "Analytical Method For Predicting the Pressure Distribution About A Nacelle At Transonic Speeds," NASA CR-2217, July, 1973, prepared by GE, Cincinnati, Ohio, for NASA-Langley Research Center.

3. Vier, W.F., QCSEE Test Results From a 14 cm Inlet for a Variable Pitch Fan Thrust Reverser. NASA CR-134867, Dec, 1975.

SECTION 15.0

NACELLE MECHANICAL DESIGN

15.1 SUMMARY

15.1.1 Flight Propulsion System

The under-the-wing flight propulsion system installation is shown in Figure 15-1. This propulsion system is designed for application to a high-wing, short-haul aircraft utilizing externally blown flaps to provide powered lift. Major installation features of this propulsion system include: a high Mach (0.79 throat Mach number) inlet; a composite, integrated nacelle/engine configuration; variable-pitch fan to provide reverse thrust; variable-geometry fan exhaust nozzle; and top-mounted engine accessories enclosed within the aircraft/engine pylon.

The top-mounted accessory configuration in combination with the integrated nacelle concept yields the following significant advantages when compared with current, conventional aircraft/propulsion system installations:

- Reduced Frontal Area - the top-mounted gearbox fits in the silhouette of the aircraft pylon and eliminates the bulge at the bottom of the nacelle which results when the accessories are mounted under the engine.

- Shorter Pipes and Wires - location of the accessories on top results in the shortest "run" from the engine to the accessories and then on to the aircraft wing, reducing system weight and improving maintainability. On current conventional aircraft installation, with accessories located beneath the engine, pipes have to be routed around the fan casing.

- Eliminates Bottom Pylon - in the absence of bottom-mounted accessories, the need for a bottom pylon is eliminated, reducing internal aerodynamic losses.

- Integrated Engine/Nacelle Structure - the high Mach inlet reduces required throat area (smaller diameter throat). The throat-to-highlight-diameter ratio required for good crosswind capability, and the highlight-to-maximum-diameter ratio consistent with aircraft Mach number requirements permits nacelle thickness and maximum diameter to be kept to a minimum. At this minimum thickness, the fan cowl (nacelle component) can be combined with the fan frame structure to complete the integration of nacelle and engine structure.

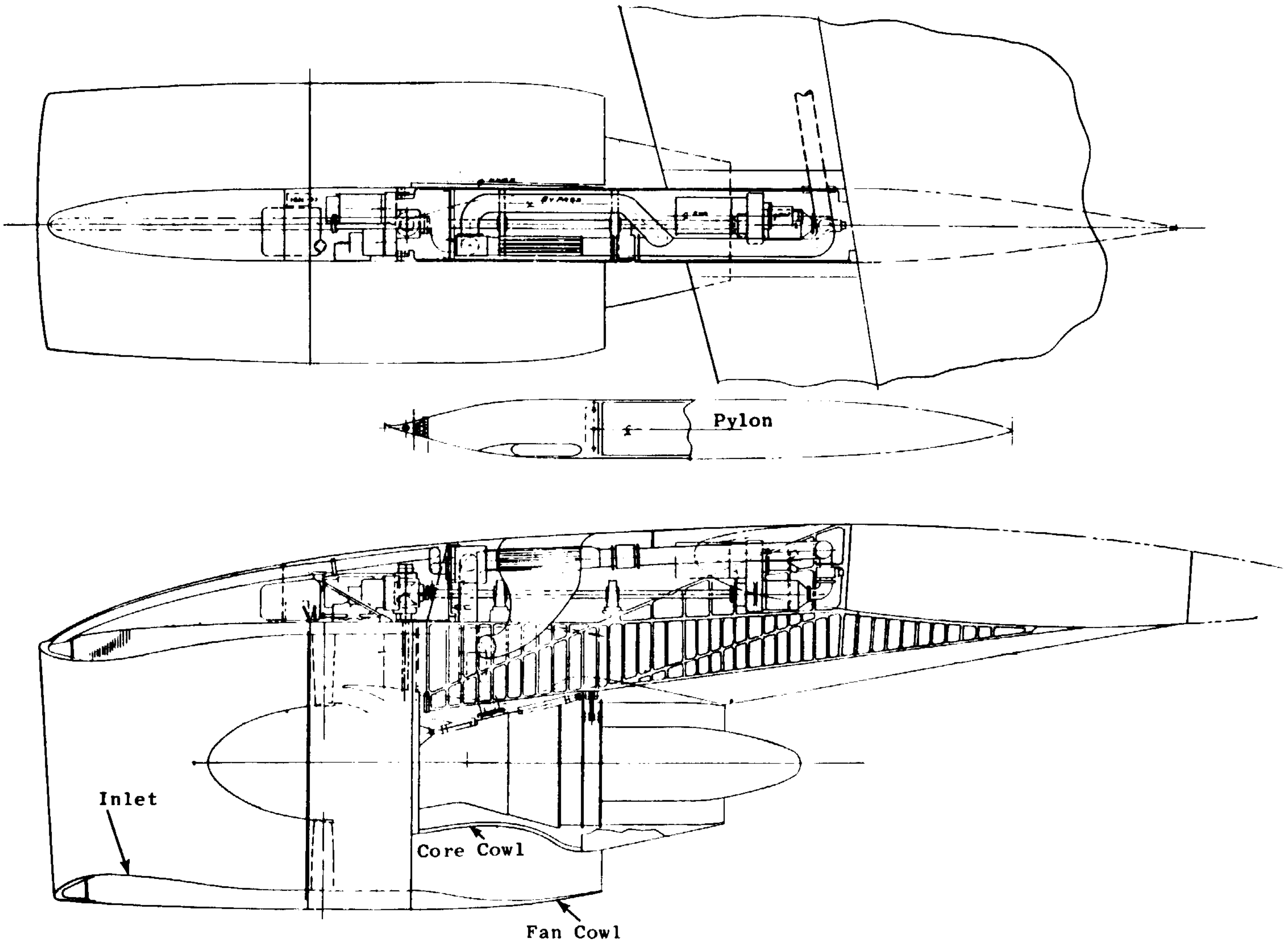
Pylon
Inlet
Core Cowl
Fan Cowl

Figure 15-1. Baseline QCSEE UTW Propulsion Unit.

The integrated engine/nacelle design approach results in thin nacelle walls [9.9 cm (3.9 in.)] uniformly around the nacelle. The walls of this configuration are in the range of 20% to 40% of the wall thickness of current aircraft nacelle configurations. The resulting nacelle maximum diameter is 198 cm (78.8 in.), and the overall length is 414 cm (163.0 in.) to the fan exhaust plane, and 563 cm (211.0 in.) to the tip of the core exhaust nozzle plug.

The aircraft installation results in a height to the bottom of the nacelle of approximately 3.05 m (10 ft). A maintenance stand is therefore required to reach the engine accessories. The accessory cover for the top gearbox rotates in halves aft to expose the engine accessories and then slides aft, as shown in Figure 15-2, to expose the aircraft accessories. This permits direct access to install or remove any component and allows visual inspection of accessories and piping joints while the engine is operating.

15.1.2 Experimental Propulsion System

The UTW experimental propulsion system is shown in Figure 15-3. The overall configuration is basically the same as the flight configuration except that a fan exhaust duct splitter has been added to meet the experimental engine acoustic objectives. The nacelle maximum diameter is the same as in the flight installation, but the overall length is 19.0 cm (7.5 in.) greater to house the 101.9 cm (40 in.) long fan exhaust splitter. The overall length is 433 cm (170.5 in.) to the fan exhaust plane and 556 cm (218.8 in.) to the core nozzle tip. Other specific design differences between the "flight" propulsion system and the experimental engine design are summarized in Table 15-I.

The initial test configuration of the UTW experimental engine will incorporate a boiler plate nacelle. Internal flow lines will be the same for the boiler plate nacelle as for the flight system; however, the external lines will be approximately 8.9 cm (3.5 in.) larger on the radius than the flight configuration. This increase in external dimensions is required for the structure to support the replaceable acoustic panels. There will be two complete sets of treated panels for noise suppression and one set of "hardwalls" for the base line noise testing. Acoustic fan exhaust splitters will be replaceable. All boiler plate nacelle hardware except inner cowl doors will be supported from the test stand to prevent overloading of the composite fan frame. Primary component attachment joints will be the same as in the flight configuration to assure normal flange air and noise leakage. Secondary joints will be provided to "break" the load path between the engine and the test-stand-mounted boiler plate components (i.e., normal engine thrust and other operating loads will be carried through the main engine mounts to the test stand.)

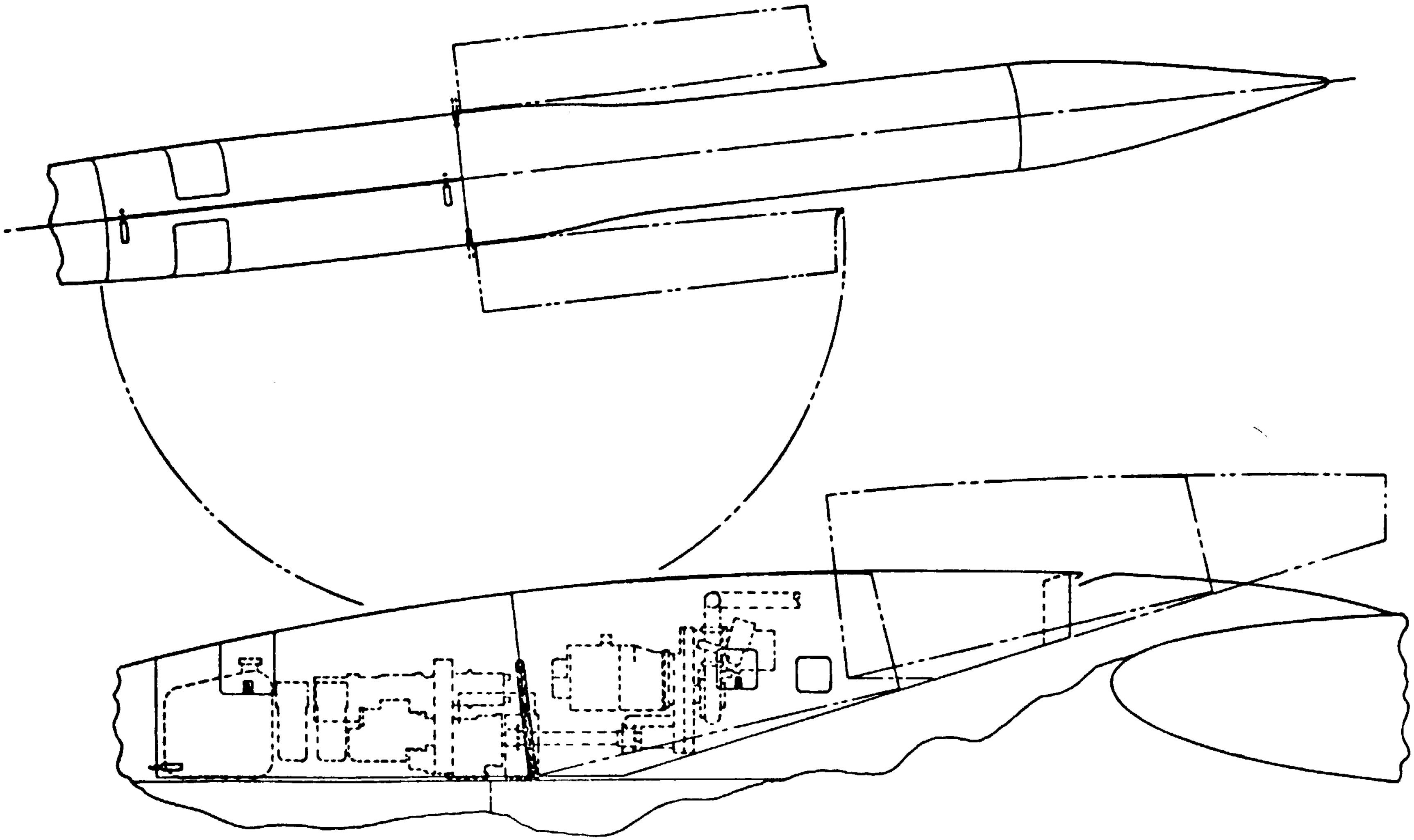

Figure 15-2. Accessory Access Provisions.

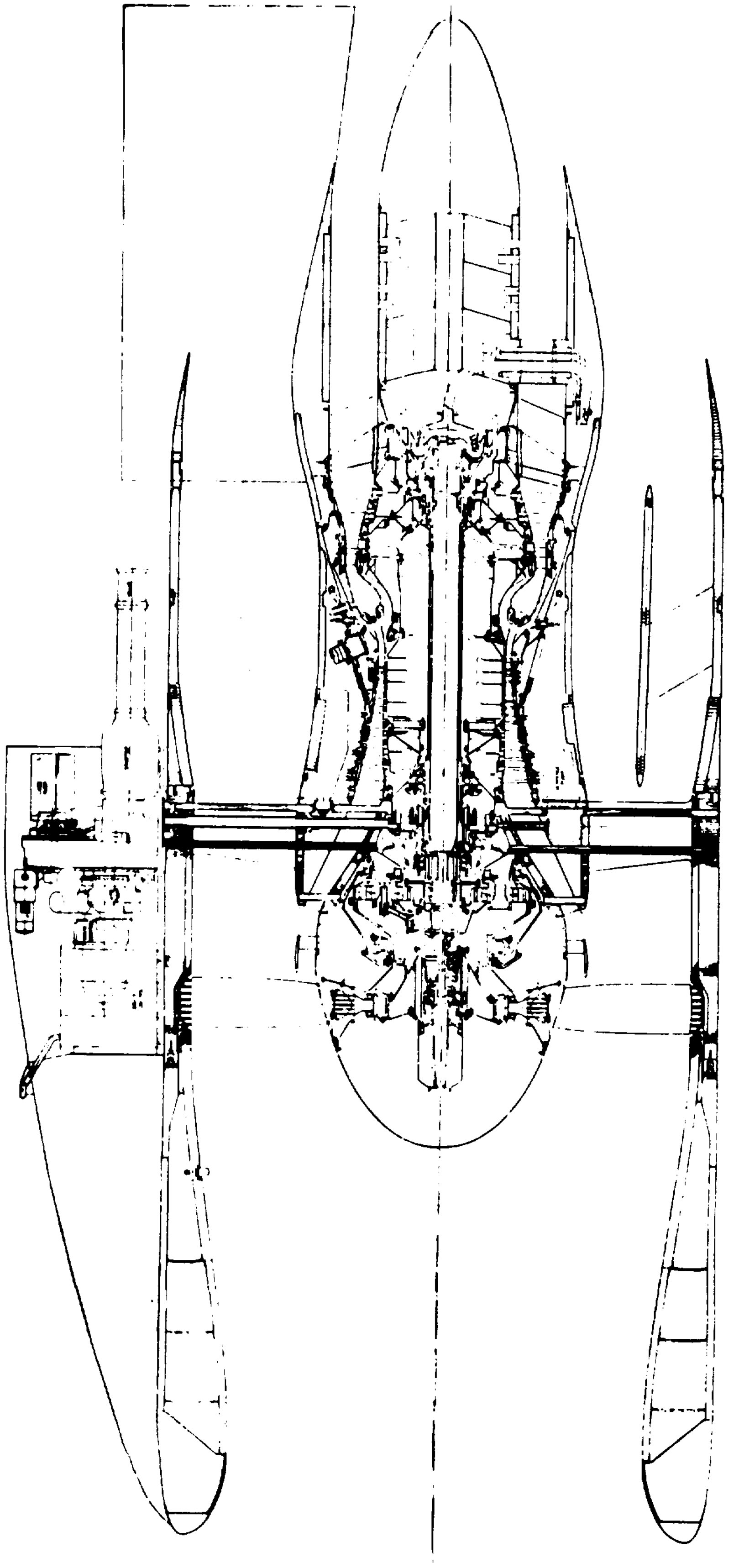

Figure 15-3. UTW Experimental Propulsion System.

Table 15-1. Experimental and Flight Propulsion System Comparison.

Areas of Differences	Experimental	Flight
Accessory Gearbox Case	Cast Aluminum	Flight Design
Oil Tank	TF39 Mod. (Facility)	Shape to Installation
Heat Exchanger	Water/Oil (LM2500 - Facility)	Fuel/Oil (Engine)
Fuel System	F101 Modified	Resized
Control System	Digital/Hydro-Mech.	Flight Design
Lube Filters	CF6/Industrial	Flight Design
Accessory Placement	Test	Aircraft
Hydraulic System	Off-Shelf	V.P. System Only
Nacelle		
Acoustic Design	609.6 m (2000-ft runway)	914.4 m (3000-ft runway)
Fan Exhaust System	Baseline	19 cm (7.5 in.) shorter
Core Exhaust System	Boiler Plate	Flight Design
Accessory Cover	Bolted	Hinged/Sliding
Test Inst. Pads	Boiler Plate	None
Maintainability and Flight Safety		
Anti-Icing	No	Yes
Fire Det. & Extinguish.	Test-Type	Flight Design
Fuel System	Single-Wall	Double Wall

Upon completion of the initial experimental engine tests with the boiler plate inlet, the required acoustic treatment will be selected and the flight weight composite nacelle components will be constructed. In these parts, the acoustic treatment will be an integral part of the nacelle structure.

15.2 DESIGN CRITERIA

All components have been designed consistent with the requirements specified in Section 2.0. Additional specific nacelle component design criteria are as follows:

Inlet

- Design of the experimental engine composite inlet is compatible with anti-icing system requirements; however, an anti-icing system components or inlet metal leading edge is included in the design.
- Design is a one-piece, 6.28-radians (360°) structure with quick-connect-and-disconnect-type fasteners. The experimental engine composite design does not include forward extension of the external pylon/accessory cover.
- Boiler plate hardware will be supported from the facility; composite hardware will be supported from the engine.

Fan Exhaust Nozzle

- Fan nozzle actuation system is submerged within the nacelle wall with required bulges faired externally on the composite nacelle. The same basic actuator mounting arrangement, with modified piping, will be used with the boiler plate cowling.
- No cowl power operating devices are included for either flight or boiler plate propulsion system hardware.
- Aft cowl to fan frame attachment is a quick-disconnect-type similar to DC-10/CF6 design.
- The variable-fan nozzle is designed to be sealed against leakage in all forward thrust conditions, i.e., fan exhaust area from 11,871 to 16,774 cm^2 (1840 to 2600 $in.^2$).
- The variable-fan nozzle is capable of withstanding inadvertent deployment to the reverse thrust position under the following operating conditions:

  - At speeds up to 154 m/sec (300 knots) from 0 to 3048 m (10,000 ft) altitude at cruise power without damage.
  - At speeds up to 193 m/sec (375 knots) above 3048 m (10,000 ft) altitude at maximum power without separation from the aircraft.
- Boiler plate cowling will be mounted from the facility. All composite hardware will be supported from the engine.

Maintainability

- The engine is capable of removal from an aircraft wing and/or facility:
  - Without disconnecting engine-to-engine configuration hardware and engine components (except for facility-mounted components and connecting hardware on the experimental engine).
  - Vertically downward (after uncoupling facility-mounted components on the experimental engine).
  - Without disassembly of fan exhaust cowl doors and variable-geometry fan nozzle.
- Propulsion system configurations are trimmable on the test stand.
- Access to boroscope ports is possible without removal of engine components or disconnecting configuration hardware.
- Engine accessories have been located for easy inspection and maintenance. In the experimental engine configuration some compromise has been made to facilitate use of existing component hardware.
- The accessory cover is hinged in halves and slid aft to expose the engine and aircraft accessories in the flight configuration. The boiler plate cover will be removable from the experimental propulsion system

15.3 COMPOSITE NACELLE DESIGN

The UTW experimental propulsion system includes an acoustically treated nacelle which is integrated with the fan frame and casing to achieve a low noise, minimum drag, lightweight design. To accomplish this integration function efficiently at minimum cost and weight, conventional metal construction is replaced with advanced composite materials.

The major portion of the nacelle, with exception of the core cowl, operates at very modest temperatures, less than 355 K (180° F), permitting use of a wide variety of composite materials. The primary composite material selected for these areas consists of a woven Kevlar 49 fabric impregnated with an epoxy resin system. This material exhibits light weight, good tensile strength, moderate stiffness, and excellent impact strength. Its major drawback is its poor compressive strength; therefore, in areas requiring higher compressive capabilities, woven glass cloth is substituted for the Kevlar. Where this is necessary, the standard 7781 weave "E" glass is used, impregnated with the same matrix system as the Kevlar.

For the core cowl, which must operate at elevated temperatures, a graphite/polyimide system is used allowing long term operation at 561 K (550° F).

The honeycomb core material in the low temperature areas is Hexcel's corrosion resistant 5052 aluminum core. For the higher temperatures in the core cowl, HRH 327 glass/polyimide core is used. The core in the acoustically treated panels is slotted to provide drainage.

The specific nacelle components which utilize composite materials are the inlet, outer cowl doors, variable fan exhaust nozzle flaps, and the inner cowl door. These are discussed individually in the following sections.

15.3.1 Inlet

Inasmuch as the detail design of the composite inlet is not complete, information presented in this section should be regarded as a design status report.

The acoustically treated inlet is the largest single piece of the overall UTW nacelle structure, being almost 178 cm (70 in.) long and nearly 200 cm (79 in.) in diameter. To reduce the weight of this large structure as much as possible, it will be constructed mainly of lightweight Kevlar/epoxy material and the acoustic treatment will be incorporated as part of the permanent structure.

The inlet consists primarily of inner and outer honeycomb sandwich walls separated and supported by circumferential stiffners as shown in Figure 15-4. The face sheets of these sandwiches are all made from Kevlar/epoxy. The inner skin of the inner wall is perforated with hole configurations that satisfy the acoustic requirements of the inlet. The inner wall thickness (honeycomb depth) is also tailored to meet the acoustic requirements. The outer wall thickness is sized to provide adequate stiffness. The honeycomb material is aluminum.

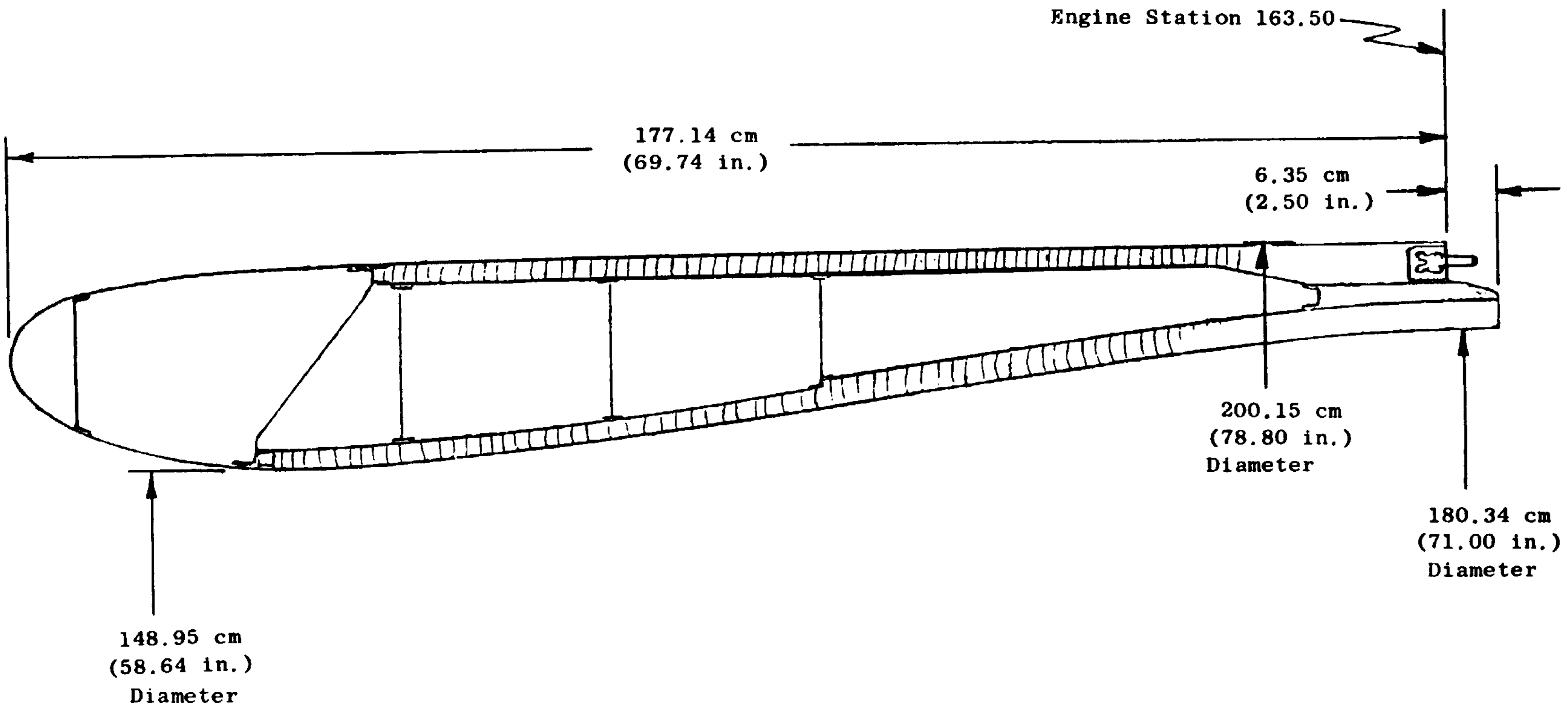
Engine Station 163.50
177.14 cm
(69.74 in.)
6.35 cm
(2.50 in.)
200.15 cm
(78.80 in.)
Diameter
180.34 cm
(71.00 in.)
Diameter
148.95 cm
(58.64 in.)
Diameter

Figure 15-4. QCSEE Inlet Axial Cross Section.

Aerodynamic loading of the inlet is far more significant than inertia loading. The primary reason for this is the large transverse load reacting on the inlet as it turns the entering engine airflow at flight conditions where the direction of the free stream air is not parallel to the inlet axis. In contrast, the lightweight structure of the inlet produces relatively low inertia loads. Th most severe aerodynamic loads occur during a 3 g aircraft stall at Mach 0.4, sea level, and with the engine operating at maximum continuous power, as shown in Table 15-II. For design analysis, the loads resulting from this condition were combined with the most severe additive inertia loads caused by dynamic landing. In addition, compressive hoop loads were considered for the sea level static takeoff power operating condition. The stress levels for these loads and this construction are shown in Table 15-II. These are based on each facing consisting of three plies of woven Kevlar/ epoxy material giving a total face sheet thickness of 0.084 cm (0.033 in.). Buckling allowables for this construction are shown in Table 15-III. The sensitivity of this configuration to local loads is shown in Figure 15-5. Stiffeners are segmented and are constructed of aluminum sheet with flanged weight reduction cutouts and with composite (Kevlar) flanges to provide bonded attachment to the walls. The stiffener flanges were designed to prevent the bearing load between the stiffener flange and sandwich wall from exceeding 2.48 x 10^6 N/m^2 (360 psi). This resulted in a flange width of 1.55 cm (0.61 in.). Using a 137.9 x 10^6 N/m^2 (20,000 psi) flange allowable bending stress results in a flange thickness of 0.1778 cm (0.07 in.).

Provision for inlet leading edge anti-icing is not included in the experimental engine inlet design. As a result the leading edge is fabricated from composite materials. In a flight engine design the leading edge would be titanium to provide anti-icing and to increase resistance to foreign object damage and erosion. A sketch of this concept is shown in Figure 15-6. A corrugated backup sheet would provide passages for the anti-icing airflow. This arrangement offers the advantages of isolating the anti-icing air from the composite material and of containing the flow for effective heat transfer and minimum air usage.

The inlet attaches to the fan frame by means of 16 rotary latches. Each of these latches is operated by turning a flush receptical. A pressure and acoustic seal is achieved at this joint by means of a thick (in the radial direction) elastomer gasket. The latch loads for this installation are shown in Table 15-IV.

As can be seen from the above analysis, the inlet is not highly stressed. The skin thicknesses selected were estimated minimum gages required for load impact during handling.

The composite inlet described above weighs 156 kg (345 lb) compared to 217 kg (479 lb) for a typical current technology metal inlet scaled to the same size.

Table 15-II. Inlet Stresses and Deflections at Maximum Combined Load Condition.*

Load			Stress				
Type	Magnitude	Direction	Type	Calculated N/cm^2 (psi)	Allowable N/cm^2 (psi)	Safety Factor	Deflection cm (in.)
Bending	69,317 Nm (613,423 in.-lb)	- -	Compression	1402 (2034)	6895 (10,000	4.9	.058 (.023)
Axial	8358 N (1879 lb)	Forward	Tension	1583 (2296)	48,265 (70,000)	30.5	
Transverse	37,119 N (8345 lb)	-	Shear	403 (584)	6895 (10,000)	17.1	.206 (.081)
Hoop	2.76 N/cm^2 (4 psi)	Burst	Tension	1806 (2620)	48,265 (70,000)	26.3	-
(Max Range Expected)	5.86 N/cm^2 (8.5 psi)	Crush	Compression	3897 (5652)	6895 (10,000)	1.8	-

*Derived from DAC "Design-To" Criteria. Aerodynamic loads from 3 G stall (M_o = 0.4 @ SL) combined with inertia loads from dynamic landing.

Table 15-III. Critical Buckling Loads.

Buckling from Bending					
	Critical Moment		Actual Max. Moment		Safety Factor
Load Conditions	Nm	(in-lb)	Nm	(in-lb)	
Moment on Outer Skins	4,557,282	(40,329,928)	69,317	(613,423)	65.7

Buckling from Compressive Hoop Load					
	Critical Pressure		Actual Pressure		Safety Factor
Load Conditions	N/cm^2	(psi)	N/cm^2	(psi)	
Pressure supported by single sandwich wall (2 skins) between 33.04 cm (13 in.) apart	154	(223)	5.9	(8.5)	26.2
Pressure supported by overall wall structure	234	(399)	5.9	(8.5)	46.9
Pressure supported by single outer aluminum nose* wall 40.64 cm (16 in.) long with stiffening corrugations	351	(509)	5.9	(8.5)	59.9
Pressure supported by single inner aluminum nose* wall aft of corrugation with corrugation sheet extended to form doubler: 6.35 cm (2.5 in.) long x 0.183 cm (0.072 in.) O/A Thk	16.2	(23.47)	5.9	(8.5)	2.76

*NOTE: Analysis was based on utilization of an aluminum nose. A subsequent decision was made to fabricate the leading edge from composite materials.

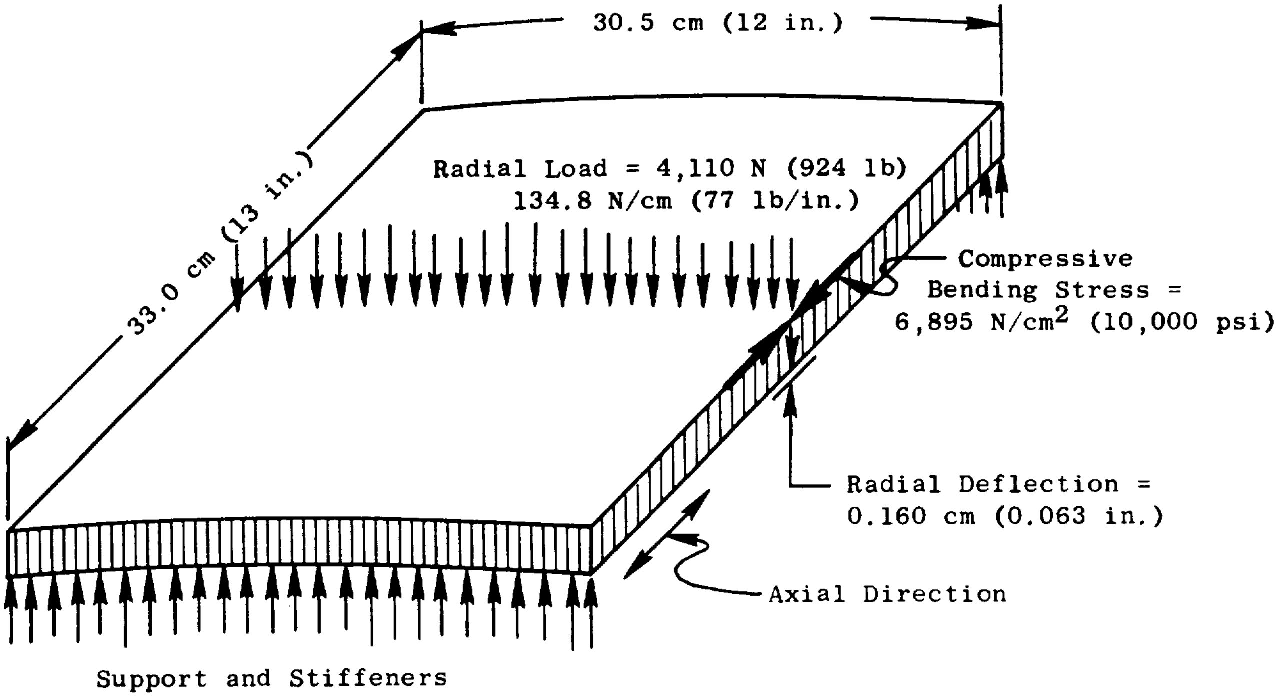
30.5 cm (12 in.)
33.0 cm (13 in.)
Radial Load = 4,110 N (924 lb)
134.8 N/cm (77 lb/in.)
Compressive
Bending Stress =
6,895 N/cm2 (10,000 psi)
Radial Deflection =
0.160 cm (0.063 in.)
Axial Direction
Support and Stiffeners

Figure 15-5. Inlet Wall Local Load Resistance.

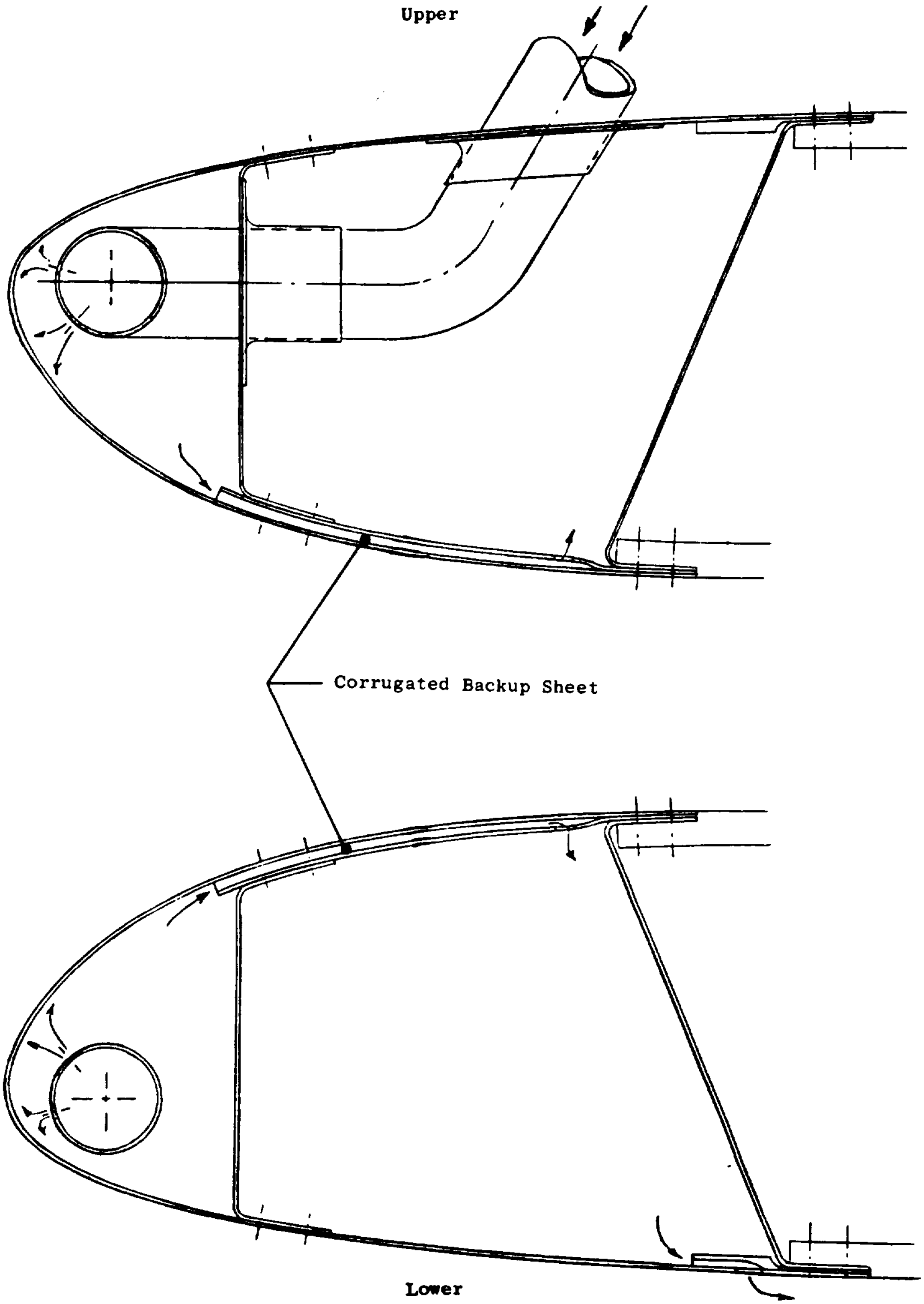
Upper
Corrugated Backup Sheet
Lower

Figure 15-6. Inlet Anti-Icing Schematic.

Table 15-IV. Inlet Latch Loads.

(@ Maximum Combined Load Condition)

Latch Configuration	Maximum Latch Load		Ultimate Latch Strength		Latch Safety Factor
	N	lb	N	lb	
All 16 Latched	9617	2162	28800	6475	3.00
One Latch Open	10737	2414	28800	6475	2.68
Two Latches Open	13135	2953	28800	6475	2.19
Six Latches Open	25073	5637	28800	6475	1.15

15.3.2 Fan Bypass Duct

The fan bypass duct and fan nozzle constitute the outer nacelle section aft of the fan frame (See Figure 15-7). These components are designed to take full advantage of advanced-type composite materials in order to provide a lightweight, thin-profile nacelle suitable for advanced air transports.

The fan bypass duct is designed as right- and left-hand sections split on the vertical center line. A roll-out view of one section is shown in Figure 15-8. Each section is attached at its upper edge to the aircraft pylon structure by means of a piano-type hinge and is sealed to the pylon as shown in Figure 15-9. The sections are fastened to each other along the bottom vertical centerline by a series of cowl latches. This allows the duct to be opened for accessibility to the core cowl, and thereby to the core engine. The duct forward "close-out" ring contains a circumferential, inward facing tongue which engages a corresponding groove in the fan frame when the duct sections are closed and latched (see Figure 15-10). The tongue and groove are tapered on the forward side (with corresponding axial free play in the piano hinge) to aid in the engagement when closing the duct. The aft surface of the joint is vertical for transmittal of the duct axial loads into the fan frame and hence through the engine mounts into the pylon.

The duct is a sandwich-type construction with Kevlar 49 face sheets and 5052 aluminum honeycomb core with stiffening rings and members were required. The inner face sheet provides a continuation of the outer wall of the fan exhaust duct and is perforated so that along with the sized honeycomb core it constitutes the sound suppression treatment in the duct. This treatment being integral with the duct, is also part of the load carrying structure. The duct outer face sheet forms the external flow surface of the nacelle and is also structural. The minimum thickness (core height) of the duct is set by the acoustic design requirements. At the forward end of the duct, where additional thickness is required to mate with the fan frame flow path, a septum sheet will be provided in the core area to maintain the proper honeycomb cell depth for acoustic treatment.

The fan nozzle actuation system will be contained within the envelope of the duct, except for external fairings locally over the actuators (three per duct half). These fairings will also be the access covers for the actuators and link system. The actuators will be mounted in cavities formed of molded pans bonded into the duct. A typical installation is shown in Figure 15-7. The aft end of the pan will contain the inner half of a track system for supporting and guiding the actuator rod-end clevis during flap operation. The outer half of the track will be mounted in the actuator access cover. Clearance holes in the duct aft close-out ring will permit free passage of the flap-to-actuator linkage during nozzle translation (see Figure 15-11). The forward actuator mount will be attached to an integral ring at the forward end of the actuator cavity, with the ring serving to distribute the

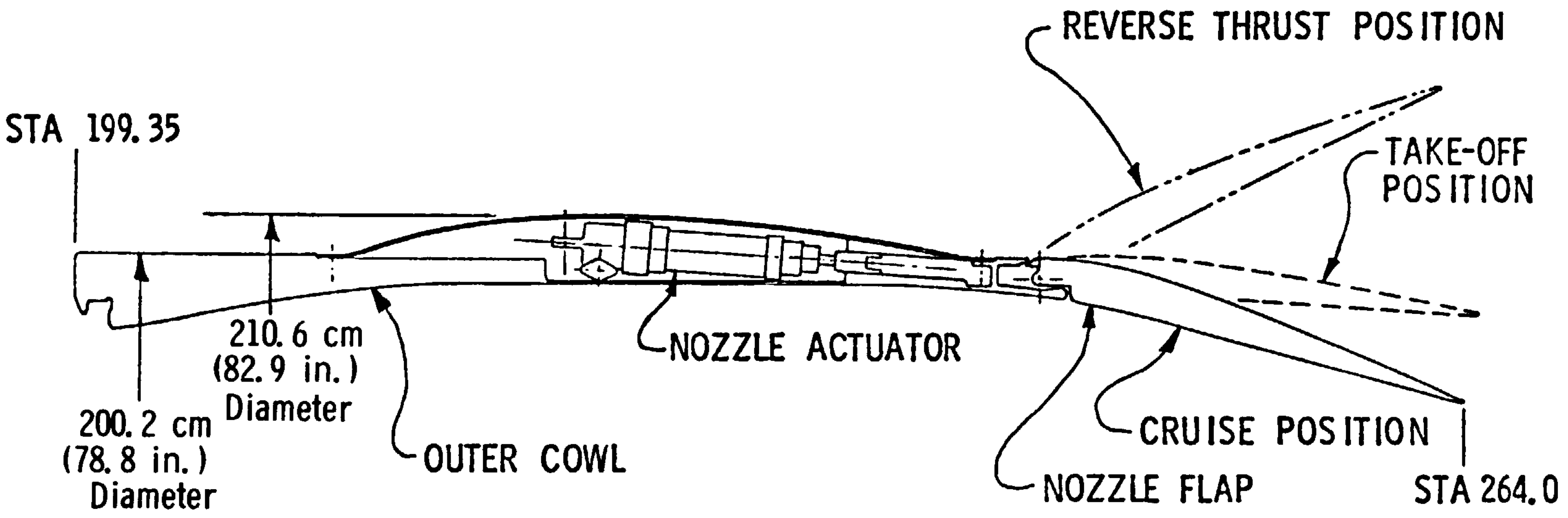
REVERSE THRUST POSITION
STA 199.35
TAKE-OFF POSITION
210.6 cm (82.9 in.) Diameter
NOZZLE ACTUATOR
200.2 cm (78.8 in.) Diameter
OUTER COWL
CRUISE POSITION
NOZZLE FLAP
STA 264.0

Figure 15-7. Outer Cowl Cross Section.

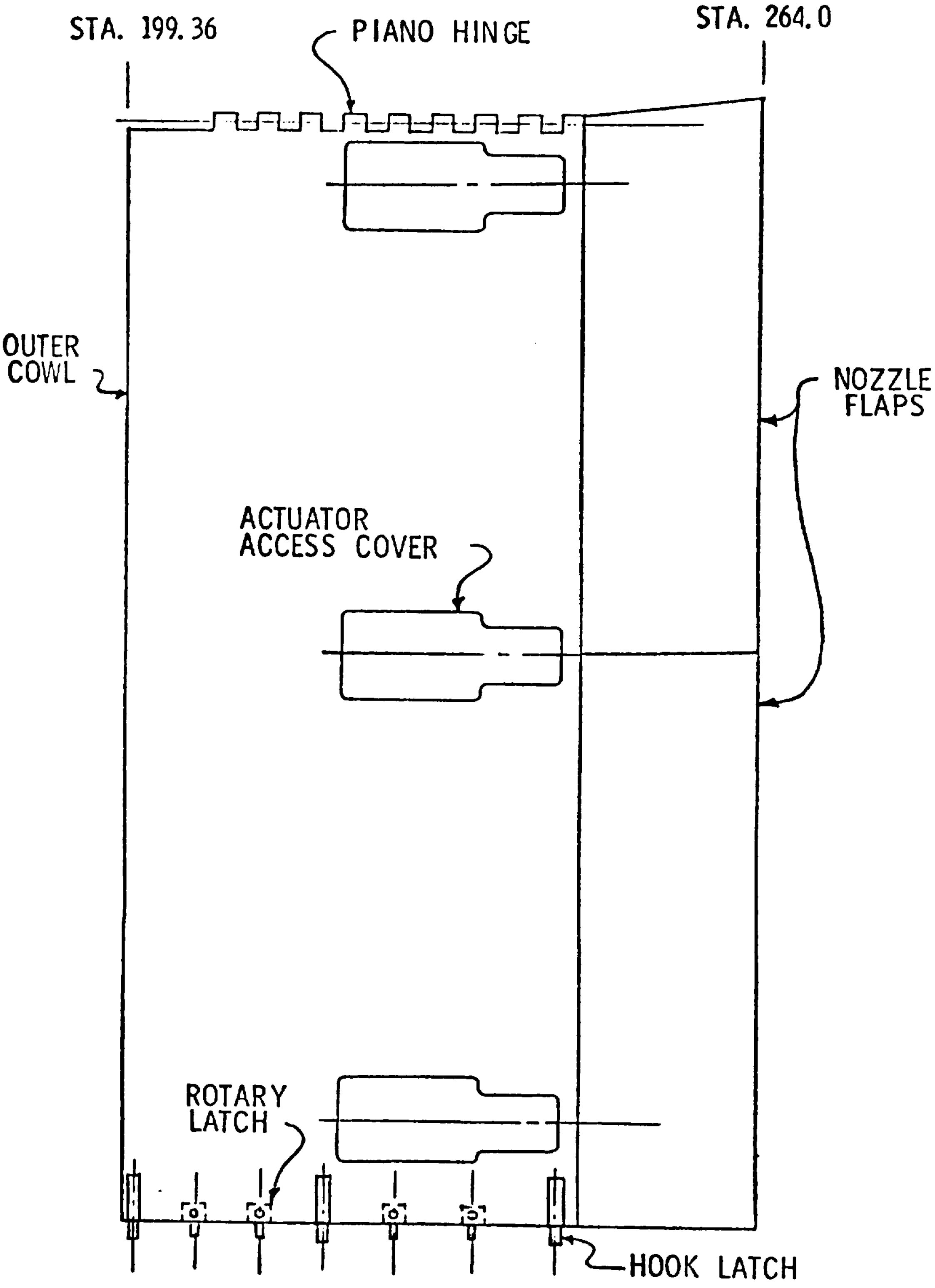
STA. 199.36
PIANO HINGE
STA. 264.0
OUTER COWL
NOZZLE FLAPS
ACTUATOR ACCESS COVER
ROTARY LATCH
HOOK LATCH

Figure 15-8. Development - Outer Cowl/Nozzle.

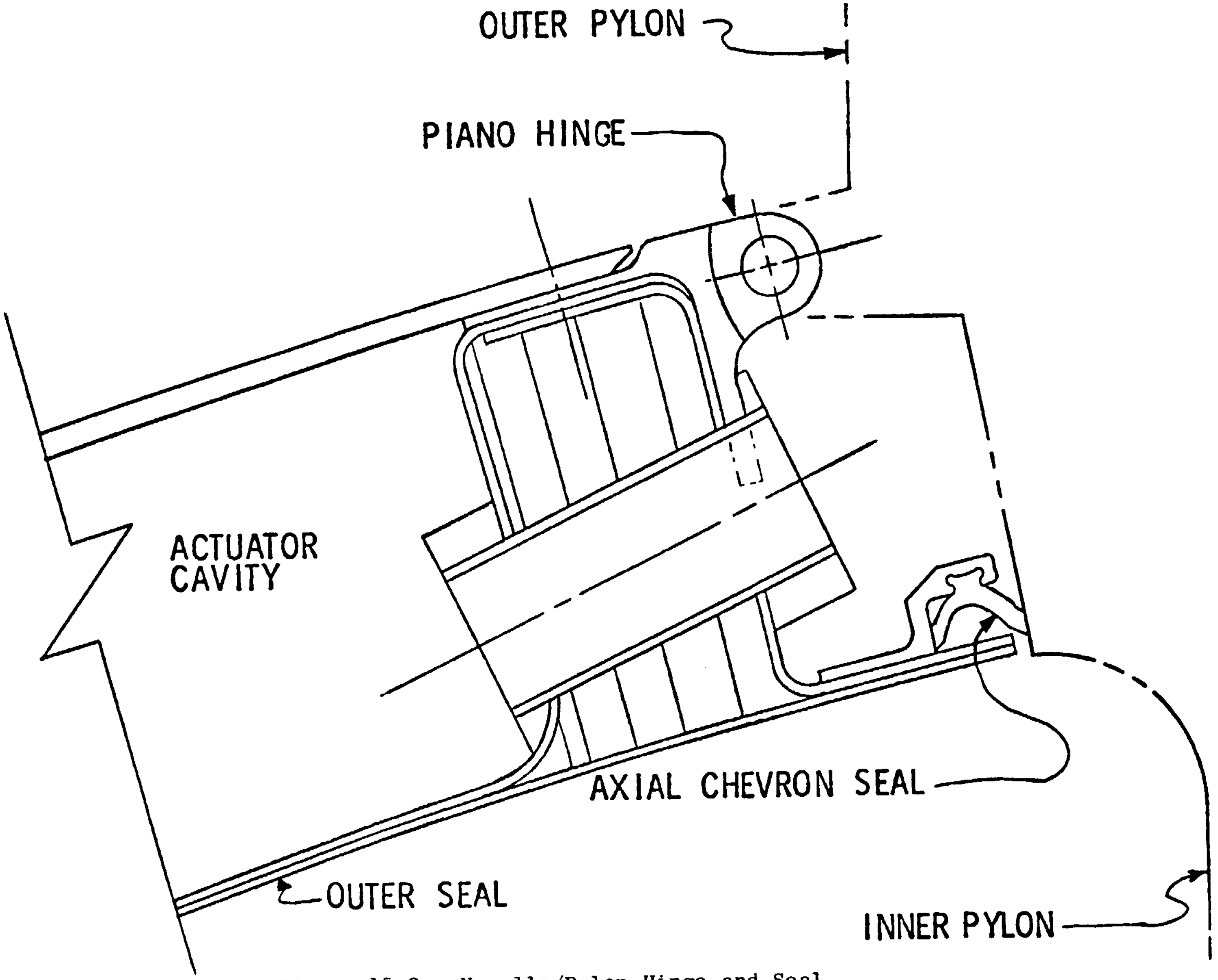
OUTER PYLON
PIANO HINGE
ACTUATOR CAVITY
AXIAL CHEVRON SEAL
OUTER SEAL
INNER PYLON

Figure 15-9. Nacelle/Pylon Hinge and Seal.

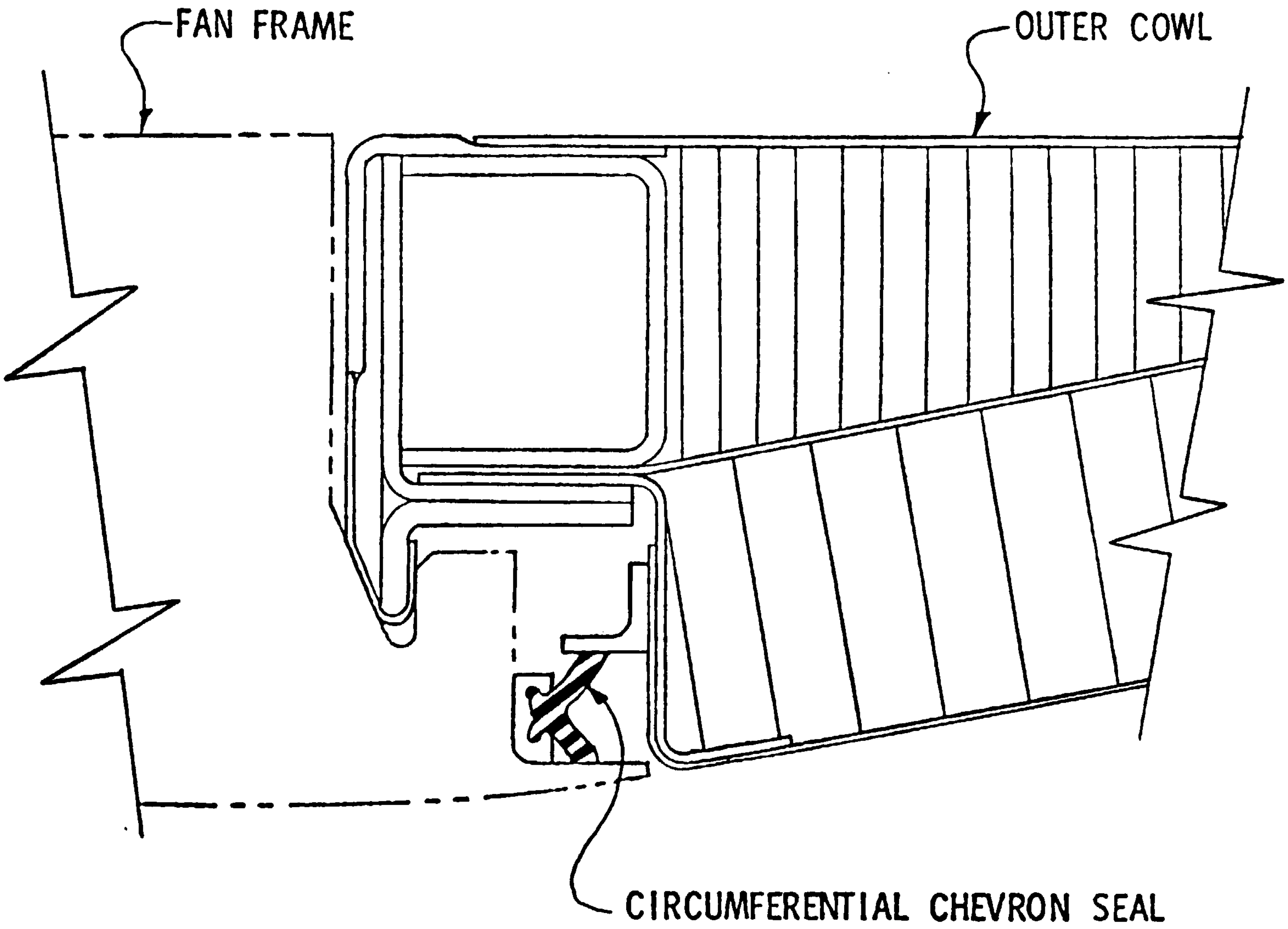
FAN FRAME
OUTER COWL
CIRCUMFERENTIAL CHEVRON SEAL

Figure 15-10. Outer Cowl/Fan Frame Attachment.

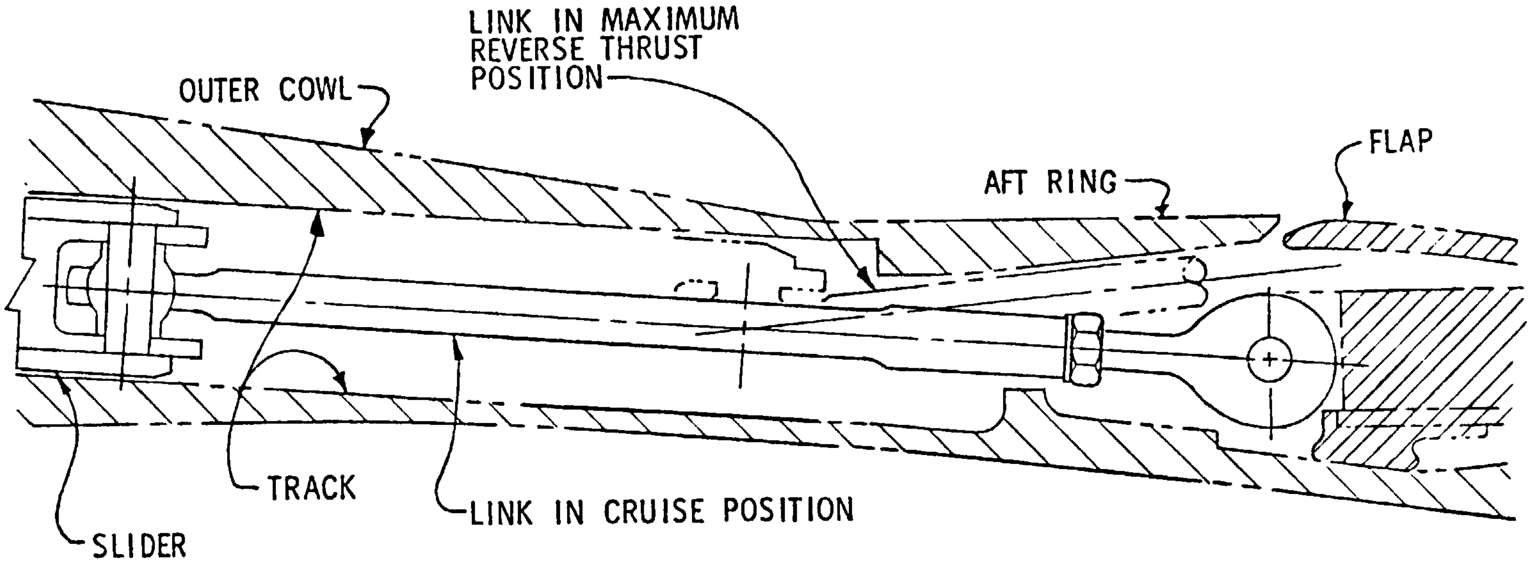
LINK IN MAXIMUM
REVERSE THRUST
POSITION
OUTER COWL
FLAP
AFT RING
TRACK
LINK IN CRUISE POSITION
SLIDER

Figure 15-11. Actuator/Flap Link Installation.

actuation loads. Tunnels formed of plastic tubing and built into the honeycomb core will serve as passages for the actuation system synchronization cable, the hydraulic rod and head end tubes and the seal drain tube. The hydraulic and drain tube passages will connect each actuator cavity and extend through both the upper and lower axial closeouts of the bondment. This will permit assembly of the tubes from either direction. The synchronization cable tunnel will extend from the upper axial bondment closeout to the center actuator cavity only.

A means for mounting the fan duct splitter will be provided as a part of the bypass duct design. At three locations on each duct half, coincident with the splitter strut foot locations, an indentation on the inner flow surface of the duct will be provided such that the foot outer surface will be flush with the duct surface forming a smooth flow path. Threaded inserts, potted in place, will be used to retain the splitter strut mechanical fasteners.

A 2024 aluminum piano hinge will be mechanically fastened along the upper edge closeout and will be continuous from the aft closeout ring to a point approximately eight inches aft of the forward ring. Figure 15-9 shows a cross section of this hinge.

The bottom latch system will consist of seven Hartwell King latches of the hook type, one at each of the three circumferential rings and the other four equally spaced between these. Figure 15-12 shows a typical latch installation. With the duct closed and latched, the duct pressure loads will be resisted by hoop tension/compression stresses with the hinge forces being reacted by the pylon support structure. Table 15-V shows the results from preliminary load and stress calculations.

15.3.3 Fan Nozzle

The composite fan nozzle is required on the first engine to test (which uses the boilerplate nacelle); therefore, this section constitutes the final design report for the fan nozzle flap system.

The fan exhaust nozzle is a fully modulating, variable-flap-type configuration that provides various nozzle exit areas for forward thrust, and is also capable of flaring outwards to provide increased area for the inlet airflow to the variable-pitch fan in the reverse mode (see Figures 15-13 and 15-14).

The nozzle consists of four hinged flaps, each 44.96 cm (17.7 in.) from hinge centerline to trailing edge. The upper flaps are 1.461 radians (83.7°) wide and the lower flaps are 1.475 radians (84.5°) wide. A hinge/actuator link clevis arrangement (see Figure 15-14) is used to position the flaps.

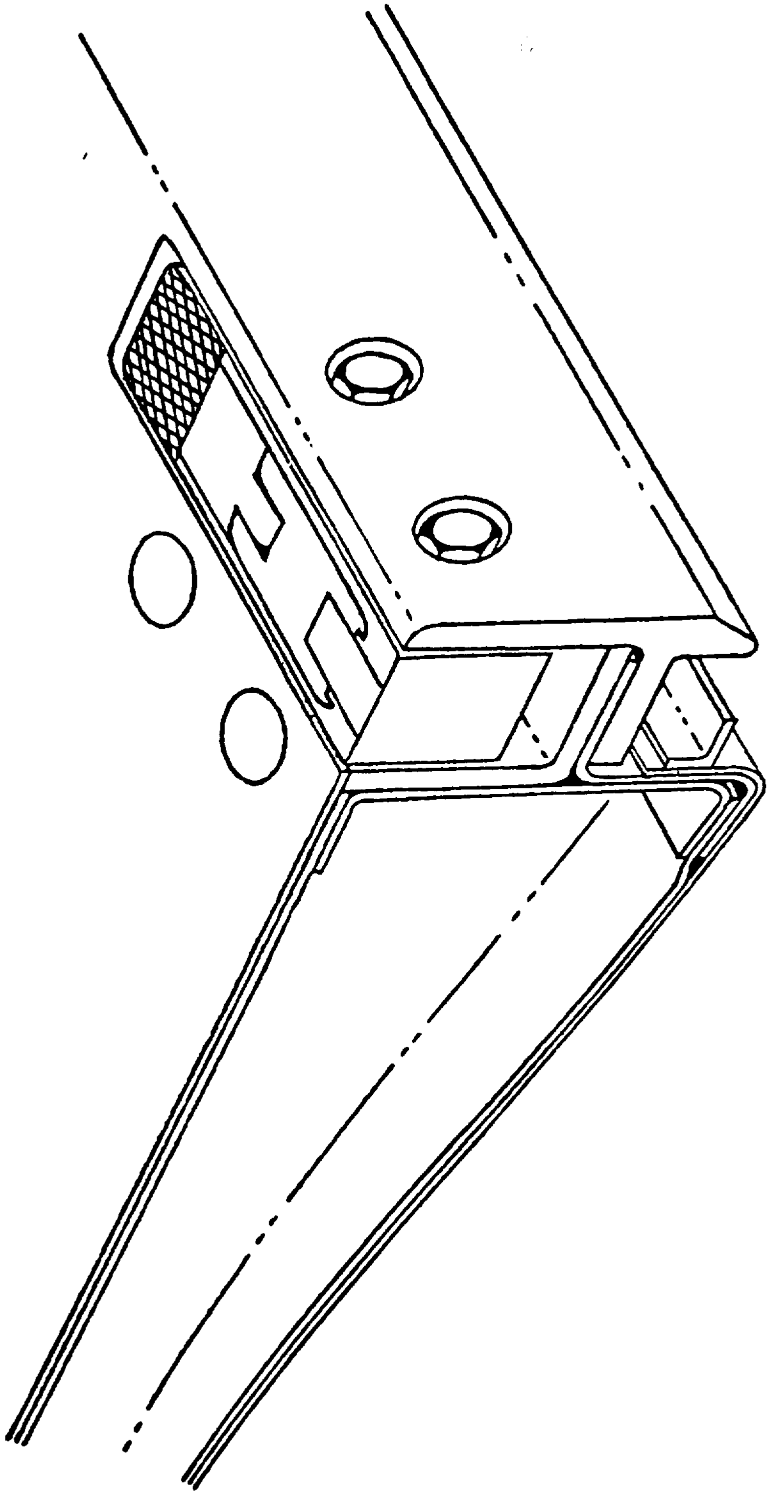

Figure 15-12. Outer Cowl, Forward Hook Latch Installation.

Table 15-V. Fan Duct Hinge/Skin Stresses.

Flight Condition	Max ΔP N/cm^2 (psi)	Hoop Load N/cm (lb/in)	Hinge Pin Brg Stress N/cm^2 (psi)	Hinge Pin Shear Stress N/cm^2 (psi)	Skin Circumferential Stress N/cm^2 (psi)	Skin Axial Stress N/cm^2 (psi)
M = 0.3 @ SL 100%	1.10 (1.60)	109 (62)	214 (310)	386 (560)	$948^{(T)}$ (1375)	$476^{(T)}$ (690)
M = 0.8 @ 9144 m (30,000 ft) MCR	2.65 (3.85)	261 (149)	548 (795)	931 (1350)	$2275^{(T)}$ (3300)	$1138^{(T)}$ (1650)
M = 0.9 @ 6096 m (20,000 ft) MRC	4.83 (7.00)	474 (271)	996 (1445)	1689 (2450)	$4137^{(T)}$ (6000)	$2069^{(T)}$ (3000)
M = 0.225 @ SL Reverse	-2.48 (-3.60)	-243 (-139)	510 (740)	869 (1260)	$2137^{(C)}$ (3100)	$1069^{(C)}$ (1550)

T - Tensile

C - Compression

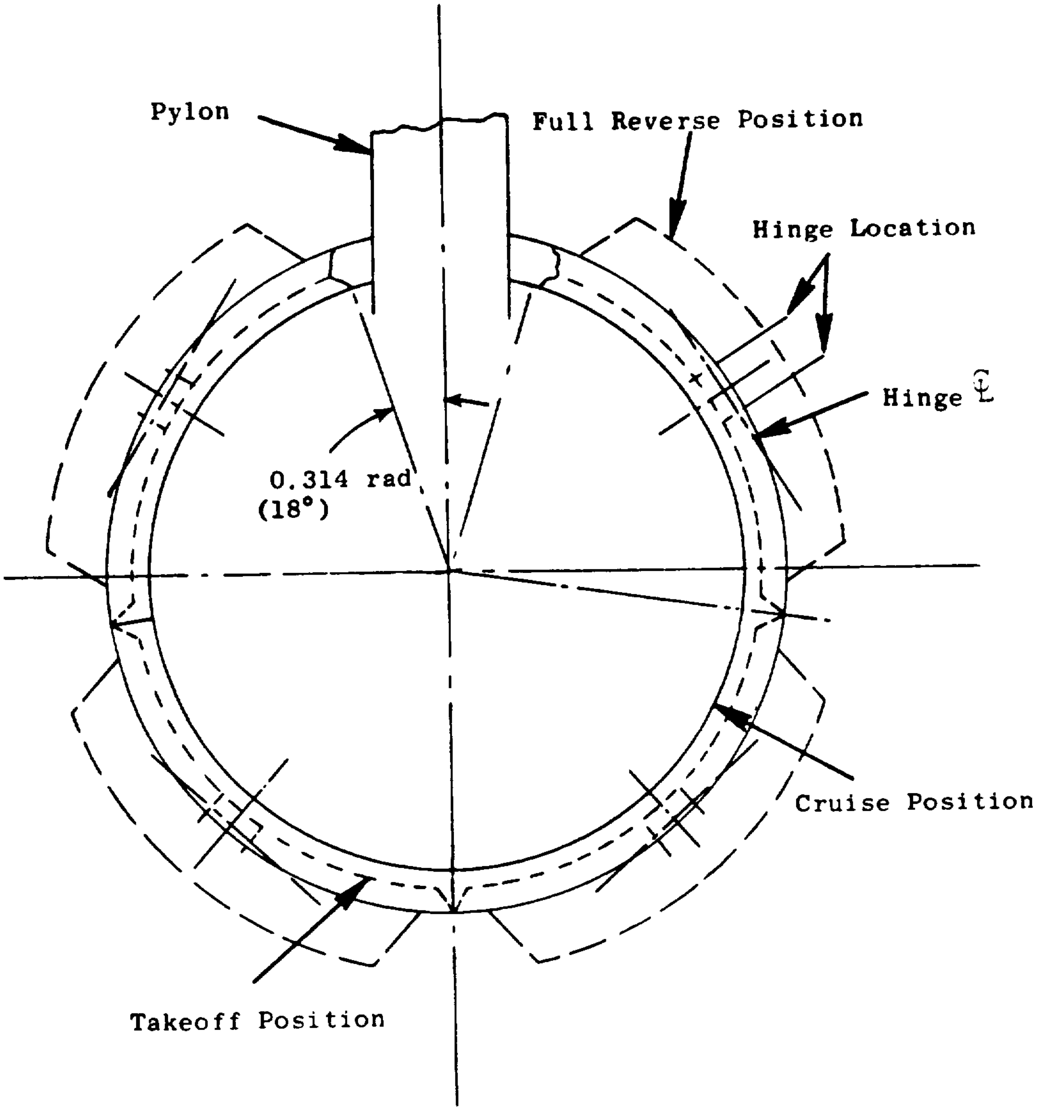
Pylon
Full Reverse Position
Hinge Location
Hinge ℄
0.314 rad
(18°)
Cruise Position
Takeoff Position

Figure 15-13. Flare Nozzle Flap Schematic.

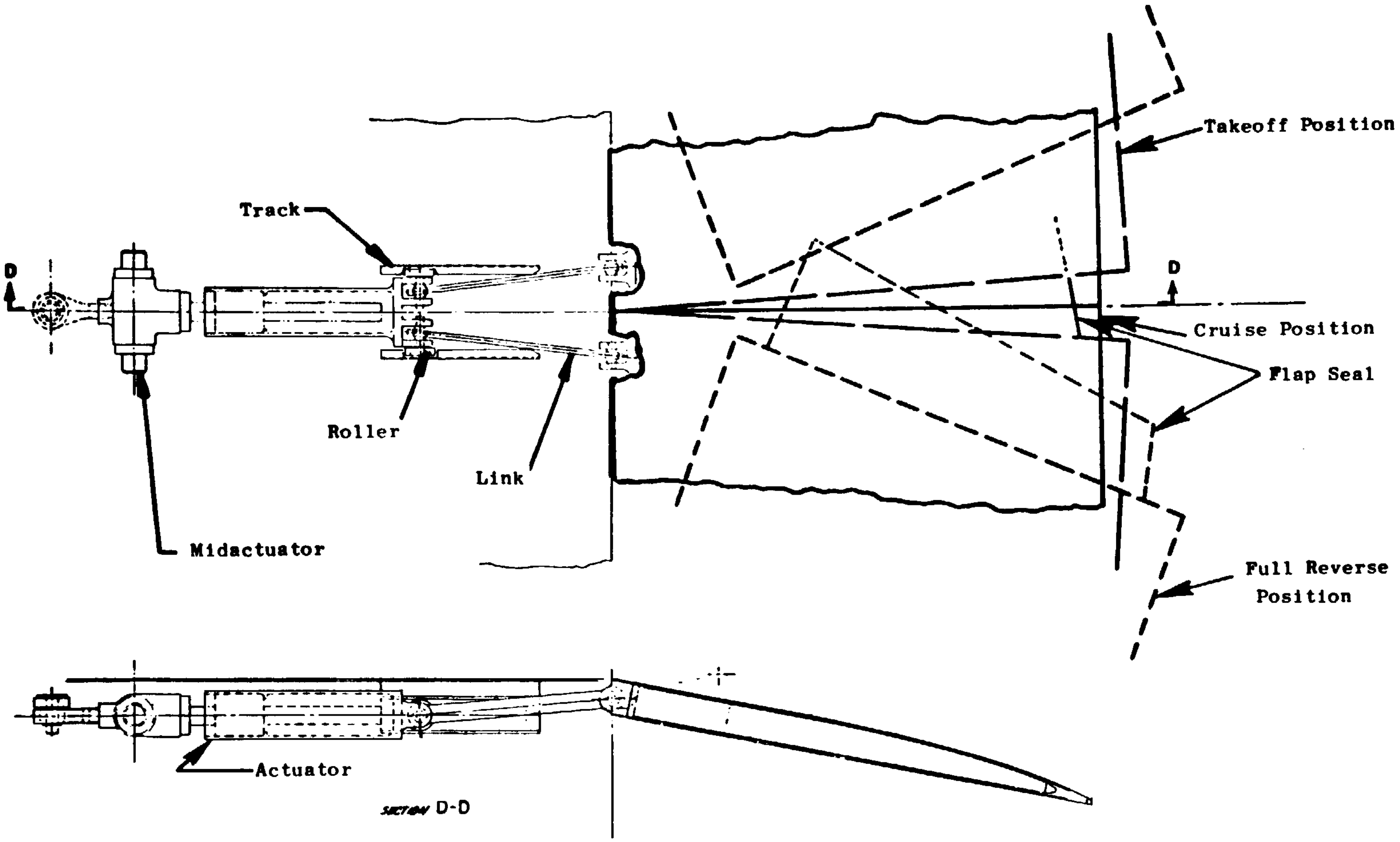
Takeoff Position
D
Track
Cruise Position
Flap Seal
D
Roller
Link
Midactuator
Full Reverse
Position
Actuator
SECTION D-D

Figure 15-14. Variable Flap Nozzle.

Each flap will be attached to the fan duct aft ring by means of a pair of hinges 30.48 cm (12 in.) apart at the flap centerline along the flap forward edge closeout. The flaps will be connected to the actuation system in the fan duct by links at link clevises which are located 0.438 radian (25.119°) outboard of each hinge. The links will have spherical bearing rod ends to preclude any binding during flap operation. The flaps are designed such that they can be rotated from an angle of about 0.227 radian (13°) in toward the engine centerline to an outward angle of approximately 0.489 radian (28°).

The synchronization of the upper and lower flaps in each duct half will be accomplished by mid-actuator which is joined to both flaps (see Figure 15-13). The synchronization between duct halves will be accomplished by the actuation system synchronization cables. The upper and lower actuators will be connected to the flaps by a single link only.

Located along the axial edges of each flap are intraflap seal assemblies (see Figure 15-15), which are designed to give full sealing from a minimum nozzle area of 11,903.2 cm^2 (1845 $in.^2$) to a maximum sealed nozzle area of 16,781 cm^2 (2601 $in.^2$). From this maximum sealed nozzle area to the full-reverse flap position the seals will be disengaged allowing a triangular-shaped void between the flaps. Sealing is not required while in the reverse mode.

The intraflap seal assemblies are spring-loaded pivoted bumpers, one of which (in each pair) has a soft face in order to provide good sealing; otherwise, the seal components are identical between seal assemblies. The spring forces are such as to cause the seals to maintain contact with each other as the flaps move outward, except that when the nozzle reaches an area of 16,781 cm^2 (2601 $in.^2$), a slot in each seal slider bottoms out against a fixed pin mounted in the seal housing, preventing further seal travel. The seals will then stay in the same position, relative to the flap they are mounted in, for any nozzle area greater than the 16,781 cm^2 (2601 $in.^2$).

A circumferential seal is also provided along the forward inner edge of each flap. This seal contacts a contoured lip extension from the aft ring of the fan outer duct (see Figure 15-16). The seal will also provide full sealing over the same range as the axial intraflap seals.

The seal at the flap/pylon interface is fixed in the axial closeout of the flap (see Figure 15-17). This seal will be adjusted at assembly of the outer duct and nozzle to the pylon to have good contact with the sealing face on the pylon. Having this seal fixed necessitates the pylon sealing face being perpendicular to the upper flap center line.

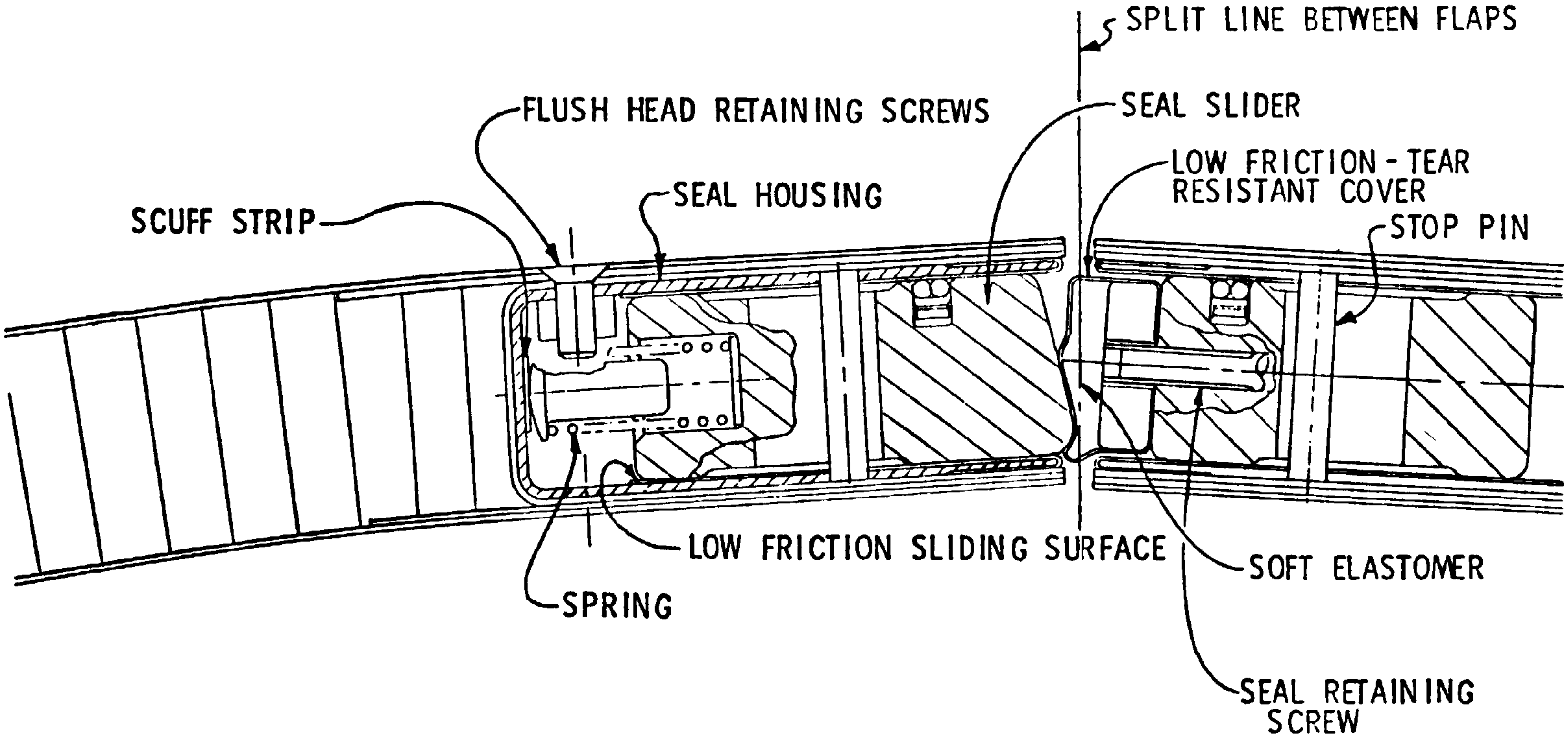
SPLIT LINE BETWEEN FLAPS
FLUSH HEAD RETAINING SCREWS
SEAL SLIDER
LOW FRICTION-TEAR RESISTANT COVER
SEAL HOUSING
SCUFF STRIP
STOP PIN
LOW FRICTION SLIDING SURFACE
SOFT ELASTOMER
SPRING
SEAL RETAINING SCREW

Figure 15-15. Intraflap Seal Schematic.

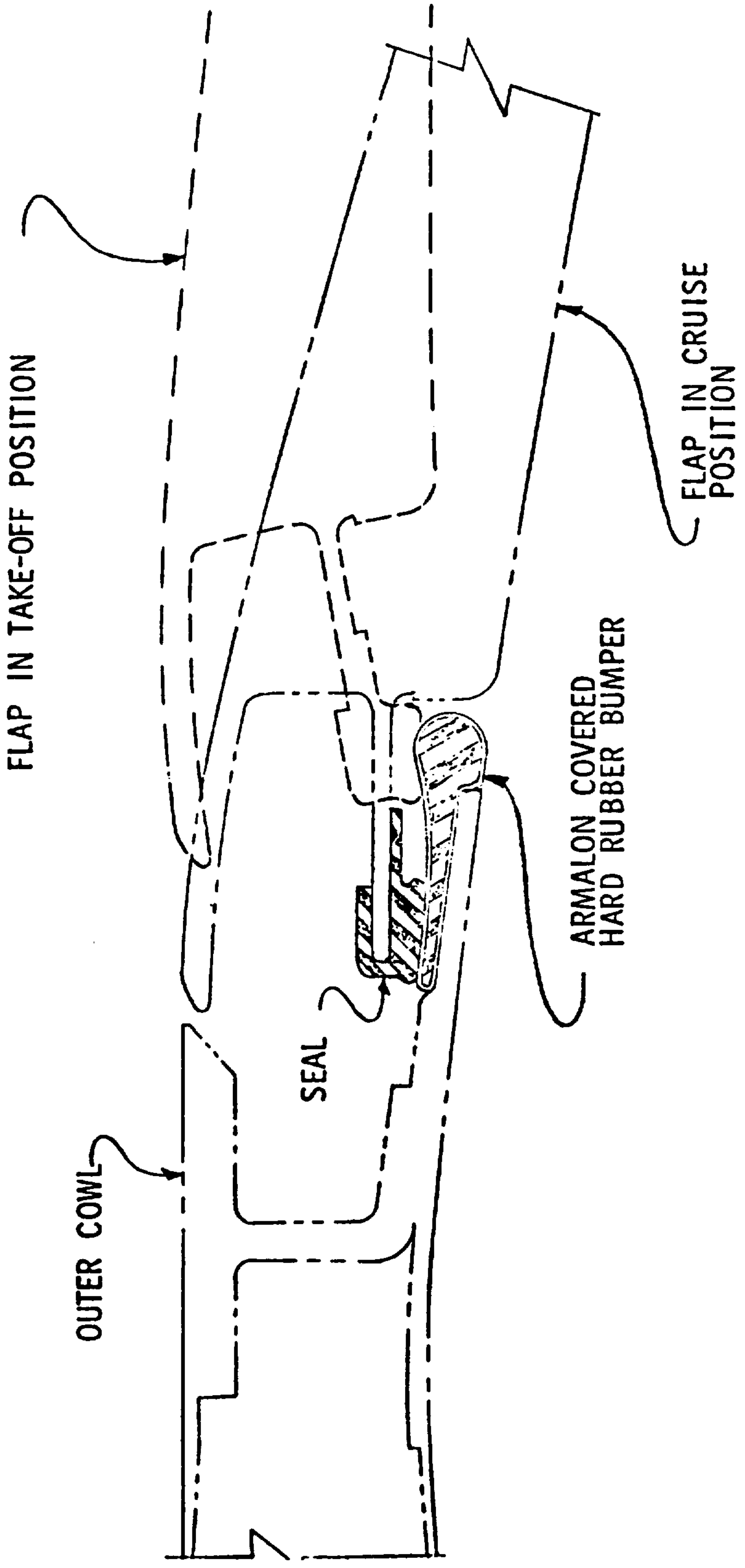
FLAP IN TAKE-OFF POSITION
FLAP IN CRUISE POSITION
ARMALON COVERED HARD RUBBER BUMPER
SEAL
OUTER COWL

Figure 15-16. Outer Cowl/Nozzle Flap Circumferential Seal.

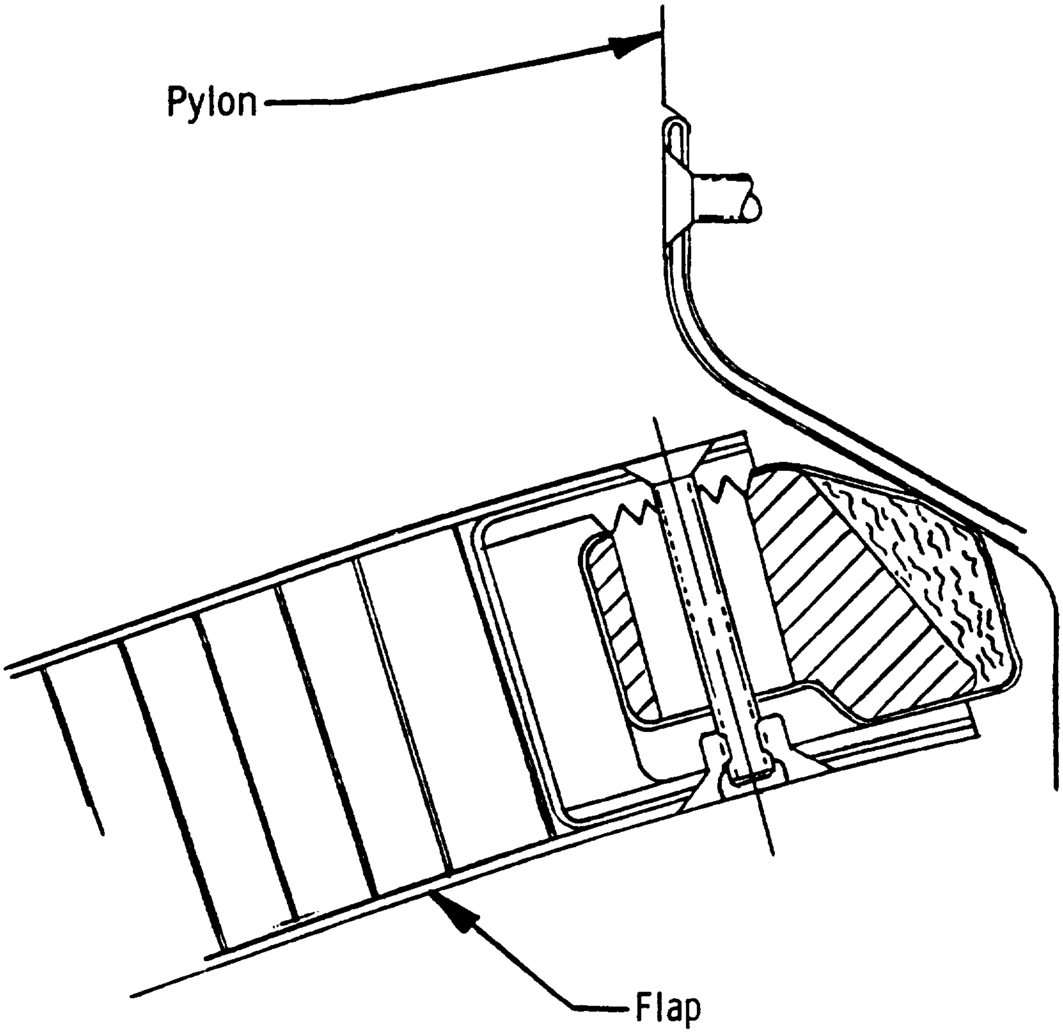

Figure 15-17. Flap/Pylon Interface Seal.

The construction of the flaps is similar to the rest of the nacelle (see Figures 15-18 and 15-19. They are of a sandwich type with Kevlar 49 face sheets and 5052 aluminum flex core honeycomb. The outer face sheet is composed of three plys oriented 90°, ±45°. The inner face sheet is perforated from the forward closeout to within 12.7 cm (5 in.) of the trailing edge, at which point the sound suppression treatment becomes ineffective due to the low height of the core. This inner sheet is made up of four plys with a 0°, ±45°, 0° orientation in order to compensate for the loss of strength due to the perforations. The forward closeout is composed of two sections, each made up of 12 graphite/epoxy laminations and bonded together. The trailing edge is built up of Kevlar 49 laminations between the inner and outer face sheets and wrapped with two plys of fiberglass to prevent delamination. Deep channel-shaped axial closeouts are provided of three plys of Kevlar 49, the cavities being deep enough to accept the axial seal assemblies. The hinges and link clevises are made integral with the bondment, each one having lugs which extend into the honeycomb, with the lugs protruding through the forward closeout. These are bonded in place and provide extensive interfaces with the face sheets and closeouts for load transfer at low stresses. In addition, doublers are provided for both the inner and outer face sheets at the forward end of the flap in order to reduce the bending stresses in this area. The outer doubler is three plys of Kevlar 49 and the inner doubler is two plys.

The flap was analyzed for the design conditions shown in Table 15-VI. The critical forward thrust case was arrived at by comparing flap differential pressures at several points along the maximum flight envelope. This study indicated that the Mach 0.92 - 6401 m (21,000 ft) case would give the greatest flap loading. The ±20 g buffet factor is based on experience obtained in the design of components for the C-5A Transport and the DC-10 aircraft. For the reverse thrust case, while the normal landing speed is 41.2 m/sec (80 knots), it was decided that the 77.17 m/sec (150 knot), M_o = 0.227 case would sufficiently cover an emergency landing or aborted takeoff condition.

The mechanical properties of the materials used are taken from several sources: metallic component allowables are taken from MIL-HDBK-5, "Metallic Materials and Elements for Flight Vehicle Structures;" graphite/ epoxy allowables are from the "Advance Composites Design Guide," as prepared for the Advanced Development Division, Air Force Materials Laboratory; and the Kevlar 49 properties are from data issued by the E.I. duPont de Nemours & Co., Inc., Wilmington, Delaware, developer and supplier of Kevlar 49. Table 15-VII shows critical calculated stresses/loads and margins of safety for the various flap components.

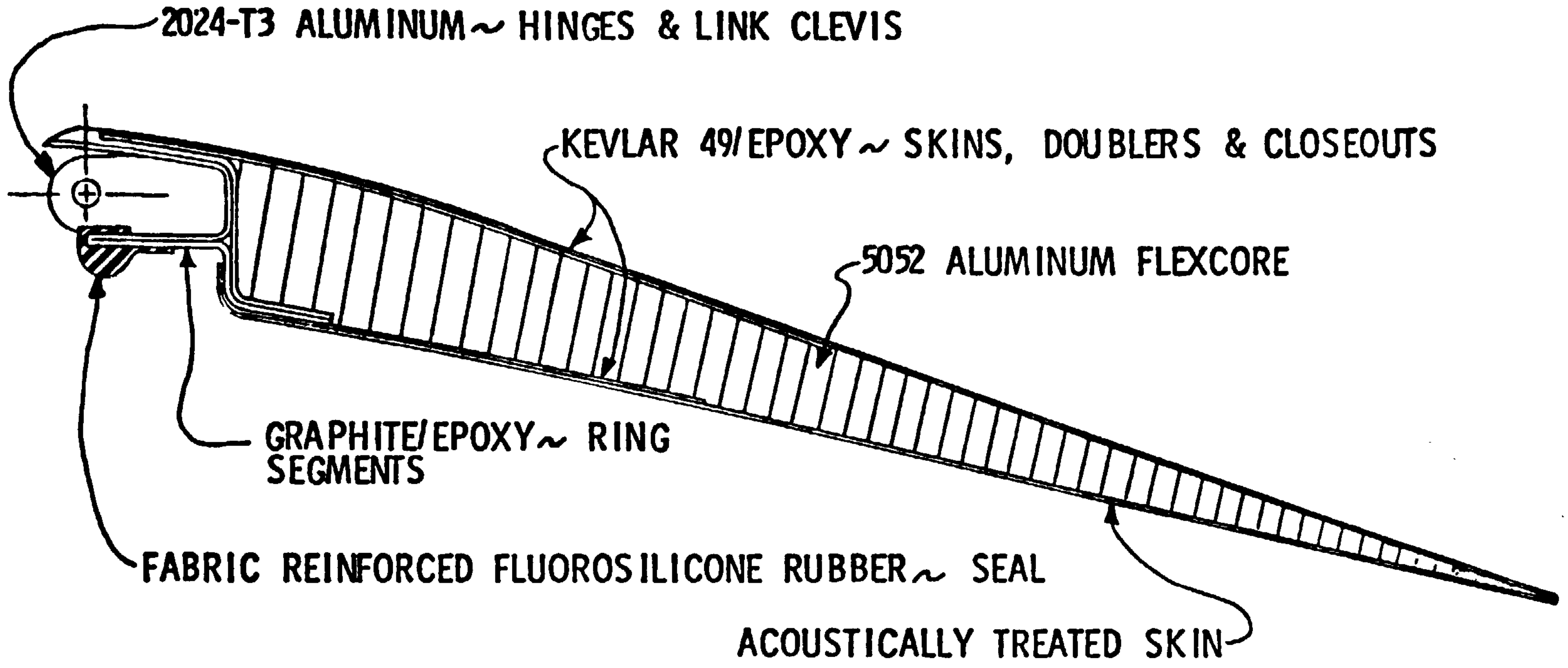
2024-T3 ALUMINUM~ HINGES & LINK CLEVIS
KEVLAR 49/EPOXY~ SKINS, DOUBLERS & CLOSEOUTS
5052 ALUMINUM FLEXCORE
GRAPHITE/EPOXY~ RING SEGMENTS
FABRIC REINFORCED FLUOROSILICONE RUBBER~ SEAL
ACOUSTICALLY TREATED SKIN

Figure 15-18. Nozzle Flap Cross Section.

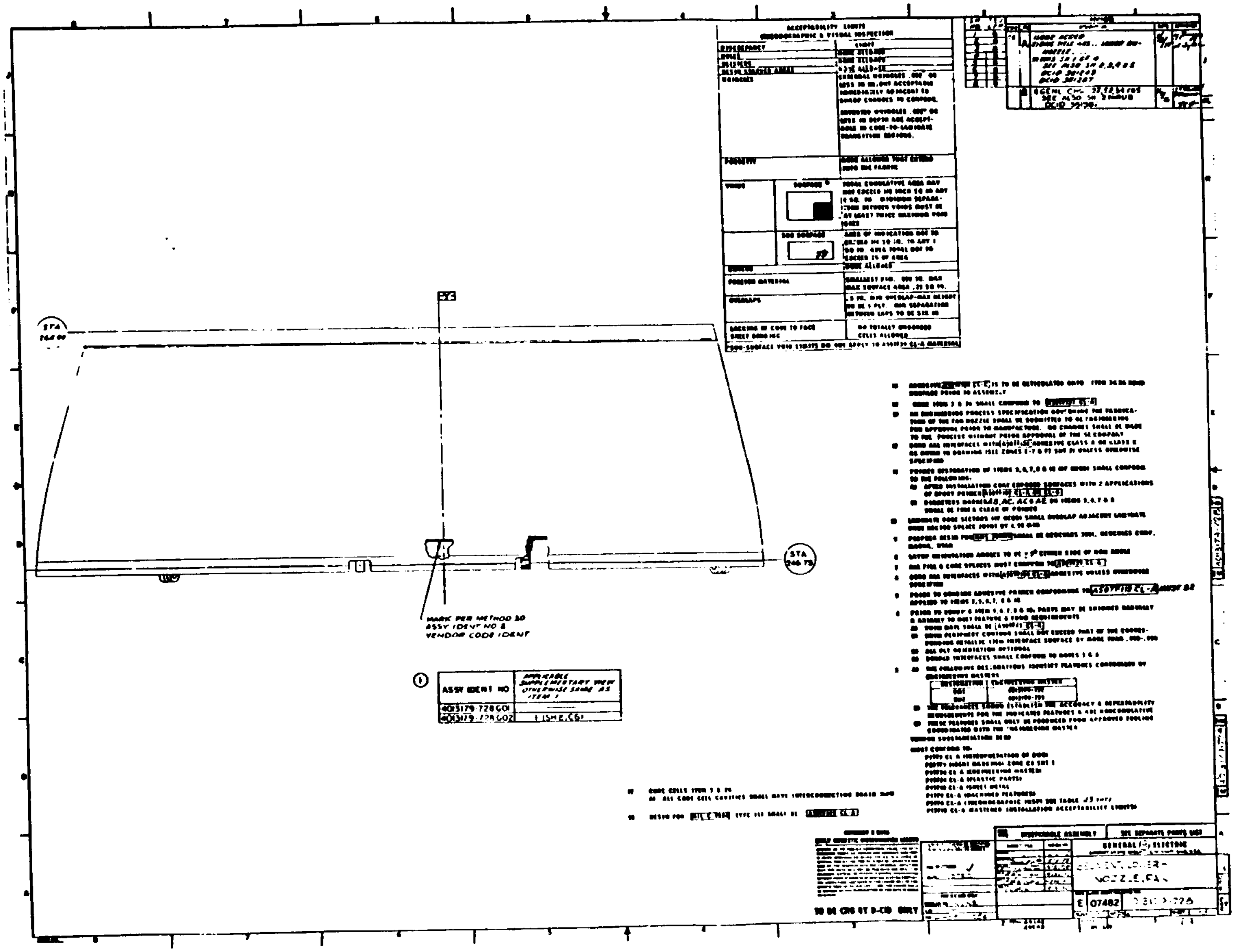
STA
MARK PER METHOD 30
ASSY IDENT NO &
VENDOR CODE IDENT
①
ASSY IDENT NO
APPLICABLE SUPPLEMENTARY VIEW OTHERWISE SAME AS ITEM 1
4013179-728G01
4013179-728G02
GENERAL ELECTRIC
NOZZLE, FAN
E
07482
TO BE CHG BY D-CID ONLY

Figure 15-19. Fan Nozzle Segment.

Table 15-VI. Nozzle Flap Design Conditions.

- Forward Thrust
  - M = 0.92 @ 6401 m (21000 ft)
  - Maneuver Loads
    - 10 g down
    - ± 2 g aft
    - 1.5 g side
  - Buffet Load
    - ± 20 g
    - C5A & DC10 experience
  - Single jammed actuator
- Reverse Thrust
  - M = 0.227 @ SL
  - Rejected T/O or emergency landing

Table 15-VII. Nozzle Critical Loads/Stress.

Component	Stress Mode	Stress/Load	Allowable Stress/Load	Margin of Safety
Flap Skin	Bending	3230 N/cm^2 (4684 psi)	10343 N/cm^2 (15000 psi)	+ 2.2 (yield)
Hinge Lug	Shearout/Bearing	48030 N (10789 lbs)	48052 N (10803 lbs)	+ 0.001 (ultimate)
Hinge Pin	Bending	165687 N/cm^2 (240300 psi)	178581 N/cm^2 (259000 psi)	+ 0.077 (ultimate)
Hinge Lug	Shear	9008 N/cm^2 (13064 psi)	22409 N/cm^2 (32500 psi)	+ 1.5 (ultimate)
Hinge Lug	Bending	10260 N/cm^2 (14880 psi)	24615 N/cm^2 (35700 psi)	+ 1.4 (ultimate)
Clevis Lug	Shearout/Bearing	11431 N (2570 lbs)	35895 N (8070 lbs)	+ 2.14 (ultimate)
Clevis Lug	Compression	19051 N/cm^2 (27630 psi)	24615 N/cm^2 (35700 psi)	+ 0.29 (yield)
Clevis Pin	Bending	92531 N/cm^2 (134200 psi)	178581 N/cm^2 259000 psi	+ 0.93 (ultimate)

Worst Case: Jammed actuator at M = 0.92 @ 6.4 km (21,000 ft)

15.3.4 Core Cowl

The core cowl doors define the inner boundary of the fan air flowpath from the fan frame to the core nozzle. They are also used as sound attenuators. Maintenance access to the core engine is also provided. A schematic of the core cowl is shown in Figure 15-20.

Temperature considerations were of primary importance in determining cowl door construction materials and configuration. The inner surfaces of the doors are exposed to radiant and convective heat from engine casings and are insulated from cooling effects of the fan air stream by the honeycomb sandwich walls. A heat transfer analysis (Figure 15-21) showed that a radiation shield plus cooling air is required to keep the maximum cowl skin temperatures within the capabilities of composite materials. Therefore, a stainless steel radiation shield is mounted off the cowl door aft of the fire wall (see Figure 15-22) at a distance of 0.635 cm (0.25 in.). Cooling air is bled in between the core cowl wall and the radiation shield and exhausted through the slip joint interface with the core nozzle. Cooling air is also bled forward from the fire wall to cool the first 12.7 cm (5 in.) forward of this point. The total amount of cooling air required to keep the maximum temperature at the desired level is approximately 0.45 kg (1 lb) per second. With the resulting temperatures, the cowl doors can be constructed of graphite/PI using Dupont's 3003 polyimide resin system or equivalent. High temperature honeycomb (HRH 327) and adhesives (FM34 or HT 434) are used to provide the required elevated temperature strength and stability.

15.3.5 Core Nozzle Design

The UTW experimental engine core exhaust nozzle is shown in Figure 15-23. It has a 70 cm (24 in.) long acoustically treated centerbody with a separate, bolted flanged cone. The outer flowpath also has a 70 cm (24 in.) long acoustically treated section with a bolted flanged fixed nozzle. A single strut assembly located on the bottom centerline of the core exhaust nozzle provides an aerodynamic fairing around the service lines that penetrate the core nozzle and are routed to the aft sump.

The inner and outer hard wall, the side branch resonator, and the stacked core acoustic treatments are shown in Figure 15-23. Recently completed acoustic tests have shown that the stacked core treatment design is more effective as a sound suppressor than the side branch resonator design. The side branch resonator design was therefore eliminated from the program. The current design effort is now directed toward updating the basic stacked core treatment (A), and designing an alternate treatment (B) which is similar in design but tuned to slightly different noise frequencies.

The stacked core acoustic treatment is designed to attenuate both high frequency turbine noise and low frequency combustion noise. The high frequency treatment consists of a honeycomb cylinder with a perforated face sheet on the flowpath side. The outer face is solid without perforations.

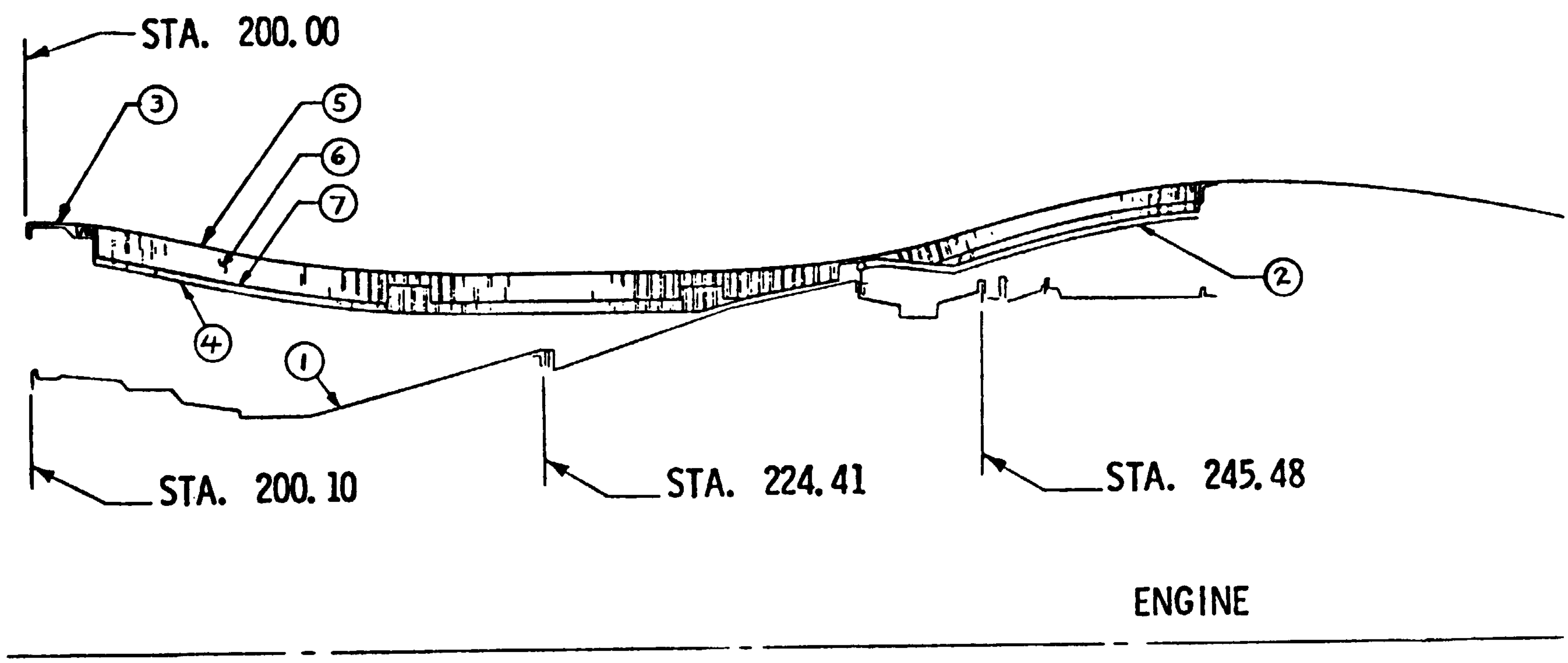
STA. 200.00
③
⑤
⑥
⑦
④
①
②
STA. 200.10
STA. 224.41
STA. 245.48
ENGINE

1. ENGINE CASING PROFILE
2. RADIATION SHIELD
3. COMPOSITE FRAME EXTENSION
4. INNER COWL I.D. FACE SHEET
5. INNER COWL O.D. FACE SHEET
6. HONEYCOMB
7. SEPTUM

Figure 15-20. Inner Cowl Schematic.

1. **Maximum** Estimated **Engine** Casing Temperature
2. **Fire Wall** Location.
3. Estimated Unshielded Cowl ID Maximum Temperature with 1 Chg/min Air.
4. Estimated Unshielded Cowl ID Maximum Temperature with 380 Chg/min Air.
5. Estimated Cowl ID Maximum Temperature with Radiation Shield and 292 Chg/min Air
6. Estimated Cowl ID Maximum Temperature with Radiation Shield, Thermal Blanket, and 180 Chg/min Air

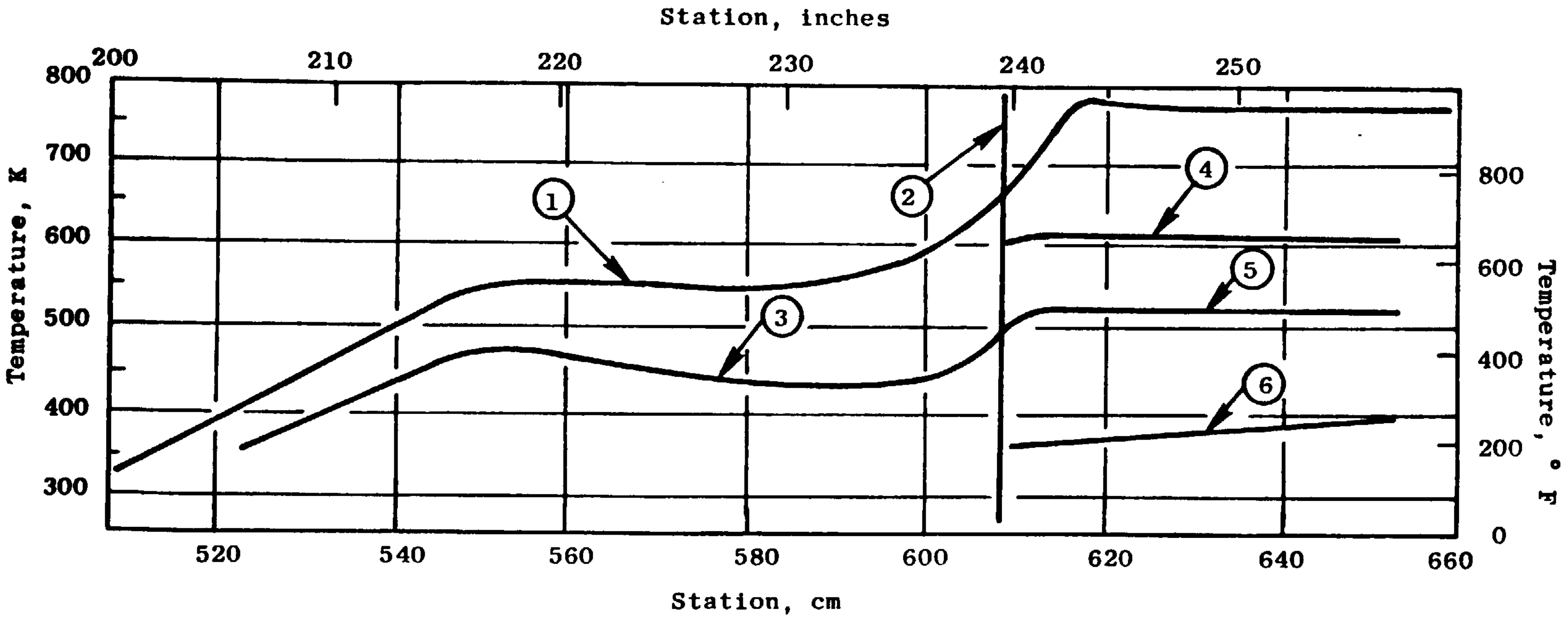

Figure 15-21. Inner Cowl Estimated Temperatures.

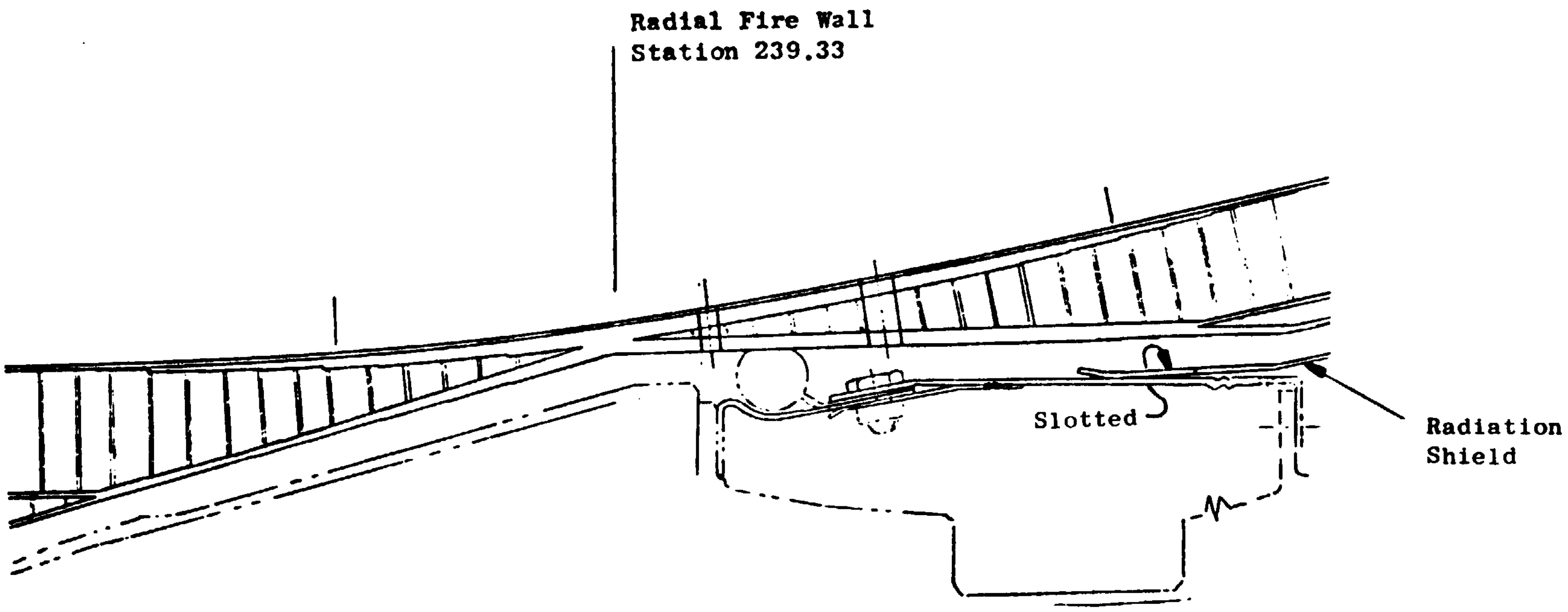
Radial Fire Wall
Station 239.33
Slotted
Radiation
Shield

Figure 15-22. Location of Air Passages and Radiation Shield.

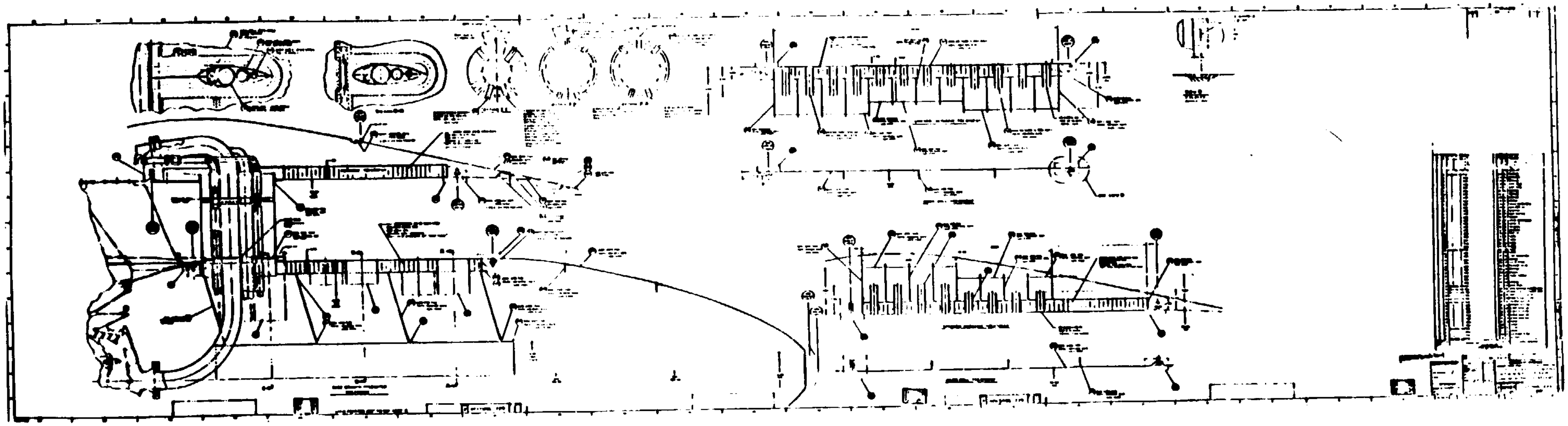

Figure 15-23. Core Exhaust Nozzle.

The honeycomb core is mechanically trapped between the inner and outer face sheet - no effort is made to bond the core to either face sheet as the honeycomb structure is required for sound attenuation only and is not required for structural integrity of the core nozzle. The low frequency noise is attenuated as it passes through the 15.9 cm (6.25 in.) diameter tubes through the honeycomb into the resonating chamber. Each section is designed for a specific frequency by varying the length of the tube and the volume of the resonating chamber. The tubes are brazed to the inner and outer face sheets and not only have a rigidizing effect on the structure but locks the core in place. The resonating chambers are fabricated by welding formed sheet metal sections into a completely enclosed and self-supporting assembly. The acoustic treatment has a bolted flange at each end to permit interchangeability between other acoustic treatment sections and the hard wall assembly.

The radial service line strut located on the bottom centerline of the core exhaust nozzle provides an aerodynamic fairing over the oil-in, oil drain, seal drain, and piston balance air lines that in the experimental engine are routed through the core nozzle to the sump. The strut is aerodynamically shaped with a 4 to 1 fineness ratio to minimize pressure loss due to flow blockage. All oil lines in the strut are insulated to minimize heat addition to the oil supply and to prevent coking of the seal drain line since the strut will operate at the core exhaust gas temperature.

Disassembly of the strut and service lines is not required to change the acoustic treatment. The strut is designed with a fishmouth seal that engages the inner and outer acoustic treatment as they are assembled to the turbine frame flange. The strut is attached to the outer turbine frame flange and has a slip joint between the strut and the centerbody to accommodate radial differential thermal expansion between the inner and outer acoustic treatment sections during transient conditions.

The core nozzle is a fixed-area nozzle; however, a ±5% area trim is provided with three separate but interchangeable conical sections that are bolted to the nozzle cone as required in the test program. Finer area control can be achieved by machining the cones to a shorter length.

Detail design of the core nozzle is still in process.

15.3.6 Mounting System

The UTW experimental engine design utilizes the same type mounting system as the flight engine configuration. Figure 15-24 shows a typical flight engine change unit or neutral engine system. The change unit includes the inlet, the engine accessories and piping, the front vertical support pin and thrust links, the rear mount assembly, the basic fan engine and core exhaust system. The flight system is designed to meet the following conditions:

- No disassembly of "engine-to-engine" piping is required on engine removal.

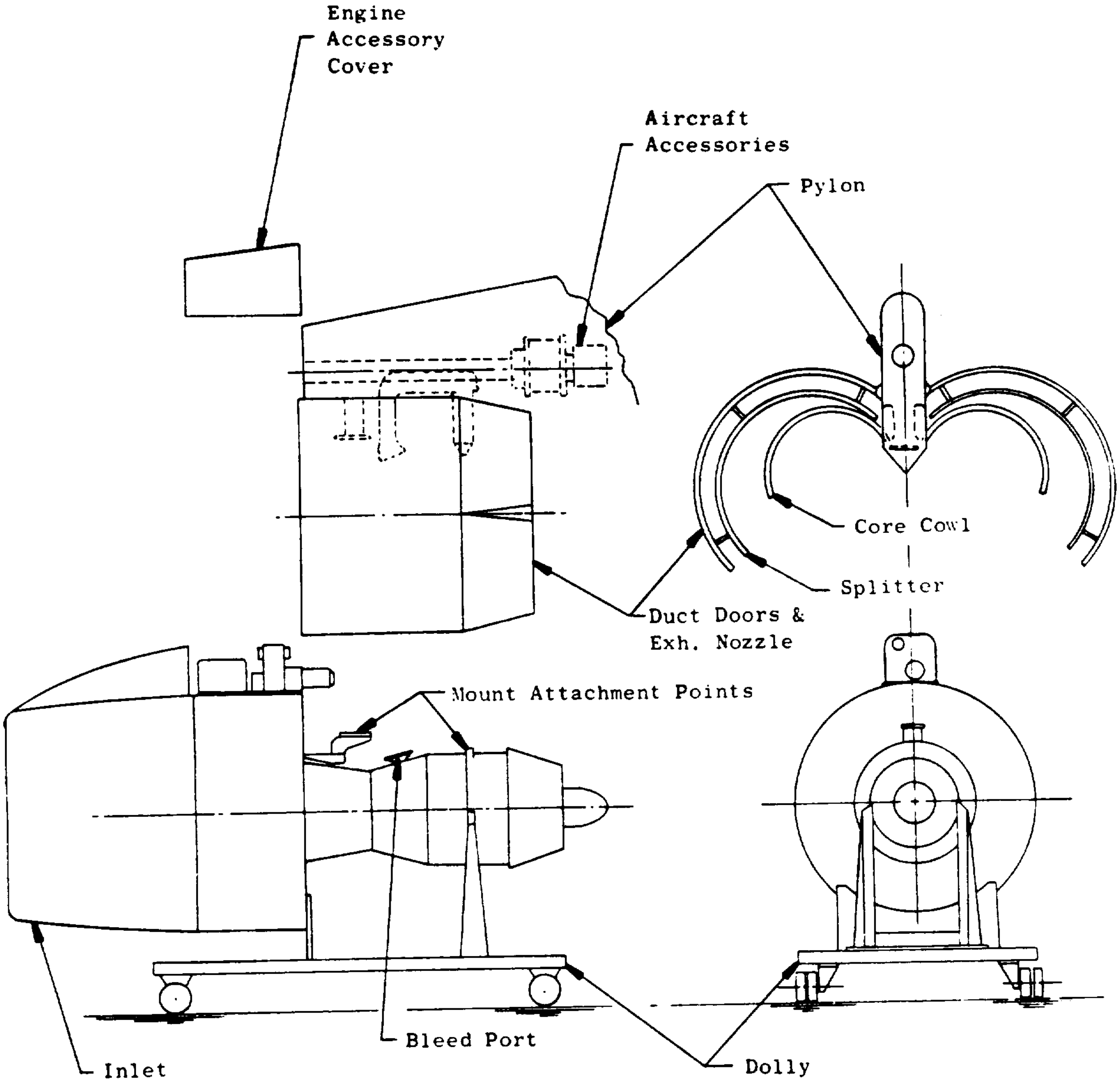
Engine Accessory Cover
Aircraft Accessories
Pylon
Core Cowl
Splitter
Duct Doors & Exh. Nozzle
Mount Attachment Points
Bleed Port
Inlet
Dolly

Figure 15-24. Engine Change Unit.

- Thrust links and rear mount, which are aircraft system hardware, remain with the engine to limit the mount system disconnect points to two.
- Fan and core cowl doors remain "on-the-wing."
- Disconnect points include:
    - Mount system - two places (4 to 7 bolts)
    - Bleed air pipe
    - Power shaft to aircraft accessories
    - Anti-icing air tube
    - Aircraft-to-engine services - pipes, lines, cables, wires, etc.

The mounting system is shown in further detail in Figure 15-25. Thrust is taken at the front frame at two points to minimize core bending due to thrust, and thereby improve rotor-to-stator clearance control. Vertical and side loads are simply supported. The mount schematic shows vertical, side, and thrust loads taken at the front mount plane on the aft ring of the fan frame and vertical, side, and torque loads taken at the rear mount plane on the outer ring of the turbine frame.

The rear engine mount system is composed of three links similar to that used on the DC-10/CF6 mount system. Uniballs at the ends of each of the links permit axial movement for differential thermal growth between the engine and the support structure.

When mounted as described, the engine and its mounting structure will withstand the flight maneuver forces described in Section 2.0. The precession rates used are consistent with the following normal commercial engine requirements:

> One radian/second in either pitch or yaw combined with the maximum resultant vertical, fore or aft, and angular acceleration loads (in the shaded area of the diagram) at zero-to-maximum thrust combined with normal cycle pressure and thermal loads.

All engine-mounted equipment such as the inlet, fan exhaust cowls, and accessories have been used to determine mount loads. A forward thrust load of 81,400 N (18,300 lb) has been used in the design.

A summary of typical mount reactions for unit maneuvers and "blade-out" loads is shown in Tables 15-VIII for the UTW "Boiler Plate" configuration with the inlet and fan cowl hung separate from the engine, supported from the facility thrust frame. Table 15-IX shows the mount reactions for the UTW composite propulsion system with the inlet and fan cowl attached to the engine system and supported through the main engine mounts.

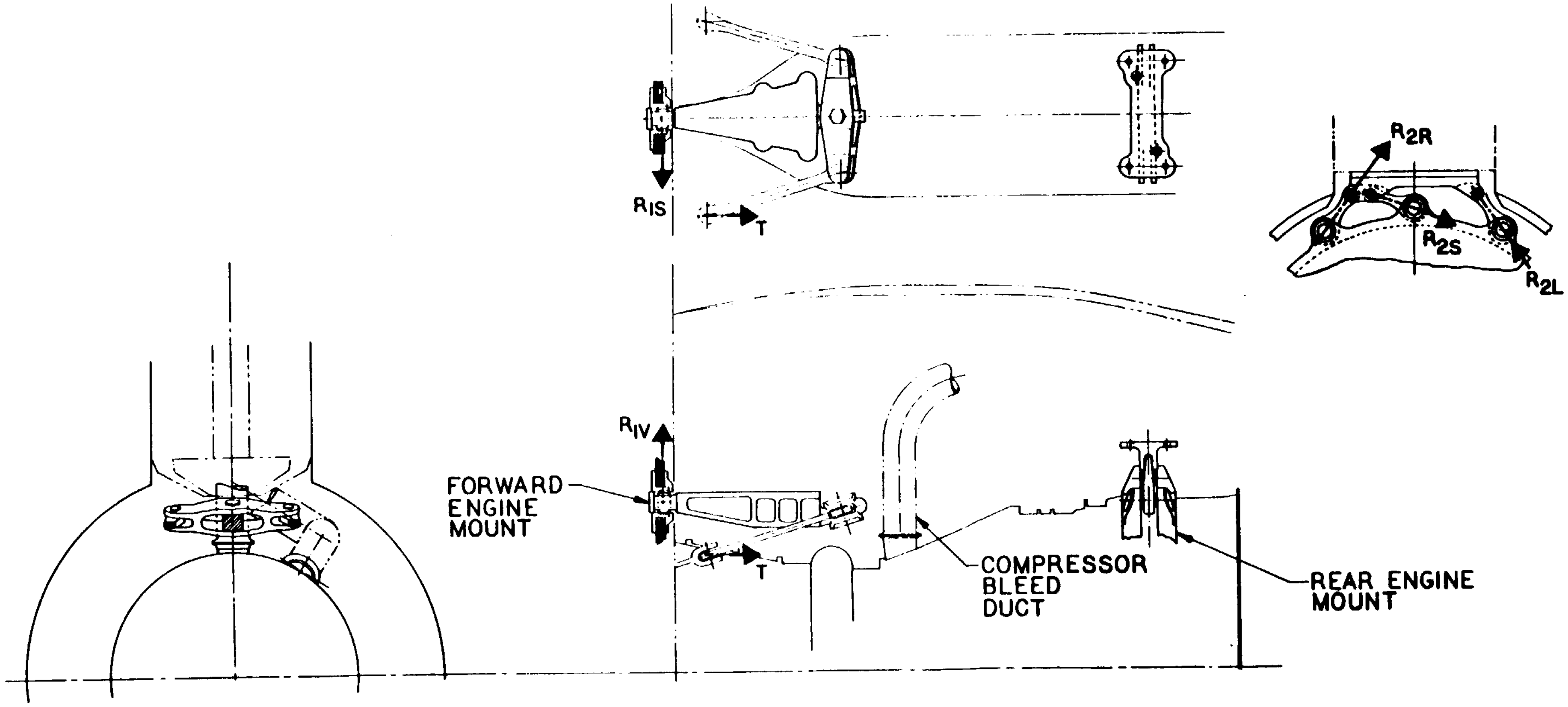
R2R
R2S
R2L
RIS
T
RIV
FORWARD ENGINE MOUNT
T
COMPRESSOR BLEED DUCT
REAR ENGINE MOUNT

Figure 15-25. Engine Mounting System.

Table 15-VIII. UTW Experimental Propulsion System Mount Loads, Boiler Plate Nacelle.

Maneuver		T	R 1V	R 1S	R 2R	R 2L	R 2S
1 G Down	N	-	+12010	-	+6295	+6295	-
	lb	-	(+2700)	-	(+1415)	(+1415)	-
1 G Side	N	-	-	±12010	∓14,635	∓30,400	∓28,560
	lb	-	-	(±2700)	(∓3290)	(∓6835)	(±6420)
1 $\dot{\theta}$ Pitch Velocity	N	-	-	±17,325	±4400	∓7450	∓21,485
	lb	-	-	(±3895)	(±990)	(∓1675)	(∓4830)
1 $\dot{\psi}$ Yaw Velocity	N	-	±17,325	-	±9560	±9560	-
	lb	-	(±3895)	-	(∓2150)	(∓2150)	-
1 $\ddot{\theta}$ Pitch Accel.	N	-	±1270	-	±690	∓690	-
	lb	-	(±285)	-	(∓155)	(∓155)	-
1 $\ddot{\psi}$ Yaw Accel	N	-	-	±1270	±535	±335	∓1580
	lb	-	-	(±285)	(±120)	(∓75)	(±355)
1000 lb Thrust	N	+2224	+980	-	-535	-535	-
	lb	(+500)	(+220)	-	(-120)	(-120)	-
(1) 2.5 Composite Blades Out	N	-	±110,780	±110,780	±60,810	±60,810	±60,810
	lb	-	(±24,906)	(±24,906)	(±13,671)	(±13,671)	(±13,671)

(1) Vertical and side loads do not act simultaneously.

Table 15-IX. UTW Experimental Propulsion System Mount Loads, Composite Nacelle.

Maneuver		T	R 1V	R 1S	R 2R	R2L	R 2S
1 G Down	N	-	+15925	-	+5200	+5200	-
	lb	-	(+3580)	-	(+1170)	(+1170)	
1 G Side	N	-	-	+15925	∓17,260	±33,690	±29,800
	lb	-	-	(±3580)	(∓3880)	(∓7575)	(±6700)
1 $\dot{\theta}$ Pitch Velocity	N	-	-	±17,325	±4400	∓7450	∓21,485
	lb	-	-	(±3895)	(±990)	(∓1675)	(∓4830)
1 $\dot{\psi}$ Yaw Velocity	N	-	±17,325	-	±9560	∓9560	-
	lb	-	(±3895)	-	(∓2150)	(∓2150)	-
1 $\ddot{\theta}$ Pitch Accel.	N	-	±1890	-	∓1050	∓1050	-
	lb	-	(±425)	-	(∓235)	(∓235)	-
1 $\ddot{\psi}$ Yaw Accel.	N	-	-	±1890	±825	∓490	∓2360
	lb	-	-	(±425)	(±185)	(∓110)	(∓530)
1000 lb Thrust	N	+2224	+980	-	-535	-535	-
	lb	(+500)	(+220)	-	(-120)	(-120)	-
(1)2.5 Composite Blades Out	N	-	±110,780	±110,780	±60,810	±60,810	±60,810
	lb	-	(±24,906)	(±24,906)	(±13,671)	(±13,671)	(±13,671)

(1) Vertical and side loads do not act simultaneously.

Load notations are defined in Figure 15-26, and load action locations are defined in Figure 15-25.

15.3.7 Accessories

The accessory arrangement for the UTW experimental propulsion system, shown in Figure 15-27, will be similar to the arrangement planned for the UTW flight system with many of the same maintenance features. To reduce cost, many of the experimental engine components in the accessory area are "off-the-shelf" items. The following list indicates the source of some of the items that are located in the top accessory area of the experimental engine:

- Main Fuel Pump and control - modified F101
- Fuel shutoff valve - non-flight design
- Water/Oil cooler from LM2500*
- Lube tank - TF39 (supply)
- Industrial scavenge filter*
- Air/Oil Separator
- Lube and Hydraulic Pumps
- Magnetic Chip Detectors from the F101
- Alternator from the F101
- Digital Control - non-flight-weight design
- Ignition Box from F101
- Control Cables - non-flight design
- Power takeoff (PTO - used for starter mounting pad on experimental engine)

Optimized configurations of the above items designed to meet flight system requirements will be mounted on the outer casing of the fan frame in the accessory area. Location of components will permit removal of the inlet without removing or uncoupling any of the engine fluid systems. Removal of the engine vertically will be possible without removing or uncoupling engine-to-engine piping for the "flight" system. On the experimental installation the piping must be uncoupled from the facility-mounted components indicated above. The experimental engine gearbox casing is cast aluminum (heavier than flight design) using gears and bearings from the F101 gearbox.

---

*Mounted to facility for experimental engine testing.

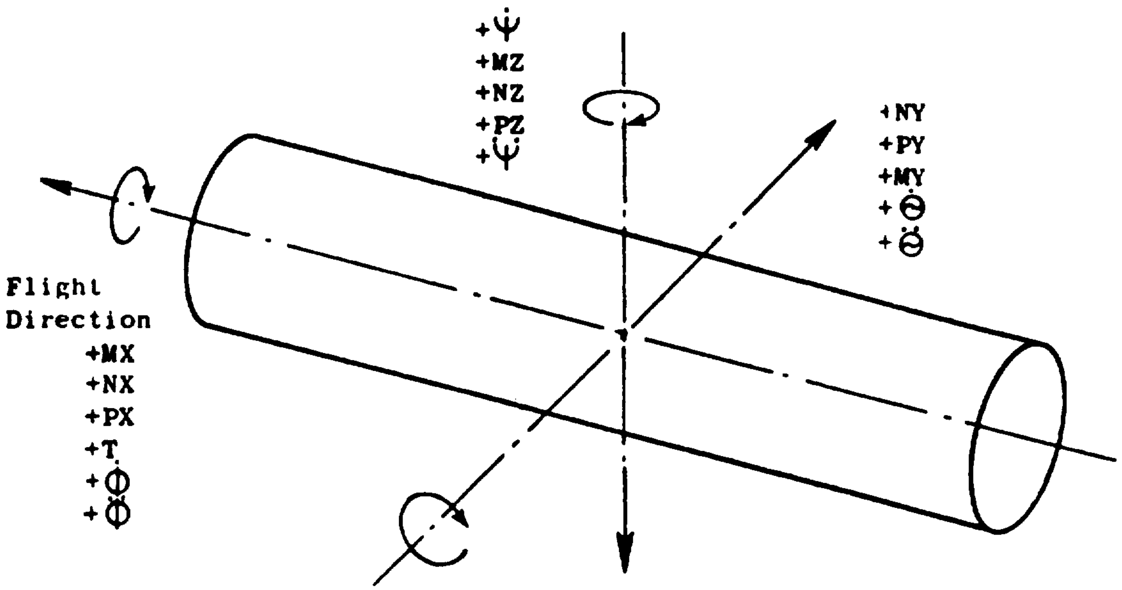
+$\dot{\Psi}$
+MZ
+NZ
+PZ
+$\ddot{\Psi}$
+NY
+PY
+MY
+$\dot{\Theta}$
+$\ddot{\Theta}$
Flight
Direction
+MX
+NX
+PX
+T
+$\dot{\Phi}$
+$\ddot{\Phi}$

Right Hand Rule for Forces, Moments, and Maneuvers

Nomenclature

NZ - Weight Acting Down

NY - Weight Acting Right Side

NX - Weight Acting Forward

T - Engine Thrust/Drag

$\dot{\Theta}$ - Angular Pitch Velocity (rad/sec)

$\ddot{\Theta}$ - Angular Pitch Acceleration (rad/sec^2)

$\dot{\Psi}$ - Angular Yaw Velocity (rad/sec)

$\ddot{\Psi}$ - Angular Yaw Acceleration (rad/sec^2)

$\dot{\Phi}$ - Angular Roll Velocity (rad/sec)

$\ddot{\Phi}$ - Angular Roll Acceleration (rad/sec^2)

PZ - Vertical Force

PY - Side Force

MZ - Moment About Vertical

MY - Moment About Side

MX - Moment About Engine Axis (Torque)

Figure 15-26. Load Nomenclature.

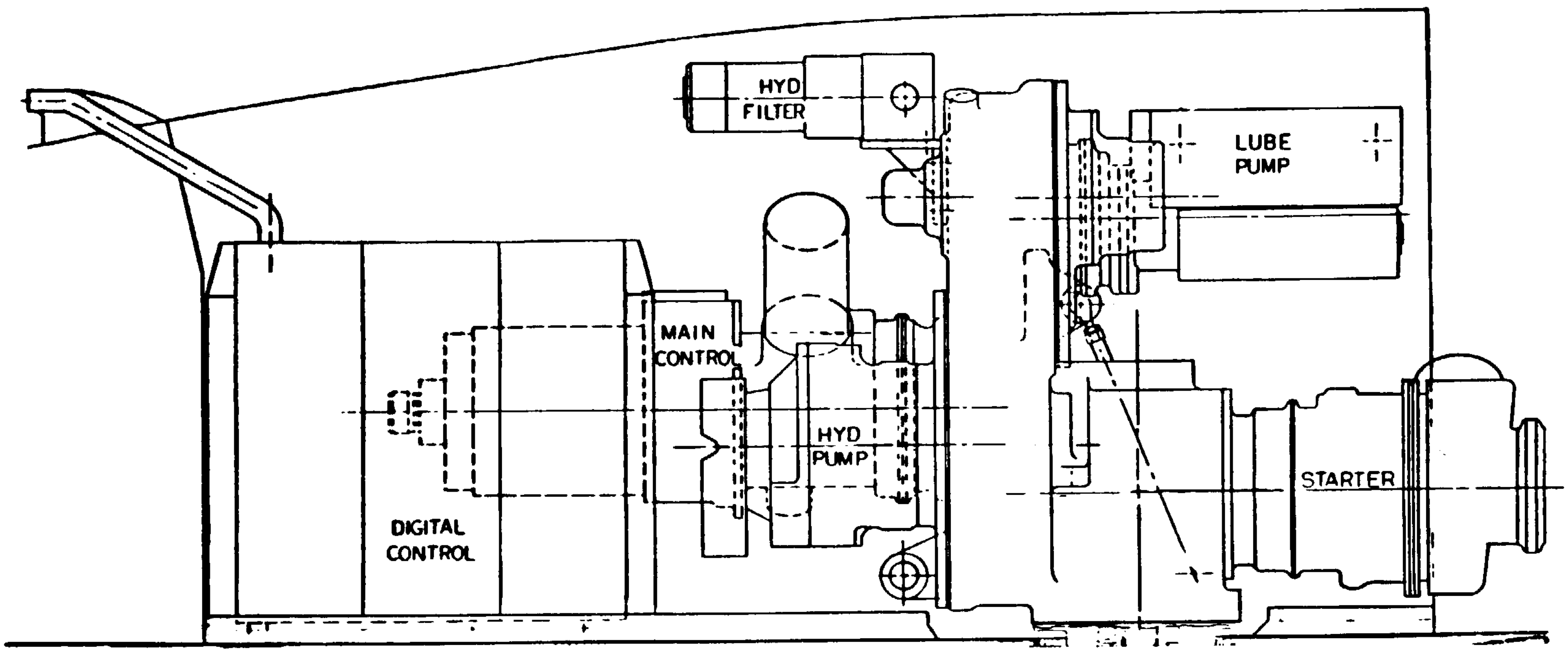
HYD
FILTER
LUBE
PUMP
MAIN
CONTROL
HYD
PUMP
STARTER
DIGITAL
CONTROL

Figure 15-27. UTW Experimental Engine Accessories.

Opening fan and core cowl doors will provide access to the core engine-mounted equipment:

- Fuel manifold, valves and tubes from the F101
- Stator actuators from the F101
- Scavenge pump
- Ignitors
- Instrumentation
- Speed sensors
- Vib sensors
- Fire detection and extinguishing (aircraft hardware mounted on the pylon)

The scavenge pump with its own inlet gearbox and radial drive is on the bottom of the engine to provide a gravity drain lube system.

The UTW flight system will include the following items not planned for the experimental engine:

- Flight-weight gearbox
- Double-wall fuel piping and manifold
- Improved replaceability of fuel injection tubes
- Flight radial drive for scavenge pump
- "Hard wall" titanium piping in place of soft hardware coupling F101 engine plumbing with accessories.

15.4 BOILER PLATE NACELLE DESIGN

Presented in this section is a discussion of the conceptual design of the "boiler plate" nacelle hardware that will be used for initial testing of the UTW propulsion system. Results of these tests will be used to establish the final acoustic configuration for the Composite Nacelle. The preliminary design review of the boiler plate nacelle and facility hardware for the UTW system was held in April of 1975. Completion of the detail design was scheduled for the fourth quarter of 1975.

15.4.1 Inlet

Planned testing of the UTW engine will require three boiler plate inlet configurations. The NASA Quiet Engine "C" bellmouth inlet shown in Figure

15-28 consists of a fiberglass/honeycomb lip and a cylindrical casing. It will be utilized for aerodynamic engine mapping and baseline acoustic evaluation. A massive inlet suppressor also from the Quiet Engine "C" program will be utilized to isolate aft-end noise and provide additional information for acoustic evaluation. An accelerating inlet featuring elevated throat Mach numbers and multiple acoustic suppression designs will be employed for the flight-type aero and acoustic evaluations. A typical inlet-to-test-stand mounting system at the Peebles test site is shown in Figure 15-29.

All inlets will be mechanically decoupled from the engine. The boiler plate nacelle components are decoupled to prevent overload of the composite fan flanges due to excessive engine motion and/or vibration. A typical decoupled or "load-break" joint is shown in Figure 15-30. The air seal is provided by a closed-cell foam, such as Scott-Foam, bonded to one-half of the flange and pressed against the other. The acoustic seal is provided by a lead foil in a vinyl cover. The two seals aerodynamically and acoustically simulate the hard joint condition of the final composite propulsion system assembly.

The accelerating inlet package, shown in Figure 15-30, includes a fiberglass/honeycomb lip and a structural shell that provides the attachment bosses for two interchangeable sets of acoustic treatment and one matched set of hard wall panels for initial UTW system testing. A typical acoustic panel fabrication will consist of an aluminum perforated face plate stretch-formed to the correct contour and bonded to a honeycomb/single-degree-of-freedom panel, which in turn is bonded to a fiberglass backing sheet.

15.4.2 Fan Bypass Duct

The UTW fan bypass duct is a hinged, two-piece structural shell that provides the attachment capability for two interchangeable sets of acoustic treatment panels and one matched set of hard wall panels. Two single-ring splitters will be procured to match the two acoustic configurations (see Figure 15-31 for a typical splitter installation). One of these splitters will be used for the composite configurations. The splitters will be built in two halves with each half supported by a fan cowl door through three airfoil-shaped struts. Core cowl access is accommodated by the hinged door construction of the outer ducting. The outer fan doors are decoupled from the fan frame and supported from the facility through the pylon and through telescoping beams (Figure 15-32).

The variable UTW fan nozzle described in Section 15.3.3 will be designed and procured as a component of the composite nacelle assembly and will be utilized in both the composite and boiler plate nacelle configurations. It attaches as an assembly to the fan duct as illustrated in Figure 15-33.

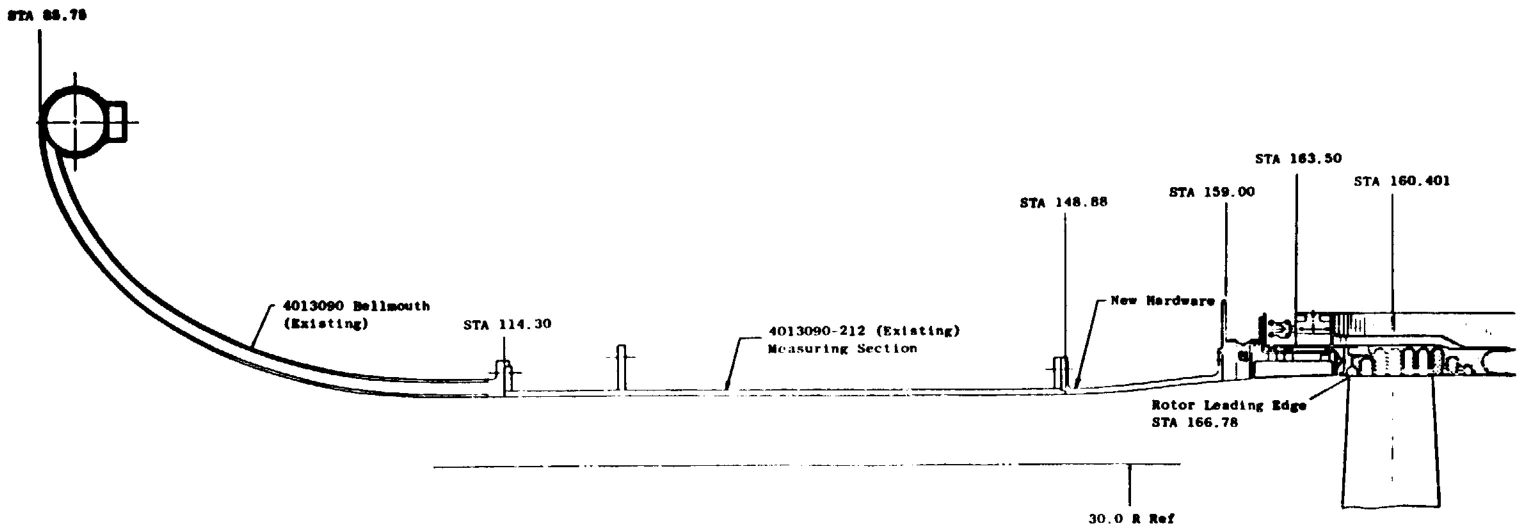
STA 88.78
4013090 Bellmouth
(Existing)
STA 114.30
4013090-212 (Existing)
Measuring Section
STA 148.88
New Hardware
STA 159.00
STA 163.50
STA 160.401
Rotor Leading Edge
STA 166.78
30.0 R Ref

Figure 15-28. Bellmouth Inlet.

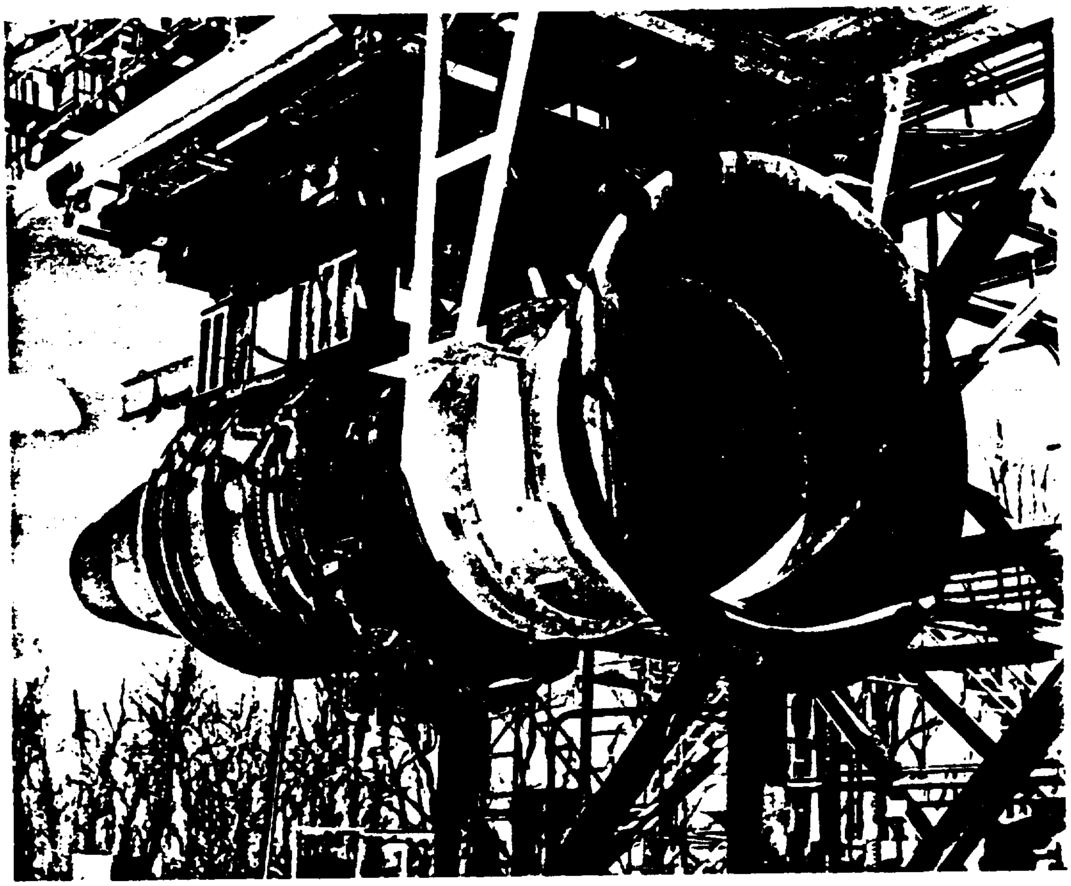

Figure 15-29. Inlet Mounted on Test Stand at Peebles Proving Grounds.

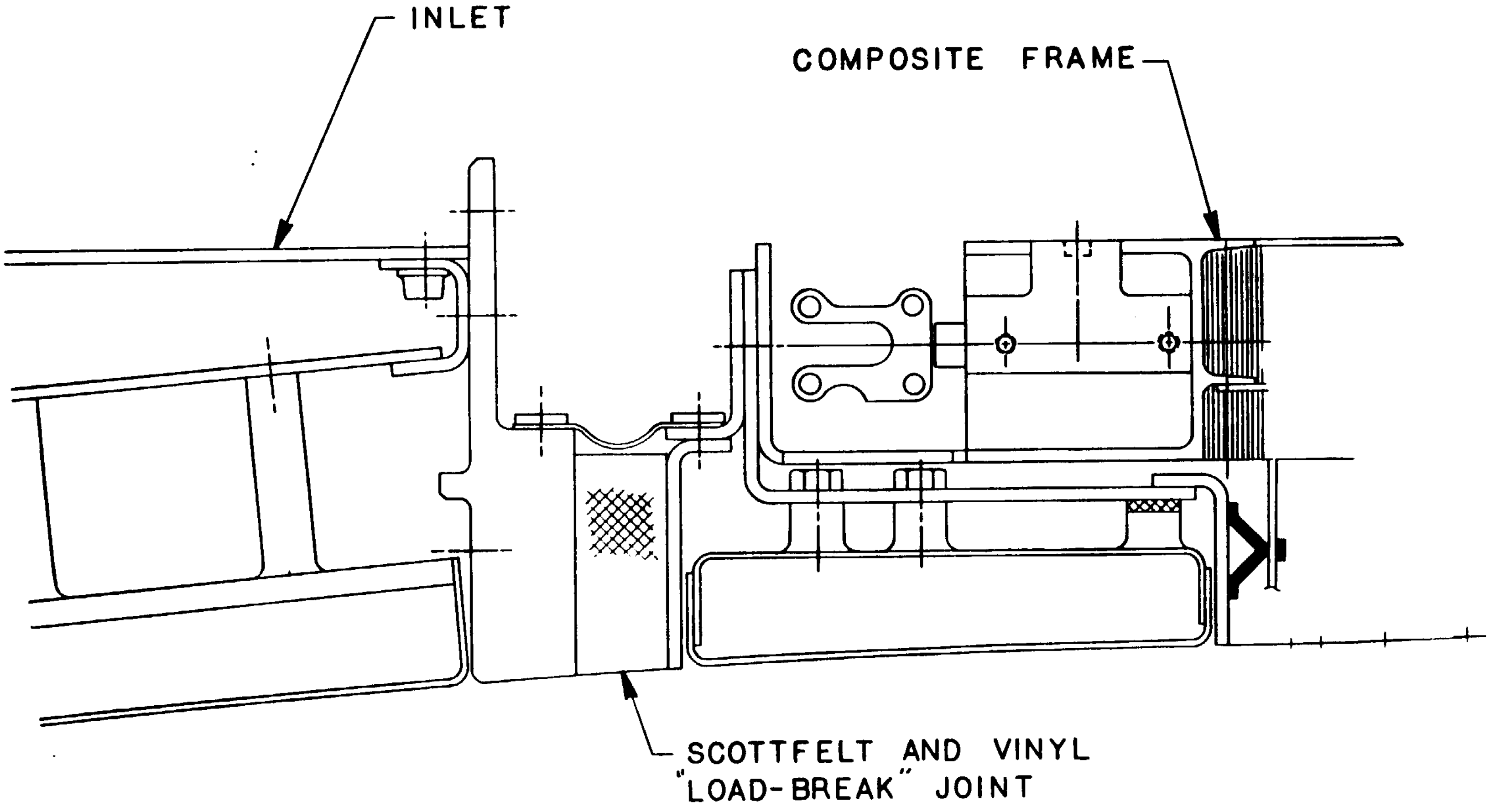
INLET
COMPOSITE FRAME
SCOTTFELT AND VINYL
"LOAD-BREAK" JOINT

Figure 15-30. Typical Decoupled ("Load Break") Joint.

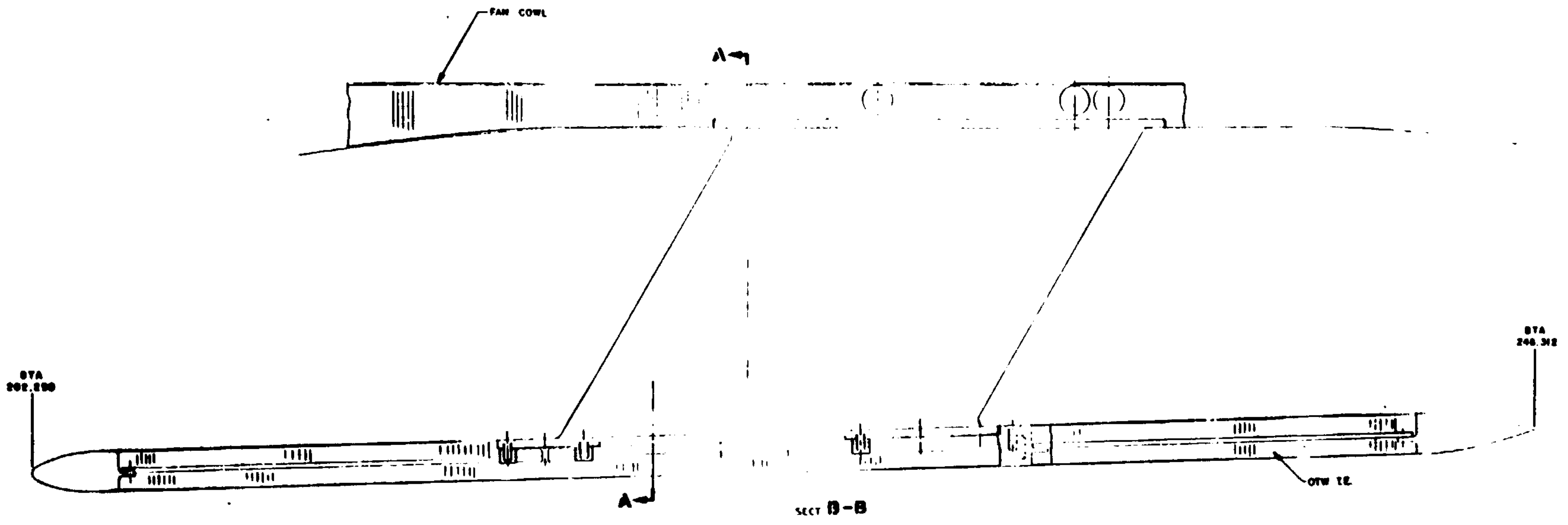
FAN COWL
A
A
BTA
202.250
SECT B-B
OTW TE
BTA
248.312

Figure 15-31. Typical Splitter Installation.

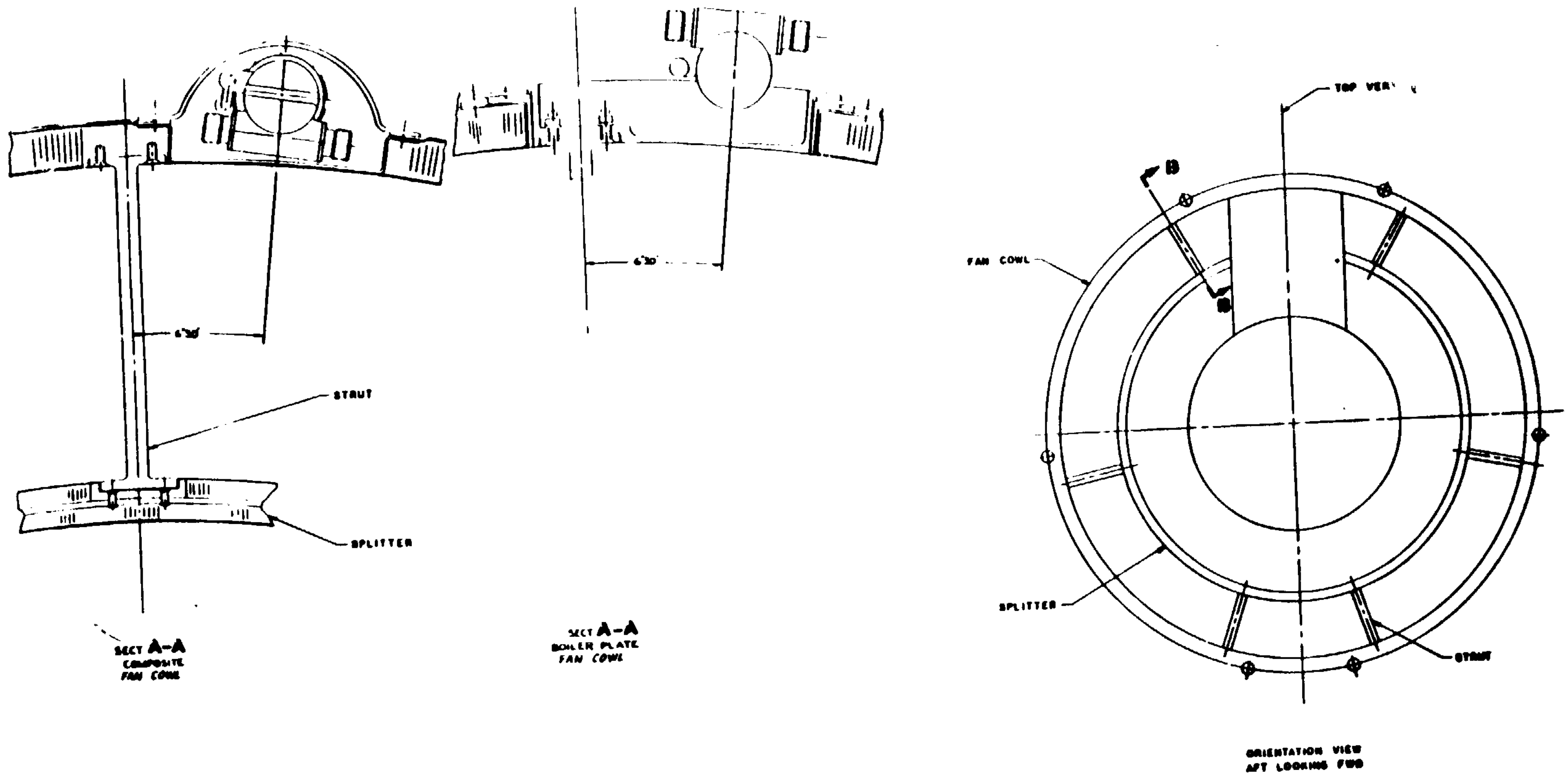
6°30'
STRUT
SPLITTER
6°30'
B
B
TOP VERT ℄
FAN COWL
SPLITTER
STRUT

SECT A-A
COMPOSITE
FAN COWL

SECT A-A
BOILER PLATE
FAN COWL

ORIENTATION VIEW
AFT LOOKING FWD

Figure 15-31. Typical Splitter Installation (Concluded).

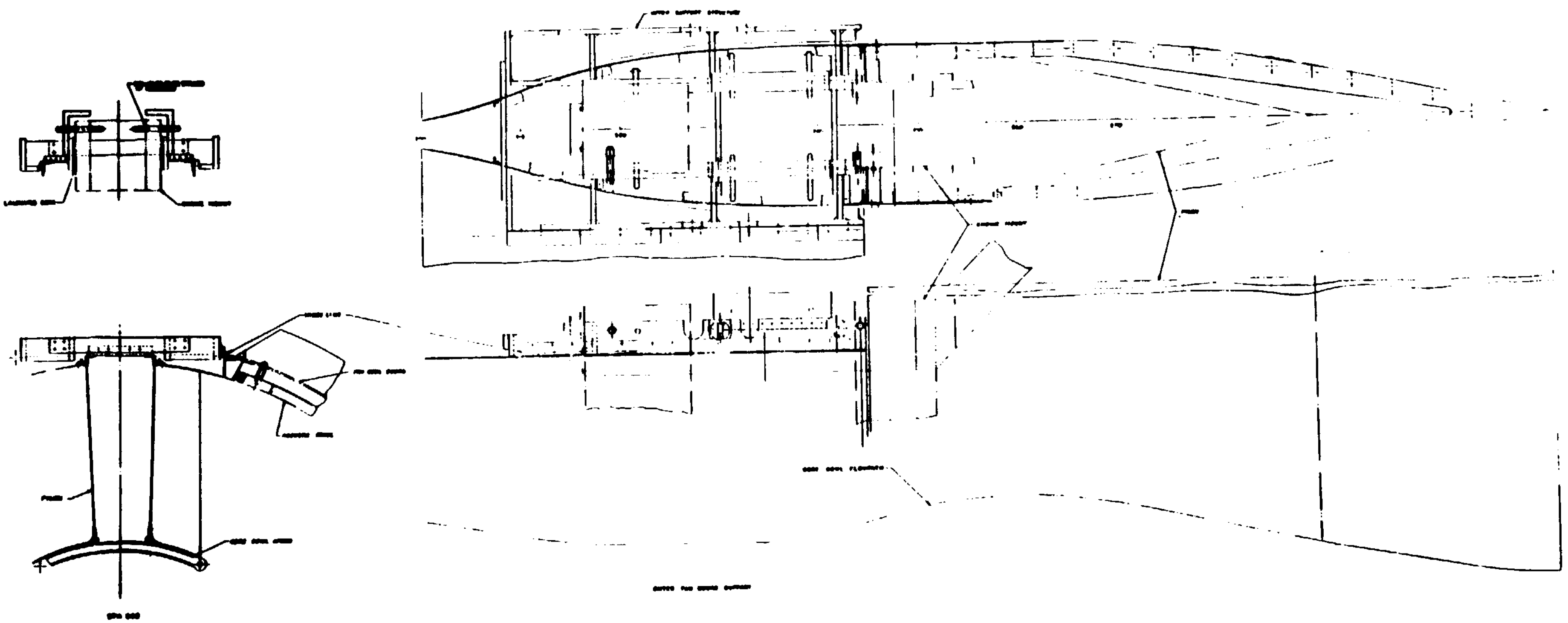

Figure 15-32. Outer Fan Doors Support.

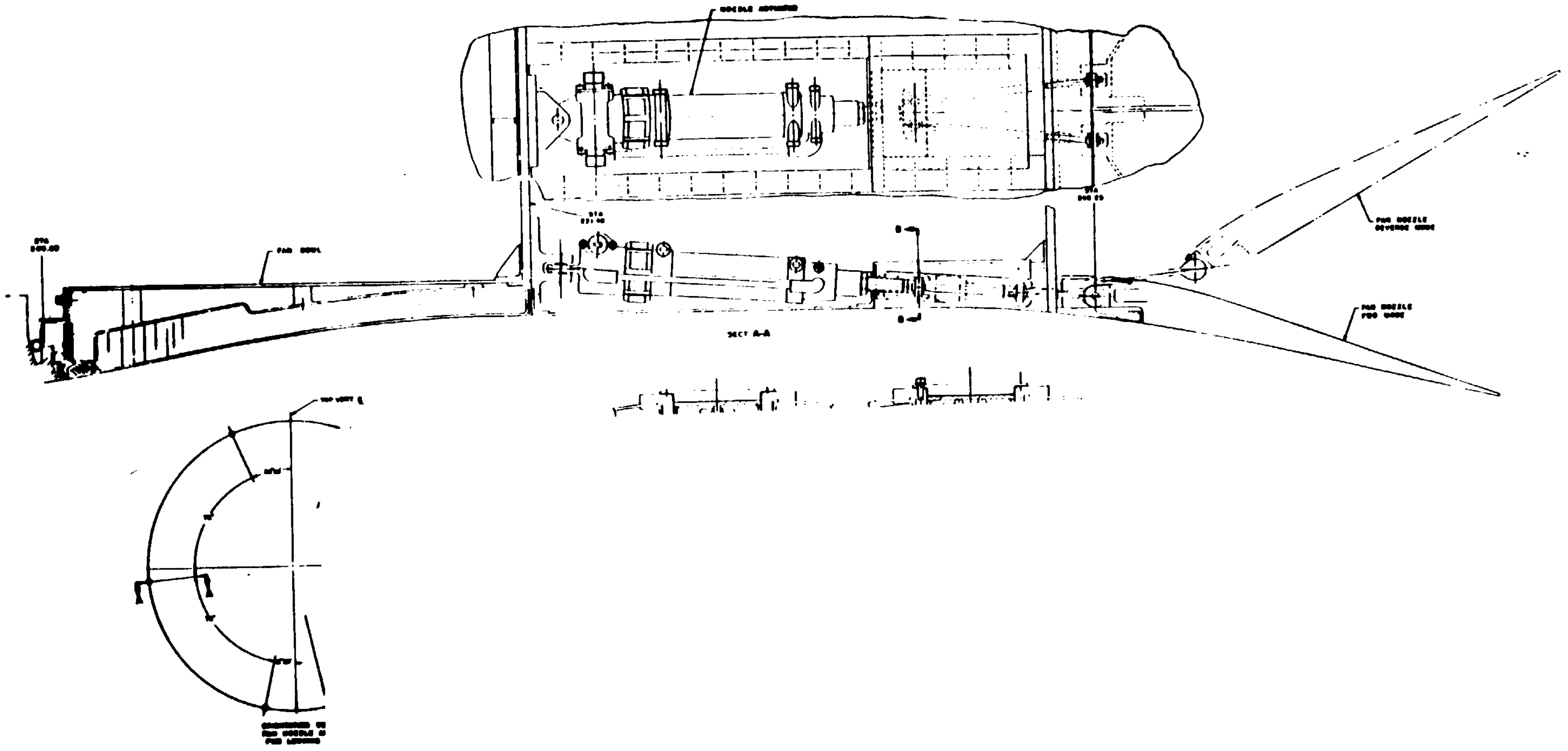
NOZZLE ACTUATOR
FAN COWL
SECT A-A
FAN NOZZLE REVERSE MODE
FAN NOZZLE FWD MODE

Figure 15-33. Fan Nozzle Assembly Attached to Fan Duct.

15.4.3 Core Cowl

The UTW core cowl embodies the same design philosophy established for the fan duct. It is a hinged, two-piece structural shell that supports two sets of interchangeable acoustic panels and one set of hard wall panels. It has a forward interface (Marman-type joint) with the fan frame and an aft interfacing slip joint with the core nozzle. Access to the compressor and turbine is provided by the hinged door construction of the core ducting. This is accomplished by first attaching the core door and skirt system to structural stringers extending down within the pylon through a set of pins (see Figure 15-34).

The core cowl will employ shop-air cooling and radiation shields to adequately cool the cowl area and ensure a safe operating environment for the epoxy resins that will be used in the construction of the acoustic panels. This method differs from the composite configuration which utilizes polyimide adhesives that provide temperature capabilities higher than epoxy resins.

The UTW core cowl structure between the fan frame and the slip joint will later be adapted for use on the OTW boiler plate core cowl with a new set of acoustic panels.

15.4.4 Boiler Plate Nacelle Pylon-Skirt Assembly

The pylon assembly is the primary structural support system for the fan exhaust duct assembly. It is always used with the boiler plate nacelle and will be delivered to NASA with the OTW engine. It is bolted to the mount system for the boiler plate nacelle and the outer door loads are transmitted directly to the facility for all conditions. The inner skirt and hinge is decoupled from the pylon during engine operation and attached to the pylon to open the core doors. Core door loads are transmitted to the fan frame during engine testing. The aerodynamic contour of the pylon is provided by a removable nonstructural fairing bolted to the structural beam. This also provides accessibility for core instrumentation inspection.

15.4.5 Composite Nacelle Pylon - Skirt Assembly

The composite nacelle pylon is similar in design to the boiler plate nacelle pylon. The main difference is that it is not bolted to the mount, and is supported by the fan cowl. All thrust loads applied to the fan ducting are transmitted to the engine mounts through the fan frame. To open the outer doors, a system of pins may be incorporated if required to couple the pylon system and the doors to the mount. The core doors function identically to the boiler plate system.

Although present plans do not include acoustic treatment of the pylon walls and core skirt, treatment could be added to the second pylon-skirt assembly that is procured for use on the composite configuration if the boiler plate nacelle does not achieve predicted noise goals.

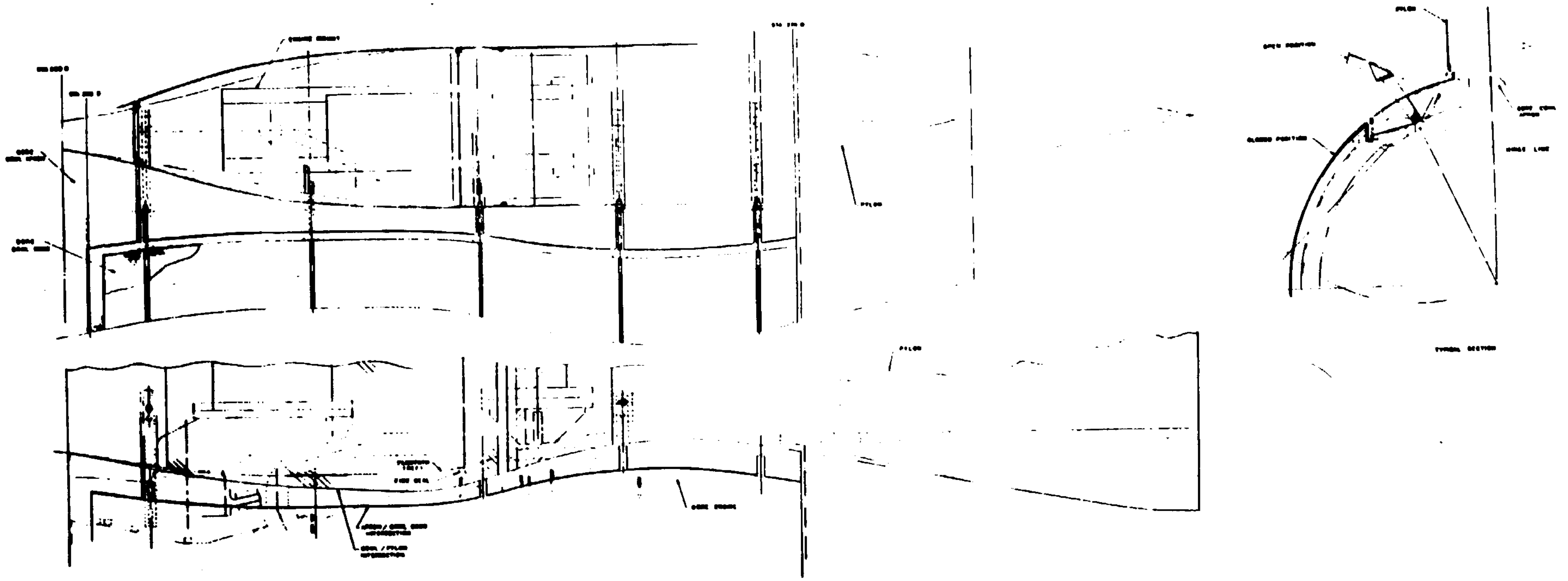

Figure 15-34. Core Cowl.

SECTION 16.0

SYSTEM VIBRATION ANALYSIS

16.1 SUMMARY

A system vibration analysis of the UTW experimental engine was performed to determine the critical speeds and corresponding amplitudes of vibration. An analysis was conducted for two configurations, the difference in configuration being in the inlet and fan cowl which are facility-mounted boilerplate for one case and engine-mounted composite for the other.

Results show that no serious vibration problems are anticipated assuming the engine rotating assemblies are balanced to within specified design tolerances using currently employed balancing technology.

16.2 DESIGN REQUIREMENTS

The propulsion system must be designed to be capable of operating within established safe operating vibration limits for excitation frequencies within all rotor speed ranges and for rotor unbalance not exceeding established allowable manufacturing tolerances. In addition, the system must be capable of withstanding, without further major structural failure, a transient loading caused by significant unbalance induced by blade loss resulting from foreign object damage (FOD). The transient consists of the time required for the pilot to recognize high vibration levels and take the necessary steps to shut down the engine.

Design vibration operating limits and the corresponding rotor balancing tolerances are established based upon the criteria that the rotor/bearing components and static structures shall not be subjected to vibratory loads in excess of those values which would reduce the life of those components below the established design life.

For the UTW propulsion system, there are actually three rotors which can serve as input sources for significant energy to excite a system mode. The three rotors are shown in Figure 16-1 along with their operating speeds. The range of frequencies for one per rev excitation is from approximately 900 rpm (15 Hz) for fan ground idle speed to 14,500 rpm (242 Hz) for maximum compressor speed. There are other sources of excitation such as gear meshing frequencies and blade passing frequencies; however, these sources do not have sufficient energy to drive the engine system modes being considered. Such component vibration is considered in the design criteria for the various engine parts by separate detail analysis of those components.

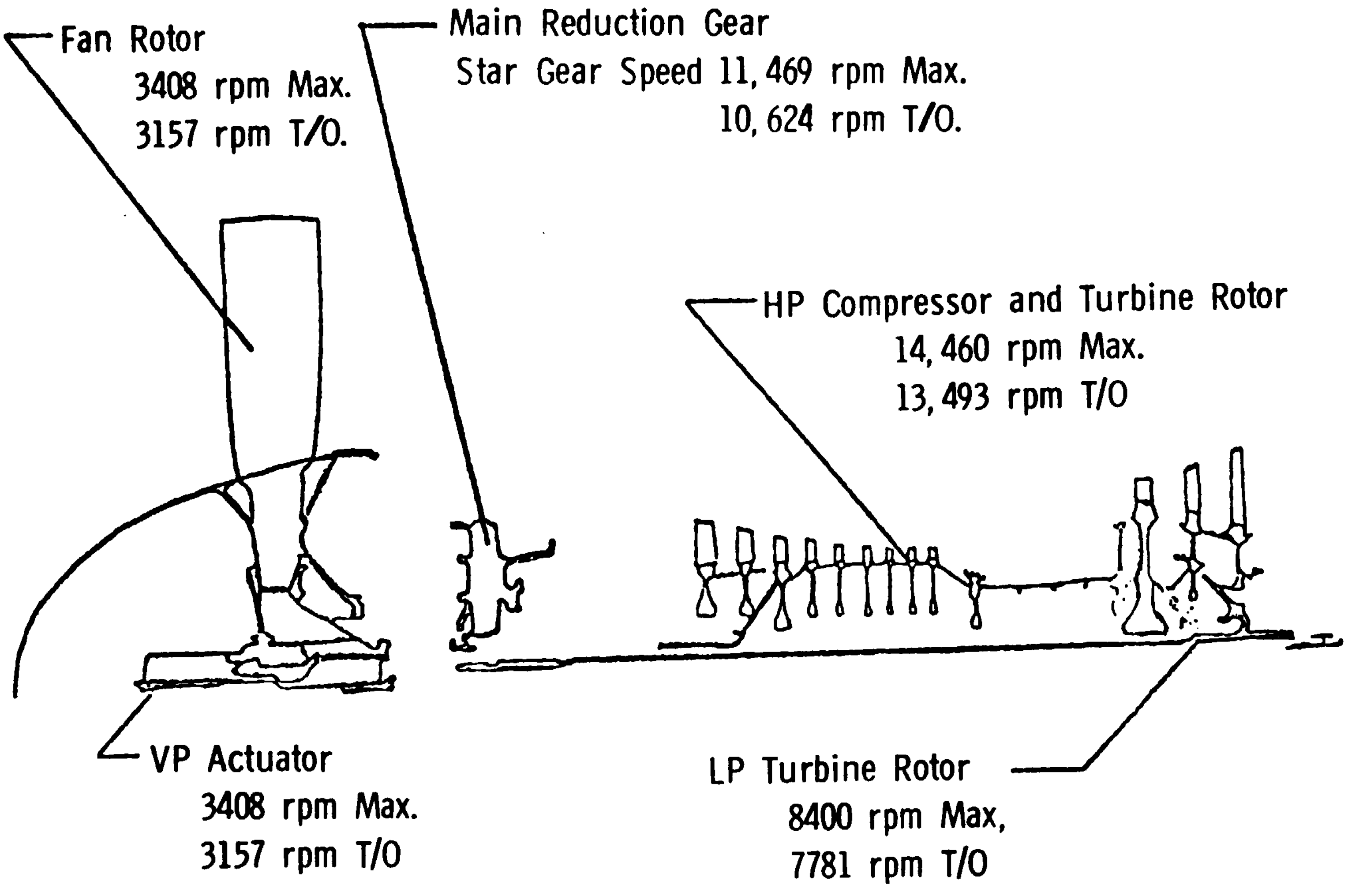
Fan Rotor
3408 rpm Max.
3157 rpm T/O.
Main Reduction Gear
Star Gear Speed 11,469 rpm Max.
10,624 rpm T/O.
HP Compressor and Turbine Rotor
14,460 rpm Max.
13,493 rpm T/O
VP Actuator
3408 rpm Max.
3157 rpm T/O
LP Turbine Rotor
8400 rpm Max,
7781 rpm T/O

Figure 16.1. UTW Engine Rotating Subsystems.

The maximum loads in the system occur when the system reaches a "critical speed" or resonance speed excited by one of the rotors. At these speeds, the amplitude of vibration for an undamped system would be infinite; however, the gas turbine propulsion system has a large amount of structural damping inherent in the various components which in practice reduces vibration levels to acceptable limits if proper balancing of rotating components has been achieved. Because of the complexity of the system, it is virtually impossible to avoid having any critical speeds in the operating range. However, there is one type of critical speed which must be avoided in order to avert possible serious problems, that being a rotor-dominated mode of the circular whirl-type where the rotor vibrates laterally or whirls at the same frequency at which it is rotating (forward synchronous precession). Therefore, the system must be carefully designed to ensure that rotor-dominated modes of the circular whirl-type do not exist in the operating speed range of the engine.

16.3 VIBRATION ANALYSIS

16.3.1 Method of Analysis

The system was analyzed by use of the General Electric computer program VAST (Vibration Analysis System) which is used to calculate system critical speeds and vibratory estimated response at critical speeds for known unbalances. The VAST program has been in use at General Electric for a number of years and has consistently demonstrated the capability of accurately predicting engine critical speeds and responses for many types of engines and test vehicles developed by General Electric. A mathematical model of the engine system is constructed which includes all rotor components plus all stator components supported from the engine mounting system. The modeling procedure consists of establishing the geometric and physical properties and representing the various components by a series of lumped (or point) masses connected by flexible beam, cone and spring elements. For more complex structures such as a fan frame or a bearing, special finite element models are constructed and/or tests of actual hardware are performed to determine their load/deflection characteristics. In summary, the basic assumptions made in VAST are as follows:

1. The structure is axisymmetric and all deflection and vibration modes will be based on beam-type behavior. No "shell modes" are considered.

2. Linear elastic behavior of materials for all elements modeled as beams or cones.

3. Elements modeled as beams follow classical beam small deflection theory in bending; shear deformation in beams is also considered.

4. All spring-type elements exhibit linear load-deflection characteristics.

5. Rotors exhibit gyroscopic stiffening due to whirling.

6. Damping coefficients are assumed to be constant. The structural damping factor is not considered to be a function of velocity.

7. Mass properties are considered as lumped at discrete points and are interconnected by massless general elastic (spring) elements.

8. A VAST analysis is based on the Prohl-Myklestad method of calculating the critical speeds of flexible rotors represented by beams.

9. The effects of flexible supports, multiple branches, and energy distribution schemes are also considered.

Critical speeds are calculated assuming an undamped system; however, estimated actual vibratory deflections and loads can be calculated including damping coefficients for the various components along with possible unbalance locations on the rotors. Damping coefficients are based primarily on past performance of similar components as well as some analytical procedures in the case of friction dampers or journal bearings which are used in some vehicles.

16.3.2 Vibration Model

The VAST system vibration model is shown in Figure 16-2 in schematic form. The various frames and bearings are represented by springs whose flexibility coefficients have been determined by a separate analysis along with past experience with similar structures. For purposes of a VAST vibration analysis, the fan and LP turbine shafts, which turn at different speeds in opposite directions are considered decoupled since no significant radial loads or shaft bending moments can be transmitted through the reduction gearing. For a torsional analysis, however, this decoupling assumption would not be true.

From a system vibration standpoint there are essentially three rotors involved due to the reduction gearing in the LP system, each rotor rotating at a different speed. Since the gyroscropic stiffening effects in the rotors depend upon the ratio of rotor speed, Ω, to the system vibratory frequency, ω, and since the source of system excitation is assumed to be an unbalance in one of the rotors causing harmonic excitation at the same frequency as the rotor speed (one per rev), it is required that three VAST vibration runs be made to determine all system criticals. Thus, the following cases are defined:

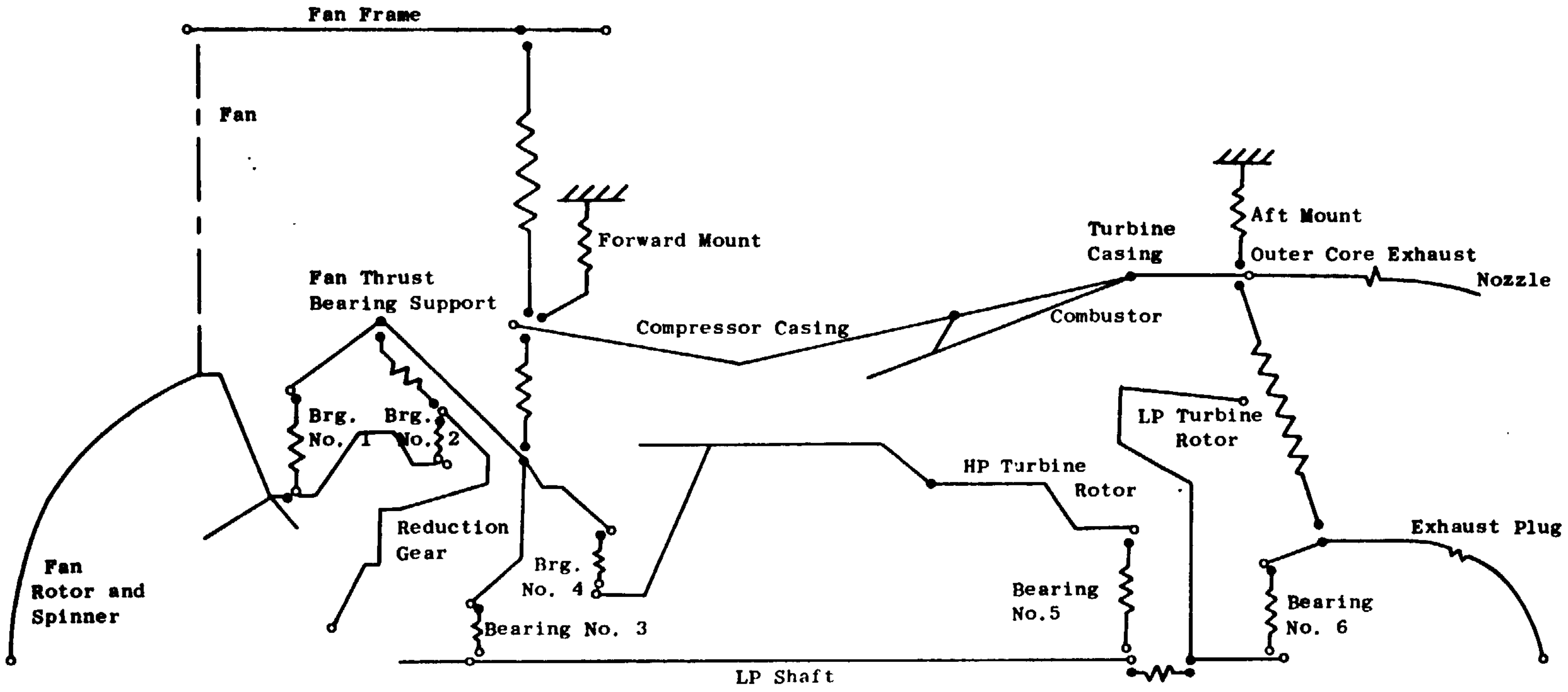
Fan Frame
Fan
Forward Mount
Fan Thrust Bearing Support
Compressor Casing
Turbine Casing
Aft Mount
Outer Core Exhaust
Nozzle
Combustor
Brg. No. 1
Brg. No. 2
LP Turbine Rotor
HP Turbine Rotor
Reduction Gear
Fan Rotor and Spinner
Brg. No. 4
Bearing No. 3
Bearing No.5
Bearing No. 6
Exhaust Plug
LP Shaft

Figure 16-2. UTW Vibration Model Installed Engine.

$R \quad = \Omega/\omega$

Fan-Excited Critical Speeds

$R_{Fan} = 1.00$

$R_{LP} = -2.46$

$R_{HP} = -4.31$

LP-Excited Reference Critical Speeds

$R_{Fan} = -0.40$

$R_{LP} = 1.00$

$R_{HP} = 1.75$

HP-Excited Reference Critical Speeds

$R_{Fan} = -0.22$

$R_{LP} = 0.57$

$R_{HP} = 1.00$

The negative sign on R represents a backward precession in whirling with respect to that component for which $R = 1$.

A series of VAST runs as outlined above was run for each of two configurations of the basic experimental engines as follows:

- Configuration 1 - Boiler plate nacelle components (inlet and fan aft duct) supported by the facility and, thus, decoupled from the engine from a vibration standpoint.
- Configuration 2 - Composite nacelle components attached to the engine system at the fan frame.

16.3.3 Analysis Results

The results of the vibration analysis are shown in tabular form giving the critical speed in rpm along with an estimated maximum system response for an unbalance of 25.4 g-cm (10 g-in.) at selected rotor planes.

Table 16-I presents the fan reference system critical speeds, excluding mount modes, for Configuration No. 1. The speed range for which criticals were calculated was 1000 to 5000 rpm.

Table 16-I. Critical Speeds, Fan Reference, UTW Configuration 1.

Mode Description	Speed rpm	Response(1) mm (Mils)
LP Rotor Bending	2333	0.001 (0.04)
Turbine Frame, Exhaust Plug, Core Casing	3036	0.028 (1.1)
Turbine Frame, Exhaust Plug, Core Casing	3918	0.018 (0.7)

(1) Single-amplitude response at point of maximum deflection, in mils, for 25.4 g-cm (10 g-in.) unbalance at fan centerline.

Table 16-II presents the LP turbine reference system critical speeds, excluding mount modes, for Configuration No. 1. The speed range for which criticals were calculated was 1000 to 9000 rpm.

Table 16-II. Critical Speeds, LP Reference, UTW Configuration 1.

Mode Description	Speed rpm	Response(1) mm (Mils)
Fan Rotor and Compressor Case	2481	0.002 (0.06)
Turbine Frame and Exhaust Plug	3368	0.028 (1.1)
Turbine Frame and Core Casing	4289	0.018 (0.7)
HP and LP Rotors	6307	0.030 (1.2)
Core Casing	8487	0.005 (0.2)

(1) Single-amplitude response at point of maximum deflection, in mils, for 25.4 g-cm (10 g-in.) unbalance in LP turbine.

Table 16-III presents the HP rotor reference critical speeds, excluding mount modes, for Configuration No. 1. The speed range for which criticals were calculated was 1000 to 15,000 rpm.

Table 16-IV presents the fan reference critical speeds, exceeding mount modes, for Configuration No. 2. The speed range for which criticals were calculated was 1000 to 5000 rpm.

Table 16-V presents the LP turbine reference critical speeds, excluding mount modes, for Configuration No. 2. The speed range for which criticals were calculated was 1000 to 9000 rpm.

Table 16-VI presents the HP rotor reference critical speeds, excluding mount modes, for Configuration No. 2. The speed range for which criticals were calculated was 1000 to 15,000 rpm.

As part of the output from VAST, a computer-generated plot of the system schematic with superimposed normalized deflection pattern is produced. Also shown on these diagrams is a percentage distribution of kinetic and potential energies. This graphic output assists in identifying deflection patterns and the energy distribution shows which parts are bending (high potential energy) and which are subject to highest g-loads (high kinetic energy). Figures 16-3 through 16-5 show typical mode shapes for various types of system modes for Configuration 1.

16.3.4 Conclusions

The results of the VAST analysis indicate the following:

1. There are no rotor one per rev flexural criticals in the engine operating range.

2. The modes and responses for Configuration 1 and Configuration 2 are very similar, the frequencies differing slightly, due mainly to weight changes.

3. The maximum responses for Configuration 1 are due to unbalance in the HP rotor which indicates 0.112 mm (4.4 mils) single amplitude at 5703 rpm and 0.097 mm (3.8 mils) single amplitude at 13,589 rpm.

4. The maximum responses for Configuration 2 are also due to unbalance in the HP rotor, and are 0.112 mm (4.4 mils) single amplitude at 5,692 rpm and 0.119 mm (4.7 mils) single amplitude at 13,179 rpm.

Table 16-III. Critical Speeds, HP Reference, UTW Configuration 1.

Mode Description	Speed rpm	Response(1) mm (Mils)	
		Unbalance at Compressor Stage 1	Unbalance at HPT
Fan Rotor Exhaust System, Core Casing	2575	0.015 (0.6)	0.008 (0.3)
Turbine Frame Exhaust System	3405	0.001 (0.04)	0.028 (1.1)
Fan Frame & Core Casing	4264	0.010 (0.4)	0.018 (0.7)
LP and HP Rotors	5703	0.013 (0.5)	0.112 (4.4)
Core Casing	8334	0.013 (0.5)	0.001 (0.03)
LP Rotor	9830	0.003 (0.1)	0.0381 (1.5)
Fan Rotor & Fan Frame	9994	0.048 (1.9)	0.003 (0.1)
LP and HP Rotors	13589	0.097 (3.8)	0.005 (0.2)

(1) Single-amplitude response at point of maximum deflection, in mils, for 25.4 g-cm (10 g-in.) unbalance at indicated location.

Table 16-IV. Critical Speeds, Fan Reference, UTW Configuration 2.

Mode Description	Speed rpm	Response(1) mm (Mils)
LP Rotor Bending	2322	0.001 (0.02)
Core Casing & Fan Duct	2360	0.001 (0.03)
Turbine Frame, Exhaust Plug, Core Casing	3597	0.014 (0.57)

(1)Single-amplitude response at point of maximum deflection, in mils, for 25.4 g-cm (10 g-in.) unbalance at fan centerline.

Table 16-V. Critical Speeds, LP Reference, UTW Configuration 2.

Mode Description	Speed rpm	Response(1) mm (Mils)
Core Casing, Inlet, Fan Duct	2321	0.005 (0.2)
Fan Rotor, Fan Frame, Inlet	2614	0.003 (0.1)
Turbine Frame & Exhaust System	3728	0.051 (2.0)
HP and LP Rotors	6280	0.028 (1.1)
Core Casing	8106	0.002 (0.09)

(1)Single-amplitude response at point of maximum deflection, in mils, for 25.4 g-cm (10 g-in.) unbalance in LP turbine.

Table 16-VI. Critical Speeds, HP Reference, UTW Configuration 2.

Mode Description	Speed rpm	Response(1) mm (Mils) Unbalance at Compressor Stage 1	Response(1) mm (Mils) Unbalance at HPT
Turbine Frame, Exhaust System, Core Casing	2338	0.015 (0.6)	0.001 (0.02)
Fan Rotor & Inlet	2725	0.003 (0.1)	0.005 (0.2)
Turbine Frame, Exhaust System	3700	0.010 (0.4)	0.053 (2.1)
LP and HP Rotors	5692	0.015 (0.6)	0.112 (4.4)
Core Casing	7995	0.005 (0.2)	0.003 (0.1)
Fan Rotor & Fan Frame	9454	0.015 (0.6)	0.003 (0.1)
LP Rotor	9858	0.079 (3.1)	0.046 (1.8)
LP and HP Rotors	13179	0.119 (4.7)	0.003 (0.1)

(1) Single-amplitude response at point of maximum deflection, in mils, for 25.5 g-cm (10 g-in.) unbalance at indicated location.

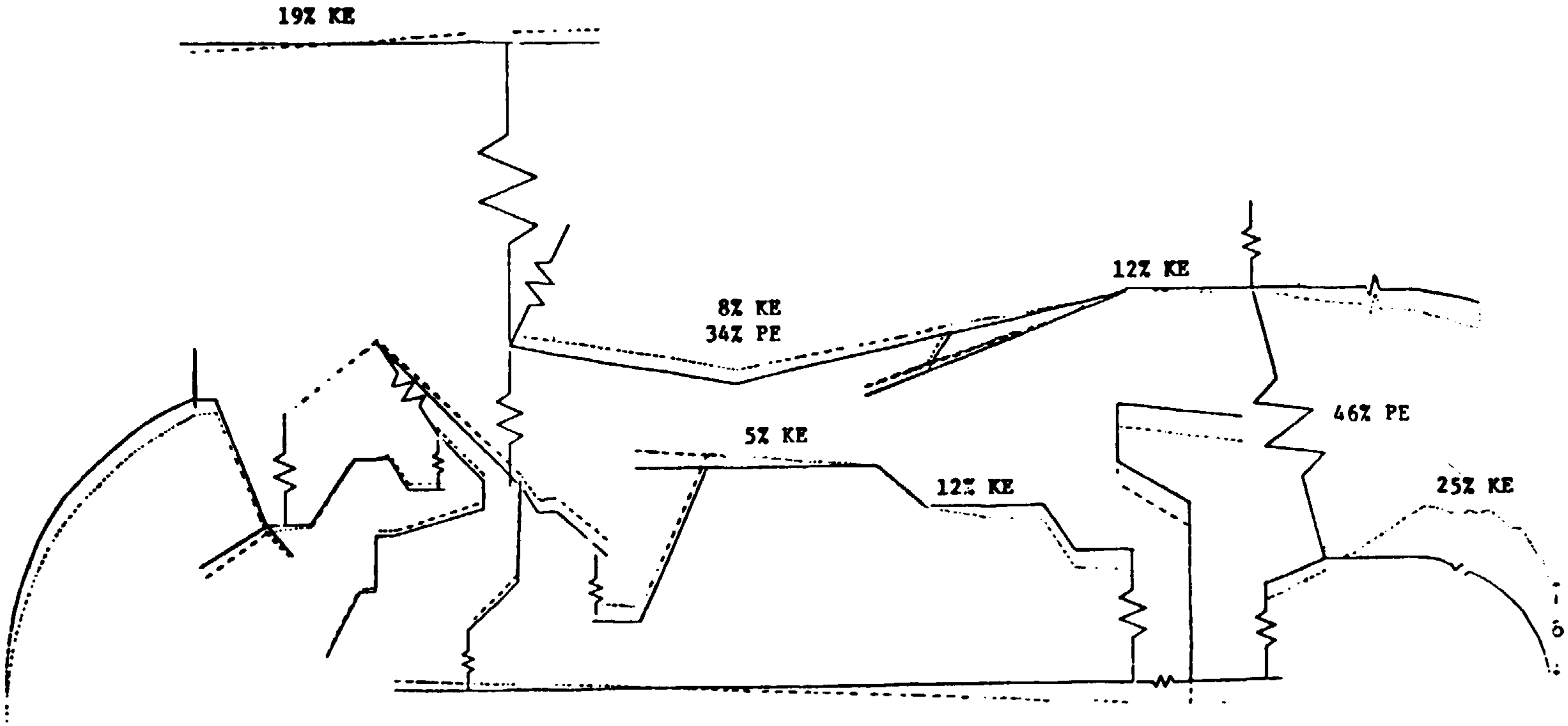
19% KE
8% KE
34% PE
12% KE
5% KE
12% KE
46% PE
25% KE

Figure 16-3. Fan Reference, Configuration 1.

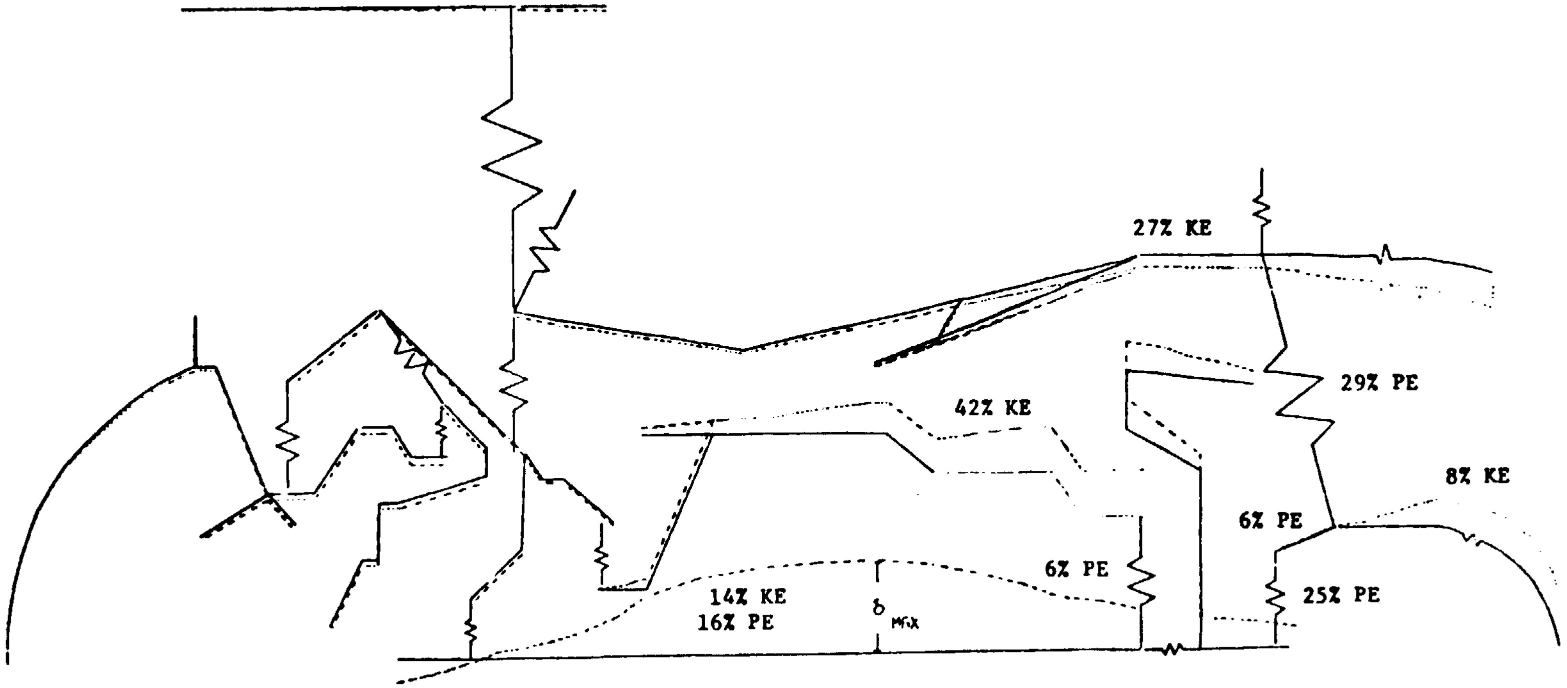
27% KE
29% PE
42% KE
8% KE
6% PE
6% PE
25% PE
14% KE
16% PE
δ_{MAX}

Figure 16-4. LP Reference, Configuration 1.

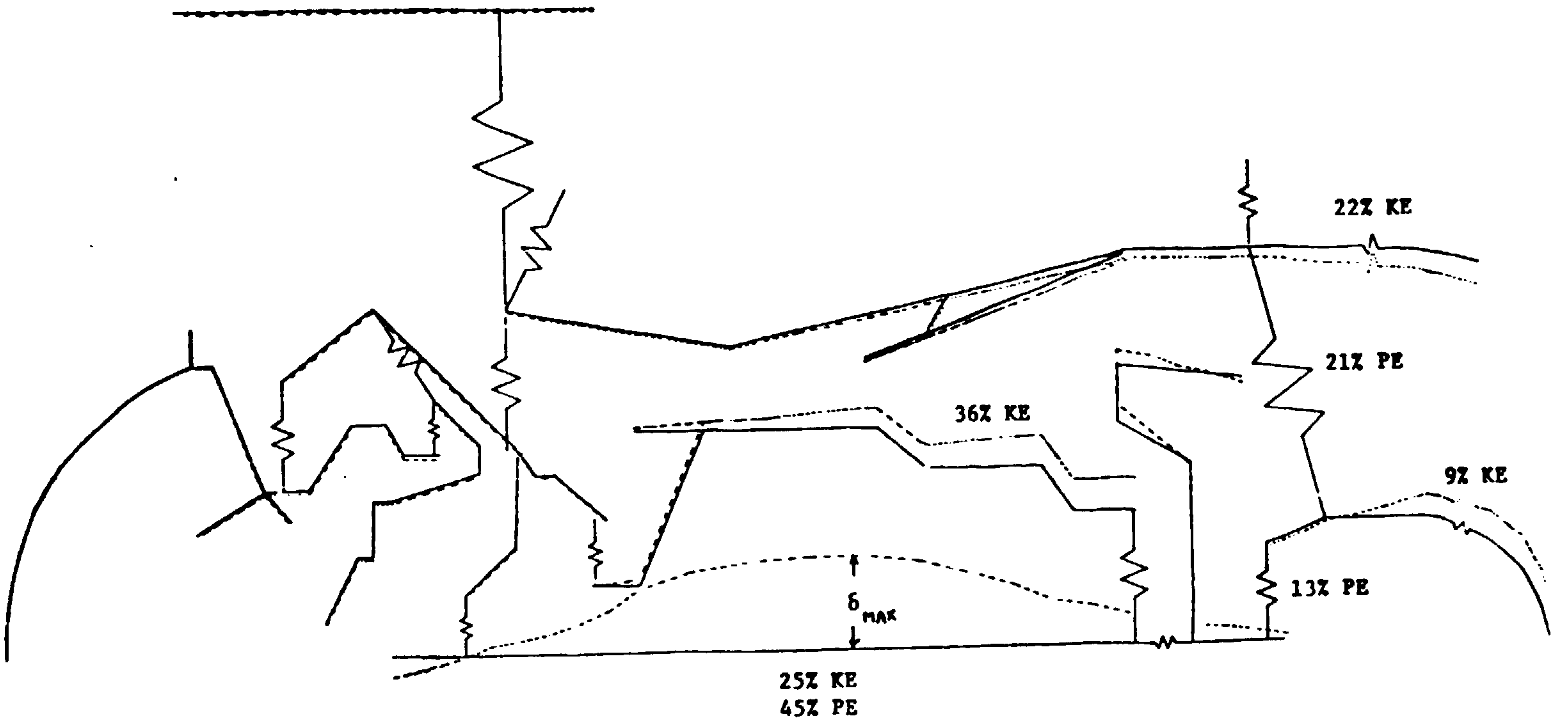
22% KE
21% PE
36% KE
9% KE
13% PE
δ_{MAX}
25% KE
45% PE

Figure 16-5. HP Reference, Configuration 1.

5. If proper rotor balancing procedures are followed, the system should not experience any serious vibration problems, since all modes involve significant bending of static or nonsynchronous rotors which contribute to dissipation of energy. Utilizing current balancing technology, the rotors can be balanced to tolerances within those required to meet design criteria.

SECTION 17.0

WEIGHT

The UTW Propulsion System weight status at the completion of the Detail Design Phase is shown in Tables 17-I and 17-II. Table 17-I shows the breakdown of engine component weights. Differences between the experimental engine and projected flight engine weights are a result of material substitutions and design changes generally made to reduce cost and lead time of the experimental hardware. These differences are covered in detail in Table 17-III.

Table 17-II itemizes the installation components which, when added to the engine weight, result in the total propulsion system weight. In the case of the installation items, both boiler plate and composite nacelle components are shown, although no particular effort has been expended to control the weight of the boiler plate hardware.

As shown, the equivalent flight UTW propulsion system is expected to meet the contract goal of 4.3 installed thrust-to-weight ratio.

Table 17-I. UTW Engine Weight.

	Experimental		Equivalent Flight	
	kg	lb	kg	lb
F101 Core	433.1	955	424.6	936
F101 LP Turbine	117.5	259	117.5	259
Mod. F101 Turbine Frame	83.9	185	52.5	115
Mod. F101 LPT Shaft	28.1	62	28.1	62
Total F101 Components	662.7	1461	622.3	1372
Fan Blades (18)	47.2	104	44.9	99
Disk and Blade Support	94.8	209	88.0	194
			(H-S 90.3	199)
Fan Shaft	35.8	79	22.7	50
Spinner and Adaptors	28.6	63	21.8	48
Total Fan	206.4	455	177.4	391
Total Reduction Gear	91.6	202	77.1	170
Fan Frame Structure	120.2	265	108.9	240
Casing and Flanges	48.1	106	48.1	106
Sump and Shields	2.7	6	2.7	6
Containment	20.9	46	20.9	46
Core OGV's	16.8	37	16.8	37
Total Fan Frame	208.7	460	197.3	435
Bearing Supports	68.0	150	36.3	80
Bearings Sumps and Seals	98.4	217	86.2	190
Accessory Drive System	64.9	143	52.6	116
Lube and Scavenge System	44.0	97	26.3	58
Total Bearings, Drives, and Lube System	275.3	607	201.4	444
Fuel System	33.6	74	21.3	47
Electrical System	26.3	58	25.4	56
V.P. Mechanism	44.9	99	39.9	88
	(H-S 52.6	166)	(H-S 40.4	89)
Piping and Wiring	36.3	80	21.8	48
Total Controls Systems	141.1	311	108.4	239
Total Engine	1585.8	3496	1383.9	3051

Table 17-II. Propulsion System Weight.

	Experimental Boiler Plate		Experimental Composite		Equivalent Flight	
	kg	lb	kg	lb	kg	lb
Inlet	567.0	1250*	156.5	345	156.5	345
Fan Duct	426.4	940*	124.7	275	73.9	163
Flare Nozzle	25.9	57	25.9	57	25.9	57
Core Cowl	244.9	540	46.7	103	44.5	98
Core Exhaust	112.0	247	112.0	247	64.4	142
Hydraulic System	11.3	25	11.3	25	11.3	21
Nozzle Actuation	20.0	44	20.0	44	20.0	44
Oil Coiler	99.8	220*	99.8	220*	18.1	40
Oil Tank	15.9	35*	15.9	35*	11.3	25
Fire Detect. & Exting.	30.8	68	30.8	68	0	0
Instrumentation	22.7	50	22.7	50	11.3	25
Drains and Vents	10.9	24	10.9	24	5.9	13
Total Installation	1587.6	3500	677.2	1493	441.4	973
Engine	1585.8	3496	1585.8	3496	1383.9	3051
Total Prop System	3173.4	6996	2263.0	4989	1825.3	4024

*Facility-Mounted Components

Thrust/Weight Uninstalled = 18300/3051 = 6.00
(Goal = 6.2)

Thrust/Weight Installed = 17400/4024 = 4.32
(Goal = 4.3)

Table 17-III. Experimental and Flight Engine Weight Differences.

Component	Weight kg	Weight lb	Justification
F101 Core	-8.6	-19	Flight engine would use QT core. Many changes not under QCSEE Projects' control, are currently being formulated. These include a single-wall combustion casing. Also, titanium can be used further back in the compressor with the subsonic operating envelope and lower fan pressure ratio. A QCSEE engine could also be designed lighter since max P_3 is 172.3 N/cm^2 (250 psia) instead of 344.8 N/cm^2 (500 psia).
Turbine Frame	-31.7	-70	The experimental frame retains the F101 structure consisting of 14 struts, uniball outer strut attachments and bolted inner strut attachments. The flight frame would be completely redesigned with 8 structural struts and 8 nonstructural vanes welded into the inner and outer casing.
Fan Blades	-2.3	-5	The flight blades will be designed to reverse in one direction only (probably through stall). This may permit an increase in hub solidity and redistribution of thickness. It is likely that a more flexible design will be needed to meet bird strike requirements. Furthermore, when flutter phenomena of composite blades are better understood, some relaxation in torsional stiffness may be permissible, reducing the boron fiber content.
Fan Disk and Blade Support	-6.8	-15	This saving reflects the 5% reduction in blade weight postulated above.
Fan Shaft	-13.2	-29	Saving is due to use of titanium in place of steel and a smaller ring gear diameter.
Spinner and Adaptors	-6.8	-15	Flight engine is assumed to use composite materials for these parts.

Table 17-III. Experimental and Flight Engine Weight Differences (Continued).

Component	Weight kg	Weight lb	Justification
Reduction Gear	-14.5	-32	Saving is due to use of titanium in place of steel for support member. Also, ring gear diameter could be reduced if common interfaces with OTW reduction gear were not a requirement.
Fan Frame Structure	-11.3	-25	A 10% reduction in structural weight has been assumed on the basis that the 3X safety factor and 5-blade-out requirement will be relaxed after more composite test experience is gained.
Bearing Supports	-31.8	-70	Saving is due to use of titanium in place of steel and using scalloped flanges.
Bearings, Sumps and Seals	-12.2	-27	Experimental engine uses a modified CF6 No. 1 bearing. It is assumed that a smaller fan bearing could be developed for a flight engine. Also, lighter thermal shields and integral oil passages would be used on all of the low pressure rotor bearings.
Accessory Drives	-12.2	-27	The experimental gearboxes use available F101 gear trains and bearings. Lighter components could be used for the reduced QCSEE accessory loads. A subsystem breakdown follows:

	Experimental		Flight	
	kg	lb	kg	lb
Accessory gearbox	44.0	97.0	37.6	83
Inlet gearbox (2)	11.9	26.3	7.3	16
Scav. Pump Drive	4.6	10.2	4.1	9
Radial Drive Shafts	4.1	9.0	3.6	8
	64.6	142.5	52.6	116

Table 17-III. Experimental and Flight Engine Weight Differences (Continued).

	Weight		
Component	kg	lb	Justification
Lube and Scavenge System	-18.6	-41	Experimental engine uses an available CF6 lube pump and scavenge filter. Flight engine would allow redesign of these components. Subsystem breakdown follows:

	Experimental		Flight	
	kg	lb	kg	lb
Lube pump	12.7	28.0	6.8	15
Scavenge pump	9.1	20.0	6.8	15
Scavenge filter	13.0	28.6	5.9	13
Supply filter	5.9	13.0	5.9	13
Check valve	3.4	7.5	0.9	2
	44.0	97.0	26.3	58

Fuel System	-12.2	-27	Most of this reduction is due to the use of an all digital control on the flight engine. A subsystem breakdown follows:

	Experimental		Flight	
	kg	lb	kg	lb
Fuel Pump	7.5	16.5	6.6	14.5
Fuel Filter	1.2	2.7	1.5	3.4
Hydromech. Control	18.6	41.0	9.1	20.0
T_{25} Sensor	0.9	1.9	-	-
Core Stator Actuators (2)	1.8	4.0	2.0	4.5
Core Stator Feedback	1.4	3.0	-	-
Drain Eductor	1.4	3.0	-	-
Eductor Flow Regulator	1.4	3.0	1.4	3.0
	34.1	75.1	20.6	45.4

Electrical System	-.9	-2	A significant saving is projected by improved packaging of the digital control, but this is largely offset by returning to a dual ignition system. The subsystem breakdown follows:

Table 17-III. Experimental and Flight Engine Weight Differences (Continued).

Component	Weight		Justification				
	kg	lb		Experimental		Flight	
				kg	lb	kg	lb
			Digital Control	16.3	36.0	11.8	26.0
			Alternator	1.6	3.5	2.0	4.5
			LPT speed sensor	0.5	1.1	0.5	1.1
			T_{12} sensor	0.2	0.5	0.2	0.5
			T_3 sensor	0.5	1.0	0.5	1.0
			Ignitor plug	2.3 (1)	5.0	3.6 (2)	8.0
			Exciter box	2.7 (1)	6.0	3.6 (2)	8.0
			Leads & brackets	2.3 (1)	5.0	3.1 (2)	6.8
				26.4	58.1	25.4	55.9
Variable Pitch Mechanism	-5.0 (12.2 (Ham.	-11 -27) Std.)	The flight engine will require only 100° blade rotation in place of 135° since reversal will be in one direction only. This will permit shorter ball splines. Hamilton Standard forecasts an 8.2 kg 18 lb reduction, mostly because of a new servovalve. It is noted however, that the H-S system will not permit as large a reduction in rotor weight as the GE system by 2.3 kg (5 lb) so the two systems are essentially a standoff.				
Piping and Wiring	-14.5	-32	Both the experimental and flight weight estimates are still very approximate. The flight engine will, however, employ titanium tubing in place of steel.				
Fan Duct	-50.8	-112	The flight duct has no acoustic splitter [required only to meet 609.6 m (2000 ft) runway requirement] and is 20.3 cm (8 in.) shorter.				
Core Cowl	-2.3	-5	Saving due to 20.3 cm (8 in.) shorter length.				
Core Exhaust	-47.6	-105	20.3 cm (8 in.) shorter, no acoustic treatment, and .038 cm (0.015 in.) stock in place of .079 cm (0.031 in.)				

Table 17-III. Experimental and Flight Engine Weight Differences (Concluded).

Component	Weight kg	Weight lb	Justification
Hydraulic System	-1.8	-4	Experimental engine uses off-the-shelf hydraulic pump, with capacity for nozzle actuators (to be supplied by aircraft hydraulic system in flight configuration). A further reduction may be appropriate for a specific aircraft where VP and VN might be operated from aircraft hydraulic systems.
Oil Cooler	-81.6	-180	Experimental engine uses slave LM2500 water/oil cooler. Flight engine uses new fuel/oil cooler.
Oil Tank	-4.5	-10	Experimental engine uses available TF39 tank.
Fire Detect. & Exting.	-30.8	-68	DACo. has agreed to include this subsystem as part of aircraft weight due to a system design and final arrangement which locates fire detectors in the pylon.
Instrumentation	-11.3	-25	Estimate based on reduced requirements in flight engine.
Drains and Vents	-5.0	-11	Reduction due to improved packaging of collector.

DISTRIBUTION LIST

AiResearch Division
Garret Corporation
F.B. Wallace
P.O. Box 5217
Phoenix, Arizona 85010

American Airlines
Maintenance and Engineering Center
K. Grayson
Tulsa, Oklahoma 74151

Andrews Air Force Base
Lt. Col. G. Strand
AFSC Headquarters
Washington, D.C. 20334

AVCO/Lycoming
S. Deckert
550 S. Main Street
Stratford, Connecticut 06497

The Boeing Company
H. Higgins
P.O. Box 3999
Seattle, Washington 98124

The Boeing Company
Wichita Division
D. Torkelson
Wichita, Kansas 67210

Bolt, Beranek and Newman, Inc.
R. Hayden
50 Moulton Street
Cambridge, Massachusetts 02138

Curtiss-Wright Corporation
Power Systems Division
W. Johnson
One Passaic Street
Wood Ridge, New Jersey 07075

Department of Transportation
NASA/DOT Joint Office of Noise Abatement
C. Foster
Office of Secretary
Washington, D. C. 20590

Detroit Diesel Allison Division of General Motors
F. Walters
Suite 312
333 West First Street
Dayton, Ohio 45402

Douglas Aircraft Company
L. Malthan
3855 Lakewood Boulevard
Long Beach, California 90801

Enivronment Protection Agency
J. Schettino
1835 "K" Street, NW
Washington, D.C. 20460

Federal Aviation Administration
Noise Abatement Division
J. Woodall
Washington, D.C. 20590

General Dynamics Convair Division
G. Nicoloff
San Diego, California 92112

Grumman Aerospace Corporation
C. Hoeltzer
South Oyster Bay Road
Bethpage, New York 11714

Hamilton Standard
Division of United Aircraft
A. Jackson
Windsor Locks, Connecticut 06096

Lockheed Aircraft Corporation
T. Higgins
Burbank, California 91503

Lockheed Georgia Company
H.S. Sweet
Marietta, Georgia 30060

NASA Installations

NASA Headquarters
N.F. Rekos
Washington, D.C. 20546

NASA-Ames Research Center
L. Roberts
Moffett Field, California 94035

NASA-Flight Research Center
D.R. Scott
Edwards, California 93523

NASA-Langley Research Center
R. Kuhn
Hampton, Virginia 23665

NASA-Lewis Research Center
21000 Brookpark Road
Cleveland, Ohio 44135

M.A. Beheim
D.N. Bowditch
L.J. Chelko
C.C. Ciepluch
E.W. Conrad
R.J. Denington
A. Ginsburg
M.J. Hartmann
R.H. Kemp
Lewis Library
R.W. Luidens
D.L. Nored
Report Control Office
L.W. Schopen
R.W. Schroeder
M.F. Valerino

NASA/Air Force Liaison
Wright Patterson Air Force Base
Dayton, Ohio 45433

L. Obery
C. Simpson
Col. C.E. Painter
G.K. Richey
G.P. Peterson

Pratt & Whitney Aircraft
Division of United Aircraft Corp.
J. Chew
20800 Center Ridge Road
Rocky River, Ohio 44116

Rohr Corporation
F. Hom
Box 878
Foot and H Street
Chula Vista, California 92012

Wyle Laboratories
L. Sutherland
128 Maryland Street
El Segundo, California 90245

Rockwell International
Los Angeles Division
Attn: D. Schlundt
International Airport
Los Angeles, California 90009